Conference Proceedings

Second ISEES International Conference On

Sustainable Energy and Environmental Challenges (SEEC-2018)

31st Dec 2017 - 3rd Jan, 2018

International Society for Energy, Environment and Sustainability

Indian Institute of Science (IISc), Bangalore, India

Conference Proceedings

Second ISEES International Conference On

Sustainable Energy and Environmental Challenges (SEEC-2018)

31st Dec 2017- 3rd Jan, 2018

International Society for Energy, Environment and Sustainability

Indian Institute of Science (IISc), Bangalore, India

Editors:

Dr. Dev Prakash Satsangi

Dr. Vikram Kumar

Dr. Nikhil Sharma

Dr. Kuppuraj Rajamanickam

Dr. Chetan Kumar Patel

Prof. Avinash Kumar Agarwal

Prof. Saptarshi Basu

Prof. Pradip Dutta

Prof. Ashok Pandey

Contents

About International Society for Energy, Environment and Sustainability (ISEES)

About the Society

The International Society for Energy, Environment and Sustainability was founded at IIT Kanpur in January, 2014 with an aim to spread knowledge in the fields of Energy, Environment, Sustainability and Combustion. In this changing environmental scenario, the time has come where more emphasis has to be laid on renewable energy resources. Moreover, in this dynamic scenario of swelling competition and reducing profits, staying environmentally responsible can be extremely challenging for any organization. More efficient systems have to be developed to meet the increasing energy demands keeping in mind its environmental impact. People have to become more aware and concerned about the environmental challenges which the world is facing today to make it a better place for us and our future generations. The Society aims to spread knowledge in the above mentioned areas among people and make them more aware about the environmental challenges which the world is facing today. The Society is involved in various activities like conducting workshops, seminars, conferences, etc. in the above mentioned domains. The society also recognizes young scientists and engineers for their contributions in this field. It comprises of experts from leading research institutions working in various domains related to energy

Aims and Objectives

1. To organize Workshops/ Symposia/ Conferences/ Lectures/ Courses for wide dissemination of knowledge to its members and society at large, in the areas related to energy, combustion, sustainability, and environment related subjects.
2. To publish technical papers, monographs, books and journals in the areas mentioned above.
3. Organizing events and activities for the benefits of the underprivileged in the society as per the capability of society members.

Journal of Energy and Environmental Sustainability (JEES)

Journal of Energy and Environmental Sustainability is official publication of the International Society for Energy, Environment and Sustainability dedicated to all the areas of conventional

and renewable energy that are relevant for environmental sustainability. The journal will publish two issues in a year and offer a platform for high-quality research in the interdisciplinary areas of energy and environmental science and engineering.

ISEES Membership

1. The Society shall have the grades of Student Member, Member, Fellow and Honorary Fellow. In addition, institutions and organizations will be given Institutional or Corporate membership on payment of dues and satisfying other eligibility criteria as specified by the executive body from time to time.
2. Fellow of the Society will be the highest grade of membership.
3. A graduate in engineering, technology, science, social sciences, humanities or having equivalent qualification as recognized by ISEES may apply for the membership of the Society. In case of unrecognized qualifications, ISEES executive committee (EC) will decide on the recognition of the qualifications. The same shall be updated in the membership documentation from time to time. Award of membership shall be at the sole discretion of the EC.
4. A member may withdraw permanently from the membership of the society at any time by giving a notice in writing to the secretary. In such cases, neither partial nor full refund of membership fee shall be done under any circumstances. There shall not be any exception to this provision.
5. The membership of any student member/ member/ fellow can be withdrawn by ISEES EC in case of unethical, immoral and criminal conduct of the individual concerned. Any action not in alignment with the objectives, interests and purpose of the society may also lead to suspension of the membership. The permanent withdrawal can only be done after an opportunity to present his/ her views to the EC has been given to the defaulting member. The decision of the ISEES EC in this regard shall be final and irrevocable in all such cases.

Privileges of Membership

1. A member whose subscription is paid up to date shall be entitled:
2. To be notified of all relevant activities of the Society.
3. To vote at all Annual General Body Meetings (AGBM) and special meetings of the Society and voting (online/ ballot) on various issues including elections and referendums.
4. Reduced registration fee in the events organized under the banner of the Society.
5. Receive a copy of the proceedings of the meetings (to the corporate members only).
6. To be included in a directory of experts along with the domain expertise to be published by the ISEES from time to time.
7. Corporate members will be able to send two delegates free/ subsidized rates to the events organized by the Society. They will also get partial fee waiver in the advertisement published in the society newsletters/ literature/ ISEES website.

Awards and Recognition

1. A member whose subscription is paid up to date shall be entitled:
2. To be notified of all relevant activities of the Society.
3. To vote at all Annual General Body Meetings (AGBM) and special meetings of the Society and voting (online/ ballot) on various issues including elections and referendums.
4. Reduced registration fee in the events organized under the banner of the Society.
5. Receive a copy of the proceedings of the meetings (to the corporate members only).
6. To be included in a directory of experts along with the domain expertise to be published by the ISEES from time to time.
7. Corporate members will be able to send two delegates free/ subsidized rates to the events organized by the Society. They will also get partial fee waiver in the advertisement published in the society newsletters/ literature/ ISEES website.

Membership Fees

	Type of membership	Annual Membership Fee	Five-Years Membership Fee	Life Membership Fee (10 Years)
India/ SAARC Countries	Student Members	1000 INR	--	--
	Member/ Fellow	2000 INR	5000 INR	10000 INR
	Corporate	10000 INR	--	50000 INR
	Honorary Fellow	0	0	0
USA, Europe and Developed Countries	Student Members	50 US$	--	--
	Member/ Fellow	100 US$	250 US$	500 US$
	Corporate	500 US$	--	2500 US$
	Honorary Fellow	0	0	0

ISEES Executive Committee

Chairman

Prof. Ashok Pandey

Secretary

Prof. A. K. Agarwal

Vice Chairman

Dr. Anirudh Gautam

Joint Secretary

Prof. B. R. Gurjar

Treasurer

Dr. Santanu De

Members

Dr. S. V. Mohan

Dr. Atul Dhar

Dr. T. Bhaskar

Dr. A. P. Singh

Committee for

Second International Conference

on

Sustainable Energy and Environmental Challenges

(SEEC-2018)

Chief Patrons:	Prof. Ashutosh Sharma, Secretary, DST Dr. V.K. Saraswat, Member, NITI Ayog
Patrons:	Prof. Sachin Chaturvedi, RIS, New Delhi Dr. Rakesh Kumar, CSIR -NEERI, Nagpur Dr. Vivek Agarwal, CDC India, Jaipur Dr. D.B Sahoo, IBSD, Imphal Dr. S.K. Barik, CSIR -NBRI, Lucknow Dr. Anjan Ray, CSIR – IIP, Dehradun Dr. R.K Malhotra, Petrofed, New Delhi Dr. Bharat Bhargava, ONGC Energy Centre Dr. Ajay Mathur, TERI, New Delhi
General Chairs:	Prof. Pradip Dutta, IISc, Bangalore Prof. Ashok Pandey, CIAB Mohali
Conference Chairs:	Prof. Saptarshi Basu, IISc Bangalore Prof. Avinash Kumar, Agarwal IIT Kanpur
Conveners:	Dr. Swetaprovo Chaudhuri, IISc Bangalore Dr. Santanu De, IIT Kanpur Dr. Atul Dhar, IIT Mandi Dr. Venkata Mohan, IICT-Hyderabad
Intl. Advisory Board Members Prof. Hugh McCann, University of Edinburgh, UK Prof. Deepak Pant, VITO, Belgium Prof. Franz Winter, Vienna University of Technology Prof. Ramesh K. Agarwal, Washington University Prof. S R Gollahalli, University of Oklahoma Prof. Kalyan Annamalai, Texas A & M University Prof. Bui Xuan Thanh, Ho Chi Minh City University of Technology Prof. Ibrahim Che Omar, Universiti Malaysia Prof. Bassim H. Hameed, Universiti Sains Malaysia Prof. Christian, Universite Clermont Auvergne, France Prof. Samir Khanal, University of Hawaii, USA	

Prof. Duu Jong Lee, National Taiwan University, Taiwan
Prof. Jonathan WC Wong, Hong Kong Baptist University, HK
Prof. Zengqiang Zhang, Northwest A&F University, Yangling, China
Prof. Edgard Gnansounou, EPFL, Lausanne, Switzerland
Prof. Mohammad Taherzadeh, University of Boras, Sweden
Prof. Huu Hao Ngo, University of Technology Sydney, Australia
Prof. Ganti S Murthy, Ganti, Oregon State University
Prof. Rajeshwar D Tyagi, INRS, Canada
Dr. Hans Oechsner, University of Hoheheim, Stuttgart, Germany
Dr. Eldon Raj, UNESCO-IHE, Netherlands
Prof. Suzana Yusuf, Universiti Teknologi Petronas, Malaysia
Dr. Zainul Akmar Zakaria, Universiti Teknologi Malaysia
Dr. S. Mani Sarathy, KAUST, Saudi Arabia
Prof. A. Krothapalli, Florida State University, USA
Prof. Mohammad Taherzadeh, University of Boras, Sweden
Prof. Samir Khanal, University of Hawaii, USA
Prof. Sankar Bhattacharya, Monash University, Malaysia
Prof. Keat Teong Lee, USM, Malaysia
Dr. Sibendu Som, ANL, USA
Prof. Michael Sauer, University of Natural Resources and Life Sciences, Vienna

National Advisory Board Members

Dr. Raja Banerjee, IIT Hyderabad
Dr. Thallada Bhaskar, CSIR-IIP, Dehradun
Dr. S. A. Channiwala, NIT Surat
Dr. Rupam Kataki, Tezpur University, Tezpur
Dr. Sunil Kumar, CSIR-NEERI, Nagpur
Dr. N. Labhsetwar, CSIR-NEERI, Nagpur
Dr. R. K. Maurya, IIT Ropar
Dr. K. Nandakumar, LPSC, ISRO, Thiruvananthapuram
Dr. S Venkat Mohan, CSIR-IICT, Hyderabad
Prof. V. S. Moholkar, IIT Guwahati
Dr. R. D. Mishra, NIT Silchar
Prof. M R Ravi, IIT Delhi
Dr. Sunita Varjani, GPCB, Gandhinagar
Dr. Satish Kumar, NIT Kurukshetra
Prof. Parimal S Parikh, SVNIT Surat
Dr. P A Laxminarayanan, Simpson Engines, Chennai
Dr. S. Somanath, LPSC, ISRO
Dr. C. Rangnayakulu, ADA, Bangalore
Dr. Debasis Chakraborty, DRDL, Hyderabad
Prof. Mahesh Panchagnula, IIT-Madras
Prof. Suman Chakraborty, IIT-Kharagpur
Prof. Swarnendu Sen, Jadavpur University
Prof. Achintya Mukhopadhyay, Jadavpur University
Prof. Vikram Jayaram, IISc Bangalore
Prof. Kamanio Chattopadhyay, IISc Bangalore
Prof. Bikramjit Basu, IISc Bangalore
Prof. K.N Lakshmisha, IISc Bangalore
Prof. S. Gopalkrishnan, IISc Bangalore
Prof. G. Jagadeesh, IISc Bangalore

SEEC-2018 ORGANISERS

Prof. Ashok Pandey
Distinguished Scientist
CSIR-Indian Institute of Toxicology Research,
Lucknow-226001, India
E-mail pandey@ciab.res.in; ashokpandey56@yahoo.co.in
Tel: +91-172-4990214
Fax: +91-172-4990204

Professor Ashok Pandey is currently Distinguished Scientist at CSIR-Indian Institute for Toxicology Research, Lucknow, India and Honorary Executive Director at the Centre for Energy and Environmental Sustainability- India. He has been Visiting Professor/Scientist and UNESCO Professor in many countries, including France, Brazil, UK, Switzerland, Malaysia, Thailand, etc. Formerly, he was Eminent Scientist at the Center of Innovative and Applied Bioprocessing, Mohali and Chief Scientist & Head of Biotechnology Division at CSIR's National Institute for Interdisciplinary Science and Technology at Trivandrum. Professor Pandey has ~ 1200 publications/communications, which include 16 patents, 54 books, 130 book chapters, 465 original and review papers, etc with h index of 84 and >29,000 citations (Goggle scholar).

Professor Pandey is the recipient of many national and international awards and fellowships, which include Life-Time Achievement Award from the International Society for Energy, Environment and Sustainability (2017); Fellow of Royal Society of Biology, UK (2016); Academician of European Academy of Sciences and Arts, Germany (2016); Fellow of International Society for Energy, Environment and Sustainability (2014); Fellow of National Academy of Science, India (2012); Fellow of Association of Microbiologists of India (2010); Fellow of International Organization of Biotechnology and Bioengineering (2008); Fellow of the Biotech Research Society, India (2005); Honorary Doctorate degree from Univesite Blaise Pascal, France (2007); Thomson Scientific India Citation Laureate Award, USA (2008); Lupin Visiting Fellowship, Best Scientific Work Achievement award, Govt of Cuba; UNESCO Professor; Raman Research Fellowship Award, CSIR; GBF, Germany and CNRS, France Fellowship; Young Scientist Award, etc.

Professor Pandey was Chairman of the International Society of Food, Agriculture and Environment, Finland (Food & Health) during 2003-2004. He is Founder President of the Biotech Research Society, India; International Coordinator of International Forum on Industrial Bioprocesses, France, Chairman of the International Society for Energy, Environment & Sustainability and Vice-President of All India Biotech Association.

Prof Pandey is Editor-in-chief of Bioresource Technology, Honorary Executive Advisors of Journal of Water Sustainability and Journal of Energy and Environmental Sustainability, Subject editor of Proceedings of National Academy of Sciences (India) and editorial board member of several international and Indian journals. He is editor-in-chief of a book series on Current Developments in Biotechnology and Bioengineering, comprising twelve volumes published by Elsevier and another series on Biomass, Biofuels and Biochemicals, comprising six volumes.

Prof. Pradip Dutta
Professor and Chairman
Department of Mechanical Engineering
Indian Institute of Science
Bangalore 560012
Phone: (080)22932512
Fax: (080)23604536
Email: pradip@iisc.ac.in
Web: http://www.mecheng.iisc.ernet.in/~pradip/

Prof. Dutta received his bachelor's degree in Mechanical Engineering from IIT Kharagpur, his master's degree from IIT Madras and Ph.D. from Columbia University. He held faculty positions at Columbia University and at the Tennessee Tech. University, before joining the Indian Institute of Science as a faculty member in 1996.

Prof. Dutta's research group focuses on development of advanced energy technologies related to solar energy, cooling of electronics, spacecraft thermal management, and on thermal technologies related to phase change.

Prof. Dutta has been elected Fellow of the ASME, and Fellow of all the four National Academies of India in science and engineering. Among several other awards, Prof. Dutta has received the VASVIK Award for Industrial Research, IISc Alumni Award for Excellence in Engineering Research, INAE Chair Professorship Award, INAE Outstanding Teacher Award, IIT Kharagpur Distinguished Alumnus Award, IIT Madras Distinguished Alumnus Award, and the J. C. Bose National Fellowship. He is serving as Associate Editors of IEEE Transactions on Components and Packaging Technology, and ASME Journal of Electronic Packaging. At IISc, he has been a co-founder of the National Facility for Semisolid Forming, co-Director of the General-Motors-IISc Collaborative Research Lab, and convenor of the Institute's solar energy initiative.

Currently, Prof. Dutta is the Chairman of the Department of Mechanical Engineering at IISc, and co-leader of the India-US Consortium called Solar Energy Research Institute for India and the United States (SERIIUS).

Dr. Saptarshi Basu
Associate Professor
Department of Mechanical Engineering
Indian Institute of Science
Bangalore 560012
Phone: 91-776-08-08825
Email: sbasu@mecheng.iisc.ernet.in

Prof. Saptarshi Basu is currently an Associate Professor in the Department of Mechanical Engineering at Indian Institute of Science.

Prof. Saptarshi basu received his M.S. and Ph. D. degrees in Mechanical Engineering from University of Connecticut in 2004 and 2007 respectively. Prof. Basu was a tenure track faculty member in the Department of Mechanical, Materials and Aerospace Engineering in University of Central Florida, USA from 2007-2010. He joined Indian Institute of Science as a faculty member in 2010.

His current research interests include combustion instability, flame-vortex interaction, droplet level transport, multiphase combustion, spray atomization and breakup, water transport characteristics in fuel cells and general areas of heat and mass transfer.

Prof. Basu is the recipient of DST Swarnajayanti Fellowship from Government of India in Engineering Sciences. He also received the K.N Seetharamu medal from Indian Society of Heat and Mass Transfer for his contributions in multiphase transport. Prof. Basu is a member of ASME, ISHMT and Combustion Institute. He is a Fellow of the Indian National Academy of Engineering.

Prof. Avinash Kumar Agarwal
Professor
Department of Mechanical Engineering
Indian Institute of Technology Kanpur
Kanpur 208016
Phone: +91-512-259 7982 (office)
Fax: +91 -512-259 7408
Email: akag@iitk.ac.in

Prof. Avinash Kumar Agarwal obtained his B.E. (Mech Engg., 1994) from Malviya Regional Engineering College, Jaipur and M.Tech. (Energy, 1996) and Ph.D. (Energy, 1999) from Indian Institute of Technology Delhi. After his Post-Doctoral Fellowship (1999 – 2001) at the Engine Research Center, University of Wisconsin, Madison, USA, he returned to India in 2001 and joined Department of Mechanical Engineering, Indian Institute of Technology Kanpur as Assistant Professor, where he is serving as a Professor currently. He was a Visiting Professor to University of Loughborough, UK, Photonics Institute, University of Vienna, Austria, Hanyang University, South Korea and Korea Advanced Institute of Science and Technology, South Korea.

At IIT Kanpur, Prof. Agarwal worked in the areas of IC engines, combustion, conventional fuels, alternative fuels, hydrogen, fuel sprays, lubricating oil tribology, optical diagnostics, laser ignition, HCCI, particulate and emission control, and large bore engines. He has developed laser fired hydrogen and CNG engines in automotive sizes and developed the first electronic fuel injection system equipped locomotive engine for Indian Railways, which improved duty-cycle fuel economy and reduced particulate emissions substantially. Currently, Prof. Agarwal is involved in development of Methanol and DME fuelled vehicles for automotive sector. He is Editor-in-Chief of Journal of Energy and Environmental Sustainability and Associate Editor of Journal of Energy Resources Technology (Transactions of ASME), International Journal of Vehicle Systems Modelling and Testing and the Journal of the Institute of Engineers (Series C).

For his outstanding contributions, Prof. Agarwal is conferred upon Clarivate Analytics India Citation Award-2017 in Engineering and Technology, Prestigious Shanti Swarup Bhatnagar Prize (2016) in Engineering Sciences, Rajib Goyal Prize in Physical Sciences (2017); NASI-Reliance Industries Platinum Jubilee Award (2012); INAE Silver Jubilee Young Engineer Award (2012); Dr. C. V. Raman Young Teachers Award (2011); SAE International's Ralph R. Teetor Educational Award (2008); INSA Young Scientist Award (2007); UICT Young Scientist Award (2007); INAE Young Engineer Award (2005); Devendra Shukla Research Fellowship (2009-12) and Poonam and Prabhu Goyal Endowed Chair Professorship (2013-16) at IIT Kanpur; AICTE Career Award for Young Tecahers (2004); DST Young Scientist Award (2002); and DST BOYSCAST Fellowship (2002). He is a Fellow of Society of Automotive Engineers International, USA (SAE; 2012), American Society of Mechanical Engineers (ASME; 2013), Indian National Academy of Engineering (INAE; 2015) and International Society for Energy, Environment and Sustainability (ISEES; 2016). At IIT Kanpur, Prof. Agarwal has established a state-of-the art "Engine Research Laboratory" (www.iitk.ac.in/erl).

ISEES FELLOWS

ISEES FELLOWS (2018)

Prof. Gautam Kalghatgi
Principal Professional, Saudi Aramco
PO Box 9290
Dhahran, Saudi Arabia 31311

Dr. Ajay Mathur
Director-General
TERI (The Energy and Resources Institute)
6C Darbari Seth Block IHC Complex, Lodhi Road
New Delhi 110003

Prof. V Ganeshan
Professor
Department of Mechanical Engineering
Indian Institute of Technology Madras

Prof. Franz Winter
Head of Chemical Process Engg and Energy Technology
Institute of Chemical, Environmental & Biological
Engineering, TU-Wien,
Getreidemarkt 9/166
1060 Vienna, Austria

Dr. Nitin Labhasetwar
Sr. Principal Scientist & Head,
Energy & Resource Management Division,
CSIR-National Environmental Engineering Research
Institute, Nehru Marg, Nagpur-440020, India

Prof. Achintya Mukhopadhyay
Professor
Mechanical Engineering Department
Jadavpur University, Kolkata, India

ISEES FELLOWS (2017)

Dr. V K Saraswat
Former Secretary Defence R&D
Member, NITI Aayog,
DRDO Guest House, Development Enclave,
Sankar Vihar Delhi Cantt., New Delhi-110010

Prof. Probir Kumar Bose
Campus Director, NSHM Knowledge Campus, GOI
Arrah, Shivtala, Via Muchipara, Durgapur - 713212

Prof. Ramesh Agarwal
William Palm Professor of Engineering
Washington University in St. Louis, USA

Prof. Bhola R. Gurjar
Professor in Civil (Environmental) Engineering, and
Head, Centre for Transportation Systems (CTRANS)
Indian Institute of Technology (I.I.T.) - Roorkee

Prof. Swarnendu Sen
Professor, Department of Mechanical
EngineeringDepartment of Mechanical Engineering,
Jadavpur University, Kolkata - 700 032

Dr. Thallada Bhaskar
Principal Scientist,
Thermocatalytic Processes Area, Bio-Fuels Division,
CSIR-Indian Institute of Petroleum, Mohkampur,
Dehradun-248005, Uttarakhand, India

Dr. Anirudh Gautam
Executive Director
Special Railway Establishment for Strategic
Technology and Holistic Advancement (SHRESHTA)
RDSO, Lucknow

ISEES FELLOWS (2016)

Prof. Avinash Kumar Agarwal
Department of Mechanical Engineering
Indian Institute of Technology Kanpur
Kanpur, 208016, UP, India

Dr. S. Venkata Mohan
Principal Scientist
Bioengineering and Environmental Sciences Lab,
EEFF Department,
CSIR-Indian Institute of Chemical Technology,
Hyderabad – 500 007, India

Prof. Ernst Wintner
Retired Professor of Applied Laser Technology
Vienna University of Technology (TU Vienna,
Photonics Institute),
Vienna, Austria

Dr. Satish Kumar
Distinguished Scientist & Chief Controller
R&D (TN) DRDO

Prof. Ryo Amano
Professor of Mechanical Engineering Department
University of Wisconsin-Milwaukee
Milwaukee, WI 53201

ISEES FELLOWS (2015)

Prof. L.M. Das
Emeritus Professor
Center for Energy Studies
IIT Delhi, Hauz Khas
New Delhi, 110016

Prof. Chang Sik Lee
Chair Professor
School of Mechanical Engineering
Hanyang University Seoul, Korea

Prof. O. N. Srivastava
Emeritus Professor
Faculty of Science, Department of Physics,
Banaras Hindu University
Varanasi

Dr. Gabriel D. Roy
CPnE Consultants,
Fairfax, VA 22030, USA

ISEES FELLOWS (2014)

Prof. Ashok Pandey
Distinguished Scientist
CSIR-Indian Institute of Toxicology Research,
Lucknow-226001, India

Prof. S. R. Gollahalli
School of Aerospace and Mechanical Engg.
University of Oklahoma
Norman. OK 73019

Dr. R. K. Malhotra
Director General
Federation of Indian Petroleum Industry (FIPI)
3rd Floor, PHD House, 4/2,
Siri Institutional Area,
August Kranti Marg,
New Delhi - 110 016

ISEES AWARDS - 2018

ISEES Young Scientist Awardees (2018)

Sunita J. Varjani

Dr. Sunita J. Varjani is a Scientific Officer in Gujarat Pollution Control Board. Dr. Varjani has worked on exploration and exploitation of indigenous hydrocarbon utilizing/ degrading and bio-surfactant producing bacterial isolates for applications in bioremediation of petroleum based hydrocarbon pollutants and microbial enhanced oil recovery (MEOR), which are considered as the burning issues. She has authored 25 peer reviewed journal papers, and 14 book chapters, and has edited 5 books. She received Fellow Award-2012 from Society for Applied Biotechnology.

Dr. Pravesh Chandra Shukla

Dr. Pravesh Chandra Shukla is a Post Doctoral Fellow at Lund University, Sweden. He has developed low-cost mixed oxide based Diesel Oxidation Catalysts to reduce gaseous and particulate emissions from diesel engine exhaust. He also conducted research on assessment of toxic potential of primary and secondary particulates/ aerosols from biodiesel, alcohol blends utilisation in heavy-duty engines and spray characterization of biodiesels. He has authored 22 peer-reviewed journal and conference papers, and two book chapters.

Dr. Murali Banavoth

Dr. Murali Banavoth is Assistant Professor in School of Chemistry at University of Hyderabad. Dr. Banavoth's research focuses on finding solutions for various energy and environmental problems using engineering and improving the performance of solar absorbers by application of nano-technology. He has authored 44 peer-reviewed journal and conference papers, and one book chapter. He is a recipient of BRICS Young Scientist Award-2017.

ISEES Best Ph.D. Thesis Awardees (2018)

Dr. Nikhil Sharma

Thesis Title: Spray, Combustion, Emissions and Particulate Investigations of a Gasohol Fuelled Gasoline Direct Injection Engine
Indian Institute of Technology Kanpur, India

Dr. Kuntal Jana

Thesis Title: Polygeneration as a Future Sustainable Energy Solution: Thermodynamic, Economic and Environmental Performance Assessment
Jadavpur University, Kolkata, India

Dr. Vishnu R Unni

Thesis Title: Dynamics of Blowout and Thermo-acoustic Instability in a Bluff-Body Stabilized Turbulent Combustor
Indian Institute of Technology Madras, India

LIST OF INVITED SPEAKERS

LIST OF INVITED SPEAKERS

Gautam Kalghatgi	Saudi Aramco, Saudi Arabia
M. Razi Nalim	Indiana University Purdue University, USA
Ramesh K. Agarwal	Washington University, St. Louis, USA
Achintya Mukhopadhyay	Jadavpur University, Kolkata
Ashoke De	IIT Kanpur
Franz Winter	Technical University of Vienna, Austria
Kalyan T Annamalai	Texas A&M University, USA
P. A. Lakshminarayanan	Simpson Engines, Chennai
N Saravanan	Mahindra Research Valley, Chennai
Rajendra Bordia	Clemson University, USA
Himanshu Tyagi	IIT Ropar
Giridhar Madras	IISc Bangalore
Gopalakrishnan Kumar	University Jillyang, Gyeongsan, South Korea
Nitin Labhasetwar	NEERI Nagpur
Alok Kumar	IISc Bangalore
Kamanio Chattopadhyay	IISc Bangalore
Sandip Kumar Saha	IIT Bombay
Pravesh C Shukla	Lund University, Sweden
Murali Banavoth	University of Hyderabad
Sunita J. Varjani	Gujarat Pollution Control Board, Gandhinagar
Nikhil Sharma	IIT Kanpur
Kuntal Jana	IIT Guwahati
Vishnu R Unni	IIT Madras
Michael Sauer	Univ. of Natural Resources & Life Sciences, Austria
Ganti S Murthy	Oregon State University, USA
Saravanamurugan S	CIAB, Mohali
Keat Teong Lee	Universiti Sains Malaysia, Pulau Pinang, Malaysia
Suzana Yusup	Universiti Teknologi PETRONAS, Perak, Malaysia
Daniel CW Tsang	Hong Kong Polytechnic University
Xuan-Thanh Bui	Ho Chi Minh City University of Technology, Vietnam
Sibendu Som	Argonne National Laboratory, USA
Kalyan K. Srinivasan	University of Alabama, USA
Tarun Gupta	IIT Kanpur
P K Bose	NSHM Knowledge Campus, Durgapur
Mahesh V. Panchagnula	IIT Madras
Debasis Chakraborty	Defence Research & Developmental Lab., Hyderabad
Gaurav Tomar	IISc, Bangalore
Anirudh Gautam	SHRESTHA, RDSO, Lucknow
Dhananjay K. Srivastava	IIT Kharagpur
Anjan Ray	CSIR-IIP, Dehradun
Suren Singh	Durban University of Technology, South Africa
Binod Parameswaran	CSIR-NIIST, Trivandrum
Santanu De	IIT Kanpur

Amit Agrawal	IIT Bombay
Teodora Emilia Motoasca	KU Leuven, Belgium
Venugopal Shankar	Mahindra Research Vally, Chennai
S L Soni	NIT Uttarakhand /MNIT Jaipur
S. Venkata Mohan	CSIR-IICT Hyderabad
Ibrahim Che Omar	Universiti Malaysia Kelantan, Malaysia
Rajeev Sukumaran	CSIR-NIIST, Trivandrum
Edgard Gnansounou	Ecole Polytechnique Fédérale de Lausanne, Switzerland
Vijayanand S Moholkar	IIT Guwahati
Jayeeta Bhaumik	CIAB, Mohali
Jong M Park	Pohang University of Science and Tech., South Korea
Deepak Pant	Central Univ. of Himachal Pradesh, Dharamshala
Thallada Bhaskar	CSIR-IIP Dehradun
Bharat Bhargava	ONGC Energy Center, Delhi
Roger Sierens	Ghent University, Belgium
Atul Dhar	IIT Mandi
Anjaneyulu Krothapalli	Florida State University, USA
Pradip Dutta	IISc Bangalore
Prodyut Chakraborty	IIT Jodhpur
Indu Shekhar Thakur	JNU, Delhi
Shantanu Bhattacharya	IIT Kanpur

BIOGRAPHIES OF PLENARY SPEAKERS

Prof. Gautam Kalghatgi
Principal Professional, Saudi Aramco
PO Box 9290
Dhahran, Saudi Arabia 31311
Phone: +966 138768171
Email: Gautam.kalghatgi@aramco.com
kalghatgig@gmail.com

Prof. Kalghatgi is currently a Principal Professional at Saudi Aramco and is also a Visiting Professor at Imperial College, London and at Oxford University. He has held similar professorial appointments in the past at KTH, Stockholm; Technical University, Eindhoven and Sheffield University. He joined Saudi Aramco in October 2010 after 31 years with Shell Research Ltd. in the U.K. He is a fellow of the Royal Academy of Engineering, SAE and I.Mech.E. and is on the editorial boards of several journals and on the International Board of Directors of the Combustion Institute. He has published around 150 papers and a recent book, "Fuel/Engine Interactions" on combustion, fuels and engine research and transport energy. He has a B.Tech. from I.I.T. Bombay (1972) and Ph.D. from Bristol University (1975) in Aeronautical Engineering. From 1975 to 1979, he did post-doctoral research in turbulent combustion at Southampton University with Prof. Ken Bray.

IS IT REALLY THE END OF COMBUSTION ENGINES AND PETROLEUM?

Currently 95% of transport energy comes from liquid fuels made from oil. The global demand for both transport energy and petrochemicals is large and is growing with increasing population and prosperity, primarily in non-OECD countries. There has been much recent comment predicting the imminent demise of internal combustion engines (ICEs) and the oil industry following speculation about electrification of the transport sector. There will be increasing electrification, particularly of light duty vehicles (LDVs) in the form of hybridization to improve the efficiency and performance of vehicles carrying ICEs. However, there are very significant environmental, economic and technical constraints on the unlimited growth of battery electric vehicles, powered only by electricity, for all transport. Other alternative transport energy sources like biofuels, natural gas, LPG, DME, methanol and hydrogen will grow but have their own constraints on fast and/or unlimited growth. Transport will continue to be largely powered by ICEs running on liquid fuels in the coming decades and it is imperative that such engines continue to improve in efficiency and cleanliness. There is great scope to achieve this is by developing fuel/engine systems in conjunction with better control and after-treatment systems through collaboration between the oil and auto industries and governments.

Dr. V K Saraswat
Former Secretary Defence R&D
Member, NITI Aayog,
DRDO Guest House, Development Enclave,
Sankar Vihar Delhi Cantt., New Delhi-110010

Dr. Vijay Kumar Saraswat, India's most gifted scientist and an accomplished researcher with more than four decades of experience spaning over several fields and areas in both basic and applied sciences of defence research. Apart from being a scientist, he is a rare combination of an innovator, technologist and visionary. Born at Gwalior on 25 May 1949, Dr. Saraswat completed his engineering from Gwalior; Master of Engineering from IISc Bangalore followed by Ph.D from Osmania University.

During his illustrious career, from Scientist to Scientific Adviser to Defence Minister, Director to Director General DRDO and Secretary to Dept of Defence R&D, Dr. Saraswat has been credited with development of Liquid Propulsion Rocket Engines and missiles namely PRITHVI, DHANUSH, PRAHAAR indigenously. He is the principal architect of the Ballistic Missile Defence programme which included major technology breakthroughs. The successive interceptions of incoming target ballistic missiles at Exo and Endo atmospheres are a testimony to his dedicated efforts and exploitation of limited technological resources. With this India joined the select nations that have the capability to develop BMD systems. Dr. Saraswat brought new dimensions to the strategic defence scenario through successful test firing of AGNI-5, SHOURYA, Initial Operational Clearance for Light Combat Aircraft TEJAS and induction of INS Arihant. Thus, today nation can boast of reaching any shores in the world with the nuclear capable missiles with different strike ranges. Under his leadership, DRDO provided the technologies developed by them for societal benefits namely Solar Powered Modular Green Shelters, Bio-Digesters, AAHAR programmes, explosive detection kit, Diagnostic Units for Dengu and Chickengunia etc.

Dr. Saraswat's pioneering efforts have taken shape into establishment of Research & Innovation Centre at IIT Madras; MILIT- Centre for Training needs of armed forces on S&T ; CERT for reporting, auditing and handling emergency response of Information Security Incidents; CHESS - futuristic technology Centre for High Energy Laser and Microwave devices; Kyrgyz-Indian Mountain Bio-Medical Research Centre at Kyrgyzstan; The new international airport and Aerospace SEZ at Hyderabad and Advanced Combustion Research Centers at IISc and IIT(M). Till recently, Dr. Saraswat was DAE Homi Bhabha Chair and initiated development of technologies for Energy Security namely Bio-Mass, Solid Waste Management, Fuel Cells, Concentrated Solar Power, Multi Junction Photovoltaic Cells, Clean Coal Technologies etc., in the country at various Industrial and Academic Institutions in addition to bringing new dimensions to Aerospace Manufacturing. Honoris Causa was conferred upon him by more than 18 Universities including Andhra University (Visakhapatnam), NIT Surat. He has also authored and presented several papers for at National & International level journals / conferences and guided eight Ph.D Scholars. Dr. Saraswat presently is the Member NITI Aayog and shouldering many honorary positions in Government and Academic Institutions.

Dr. Baldev Raj FTWAS, FNAE, FNA, FASc, FNASc
Director, National Institute of Advanced Studies
(www.nias.res.in)
Chancellor, Academy of Scientific and Innovative Research
(AcSIR)
Distinguished Scientist and Former Director, Indira Gandhi
Centre for Atomic Research
Chairman, Research Council of Gas Turbine Research
Establishment, DRDO
Past President, Indian National Academy of Engineering
Past President, International Council of Academies of
Engineering & Technological Sciences

Pursuits of Prof Baldev Raj in basic science and applications with multi and interdisciplinary approaches and teams have found expressions of merit in materials science and technologies, cultural heritage, medical technologies and policies. He has provided unique interpretations and solutions to challenges in energy, water, healthcare, manufacturing and national strategic unsolvables in a large measure, with clear impact, distinctions and awards. He is acclaimed for his contributions to Science and Technology of measurements and Sodium Fast Reactors and Associated Fuel Cycle.

Prof Baldev Raj is known for overcoming the barriers of academic research and industry with acumens of leadership and experiences. His work on non-destructive evaluation, different aspects of materials (welding corrosion, mechanics), nuclear systems science and technology, ferrofluids and sensors has earned for him to be among the national and world leaders by virtue of his 1300 plus publications, 80 plus books, 100 plus articles in encyclopedia and handbooks, technologies, patents, standards, etc.

Prof Baldev Raj has been selected for eminent positions, as evidenced by awards, fellowships of all the four academies of Sciences and Engineering in the country, International Nuclear Energy Academy, Institute of Directors, Indian Academy of Social Sciences, Academy of NDT International, American Society of Metals, German Academy of Science, The World Academy of Sciences etc. etc.. He is Honorary Fellow of International Medical Sciences Academy, Indian Institute of Metals, Indian Society of NDT, Indian Institute of Welding International Committee on NDT etc. With invitations for about 500 plenary, keynote, invited speeches; Chairs and Members of some of the most eminent Committees, Councils and Bodies in the country and more than 30 countries worldwide, he has steered several large high impact collaborative programmes with almost all important countries in the world. His contributions to science policy and science diplomacy are recognized worldwide. He has been honored with Homi Bhabha Gold Medal; H K Firodia Award; Om Prakash Bhasin Award; Vasvik Award, National Metallurgist Award; Lifetime Achievement Award of Indian Nuclear Society, Distinguished Material Scientist Award; Padma Shri; Distinguished Alumni of Indian Institute of Science, among many other distinct honors.

Prof Baldev Raj has a passion for interacting with students and young professionals for mutual inspirations and service to society.

BIOGRAPHIES AND ABSTRACTS OF INVITED SPEAKERS

PRESSURE-GAIN AND WORK-PRODUCING COMBUSTION FOR HIGH-EFFICIENCY LIGHT-WEIGHT ENGINES

M. Razi Nalim

Department of Mechanical Engineering,
Purdue School of Engineering & Technology,
Indiana University Purdue University Indianapolis
USA

There is continuing interest in pressure gain combustion in applications that traditionally used continuous flow nominally constant-pressure combustors. Thermodynamic analysis indicates potential for greatly improved specific power and thermal efficiency in combustion engines used for propulsion and power applications, after allowing for a realistic level of component losses. Specific-fuel-consumption improvements in excess of 30% over those of a conventional Brayton cycle are indicated for medium and small-size gas turbine engine applications. Combustion approaches for achieving pressure-gain include deflagrative combustion in wave rotor devices and pulse combustors, and detonative combustion in rotating-detonation and pulse-detonation devices. The opportunities and challenges of each of these types is discussed. Wave-rotor devices also offer the option of work production by the combustor device, which is explored in more detail. The fundamentals of the ignition process by a hot-gas traversing jet in a wave rotor are presented. The technology development status of pressure-gain and work-producing combustors is summarized.

Prof. M. Razi Nalim
Professor
Department of Mechanical Engineering
Purdue School of Engineering & Technology
Indiana University Purdue University Indianapolis
Email: mnalim@iupui.edu

Prof. M. Razi Nalim has completed his B.Tech. in mechachanical engineering from IIT Kanpur (1983), masters in mechanical engineering (1985) and PhD in aerospace engineering (1994) from Cornell University.

He has worked as expertise in field of combustion; unsteady compressible gasdynamics; energy conversion; combustion engines; energy efficiency; computational fluid mechanics; heat transfer; thermodynamics; aircraft and space propulsion; biofluid mechanics; engineering education; graduate education, research administration.

His area of interests are pollution control; innovative powerplants; wave rotors; combustion and turbulence modeling; ignition processes; design methodology and optimization; unsteady biofluid flow; biomedical engineering; aerospace education.

TRANSIENT COLD FLOW SIMULATION OF A FAST FLUIDIZED BED FUEL REACTOR FOR CHEMICAL LOOPING COMBUSTION

Ramesh K. Agarwal

William Palm Professor of Engineering,
Washington University in St. Louis, USA

Abstract

Circulating fluidized bed (CFB) in chemical looping combustion (CLC) is a novel carbon capture technology which offers great advantage for high efficiency and low cost. To obtain a thorough understanding of the hydrodynamics behavior inside the reactors as well as CLC process, numerical simulations are conducted. Computational Fluid Dynamics (CFD) simulations are performed with Dense Discrete Phase model (DDPM) to simulate the gas-solid interactions. CFD commercial software ANSYS Fluent is applied for the simulations. Two bed materials of different particle density and diameter, namely the molochite and Fe100, are used in studying the hydrodynamics and particle behavior in a fuel reactor corresponding to the experimental set up of Haider et al. at Cranfield University in U.K. Both the simulations reach satisfactory agreement with the experimental data concerning both the static pressure and volume fraction at various heights above the gas inlet inside the reactor. It is found that an appropriate drag law should be used in the simulation depending on the particle size and flow conditions to obtain accurate results. The simulations demonstrate the ability of CFD/DDPM to accurately capture the physics of CFB based CLC process at pilot scale which can be extended to industrial scale applications.

Prof. Ramesh K. Agarwal
William Palm Professor of Engineering
Washington University in St. Louis, USA
Phone: +1-314-935-6091
Fax: +1-314-935-4014
Email: rka@wustl.edu

Dr. Ramesh K. Agarwal is the William Palm Professor of Engineering in the department of Mechanical Engineering and Materials Science at Washington University in St. Louis. From 1994 to 2001, he was the Sam Bloomfield Distinguished Professor and Executive Director of the National Institute for Aviation Research at Wichita State University in Kansas. From 1978 to 1994, he was the Program Director and McDonnell Douglas Fellow at McDonnell Douglas Research Laboratories in St. Louis. Dr. Agarwal received PhD in Aeronautical Sciences from Stanford University in 1975, M.S. in Aeronautical Engineering from the University of Minnesota in 1969 and B.S. in Mechanical Engineering from Indian Institute of Technology, Kharagpur, India in 1968. Over a period of 40 years, Professor Agarwal has worked in various areas of Computational Science and Engineering - Computational Fluid Dynamics (CFD), Computational Acoustics and Electromagnetics, Multi-disciplinary Design Optimization and Clean and Renewable Energy. He is the author and coauthor of over 250 archival and 600 conference publications. He has given many plenary, keynote and invited lectures at various national and international conferences worldwide in over sixty countries. Dr. Agarwal is a Fellow of eighteen societies including the American Physical Society, American Society of Mechanical Engineers, Institute of Electrical and Electronics Engineers, American Institute of Aeronautics and Astronautics, Royal Aeronautical Society and Chinese Society of Aeronautics and Astronautics. He has received many prestigious honors and awards from various organizations for his research contributions.

NUMERICAL SIMULATION OF DIRECT CONTACT CONDENSATION

Achintya Mukhopadhyay
Mechanical Engineering Department,
Jadavpur University, Kolkata 700032, India

Abstract

Direct contact condensation is a phenomenon that is experienced in many applications in thermal, chemical, and nuclear engineering, particularly in energy generation devices. Under certain situations, it can lead to violent condensation resulting in rapid pressure transients which could have serious implications on structural integrity and safety especially in nuclear plants. Direct contact condensation is a complex physical phenomenon involving multiple scales. In this presentation, some recent work in our group would be presented which deals with both system level modeling and also direct simulation of phenomena at the scale of individual liquid-vapour interfaces. At the interfacial scale, a novel energy balance at the interface has been proposed, which accurately simulates the dynamics of individual condensing bubbles. On the other hand, at the system level, appropriate closure relations are used to model the phenomena including very high pressure peaks and transients.

Prof. Achintya Mukhopadhyay
Professor
Mechanical Engineering Department
Jadavpur University Kolkata India
Phone: +91-33-24572468
Fax: +91-33-24146532
Email: achintya.mukho@gmail.com

Dr. Achintya Mukhopadhyay is a Professor of Mechanical Engineering at Jadavpur University, Kolkata. He also served as Professor of Mechanical Engineering at Indian Institute of Technology Madras and held visiting positions at Technical University of Munich where he was an Alexander von Humboldt Fellow and University of Illinois at Chicago. He obtained his Bachelors, Masters and doctoral degrees from Jadavpur University, Indian Institute of Science, Bangalore and Jadavpur University, all in Mechanical Engineering. Dr. Mukhopadhyay's major research interests are chemically reacting flows, multiphase flow and heat transfer anddynamics of thermal systems. His current research activities include droplet and spray combustion, structure and dynamics of partially premixed flames, nonlinear dynamics and chaos in combustion systems, instability of liquid sheets and atomization and spray impingement heat transfer. Dr. Mukhopadhyay has over 270 research publications including nearly 100 international journal publications and has advised a number of masters and doctoral thesis. He has also served as reviewer of a number of international journals. Dr. Mukhopadhyay is a Fellow of the West Bengal Academy of Science and Technology and life member of Indian Society of Heat and Mass Transfer, International Society for Energy, Environment and Sustainability and Indian section of the Combustion Institute and a member of the Society of Automotive Engineers (India).

INVESTIGATION OF NOX IN PILOT STABILIZED CH4-AIR DIFFUSION FLAMES

Ashoke De
Department of Aerospace Engineering,
Indian Institute of Technology Kanpur,
Kanpur 208016, India

Abstract

The present work aims to numerically investigate NOx in three turbulent piloted diffusion flames (Sandia D, E, and F) of different levels of extinction with fairly detailed chemistry, i.e. GRI 3.0 mechanism. The main focus of the study is to analyze the effects of the two different combustion model approaches, such as infinitely fast chemistry based unsteady flamelet and finite rate chemistry based EDC. The EDC approach is able to predict the passive scalar quantities but shows over-prediction in the reactive scalar quantities and NO prediction, while the unsteady flamelet modeling is found to be essential in predicting the accurate formation of slow kinetic species like NOx. The inability of flamelet and EDC approach in capturing localized flame extinction is observed, which lead to an over-prediction of NOx at larger downstream locations. Further, the dominance of NOx formation pathways is investigated in all three flames.

Dr. Ashoke De
Associate Professor
Propulsion Laboratory
Department of Aerospace Engineering
Indian Institute of Technology Kanpur
Kanpur, India
Phone: +91-512-259-7863
Email: ashoke@iitk.ac.in
Web: http://home.iitk.ac.in/~ashoke

Dr. Ashoke De is currently working as Associate Professor in the Department of Aerospace Engineering at Indian Institute of Technology Kanpur. He is the recipient of IEI-Young Engineer's Award-2014, DST Young Scientist award-2015, and P K Kelkar Research Fellowship from IIT Kanpur. He is a member of ASME, SIAM, FMFP, ISHMT and Combustion Institute. Dr. De received his Masters' degree in Aerospace Engineering from IIT Kanpur in 2004, and PhD degree in Mechanical Engineering from Louisiana State University, USA in 2009. Before joining IIT Kanpur, he has worked as post-doctoral scholar at Technical University of Delft (TU-Delft), Netherlands and as Research Engineer in GE Global research at Bangalore. Dr. De leads large scale initiatives in the modeling of turbulent reacting and non-reacting flows at IIT Kanpur. So far, he has authored more than 80 peer reviewed articles in journals and conferences. His current research interests include combustion modeling, hybrid RANS/LES model development, supersonic flows and Fluid-Structure interactions (FSI). He is actively pursuing research projects from various organizations like ISRO, ARDB, DST and PWC. His primary research focus is the emerging field of computational mechanics with particular interest in combustion and turbulent flows.

WASTE INCINERATION IN AUSTRIA: AN OPPORTUNITY FOR URBAN MINING

Franz Winter, Jakob Weber
Environmental & Biological Engineering,
TU-Wien, Getreidemarkt 9/166
1060 Vienna, Austria

Abstract

One of the most challenging fuels in terms of combustion is waste. Various types of waste differ in amount, composition and legal limitations. The thermal treatment of municipal solid waste, sewage sludge and hazardous waste in large, centralized waste incineration plants with state of the art flue-gas cleaning is a good implementation for this type of fuel. These facilities use different kinds of incineration technologies, each proven and tested. The used techniques in Austria are: grate furnace incineration (for municipal solid waste), fluidized bed combustion (for pretreated municipal solid waste and sewage sludge) and the combustion in rotary kilns (for hazardous waste). In addition to the combustion process itself, also the steps of fuel preparation (e.g. sorting, shredding, etc.), flue gas cleaning and residue management need to be optimized. However, the waste of a country may also contain valuable materials in economically relevant amounts, which can be of importance for urban mining.

This work discusses the importance of waste incineration in Austria and its general potential for urban mining.

Prof. Franz Winter
Head of Chemical Process Engineering and
Energy Technology Institute of Chemical,
Environmental &
Biological Engineering, TU-Wien, Getreidemarkt
9/166
1060 Vienna, Austria
Phone: +43-1-58801-166301
Fax: +43-1-58801-16699
Email: franz.winter@tuwien.ac.at
https://www.vt.tuwien.ac.at/chemical_process_eng
ineering_and_energy_technology/EN/

Prof. Franz Winter finished his PhD in 1995 in Chemical Engineering at the TU Wien, Vienna, Austria and – after habilitation – he became Associate Professor at TU Wien in 2000. He headed the Christian Doppler Laboratory for Chemical Engineering at High Temperatures from 2001-2008.

Currently he is the Head of the Research Division Chemical Process Engineering & Energy Technology at the Institute of Chemical, Environmental & Biological Engineering at TU Wien. He has been published 100 scientific papers in international peer reviewed journals and was chairman of several international conferences as well of the International Energy Agency Fluidized Bed Conversion programme.

BIOMASS ENERGY: AGRICULTURAL AND NON-AGRICULTURAL SOURCES, UPGRADING AND CONVERSION PROCESSES, BENEFITS AND PROBLEMS

Kalyan Annamalai

Texas A&M University,
College Station, TX 77843-3123, USA

Abstract

Energy is the most important prime mover of economy of a country involving stationary and transportation liquid and gaseous fuels. Since fossil based fuels result in emission of carbon dioxide (CO2), a global warming gas, biomass based fuels are proposed as future fuels to mitigate the release of CO2. The review summarizes the various agricultural and non-agricultural biomass (AB, and NAB) fuels, upgrading processes to improve the quality of fuels includes drying and torrefaction. The NAB includes manure based biomass fuels (animal and sewage sludge), mortality biomass (MB) and municipal solid wastes (MSW). The conversion processes include thermochemical conversion in the production of gaseous and liquid fuels, non-thermal conversion via aqueous-phase and direct energy conversion via combustion, cofiring and incineration. The recent respiratory quotient (RQ) technique is used to rank the CO2 emitting potential of various fuels. While the woody wastes left over land may be carbon neutral the "CO2 processing" cost of biomass fuels increase RQ of biomass fuels above that of coal. Results are presented for fuel properties of AB, NAB and MB fuels, performance under gasification, cofiring and reburn for reduction of NOx including pilot scale test results.

Prof. Kalyan Annamalai
Paul Pepper Professor (Retd.)
Organization and Address: Texas A&M University,
College Station, TX 77843-3123, USA
Phone: 979.845.1252
Fax: 979.862.3989
Email: k-annamalai@tamu.edu;
kal.annamalai@gmail.com
Web::
http://www.crcpress.com/product/isbn/9781439805725

Dr. Kalyan Annamalai received his BS from College of Engineering (Anna University) at Guindy, Chennai, MS from Indian Inst. of Science, Bangalore, and Ph.D. from the Georgia Institute of Technology, Atlanta and worked at Brown University, Providence and later at AVCO Everett Research Laboratory, Revere, Mass. He joined Texas A&M in 1981 as an Assistant Professor and was appointed as Paul Pepper Professor of Mechanical Engineering in 2005. In fall 2013, he was visiting scholar at MIT Energy laboratory and McMaster Univ., Canada. He is also a Senior TEES Fellow of College of Engineering, Texas A&M. He is the author of books on "Advanced Thermodynamics," Taylor and Francis (2nd Ed, 2011) and "Combustion Science and Engineering" (Taylor and Francis, 2007). His research projects dealt with Energy Conversion from Coal and biomass (Agricultural and Animal wastes), group Combustion, Alternate/Bio-fuels, Gasification, and Emission of NOx and Hg. He is the author of about 150 journal and reviewed conference publications mostly in the area of combustion and gasification of coal and biomass, and emissions from fossil fuels. He had developed respiratory quotient method of ranking of fossil fuels based on CO_2 emission. Recently he was involved with transferring results from combustion and thermodynamics in engineering to biology field involving metabolism and entropy generation within human body in predicting organ stress and life span. He is a member of combustion institute and a fellow of American Society of Mechanical Engineers. He serves on the editorial boards of several journals.

TWO CYLINDER AND SINGLE CYLINDER COMPACT ENGINES FOR OFF-ROAD APPLICATIONS

P.A. Lakshminarayanan
Technical Adviser,
Simpson and Co. Ltd. Chennai

Abstract

The design and development of a new four-stroke two-cylinder diesel engine family of 1.29 litre capacity for off road are discussed. The engine is in naturally aspirated and turbocharged and intercooled versions and rated from 11.9 kW/1500 rpm to 25.7 kW/2500 rpm. The engines were tuned for air and fuel flows, air utilisation, fuel air mixing, performance and emissions at steady state at a development lab and later certified in national labs. The high altitude capability of the TCIC was checked using a model. The engines rated at less than 19 kW satisfy India Generator set and off road norms of India and Europe equivalent to USTier4 standard, and at higher ratings, standard equivalent to US Tier4-interim. In the second part of the paper, the design of coolant and oil pumps, oil cooler for TCIC engine and the piston with steel oil control ring are discussed. The higher loaded TCIC engines use fillet hardened crankshafts of chromium molybdenum steel. The crankcase integrated with the flywheel housing and the timing case at the front, in conjunction with a cast iron sump makes the engine rigid against torsion and bending in an agricultural tractor. The firing order 0°-360° with the two pistons moving in phase allows lower cyclic irregularity and a light flywheel as well as turbocharging. The resultant primary reciprocating inertia force is neutralized by a counter-rotating balancer shaft and the fluctuations in crankcase pressure are taken care by a valve in the breather to avoid oil carry over.

The single cylinder naturally aspirated engine rated at 12.5 kW at 2800 rpm with a swept volume of 0.745 litre was developed for mini tractors. This satisfies India TREM3A emission norms as well as proposed TREM3B norms of 2023. This engine is 100% balanced internally for primary reciprocating forces and is electronically governed. Setting rated speed, power as well as torque is to closer tolerances than with a conventional mechanical governor. Further, at all operating speeds the governing is isochronous which is much desired in off road applications.

Dr. P. A. Lakshminarayanan
Technical Adviser
Simpson and Co. Ltd. Chennai
Phone: 9840850068
Email: pal@simpson.co.in

Dr. P. A. Lakshminarayanan studied at Indian Institute of Technology, Madras for his B. Tech., M.S. and Ph.D. degrees. He worked at Loughborough University of Technology and Kirloskar Oil Engines Ltd. for five and 20 years respectively. In 2002, he was called to head the Engine R&D in Ashok Leyland. In 2011, he became Chief Technical Officer at Simpson and Co. Ltd. From 2017 he is a Technical Adviser to Simpson.

With his teams, he has developed more than eight diesel and CNG engine platforms and 150 types of engines commercially successful for the efficiency and cost effectiveness. Two engines received prizes from the Institute of Directors (India). He has authored 50 research papers in journals and conferences of international repute. Four of them received the prizes for integrity and quality of the contents from the SAE (intl.), Combustion Society (India), AVL (Graz) and AVL (Pune) in 1983, 1993, 2005 and 2010 respectively. He has co-authored a book on "Modeling Diesel Combustion" published by Springer Verlag (2010). His next book "Critical Component Wear of Parts in heavy Duty Engines" was published in 2011 by John Wiley International. He is a fellow of SAE and a fellow of Indian National Academy of Engineering.

SUSTAINABILITY IN PRODUCT DEVELOPMENT – AN AUTOMOTIVE PERSPECTIVE

N Saravanan
Mahindra Research Valley,
Mahindra World City, Plot 41/1, Anjur Post,
Chengalpattu, Kancheepuram 603004

Abstract

Sustainable product development generally have the consideration of Environmental, Social, Regulation and Socio Economic factors involved in the different phases of development, production, use, and ultimate disposal/recycle of the products. The greater opportunities for improving the sustainability performance of a product are in the adoption of early stages in the product development process, in which the degrees of freedom are higher. The success of integrating these several aspects into product Design and Development in an organization is felicitated by the involvement of relevant functions such as Design, Innovation, Engineering, Sales, Marketing, Quality, Planning, Manufacturing, Sourcing, Service etc. To measure overall impact, there are two approaches followed a) End of Life Vehicle (ELV) b) Life Cycle Assessment (LCA) of the product. The ELV deals with how to minimize the impact of end–of–life vehicles on environment by restricting the use of four heavy elements: lead, hexavalent chromium, mercury, and cadmium less than stipulated limits. This directive (2000-53-EC) also demands to ensure certain minimum levels of recyclability and recoverability of vehicles. The Directive lays down the mandatory targets of minimum 85% recyclability, minimum 95% recoverability, and maximum 5% landfill rates along with restricted use of heavy elements in the vehicles.

Life-cycle assessment (LCA), is a technique to assess environmental impacts associated with all the stages of a product's life (cradle to grave approach) from raw material extraction through materials processing, manufacture, distribution, use, repair & maintenance, disposal or recycling. LCAs can help avoid environmental concerns by having overall perspective on emissions in different phases of the product. Life cycle thinking enables the transition towards the circular economy. The integration of sustainability into business and product development has, therefore, a strong potential to increase the sustainability performance of products across their entire life cycle, making good business sense and enabling a positive impact in the society.

Dr. N Saravanan
Principal Engineer, Mahindra & Mahindra Limited,
Mahindra Research Valley, Mahindra World City, Plot
41/1, Anjur Post, Chengalpattu, Kancheepuram 603004
Phone: 044-67038751 , 9500042649
Email: n.saravanan@mahindra.com
Web: http://www.mahindra.com

Dr. N. Saravanan has completed his doctorate in the field of Hydrogen fuel Injection in Diesel engines. He has published several publications; 26 International journals, 25 International conferences and in several national conferences. He is working as Principal Engineer in Technology Innovation, Sustainability & Capability Building (MTA) in MRV. He handled several projects such as Hydrogen diesel dual fuel development, Smart Rotavators, Hyalfa hydrogen powered 3 wheeler development, Hydrogen multicylinder vehicle development, HCNG development, Fuel cell development, Direct injection CNG development etc. He has published his development work in several SAE world congress, SIAT and in other International conferences. He also owns 7 patents for his contributions on Hydrogen, CNG, Implements developments. He is also involved in Sustainable product development and CO2 reduction technology and in the formation of Competency Development for IPR. He has been awarded prestigious Young Engineer Award 2013 from Institute of Engineers, India for his contribution in hydrogen & alternative fuels developments. He also receiptant for Mahesh Modi award for developing India's first Hydrogen TC Minibus in SIAT 2015 @ ARAI, Pune. He is also the receiptant of Excellence in Innovation Technology Award for the innovation work done on Hydrogen Vehicles developments from World Innovation and Congress & Awards 2016.

HIERARCHICAL POROUS CERAMICS FOR ENERGY CONVERSION AND STORAGE

Rajendra K. Bordia, Franziska Scheffler, Michael Scheffler
Materials Science and Engineering,
Clemson University, Clemson, SC 29634 USA

Abstract

Our current research is focused on developing processing strategies to control the microstructure of ceramics at different length scales. One of the focal areas is porous ceramics. Many of the applications of porous ceramics demand optimization of a multitude of properties some of which have conflicting requirements on the microstructure. Materials with designed anisotropic and/or hierarchical microstructures have the potential to optimally address these requirements.

We will first present a broad overview of the use of porous ceramics in advanced energy conversion and storage applications including the property requirements. Next, we will present results from our collaborative projects focused on microstructural control in hierarchical, i.e. micro/macroporous, and/or anisotropic porous ceramics.

Porous ceramics are used in a broad range of technologies of interest to energy conversion and storage including electrochemical applications like electrodes for solid oxide fuel cells, high temperature insulators, thermal energy storage and electrochemical energy storage. In these applications, a multitude of properties are of interest. For specific applications, a subset of mechanical, thermal, electrical properties, ionic conductivity, gas diffusion and chemical reactivity need to be optimized. In this presentation, results will be presented on the processing approaches to make these designed microstructures, the quantification of the 3D microstructure at different length scales and simulations to design optimal microstructures for specific applications.

Prof. Rajendra K. Bordia
Clemson University
Materials Science and Engr.
161 Sirrine Hall, Clemson University
Clemson, SC, USA, 1-864-656-5228
rbordia@clemson.edu
https://www.clemson.edu/cecas/departments/mse/peo
ple/faculty/bordia.html

Prof. Rajendra K. Bordia is currently a Professor and Chair of the Materials Science and Engineering Department at Clemson University in Clemson, SC, USA (since April 2013). He was a faculty member at the University of Washington (1991-2013) and a Research Scientist in DuPont Co. (1986 to 1991). He received his B.Tech from IIT, Kanpur, India (1979), and his M.S. (1981) and Ph.D. (1986) from Cornell University, Ithaca, NY, USA.

His research is at the intersection of materials and mechanics and is focused on fundamental and applied studies in the processing and properties of complex material systems for energy, environmental and medical applications. He has authored or co-authored over 135 peer-reviewed technical publications.

He was elected as the Fellow of the American Ceramic Society (2002); the Fellow of the Indian Institute of Metals (2010); and an Academician in the World Academy of Ceramics (2012). Other significant awards include: the Humboldt Research award from the Alexander von Humboldt Foundation, Germany (2007); and the Outstanding Educator Award of the American Ceramic Society (2012). He is an Associate Editor of the Journal of the American Ceramic Society (1988-Present); Editor of the Journal of Ceramic Processing Research (1999-Present); and Editor-in-Chief of the Ceramics International Journal (2009 – Present).

USE OF NANOPARTICLES FOR HARNESSING SOLAR THERMAL ENERGY AND APPLICATIONS IN ENERGY EFFICIENT BUILDINGS

Himanshu Tyagi
School of Mechanical, Materials and Energy Engineering
Indian Institute of Technology Ropar,
Nangal Road, Rupnagar - 140001, Punjab, India

Abstract

Solar energy is abundantly available and is harnessed using solar thermal systems for several applications. The range of temperatures at which the output fluid is needed determines the specific type of solar thermal collector being used – starting from non-concentrating type collectors (for low temperatures), to highly concentrated collectors (for medium to high temperatures). Conventional surface-based collectors absorb the sunlight using a black solar-selective surface. The heat is then transferred to the fluid flowing through the system. On the other hand a volumetric nanoparticle-based direct absorption solar collector absorbs the solar energy directly within the fluid, hence improving the other all efficiency of the system. The thermal energy gained by the fluid can be used for various applications – industrial processing, domestic usage, heating of buildings. Large portion of energy requirements for heating of buildings can be provided by such solar thermal systems.

Dr. Himanshu Tyagi
School of Mechanical, Materials and Energy
Engineering
Indian Institute of Technology Ropar
Nangal Road, Rupnagar - 140001, Punjab, India
Phone: +91-97796-12972
Fax: +91-1881-223395
Email: himanshu.tyagi@iitrpr.ac.in
Web: http://www.iitrpr.ac.in/smmee/himanshutyagi

Himanshu Tyagi obtained his PhD from Arizona State University, USA in the field of heat transfer. Prior to his PhD he obtained his masters from University of Windsor, Canada and his bachelors from I.I.T. Delhi both in the field of Mechanical Engineering. He has been working at IIT Ropar since 2009, working to develop nanotechnology-based clean and sustainable energy sources with a team of several PhD and undergraduate students. He has previously worked in the Steam Turbine Design Division of Siemens (in Germany and India) and in the Thermal and Fluids Core Competency group of Intel Corp (in USA). His research interests include thermo-fluids engineering, bio-heat transfer, radiative and ignition properties of nanofluids, nanoscale heat transfer and its applications in energy harvesting.

Prof. Gridhar Madras
Department of Chemical Engineering
Indian Institute of Science
Bengaluru, Karnataka. – 560012.
Phone: 080-22932321
Email: giridharmadras@gmail.com
Web:
ttp://chemeng.iisc.ac.in/chemeweb/faculty_giridhar.h
tm

Giridhar Madras received his chemical engineering degree from Indian Institute of Technology, Madras in 1990. He obtained his Ph.D. in chemical engineering from Texas A&M University, USA, in 1994. Subsequently, he worked in the University of California at Davis, USA. He returned to India as an Assistant Professor of chemical engineering at the Indian Institute of Science, Bangalore in 1998. Since 2007, he has been a Full Professor at the Chemical Engineering Department. He is also an associate faculty in Solid State and Structural Chemistry and the chairman of the Interdisciplinary Center for Energy Research (ICER). He has successfully executed various projects worth several crores from various governmental agencies such as DST, DBT etc. and numerous industries such as BHEL, FMC, GAIL etc. In recognition of his early work, he received the Scopus Young Scientist Award from Elsevier for being the most cited young author in engineering. Based on his overall work, he was awarded the Presidential Swarnajayanthi fellowship by the Department of Science and Technology, India, in 2006 and the S.S. Bhatnagar prize from CSIR, India in 2009 from the prime minister of India and the J.C. Bose National fellowship in 2014. He is currently the associate editor of several journals with various publishers including RSC advances (RSC), Advanced powder technology (Elsevier), Bulletin of Material Science (Springer), Current Science (Indian Academy) and International journal of polymer science (Hindawi). His research interests are in the area of reaction engineering applied to polymers, supercritical fluids, and catalysis. The research group's approach is to develop several new materials that are used as catalysts for known reactions. He proposes new reaction pathways/ mechanisms providing the research community with a method to develop new materials with superior properties. In this regard, his research group has synthesized new materials that work as photocatalysts for the degradation of a wide variety of dyes and organics that are common pollutants in waste water. He has also developed new catalysts for the three-way catalysis for the NO+CO reaction and CO and hydrocarbon

oxidation and proposed new mechanisms governing these reactions. His studies on polymer degradation wherein the polymers are converted to useful products such as the monomers or fuel oils have been well cited and known in the field.

BIOENERGY PRODUCTION FROM MICRO AND MACRO (MARINE) ALGAE BIOMASS: TRENDS AND VIEWS TOWARDS SUSTAINABILITY ALONG WITH THE INTEGRATION OF BIO-REFINERY

Gopalakrishnan Kumar, Hour Huy
Department of Environmental Engineering,
Daegu University, Jillyang, Gyeongsan 712-714
South Korea

Abstract

Dwindling fossil fuel resources and the ever increasing energy demands due to the sustained growth of industrial sectors have forced the energy scientists towards the prospecting of renewable energy resources, that are green, clean and pollution free. Biofuel production from various cellulose biomass has been practiced for long time, however, owing to the expensive pretreatment techniques, concluded as not sustainable. In this spotlight, liquid biofuel production from micro and macro algae biomass are highly promising, because of their bio- refinery products (mainly chemicals and value added products, etc), additionally, these feedstocks are attained at low cost and also bearing enormous amount of bio-moieties ranging from carbohydrate, protein and lipid, that could be converted to various chemicals such as volatile fatty acids and pigments. Further, conversion of left over residues for the biofuel production could create a sustainable and economical industrial sector. This talk would cover the trends of biofuel production from various micro and macro algae biomass that includes the production of biodiesel, ethanol, hydrogen and methane. Besides, sustainable scheme of bio-refinery concept for the production of biochemicals and the residual conversion would be highlighted for the sustainable future.

Prof. Gopalakrishnan Kumar
Department of Environmental Engineering, Daegu
University, Jillyang, Gyeongsan 712-714 South Korea

Dr.Gopalakrishnan Kumar, graduated from Feng Chia University, Taiwan and had post doc experiences in UNAM, Mexico, Daegu University, Korea, JSPS post doc at NIES, Japan prior to his current position. Additionally, he is also Adjunct Prof & head in Ton Duc Thang University, Vietnam. His major research area includes, Microalgae biofuel technologies, wastewater treatment, Biofuels (H2, Ethanol, CH4) production from LCB/solid waste and wastewater, Environmental Remediation & green NP synthesis.

ENERGY-AIR POLLUTION NEXUS: NEED FOR MORE EFFECTIVE TECHNOLOGICAL SOLUTIONS AND ENFORCEMENT

Nitin Labhasetwar
Energy & Resource Management Division,
CSIR-National Environmental Engineering Research Institute,
Nehru Marg, Nagpur-440020, India

Abstract

India is projected to witness highest growth rate in energy demand, production and consumption with as much as quarter of total global energy demand will come from India by 2040. Despite that, the energy demand in India will still be 40% below world-average, therefore such estimates could be even conservative. More importantly however, the fuel-mix projections infer that majority of this energy even in 2040 will come from carbon and hydrocarbon based fuels. As we are entering late in to foray of major energy producers and consumers, India will have certain advantages with respect to availability of advanced technologies for achieving better energy efficiency and reduced environmental footprint, but at the same time of facing serious challenges of depleted assimilative capacity to accommodate more emissions, especially related to CO_2 NOx and PM. Balancing these issues in a techno-economically feasible manner will be a key guideline for India's energy programme. There are two basic issues related to so called Energy-Air Pollution Nexus- The related Health impacts primarily due to PM, NOx and other emissions, and second the GHG impacts. These will be discussed along with our research works related to the cleaner energy generation as well control of emissions from automobile exhaust.

Dr. Nitin Labhasetwar
Sr. Principal Scientist & Head,
Energy & Resource Management Division,
CSIR-National Environmental Engineering Research
Institute, Nehru Marg, Nagpur-440020, India
Phone: 9850316799; Fax: 0712-2249900
Email: nk_labhsetwar@neeri.res.in
Web: http://www.neeri.res.in

Dr. Nitin Labhasetwar is a Ph.D. in Chemistry with 31 years of research experience in environmental and energy related research. He has worked as STA/JSPS Fellow and Visiting Overseas Researcher at NIMS, Tsukuba, Japan and as a Visiting Professor at Kyushu University, Japan under the GCOE programme. He has also worked at other International Laboratories on development of materials and processes including low cost and nano-materials for their applications in energy & environmental applications, vehicular emission control, photocatalysis, GHG emission control, cleaner energy generation, heterogeneous catalysis etc. He has over 155 research publications with over 4300 citations and 22 international patents in addition to a few contributions in books. He has received 9 awards for excellence in research and also received various fellowships in India and abroad. He is a reviewer for more than ten SCI journals and member of Editorial Advisory Boards of two international journals. He has supervised 15 students for PhD and several others for Master courses. He is currently involved in more than 15 R&D projects.

COLLOIDAL STREAMER FORMATION IN MICROSCALE FLOWS

Aloke Kumar

Department of Mechanical Engineering,
Indian Institute of Science

Abstract

Flow of colloidal dispersions through porous media is a topic of substantial contemporary interest due to its applications in areas such as environmental science and engineering. Here we present the generalization of a previously known biophysical phenomenon – the formation of slender bacterial aggregates in systems with sustained hydrodynamic flow. This phenomenon known by the name of bacterial streamers is extended to a biotic system, by demonstrating the formation of morphologically similar structures formed during particle laden polymeric flows through artificial porous media. We show that when a polyacrylamide (PAM) solution, laden with polystyrene (PS) beads is introduced into a microfluidic device containing an array of micropillars, localized particle aggregation is found to occur under certain flow regimes. These aggregates initially have a string-like morphology and are tethered at their ends to the micropillar walls, while the structure remains suspended in the fluid medium. We also discuss the implications of our finding.

Dr. Aloke Kumar
Assistant Professor
Department of Mechanical Engineering,
Indian Institute of Science, Bangalore
Email: aloke@mecheng.iisc.ernet.in

Dr. Aloke Kumar has completed his B. Tech & M. Tech (2000-2005) from Indian Institute of Technology, Kharagpur and PhD (2005-2010) from Purdue University. He has awarded Canada Research Chair (Tier II) in Microfluidics for Biological Systems, NSERC, Canada (2014-2017) Eugene P. Wigner Fellowship, Oak Ridge National Laboratory, USA (2010-Present) DeKármán Fellowship, Josephine DeKármán Fellowship Trust, California, USA (2009-2010), Bilsland Dissertation Fellowship, Purdue University, USA (2009-2010), Adelberg Fellowship, Purdue University, USA (2007-2008), Ross Fellowship, Purdue University, USA (2005-2006).

SUSTIANBLE ENERGY SYSTEM WITH HYDROGEN

Anjaneyulu Krothapalli
Department of Mechanical Engineering
Florida State University,
2525 Pottsdamer Street, Tallahassee, Fl 32310

Abstract

The energy sectors that are most important to human development are the electricity supply and the energy for transportation. The growth in demand for energy is primarily the result of increasing electricity demand and rapidly expanding transport use. A high-renewables scenario for an energy road map aims for 85% energy coming from renewable energy sources such wind, solar and biomass. Meeting this target requires a significant increase in demand for energy storage. While a variety of technologies will be used to fulfill the storage needs, hydrogen plays an essential role in different areas of supply and distribution chain for renewably-sourced energy mainly because of its benefits of scalability. At current levels of increase, CO2 emissions from the transport sector are projected to rise and the rate of increase constitutes one of the fastest growing and most threatening contributors to global warming. Hydrogen is a promising alternative energy source for transportation, especially when it is produced using renewable energy technologies. As a transportation fuel, use of hydrogen will have a significantly positive impact on future CO_2 emissions and an immediate impact on fuel economy. The successful use of hydrogen within the transportation sector is dependent on the development and commercialization of affordable fuel cell vehicles (FCVs). Harnessing the full power of renewable energy with hydrogen will help support a clean and efficient sustainable energy system.

Anjaneyulu Krothapalli
Don Fuqua Eminent Scholar Professor Emeritus,
Department of Mechanical Engineering
Florida State University
2525 Pottsdamer Street
Tallahassee, Fl 32310
Phone: +1 850 339 0428
Email: akrothapalli@fsu.edu

Prof. Krothapalli was the Don Fuqua Eminent Scholar Chair & Professor Emeritus of mechanical engineering at Florida State University (FSU), USA and an Affiliated Professor of Energy at Royal Institute of Technology (KTH), Sweden. He was the founding member and Chairman of the Mechanical engineering department at FSU from 1983 to 2002. He was on the faculty of Aeronautics & Astronautics at Stanford University from 1981-1983. He obtained his M.S. and Ph.D. degrees from Stanford University in 1978 and 1979 respectively. As an entrepreneur, he founded five start-up companies in California and Florida. Dr. Krothapalli is an expert engineer/scientist in the fields of Aeronautics and Renewable Energy with 5 US patents and over 200 scientific papers.

MOVING BOUNDARY MODELING FOR WORKING FLUID PHASE CHANGE TRACKING AND ADVANCED CONTROL OF SOLAR THERMAL SYSTEMS

Sandip Kumar Saha

Indian Institute of Technology Bombay,
Powai, Mumbai- 400076, INDIA

Abstract

Scarcity of proper analytical solutions pertinent to heat flow and diffusion involving phase change in solar thermal applications in the published literature has resulted in the moving boundary models coming into prominence. Smaller order and typically high computational speed make moving boundary models interesting candidates for describing dynamic characteristics of evaporators pertinent to the ORC system. While simplified reduced order quasi-steady models have been utilized to predict the phase change characteristics and suitable mass flow ranges of the ORC working fluid (e.g. R134a) for different steady state bulk heat transfer fluid (e.g. Duratherm FG) temperatures, dynamic models are needed to ensure advanced control as well as the improved performance and efficiency in the medium temperature (150-300 oC) solar thermal systems. Dynamic model enables us in capturing the sharp time-varying phase change characteristics of the system (time scale ~ few seconds). Possible fluctuations may appear in the form of temporal variation in ORC inlet conditions as well as the transient changes in average temperature of the heat transfer fluid. An effective way of dynamic modeling can be done by considers the time-varying pressure on the subcooled ORC working fluid (refrigerant) at the heat exchanger entry to be the sole independent variable and all other physical as well as thermodynamic variables of interest are treated as dependent variables that change with any variation in the aforesaid pressure. Computational results hint at mitigation of the extent of fluctuation in the wall temperature of the narrow tube that carries the working fluid refrigerant in the heat exchanger with increasing mass flow rates. Perturbation in the working fluid pressure causes a larger amount of perturbation in the wall temperature for lower mass flow rates. Thus the simulation results serve as a good platform and pave way for further optimization of the thermal performance cycle of a real-life system.

Dr. Sandip Kumar Saha
Associate Professor
Indian Institute of Technology Bombay,
Powai, Mumbai- 400076, INDIA.
Phone: +91 22 2576 7392
Fax: +91 22 2572 6875
Email: sandip.saha@iitb.ac.in
Web: http://sandipksaha.tk

Dr. Sandip K. Saha is an Associate Professor of Mechanical Engineering at Indian Institute of Technology Bombay, INDIA. He received his B.E. degree in Mechanical Engineering from Jadavpur University, Kolkata, India and the M.Sc. (Engg.) and Ph.D. degrees from Indian Institute of Science, Bangalore, India, respectively. His doctoral research work was on the applications of solid-liquid phase change materials in thermal management of electronics. Prior to joining Indian Institute of Technology Bombay, he was with R&D TATA Steel, India, as a Researcher and Applied Mechanics and Energy Conversion, Department of Mechanical Engineering, Katholieke Universiteit of Leuven, Leuven, Belgium, as a Post-Doctoral Fellow. His research interests include heat transfer, thermal management of electronics, thermal storage system for solar thermal applications, thermal management of buildings and computational fluid dynamics. He is working on the development and implementation of latent heat thermal energy storage for small and medium power (10-100 kW) and medium temperature (~ 200 $\square$C) solar thermal power plant.

NUMERICAL ANALYSIS OF FIN ORIENTATION TO ENHANCE THERMAL PERFORMANCE IN LATENT HEAT STORAGE DEVICE FOR CONCENTRATED SOLAR COOKER

Prodyut Ranjan Chakraborty
Department of Mechanical Engineering,
Indian Institute of Technology Jodhpur

Abstract

Solar energy is a clean and bountiful renewable energy source which can solve some serious problems like pollution and deforestation. Using concentrated solar cooker is one of the ways to utilize this solar energy for cooking at high temperature range of 250-350. But the only limitation is the absence of maximum heat flux during early morning or evening which is the preferable cooking time in India. This issue can be solved by storing thermal energy during noon (timing of maximum heat flux) and utilizing it later after sundown for cooking by using Phase change materials(PCM) for storing thermal energy in the form of latent heat. The PCM can be obtained in the form of composites by soaking it within Compressed Expanded Graphite (CEG) matrix to enhance the otherwise low thermal conductivity of PCM. Further enhancement of heat transport capability of the storage unit can be obtained by the addition of fins within the storage medium. The present work focuses on arrangement and orientation of fins in order to have minimum charging time for the entire storage medium, while charging is considered to be complete when the entire PCM present within the heat storage unit melts. The charging process of the vessel has been numerically investigated for concentrated solar cooker unit with a paraboloid reflector while considering various axisymmetric arrangements of fins within the storage medium.

Prodyut Ranjan Chakraborty
Associate Professor
Department of Mechanical Engineering
Indian Institute of Technology Jodhpur
Phone: +91 291 2449058
Email: pchakraborty@iitj,ac,in
Web: http://home.iitj.ac.in/~pchakraborty

Dr. Prodyut Ranjan Chakraborty is currently working as Associate Professor of Mechanical Engineering at Indian Institute of Technology Jodhpur. He has previously worked in German Aerospace Center (DLR) Cologne and G.E. Global Research Center Bangalore (India). He received his PhD and Masters from the Department of Mechanical Engineering, Indian Institute of Science Bangalore, and his bachelors from North Bengal University. His primary areas of research are numerical modeling of alloy solidification, latent heat based energy storage systems for high temperature applications, Thermal management and thermal comfort, and sorption cooling.

PARTICLE EMISSION FROM DIESEL ENGINES AND ITS CHARACTERIZATION

Pravesh Chandra Shukla
Division of Combustion Engines,
Department of Energy Scieces
Lund University, Sweden

Abstract

Particulate emissions from the diesel engines are one of the major environmental concerns these days with increasing vehicle density on roads. Most of the countries around the world have implemented vehicular emission regulations. These emission regulations define the limit of the pollutants emitted from the engines namely CO, NOx, THC and PM, depending on the type and power rating of the vehicles. PM emissions are regulated by the mass emissions. In modern engines, PM emission has drastically reduced compared to the emission levels of older diesel vehicles. Particle number emission should also be major criteria for particle emissions from diesel engines. In a modern diesel engine, particle number emission can be significantly higher despite of having lower particulate mass emission. Smaller particles can easily penetrate deeper into the human lungs and can reach the blood stream. These tiny particles are considered carcinogenic for the human health.

Dr. Pravesh Chandra Shukla
Postdoctoral Researcher
Division of Combustion Engines
Department of Energy Sciences
Lund University, Sweden
Phone: +46-764361519
Email: shukla.pravesh@gmail.com

Dr. Pravesh Chandra Shukla is a Postdoctoral researcher in the Department of Energy Sciences, Lund University, working in the field of Internal Combustion engines.I has completed my PhD from Indian Institute of Technology Kanpur, India in February, 2016. My main research interests include Alternative fuels for combustion engines, Diesel engine exhaust emission characterization, Engine exhaust aftertreatment devices etc. With an interdisciplinary research experience and background in mechanical and environmental engineering, I have strength to link two major mutually related research fields of engine research and its environmental aspects. Modern world is dependent on various modes of power generation units out of which diesel engines contribute significant fraction. These engines are efficient, easily movable and durable, however infamous for their emissions. Utilization of favorable alternative fuels, optimized advanced combustion processes, emission control devices etc. make them much efficient and environment friendly.

ORGANIC AND PEROVSKITE PV: A PARADIGM FOR SOLAR FUTURE LCA

Murali Banavoth

School of Chemistry, University of Hyderabad

Prof. C R Rao Road, Gachibowli, Hyderabad,

Hyderabad Telangana, India, 500046

Abstract

Growing demand for the energy has turned to be a bottleneck for survival present and future days. Inexhaustible solar energy, which provides a clean, economical and green energy, seems to be an alternative solution, for current and future terawatt level energy demands. The challenges imposed and the quest for more affordable and efficient clean energy production to find a cheaper alternative led to the development of perovskite and organic bulk heterojunction based solar cells. The planning, conducting and dissemination of research undertaken will address the most preliminary issues by investigating various solar cells. In each, case the organic–inorganic metal trihalide perovskites having both abundant and cheap starting materials, which are easily processed at low temperatures. The focus would lay on a) Enhancing the efficiency in cost-effective ways by integrating newer perovskite crystals in devices. b) Improving the carrier lifetimes of lead free perovskites from few hundreds of nm to micrometer range. c) Engineering the electron and hole transporting layers in inverted BHJ cells. d) Perform the life cycle device statistics and encapsulation ways to cheap, safe, durable, and capable of being manufactured in large panels.

Dr. Murali Banavoth
Assistant Professor
School of Chemistry, University of Hyderabad
Prof. C R Rao Road, Gachibowli, Hyderabad,
Hyderabad Telangana, India, 500046
Phone   : +91 40 23134828
Fax: +91 4023012460

Dr. Murali Banavoth, an Assistant Professor at School of Chemistry, University of Hyderabad, with expertise in the fabrication of thin film solar cells, has contributed to the advancement of science in the field of photovoltaics, which has conferred upon him the recent BRICS Young Scientist Award. He has published over 45 refereed journal papers, has an h-factor of 18, I-10 index of 28 and was cited over 1400 times during 2015-2017. He is currently the editor of reputed international journals like Frontiers in Optics and Photonics, Frontiers in Physics, etc. Few of his research outcomes are selected for the cover pages of reputed journals like Advanced Energy Materials, ACS Energy Letters and Dalton Transactions and few also selected as the 'Renewable Energy Global Innovation Award' (REGI). Dr. Banavoth has made significant contributions to the development of solar absorber layers by the novel, simple and cost effective techniques. His recent studies on the lead halide perovskites ($MAPbX_3$, $FAPbX_3$ and $CsPbX_3$ where X= I^-/Br^-/Cl^-) thin film/single crystal photovoltaics, are published in reputed journals like few Nature, JACS, Angew Chem, Advanced Materials, Advanced Energy Materials etc. He also studies the engineering of the electron transport layers (ETL), i.e., TiO_2/ZnO and doped TiO_2/AZnO (Yt, Zr, Al, Ga, In) for efficiency enhancement by cost-effective solution processes.

MICROBIAL ENHANCED OIL RECOVERY AND BIOREMEDIATION OF PETROLEUM HYDROCARBON POLLUTANTS

Sunita J. Varjani

Gujarat Pollution Control Board,
Gandhinagar - 382010, Gujarat, India

Abstract

In recent years, there has been increasing concern over public health threats posed due to the introduction of different xenobiotic compounds in environment due to anthropogenic activities to a greater extent and natural processes to some extent. There has been an increasing attention about human health and environmental risk of pollutants present in solid waste or effluent generated by anthropogenic activities. Petroleum industry is one of the big industrial sector which supply energy demands and petrochemical intermediates needed in day to day life. The increasing demand for petroleum products in the world coupled with stringent environmental laws piled technical as well as economical pressure upon petroleum industry to further improve petroleum crude recovery keeping in mind reduced level of environmental pollutants. Remediation of polluted sites by applying various physical, chemical, thermal and biological techniques are in practice. Many conventional engineering based physico-chemical decontamination methods for remediation of these xenobiotic compounds are expensive. Hence, it can be said that petroleum industry is facing two major burning issues such as remediation of petroleum hydrocarbons polluted site(s) and oil recovery. The increasing costs and limited efficiency of traditional physico-chemical treatments have spurred the development of green technologies, which ultimately leads the sustainable development of environment. Biological methods with the aid of biotechnology provide viable option to physico-chemical methods used for remediation of petroleum hydrocarbon pollutants. Bioremediation using microbes has emerged as the best successful initiative to mitigate pollution and also help to recover polluted sites. In addition, different conventional enhanced oil recovery processes are currently employed in petroleum industry to extract trapped reservoir oil viz. thermal, chemical and injection of gas. In search of environment-friendly and economical solutions, attention has been given to biotechnological techniques such as use of microbial enhanced oil recovery (MEOR). Detailed results of laboratory simulation experiment for bioremediation of petroleum hydrocarbons polluted soil of Ankleshwar, Gujarat by locally isolated consortium of six microbes to degrade crude oil will be presented. This study highlights challenges that need to overcome for making MEOR commercially successful. The study will also discuss in detail application of rhamnolipid producing halotolerant Pseudomonas aeruginosa NCIM 5514 in MEOR study.

Dr. Sunita J. Varjani
Scientific Officer
Gujarat Pollution Control Board,
Gandhinagar - 382010, Gujarat, India
Email: drsvs18@gmail.com

Dr. Sunita Varjani is Scientific Officer at Gujarat Pollution Control Board, Gandhinagar, Gujarat, India. She holds M.Sc. degree in Microbiology and Ph.D. in Biotechnology. Her major areas of research are Industrial and Environmental Microbiology/Biotechnology and Molecular biology. Dr. Varjani has authored 44 publications, including original research papers, reviews, books and book chapters. She has won several awards and honours, including Young Scientist Award at AFRO-ASIAN Congress on Microbes for Human and Environmental Health, New Delhi (2014) and Best Paper Awards for oral presentations in national and international conferences in 2008, 2012 and 2013. She is member of editorial board of Journal of Energy and Environmental Sustainability. She has delivered talks as invited speaker in many international conferences including the countries India and China. She has served as guest editor of Bioresource Technology journal for a special issue (2017). She is recipient of visiting scientist fellowship from EPFL, Lausanne, Switzerland (2017).

SPRAY, COMBUSTION, EMISSIONS AND PARTICULATE INVESTIGATIONS OF A GASOHOL FUELLED GASOLINE DIRECT INJECTION ENGINE

Nikhil Sharma
Department of Mechanical Engineering,
Indian Institute of Technology Kanpur,
Kanpur, 208016, India

Abstract

Test fuels selected for this study were gasohols [15% (v/v) blends of ethanol/ methanol/ butanol with 85% (v/v) gasoline] and baseline gasoline. Macroscopic spray investigation was performed to find out spray penetration length and cone angle. A section of this thesis focuses on microscopic spray investigations using phase Doppler interferometry (PDI) technique for measurement of various spray characteristics. After performing spray experiments, same test fuels were experimentally investigated in the engine. In optical engine investigations, phase Doppler interferometry (PDI) was implemented in the engine cylinder to evaluate real time spray droplet velocity distribution and spray droplet diameter distribution under various engine operating conditions. Many questions were answered by these comprehensive experiments, which otherwise remained unanswered in a constant volume spray chamber experiment. The results obtained from these experiments were helpful in optimizing parameters for engine experiments with thermal head. Effect in variation in spark timings (ST), fuel injection pressures (FIP), engine loads and engine speed (rpm) on combustion, performance and emission characteristics were investigated experimentally. In engine experiments with thermal head, detailed investigations to evaluate engine performance, combustion and emission characteristics were conducted for the test fuels.

Dr. Nikhil Sharma
Senior Project Engineer
Department of Mechanical Engineering,
Indian Institute of Technology Kanpur,
Kanpur, 208016, India.
Phone: 9455504117
Email: snikhil@iitk.ac.in

Dr. Nikhil Sharma is currently working as Senior Project Engineer at Indian Institute of Technology Kanpur, India. Dr. Sharma received his Ph.D. in Mechanical Engineering from Indian Institute of Technology Kanpur, India in 2017 and Masters in Mechanical Engineering from NIT Hamirpur in 2012. Dr. Sharma has worked as an Assistant Professor at Amity University, Noida from July 2012- June 2013. His areas of research include spray characteristics, alternative fuels for internal combustion engines (biodiesel, alcohols), engine emission measurement and their control, combustion diagnostics, particulate characterization and their control. During his Ph.D. he worked on "Spray, combustion, emissions and particulate investigations of a gasohol fuelled gasoline direct injection engine.

POLYGENERATION AS A FUTURE SUSTAINABLE ENERGY SOLUTION

Kuntal Jana
Indian Institute of Technology Guwahati,
Guwahati-781039

Abstract

In the present context of energy security and environmental degradation, distributed energy generation using locally available renewable resources may be a possible solution. However, the energy system should be economically feasible, socially acceptable and environmentally acceptable to be a sustainable energy solution. On the other hand, long route transportation of utility outputs may not be feasible for distributed energy system. Hence, utility outputs should cater to the needs of local people. Integrating multi-utility system in a single unit, named as polygeneration is a possible path of delivering multiple utilities to cater to the secondary energy needs of the local people. However, efficient process integration increases thermodynamic, economic and environmental performance of the energy system. In the context of global warming, biomass based polygeneration with carbon capture and storage gives the opportunity of net-CO_2 negative energy system. Life cycle assessment (LCA) is the most useful scientific tool for estimating the net CO_2 emission from the energy system. As polygeneration delivers different types of utilities from a single unit (e.g. energy services, materials), developing performance assessment parameters is another challenging task.

Dr. Kuntal Jana
SERB National Post Doctoral Fellow
Indian Institute of Technology Guwahati,
Guwahati-781039
Phone: +91 9874126675
Email: kuntaljana@gmail.com

Dr. Kuntal Jana is presently working as a SERB National Post-Doctoral Fellow at Indian Institute of Technology Guwahati. He completed his Master of Mechanical Engineering and PhD in Engineering both from Jadavpur University, Kolkata. His PhD thesis was based on performance assessment of polygeneration energy systems. Sustainable energy system is the broad area of his research. Energy system modeling, simulation and assessment, bioenergy, carbon capture and utilization, distributed energy system are the specific areas of his interest. He has authored 15 papers published in international journals, 12 international conference papers and 3 book chapters.

COMPLEX SYSTEMS THEORY TO STUDY THE DYNAMIC TRANSITIONS IN A TURBULENT COMBUSTOR

Vishnu R. Unni

Indian Institute of Technology Madras,
Chennai, India

Abstract

Gas turbine engines are operated in near fuel lean limits to reduce the emissions. However, at these conditions, combustors are susceptible to flame blowout and thermoacoustic instability due to the increased sensitivity of the flame to the flow perturbations. The main focus of the talk is to characterize the complex dynamics that a dump combustor with a bluff-body stabilized turbulent flame exhibits during transition from stable combustion to lean blowout. These different dynamic transitions are characterized using tools such as Multifractal Detrended Fluctuation Analysis (MFDFA), recurrence quantification analysis (RQA) and symbolic time series analysis and a unifying framework based on multifractality is proposed to describe both flame blowout and onset of thermoacoustic instability. Fractal measures and recurrence quantities were shown to be viable precursors for an impending thermoacoustic instability and flame blowout. A phenomenological model based on population dynamics of flamelets is introduced to study flame blowout as a threshold like transition to an absorbing phase.

Dr. Vishnu R. Unni
Senior Scientist
Indian Institute of Technology Madras,
Chennai, India
Phone: 9677140931
Email: vishnu.runni@gmail.com

Dr. Vishnu R. Unni, is a Senior Scientist at Department of Aerospace Engineering, Indian Institute of Technology Madras. Primary focus of his research is on turbulent combustion. During his Ph. D, at IIT Madras, he applied complex systems theory to study the various dynamics that a combustor exhibits at different operational regimes. He was able to successfully devise techniques for early warning of onset of thermoacoustic instability and flame blowout. Currently, he is focused on devising passive control strategies to mitigate oscillatory instabilities in turbulent combustors.

SYNTHETIC AND DIVERSE - MICROBIOLOGY ON DUTY IN INDUSTRY

Michael Sauer
CD Laboratory of Biotechnology of Glycerol
Department of Biotechnology BOKU-VIBT
University of Natural Resources and Life Sciences,
Vienna, Austria

Abstract

In our societies quest to mitigate greenhouse gas emissions and petroleum use, industrial microbiology plays a key-role for the provision of processes for fuel and chemical production from renewable resources.

Clearly, the microorganism is in the center of the process and care should be taken for its choice. Industrial production conditions are generally very harsh for the microorganism. Nevertheless, the host cells should be very efficient, which opens a vast area of conflict for the industrial microbiologist. Synthetic biology and metabolic engineering provide optimal tools for the rational design of biocatalysts. However, biodiversity is a major resource which should be tapped first. Nature solved many problems, which we face in industrial context – be it natural stress resistance or efficiency of metabolic pathways. However, all too often the rich source of natural diversity is neglected in favor of "pet" or model organisms. I propose that the fastest and most reliable path to efficient and economically viable microbial production processes uses both – natural diversity and synthetic biology. This concept shall be exemplified with bacterial and yeast host systems for the production of 1,3-propanediol, or sugar alcohols, respectively.

Prof. Michael Sauer
University of Natural Resources and Life Sciences
Department of Biotechnology
Muthgasse 18, 1190 Vienna, Austria
Phone: +43 1 47654 79105
Email: michael.sauer@boku.ac.at
Web:
https://www.biotec.boku.ac.at/arbeitsgruppenresear
ch-groups/research-group-mattanovich-gasser-
sauer/research/microbial-chemical-production/

Prof. Michael Sauer has studied his bachelor from Biotechnology at the Swiss Federal Institute of Technology (ETH Zürich), Doctorate (Biochemistry) at University of Vienna and Postdoctoral experience at the University of Milano Bicocca. He is team leader and PI at the Department of Biotechnology of BOKU-University of Natural Resources and Life Sciences. He is Head of the Christian Doppler Laboratory for Biotechnology of Glycerol.

A SYSTEMS PERSPECTIVE ON EMERGING BIOECONOMY IN THE CONTEXT OF FOOD-ENERGY-WATER

Ganti S Murthy
Biological and Ecological Engineering,
Oregon State University, USA

Abstract

We live in a resource-constrained world subjected to uncertain climate variations. We must address the challenges of meeting increasing demands of water, food and land from growing populations in the context of food-energy-water nexus. Emerging bioeconomy has potential to address some of these challenges through sustainable technologies and resilient strategies. A systems perspective considering the interaction of technology, economic, environment and policy will be discussed. The focus will be to present the linkages to enable integrated analysis to facilitate the development of sustainable technologies and resilient strategies. The first example will focus on a scenario analysis for advanced biofuel production in the Hawaiian Islands. The second example will emphasize the food-energy-water nexus in Columbia River basin in Pacific North-Western United States. Finally, a case study on the algal biofuels and biofertilizers will be presented. Through these examples, the trade-offs between techno-economic feasibility, environmental impacts and resource sustainability will be explored.

Prof. Ganti S Murthy
Professor
Biological and Ecological Engineering,
Oregon State University, Corvallis, OR-97331
Phone: 541-737-6291
Fax: 541-737-2082
Email: Ganti.murthy@oregonstate.edu
Website: http://agsci-labs.oregonstate.edu/stlab/

Ganti S. Murthy completed his B.Tech in Agricultural Engineering from NERIST, Arunachal Pradesh and M.Tech in Dairy and Food Engineering from IIT-Kharagpur. He then went to pursue PhD at Univ. of Illinois at Urbana–Champaign and obtained his PhD in Dec., 2006. He joined Oregon State University as a tenure track assistant professor in Jan., 2007. He was tenured and promoted to associate professor in Jul, 2013. He is currently a tenured full professor in Biological and Ecological Engineering Department at Oregon State University.

Dr. Murthy's research is broadly focused on development and evaluation of biofuels and bioproduct production technologies with a strong focus on all aspects of sustainability. For any proposed technology or policy, they seek to answer the question: "Is this approach technically feasible, economic viable, resource sustainable and has lower environmental impacts compared to alternatives? If not, how can we make it so?" His group employs a combination of experimental and theoretical approaches using control theory, systems biology, process modeling, economic analysis and life cycle assessment (LCA) techniques to conduct molecular, cellular, industrial scale and systems level analyses of technologies to establish a sustainable bioeconomy. They have developed technologies for fermentation control in corn ethanol plants, high solids fermentation for lignocellulosic biomass, advanced process control algorithms for algal production systems, low cost algal based waste water treatment systems and treatment of landfill leachate. Recently, Murthy group has been trying to understand the nutrient-energy-water nexus at regional and global scale with particular focus on building resilience of agro-ecological systems to pulse and pressure disturbances.

MEMBRANE BIOREACTOR VERSUS ITS REMOVAL OF ANTIBIOTICS

Xuan-Thanh Bui

Ho Chi Minh City University of Technology - Vietnam

Abstract

Recently, membrane bioreactor (MBR) has become an advanced technology for water and wastewater treatment. There are several advantages compared to conventional biological treatment processes such as activated sludge process, trickling filter, oxidation ditch, bio-filter, rotating biological contactor, wetland, etc. Although many advantages of MBR such as higher loading rate, longer sludge retention time, good treated water quality, less footprint, better removal of micro pollutants, etc. are clearly observed in recent research works, membrane fouling still remains an its drawback. Since then, MBR has been developed and upgraded with many modifications for fouling alleviation. Fouling was controlled by a number of methods such as using various membrane configurations, operating conditions, addition of various flocculants/media into membrane tank, use of special microbial species, applying different physical and/or chemical cleanings.

Nowadays, micro-pollutants (antibiotics) in both surface and ground waters becomes a major concern due to their potential eco-toxicity, causing water quality and impart a toxic effect on living organisms. MBR technology are not merely advantageous for organic and nutrient removal, but also likely promote a higher biodegradation efficiency of micro pollutants. The removal of antibiotics in MBRs is better due to the relatively long sludge retention time, which leads to the development of distinct microbial communities in the reactor compared to other conventional processes. This review focus on the recent development of MBR and its performance on antibiotics removal.

Prof. Xuan-Thanh Bui
Ho Chi Minh City University of Technology,
Vietnam
Phone: +84-965376073
Email: bxthanh@hcmut.edu.vn
Web: http://www.buixuanthanh.com

Bui Xuan Thanh received the Ph.D. degree in environmental engineering from an exchange program between the Asian Institute of Technology (AIT) - Thailand and the Institute National des Sciences Appliquées (INSA), Toulouse - France. Currently, he is an Associate Professor at the Faculty of Environment and Natural Resources, Ho Chi Minh City University of Technology, Vietnam. In addition, he also serves as a chairman of Department of Water Science and Technology in the Faculty. His research interests include membrane separation processes, water and wastewater treatment technologies and biological treatment processes. He has published more than 45 SCI/SCIE journal papers, 10 books/book chapters and 01 US patent. In addition, he has played a role of project investigator of more than 45 international/national research projects in the field.

BIOETHANOL PRODUCTION FROM THE MICROWAVE ACID HYDROLYSATE OF RED MACROAGLAGE EUCHEUMA DENTICULATUM

Lee Keat Teong, Teh Yong Yi
School of Chemical Engineering,
Universiti Sains Malaysia, Engineering Campus,
Seri Ampangan, 14300 Nibong Tebal,
Pulau Pinang, Malaysia

Abstract

This study aims to produce bioethanol from macroalgae hydrolysate obtained from microwave-assisted acid hydrolysis with sulfuric acid concentrations of 0.1 and 0.2 M, reaction temperatures of 150–170 °C and a heating time of 10 min. The main components of carrageenan in macroalgae can be hydrolysed and fermented with baking yeast. Higher yield of bioethanol and shorter optimum time taken were attained when dilute sulphuric acid was added.

Dr. Lee Keat Teong
School of Chemical Engineering,
Universiti Sains Malaysia, Engineering Campus,
Seri Ampangan, 14300 Nibong Tebal,
Pulau Pinang, Malaysia.
Phone: 604 6536533
Fax: 604 6536553
Email: ktlee@usm.my
Web: http://chemical.eng.usm.my/notes/ktlee/

Dr. Lee Keat Teong obtained his Ph.D in Chemical Engineering from Universiti Sains Malaysia (USM) in 2004. He is currently holding the position of Professor at the School of Chemical Engineering and he is also the Director of Research Creativity & Management Office and International Collaboration Center, Universiti Sains Malaysia. Dr. Lee has co-authored 2 books, 10 book chapters, 30 review papers and more than 100 research papers in peer reviewed international journals. Dr. Lee is currently the Co-Editor for Energy Conversion and Management (Elsevier) and Editorial Board Member for Bioresource Technology (Elsevier) and Energy Science & Engineering (Wiley). He has also won numerous awards including Young Scientist Award 2011 by The International Forum on Industrial Bioprocess and 2012 Top Research Scientists Malaysia by the Academy Sciences of Malaysia. Recently he is one of the four Malaysian researchers that was recognized as the most cited researchers in the latest Shanghai Academic Ranking of World Universities 2016 by Subjects (Energy Science & Engineering).

NATURAL LOW TRANSITION TEMPERATURE MIXTURES (LTTMS) AS NEXT GENERATION GREEN SOLVENTS FOR BIOMASS DELIGNIFICATION

Suzana Yusup
Chemical Engineering Department,
Universiti Teknologi PETRONAS,
32610 Bandar Seri Iskandar,
Perak, Malaysia

Presently, the concept of sustainable and green process has received a significant level of attention in the field of energy and environmental science. In this context, the challenge of searching green solvents for biomass pretreatment became a foregoing goal in producing renewable biofuels. Deep eutectic solvents (DESs) or low-transition-temperature mixtures (LTTMs) came up as promising alternative to conventional pretreatment technologies and the use of IL. Herein, solvents named as low transition temperature mixtures (LTTMs) by utilizing the malic acid from plants as hydrogen bond donor (HBD) and sucrose as hydrogen bond acceptor (HBA) were proposed. The crystallinity index of the biomass increased after delignification due to removal of amorphous hemicellulose and lignin resulted in an overall more crystalline substrate. LTTMs-delignified biomass also exhibited higher decomposition temperature and enhanced thermal stability due to transformation of cellulose I to cellulose II. Besides, pretreatment also removed the minerals in biomass and led to an enhanced thermal stability.

Prof. Suzana Yusup
Chemical Engineering Department,
Universiti Teknologi PETRONAS,
32610 Bandar Seri Iskandar, Perak, Malaysia
Phone: +605-3687642
Fax: +605-3688205
Email: drsuzana_yusuf@utp.edu.my
Web: https://www.utp.edu.my/SitePages/Home.aspx

Prof. Suzana Yusup is the pioneer in developing biomass research areas at Universiti Teknologi PETRONAS. She has published in numerous journals, articles and conferences and lead several research grants at national and international levels. She is also a reviewer for refereed journals and also technical committee at both national and international levels. She was the recipients of research product awards from Belgium, USA and Malaysia. Among important awards won are Malaysian Research Star Award (2017), Malaysian Rising Star Award (2016), Elsevier Green and Sustainable Chemistry Challenge (2016), Top Research Scientist Malaysia (2016), Asia Research Award (2012) from The Society of Chemical Engineers, Japan (SCEJ).

GREEN SOLVENTS FOR VALORISATION OF STARCH-RICH FOOD WASTE INTO VALUE-ADDED CHEMICALS

Daniel CW Tsang
Department of Civil and Environmental Engineering,
Faculty of Construction and Environment,
Hong Kong Polytechnic University, Hung Hom,
Kowloon, Hong Kong

Abstract

The carbohydrate-rich food waste is a potential renewable feedstock for biorefinery producing value-added chemicals such as hydroxymethylfurfural (HMF). This study aimed to examine the effect of γ-valerolactone (GVL) and propylene carbonate (PC) as the green solvents on conversion of bread waste to HMF over $SnCl_4$ as the catalyst under microwave heating at 120oC. Results showed that the maximum HMF yield of ~20 mol% was reached at 10 and 20 min in PC/H_2O and GVL/H_2O (1:1 v/v), respectively. In comparison, water produced 59 mol% glucose as the major product at 10 min. These results suggested that starch hydrolysis, glucose isomerisation, and fructose dehydration were efficient in the presence of PC and GVL, while glucose conversion was hindered in water. White particles appeared after heating $SnCl_4$-containing water, which were possibly SnO_2 as revealed by XRD analysis, implying that PC/H_2O and GVL/H_2O maintained Sn in an active form for catalysing glucose isomerisation.

Dr. Daniel CW Tsang
Department of Civil and Environmental Engineering
Faculty of Construction and Environment
Hong Kong Polytechnic University
Hung Hom, Kowloon, Hong Kong
Phone: 852-2766-6072
Email: dan.tsang@polyu.edu.hk

Dr. Daniel Tsang is currently an Associate Professor in the Department of Civil and Environmental Engineering at the Hong Kong Polytechnic University (HK PolyU). He was an IMETE Visiting Scholar at Ghent University in Belgium (2015), Visiting Scholar at Stanford University in the US (2011-2013), Senior Lecturer (2011-2012) and Lecturer (2008-2010) at the University of Canterbury in New Zealand, and Post-doctoral Fellow at Imperial College London in the UK (2007-2008) and the Hong Kong University of Science and Technology (2006-2007). Dan holds BEng (2002) and PhD (2006) from the Hong Kong University of Science and Technology. With a strong link to real-world environmental challenges, Dan's research group strives to develop cost-effective and low-impact solutions to ensure sustainable urban development, enhance the engineering infrastructure, and create new ways in which we manage contaminated soils/sediments, municipal solid waste, and urban waters. Dan has published over 130 SCI journal papers, and he is chair/co-chair and organizer of 2nd Biological Waste as Resource Conference (BWR2017, Hong Kong), 2nd International Conference on Bioresources, Energy, Environment, and Materials Technology (BEEM2018, Korea), and 4th Contaminated Land, Ecological Assessment and Remediation Conference (CLEAR2018, Hong Kong).

ZEOLITE CATALYSED GLUCOSE ISOMERISATION AND ITS DIRECT CONVERSION TO ALKYL LEVULINATE

S. Saravanamurugan

Center of Innovative and Applied Bioprocessing (CIAB),
Department of Biotechnology, Govt. of India,
Sector 81 (Knowledge City), PO Manauli,
SAS Nagar, Mohali 140 360,
Punjab, India

Abstract

Limited petroleum reserves are steadily diminishing as the world population and energy demand ascends to a large extent, making researchers and chemical industry to find alternative ways to transform biomass into potential chemicals and fuels, that can substitute the fossil based chemicals. In connection with this, we present a new reaction protocol for getting a high yield of fructose (> 50%) from glucose isomerisation in one-pot two-step in aqueous and alcoholic mixture with zeolites as catalysts. The best reaction results were obtained using the large pore zeolites H-USY (6) and H-beta (12.5) affording high fructose yields of 55 and 40 %, respectively. The direct conversion of carbohydrates to levulinic acid esters was also studied with the same zeolites to investigate their activity for catalyzing isomerization followed by subsequent dehydration and rehydration to obtain alkyl levulinate. Notably, H-USY (6) and (30) yielded 49 and 37 % of MLevu, respectively.

Dr. S. Saravanamurugan
Scientist-E
Center of Innovative and Applied Bioprocessing
Department of Biotechnology, Govt. of India
Sector 81 (Knowledge City)
PO Manauli, SAS Nagar
Mohali 140 360, Punjab, India
Phone: 0091-1725221538
Email: saravana@ciab.res.in; rsaravana78@gmail.com
Web: http://ciab.res.in/page.aspx?id=34

Dr. S. Saravanamurugan is currently Scientist-E at Center of Innovative and Applied Bioprocessing (CIAB) (Department of Biotechnology, Govt. of India), Mohali, India. Formerly, he was working as Senior Researcher at Centre for Catalysis and Sustainable Chemistry, Technical University of Denmark (DTU), Denmark since 2010. He moved to Korea Advanced Institute of Science and Technology (KAIST) in South Korea as Research Scientist in 2005 after obtaining his Ph.D from Anna University, Chennai in the same year. He also worked as post-doctoral fellow at Inha University, South Korea between 2006 and 2007 before moving to Denmark in January 2008. He has more than sixteen years of research experience and his main research topics include synthesis and modification of porous materials and biomass transformations. He has more than 50 peer reviewed publications, two book chapters and eight patents filed/granted with more than 2000 citations (h Index 21). He has co-authored an article in the prestigious journal Science in 2010, related to conversion of sugars to lactic acid derivatives with Lewis acid containing zeolites. He received a DST-DAAD Fellowship during his doctoral studies in 2004.

HIGH-PERFORMANCE COMPUTING ACCELERATING FUEL-ENGINE CO-OPTIMIZATION

Sibendu Som
Argonne National Laboratory, USA

Abstract

Vehicles powered by Internal Combustion Engines (ICEs), operating on a variety of fuels, are expected to remain as the primary mode of transportation in the foreseeable future. With the advent of High Performance Computing, simulation-based tools are becoming extremely important for providing unique insights into ICE design and operation. The latest developments in scaling and load-balancing of engine simulations which enabled the largest engine calculation ever, at the Mira supercomputer at Argonne will be shown first. Recent model developments for two-phase flow, combustion, and emission modeling along with extensive validation will be shown next. Our approach towards capturing cycle-to-cycle variability in engines will be highlighted. We have also been pioneering the use of Uncertainty Analysis and Machine Learning tools for ICE simulations and recent applications of this technique towards combustion applications will be demonstrated. Applications of the above mentioned tools towards US Department of Energy's Co-Optima program will be shown.

Dr. Sibendu Som
Group Leader & Principal Computational Scientist
Argonne National Laboratory
Argonne, IL 60439, USA
Phone: (630)252-5273
Fax: (630)252-3443
Email: ssom@anl.gov
Web: http://verifi.anl.gov

Dr. Sibendu Som has over a decade of experience in enabling technologies for more efficient engine combustion using computational tools. He leads a CFD team at Argonne National Laboratory with research focus on the development of nozzle-flow, spray, and combustion models, HPC for ICE applications. His team is responsible for developing predictive simulation capabilities for OEMs to develop advanced high-efficiency low-emission engines. Dr. Som's group is pioneering the implementation of uncertainty quantification and machine learning tools for engine simulations. He is a co-founder and technical lead on Argonne's Virtual Engine Research Institute and Fuels Initiative (VERIFI) program which is aimed at providing predictive simulations for OEMs. Dr. Som is the recipient of HPC Innovation Excellence Award by IDC in 2014, winner of the Federal Laboratory Consortium Award for Excellence in Technology transfer by DOE in 2015, and "best postdoctoral supervisor award" from Argonne in 2016. Dr. Som has authored more than 100 papers with more than 50 each in journals and peer-reviewed conferences with more than 2600 citations. Dr. Som received a Master of Science (2005) and Doctor of Philosophy (2009) degrees in Mechanical Engineering from University of Illinois at Chicago.

STRATEGIES TO ACHIEVE HIGH BRAKE THERMAL EFFICIENCIES IN LOW TEMPERATURE DUAL FUEL COMBUSTION ENGINES

Kalyan Kumar Srinivasan
Department of Mechanical Engineering,
The University of Alabama
286 Hardaway Hall 401 7th Ave.
Tuscaloosa, AL 35401, USA

Abstract
The latest US DOE estimates indicate that the transportation sector has overtaken the power plants as the largest contributor to net global CO_2 emissions in the continental USA. This is a clarion call to increase the efficiency of the transportation. The quest for increased efficiency should begin with the examination of the internal combustion (IC) engine. Advanced low temperature combustion technologies can achieve high efficiency in IC engines. Low temperature Dual fuel combustion or Reactivity Controlled Compression Ignition (RCCI) is a promising strategy to achieve high efficiency with low engine-out emissions. Our experiments indicate that it is possible to achieve high closed-cycle efficiencies by adjusting the relative amounts of diesel and methane; however, this window of opportunity is limited by knock at high diesel substitutions and at high methane substitutions. We further postulate high efficiency enablers include dilution, optimized CA50, high cylinder pressures, and short combustion durations.

Prof. Kalyan Kumar Srinivasan
Department of Mechanical Engineering
The University of Alabama
286 Hardaway Hall
401 7th Ave.
Tuscaloosa, AL 35401, USA.
Phone +1 205 348 6582
Fax +1 205 348 6419
Email ksrinivasan@eng.ua.edu
Web http://me.eng.ua.edu/people/ksrinivasan/

Dr. Srinivasan's expertise is in pollutant mitigation from internal combustion engines for transportation and stationary power generation. He uses both experimental methods and numerical simulations to develop novel combustion engine concepts that burn both conventional fossil fuels and alternative fuels such as natural gas, propane, syngas and other renewable biofuels. He has published over 56 peer-reviewed research articles that discuss innovative pathways to realize high fuel efficiencies while simultaneously reducing harmful environmental pollutants. Srinivasan is currently supervising 1 Ph.D. student and co-directing 2 Ph.D. students. He has directed / co-directed 4 Ph. D. students and 19 MS students over his eleven year academic career. Dr. Srinivasan's research has been funded by a variety of federal and industrial sources including PACCAR Engines, EATON Corporate Technology and Research Center, US DOE VTO, US DOE EERE, ARPA-E, Propane Education and Research Council (PERC), Mississippi Technology Alliance, DENSO N.A. Foundation, etc. Dr. Srinivasan continues to actively serve the ASME Internal Combustion Engine Division (ICED) in the capacity of the Vice Chair Elect of the ICED Executive Committee. He has been associated with the ASME ICED for the last 12 years and served as the overall conference chair of the ASME Internal Combustion Engine Fall Conference in 2016 and 2017.

COMPARISON OF ARTIFICIAL INTELLIGENCE (AI) BASED PREDICTION MODELS OF PERFORMANCES AND EMISSIONS OF COMPRESSION IGNITION ENGINE FUELED WITH DIESEL-KEROSENE-ETHANOL

Probir Kumar Bose
NSHM Knowledge Campus,
Durgapur, India

Abstract

The present study investigates the effects of oxygen containing bio-based Ethanol inclusion on the performances and exhaust fumes of a single cylinder off-road indirect injection (IDI) Diesel engine fueled with adulterated Diesel fuel. In the first phase of this study, mineral Diesel fuel has been adulterated by including subsidized Kerosene in the volumetric proportions of 5% and 10%. Adulterated Diesel fuel reduced the NOX emissions of the IDI engine with the penalties of lower brake thermal efficiency (BTE), higher brake specific energy consumption (BSEC), higher unburnt hydrocarbon (UBHC) and carbon monoxide (CO) emissions. Besides, oxygenated fuel inclusion in adulterated Diesel fuel considerably enhanced engine exhaust emissions without altering performances parameters. In the second phase, based on engine experimental datasets, two Artificial Intelligence (AI) based models viz. Artificial Neural Network (ANN) and Adaptive-Neuro Fuzzy Inference System (ANFIS) have been developed for mapping IDI engine performance-emission paradigms. BTE, BSEC, NOX, UBHC and CO have been chosen as output variables of the proposed AI based models, while load, Kerosene volume percentage and Ethanol volume percentage as input of the models. Both the AI based models have the capability for mapping IDI engine performance-emission parameters with high fidelity. For ANN model, Levenberg–Marquardt feed-forward back propagation (trainlm) with a topology of (3-6-5) has been found to the most advantageous than other training functions. To this end, a comparative study has been done, wherein ability of ANFIS model prediction has been observed to be higher accurate than ANN model.

Prof. Probir Kumar Bose
Campus Director
NSHM Knowledge Campus, GOI
Arrah, Shivtala, Via Muchipara
Durgapur - 713212
Phone : 0343-2533813(O), +91   9830054970(M)
Fax : 0343-2534025
Email : pkb32@yahoo.com
Web : http://www.nshm.com

Prof. P.K. Bose in his long professional career has several proven achievements and Excellency in Research and Development, Teaching and Academic Administration at the highest order of magnitude. Due to his outstanding contribution in Higher Education and Administrative capabilities, Ministry of Human Resource Development has given him additional charge, Director of N.I. T. Silchar and also as the Mentor Director for N.I.T. Manipur and Nagaland for creating and nurturing those N.I.T.s during their formation stage. At one point of time Prof. Bose had the responsibility to head four N.I.Ts and he efficiently delivered the responsibilities entrusted upon him. In which is rear achievement in the field of Educational Administration in the country.

Prof. Bose as Director School of Automotive Engineering, Jadavpur University, had established R and D and Innovation Centre for Howrah Foundry Cluster. The program is supported under TIFAC (D.S.T.) His pledge to revitalize the indices of education not only in the field of technical subjects but also in the conventional science and management subjects through its various tributaries of M. Sc. and MBA programmes are but a few examples of his holistic approach to the cause of academic and social prosperity of the North East. As eminent visionary and an administrator per excellence Dr. Bose obtained 07 patents and 03 International Patents, 40 numbers Ph.D. guidance and more than 224 nos of publications. 15 nos. of books/book chapter and completion 18 sponsor's projects along with academic leadership proved his Engineering Excellence.

TEMPORAL AND SPATIAL MICROSTRUCTURE OF A SPRAY

Dhivyaraja Kumaran, Sri Vallabha Deevi, Mahesh V. Panchagnula
Dept. of Applied Mechanics,
IIT Madras

Abstract

Sprays are widely used in a variety of industrial applications – for cooling, combustion and mixing. A spray is usually described by quantities such as Sauter mean diameter (SMD), which is a global average of the spatial as well as temporal unsteadiness inherent to sprays. We present results from statistical analysis of droplet size and velocity measurements that reveal valuable insights into the microstructure of the spray. Conditional probability analysis of spray data shows that apart from velocity clustering, there is significant size clustering in spray, with droplets of similar sizes following each other. Analysis using time series techniques show that the effect of a droplet is felt upto four/five droplets downstream for velocity and diameter. We propose a metric to quantify ordering in sprays. Analysis of airblast atomizer using this metric shows increasing ordering towards the edge. Further, results from single and intersecting sprays are compared to identify variations in temporal and spatial microstructure due to droplet collisions.

Dr. Mahesh V. Panchagnula
Department of Applied Mechanics
Indian Institute of Technology Madras
044 2257 4056
044 2257 4052
mvp@iitm.ac.in
https://apm.iitm.ac.in/fmlab/mvp/

Mahesh V. Panchagnula graduated from IIT Madras in 1992 with a B. Tech in Mechanical Engineering. He subsequently obtained an MSME in 1994 and Ph.D. in ME in 1997, both from Purdue University. He has since worked in industrial research positions with Goodrich Aerospace and Excel India till 2004. He has served as a Research Fellow at Lehigh University and as an Assistant Professor of Mechanical Engineering at Tennessee Technological University from 2005 to 2010. He has been on the faculty of the Department of Applied Mechanics, Indian Institute of Technology Madras since 2010 and in the current rank since 2014. He is also the faculty advisor to IIT Madras Pre-incubator Nirmaan and the associate faculty-in-charge of the IIT Madras Incubation Cell, which advises faculty and the student's entrepreneurship activities.

Prof. Panchagnula's current research broadly focuses on fundamental interdisciplinary multiphase thermal/fluid phenomena including wetting, hysteresis in natural systems, spray formation physics, pulmonary aerosol transport, liquid-liquid wetting and spray combustion. His lab employs both experimental as well as theoretical inquiry techniques. He has worked on the problem of contact angle and shown that it is an effect originating at the contact line. In addition, he has worked on wetting in partially miscible liquid-liquid systems such as oil/water thin film dynamics with Marangoni effects. His recent research has focused on applying simulation and data analytics tools to fluid mechanics problems such as the behavior of large crowds and turbulence. His complete list of published work can be found on Google Scholar.

ASSESSMENT OF DROPLET BREAKUP MODELS IN HIGH SPEED CROSS FLOWS

Debasis Chakraborty

Directorate of Computational Dynamics,
Defence Research and Developmental Laboratory,
Kanchanbagh P.O. Hyderabad-500058, India

Abstract

Modelling of liquid atomization is important in various engineering applications including aerospace propulsion systems, automotive engines, food processing, inkjet printing etc. Turbulent spray includes multi-scale physical processes. The liquid column disintegrates into ligaments and the droplets form sprays. Column breakup and surface breakup are two basic mechanisms of droplet formation. Droplet breakup process in quiescent atmosphere and high speed cross flow is numerically simulated by solving three dimensional RANS equations with K-ε turbulence model using commercial CFD softwares. Different droplet breakup models namely, TAB, ETAB, Ritz-Diwakar, KH-RT models are studied to access their predictive capability in characterising spray in high speed cross flows. The validation test cases include liquid injection into quiescent atmosphere, subsonic cross flow and supersonic cross flow. Computed droplet velocity, droplet size and spray structure compare well with the experimental /numerical data available in literature. Validated droplet models are employed to design hydrocarbon fuelled scramjet combustor.

Dr. Debasis Chakraborty
Scientist 'H'/ Outstanding Scientist
Directorate Of Computational Dynamics
Defence Research and Developmental laboratory
Kanchanbagh P.O. Hyderabad-500058, India
email: debasis_cfd@drdl.drdo.in

Dr. Debasis Chakraborty obtained his B.E. (Mechanical Engineering) degree from B. E. College, Shibpore (Presently BESU, IIEST) in the year 1980 and Master of Science (M.Sc.) in 1992 in SME (Noise & Vibrations) from Cranfield Institute of Technology, U.K. He has joined DRDO at the Laboratory NSTL, Vishakhapatnam as Scientist 'C' through UPSC on 15th July 1985. During his tenure at NSTL from 1985 till end 2015, he has worked on the projects Triple Tube Torpedo Launcher (TTL), Drill & Practice Torpedoes, Torpedo advanced light weight (TAL), Advanced Light weight torpedo (ALWT), Varunastra (Advanced Heavy weight torpedo), Mareech (Torpedo decoy system), Frontal Sealing systems in torpedoes, Sahayak emergency pay load delivery system and CRITECH (Critical Technology Development) Projects.

Dr. Debasis Chakraborty has been elevated to the level of Outstanding Scientist (OS) in the year 2015. Subsequently he has been assigned by DRDO to lead ADRDE (Aerial Delivery Research & Development Establishment) Agra, as Director from 18th November 2015. He has published numerous papers/technical reports to his credit in various International National journals/conference/seminars. Dr. Debasis Chakraborty is the Chairman of the Agra Chapter of Aeronautical Society of India and of the Agra Chapter of INSARM & Fellow of Indian Institution of Engineers.

Dr. Gaurav Tomar
Associate Professor
Department of Mechanical Engineering
Indian Institute of Science
Bangalore 560012
Phone: +91-80-22933062
Email: gtom@mecheng.iisc.ernet.in

Dr. Gaurav Tomar has completed his B.Tech (2003) and Ph.D (2008) from IIT Kanpur. His research areas are Multiscale simulations, Two-phase flows, Heat and Mass Transfer and Thin films.

Research in Their laboratory focuses on simulations of two phase flows. They use various numerical tools to study two-phase flow phenomena. An in-house Volume of Fluid method based two-phase flow solver is used for two dimensional and axisymmetric simulations of electrohydrodynamic flows. A meshless particle based method, namely, Smooth Particle Hydrodynamics, is used to simulate two and three dimensional free surface and fluid-structure interaction flows. Using these tools, we study various two-phase flow phenomena: droplet and bubble dynamics in electric field, undular hydraulic jumps, atomization of a liquid jet and water entry of projectiles.

DEVELOPMENT OF A METHANOL FUELLED LOCOMOTIVE FOR INDIAN RAILWAYS

Anirudh Gautam

Special Railway Establishment for Strategic Technology and Holistic Advancement (SHRESHTA), RDSO, Lucknow

Abstract

A detailed roadmap for design, development and retro-fitment of a methanol locomotive is presented in the paper. The paper takes into account different technologies, which have been explored earlier for conversion of CI engines to run on methanol. These technologies include a wide range starting from fumigation, port injection, direct injection, high pressure direct injection to ignition improver additized methanol. Locomotive diesel engine is a large-bore, medium-speed, compression ignition diesel fuelled engine. Using a high octane fuel such as methanol in this configuration is a technical challenge and requires elaborated R&D and retro-fitment.

Methanol poses several technical issues when used as a transportation fuel. Fortunately, most of these issues have already been resolved by early researchers. Methanol is an extensively corrosive and toxic fluid, if contacted in large quantities. At the same time, it is highly bio-degradable. Although it is completely miscible in water, its short life-span in water and in air, in the event of an accident does not pose any significant risk to the ambient and marine environment. Its use as a transportation fuel is being actively practiced in various parts of the world such as China, and European Union. In China, methanol is being increasingly produced by gasification of coal. India can also do the same by converting its large domestic reserves of high ash coal (which cannot be used for power generation) into methanol and use it for the transportation fuel. Indian Railways can emerge as one of the first large user of the methanol since it is under a single management and owns more than 5000 diesel locomotives with potential for conversion to methanol. This approach has vast potential for reducing life-cycle energy usage, and reduce green-house gas emissions and toxic emissions from locomotive engines compared to diesel and electric locomotives. Of the various technologies surveyed, two technologies are found to be suitable for IR diesel locomotives and duty-cycles. These are high pressure direct injection of methanol with pilot injection of diesel and use of additized methanol and these are discussed in detail to narrow down the choice to most suitable technology.

Dr. Anirudh Gautam
Executive Director
Special Railway Establishment for Strategic
Technology and Holistic Advancement (SHRESHTA)
RDSO , Lucknow
Email: gautam.anirudh@gov.in
Web:http://www.indianrail.gov.in/

Dr. Anirudh Gautam is a mechanical and electrical engineer from prestigious SCRA scheme of Indian Railways. He has served initial years on the Indian Railways in the maintenance of the carriage and wagon, maintenance and operation of steam locomotives, operation and maintenance of diesel locomotives and train and crew management in the challenging Eastern Sector of Indian Railways. He then worked in the area of manufacture of diesel locomotives at Diesel Locomotive Works, Varanasi and moved to the niche area of design and development of diesel engines for the locomotives. He is credited with design of the first hotel load feature on an export locomotive and was instrumental in building the first indigenous EMD design locomotive in India at DLW. He has developed the worlds first ALCO locomotive electronic fuel injection system which has been commercially successful. He developed the mobile Emission Test Car which has been used for measuring pollutants levels from diesel locomotives of Indian Railways. He has been working on the research and development of alternate and advanced propulsion systems. His main areas of interest are energy production devices, fuel cells, hybrid power trains and sustainable motive power systems, control systems development and structures optimization.

Dr. Gautam is recipient of various awards by the Ministry of Railways, including the coveted National Award for Outstanding service by the Minister of Railways. He is currently working on development of highly fuel efficient engine technologies for locomotive engines, design and development of natural gas engine technologies, use of methanol on locomotive engines and reduction of emissions from locomotive engines. He is working on developing fuelcell based hybrid trainsets which is the future of railway traction. He holds a Masters in Quality management from BITS Pilani, a Masters of Engineering in Engine Systems from University of Wisconsin, Madison, USA and a PhD in renewable energy and transportation from IIT Kanpur.

DEVELOPMENT OF VARIABLE VALVE CONTROL SYSTEM FOR SPARK IGNITION ENGINE

Dhananjay Kumar Srivastava
Department of Mechanical Engineering,
Indian Institute of Technology Kharagpur, Kharagpur - 721302

The valvetrain coordinates the intake of fresh charge/air and exhaust of combustion products in an IC engine. The power developed by an engine increases with increase in the amount of intake charge. Allowing the engine to draw in more charge will increase the power output of the engine. However, at the same time expelling the exhaust gas at the right time helps reduce the pumping work. Hence a proper trade-off between expansion work and pumping work helps improve the net power output. Tuning of the valve timing and lift thus plays a crucial role in improving the power output as well as the efficiency of an IC engine.

In most reciprocating IC engines, the timing and lift of the intake and exhaust valves are controlled by a camshaft. Being mechanically driven by the crankshaft, a camshaft simplifies the valve actuation process. However, it also means that the valve timing and lift do not vary with speed. As a result, a camshaft driven valvetrain can be optimized for only a narrow speed range resulting in poor performance at speeds outside the optimized range. Hence, the power and torque curves of engines using camshaft driven valvetrains exhibit a peak at a particular speed, on either side of which power and torque drops. While, there do exist camshaft driven variable valve timing and lift systems, they usually offer few discrete modes of operation according to discrete speed ranges. Continuous variation of valve timing and lift with speed is usually not encountered, thus motivating the development of an independent valve timing and lift control system.

Dr. Dhananjay Kumar Srivastava
Assistant Professor
Department of Mechanical Engineering
Indian Institute of Technology Kharagpur
Kharagpur - 721302
Phone: 03222-282930
Email: srivastava@mech.iitkgp.ernet.in

Dr. Dhananjay Kumar Srivastava is currently working as Assistant Professor in the Department of Mechanical Engineering, IIT Kharagpur, since April 2015. He has done Doctor of Philosophy from Engine Research Laboratory, IIT Kanpur, in 2013. He was a Research Fellow at University of Birmingham, UK, in 2014. He was also a Visiting Researcher at University of Vienna, Austria, in 2004. His areas of expertise include laser ignition of engine, combustion visualization, emission control, engine calibration, gasoline direct injection. He is the recipient of Gandhian Young Technological Innovation Award in March 2013, Pool Scientist Fellowship by CSIR, India, from 2010 to 2013.

NON-FOSSIL CARBON SOURCES AND CONVERSION PATHWAYS TO FUELS FOR REDUCTION OF FOSSIL FUEL IMPORTS AND GHG EMISSIONS IN INDIA

Anjan Ray, Jasvinder Singh

CSIR-Indian Institute of Petroleum, Dehradun

Abstract

The current energy profile in India continues to be significantly dependent on fossil fuels, though the renewable content of the overall energy mix is increasing steadily. The adoption of renewable fuels requires identification, conversion and efficient as well as cost-effective application of fuels derived from domestic non-fossil carbon sources. Anthropogenic carbon is abundantly available in India but conversion and application efforts have yet to leverage the full spectrum of possibilities.

Sustainable production and application of fuels from widely different sources such as biomass, municipal solid waste (MSW), sewage and carbon-containing gases can not only enable India to significantly reduce fossil fuel imports but also move forward in the direction of national commitments (INDC) to the COP-21 UNFCCC greenhouse gas (GHG) reduction targets, enhance economic and ecological benefits along the value chain from generated anthropogenic carbon to utilizable fuels derived from such sources. Case studies indicate that technology-neutral policy interventions to widespread deployment of anthropogenic carbon-based fuel technologies could be broadly beneficial for India.

Dr Anjan Ray
Director
CSIR-Indian Institute of Petroleum,
P.O. IIP Mohkampur, Dehradun
Phone: +91 9810208092
Fax: 0135 2660098
Email : director@iip.res.in, anjan.ray@iip.res.in
Web: www.iip.res.in

Anjan Ray received his Doctorate in Chemistry from the University of Pennsylvania under the guidance of Nobel Laureate Prof. Alan MacDiarmid. He then moved to the chemical industry and worked for over 25 year across functions ranging from Quality Control, Technical Service, R&D and Marketing to General Management, Mergers & Acquisitions and Corporate Strategy.

His professional interests have spanned fields as diverse as surfactants, oleochemicals, paints, adhesives, textiles, cosmetics, pharmaceuticals, water treatment, energy efficiency, biofuels and renewable energy policy. Currently, he holds the position of Director – CSIR-Indian Institute of Petroleum and Head, Research Project Planning and Business Development Directorate (RPPBDD), Council of Scientific & Industrial Research (CSIR) Headquarters (Additional Charge), New Delhi. Apart from his professional career in chemical technology, Dr Ray has had an active interest in media, education, heritage and environmental conservation for over 3 decades.

INTEGRATIVE ENZYMATIC BIOREMEDIATION APPROACHES FOR ENVIRONMENTAL SUSTAINABILITY

**Bibhuti Ranjan, Santhosh Pillai,
Kugenthiren Permaul and Suren Singh**
Department of Biotechnology and Food Technology,
Faculty of Applied Sciences,
Durban University Of Technology
Steve Biko Road Durban, South Africa

Absract

Cyanide toxicity poses environmental problems globally and is also relevant in South African context due to its frequent use in industry for the extraction of precious metals. Owing to its potential toxic nature, there is an essential need to find the process, which is cost-effective and environmental friendly for cyanide remediation. Microbial enzymes are promptly gaining interest in bio-remediation because of lower process time, requirement of lower energy, cost-effective, nontoxic and eco-friendly characteristics. Although, production and properties of enzymes can be enhanced and modified according to the need, via genetic- and protein-engineering approaches. However, the high cost of up- and down-stream processing of enzymes and difficulty in separation from reaction mixture for subsequent reuse may discourage the use of enzymes from the economic prospects. Consequently, enzyme immobilization offers an alternative to resolve the challenges associated with the reusability of enzymes coupled with the several other advantages, such as, enhanced thermal stability and ease of separation. In addition, with the increasing consideration paid to enzymatic cascade reactions towards bio-remediation, it is possible that co-immobilization of multiple enzymes on nanoparticles could be achieved for the economical, efficient and sustainable bio-remediation.

Cyanase is an enzyme that catalyzes the decomposition of cyanate in bicarbonate-dependent reaction, however, the requirement of bicarbonate is a major drawback for its effective utilization in large-scale applications. Therefore, in the present investigation, we have developed a novel strategy to limit the bicarbonate utilization in cyanate remediation, by the co-immobilization of two recombinant enzymes, cyanase (rTl-Cyn) and carbonic anhydrase (rTl-CA) from the thermophilic fungus Thermomyces lanuginosus on magnetic nanoparticles. Of significance is that this integrative approach resulted in the complete degradation of cyanate using 80% less bicarbonate, compared to rTl-Cyn alone. Further, we have also evaluated the reusability of immobilized enzymes, and observed that after 10 cycle more than 90% of activity was retained. In addition, we have also evaluated the efficacy of immobilized enzymes on simulated wastewater system at laboratory-scale with great success.

Prof. Suren Singh
Executive Dean – Faculty Of Applied Sciences
Leader; Enzyme Technology Research Group
Durban University Of Technology Steve Biko
Road Durban
South Africa
Phone: +27 834684292
Email: singhs@dut.ac.za

Prof. Suren Singh is currently the Executive Dean of Applied Sciences since 2014, at the Durban University of Technology (DUT) in South Africa. He was previously Head of Department of Biotechnology & Food Technology at DUT and holds a professorial appointment in the department. He has published over 100 papers in international journals mainly in the field of enzyme production and application with emphasis on extreme properties that such enzymes could be modified and expressed accordingly. His initial work began with a unique thermophilic fungus, Thermomyces lanuginosus and this has been the hallmark of all his current work. The genome has been sequenced and more than 100 clones as potential carbohydrases are currently being expressed. Collaborations of his group has been extensive in Europe, USA, China and India for more than 10 years.

LIGNOCELLULOSIC BIOMASS FOR A SUSTAINABLE BIO-BASED ECONOMY

Parameswaran Binod
CSIR-National Institute for Interdisciplinary Science and Technology,
Industrial Estate PO, Pappanamcode,
Trivandrum – 695019, Kerala, India

Abstract

The biorefinery approach for conversion of lignocellulosic agro-residues into valuable chemical building blocks is the emerging trend in biomass conversion. The pretreatment and enzymatic hydrolysis of lignocellulosic biomass results in fermentable sugars that can be utilized in microbial fermentation for the production of high value chemicals. The present study aims to produce high value chemicals like 1,3 propanediol, 2,3 butanediol and 2,5 furan dicarboxylic acid. We have demonstrated the production of 1,3 propanediol by a isolated Lactobacillus strains utilizing the crude glycerol generated from biodiesel industry as raw material. Bioconversion of glucose to 2,3-butanediol (BDO) by Enterobacter sp SG1 has been carried out and it was found that the BDO production is growth independent process and majorly depends on the glucose concentration in the media. The present study also discusses the approaches to develop an eco-friendly biological process for the production of FDCA from hydroxymethyl furfural (HMF) using microorganisms.

Dr. P. Binod
CSIR-National Institute for Interdisciplinary
Science and Technology,
Industrial Estate PO, Pappanamcode,
Trivandrum – 695019, Kerala, India
Phone: +91-471-2515361
Fax: +91-471-2491712
Email: binodkannur@niist.res.in
Web: http://www.niist.res.in/english/scientists/binod-
parameswaran-/academic-qualifications.html

Dr. Parameswaran Binod is currently working as a Scientist in the Microbial Processes and Technology Division of CSIR-National Institute for Interdisciplinary Science and Technology, Trivandrum, India. He obtained his PhD in Biotechnology from Kerala University, Trivandrum in 2008 and after that he did his post Doctoral studies at Korea Institute of Energy Research, Daejeon, South Korea in the area of lignocellulosic biofuels. He has nearly 85 publications including research papers, reviews and book chapters. In 2001 he received Young Scientist Award from International Forum on Industrial Bioprocesses (IFIBiop) and in 2014 he received Kerala State Young Scientist Award. His research interest includes bioprocess and bio-products including biofuels, biopolymers and biochemicals of industrial importance.

LARGE EDDY SIMULATION OF A HYDROGEN-FUELLED SCRAMJET COMBUSTORSANJEEV

Santanu De

Department of Mechanical Engineering,
IIT Kanpur, Kanpur-208016, India

Abstract

Large eddy simulation is performed for the German aerospace center (DLR) scramjet combustor with strut based injectors. Numerical simulations of both reacting and nonreacting cases are performed using a pressure-based solver in OpenFoam. Oxidizer enters the combustor at a Mach number of 2, whereas H2 is injected in the wake created by the strut at unity Mach number. Numerical results of pressure, velocity and temperature are compared with the experimental data at different cross sections for different turbulence and combustion models. Effects of LES turbulence models in supersonic flow field have been studied and compared for four different subgrid-scale models, namely Smagorinsky (zero equation), k-equation (one equation), dynamic Smagorinsky with Lagrangian averaging (DLM), and delayed detached eddy simulation (DDES) models. In order to model complex turbulence-chemistry interaction, flamelet models are used. Two different variants of flamelet models are used based on scalar dissipation rate and flamelet progress variable (FPV) approach. A detailed chemical kinetics with 9 species and 27 reversible reactions is used for H2-O2 combustion. Performance of the flamelet models is compared with partially stirred reactor (PaSR) model based on single-step global reaction. Contours of pressure, velocity, density, H2O mass fraction, and temperature are also examined.

Dr. Santanu De
Assistant Professor
Department of Mechanical Engineering
Indian Institute of Technology Kanpur
Kanpur, U.P. – 208 016
Phone: 0512 259 6478
Fax: 0512 259 7408
Email: sde@iitk.ac.in
Web: http://home.iitk.ac.in/~sde

Dr. Santanu De is an Assistant Professor in the Mechanical Engineering, IIT Kanpur since December 2014. He received a Bachelor of Engineering from the North Bengal University in 2002, and an M.Tech. from the IIT Kanpur in 2004, both in Mechanical Engineering. He received his Ph.D. in Aerospace Engineering from the Indian Institute of Science, Bangalore in 2012. Prior to his joining at IIT Kanpur, he served two years at the Michigan Technological University as a postdoctoral research associate, and one year at the Institute of Combustion Technology (ITV), University of Stuttgart. He also worked as a scientist at the Liquid Propulsion Systems Center, Indian Space Research Organization between years 2004 and 2005. His primary area of research is numerical modeling of turbulent combustion, spray atomization and combustion, coal gasification and combustion.

SEARCH FOR HIGHER-ORDER CONTINUUM TRANSPORT EQUATIONS

Amit Agrawal

Department of Mechanical Engineering

Indian Institute of Technology Bombay,

Powai, Mumbai 4000076

Abstract

There is evidence in the literature as well as experimental data from our lab suggesting that the Navier-Stokes-Fourier equations are inadequate to explain several observations with low-pressure gas flows. There seems to be no satisfactory alternative to theoretically describe the flow when the mean free path of the gas is of the order of the characteristic length scale. The two well established approaches of solving the Boltzmann equation yields the Burnett and Grad 13-moments equations. However, several shortcomings of these equations are known by now. This motivated us to explore alternate ways to derive higher-order continuum transport equations. In this context, we have employed a phase density function consistent with the principles of nonequilibrium thermodynamics and satisfying collision invariance properties, to derive new set of generalized transport equations. The phase density function satisfies the linearized Boltzmann equation and provides the correct value of the Prandtl number for monatomic gas. We term these new equations OBurnett and O13 equations ('O' for Onsager, as these equations are consistent with Onsager's symmetry principle).

The proposed OBurnett equation involve cross single derivatives of field variables such as temperature and velocity, with no higher-order derivative in higher-order terms. This is remarkable feature of the equations as the number of boundary conditions required is the same as needed for conventional Navier-Stokes equations. Linear stability analysis of the OBurnett equations is performed, which shows that the derived equations are unconditionally stable. Similarly, it is noted that the proposed O13 equations require same number of boundary conditions as compared to the Grad equations, and fewer than the regularized 13-moment equations. The Knudsen number envelope which can be covered to describe flows with these equations is expected to be much larger as compared to the earlier equations. In this talk, I will present these newly derived equations and our current efforts in verifying these equations. The results from the OBurnett equations have been verified for force-driven compressible plane Poiseuille flow problem. I will also present the first analytical solution of the Burnett equations for any configuration. I will also point out the relation between Grad and Cattenao equations (a popular non-Fourier model).

Prof. Amit Agrawal
Professor
Department of Mechanical Engineering
Indian Institute of Technology Bombay,
Powai, Mumbai 4000076
Email: amit.agrawal@iitb.ac.in

Prof. Amit Agrawal work in the fields of Fluid Mechanics and Heat Transfer using experimental, theoretical and simulations tools. His research group's problems are mainly drawn from the areas of Microfluidics and Turbulent flows. Among their research interests are: development of innovative microdevices for various applications; theoretical development of higher-order continuum transport equations and related experiments; synthetic jet and microchannel based cooling of electronic devices; wake interaction from multiple bodies; etc.

They have developed a microdevice for blood-plasma separation; also microdevices for three-dimensional hydrodynamic focusing, and for maintaining constant wall temperature. They have provided the first analytical solution of the Burnett equation (a higher-order continuum transport equation), for any configuration. Further, keeping the limitations of Burnett and Grad equations in mind, we derived a new set of Onsager-consistent equations, which are supposedly more general continuum transport equations then the Navier-Stokes equations. They have demonstrated synthetic jet and microchannel based device for cooling of electronic devices requiring small working distance and input power.

Their research work is documented in over 125 journal articles. The work has appeared on the cover page of prestigious journals such as the Journal of Fluid Mechanics and highlighted in the media. The work has been conducted by 13 PhD and 50 MTech students (who are all well placed in various Industry/Academia), along with 4 Postdoctoral Fellows. Currently, he has an active research group comprising several very dedicated students, postdocs and project staff. He is also serving as the Editor of Experimental Thermal and Fluid Science and Sadhana; also as Editorial Board Member of Nature Scientific Reports along with two other journals.

AIMING AT SUSTAINABLE ENERGY: HOW SUSTAINABLE ARE THE RENEWABLE ENERGY SOURCES?

Teodora Emilia Motoasca
KU Leuven, Department of Electrical Engineering,
Energy & Automation (E&A)
Faculty of Engineering Technology – TC Ghent

Abstract

A possible short-, mid- and long-term solution for the worldwide energy shortage is the more extensive and intensive application of renewable energy sources, like sun, wind, water and biomass. However, a closer look at their sustainability reveals that not all of them are sustainable when it comes to the long-term evaluation of social, economic and environmental sustainability parameters. Calculation of the environmental impact of renewable energy should start from the energy cost and the environmental impact of production, transport, installation, maintenance and recycling of all devices needed for renewable energy production. The evaluation of social and economic sustainability may seem sometimes straight forward, but it is a diverse and complex problem where long-term maximization of the workers' and local communities' welfare together with economic growth is aimed at.

Renewable energy application is not always socially, environmentally and economically sustainable. This work presents some lessons learned from current renewable energy projects and some proposals for sustainability improvement.

Prof. Teodora Emilia Motoasca
KU Leuven, Department of Electrical Engineering
Energy & Automation (E&A)
Faculty of Engineering Technology – TC Ghent
Gebroeders Desmetstraat 1,
BE-9000 Ghent, Belgium
Phone: + 32 9 3316567
Email: emilia.motoasca@kuleuven.be
Web: www.iiw.kuleuven.be/gent

Emilia Motoasca obtained a PhD-degree in electrical engineering from Delft University of Technology (the Netherlands) in 2003. Between 2003 and 2013 she worked at the Eindhoven University of Technology (the Netherlands), Faculty of Electrical Engineering, as post doc and later on as assistant professor. Nowadays she is member of the research group Energy and Automation from Department of Electrical Engineering of KU Leuven (Belgium) at Technology Campus Ghent. Her research interests include design and modelling of electric motors, hydraulic and electric drives, heat flow in smart systems with a wide range of application to robotics, e-mobility, sustainable energy harvesting and usage, and to industrial processes.

CREATING SUSTAINABLE MOBILITY TECHNOLOGIES – OPPORTUNITIES AND CHALLENGES

Shankar Venugopal, Shantha Shankar
Mahindra Research Valley,
Mahindra World City, Chennai

Abstract

Sustainable mobility for the future is all about creating automotive technologies that are clean, safe and fast. If we look at the urban mobility scenario today, there are three problem areas that need attention (a) pollution due to vehicular emission (b) vehicular accidents and (c) loss of productivity due to difficulty in navigating through dense traffic. Electric Vehicles are emerging as the future clean vehicle technology and will remove concerns around rising vehicular emissions. Autonomous cars have demonstrated accident-free performance for more than a million miles. Connected vehicles that can proactively communicated with signals, parking lots and other vehicles on the road are fast emerging as the solution for handling traffic jabs in the cities.

The opportunities in the short-term include introducing battery powered electric vehicles (that are powered by a mix of solar and fossil fuel), autonomous tractors and border patrol vehicles and connected vehicles whose location and performance can be monitored remotely. In the medium term, electric vehicles fully powered by solar, autonomous trucks that can move on dedicated tracks on the highways to transport goods and connected vehicles that can talk to signals and parking spaces. In the long term, we visualize emergence of electric vehicles that will not need energy storage (create and use electrical energy on the go), autonomous cars on the road and connected vehicles that can talk to each other, plan their route and coordinate their movement. The challenges in realizing these three technologies – electric, autonomous and connected vehicles – are three fold. The first is the materials challenge – the scarcity of materials such as Lithium for battery, Rare Earth minerals for magnets in the motors, Cobalt etc may become bottlenecks for scaling up these technologies. The second challenge is about Intellectual Property (IP) – since these technologies are exponentially growing and converging, there is a need to accelerate the creation and commercialization of IP. For instance, if it takes more than five years to secure IP for a technology invention, then the technology may become obsolete by that time. The third challenge is to get the ecosystem ready for effective diffusion of these technologies. For instance, electric vehicles will need charging infrastructure, autonomous vehicles will need favorable legal framework and connected vehicles will need seamless internet availability. The talk will describe the potential opportunity to create sustainable mobility for the future by investing in the development of electric vehicle, autonomous vehicle and connected vehicle technologies. We will also discuss the challenges associated with critical materials, intellectual property and ecosystem readiness.

Dr. Venugopal Shankar
Vice President
Mahindra & Mahindra Limited,
Mahindra Research Valley,
Mahindra World City
Plot 41/1, Anjur Post,
Chengalpattu, Kancheepuram 603004
Phone: 044-67037346,
Email: venugopal.shankar@mahindra.com
Web: http://www.mahindra.com 603004

Dr. Shankar leads technology innovation for the Automotive & Farm services business (AFS). He heads the intellectual property (Patents) and knowledge management functions. He is also the Dean of the Mahindra Technical Academy. Shankar is passionate about developing sustainable urban mobility solutions and his current interests span across electric vehicles, connected vehicles and autonomous vehicles.

Prior to joining Mahindra & Mahindra, Shankar has held technology innovation leadership roles at GE, Dow, Honeywell and Cummins. He holds ten international patents and numerous new product innovation awards. He has developed a proprietary innovation methodology – Innovation FLOW – and trained 1000 + inventors and innovators.

Shankar obtained a Ph.D in Materials Science and a gold medal for the best doctoral thesis from the Indian Institute of Science, Bangalore. He completed his executive management program from the Indian Institute of Management, Bangalore. Shankar is an avid reader and is interested in physics, philosophy and psychology. He teaches technology innovation management at premier engineering & management institutes in India & abroad.

EMISSION REDUCTION TECHNIQUES IN AUTOMOBILES

Pradeep Kumar Gupta, Shyam Lal Soni and Dilip Sharma

National Institute of Technology Uttarakhand

Abstract

Controlling of exhaust emissions in transportation sector is seriously felt. Though strict automotive emission norms are being implemented by all countries, still the road worthiness of vehicles is tested as per the year of manufacture. Old vehicles (Euro III and earlier) will continue to ply on roads, fulfilling the emission norms of their respective year of manufacture, especially in developing nations. Nitrogen oxides (NOx) and particulate matter (PM) emissions from diesel engines require more attention. While studies have been conducted on constant speed stationary engines and modern engines, this study tried to analyze the effectiveness of an uncoated (uncatalyzed) wall-flow type ceramic diesel particulate filter and an electronic control unit (ECU) controlled exhaust gas recirculation valve on a Euro-1, 4-cylinder, water-cooled, direct injection, variable speed, automotive compression ignition engine in a laboratory set-up in India. Also, this study focused on diesel particulate filter regeneration by two methods: active regeneration by diesel injection in the particulate filter using an electronic control unit; and off-board regeneration by taking out and heating the diesel particulate filter in an electrical resistance furnace at 650°C for 10 hours. The results, in the form of smoke emission, NOx emission and engine performance, obtained using both the regeneration methods were analyzed and conclusions were drawn. It was found that using diesel particulate filter; particulate matter emissions (smoke) were almost entirely eliminated. It was also found that off-board regeneration had numerous advantages compared to active regeneration. Since a furnace would be needed for off-board regeneration, an exchange process for diesel particulate filter is suggested. Reduction of NOx was achieved by testing an EGR valve running the engine on different speeds; with different torques, as also with varying EGR percentages. It was found that using EGR, NOx emissions were substantially reduced (average 45% reduction), however slightly impacting the engine performance. Also, smoke emission increased with EGR. In order to counter the adverse effects, additional emission reduction technologies should be used in tandem with EGR like DPF. DPF and EGR were used in tandem on the same engine giving the desired results of substantial reduction in NOx as well as smoke compared to base case. Effect of vehicle weight on emission was also studied and conclusions were drawn. Various researchers have come out with different empirical formulae for CO_2 emission with vehicle weight which shows a linear relationship between the two. i.e. CO_2 emissions increase proportionally with increase in vehicle weight keeping other parameters constant. However, no straight relationship could be found between vehicle weight and other emissions though it is certain that other emissions also reduce on reduction in vehicle weight. Various ERTs were studied and relative importance of ERTs w.r.t. future BS norms was predicted concluding that DPF / GPF will be a must post BS IV (BS VI onwards).

Prof. Shyam Lal Soni
Director
National Institute of Technology Uttarakhand
Srinagar, Pauri-Garhwal
Phone: 9829128150
Fax: 01346251095
Email: shyamlalsoni@gmail.com

Dr. Shyam Lal Soni is the Director of National Institute of Technology Uttarakhand. Before joining the post of the Director at NIT UK he was Professor at MNIT Jaipur. He served as Dean Research and Consultancy, Faculty Coordinator Training and Placement, Chairperson Golden Jubilee Year Celebrations, Chief Vigilance Officer, Registrar, Head in the Department of Mechanical Engineering at Malaviya National Institute of Technology Jaipur. Dr. Soni passed his B.E. from MREC with honours in 1979. He did his M.Tech. from IIT Delhi with CGPA of 9.6 and also obtained Ph.D. from IIT Delhi. His field of specialization is alternate fuels in I.C. engines. He has more than 37 years of teaching experience at MNIT Jaipur. He has published more than 80 research papers in National and International journals and conferences. He has guided seven research works leading to award of PhDs, four more have submitted their thesis and six more Doctoral research works are under progress in his supervision. He is founder Faculty Advisor of SAE student chapter at MNIT Jaipur. He recently received the Guru Award 2016-17 from SAEINDIA Foundation.

He has developed the I.C. engines laboratory by up grading of the laboratory equipment conforming to Industrial requirement, setting up of new experiments to facilitate graduate and other research projects of PhD level at MNIT Jaipur. As in charge I.C. Engines Laboratory he had very actively worked in the field of I.C. engine technology, fuel quality and alternate fuels for S.I. and C.I engines. The laboratory has been developed to have facilities at par with IIT laboratory to carry out any research work. As Chairperson Golden Jubilee Year Celebrations at MNIT he could manage to organize more than 30 International and National Conferences at MNIT Jaipur.

SUSTAINABLE WASTE MANAGEMENT THROUGH CLOSING THE LOOP APPROACH

S. Venkata Mohan

Bioengineering and Environmental Sciences Lab,
EEFF Department
CSIR-Indian Institute of Chemical Technology (CSIR-IICT),
Hyderabad-500 007

Abstract

Waste as the core element and feedstock advocates sustainable development in the circular economy mode contrary to the fossil based linear economy. In this realm, our research is aimed at waste management and resource recovery in a integrated way by developing sustainable waste remediation strategies for the production of biofuels and platform chemicals in the closed loop approach. CSIR-IICT designed and a state of art pilot plant facility (10,000 liters capacity) for the production of biohydrogen from waste/wastewater with the funding from Ministry of New and Renewable Energy, Government of India. The pilot plant facility has acidogenic reactor at focal point inter-connected with seven unit operations each with a defined function i.e. inoculum preparation, redox control, buffering/pre-treatment, biogas holding, anaerobic digestion, auto biogas-flare and water storage/waste feeding. The pilot plant was operated with the food waste after pre-hydrolysis in a acidic microenvironment using selectively enriched consortia as biocatalyst with 48 hours of retention time. For the production of biobased products a biorefinery with a closed loop approach was designed and operated. The pilot plant was integrated with a waste biorefinery platform designed and constructed by CSIR-IICT (funded by CSIR, Government of India; 12 FYP-CSC-0113) with operation capacity of 10,000 liters. The facility consist of anaerobic reactors (2 no), algal race way ponds (2 no), ecological engineered living system (three stages), PDBR system(anoxic/aerobic) and bio-electrochemical treatment system connected in a defined/sequential order to recover biobased products in a cascading way by passing wastewater in a closed loop from biohydrogen production (for dilution) to organic farming. This communication make an holistic attempt to establish a systematic link between waste remediation and biobased products in closed loop approach.

Dr. S. Venkata Mohan
Principal Scientist
Bioengineering and Environmental Sciences
Lab, EEFF Department
CSIR-Indian Institute of Chemical Technology
Hyderabad – 500 007, India
E-mail: vmohan_s@yahoo.com

Dr. S.Venkata Mohan is currently working as Principal Scientist in CSIR-Indian Institute of Chemical Technology, Hyderabad since 1998. His main research interests are in the domain of Environmental Bioengineering and Biofuels specifically in the areas of Advance waste remediation, Aciodogenesis, Microbial electrochemical systems, Waste Biorefinery, and photosynthetic fuels. He has authored more than 300 research articles, 36 chapters for books and has 9 patents. His publications have so far has more than 12,000 citations, and have an h-index of 61 (Google Scholar). He has guided 21 PhDs., 2 M.Phils and more than 90 M.Tech./B.Tech./M.Sc. students. He carried out various industrial and consultancy projects in the area of environment and management. Recently, Dr Mohan constructed and operated successfully a pilot plant for biohydrogen production from waste and waste fed biorefinery platform. Dr Mohan worked as Visiting Professor at Kyoto University (2005) and Alexander von Humboldt (AvH) Fellow at Technical University of Munich, Germany (2001-02). Dr Mohan is recipient of coveted 'Shanti Swarup Bhatnagar (SSB) Prize' for the year 2014 in Engineering Sciences. He also received several awards and honours, such as 'National Bioscience award-2012' by DBT, Government of India, SERB-IGCW 2017 for biohydrogen Technology, 'Prosper.net-Scopus Young Researcher Award in Sustainable Development -2010' under Energy Category by United Nations University and Elsevier, 'NASI-Scopus Young Scientist Award- 2010' in Earth, Oceanographic & Environmental Sciences by NASI and Elsevier, Nawab Zain Yar Jung Bahadur Memorial Prize-1994 by The Institution of Engineers (India), etc. Dr Mohan is a elected fellow of National Academy of Engineering, Biotech Research Society of India, Telangana Akademy of Sciences, International Forum on Industrial Bioprocesses, Institution of Engineers and International Society for Energy, Environment and Sustainability, etc. Dr Mohan is subject Editor for the Journal of Energy, Associate Editor for Frontiers in Environmental Science and Frontiers in Energy Research and is serving on editorial board of several journals viz., Bioresource Technology, Advances in Energy Research, The Open Waste Management, etc.

ENTREPRENEURIAL CREATION OF WEALTH THROUGH THE SUSTAINABLE EXPLOITATION OF BIO-WASTE MATERIALS AND THE BIO-BUSINESS MANAGEMENT

Ibrahim Che Omar
Universiti Malaysia Kelantan,
Locked Bag 36, 16100 Pengkalan Chepa, Kota Bharu,
Kelantan, Malaysia

Abstract

Malaysia produces large volumes of bio-wastes and agro-biomass forms one of the largest waste-products from the agricultural sector. Without suitable management systems, the bio-wastes may cause numerous detrimental effects to the environment and therefore it is mandatory that these bio-wastes must be recycled and reused for the production of high value products complementing the agenda of high income and economic generation. The production of new products, processes and technologies involved the application of chemical and/or biological transformational methods which are friendly to the environment and human health. Our research so far has shown that based on the use of biological approaches and methodologies, various products and processes which have high commercial values can be produced. Some of the products include enzymes, organic acid, bio-pesticides, compost and fertilizers, mushroom and new food, animal feed, flavouring compounds, anti-oxidants, detergents, food additives, bioplastics, biofuel, absorbents, and plant based products. The bio-processes or known as transformation processes include the use of biocatalysts for environmental management, dye degradation, solid waste decomposition, petroleum degradation, enzymatic deinking system, and production of new compounds. The bioprocesses, also on the other hand, produce another set of new products which can be translated to products for commercialization and entrepreneurship.

Prof. Ibrahim Che Omar
Universiti Malaysia Kelantan,
Locked Bag 36, 16100 Pengkalan Chepa,
Kota Bharu, Kelantan, Malaysia
Phone: 609- 771-7090
Fax: 609-771-7112
Email: Ibrahim@umk.edu.my
Web: http://www.umk.edu.my

Professor Dato' Dr. Hj. Ibrahim Che Omar, is currently the Deputy Vice Chancellor (Research and Innovation) Universiti Malaysia Kelantan, a senior professor in Industrial Biotechnology and the Fellow, Science Academy Malaysia (ASM). He holds Bachelor of Science (First Class), Master of Engineering and Doctor of Engineering (DEng) from Hiroshima University, Japan. As a researcher in his specialization of Industrial Biotechnology, he has completed over 30 research projects with 26 research awards, 10 academic awards, 5 patents and over 50 post graduates. He has published over 15 books and 400 research articles in journals and research proceedings. Besides as a recipient of Language Award by Malaysian Linguistic Society-Public Bank for his contribution in scientific writing, is also a fellow of The National Institute on Higher Education Research (IPPTN). As an expert in his area, he is involved in over 100 committees around the country and abroad as examiner, reviewer, evaluator, assessor, invited/keynote speakers, research panels, consultant, and discussant. A founder of the Malaysian Journal of Microbiology (MJM), Advisory Board of MJM and Asian Federation of Biotechnology, and as Editorial Board of 8 international journals. Currently, he is actively involved in translational research and entrepreneurship.

CHALLENGES IN THE DEVELOPMENT OF ENZYMES FOR BIOMASS HYDROLYSIS

Rajeev Kumar Sukumaran
Biofuels and Biorefineries Section,
Microbial Processes and Technology Division,
CSIR-National Institute for Interdisciplinary Science and Technology,
Industrial Estate P.O., Pappanamcode
Thiruvananthapuram 695019

Abstract

The key to biomass conversion to ethanol is its hydrolysis to sugars, mediated by lignocellulose hydrolysing enzymes. Cellulose and hemicellulose hydrolysing enzymes have been identified as the major contributors to the cost of bioethanol and efforts are underway in different laboratories and companies across the world to bring down the cost of these enzymes, despite the fact that there are commercial biomass-hydrolysing enzymes available in the market. Most of the current commercial cellulases are sourced from the filamentous fungus – Trichoderma reesei RUT C30, though the fungus is known to have lesser expression of β-glucosidase (BGL) the rate limiting enzyme in cellulose digestion cascade. Also this enzyme is inhibited by its product glucose, making it difficult to attaining high sugar concentrations and hence high ethanol yield. Most of the commercial blends therefore contain heterogeneous BGL added into them.

The challenges in enzyme development for biomass hydrolysis include the attainment of cost efficiency, higher specific activity, improved yields, storage and thermal stability in addition to be able to achieve high turnovers in minimal time. These challenges are discussed in the context of biomass hydrolysis and the multiple approaches followed to reduce the production cost of cellulases and improving their efficiency are described.

The efforts are CSIR-NIIST – Centre for Biofuels are elaborated and our work on cellulases and beta glucosidases are discussed in detail. Strategies for reducing production cost and developing effective enzyme cocktails are discussed and case studies on cocktail development to improve biomass hydrolytic efficiency are presented.

Dr. Rajeev Kumar Sukumaran
Senior Scientist & Head
Biofuels and Biorefineries Section
Microbial Processes and Technology Division
CSIR-National Institute for Interdisciplinary
Science and Technology,
Industrial Estate P.O., Pappanamcode
Thiruvananthapuram 695019
Phone: +91 471 2515368 (O)
Fax: +91 471 2491712
Email: rajeevs@niist.res.in
Web: http://www.niist.res.in

Dr. Rajeev Sukumaran is currently heading the Biofuels and Biorefineries Section, of the Microbial Processes and Technology Division of CSIR- NIIST. He did his Masters and PhD in Biotechnology from Cochin University of Science and Technology, Kochi, India (1993-2000). He had a short stint in industry where he worked as technical member of Bigtec Pvt Ltd, Bangalore, where he additionally served as consultant to the Vittal Mallya Scientific Research Foundation (United Breweries Group R&D). He then did post doctoral trainings in Molecular Immunology and Stem Cell Biology at the Mount Sinai School of Medicine, New York, USA and National University Hospital, Singapore respectively before joining CSIR in November 2004. Since then, he has been working on enzymes for biomass conversion and lignocellulosic ethanol.

He played a leading role in setting up the CBF's lignocellulosic ethanol pilot plant, and the solid state enzyme production pilot plant at NIIST. His work on cellulases has lead to a technology transfer on the production of this enzyme. He received the SB Chincholkar memorial award for outstanding contributions in the area of Microbial and Enzyme Technology in 2015 from Biotech Research Society India (BRSI). He has a total of 80 publications in International Journals, about 120 conference papers, besides several book chapters and reports.

COMPARATIVE SUSTAINABILITY ASSESSMENT OF BIOREFINERIES: AN INTEGRATED FRAMEWORK

Edgard Gnansounou

Bioenergy and Energy Planning Research Group,
Civil Engineering Institute
School of Archit., Civil and Environ. Engineering,
Ecole Polytechnique Fédérale de Lausanne (EPF)

Abstract

Several researchers undertake works on comparative sustainability assessment of biorefineries and find out that some biorefineries outperform on certain environmental aspects while fail with regard to other criteria. Whereas rigorous numerical evaluations support these conclusions, the meaningfulness and relevance of the assessments are often discussable. This talk points out the need for a stronger foundation of the Comparative Sustainability Assessment of biorefineries. After presenting the typology of biorefineries, the speaker addresses the necessity for comparison based on the same services and within a well-defined context. The talk is illustrated by a methodology proposed by the Bioenergy and Energy Planning Research Group (BPE) of the Swiss Federal Institute of Technology Lausanne (EPFL) that was used to compare selected sugarcane biorefineries. The speaker concludes by proposing few principles aiming at assuring the usefulness of such assessments.

Prof. Edgard Gnansounou
Bioenergy and Energy Planning Research
Group
Civil Engineering Institute
School of Archit., Civil and Environ.
Engineering
Ecole Polytechnique Fédérale de Lausanne
(EPF)
Phone: 0041216930627
Fax: 0041216932863
Email: edgard.gnansounou@epfl.ch
Web: http://bpe.epfl.ch

Dr. Gnansounou is Professor of modelling and planning of Energy Systems at the Swiss Federal Institute of Technology, Lausanne (EPFL) where he is Director of the Bioenergy and Energy Planning Research Group. His current research works comprise techno-economic and environmental assessment of bio-refinery schemes based on conversion of agricultural residues. He has led research projects in that field in several countries including China, Brazil, and South Africa. Edgard Gnansounou is credited with numerous papers in high impact scientific journals. He is member of the editorial board of Bioresource Technology. He graduated with a M.S. in Civil Engineering and Ph.D. in Energy Systems at the Swiss Federal Institute of Technology Lausanne. He was a visiting researcher at the Thayer College, Dartmouth School of Engineering with Professor Charles Wyman (USA), at Polytech of Clermont-Ferrand, University Blaise Pascal (France) and at the Center of Biofuels, the National Institute for Interdisciplinary Science and Technology, with Prof. Ashok Pandey, Trivandrum (India). He was also a visiting Professor of the African University of Science of Technology (Abuja, Nigeria). He is a citizen of Benin (Africa) and Switzerland.

INVESTIGATIONS IN SONICATION–INDUCED INTENSIFICATION OF CRUDE GLYCEROL FERMENTATION TO DIHYDROXYACETONE BY FREE AND IMMOBILIZED GLUCONOBACTER OXYDANS

Vijayanand S. Moholkar
Department of Chemical Engineering and Center for Energy,
Indian Institute of Technology Guwahati,
Guwahati –781 039, Assam, India

Abstract

The present study has dealt with fermentation of crude glycerol by G. oxydans for production of dihydroxyacetone (DHA), and intensification of this process with sonication. Both free and immobilized cells of G. oxydans have been used for fermentation. Application of sonication during fermentation was revealed to boost glycerol consumption rate by 60–84%. The kinetic constant of fermentation increased 1.4×–2.9×. Lesser DHA yield for crude glycerol (as compared to pure glycerol) was attributed to possible formation of sodium glycerate by G. oxydans due to alkali (Na+) impurities in crude glycerol. Slight reduction in DHA yield for initial substrate concentration of 50 g/L was attributed to substrate inhibition effect. Flow cytometric analysis of ultrasound–treated cells at 20% duty cycle did not reveal any morphological change. The circular dichroism analysis of intracellular proteins obtained from ultrasound–treated G. oxydans revealed significant reduction in α–helix and β–sheet content. These conformational changes in protein structure were possibly induced by strong micro–convection generated by sonication, and could lead to augmentation of activity and substrate affinity of the intracellular enzyme glycerol dehydrogenase. This phenomenon is essentially manifested in terms of enhanced kinetics of glycerol fermentation by G. oxydans.

Dr. Vijayanand S. Moholkar
Professor and Head, Center for Energy
Indian Institute of Technology Guwahati
Guwahati – 781 039, Assam, INDIA
Phone: +91 361 258 2258/3126/3150 (landline)
     + 91 9954709058 (mobile)
Fax: +91 361 258 2291
Email: vmoholkar@iitg.ernet.in,
vmoholkar1972@gmail.com

Dr. V. S. Moholkar is a Full Professor of Chemical Engineering and Head of Center for Energy at Indian Institute of Technology (IIT) Guwahati. He received Bachelors (1993) and Masters (1996) degree in chemical engineering from Institute of Chemical Technology (ICT) Mumbai, followed by Ph.D. from University of Twente in 2002. He has been Head of the Chemical Engineering Department at IIT Guwahati between 2012-2015. His main research interests are sonochemistry, cavitation assisted physical, chemical and biological processing, and thermo- and biochemical routes to biofuels. As of June 2017, he has published more than 120 papers in renowned international journals that have received more than 4000 citations (with h-index of 39). He has also filed 2 US patents (in collaboration with CTI Nanotech, CA, USA) on application of hydrodynamic cavitation reactors for biomass pretreatment and bioalcohol synthesis. He has graduated 10 Ph.D. and 24 M.Tech. students. He has been elected as Fellow of Royal Society of Chemistry (FRSC) in July 2016. He was admitted as Senior Member of American Institute of Chemical Engineers (MAIChE (Sr.)) in August 2016. He is a chartered member of Institution of Chemical Engineers, UK, and Chartered Engineer (CEng) registered with Engineering Council of UK.

BOIMASS DERIVED NANO-LIGGNIN COMPLEXES: BEST OUT OF THE WASTE FOR VERSATILE APPLICATIONS

Jayeeta Bhaumik
Center of Innovative and Applied Bioprocessing (CIAB)
Mohli, India

Abstract

Lignin is one of the major components of agricultural waste. Lignin mainly contains polyphenols which can act as reducing, stabilizing and capping agents during the synthesis of noble metal nanoparticles (MNPs) namely silver and gold nanoparticles. Lignin was therefore utilized in the synthesis of silver and gold nanoparticles with optimum size. The metal nanoparticles were characterized by various analytical techniques such as absorption spectroscopy, DLS, SEM and FTIR. These nanoparticles were evaluated for their anti-oxidant potential, therapeutic potential and catalytic efficiency. The therapeutic potential was evaluated after conjugation of various therapeutic dyes on these nanoparticles and the catalytic efficiency was evaluated after enzyme immobilization and degradation of organic pollutants (such as dyes). By this means, lignin waste generated from agricultural biomass as well as from various industries can be transformed into valorized products.

Jayeeta Bhaumik
Scientist D
Center of Innovative and Applied Bioprocessing (CIAB)
(Department of Biotechnology, Government of India)
Knowledge City, Sector 81, Mohali 140306,
Punjab, India

Jayeeta Bhaumik obtained Ph.D. in Organic Chemistry from North Carolina State University, Raleigh, USA in 2007. She carried out NIH postdoctoral fellowship at Harvard Medical School (2007-2011). Dr. Bhaumik returned to India and joined NIPER, Mohali as DST-sponsored Scientist and worked there from 2012 till 2015. She also served as a Visiting Scientist of Harvard Medical School form year 2012 to 2013. Later, she worked as an Assistant Professor of Medicinal Chemistry at NIPER, Kolkata (2016). Currently, she is Scientist D (Senior Scientist) at Center of Innovative and Applied Bioprocessing (DBT-CIAB) and pursuing research in the field of bioorganic chemistry and nanobiotechnology for the valorization of agricultural biomass. She has co-authored more than 25 research articles which are published in various peer-reviewed journals and published two book chapters. Her research publications include, ACS Sustainable Chemistry and Engineering, ACS Biomaterials Science and Engineering, Bioresource Technology, Nano Research, Nature Oncogene, PNAS, Journal Organic Chemistry, Molecular Oncology, Cancer letters and several others.

MICROBIAL LIPID PRODUCTION FROM LOW-COST ORGANIC WASTES

Jong M Park

Pohang University of Science and Technology,
South Korea

Abstract

The use of biodiesel is a promising alternative to circumventing the environmental issues of petroleum-based diesel. Recent advances in microbial lipid production technology using oleaginous microorganisms have attracted significant attention, but its commercialization remains challenging because of the high cost of feedstock or low lipid yield. In general, the lipid yield of oleaginous microorganisms can be increased by using sufficient concentration of organic carbon sources; therefore, using organic wastes can solve the problems at minimal cost because it is a rich source of organic carbon sources. However, the characterisitcs of each microorganism and each substrate should be considered simultaneously for effective bioconversion of low-cost substrates to microbial lipids. The quality of biodiesel is also influenced by their production processes. In this talk, recent achievements in microbial lipid production by various oleaginous microorganisms from low-cost organic wastes will be presented.

Prof. Jong Moon Park
POSTECH, 77 Cheongam-ro, Nam-gu,
Pohang, Gyeongbuk, Korea 37673
Phone: +82-54-279-2275
Fax: +82-54-279-8299
Email: jmpark@postech.ac.kr
Web: http://great.postech.ac.kr

Prof. J M Park is a pioneer in the environmental biotechnology of Korea. He joined Pohang University of Science and Technology (POSTECH) in 1989 and still stays in POSTECH as a professor of multiple departments of Chemical Engineering, Environmental Science and Engineering, and Nuclear Engineering.

However, his main research activity remains in the area of environmental biotechnology and recent research forwards to bioenergy mainly liquid biofuels such as biodiesel. He is trying to transfer technologies developed in the laboratory to the industries. Within short period of time, he is expected to realize the technology transfer successfully.

VALUE ADDITION IN WASTE PLASTIC THROUGH DEPOLYMERIZATION

Deepak Pant
Mechanical Department of Environmental Sciences,
Central University of Himachal Pradesh,
Dharamshala– 176215,
Himachal Pradesh India

Abstract

Recycling of polymer to value added product is one of the fascinating areas of research for the management of plastic waste by chemolysis. Value addition can provide the sustainability towards recycling and protect petroleum resources from depletion. Chemical recycling/ depolymerization fundamentally involve transformation of polymer chain. The polymer backbone is depolymerized into monomer units along with oligomers (randomly raptured larger chain fragments) with related formation of gaseous products. These products were used for the composition of many coating applications. Current research reports the value addition technique of glycolized products of waste PC, PU and PET.

Dr. Deepak Pant
Dean and Head,
Dean and Head, Environmental Science,
Central University of Himchal Pradesh,
Dharamshala, Himachal Pradesh
Phone: 9816639032
Email: dpant2003 @gamil.com

Dr. Deepak Pant currently working as Dean and Head, Environmental Science, Central University of Himchal Pradesh, Dharamshala, Himachal Pradesh is the recipient of Silver Jubilee Research Fellowship award for the year 2003 by Kumaun University, Nainital (India); UCOST Young Scientist Award 2009, INSA Fallow 2010, DST-SERC Visiting Fallow 2010 and DST- SERC Young Scientist Award 2011 for his research activities. He is also the chairman of Innovation club and active member for HP state innovation activities.

Dr Pant has 05 patents in the area of waste management by green techniques and published 10 books, 50 research papers in various national and international journals. He has guided 02 M.Phil, 04 Ph. D. thesis and 48 M. Sc. dissertations. He is in the editorial board of The Journal of Environmental Science and Sustainability (JESS). Dr Pant recently awarded by Visitor award 2017 by president of India for his innovation in the area of waste management.

INTEGRATED THERMOCHEMICAL PROCESSES FOR SUSTAINABLE UTILIZATION OF LIGNOCELLULOSIC BIOMASS

Thallada Bhaskar

CSIR-Indian Institute of Petroleum,

Dehradun-248005,

Uttarakhand, India

Abstract

The increasing concerns over the depletion of fossil resources and its associated geo-political issues have driven the entire world to move towards sustainable and alternative forms of energy and resources. Researchers all over the world are trying to develop processes to utilize waste and renewable resources as they do not cause the climate change issues for the production of energy. Solar, wind, tidal, geothermal energy etc. can be used for the production of power/ electricity but the organic carbon required for the production of liquid hydrocarbons cannot be obtained from the above. Biomass or biobased products and plastics are the major components of municipal solid waste, which is a good source for the carbon for production high value hydrocarbons including transportation fuels and petrochemical feedstock. Biomass is the only renewable and sustainable source of organic carbon which can be obtained from any living or recently living biological material. Thermo-chemical methods of conversion have some advantages and are complementary with bio-chemical routes, as the thermochemical methods requires shorter processing times, flexibility in feed handling, complete utilization of feedstock, wide range of product slate etc. Under the umbrella of thermo-chemical methods, several processes can be utilized depending on the feedstock availability/ characteristics and end product requirement. The integration processes within thermochemical platform can provide the energy and high value chemicals in a sustainable way.

Dr. Thallada Bhaskar
Principal Scientist
Thermocatalytic Processes Area
Bio-Fuels Division
CSIR-Indian Institute of Petroleum
Mohkampur, Dehradun-248005,
Uttarakhand, India
Phone: 0135-2525 820/824
Email: tbhaskar@iip.res.in
Web: http://thalladabhaskar.weebly.com

Dr. Thallada Bhaskar received Ph.D. for his work at CSIR-Indian Institute of Chemical Technology (IICT), Hyderabad. He carried out Postdoctoral Research at Okayama University, Okayama, Japan after which he joined as Faculty at the level of research assistant professor for ~7 years and worked as a visiting scientist at Tokyo Institute of Technology (TIT), Tokyo, Japan; SINTEF Materials & Chemistry, Oslo; Dalian Institute of chemical physics (DICP), China. He has over 130 publications in SCI journals of international repute, an h-index of 33 and around 3800 citations. He has contributed 22 book chapters to renowned publishers (Elsevier, ACS, John Wiley, Woodhead Publishing, CRC Press, Asiatech, etc.) and 13 patents in his field of expertise in addition to 250 national and international symposia presentations. His 24 years of research experience cover various fields of science revolving around his expertise in heterogeneous catalysis, thermo-chemical conversion of biomass (lignocellulosic and aquatic biomass including macro and micro algae) waste plastics and e-waste (WEEE) plastics into value-added hydrocarbons.

THERMOCHEMICAL SPLITTING OF WATER TO PRODUCE HYDROGEN

Bharat Bhargava
ONGC Energy Centre,
Core 3&4, 8th Floor, Laxmi Nagar,
Delhi 110092

Abstract

Hydrogen is a clean energy carrier. It is abundant on earth, but in combined form in several compounds, the most common being water. There are several methods to produce Hydrogen, mainly from hydrocarbons; which may not be a sustainable source in future. Therefore, considering the emerging demand for hydrogen as a fuel, it is imperative to research methods to generate hydrogen from water in an efficient manner.

ONGC Energy Centre (OEC) has been working on development of thermochemical processes for generation of Hydrogen by splitting of water utilizing high temperatures, which may be obtained from solar or nuclear sources as heat. From among various possible options, development of closed-loop Copper-Chlorine (Cu-Cl) and closed / open-loop Iodine - Sulfur (I-S) cycles have been taken up under this programme. OEC has now successfully completed indigenous development of a new patented thermochemical process for splitting of water into Hydrogen and Oxygen. Several equipment and materials required for Cu-Cl and I-S cycles have also been indigenously designed and developed.

This paper presents an outline of the R&D work by ONGC Energy Centre and highlight the key progress achieved in this research initiative. This work has been carried out by ONGC Energy Centre in association with some of the leading research and academic institutions.

Dr. Bharat Bhargava
Director General
ONGC Energy Centre
Core 3&4, 8th Floor, Laxmi Nagar, Delhi 110092
Phone: 011220406040
Fax: 01122011783
Email: bhargavabh@ongc.co.in
Web: http://ongcindi.com/ongcenergycentre

Dr. Bharat Bhargava is Director General, ONGC Energy Centre since January, 2013, working on various clean energy options including hydrogen energy, solar energy, geothermal energy, biotechnology and uranium exploration and recovery by In Situ Leaching etc.

Dr. Bhargava has worked at the National Physical Laboratory, New Delhi for his Ph.D. in Physics (thin films). He holds several patents and published a number of papers in international and national journals. He has been recognized by several international and national institutions for his contributions in clean energy technologies.

In 1976 he joined Central Electronics Limited (CEL), and developed large area solar cell and module technology in the country. He was also involved in development of a number of solar applications in the country, most notable being solar lantern. Thereafter, he was in the Ministry of New and Renewable Energy, Government of India from 1989 to 2011, mainly working on Solar Energy and Hydrogen Energy. Dr. B. Bhargava is one of the main architects of the Jawaharlal Nehru National Solar Mission, launched in 2010, which has given the Indian solar programme much needed thrust. Dr. B. Bhargava has over 45 years' experience in policy, planning, management, research, product development, quality assurance and production in energy sector, working in a research laboratory, industry and the Government.

HYDROGEN "THE" FUEL FOR INTERNAL COMBUSTION ENGINES.

Roger Sierens
Laboratory of Transport Technology,
Ghent University, Belgium

Abstract

Hydrogen as a fuel in internal combustion engines (ICE's) is still a solution for the near future to realize zero CO_2 emissions for traffic applications in spite of the competition with electrical vehicles and fuel cells. And the hydrogen fueled IC engine is ready for that competition. IC engines will not disappear in the next decades. The advantages and disadvantages are given briefly. Load control strategies for high power output and high efficiencies are discussed. Recently the interest is mainly on direct injection hydrogen IC engines. But the storage and production of hydrogen and to build the necessary infrastructure, are the real shortcomings in the general use of hydrogen in IC engines.

Prof. Roger Sierens
Laboratory of Transport Technology
Ghent University, Belgium

Roger Sierns in Professor at the University of Ghent, Belgium and Previous Chairman of the Department of Flow, Heat and Combustion Mechanics and director of the Laboratory of Transport Technology.

He obtained several awards: Dugald Clerk Prize (Institution of Mechanical Engineers, England), Erskine Fellowship (New Zealand), I. Akerman Prize (Atlas Copco), Professor Onorific (Romaina), Outstanding Scientific Achievement award by the Int. Association of Hydrogen Energy, Dr. H.C University of Havana (CUJAE) and published nearly 200 international papers on IC Engines.

SYNERGETIC APPLICATION OF HYDROGEN IN INTERNAL COMBUSTION ENGINES

Atul Dhar
School of Engineering,
IIT Mandi, Himachal Pradesh , India

Abstract

The world is facing twin crises of energy scarcity and environmental degradation. Plummeting fossil fuel reserves is influencing the global economics and setting the fractal hierarchy amongst the countries. Even though divided as developed and undeveloped, still, the countries are aligned on the issue of curbing the pollution arising due to use of fossil fuels. The harm caused by the pollution is not limited just to the local ecosphere. The global impact is felt in the form of climate change and global warming. Internal combustion (IC) engines are considered as forefront cause of pollution in cities and have become a victim of their success. However, the versatility offered by these engines allow them to dominate as power plants in both transportation and power sectors. So it is essential to hasten the quest for renewable sources of fuel with clean-burning properties. Hydrogen offers potential solution to these problems by its clean-burning properties and renewable production routes. Researchers have explored various methods for application of hydrogen in IC engines. The use of hydrogen as a fuel for both spark ignition engines and compression ignition engines have become established technologies. Moreover, hydrogen use as fuel for advanced combustion technologies like homogenous charge compression ignition, low temperature combustion and dual fuel have significantly been researched upon in last decade. Most of these techniques show promising results in emission reduction. Further, Hydrogen use in selective catalytic reduction of NOx show a glimmer towards its use in reduction of the only polluting emission arising out of hydrogen combustion. This work attempts to present the level of technological development attained in hydrogen-fuelled IC engines and their possibility in bridging the gap between all-electric transport future (till large scale storage infrastructure becomes feasible).

Dr. Atul Dhar
Assistant Professor,
School of Engineering, IIT Mandi
Himachal Pradesh , India
Phone: +91-1905267143
Fax: +91-1905267143
Email: add@iitmandi.ac.in
Web: http:// se.iitmandi.ac.in/facprofile.php?user=add

Dr. Atul Dhar is Assistant Professor at Indian Institute of Technology Mandi since 2013. He received his M.Tech. and PhD degrees from Department of Mechanical Engineering, Indian Institute of Technology Kanpur in 2006 and 2013 respectively. Atul Dhar graduated in mechanical engineering from Harcourt Butler Technological Institute, Kanpur in 2004. He was awarded the Erasmus Mundus fellowship of European Union for pursuing postdoctoral research at Ecole Centrale de Nantes, France in 2013. He is the recipient of young scientist award from International Society for Energy, Environment and Sustainability in 2015. He also worked at Mahindra & Mahindra, Automotive Sector in 2006 for getting exposure of industrial working environment. His areas of interests include reciprocating internal combustion engines, emission control technologies, alternative fuels and lubricating oil tribology. Till now he has published more than thirty international peer-reviewed journal papers.

THE INFLUENCE OF ENVIRONMENTAL POLLUTION ON PERFORMANCE OF PHOTOVOLTAIC SOLAR CELL UNDER URBAN CONDITION: A CASE STUDY OF CITY OF BANGALORE

Kamanio Chattopadhyay
Department of Materials Engineering,
Indian Institute of Science, Bengaluru

Dr. Kamanio Chattopadhyay
Honorary Professor
DEPARTMENT OF MATERIALS ENGINEERING
Indian Institute of Science, Bengaluru
Karnataka – 560012
Phone: 91 80 22932262 (office), 91 80 22932678 (lab)
Fax: 91 80 23600472, 91 80 23061991
Email: kamanio@materials.iisc.ernet.in
Web: http://materials.iisc.ac.in/~kamanio/

Prof. Kamanio Chattopadhyay received his Bachelors of Engineering Degree in Metallurgical Engineering from Burdwan University in 1971 and M.Sc.(Eng.) and Ph.D. from Banaras Hindu University in 1973 and 1978 respectively. Appointed faculty member (Lecturer) at Banaras Hindu University in 1975, he later joined Indian Institute of Science in 1983 as an Assistant Professor. He is currently an Honorary Professor at the Materials Engineering Department. Recipient of the prestigious Shanti Swaroop Bhatnagar Award in 1995, he is also a recipient of The Medal of the Materials Research Society of India, the Birla Gold Medal of the Indian Institute of Metals, the National Metallurgist Award of Government of India for life time contribution to the metallurgical profession and the Life Time Achievement Award of the Electron Microscope Society of India. He is a fellow of Indian National Science Academy (INSA), Indian Academy of Science (IASc) and Indian National Academy of Engineering (INAE). He is also a life fellow and the Vice President of the Indian Institute of Metals. He served as the Chair of the International Committee on the Rapidly Quenched and Metastable Materials and the Chairman of the International Committee on Nanostructured Materials. He was a member of the International Committee on Quasicrystal, International Affair Committee of the Materials Research Society, Boston and member of the award committee of the American Society for Mining and Metallurgy. The research work of Professor Chattopadhyay primarily aims at synthesizing newer materials through non-equilibrium processing and understanding their structure and stability at different length scales. The processing techniques utilized by him include techniques of rapid solidification and undercooling of the melt, mechanical alloying of solids, laser ablation and laser/electron beam processing. His current research thrust revolves around developing new high temperature materials.

SUPERCRITICAL CARBON DIOXIDE BRAYTON CYCLE FOR POWER GENERATION: MAJOR R & D EFFORTS AND DIRECTIONS

Pradip Dutta
Department of Mechanical Engineering,
Indian Institute of Science, Bangalore-560012

Abstract

In this presentation, the potential of supercritical CO_2 Brayton cycle to replace steam in conventional thermal power plants, solar thermal as well as nuclear plants, is examined. The major advantages of S-CO_2 Brayton cycle over steam Rankine cycle is noted, followed by assessments of international and national status of the technology. In the case of concentrating solar power (CSP), the demand for distributed and scalable solar thermal power plants necessitates the use of novel power cycles such as S-CO_2 Brayton, which are efficient and cost effective at low to medium scales. However, development of components and systems for such high pressure and high temprature power cycles, such as turbomachinery, solar receivers, recuperators and storage systems involve significant materials as well as heat transfer challenges which are highlighted in this presentation. Major indigenous R&D efforts towards development of technologies related to S-CO_2 power plants are discussed.

Prof. Pradip Dutta
Professor and Chairman
Department of Mechanical Engineering
Indian Institute of Science
Bangalore 560012
Phone: (080)22932512
Fax: (080)23604536
Email: pradip@iisc.ac.in
Web: http://www.mecheng.iisc.ernet.in/~pradip/

Prof. Dutta received his bachelor's degree in Mechanical Engineering from IIT Kharagpur, his master's degree from IIT Madras and Ph.D. from Columbia University. He held faculty positions at Columbia University and at the Tennessee Tech. University, before joining the Indian Institute of Science as a faculty member in 1996.

Prof. Dutta's research group focuses on development of advanced energy technologies related to solar energy, cooling of electronics, spacecraft thermal management, and on thermal technologies related to phase change.

Prof. Dutta has been elected Fellow of the ASME, and Fellow of all the four National Academies of India in science and engineering. Among several other awards, Prof. Dutta has received the VASVIK Award for Industrial Research, IISc Alumni Award for Excellence in Engineering Research, INAE Chair Professorship Award, INAE Outstanding Teacher Award, IIT Kharagpur Distinguished Alumnus Award, IIT Madras Distinguished Alumnus Award, and the J. C. Bose National Fellowship. He is serving as Associate Editors of IEEE Transactions on Components and Packaging Technology, and ASME Journal of Electronic Packaging. At IISc, he has been a co-founder of the National Facility for Semisolid Forming, co-Director of the General-Motors-IISc Collaborative Research Lab, and convenor of the Institute's solar energy initiative. Currently, Prof. Dutta is the Chairman of the Department of Mechanical Engineering at IISc, and co-leader of the India-US Consortium called Solar Energy Research Institute for India and the United States (SERIIUS).

BIOLOGICAL NUTRIENT REMOVAL FROM WASTEWATER ALONG WITH EXOPOLYMERIC SUBSTANCE PRODUCTION BY A DENITRIFIER PARACOCCUS DENITRIFICANS ISTOD110

Kristina Medhi, Indu Shekhar Thakur
School of Environmental Sciences,
Jawaharlal Nehru University,
New Delhi-110067, India

Abstract

Eutrophication is a natural ageing process occurring in water bodies through introduction of plant nutrients like phosphorus and nitrogen, causing algal blooms, detrimental to aquatic life as well as decrease of water quality. Microorganisms play a vital role in biological based treatment and converting organic materials into some by-products such as extracellular polymeric substances (EPS). This study focuses on both N & P removal achieved by an aerobic denitrifier Paracoccus. denitrificans ISTOD1 showing that it could remove 60.5% NO3-N and 93% ortho-P within 72 h, suggesting the strain as a potential denitrifying phosphorus accumulating organism (DPAO). Moreover, EPS production capability by strain ISTOD1 was also observed between late exponential- stationary phase, which was extracted by methanol at 120 h. Assessment on real wastewater was also studied where domestic wastewater was combined with 5% molasses to observe the role of ISTOD1 in ammonia and total phosphorus removal along with EPS production.

Dr. Indu Shekhar Thakur FNASc, FNAAS, FIBA, FBRS, FNESA
Professor and Former Dean
School of Environmental, Sciences, Jawaharlal Nehru
University, New Delhi, India
Phone: 01126742370®, 9868558865(M)
Email: indushekhart@gmail.com: isthakur@jnu.ac.in;
isthakur@hotmail.com

Professor Thakur is working on bioremediation, biovalorization and detoxification of natural and organic compounds. Developed bacterial consortium by genetic breeding, characterized catabolic genes and proteins, proteomics, genomics analysis for carbon dioxide sequestration for production of biomass, enzymes, biodiesel, bioflocculant, bioplastic, biomaterials. Bacteria consisting carboxylating enzymes including RuBisCO and municipal sludge, scaled to 200 litre bioreactors for cost effective biodiesel production, energy efficiency, sensitivity,emission and engine testing. Bacteria applied for degradation of pentachlorophenol in tannery, lignin in pulp and paper mill, melanoidin in distillery, dioxin-like compounds, ecoestrogens and emerging contaminants in municipal solid sludge, landfill leachates, pesticides in agriculture field and recovery of nitrogen and phosphorus in waste water. Persistence of phthalates, risk assessment and characterization carried out. Recovery of chromium III for tanning and leather preparation with protease and lipase enzymes and chromium VI from electroplating effluent by fungi and bacteria and detoxification by human cell lines performed. Lignocellulose valorization by bacteria and fungi for colour removal, biopulp, bioethanol, biobleaching and chemicals, and used Leucaena leucocephala seeds and wood for lipase production and biorefinery processes. Lipase immobilized on charcoal for enhanced production of biodiesels from bacteria, Leptolyngbya sp. and Scenedesmus sp. Metaproteogenome characterized for carbon dioxide utilization and biomaterials.

A STORY REVEALED BY AMBIENT PM₁: ENHANCEMENT OF WINTERTIME POLLUTION IN IGP DUE TO HIGH MOISTURE CONTENT

Tarun Gupta

Department of Civil Engineering,
Indian Institute of Technology, Kanpur

Abstract

A study was carried out at Kanpur situated within Indo-Gangetic Plain (IGP) to understand secondary aerosol formation and their fog-processing via measurement of PM1-bound species (PM1: particulate matter of aerodynamic diameter $\leq$ 1.0 µm) during wintertime. PM1 mass concentration during non-foggy episodes varied from 24–393 µg m−3, whereas during foggy condition it ranged from 42–243 µg m−3. Foggy conditions were associated with higher contribution of organic matter (OM, by 23%). However, lower fractional contribution of sulphate, nitrate and ammonium during foggy conditions is attributable to wet-scavenging owing to their high affinity to water. Significant influence of fog-processing on organic aerosols composition is also reflected by co-enhancement in OC/EC and WSOC/OC ratio during foggy condition. Source apportionment carried out via Positive matrix factorization (PMF) resolved seven sources: biomass burning (19.4%), coal combustion (1.1%), vehicular emission (3%), industrial activities (6.1%), leather tanneries (4%), secondary transformations (46.2%) and mineral dust (20.2%).

Dr. Tarun Gupta
Professor
Department of Civil Engineering
Indian Institute of Technology, Kanpur
Phone: 05122597128
Fax: 05122597395
Email: tarun@iitk.ac.in; tarunelectric@gmail.com
Web: http://www.researchgate.net/profile/Tarun_Gupta5

Dr. Tarun Gupta Tarun Gupta is doctorate from Harvard University & MTech from IIT Bombay. He has authored >100 publications, 6 book chapters, 4 patents, 4 design, 1 technology transfer to industry & reviewer of >35 ISI indexed journals. He has graduated 6 PhD and 32 M.Tech. students. A submicron aerosol sampler designed, developed and evaluated by him at IIT Kanpur has been commercialized by Envirotech (Delhi). He has developed several low flow rate as well as high flow rate impaction based samplers and a non-selective membrane based diffusion denuder. He is currently P K Kelkar research fellow and selected member of INYAS and INAE Associate. He won INSA Medal for Young Scientist & INAE & IEI Young Engineer Award and NASI-SCOPUS Award.

Novel Photo-Catalytic Solution through Nano-Technology for Industrial Water Remediation

Shantanu Bhattacharya
Department of Mechanical Engineering,
IIT Kanpur

Abstract

Indian Institute of Technology Kanpur, Uttar Pradesh-208016Nano-structured materials exhibit distinct properties by virtue of nano scale morphological variations which lead to novel and interesting applications. In this work, several nano-fabrication strategies have been explored to realize highly porous as well as high aspect ratio structures. These nano-structures have been utilized for applications like visible/ UV light based catalysis causing dye remediation in industrial water samples and other antimicrobial and bio sensing properties. In this talk I will be providing a glimpse of some of these applications and some discussions of how to realize these nano-structures in an easy and inexpensive manner using wet chemistry.

Prof. Shantanu Bhattacharya
Department of Mechanical Engineering
Indian Institute of Technology Kanpur
Uttar Pradesh-208016
Phone: 0512-259-6056
Fax: 0512-259-7408
Email: bhattacs@iitk.ac.in
Web: http://home.iitk.ac.in/~bhattacs/

Dr. Shantanu Bhattacharya is a faculty of Mechanical Engineering at IIT Kanpur since July 2007. He received his MS from Texas Tech in 2003 and earned his doctorate from University of Missouri, Columbia in 2006. Before moving to India, he spent about a year at Birck Nanotechnology Center, Purdue University, West Lafayette, Indiana as a Post-doctoral Research Associate. Dr. Bhattacharya has developed strong thrusts at IIT Kanpur spanning from nucleic acid analysis, surface-electrophoresis, micromixers for microfluidics, cell trap devices, photo-catalytic solutions for water remediation etc. He has 5 US and 6 Indian patents and has authored more than 65 International Journal papers, a number of review articles and has written three books on miniaturized nucliec acid analysis, water remediation and Medical, chemical and environmental sensors.

He serves on Editorial Board of the Journal of Green Nanotechnology and is also an associate editor of the journal Nanotechnology and Nanoscience. Dr. Bhattacharya received Young Engineers Award from the Institution of Engineers (India) in 2009, the ISSS young scientist award in 2013, the NDRF best mechanical engineering design award of 2014, Boeing outstanding Leadership award of 2011 etc. He is also a fellow of the Institution of Engineers (India).

Contributed Papers

SEEC-2018-002

Environmental Protection and Sustainability:

A Case Study of the Sompeta Thermal Power Plant

Varigonda Kesava Chandra
Ph.D. Candidate
South Asian Studies Programme,
National University of Singapore
Email: kesavachandra@gmail.com

EXTENDED ABSTRACT

What constitutes 'environmental protection and sustainability' in the context of energy security? Who are the stakeholders in ensuring environmental protection and sustainability with regards to coal-fired thermal plants in India? These are the questions this paper hopes to address.

Through an in-depth case study of the proposed coal-fired thermal power plant in Sompeta, and the resultant widespread opposition movement, the paper hopes to answer the central questions.

The primary stakeholders charged by the Indian Constitution with ensuring sustainable development of coal-fired plants in India are: the central government (represented by the Ministry of Environment and Forests),

the State government and its State pollution board; the private firm in charge of plant construction and operation; the independent judiciary, particularly the National Green Tribunal, tasked with adjudicating cases related to environmental protection.

The three constituents of sustainable development are environmental, social, and economic. It is discerned by minimal adverse impact on the surrounding environment; salutary impact on the lives, health and livelihoods of the surrounding populace. The thermal plant at Sompeta is detrimental to the three facets of sustainable development.

However, the proposal for the plant as put forth by the private firm was deemed suitable by the State and central government functionaries.

An additional stakeholder is the civil society. While only given marginal powers constitutionally, in the case of the Sompeta thermal power plant, the civil society, along with the judiciary, has played a crucial role in preventing the inception of the plant, and thereby ensuring sustainable development is not compromised.

Keywords: Coal-fired thermal power plant; Sustainable development; Civil society

Coal-fired thermal plants and sustainable development

The International Energy Agency (IEA), of which India is a member, defines energy security as, "the uninterrupted availability of energy sources at an affordable price" (International Energy Agency). This includes electricity, an important secondary energy source, whose supply security is deemed imperative for a country's economic development.

Energy security in India, particularly with regards to electricity supply has, since independence, been inordinately dependent on coal-based thermal power. In spite of the steep increase in renewable energy-based generation, the installed capacity of coal-based thermal power plants, as of 2017, stands at nearly 60 percent of the total installed capacity for power generation (Ministry of Power, 2017). Thermal plants (coal and gas inclusive)

contribute to over 75 percent of electricity generated (Central Electricity Authority, 2017).

Sustainable development is defined by the Brundtland Commission in 1987 as, "development that meets the needs of the present without compromising the ability of future generations to meet their own needs" (UN Documents, 1987). Along with societal and economic sustainability, environmental sustainability is deemed a key aspect of sustainable development.

The Exergy framework and the energy security and sustainable development (ESSD) framework link energy, environment and sustainable development. The ESSD framework puts forth three aspects of sustainable development: social, economic and environmental; it further lists four aspects of environmental sustainability, as related to energy security: climate change, air pollution, water pollution and land pollution (Indriyanto et al., 2010).

Energy generation, especially from coal-fired power plants, is inherently detrimental to environmental sustainability. Greenhouse gases (GHG) including carbon dioxide released by coal-fired plants contribute as much as 60 percent of the GHGs in the atmosphere; they are the primary cause of climate change. The Kyoto Protocol 1997, of which India is signatory, advocates reduction of

fossil fuel combustion as an urgent means of climate change mitigation.

In addition, discharges of fly ash and other particulate matter into the air, discharges of water and pollutants into water bodies and the sea, cause more immediate damage to the environment. This has a direct and adverse bearing on the health, lives and livelihoods of the surrounding populace – particularly those that rely on water bodies for farming and fishing, and daily consumption.

Therefore, while it is argued that power generated from thermal plants drive the country's economy, it is detrimental to the socio-economic sustainability of the populace in the vicinity of the plant.

Sustainable development and Sompeta Thermal Plant

In late 2000s, the Nagarjuna Construction Company (NCC), a private firm, sought permission to construct a thermal power plant in the coastal villages in Sompeta, a town in the Srikakulam district of Andhra Pradesh. The location seemed ideal for a coal-fired thermal power plant: the Beela, a freshwater lake that was just beside the earmarked land would provide a constant water source for plant operations. The sea, which was also just over a kilometre from the plant, would be ideal for the dispelling of affluent.

In February 2009, the Andhra Pradesh State government gave the government order confirming the sales of state and private lands in the region for the construction of the thermal plant, after a 'no objection' certificate was granted by the local bureaucracy. In December 2009, India's Ministry of Environment and Forests (MoEF) issued an Environmental Clearance (EC) after the conductance of the Environmental Impact Assessment (EIA), and after the Andhra Pradesh State Pollution Board's conductance of a public hearing.

In response, the populace around the Beela lake: rural and urban; fishermen and farmers came together in protest against the thermal plant. The larger surrounding region constituted over a hundred thousand residents. Their contended that the coal-fired thermal plant would be catastrophic to the environment: it would dilute the lake and pollute the sea. By extension, it would equally be catastrophic to the livelihoods of farmers, who were intimately dependent on the Beela for watering their crops, and to those of fishermen, who depended upon fishing in the open sea. In addition, the fragile ecology that the Beela lake had nurtured would be devastated.

Led by the Paryavarana Parirakshana Samiti (PPS), an umbrella organisation formed by environmental activists in the Sompeta town, and affiliated with the farming and fishing communities in the region, the populace of that

region began a relay hunger strike in protest against the thermal plant, in 2009. Over 10,000 people, from over 11 surrounding villages, were involved. In July 2010, State government sent in the police to quell the protests, resulting in violent altercations and police firing, in which four villagers were killed.

In 2010, the PPS, along with various affected villagers and environmental activist groups, filed a case against the State government (along with the NCC and MoEF) in the Andhra Pradesh High Court. In the immediate aftermath of the violence of July 2010, the High Court gave a stay order to the construction of the thermal plant. In 2012, the NGT overruled an appeal by NCC, precluding the construction of a thermal power plant in the region. By September 2015, the Andhra Pradesh State government, then led by the Telugu Desam Party (TDP), added a caveat to its land transfer order, stating that the NCC could only carry out agricultural development in the allotted land.

Conclusion

Who are the stakeholders in determining, and ensuring, the environmental and socio-economic sustainability of coal-fired thermal power plants? This paper tackles this question through an in-depth case study of the Sompeta thermal power plant. It first at the hierarchy of stakeholders: the central government, State government, and the private owner of the plant. It then looks at how the civil society is

a key, if overlooked, actor, as well as the important role played by the judiciary.

Finally, the paper concludes with a look at present and future trends of coal-fired power plants, especially in light of the rapid growth of renewable energy as a more environmentally sustainable option.

References

[1] International Energy Agency, "Energy Security," https://www.iea.org/topics/energysecurity/.

[2] UN Documents, *Report of the World Commission on Environment and Development: Our Common Future*, 1987, http://www.un-documents.net/our-common-future.pdf.

[3] Ministry of Power, Government of India, "Power sector at a glance: All India," 2017, http://powermin.nic.in/en/content/power-sector-glance-all-india.

[4] Central Electricity Authority, "Energy generation, programme, and plant load factor," 2017, http://cea.nic.in/reports/monthly/generation/2017/June/actual/opm_01.pdf.

[5] Aclepias Indriyanto, Dwi Ari Fauzi and Alfa Firdaus, "The sustainable development dimention of energy security," in Benjamin Sovacool, ed., *The Routledge Handbook of Energy Security*, Oxford: Routledge, 2010: 96-113.

PERFORMANCE ANALYSIS OF TRIPLE EFFECT SOLAR STILL WITH EVACUATED TUBES

Hitesh Panchal
Mechanical Engineering Department
Government Engineering College Patan
Email: engineerhitesh2000@gmail.com

Kamlesh Pansal
Mechanical Engineering Department
Government Engineering College Patan
Email : kamlesh_er@yahoo.co.in

Hitesh Bhargav
Mechanical Engineering Department
BVM Engineering College, VV Nagar
Email : bhargav_hitesh@yahoo.com

Anuradha Awasthi
PhD Scholar
CSIR- NEERI, Nagpur
Email : anu17awasthi@gmail.com

ABSTRACT

Drinkable water is one of the most essential requirements for humanity, and the rise in human population growth has to lead to water pollution to the river and underground water reservoirs. To overcome the demand concerning about potable water, many researchers from all around the world have tried various new technologies. Solar distillation is the simple and cost-effective technology for changing of contaminated water to potable water. In this present research work, efforts are applied to make solar still with enhanced distillate output with the help of attachment of Evacuated tubes. Hence, triple effect solar still has been fabricated and tested to see its performance. Experiments on the present solar still have been carried out for three days in climate conditions of Patan, Gujarat. From the research work, it has been evaluated that, the increment of distillate water production and energy payback time found 700% and 72 days only. It has also found that the present solar still is capable of producing 20 litres of distillate production of water from saline or brackish water. Hence, it is the best solar still for potable water requirement.

Keywords: Triple effect solar still, Evacuated tubes, output.

1. INTRODUCTION

Solar still is a single basin solar still this is a famous device which is used in solar distillation and desalination for the conversion of available blackish water or wastewater into potable water [1]. Panchal et al. [2] found improvement in efficiency and productivity many materials were used like- coupling with reflectors has been used. Parameters can play the vital role in location, solar radiation intensity, and wind velocity, water depth in the basin, solar angle, wind, inclination and most significant heat capacity of still. Whereas active solar still requires the different type of mechanical support for maximum output by making the essential improvement to get the better rate of heat transfer we can obtain enhancement in the distilled production. Abdel-Rahim and Lasheen [3] proved that coupling of solar still with parabolic through collector focal pipe heat collector increases the production of solar still 18%. Rai and Tiwari [4] have worked on the solar still integrated with flat plate and concentrating collector to improve the efficiency around 24% compared with conventional solar still. Tiris et al. [5] proved that coupling of flat plate collector with single basin increases the efficiency 51% compare with single basin. The effect of coupling a flat-plate collector on the solar still productivity in desalination, work was investigated by Barden et al. [6-11]. They found enhancement of around 29% compared with conventional solar still. Velmurgan and Srithar [12-13] integrated solar pond with conventional solar still to enhance water temperature inside basin. They found 26.6% increment of distillate output compared with conventional solar still. They have also carried out theoretical analysis and compared with experimental study and found impressive similarity in results. Dimri et al. [14] evaluated that, the integration of flat plate collector with higher thermal conductivity materials improve the distilled output compare with the single slope solar still. To reduce inner glass cover temperature was determined by Kumar and Bai [15] gained that 30% improvement in distillate output

compared with conventional solar still. Integration of black wire helical springs have used by Khaled and Eldalil, [16] and found 32% increment.

Panchal et al. [17] proved that coupling of flat plate collector with single basin increases the 29%. Single sloped solar still using Lauric acid (PCM) increases the output 36% .

From the literature review, it has been found that the distillate output improvement is required in solar still. Many researchers have introduced various devices like flat plat collector, Evacuated tubes, parabolic trough collector etc. But the design of solar still requires attention along with the use of above tools with it. Hence, the primary aim of the present research work is to fabricate triple effect solar still with Evacuated tubes and tested in climate conditions of Patan to see its performance and increase distillate output.

2. EXPERIMENTAL SET UP

Fig.1 Experimental set up of triple effect solar still

During starting of research work on solar still, water is filled in the storage tank after that basin is filled up to 3 cm of height on night time through the inlet pipe which is directly connected to the upper basin. The glass, which covers the top basin, is cleaned daily in the morning for removal of extra dust and particles which is deposited on the upper surface of glass before stating the setup. The experiment setup was set in the November and March month from 10 to 24 November 2015 and 10 to 30 March in 2016. The reading was recorded and taken from morning 9 am to evening 6 pm. The important variables in present research work like basins water temperature (Tw), the upper surface temperature of glass (To), evacuated tube outside temperature(Teo), ambient temperature (Ta) and solar radiation on the still (Ig) and output.

3. RESULT AND DISCUSSION

An experimental setup was set in the month of November 10/11/2015 to 24/11/2015 and in March 20/03/2016 to 30/03/2016. The observation was monitored and analyzed on daily basis Daily Total by 15 days regular monitoring in November show that the maximum distilled output was recorded 15, 16 and 17 November, 2015. The main reason for choosing of three days is that; the average global solar radiations are found nearly same during above said three days. 10 days routine monitoring in March shows that the maximum distilled output was recorded in 23, 24 and 25 March. Therefore, for further study, these three days in November consider for detail study.

3.1 Effect of Ambient temperature and solar intensity with time on triple basin solar still.
Solar still distilled output is directly depending upon the weather condition of that place and time. The ambient temperature and solar intensity play a key role in the distillation process. Figure 2
The basin temperature was recorded maximum at 12 pm to 3 pm. The solar radiation gradually increases from early morning to 1 pm due to brilliant sun and then cut back towards evening due to low sunshine. It gets to maximum value of 900 W/m2 on 17/11/2015 at 1:00 pm. But the variation in ambient temperature was found as its minimum 17°C at early 9 am morning in 17/11/2015 and gained the maximum of 25 °C at 2pm on 16/11/2015 and 26 °C on 17/11/2015, but on 15/11/2015 the ambient temperature was maximum at 1:00 pm found 27 °C.
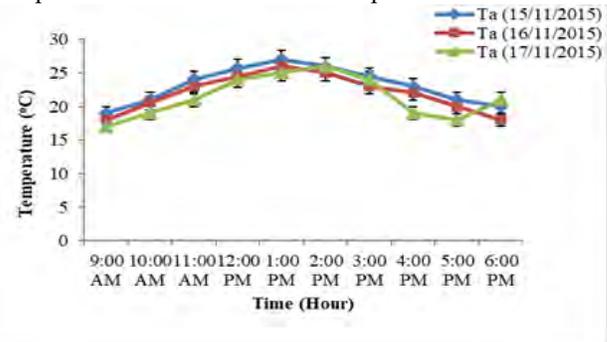
Fig.2 Variation of ambient temperature with time

3.2 Enhancement in the of distilled output coupling with evacuated tubes.
The distillate water increases from 2 pm to 5 pm. It reaches a maximum value of distillate water 1670 mL during 5 pm on 15/11/2015 and the minimum amount of 843 mL during 3 pm on 17/11/2015. The maximum value of water was found on 16/11/2015, and the minimum value of water was found on 17/11/2015

3.2 Enhancement in the of distilled output coupling with evacuated tubes.
The distillate water increases from 2 pm to 5 pm. It reaches a maximum value of distillate water 1670 mL during 5 pm on 15/11/2015 and the minimum amount of 843 mL during 3 pm on 17/11/2015. The maximum value of water was found on 16/11/2015, and the minimum value of water was found on 17/11/2015.
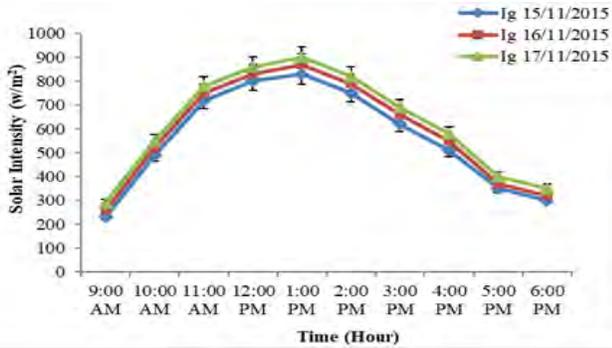
Fig.3 Variation of solar radiation with **time**
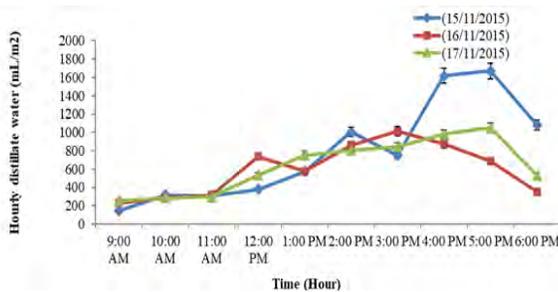
Fig. 4. Hourly variation of distilled output with time

3.3 Total (Day & Night) Distilled water output
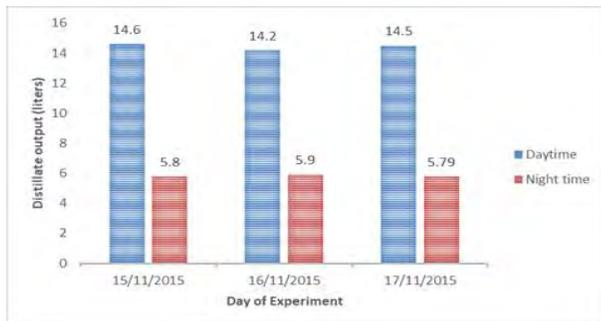
Fig.5. Day and night collection of distilled water

The slight variation of distilled output in sun-shine and off-sunshine hours was recorded on 15/11/2015, but in 16/11/2015 and 17/11/2015, the extracted output was maximum at night time.

3.4 Comparison of output efficiency of present research work

Before current solar still in the market, the comparison study is required. It gives the idea of present work compared with other researchers work. Table 1 shows the comparison of various researchers works compared to present research work in terms of increase in distillate output of water. For comparison with other researchers work, average distillate output of conventional solar still is take as 3 liters.

Sr. No.	References	Experiment work Type of Augmentation with solar still	Increase in distillate water (%)
1	Rai et al., 1983	Single basin Solar still coupled with Flat plate collector	18
2	Adbel-Rehim et al., 2007	Experimental and Therotical Analysis solar still Augmented with Parabolic collector	24
3.	Velmurgan and Srithar, 2007	Solar still Integrated with a Mini Solar Pond.	26.6
4	Badran et al., 2005	The effect of coupling a flat-plate collector on the solar still productivity. Desalination	29
5	Kumar and Bai, 2008	Solar still condensation	30
6	Srithar, 2010	Solar still coupled with activated carbon and methanol with sponge and sand	32.32
7	Panchal, 2013	Actual performance analysis of flat plate collector coupled with passive solar still with Flat plate collector	36
8	Sampathkumar, 2013	An experimental study on single basin solar still augmented with evacuated tubes	49.7
9	Panchal et al., 2014	Enhancement of distillate output of double basin solar still with vacuum tubes	266.67
10	**Present work**	**Triple basin solar still with Evacuated tube collector**	**700**

Table 1 : Comparison of various researchers work on solar still in terms of percentage of distillate output

3.5 Economic analysis of the solar still

₹1 USD	INR. 63 (Assume)
Cost of Fabrication	₹-19640
Cost of Operation	₹-5/day
Cost of Maintenance	₹-5/day
Feed water cost	₹-1
Cost of distilled water	₹12/Litre
Cost of water produced / day	₹-264/day
Subsidized cost given by government	4% = ₹-785
Net profit = (Cost of water produced / day) –Cost of Operation – Cost of Maintenance - Cost of feed water	₹253.
Payback period = (Investment - Subsidized cost) / Net profit	74 Days

Table 2 : Economic analysis of solar still

Payback period of triple basin solar still coupled with evacuated tubes depends on the various cost like- cost of fabrication, cost of feed water maintains and operating cost and also the financial subsidy are offered by the Government. Table 2 Shows the economic analysis of solar still.

4. CONCLUSION

.From the research work, following points are concluded:

❖ Design and development of solar still with modified three basins increase the output.

❖ The present solar still can generate freshwater not only in the daytime but also in the night, with maximum freshwater yield amounting to 20 liter.

❖ Present solar still is not only producing the distillate water from the lower basin but also from top and middle basin. Hence, distillate output will be remains higher as compared with conventional solar still.

❖ Evacuated tubes coupled with lower basin, hence lower basin temperature always remain higher compared with middle and upper basin. It provides thermal force to transfer heat from lower basin to middle and top basin to get higher distillate output.

❖ Presence of maximum amount of solar intensity and ambient temperature increases the distilled output.

❖ Present solar still increased distillate output around 700% compared with conventional solar still distillate output.

❖ Temperature of water is not only remains higher during sunshine hours but also in night time. Hence, present solar still provides continuous supply of fresh water from day to night.

❖ After the experiment this distilled water can be utilized as potable water.

❖ This technology can be referred as environmental friendly and low cost technology for water purification

Acknowledgement:

References:

[1] Bassam A, K., Abu-Hijileh., Himzeh M Rababa'h., (2006). Experimental analysis of solar still with different materials, Energy Coversion and Management, 33 : 1411-1418.

[2] Panchal, Hitesh, and Pravin Shah. (2013a). "Performance Improvement of Solar Stills via Experimental Investigation." International Journal of Advanced Design and Manufacturing Technology 5 (5): 19–23.

[3] Panchal, Hitesh, and Pravin Shah. (2013b) "Performance Analysis of Double Basin Solar Still with Evacuated Tubes." Applied Solar Energy 49 (3): 174–179.

[4] Panchal, Hitesh, and Pravin Shah. (2014a) "Enhancement of Distillate Output of Double Basin Solar Still With Vacuum Tubes." Frontiers in Energy 8 (1): 101–109.

[5] Panchal, Hitesh, and Pravin Shah. (2014b) "Enhancement of Upper Basin Distillate Output by Attachment of Vacuum Tubes with Double-Basin Solar Still." Desalination and Water Treatment 55 (3): 587–595. doi:10.1080/194 43994.2014.913997.

[6] Panchal, Hitesh, and Pravin Shah. (2014c). "Improvement of Solar Still Productivity by Energy Absorbing Plates." Journal of Renewable Energy and Environment 1 (1): 1–7.

[7] Panchal, Hitesh, and Pravin Shah. (2014d). "Investigation on Performance Analysis of Novel Design of Vacuum Tube-Assisted Double Basin Solar Still: An Experimental Approach." International Journal of Ambient Energy 37 (3): 220–226. doi:10.1080/01430750.2014.924435.

[8] Panchal, Hitesh, and Patel Sanjay. (2017). "An Extensive Review on Different Design and Climatic Parameters to Increase Distillate Output of Solar Still." Renewable and Sustainable Energy Reviews 69: 750–758.

[9] Panchal, Hitesh, and Pravin Shah. (2011a). "Char Performance Analysis of Different Energy Absorbing Plates on Solar Stills." Iranica Journal of Energy & Environment 2 (4): 297–301.

[10] Panchal, Hitesh, and Pravin Shah. (2011b). "Modelling and Verification of Single Slope Solar Still Using ANSYS-CFX." International Journal of Energy and Environment 2 (6): 985–998.

[11] Abdel-Rahim and Lasheen, (1981). "Experimental and theoretical study of solar desalination" Desalination, 37 : 325-342.

[12] Rai S. N. and Tiwari G. N. (1983). "Single basin solar still coupled with flat plate collector". Energy Conversion and Management, 23(3):145–149.

[13] C. tiris, M. tiris, Y. Erdalli and M. Somhen, (1996). "Experimental studies on a solar still coupled with a flat plate collector and single basin solar still". Energy Conversion and Management, 39(8) : 853-856.

[14] Badran, O.O., Al–Tahainesh, (2005). A solar still augmented with a flat plate collector. Desalination 172, 227–234.

[15] V Velmurugan, and K Srithar (2007). " Solar stills integrated with a mini solar pond—analytical simulation and experimental validation". Desalination, 216(1) : 232-241

[16] Panchal H. N. (2011). "Actual performance analysis of flat plate collector coupled with passive solar still". International Journal of Engineering Studies, 3: 51–60.

[17] Panchal H. N. (2013). "Enhancement of distillate output of double basin solar still with vacuum tubes". Journal of King Saud University-Engineering Sciences,27(2) 170-175.

SEEC-2018-005

COMBUSTION ANALYSIS OF A DIRECT INJECTION DIESEL ENGINE FUELED WITH WASTE CHICKEN FAT DERIVED FUEL-DIESEL BLEND

Debabrata Barik
Department of Mechanical
Engineering, Karpagam University,
Coimbatore-641021, India.
Email: debabrata93@gmail.com

Madhavan R.
Department of Automobile
Engineering, Karpagam University,
Coimbatore-641021, India.
Email: madhavanamku@gmail.com

Susmita Samal
Department of Electrical and Electronics
Engineering, Government College of
Technology, Coimbatore 641013, India.
Email: susmitasamal95@gmail.com

ABSTRACT

In the present investigation, chicken fat methyl ester (CFME) was produced from the transesterification of waste chicken fat obtained from various meat processing industries. For transesterification Na_2O_3Si was used as catalyst. The quality of the CFME was examined according to ASTM 6751: biodiesel standard and testing method. Important fuel properties such as heating value, cetane index, viscosity, density, and others were also investigated. Four types of blends were prepared with diesel-CFME, such as DCFME10 (90%-diesel, 10%-CFME), DCFME20 (80%-diesel, 20%-CFME), DCFME30 (70%-diesel, 30%-CFME), and DCFME40 (60%-diesel, 40%-CFME). The blends were tested in a direct injection (DI) diesel engine of rated power 3.7 kW, runs at 1500 rpm, and compression ratio of 17.5, to examine the critical phenomenon for combustion characteristics. The analysis of result showed that, for DCFME blends the cylinder pressure was marginally higher but, the heat release rate (HRR) was lower in comparison to that of diesel at full load. The ignition delay was shorter for DCFME blends whereas, the combustion duration was marginally longer in comparison with diesel throughout the load spectrum.

Keywords: Chicken fat methyl ester, Diesel engine, Combustion, Cylinder Pressure, Heat Release Rate, Transesterification.

INTRODUCTION

Currently, the world is facing a major crisis of fuel depletion and environmental degradation due to over consumption of fossil fuels, and it resulted in global degradation effects such as ozone depletion and acid rain. This also led to the reduction of underground carbon energy sources and increased CO_2 levels in the atmosphere [1,2]. The increase in population, setup of new power plants, industrialization, and increase in automotive vehicles demand for the huge consumption of fossil-based fuels, which is depleting day by day. The use of bio-fuels in substitution to fossil-based fuels can increasingly satisfy the energy needs, in an environmental friendly and cost-effective manner, while reduces the dependence on the import of fossil-based fuels and thereby provides a higher degree of National Energy Security (NES) to the nation [3]. The Indian approach to bio-fuels is based totally on non-food feedstock to be raised on degraded or wastelands which are not suited to agriculture, thus avoiding a possible conflict of food crisis [4].

Biodiesel is a renewable, non- toxic, biodegradable and environmental friendly fuel, which can be produced from several of feedstocks which include waste cooking oil, edible and non-edible vegetable oils, and animal fats [5]. Nowadays biodiesel has become the most preferred and promising alternative fuel that can be directly used in diesel engines in substitute to diesel or a blend with diesel. The marginal production of feedstock and unskilled technology employed for biodiesel research is the main key to increase its price in comparison to diesel. The economic feasibility of biodiesel mainly depends on the availability of low-cost feedstocks [4,5]. As a result, animal fats increasingly play an important role to turn biodiesel competitive as this is a waste from meat processing industries and is abundance available at a relatively low

price. The animal fat waste is increasing gradually with the growing annual meat consumption rate [6,7]. The improper disposal of these wastes causes environmental degradation by generating bacterial toxins, methane (about 37% anthropogenic), excessive amounts of nitrogen, phosphorus and heavy metals (such as zinc, copper, chromium, arsenic, cadmium, and lead). These pollutants cause severe respiratory and cardiac disorders [8,9]. The ammonia from waste animal fat slurry breeds bacteria, which creates acid that evaporates and combines with nitrous oxide in the air to form nitric acid rain. This acid despoils forest habitats and aquatic ecosystems [10,11]. The environmental degradation caused by the meat industries waste (animal fat) can be minimized by extracting biodiesel from it in an esterification reactor.

Among animal fat, chicken fat is abundantly available from meat processing industries and also from small chicken firms. Chicken fat is extracted from chicken wastes such as feather meal, chicken feathers, blood, offal and trims after rendering process. Feather meal contains a significant amount of chicken fat. The fat content of the feather meal varies from 2-12% depending on the kind of used feathers [12,13]. Chicken fat methyl ester (CFME) can be extracted from chicken fat oil, which is a promising alternative fuel. CFME has many benefits in comparison to diesel, and it plays an important role in meeting future energy demand and waste minimization from meat processing industries.

The CFME production process can become economical by choosing low-grade chicken fats, which usually contains high free fatty acid (FFA) and a usual waste from meat processing industries. But, these low-grade fats contain high FFAs, which react with alkaline catalyst, and forms soap, and prevent the separation of glycerin, and ester and reduce the quantity of CFME yield. However, this problem can overcome by using alcohols such as ethanol, methanol, and butanol during transesterification process [14,15]. The use of a good catalyst can also yield the production of CFME. Acid catalysts are considered to be slow for converting triglycerides to biodiesel but, it appears to be quite effective for converting high FFAs to esters. The most commonly preferred acid catalysts are sulfuric acid, sulfonic acid, and hydrochloric acids [16,17]. However, highly reactive homogeneous bronsted liquid acid catalysts are also efficient for chicken fat based FFAs, but they suffer from serious contamination and corrosion issues because of the formation of toxic compounds. However, the use of the solid acid catalyst in place of the liquid acid catalyst can overcome the generation of toxic wastes and easily separates the ester and glycerin [18,19].

Many researchers have investigated the production of biodiesel from animal fats [12-17,20]. However, very few researchers have worked on its application in diesel engines either as raw oil or blend with diesel [6,21-27]. Awad et al. [21] reported that the use of raw animal fat biodiesel in diesel engine gives a drop in brake thermal efficiency (BTE) of about 9% than that of normal diesel operation. But, the unburned hydrocarbon (HC) emission was lower by about 32%. The particulate matter (PM) emission was also marginally reduced at low and intermediate load ranges, but at full load operation, it was a similar trend to diesel. The NOx emission was increased at part loads by about 20%, but at full load decreased by about 4% in comparison to diesel. Also, they observed that animal fat biodiesel gives earlier start of combustion and longer combustion duration at low loads, and shorter combustion duration at high loads [21]. Ballesteros et al. [22] observed that the use of animal fat biodiesel in diesel engine gave carbonyl emission higher than that of diesel. Alptekin et al. [6] documented the results of animal fat biodiesel utilization in a direct injection diesel engine, with diesel as a reference fuel. They observed that the brake specific fuel consumption (BSFC) for animal fat biodiesel was about 16% higher than that of diesel. The maximum cylinder pressure during animal fat biodiesel operation was about 1.2 % higher, and the ignition delay was shorter than that of diesel. The CO emission for animal fat biodiesel was lower, but the NOx, and CO2 emission was reportedly higher than diesel. Barrios et al. [23] investigated the use of animal fat biodiesel and its diesel blend in a turbocharged diesel engine. They observed that the NOx emission was increased and the PM emission was decreased significantly when the concentration of animal fat biodiesel was more than 25% in the blend. Kleinova et al. [24] investigated the usability of animal fat oil in a diesel turbocharged passenger car VW Touareg R5 2.5 UI (Unit Injection) system. They observed that the engine performance was decreased by about 12-13% for animal fat oil. The concentration of PM, CO, and HC emissions were lower, but the NOx emission was reportedly higher. Behçet et al. [25] reported that the use of animal fat biodiesel in diesel engine gave lower brake power (BP), and lower torque. The tailpipe emissions such as CO, HC and carbon dioxide (CO2) concentrations were also lower, while the NOx and BSFC increased in comparison to diesel.

In this present investigation, waste chicken fat, a potential animal bases waste originated from meat processing industries was exploited as a feedstock for the production of biodiesel, to minimize stagnant environmental and waste disposal issues. The biodiesel i.e. chicken fat methyl ester (CFME) was extracted from the waste chicken fat oil by the transesterification process. Then the CFME was blended with diesel in different proportions (10-40% in steps of 10% each), and the diesel-CFME (DCFME) blends were prepaired. Further, DCFME blends were utilized as alternative fuels in a single cylinder direct injection diesel engine. The combustion,

performance and emission characteristics of the engine fueled with DCFME blends were analyzed and compared with those of diesel operation and presented in this paper.

METHODOLOGIES AND EXPERIMENTAL DETAILS

Fuel Production

The waste chicken fat was collected from a local chicken farm located near to Karpagam University, Coimbatore. Sodium silicate (Na_2O_3Si) and methanol were collected from a fuel and chemical supplier. For the transesterification reaction of waste chicken fat, Na_2O_3Si was used as catalyst and methanol was used as alcohol. Na_2O_3Si was chosen as a catalyst because it offers certain advantages over other catalysts. It does not saponify during the transesterification reactions with the feedstock having very high FFA content. Also, Na_2O_3Si is corrosion resistant, reusable and can be easily separated from the product. Methanol gives certain advantages of low price and polar shortest chain alcohol.

Initially, the waste chicken fat was washed using water. To remove the water and moisture content, the cleaned waste chicken fat was warmed for 10 minutes at a temperature of 100°C. Then the waste chicken fat was heated at a temperature of 220-240°C for 35 minutes using a microwave heater. By the application of heat, the waste chicken fat dissociated and collected in the form of fat oil. Then the acid value and FFA percentage were analyzed using titration method. For titration, initially, titrant was prepared by adding 1 gram of KOH in one liter of water. A phenolphthalein indicator was also prepared by mixing 0.05 g of phenolphthalein and 50 ml of ethanol. Then the chicken fat oil of 1 ml was mixed with 10 ml of isopropanol, and placed on a hot magnetic stirrer. To prevent solidification of the sample stirrer temperature was maintained at 60 °C. Then the prepared phenolphthalein solution and KOH solution was added drop by drop to the isopropanol-chicken fat oil mixture until the color changes to pinkish. From this, the volume of KOH required to neutralize was calculated. The FFA content was calculated using the following formula:

$$Percentage\ FFA = \frac{V \times M \times W}{m} \times 100 \qquad (1)$$

where, M and V are the molarity (mol/1000 ml) of KOH and volume in ml respectively. W is the molar weight (g/mol) of the fatty acid in chick fat oil, and m is the mass (g) of sample considered for analysis. The FFA composition of CFME is given in Table 1.

A trial and error method for chicken fat oil to alcohol molar ratio was carriedout in the range of 1:4 to 1:8, and finally molar ratio of 6:1 was chosen for high yield during the transesterification reaction.

TABLE 1 Fatty acid composition of CFME.

Fatty acid	% in CFME
Myristic 14:0	2
Palmitic 16:0	25
Palmitoleic 16:1	8
Stearic 18:0	6
Oleic 18:1	41
Linoleic 18:2	18

The catalyst amount was selected as 1% of the weight of the initial amount of fat in the chicken fat oil, with the neutralization amount calculated from the titration. The transesterification reaction was carried out in 250 ml three-necked round-bottom flasks equipped with a reflux condenser, a thermometer, and a heating mantle with a magnetic stirrer. Initially, the flask was loaded with 100 ml of chicken fat oil, and it was heated to the temperature of 200°C and the magnetic stirring was started. Then separately in a 100 ml beaker, a specified amount of Na_2O_3Si was dissolved with methanol under magnetic stirring. The prepared solution of Na_2O_3Si was then added to the pre-heated fat oil and steered continuously till the oil and glycerin separates from each other. After the transesterification reaction, the glycerin layer was separated in a separating funnel. Then the ester layer was washed with the warm water. The washing was repeated for thrice to obtain pure methyl ester. To remove the excess alcohol and water, the methyl ester was heated to a temperature of 110°C and then filtered. The obtained methyl ester was characterized to ensure its fuel properties for its suitable application. The photograph of CFME production setup is illustrated in Figure 1. The important properties of CFME in comparison with other animal fat waste are given in Table 2.

FIGURE 1 Photograph of CFME production setup.

TABLE 2 Properties of CFME in comparison with other animal fat waste.

Properties	Test method, ASTM	CFME	Fish oil methyl ester (FOME) [25]	All Animal fat mixture [22,26]	Fleshing oil biodiesel [6]	Chicken fat biodiesel [12]
Density, kg/m^3	D 4052	886	881	877	876.7	889.7
Lower heating value, kJ/kg	D 4809	40100	40546	36830	37300	37100
Kinematic viscosity, at 40 °C cSt	D 445	4.8	4.7	4.42	5.5	5.3
Auto-ignition temperature, °C	E 659	150-280	-	-	-	-
Flash point, °C	D 93	150	155	-	168	169
Pour point, °C	D 97	-3	-	-	-	-
Fire point, °C	D 93	250	-	-	-	-
Cetane number	D 613	57.5	52.4	65.6	58.8	52.3
Carbon, wt.%	D 3178	72.71	-	76.14	-	-
Hydrogen, wt.%	D 3178	9.27	-	12.83	-	-
Nitrogen, wt.%	D 3228	0.064	-	0.00	-	-
Sulphur, wt.%	D 3177	0.011	-	0.00	-	-
Oxygen, wt.%	E 385	17.69	-	11.03	-	-

Test Fuel Properties

The experimental investigation was carried out with four blends of diesel-CFME in different proportions named as DCFME10 (90% diesel with 10% CFME), followed by DCFME20, DCFME30, and DCFME40. Pure diesel was also used as a fuel for the comparative analysis of the results with the blends. The important physical properties of diesel and diesel-CFME blends are given in Table 3.

Experimental Setup

The experimental investigation was carried out at the Internal Combustion (IC) engines laboratory of Karpagam University, Coimbatore, India. Figure 2 shows the schematic representation of the experimental setup. Table 4 gives the detail technical specification of the engine used for the investigation. For loading the engine an eddy current dynamometer was coupled to the engine. A cantilever type load cell was mounted on the loading end of the dynamometer. As the loading arm hits the load cell the sensor senses the load and displays in the digital torque indicator. The air consumption by the engine was measured with the help of an orifice meter fitted on the intake air flow duct of the air box. The fuel consumption by the engine was measured with the help of a burette fitted with two optical fuel level sensors. One was at a higher level and the other was at a lower level (the higher to lower level effective measurement volume was 30 cm^3). The optical fuel level sensor gave an input to the control panel from which, the time taken for the consumption of fuel for a fixed volume was calculated at a particular load.

TABLE 3 Properties of diesel and diesel-CFME blend.

Properties	Test method, ASTM	Diesel	DCFME10	DCFME20	DCFME30	DCFME40
Density, kg/m^3	D 4052	830	835.6	841.2	846.8	852.4
Lower heating value, kJ/kg	D 4809	43800	43430	43060	42690	42320
Kinematic viscosity, at 40 °C cSt	D 445	3.5	3.63	3.76	3.89	4.02
Auto-ignition temperature, °C	E 659	210-350	204-343	198-336	192-329	186-322
Flash point, °C	D 93	50	60	70	80	90
Pour point, °C	D 97	-6	-5.7	-5.4	-5.1	-4.8
Fire point, °C	D 93	56	75.4	94.8	114.2	133.6
Cetane number	D 613	50	50.75	51.5	52.25	53
Carbon, wt.%	D 3178	85.3	77.9	76.47	75.23	73.95
Hydrogen, wt.%	D 3178	13.19	10.8	10.4	10.0	9.66
Nitrogen, wt.%	D 3228	1.21	0.52	0.40	0.29	0.17
Sulphur, wt.%	D 3177	0.3	0.18	0.21	0.24	0.27
Oxygen, wt.%	E 385	Nil	10.6	12.52	14.24	15.95

A turbine type water flow sensor was used to measure the water flow rate to the engine casing water jacket and to the exhaust gas calorimeter. Fine control stainless steel ball valves were used to control the water flow rate to the engine head jacket, exhaust gas calorimeter and the pressure sensor cooling adopter. The exhaust manifold line of the engine was well insulated with ceramic rope to reduce the heat loss by radiation, which helped to measure the exact temperature of the exhaust gas. A piezotronic pressure sensor was mounted on the engine head to measure the rate of pressure rise (ROPR) and combustion

pressure and at every one degree crank angle interval. The pressure sensor was connected to a charge amplifier and flushed into the clearance volume, to measure the instantaneous cylinder volume and pressure with respect to crank angle. A water cooling adopter was connected to the piezotronic pressure sensor for its cooling purpose. A low noise cable was connected to the pressure sensor and the signal conditioner for data transformation. A rotary encoder was mounted near the coupling with a reference for measuring the engine speed, TDC position of the piston and crank angle of the engine.
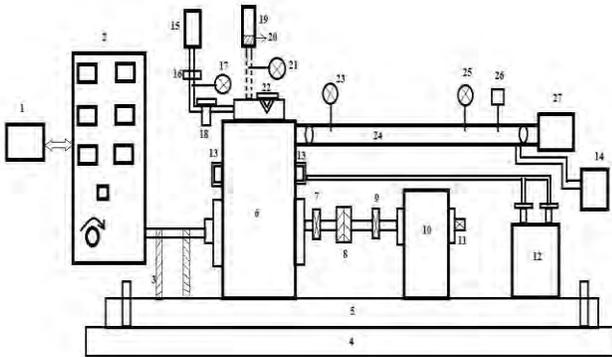
FIGURE 2 Schematic diagram of the experimental setup. 1. Data acquisition system, 2. Digital display unit, 3. Insulated cable box, 4. Engine bed, 5. Base frame vibration absorber, 6. Single cylinder CI engine, 7. Crank angle sensor, 8. Flywheel coupling, 9. Speed sensor, 10. Eddy current dynamometer, 11. Load cell, 12. Water lever controller, 13. Pressure sensor with water cooling arrangement, 14. Exhaust gas analyzer, 15. Fuel tank, 16. Filter, 17. Fuel flow sensor, 18. Fuel pump, 19. Air box, 20. Pressure transducer, 21. Air flow sensor, 22. Fuel injector, 23. K-type thermocouple 1, 24. Exhaust gas calorimeter, 25. K-type thermocouple 2, 26. Exhaust gas sensor, 27. Smoke meter.

For every cycle, a total of 720 data points for both cylinder volume and pressure were recorded at each load. Twenty cycles were considered for calculating the heat release rate at a particular load. The heat release rate calculation is broadly provided in Section 3.1. Furthermore, the instantaneous pressure data were smoothed by using the following correlation:

$$P_n = \frac{[(P_{n-1}) + 2(P_n) + (P_{n+1})]}{4} \tag{2}$$

For every crank angle, the change of pressure was determined by using the equation

$$\frac{dP}{d\theta} = \frac{[(P_{n-2}) - 8(P_{n-1}) + 8(P_{n+1}) - (P_{n+2})]}{[12(\Delta\theta)]} \tag{3}$$

The signals from the crank angle encoder and pressure sensor were trapped to the charge amplifier for the in-cylinder combustion analysis. A data acquisition system (DAS) was used for collecting the data, and the acquired data stored in the computer for analysis. A combustion analyzer kit was used to analyzes heat release rate (HRR), ignition delay (ID), start of combustion (SOC), mass fraction burned (MFB) inside the cylinder. A multi-channel temperature indicator with K- type thermocouples were used for sensing the exhaust gas temperature, intake air temperature, water inlet temperature and outlet temperature.

The engine exhaust emissions such as CO, HC, NO, CO_2, and O_2 were measured with a five-gas analyzer (AVL 444). The ASTM D6522 standard was followed during emission measurement. At each module of experiment, during steady state operation of the engine, the exhaust gas was allowed to surge through the probe, and then filtered and became moisture free by a condensation trap. The moisture free dry exhaust gas was passed to the NDIR (Non-dispersive infrared) sensor for CO, HC and CO_2 measurement. The NO emission was measured with the help of an electro chemical sensor. The intensity of smoke emission was measured with the help of a diesel smoke meter (AVL 437C).

TABLE 4 Test engine specifications.

Make/model	Kirloskar, variable compression ratio (VCR)
Engine type	Single cylinder, four stroke, CI, naturally aspirated
Fuel type	Multi fuel engine
Type of injection	Direct
Brake power, kW	3.7
Rated speed, rpm	1500
Cooling system	Water
Displacement volume, cm^3	551 (stroke 11 cm, bore 8 cm)
Injection nozzle hole	5-hole
Nozzle opening pressure, bar	180
Injection timing , ^{o}CA bTDC	23
Compression ratio	17.5
Dynamometer type	Eddy current dynamometer

Experimental Design

The engine was first run up to the warm up condition with diesel to ensure the steady state operation. During steady state condition, the combustion, performance and emission data for diesel were collected. Then the engine was allowed to run with the DCFME blends (10-40%) in steps of 10 each. During investigation the fuel injection pressure, compression ratio and engine speed were held constant at 180 bar, 17.5, and 1500 rpm respectively. In both the diesel and DCFME operation, the fuel injection timing was kept constant at 23 ^{o}CA bTDC. During the

experimental investigation, the engine was loaded from 0% load to 100% load in steps of 25%. The experimental test conditions detail are given in Table 5. The fuel injection quantities in diesel and DCFME operation were controlled by the governor, with variations in the engine load. The test engine was operated at 35 ± 2 °C of ambient temperature under all the modes of operations. The acronyms used for the diesel, DCFME operations are given in Table 6.

TABLE 5 Experimental test conditions.

Test fuels	Diesel, DCFME10, DCFME20, DCFME30, DCFME40
Engine speed, rpm	1500 (constant)
Ambient temperature, °C	35 ± 2
Fuel injection pressure, bar	180
Compression ratio	17.5
Engine load variation, %	0, 25, 50, 75, 100

TABLE 6 Test matrix and acronyms used for the fuels.

Mode	CR	IT, °CA bTDC	Acronyms used
Diesel (100%)	17.5	23	Diesel
Diesel+CFME (10%)	17.5	23	DCFME10
Diesel+CFME (20%)	17.5	23	DCFME20
Diesel+CFME (30%)	17.5	23	DCFME30
Diesel+CFME (40%)	17.5	23	DCFME40

Uncertainty Analysis And Instrument Details

Uncertainty is the means for measuring the error of a result or an instrument. Without such measure it is impossible to judge the fitness value. To estimate the bounds on the accuracy of an estimated parameter, the uncertainty analysis is highly recommended. The evaluation of uncertainty from some known physical value can be obtained by using the formula described by Coleman and Steele [28]. Table 7 lists the uncertainties of the instruments used in the present investigation.

$$U_R = (B_R^2 + P_R^2)^{1/2} \qquad (4)$$

U_R is the uncertainty of the physical parameter considering 5% significance [29]. B_R and P_R are the systematic and random uncertainties respectively [30].

$$\frac{B_R}{R} = \left[\sum_{i=1}^{n}\left(\frac{1}{R}\frac{\partial R}{\partial X_i}B_i\right)^2\right]^{1/2} \qquad (5)$$

$$\frac{P_R}{R} = \left[\sum_{i=1}^{n}\left(\frac{1}{R}\frac{\partial R}{\partial X_i}P_i\right)^2\right]^{1/2} \qquad (6)$$

In the equation cited, R is the physical parameter that depends on the variable X_i. The symbols P_R and P_i denote the uncertainty in R and the measurement level, respectively. For the uncertainty analysis 20 sets of observation have been taken in the same engine and same operating condition, and as a result, the maximum uncertainty of the instruments obtained was $\pm 1.13\%$.

TABLE 7 Range, accuracy, and uncertainty of the instruments used [30].

Instruments used	Parameter measured with units	Range	Accuracy	Uncertainty, %
Load cell	Engine load, watt	250-6000	±10	±0.2
Thermocouple	Temperature, °C	0-900	±1	±0.15
Burette	Fuel consumption, cm³	1-30	±0.2	±0.5
Orifice meter	Air consumption, m³/min	0.5-50	±0.1	±0.5
Speed sensor	Engine speed, rpm	0-10,000	±10	±1
Pressure transducer	In-cylinder pressure, bar	0-110	±0.1	±0.15
Crank angle encoder	Crank position, °CA	0-720	±0.6	±0.01
Smoke meter	Smoke opacity, %	0-100	±1	±1
Exhaust gas analyzer	Exhaust emission			
	NO, ppm	NO: 0-5,000	<500 ppm vol: ±50 ppm vol. P500 ppm vol: ±10% of initial value	±1
	HC, ppm	HC: 0-20,000	<200 ppm vol: ±10 ppm vol. P200 ppm vol: ±5% of initial value	±0.5
	CO, vol.%	CO: 0-10	<0.6% vol: ±0.03vol.% P0.6% vol: ±5% of initial value	±0.03

Combustion Efficiency

In this investigation, the increase in percentage of CFME in the blend affects the combustion efficiency and pollutant emissions. Because, under fuel-rich operating conditions the availability of oxygen, increase in viscosity, and the decrease in lower heating value (LHV) of the blends may result in a more incomplete combustion and a fraction of the fuel's chemical energy not released during the combustion process. In the diesel operation, the combustion efficiency is generally in the range of 98-99% [31,32].

The DCFME blend affects the combustion efficiency at relatively low and part load operations. The combustion efficiency is defined as the ratio between the accumulated heat release and the gross heat supplied by the total fuel. However, the gross total heat released in the cylinder is hard to measure accurately in practice. So, the combustion efficiency is calculated from the exhaust components like CO, H_2 and HC. The higher amounts of these species reflect the combustion efficiency [33]. The combustion efficiency in a DCFME fueled diesel engine can be quantified as follows:

$$\eta_{comb} = \left[1 - \frac{\sum_i e_i LHV_i}{\left[\frac{(m_D.LHV_D + m_{CFME}.LHV_{CFME})}{(m_{air} + m_D.LHV_D + m_{CFME}.LHV_{CFME})}\right]} \right] \times 100 \quad (7)$$

where, η_{comb} is the combustion efficiency (%). e_i is the mass fraction of HC, CO, H_2 and particulates in the exhaust gas (kg). LHV_i is the lower heating value of each exhaust components (kJ/kg). The fraction of H_2 can be calculated from the combustion reaction kinetics.

RESULTS AND DISCUSSION

Combustion Analysis

In-Cylinder Pressure

Figure 3 portrays the variation of cylinder pressure with crank angle for diesel, DCFME10, DCFME20, DCFME30, and DCFME40 at full load. The cylinder pressure vs crank angle history is an important parameter to analyze the combustion characteristics of the engine because the increase and decrease in cylinder pressure directly influence the exhaust emissions and performance parameters of the engine. It can be observed from the figure that, the peak cylinder pressure for diesel is 75.7 bar, occur at 7.41 ^oCA aTDC. For DCFME10, DCFME20, DCFME30, and DCFME 40 the peak cylinder pressure is 78 bar, 76.5 bar, 78.6 bar and 79.7 bar, which occur at 7.26 ^oCA aTDC, 5.26 ^oCA aTDC, 3.77 ^oCA aTDC, and 1.48 ^oCA aTDC respectively. DCFME40 gives higher cylinder pressure than that of DCFME10, DCFME20, and DCFME30. This may be due to the higher percentage of CFME in the blend, contributes higher dissolved oxygen concentration and high cetane index in the fuel, which inhibited earlier start of combustion of fuel in the premixed combustion phase, and lead to a rapid increase in cylinder pressure in the diffusion combustion phase [34]. Another possible reason for higher cylinder pressure for DCFME40 may be due to the higher viscosity of CFME, which results in poor spray droplet and forms a premix fuel rich zone inside the combustion chamber because viscous fuels have a tendency to form large droplets within the fuel jet leading to a lower mixing [27]. The premix fuel burns out sharply because of the abundance oxygen and the high contact surface between air and fuel droplets. The premix combustion phase ends before the end of fuel injection. Thus the fuel injected by injector burns in diffusion phase and continues in the late combustion phase [21,35]. For the DCFME40 maximum amount of fuel burns before TDC and the peak cylinder pressure moves closer to TDC. It is also evident that the peak cylinder pressure decreases with the decrease in CFME percentage in the blend. At full load operation, diesel gives low cylinder pressure than those of DCFME10, DCFME20, DCFME30, and DCFME40. This is due to the high volatility of diesel and has an exquisite tendency to mix with air, which reduces the chance of forming fuel-rich pockets in the burning zone of combustion chamber [35].
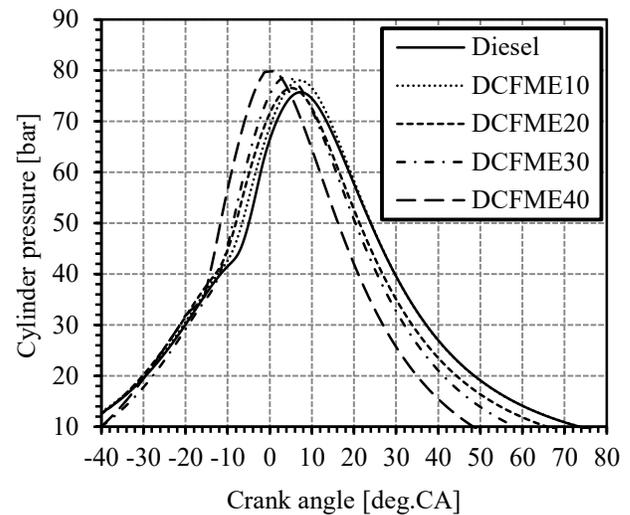
FIGURE 3 Variation of cylinder pressure for diesel and DCFME blends at full load.

Heat Release Rate

Figure 4 illustrates the variation of heat release rate with crank angle at full load. It can be observed from the figure that, a maximum heat release rate of 56.5 J/^oCA is noticed for diesel, which occurs at 8.9 ^oCA aTDC. This is due to the higher energy density of diesel [36,21]. Another possible reason for higher heat release rate in diesel may be attributed to the increased accumulation of fuel during the relatively longer delay period, which forms a significantly flammable zone in the premix combustion phase [37]. For DCFME operation, with the increase in CFME percentage in the blend, the heat release rate gradually decreases. This is obvious, due to the decrease in heating value of the fuel blends [36]. Another possible reason for the decrease in heat release rate is due to the high cetane number of the CFME in the blend that leads to an earlier start of combustion. However, the high viscosity and low volatility of CFME gives poor atomization and mixing of fuel with air. Hence, less fuel burns in the premix combustion zone. And rich fuel pockets are formed in the diffusion combustion zone, and fuel continues its combustion in the

late combustion zone and decreases the heat release rate [21]. DCFME10 gives a higher heat release rate of 56.31 J/°CA in comparison to DCFME20, DCFME30, and DCFME40, which occurs at 7.07 °CA aTDC at full load. The heat release rate for DCFME20, DCFME30 and DCFME40 is 55.41 J/°CA, 55.11 J/°CA, and 54.21 J/°CA, which occur at 5 °CA aTDC, 4.27 °CA aTDC, and 2.31 °CA aTDC respectively at full load. A drop in heat release rate of 0.3 %, 1.9 %, 2.4 %, and 4 % is observed for DCFME10, DCFME20, DCFME30, and DCFME40 in comparison to diesel at full load respectively.
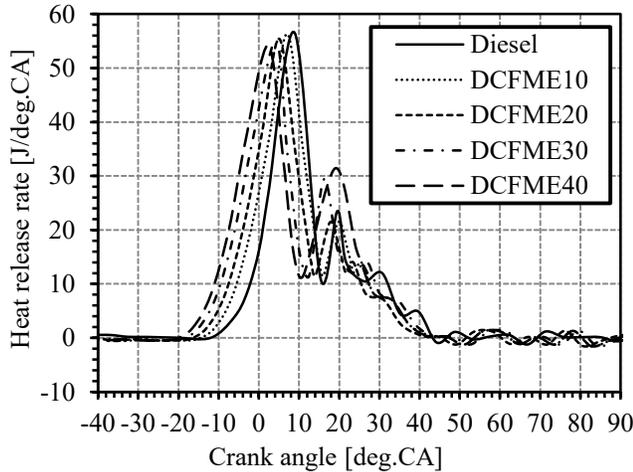
FIGURE 4 Variation of heat release rate for diesel and DCFME blends at full load.

Ignition Delay

The variation of ignition delay with the variation in load for diesel, DCFME10, DCFME20, DCFME30, and DCFME40 is depicted in Figure 5. It can be observed from the figure that, the ignition delay decreases with the increase in load irrespective of the fuels used. This is due to the higher combustion chamber wall temperature, high residual gas temperature and reduced exhaust gas dilution at high loads [38]. DCFME10, DCFME20, DCFME30, and DCFME40 exhibit a shorter ignition delay than that of diesel throughout the load spectrum. This is due to the higher cetane number of CFME and the existence of oxygen in the fuel that leads earlier start of combustion. The ignition delay for diesel is about 11.5 °CA whereas; in DCFME operation it is shorter by about 1-1.9 °CA at full load. DCFME10, DCFME20, DCFME30, and DCFME 40 gives shorter ignition delay of 11.3 °CA, 10.8 °CA, 10.1 °CA, and 9.6 °CA than that of diesel, at full load respectively.

Combustion Duration

Combustion duration is defined as the crank angle interval between the points at which the heat release rate

becomes positive (as depicted in Figure 4) and the point at which 90% of the heat release taken place.
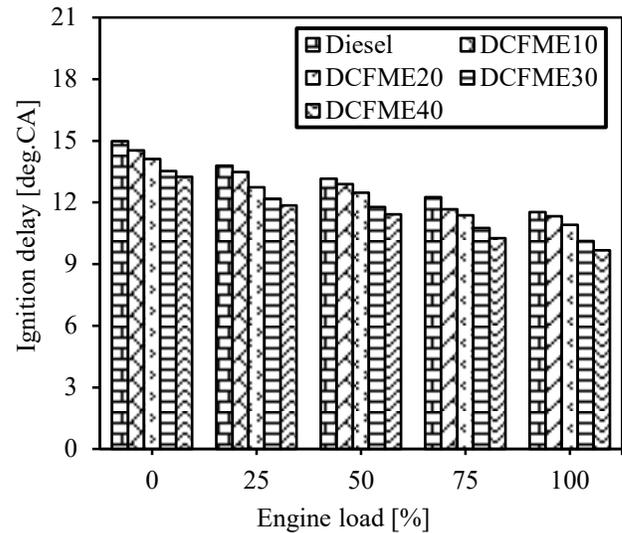
FIGURE 5 Variation of ignition delay with load for diesel and DCFME blends.
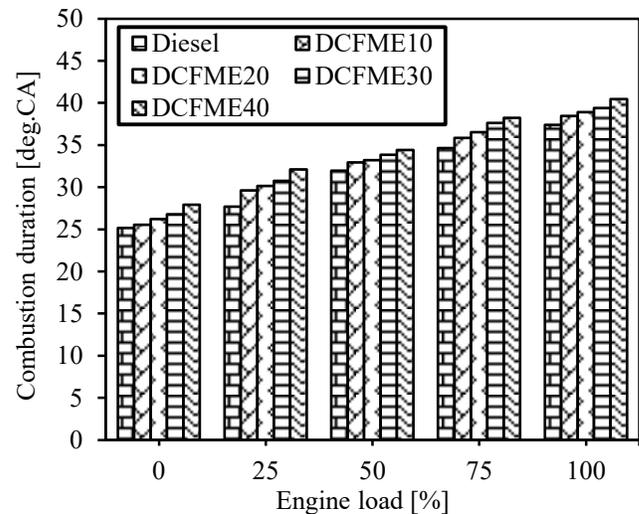
FIGURE 6 Variation of combustion duration with load for diesel and DCFME blends.

It can be observed that the combustion duration increases with the increase in load irrespective of the fuels used. This is due to the consumption of more quantity of fuel at relatively higher loads [39]. The combustion duration for diesel, is found to be 37.4 °CA at full load. For DCFME10, DCFME20, DCFME30, and DCFME40 the combustion duration is found to be 38.4 °CA, 38.9 °CA, 39.4 °CA, and 40.4 °CA at full load, respectively. The reason for the increase in combustion duration for DCFME operations than that of diesel is due to the high viscosity and low volatility of CFME, which gives poor atomization and mixing of fuel with the air and causes a slower rate of burning of the blend. It can also be observed from the

figure that, the combustion duration for DCFME40 increases drastically in comparison to DCFME30 at full load. This is due to the higher blend percentage of CFME, which alters the physical properties of the charge being compressed and causes slower diffusion combustion, and results in prolonged combustion duration. For diesel and DCFME operations, shorter combustion duration is noticed at low load; this may be due to the consumption of less fuel at relatively low load operations.

Maximum Cylinder Pressure

It can be observed from the figure that, the cylinder pressure increases with the increase in engine load, as expected. The maximum cylinder pressure for diesel is about 75.7 bar, at full load. For DCFME10, DCFME20, DCFME30, and DCFME40 the maximum cylinder pressure is 76.5 bar, 77.8 bar, 78.6 bar, and 80.2 bar respectively at full load. The increase in maximum cylinder pressure for DCFME operations than that of diesel is due to the higher viscosity of CFME, which results in poor spray droplet and forms a premix fuel rich zone inside the combustion chamber, because viscous fuels have a tendency to form large droplets within the fuel jet leading to an increase in under mixing [27]. The under premix fuel burns sharply and increases the cylinder pressure.
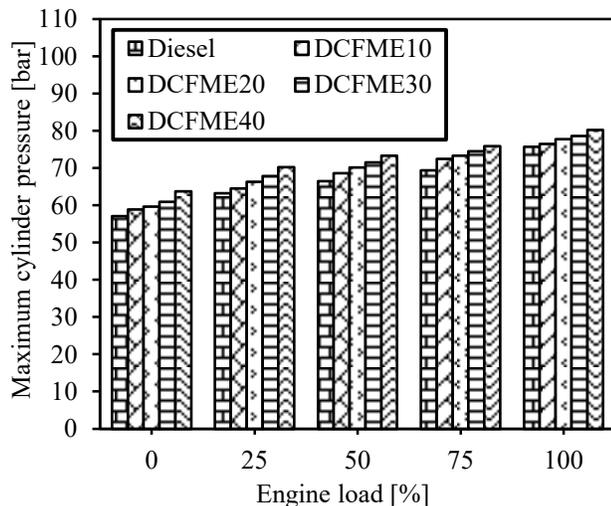
FIGURE 7 Variation of maximum cylinder pressure with load for diesel and DCFME blends.

Mass Fraction Burned

Figure 8 portrays the variation of mass fraction burn with the variation in crank angle for diesel and DCFME operations. The energy conversion during a specific combustion cycle can be expressed by the fraction of mass of fuel burned at a specific crank angle. The mass fraction burned at each individual combustion cycle is a normalized quantity with a scale 0-1, describing the process for the conversion of fuel's chemical energy into work, as a

function of crank angle [39]. This is also indicative of the start and end of combustion [31].

It can be observed from the figure that, the mass fraction burn for DCFME blends is marginally higher than that of diesel at full load. This is due to the high cetane index of CFME that gives earlier start of combustion and advances the heat release start point hence, maximum amount of fuel burns close to the top dead center (TDC) [39]. It is also observed that crank angles at which 10% mass fraction burned for DCFME blends is earlier than that of diesel at full load. But at crank angles of 90% mass fraction burned the difference between diesel and DCFME blends is nearly equal. This may be due to the slower combustion rate in the premixed burning phase of DCFME blends and longer diffusion phase which increases the total combustion duration. The high volatility nature of diesel enhances its rate of combustion and increases the mass fraction burn with respect to crank angle, at full load [31,37]. The occurrence of 90% mass fraction burn for diesel, DCFME10, DCFME20, DCFME30, and DCFME40 is noticed at 31.1 °CA aTDC, 30.3 °CA aTDC, 29.8 °CA aTDC, 29.2 °CA aTDC, and 28.5 °CA aTDC at full load, respectively.
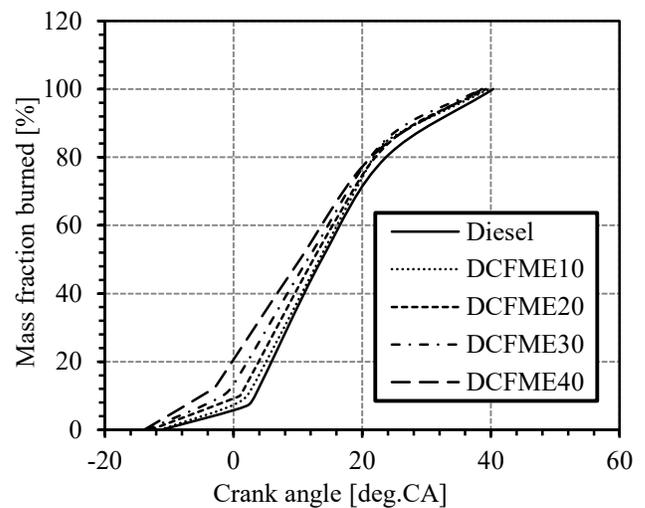
FIGURE 8 Variation of mass fraction burned with crank angle for diesel and DCFME blends.

CONCLUSIONS

The conclusions of the results obtained from the investigation are as follows:

- The peak cylinder pressure for DCFME30 is about 78.6 bar, which occur at 3.77 °CA aTDC.
- DCFME30 gave optimum results in combustion, performance and emission in comparison to DCFME10, DCFME20, and DCFME40.

- DCFME30 gave a shorter ignition delay and longer combustion duration of 1-1.9 ^{o}CA in comparison with diesel, at full load respectively.
- For DCFME30 the combustion duration is found to be 39.4 ^{o}CA at full load, respectively.
- The occurrence of 90% mass fraction burn for DCFME30 is noticed at 29.2 ^{o}CA aTDC, at full load.

REFERENCES

[1] Maddalena Zucali, Alberto Tamburini, Anna Sandrucci, Luciana Bava. Global warming and mitigation potential of milk and meat production in Lombardy (Italy). Journal of Cleaner Production (2016), http://dx.doi.org/10.1016/j.jclepro.2016.11.037.

[2] G. Pratibha, I. Srinivas, K.V. Rao, Arun K. Shanker, B.M.K. Raju, Deepak K. Choudhary, K. Srinivas Rao, Ch. Srinivasarao, M. Maheswari. Net global warming potential and greenhouse gas intensity of conventional and conservation agriculture system in rainfed semi-arid tropics of India. Atmospheric Environment 2016;145:239-250.

[3] Irina Naroznova, Jacob Møller, Charlotte Scheutz. Global warming potential of material fractions occurring in source-separated organic household waste treated by anaerobic digestion or incineration under different framework conditions. Waste Management 2016;58:397-407.

[4] Gita Surie. Innovating via emergent technology and distributed organization: A case of biofuel production in India. Technological Forecasting & Social Change 2013;80:253-266.

[5] Aliakbar Roosta, Iman Sabzpooshan. Modeling the effects of cosolvents on biodiesel production. Fuel 2016;186:779-786.

[6] Ertan Alptekin, Mustafa Canakci, Ahmet Necati Ozsezen, Ali Turkcan, Huseyin Sanli. Using waste animal fat based biodiesels–bioethanol–diesel fuel blends in a DI diesel engine. Fuel 2015;157:245–254.

[7] Metin Guru, Atilla Koca, Ozer Can, Can Cınar, Fatih Sahin. Biodiesel production from waste chicken fat based sources and evaluation with Mg based additive in a diesel engine. Renewable Energy 2010;35:637–643.

[8] Kate Ryder, Alaa El-Din Bekhit, Michelle McConnell, Alan Carne. Towards generation of bioactive peptides from meat industry waste proteins: Generation of peptides using commercial microbial proteases. Food Chemistry 2016;208:42-50.

[9] Alberto Oliveros-Bastidas, María Pía Calcagno-Pissarelli, Marlene Naya, Jorge Luis Ávila-Núñez, Miguel E. Alonso-Amelot. Human gastric cancer, Helicobacter pylori and bracken carcinogens: A connecting hypothesis. Medical Hypotheses 2016;88:91-99.

[10] Ciro Fernando Bustillo-Lecompte, Mehrab Mehrvar. Treatment of actual slaughterhouse wastewater by combined anaerobic–aerobic processes for biogas generation and removal of organics and nutrients: An optimization study towards a cleaner production in the meat processing industry. Journal of Cleaner Production 2017;141:278-289.

[11] A.M. Kooijman, C. Bakker. The acidification capacity of wetland bryophytes as influenced by simulated clean and polluted rain. Aquatic Botany 1994;48:133-144.

[12] Ertan Alptekin, Mustafa Canakci. Optimization of transesterification for methyl ester production from chicken fat. Fuel 2011;90:2630–2638.

[13] Kondamudi N, Strull J, Misra M, Mohapatra SK. A green process for producing biodiesel from feather meal. Journal of Agricultural and Food Chemistry 2009;57:6163–6166.

[14] Muhammad Farooq, Anita Ramli, Abdul Naeem. Biodiesel production from low FFA waste cooking oil using heterogeneous catalyst derived from chicken bones. Renewable Energy 2015;76:362-368.

[15] Praful Nair, B. Singh, S.N. Upadhyay, Y.C. Sharma. Synthesis of biodiesel from low FFA waste frying oil using calcium oxide derived from Mereterix mereterix as a heterogeneous catalyst. Journal of Cleaner Production 2012;29-30:82-90.

[16] Lubomir Sanek, Jiri Pecha, Karel Kolomaznik, Michaela Barinova. Pilot-scale production of biodiesel from waste fats and oils using tetramethylammonium hydroxide. Waste Management 2016;48:630–637.

[17] Ertan Alptekin, Mustafa Canakci. Optimization of pretreatment reaction for methyl ester production from chicken fat. Fuel 2010;89:4035–4039.

[18] Jabbar Gardy, Ali Hassanpour, Xiaojun Lai, Mukhtar H. Ahmed. Synthesis of Ti(SO$_4$)O solid acid nano-catalyst and its application for biodiesel production from used cooking oil. Applied Catalysis A: General 2016;527:81-95.

[19] Fang Su, Yihang Guo. Advancements in solid acid catalysts for biodiesel production. Green Chemistry 2014,16, 2934-2957.

[20] Rajat Chakraborty, Abhishek.K. Gupta, Ratul Chowdhury. Conversion of slaughterhouse and poultry farm animal fats and wastes to biodiesel: Parametric sensitivity and fuel quality assessment. Renewable and Sustainable Energy Reviews 2014;29:120-134.

[21] Sary Awad, Khaled Loubar, Mohand Tazerout. Experimental investigation on the combustion, performance and pollutant emissions of biodiesel from animal fat residues on a direct injection diesel engine. Energy 2014;69:826-836.

[22] R. Ballesteros, J. Guillen-Flores, J.D. Martinez. Carbonyl emission and toxicity profile of diesel

blends with an animal-fat biodiesel and a tire pyrolysis liquid fuel. Chemosphere 2014;96:155–166.

[23] Carmen C. Barrios, Aida Domínguez-Sáez, Carlos Martín, Paloma Álvarez. Effects of animal fat based biodiesel on a TDI diesel engine performance, combustion characteristics and particle number and size distribution emissions. Fuel 2014;117:618–623.

[24] A. Kleinova, I. Vailing, J. Labaj, J. Mikulec, J. Cvengros. Vegetable oils and animal fats as alternative fuels for diesel engines with dual fuel operation. Fuel Processing Technology 2011;92:1980-1986.

[25] Rasim Behçet, Hasan Oktay, Abdulvahap Çakmak, Hüseyin Aydin. Comparison of exhaust emissions of biodiesel-diesel fuel blends produced from animal fats. Renewable and Sustainable Energy Reviews 2015;46:157-165.

[26] Ángel Ramos, Reyes García-Contreras, Octavio Armas. Performance, combustion timing and emissions from a light duty vehicle at different altitudes fueled with animal fat biodiesel, GTL and diesel fuels. Applied Energy 2016;182:507–517.

[27] Eliezer Ahmed Melo-Espinosa, Ramón Piloto-Rodríguez, Leonardo Goyos-Pérez, Roger Sierens, Sebastian Verhelst. Emulsification of animal fats and vegetable oils for their use as a diesel engine fuel: An overview. Renewable and Sustainable Energy Reviews 2015;47:623-633.

[28] Coleman HW, Steele Jr WG. Experimentation and uncertainty analysis for engineers. New York: John Wiley & Sons; 1989.

[29] Kyunghyun R. Effects of pilot injection timing on the combustion and emissions characteristics in a diesel engine using biodiesel–CNG dual fuel. Applied Energy 2013;111:721–730.

[30] Debabrata Barik, S. Murugan. Effects of diethyl ether (DEE) injection on combustion performance and emission characteristics of Karanja methyl ester (KME)–biogas fueled dual fuel diesel engine. Fuel 2016;164:286–296.

[31] Debabrata Barik, S. Murugan. Experimental investigation on the behavior of a DI diesel engine fueled with raw biogas-diesel dual fuel at different injection timing. Journal of the Energy Institute 2016;89:373-388.

[32] J.B. Heywood, Internal Combustion Engine Fundamentals, McGraw-Hill, New York, 1988.

[33] M. Yao, Z. Chen, Z. Zheng, B. Zhang, Y. Xing, Study on the controlling strategies of homogeneous charge compression ignition combustion with fuel of dimethyl ether and methanol, Fuel 2006;85:2046-2056.

[34] Gill SS, Tsolakis A, Dearn KD, Rodriguez-Fernandez J. Combustion characteristics and emissions of Fischer-Tropsch diesel fuels in IC engines. Progresses in Energy Combust Science 2011;37:503-523.

[35] Qi D, Bae C, Feng Y, Jia C, Bian Y. Preparation, characterization, engine combustion and emission characteristics of rapeseed oil based hybrid fuels. Renewable Energy 2013;60:98-106.

[36] Rakopoulos DC. Heat release analysis of combustion in heavy-duty turbocharged diesel engine operating on blends of diesel fuel with cottonseed or sunflower oils and their biodiesel. Fuel 2012;96:524-534.

[37] R. Prakash, R.K. Singh, S. Murugan. Experimental studies on combustion, performance and emission characteristics of diesel engine using different biodiesel bio oil emulsions. Journal of the Energy Institute 2015;88:64-75.

[38] S. Jaichandar, K. Annamalai. Combined impact of injection pressure and combustion chamber geometry on the performance of a biodiesel fueled diesel engine. Energy 2013;55:330-339.

[39] Debabrata Barik, Ashok Kumar Satapathy, S. Murugan. Combustion analysis of the diesel–biogas dual fuel direct injection diesel engine-the gas diesel engine. International Journal of Ambient Energy 2017;38:259-266.

DEVELOPMENT OF A COMPUTATIONAL MODEL FOR DIRECT INJECTION SPARK IGNITION ENGINE USING CFD APPROACH

SrinibasTripathy
School of Energy Science & Engineering
IIT Kharagpur
Email: srinibas@iitkgp.ac.in

Sridhar Sahoo
School of Energy Science & Engineering
IIT Kharagpur
Email: sridharsahoo366@iitkgp.ac.in

Dhananjay Kumar Srivastava
Mechanical Engineering Department
IIT Kharagpur
Email: srivastava@mech.iitkgp.ernet.in

ABSTRACT

A numerical model was developed for a single cylinder VCR direct injection spark ignition engine using a highly efficient CFD tool ANSYS Forte 18.0. Prior to numerical modeling, intake and exhaust port were scanned and redesigned using CAD software to develop the fluid domain. Decomposition of the fluid domain was performed, and refinement technique was applied to various critical regions of the geometry. Mesh sensitivity was checked at different global mesh size. RNG K-Ɛ turbulence model was used to capture the dynamically varying spatial and temporal in-cylinder flow. An advanced hybrid KH-RT spray breakup model was coupled with an unsteady gas jet model to predict the improved gas entrainment rate. The discrete particle ignition kernel (DPIK) flame model was used for flame initiation modeling followed by a G-equation model to track the turbulent flame speed. To validate the numerical model, the experimental analysis was performed on port fuel injection (PFI) gasoline engine at different operating conditions. The measured performance parameter for premixed combustion of PFI engine shows a good agreement with the simulation results. The validated model is then used to investigate the performance and combustion analysis of a spray-guided GDI engine.

Keywords: *Numerical model, Spray, Combustion*

NOMENCLATURE

μ_{eff}	Effective viscosity
η	Strain rate
B_{KH}	KH model break up constant
Λ_{KH}	Wavelength of the fastest growing wave
C_b	RT model breakup constant
d_{noz}	Diameter of the nozzle
ρ_l	Density of liquid
ρ_g	Density of gas
τ_{RT}	Characteristic time to break parent droplet
r_k	flame kernel radius
ρ_u	local unburnt gas density
ρ_k	gas density inside kernel region
S_{plasma}	Velocity of plasma
S_T	Turbulent flame speed
C_{m1}	kernel flame modelto G-equation switch constant
$\vec{v}_f$	flame velocity vector
s_t^0	turbulent burning velocity
$\bar{\rho}_u$	unburned mass density
$\bar{\rho}$	mass density in meanflamefront location

INTRODUCTION

The performance of an internal combustion engine is greatly influenced by the complex fluid dynamic interactions of air-fuel mixture formation inside the combustion chamber. The experimental analysis for an in-cylinder mixture formation and combustion process visualization is more complex and tedious as compared to numerical analysis. CFD package can offer an in-depth analysis of geometry creation from the actual engine, the dynamic meshing of the decomposed geometry, initial and boundary conditions, a set of numerical models describing the fluids interaction and combustion mechanism with various solution approaches.

Various researchers developed their CFD code to computationally model the mixture formation and combustion processes of a direct injection spark ignition engine. However, numerical simulation includes the traditional method of decomposition and discretization, lack of mesh and time step dependency study, conventional spray and chemical kinetics reaction modeling. This leads to higher computational cost to solution accuracy [1].

In the present study, a highly efficient CFD tool ANSYS Forte 18.0 is used to develop a computational model to investigate the mixture formation and combustion analysis in a direct injection spark ignition engine. The fluid domain was developed by accurately scanning the cylinder head using advanced scanning technique.CFD code has the ability to employ state of the art, on the fly, fully automatic mesh generation technique in which the dynamic volume mesh is generated during the simulation. The advanced spray model has the potential to reduce the mesh and time step dependency dramatically compared to the existing CFD approaches.

GEOMETRY MODELING

Numerical modeling of the air-fuel mixture formation and combustion process requires an accurate designing of a 3D fluid domain. So, care was taken in designing the intake and exhaust port, piston, valves, cylinder head, and liner. Details about the engine can be found in the Tab. 1.

TABLE 1: ENGINE SPECIFICATIONS

Sl No	Engine Specification	Remarks
1	Engine model	Kirloskar TV1
2	Engine type	Single cylinder
3	Bore × Stroke	87.5 mm × 110 mm
4	Connecting rod length	234 mm
5	Intake valve open	4.5^0BTDC
6	Intake valve close	35.5^0 ATDC
7	Exhaust valve open	35.5^0 BBDC
8	Exhaust valve close	4.5^0ATDC

In this study, cylinder head of a single cylinder VCR engine was cut in wire EDM machine, and the intake port was extracted. The section was scanned by phoenix v|tome|x s industrial non-destructive micro-computed tomography scanner with scanning with accuracy ±0.2mm. The output generated from the scanning was in the stereolithography format, which describes the surface of the section without any representation of texture, color or any common attributes of CAD model. A reverse engineering tool of Geomagic Design X was used in this study to convert the scanned stereolithography file format into 3D solid CAD model. The 3D solid CAD model contains all the features of the intake port section and redesigned by CAD tool of SOLIDWORKS. The similar procedure was also followed for the intake & exhaust valves, and dimensions were extracted for solid modeling.

In addition to the above, hemispherical piston dome and cylinder head were designed by SOLIDWORKS CAD tool. Finally, all the CAD attributes were assembled, and the fluid domain was developed as shown in Fig. 1.
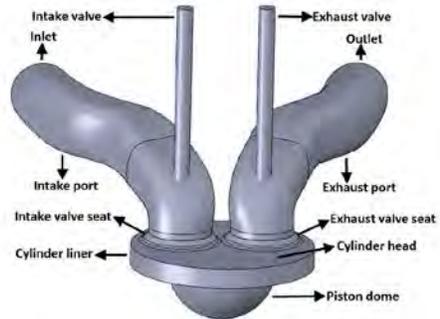
FIGURE 1. COMPUTATIONAL FLUIDDOMAIN

DISCRETIZATION

ANSYS Forte employs state of the art, on the fly, fully automatic mesh generation technique in which the dynamic volume mesh is generated during the simulation. Automatic mesh generation with geometry-based adaptive mesh refinement (AMR) and solution-adaptive mesh refinement (SAM) are used to dynamically generate a Cartesian cell mesh across the critical flow regions of the geometry for full engine full cycle simulation. The mesh generations with moving boundaries are performed automatically by a predefined global mesh size and immersed boundary method. An input surface mesh was used to establish the bounding surfaces and volumetric domain [2].

To capture the flow physics near the walls, a single cell layer at each wall is set half of that global mesh size. To refine the mesh that intersects the open boundaries, two extended layers are required to make sure that the inlet and outlet have smooth refinement, where they intersect the wall boundary. Intake and exhaust valve stems were refined 10 layers of refinement to properly describe the flow at this location. For similar reasons, refinement is done near the valve ends which seat the port. The mesh resolution within the valve gaps is dynamically controlled by valve lift profiles and user-specified minimum lift thresholds. At the top dead center, the mesh must be refined such that some of the cells separate the head and piston surfaces. To properly capture the chemistry around the spark, a point refinement is applied in which a sphere of mesh is defined within a radius of application during a specified crank angle.

SAM allows refinement of certain regions in the mesh based on a solution field (or gradient) during the numerical solution of the CFD governing equations. In the present study, based on the refinement criterion and refinement level, the gradients of velocity and temperature have been used to refine the mesh during the transient simulation.

TURBULENCE MODELING

The unsteady, non-periodic, fluctuating and chaotic fluid motion inside the cylinder referred as turbulent flow violently mixes the air-fuel mixture and enhances the combustion rate. The dynamically varying spatial and temporal turbulent length scales need to be captured for predicting the fluctuating transport properties.

ANSYS Forte employs a time-averaged RANS based RNG K-Ɛ model for turbulence modeling. The model is validated for a wider class of flows for accurately predicting the highly strained flows as compared to the standard K-Ɛ model. For complex and high turbulence flows, instantaneous quantity is decomposed into its time-averaged and fluctuating quantities. The time averaging of the momentum equations lead to an extra term in the NS equation,i.e., Reynolds stresses needed to be modeled. The eddy viscosity to predict turbulent stress in the Reynolds stress equation is modeled by solving two transport equations of turbulent kinetic energy (K) and dissipation rate (Ɛ). The additional term in the dissipation rate (Ɛ) equation helps to predict the mean strain rate during the separation or near wall regions [3]. The transport equations for K and Ɛ for RNG K-Ɛ model is given by Eqn. (1-3) as

$$\frac{\partial}{\partial t}(\rho k) + \Delta \cdot \rho k \vec{u} = \Delta[\alpha_k \mu_{eff} \operatorname{grad} k] + G_k - \rho\varepsilon \qquad (1)$$

$$\frac{\partial}{\partial t}(\rho\varepsilon) + \Delta \cdot \rho\varepsilon\vec{u} = \Delta\left[\alpha_\varepsilon \mu_{eff} \operatorname{grad} \varepsilon\right] + C_{1\varepsilon}\frac{\varepsilon}{k}G_k - C_{2\varepsilon}^*\rho\frac{\varepsilon^2}{k} \qquad (2)$$

Where

$$C_{2\varepsilon}^* = C_{2\varepsilon} + \frac{C_\mu \rho \eta^3\left(1-\frac{\eta}{\eta_0}\right)}{1+\beta\eta^3} \qquad (3)$$

In the regions of large strain rate $\eta > \eta_0$, $C_{2\varepsilon}^*$ is less than $C_{2\varepsilon}$. Hence in comparison to standard K-Ɛ model, the destruction of turbulent dissipation rate reduces the turbulent kinetic energy which reduces the effective viscosity.

SPRAY MODELING

The droplet breakup and spray atomization were modeled by Kelvin-Helmholtz (KH) and Rayleigh-Taylor (RT) hybrid model along with a discharge coefficient model to predict the primary and secondary breakup processes. The discharge coefficient model predicts the injection velocity and initial droplet size at the nozzle exit. The blob injection model injects liquid drops with a diameter equivalent to the effective nozzle diameter. KH model is used to predict the initial break-up of the injected "blobs" or the intact liquid core, and Rayleigh-Taylor model is then used in conjunction with the KH model to predict the secondary breakup of the droplets [4]. Aerodynamic breakup within the liquid core is computed based on the KH breakup model; however outside the liquid core, higher droplet acceleration makes the RT instability to grow faster for higher Weber number sprays.

The breakup of droplet parcels is calculated by assuming that the radius of newly formed droplets is proportional to the frequency of the fastest growing surface wave and its corresponding wavelength. The radius of new droplets (r_c) formed from the parent droplets radius (r_p) is given by Eqn. (4) as

$$r_c = B_{KH}\Lambda_{KH} \qquad (4)$$

Beyond the breakup length from the nozzle exit, RT model is used to describe the secondary breakup of the spray droplets. According to Levich theory, length of the liquid core (L_{brk}) is expanded in Eqn. (5) as

$$L_{brk} = C_b d_{noz} \sqrt{\frac{\rho_l}{\rho_g}} \qquad (5)$$

To reduce the time step dependency of the RT model, the RT breakup process is modeled by a rate equation similar to that of the KH model is given by Eqn. (6) as

$$\frac{dr_p}{dt} = -\frac{r_p - r_c}{\tau_{RT}} \qquad (6)$$

In practice, the rate equation for both KH and RT model cannot be solved analytically. Since r_c and τ_{RT} changes with time, liquid-gas relative velocity can change significantly. Therefore, a sub cycle approach is used to solve these rate equations to eliminate time-step dependency.

The mesh dependency of the KH-RT breakup model is greatly influenced by the liquid-gas relative velocity calculation, where the $\vec{V}_{gas}$ is taken to be the CFD cell gas velocity. A separate unsteady gas jet model is used along with the KH-RT model to remove the mesh-size dependency for the liquid droplet-ambient gas coupling. The unsteady gas jet theory of gas jet model reveals that the axial droplet-gas relative velocity is modeled without using discretization on the CFD mesh [5].

The radius of influence (ROI) collision model is used to remove numerical dependencies on mesh-size and time-step in droplet collision process. The theory states that one particle is allowed to collide with other only if this particle resides within the radius of influence of other. A discrete multi-component vaporization model is used to track the individual components of the fuel during evaporation process and allows coupling with the reaction kinetics of individual fuel components.

COMBUSTION MODELING

The detailed chemical reaction kinetics of a spark ignition engine is characterized by flame initiation around the spark location followed by flame propagation into the combustion chamber. The discrete particle ignition kernel (DPIK) flame model was used for flame initiation modeling followed by a G-equation model to track the

turbulent flame speed. A switch constant, determined from mesh size and turbulence models, used for calculating the switch between kernel flame to G-equation model. After spark initiation, a flame kernel of certain radius produces, which is of order 3 to 4 times smaller than the average computational mesh size. DPIK model proposed by Tan et al. [6] uses a Lagrangian marker to track the particle flame growth of initial flame kernel development. Particles present in the computational cells are tracked in order to track the flame kernel surface position. Therefore, the requirement of the fine computational mesh is reduced, and flame growth can be captured accurately in coarse mesh too, reducing the mesh size dependency. The growth rate of flame kernel radius is dependent on plasma velocity, and turbulent flame velocity is given by Eqn. (7) as

$$\frac{dr_k}{dt} = \frac{\rho_u}{\rho_k}\left(S_{plasma} + S_T\right) \tag{7}$$

Effect of turbulent burning velocity in this equation is very significant, which is found in Peter [6-7].Laminar flame speed Model governs the flame speed behavior with the varying conditions of temperature, pressure and equivalence ratio inside the combustion chamber.Switching from ignition model to combustion model takes place after a threshold flame kernel radius limit, which is related to integral turbulent length scale as given by Eqn.(8). After that, DPIK model is inactive, and G-equation model plays a dominant role in combustion modeling.

$$r_k \geq C_{m1}.l = C_{m1} * 0.16\frac{k^{\frac{3}{2}}}{\varepsilon} \tag{8}$$

After the flame kernel development inside the cylinder, the complete combustion mechanism is ready to take place. On a fully developed flame, It is assumed that the mean flame front has zero thickness separating unburned region from burned one. Turbulence formed within the cylinder creates very small turbulent eddies that make the flame front more distorted and strained which makes it different than laminar flame.Therefore, arbitrarily shaped turbulence flame contour propagates till it quenches or extinct near the cylinder wall. The mean flame front is the ensemble average of the instantaneous location of all the flame particles present in the flame surface boundary. To determine the exact location of the turbulent flame front, G-equation is used, where G is a scalar function of space and time. Transport of this scalar function models the flame propagation and accumulation of unburned charge as flame continues to move. It is assumed that mixture is completely burned behind the flame front. Along with G-equation model, flamelet concept of Peter [8] gives mass conservation of individual species after the chemical reaction that takes place, to form combustion products. This states the flow transport and species conservation is individually solved by G-equation and continuity equationrespectively.The governing equation for transportation of turbulent flame front by Peter is given by Eqn. (9) as [9]

$$\frac{\partial \tilde{G}}{\partial t} + \tilde{\vec{v}}_f \cdot |\nabla \tilde{G}| = \frac{\bar{\rho}_u}{\bar{\rho}} s_t^0 \nabla \tilde{G} - D_t \tilde{k}_M |\nabla \tilde{G} \tag{9}$$

A value of $G(\vec{x}, t)$=0 is defined for turbulent flame front. $G > 0$ indicates burned gas regime on the other hand$G < 0$ indicates unburned regime.

SAMPLE OF RESULTS

The simulation was performed with the developed numerical model at 2000 rpm and compression ratio 8 in a spark ignition gasoline premixed combustion engine. The global mesh size was varied from 2.5 mm to 4 mm for mesh sensitivity analysis. Figure 2 shows the optimized mesh size for numerical simulation.
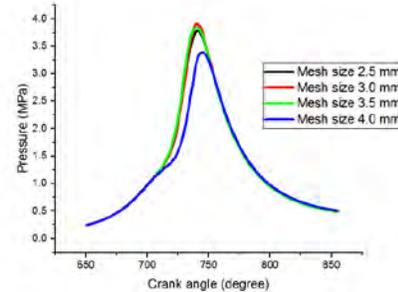
FIGURE 2. MESH SENSITIVITY ANALYSIS

REFERENCES

[1] Huang, Y., 2014. "Development of a numerical model for investigating the EDI+GPI engine". 19th Australasian Fluid Mechanics Conference, Melbourne, Australia.

[2] Yakhot, V., Orszag, S.A., Thangam, S., Gatski, T.B. and Speziale, 1992. "Development of turbulence models for shear flows by a double expansion technique". Physics of Fluids A: Fluid Dynamics, 4, July, pp. 1510-1520.

[3] Verma, I., 2016. "CFD modeling of spark ignited gasoline engines-part 2: Modeling the engine in direct injection mode along with spray validation". SAE Technical paper, 2016-01-0579.

[4] Bellman, R., and Reitz, R., 1999. "Modeling spray atomization with the Kelvin-Helmholtz / Rayleigh-Taylor hybrid model". Atomization and spray, 9, pp. 623-650.

[5] Abani, N., and Reitz, R., 2007. "Unstaedy turbulent round jets and vortex motion". Physics of Fluids, 19, 125102.

[6] Tan, Z., and Reitz, R., 2006. "An ignition and combustion model based on the level-set method for spark ignition engine multidimensional modeling".Combustion and Flame, 145, April, pp. 1-15.

[7] Peters, N., 1999. "The turbulent burning velocity for large-scale and small-scale turbulence". Journal of Fluid Mechanics, 384, April, pp. 107-132.

[8] Peters, N., 1988. "Laminar flamelet concepts in turbulent combustion". Symposium (International) on combustion, 21, pp. 1231-1250.

[9] Peters, N., 2001. "Turbulent combustion". Cambridge University Press, Cambridge, Chap. 2, pp. 66–169.

FUNCTIONAL GROUP BASED ARTIFICIAL NEURAL NETWORK FOR PREDICTING OCTANE NUMBER OF OXYGENATED FUELS

Abdul Gani Abdul Jameel
King Abdullah University of Science and
Technology, Clean Combustion Research Center,
Thuwal, Saudi Arabia
Email: abdulgani.abduljameel@kaust.edu.sa

Mani S.Sarathy
King Abdullah University of Science and
Technology, Clean Combustion Research Center,
(KAUST), Thuwal, KSA
Email: mani.sarathy@kaust.edu.sa

Vincent V. Oudenhoven
King Abdullah University of Science and
Technology, Clean Combustion
Research Center, Thuwal, Saudi Arabia
&
University of Waterloo
Email:
vincentvanoudenhoven@gmail.com

ABSTRACT

A model for the prediction of research octane number (RON) and motor octane number (MON) of gasoline fuels containing oxygenates has been developed using artificial neural networks (ANN) and ^{1}H nuclear Magnetic Resonance (NMR) spectroscopy. RON and MON of 125 pure compounds and 150 blends of hydrocarbons of known composition, FACE (fuels for advanced combustion engines) gasolines and ethanol were utilized as a dataset. The effect of weight % of functional groups such as paraffinic CH_3 groups, paraffinic CH_2 groups, paraffinic CH groups, olefinic $CH-CH_2$ groups, naphthenic $CH-CH_2$ groups, aromatic C-CH groups and alcoholic OH groups on RON and MON was studied. The effect of branching (i.e., methyl substitution) on RON and MON was also studied, and a parameter denoted as the branching index (BI) was introduced to quantify this effect. The developed ANN model was validated against experimentally measured RON and MON of gasoline-ethanol blends; the absolute predicted values matched well with the experimental data with an absolute error of 1.58 for RON and 1.32 for MON.

Keywords: research octane number (RON), motor octane number (MON), functional group, ANN.

INTRODUCTION

Octane number is a measure of a fuel's resistance to knocking. Gasolines with high octane numbers can withstand higher compression ratios inside an engine, and therefore are used in high performance engines. Ethanol is used as an octane booster and blended with gasoline worldwide to meet the demand for high octane fuels. Research octane number (RON) and motor octane number (MON) are the two most commonly employed octane ratings used today. RON of a gasoline is measured by running the fuel in a cooperative fuel research engine (CFR) and comparing the results obtained with blends of n-heptane and iso-octane as specified by ASTM D2699-16 method [1]. MON is also measured in a CFR engine but under more intense conditions of engine speed, variable spark timing and with a preheated fuel mixture as specified by ASTM D2700-16a method [2]. Both these methods employed for measurement of RON and MON are time consuming, expensive, and labour intensive.

The aim of the present work is to develop a new model for the prediction of RON and MON of gasoline fuels containing alcoholoic oxygenates using ^{1}H NMR spectroscopy. RON and MON of of 125 pure compounds and 150 blends comprising n-heptane, iso-octane, toluene, 1-hexene, cyclopentane, 1,2,4-trimethylbenzene, FACE F

gasoline, FACE G gasoline and ethanol were measured or obtained from literature. The dataset was used to study the relationship between RON and MON and the eight functional groups calculated from their composition. The eight parameters include weight % of paraffinic CH_3 groups, paraffinic CH_2 groups, paraffinic CH groups, olefinic CH-CH_2 groups, naphthenic CH-CH_2 groups, aromatic C-CH groups, ethanol content and a new parameter called as branching index (BI) introduced by Abdul Jameel et al. [3]. Artificial neural networks (ANN) were used to analyze the relationship between the nine parameters and RON and MON. There is a non-linear increase in RON and MON of a gasoline when ethanol (an octane booster) is added to it [4]. Sennot et al. [5] developed a ANN model to predict the cetane number of biofuel candidates using the molecular structure. Abdul Jameel et al. [6] developed a correlation to predict RON and MON of gasoline-ethnaol blends using MLR, whose accuracy was limited.Therefore, ANN were used for this study because they are able to capture non-linear, and complex relationships between input features and the output of interest (RON and MON) effectively. Pasadakis et al. [7] have developed an ANN model to predict RON of gasoline blends using the chemical classes in the fuel as inputs. Meusinger et al. [8] have also developed asn ANN based based to predict ON using the information from ^{13}C NMR spectroscopy. ANN are computational models consisting of interconnected nodes, loosely comparable to neurons in the brain, which in turn represent 'features' or attributes of the analyzed dataset. These nodes are structured in layers and this allows for the learning of complex relations between the given input and output.

METHODOLOGY: ANN

In order to capture the non-linearity, and the presumed complexity between the input features and the respective output, whilst keeping prediction as priority, neural networks were the tool of choice for this problem. A feedforward ANN was used, minimizing the errors using backpropagation. Multiple architectures were tested to arrive at the best model that produced the least error. The data used was split up randomly in to test and train sets, 25% and 75%, respectively. The test set is fixed, and was used for the evaluation of each algorithm, for both RON and MON. Due to the limited dataset, having a separate validation set would lead to a significant drop in overall learning capabilities – instead K-fold Cross. Validation was used for model selection. The basic principle is to split up the training set in to K subsamples, of which one is chosen as the validation set, and the others make up the train set; this is rotated until each sample has been tested on. The evaluation of the model consists of the average over the tested folds. Finally the accuracy of the model is evaluated on the test set that was separated from the beginning. This leads to a robust, and more general model, while at the same time having a realistic measurement of the expected accuracy. Neglecting a validation set, optimizing hyper parameters

and extending number of units in each layer can lead to indirect overfitting. Although changes to such parameters are critical for obtaining the ideal solution – it is possible to obtain seemingly good results by mere chance that do not generalize well. Additionally, since the dataset has a relatively high number of parameters spanning large ranges in comparison to training examples, it is implausible to encompass fully representative information in to subsets of the data. Using K-fold CV avoids this problem and overcomes the innate variance of the dataset, without prioritizing particular examples over others.

EXPERIMENTAL

All ^1H NMR experiments were recorded at 298 K using Bruker 700 AVANAC III spectrometer equipped with Bruker CP TCI multinuclear CryoProbe (BrukerBioSpin, Rheinstetten, Germany). The sample was prepared by dissolving 50 µl of the fuel sample in 700 µl of deuterated chloroform CDCl3. The samples were vortexed for 30 seconds and then 600 µl of the solution was transferred to 5 mm NMR tubes. 1H NMR spectra were recorded by collecting 128 scans with a recycle delay time of 5s, using standard 1D 90o pulse sequence using standard (zg) program from Bruker pulse library. Chemical shifts were adjusted using Tetramethylsilane (TMS) as an internal chemical shift reference. The spectra were collected with spectral width of 20 ppm corresponding to 14098 Hz digitized into 64k data points. An exponential function equivalent to a 0.3 Hz line broadening was applied before Fourier transform. Table 1 shows he chemical shifts used in the present work.

TABLE 1: ^1H NMR ASSIGNMENTS

Chemical shift region (ppm)	H type
6.42 – 8.99	Aromatics
4.50 – 6.42	Olefinic CH and CH_2 groups
3.78 – 3.68	Alcohol OH groups
2.88 – 3.40	α-CH
2.64 – 2.88	α-CH_2
2.04 – 2.64	α-CH_3
1.57 – 1.96	Naphthenic CH and CH_2 groups
1.39 – 1.57	Paraffinic CH groups
0.94 – 1.39	Paraffinic CH_2 groups
0.25 – 0.94	Paraffinic CH_3 groups
0.84 – 0.87	Paraffinic CH_3 groups connected to the longest chain towards the interior
1.35 – 1.39	Paraffinic CH_2 groups connected to the longest chain towards the interior
2.31 – 2.34	α-CH_3 groups in the meta position with respect to other α-CH_3 groups
2.17 – 2.19	α-CH_3 groups in the para position with respect to other α-CH_3 groups

RESULTS & DISCUSSION

The effect of each of the functional groups on RON and MON was studied from the developed dataset and is presented below.

Parraffinic CH₃

The ignition quality of paraffinic fuels depends on the presence and the degree of the methyl substitution. Experiments conducted in a constant volume combustion chamber with blends of different C16 iso-paraffins show increased ignition delays with increasing number of methyl branches. Fig. 1. Shows the effect of paraffinic CH_3 content on RON and MON of the blends. It can be observed that as the paraffinic CH_3 content in the blends increases both RON and MON decrease quite rapidly. However, in the blends containing 1,2,4-trimethylbenzene and ethanol we see that an increase of paraffinic CH_3 content increases both the RON and MON. This is because ethanol is a better octane booster than 1,2,4-trimethylbenzene. As the ethanol content is gradually increased in the blend, the net RON and MON of the blends decreases and so does the methyl groups connected to 1,2,4-trimethylbenzene.
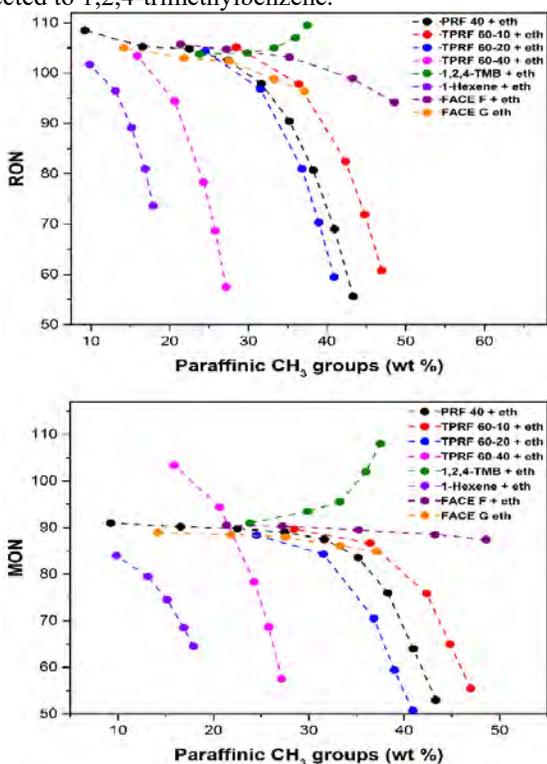
FIGURE 1: Effect of paraffinic CH_3 groups on RON and MON of the blends

Parraffinic CH₂

It has been experimentally demonstrated that mass fractions of paraffinic CH_3 and paraffinic CH_2 groups in paraffinic fuels has a significant effect on their combustion characteristics. Lapuerta et al. [9] have shown that blends of C16 iso-paraffin isomers that possess the same CH_2/CH_3 mass ratio have the same IDT which indicates that CH_2/CH_3 ratio as an important factor that effects ignition. Fig. 2. Shows the effect of the paraffinic CH_2 content on RON and MON of the blends. It can be observed from the figure that as the paraffinic CH_2 content of the blend increases the RON and MON decreases steadily for all the blends.

Parraffinic CH

The effect of paraffinic CH groups on RON and MON of the blends is shown in Fig. 3. It can be observed from the figure that as the paraffinic CH content of the blend increases the RON and MON decreases rapidly for all the blends. The decrease in RON and MON is rapid especially for the blends containing TPRF and ethanol. The increase in CH groups is an indication of the increase in the degree of branching of the molecules. Ghosh et al. [10] have showed for molecules with an increasing degree of branching the RON and MON increases. We see an opposing trend here. This is because the composition of the blends has a high percentage of ethanol content that is devoid of any paraffinic CH groups. Therefore, the true effect of branching is masked. This also shows that the ethanol content has a more severe effect on RON and MON than all the other paraffinic groups discussed above.
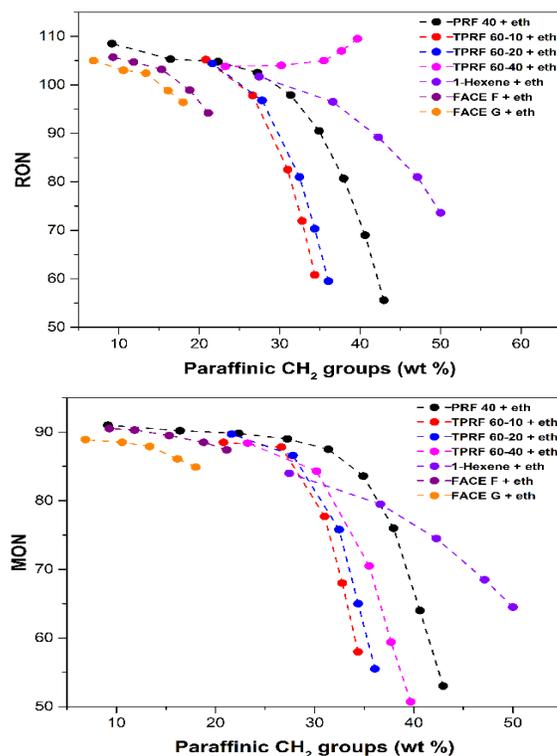
FIGURE 2. Effect of paraffinic CH_2 groups on RON and MON of the blends
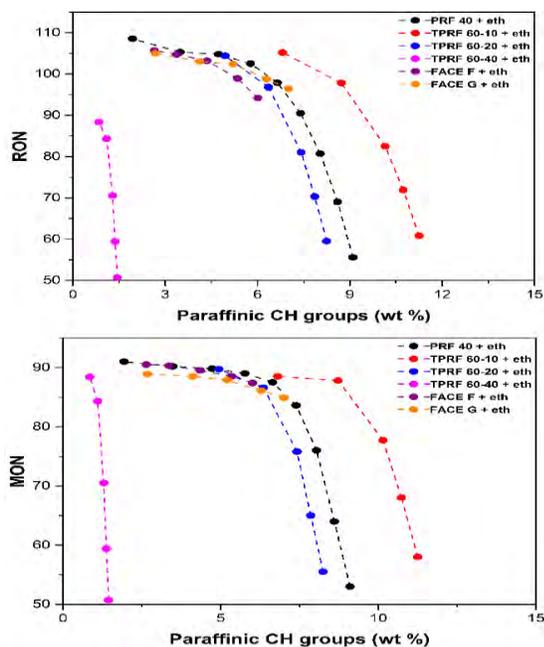
FIGURE 3. Effect of paraffinic CH groups on RON and MON of the blends

Validation

The test data comprised of 62 points (25 % of the dataset) that was randomly selected to validate the developed ANN model comprising of pure compounds, blends of known compoistions and test FACE gasoline –ethanol blends. There is good comparison between the experimental and the predicted values of RON and MON as shown in Fig. 4. The value of R^2 obtained for both the cases was 0.98. Some of the points showed an absolute error of prediction of upto 6.5. This could be due to a number of reasons like experimental error, purity of the components tested etc.
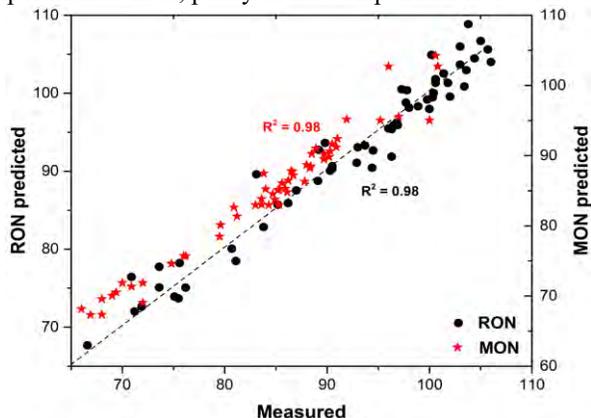
FIGURE 4: Comparison of experimental and predicted RON and MON values

The average error of predicton for RON and MON was found to be 1.58 and 1.32 which is well within the experimental eror of RON/MON measurement using the CFR engine. The developed model can be used to predict the octane numbers of pure compounds and blends. It can also be used to design fuels of a specified RON and MON. The RON/MON of oxygenated gasoline fuels can be predicted with a knowledge of the ^{1}H NMR spectra.

CONCLUSION

In the present work an ANN model was developed to predict the RON and MON of pure compounds, blends and oxygenated gasolione fuels using ^{1}H NMR spectra of the fuel. RON and MON values of 125 pure compounds and 150 blends of hydrocarbons and gasoline's with ethanol was formulated and this was used as a dataset to study the relationship between the ON and eight functional groups. The developed model was validated with FACE gasoline's blended with ethanol. There was a good correlation (R^2 =0.98) between the measured and the predicted values.

ACKNOWLEDGEMENT

REFERENCES

[1]   ASTM Int., Standard Test Method for Research Octane Number of Spark-Ignition Engine Fuel 1, 2012.

[2]   ASTM Int., Standard Test Method for Motor Octane Number of Spark-Ignition Engine Fuel 1, 2011.

[3]   A.G. Abdul Jameel, N. Naser, A.-H. Emwas, S. Dooley, S.M. Sarathy, Predicting Fuel Ignition Quality Using 1 H NMR Spectroscopy and Multiple Linear Regression, Energy & Fuels. 30 (2016) 9819–9835.

[4]   J. Badra, A.S. AlRamadan, S.M. Sarathy, Optimization of the octane response of gasoline/ethanol blends, Appl. Energy. 203 (2017) 778–793.

[5]   T. Sennott, C. Gotianun, R. Serres, M. Ziabasharhagh, J.H. Mack, R. Dibble, Artificial Neural Network for Predicting Cetane Number of Biofuel Candidates Based on Molecular Structure, in: Vol. 2 Fuels; Numer. Simulation; Engine Des. Lubr. Appl., ASME, 2013: p. V002T02A009.

[6]   A.G. Abdul Jameel, S.M. Sarathy, Prediction of RON and MON of gasoline-ethanol using 1 H NMR spectroscopy, in: Proc. Eur. Combust. Meet. 2017.

[7]   N. Pasadakis, V. Gaganis, C. Foteinopoulos, Octane number prediction for gasoline blends, Fuel Process. Technol. 87 (2006) 505–509.

[8]   R. Meusinger, R. Moros, Determination of octane numbers of gasoline compounds from their chemical structure by 13C NMR spectroscopy and neural networks, Fuel. 80 (2001) 613–621.

[9]   M. Lapuerta, J.J. Hernández, S.M. Sarathy, Effects of methyl substitution on the auto-ignition of C16 alkanes, Combust. Flame. 164 (2016) 259–269.

[10]   P. Ghosh, K.J. Hickey, S.B. Jaffe, Development of a Detailed Gasoline Composition-Based Octane Model, (2006) 337–345.

SEEC-2018-009

PERFORMANCE ANALYSIS OF SOLAR AIR HEATER WITH FINS AND PERFORATED TWISTED TAPE INSERTS

Rajesh Kumar	Prabha Chand
Department of Mechanical Engineering	Department of Mechanical Engineering
National Institute of Technology, Jamshedpur,	National Institute of Technology, Jamshedpur,
Jharkhand, India-831014	Jharkhand, India-831014
Email: rjsh.nitjsr@ gmail.com	Email: pchand.me@nitjsr.ac.in

ABSTRACT

The present paper deals with analytical investigation on the thermal and thermo-hydraulic performance of the solar air collector fitted with fins and perforated twisted tapes (PTT) of twist ratio 2 with different axial pitch ratio (S_x / p). The mathematical models are presented and the effect of mass flow rate and axial pitch ratios on the thermal and effective efficiency has been discussed. The results obtained are compared with the results of the solar air heater without fins and twisted tapes. Results conveyed that the collectors with fins and perforated twisted tape perform better but at the expense of increased pressure drop. Also, twisted tape with minimum axial pitch ratio is found to be more efficient than others.

Keywords: **Solar air heater, Thermal efficiency, Twisted tape, axial pitch ratio.**

NOMENCLATURE

Nomenclature	
A_P	Absorber plate area(m^2)
I	intensity of solar radiation (W/m^2)
$\dot{m}$	mass flow rate(kg/s)
N	Nuber of fins.
η_{th}	thermal efficiency
(S_x / p)	different axial pitch ratio.
$T_g, T_p,$ T_f, T_b	mean temperature of glass cover, absorber plate,air and bottom plate respectively(K)

INTRODUCTION

Solar air heater is a special kind of heat exchanger which absorbs the sun radiation and transfer air to the flowing air inside the duct. The heated air is used for space heating, crop drying, seasoning of timber etc. [1]. The heat transfer can be augmented by use of various passive techniques e.g. fins, ribs, roughness, twisted tape inserts etc. [2]. Yao et al. [3] evaluated the performance of all-glass evacuated tube solar water heater with twist tape inserts and showed that the twist tape inserts augment heat transfer at comparatively higher temperature. Ghadirijafarbeigloo et al. [4] worked with louvered twisted-tape in a receiver tube of solar parabolic trough concentrator. Jaisankar [5] performed experimental analysis on heat transfer and friction factor characteristics of forced circulation solar water heater system fitted with helical twisted tapes and developed correlations for Nusselt number and friction factor with various twist ratios. Raja Sekhar et al. [6] studied the performance of solar thermal heater with Al$_2$O$_3$ nano-fluids and twisted tapes in a pipe. Saha and co-workers [7–8] did an experimental analysis of laminar flow through square and rectangular ducts with twisted tapes types vortex generator along with oblique teeth, axial corrugations, transverse ribs and wire coil inserts.

The present work focuses on the theoretical investigation of the performance of solar air heater with fins and twisted tape inserts.

THEORETICAL ANALYSIS

Fig.1. shows the schematic diagram of solar air heater fitted with fins and twisted tape inserts below the absorber plate.

A. ENERGY BALANCE EQUATIONS:

Steady state energy balance equation for different components of solar air heater can be written as:

Glass cover:

$$\alpha_g I + (h_{r,pg} + h_{c,pg})(T_p - T_g) = (h_w + h_{r,ga})(T_g - T_a)$$

$$(1)$$

Absorber plate:

$$I\alpha_p\tau_g = (h_{r,pg} + h_{c,pg})(T_p - T_g) + h_{r,pb}(T_p - T_b)$$
$$+ h_{c,pf}(T_p - T_f) + (NA_3 / A_p)(T_p - T_f) \tag{2}$$

Bottom plate:

$$h_{r,pb}(T_p - T_b) + h_{c,fb}(T_f - T_b) = U_b(T_b - T_a) \tag{3}$$

Air:

$$h_{c,pf}(T_p - T_f) + (NA_3 / A_p)(T_p - T_f)$$
$$= 2(\dot{m}c_p / A_p)(T_f - T_i) + h_{c,fb}(T_f - T_b) \tag{4}$$

where, $A_3 = \dfrac{mk_{fn}A_{fn}\left[\sinh A_1 + A_2\cosh A_1\right]}{\cosh A_1 + A_2\sinh A_1}$

in which $A_1 = mH_f$ and $A_2 = h_{c,pf} / mk_{fn}$
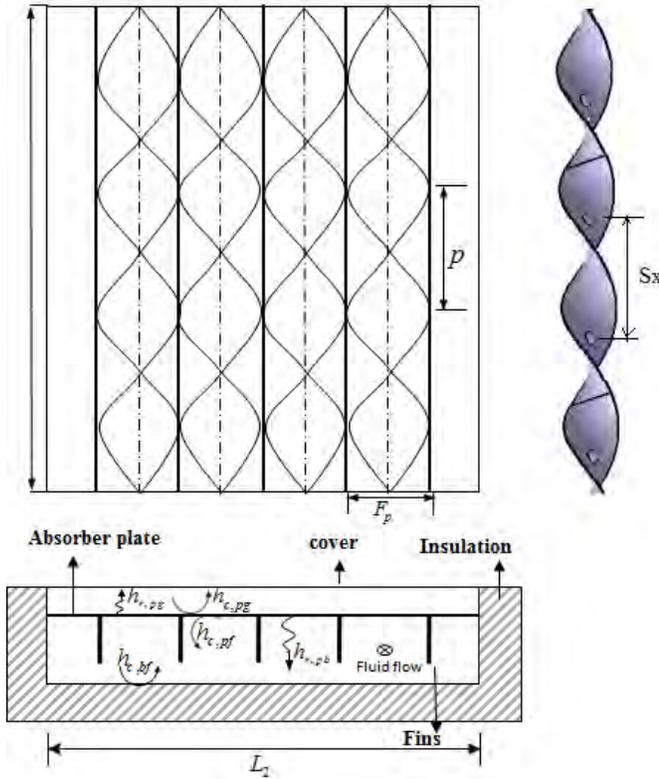
Absorber plate   **cover**   **Insulation**

FIG. 1 SCHEMATIC DIAGRAM OF SOLAR AIR
HEATER WITH FINS AND PERFORATED TWISTED
TAPE INSERTS

Eqns. (1)-(4) can be arranged in the form of 4x4 matix in the form of $[A]\,[T] = [C]$

$$\begin{bmatrix} a_{11} & a_{12} & 0 & 0 \\ a_{21} & a_{22} & a_{23} & a_{24} \\ 0 & a_{32} & a_{33} & a_{34} \\ 0 & a_{42} & a_{43} & a_{44} \end{bmatrix} \begin{bmatrix} T_g \\ T_p \\ T_b \\ T_f \end{bmatrix} = \begin{bmatrix} C_1 \\ C_2 \\ C_3 \\ C_4 \end{bmatrix} \tag{5}$$

$a_{11} = h_{r,pg} + h_{c,pg} + h_w + h_{r,ga}T_g$, $a_{12} = -(h_{r,pg} + h_{c,pg}) = -a_{21}$

$a_{22} = h_{r,pg} + h_{c,pg} + h_{r,pb} + h_{c,pf}$, $a_{23} = h_{r,pb} = a_{32}$

$a_{24} = h_{c,pf} + (NA_3 / A_p) = -a_{12}$, $a_{33} = -(h_{r,pb} + h_{c,fb} + U_b)$,

$a_{34} = h_{c,fb} = a_{43}$, $a_{44} = -(NA_3 / A_p + 2(\dot{m}c_p / A_p) + h_{c,fb})$

$C_1 = \alpha_g I + (h_w + h_{r,ga})T_a$ $C_2 = I\tau_g\alpha_p$, $C_3 = -U_bT_a$,

$C_{44} = 2\dot{m}c_p / A_p$

The four unknown Tg, Tp, Tb, and Tf can be determined by inverse matrix $[T] = [A]^{-1}[C]$

B. HEAT TRANSFER COEFFICIENTS:

Convective heat transfer coefficient due to wind velocity can be given by the relation [9]

$$h_w = 2.8 + 3.0V_w \tag{6}$$

The radiative heat transfer coefficient between the glass cover and ambient air, absorber plate and glass cover, absorber plate and bottom plate and free convection heat transfer coefficient of air between glass cover and absorber plate can be written as: [10]

$$h_{r,ga} = \sigma\varepsilon_g(T_g^4 - T_s^4) / (T_g - T_a) \tag{7}$$

where T_s is sky temperature and is given by [11]

$$T_s = 0.0552T_a^{1.5} \tag{8}$$

$$h_{r,pg} = \frac{\sigma(T_p^2 + T_g^2)(T_p + T_g)}{1/\varepsilon_p + 1/\varepsilon_g - 1} \tag{9}$$

$$h_{r,pb} = \frac{\sigma(T_p^2 + T_b^2)(T_p + T_b)}{1/\varepsilon_p + 1/\varepsilon_b - 1} \tag{10}$$

$$h_{c,pg} = Nu_{pg} / L \tag{11}$$

Nu_{pg} is the Nusselt number between absorber plate and glass cover and can be determined as [12]

$$Nu_{pg} = 1 + 1.44\left[1 - (1708(\sin 1.8\beta)^{1.6} / Ra\cos\beta)\right]$$
$$\left[1 - (1708 / Ra\cos\beta)\right]^{+}\left[\left(Ra\cos\beta / 5803\right)^{1/3} - 1\right]^{+} \tag{12}$$

where β is plate tilt angle and + superscript means only positive value is to be used for the terms in the square bracket.

The Rayleigh number Ra can be expressed as

$$Ra = g\beta'(T_p - T_g)L^3 / v\alpha \tag{13}$$

where β' is the volumetric coefficients of expansion given by $\beta' = 1/T$ in which $T = (T_p + T_g)/2$ (in Kelvin)

For calculating the Ra, properties are taken at mean temperature of plate and glass temperature.

Correlations are required to determine the heat transfer coefficient of heated air in the duct.

For turbulent flow in rectangular channel, the correlation based on Kay's data [13] is used to determine the heat transfer coefficient

$$Nu_{pb} = 0.00158(\text{Re})^{0.8} \tag{14}$$

For turbulent flow inside the channel with perforated twisted tape the equation given by Yaningsih et al [14] can

be used to predict heat transfer coefficients.

$$Nu_{pb} = 0.03\,\mathrm{Re}^{0.842}\,\mathrm{Pr}^{0.3}(S_x/\mathrm{p})^{-0.195} \qquad (15)$$

Convective heat transfer coefficient for air between absorber plate and bottom plate can be calculated as follow:

$$h_{c,pf} = h_{c,bf} = Nu_{pb}k_{air}/D_h \qquad (16)$$

The pressure drop across the duct can be calculated by the expression

$$\Delta p = 4f\rho L_1 V^2/2D_h \qquad (17)$$

in which 'f' is the fanning friction factor and can be determined by the following expression:
For turbulent flow in the duct with twisted tape the relation Yaningsih et al [14] can be used

$$f = 8.009\,\mathrm{Re}^{-0.46}(S_x/\mathrm{p})^{-0.173} \qquad (18)$$

For the duct without twisted tape inserts the following relation can be used to predict the friction factor.

$$f = 0.079\,\mathrm{Re}^{-0.25} \qquad (19)$$

A. Performance of solar air heater:

Thermal efficiency of the solar collector is the ratio of useful heat energy gain to the total incident radiation on the collector during any period of time.

$$\eta_{th} = Q_u/IA_c \qquad (20)$$

The useful heat gain can be obtained from the expression

$$Q_u = 2\dot{m}c_p(T_f - T_i) \qquad (21)$$

in which T_f is mean temperature of working fluid.
The real economic performance of solar collector is evaluated in terms of thermohydraulic efficiency or effective efficiency defined as [15]

$$\eta_{eff} = \frac{Q_u - (P_{mech}/C)}{IA_c} \qquad (22)$$

where P_{mech} is the mechanical power required to overcome the pressure loss across the duct.

$$P_{mech} = \dot{m}\Delta P/\rho \qquad (23)$$

C is conversion factor which represents the conversion of thermal power to mechanical power of fan or blower. The recommended value of C is 0.18 [15].

RESULTS AND DISCUSSIONS

To study the present model numerical calculation has been made. For this codes have been developed in MATLAB-14 using the following fixed system and design parameters:
$L_1 = 1.2\,\mathrm{m}$, $L_2 = 0.4\,\mathrm{m}$, $H = 0.03\,\mathrm{m}$, $L = 0.04\,\mathrm{m}$,

$H_f = 0.03\,\mathrm{m}$, $t_{ins} = 0.006\,\mathrm{m}$, $t_f = 0.001\,\mathrm{m}$, $F_p = 3\mathrm{cm}$,

$V_w = 2.5\,\mathrm{m/s}$, $k_{ins} = 0.05\mathrm{W/mK}$, $k_{fn} = 50\mathrm{W/mK}$, $I = 900\mathrm{W/m}^2$

$\dot{m} = 0.019 - 0.07\,\mathrm{kg/s}$, $T_i = 303\mathrm{K}$, $T_a = 300\mathrm{K}$, $\alpha_g = 0.11$,

$\alpha_p = 0.96$, $\varepsilon_p = 0.95$.

Fig.2 shows the variation of Nusselt number with mass flow rate for smooth and PTT solar air heater for various axial pitch ratios. As mass flow rate increases Nusselt number increase for all axial pitch ratios this is due to increase velocity of air at higher mass flow rate. Also at lowest axial pitch ratio Sx/p=0.5 highest Nusselt number is observed.
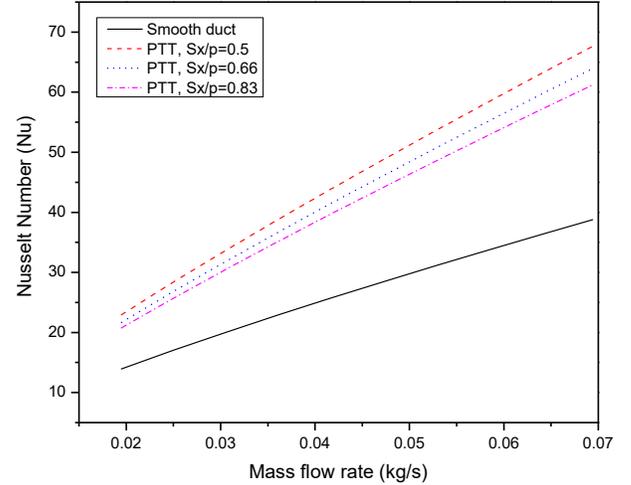
FIG. 2 VARIATION OF NUSSELT NUMBER WITH MASS FLOW RATE.

The thermal efficiency as a function of mass flow rate is plotted in fig.3 for smooth as well twisted tape absorber solar air heater for different axial pitch ratios. From fig it is observed that the thermal efficiency rises with increasing mass flow rate. This is attributed to increased Nusselt number at higher mass flow rate as depicted by fig.2. The thermal efficiency increases with decrease in axial pitch ratios. At fixed mass flow rate of 0.036 kg/s, addition of perforated twisted tape of axial pitch ratio 0.5 enhances the thermal effficency by18%.
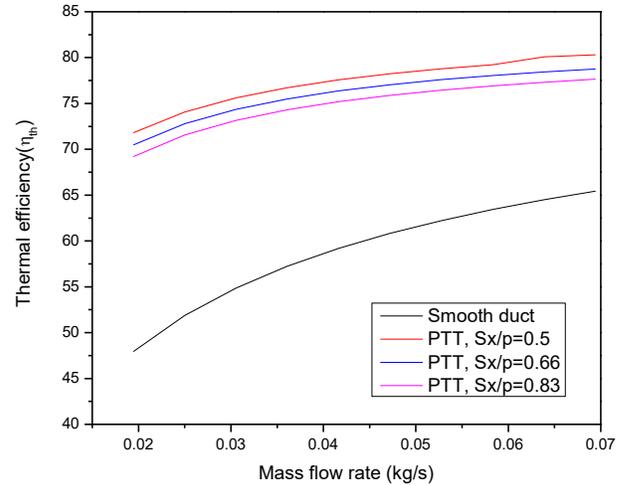
FIG. 3 THERMAL EFFICIENCY AS A FUNCTION OF MASS FLOW RATE.

The effect of mass flow rate on pressure drop across the duct fitted with fins and perforated twisted tape inserts for

different axial pitch ratio is shown in fig.4. The figure shows that with increasing air flow rate the pressure loss increases and for a given mass flow rate, the pressure loss for the solar air heater fitted with Perforated twisted tape is higher than that of without fins and twisted tapes. This is due to flow mixing and formation of vortex inside the duct. Decrease in axial pitch ratio results in increased pressure drop.
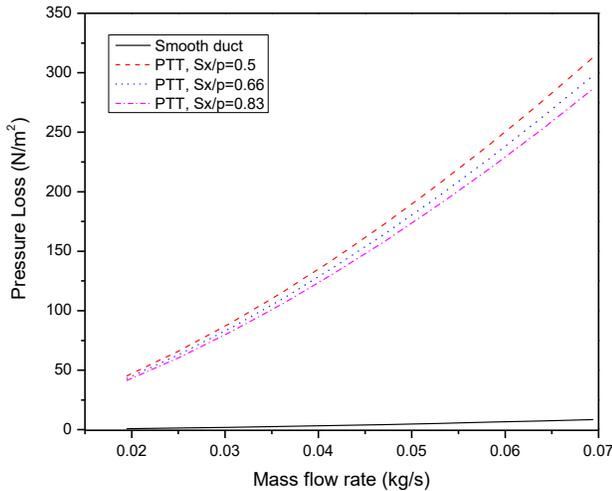
FIG. 4. EFFECT OF MASS FLOW RATE ON THE
PRESSURE LOSS ACROSS THE DUCT.
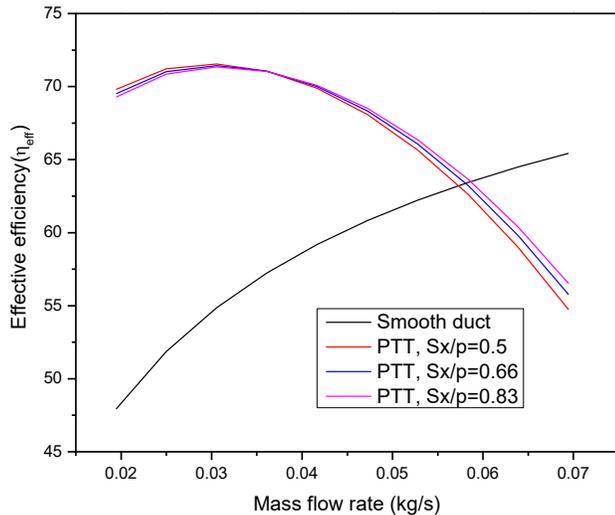
FIG. 5 VARIATION OF EFFECTIVE EFFICIENCY
WITH RESPECT TO MASS FLOW RATE.

The influence of perforated twisted tapes with three axial pitch ratios (Sx/p = 0.5, 0.66 and 0.83) on the thermo-hydraulic or effective efficiency with mass flow rate is shown in fig.5. The effective efficiency of smooth solar air heater is also plotted for comparison. For all cases except for the smooth solar air heater the effective efficiency first rise up to mass flow rate of 0.03 kg/s and then they drop. This is because of the fact that as the mass flow rate increases both the useful heat gain and pressure drop increase but for lower

range of mass flow rate increase in useful heat gain dominates over increase in pressure drop so effective efficiency increases whereas at higher mass flow rate increase in pressure drop across the duct dominate over the rate of increase in useful heat gain and hence effective efficiency decline. In smooth solar air heater pressure loss is not much more pronounced so effective efficiency goes on increasing.

CONCLUSIONS

The theoretical analysis has been carried out to investigate the performance of solar air heater fitted with fins and perforated twisted tape of twist ratio 2 and various axial pitch ratios (Sx/p) of 0.5, 0.66 and 0.83. Based on the results obtained it may be concluded that addition of fins and perforate twisted tapes result in substantial enhancement in the thermal efficiency due better fluid mixing, however, the pressure loss associated with the duct increases. Twisted tape with lowest axial pitch ratio performs thermally better than that of higher axial pitch ratio.

REFERENCES

[1]. Duffie JA, Beckman WA. Solar Engineering of Thermal Processes. Wiley, New York; 1980.
[2]. Webb RL, Kim NH. Principles of Enhanced Heat Transfer. Wiley, New York; 1994.
[3]. Yao K, Li T, Tao H, Wei J, Feng K. Performance evaluation of all-glass evacuated tube solar water heater with twist tape inserts using CFD, Energy Procedia, vol. 70, pp. 332-339, 2015
[4]. Ghadirijafarbeigloo S, Zamzamian AH, Yaghoubi M. 3-D numerical simulation of heat transfer and turbulent flow in a receiver tube of solar parabolic trough concentrator with louvered twisted- tape inserts. Energy Procedia, vol. 49, pp. 373-380, 2014.
[5]. Jaisankar S, Radhakrishnan TK. Sheeba KN, "Experimental studies on heat transfer and friction actor characteristics of forced circulation solar water heater system fitted with helical twisted tapes," Solar Energy, vol. 83, pp. 1943-1952, 2009.
[6]. Raja Sekhar, Y. Sharma, K. V. and Thundil Karupparaj, R., "Heat Transfer Enhancement with Al2O3 Nanofluids and Twisted Tapes in a Pipe for Solar Thermal Applications," Procedia Engineering, vol. 64, pp. 1474-1484. 2013.
[7]. Pramanik D. Saha, S K., "Thermohydraulics of laminar flow through rectangular and square ducts with transverse ribs and twisted tapes," ASME J. Heat Transfer, vol. 128, no. 10, pp. 1070–1080, 2006.
[8]. Saha SK. "Thermohydraulics of laminar flow through rectangular and square ducts with axial corrugation roughness and twisted tapes with oblique teeth," ASME J. Heat Transfer, vol. 132, no. 8, pp. 081701(1–12), 2010.

[9]. Watmuff JH, Charters WWS, Proctor D. Solar and wind induced external coefficients for solar collectors. COMPLES 1977; 2:56.

[10]. Garh HP, Jha R, Choudhry C, Datta G. Theoretical analysis on a new finned type solar air heater. Energy 1991; 16:1231-1238

[11]. Mohammadi K, Sabzpooshani. Comprehensive performance evaluation and parametric studies of single pass solar air heater with fins and baffles attached over the absorber plate. Energy 2013; 57:741-750.

[12]. Yeh HM, Ho CD. Effect of external recycle on the performances of flat-plate solar air heaters with internal fins attached. Renewable Energy 2009; 34:1340-1347

[13]. Kays WM. Convective heat and mass transfer. New York: McGraw-Hill; 1980.

[14]. Yaningsih I, Istanto T, Wijayanta AT. ”Experimental Study of Heat Transfer Enhancement in a Concentric Double Pipe Heat Exchanger with Different Axial Pitch Ratio Of Perforated Twisted Tape Inserts,” in International Conference and Exhibition Sustainable Energy and Advanced Material (ICESEAM) 2015, AIP Conference Proceedings 1737, edited by Triyono et al (American Institute of Physics, Melville, NY, 2016), pp. 030012-1 – 030012-10.

[15]. Apurba Layek. Optimal thermo-hydraulic performance of solar air heater having chamfered rib-groove roughness on absorber plate. International Journal of Energy and Environment 2010; 4: 683-696.

SEEC-2018-010

AN EFFECTIVE APPROACH TO PREDICT THE OCCURRENCE OF COLUMN SEPARATION LEADING TO POTENTIAL CAVITATION EROSION IN DIESEL PUMPS

Ranjit Kumar TA
Bosch Limited, India

Email: ranjit.kumarta@in.bosch.com

Shashi Kanth N
Bosch Limited, India

Email:
Shashikanth.N@in.bosch.com

ABSTRACT

Cavitation is the formation of vapor bubbles in a liquid medium, which is formed as the liquid pressure reaches the vapor pressure. There are multitude of mechanisms that can lead to cavitation (inertial and non-inertial cavitation). The present work deals with non-inertial cavitation. Column separation effect is one of the main phenomenon which leads to the non-inertial cavitation. Column separation occurs due to water hammer event. During a water hammer, intense shock waves generation and propagation occurs due to sudden closure of a boundary. This phenomenon may occur in case of diesel pumps, where the liquid is forced to rapid pressure changes during the valve opening/closure. This leads to the stretching of liquid medium (diesel), during which the vapor bubbles are formed. Simultaneously, the pressure wave travels downstream, hits a wall and reflects back. The reflected waves implodes the existing bubbles on to the nearest wall on its way. This leads to cavitation erosion.

A simple model is established to assess the effects of cavitation due to column separation, using Magnitude of transient number 'M'. The model is verified with two different high pressure diesel pump(Pump1 and Pump2). A hydraulic simulation (AMESim) is performed to extract the parameters like fluid velocity and pressure, to estimate the Magnitude of transient (M). The predicted Magnitude of transient (M) is low for Pump1 and whereas for Pump2 M value is high..

Observations in the field forPump1 shows no occurance of cavitation erosion and whereas Pump2 shows occurrence of cavitation erosion, this is matching with model prediction i.e., higher the M value, higher the cavition.

As future demands for higher pump speeds, the possibility of occurrence of cavitation erosion may be high. Magnitude of transient (M) value can therefore be a very handy in predicting cavitation (during design stages) and reduce cavitation.. The proposed model would reduce the design and testing iterations, thereby reducing the lead time of product development.

*Keywords***:** Cavitation erosion, Column separation, Magnitude of transient (M), Vapor pressure, Water hammer **.**

NOMENCLATURE

Jp	Joukowsky Pressure, bar
ρ	Density, Kg/m3
c	Velocity of sound, m/s
Vfluid	Fluid velocity, m/s
Sp	System pressure
M	Magnitude of Transient, No unit

INTRODUCTION

Cavitation is the formation of empty cavities in a liquid, followed by their immediate and sudden implosion. Cavitation is a common problem encountered in pumps and control valves; one that causes serious wear and tear and can reduce a component's time-in-service dramatically. The primary causes for their formation include vaporization at low pressure, air ingestion, flow turbulence, and internal re-

circulation. If the pressure in the hydraulic circuit (Pump, Turbine etc.) falls below the vapour pressure of the liquid at the prevailing temperature, then the liquid will form bubbles. These are carried down stream until they reach an area of higher pressure, where they collapse or implode.

There are two types of cavitation in general i.e., inertial and non-inertial cavitation. The current work focus on non-inertial cavitation.

The non-inertial cavitation is induced by pressure wave interferences or high speed boundary movements. The phenomenon known as column separation occurs in fluid conveyance systems when fluid vaporization pressure is attained and liquid is converted to vapor in a section of the pipeline. Column separation is a transient phenomenon and is the result of changes in the boundary conditions of the system. The boundary condition changes that can lead to column separation are: downstream valve closures, sudden downstream fluid demands, upstream valve closures, accidental or planned pump shutdowns, and in very extreme cases, pipe ruptures [1]. Investigations from 1 & 2 shows that the shock wave induced by a bubble rebound could be stronger than the shock wave induced by the bubble collapse itself. The bubble rebound can produce upto 2200 N/mm2 of shock wave. The bubble collapse onto the wall, leads to the release of very high energies which erodes the material

NON-INERTIAL CAVITATION DUE TO COLUMN SEPARATION

One of the non-inertial cavitation mechanism which is occurs in valves of high pressure diesel pump is discussed here. Figure 2 illustrates a common mechanism of erosion due to non-inertial cavitation during valve closure.

A simple 2D pipe model is used for representing the non-inertial cavitation mechanism in a valve. Initially the valve is in closed condition. When the valve is open, the fluid flows from region 1 to region 2. When the valve closes suddenly, the fluid medium in region 2, just behind the valve body, stretches. This leads to the column separation and subsequent creation of the vapor bubbles due to the drop in pressure less than the vapor pressure. The sudden closure, leads to the creation of the pressure waves downstream from the valve in region 2. This pressure surge is termed as the Joukowsky pressure [2,3]. This pressure waves travels at the speed of sound in fluid medium. It reflects at the nearest wall downstream and travels back to wards the valve. This incoming pressure waves, implodes the vapor bubbles on to the valve body or anyother wall on its path leading to bubble implosion. This implosion can release very high energies on to the valve.

In a typical high pressure diesel pump, valve operates at high frequencies. This leads to repeated bubble implosion with every valve cycle and subsequently material erosion. In

due time, the erosion can intensify and may affect the valve operation due to leakage.

Magnitude of transient (M): Dimensionless number

Autrique *et. al* [4] discuss the results of experimental studies of water column separation following an upstream valve closure. Column separation is a transient phenomenon that can be explained and classified using dimensionless parameter, M [3]. It is the ratio of the Joukowsky pressure to the system pressure.

$$M = \frac{Jp}{Sp} \qquad (1)$$

Where, Jp is the Joukowsky pressure = $\rho c V_{fluid}$

Sp is the pressure at that instant of valve closure

ρ is the density of the fluid

c is the velocity of the sound in fluid medium

V_{fluid} is the velocity of the fluid

Very long cavities, both in length and time, were obtained for large magnitude (M) transients with low initial heads and large water velocities [3].

Prediction of non-inertial cavitation: High pressure diesel pump case study

In the present study, two high pressure diesel pump samples are considered. The main difference between the two pump samples under investigation is the cam profile. The inlet valve, in particular, is considered for the cavitation study.

A 1D hydraulic tool (AMESim) is used to model the two high pressure diesel pumps under consideration. The flow rate, pressure of the diesel above and below the inlet valve with respect to the valve lift is obtained from the simulation. Equation 1 is used to calculate the magnitude of transient (M) for each corresponding lift.

Figure 3 shows the inlet valve lift with respect to the cam angle in dimensionless quantities for the two high pressure diesel pump sample. The operating condition of both the pumps are same. Figure 4 shows the diesel flow rate across the inlet valve with respect to the cam angle. It can be noted that the two samples, indicate the flow in the negative Y axis before the valve closure. This is referred as the reverse flow. The reverse flow is due to the high pressure leakage from the element chamber, forcing the inlet valve to close. It is worthwhile to note that the Inlet valves are mechanically actuated.

The inlet valve is mainly susceptible for erosion due to non-inertial cavitation during the valve closure. 'M' number is calculated for both the cases during the valve closure.. A

'M' curve is generated with the obtained M values for various lift.

Figure 5 shows the plot of M curve with respect to various valve lifts. It can be seen that the M curve peaks out at a point, which indicates the possible high magnitude pressure wave generation. The 'M' curve of high pressure diesel pump1 is compared against the 'M' curve of the high pressure diesel pump2. The maximum 'M' number in the 'M' curve of high pressure diesel pump1 is 9.3 times more compared to the high pressure diesel pump2. This may indicate that the high pressure diesel pump1 is more susceptible for non-inertial cavitation due to column separation compared to the high pressure diesel pump2.

Test trials are carried out to identify the cavitation erosion intensity in both the pump sample under study. Trials indicate that the high pressure diesel pump1 shows cavitation erosion in the inlet valve. No erosion or very negligible erosion is observed in the inlet valve of the high pressure diesel pump2 sample.

Thus the dimensionless 'M' number shows a very strong correlation for the non-inertial cavitation. It can be observed that the 'M' number for high pressure.

CONCLUSION

Non-inertial cavitation in the inlet valve of high pressure diesel pump is investigated. Column separation is a transient phenomenon which may lead to erosion due to non-inertial cavitation. Components like inlet valves, etc are prone for non-inertial cavitation due to sudden change in boundaries at higher speeds.Magnitude of Transient (M) is a dimensionless number used to estimate the non-inertial cavitation due to column separation. Maximum magnitude of transient represents higher column separation and Vice Versa. Inlet valves of two high pressure diesel pumps (Pump1 and Pump2) are investigated for non-inertial cavitation. An AMESim simulation is built to generate the flow rate across the inlet valve, Lift of the inlet valve and pressure below the inlet valve. These data are use to estimate the Joukowsky pressure and subsequently to estimate the 'M' number.

Results indicate that the 'M' number of high pressure diesel pump1 is significantly higher (9,3 times) compared to the high pressure diesel pump2. Thus the inlet valve of high pressure diesel pump1 is more susceptible for non-inertial cavitation due to column separation. The observation from 'M' number estimation correlates with the test trails where erosion is observed in the inlet valve of high pressure diesel pump1.

As the future demands for very high pump speeds and delivery pressures, the possibility of occurrence of cavitation erosion may be very high. Magnitude of transient (M) curve estimation can therefore be a very handy method for the practicing engineers (during design stages), to detect and reduce cavitation and its effects. Thus one feels, this would reduce the testing of samples to a large extent, thereby reducing the lead time of product development.
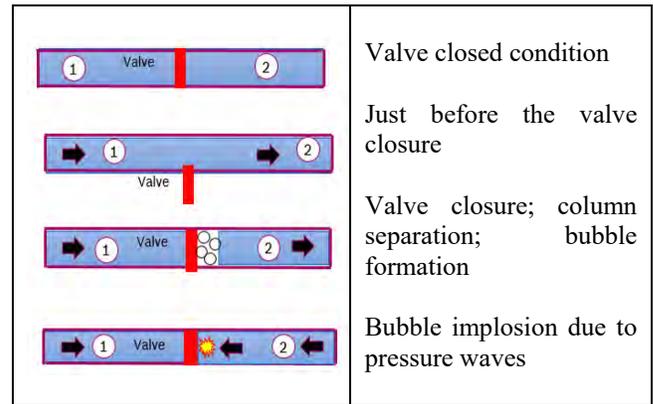
FIGURE 2. 1D REPRESENTATION OF NON-INERTIAL CAVITATION IN VALVES
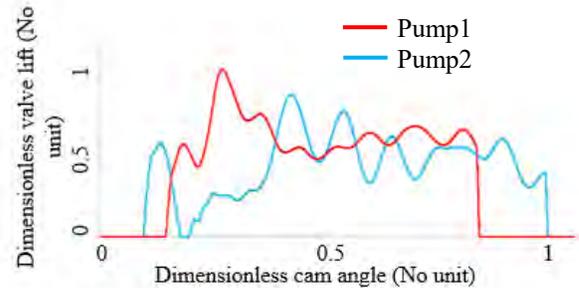
FIGURE 3. DIMENSIONLESS LIFT OF THE INLET VALVE
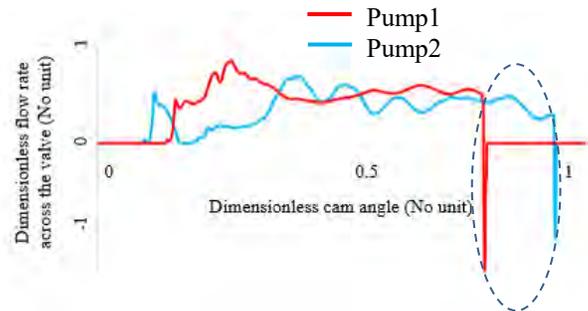
FIGURE 4. DIMENSIONLESS FLOW RATE ACROSS THE INLET VALVE
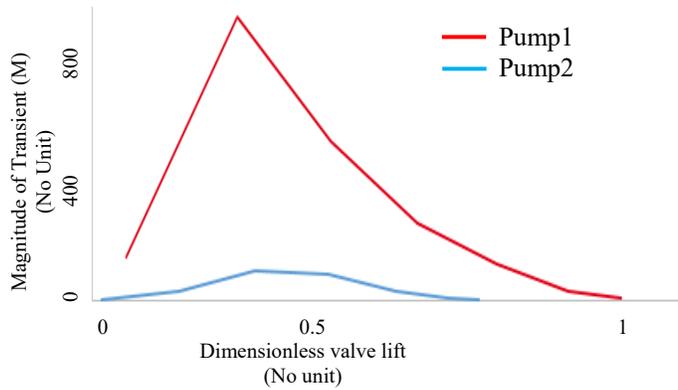
FIGURE 5. MAGNITUDE OF TRANSIENT (M) CURVE

REFERENCES

[1] Autrique R *et. al* ., 2012. Physical model studies of water column separation, "IOP Conf. Series: Earth and Environmental Science" 15 (2012) 022014

[2] Joukowsky N., 1904. "Water Hammer". St. Louis AWWA.

[3] Bergent A, Simpson A R and Tijsseling A S., 2006, "Journal of Fluids and Structures". 22 135 - 171..

[4] Autrique R and Rodal E., 2013, Laboratory studies of water column separation "IOP Conf. Series: Material Science and Engineering" 51 (2013) 022022

THERMAL AND CATALYTIC PYROLYSIS OF *MADHUCA INDICA* SEEDS: A POSSIBLE ROUTE FOR PRODUCTION OF CLEAN FUEL AND VALUABLE CHEMICALS

Ranjeet Kumar Mishra
Department of Chemical Engineering
IIT Guwahati, Assam India
Email: m.ranjeet@iitg.ernet.in

Kaustubha Mohanty
Department of Chemical Enginerring
IIT Guwahati, Assam India
Email: kmohanty@iitg.ernet.in

ABSTRACT

As an alternative energy source, Madhuca indica is a promising biomass resource. The physiochemical characterization of Madhuca indica seed confirmed that it is suitable feedstock for pyrolysis. Thermal and catalytic pyrolysis was carried out at optimum operating condition (500 ^{o}C temperature, 80 ^{o}C min^{-1} heating rate, and 80 ml min^{-1} nitrogen gas flow rate) with different biomass to catalyst ratio (3:1, 6:1, 8:1, 10:1 and 12:1). The results showed that maximum pyrolytic liquid was obtained (56.60 wt. %) at the thermal condition, however, at catalytic pyrolysis oil yield is decreased, only in case of TiO$_2$ catalyst oil yield was increased. Characterization of pyrolytic liquid confirmed that use of these catalyst significantly pH, moisture content, density, and calorific value increased while viscosity and specific gravity decreased. GC-MS analysis of pyrolytic liquid confirmed that use of these catalyst area percentage of alcohol, aldehyde, and hydrocarbons significantly increased and formation of acids reduced.

Keywords: **Lignocellulosic waste biomass, Pyrolysis, Renewable fuel, characterization of pyrolytic liquid.**

NOMENCLATURE
FTIR   Fourier-transform infrared spectroscopy
GC-MS Gas chromatography-mass spectrometry
TGA Thermogravimetric analysis

INTRODUCTION

Energy is the important factor for the development of human civilization. It is the major input almost all the transportation, production and consumption sectors [1]. International energy agency (2015) has reported that global energy consumption distributed into power sources such as oil 31.1 %, coal/peat 28.9 %, natural gas 21.4 %, biofuel/waste 10.2 %, nuclear (4.8 %, hydro 2.4 % and other renewable energy sources such as wind power, solar energy, tidal energy etc, 1.2 % [2]. The extraction rate was much higher than replacement so it can be predicted that energy will be exhausted soon. Substantially increments of greenhouses gases become a challenge. To mitigate the greenhouse emission, either replaced fossil fuel with alternative fuels or improves the efficiency of utilization of fossil fuel. Due to limited fossil fuel resources, the development of renewable energy sources becomes essential as it is the best alternative way to reduce greenhouse emission. Further, renewable energy sources do not fulfill only energy deficiency gap but it is also environmental eco-friendly and cost-effective [3].

Among all the renewable energy sources such as wind power, solar energy, tidal energy, hydrothermal energy, etc., biomass is considered best possible sources due to its environmental advantages and wide availability across the worlds. Grown and waste biomass was used for energy production, and almost 10-14 % energy requirements meet from the biomass [4].

There are two major routes for conversion of biomass into fuel: Biochemical and Thermochemical process. During thermochemical conversion, biomass split into smaller compound within few seconds. Combustion, gasification, pyrolysis liquefication and co-firing are the main thermochemical process. Among all thermochemical process, pyrolysis has greater attention due to its simple operation and suitability for fuel production. Pyrolysis turns biomass into solid (biochar), liquid (liquid fuel) and gases (noncondensable gases). Decomposition of biomass in the absence of oxygen at moderate temperature is known as pyrolysis. Compared with other biomass to energy conversion process, pyrolysis has gained more interest from the viewpoint of producing liquid fuel from various biomass

such as woody biomass, bagasse, straw, miscanthus, municipal soil waste, non-edible seeds, etc.

Use of catalyst during pyrolysis increase the reaction rate, products yield and improves properties of products yield. Also, it increases the pyrolysis reaction kinetics by the cracking of higher molecular weight compounds into lower molecular weight compounds such as hydrocarbons. Use of appropriate catalyst during pyrolysis can boost the conversion efficiency, reduced tar formation and increase the desired products.

Although a number of work has been done on Mahua seed for the production of fuel and chemicals through thermal pyrolysis but never has been attempt to observe the effect of zeolite, potassium carbonate, and titanium oxide as catalysts on the production of fuel and chemical on Mahua seed. Also, the effect of process parameters such as temperature heating rate and B/C ratio was studied.

MATERIALS AND METHODS

Sample collection and preparation

Mahua seed was collected from Basti district (26° 23' and 27° 30' North Latitude and 82° 17' and 83° 20' East longitude) Uttar Pradesh, India. The Mahua seed was sun-dried for 48 h (according to climate condition) and placed in the plastic container to prevents moisture observed. Dried biomass was pulverized into desired particle size (less than 1 mm particle size). Smaller particle sized offer greater heat and mass transfer during the thermochemical process while higher particle size biomass created heat and mass transfer limitation due to the lower surface area and required higher activation energy to start the process.

Catalysts

Four catalysts such as K_2CO_3, Zeolite, TiO_2 and MgO was used in this study. The particle size of the catalyst was varied from 0.05-0.07 mm and used without any pre-treatment. Biomass to catalyst loading is one of the important parameters which results in the maximum production of pyrolytic liquid. Therefore, optimization of B/C ratio becomes essential. The catalyst to biomass ratio varied with different proportions (3:1, 6:1, 8:1, 10:1, and, 12:1) in this study.

Characterization and raw biomass were done by using TGA, FTIR, proximate analysis, ultimate analysis, and calorific value. The pyrolysis experiment was carried out in a semi-batch reactor under the inert atmosphere at optimized conditions (500 °C temperature, 80 °C min^{-1} heating rate, and 80 ml min^{-1} nitrogen gas flow rate). The desired amount of biomass was placed in the reactor and placed in the furnace. Temperature and heating rate was controlled by using external PID controller. As temperature

increases, biomass decomposed and released volatiles in the form of gases. A condenser was connected at the top of the reactor which condensed all the condensable volatiles at temperature 4-6 °C. At the end of experiment rector cool down at room temperature, char was removed from the reactor. Pyrolysis experiment was carried out in an inert atmosphere (nitrogen gas), and purging of the reactor was started before 15 min before the experiments to evacuate all the unwanted gases.

The pyrolytic liquid was obtained from the experiment was found to be black and brown color with irritative small.The pyrolytic liquid contains 17-22 % of water content. Aquoes phase was separated from the pyrolytic oil by using separating funnel due to density difference. The separated pyrolytic liquid was characterization by using pH meter, density meter, oxygen bomb calorimeter, Interfacial rheometer, Kerl-Fischer titration, and GC-Ms analysis.

RESULTS AND DISCUSSION

The physiochemical characterization confirmed that mahua seed has potential to produce fuel and chemicals. Mahua seed contains higher volatile matter (76.0 %) and lower ash content (3.08 %) while ultimate analysis confirmed the presence of higher carbon content (60.48 %) and lower nitrogen and sulfur content which made mahua seed suitable feedstocks for pyrolysis. Thermal analysis of biomass confirmed that biomass splits into three major stage: Drying, devolatilization and char formation. The first stage up to 150 °C temperature removal of moisture content and lower molecular weight compounds occurred, and it is known as drying zone. In second stage volatilization takes place where maximum decomposition occurred. In this zone higher molecular weight compounds fragmented into lower molecular weight compound by the continuous supply of heat. Further, the aliphatic chain gets fragment into gases by using heat. In the third stage, lignin decomposed at the higher temperature >500 °C due to the presence of phenolic hydroxyl groups. This stage is known as char formation zone. FTIR analysis confirmed the presence of hemicellulose cellulose and lignin content.

Thermal and catalytic pyrolysis of mahua seed at different biomass to catalyst ratio was done, and results indicate that during catalytic pyrolysis oil yield decreased. However in case of TiO_2 catalyst oil yield was slightly increased. It was also observed that catalytic pyrolysis produced higher water content than thermal pyrolysis.The hydrogen molecules get reacts with oxygen molecules during pyrolysis and formed water contents.

Characterization of pyrolytic liquid confirmed that use of catalyst increased pH, density, calorific value, and moisture content while viscosity and specific gravity decreased significantly. The FTIR analysis confirmed the

presence of phenols, esters, ethers, and aromatics. GC-Ms analysis confirmed the presence of useful function groups such as hydrocarbons, acids, esters, ethers, alcohols aldehyde amide and nitrogen containing groups. Combining these results together. It can be concluded that mahua seed has potential to produce clean fuel and chemicals.

FIGURES AND TABLES
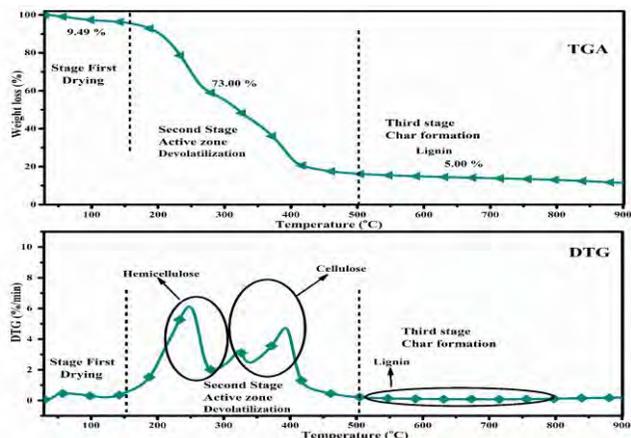
FIGURE 1. TGA AND DTG ANALYSIS OF RAW BIOMA
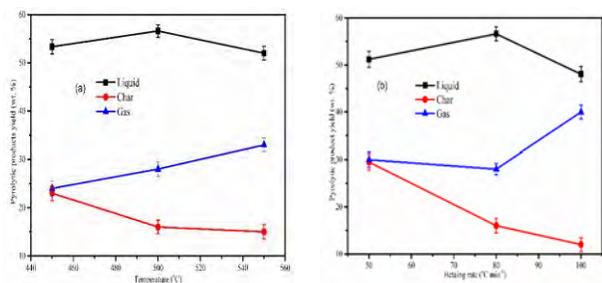
FIGURE 2. (A) EFFECT OF TEMPERATURE AND (B) EFFECT OF HEATING RATE ON PYROLYSIS
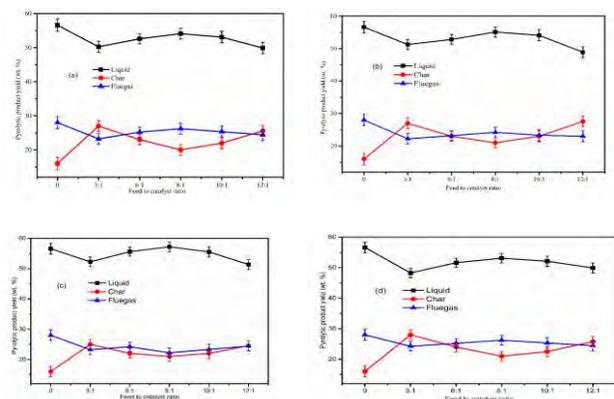
FIG. 5. EFFECT OF B/C RATIO ON PYROLYTIC YIELD (a) K_2CO_3 (b) ZEOLITE (c) TiO_2 (D) MgO.
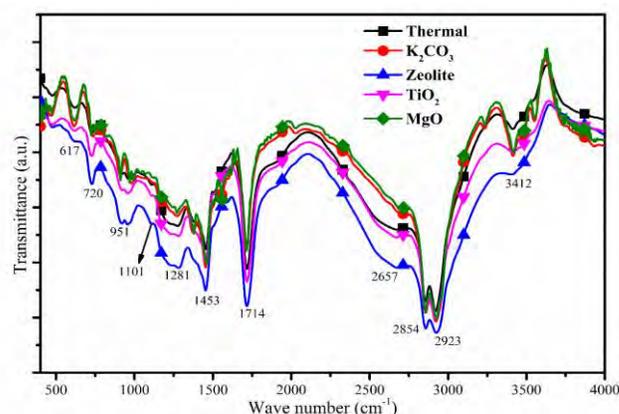
FIGURE 3. FTIR ANALYSIS OF THERMAL AND CATALYTIC PYROLYTIC LIQUID AT OPTIMIZED CONDITIONS.
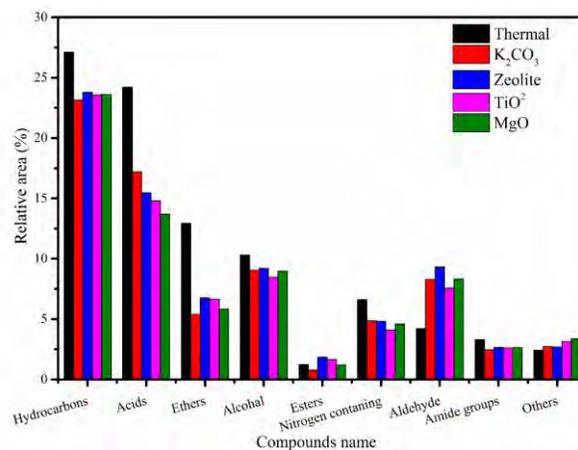
FIGURE 4. GC-MS ANALYSIS OF THERMAL AND CATALYTIC PYROLYTIC LIQUID AT OPTIMIZED CONDITIONS

TABLE 1. CHARACTERISTICS OF MAHUA SEED ALONG WITH OTHER NON-EDIBLE SEED.

Characteristics	Mahua seed	Jatropha seed [5]	Coaster seed [6]	Cascabela thevetia [7]
Proximate analysis (wt. %)				
Moisture content	7.88±0.2	7.5±0.12	7.24	5.10
Volatile matter	76.05±0.82	77.1±0.95	65.21	73.81
Ash content	3.08±0.51	5.9±0.55	4.22	4.20
Fixed Carbon	12.63±0.43	9.4±0.53	23.33	16.82

Ultimate analysis (wt. %)				
Carbon	60.48	53.7	48.96	46.08
Hydrogen	9.69	8.0	5.52	7.20
Oxygen	26.86	27.9	42.61	40.29
Nitrogen	2.62	4.5	2.79	6.43
Sulphur	0.34	-	0.12	-
Calorific value (MJ/kg)	22.78±0.30	24.0±0.24	22.75	19.25
Compositional analysis (wt. %)				
Extractives	59.52	44.6	16.07	-
Hexane/Water	51.49	15.5	-	-
Ethanol	8.03	29.1	-	-
Chemical analysis (wt. %)	80.25	26.1	83.86	-
Hemicellulose	27.33	-	4.6	-
Cellulose	38.72	-	46.95	-
Lignin	14.20	26.1	32.31	-

TABLE 2. THERMAL AND CATALYTIC PROPERTIES OF PYROLYTIC LIQUID

	Thermal	K_2CO_3	Zeolite	TiO_2	MgO	Diesel
Thermal	41	38	38.6	37.56	41	
Viscosity (cst) at 40 ℃	4.2	9.6	8.6	9.2	10.2	-
pH	1.2	1.32	1.35	1.25	1.26	-
Moisture content (%)	904	912	920	915	919	-
Density (kg/m^3)	0.905	0.884	0.885	0.883	0.882	828
Specific gravity	37.73	39.3	41.65	40.86	39.65	0.828
Calorific value (MJ/kg)						44.5

REFERENCES

[1] N.H. Afgan, D. Al Gobaisi, M.G. Carvalho and M. Cumo, *Renewable and sustainable energy reviews*, 2, (1998) 235.

[2] I.E. Agency, *Key world energy statistics*, International Energy Agency, 2007, p.

[3] B.E. Dale and R.G. Ong, *Biotechnology progress*, 28, (2012) 893.

[4] P. McKendry, *Bioresource technology*, 83, (2002) 37.

[5] J. Kongkasawan, H. Nam and S.C. Capareda, *Energy*, 113, (2016) 631.

[6] N.A. Santos, Z.M. Magriotis, A.A. Saczk, G.T. Fássio and S.S. Vieira, *Energy & Fuels*, 29, (2015) 2351.

[7] D. Sut, R.S. Chutia, N. Bordoloi, R. Narzari and R. Kataki, *Bioresource technology*, 213, (2016) 111.

Influence of Compression Ratio on the Combustion Characteristics of a Diesel Engine Running with Tyre Pyrolysis Oil Blend

Abhishek Sharma [a],*, Utkarsh Dixit[a], Vishal Gupta [b], S Murugan [c]

[a]Department of Mechanical & Automation Engineering, Amity School of Engineering & Technology, Amity University Gwalior, Madhya Pradesh, India,
drasharma58@gmail.com
[b]Department of Mechanical Engineering, Radharaman Engineering College, Bhopal, Madhya Pradesh, India, vishalgupta.manit@gmail.com
[c]Department of Mechanical Engineering, National Institute of Technology Rourkela, Rourkela, Orissa, India, smurugan@nitrkl.ac.in
*Corresponding Author

Abstract:

One of the major environmental problems faced by world is the accumulation of waste tyres which is quite inappropriate and one of the major culprit for anthropogenic air pollution. Waste automobile tyre is an organic waste from which useful energy in the form of liquid, gas or solid can be derived. Pyrolysis is an encouraging technology to challenge the waste tyre disposal problem via converting the waste tyres into useful products i.e. pyrolysis oil, solid char and remaining fraction as non-condensable gases. The TPO, a dark-brown/black coloured liquid is used as a fuel in compression ignition (CI) engines, industrial furnaces and power plants etc. The TPO contains compounds of different hydrocarbon from C_5-C_{20}. The utilization of TPO as an alternate source of energy may help to reduce the consumption of petroleum fuels and their rising trend in prices. Also, the potential energy content of TPO possesses many benefits such as the possibility of recycling carbon dioxide (CO_2) with subsequent fall in greenhouse gas emission (GHG) emissions, less environment pollution compared to burning of waste tyres in open atmosphere, value added chemicals etc. But the 100% TPO as a transportation fuel is not possible due to its poor fuel properties such as high moisture content, poor ignition temperature, high kinematic viscosity, lower cetane number etc.

In this study, tyre pyrolysis oil produced from waste automobiles tyres by the pyrolysis was blended with Jatropha biodiesel and used as an alternative fuel for diesel engine. It may be mentioned that the typical design of a diesel engine is not fit for a fuel of different origin. Numerous research works have already been documented on the optimum design parameters such as start of injection timing (IT), nozzle opening pressure (NOP), nozzle geometry, compression ratio and design of combustion chamber etc. for CI engines run on biodiesel/biodiesel blend, because the conventional CI engine is considered only for mineral diesel. In this regard, eexperimental investigations were carriedout in a single cylinder, four stroke air cooled, diesel engine to analysis the effects of varying the compression ratio from 16.5 to 18.5. The combustion parameters of the diesel engine were evaluated in terms of cylinder pressure-crank angle diagram,

cumulative heat release, maximum heat release rate, maximum cylinder pressure and mass fraction burned. The experimental test results showed that, the maximum cylinder pressure and cumulative heat release rate were marginally higher for the higher compression ratio in comparison with the original compression ratio.

Key words: Alternative Energy Source, Diesel Engine, Tyre Pyrolysis Oil, Combustion
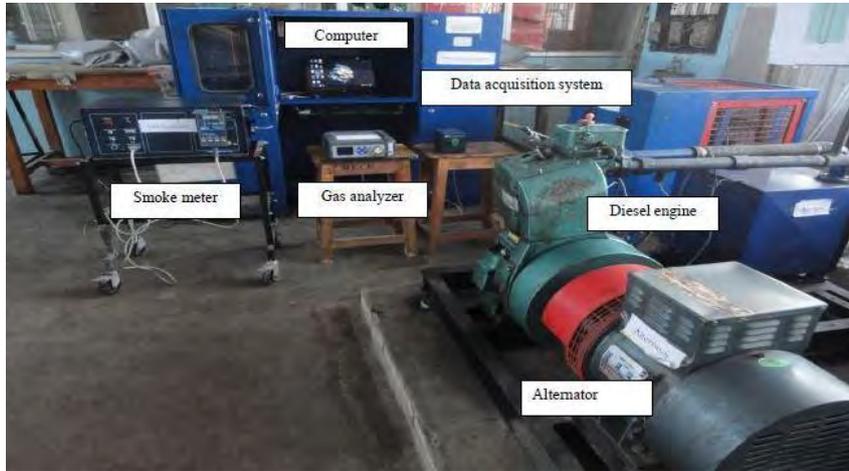
Photograph of the test engine
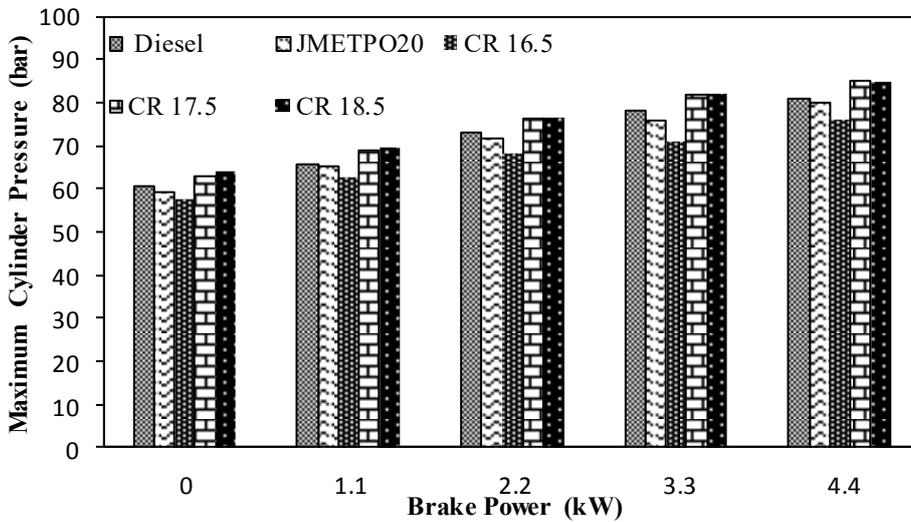
Variation of maximum cylinder pressure for test fuels at different compression ratio

PYROLYSIS OF PE AND PVC IN A TWO-STAGE PYROLYSIS

Ki-Bum PARK
Department of Energy and Environmental System Engineering, Univ. of Seoul, 163 Siripdaero, Dongdaemun-Gu, Seoul
Email: pkb7023@uos.ac.kr

Joo-Sik Kim
Department of Energy and Environmental System Engineering, Univ. of Seoul, 163 Siripdaero, Dongdaemun-Gu, Seoul
Email: joosik@uos.ac.kr

ABSTRACT

In this research, a two-stage pyrolysis process developed to separate contaminants in waste plastic in advance was applied. During pyrolysis of waste plastic containing PVC (polyvinyl chloride), harmful chlorinated compounds like HCl is generated to damage pyrolysis processes. The pyrolysis using the two-stage pyrolyzer consisting of an auger reactor and fluidized bed reactor in series is a new approach to remove HCl before the main pyrolysis. In the auger reactor which usually operates around at 300-400°C, HCl is released from PVC due to the relatively lower bonding energy of C-Cl. The residue leaving the auger reactor is then fed into the fluidized bed reactor where the main pyrolysis occurs. In the experiments, the reduction of Cl in pyrolysis oil was limited only when the two-stage pyrolyzer was applied. However, the two-stage pyrolysis together with a CaO filter turned out to be very effective in removing HCl from the pyrolysis vapor.

Keywords: *Pyrolysis, Plastic, PE, PVC*
.

INTRODUCTION

Different types of plastics are widely used in our daily lives. Consequently, the global production of waste plastic has been gradually increasing [1]. In Korea, waste plastic is usually transformed into fuel for combustion or mechanically recycled. When waste plastic is combusted, it is hard to control contaminants such as dioxins, fly ash, and NOx.

Gasification and pyrolysis can be alternatives in waste plastic management. Gasification is a process of converting waste plastic mainly into a combustible gas called producer

reactor has a function to remove contaminants in advance of the main pyrolysis in the fluidized bed reactor.

MATERIALS AND METHODS

- SAMPLE CHARACTERISTICS

Pellet type PE and PVC with a diameter of 2-4 mm was used in this study. They were mechanically mixed and then fed into the process. In order to figure out the characteristics of feed material, several analyses with the feed material were carried out. To confirm the C, H, N, S and O contents in the feed material, we conducted the ultimate analysis. Also, proximate analysis and TGA (Thermogravimetric Analysis) were conducted.
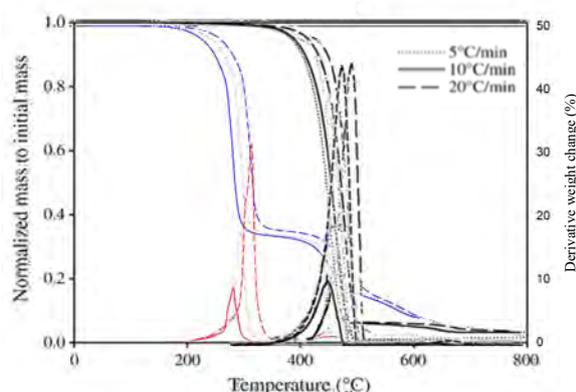
Figure 1. TG and DTG graphs of PE and PVC

Figure 1 represents the thermal characteristics of PE and PVC. Red and blue graphs are the TG and DTG peaks of PVC. Grey graphs represent the PE thermal degradation peaks. As shown in Figure 1, PVC has two characteristic peaks: the first one around at 300°C is the HCl release peak, and the other is the polyene degradation peak. The degradation peak of PE overlapped the second peak of PVC. The TGA shows that HCl can be separated in advance if reactor temperatures of the two-stage pyrolyzer are optimally controlled.

- EXPERIMENTAL METHOD

The mixed feed material consists of PE 98 % and PVC 2 %. As shown in Figure 2, the two-stage pyrolysis process was equipped with separate collection systems for the pyrolysis vapors generated from the auger and fluidized bed reactors. Each collection system consists of mainly a cyclone, condensers, and an electrostatic separator. The uncondensed vapor of the fluidized reactor part was used as the fluidizing medium for the fluidized reactor. The pyrolysis process operated at a pressure of 20 kPa with a fluidizing medium flow rate of 15 NL/min.
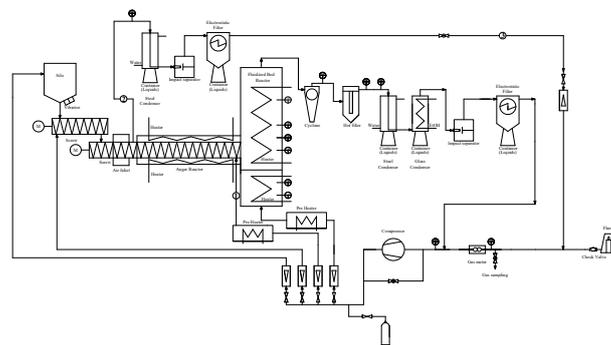
Figure 2. Schematic diagram of two-stage pyrolysis process

TABLE 1: Experimental conditions

Parameter	Run 1	Run 2	Run 3	Run 4	Run 5	Run 6
Auger reactor temperature (°C)	300	300	400	0	300	300
Fluidized reactor temperature (°C)	600	700	700	700	700	700
Feed rate (g/min)	2	2	2	2	2	2
Auger reactor retention time (min)	10	10	10	10	10	10
Additive	-	-	-	-	CaO[a]	CaO[b]

Table 1 shows the experimental conditions. The influence of temperatures of the auger and fluidized bed reactors on the product characteristics was mainly investigated. The temperature range of the auger reactor was 300−400°C, whereas that of the fluidized bed reactor was 600−700°C. Also, the effect of CaO on the removal of HCl was also examined. In Run 5, CaO was fed together with feed material from the silo into the reactors. In Run 6, a CaO filled hot filter located after the fluidized bed reactor was used. CaO used in work had a diameter of 1-2 mm. Chlorine content in oil was measured by a combustion IC (Ion Chromatography)

RESULTS AND DISCUSSION

In Run2, the Cl content of the oil from the auger reactor was 443 ppm, and that from the fluidized bed reactor oil was 367 ppm. The HCl removal in advance by the auger reactor appeared to take place, but the extent was not huge. The HCl generation from PVC in the auger reactor appeared to be limited mainly due to low thermal conductivity of the plastics.

In Run 5, where CaO was fed together with feed material, the Cl content of oil obtained from the fluidized bed oil was high compared to Run 3. It seemed that CaCl$_2$ formed in the auger reactor was dissociated to generate HCl in the fluidized bed reactor. However, In Run 6, a pyrolysis oil with a low Cl content could be obtained. A CaO filter along with a two-stage pyrolyzer could produce a pyrolysis oil with a low Cl content.

Table 2 shows mass balances of the experiments. A very interesting result was the high yields of ethene and propene, monomers of PE and PP (polypropylene). It was mainly caused by the fact that polymer molecules in the melt in the auger reactor was in higher vibrational states and was cracked more easily in the fluidized bed reactor to abundantly produce molecules with low molecular weights like ethene and propene.

REFERENCES
[1] PlasticsEurope, 2016. the Fact 2016
[2] S.M. Al-Salem., 2014, Techno-economic assessment of thermo-chemical treatment (TCT), Chemical Engineering Journal 248, pp. 253–263.

TABLE 2: Product yield of experiment

Reactor type	Products	Yield (wt. %)
Auger reactor	**Gases**	**17.80**
	Oil+wax	**6.22**
: ~300 °C	**Residues**	**5.00**
	Gases (sum)	**46.59**
	Hydrogen	0.24
	Methane	14.29
	Ethane	3.61
	Ethene	18.56
	Propene	6.26
	Butenes	1.24
	1,3-butadiene	1.58
	Oils (sum)	**20.76**
	Aliphatics (sum)	0.02
Fluidized bed	Cyclooctatetraene	0.01
	Other aliphatics	0.01
reactor	Aromatics (sum)	19.55
	Monoaromatics	9.12
: ~ 700 °C	Benzene	0.06
	Toluene	0.91
	Ethylbenzene	0.21
	o-Xylene	0.18
	Styrene	2.14
	Other mono	5.62
	Polyaromatics (sum)	10.86
	Naphthalene	4.02
	Other polyaromatics	5.33
	Unknowns	**1.19**
	Char	**3.64**

COMPUTATIONAL AND EXPERIMENTAL INVESTIGATION OF FLUID FLOW BEHAVIOR IN FILM COOLING ORIFICE OF LIQUID ROCKET ENGINE UNDER BACK PRESSURE CONDITIONS

*Amit K Yadav, Rafeeque TA
Liquid Propulsion System Center, Trivandrum

Shibu Mathew, G Mahesh, Nandakumar K
Liquid Propulsion System Center, Trivandrum

ABSTRACT

This study is to investigate the effect of the configuration of the orifice on fluid flow behavior under back pressure conditions as seen in the actual rocket engine working environment. Fluid flow behavior of two different configurations of orifices is investigated experimentally as well as computationally under various back pressure conditions from 0.1 to 1 MPa. The flow behaviour is simulated using water at 300 K as working fluid and gaseous nitrogen (GN_2) for providing the back pressure. The investigated parameters are coefficient of discharge (C_d), velocity acquired by the fluid for a given mass flow rate and pressure difference across the orifice. Due to the losses inside the flow passage, there are areas where cavitation occurs. This study has looked into the conditions which prompt the formation of cavitation and has estimated the cavitation margins available for the orifice configurations. Computational simulation using CFD is also carried out and results are discussed. Based on the above investigation, it is found that the orifice with downstream diverging shape have 15% higher coefficient of discharge (C_d) and better spread of flow pattern compared to sharp edged orifice. However the cavitation margin for the diverging shape orifice is lower than the sharp edged orifice.

*Corresponding Author: Amit Kumar Yadav
LPSC/ISRO Valiamala, Trivandrum, Kerala
Email: amitkumar@lpsc.gov.in/amit66459@gmail.com
Contact no 04712567743

NOMENCLATURE

LRE	Liquid Rocket Engine
CFD	Computational Fluid Dynamics
ρ	Density
p	Secondary phase
k	Primary phase
DAQ	Data Acquisition System
Cd	Coefficient of discharge
α	Volume fraction
MFR	Mass Flow Rate
Pi	Inlet pressure
Pb	Back Pressure

1. INTRODUCTION

Film cooling is an important aspect of thrust chambers, which determines the performance, life and survivability of liquid rocket engines [1]. It is not only the size but also the configuration of the orifice that plays a vital role in dictating the optimum performance of the engine. The configuration of the orifice needs to provide an optimum flow rate at a minimum pressure drop with a spreading flow pattern to optimize the cooling of the trust chamber [2]. Since film cooling orifice of the rocket thrust chamber is a part where propellant flows with acceleration from manifold, there is a need to quantify the relation between pressure drops available across the orifice for a prescribed flow rate to avoid the cavitations as accelerating flows are prone for cavitaion [3-6]. Not only this, during the transient conditions of engine start and shut-off the film cooling orifices are exposed to varying back pressures which may lead to the conditions where flow may cavitate. Cavitating flow through film cooling orifice may cause severe damage to the rocket thrust chamber as it may lead higher pressure drop, lower flow rate and hence inefficient cooling. To quantify the effect of configuration and size of the orifices on flow behaviour through it, two orifices were realised. One had higher diameter and sharp edge entry and

exit, whereas the other one had lower diameter and sharp edge entry but diverging exit figure -1. Flow simulations were carried out on these orifices. Since the application of these orifices are under back pressure conditions simulation were carried out under various back pressure conditions. Later on experiments were also conducted on both the offices under various back pressure conditions from 0.1 MPa to 1 MPa and flow behaviour was studied experimentally.
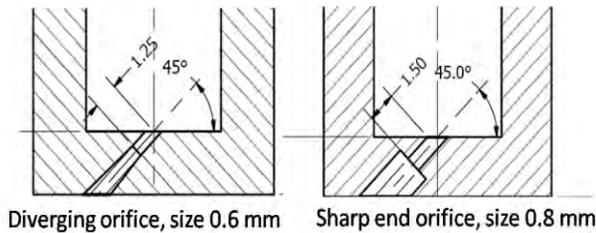
Figure1: Detail of orifice configuration

2. NUMERICAL APPROACH

Commercial software ANSYS solver, Fluent -16 is used to model the flow in the orifices. For mixture model was used to model the flow during the cavitation. Mixture model is employed. Water is taken as the working fluid for simulation, with the assumptions of steady state, incompressible, Newtonian flow. The properties of the water are assumed to be constant. The flow is considered isothermal without any heat transfer from the surrounding. No slip velocity is permitted between the liquid and vapor phase during the cavitation phenomenon. The mixture model solves the continuity equation for the mixture, the momentum equation for the mixture, energy equation for the mixture, and the volume fraction equation for the secondary phases, as well as algebraic expressions for the relative velocities. (If the phases are moving at different Velocities) [7]

Continuity equation

$$\frac{\partial}{\partial t}(\rho_m) + \nabla.(\rho_m \vec{v}_m) = 0 ....(1)$$

$$\vec{v}_m = \frac{\sum_{k=1}^{n} \alpha_k \rho_k \vec{v}_k}{\rho_m} ....(2)$$

$$\rho_m = \sum_{k=1}^{n} \alpha_k \rho_k ....(3)$$

Where $\vec{v}_m$ is mass averaged velocity and ρ_m is mixture density and α_k is volume fraction of phase k and n is number of phases.

Momentum equation

$$\frac{\partial}{\partial t}(\rho_m \vec{v}_m) + \nabla.(\rho_m \vec{v}_m \vec{v}_m) = -\nabla p + \nabla.[\mu_m(\nabla \vec{v}_m + \nabla \vec{v}_m^T)].......(4)$$

Where μ_m is mixture viscosity which is expressed by equation 5

$$\mu_m = \sum_{k=1}^{n} \alpha_k \mu_k ....(5)$$

Energy equation

$$\frac{\partial}{\partial t}\sum_{k=1}^{n}(\alpha_k \rho_m E_k) + \nabla.\sum_{k=1}^{n}(\alpha_k \vec{v}_k(\rho_k E_k + p)) = \nabla(k_{eff}\nabla T).......(6)$$

Where k_{eff} is the effective thermal conductivity of the material of phase k in addition to the thermal conductivity because of the turbulence.

To calculate the volume fraction of secondary phase (p) (vapor phase) equation 7 is solved

$$\frac{\partial}{\partial t}(\alpha_p \rho_p) + \nabla.(\alpha_p \rho_p \vec{v}_p) = \sum_{q=1}^{n}(\dot{m}_{qp} - \dot{m}_{pq}) ....(7)$$

Since the flow is turbulent in nature the turbulence is solved using k-ε, two equation model, for solving the cavitation

Cavitation phenomenon is modeled using schnerr and Sauer Model. As per this model the net mass transfer from liquid to vapor is computed using following equations. The equation for vapor volume fraction has the following general form

$$\frac{\partial}{\partial t}(\alpha \rho_v) + \nabla.(\alpha \rho_p V) = R.................(8)$$

Here the net mass source term R is defined as follows

$$R = \frac{\rho_v \rho_l d\alpha}{\rho dt}$$

$$\alpha = \frac{n_b \frac{4}{3}\pi R_B^3}{1 + n_b \frac{4}{3}\pi R_B^3}$$

$$R = \frac{\rho_v \rho_l \alpha}{\rho}(1-\alpha)\frac{3}{R_B}(\frac{2}{3}\frac{(p_v - p)}{\rho_l})$$

$$R_B = (\frac{\alpha}{1-\alpha}\frac{3}{4\pi}\frac{1}{n})^{\frac{1}{3}}$$

R is equal to source term which is computed by using bubble radius ie, R_B and number of bubble density (nb) which depends on vapor pressure of the water and local pressure.

At first case, 3 D geometry is prepared and a fine mesh is generated. The number of elements is 133687 for diverging orifice and 125161 for sharp edge exit orifice. The quality of the mesh is maintained same in both the cases. The Boundary conditions and flow domain is shown in figure-2. Pressure inlet (Pi) and Pressure out let (P b) boundary conditions are applied at the inlet and out let of the computational domain. The constant wall temperature of 300K is maintained at the wall.
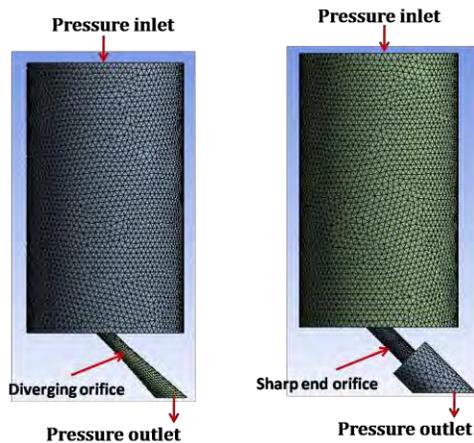
Figure 2: Mesh and boundary conditions

3. EXPERIMENTAL APPROACH:

For visual inspection of the flow behavior inside the orifices, orifices are made of Perspex as shown in figure-3. To visualize the flow inside the orifice a high speed camera was employed and data were recorded with 5000 fps.

Figure 3: Diverging orifice (left) Sharp exit orifice (right)

Full experimental set up is shown in figure-4. The important flow parameters like mass flow rate, Injection pressure and backpressure were acquired using a data acquisition (DAQ) system and the relevant images are captured using a high speed imager in synchronization with DAQ. Pressurized DM water was fed from a high pressure

storage run tank and backpressure gas (Nitrogen gas) was supplied from a chamber of $0.8m^3$.
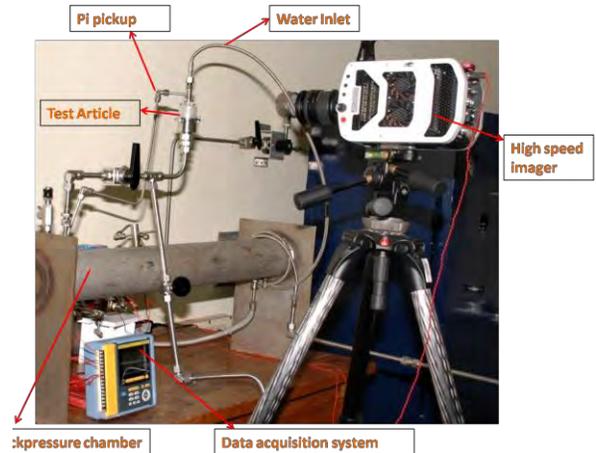
Figure 4: Complete experimental set up

Pressure was measured using pressure transmitters with a range of 0-2 MPa and flow rate measured using Micro Motion make mass flow meter with a range of 0-50 g/s . The water feed line was regulated by manual ball valves and backpressure using pressure regulators and ball valves. The experiment was performed with following conditions which are similar to actual working conditions of orifice. The injection pressure (Pi) was kept between 1.1-1.2 MPa to match with the actual engine operating value Chamber pressure (Pc) was kept at 0.68-0.85 MPa to simulate real working pressure and it was raised to this value at different rates to study the transition effects.

4. RESULTS AND DISCUSSION:

The study compared the following aspects of the jets on these two configurations

1. Flow behavior inside the orifices under different backpressure conditions.
2. Flow transitions from liquid phase to two phase (liquid and vapor) due to cavitation

4.1 Flow behavior inside the orifices

The pressure drop across the orifices in actual working conditions of the engine is ~0.3 MPa (1.1-1.15 MPa injection pressure and 0.83 MPa chamber pressure). The initial study was started with maintaining the 0.3 MPa pressure drop across the injector by setting up the upstream pressure at ~0.4 MPa and downstream at ambient pressure (0.1 MPa). The prediction made with computational analysis indicated the presence of cavitation in the orifice figure-5 (left column). Same results were obtained during the experiments also as shown in figure 5 (right column).

The white portion seen in figure -5 (right column) shown inside the ellipse is showing the vapor and liquid mixed flow and transparent portion is water alone.
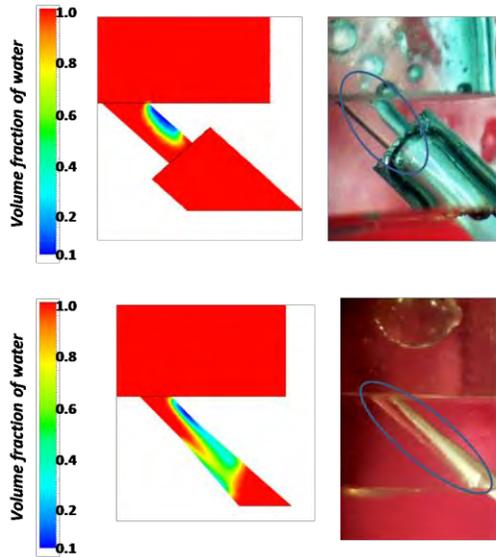
Figure 5: Cavitation observed in sharp exit film cooling Orifice and diverging film cooling orifice under 1atm back pressure condition computational results (left column) and experimental results (right column)

Since cavitation was observed during the above simulations the upstream pressure is increased to engine operating injection pressure i.e. 1.15 MPa and downstream pressure was varied from 0.1 MPa (ambient pressure) to 0.85 MPa for both the orifices. In sharp edge orifice cavitation was observed up to a back pressure of 0.4 MPa. Above this the cavitation phenomenon was not seen. Whereas in diverging orifice cavitation was present up to 0.7 MPa back pressure. Similar observation was recorded during the experiments also (figure-6). This indicates that the cavitation margin available for sharp edge cooling orifice is higher than diverging cooling orifice.

Parameters	Sharp edge orifice		Diverging orifice	
	Exp.Res.	Num Res.	Exp.Res.	Num Res.
MFR (g/s)	15.3	12.9	8.37	7.44
Pi (MPa)	1.2	1.1	1.2	1.1
P_b(MPa)	0.4	0.4	0.7	0.7

Table-1 Flow parameters conditions to eliminate the cavitations

Due to back pressure the cavitaion of the fluid is eliminated and for a given pressure drop across the injector orifice mass flow rate is constant and not increasing with increase in back pressure. The test results after cavitation

phenomenon is eliminated are given in Table-1. The experiments were repeated with varying rate of rising backpressure (up to 0.8 MPa) i.e. 0.027MPa/s, 0.053 MPa/s and 0.32 MPa/s. All the test data shows a steady rise of Cd followed by a sudden attachment. Computed value of Cd of sharp edge film cooling orifice is 0.79 and for diverging film cooling it is 0.92 during the full flow conditions (without cavitation).
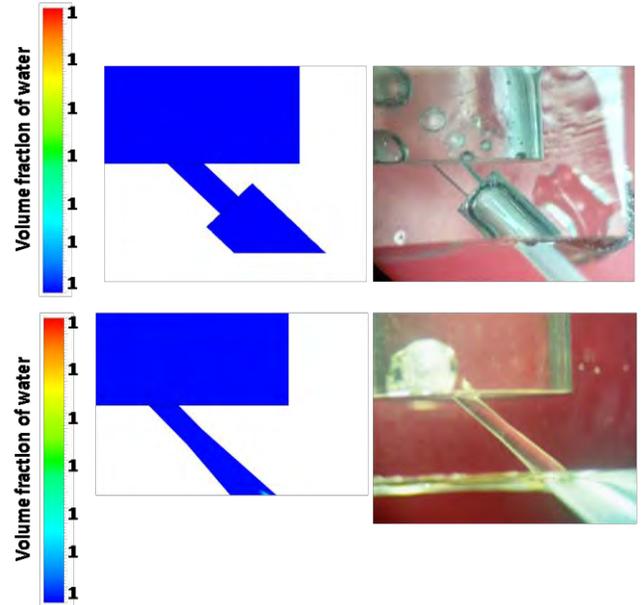
Figure 6: Absence of cavitation in sharp exit film cooling orifice and diverging film cooling orifice under high back pressure condition computational results (left column) and experimental results (right column)

5. Conclusion:

Diverging orifice has higher Cd (0.91) at 7 bar back pressure, compared to sharp exit orifice (Cd=0.79). Diverging orifice also shows lower exit velocity and better spreading pattern over chamber wall. The cavitation margin available for diverging film cooling orifices is less compared to sharp exit orifice because it is seen to cavitate up to a back pressure of 0.7 MPa whereas for sharp edge film cooling orifice cavitation is getting eliminated at a back pressure of 0.4 MPa. The low cavitation margin available for diverging cooling orifices may cause some or all the orifices to cavitate during engine hot tests (because of higher vapor pressure due to higher temperature of the fuel). This can cause bubble formation due to localized boiling of fuel inside the orifice. This in turn can reduce the total mass flow rate and hence reducing the cooling provided by the regenerative coolant. Such a situation can lead to undesirable heating and even failure of the rocket engine.

6. ACKNOWLEDGMENTS

6. REFERENCES:

[1] Eldon L. Knuth, "The Mechanics of Film Cooling," Jet Propulsion, November-December, 1954 publication no. 5 8

[2] A. Lakshya Kumar J. C. Pisharady · S. R. Shine, "Effect of injector configuration in rocket nozzle film cooling "Heat Mass Transfer DOI 10.1007/s00231-015-1590-7

[3] G. Palau-Salvador, P. González and J.A Valverde, "Numerical modeling of cavitating flows for simple geometries using FLUENT V6."Spanish Journal of Agricultural Research 2007 5(4), 460-469

[4] Smith Eiamsa, Artit Ridluan, Prachya Somravysin, and Pongjet Promvonge "Numerical investigation of turbulent flow through a circular orifice KMITL Sci. J. Vol.8No.1 January – June, 2008

[5] Manmatha K. Roul, Sukanta K. Dash "Single-Phase and Two-Phase Flow Through Thin and Thick orifices in horizontal pipes" Journal of Fluids Engineering SEPTEMBER 2012, Vol. 134 / 091301-1

[6] S I Bernad, Romeo Susan, "Numerical Model for Cavitational Flow in Hydraulic Poppet Valves" Hindawi Publishing Corporation Modeling and Simulation in Engineering Volume 2012, Article ID 742162, 10 pagesdoi:10.1155/2012/742162

[7] ANSYS Fluent Theory Guide .Release 15.0 November 2013

SEEC-2018-016

COMBUSTION CHARACTERISTICS OF ISROSENE ALUMINUM NANOFLUID

Amit Kumar Yadav
Liquid propulsion system center,
ISRO,Thiruvananthapuram,Kerala,India
amitkumar@lpsc.gov.in

Atul Srivastava
Indian institute of technology Bombay, Mumbai,
Maharashtra, India
atulsr@iitb.ac.in

Arindrajit Chowdhury
Indian institute of technology Bombay, Mumbai,
Maharashtra, India
arindra@iitb.ac.in

Nandakumar K
Liquid propulsion system center,
ISRO,Thiruvananthapuram,Kerala,India
nandakumar_k@lpsc.gov.in

ABSTRACT

Combustion characteristics of Isrosene and Isrosene loaded with aluminum nanoparticles (ANP) are studied using suspended droplet combustion technique. Isrosene is refined kerosene, suitable fuel for rocket application with liquid oxygen as an oxidizer. Mass loading of ANP in Isrosene is varied from 0.5 % to 4% and combustion of the droplets were recorded employing a high speed camera. The synthesis of nanofluid was carried out using two step method. No surfactant was added during the preparation of nanofluid.

Similarity and difference of burning characteristics between the pure isrosene droplets and ANP loaded Isrosene droplets are explained. It is found that by addition of ANP in Isrosene the mass burning rate of the Isrosene is first reduces followed by an increase. A maximum of 13.3 % increase in burning rate constant is observed for ANP mass loading of 4%. At higher mass loading the droplet combustion does not obey the D^2-t law. Intermittently during the combustion and towards the end of the combustion of ANP-Isrosene nanofluid droplets micro explosions are seen which causes the increase in burning rate.

Keywords: Nanofluid, Droplet combustion, Isrosene burning rate, D^2-t curve, Micro-explosion

NOMENCLATURE

ANP	Aluminum Nano Particles
v_e	Volume of ellipsoidal droplet (mm^3)
d_{max}	Major diameter of ellipsoidal (mm)
d_{min}	Minor diameter of ellipsoidal (mm)
d	Instantaneous diameter of the droplet (mm)
d_0	Initial diameter of droplet (mm)
k	Burning rate constant (mm^2/s)
$\dot{m}$	Mass burning rate (mg/s)
ρ_l	Density of fuel

INTRODUCTION

Nanofluids have made a fairly good impact in research community where majority of the work conducted is limited to improve the heat transfer characteristics of the fuel [1-3].The application of nanofluids in rocket engines to achieve better heat transfer characteristics necessitates the study of their combustion characteristics. The combustion characteristics are important as the fuel is combusted in the chamber after being used as a coolant. A comparison also needs to be made with the base fuels.

Gan et al. [4] studied the burning characteristics of ethanol and n-decane by addition of nanometer sized and micron sized aluminium particles. Javed et al [5] studied the ignition and combustion characteristics of kerosene and aluminium at elevated temperatures and reported a significant enhancement in burning rate by addition of aluminium nanoparticles. Guerieri et al [6] reported the

reduction in the burning rate of kerosene loaded with aluminium nanoparticles. Gan et al [7] studied the combustion characteristics of boron and iron nanoparticles added to ethanol and n-decane, where they explained differences in the flame structure. Chen et al [8] studied the evaporation characteristics of Leponite, (ferric oxide) and silver nanoparticles added to water separately and concluded that there is remarkable increase in evaporation rate. In the present study combustion characteristics of ANP-Isrosene Nanofluid was determined using suspended droplet combustion technique. Isrosene is refined kerosene, suitable fuel for rocket application with liquid oxygen as an oxidizer. ANP having the specific surface area (SSA) of 40 m^2/g and the particle size of 80 nm was added in different proportions by mass (0.05 to 4%) in Isrosene. No surfactant was added during the preparation of the nanofluid to avoid its influence on combustion. The methodology of droplet combustion is adopted because it is a simple, one-dimensional and fairly accurate way to study the spray combustion [9-12]. The effect of ANP on mass burning rate, burning rate constant, and flame temperature were investigated

2. EXPERIMENTAL METHOD

2.1 Fuel preparation:

The experimental setup and procedure to prepare nanofluid has been explained in detail elsewhere [2, 3]. A two-step method was applied for preparation of the nanofluid. The packets of aluminium nanoparticles were purchased from NaBond Technologies CO. LTD. China. The average particle size of nanoparticles was 18 nm, varying from few nm to 50 nm. The specific surface area prescribed by the supplier was 40-60 m^2/g. The purity was reported as 99.9%. ANP was added in desired quantity i.e of 0.25, 0.5, 1, 1.5 and 2 grams in a measured quantity of Isrosene (50 grams). After initial mechanical stirring, the solutions were ultra-sonicated for the minimum of two hours in a constant temperature chamber. Once the nanoparticles were fully mixed in Isrosene, the droplet combustion experiments were conducted within half an hour to avoid agglomeration of nanoparticles. No surfactant was added during the preparation of the nano-fluid.

2.2 Experimental setup of droplet combustion:

The experimental set up of droplet combustion for conducting the experiments has been detailed elsewhere [13]. It consists of a combustion chamber with a volume more than 50 times of the droplet volume to avoid oxygen depletion during the combustion of the droplet.

There are three glass windows and ten ports, for optical accessibility and various in and out flow of fluids to the chamber. A 5 cm long 0.32 mm diameter quartz rod was used for suspension of droplets approximately 1.28 mm in diameter. A 10 µl micro syringe was used to deposit the droplets on the tip of the quartz rod. The droplet was ignited by a spark approximately 3 mm below the bottom

tip of the droplet using two electrodes. The spark was generated using an ignition transformer for duration approximately 0.30 s which was just sufficient for the ignition of the droplets.

To capture the variation of droplet size with time, a Phantom make high-speed imager (v 1210) with a resolution of 1280x800 pixels with backlight was employed. Combustion was recorded at 3000 frames per second (fps). To observe the change of flame structure and flame diameter, the FLIR make thermal imaging camera (X6540-X6550 SC) was used. Combustion was recorded at 100 fps by this camera.

After each experiment, the suspension rod was cleaned to ensure the absence of any carbon deposits on it. Each experiment was repeated two times to ensure the repeatability of the acquired data
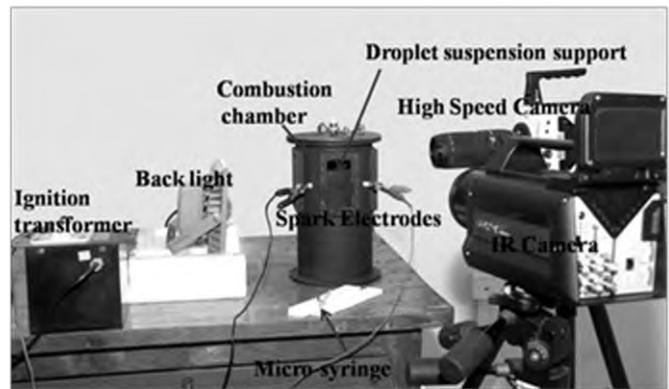
Figure-1 Droplet combustion experimental setup

2.3 Data reduction procedure:

Once the set of experiments was completed, the recorded sequence of images of droplet surface history from the high-speed imager and flame temperature sequence of images from thermal imager was analysed. Analysis involves plotting the D^2-t curve and determining the slope of the curve i.e. burning rate constant [12]. Droplet diameter was determined using Equations 1 and 2 and the D^2-t curve was plotted. Once the burning rate constant was computed, the initial mass burning rate was also computed using Equation 4 [9].

$$v_e = \frac{\pi}{6} \times d_{max} \times (d_{min})^2 \dots\dots(1)$$

$$d = (\frac{6}{\pi} v_e)^{1/3} \dots\dots(2)$$

$$d^2 = d_0^2 - kt \dots\dots(3)$$

$$\dot{m} = \frac{\pi \rho_l d_0 k}{4} \dots\dots(4)$$

Here v_e is the volume of ellipsoidal droplet, d_{max} major diameter, d_{min} minor diameter, d Instantaneous diameter, d_0

Initial diameter of droplet k burning rate constant $\dot{m}$ mass burning rate and ρ_l Density of fuel

3. RESULTS AND DISCUSSION:

3.1 Difference in burning characteristics of pure Isrosene droplet and ANP loaded Isrosene droplet by visual observation:

The burning characteristics of Isrosene droplets loaded with ANP were found to be different compared to those of pure Isrosene droplets. Figure 2 shows the sequence of images of burning pure Isrosene droplet. It may be observed that the shape and size is similar at various time instants except at the beginning and end of the event. The flame size is a transient property that increases with time because of the increase in heat available for evaporation of the fuel. During the initial phase of the event heat is utilized in inert heating of the droplet. Once the droplet temperature reaches the boiling temperature of the fuel the total heat of combustion is utilized for evaporating the fuel.
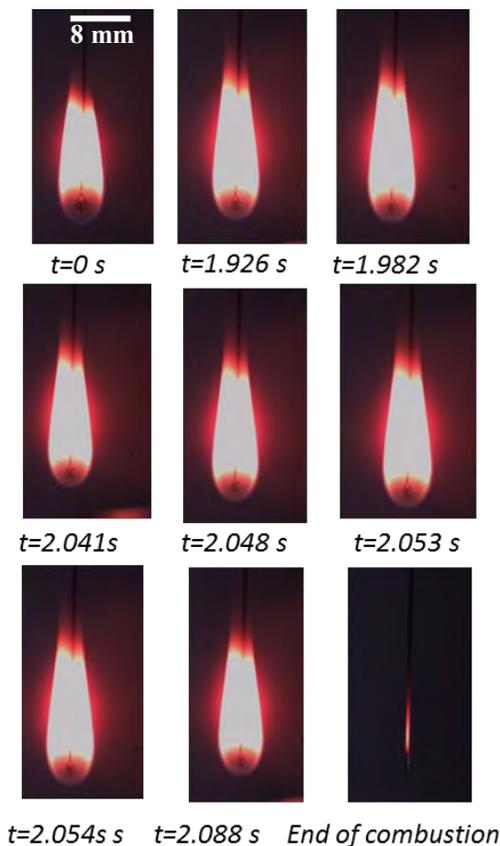
Figure 2 Steady state flame during the Combustion of pure Isrosene droplet (absence of micro explosion

Figure 3 shows the sequence of the images from the burning droplet of Isrosene loaded with ANP. The

combustion process was smooth up to 75% of the total burning time and the flame was similar to the burning of pure Isrosene droplets. However at t =1.926 s and 1.982 s low intensity micro explosions were observed. Towards the end of the combustion process, a high intensity micro explosion phenomenon was observed at t = 2.05 s, which changed the flame shape. The high intensity micro explosion was survived to 20 ms . In micro explosion phenomenon during the combustion of ANP loaded droplet, the inner portion of the droplet get heated up by the flame higher to boiling temperature of fuel which starts the nucleate boiling inside the droplet results in bulging and explosion of the droplet in small droplets which combusted individually or unison with the main flame. Such small combusting droplets are shown by enclosed circles in figure-3.
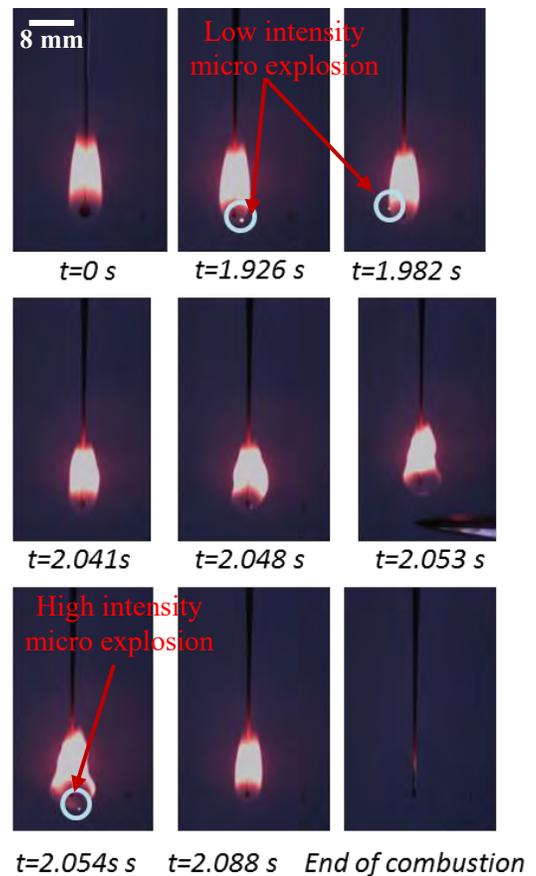
Figure-3 Unsteady flame and presence of low and high intensity micro explosion during the combustion of nanofluid droplet

3.2 D^2-t curve and burning rate constant:

The surface history of the droplet with time was computed and non-dimensionilzed surface history with normalised time is shown in figure-4. From the figure it

can be seen that for pure isrosene droplet the combustion process was smooth and the surface regression was linear with time following the D^2 law. For the ANP loaded Isrosene droplets also the surface regression was as per the D^2 law up to the loading of 2%. Intermittently low intensity micro explosion were observed for 2% mass loading but it could not made any irregularities in surface regression. For the higher mass loading i.e. 3 % and 4 % the surface regression is not obeying the D^2 law throughout the burning time. In case of 3 % mass loading of the ANP droplet surface regression is obeying the D^2 law but towards end of the combustion fluctuations are seen due to micro explosion. The diameter of the droplet is almost increases double to the exiting diameter followed by reduction. In case of 4 % mass loading the droplet surface regression is not obeying the D^2- law. It can be seen that the reduction in droplet diameter is higher at the beginning followed by a reduction. The slope of the curve is representing the burning rate constant. It can be seen there is decrease in burning rate constant by addition of ANP followed by increase.
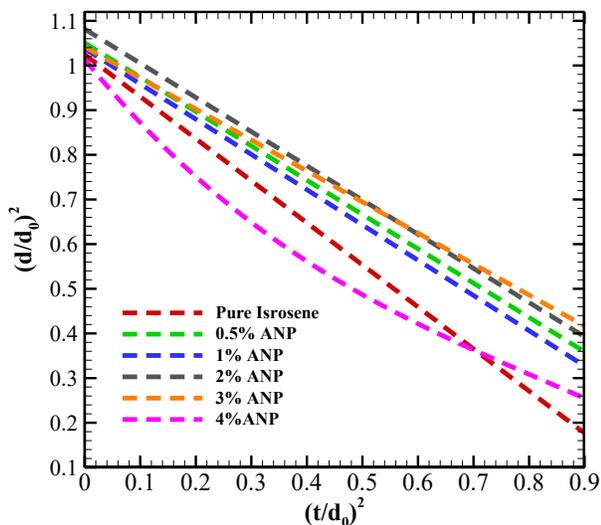
Figure-4 D^2-t curve for Isrosene and ANP loaded Isrosene droplets

The maximum increase in burning rate is observed to be 13.3% for the mass loading of 4%. Since in case of 4% mass loading the surface regression does not follow the D^2-law there are 2 burning rate constant. Initial burning rate constant is higher than pure isrosene burning rate constant but towards the end the burning rate is almost equal to pure Isrosene.
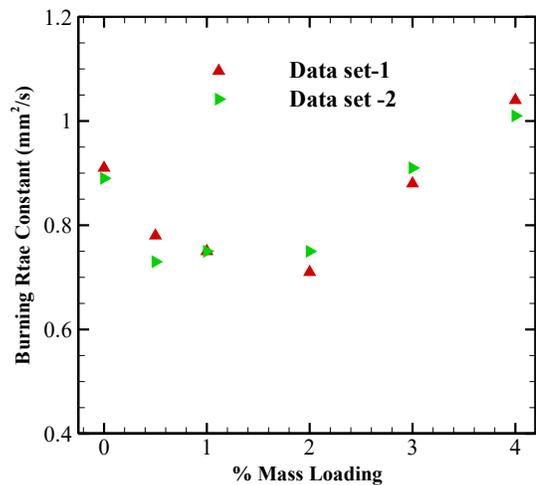
Figure-5 Variation of burning rate constant with % mass loading of ANP

4. CONCLUSIONS:

Combustion characteristics of ANP+Irosene Nano-fluid are studied using droplet combustion methodology. The major highlights of results out are listed below.

- Droplet combustion of ANP+Isrosene droplets follows the D^2-t curve for lower mass loading but deviate from it for higher mass loading.
- Addition of ANP in Isrosene reduces the burning rate constant and then increases. The maximum increase is 13.33% for a mass loading of 4 %.
- Phenomenon of micro explosion is witnessed during the combustion of ANP+Isrosene Nano-fluid droplets.

5. ACKNOWLEDGMENTS

6. REFERENCES:

[1] S.U.S. Choi, "Enhancing thermal conductivity of fluids with nanoparticles," The Proceedings of the 1995 ASME Int. Mechanical Engineering Congress and Exposition, ASME, San Francisco, USA, 1995, pp. 99e105

[2] Agarwal D. K, Vaidyanathan A., Kumar S. S., "Synthesis and characterization of kerosene-alumina Nano-fluids" Applied Thermal Engineering 60 (2013) 275-284.

[3] Agarwal D. K, Vaidyanathan A., Kumar S. S., "Experimental Investigation on Thermal Performance of Kerosene-Graphene Nano fluid", Experimental Fluid and Thermal Science 71 (2016) 126-137

[4] Y. Gan and Li Qiao, "Combustion characteristics of fuel droplets with addition of nano and micron-sized aluminum particles" Combustion and Flame 158 (2011) 354–368

[5] Irfan Javed, Seung Wook Baek, Khalid Waheed, "Autoignition and combustion characteristics of kerosene droplets with dilute concentrations of aluminum Nano-particles at elevated temperatures" Combustion and Flame 162 (2015) 774–787.

[6] Philip M Guerieri, Jeffery B Delisio, Michal R Zachariah, "Nanoaluminum/Nitrocellulose micro particles addition for burn enhancement of liquid fuels." Combustion and Flame 176 (2017) 220–228

[7] Yanan Gan, Yi Syuen Lim, Li Qiao "Combustion of Nanofluid fuels with the addition of boron and iron particles at dilute and dense concentrations" Combustion and Flame 159 (2012) 1732–1740.

[8] Ruey-Hung Chen, Tran X. Phuoc, Donald Martello, "Effects of nanoparticles on nanofluid droplet evaporation" International Journal of Heat and Mass Transfer 53 (2010) 3677–3682.

[9] A Ambekar, A Chowdhury, S Challa, D Radhakrishna, "Droplet combustion studies of hydrocarbon-monopropellant blends", Fuel 115 (2014) 697–705

[10] T. Farouk , F. L. Dryer, "Microgravity droplet combustion: effect of tethering fiber on burning ate and flame structure "Combustion Theory and Modeling Vol. 15, No. 4, 2011, 487–515

[11] Ambekar, A., A. Chowdhury. "Experimental Prediction of Intrinsic Burning Rate Constants of Liquid Fuel Droplets". ASPACC 2015 - 10th Asia-Pacific Conference on Combustion. SCOPUS. Web. 22 May 2016

[12] SR Turns. "Introduction to combustion Concepts and Applications" McGraw-Hill 2000, 2nd edition,Chapter-10,362-421

[13] Amit Kumar Yadav, Arindrajit Chowdhury, Atul Srivastav, Nandakumar K "Combustion characteristics of isrosene graphene nanofluid" Proceedings of the International Conference on Sustainable Energy and Environmental Challenges (SEEC-2017) 26 – 28 February, 2017, Mohali, India, Paper ID 13

SEEC-2018-017

IDENTIFICATION OF SUSTAINABLE ENERGY SOURCE FOR INDIAN CLIMATIC CONDITIONS: A MCDM APPROACH

S. K. Saraswat
Mechanical Engineering Department,
Birla Institute of Technology & Science, Pilani
santosh.saraswat738@gmail.com

Dr. Abhijeet K Digalwar
Mechanical Engineering Department,
Birla Institute of Technology & Science, Pilani
akdigalwar@gmail.com

ABSTRACT

The electricity requirements of India are increasing at alarming rate and power demand is running quiet ahead of power supply. In current energy scenario, India 66.67% power generation is using conventional (coal, petroleum, gas etc.) energy sources. The problem associated with conventional energy sources are limited reserve of fossil fuels and their environmental impacts. To overcome these problems and fulfill the energy demand, it is necessity to develop Non-conventional/Renewable Energy Sources. In renewable energy source for Indian climatic conditions, solar energy is having huge potential due to its location (8° to 38° latitude) in global solar belt with more than 300 days clear sunny days.

The aim of this work is to find out best source of power in between conventional power source (thermal) and renewable (solar) power source for sustainable power in India. In this work, current issues, strengths, weaknesses, threats, challenges and opportunities associated with conventional power source and renewable power source are discussed. Based on the literature available, eight criteria/ drivers are selected to obtain sustainable power source. As an experts to give weightage to select criteria, academicians and practitioners from energy sector are chosen. For analysis and weightage to the expert remarks, Multi Criteria Decision Making (MCDM) Fuzzy TOPSIS is used. It is obtained that renewable energy is most suitable power source with highest confidence level of 0.530363 than conventional power source with 0.469075 for Indian climatic conditions.

Keywords
MCDM,

NOMENCLATURE
A1   Solar Power
A2   Thermal Power

INTRODUCTION

India is third largest (1217.709 BkWh) producer of electricity in the world after the China and United States [1]. According to government of India as on January 2017, per capita electricity consumption is 1075 kWh and it will reach 1500 kWh till 2022 [2]. In India, electricity demand is continuously increasing because of better living standard and increase in population. It is expected, electricity demand will reach around 4500 BkWh by 2031-32 [3]. India is mainly dependent on Non-conventional power sources, in total installed (329226.27 MW) power 66.67% power is fulfilled by Non-conventional power sources [4]. Due to environmental pollution and depletion of fossil fuels, government major concern on renewable energy sources.

India has huge potential of renewable energy sources of about 900 GW from commercially exploitable source. In overall potential Solar energy having major portion of 750 GW (assuming 3% waste land) and remaining portion is covered by Wind energy 102 GW (assuming hub height at 80 m), Bio-energy 25 GW and Small Hydro 20 GW [5].

Sonal et al. [6] discussed Strength-Weakness-Opportunity-Challenges (SWOC) of solar energy deployment for indian climatic conditions. They applied Analytical Hierarchy Process (AHP) technique to prioritize the SWOC variables. They found opportunity factor as most dominant factor and weakness as least dominant factor for deployment of solar energy. Manju and Sagar [7] done a critical review on current status, applications, developmental barrier and prospects of solar photovoltaic systems in India. They discussed various applications of solar energy such as water heater, dryer, cooker, desalination, air conditioning units, water pumps and grid connected PV plants for Indian Scenario. They found

Market & Policy issues, Financial issues and Technological issues works as barrier in the growth of renewable energy. Ansari et al. [8] selected thirteen relevant barriers based on literature and subsequent discussions with experts from academia and industry. They developed interpretive structural modeling (ISM) to obtain a contextual relationship among these barriers. They classified the barriers using MICMAC analysis. They identified one barrier as top level barrier and six as bottom level barriers. They also suggested the way of removal of these barriers. Sonal et al. [9] applied integrated ISM and Fuzzy MICMAC approach to identification and analysis the barrier in implementation of solar energy in Indian rural sector. They classified the barriers in major five categories such as Investment, Technical, Financial, Social & Environmental and Marketing & Policy barriers. They found Social & Environmental barrier as dependent and Marketing & Policy barriers as independent barrier for implementation of solar energy in Indian rural sector.

The study involves the comparison of leading solar and coal based power generation in India. The selected drivers mainly covers competitive strategy, share in total power generation, sustainability, cost, transmission efficiency, ease of installation, land area utilization and the kind of resources used to generate electricity. The impact of different power generating plants on the environment and people has been given prime importance while meeting the electricity need i.e transition from conventional sources of energy to green sources of energy.

METHODOLOGY

The proposed methodology is comprised of two approaches. The first stage discusses the current issues of thermal power and solar power i.e SWOT analysis with respect to Indian perspective. The second stage deals with the comparative analysis of drivers or criteria like competitive strategy, share in total power generation, sustainability, cost, transmission efficiency, ease of installation and land area utilization for solar and coal based power generation and generating rank matrix. The third stage deals with the application of MCDM tools to the generated matrix in the second stage.

SWOT Analysis

In first step, we are performing a SWOT (Strengths, Weaknesses, Opportunities and Threats) analysis. The SWOT analysis is a strategic analysis tool that combines both internal assessment (strength and weakness) and external assessment (opportunities and threats) of any system/organization/sector/territory. The aim of this tool is to maximize the potential of strength and opportunities while minimizing the effects of weaknees and threats [10-11].

TABLE 1: SWOT ANALYSIS OF COAL BASED THERMAL POWER PLANT IN INDIA

Strengths	• Efficient Production with large capacity plants • Major Contributor to electricity in India • Huge scope of employment • Most matured technology
Weaknesses	• Depleting natural resources/fossil fuels • Government intervention can often cause disruptions in operations • Rising cost of raw material and power production
Opportunities	• Huge demand and supply gap • Large opportunity in energy consultancy service • Technological upgradation • Employability
Threats	• Prices are regulated by central and state goverments of India • Depletion of fossil fuels • More rigorous environmental regulations • Development of cheaper and more efficient sources of energy

TABLE 2: SWOT ANALYSIS OF SOLAR POWER PLANT IN INDIA

Strengths	• India is having appropriate geographical locations for installing solar PV panels • Reduce Green House Gas emission • Government subsidy for all solar power plants • Suitable for small to large scale entrepreneurs. • Replace a large percentage of fossil fuels. • No operation & maintenance costs
Weaknesses	• High transmission losses • Solar Power is land-intensive (require 4–6 acres for 1 MW PV plant) • High production cost (Rs./kWh) as compared to conventional sources in India. • Lack of awareness among the peoples • Unavailability of solar energy in rainy and cloudy weather. • Lack of technical support at remote locations.
Opportunities	• New employment opportunities and economic benefits • Constant/decreasing PV panels prices • By-products of Solar Power can be used for drying, cooking and desalination. So there is large future research scope
Threats	• Relatively new market and small market share. • Due to huge investment in installation, maintenance and distribution only large investers are interested • Technology is not yet matured

Comparative Analysis of Drivers and Rank Matrix Generation

TABLE 3: RANK MATRIX IS GENERATED BASED ON THE CONSENSUS OF THE EXPERTS

Drivers / Power Source	Electricity Production Cost	Land area Required (per MW production)	Impact on environment	Plant Installation cost	Maintenance cost	Input Fuel Cost	Plant Efficiency	Future Availability of resource
Coal Based Thermal Power	3	3	5	4	4	4	3	2
Solar Power	3	4	1	4	3	1	4	5

MCDM TECHNIQUE : FUZZY TOPSIS

Multi Criteria Decision Making technique consists of a finite set of criterias among which a decision maker has to prioritize or select the criterias. Criterias are weighted based on their Social, Environmental and Economical point of view. Fuzzy TOPSIS technique is used to maximize the benefical criterias and minimize the cost associated criterias [12].

TABLE 4: CRITERIA USED TO EVALUATE ALTERNATIVES IN THE ANALYSIS

Criteria	Description
C1	Minimum electricity production cost
C2	Minimum land area required per MW energy produced
C3	Minimal impact on environment
C4	Low plant installation cost
C5	Low maintenance cost
C6	Minimal input fuel cost
C7	High plant efficiency
C8	Future availability of resource

Experts E1, E2 and E3 rated the criterion and alternatives under each criteria. Alternatives on a linguistic variable having five values, importance weight in fuzzy terms and the crisp values are shown in the Table .

Crisp value, P(A) is calculated using equation (1)

$$P(A) = \frac{(a_1 + 4a_2 + a_3)}{6} \qquad (1)$$

TABLE 5: LINGUISTIC VARIABLES FOR THE IMPORTANCE WEIGHT OF EACH CRITERION AND ITS CRISP VALUE

Linguistic variable	Importance weight of criteria	Crisp values, P(A)
Very Low (VL)	(0, 0.1, 0.3)	0.1167
Low (L)	(0.1, 0.3, 0.5)	0.3000
Medium (M)	(0.3, 0.5, 0.7)	0.5000
High (H)	(0.5, 0.7, 0.9)	0.7000
Very High (VH)	(0.7, 0.9, 1.0)	0.8833

TABLE 6: LINGUISTIC VARIABLES FOR RATINGS AND THEIR CRISP VALUE

Linguistic variable	Importance weight of criteria	Crisp values, P(A)
Very poor (VP)	(0, 0, 3)	0.5000
Poor (P)	(0, 3, 5)	2.8333
Fair (F)	(2, 5, 8)	5.000
Good (G)	(5, 7, 10)	7.1667
Very Good (VG)	(7, 10, 1.0)	9.5000

TABLE 7: IMPORTANCE WEIGHT OF THE CRITERIA BY THE EXPERTS

	Expert 1 (E1)	Expert 2 (E2)	Expert 3 (E3)
C1	H	VH	VH
C2	H	M	H
C3	VH	VH	H
C4	H	H	H
C5	H	VH	M
C6	H	H	H
C7	M	H	H
C8	VH	VH	VH

Calculate the weight for each criteria based on experts opinion and crisp values in table 8 using the equation (2)

$$W_j = \frac{\sum_{t=1}^{k} W_{jt}}{k} \qquad (2)$$

where j is the row number, t is the column number and k is the total number of experts in table 9

TABLE 8: CRITERIA AND THEIR WEIGHT

Criteria	Weight (W_j)
C1	0.8222
C2	0.6333
C3	0.8222
C4	0.7000
C5	0.6944
C6	0.7000
C7	0.6333
C8	0.8833

TABLE 9: EXPERTS RATING OF ALTERNATIVES UNDER DIFFERENT CRITERION

Criteria	Alternatives	Expert 1 (E1)	Expert 2 (E2)	Expert 3 (E3)	Weight (W_j)
C1	A1	P	F	F	4.2777
	A2	G	VG	G	7.9444
C2	A1	P	F	F	4.2777
	A2	G	F	G	6.4444
C3	A1	VG	VG	VG	9.5000
	A2	VP	P	VP	1.2777
C4	A1	F	F	P	4.2777
	A2	G	F	G	6.4444
C5	A1	VG	G	VG	8.7222
	A2	F	G	F	5.7222
C6	A1	VG	VG	VG	9.5000
	A2	F	G	P	5.0000
C7	A1	F	F	G	5.7222
	A2	F	G	F	5.7222
C8	A1	VG	VG	VG	9.5000
	A2	P	P	F	3.5555

Aggregated rating R_{ij} of alternatives A_i with respect to criteria C_j is obtained using the equation (3)

$$R_{ij} = \frac{\sum_{t=1}^{k} r'_{ijt}}{k_i} \qquad (3)$$

TABLE 10: AGGREGATED RATING (R_{ij})

	C1	C2	C3	C4	C5	C6	C7	C8
A1	4.278	4.278	9.500	4.278	8.722	9.500	5.722	9.500
A2	7.944	6.44	1.278	6.44	5.722	5.000	5.722	3.555

Now, the decision matrix is obtained by multiplying weight with aggregated rating ($W_j * R_{ij}$)

TABLE 11: DECISION MATRIX

	C1	C2	C3	C4	C5	C6	C7	C8
A1	3.517	2.709	7.811	2.994	6.057	6.650	3.624	8.391
A2	6.532	4.081	1.050	4.511	3.973	3.500	3.624	3.140

TABLE 12: NORMALIZED WEIGHT OF CRITERION

C1	C2	C3	C4	C5	C6	C7	C8
0.1396	0.1075	0.1396	0.1189	0.1179	0.1189	0.10754	0.14999

Further, apply TOPSIS MCDM method in the decision matrix shown in table 13.
Multiply the normalized weights obtained in table 14 to the respective decision matrix in table 13.

TABLE 13: WEIGHTED DECISION MATRIX

	C1(-)	C2 (-)	C3 (-)	C4 (-)	C5 (-)	C6 (-)	C7 (+)	C8 (+)
A1	0.491	0.291	1.09	0.355	0.714	0.791	0.389	1.258
A2	0.911	0.438	0.146	0.536	0.468	0.416	0.389	0.470

Ideal Solution, X_j: {0.49105, 0.29132, 0.14667, 0.3559, 0.46854, 0.41604, 0.38970, 1.25861}
Negative Ideal Solution, X_k: {0.91198, 0.43885, 1.0905, 0.5362, 0.71419, 0.79048, 0.38970, 0.47098}

Positive and negative sum (S^* and $S)'$ of alternatives (A1 and A2) are obtained using the equations (4) and (5) respectively

$$S^* = \sqrt{\sum(w_{ij} - x_j)^2} \qquad (4)$$

$$S' = \sqrt{\sum(w_{ij} - x_k)^2} \qquad (5)$$

TABLE 14: POSITIVE AND NEGATIVE SUM OF ALTERNATIVES

	S^*	S'
A1	0.92291	1.0446
A2	1.0446	0.92291

Calculation of confidence level, S^*

$$S^* = \left(\frac{s'}{s' + s^*}\right) \qquad (6)$$

The highest confidence level index is considered as the best alternative. A1 and A2 are having confidence level of 0.530363 and 0.469075 respectively. So, solar enery is considered a better sustainable source than Thermal energy.

CONCLUSIONS

In this research study, status of power generation from both conventional and non-conventional (renewable) are discussed. Major portion of demand is fulfilled by the conventional sources but renewable energy sources are also being increasingly sharply due to government policies and incentives. SWOT (Strength, Weakness, Opportunities and Threats) analysis is performed for conventional and renewable energy system. Academia and industry experts are chosen to find out best source of sustainable power in India. 12 different criterias are selected based on literature for analysis. Multi Criteria Decision Making (MCDM) technique: Fuzzy TOPSIS is applied on given remarks of the experts. By analysing, solar energy is found to be more sustainable power source for indian climatic conditions with a confidence level of 0.530363. Thermal energy obtained a confidence level of 0.469075.

REFERENCES

[1] International Energy Agency, https://www.eia.gov/beta/international/, Sept. 2017.
[2] Press Information Bureau, Government of India, http://pib.nic.in/newsite/PrintRelease.aspx?relid=155612, September 2017.
[3] Tripathi, L., Mishra, A. K., Dubey, A. K., Tripathi, C. B., Baredar, P., 2016. "Renewable Energy: An Overview on its Contribution in Current Energy Scenario of India". Renewable and Sustainable Energy Reviews, vol. 60, Jan. 2016, pp. 226-233.
[4] A Report of Central Electricity Authority, GOI, http://www.cea.nic.in/reports/monthly/installedcapacity/2017/installed_capacity-08.pdf, September 2017.
[5] Overview of Potential of Renewable Energy, https://www.geni.org/globalenergy/library/energytrends/currentusage/renewable/Renewable-Energy-Potential-for-India.pdf, Sept. 2017.
[6] Sindhu, S., Nehra, V., and Luthra S., 2017. "Solar Energy Deployment for Sustainable Future of India: Hybrid SWOC-AHP Analysis". Renewable and Sustainable Energy Reviews, vol. 72, May, pp. 1138-1151.
[7] Manju, S., and Sagar N., 2017. "Progressive Towards the Development of Sustainable Energy: A Critical Review on the Current Status, Applications, Developmental Barriers and Prospects of Solar Photovoltaic System in India". Renewable and Sustainable Energy Reviews, vol. 70, pp. 298-313.
[8] Ansari, F., Khrab, R. V., Luthra, S., Shimmi, S. L., and Chatterji, S., 2013. "Analysis of Barriers to Implement Solar Power Installation in India Using Interpretive Structural Modeling Technique". Renewable and Sustainable Energy Reviews, vol. 27, pp. 163-174.
[9] Sindhu, S., Nehra, V., and Luthra S., 2017. "Identification and Analysis of Barriers in Implementation of Solar Energy in India Rural Sector Using Integrated ISM And Fuzzy MICMAC Approach". Renewable and Sustainable Energy Reviews, vol. 62, pp. 70-88.
[10] Fertal, C., Bhan, O., Vaillancout, K., and Waaub, J., 2013. "Canadian Energy and Climate Policies: A SWOT Analysis in Search of Federal/Provincial Coherence". Energy Policy, vol. 63, pp. 1139-1150.
[11] Chen, W., Kim, H., and Yamaguchi, H., 2014. "Renewable Energy in Eastern Asia: Renewable Energy Policy Review and Comparative SWOT Analysis for Promoting Renewable Energy in Japan, South Korea and Taiwan". Energy Policy, vol. 74, pp. 319-329.
[12] 5th International & 26th All India Manufacturing Technology, Design and Research Conference, AIMTDR, ed., 2014., "Integrated AHP and fuzzy TOPSIS Approach for the Selection of a Rapid Prototyping Process under Multi-Criteria Perspective" IIT Guwahati, Assam, India

SEEC-2018-018

INVESTIGATING THE ANTAGONISTIC BLENDING EFFECTS ON DCN OF GASOLINE-ALCOHOL MIXTURES

Fabiyan A S, Nimal Naser, S. Mani Sarathy
King Abdullah University of Technology
Clean Combustion Research Centre
Email: fabiyan.angikathshamsudheen@kaust.edu.sa

ABSTRACT

Studying the ignition response alcohol blending with petroleum fuels is a subject of practical and research interest. Analogous to the octane number, Derived Cetane Number (DCN) of gasoline fuels non-linearly decreases with the addition of lower carbon number alcohols. However, predicting the extent of the non-linearity is not fully established as it involves unknown inter-molecular interactions between base fuel components and the blended alcohol. There is clear evidence that the non-linearity depends on the structural composition of base fuel considered and the type of alcohol chosen. Gasoline fuels containing hundreds of different compounds making it challenging to clearly understand the antagonistic effect observed in the blending studies. In this study, the DCN of Primary Reference Fuels PRF 60, 70 and 84 and three Fuels for Advance Combustion Engines (FACE) gasoline namely FACE I, A and J were blended with two alcohols - propan-1-ol and butan-1-ol, and measured using Ignition Quality Tester (IQT) following ASTM D6890 method. A molar based Gaussian fit was used to model the antagonistic effect and it has successfully fitted the data to greater than $R^2 = 99\%$. By analysing the Gaussian parameters and formulating crucial equations, the antagonistic effect of different combination of fuels is clearly explained. Finally, a linear regression tool was considered to give insights into the effects of structural composition on antagonistic blending effects.

***Keywords* :** ethanol, propan-1-ol, butan-1-ol, biofuel, Gaussian fit, inflection point, antagonistic effect.
.

NOMENCLATURE
Symbols

a,b,c	Gaussian parameters
x	mole fraction
x^*	molefraction at inflection point
DCN^*	normalized derived cetane number
$\rho *$	specific density
AD^*	antagonistic distance at inflection point.
V_a	volume at inflection point.
$a_0, a_1 \ldots \ldots a_7$	linear regression coefficients

INTRODUCTION

A key advantage of blending of gasoline fuels with alcohols such as ethanol and butan-1-ol is the ability to meet the demand for higher octane numbers in modern downsized spark ignition (SI) engines[1]. Higher octane numbers allow engine operations at higher compression ratios and hence greater thermal efficiencies. Addition of ethanol also could potentially lead to lower CO2 emissions [1]. Many nations have came forward to increase the content of biofuels to favour more sustainable energy source.

Another advantage of using simple alcohols in SI engines is their high latent heat of vaporization. This enables the cooling down of SI engines which in turn hinders the knocking effect, commonly known as the charge cooling effect[2]. Alcohol components with higher carbon content such as propanol and butan-1ol have higher latent heat of vaporization and energy density when compared to ethanol with similar octane number boost. Engine knocking is a phenomena that occurs in SI engines

when auto-ignition of fuel-air mixture at the flame end autoignites, creating unstable pressure waves that could harm the engine[3]. It is well known that the addition of ethanol to gasoline suppresses the engine knock tendency [4]. However, limited information is available on the effect of adding simpler alcohols other than ethanol. Analogous to the octane boost, alcohol addition decreases cetane number. The fuels tendency to autoignite is described by the derived cetane number (DCN) which can be obtained using Ignition Quality Tester (IQT) whose specifications are described in ASTM D6890[5]. The octane number and cetane number are observed to have an inverse relationship [6]. The main motivation of this study is to compare the DCN dependence on the structural composition of base fuels and the type of alcohol added. The similarities with research octane number (RON –specification in ASTM D2699[7]) dependence on the PIONA (Paraffin, Iso-Paraffin, Olefin, Naphthene, Aromatics) will also be discussed. This information is highly helpful in designing fuel formulations which favour higher engine efficiency and it is in parallel to reductions of net life cycle greenhouse gases (GHG).

BACKGROUND

There have been several models developed on RON estimation of blended fuels. Recently, Anderson et al. [8], Foong et al. and Aronsson et al [9]reported volumetric and molar non-linearity of ethanol addition to gasoline, suggesting a synergistic effect and this depends on the base fuel composition. Al-Ramadan et al. [10] proposed a molar based blending model to predict the octane response of toluene primary reference fuels (TPRF) mixtures with ethanol. Recently, Badra et al [11] proposed a more detailed ON model with an attempt to correlate ethanol synergism with 8 different classes of gasoline components. They commenced with the pure components Heptane, Iso-pentane, hex-1-ene, cyclo-pentane and 1,2,3,trimethyl benzene that represent the Paraffin, Iso-paraffin, Olefin, Naphthene and Aromatic (PIONA) classes of gasoline, blended with ethanol at different proportions. From these measurements, they developed a molar based model that was validated by FACE fuels/ethanol blends. They concluded that the synergism is proportional to paraffinic and iso-paraffinic content in the base fuel, while it declines with aromaticity and olefins and naphthenes are observed to show linear blending effects.

The models were able to suggest synergistic effect and give possible relations to the base fuel composition. The present work studies on reduction in derived cetane number on blending with alcohols. The reduction in DCN does not follow the linear trend, instead it follows non-

linear behavior and shows a magnitude less than the corresponding linear value. This study focuses on blending of primary reference fuels (PRF 60,70,84) and 3 Fuels for advanced combustion engines (FACE I,A,J) with alcohols. Propan-1-ol(POH) and butan-1-ol(BOH) are the considered blending agents. The motivation to give preference to these alcohols over ethanol is because of their high latent heat of vaporization and high energy density per volume. The whole study can be summarized into 3 key points.

- Quantify the anatagonistic effect of blending and finds its dependence on structural composition of base fuel.
- Compare the antagonistic effect of the alcohols studied.
- Find an optimum volume or mole fraction of alcohols that maximize the blending effect.

EXPERIMENTAL METHODOLOGY

Experiments was done on Ignition Quality Tester as per ASTM D6890[3]. For a constructive fitting of data, seven volumes of propan-1-ol and butan-1-ol such as 5,10,15,20,30,50,70% on a gravimetric basis were considered for the experiment which then translated later into mole-fractions.

GAUSSIAN MODEL FOR BLENDED FUELS

In Mathematics, a Gaussian Equation is expressed as follows [12].

$$f(x) = a.e^{\frac{-(x-b)^2}{2c^2}} \qquad -(3)$$

For arbitrary real constants a, b and c. The graph of a Gaussian is a characteristic symmetric Bell curve shape.

- The parameter „a" is the height of curve's peak.

    $At\ x = b, f(x) = f(b) = a.e^{-0} = a.$

- The parameter „b" is the value of variable „x" at which the curve reaches the peak.
- The parameter „c" tells about the width of the curve or extend of deviation (standard deviation, sometimes called the Gaussian RMS width) from the mean point $f(b) = a$.

Inflection Point (IP)

In differential calculus, the inflection point is the point at which the direction of curvature changes its sign while a tangent still exists. If the function is double differentiable, the value at which the second derivative becomes zero is the inflection point. In a Gaussian curve,

$$f''(x) = 0 => IP, x = b \pm c. \qquad -(4)$$

In this study, only the right hand coordinate is considered, thus one IP $(x = b + c)$. At this IP, the sign of $f''(x)$ changes from $'-\ to +'$. Here, in graphical terms, the inflection point is the starting point where curvature

changes from steep to moderate.

At $x^* = b+c$, $f(x^*) = \dfrac{a}{1.6487}$ - (5)

This shows that the value at inflection point depends only on the peak value of the curve (a).

Normalized DCN (DCN*)

In order to fit Guassian model to blending studies, normalized (DCN*) vs molefraction (x) is plotted.

$$DCN^* = \frac{DCN_{d(m)} - DCN_{ol(a)}}{DCN_{b(b)} - DCN_{ol(a)}} \qquad -(6)$$

where,

- $DCN_{blend(mix)}$ - Blended derived cetane number of fuels of known mole-fractions.
- $DCN_{Alcohol(a)}$ - DCN of pure alcohol component.
- $DCN_{base(b)}$ - DCN of pure base fuel taken.

At mole fraction x=0 or no alcohol is added to the base fuel, $DCN_{mix} = DCN_b$. So, $DCN^* = 1$. At mole fraction x =1, $DCN_{mix} = DCN_a$ or $DCN^* = 0$. Therefore, the y axis or DCN^* runs between 0 to 1 in all blended fuel cases and provides platform for effective comparison between different combinations chosen. If an assumption is carried out such that DCN of blended fuels follows a linear relationship, then,

$$DCN_{blend(mix)} = x.DCNa + (1-x)*DCNb \qquad -(7)$$

Substituting (7) in (6)

$$DCN^*_{Linear} = \frac{(x.DCNa + (1-x)*DCNb) - DCN_{(a)}}{DCN_{(b)} - DCN_{(a)}} = (1-x) \quad -(8)$$

This means that when normalized, the linear trend follows the equation $x + y = 1$.

In normalized terms, the parameter „a"~1. Thus Eq(5) can be rewritten, $f(x^*) = 0.6065$. The following plots show the common line at $DCN^* = 0.6065$, and the lines to the corresponding IP's in the x-axis .
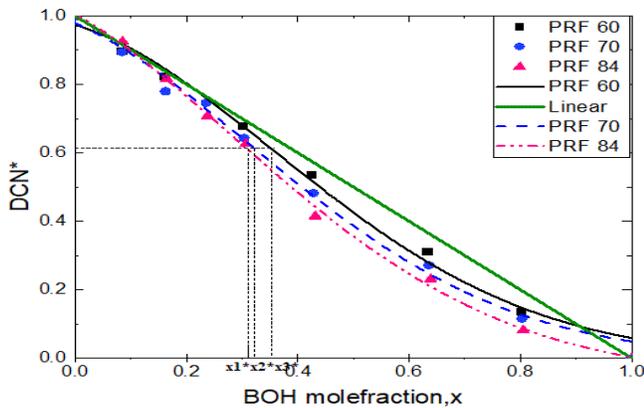
Figure 1: DCN* vs Butan1-ol (BOH) mole-fraction for PRF 60, PRF 70 and PRF 84. The scattered points, Gaussian fitting

(curve) and linear change of DCN* from Eq (8) are shown in the plot. The IP's x1*,x2*,x3* corresponds to PRF 84,70,60 respectively.
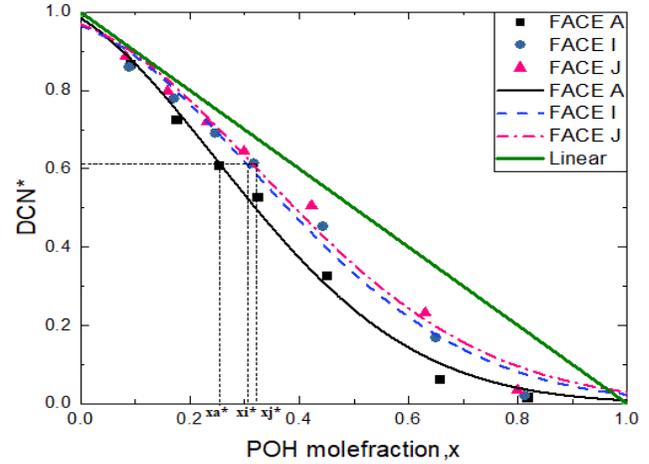
Figure 2: DCN* vs Propan-1-ol (POH) mole-fraction for Face I, A, J. The IP's xa*,xb*,xj* corresponds to Face A,I,J respectively.

DISCUSSIONS

Our method shows that fitting normalized scattered DCN* points with Gaussian curve works well in all cases of blending. In all the curves, the DCN$_{mix}$ is lower than its corresponding linear trend from eq(8). In other terms, there is antagonistic blending effects.

The curve changes the direction at inflection point from steep to moderate. So for fuel designers, it is profitable to blend until molefraction of alcohol =IP, thereby optimizing the alcohol blending effect. In other terms blending effect is strongest until IP and then it eventually degrades.With the help of Gaussian fitting, the DCN$_{mix}$ at inflection point of any blend can be unmasked. This is because for all blends, DCN* at x=IP is approximately constant (as defined in modified eq5). In simple terms, with a known DCN of fuel and alcohol, the optimum DCN$_{mix}$ can be determined from the DCN*. This optimises the amount of alcohol required, energy content of the blend, and DCN hindrance or the octane boost in improving the anti-knock properties of gasoline blends.

From Table 1, the general trend is that a lower inflection point results in higher antagonistic nature because the normal distance between linear and the curve(AD*) is higher. Also by converting mole fraction at IP to volume (Va*), the lowest volume of alcohol at IP can be obtained for higher antagonistic blends.

Among the primary reference fuels, the antagonistic trend is as follows PRF84 > PRF70> PRF 60. The same was observed in Figure 1 for BOH.Among the FACE fuels, FACEA>FACE I>FACE J. The same can be observed in Figure 2 for propan-1-ol (POH). The antagonistic behaviour is observed higher for POH than BOH. This shows that POH is a better blending agent than BOH.

Table 1: Summarizing the blending effect properties of fuels (IP, volume of alcohol at IP, AD*) with POH(propan-1-ol)

Fuel	DCN$_b$	Fuel Composition (mole%)						fit(R^2%)	IP (x* = b+c)	POH vol at x*= Va* (ml)	Antagonistic distance(AD*) *10^{-2}
		Para	I-Para	Arom	Naph	Olef	BI				
PRF 60	36.3	41.8	58.2	0.0	0.0	0.0	0.36	99.5	0.333	19.1	6.0
PRF 70	31.6	32.5	67.5	0.0	0.0	0.0	0.42	99.4	0.324	18.3	7.5
PRF 84	26.4	17.5	82.4	0.0	0.0	0.0	0.5	99.4	0.263	14.1	12.0
Face A	25.6	13.2	83.7	0.3	2.4	0.4	0.42	99.6	0.247	14.6	12.7
Face I	31.8	14.4	69.7	4.9	4.1	6.8	0.38	99.4	0.314	19.8	8.9
Face J	28.6	31.5	32.4	32.9	2.3	0.6	0.68	98.6	0.331	22.5	5.1

From Table 1, comparing antagonistic distance, AD*, provides information on the blending performance trend. It follows that FACE A>PRF 84>FACE I>PRF 70>PRF 60>FACE J.Though the DCN of some of base fuels are closer (FACE A, PRF 84) and (FACE I,PRF 70), the antagonistic blending features are different. The performance is unique for a type of fuel and alcohol chosen suggesting that structural composition of base fuel has a clear role.

Linear Regression

Linear Regression of AD* with repect to structural composition of base fuels is carried out to analyse their effect on blending performance. At global minima of rms = 2.468, the dependence on structural parameters is described

$$A_D^* = -0.31 + 0.024 * [para] + 0.086 * [Iso] - 0.245 * [Arom] + 0.97 * [Naph] - 0.109 * [Olef] + 22.43 * B.I - 0.93 * [DCN_a] \qquad -(9)$$

CONCLUSIONS

The Gaussian fit model helps to optimize the blending effect. Its profitable to blend till the inflection point and after that it starts to degrade. Propanol is considered to be a better blending agent than butan-1-ol. The blending performance is unique for a type of fuel and alcohol chosen suggesting that the antagonistic effect strongly depends on structural composition of fuel. The most significant positive term in Eq 9 is the branching index (B.I) of the base fuel implying that more the branching, more the A_D^*. Indirectly it gives clue that iso-paraffinity presence causes DCN hindrance.The contribution of aromatics and olefins to the antagonistic behavior is shown to be negative. The presence of double bonds is responding opposite to para and iso-para making the blending effect closer to linear. FACE J fuel with maximum presence of aromatics shows the least antagonistic performance in blending.

ACKNOWLEDGMENTS

REFERENCES

[1] Anderson JE, DiCicco DM, Ginder JM, Kramer U, Leone TG, Raney-Pablo HE,et al. High octane number ethanol–gasoline blends: Quantifying the potentialbenefits in the United States. *Fuel 2012;97:585–94*.

[2] Stein RA, House CJ, Leone TG. Optimal use of E85 in a turbocharged direct injection engine. SAE Int J Fuels Lubr 2009;2:670–82.

[3] Heywood JB. Internal combustion engine fundamentals. New York: Mcgrawhill;1988.

[4] Da Silva R, Cataluna R, de Menezes EW, Samios D, Piatnicki CMS. Effect of additives on the antiknock properties and Reid vapor pressure of gasoline, *Fuel 2005;84:951–9.*

[5] ASTM D6890 Standard Test Method for Determination of Ignition Delay and Derived Cetane Number (DCN) of Diesel Fuel Oils by Combustion in a Constant Volume Chamber;2013**.**

[6] Naser,N.,Yang,S(2017).Relating the octane numbers of fuels to ignition delay times measured in an ignition quality tester (IQT).*Fuel,187,117-127.*

[7] Standard test method for research octane number of spark-ignition engine fuel. *ASTM D 2699 - 13b; 2013*.

[8] Anderson J, Kramer U, Mueller S, Wallington T. Octane numbers of ethanol and methanol gasoline blends estimated from molar concentrations. *Energy Fuels 2010; 24:6576–85.*

[9] Solaka Aronsson et al. Using oxygenated gasoline surrogate compositions to map RON and MON. SAE International, *SAE Technical Paper 2014-01-1303; 2014*.

[10] AlRamadan AS, Sarathy SM, Khurshid M, Badra J. A blending rule for octane numbers of PRFs and TPRFs with ethanol. *Fuel 2016;180:175–86.*

[11] J. Badra, A. S. AlRamadan, and S. M. Sarathy, "Optimization of the octane response of gasoline/ethanol blends," *Appl. Energy*, 2017.

[12] C.Walcke, Handbook on statistical distributions for experimentalists,ch34,pg119.

An approach for bioremediation of distillery spent wash and biomass production using Microbial Fuel Cell

Jagdeep Kumar Nayak[1] (Research Scholar), Uttam Kumar Ghosh*[1] (Associate Professor)

[1]Department of Polymer and Process Engineering, Indian Institute of Technology Roorkee, India.

* Corresponding author: Uttam Kumar Ghosh

E-mail: uttamghosh.iitr@gmail.com

Distillery spent wash (DSW) has become a major source of environmental pollution due to the presence of organic, inorganic pollutants and heavy colour load in it. DSW is a good source of high organic matter and nutrients for microorganism growth. In the present study, bio-electrochemical treatment approach was made to treat DSW using microbial fuel cell (MFC) system. In anaerobic environment DSW was used as substrate in anodic compartment and cathodic compartment was filled with BBM media and *Scenedesmus abundans*. CO_2 generated during breakdown of organic substrates by anaerobes present in DSW was utilized by microalga *Scenedesmus abundans* for photosynthesis. DSW was treated for 21 days using a mixture of two anaerobic bacteria. Significant reduction in COD (10% to 70%), total dissolved solid (30%) and suspended solid (69%) has been achieved. A power density of 180 mW/m^2 and open circuit voltage (OCV) of 351 mV were obtained along with biomass concentration of 516 mg/L.

Keywords: Microbial Fuel Cell, Distillery spent wash, Bioelectricity, Microalgae

1. Introduction:

The extensive use of fossil fuels, especially oil and gas, in recent years has triggers a global energy crisis which causes depletion of fossil fuels, environmental pollution and efficient development of renewable energy sources. Renewable bio energy is viewed as one of the ways to improve the current global warming crisis [1].

Microbial fuel cell (MFCs) is an emerging technology which use microbial interaction to convert chemical energy to electric energy and value added product through the metabolic activity of microorganisms [2, 1, and 3]. A general design of a two chambered MFC is consist of both anodic and cathodic compartment, microorganisms (Fig. 1). The electrons produced in anodic chamber, passing through external circuit and along with protons passing through a proton exchange membrane (PEM) react with an oxidizing agent, such as oxygen, at the cathode surface which leads to close the circuit.

During the process of ethanol production in alcohol distillery industries, a large volume of liquid waste effluent rejects comes out of the distillery industry as spent wash. This high strength toxic liquid waste is a discharge from the fermentative production of ethanol [4]. Brewery wastewater containing COD of 2000 mg/l was treated in dual chambered (rectangular) MFCs (0.2 L anode volume), to obtain power density of 305 mW/m2 at 30 ± 2 °C with 80% removal of COD [5].

2. Materials and Methods:

2.1 Bacterial Culture and *Scenedesmus* sp. Cultivation

Scenedesmus abundance was procured from NCCS Pune and store in 4°C. Before inoculation in standardized BBM (Bolds Basal medium), media was sterilized for 30 mins by maintaining 120°C at 150 lb [6]. *Pseudomonas aeruginosa* and *Bacillus subtilis* was obtained from NCL, Pune. Both the bacteria were cultured in agar media at 25 °C. The effluent was collected from malt based distillation plant and was preserved in 4°C prior using. Pre-treatment of distillery effluent by sterilization was done before experiment.

2.2 Experimental Setup

The experimental setup of MFC was designed and fabricated using Plexiglas. The constructed MFC contain two cylindrical chamber with a working volume 900ml each separated by proton exchange membrane (Nafion) from DuPont international. Both the electrode were graphite. The two chamber was connected with an outlet to pass gasses produced from anode chamber during anaerobic respiration. The whole set up was operated in batch mode.
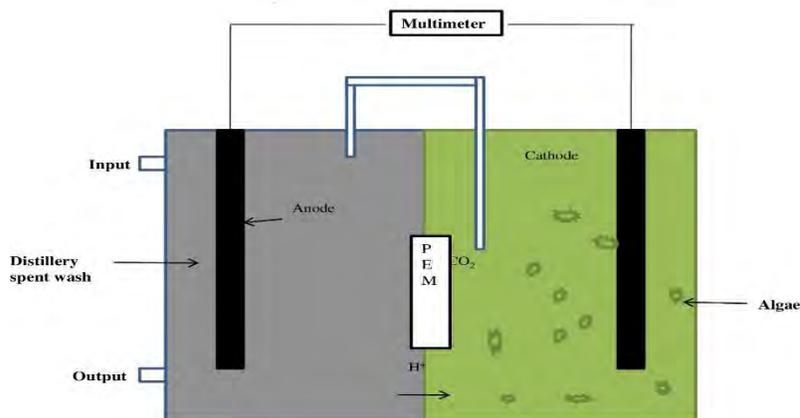
Fig 1. Experimental set used in this study

2.3 Electro chemical Analysis and Calculation

Power was calculated by using Ohm's formula; $P = V^2/R$ where V and R is the Voltage and Resistance respectively. The power was normalized to the anode surface in order to calculate power density (mW/A^2). Power density was calculated according to the electrode surface area; $PD = P/A$ where A is the total surface area of electrode in m^2. The COD removal efficiency (% age) was calculated using Eq. (1).

$$\text{COD Removal (\% age)} = \frac{c_i - c_f}{c_i} \times 100 \qquad \text{(Eq. 1)}$$

Several parameter including COD, TDS, TSS, TS were characterized of the sample in each day as per the Standard methods (APHA, 1998).

Table 4. Physiochemical parameters of distillery spent wash

Parameters	Color	Odor	pH	COD	TDS	TSS	TS	Total Alkalinity	Chloride	Calcium	Magnesium	Total Phosphorous	Total Potassium
Distillery spent wash (DSW)	Dark brown	Unpleasant	4.5± 1.5	65000 - 75000	37500	6500	44000	2160	4900	1850	1100	14680	1000

2.4 Algal growth

The concentration of algae biomass was collected in every day basis and was measured by UV spectrophotometer at 680 nm and converted in to biomass curve using standard. The sample was collected and centrifuged at 6200 rpm for 5 min and vacuum dried overnight at 104 °C. Dry mass was estimated by gravimetric process.

3. Results

3.1 Electricity generation

MFCs were operated in a proper anaerobic condition in anodic chamber with precautions for 21 days. The output data of voltage was monitored in multimeter and illustrated in fig.3 with resistance (100 Ω).Stable voltage growth was seen after 12-14 days which indicates the highest degradation of organic substances after this period. The output of 100% DSW also showed higher power density from the other studies. The peak power density and COD removal efficiency was observed as 180 mW/m2 and 70% at optimum environment (Fig.2). The distillery
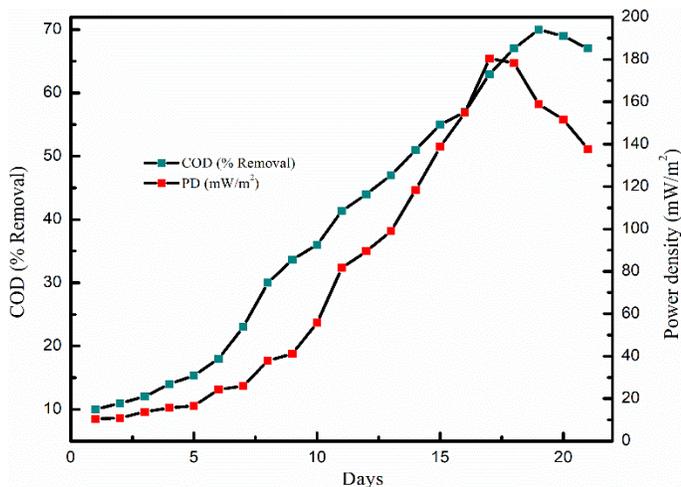
Fig 2. Effect of COD (% Removal) with PD (power density)
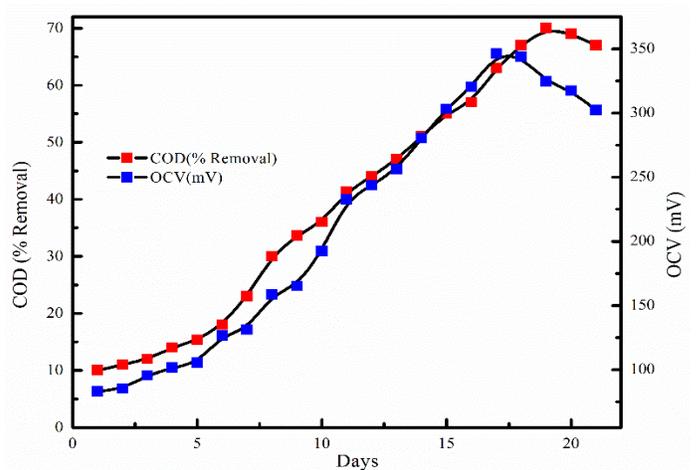
Fig 3. Relation between COD (% removal) and OCV (mV)

effluent was utilized as an organic substrate for bacterial biocatalyst and produces electrons (e-) and protons (H+) through redox reaction which facilitating power generation [7]. After 10 days, the MFCs yielded a relatively stable operating potential of 193.33 mV in 100% distillery effluent. The generation of maximum voltage and power density of 346.2 mV and 180.42 mW/m2, respectively (Fig. 3) was noticed on 17th day and the output was quite high than previous studies.

3.2 Substrate degradation analysis

The correlation between voltage outputs and COD concentration over incubation period of the distillery spent wash was monitored (Fig. 4). The steady incline in COD reduction percentage with an increase in cell voltage over time, indicates the capability of the inoculated consortia culture to remove COD of the distillery spent wash and generate electricity. After successful run, effective wastewater treatment was noticed as well as power generation. COD removal along with TDS, TSS (30% and 69%) and other component reduction was observed (Fig. 5). The value of voltage was decreased after a steady removal efficiency of COD due to unavailability of organic nutrient. Distillery effluent showed lowest removal efficiency of 65% due to presence of high organic load. It was difficult to sustain microbes in high COD. Time taken by microbes in lag phase was around 5th-8th days. After acclimatized with sample the growth of microbes and removal of COD was quite increased up to 16th-19th days.
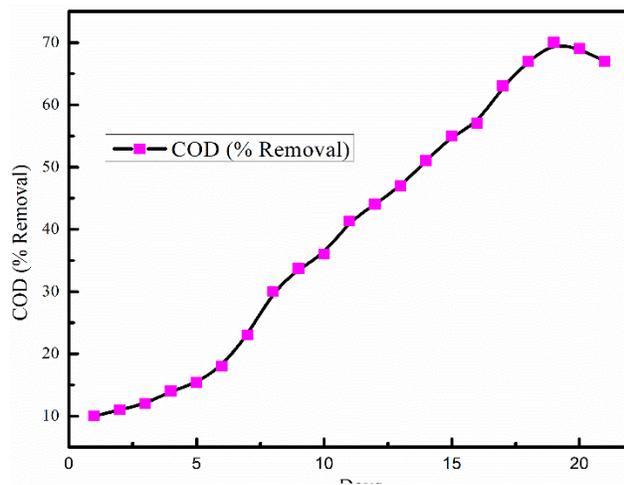
Fig 4. COD (% removal) in the incubation period
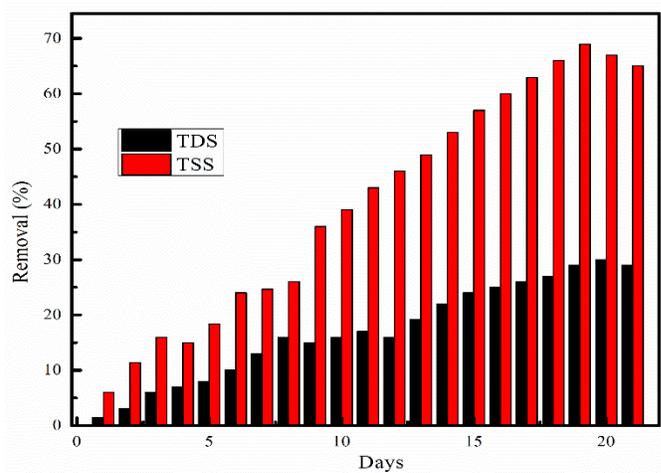
Fig 5. TDS and TSS removal (%) during 21 days of the incubation

3.3 Biomass production

In this study, the culture conditions are same but CO_2 for algae growth was supplied from the anode chamber of different concentration to the cathode chamber in which algae was cultured and the growth of microalgae was observed. *Scenedesmus abundans* showed the maximum biomass productivity of 0.516 g/Ld^{-1}in 50% dilution of distillery experimental setup on 21th day of cultivation period as shown in fig 6, which indicates the maximum anaerobic digestion in anodic chamber. *Scenedesmus abundans* has a lag phase of 5 days before going to the exponential phase. It attained the stationary phase at 21th day of cultivation period.
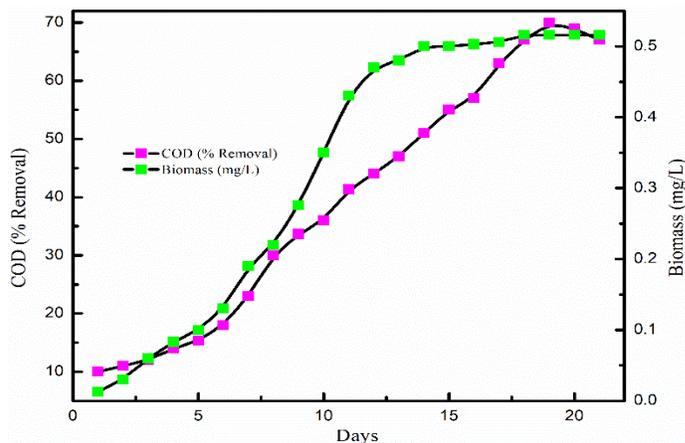
Fig 6. Relation between COD (% removal) and Biomass production (g/L)

4. Conclusion

In this study, the efficiency of H-type two chamber MFC using mixture of distillery wastewater and sewage wastewater as a substrate was systematically observed. The feasibility of power generation using microalgae was demonstrated. The maximum power density (180 mW/m^2) and maximum OCV (351 mV) in this study were found relatively higher as compared to other reports. The production of CO_2 by the degradation of organic and inorganic compound could be used by microalgae to promote their growth as well as oxygen generation at cathode. The maximum growth of biomass 516 mg/L was noticed. This study suggests that proper dilution of distillery wastewater and optimized condition for microalgae growth can be a promising way for high power generation in MFC operation.

References

[1] Du, Z., Li, H., Gu, T., 2007. A state of the art review on microbial fuel cells: A promising technology for wastewater treatment and bioenergy. Biotechnol. Adv. 25, 464–482.

[2] Pant, D., Van Bogaert, G., Diels, L., Vanbroekhoven, K., 2010. A review of the substrates used in microbial fuel cells (MFCs) for sustainable energy production. Bioresour. Technol. 101, 1533–1543.

[3] Xiao, L., He, Z., 2014. Applications and perspectives of phototrophic microorganisms for electricity generation from organic compounds in microbial fuel cells. Renew. Sustain. Energy Rev. 37, 550–559.

[4] David, C., Arivazhagan, M., Tuvakara, F., 2015. Decolorization of distillery spent wash effluent by electro oxidation (EC and EF) and Fenton processes: A comparative study. Ecotoxicol. Environ. Saf. 121, 142–148.

[5] Miran, W., Nawaz, M., Kadam, A., Shin, S., Heo, J., Jang, J., Lee, D.S., 2015. Microbial community structure in a dual chamber microbial fuel cell fed with brewery waste for azo dye degradation and electricity generation. Environ. Sci. Pollut. Res. 22, 13477–13485.

[6] Kondaveeti, S., Choi, K.S., Kakarla, R., Min, B., 2014. Microalgae Scenedesmus obliquus as renewable biomass feedstock for electricity generation in microbial fuel cells (MFCs). Front. Environ. Sci. Eng. 8, 784–791.

[7] Mohanakrishna, G., Venkata Mohan, S., Sarma, P.N., 2010. Bio-electrochemical treatment of distillery wastewater in microbial fuel cell facilitating decolorization and desalination along with power generation. J. Hazard. Mater. 177, 487–494.

SEEC-2018-0021

LIFE CYCLE SUSTAINABILITY ANALYSIS OF JATROPHA BIODIESEL

M.Tech Automotive Engineering
VIT University- Vellore
Email[1]: vignesh.s2017@vitstudent.ac.in
Email[2]: m.mahesh2017@vitstudent.ac.in

Thangaraja J[3]
Associate Professor, SMEC
VIT University – Vellore
Email[3]: thangaraja.j@vit.ac.in

ABSTRACT

Biodiesel is one of the promising alternative fuel for compression ignition engines and numerous research has been carried out to evaluate their performance and emission characteristics. However, India is not able to meet its ambitious target of substituting 20% of fossil diesel consumption by biodiesel within the planned timeline[4]. Further, substitution of biodiesel fuels has created uncertainty over sustainable development goal (SDG) number 7[8]. A plethora of resources, over 32 million hectares of Indian land for crop cultivation also raises concern about the food versus fuel contest[14]. Hence, this paper attempts to evaluate the energy, environmental, economical and social indicators for promoting jatropha biodiesel with respect to Indian scenario. The energy balance and net carbon dioxide analysis for cultivating jatropha as a biofeedstock is carried out using the commercial GREET software. Further, the benefit to cost ratio[1] for jatropha is compared with the conventional diesel fuel. Though earlier studies have mentioned the cost of jatropha oil around 30 rupees per litre[5], the current market rate has quadrupled.

***Keywords:** Life cycle sustainability, GREET, Benefit to Cost ratio, Jatropha.*

NOMENCLATURE

BCR   Benefit to Cost Ratio
FER   Fossil Energy Ratio
NEG   Net Energy Gain
NER   Net Energy Ratio

INTRODUCTION

Mobility has become essential etiquettes in day to day life. Transportation sector handed a new life to automobiles since last decade. With booming population in India, requirement of fuel has created uncertainty in sustainability for future generations to take over. But the fuels used today are fossil based courtesy to its exhaustive nature.

According to estimated wasteland reports, there are about 50 million hectares available in India in the form of waste lands [18]. Ever since Jatropha has become a corner stone for one of the alternate fuels which can be renewable, non toxic, biodegradable [20] and thus Government of India has announced the biodiesel mission phase 1 i.e. 5% blend of biodiesel [5]. The demands are expected to rise by 6-8 percent in future. India's energy security would remain in risk until alternative fuels are developed[18].

India is focusing more on feedstocks like Jathropha, Karanja, and Algae etc. The Planning Commission Report has proposed of blending 5 percent of biodiesel with diesel from 2006-2007 and further rise of blend to 20 per cent in 2011-2012[5]. The National Mission on Biodiesel was proposed in two phases. Phase I consists of introduction of the project to be implemented by the year 2006-2007. This involves expansion of plantation and other related infrastructure for meeting the 20 per cent blending target in year 2011-2012[4].Purchase price was estimated to be 26.50 per litre. The self-sustaining phase of the National Mission was to bring in about 11.2 million ha of land under jatropha plantation by 2011–12 in order to meet the 20 per cent target [15].The government has also made Rural Employment Guarantee Act (NREGA), eligible for feedstock cultivation of Jatropha[19].

METHODOLOGY
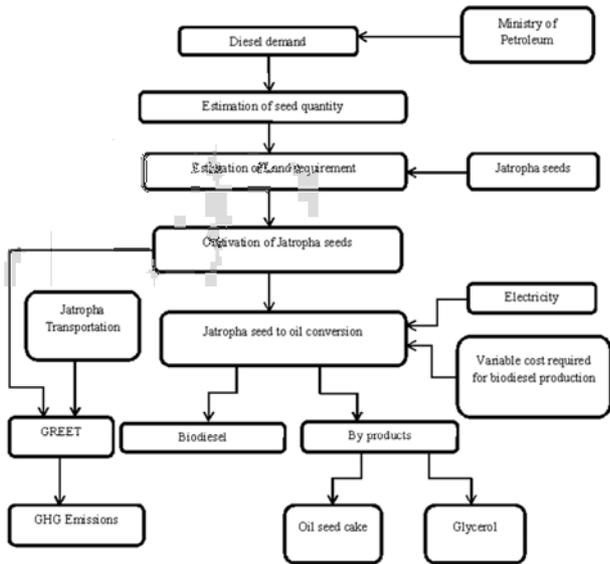
FIGURE. 1 Flow chart representing the sequence of biodiesel production

The diesel demand is obtained from Ministry of Petroleum & Natural Gas, India. By fixing the diesel demand, the quantity of jatropha seeds required is calculated. Depending on the quantity of seeds the land required for cultivation is estimated. This contributes the cost of cultivation for jatropha seeds. Then the seeds is converted to oil by crushing and it is transesterified with Methanol and Sodium hydroxide, the byproducts are Oil seed cake and Glycerol. The emissions released during the Jatropha oil production is simulated in GREET software. The complete pathway is divided into three processes namely Jatropha cultivation, Jatropha transportation and Jatropha to Jatropha oil conversion. After providing the inputs to the software the emissions are simulated.

$$\text{Net Energy Gain} = \text{Energy Output} - \text{Energy Input} \quad (1)$$

$$\text{Net Energy Ratio (NER)} = \frac{\text{Energy output}}{\text{Enegry input}} \quad (2)$$

$$\text{Fossil Energy Ratio} = \frac{\text{Renewable energy otuput}}{\text{Fossil energy input}} \quad (3)$$

$$\text{Specific Energy} = \frac{\text{Output energy}}{\text{No. of seeds}} \quad (4)$$

$$\text{Enegry productivity} = \frac{\text{Yield}}{\text{Input energy}} \quad (5)$$

$$\text{Energy Intensiveness Value} = \frac{\text{Total energy obtained}}{\text{Gross Production Value}} \quad (6)$$

$$\text{Benefit to Cost ratio} = \frac{\text{Gross Production Value}}{\text{Total Production cost}} \quad (7)$$

$$\text{Energy Cost Ratio} = \frac{\text{Total energy cost}}{\text{Total Production cost}} \quad (8)$$

$$\text{Total Energy} = \text{Output Energy} + \text{Input Energy} \quad (9)$$

$$\text{Total Energy cost} = \text{Total Energy} \times \text{Cost of energy/kWh} \quad (10)$$

$$\text{Energy Intensity Cost} = \frac{\text{Total cost}}{\text{Yield}} \quad (11)$$

$$\text{Energy Intensiveness} = \frac{\text{Input energy}}{\text{Total cost of production/litre}} \quad (12)$$

TABLE 1 CALORIFIC VALUES OF DIFFERENT CONSTITUENTS

Product	Calorific Value
Jatropha biodiesel	38.5 MJ/Kg.[5]
Diesel	45.34 MJ/Kg.[5]
Oil Cake	19.63 MJ/Kg.[23]
Glycerol	19 MJ/Kg.[17]
Ethanol	29.67 MJ/Kg.[3]
Sodium Hydroxide (NaOH)	19.87 MJ/Kg.[1]

Results and Discussion

The land requirement calculation is based on the quantity of seeds required. The plant density for optimum yield of jatropha is 1517 to 1518 plants per hectare. 2 Kg of Jatropha seeds per plant is the case where minimum land is required for cultivation. Net benefit is the actual cost remaining after processing the byproducts. By fixing zero net benefit, the optimum yield is figured out.

TABLE 2 REPRESENTATION OF YIELD OF JATROPHA SEEDS WITH AREA AND NET BENEFIT

Yield (tonne/Hectare)	Area 20% Jatropha (Million Hectares)	Net benefit 20% Jatropha in Billion Rs.
3.0340	21.211	-0.100
3.0347	21.206	0
3.0350	21.204	0.039

From Table 2 , the optimum yield (with zero net benefit)for jatropha seeds is taken for calculating area required, cost of production and energy calculations.
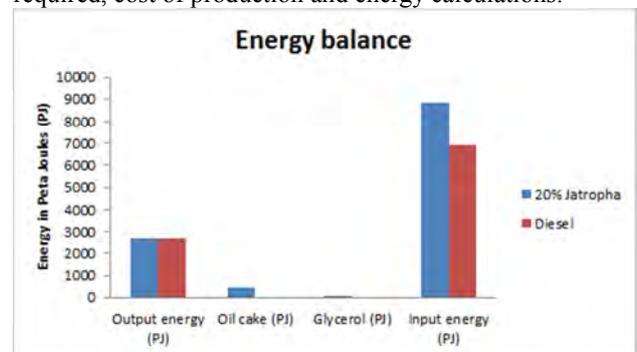
FIGURE.2 Energy obtained from jatropha biodiesel

National energy requirement is taken as the total output for both 20% Jatropha blend and convetional diesel in Fig.2. After fixing the output energy the inputs energy is calculated. Jatropha blend requires more input energy than conventional diesel.
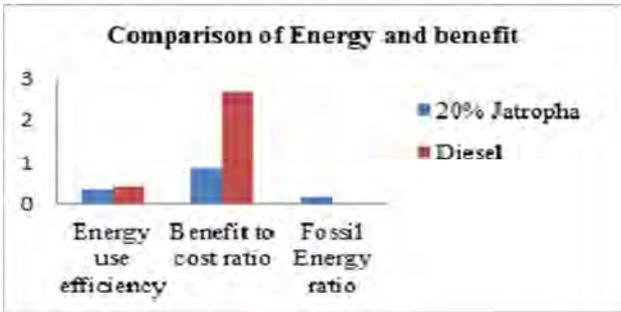
FIGURE 3 Comparison of Energy and cost parameters

From Fig.3 the BCR is low because the cost of production for jatropha biodiesel is higher than diesel.The fossil energy ratio is zero for diesel since there is no renewable energy.For jatropha biodiesel 20% is renewable.Energy use efficiency is 0.36 for jatropha biodiesel and 0.39 for diesel and this is due to higher input energy reqirements for jatropha.
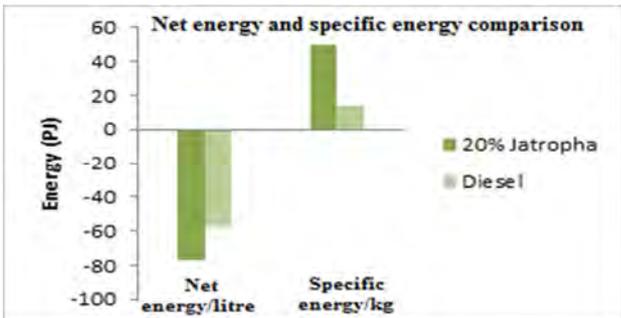
FIGURE 4 Comparison of Net energy and Specific energy

Referring to Fig.4 the net energy of jatropha biodiesel is much lower than diesel because the energy input is high. However the specific energy is high when compared with diesel.
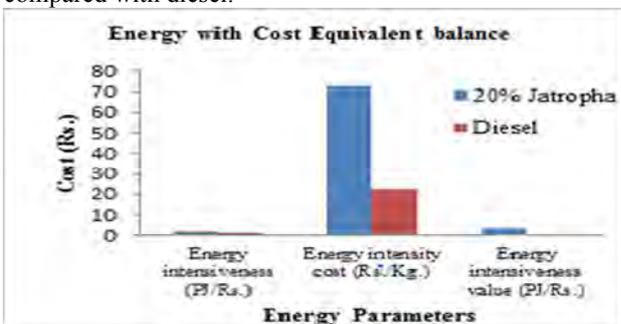
FIGURE 5 Comparison of Economic parameters

Referring to Fig.5 the energy involved in production of biodiesel when converted in to cost equivalent proves to be beneficial when compared with fossil diesel.

Emission balance is calculated for extraction Jatropha oil from 1kg of Jatropha seeds. To estimate the emissions released during the cultivation and the oil extraction process Greet software is used. The emissions were simulated by the software. The GHG(Green House Gases) of 80.08 gram is released to produce MJ of Jatropha oil. Moreover the CO_2 emissions were estimated to be nearly 49.86 g/MJ of Jatropha oil.

Conclusion

India requires 73.215 billion litres of diesel per year. Substituting with 20% Jatropha biodiesel needs 14.643 billion litres extracted from Jatropha oil itself. The land required is 21.206 million hectares for cultivation which serves to be one third of the forest lands available in India. Going with land availability for cultivation India is in a safe position to meet food demands also which compliments as well with Sustainability Development Goal 7[8].On yield basis, 3.034 tonnes of Jatropha seeds per hectare claims break even cost for production. Hence going with optimum yield of 3.034 tonnes per hectare the cost per litre works out to be Rs.61.47. And this is Rs.1.33 higher than the actual cost of diesel.

Net Energy Ratio is lower for Jatropha due to its lower calorific value. Specific energy of biodiesel is 50.183 PJ/Kg. The specific energy for fossil diesel is nowhere near to biodiesel. Energy Cost Ratio is in the positive side when compared with diesel.

The GHG gases released during the Jatropha oil production is simulated in GREET software. From the simulation the GHG-100 released for production of 1MJ of Jatropha oil is nearly 80.7 grams/MJ.

Thus National Biodiesel Mission Phase – 2 is within the reachable limits but the cost wise jatropha biodiesel is slightly higher than diesel. The cost per litre can be fixed as permanent one only when maximum yield is considered. Energy wise the lower calorific value of jatropha seeds impacts in higher quantity of seed requirements thus increases the cost of cultivation. Land availability is not an issue for cultivation of seeds. It is also recommended to have an alternate source with nearby calorific value of diesel.

References

[1] Ahmad Mohmmadshirazhi, Asadolah Akram, Shahin Rafiee, Elnaz Bagheri Kalhor "Energy and cost analyses of biodiesel production from waste cooking oil" –Renewable and Sustainable Energy Reviews · May 2014

3

[2] Mr. Soumitra Biswas, Mr. Gudavalli Srikanth, Ms. Nirmala Koushik "Biodiesel Fuel for the future?" – TIFAC CORE, India.

[3] Alternative Fuels Data Centre – Fuel properties comparison www.afdc.energy.gov

[4] Indian railways organisation for alternate fuels , Ministry of railways , Government of India ,New Delhi . A concept Paper on Alternate fuels for Indian Railways, May- 2013.

[5] Sunil Kumar, Alok Chaube, Shashi Kumar Jain "Sustainability issues for promotion of Jatropha biodiesel in Indian scenario: A review" - Renewable and Sustainable Energy Reviews 16 (2012) 1089– 1098

[6] S.Antony Raja, D.S.Robinson smart, and C.Lindon Robert Lee "Biodiesel production from jatropha oil and its characterization" - Research Journal of Chemical Sciences Vol. 1 (1) April (2011)

[7] Tingting Zhang, Xiaomin Xie, and Zhen Huang "Life Cycle Land Requirement, Energy Consumption and GHG Emissions of Biodiesel Derived from Microalgae and Jatropha *curcas* Seeds in China"– SAE 2014-01-1964

[8] Michael Acheamponga, Funda Cansu Ertem, Benjamin Kappler, Peter Neubauer "In pursuit of Sustainable Development Goal (SDG) number 7: Will biofuels be reliable ?" - Renewable and Sustainable Energy Reviews 75 (2017) 927–937

[9] Samodini S. Nevase, P.S. Dharpal, K.N. Barse and S.R. Gadge "Economic Feasibility of Jatropha Oil as Biodiesel" - Economic Affairs, Vol. 61, No. 4, pp. 667-670, December 2016

[10] Total forest and Tree cover has increased; Increase in Carbon stock an assurance to negotiators at Cop 21: Javadekar- Environment Minister Releases India State of Forest Report 2015

[11] Avelino Corma, Laurent Sauvanaud, Yannick Mathieu, Saad Al-Bogami, Abdennour Bourane, Musaed Al-Ghrami "Direct crude oil cracking for producing chemicals: Thermal cracking modeling" - Fuel 211 (2018) 726–736.

[12] Indian Oil Product prices – 24/10/2017.

[13] Previous prices of diesel, Indian Oil Corporation Limited – 28/10/2017.

[14] Atta Ajayebi, Edgard Gnansounou, Jegannathan Kenthorai Raman "Comparative life cycle assessment of biodiesel from algae and jatropha: A case study of India" - Bioresource Technology 150 (2013) 429–437

[15] "Biofuel Promotion in India for Transport: Exploring the Grey Areas" Policy Brief – The Energy and Resources Institute – February 2015

[16] Samodini S. Nevase1, S.R. Gadge, A.K. Dubey and B.D. Kadu "Economics of biodiesel production from Jatropha oil" - Journal of Agricultural Technology 2012 Vol. 8(2): 657-662

[17] N.H.Ravindranath,C.SitaLakshmi,Ritumbra Manuvie, P.Balachandra "Biofuel production and implications for land use, food production and environment in India" - Energy Policy 39 (2011) 5737–5745

[18] Wouter M.J. Achten, Joana Almeida, Vincent Fobelets, Evelien Bolle, Erik Mathijs, Virendra P. Singh, Dina N. Tewari, Louis V. Verchot, Bart Muys "Life cycle assessment of Jatropha biodiesel as transportation fuel in rural India" - Applied Energy 87 (2010) 3652–3660

[19] Sunil Kumar , Alok Chaube , and Shashi Kumar Jain ,Chapter 2 "Importance of Jatropha curcas for Indian Economy" N. Carels et al. (eds.), Jatropha, Challenges for a New Energy Crop: Volume 1: 13 Farming Economics and Biofuel.

[20] Owolabi R.U., Adejumo A.L., Aderibigbe A.F" "Biodiesel: Fuel for the Future (A Brief Review)" - International Journal of Energy Engineering 2012, 2(5): 223-231

[21] Kishore Chandra Swain "Biofuel Production in India: Potential, Prospectus and Technology" - Fundamentals of Renewable Energy and Applications 2014

[22] India Biofuels Annual 2017 www.usda.gov.in

[23] J. Ružbarský1, M. Müller and P. Hrab "Analysis of physical and mechanical properties and of gross calorific value of Jatropha curcas seeds and waste from pressing process" - Agronomy Research 12(2), 603–610, 2014

[24] Annual Report 2016-2017, Ministry of Petroleum and Natural gas, Government of India.

Appendix

Diesel demand = 73.215billion litres/year.[24]

Cost of diesel per litre = 60.14 Rs. [12,13]

Cost spent for diesel per day = 4403 billion Rs./year

Density of Jatropha biodiesel = 879 Kg/m^3 [5]

Density of Diesel = 840 Kg/m^3 [5]

Density of Crude Oil = 920 Kg/m^3 [11]

Yield of Jatropha = 5 Kg. of seeds are required to produce 1 kg. of oil [2]

Plant density = 1100 to 2500 plants/Hectare[2]

Yield = 1 to 2 Kg. of seeds from one Jatropha plant[2]

Cultivation cost = 20000 Rs/Ha.[2]

Jatropha Oil Production = 43 Rs/Kg. of Oil[9]

Electricity cost = 4 Rs/Kwh.[9,16]

1 Metric Tonne of Jatropha Oil produces 1.9 Metric Tonne of Oil seed cake[2] and 1 Metric Tonne of Jatropha Oil produces 0.095 Metric Tonne of Glycerol[2]

Oil seed cake = 1 Rs/Kg [5].

Glycerol = 60 Rs/litre[9]

NUMERICAL INVESTIGATION OF VORTEX SHEDDING FROM A BLUFF BODY STABILIZED FLAME WITH CROSS INJECTION

Sombuddha Bagchi
Mechanical Engineering Dept.
Jadavpur University
Email: sombuddha.bagchi@gmail.com

Sourav Sarkar
Mechanical Engineering Dept.
Jadavpur University
Email: souravsarkar.iitm@gmail.com

Uddalok Sen
University of Illinois at Chicago
Email: uddalok.sen.us@gmail.com

Achintya Mukhopadhyay
Mechanical Engineering Dept.
Jadavpur University
Email: achintya.mukho@gmail.com

Swarnendu Sen
Mechanical Engineering Dept.
Jadavpur University
Email: sen.swarnendu@gmail.com

ABSTRACT

A laminar, two dimensional flow past a cylindrical bluff body is simulated with methane injection perpendicular to the free stream flow using an unstructured grid finite volume method. The numerical simulations are carried out using a commercial CFD package ANSYS Fluent 14.5. First ignition is carried out and then the mass fraction of methane injected through the slots are regulated. Comparisons are drawn between the lean and rich combustion of methane and the results are studied both qualitatively and quantitatively. The lean combustion is observed to be stable and the flame is anchored. The lean combustion is observed to oscillate at two dominant frequencies, one at that of the rich combustion and another at a higher frequency, almost 60 times greater than the rich combustion. Some noise is also observed.

Keywords:
Vortex shedding, flow past a cylinder, flame stabiliser
.

INTRODUCTION

NOx emission control has become a primary concern of aerospace and automobile industries due to the stringency of emission control rules and regulations in recent times. The primary source of NOx formation is identified to be combustion at high temperature.. So often lean combustion is preferred over rich combustion to reduce NOx emission. However unstablility is an important disadvantage of lean combustion which leads to large-amplitude oscillations, unacceptable noise and even structural damage of the combustion systems [1,2]. Bluffbody flame stabilizer are installed in practical combustor like ramjet and turbojet afterburner. Mixing shear layer formed at the downstream of the bluffbody helps to stabilize the flame. However the flow pattern in the wake behind is complex and has different interesting flow features and it is identified as one of the classical problem of fluid mechanics. Asymetrical Von Karman vortex shedding pattern at certain values of Reynolds number is one of the most interesting feature in flow past a cylinder situationwhich is of prime importance in bluff body stabilized combustors. Zhu et al.[3] studied

the simulation of vortex shedding behind a bluff-body (triangular) flame stabilizer using a hybrid U-RANS/PDF method. Mondal et. al [4] experimentally studied a bluffbody stabilized laboratory-scale pulse combustor to investigate the effects of different parameters on combustion instability. Raghavan et al. [5] did a considerable amount of work in flame stabilisation in a combustor having vortices generated by flame holding devices and flame–vortex interactions in separated methane–air cross flow flames established behind three bluff bodies. Uddalok et al. [6] studied the transient, 2-D laminar flow past a circular cylinder with injection of methane.

In our present work, transient flow past a circular cylinder has been studied.. The bluff body i.e. the cylinder has two slots perpendicular to the direction of the flow, both of them 180º apart which is referred to as a cross-flow arrangement. At a particular velocity, methane is injected through the two slots. Here, a comparison of the flow has been done between two cases. First, the flow past a circular cylinder has been done at rich combustion. Second, the flow past the cylinder is studied at lean combustion. The commercial CFD package ANSYS Fluent 14.5 has been used to carry out the simulations at a free stream Reynolds number of 100. To determine the frequency of vortex shedding, a Fast Fourier Transform is done for both cases.

PROBLEM GEOMETRY

A rectangular unconfined flow domain (200 mm x 200mm) is considered and the slotted cylinder is placed centrally within the flow domain. The maximum diameter of the cylinder is 6 mm and two diametrically opposite slots are placed perpendicular to the direction of the flow 180º apart. Schematic of geometry is presented in figure 1. The free stream Reynolds number of 100 is considered for the present study. A velocity inlet condition is specified at the inlet, pressure-outlet condition at the outlet and a specified shear of zero magnitude at the two walls. The ratio of magnitude of injection velocity of methane to that of magnitude of velocity of the free stream is denoted as ε and the ratio of the mass of methane to that of nitrogen is denoted as ϕ. In this configuration, the direction of injection velocity of methane is along the positive and negative y-direction and has a value of 0.73m/s or $\varepsilon=3$. The ϕ is changed from 1 to 0.75 and the effects of this change on the combustion is observed.
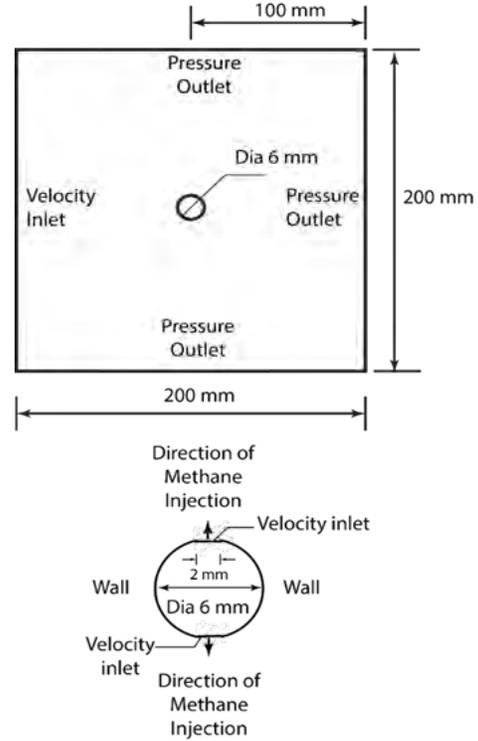
Fig 1: Geometry and boundary conditions

EQUATIONS

For incompressible, laminar, 2-D transient flow the following governing equations has been used:
Continuity:

$$\frac{\partial \rho}{\partial t} + \nabla.\left(\rho \vec{V}\right) = 0 \qquad (1)$$

Momentum:

$$\frac{\partial (\rho \vec{V})}{\partial t} + \nabla.\left(\rho \vec{V}\vec{V}\right) = -\nabla p + \nabla.\vec{\tau} + \rho \vec{g} \qquad (2)$$

where p is the static pressure, $\vec{\tau}$ is the stress tensor, $\rho \vec{g}$ is the gravitational body force and $\vec{F}$ is any other external body force such as that arising from interaction with the discrete phase.
The stress tensor is given by

$$\vec{\tau} = \mu \left[(\nabla \vec{V} + \nabla \vec{V}^T) - \frac{2}{3} (\vec{V} I) \right]$$

Energy Equation:

$$\frac{\partial (\rho E)}{\partial t} + \nabla.\left[\vec{V}(\rho E + p)\right] = \nabla.\left[(k \nabla T) - \sum_j h_j J_j + \nabla.\left(\vec{\tau}\vec{V}\right)\right] + S_h \qquad (3)$$

The energy is given by

$$E = h - \frac{p}{\rho} + \frac{V^2}{2}$$

where

$$h = \sum_j Y_j h_j + \frac{p}{\rho}$$

$$h_j = \int_{T_{ref}}^{T} C_{p,j} \; dT$$

The reference temperature was taken to be 298.15 K.

Species Transport Equation:

$$\frac{\partial(\rho Y_i)}{\partial t} + \nabla.\left(\rho \vec{V} Y_i\right) = -\nabla.J_i + R_i + S_i \qquad (4)$$

Where R_i is a reaction source term and S_i represents other source terms, which is generated from the discrete phase. For N species, generally N - 1 species equations are solved. The Nth species mass fraction is determined by subtracting from 1. Nitrogen is taken to be the Nth species.

J_i is the diffusion flux of species i

$$J_i = -\rho D_{i,m} \nabla Y_i - D_{T,i} \frac{\nabla T}{T} \qquad (5)$$

The Laminar finite rate model was used to calculate source term R_i. As gas flows are laminar in this study, laminar finite rate model is chosen. For a reversible reaction, the molar rate of generation of a species i in reaction r is given by the expression

$$R_i = \Gamma(v_i'' - v_i')\left[k_{f,r}\prod_{j=1}^{N} C_{j,r}^{v_{j,r}'} - k_{b,r}\prod_{j=1}^{N} C_{j,r}^{v_{j,r}''}\right]$$

$$(6)$$

The rate constants are calculated as

$$k_{f,r} = A_r \, T^{\beta_r} e^{\frac{E_r}{RT}}$$

$$k_{b,r} = {k_{f,r}}\big/{k_r}$$

Where k_r is the equilibrium constant of the rth reaction calculated from enthalpy and entropy of the species evaluated at the respective temperature and pressure. A reduced reaction mechanism with 16 species and 46 reactions was used to model chemistry of the combustion phenomena.. All the other data for evaluation of the rate constants are provided through the thermodynamic and transport database files in FLUENT.

NUMERICAL SIMULATION AND VALIDATION

A finite volume based CFD code ANSYS Fluent 14.5 has been used to perform the required numerical simulations. The laminar viscous model is used as the Reynolds number of the flow is 100. The pressure based solver has been chosen as the numerical scheme, and second order implicit transient solutions are performed. A least squares cell based scheme is employed for gradient calculations. SIMPLE scheme is used for pressure-velocity coupling and QUICK scheme was used for discretization of momentum equation. The convergence criteria for continuity and momentum equations were set at 10^{-8}.

The ANSYS Meshing package is used to create a triangle based unstructured grid. For better results and finer meshing around the central region, inflation is carried out with least element size of $10^{-7} \, m$ having 80 layers and a growth rate of 1.5. Grid independence study slong with time independence is carried out to select the optimum mesh and time step for simulation. It is carried out by replacing the bluff body by a regular cylinder of the same diameter.The Reynolds number of the free stream is 100. Grid independence study was again carried out post combustion to validate the mesh.

This mesh and a time step size of 0.001 is considered to be optimum for simulation to reduce the computational time without any considerable loss in accuracy.

RESULTS AND DISCUSSION

.The velocity, temperature and mass fraction of methane contours for $\varepsilon=3$ and mass fraction of methane $\phi=1$ and $\phi=0.75$ has been compared and shown in the Fig. 2 and 3. The vortex shedding is observed to be more compact in case of $\phi=0.75$ than $\phi=1$.
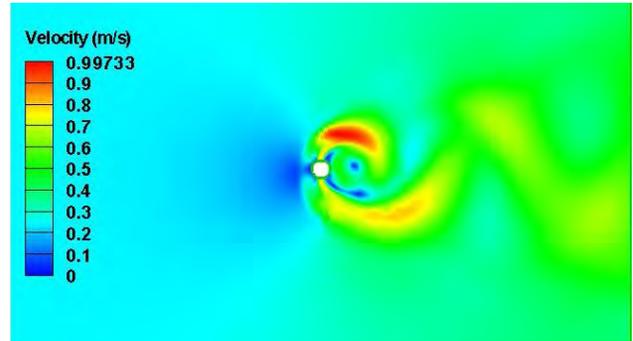
Fig. 2: Velocity contours for $\phi=1$
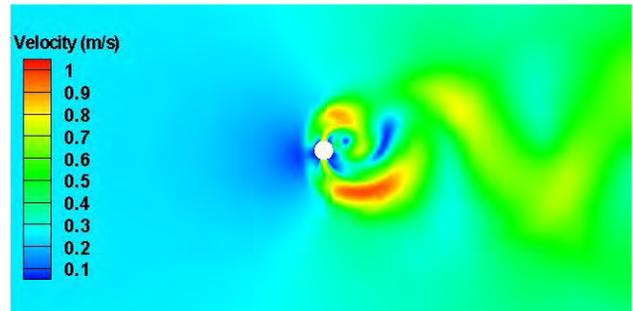
Fig. 3: Velocity contours for $\phi=0.75$
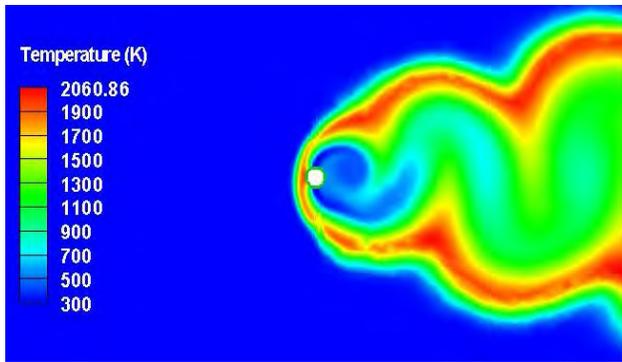
Fig. 4: Temperature contours for φ=1
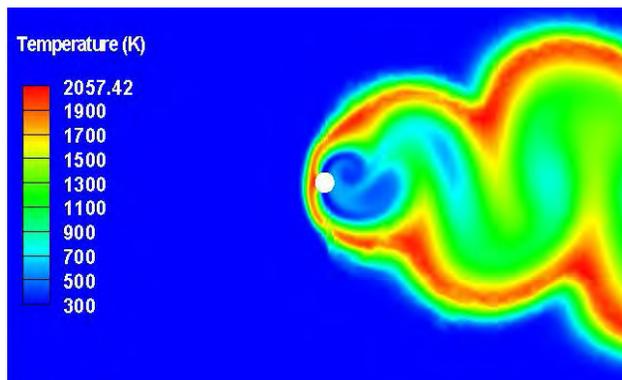
Fig. 5: Temperature contours for φ=0.75
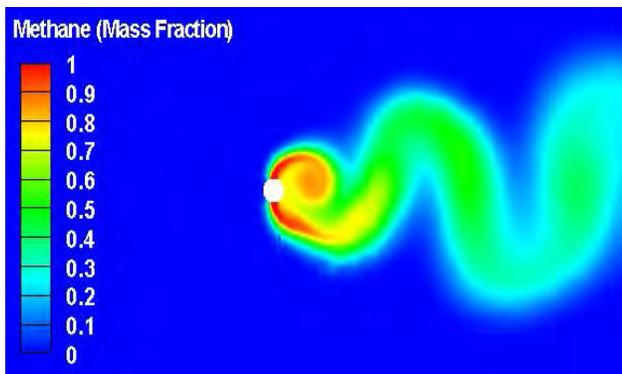
Fig. 6: Methane mole fraction contours for φ=1
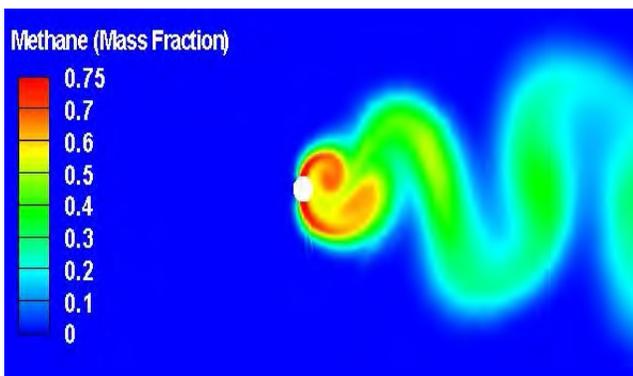
Fig. 7: Methane mole fraction contours for φ=0.75

The lift coefficient of the flow is monitored and Fast Fourier Transform (FFT) is done on the results achieved. The corresponding FFT plots are shown as follows (Fig. 8 & 9). The Strouhal number calculated from the corresponding frequencies in the FFT plots. In case of ε=3 and φ=1 only one dominant peak is observed at 7.83Hz (St=0.193) whereas in case of φ=0.75 two dominant peaks are observed at 7.83Hz (St=0.193) and 484.02Hz (St=11.93).as is evident from the FFT plots done in MATLAB.
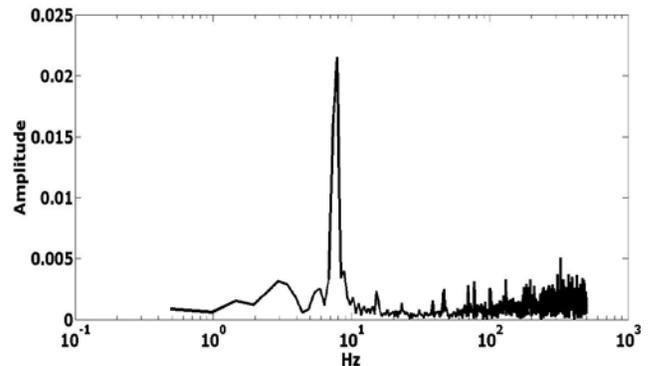
Fig. 8: Fast Fourier Transform plot for φ=1
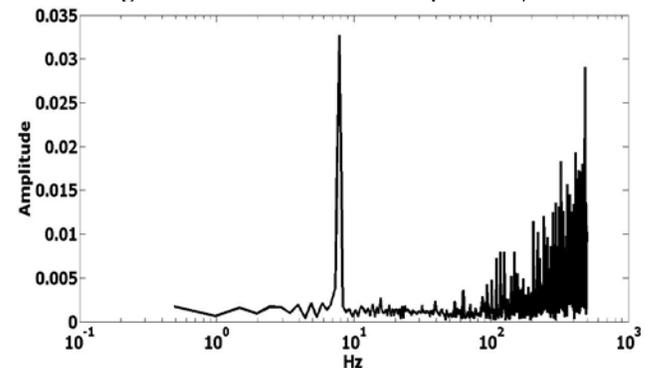
Fig. 9: Fast Fourier Transform plot for φ=0.75

CONCLUSIONS

The flame persists and is anchored right in front of the cylinder for both φ=1 and 0.75. The combustion characteristics are almost the same for both the lean and rich combustion. The flame is stable and continues to burn without losing heat. The lean combustion oscillates at predominantly two frequencies, one of that of the rich combustion, and other around 60 times of the rich combustion. Some noise is also observed in case of lean combustion.

REFERENCES

[1] Thevenin D., Renard P.H., Fiechtner G.J., Gord J.R.,Rolon J.C., 2000. "Regimes of non-premixed flames vortex interactions". Proc. Energy Combust. Sci. 26(3), 225–282

[2] Candel, S., 2002, "Combustion dynamics and control: Progress and challenges" Proc. Combust. Inst. Vol. 29, 1-28.

[3] Zhu M.M., Zhao P.H.,Ge H.W., Chen Y.L. 2012, "Simulation of vortex shedding behind a bluff body flame stabilizer using a hybrid U-RANS/PDF method" Acta Mech. Sin., Vol. 28, 348-358.

[4] Mondal S., Mukhopadhyay A., Sen S., 2014, "Dynamic Characterization of a Laboratory-Scale Pulse Combustor" Combust. Sci. and Tech., Vol. 186.2: 139-152.

[5] Raghavan V., Shijin P.K., Babu V., 2016, "Numerical investigation of flame–vortex interactions in laminar cross-flow non-premixed flames in the presence of bluff bodies", Combust. Theo. and Model., Vol. 20, 683-706.

[6] Sen U., Mukhopadhyay A., Sen S., 2017, " Effects of fluid injection on dynamics of flow past a circular cylinder", Eur. J. Mech. B/Fluids., Vol. 61, 187-199.

SEEC-2018-024

PARTICLES EXPOSURE LEVEL AND RESPIRATORY DEPOSITION DOSE WHILE COOKING USING DIFFERENT FUELS TYPE UNDER DIFFERENT SCENARIOS

Sandeep Kumar Chaudhry
Environmental Science and Engineering
Research Scholar
IIT (ISM), Dhanbad
Email:
krsandeep2006@gmail.com

Anil Kumar
Environmental Science and Engineering
Research Scholar
IIT (ISM), Dhanbad
Email:
akumarmjmc@gmail.com

Suresh Pandian Elumalai
Environmental Science and Engineering
Assistant Professor
IIT (ISM), Dhanbad
Email:
espandian@iitism.ac.in

Abstract:

Exposure towards particulate matter (PM) emitted while cooking is related to adverse human health effects. PM emission during cooking varies due to several reasons like fuel used for cooking (coal, wood and liquefied petroleum gas (LPG)), meteorological condition, ventilation and position of cooking pan on stove. In this study, respiratory deposition dose (RDD) in head airway (HD), tracheobronchial (TB), and alveolar (AL) regions of various PM size fraction (<10, <2.5 and <1 μm; PM_{10}, $PM_{2.5}$, and PM_1) were estimated for male and female cook in three different scenarios. As per of current study, RDD in HD for PM_{10} and PM_1 is maximum while cooking over coal as fuel i.e., 0.99 (0.82) and 1.78 (1.48) μg min^{-1} in close kitchen while for $PM_{2.5}$ is maximum when cooking on LPG i.e., 0.64 (0.53) μg min^{-1} for male (female) respectively. The RDD values in HD region were significantly highest in PM_{10} (96%) while RDD values for TB and AL were highest in PM2.5 and PM1 (7% and 29%) respectively.

Keywords: Particulate matter, Respiratory deposition dose, Cooking, Fuel type

Nomenclature
BG: Background
CK: Cooking
ACK: After cooking

Introduction:
Airborne PM is among primary pollutants monitored by U.S. Environmental Protection Agency (EPA) through the Clean Air Act "[1]".. While people spent most of the time in doing indoor work like study, watching television or cooking so, air quality inside house is also a matter of concern like outdoor air quality. As, exposure of insiders towards the coarser pollutants (PM>2.5 μm) and ultra fine particles (UFP) (PM<0.1 μm) depends upon their inside house activities like cooking. Many studies conclude that human exposure towards PM2.5 and UFP is due to cooking emissions in a residential or commercial kitchen "[2-3]".

In India many population resides in rural areas where they still using solid fuel for cooking like firewood, crop residues, charcoal and coal while population resides in urban areas are using liquefied petroleum gas (LPG) in

houses. Rural areas still don't have proper ventilated kitchens which lead them to suffer from various diseases causes due to their exposure towards fuel pollutants like PM. Many epidemiological studies have confirmed that continuous exposure to high concentrations of PM, particularly fine PM (such as PM2.5 and finer particles), is closely correlated with human health risk (eg., increasing morbidity and mortality rates) of various respiratory and cardiovascular diseases "[4-5]".

In this study PM concentration is measured at three different locations under different working scenarios where and also using different types of fuel for cooking (LPG, Coal and wood). Particulates concentration is monitored at before cooking, at cooking and after cooking with an optical particular counter (Grimm model 1.109; XX, Germany) in Dhanbad. This study focus mainly on PM concentration in indoors and its association with respiratory deposition dose (RDD) at during cooking.

Estimation of respiratory deposition doses

Respiratory deposition of particulate matter calculated by following equations which is adapted from International Commission on Radiological Protection "[6-7]" and has been used in early studies "[7]".

$$RDD = (V_T \times f) \times DF_i \times PM_i \tag{1}$$

Where V_T is the tidal volume (m^3 breath^{-1}), f is the typical breathing frequency (breath min^{-1}), DF_i is a deposition fraction of a size fraction i, and PM_i was the mass concentration in different size ranges. The DF for HD was calculated using eq 2

$$DF_{HD} = IF\left(\frac{1}{1+\exp(6.84+1.183\,lndp)} + \frac{1}{1+\exp(0.924-1.885\,lndp)}\right) \tag{2}$$

Where d_p is particle size in µm and IF is the inhalable fraction as used by ICRP model (eq 3)

$$IF = 1-0.5\left(1-\frac{1}{1+0.00076\,dp^{2.8}}\right) \tag{3}$$

The deposition fraction for the tracheobronchial region DF_{TB} is given by eq 4

$$DF_{TB} = \left(\frac{0.00352}{d_p}\right)[\exp(-0.234(\ln d_p + 3.40)^2) + (63.9\exp(-0.819(\ln d_p - 1.362)^2)] \tag{4}$$

The deposition fraction for the alveolar region DF_{AL} is given by eq 5

$$DF_{AL} = \left(\frac{0.0155}{d_p}\right)[\exp(-0.416(\ln d_p + 2.84)^2) + 19.11\exp(-0.482(\ln d_p - 1.362)^2)] \tag{5}$$

The V_T and f depends on the person's gender and physical activity. For light work V_T and f are considered equal to 12.5 X 10^{-4} (9.9 X 10^{-4}) m^3 per breath and 20 (21) breaths per minute for male (female), respectively.

Results and discussions:

A range of highly time-resolved measurements of particulate emissions due to burning of coal, wood and LPG is measured in different indoor environments in real time working scenario. Particulate concentration due to burning of coal is measured at open environment with no walls and in closed kitchen with no electric exhaust system while for wood and LPG cooking fuel particulate concentrations are monitored inside closed kitchens having electric exhaust system. Table 1 Shows the average PM concentration of different sizes (10, 2.5 and 1 µm) while cooking with the use of different fuel type.

Table 1: Average PM concentration due to uses of different cooking fuel

Fuel type	Concentration (µg m^{-3})								
	BG			CK			ACK		
	PM$_{10}$±SD	PM$_{2.5}$±SD	PM$_1$±SD	PM$_{10}$±SD	PM$_{2.5}$±SD	PM$_1$±SD	PM$_{10}$±SD	PM$_{2.5}$±SD	PM$_1$±SD
LPG	73.5±28.2	43.2±8.6	28.2±3.9	138.3±31.7	102.9±24.2	65.7±8.4	120.2±24.6	82.8±9	47.2±7.8
Coal (open)	78.7±13.7	61.3±7.4	54.6±6.04	348±116	328±109	320±106	37.9±12.8	26.8±7.3	21.5±4.2
Coal	111.4±53.7	72.6±13.3	62.7±9.9	264.7±86.7	215.6±69.8	203.5±71.2	165.4±99.5	115.1±36.6	102.3±36.4
Wood	134.1±50.4	103.1±34.17	88.7±25.9	174.9±162.5	126.4±113.3	99.6±60.4	176.9±135.4	119.6±89.02	91.4±48.2

Respiratory deposition dose:

RDD is calculated for three different cases headway (HD), tracheobronchial (TB) and alveolar (AL) regions for PM_{10}, $PM_{2.5}$ and PM_1 under different cooking fuel. Figure 1 shows the variation of different RDD values in different scenarios.
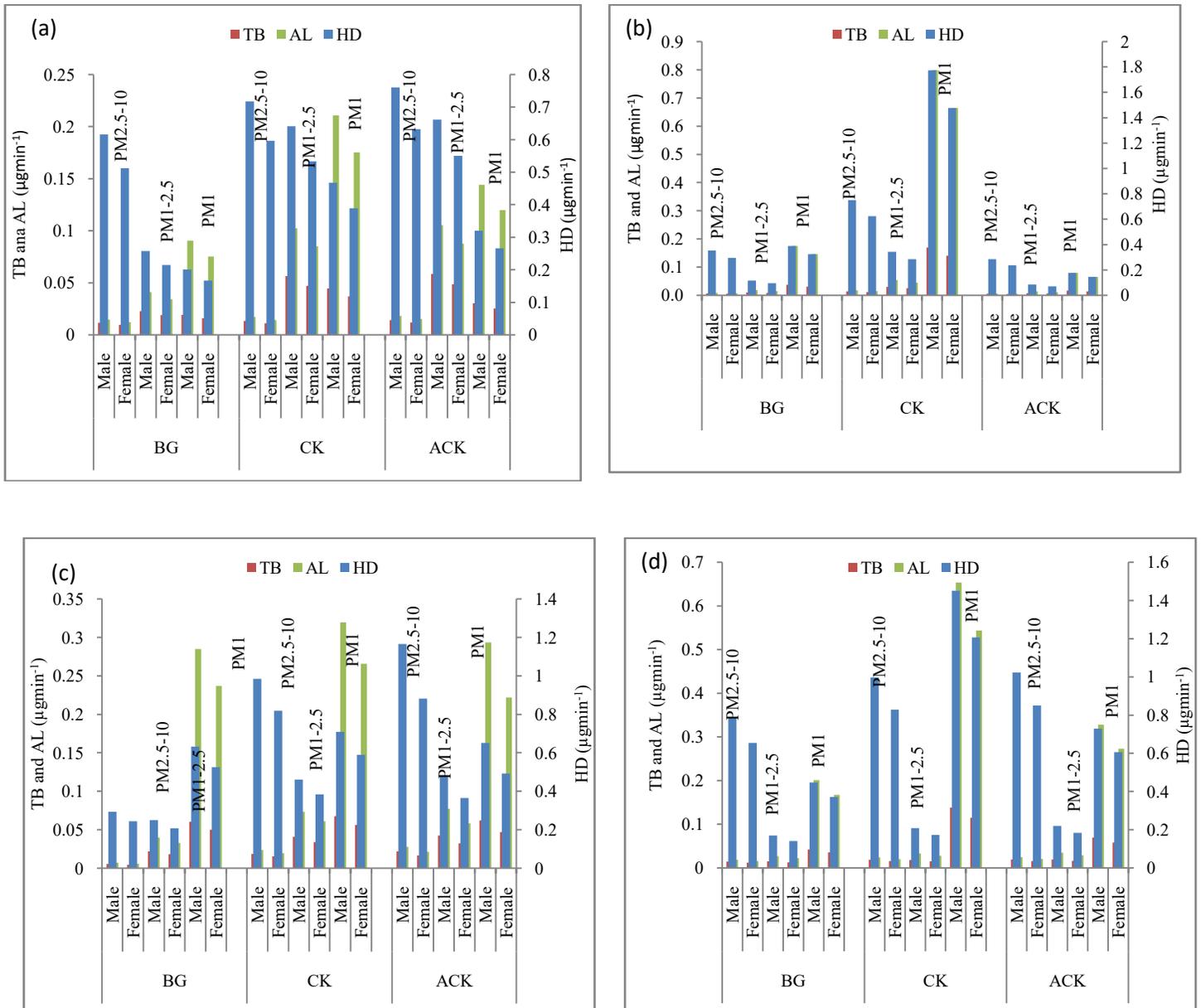
Figure 1: Three levels of respiratory deposition doses (RDD) of PM fraction in four different cases under different cooking environment (a) using LPG for cooking inside house kitchen, (b) using coal for cooking in an open environment, (c) using coal for cooking inside kitchen and (d) using wood as an fuel for cooking inside kitchen.

PM concentration not only depends upon type of fuel uses for cooking but also depends on type of cooking oil, metrological condition, nearby ongoing activity and ventilation at the measuring locations and nearby ongoing activity. This study caries out at four different locations:

1. At house kitchen using LPG for cooking and having one running electric exhaust and open windows for ventilation.
2. At hotel closed kitchen using coal for cooking with no electric exhaust but having windows for ventilation.
3. At open environment cooking uses coal for cooking.
4. In restaurant kitchen uses wood as fuel with 3 electric exhaust fan and sufficient windows for ventilation.

In this study it has been found that PM emission while cooking is maximum when we uses coal as an fuel followed by wood and minimum in the case of LPG for PM_{10} (0.99(0.82), 0.98(0.81) and 0.71(0.59) µgmin^{-1} for mail (female) for coal, wood and LPG respectively) while for $PM_{2.5}$ maximum emission is for LPG then that of coal and wood (0.64(0.53), 0.46(0.38) and 0.34(0.28) µgmin^{-1} for male(female) under LPG, wood and coal as fuel respectively) while for PM_1 maximum concentration is recorded for coal followed by wood and minimum for LPG fuels (1.7(1.47), 070(0.59) and 0.47(0.39) µgmin^{-1} for male(female) under coal, wood and LPG as fuel respectively).

References:
1. EPA, 2014. What Are the Six Common Air Pollutants. Office of Air and Radiation, U.S. Environmental Protection Agency, Washington, DC (updated 20 April 2012).
2. Abdullahi, K., Delgado-Saborit, J., Harrison, R., 2013. Emissions and indoor concentrations of particulate matter and its speci fic chemical components from cooking: a review. Atmos. Environ. 71, 260 –294.
3. Wan, M., Wu, C., Ton, G.S., Chan, T., Chao, C.Y., 2011. Ultra fine particles, and PM2.5 generated from cooking in homes. Atmos. Environ. 45, 6141 –6148.
4. Smith, K.R., Bruce, N., Balakrishnan, K., Adair-Rohani, H., Balmes, J., Chafe, Z., et al., 2014. Millions dead: how do we know and what does it mean? Methods used in the comparative risk assessment of household air pollution. Annu. Rev. Public Health 35, 185-206.
5. Apte, J.S., Marshall, J.D., Cohen, A.j., Brauer, M., 2015. Addressing global mortality from ambient $PM_{2.5}$. Environ. Sci. Technol. 49 (13), 8057-8066.
6. International Commission on Radiological Protection (ICRP), 1994. Human respiratory track model for radiological protection: A report of a task group of the International Commission on Radiological Protection. ICRP publication 66. Ottawa, Ontario, Canada: International Commission on Radiological Protection
7. Hinds, W.C. 1999.Aerosol Technology: Properties, Behaviour and Measurement of Airborne Particles, 2nd ed. New York: John Wiley & Sons
8. Gupta, S.K., Elumalai, S.P., 2017. Size-segregated particulate matter and its association with respiratory deposition doses among outdoor exercisers in Dhanbad City, India. Journal of the Air & Waste Management Association. 67 (10), 1137-1145.

SEEC-2018-026

NUMERICAL MODELLING OF SOLAR THERMAL ENERGY STORAGE WITH PHASE CHANGE MATERIALS

Swapnil S. Salvi
School of Mechanical, Materials and
Energy Engineering
Indian Institute of Technology Ropar
Rupnagar, Punjab, India
swapnil.salvi@iitrpr.ac.in

Vikrant Khullar
Mechanical Engineering
Department
Thapar University
Patiala, Punjab, India
vikrant.khullar@thapar.edu

Himanshu Tyagi
School of Mechanical, Materials and
Energy Engineering
Indian Institute of Technology Ropar
Rupnagar, Punjab, India
himanshu.tyagi@iitrpr.ac.in

ABSTRACT

Due to the efficient performance in energy storage density, solar thermal energy storage (especially latent type) applications are drawing more attention in the research field of solar energy. Among all of the types of solar thermal storage technologies, latent heat storage system using phase change materials is the most efficient way of storing thermal energy. It has some dominant factors like high density energy storage and isothermal operations, i.e., very small temperature range for heat storage and removal. Thus, latent heat storage systems have greater applicability over the other types of thermal energy storage systems. This paper presents an analysis of latent type solar thermal energy storage system involving cases consisting application of ambient conditions, consideration of natural convection along with conduction, with various geometries and working conditions. The analysis is carried out in MATLAB and COMSOL, which contains transient simulations of latent heat storage functioning with 1D and 2D modelling. It comprises validation of numerical 1D analysis with corresponding analytical solution, observation of change in thermophysical properties at melting point, effects of convective losses from end surfaces and comparison between a problem considering gravitational-buoyancy forces (accounting natural convection) and a problem considering only conduction.

Keywords: Solar energy; Thermal energy storage; Heat transfer; Phase change material; Numerical modelling.

NOMENCLATURE

a	constant value of radii
C_p	specific heat
H	height
h	convective heat transfer coefficient
k	thermal conductivity
L	latent heat of fusion
R	phase front location (cylindrical coordinates)
r	radial variable
T	temperature
t	time variable
X	phase front location (Cartesian coordinates)
x	spatial variable
ρ	density
μ	dynamic viscosity
α	thermal diffusivity
β	root of interfacial melting front equation

SUBSCRIPTS

end	end surface
i	initial
in	inner wall
l	liquid
m	melting
out	outer wall
S	surface
W	wall

INTRODUCTION

Global problems like increasing modeling fossil fuel and higher greenhouse gas emissions could be tackled by effective utilization of renewable energy forms. Earth's surface experiences solar radiation for a significant time period of the day, which can be converted into thermal energy directly or into electricity using solar PV. Solar thermal energy storage techniques are becoming a fundamental requisite, to reduce the adverse effects of fluctuations in solar radiative energy due to cloud cover, day-night cycle, seasonal variations, etc.

It has been recognized by Kuravi et al. [1] that, thermal energy storage (TES) incurs lower capital cost as compared to mechanical and electrical energy storage technologies, along with higher operational efficiencies. TES is implemented to balance out the low solar energy supply and periodic higher demand rates. Zalba et al. [2] have stated that, TES also ensures the security of energy supply and storage. TES system can allow the power plant to run on its full capacity regularly, even if the demand rate isn't matching with thermal energy production.

Different forms of thermal energy storages are sensible heat storage, latent heat storage and thermochemical storage [3]. The properties like high thermal storage density as well as the isothermal nature of the operation leads to employ phase change materials (PCMs) in latent heat storage system. Storage of energy by any means other than thermal, requires the usage of an extra equipment like electric battery; whereas in case of latent heat storage, it can be reduced or eliminated [2].

Zhao et al. [4] stipulated that, the major issue regarding PCM is its low thermal conductivity, which usually ranges from 0.2 to 0.7 W/m-K. This is much lower as compared to heat storage mediums in sensible heat storage systems. Low thermal conductivity will result into slow disposal rate of the stored heat energy, thus it leads to sub-optimal performance of PCM-latent heat storage system. It is a very important and desired quality required as far as thermal storages are concerned. For improving the thermal performance of PCM storage system, fins are incorporated in the system [5] or high thermal conductivity particles are introduced into the PCM.

In this study, analysis of latent thermal storage models has been carried out. Various cases consisting of different working conditions are applied on the 1D and 2D geometries. Three cases have been considered. In first case (Case 1), validation of numerical solution has been carried out with analytical solution of simple 1D Cartesian geometry, using MATLAB and COMSOL codes. Case 2 comprehends the temperature distribution for Cartesian and cylindrical models when heated from ambient-like conditions to a higher temperature above PCM's melting point. At last, Case 3 includes a comparison between two different cases, in first case only conduction hear transfer is considered along with the phase transfer process, whereas in second case conduction plus natural convection is also considered along with phase transformation. Corresponding results are presented and illustrated in the comparison between two cases mentioned. Cases 2 and 3 uses COMSOL based simulation of a PCM melting process.

THEORETICAL MODEL

Phase change material for all cases selected is octadecane ($C_{18}H_{38}$) which is being used as encapsulated PCM in building structures [6], having the following properties [7][8]:-

Table 1. Thermophysical properties of octadecane.

Properties	Solid	Liquid
Melting temperature (T_m)	27.5 ℃	
Latent heat of fusion (L)	244 kJ/kg	
Density (ρ)	814 kg/m^3	774 kg/m^3
Dynamic viscosity (μ)	10^8 Pa-s (Infinite)	0.0039 Pa-s
Thermal conductivity (k)	0.358 W/mK	0.152 W/mK
Specific heat (C_P)	2150 J/kgK	2180 J/kgK

For first 2 cases, numerical study considers only conduction as a mode of heat transfer, and neglects the effect of natural convection. The assumption of only conduction is valid for small PCM passages.

Case 1:-

In this case, validation of numerical against analytical solution is carried out. Schematic is shown in figure 2.
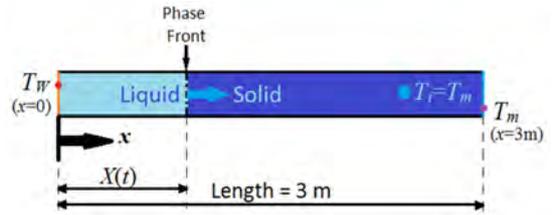
Figure 1. Schematic model for Case 1.

Analytical solution for 1D model [9] gives the following temperature distribution equation (1) for liquid region in PCM slab-

$$T_l(x,t) = T_W + (T_m - T_W) \times \frac{erf\left[\frac{x}{2\sqrt{A_l \times t}}\right]}{erf[B]} \quad (1)$$

where, T_l is the spatial temperature of liquid PCM, T_W and T_m are left side wall temperature and melting point of PCM respectively, α_l is thermal diffusivity of liquid PCM, x and t are spatial and time variables respectively.

β is the root of interfacial melting front equation (2)

$$B e^B erf(B) = \frac{C_{Pl}(T_W - T_m)}{L\sqrt{P}} \quad (2)$$

where, C_{Pl} is specific heat of liquid PCM, L is latent heat of fusion.

Phase front location (X) also depends on β,

$$X = 2B\sqrt{A_l t} \quad (3)$$

Selected parameters for the problem in case 1 for numerical as well as analytical solution, are as follows:-

- Length = 3 m
- Initial temperature, $T_i = 27.5°C$
- Left wall temperature, $T_W = 50°C$
- Mesh = Custom (Max element size=0.5mm)
- Time range = (0:5:600) seconds

Case 2:-

In this case, numerical solution gives the temperature distribution for Cartesian and cylindrical coordinates, melting the PCM from ambient like conditions to a higher temperature. The schematics for Cartesian and cylindrical problem are illustrated in figure 3 and figure 4 respectively.
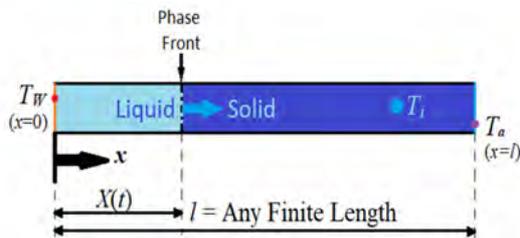
Figure 2. Schematic for Cartesian problem case 2.
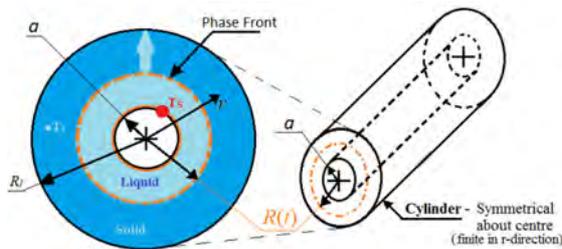
Figure 3. Schematic for cylindrical problem case 2.

where, X and R are phase front locations in Cartesian and Cylindrical coordinates resp.

Technical parameters for the problem in case 2 for numerical analysis, are as follows:-

Cartesian:-

- Length = 200 mm
- Initial temperature, $T_i = 20°C$
- Left wall temperature, $T_W = 40°C$
- Mesh = Extremely fine
- Time range = (0:20:2400) seconds

Cylindrical:-

- Inner radius = 10 mm
- Outer radius = 30 mm
- Initial temperature, $T_i = 20°C$
- Inner wall temperature, $T_S = 40°C$
- Mesh = Extremely fine
- Time range = (0:20:2400) seconds

Case 3:-

Modules used for analysis purpose of third case are Laminar Flow and Heat Transfer in Fluid with Transient analysis, which will be compared with a problem with conduction only (neglecting convection). Laminar flow is driven by the body force due to natural convection.

It is being assumed that the cylinder is kept in horizontal position lengthwise, thus the buoyancy forces are developed in the plane perpendicular to the axis of cylinder (in vertical direction). Selected parameters while defining the problem are as follows:-

- Inner radius = 25 mm
- Outer radius = 50 mm
- Initial temperature, $T_i = 27.5°C$
- Inner wall temperature, $T_{in} = 60°C$
- Outer wall temperature, $T_{out} = 30°C$
- Convective heat transfer coefficients, h $h_{in} = 20$ W/m^2-K & $h_{out} = 10$ W/m^2-K
- Mesh = Finer
- Time range = (0:1:200) minutes

RESULTS AND DISCUSSIONS

Case 1:-

From the results, we can validate the numerical method. Figures 5 and 6 show that the temperature distribution and phase front location of numerical method is fairly matching with the analytical solution.
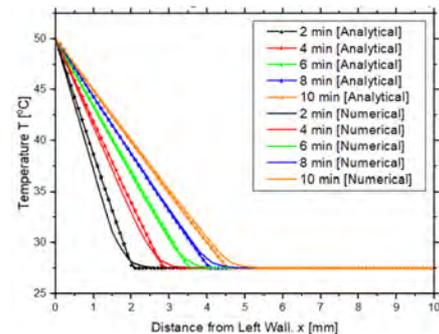
Figure 4. Comparison of temperature distribution of numerical vs. analytical method – Case1.
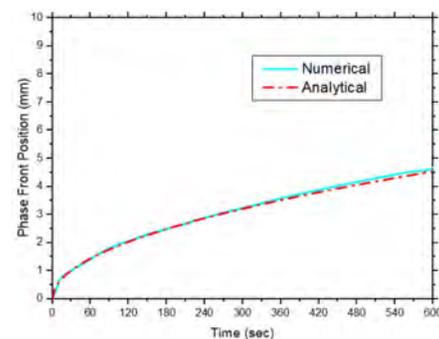
Figure 5. Comparison of phase front position of numerical vs. analytical method – Case 1.

Case 2:-

In this case, we can observe the change in slope in temperature distribution curves at melting point of PCM as the thermophysical properties changes when state of the PCM changes from solid to liquid.
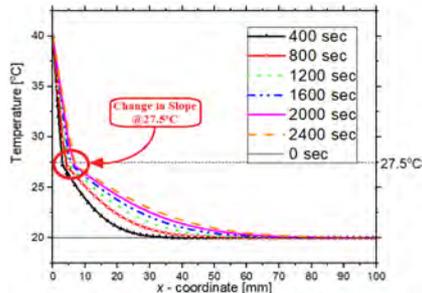
Figure 6. Temperature distribution for PCM (Cartesian coordinates) - Case 2.
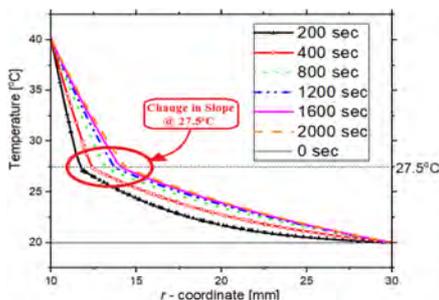
Figure 7. Temperature distribution of PCM (Cylindrical coordinates) - Case 2.

Case 3:-

The only case in which natural convection is accounted with phase transformation process. This case gives the comparison of phase transformation with and without the consideration of natural convection.
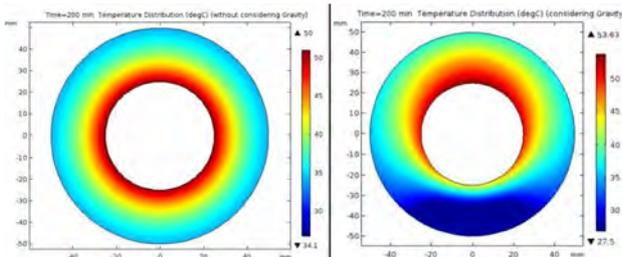
Figure 8. Comparison of temperature distributions -case 3.

It can be observed from figure 8 that initially due to dominant convective currents the melting rate is higher in the problem in which gravity is accounted. However, in the problem accounting natural convection, the heat accumulates in the upper part of the geometry. Due to which the bottom part of cylinder takes comparatively more time to melt than that of upper part, because most of the heat transferred to the bottom part is through conduction only.

CONCLUSION

The results of comparison of analytical and numerical solution in Case 1 shows that the numerical results are fairly validated using the analytical method results. Case 2 shows change in slope in temperature distributions at the melting temperature of PCM due change in properties of PCM while converting from solid to liquid state. Case 3 depicts the effects of considering natural convection or effects of gravity with cylindrical 2D geometry. It has been observed that the hot liquid octadecane is getting accumulated in the upper area due to set up of convective eddy currents / density differences, thus it results in maximum solid octadecane melting in the upper region first.

REFERENCES

[1] Kuravi, S., Trahan, J., Goswami, D. Y., Rahman, M. M., and Stefanakos, E. K., 2013, "Thermal Energy Storage Technologies and Systems for Concentrating Solar Power Plants," Prog. Energy Combust. Sci., **39**(4), pp. 285–319.

[2] Zalba, B., Marín, J. M., Cabeza, L. F., and Mehling, H., 2003, "Review on Thermal Energy Storage with Phase Change: Materials, Heat Transfer Analysis and Applications," Appl. Therm. Eng., **23**(3), pp. 251–283.

[3] Duffie, J., and Beckman, W., 2013, *Solar Engineering of Thermal Processes, 4th Ed.*

[4] Zhao, C. Y., Lu, W., and Tian, Y., 2010, "Heat Transfer Enhancement for Thermal Energy Storage Using Metal Foams Embedded within Phase Change Materials (PCMs)," Sol. Energy, **84**(8), pp. 1402–1412.

[5] Velraj, R., Seeniraj, R. V., Hafner, B., Faber, C., and Schwarzer, K., 1999, "Heat Transfer Enhancement in a Latent Heat Storage System," Sol. Energy, **65**(3), pp. 171–180.

[6] Khudhair, A. M., and Farid, M. M., 2004, "A Review on Energy Conservation in Building Applications with Thermal Storage by Latent Heat Using Phase Change Materials," Energy Convers. Manag., **45**(2), pp. 263–275.

[7] Hale, B. D. V, Hoover, M. M. J., Lockheed, N., Huntsville, B. D., September, E., Cha, P., Co, S., Marshall, F., Space, A., and Space, N. M., 2017, *Nasa Contractor Report Nasa Cr-51363*.

[8] Humphries, W. R., and Griggs, E. I., 1977, *A Design Handbook for Phase Change Thermal Control and Energy Storage Devices- NASA*.

[9] Carslaw, H. S., and Jaeger, J. C., 1986, *Conduction of Heat in Solids*, Clarendon Press.

SEEC-2018-027

THERMO-GRAVIMETRIC ANALYZER STUDIES ON DIRECT COAL FUELLED CHEMICAL LOOPING COMBUSTION UNDER N_2 AND CO_2 ATMOSPHERE

Barnali Bhui
Chemical Engineering Department
IIT Guwahati
Email: barnali.bhui@iitg.ernet.in

Prabu Vairakannu
Chemical Engineering Department
IIT Guwahati
Email: v.prabu@iitg.ernet.in

ABSTRACT

Chemical looping combustion (CLC) is a promising technology for the inherent capture of CO_2. Metal oxide particles act as the oxygen carriers for fuel combustion and produces a pure stream of CO_2, which can be sequestered without any treatment. The reactivity of low ash North East Indian coal under CLC conditions is examined in a thermo-gravimetric analyser (TGA) using NiO and Fe_2O_3 as the oxygen carrier. The reactivity and the conversion of coal were assessed in N_2 and CO_2 atmosphere under non-isothermal conditions. Both the metal oxides initiated their reaction at 400°C with volatile matters of the coal. NiO showed a maximum reactivity of $5x10^{-4}$ s^{-1} while Fe_2O_3 displayed $1x10^{-5}$ s^{-1} under N_2 atmosphere at 400-600°C. Whereas, in CO_2 atmosphere, a low reactivity is observed in this temperature range for Fe_2O_3 as similar to N_2 atmosphere. However, above 800°C, a high reactivity between CO_2-char-metal oxide is estimated under CO_2 atmosphere.

Keywords: *chemical looping combustion (CLC):* coal, oxygen carriers, TGA study.

NOMENCLATURE

r_{inst}	Instantaneous reactivity (s^{-1})
α	Conversion
Δm	Weight loss during the time interval Δt (mg)
m_{Re}	Mass retained within the crucible at time Δt (mg)
m_0	Initial mass fed into the crucible (mg)
m_i	Instantaneous mass (mg)
m_{ash}	Mass of the ash present in the coal (mg)
m_{Me}	Mass of the Me present in the crucible (mg)

INTRODUCTION

Around 61% of the total energy demand of India is fulfilled by coal-fuelled power plants [1]. Coal on combustion releases greenhouse gases into the atmosphere. As a result, global warming is caused and, this serious issue can be rectified by carbon capture and storage methods (CCS). Conventional methods of coal combustion cause huge energy penalty for the capture of CO_2 and thus, the overall net thermal efficiency of power plants is reduced. Pre-combustion, post-combustion and oxy-fuel combustion are energy intensive CCS methods. Alternatively, chemical looping combustion (CLC) is a recent advanced technology for the inherent capture of CO_2 with less energy penalty as compared to conventional methods.

CLC process consists of two interconnected reactors such as a fuel reactor (FR) and an air reactor (AR). Metal oxides are the oxygen carriers (OC) that are cheaply available source for oxygen separation from air. Metal particles undergo oxidation process in the AR and get reduced in the FR during metal-oxy combustion reactions. These metal/metal oxides are circulated in a loop between both the reactors. CLC of gaseous fuels is not complex as compared to solid fuel based operation. Gaseous fuels such as CO, H_2 and CH_4 can interact easily with metal oxides in a fluidized bed reactor and achieve high conversion. Whereas, the direct use of soild fuels such as coal and biomass in a CLC operation makes the process inefficient as it involves the interaction of

solid-solid reactants (coal-metal oxides). Hence, a gasifying medium is required to gasify the solid fuels into syngas. Solid fuels can be converted into syngas either using a separate gasifier or by *insitu* gasification CLC (ig-CLC) process. The simultaneous gasification of solid fuel (Rxn. 1) with metal-oxy combustion of syngas (Rxn. 2) in a single reactor is referred as ig-CLC process. The re-oxidation of the reduced metal oxides is carried out in the AR using atmospheric air (Rxn. 3). This process eliminates the utilization of pure oxygen in the CLC process. Whereas, the use of a separate gasifier requires pure oxygen for gasification.

$$Coal + CO_2 \rightarrow CO + H_2 \tag{1}$$

$$CO + H_2 + Me_xO_y \rightarrow Me_xO_{y-1} + H_2O + CO_2 \tag{2}$$

$$Me_xO_{y-1} + 1/2\, O_2(air) \rightarrow Me_xO_y \tag{3}$$
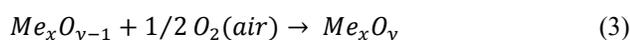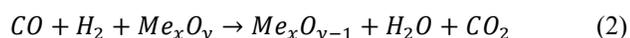
The reactivity of oxygen carriers such as NiO, CuO, CoO, MnO etc. with gaseous fuels is extensively reported in the literature using various reactors with different contacting patterns [2-6]. Also, thermo gravimetric analysis (TGA) studies were reported in the literature concerning the reactivity of metal oxides with gaseous fuels over a range of temperatures. However, there is not much studies available on coal based ig-CLC process. In the present study, TGA studies are carried out using CO_2 as a gasification agent for low ash coals. NiO and Fe_2O_3 are used as metal oxides. These metal oxides are selected on the basis of their higher melting point, higher reactivity, low agglomeration etc. Fe_2O_3 is a cheap source of metal oxides and abundantly available in the form of ores.

EXPERIMENTAL DETAILS

A low ash coal (~2% ash) is used in the present study. Fe_2O_3 and NiO in pure form (>99% pure) is utilized in the TGA studies. A 14 mg reaction mixture (coal+metal oxide) was analyzed using a TGA under N_2 and CO_2 atmosphere. Table 1 shows the proximate and ultimate analysis of the used coal. It can be seen that a significant proportion of volatile matter and sulfur is present in the coal. The calorific value of the coal is estimated using a bomb calorimeter.

TABLE 1: PROXIMATE AND ULTIMATE ANALYSIS OF COAL

Coal	Weight (%)
Ash	2.0
Voaltile matter	39.0
Moisture	11.0
Fixed carbon	48.0
Carbon	78.3
Hydrogen	5.5
Oxygen	12.0
Nitrogen	2.4
Sulphur	1.8
HHV (MJ/kg)	31.9

TGA studies are conducted under non isothermal conditions in the temperature range of 30°C to 1000°C. The mass loss with respect to temperature is recorded. The reactivity of metal oxides with coal under pyrolysis and gasification condition is estimated under N_2 and CO_2 atmosphere, respectively. The reactivity of fuel with metal oxides is calculated using the following equations (4) & (5). The instantaneous reactivity (r_{inst}) is defined by Equation (3) [7].

Instantaneous reactivity is defined as the ratio of mass loss during a time interval 't' to the active reactive mass retained at the end of the time interval in the reaction mixture per unit time.

$$r_{inst} = \frac{1}{m_{Re} - m_{ash} - m_{Me}} \frac{\Delta m}{\Delta t} \tag{4}$$

The conversion (α) is defined as the ratio of total mass loss at any time 't' to the total reactive mass of the initial sample.

$$\alpha = \frac{m_0 - m_i}{m_0 - m_{ash} - m_{Me}} \tag{5}$$

RESULT AND DISCUSSION

Figure 1 shows the instantaneous reactivity of the coal with the chosen metal oxides under N_2 atmosphere. It can be seen that NiO has shown higher reactivity than Fe_2O_3. Four distinct peak zones are observed in the instantaneous reactivity curve. The first zone below 200°C shows the liberation of moisture content and, the second zone between 300°C to 500°C depicts the reactivity of metal oxides with volatile matters. The third zone between 600°C and 800°C indicates the decomposition and the reactivity of tar molecules with metal oxides. The reactivity of char with metal oxides can be seen in the fourth zone at above 800°C. The difference in reactivity between the pyrolysis curve (coal+N_2) and NiO reactivity curve (coal+N_2+NiO) indicates the interaction of solid-soild particles (char-metal oxide) at elevated temperature. NiO and Fe_2O_3 have shown a reactivity as high as 5×10^{-4} s^{-1} and 1×10^{-4} s^{-1}, respectively, under N_2 atmosphere during the release of volatile matters at 400-600°C. Char- metal oxide shows a reactivity of 5×10^{-4} s^{-1} and 8×10^{-5} s^{-1} for NiO and Fe_2O_3, respectively.
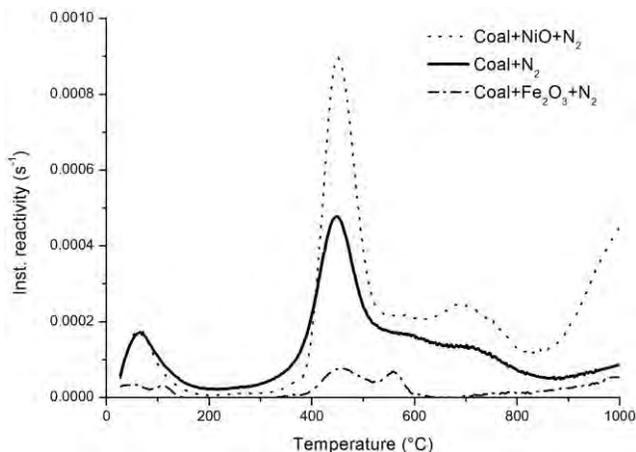
FIGURE 1. Instantaneous reactivity of low ash coal with Fe_2O_3 and NiO in N_2 atmosphere

Figure 2 depicts the instantaneous reactivity of coal-metal oxide under CO_2 atmosphere. It showed a different trend as compared to N_2 atmosphere. At high operating temperatures above 800°C, Fe_2O_3 achieves a higher reactivity than NiO. This shows that the reaction of Fe_2O_3 with CO (due to Boudouard reaction) requires a high activation energy. whereas NiO has shown a high reactivity even at low temperature 400 to 600°C due to the reaction with volatile matters. Also, the oxygen carring capacity of Fe ($Fe_2O_3 \rightarrow Fe$) is higher than Ni (NiO$\rightarrow$Ni). As a result, at high temperatures, a high reactivity is shown for Fe_2O_3 as compared to NiO.
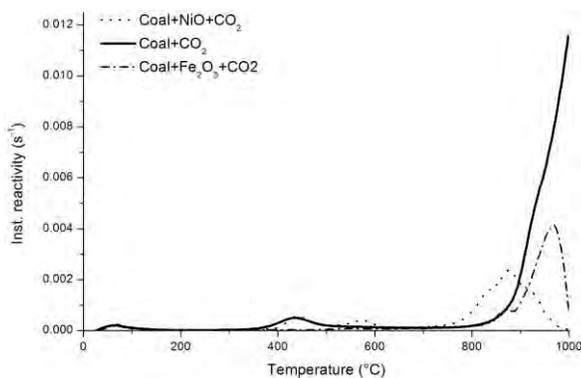
FIGURE 2. Instantaneous reactivity of low ash coal with Fe_2O_3 and NiO in CO_2 atmosphere

The conversion of coal-metal oxide under N_2 and CO_2 atmosphere is shown in Figure 3 and 4, respectively. Further, the conversion of pure coal under N_2 and CO_2 atmosphere is plotted in the same graph and compared. It can be observed that a low conversion is achieved using Fe_2O_3 in the temperature range of 400-600°C. This may be due to the diffusional resistance of Fe_2O_3 for the release of volatile matters. Whereas, NiO has shown an increase in the

conversion of about 10% as compared to coal pyrolysis under N_2 atmosphere (Figure 3). It evidences the reactivity of NiO with volatile matters at the low temperartures.
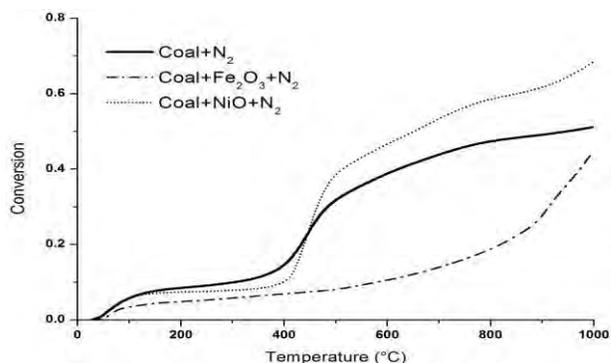
FIGURE 3. Conversion of NiO-coal and Fe_2O_3-coal mixture in N_2 atmosphere

The reactivity of coal-NiO followed a similar trend in both the atmosphere. However, at 700-900°C, under CO_2 atmosphere, it is evident that NiO has shown reactivity with coal, which might be due to tar cracking reactions. In the case of coal-Fe_2O_3, the conversion steeply increased above 800°C under both atmospheres. It is found that, under CO_2 atmosphere, 88% conversion is achieved in the case of NiO whereas 50% conversion is observed for Fe_2O_3 oxygen carriers.
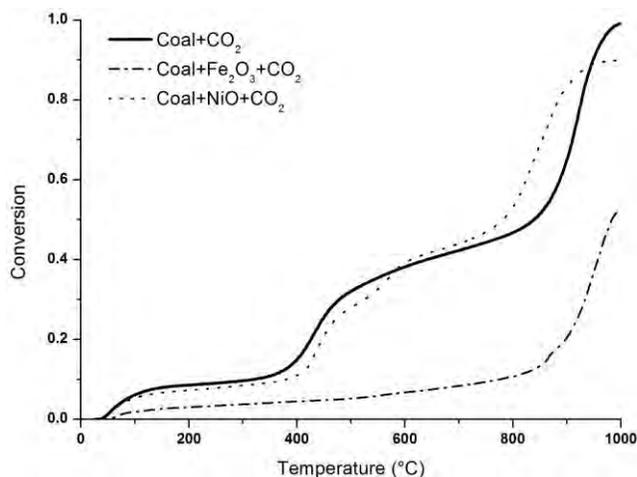
FIGURE 4. Conversion of NiO-coal and Fe_2O_3-coal mixture in CO_2 atmosphere

CONCLUSION

NiO exhibited higher reactivity than Fe_2O_3 at low temperature in both the N_2 and CO_2 atmosphere. However, the reactivity of Fe_2O_3 sharply increased at high temperatures. At low tempeartures, Fe_2O_3 exhibited diffusional resistance for the release of volatile matters. Also, Fe_2O_3 has shown 50% conversion under CO_2

atmosphere. Further studies are required under isothermal conditions for evaluating the maximum conversion efficiency. Future studies are to be focused on selecting oxygen carriers, which are derived from industrial waste or natural ore for mitigating the cost issue. The TGA results clearly indicate that the direct utilization of coal in CLC technology is feasible using CO_2 as a gasification agent.

REFERENCES

[1] Kumar, K.V., Bharath, M., Raghavan, V., Prasad, B.V.S.S.S., Chakravarthy, S.R. and Sundararajan, T., 2017. Gasification of high-ash Indian coal in bubbling fluidized bed using air and steam–An experimental study. Applied Thermal Engineering, 116, pp. 372-381.

[2] Mei, D., Abad, A., Zhao, H., Adánez, J. and Zheng, C., 2014. On a highly reactive Fe_2O_3/Al_2O_3 oxygen carrier for in situ gasification chemical looping combustion. Energy & Fuels, *28*(11), pp.7043-7052.

[3] Shen, L., Wu, J., Xiao, J., Song, Q. and Xiao, R., 2009. Chemical-looping combustion of biomass in a 10 kWth reactor with iron oxide as an oxygen carrier. Energy & Fuels, 23(5), pp.2498-2505.

[4] Leion, H., Lyngfelt, A. and Mattisson, T., 2009. Solid fuels in chemical-looping combustion using a NiO-based oxygen carrier. Chemical Engineering Research and Design, 87(11), pp.1543-1550.

[5] Cao, Y. and Pan, W.P., 2006. Investigation of chemical looping combustion by solid fuels. 1. Process analysis. *Energy & Fuels*, *20*(5), pp.1836-1844.

[6] Arjmand, M., Leion, H., Lyngfelt, A. and Mattisson, T., 2012. Use of manganese ore in chemical-looping combustion (CLC)—Effect on steam gasification. *International Journal of Greenhouse Gas Control*, *8*, pp.56-60.

[7] Saha, C. and Bhattacharya, S., 2012. Chemical looping combustion of low-ash and high-ash low rank coals using different metal oxides–A thermogravimetric analyser study. *Fuel*, *97*, pp.137-150.

[8] Siriwardane, R., Tian, H., Richards, G., Simonyi, T. and Poston, J., 2009. Chemical-looping combustion of coal with metal oxide oxygen carriers. *Energy & Fuels*, *23*(8), pp.3885-3892.

MOLECULAR SIMULATION OF ADSORPTIVE CO_2 CAPTURE USING Zr-BASED METAL-ORGANIC FRAMEWORKS

Kishant Kumar
Department of Chemical Engineering
Indian Institute of Technology Guwahati
Guwahati, Assam 781039, India.
Email: kishant@iitg.ernet.in

Amit Kumar
Department of Chemical Engineering
Indian Institute of Technology Guwahati
Guwahati, Assam 781039, India.
Email: amitkumar@iitg.ernet.in

ABSTRACT

Metal-organic frameworks (MOFs) consist of inorganic metal atoms coordinated by multiple organic linkers to form a regular, porous three-dimensional framework. MOFs possess a number of interesting properties such as high surface area, tunable pore size and available pore volume [1] which makes them attractive for gas separation and storage. Zirconium-based MOFs UiO-66/67/68 show remarkable structural stability at high temperatures in addition to high surface areas and tunable pore size [2]. Separation of CO_2/N_2 mixture is important with regard to CO_2 capture from flue gas, and adsorptive separation using MOFs provides an attractive alternative to conventional amine-based absorption which is energy-intensive. In the present work, we report grand canonical Monte Carlo (GCMC) simulation study of adsorptive separation of CO2 from N2 using two different zirconium-based MOFs, namely UiO-66 and UiO-67. The two MOFs studied in this work are topologically similar but have cages and windows of different sizes. Isosteric heats of adsorption and gas loading in the low pressure region (upto 1 bar) were found to be higher for UiO-66 than UiO-67 for both CO_2 and N_2. This can be attributed to the presence of smaller cages and hence, stronger interactions, in UiO-66. However, at higher pressures, gas uptake in UiO-67 was found to be more (than in UiO-66) due to the presence of larger cages. The adsorption behavior of CO_2 was explored in detail, using CO_2 density distribution inside the cages and radial distribution functions, to identify favorable sites for adsorption. The preferential sites for CO_2 adsorption were observed to be in the vicinity of the carbon atoms of organic linkers in the smaller cages of the MOFs. The selectivity of CO_2 in binary CO_2/N_2 mixtures was studied over a range of pressures. Binary mixture simulations revealed that both MOFs were more selective toward CO_2 than N_2. The CO_2/N_2 selectivity was significantly higher in the case of UiO-66 primarily due to the presence of smaller cages and narrow windows which result in stronger interactions. In both UiO-66 and UiO-67, the selectivity was observed to decrease with increasing temperature.

REFERENCES

[1] Furukawa, H., Cordova, K.E., O'Keeffe, M., and Yaghi, O.M., 2013. "The Chemistry and Applications of Metal-Organic Frameworks". Science, 341(6149), Aug, pp. 1230444.

[2] Cavka, J.H., Jakobsen, S., Olsbye, U., Guillou, N., Lamberti, C., Bordiga, S., and Lillerud, K.P., 2008. "A New Zirconium Inorganic Building Brick Forming Metal Organic Frameworks with Exceptional Stability". J. Am. Chem. Soc., 130(42), Sep, pp. 13850–13851.

SEEC-2018-029

Biodiesel Spray Characteristics and its Correlation with Engine Performance, Combustion and Emission Characteristics

Akhilendra Pratap Singh, Avinash Kumar Agarwal*

Engine Research Laboratory, Department of Mechanical Engineering

Indian Institute of Technology Kanpur, Kanpur-208016, India
*Corresponding Author: akag@iitk.ac.in

Abstract

Spray pattern is the shape of spray leaving the injector nozzle. Optimized spray pattern significantly affects fuel-air mixing in the combustion chamber. Spray pattern was obtained by capturing the spray images in a constant volume spray chamber (CVSC) using a high speed camera. Spray patterns were obtained for different biodiesel blends and mineral diesel at different fuel injection pressures (FIPs) and ambient pressures (APs). Spray pattern analysis was carried out to characterize the spray shape and spray evolution, which affected fuel-air mixing. Results show that increasing FIP resulted in relatively higher fuel spray penetration length and reduced spray cone angle. Increasing AP resulted in smaller fuel spray penetration length and increased spray cone angle. Increasing biodiesel content in test fuels improved spray characteristics however higher biodiesel blends resulted in slightly inferior spray characteristics. To verify these findings, engine experiments were also carried out to investigate the engine performance, combustion and emission characteristics in a single cylinder research engine. Experiments were performed at same FIPs using same test fuels. Engine combustion results showed that lower blends of biodiesel resulted in similar combustion characteristics however higher blends of biodiesel resulted in relatively inferior performance and emissions compared to mineral diesel. Results of engine experiments were in good agreement with spray results.

Keywords: Spray characteristics, Fuel atomization, Biodiesel, Spray evolution, Combustion.

SEEC-2018-030

Methanol Utilization in Reactivity Controlled Compression Ignition Combustion Engine

Akhilendra Pratap Singh, Tushar Agarwal, Avinash Kumar Agarwal*

Engine Research Laboratory, Department of Mechanical Engineering

Indian Institute of Technology Kanpur, Kanpur-208016, India

Corresponding Author: akag@iitk.ac.in

Abstract

Diesel engines are widely used for transportation and power generation applications because of their high fuel efficiency. However, diesel engines can cause environmental pollution owing to their high oxides of nitrogen (NOx) and soot emissions. Many researchers have shown that homogeneous charge compression ignition (HCCI) and premixed charge compression ignition (PCCI) concepts are promising techniques for simultaneous NOx and soot reduction however HCCI and PCCI combustion generally suffer from high levels of carbon monoxide (CO) and unburnt hydrocarbon (UHC) emissions. Therefore a new combustion technique namely reactivity controlled compression ignition (RCCI) has been introduced. RCCI is a dual fuel engine combustion technology that uses in-cylinder fuel blending with at least two fuels of different reactivity, and multiple injections to control the in-cylinder fuel reactivity to optimize the combustion phasing, duration and magnitude. The process involved in RCCI includes the introduction of a low reactivity fuel into the cylinder to create a well-mixed charge of low reactivity fuel, air and recirculated exhaust gases. The high reactivity fuel is then injected before ignition of the premixed fuel directly into the combustion chamber. In this study, methanol was used as low reactivity fuel and mineral diesel was used as high reactivity fuel. Experiments were performed at different premixed ratios of methanol with respect to mineral diesel. CCI combustion, performance and emission characteristics were investigated at four different engine loads (25%, 50%, 75% and 100%).

Keywords: Reactivity controlled compression ignition, Methanol, Combustion, Particulate emission.

SEEC-2018-031

AIR POLLUTION IN DELHI: A MAJOR ENVIRONMENTAL AND PUBLIC HEALTH CHALLENGE

Indian Institute of Technology Kanpur, Kanpur-208016, India
Email: snikhil@iitk.ac.in

Manish Trivedi
Engine Research Laboratory,
Department of Mechanical
Engineering,
Indian Institute of Technology
Kanpur, Kanpur-208016, India
Email: manishtr@iitk.ac.in

Avinash Kumar Agarwal*
Engine Research Laboratory,
Department of Mechanical
Engineering,
Indian Institute of Technology
Kanpur, Kanpur-208016, India
*Email:akag@iitk.ac.in

ABSTRACT

Delhi has made development in sectors such as industry, transport and housing. All these sectors in one or other way contribute to air pollution in Delhi. The spectrum of the adverse health effect due to air pollution from vehicles is now a matter of concern and has become more serious, than was evident two decades ago. This is because of industrialization, migration of population from rural area to Delhi and increase in number of vehicle. Megacities like Shanghai, Tokyo, Seoul, Bangkok, Cairo, Delhi and Mexico experience/share almost same kind of adverse health problems due to air pollution. The government has not framed any foolproof policy so that these cities are pollution free in the foreseeable future. This is because pollution is a global problem and not related to specific city or area. In this context, if timely measures are not taken the existing environment will deteriorate and air is likely to become unbearable. Before making any policy it becomes necessary to understand varying needs, expectations, and perceptions of people across Delhi. In this paper, a discussion is made about the vehicle pollution, winter pollution, public transport connectivity in national capital region (NCR), recommendations/suggestions to improve the air quality of Delhi.

Keywords: Delhi, Vehicle Pollution, Control, monitor

INTRODUCTION

Rapid industrialization in combination with incompetent planning of metro city like Delhi has resulted in unmanaged air pollution particularly from vehicles. Expanding area of cities, rising traffic jams, higher energy consumption, rapid economic development are directly associated to air pollution. Air pollution may be defined as the presence of undesirable material such as motor vehicle exhaust, exhaust from factories, construction etc in atmosphere which is large enough in quantity to produce adverse health effect to all living organisms and cause damage to property of an individual. Air pollution is harmful even when it is not visible by naked eye. There are primarily two sources of air pollution in the atmosphere; (1) Natural emissions; and (2) Anthropogenic emissions. Anthropogenic emissions are produced by internal combustion (IC) engines and furnaces via combustion. On a global scale, each year more than 25 billion tons of carbon dioxide (CO_2) is produced worldwide by anthropogenic activities [1]. Likewise, air pollution in Delhi is mainly produced because of enlarge anthropogenic activities since past few decades. In addition to this, transport sector emits large fraction of greenhouse gas (GHG) that contributes to climate change. Due to increasing number of vehicles and traffic jams in Delhi, this sector is emerging as a major contributor of GHG emissions and other harmful pollutant species in urban and rural areas of Delhi.
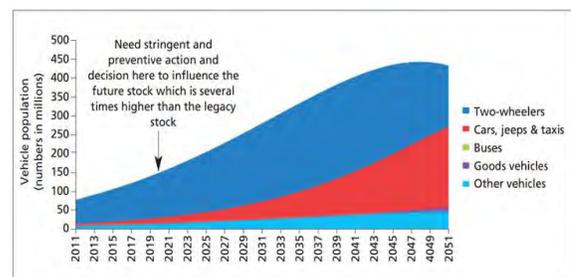
Figure 1: Estimated vehicle population with year [2]

Air pollution in Delhi is mainly due to large concentration of vehicles on road. Vehicles in Delhi are beyond the carrying capacity of roads which has results in increase in air pollution due to increase in traffic jams, increased travel time and also decrease of speed. But transport sector is critical for economic development and human welfare. Figure 1 shows the expected increase in number of vehicle by the year 2051 for two wheelers, cars, jeeeps and taxis, buses, goods vehicles. This increase in vehicle cannot be stopped as they are necessary for growth of country. Moreover, the vehicles have become affordable to more number of people and have led to increase in air pollution. Because of this reason global energy consumption in transport sector is expected to increase [3]. At present the general trend is to produce emissions by industrial activities and from vehicle and later control these emissions. If timely measures are not taken up by government and people of Delhi, pollution will exponentially increase. The control of pollution should be from a global solution rather than a local solution. On the other hand, the car ownership of Delhi is low as compared to many European cities [4]. Despite of this fact Delhi roads experiences long hour traffic jams leading to pollution due to in efficient fuel combustion [5]. There are some additional factors responsible for pollution in Delhi in addition to increase in vehicle. These include types of engines used, age of vehicles, poor road conditions, outdated engine design and automotive technologies, ill maintained vehicles, congested traffic and traffic management systems, unorganized road network leading to longer routes, slow moving traffic. In fact, three-quarters of transport-related emissions are from road traffic [6]. Government of Delhi should plan for a long term keeping a note of these points.

The focus of this paper is Delhi. Delhi is jointly administered by central and state government. It is the 18th most populated state in India and covers 1483 square km area [7]. According to 2011 census pollution of Delhi was 167.5 lakh. Out of this total population 97.50 % live in urban area and the literacy rate of Delhi in urban region was 86.32 in 2011. Delhi is geographically located in North India within the latitude 28°24'17" and 28°53'00''N, and longitude 77°45'30" and 77°21'30''E. The migration of population from rural areas to Delhi in search of jobs and lack of government policies to handle this has led to unplanned rural and urban development specifically at the border area of Delhi. The green areas in the outer of Delhi or neighboring states have been converted to residential towers. Polluting devices have increased and green area has been converted to buildings despite of the well-known fact that the oxygen available in the atmosphere is made by green plants using the equation:

$nCo_2 + nH_2O + light = (CH_2O)n + nO_2$
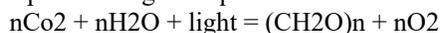
World Health Organization (WHO) listed Delhi among the top 20 cities with the worst air pollution [8]. Delhi being one of the populated and capital regions has grown in all sectors including industry, transport and housing. Because of this reason ambient PM2.5 concentration exceeds the national air quality standard by more than 300% in Delhi [8, 9]. In developing countries like India, urbanization is linked with an increased adverse health effect leading to non-communicable diseases [10]. Few classical studies also showed that extended exposure to large concentration of PM from IC engine have a symbolic effect on mortality and morbidity rates in a city [11, 12].

If this matter is so severe, what is our government doing to control this? Air pollution problem in Delhi was recognized long time back and several measures were taken to control the pollution. Most of the laws made by Delhi government are based on the thinking that air pollution is a local problem of Delhi. People of Delhi think that after election newly elected government will change the policy and pollution would also be reduced. Pollution is a global problem and will not be reduced by any local solution such as changing bused or cars to CNG etc. Problems like acid rains may cross the boundaries of a state and no government can settle this problems. Converting the buses to CNG in 1990 has not yet solved the problems of pollution in Delhi. In fact Delhi still ranks among the world's most polluted cities. Another policy was to reduce the volume of traffic in Delhi by implementation of odd and even number plates that could enter the city on alternate days. Another solution proposed by Delhi is subsidizing CNG kits. All these are not a solution to the global problem. Only one feasible solution implement by government is increasing the public transport such as metros in Delhi city. But due to inadequate public transport system people are forced to arrange their own ride. Although it is a global problem, some of the highest air pollution levels are found in rapidly expanding cities in India and China. It's the people of Delhi who can change the air pollution scenario by taking imitative and responsibility of creating clean environment.

WHY THE SUDDEN RISE IN INTEREST FOR DELHI?

Urban living, high life style is the foundation of modern society particularly in metro cities like Delhi. Air pollution control is considered as a luxury and people with sufficient money living in a metro city want to breathe fresh air. The priority of poor man is to work and arrange meal for the day for his family. His priority is not to spend money to breath fresh air. Poor people do not want to control air pollution and have no interest in this. The literacy rate of Delhi was urban region was 86.32% in 2011 which make this clear that public has become aware and people want sustainable development. The awareness has come through media and newspaper and they want a healthy life style. They want that at least next generation; people going to school should not inhale polluted air and become pray to deceases. Direct evidence of people dying due to air pollution is very less. For example: people dying

due to chikungunya in Delhi is accountable immediately however people dying due to pollution is not well understood to common man and it has a long term effect. A particulate inhaled by a person may be a cause of cancer after many years. Climate change and air pollution are interrelated. Climate change is most critical threat to sustainable development. CO2, N2O, CH4 are considered as GHG and major air pollutants like ozone, CO, and black carbon (BC) particles come from a variety of sources.

WINTER POLLUTION IN DELHI

Fog is a persistent winter phenomenon that happens in Delhi almost every winter of a year by late November or early December [13]. Due to pollution fog is persistent in urban areas like Delhi than in rural areas. This is because of increased air pollution from various sources in Delhi. In a report by Delhi Pollution Control Committee written by Sharma and Dixit in the year 2016 estimated that average daily concentration of PM2.5 in winter remains about 375 μg/m3 against the permissible limit of 60 μg/m3 [14]. During winters average minimum temperatures of Delhi is about 7°C and cold and dry air is near to ground level with relatively low wind velocity. The direction of wind in Delhi is towards northwest in summers, west during spring and southwest during winter.

Winter of Delhi was once considered as a good time of the year. People would go out in parks with their children during weekends. But today, doctors' advice is to be in house throughout the winter season. This is because majority of the people suffer from cough and burning eyes. Most of the schools are shut down. Wind direction from the Punjab and Haryana is towards Delhi during winters. During this period, framers burn straw from rice in their fields and make the land ready for wheat. Ali et al. [13] reported that the anthropogenic species are higher during winter period in Delhi. This may be because of burning of wood, kerosene and plants to protect themselves from cold. Due to zero-visibility caused by dense fog many flights are cancelled in winters and airplanes traffic suffer the most. On a single day in December (Dec) 2014 at IGI Airport, New Delhi approximately 100 flights were affected [15]. In winters the pollution concentration is at least double the annual averages. This is because of relatively higher air pollution from heating and unfavorable meteorological conditions [16].

However, a variety of other sources in the surrounding areas of NCR also contribute to total emissions. As mentioned earlier all the pollution from burning of straw come to Delhi and creates thick layer of air pollution. Winters are normally calm and cool and air pollution makes this air heavy. The 52% velocity of wind is below 2.1 m/s in Delhi [17]. As a result this thick stagnant layer is not able to move outside Delhi. This gives a message that government of Delhi is not capable to provide pollution free air to breath. Public should be aware of this and become responsible for their action. Winters with polluted air are extremely dangers for people suffering from asthma and heart diseases. Children and elderly people suffer the most and many elderly people even die without knowing the real cause.

PUBLIC TRANSPORT CONNECTIVITY IN NCR

Population of people living in border areas of Delhi has increased since past few years. The industrial area in states has of Haryana, Uttar Pradesh, Rajasthan has seen a growth because the border touches with Delhi. There is a large group of people traveling from this border to Delhi and vice-versa. With increase in population, frequency of buses and trains has not increased. There is less facility of public transport from this area to Delhi. This has bound the people of these areas to use personal cars and taxis. Another reason is ill maintained public transport. Due to low per-capita income in India as compared to North American or European countries, India has been forced to keep its public transport fares extremely low. Because of which they are not well maintained. This aspect is completely ignored while making the blue print of buses frequencies. The government from different states must contribute and come to a solution of this category of people traveling interstate. The government has changed and not the situation. The next part of the paper deals with recommendations which must be implemented.

RECOMMENDATIONS/ SUGGESTIONS TO IMPROVE THE AIR QUALITY OF DELHI

Based on the above discussion, there are following recommendations specifically for Delhi:
1. One must understand that pollution is a global issue and not an area specific problem. Policies like odd even and introducing CNG vehicles may decrease the emissions to some extent and for some time only. Another point is, changing the Delhi government after election will certainly not decrease air pollution in Delhi. It is the people of Delhi, who must be responsible for increase or decrease of air pollution. One must have a global vision and not a short term goal.
2. After creating a global vision among Delhi residents, a large funding and a strong technical expert committees should be hired for a long term vision and goal.
3. As per the emission norms, the manufactures should be told to implement emission control techniques such as in cylinder or after treatment devices. Diesel particulate filter (DPF), Gasoline particulate filter (GPF) or other devices must be installed and maintained. Pollution control certificate must be must be checked after every 6 months to verify that vehicle is maintained by owner. This is responsibility of individual and one should not blame the government if air pollution is produced by his/ her vehicle.
4. A third party may be hired and pollution must be monitored and recorded at various places of Delhi at

least twice a day. Based on the reading, the pollution control strategy may be framed. Additional sources of air pollution such as construction sites, industries, weather condition, festivals, wind direction and wind speed may play a vital role in changing these reading from place to place in Delhi.

5. Limits such as; a family can have only one vehicles may be imposed.
6. Old vehicles pollute to a great extent and must be stopped as early as possible. Rather they should be held by government and should be damaged after giving a reasonable compensation.
7. Public transport may be improved. The service quality of Delhi buses may be improved. Fares of public transport and buses may be revised/ increased from time to time.
8. Traffic signals are a great source of air pollution. Reduced idle time by proper co-ordination may be reducing air pollution.
9. Government offices, private companies and industries should have subsidized pick and drop facility compulsory for their employees. This can reduce traffic on road and hence pollution in morning and evening office timing.
10. Trees must be planted on dividers and on sides of road to reduce pollution. This tress will help to reduce pollution particularly at traffic junction and traffic signals.
11. Awareness through radio, TV, newspaper must be spread to public of Delhi to reduce air pollution. As mentioned earlier, people also play a vital role in reducing pollution and not only the government.
12. Electric vehicles must be subsidized by government and must be promoted to reduce pollution. Research on batteries in terms of life, working hours and charging time should be promoted.
13. Children in schools must be educated about sustainable development as they will play a vital role in the coming years. New license holders must be made aware about such issues and they should be requested to contribute to reduce and control air pollution.

REFERENCES

[1] Abbasi T, Abbasi S. Decarbonization of fossil fuels as a strategy to control global warming. Renewable and Sustainable Energy Reviews. 2011;15:1828-34.

[2] http://www.cseindia.org/userfiles/DelhiCleanAirActionPlan.pdf

[3] Nakicenovic N, Jefferson M. Global energy perspectives to 2050 and beyond. 1995.

[4] Thynell M, Mohan D, Tiwari G. Sustainable transport and the modernisation of urban transport in Delhi and Stockholm. Cities. 2010;27:421-9.

[5] Tiwari G. Urban transport priorities: meeting the challenge of socio-economic diversity in cities, a case study of Delhi, India. Cities. 2002;19:95-103.

[6] Ribeiro SK, Kobayashi S, Beuthe M, Gasca J, Greene D, Lee DS, et al. Transportation and its infrastructure. Institute of Transportation Studies. 2007.

[7] Guttikunda SK, Calori G. A GIS based emissions inventory at 1 km× 1 km spatial resolution for air pollution analysis in Delhi, India. Atmospheric Environment. 2013;67:101-11.

[8] Guttikunda SK, Goel R. Health impacts of particulate pollution in a megacity—Delhi, India. Environmental Development. 2013;6:8-20.

[9] Dey S, Di Girolamo L, van Donkelaar A, Tripathi S, Gupta T, Mohan M. Variability of outdoor fine particulate (PM 2.5) concentration in the Indian subcontinent: a remote sensing approach. Remote Sensing of Environment. 2012;127:153-61.

[10] Kumar R, Singh MC, Ahlawat SK, Thakur JS, Srivastava A, Sharma MK, et al. Urbanization and coronary heart disease: a study of urban-rural differences in northern India. Indian heart journal. 2006;58:126-30.

[11] Vincent JR, Ali RM, Tan C, Yahaya J, Rahim K, Ghee L, et al. Environment and development in a resource-rich economy: Malaysia under the New Economic Policy: Harvard Institute for International Development, Harvard University; 1997.

[12] Small KA, Kazimi C. On the costs of air pollution from motor vehicles. Journal of Transport Economics and policy. 1995:7-32.

[13] Ali K, Momin G, Tiwari S, Safai P, Chate D, Rao P. Fog and precipitation chemistry at Delhi, North India. Atmospheric Environment. 2004;38:4215-22.

[14] Sharma M, Dikshit O. Comprehensive Study on Air Pollution and Green House Gases (GHGs) in Delhi. A report submitted to Government of NCT Delhi and DPCC Delhi. 2016:1-334.

[15] Tyagi S, Tiwari S, Mishra A, Singh S, Hopke PK, Singh S, et al. Characteristics of absorbing aerosols during winter foggy period over the National Capital Region of Delhi: Impact of planetary boundary layer dynamics and solar radiation flux. Atmospheric Research. 2017;188:1-10.

[16] Guttikunda SK, Gurjar BR. Role of meteorology in seasonality of air pollution in megacity Delhi, India. Environmental monitoring and assessment. 2012;184:3199-211.

[17] Mohan M, Bhati S. Why is megacity Delhi prone to high atmospheric pollution potential. TFMM-TF HTAP Joint Workshop, Paris2009.

SEEC-2018-032

OPTIMIZATION OF FUEL INJECTION TIMING OF GASOLINE DIRECT INJECTION (GDI) ENGINE IN HOMOGENEOUS MODE OF COMBUSTION

Nikhil Sharma
Engine Research Laboratory,
Department of Mechanical Engineering,
Indian Institute of Technology Kanpur, Kanpur-208016, India
Email: snikhil@iitk.ac.in

Avinash Kumar Agarwal*
Engine Research Laboratory,
Department of Mechanical Engineering,
Indian Institute of Technology Kanpur, Kanpur-208016, India
*Email:akag@iitk.ac.in

ABSTRACT

Gasoline direct injection (GDI) vehicles have become popular choice among buyers due to its superior power output. GDI injectors have undergone immense improvements in delivering fuel at higher pressure. But, significant high pressure may cause particulate emission from a GDI engine due to fuel impingement in the piston or cylinder walls. Therefore, it becomes necessary to understand the effect of fuel injection timing of a GDI engine on particulate emission. An experimental study was carried out to optimize start of injection (SOI) timing using gasoline as a test fuel. Five SOI timing 230, 250, 270, 290 and 310˚ bTDC was selected for this study. Particle size-number distributions were determined using an Engine Exhaust Particle Size Analyzer (EEPS) at these SOI timing. The experiments demonstrated that optimized SOI timing showed the minimum particulate emission. It was found that lower count mean diameter (CMD) and higher total particle number concentration are more prone to adverse health effect.

Keywords: GDI, Start of injection, PN/ PM distributions

INTRODUCTION

The gasoline direct injection (GDI) engine has been a key area of research since the recent decade because of its advantages in terms of fuel economy and power output [1]. But, relatively high level of PM from GDI engine is a matter of concern due to stricter emission legislation. Moreover, GDI engine emit large quantity of nanoparticle compared to diesel engine and therefore is considered to be more harmful [2]. These fine particles have more retention time in atmosphere and therefore are responsible for deteriorating air quality. They also penetrate deep into the human respiratory system on inhalation causing adverse health effect such as asthma and respiratory issues and cardiopulmonary morbidity and mortality [3-5].

Piston geometry and SoI timing are the two important key points which play critical role in reducing PM emission from GDI engine [6]. As the fuel is injected directly inside the combustion chamber, there is a high possibility of fuel impingement on the piston surface and liner. This is due to higher injection pressures and resulting in higher penetration velocity and distance [7]. Further, advancing SoI timing may increase this phenomenon [8].

High temperature on the surface of piston creates a vapor film which slows evaporation of the rest of the fuel adjustment to vapor film. This process results in diffusion combustion or pool fire responsible for high PM emission [9].This PM produced from the GDI engine can be reduced by combustion process or with after-treatment systems such as gasoline particulate filters (GPF) [10]. In a study, Keskinen [11] reported that fuel-air mixing inside combustion chamber was highly sensitive to SoI timing and slightly influenced by FIP.

In this paper, an experimental study was carried out to optimize start of injection (SOI) timing using gasoline as a test fuel. Five SOI timing 230, 250, 270, 290 and 310˚ bTDC was selected for this study. Particle size-number distributions were determined using an Engine Exhaust Particle Size Analyzer (EEPS) at these SOI timing.

EXPERIMENTAL SETUP AND PROCEDURE

A single cylinder 500cc GDI engine capable to deliver a rate toque of 30 Nm @ 2000 rpm engine speed was selected for this study. A 36 kW transient dynamometer (Dynomerk Controls; 6-2013) was connected with this engine. Table 2 shows specifications and figure 2 shows the schematic of the experimental setup.

An optical crank angle encoder (AVL; 365C) was coupled which delivered 720 pulses in each revolution of the crankshaft. The other end of encoder was directly connected to the DAQ system (AVL, Indimicro) through a signal conditioning unit (AVL; 365-C). An indicating spark plug (AVL; ZI31_Y5S) was mounted on the engine cylinder head and output pressure signals is plugged into the DAQ system. Programmable ECU (MOTEC; m400) was part of engine test cell which controlled SoI, ST and injector pulse width. GDI injector peak and hold driver (Zenobalti; ZB-5100G) was used to inject fuel which received trigger signal from the optical encoder. EEPS-3090 was used to obtain particulate number-size, mass-size, and surface area-size distributions. Technical specifications of EEPS-3090 are listed in Table 3.
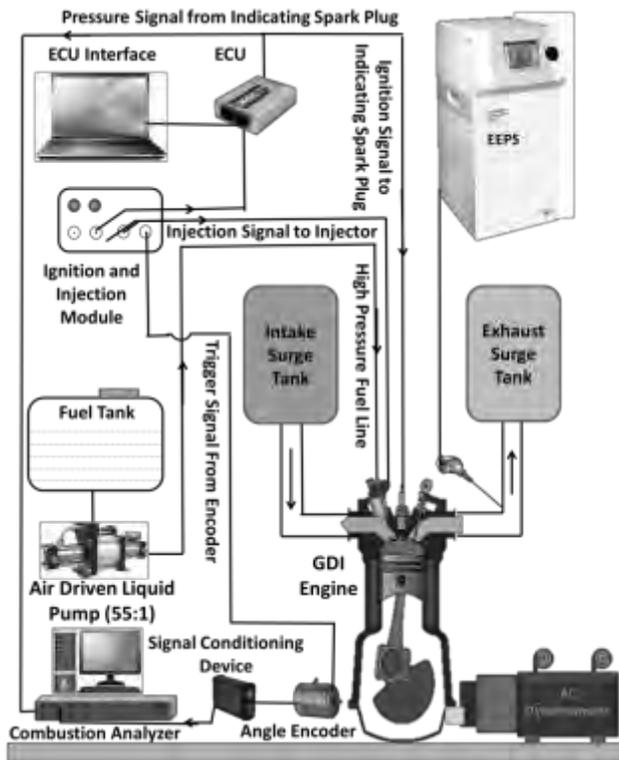
Figure 1: Schematic of experimental setup

Table 2: Engine specifications

Engine type	Single Cylinder GDI engine
Bore/ Stroke	86 mm/ 86 mm
Displacement	500 cc
Connecting rod length	196 mm
Compression ratio	10.5
Maximum power	10 KW @ 3000 rpm
Maximum torque	32 Nm @ 3000 rpm
No. of Injector holes	6

Table 3: Technical specifications of EEPS 3090

Particle size range	5.6-560 nm
Particle size resolution	16 channels per decade
Electrometer channels	22
Charger mode of operation	Unipolar diffusion charger
Inlet cyclone 50% cut-point	1μm
Maximum data rate (Hz)	10

RESEARCH AND DISCUSSION

The present experimental investigation provides detailed insight of particle size-number distributions for the GDI engine fuelled by gasoline from different SoI timings. Particle size distribution was divided into nuclei mode particle (Dp; 5 - 50 nm), nano-particles (Dp < 50 nm), ultrafine particles (Dp < 5 0 nm), accumulation mode particle (Dp; 100 - 300 nm) and coarse mode particles (Dp < 10 μm). The purpose of this investigation was to find out the optimum SoI timing. Particle number size, Particle size-mass and Particle surface area distribution are discussed in this section.

Particle Number-Size Distribution
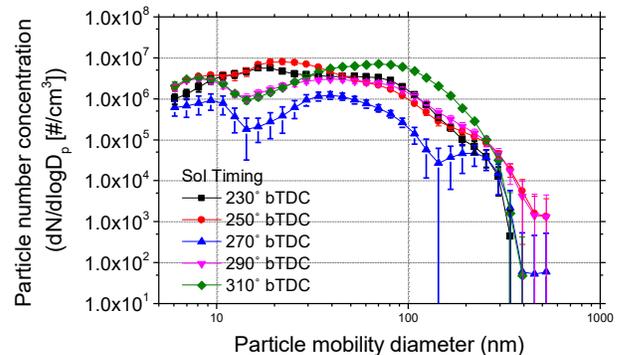
Figure 2: Particle number size distribution vs particle mobility diameter (nm)

The PN concentration was calculated by the following formula:-

$$ n = \frac{c}{tQ}\frac{\varphi}{\eta} $$

Where, η = sample efficiency factor per channel, n = number weighted concentration per channel, c = particle counts per channel, φ = sample dilution factor, t = sampling time, Q = sample flow rate.

Figure 2 shows particle number size distribution for five different SoI timings. SoI timing of 270 ° bTDC showed lowest particle number concentration and was clearly

distinguished from other SoI timing. On the other hand, for SoI timing of 310° bTDC showed highest particle number concentration @ 100 nm particle size. No clear distinguished trend among different SoI was noticed for particle size < 30nm. Particles in the size range of 500–1000 nm are not emitted in this GDI engine. It was probably because of high FIP which results in superior atomization of fuel droplets. Another reason could be because of fuel properties such as lower density and viscosity of gasoline. The atomized fuel droplet led to better mixing and evaporation. In all this process, pyrolysis of rich mixture does not occur and large size particles are not formed. It was found that 270 ° bTDC was optimum SoI timing because fuel impingement on the cylinder and piston surface was less or did not occur at all.

Particle mass distribution

The PM was calculated by the following formula:-

$$m = \rho v$$

Where, ρ = particle density, v = volume weighted concentration per channel, m = mass weighted concentration per channel.
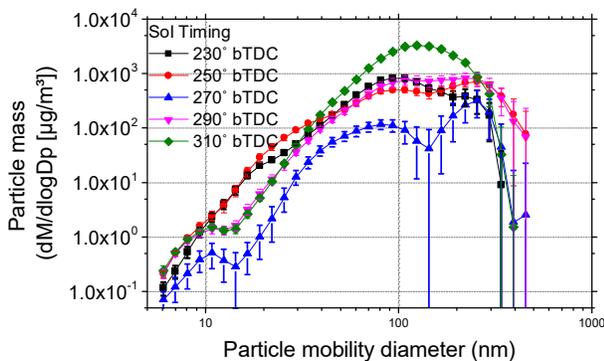
Figure 3: Particle size-mass distribution vs particle mobility

Figure 3 shows particle mass distribution for five different SoI timings. For SoI timing of 270 ° bTDC particle mass concentration was found to be lowest and was clearly distinguished from other SoI timing. On the other hand, for SoI timing of 310° bTDC particle mass was found to be highest @ 100 nm particle size. Physical significance of this graph lies in the fact that particles with heavier mass will have less retention time in atmosphere and will settle quickly. But the lighter particle will stay in atmosphere and eventually penetrate into the human body. On the other hand heavier particles mostly get filtered through hairs in the nose. In a nutshell, particles with lower mass are considered to be more toxic for human health.

Particle surface area distribution

The particle surface area distribution was calculated by the following formula:-

$$s = \pi D_P^2 n$$

Where, n = number weighted concentration per channel, Dp = particle diameter (channel midpoint), s = surface area weighted concentration per channel
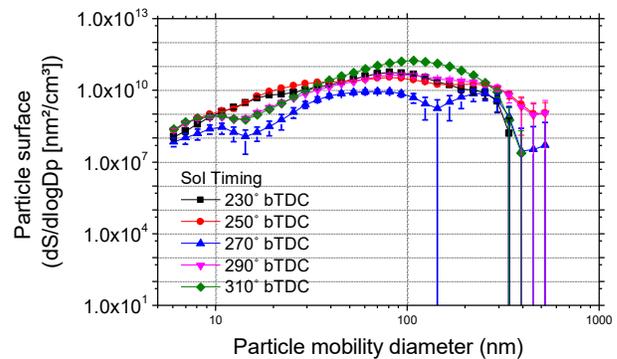
Figure 4: Particle surface area distribution vs particle mobility diameter (nm)

Figure 4 shows particle surface area distribution for five different SoI timings. For SoI timing of 270 ° bTDC particle surface area distribution was found to be lowest and was clearly distinguished from other SoI timing. On the other hand, for SoI timing of 310° bTDC particle surface area was found to be highest @ 100 nm particle size. The significance of particle surface area lies in the fact that particles with an increased surface area will have higher probability of adsorption of toxic compounds. Moreover, potential sites for adsorption of toxic compounds for agglomerates are relatively higher than spherical particles. The toxic compounds adsorbed on the surface may penetrate into the blood stream and are considered to be potentially carcinogenic. Particulate emissions can be reduced by optimizing SoI timings and spray characteristics.

Count mean diameter (CMD) and total particle distribution
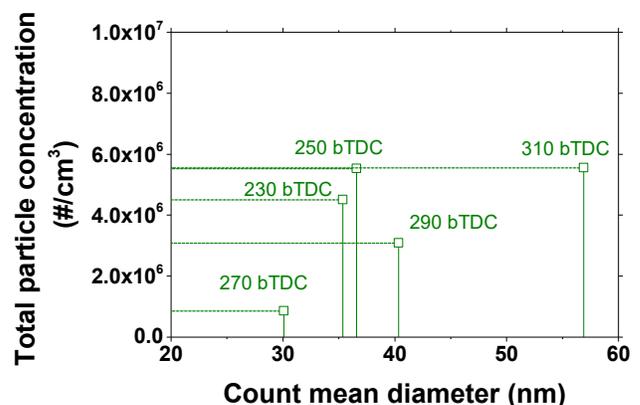
Figure 5: Co-relation between total particle concentration and count mean diameter

CMD gave a clear relationship between engine out particle emissions and adverse health effects w.r.t. different SoI timing. For comparison CMD was calculated and plotted against total particle distribution with different SoI timing. This clearly showed that 270 ˚bTDC resulted in lower CMD and lower total particle number concentration. Also, total particle concentrations for 230, 250, and 310˚ bTDC were nearly the same but CMD was significantly lower for advance SoI timing. If CMD is low and total particle number concentration is high then PM is more prone to adverse health effect.

CONCLUSION

The purpose of this investigation was to find out the optimum SoI timing for gasoline fuel. If the SoI is not optimized than there are more PM emissions due to pool firing or fuel impingement on the piston and cylinder wall. Experiments were performed on five SoI timing 230, 250, 270, 290 and 310˚ bTDC to measure particle number size, particle size-mass and particle surface area distribution. It was found that too advance or too restarted SoI timing resulted in relatively higher PM/PN emission. 270˚ bTDC was found to be the optimum SoI timing were PM/PN emissions were minimum.

ACKNOWLEDGMENTS

DEFINITIONS/ABBREVIATIONS

Bu15   15% (v/v) Butanol blended with 85% (v/v) Gasoline
ECU   Electronic Control Unit
EEPS   Engine Exhaust Particle Size
FIP   Fuel Injection Pressure
GDI   Gasoline Direct Injection
IC   Internal Combustion
IMEP   Indicated Mean Effective Pressure
PM   Particle Mass
PN   Particle Number

REFERENCE

[1] Zhao F, Lai M-C, Harrington DL. Automotive spark-ignited direct-injection gasoline engines. Progress in energy and combustion science. 1999;25:437-562.
[2] Bergvall C, Westerholm R. Determination of highly carcinogenic dibenzopyrene isomers in particulate emissions from two diesel-and two gasoline-fuelled light-duty vehicles. Atmospheric Environment. 2009;43:3883-90.
[3] Pope III CA, Dockery DW. Health effects of fine particulate air pollution: lines that connect. Journal of the air & waste management association. 2006;56:709-42.
[4] Kim K-H, Kabir E, Kabir S. A review on the human health impact of airborne particulate matter. Environment international. 2015;74:136-43.
[5] Mimura T, Ichinose T, Yamagami S, Fujishima H, Kamei Y, Goto M, et al. Airborne particulate matter (PM2. 5) and the prevalence of allergic conjunctivitis in Japan. Science of the Total Environment. 2014;487:493-9.
[6] Wang X, Zhao H, Xie H. Effect of piston shapes and fuel injection strategies on stoichiometric stratified flame ignition (SFI) hybrid combustion in a PFI/DI gasoline engine by numerical simulations. Energy Conversion and Management. 2015;98:387-400.
[7] Ventura R, Samuel S. Optimization of fuel injection in GDI engine using economic order quantity and Lambert W function. Applied Thermal Engineering. 2016;101:112-20.
[8] Karlsson RB. Piston fuel film observations in an optical access GDI engine: Massachusetts Institute of Technology; 2000.
[9] Eastwood P. Particulate emissions from vehicles: John Wiley & Sons; 2008.
[10] Chan TW, Meloche E, Kubsh J, Rosenblatt D, Brezny R, Rideout G. Evaluation of a gasoline particulate filter to reduce particle emissions from a gasoline direct injection vehicle. SAE International Journal of Fuels and Lubricants. 2012;5:1277-90.
[11] Keskinen K, Kaario O, Nuutinen M, Vuorinen V, Künsch Z, Liavåg LO, et al. Mixture formation in a direct injection gas engine: Numerical study on nozzle type, injection pressure and injection timing effects. Energy. 2016;94:542-56.

SEEC-2018-033

ROLE OF MISCIBILITY ADDITIVES ON COMBUSTION AND NOISE CHARACTERISTICS OF A DIESEL ENGINE FUELLED ON DIESEL/METHANOL BLENDS

Dev Prakash Satsangi
Department of Mechanical Engineering
Indian Institute of Technology Kanpur
Email: satsangi@iitk.ac.in

Nachiketa Tiwari
Department of Mechanical Engineering
Indian Institute of Technology Kanpur
Email: ntiwari@iitk.ac.in

Avinash kumar Agarwal
Department of Mechanical Engineering
Indian Institute of Technology Kanpur
Email: akag@iitk.ac.in

ABSTRACT

Diesel engines fuelled on alcohols have considerable emissions advantages over diesel fuel. This is because the presence of inherent oxygen increases oxygen/fuel ratio and hence improve the in-cylinder combustion process. Miscibility additives (n-butanol and 1-dodecanol) were explored in context of diesel engine's combustion and noise characteristics. In current study oxygen content of the diesel/methanol blends were fixed to 2% by weight. For the experimental purpose a single-cylinder, 4-stroke, naturally aspirated direct injection diesel engine was used at 1500 rpm, and at six different engine loads. It has been found that the blend which uses n-butanol as an additive exhibits more or less same combustion and noise characteritics with referecnce to diesel. Noises were also reduced for blends which have n-butanol as an additive into it compared to 1-dodecanol.

Keywords: A-Weighting (dBA) filter, one-third octave band, compression ignition engine, diesohols, methanol, n-butanol, 1-dodecanol.

INTRODUCTION

Diesel engines are widely used in transportation, industries and agricultural field. The contribution of diesel vehicles to environmental pollution is increasing due to their increasing demand. Stationary diesel engines conventionally use diesel as a fuel. The massive use of diesel fuel in the engine is responsible for economic as well as environmental concerns. In recent years, researchers have tried a number of alternative fuels (alcohols, vegetable oils, gaseous fuels, and ethers etc.) in diesel engines and found alcohols to be a promising solution [1-2]. Alcohols can also be used as a fuel in unmodified engines or engines with minimal modifications [3-5].

Many resreachers have encountered the problem of phase separation while blending alcohol and diesel. Gerdes et al. [6] have reported that solubility of alcohols in diesel to be a function of temperature, additive concentration, water content, and specific gravity of diesel. Among primary alcohols (methanol, ethanol, propanol and butanol), menthol possesses highest concentration of inherent oxygen in it i.e. ~50% by weight which is an important factor for smother combustion. Being oxygenated fuel, the presence of oxygen at the time of combustion plays a significant role and affects the engine characteristics.

Guo et al. [7] have investigated combustion characteristics of a direct injection diesel engine using methanol blends. They reported a decrease in peak value of cylinder pressure due to lower heating value of blends compared to diesel. In another study Li et al. [8] have

investigated combustion characteristics in a reactivity controlled compression ignition engine using numerical approach when fuelled on methanol blends. They reported decrease in peak value of heat release rate due to combined effect of ignition delay, inherent oxygen content, and reduction of combustion rate in initial combustion stage. Uludamar et al. [9] have experimentally investigated noise in an unmodified diesel engine using different biodiesel blends. They conducted regression analysis of linear and non-linear models to predict the relationship between fuel properties with noise characteristics of the diesel engine.

It is seen that a significant amount of research work has been conducted on performance and emissions characteristics of methanol blended fuels in diesel engine. However there is a very less work reported on noise, and combustion characteristics. This work seeks to fill this gap by assessing the behavior of a diesel engine. The work address engine combustion, and noise, aspects of the diesel engine for different methanol blends using different miscibility additives and their influence on these characteristics.

EXPERIMENTAL APPARATUS AND METHODS

Present research uses a vertical, single cylinder, water-cooled, 4-stroke, direct injection diesel genset (DM-10). It has a capacity of 7.4 KVA, and its rated rpm is 1500. The schematic of the experimental setup is shown in Figure 1.
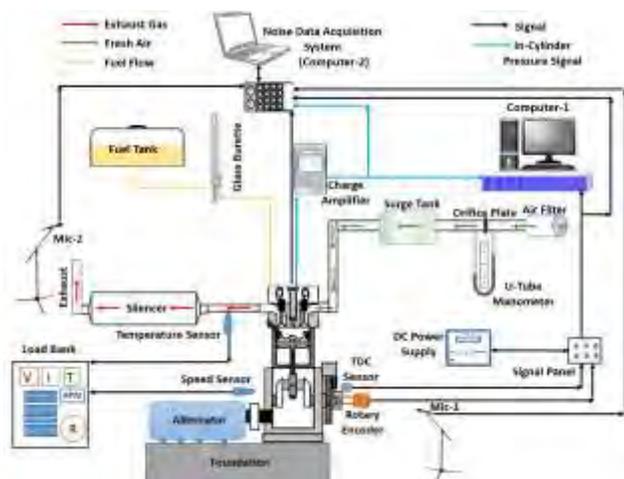
Figure 1. Schematic of experimental set-up

In-cylinder pressure signal was acquired using a piezoelectric pressure transducer along with crank angle rotation for combustion analysis. Total and exhaust noises were measured consistent with ISO 9614-2 and SAE-J1287 respectively using two microphones at sampling frequency of 25.6 kHz. Experiments were conducted at

1500 RPM, injection pressure of 200 bar. Measurement was done at six engine loads (0-100% in steps of 20%). In-cylinder pressure signal was acquired for 250 cycles to minimize cyclic variations.

Test Fuel Preparation and their Characterization

Blends of alcohol and diesel are referred as "Diesohol". Co-solvents, 1-dodecanol and n-butanol were used to avoid phase separation between methanol and diesel. Both blends were prepared by fixing 2% of inherent oxygen content by weight. Compostion of test fuels and their properties are shown in Table 1.

TABLE 1: Test Fuel Characterization

Test fuel	Density (kg/m^3@30°C)	Kinematic Viscosity (m^2/s@40°C)	Calorific value (MJ/kg)
Diesel	830	2.89e-6	43.86
DMDOD2	829	2.87e-6	43.12
DMB2	828	2.87e-6	43.10

RESULTS AND DISCUSSION
Combustion

Figure 2 shows variation of in-cylinder pressure with respect to engine load. It shows that in-cylinder pressure increases with increasing engine load for all test fuels. It can be seen that DMDOD2 shows slightly increased peak pressure relative to diesel compared to DMB2. This is attributable to fuel's cetane number, and the engine load.
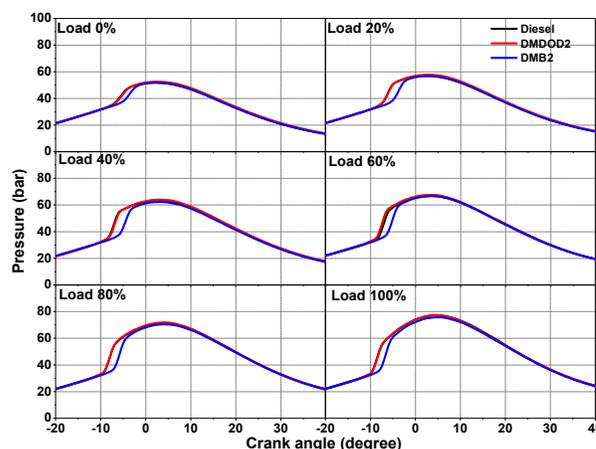
Figure 2. Pressure variation with CAD and engine load

In-cylinder pressure derivative with respect to crank angle position is referred as rate of pressure rise (RoPR). The amount of combustible fuel accumulated during ignition delay period when burns during pre-mixed

combustion phase leads to RoPR [10 RoPR is one of the crucial combustion parameter which is responsible for generation of noise in the engine. Figure 3 shows variation of RoPR for test fuels with CAD and engine load. For engine load below 60% RoPR increases with increasing engine load decrees therafter above 60%, irrespective of test fuels. Here also, DMDOD2 shows slightly increased RoPR$_{max}$ relative to diesel compared to DMB2.
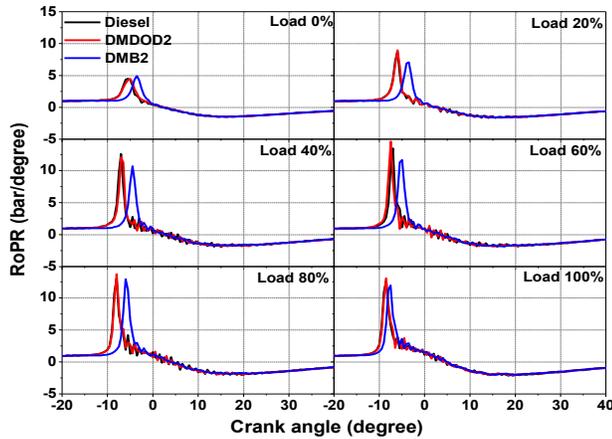
Figure 3. RoPR variation with CAD and engine load

Figure 4 show heat release rate (HRR) trend for all test fuels as a function of CAD and engine load. It is seen that peak values of HRR increases with increasing engine load irrespective of the test fuels. This is attributable to combustion of progressively richer fuel-air mixture with increasing the engine load. A partial correlation was found between RoPR$_{max}$ and HRR$_{max}$.
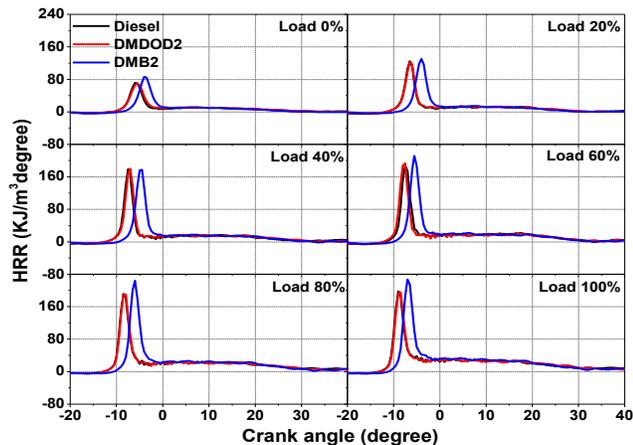
Figure 4. HRR variation with CAD and engine load
Noise

Combustion noise from a genset engine is produced due to rapid fluctuations of in-cylinder pressure developed by spontaneous ignition of fuel inside the combustion chamber [11]. Figure 5 shows generated combustion noise due to ignition of fuel which leads to
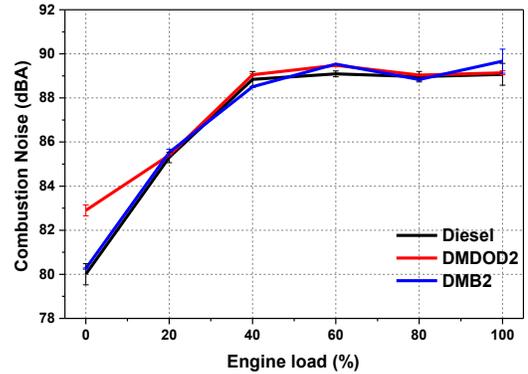
Figure 5. Variation of combuastion noise with engine loads

RoPR. For calculation of combustion noise in-cylinder pressure signals were processed through engine structural attenuation delay (Lucas filter) and A-weighting filters [12]. The combustion noise level was observed in the range of 80 to 90 dBA. DMDOD2 shows increase in combustion noise level compared to DMB2 relative to diesel. Combustion noise increases with engine load for engine load below 60% irrespective of test fuels. However, above 60% engine load combustion noise flatten for all test fuels and shows more or less same noise level. A good coorelation has been observed between RoPR$_{max}$ and combustion noise.
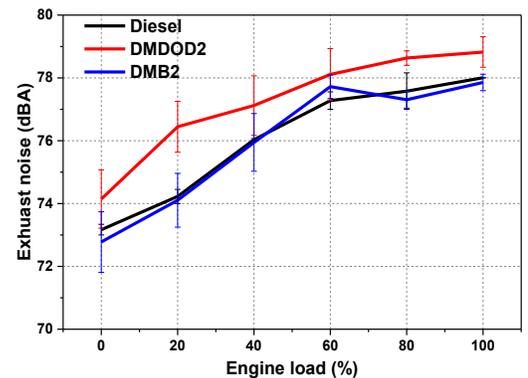
Figure 6. Variation of exhaust noise with engine loads

The exhaust noise gets weaken while travelling through exhaust manifold to the outside via silencer. Consisted with the industry standards the exhaust pressure signal was A-

weighted for one-third octave bands. Figure 6 shows the exhaust noise plot for methanol blends compared to diesel for different engine loads. It is seen that exhaust noise gradually increased with increasing engine load. Overall the exhaust noise of all test fuels was observed in the range of 72-79 dBA. Less cetane index leads to longer ignition delay i.e. more time for fuel to get injected inside the cylinder chamber. This leads to not only high RoPR, but also higher knocking, and as a consequence, more noise levels. Exhaust noise of DMDOD2 has been observed to be higher compared to DMB2 vis-à-vis diesel.

Total noise is shown in Figure 7. It comprises of combustion, mechanical and ambient noises. It is seen that
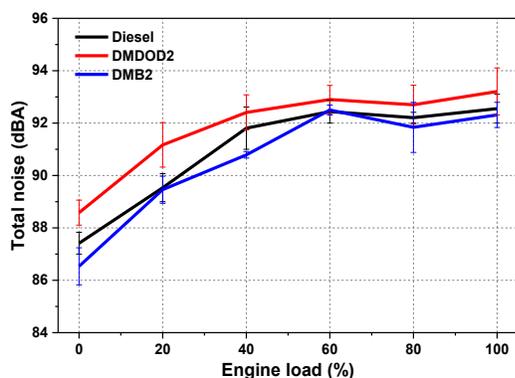
Figure 7. Total engine noise variation at different engine loads

the characteristics of total noise were similar to that of the exhaust noise. However, the overall level of total noise was more than that of the exhaust noise. Total noise emitted by test fuels lies in the range of 86-94 dBA. It is seen that DMDOD2 shows maximum total noise while DMB2 shows least total noise.

CONCULSIONS

Present research involves the role of miscibility additives on noise and combustion characteristics in a 7.4 kW genset diesel engine fuelled on diesel/methanol blends. Being consistent in oxygen content, density, kinematic viscosity, and calorific value of DMDOD2 and DMB2. It is seen that the blend which uses 1-dodecanol as an additive shows increased value of pressure, RoPR, HRR, and various noises compared to that of blend which uses n-butanol as an additive.

Spectrum curves of in-cyinder pressure, exhaust noise and total noise exhibit the dominant nature of 12.5 and 25 Hz frequencies and their harmonics. The 12.5 Hz and 25

Hz frequency corresponds to the combustion cyclicity and engine speed respectively. Combustion noise and ROPR$_{max}$ were correlated well with each other irrespective of test fuel and engine load.

REFERENCES

[1]   Balat M, Balat H. Recent trends in global production and utilization of bioethanol fuel. Appl Energy November 2009;86(11):2273-82.

[2]   Reijnders L. The life cycle emission of greenhouse gases associated with plant oils used as biofuel. Renew Energy February 2011;36(2):879-80.

[3]   Agarwal, AK. "Biofuels (alcohols and biodiesel) applications as fuels for internal combustion engines." Progress in energy and combustion science, 2007; 33(3) ;233-271.

[4]   Sharma A, Murugan S. "Combustion, performance and emission characteristics of a DI diesel engine fuelled with non-petroleum fuel: a study on the role of fuel injection timing". J Energy Inst 2014;88:364-75.

[5]   Muthukumaran N, Saravanan CG, Prasanna Raj Yadav S, Vallinayagam R, Vedharaj S, Roberts WL. "Synthesis of cracked Calophyllum inophyllum oil using fly ash catalyst for diesel engine application". Fuel 2015;155:68-76.

[6]   Gerdes, KR. and Suppes, GJ. Miscibility of ethanol in diesel fuels. Industrial & engineering chemistry research. 2001; 40(3): 949-956.

[7]   Guo, Z., Li, T., Dong, J., Chen, R., Xue, P. and Wei, X. Combustion and emission characteristics of blends of diesel fuel and methanol-to-diesel. Fuel. 2011; 90(3): 1305-1308.

[8]   Li, Y., Jia, M., Liu, Y. and Xie, M. Numerical study on the combustion and emission characteristics of a methanol/diesel reactivity controlled compression ignition (RCCI) engine. Applied energy. 2013; 106: 184-197.

[9]   Uludamar, E., Tosun, E., & Aydın, K., Experimental and regression analysis of noise and vibration of a compression ignition engine fuelled with various biodiesels. Fuel, 2016; 177, 326-333.

[10]   Taghizadeh-Alisaraei, A, Ghobadian, B., Tavakoli-Hashjin, T., Mohtasebi, SS. "Vibration analysis of a diesel engine using biodiesel and petrodiesel fuel blends" Fuel,2012 ;102 : 414-422.

[11]   Seifi, M.R., Hassan-Beygi, S.R., Ghobadian, B., Desideri, U. and Antonelli, M. Experimental investigation of a diesel engine power, torque and noise emission using water–diesel emulsions. Fuel. 2016; 166: 392-399.

[12]   Söderberg, A. "Definition of structural attenuation from engine block using loudspeaker tests and acoustic camera." 2013.

H$_2$ Enriched CNG as Alternative fuel for Internal Combustion Engine

Rajesh Kumar Prasad, Avinash Kumar Agarwal*

Engine Research Laboratory, Department of Mechanical Engineering,
Indian Institute of Technology Kanpur, Kanpur-208016, India
Corresponding Author's Email: akag@iitk.ac.in

Abstract

Transport policies in the world have been mainly driven by the need to reduce the harmful effects of automobile emissions, particularly in urban areas. A complex combination of several factors such as fluctuating prices of petroleum products, undesirable pollutant emissions and resultant ecological imbalances has forced focus on alternative fuels. Thus, GHG emissions reduction and security of energy supply are the two main drivers for development of alternative fuels globally. In an optimized development scenario, the possible contribution of biofuels, natural gas and hydrogen (H$_2$) towards reduction of environmental complications have been identified. Amongst all alternative fuels, natural gas is readily available in large quantities, therefore, no production units are needed like biofuels, cheapest alternative fuel, and quicker commercial implementation to market with slight modification. Lean burn concept is an effective approach to enhance engine's thermal efficiency and reduce exhaust emissions but combustion and performance were decreased due to slower flame speed and more cyclic fluctuation results. Increasing turbulence and using multiple spark plugs are conventional approach to increase flame speed but at the expense of volumetric efficiency and electrode erosion due to increased energy. Therefore, enriching H$_2$ with natural gas is an effective way to increase flame speed with reduction in ignition energy. H$_2$ has a very low energy density per unit volume and as a result, volumetric heating value of HCNG decreases if proportion of H$_2$ is increased in the mixture. Therefore, for the same power output, complete combustion of HCNG reduces HC and CO and NOx emissions. Using laser spark instead of conventional spark system, the lean operation limit extends 1.7 and 1.8 for 30HCNG and 40HCNG respectively. Extended lean limit operation results lower emissions. A major challenge with HCNG as a fuel is the variation of the fraction of H$_2$ during engine operation. For this, a dedicated dynamic mixing system is needed to vary the H$_2$ fraction and optimize engine behavior at desired conditions.

SEEC-2018-035

Effect of spark timing on Combustion, Performance and Emissions Parameters of SI as well as LI Ignited Single Cylinder Engine Fuelled with HCNG

Rajesh Kumar Prasad, Avinash Kumar Agarwal*
Engine Research Laboratory, Department of Mechanical Engineering,
Indian Institute of Technology Kanpur, Kanpur-208016, India

*Corresponding Author's Email: akag@iitk.ac.in

Abstract

For an internal combustion engine there exists optimal spark timing, called maximum brake torque (MBT), which maximizes the output torque, efficiency of the engine and minimizes emissions. MBT timing is extremely important because it affects the start of combustion (SoC). If SoC is too early, work is done against piston and if too late then combustion peak pressure is reduced. In this study, the engine was fuelled with dynamically blended HCNG in vol. % and running at 1500 rpm, λ = 1.2 and spark timing were varied from 22° CA bTDC to 46° CA bTDC, with an interval of 3°CA. The optimum torque for all HCNG blends was noticed at 31° CA bTDC. It was observed that 10% MFB duration decreases with advancing ignition timing till 31° CA bTDC then again increasing with increased ignition timing. For particular ignition timing, the 10% MFB and 90% MFB duration decreases with increase of hydrogen in the HCNG blends, indicating that hydrogen addition can speed up flame kernel displacement and its propagation during initial stage of combustion. In order to achieve improved engine efficiency and lower regulated emissions using lean burning, it is important to secure cyclic variation at higher λ. Unstable lean burning may cause deteriorates engine efficiency and increased HC emissions. The COV_{IMEP} values for different HCNG blends for both SI and LI modes of combustion for varying λ. It was observed LI shows lower variation in COV_{IMEP} compared to SI. It was observed that for all HCNG blends COVimep were lower upto λ = 1.2 then increases but within 6% and minimum variation was observed for 31° CA bTDC (< 2%) compared to 28° CA BTDC and 34° CA BTDC. It was observed that brake thermal efficiency decreases with H_2 enrichment with CNG for any spark timing. This is indirect indication of reducing spark timing with H_2 addition.

SEEC-2018-036

In-cylinder Spray and Combustion investigations in a heavy duty optical diesel engine fueled with Waste cooking oil, Jatropha and Karanja Biodiesels

Chetankumar Patel[a], Joonsik Hwang[b],Krishn Chandra[a], Choongsik Bae[b], Tarun Gupta[a], Avinash Kumar Agarwal[a]

Engine Research Laboratory[a], Department of Mechanical Engineering,

Indian Institute of Technology Kanpur, Kanpur-208016, India

Engine Lab[b], Department of Mechanical and Aerospace engineering,

Korea Advanced Institute of Science and Technology (KAIST), Daejeon, South Korea

*Corresponding Author's Email: akag@iitk.ac.in

Abstract:

In this experimental study, spray and combustion characteristics inside the single cylinder optical engine was carried out by varying injection pressures 40, 80 and 120 MPa. Karanja, Jatropha and Waste cooking oil biodiesel were utilized as test fuels and the results were compared with conventional diesel fuel. There was no significant difference observed in spray tip penetration among the test fuels. However, spray angle found slightly wider for biodiesel. Diesel fuel showed relatively shorter injection delay than biodiesel fuels at the injection pressure of 40 and 80 MPa. Jatropha and Karanja oil biodiesel showed higher flame luminosity for all injection pressure, while waste cooking oil biodiesel showed lower flame luminosity especially at higher injection pressure of 80 and 120 MPa due to comparatively lower viscosity among the biodiesel fuels. Flame spatial fluctuation (FSF) and flame non-homogeneity (FNH) observed higher for all biodiesel at lower injection pressure of 40 MPa. Karanja and Jatropha biodiesel also showed higher FSF and FNH at higher injection pressure, while Waste cooking oil biodiesel showed lower values of FSF and FNH at higher injection pressure.

SEEC-2018-037

Spray atomization characteristics for biodiesel at varying injection pressure and at different locations after break-up length

Chetankumar Patel[a], Joonsik Hwang[b], Choongsik Bae[b], Tarun Gupta[a], Avinash Kumar Agarwal[a],*

a) Engine Research Laboratory, Department of Mechanical Engineering, Indian Institute of Technology Kanpur, Kanpur-208016, India

b) Department of Mechanical Engineering, Korea Advanced Institute of Science and Technology,
*Corresponding Author: akag@iitk.ac.in

Abstract

Biodiesel gaining popularity as a alternative fuels for small and large power generation diesel engines. As higher viscosity of biodiesel significantly affect the fuel atomization characteristics. It is important to investigate the fuel atomization properties of biodiesel compared to diesel. Fuel atomization characteristics are generally represented by droplet size distribution, sauter mean diameter (SMD) and velocity investigations. This investigation was carried out to with common rail direct injection system (CRDI) at 400, 600 and 800 bar Fuel injection Pressure (FIP) at atmospheric condition. The test fuels for this experiment were Karanja, Jatropha and Waste cooking oil biodiesel and mineral diesel. The droplet size was measured at total 16 points after the breakup length 60 mm. The location was changed by 1 mm and 10 mm along the horizontal and vertical axis respectively. SMD decreased with increase in injection pressure. SMD also decreased along the axial direction regardless of fuel type. Higher SMD observed for biodiesel compared to baseline mineral diesel.

Keywords: Spray characteristics, SMD, Fuel atomization, Biodiesel, FIP, Combustion.

SEEC-2018-038

TRIBOLOGICAL INVESTIGATION OF HARD COATING ON STEEL

Vikram Kumar
Dept. of Mechanical Engg.
Indian Institute of Technology Kanpur
Email: vikramk@iitk.ac.in

Sujeet K. Sinha
Dept. of Mechanical Engg.
Indian Institute of Technology Delhi
Email:sks@mech.iitd.ac.in

Avinash K. Agarwal
Dept. of Mechanical Engg.
Indian Institute of Technology Kanpur
Email:akag@iitk.ac.in

ABSTRACT

The main objective of this investigation is to evaluate the tribological performances of hard-coatings like diamond like carbon(DLC), tungsten carbidE (WC) and titanium aluminium nitride (TiAlN) deposited on D2 steel for extreme condition applications such as engine piston rings and bearing. The hard-coatings were applied on cylindrical specimen (D2 steel) of 40 mm diameter and a steel ball of 4 mm diameter was used as the counterface for tribological tests. The tests were conducted at 10 N normal loads, and 0.63 m/s linear sliding speed. Among all hard-coatings, the DLC layer provided the lowest coefficient of friction of 0.075.

Keywords: DLC, *WC*, TiAlN, Lubrication.

INTRODUCTION

Tribological significance of many of hard coatings is not very good due to higher frictional coefficient, poor bonding strength with substrate because of residual stresses and brittleness [1]. Hence there is a requirement of low wear and low friction with high load bearing capacity tribological coatings. The load bearing capacity can be enhanced by applying hard film coating over the substrate and lubricating property of coating enhance tribological properties. By using hard self-lubricating coating, friction is controlled by lubricating properties of coating. Many researchers have studied hard coatings followed by solid lubricant coatings [2, 3]. The coefficient of friction of steel sliding against steel in dry condition is in the range of 0.6-0.9 in ambient condition and with an ordinary lubricant, it is around 0.1 with similar material pair. Various coating materials that have been used against steel counter-face for low coefficient of friction (around 0.2) such as diamond like carbon (DLC), molybdenum disulphide (MoS2), various metal carbides such as, tungsten carbide (WC), titanium carbide (TiC), chromium carbide (CrC), and many physical vapor deposition (PVD) coatings like, titanium aluminum nitride (TiAlN), chromium aluminum nitride (CrAlN), titanium dioxide (TiO2), alumina (Al2O3) etc. [4, 5, 6, 7, 8, and 9]. Low coefficient of friction and wear rate of Metal nitride (MoN) Cu doped coating is due to formation of CuMoO4 tribo-film [10]. Metal alloy (TiAlC) coatings reduce the coefficient of friction by forming the transfer film layer (tribo-film) due to graphitization (carbide transformation into amorphous carbon which attributed to graphitization) [11, 12].

Although various coatings, as mention by literature survey as above, it can be concluded that low friction coating can be achieve by replacing conventional lubrication with self lubricating coating.

2. EXPERIMENTAL PROCEDURE
2.1 MATERIALS

Cylindrical shaft (diameter = 40 mm width ~12 mm and roughness ~ 0.40 micron) of D2 steel was coated by material DLC, WC and TiAlN (Oerlikon Balzers Coating India Private Limited). The counterface for all tribological tests is stainless steel (SAE 52100) ball of 4 mm diameter. For base oil lubricated tests, SN 150 (provided by Indian oil Corporation Limited) of Group-I having viscosity index 95 was used under boundary lubrication condition.

2.2 SAMPLE PREPARATION

Cylindrical shaft of D2 steel with specifications as mention above was hardened by heat treatment to hardness of 2.75 ± 0.05 GPa. After the heat treatment, cylindrical

soft were cleaned. The specimen was then coated with different hard coating materials (DLC, WC and TiAlN) using Physical Vapor Deposition (PVD) method. The hard layer coating thicknesses was between 6 – 10 μm

2.3 Surface Properties Hard Coatings

Hardness of the hard coatings and the dual-coatings were measured using Vickers hardness tester, and the data is given in Tables 1 shows that the hardness of all hard coated samples had hardness in the range of 11.50 – 12.58 GPa, which was nearly four times that of the D2 steel, and WC coating had the maximum hardness (12.58 GPa), followed by TiAlN (11.86 GPa) and DLC (11.5 GPa). Surface roughness of hard coated surfaces are given in Table 1. Surface roughness was the least for DLC coating.

Table 1: Hardness (GPa) of three hard (DLC/, WC and TiAlN) coatings on D2 steel.

Coating Material	DLC	WC	TiAlN
Hardness (GPa)	11.50 ± 0.75	12.58 ± 0.59	11.86 ± 0.11
Surface Roughness (μm)	0.126 ± 0.029	0.205 ± 0.075	0.134 ± 0.032

2.4 TRIBOLOGICAL CHARACTERIZATION

Dry and lubricated (in base oil SN 150) friction and wear tests have been carried out using lab-fabricated ball-on-cylinder tribometer setup (Figure 1). The tests have been conducted at different normal load 10 N and at sliding speed of 0.63 m/s (300 rpm) for maximum number of cycles till the coefficient of friction (CoF) reached 0.3 at room temperature (25^0C) and relative humidity of 45 %.
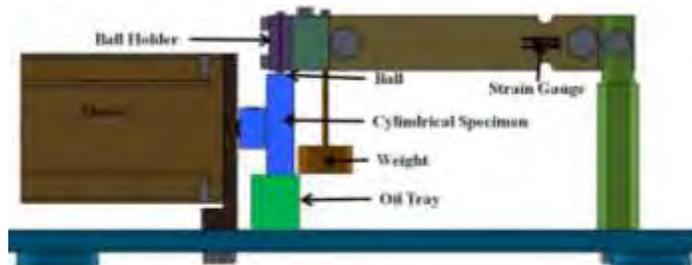
FIGURE 1. Ball-on-cylinder type tribometer.

3. RESULTS AND DISCUSSION

Tribological investigations of hard coated D2 steel were performed on ball-on-cylinder tribometer under following conditions:

3.1 TRIBOLOGICAL ANALYSIS UNDER DRY CONDITION

Dry tests of hard coatings at 0.63 m/s speed and 10 N normal load were performed for 4 x 10⁴ cycles for DLC and WC, and only 1500 cycles for TiAlN since it wore out the counterface ball rapidly.

(a)

(b)
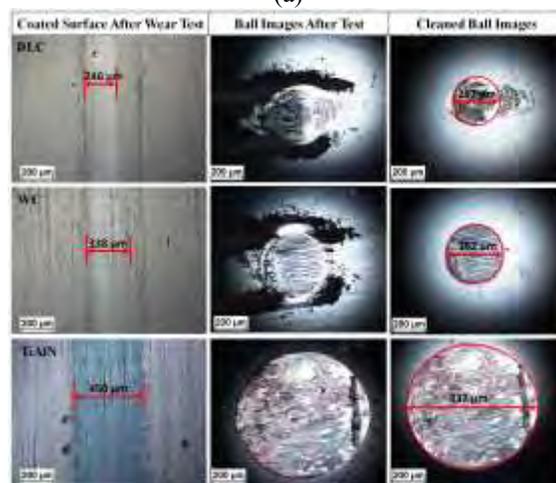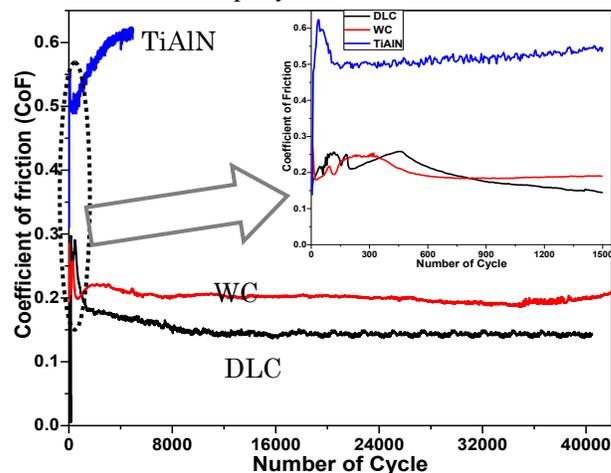
FIGURE 2. (a) Variations in coefficient of friction with the number of cycles, (b) the worn surface of coatings and ball images after test under dry condition.

Variations of the coefficient of friction with number of cycle for hard coatings over D2 steel are shown in Figure 2a and worn surface of coatings and the corresponding ball counterface are shown in Figure 2b. Enlarged view of initial coefficient of friction variations is shown in the inset of Figure 2a for 1500 cycles. The coefficient of friction of DLC coating initially increased and then decreased after few cycles due to formation of tribo-film (transfer film), which acted as self-lubricating film. DLC hard coating showed the lowest steady-state coefficient of friction (~0.14) due to the formation of amorphous carbon

hydroxide. Similar trend for coefficient of friction was observed with WC coating which exhibited steady-state coefficient of friction (0.20). The carbon present in the transfer film lowered the coefficient of friction, depending on the quality of transfer film.

3.2 TRIBOLOGICAL ANALYSIS UNDER LUBRICATED CONDITION

Tribological tests of hard (DLC, WC and TiAlN) coatings over D2 steel at 0.63 m/s linear sliding speed and 10 N normal loads were performed for 2×10^5 cycles under base oil lubrication.
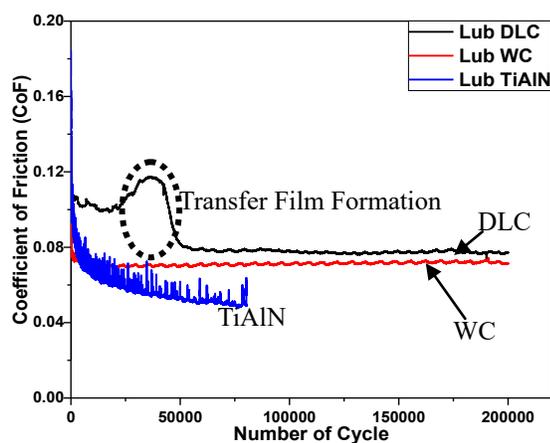
(a)
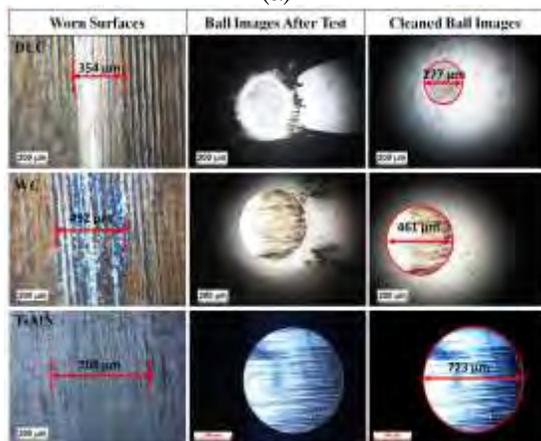
(b)

FIGURE 3. (a) Variations in coefficient of friction with number of cycles (b) Worn surface and corresponding ball image after wear test under base oil (SN150) lubricated condition at 10 N load and 0.63 m/s (300 rpm)sliding speed under lubricated condition.

The variations in coefficient of friction with the number of cycles are shown in Figure 3(a) at 10 N normal load. The coefficient of friction of DLC coating initially exhibited slightly higher value (~0.10) which further increased to ~0.12 (marked by dotted circle). As the wear

of DLC coating took place, a thin transfer film formed on the wear track, which reduced the coefficient of friction to ~0.08 at normal load of 10 N. The transfer film on DLC coating formed after different number of cycles at two different loads of 10 N as shown in Figure 3a. The coefficient of friction for WC coating was observed to be the lowest at 0.075 at the normal loads of 10 N, and the coefficient of friction remained constant throughout the test. The coefficient of friction for TiAlN coating was initially observed to be the highest (~0.19) which reduced to be the lowest (~0.06) amongst all the coatings at 10 N normal load. The optical images of worn surface of coatings and ball counterface after sliding test and after cleaning are shown in Figure 3b.

4. CONCLUSION

Hard coatings of DLC, WC and TiAlN were applied on the D2 steel and their friction coefficient and wear life were evaluated under dry and lubricated conditions at 10 N normal load and 0.063 m/s linear sliding speed. Amongst all the three hard coatings, DLC exhibited the lowest coefficient of friction (0.14) under dry condition at 10 N load, whereas under lubricated condition, WC coating exhibited the least coefficient of friction (0.075) at normal loads of 10 N.

REFERENCES

[1] Neville A, Morina T, Haque and Voong M, Compatibility between tribological surfaces and lubricant additives- How friction and wear reduction can be controlled by surface/lube synergies, Tribology International 2007; 40:1680-1695.
[2] Sherbiney MA, Halling J. Friction and Wear of Ion-Plated Soft Metallic Films. Wear 1977; 45:211 – 220.
[3] Erdemir A, Busch DE, Erck RA, Fenske GR, Lee R. Lubrication Engineering 1991; 47 (10) 863.
[4] Erdemir A, Nichols FA, Pan XZ. Friction and wear performance of ion-beam deposited diamond-like carbon films on steel substrates. Diamond and Related Materials 1994; 3:119–125.
[5] Gahlin R, Larsson M, Hedenqvist P, Jacobson S, Hogmark S. The crater grinder methods as a means for coating wear evaluation –an update. Surface and Coatings Technology 1997; 90:107–l 14.

[6] Grill A. Tribology of diamond like carbon and related materials: an updated review, Surface and Coatings Technology 1997; 94-95:507–513.

[7] Gilmore R, Baker MA, Gibson PN, Gissler W, Stoiber M, Losbichler P, Mitterer C. Low-friction TiN-MoS2 coatings produced by dc magnetron co deposition. Surface and coatings technology 1998; 108:345–351.

[8] Voevodin AA, O´Neill JP, Sabinski JS. Tribological performance and tribochemistry of nanocrystalline WC/amorphous diamond-like carbon composites. Thin solid films 1999; 342:194–200.

[9] Martınez E, Wiklund U, Esteve J, Montala F, Carreras LL. Tribological performance of TiN supported molybdenum and tantalum carbide coatings in abrasion and sliding contact. Wear 2002; 253(11):1182–1187.

[10] Ozturk A, Ezirmik KV, Kazmanlıa K, Urgen M, Eryılmaz OL, Erdemir A. Comparative tribological behaviors of TiN, CrN, and MoN–Cu nanocomposite coatings. Tribology International 2008; 41:49–59.

[11] Wang X, Kwon PY, Schrock D. Friction coefficient and sliding wear of AlTiN coating under various lubrication conditions. Wear 2013; 304:67–76.

[12] Lindquist M, Wilhelmssonb O, Janssonb U, Wiklunda U. Tribofilm formation and tribological properties of TiC and nanocomposite TiAlC coatings. Wear 2009; 266:379–387.

[13] Kumar, V., Sinha, SK., Agarwal, AK., 2017. "Tribological studies of epoxy composites with solid and liquid fillers". Tribology international, 105, 27-36.

SEEC-2018-039

EPOXY COMPOSITE COATINGS FOR ENGINE APPLICATIONS

Vikram Kumar
Dept. of Mechanical Engg.
Indian Institute of Technology Kanpur
Email: vikramk@iitk.ac.in

Sujeet K. Sinha
Dept. of Mechanical Engg.
Indian Institute of Technology Delhi
Email:sks@mech.iitd.ac.in

Avinash K. Agarwal
Dept. of Mechanical Engg.
Indian Institute of Technology Kanpur
Email:akag@iitk.ac.in

ABSTRACT

Engine piston rings are coated with hard materials such as tungsten carbide (WC) and epoxy composite coatings have been applied over them, and their wear analysis was carried out on in a firing internal combustion (IC) engine to protect and enhance the tribological properties. Wear test of rings were performed in firing single cylinder diesel engine. The wear rate of dual-coated(hard and soft coating) top piston ring has was 2.11 x 10^{-12} mm^3/ N-m.

Keywords: *Engine, Piston Rings, WC, Dual-coating*.

INTRODUCTION

The main drawbacks of IC engines are their low mechanical and thermal efficiencies. Frictional loss in engine alone is in the range of 4-15% of total energy losses. Large amount of fuel energy is wasted in the form of heat. From the tribological point of view, there is a requirement to develop coating or lubrication techniques, which lower the friction in engine component such as piston assembly, valve-train and bearings, which are also durable under enhanced loading, high speeds and temperatures.Piston ring assembly is one of the main contributors to frictional losses [1]. Piston-rings are exposed to very rapid and large variations in speed, load, temperature and lubricant availability [2]. The frictional force of the piston rings is based on the shear force calculation under mixed lubrication regime. But it is very difficult to predict exact nature of tribological behaviour of piston ring assembly [3, 4]. Design and wear behaviour of the engine piston rings assembly have been investigated and it is reported that maximum wear takes place in the compression rings. There is no exact mechanism to explain the wear of engine piston rings. However, Lancaster [5]

and Priest [6] proposed the Archard equation for wear calculations which is as follows:

$$V = k\ WL \qquad (1)$$

where,

V = worn volume (m^3),
k = wear factor (m^3/N-m),
W = load (N),
L = sliding distance (m)

2. EXPERIMENTAL PROCEDURE
2.1 MATERIALS

Piston rings (Kirloskar India) of IC engine have been used to coat epoxy (Araldite AY 103 and hardener HY 951; Huntsman Advanced Material Pvt. Ltd) filled graphene(RN-TE-GN-G01; Reinste nano ventures Pvt. Ltd). The counterface is cylinder liner of gray cast iron with 102 mm diameter.

2.2 SAMPLE PREPARATION

A set of piston rings (DM-10 diesel engine) with outer diameter of 102 mm, width of 3 mm and thickness of 4 mm were coated with hard coating material (WC) using physical vapor deposition (PVD) method, which is discussed previously. After that, polymer composite (epoxy/graphene/SN150) coating was applied by using dip and rotate coating machine and cured. Curing of epoxy composite coating have been performed 16 hours at room temperature then thermally cured at 80 °C for four hours. Before the application of epoxy composite coatings, surface was cleaned thoroughly cleaned with acetone and dried at room temperature **[7]**. The thickness of coating varied in the range of ~50 – 60 μm.

2.4 WEAR TEST OF ENGINE PISTON RINGS

The engine (single cylinder, four-stroke diesel engine) tests were carried out for 4 h (3.6 x 10^5 cycles) at 1500 rpm engine speed and 50% engine load and the results were compared with true uncoated piston rings exposed to identical test conditions. Specific wear rate has been calculated by measuring the wear track profiles using an optical surface profiler.

Table 1: Technical specification of Internal Combustion diesel engine.

Manufacturer/ Model	Kirloskar Oil Engines Limited/ DM 10
Engine type	Four stroke water cooled diesel engine
Number of cylinder	1
Compression ratio	17.5
Combustion system	Direct injection
Bore/ stroke	102/ 116 mm
Swept volume	948 cc
Liner type	Cast iron replaceable wet liner
Fuel injection timing	(SOI) $17 \pm 1°$ BTDC
Rated power	10 hp at 1500 rpm
Maximum torque	48 N-m @1500 rpm
Direction of rotation	Clockwise from flywheel side
Oil sump capacity	3.7 liters
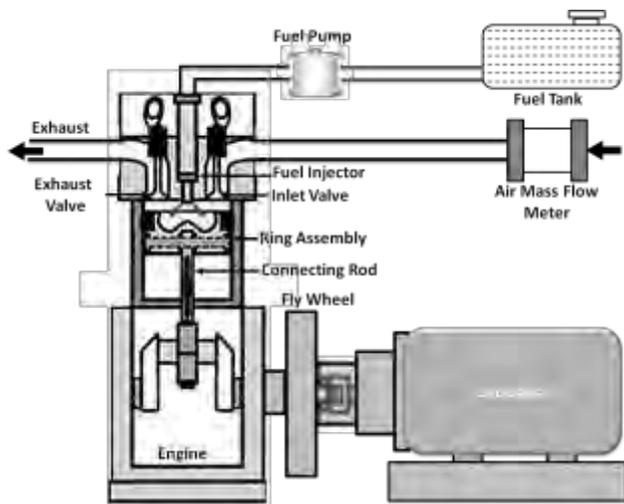
FIGURE 1. Schematic of test engine

3. RESULTS AND DISCUSSION

Dual coatings of (epoxy/ graphene/ SN150) composites with film thickness ~60 μm have been formed on engine piston rings. Wear tests of dual coatings have been carried out on engine firing conditions. The following results have been obtained.

3.1 SURFACE ROUGHNESS

Roughness of dual coatings was measured by 3D-optical profilometer (Bruker, USA Model: Counter GTK). The roughness of the piston rings was evaluated before and after test, and is reported in Table 2. Roughness of the coated surfaces was increased due to wear of the piston rings. The top ring had the least roughness value (0.21 before test and 0.73 after test) among all three (top, middle and lower).

Table 3: Surface roughness of WC/ EGNSN dual-coated rings before and after wear test.

Ring Type	Roughness (R_a) Before Test (μm)	Roughness (R_a) After Test (μm)
Top Ring	0.21	0.703
Middle Ring	0.31	1.35
Lower Ring	0.53	1.91

3.2 THERMO-GRAVIMETRIC ANALYSIS (TGA)

Thermal stability of epoxy composite coatings were evaluated by using high temperature simultaneous TGA (STA 800 Perkin Elmer Limited). With the TGA, thermal decomposition temperature of materials was investigated before and after engine test.
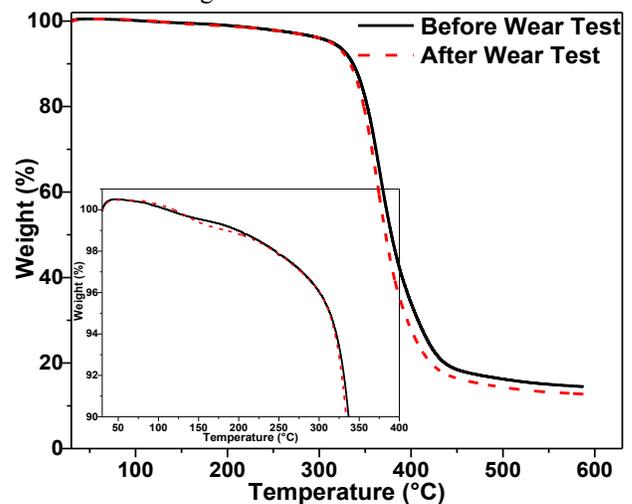
FIGURE 2. TGA of epoxy/ graphene/ SN150 composite before and after the engine test.

The tests were conducted by heating the composite at the rate of 10°C/ min from 30°C to 600°C and holding for 5.0 min at 600°C and then cooling at 30°C/ min from 600°C to 30°C. Any peak in the plot shows the phase transformation of material. From Figure 2, the decomposition temperature for epoxy/ graphene/ SN150 composite is nearly 335°C. Since the average temperature inside the combustion chamber is in the range of 180°C to 200°C. Hence, it is expected that no degradation of epoxy composite coating would take place over the top of piston rings. Also there would be no further curing of epoxy composite during the test as a result of thermal effects.

3.3 WEAR ANALYSIS

After the wear test, there were turning marks left on the surfaces. Hence, the piston rings surfaces wore out dramatically during the running-in of diesel engine firing test. After the firing test of the engine, the wear volume of the engine piston rings was calculated by measuring the mass loss and density epoxy composite and specific wear rates were computed using Equation 1. The wear rates of uncoated and dual-coated rings are shown in Figure 3 and explained in the following paragraphs.
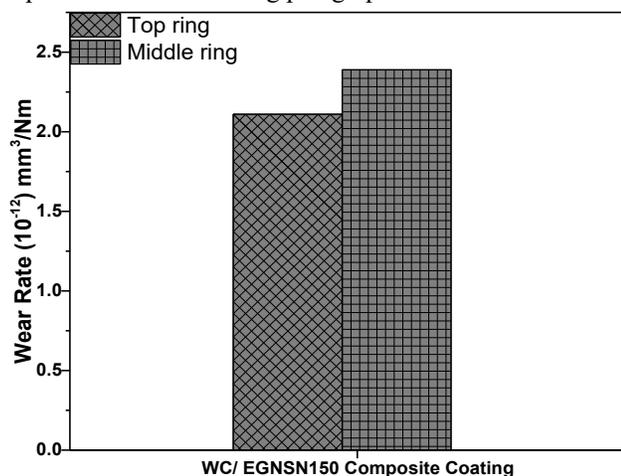
FIGURE 3. Wear rate of dual coating on engine piston ring after engine firing test.

FIGURE 4. Worn surface of dual coated top piston ring

Top dual coated-piston ring survived severe temperature encountered during firing engine conditions There was no delamination of soft top coatings over WC

intermediate layer, as shown in **Figure 4**. However, there was some burning of top soft layer of WC/ EGNSN dual-coating (**Figure 4**). Top dual coated piston ring had the the wear rate 2.11 x 10^{-12} mm^3/ N-m.

4. CONCLUSION

It is to be noted that wear of rings cast iron surface was negligible for dual-coatings, which did not delaminate, on the top and middle rings. For the exhaustive series of experiments, it can be concluded that epoxy/graphene/SN150 is a potential coating of steel surfaces, which can give low friction and long wear life under dry and base oil lubricated conditions, for severe condition of load and temperature, typical of an IC engine. Overall, liquid-filled epoxy-based composites are suitable as tribological coatings and they were further improved by providing DLC as an intermediate coating layer, which offered negligible wear and was successfully applied on the piston rings. The coatings survived the harsh thermal and stress conditions typical of an IC engine and protected the base metal of rings (cast iron).

ACKNOWLEDGEMENT

REFERENCES
[1] Andersson BS., 1991. Company's perspective in vehicle tribology. Leeds-Lyon Symposium on tribology, 503–506.
[2] Dowson D., 1993. Piston assemblies: background and lubrication analysis, (C.M. Taylor Ed.), Engine Tribology, Tribology Series 26, Elsevier.
[3] Priest M., Taylor CM., 2000. Automobile engine tribology — approaching the surface. Wear, 241:193–203.
[4] Tayler CM., 1998. Automobile engine tribology— design considerations for efficiency and durability, Wear, 221:1–8.
[5] Lancaster JK., 19973. Basic mechanisms of friction and wear of polymers. Plastics and Polymers, 41:297–306.
[6] Priest M., 1996. The Wear and Lubrication of Piston Rings. Ph.D. Thesis, University of Leeds.
[7] Kumar, V., Sinha, SK., Agarwal, AK., 2017. ―Tribological studies of epoxy composites with solid and liquid fillers". Tribology international, 105, 27-36.

SEEC-2018-041

EXTRACTION OF CHITIN FROM SHRIMP EXOSKELETON USING 2^K FULL FACTORIAL METHOD

B. Shankaranarayanan
Department of Biotechnology
Sri Venkateswara College of
Engineering (Autonomous)
Sriperumbudur Tk – 602 117
Email id: shankbalaji@gmail.com

S. Naga Vignesh
Department of Biotechnology
Sri Venkateswara College of
Engineering (Autonomous)
Sriperumbudur Tk – 602 117
Email id: nagavignesh@svce.ac.in

E. Nakkeeran
Department of Biotechnology
Sri Venkateswara College of
Engineering (Autonomous)
Sriperumbudur Tk – 602 117
Email id: nakkeeran@svce.ac.in

ABSTRACT

In recent years, the disposal level of shrimp processing industry wastes has been increasing. Its main contents composed of the head/exoskeleton can be utilized to produce chitin, a biopolymer. The existing extraction methods of chtin are not efficient and has resulted in release of chemicals such as HCl, acetic acid, and NaOH as toxic effluents after the extraction process. The current approach targets towards developing an alternative extraction process to replace HCl with citric acid. Compared to the existing extraction method with HCl, the developed method was found to be highly efficient with maximum recovery and purity of 87% and 69% respectively. Chtin could be obtained without deproteinization step when 1% citric acid was used at a temperature of 121°C for a period of 1 h. The results revealed the suitability of citric acid in obtaining high purity chitin from shrimp shells.

Keywords: Shrimp shell, Demineralization, HCl, Citric acid
.

INTRODUCTION

Aquaculture is the world's fastest growing food production sector in recent years. Shrimp is a high value aquacultural product, and is processed for the meat, leaving the carapace and head as waste. These wastes are dumped either in landfills or discarded in sea water. The Indian shrimp processing industry alone produces more than 100,000 tonnes of wastes making it as the single largest waste in the country [1]. Being light in weight, they accumulate on the surface thereby causing surface pollution and unpleasant smell in coastal areas. Hence constitutes an important concern of environmental pollution.

The head/exoskeleton can be harvested for the production of products of great economical viability such as chitin and chitosan. Chtin is the second largest biopolymer in the world after cellulose [2]. The polymers formed by chitin are natural amino polysaccharides having unique structures, functions and wide applications in biomedical and other industries. Chitin and its derivatives hold great economic value because of their versatility, biocompatibility, biodegradability and agrochemical applications [3]. Due to its high tensile strength, it can very well be used in wound dressing and other medical textiles [4]. It can be used to immobilize enzymes and whole cells and thus finds its applications in various food processing and diary industries.

The principle behind extraction of chitin is the removal of protein and minerals (especially calcium carbonate) and other compounds (including pigments like astaxanthin) from the shells and later drying [5]. Currently, chitin is extracted using HCl as the demineralizing agent. Using this method, approximately 10^{10}-10^{12} tons of chtin is produced annually by the concerned industries [6]. This poses issues of disposal which contributes to polluting the environment. HCl is also found to degrade the chitin powder, hence, reducing the overall recovery of chitin from the shell.

In view of the above, this study focused to optimize the extraction of chitin using an alternate demineralizing agent, citric acid in order to improve the recovery and purity of chitin from shrimp shell.

MATERIALS AND METHODS

PREPARATION OF SHRIMP SHELL

The shrimp head wastes were obtained from local fish market and the meal was removed. The resulting shell was washed thoroughly with distilled water and stored at -80°C for further use.

EXTRACTION OF CHITIN USING CITRIC ACID

The shell was washed and dried. The dried shells were subjected to soaking at different concentrations of citric acid for demineralization. Subsequently, deproteinization was carried out using sodium hydroxide of various concentrations. Further, the shells were subjected to decolourization to remove the residual colours present in the shell using sodium hypochloride. The shells were dried, pulverized and sieved to obtain chitin. The experimental design used is described in the experimental design table (Tab.1). Attempts were also made to eliminate deproteinization step.

TABLE 1: EXPERIMENTAL DESIGN

Independent Variable	Coded Symbol	Range and level	
		-1	+1
Citric Acid (%)	A	1	2
NaOH (%)	B	0.1	1
NaOCl (%)	C	1	2
Temperature (°C)	D	37	121
Time (h)	E	1	24

ESTIMATION OF CHITIN CONTENT

The chitin content was estimated using the following formula:

Where, the impurities include mineral and protein content. The mineral and protein content was estimated using ash test [7] and Lowry's method [8] respectively.

CALCULATION OF CHITIN RECOVERY AND PURITY

The recovery and purity of chitin were calculated using the following formulae:

RESULTS AND DISCUSSION
FACTOR SCREENING AND OPTIMIZATION

Various factors that influenced the recovery as well as purity of chitin were considered in the experimental design. A number of variables influencing the extraction process such as concentrations of citric acid, sodium hydroxide and sodium hypochloride, incubation time and temperature were selected. The levels of each parameters are represented in experimental design table (Tab. 1). The recovery and purity of chitin powder were considered as the response parameters. Once the variables and their experimental design were selected, the influence of variables and their interactions on the response factors were assessed using 2^k factorial method. MINITAB 16 software was used to design the experiments.

NORMAL PROBABILITY PLOT

In order to understand the role of each factor and its interaction and the effect it causes on the response factor, a normal probability plot of standard effects is presented. The plot is devised based on the central limit theorem wherein identified whether the results are either real or false positive. The effects were divided into two regions: the region below 50%, where the factors and their interactions present negative coefficient and the region above 50%, where the factors and their interactions present a positive coefficient [9].

The normal probability plots (Fig.1 and Fig.2) showed that the concentration of citric acid used and the time of incubation played a major role in affecting the recovery as well as purity of chitin. The combination of citric acid concentration, temperature and incubation time was directly proportional to the recovery and purity of chitin. It showed a positive effect of over 85% showing the importance of three parameters. It was also identified that the citric acid concentration and time of incubation was inversely proportional to the recovery of chitin. Both the factors showed a maximum negative correlation effect of 30% and 15% respectively on both the responses. It was concluded from the plots that time and concentration of citric acid must be maintained as low as possible in order to obtain maximum recovery and purity. Contrary to the insignificance of temperature in chitin recovery, it was found to be highly significant and highly crucial in affecting the purity of chitin. It was also identified that the concentration of sodium hypochloride coupled with incubation time and temperature played positive effect on the chitin purity. Thus, it was identified that the concentration of the bleaching agent also exhibited crucial role in the purification of chitin.

DESIRABILITY FUNCTION AND OPTIMIZATION

One of the main objectives of this study was to determine the optimum conditions in order to maximize the recovery as well as purity of chitn obtained from shrimp shell wastes. Thus, desirability function study using a

response optimizer was carried out. The desirability function approach is one of the most widely used methods in industrial applications for the optimization of multiple response processes. It is based on the idea that the quality of a product or process that has multiple quality characteristics, with one of them outside of some desired limits, is completely unacceptable. The method finds operating conditions that provide the most desirable response values. In this case, the objective was to maximize the recovery as well as purity of chitin powder obtained from shrimp shell wastes [10].
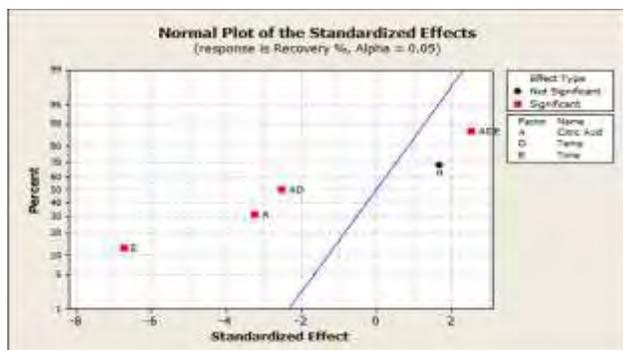
FIGURE 1. NORMAL PLOT FOR RECOVERY (%) OF CHITIN (R-Sq : 73%)
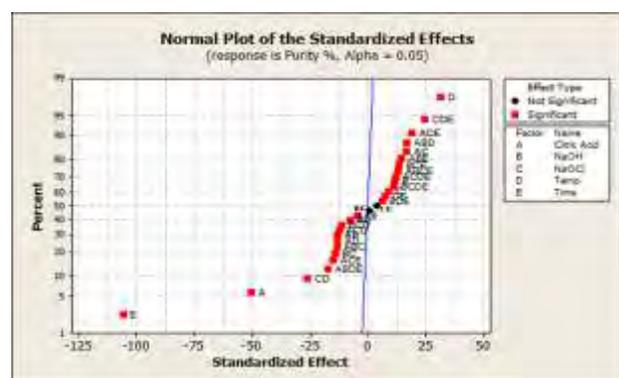
FIGURE 2. NORMAL PLOT FOR PURITY (%) OF CHITIN (R-Sq : 98%)

Hence, maximization algorithm was used to find the desirability. From the response optimization plot (Fig. 3) it was found that a maximum recovery of 73% could be obtained with a desirability value of 1.0 when 1% of citric acid was used at a temperature of 121°C for an incubation time of 1h. Since concentrations of sodium hydroxide and sodium hypochloride were insignificant in affecting the recovery, they were not considered. It was found that the maximum purity of 78% with 0.93 level of desirability could be obtained when 1% of citric acid was used with 1% of NaOH and 2% of NaOCl at a temperature of 121°C for 1 h (Fig. 4).

The results were comparable with the results reported by Pacheco *et al* [10]. They reported that the temperature and time played a major role in the extraction process. Also, the currently followed chemical method of chitin extraction reported by Khanfari *et al* [11] used 4% NaOH and 4% HCl for deproteinization and demineralization, respectively. Upon using the method, only 39% of chitin could be recovered with a purity of 50%.

Subsequently, changes were made in the demineralization process by replacing the HCl with organic acids like citric acid. Citric acid was selected based on the reports of Setoguchi *et al* [12]. They reported that citric acid acts as a chelating agent on shrimp shells aiding in the removal of minerals and also some of the pigments present in the shell. 2^K factorial method of optimization was applied to optimize the overall chitin extraction process. The optimization procedure followed by Ponnusami *et al* [13] was used in this statistical tool as a model. Based on the above study, five parameters were selected including concentration of demineralizing agent, deproteinization agent, decolourization agent, time and temperature for the optimization of extraction process to obtain maximum recovery and purity of chitin.
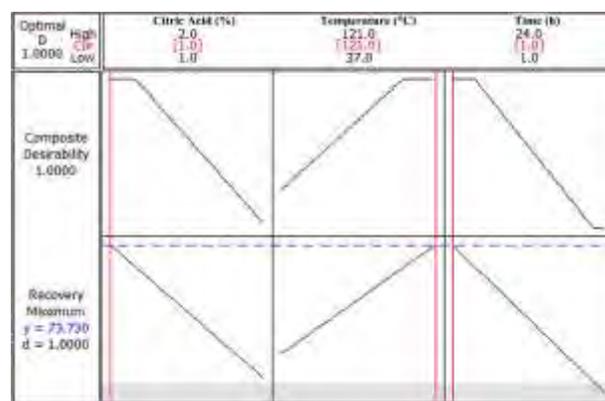
FIGURE 3. RESPONSE OPTIMIZATION PLOT FOR RECOVERY OF CHITIN
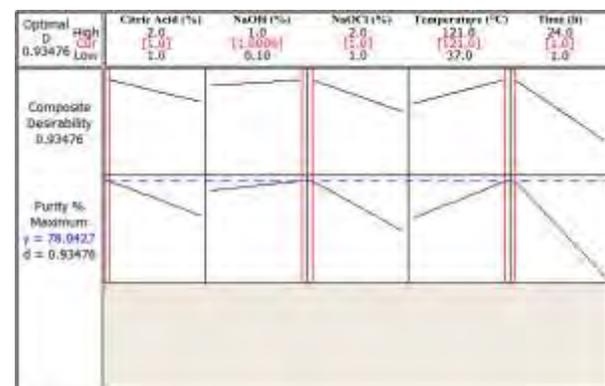
FIGURE 4. RESPONSE OPTIMIZATION PLOT FOR PURITY OF CHITIN

CONCLUSIONS

Chitin as a biopolymer has several applications in food and pharmaceutical industries. Due to the existing harsh treatments, the overall purity and quality of chitin is affected. The treatment of the effluents after each step becomes a challenge. Extraction of chitn from shrimp shell wastes using an alternative demineralizing agent was attempted in this study. The influence of parameters for the extraction of chitin was initially studied. Overall, the temperature, time and concentration of demineralizing agent, citric acid was found to largely influence the extraction process. When citric acid was used as demineralization agent, a maximum recovery of 87% with a purity level of 69% was obtained. It was concluded that citric acid could be used as an alternative to HCl for the efficient extraction of chitin from shrimp shell wastes. The possibilities of eliminating deproteinization step after demineralization with citric acid was also studied. It was found that citric acid was efficient to remove the proteins present in the shell and hence, use of NaOH for deproteinization could be eliminated.

REFERENCES

[1] Fanmino, A.O., Odugwa, O.O., Onifade, A.O., Olutunde, T.O., 2000 "Protein quality of shrimp-waste meal". Bioresource Technology, 72, pp. 185-188

[2] Oh, K.T., Kim, Y.J., Nguyen, N.V., Jung, W.J and Park, R.D., 2008 "Effect of crab shell size on biodemineralization with lactic acid producing bacterium *Lactobacillus paracasei* subsp. Tolerans KCTC-3074". Enzyme and Microbial Technology, 27, pp. 3-10

[3] Younes, I., Bellaaj, I.O., Nasri, R., Chaabouni, M., Rinaudo, M and Nasri, M., 2012 "Chitin and chitosan preparation from shrimp shells using optimized enzymatic deproteinization". Process Biochemistry, 47, pp. 2032-2039

[4] Pillai, C.K.S., Paul, W and Sharma, C.P., 2009 "Chitin and chitosan polymers : Chemistry, solubility and fiber formation". Progress in Polymer Science, 34, pp. 641-678

[5] Puvvada, Y.S., Vankayalapati, S and Sukhavasi, S., 2012 "Extraction of chitin from chitosan from exoskeleton of shrimp for application in the pharmaceutical industry". International Current Pharmaceutical Journal, 1(9), pp. 258-263

[6] Gortari, M.C and Hours, R.A., 2013 "Biotechnological processes for chitin recovery out of crustacean waste: A mini-review". Electronic Journal of Biotechnology, 16 (3), pp. 1-10

[7] Bhaskar, N., Suresh, P.V., Sakhare, P.Z and Sachindra, N.M., 2007 "Shrimp biowaste fermentation with *Pediococcus acidolactici* CFR2182: Optimization of fermentation conditions by response surface methodology and effect of optimized conditions on deproteination/demineralization and carotenoid recovery". Enzyme and Microbial Technology, 40, pp. 1427-1434

[8] Markwell, M.A.K., Haas, S.M., Bieber, L.L., Tolbert, N.E., 1978 "A Modification of the Lowry Procedure to Simplify Protein Determination in Membrane and Lipoprotein Samples". Analytical Biochemistry , 87, pp. 206-210

[9] Croarkin, C., 2012. E-Handbook of Statistical Methods, 2012. www. Itl.nist.gov/div898/handbook

[10] Pacheco, N., Gonzalez, M.G., Hernandez, J.Y.R., Albino, B.F., Gimeno, M., Barzana, E and Shirai, K., 2009 "Effect of temperature on chitin and astaxanthin recoveries from shrimp waste using lactic acid bacteria". Bioresource Technology, 100, pp. 2849-2854

[11] Khanafari, A., Marandi, H and Sanatei, S.H., 2008 "Recovery of Chitin and Chitosan From Shrimp Waste by Chemical and Microbial methods". Iran Journal of Environmental Health, 5, pp.19-24

[12] Setoguchi, T., Kato, T., Yamamoto, K and Kadokawa, J.I.,2012 "Facile production of chitin from crab shells using ionic liquid and citric acid". International Journal of Biological Macromolecules, 50, pp. 861-864

[13] Ponnusami, V., Krithika, V., Madhuram, R and Srivatsava,S.N., 2007 "Biosorption of reactive dye using acid treated rice husk : factorial design analysis". Journal of Hazardous Materials, 142, pp. 397-403

CHARACTERISATION OF SOOT PARTICLES FROM VEHICULAR EXHAUST

Shweta Kumari	Suresh P andian Elumal ai	Manish Kumar J ain
Department of Environmental Science and Engineering, IIT (ISM), Dhanbad	Department of Environmental Science and Engineering, IIT (ISM), Dhanbad	Department of Environmental Science and Engineering, IIT (ISM), Dhanbad
Research scholar	Assistant professor	Associate Professor
kanth.shweta@gmail.com	espandian@iitism.ac.in	manishjkm@gmail.com

ABSTRACT

Diesel driven vehicles are the main source of air quality issues of urban areas especially at roadways and intersections. The main drawback is the release of harmful gases and particulate matter (PM). The PM is mainly composed of soot, soluble organic fraction, sulphates and ash. PM released from vehicles are harmful to human and nearby natives. Amount of particulate matter (PM) released from vehicle depends on fuel type. In the present study, the result shows that the diesel engines emit more soot particles in comparison to gasoline engines per unit distance travelled.

Keywords: Vehicular Exhaust, Soot, Diesel

INTRODUCTION

Nowadays, air pollution is the most serious global incident which affects both biotic and abiotic components of the biosphere. Road vehicles are an important source of atmospheric particulate matter (PM), CO, NOx and volatile organic compounds [1]. In road traffic, PM is emitted mainly from tailpipe exhaust [2]. PM or soot particulates are the result of incomplete combustion of fuel in engines, being introduced to the environment through the emitted exhaust from the tailpipes of the vehicles. Diesel engine vehicles emit more pollutants than the gasoline driven vehicles due to the presence of unburned fuel in the exhaust [3]. Exhaust emission is affected by engine type and technology where the necessary combustion of the fuel in the presence of air takes place, generating the soot or PM and gaseous pollutants. The physical and chemical characteristics of the vehicle exhaust depend on many factors such as vehicle characteristics, driving cycle, driving behaviour, fuel quality, and environmental conditions are affecting factors like road characteristics, ambient conditions [4]. The emissions from traffic have been continuously adding pollutants to urban soils where they will remain present for many years even if the pollution sources are removed. For controlling these pollutants from emitting it is important to know the main components which are being released from the tail pipe with the help of different physical and chemical characterisation.

METHODS

Diesel and gasoline are the most common fuel used in vehicles. In the present study diesel driven shared auto and gasoline driven passenger car were selected. Vehicular exhaust was made to deposit on soil with the help of self-fabricated set-up. The collected samples were used for characterisation. The list of instruments used and its principals for this characterisation are mentioned below in Table 1:-

TABLE 1 : INSTRUMENTS USED FOR CHARACTERISATION

Sl. No.	Instru ment	Chara cterisat ion done for
1.	Field emission scanning electron microscope (FESEM)	Morphological features i.e., size, fractal structure of agglomerates, etc
2.	Energy-dispersive X-ray spectroscopy (EDS)	Elemental composition in samples in %wt

RESULTS

The elemental composition results are shown in figure 1. It clearly indicates high carbon content of exposed soil sample in comparison to unexposed soil samples. It shows that the carbon content is more in diesel sample than gasoline samples. Significant morphological difference was found in the exposed soil samples in comparison to unexposed sample in FESEM images. It was observed that the microgragh of diesel exposed sample having smooth surface in comparison to exposed sample of gasoline may be due to presence of more carbon content. The size of the individual particles was found between 30-50 nm making them dangerous when inhaled, as they can reach deep inside the respiratory tract and get incorporated into the blood stream causing further damage to other internal organs.
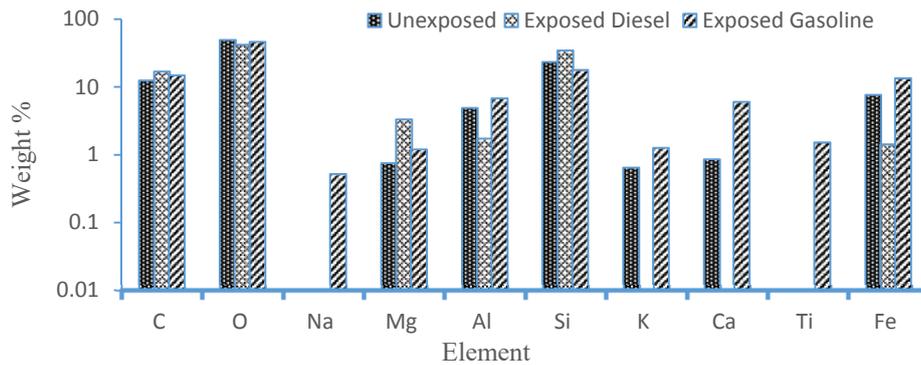
FIGURE 1. GRAPHICAL REPRESENTATION OF ELEMENTAL COMPOSITION OF UNEXPOSED, EXPOSED TO DIESEL AND EXPOSED TO GASOLINE SAMPLES OBTAINED BY ENERGY -DISPERSIVE X-RAY SPECTROSCOPY
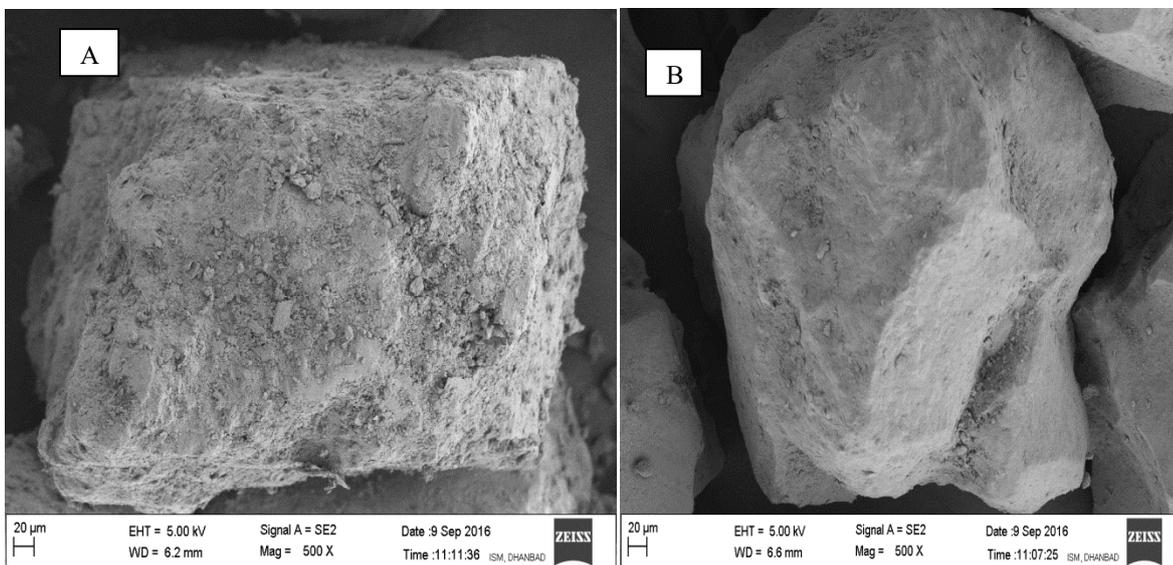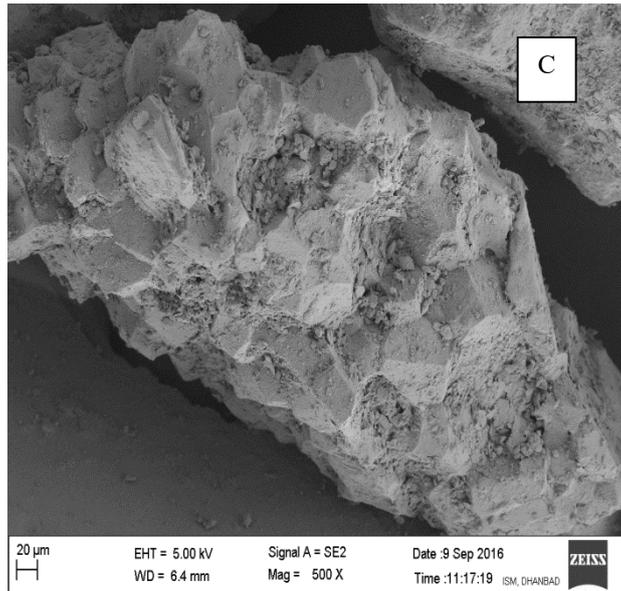
FIGURE 2 . SEM images of A. Unexposed soil sample (Background) B. Soil exposed to diesel engine C. Soil exposed to gasoline engine

CONCLU SIONS

This study concludes that diesel driven vehicle emit more PM than gasoline driven vehicles. As carbon content of exposed soil samples were high for diesel vehicles, this suggests role of vehicular emission in increasing the the carbonaceous particulate matter in atmosphere. These carbon particles affect the climate directly or indirectly, hence necessitates further characterisation of PM from vehicular exhaust for their radiative properties.

.

REFERENC ES

[1] Hung-Lung, C., Yao-Sheng, H. (2009). Particulate matter emissions from on-road vehicles in a freeway tunnel study. Atmospheric Environment,43(26), 4014-4022.

[2] Harrison, R. M., Deacon, A. R., Jones, M. R., & Appleby, R. S. (1997). Sources and processes affecting concentrations of PM10 and PM2. 5 particulate matter in Birmingham (UK). Atmospheric Environment, 31(24), 4103-4117.

[3] Kittelson, D. B. (1998). Engines and nanoparticles: a review. Journal of aerosol science, 29(5), 575-588.

[4] Lin, R., Li, B., Hou, Y. P., & Ma, J. M. (2009). Investigation of dynamic driving cycle effect on performance degradation and micro-structure change of PEM fuel cell. International Journal of Hydrogen Energy, 34(5), 2369-2376.

SEEC-2018-044

STUDY OF TEMPERATURE VARIATIONS ON PHOTO-VOLTAIC MODULE - A NUMERICAL EXPERIMENT

Balkrishna Mehta
Department of Mechanical Engineering
Indian Institute of Technology Guwahati
Guwahati, Assam-781039, India
krishnab@iitg.ernet.in

Pradeep Kumar
Numerical Experiment Laboratory
(Radiation & Fluid Flow Physics)
Indian Institute of Technology Mandi
Mandi, Himachal Pradesh-175005, India
pradeepkumar@iitmandi.ac.in

ABSTRACT

The higher operating temperature of photovoltaic (PV) module above the standard operating temperature, usually 25^oC, adversely affects the panels efficiency. Therefore, it demands the careful analysis of thermal characteristics of photovoltaic module under the actual environmental parameters. Performing the numerical experiment, this work is an attempt to investigate the temperature variation on a photovoltaic module under practical condition by including the radiative heat transfer along with the forced convection. Here, in the first step, steady state simulation with solar insolation at particular location (Jaipur, Rajasthan), day (21 June) and time (13:00 hours) has been calculated by solar load model of ANSYS Fluent. Further, this data will be provided as boundary condition to the full three dimensional fluid flow and heat transfer models where in, radiative heat exchange is also included between the surfaces of photovoltaic module and surroundings and comparison is made with the simulation results without radiation model. It has been observed that simulation with radiation model provides accurate value of temperature.

1 INTRODUCTION

With the increasing energy demands to improve the living conditions and sustainable growth of the human being, technology has made a shift to develop the methodologies to use renewable sources of energy like solar, wind, tidal and geo-thermal etc. Generating electricity using solar Photovoltaic (PV) systems is one of the state of the art technology in recent times, where maintaining the system temperature within the operating range is essential for maximizing the performance of such PV systems. The operating temperature plays a key role in the PV conversion process. The performance of a solar PV cell decreases with increasing temperature due to increased internal carrier recombination rates, caused by increased carrier concentrations. It is well known that electrical conversion efficiency decreases with increase of solar cell temperature resulting from absorption of nearly 50% of other spectrum band of radiation than necessary of the total incident energy falling on the surface of the solar cell [1, 2]. For example, the efficiency of a typical PV system with c-Si cells decreases by 0.45% for every 1^oC increase of the working temperature [3]. Therefore, thermal exchange analysis of solar photovoltaic cell is an important step to obtain the temperature distribution in the various parts of the module to predict the efficiency with reasonable accuracy.

When we look at the heat interaction of PV module, it is clear that the incident solar radiation is absorbed according to the optical properties of the material like absorption coefficient, reflection coefficient and transmission coefficient. The part of this incident radiation is converted in electrical energy and rest is absorbed as thermal energy which increases the temperature of the PV module. To keep the operating temperature of the PV module closer to the maximum efficient point, the absorbed heat need to be dissipated. In general, the dissipation takes place by
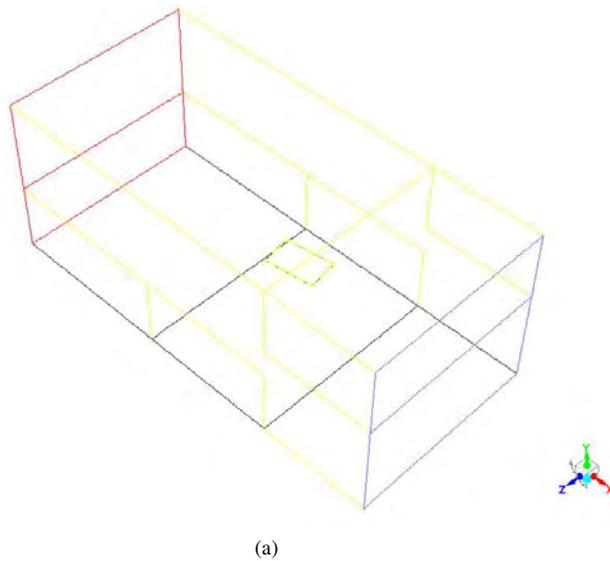
(a)
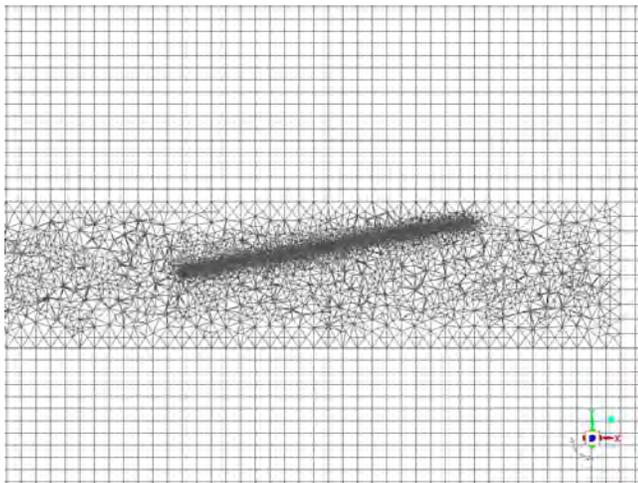
(b)

FIGURE 1: Computation geometry (1a) and grid (1b) around the PV module in z-plane

FIGURE 2: Solar heat flux (W/m^2) distribution on the ground

convective and radiative heat exchange. Evaluation of heat dissipation by convection is not so difficult but the heat exchange by radiation is quite involved phenomenon because radiative heat exchange may/may not be unidirectional and coupled. At the same time, radiative heat exchange between ground surface and PV module is as important as radiative exchange between PV module and environment. Hence, understanding the temperature distribution of PV module in presence of convective and radiative heat exchange is very important to predict the efficiency of PV module. Therefore, focus of this work is an attempt to understand the temperature distribution in the various parts of PV module in presence of both convective and radiative heat exchange especially, considering the radiative heat interaction between the ground surface and PV module.

2   COMPUTATIONAL DOMAIN, GRID, MATHEMATICAL MODELING and BOUNDARY CONDITIONS

The full–scale geometry of PV module of dimension $2 \times 1m^2$ with five layers of glass, ethylene vinyl acetate (eva) film, solar cell and tedlar composite of thicknesses 3 mm, 0.5 mm, 0.3 mm and 0.5 mm [2] have been constructed as shown in figure 1a. The PV module has been rotated to 10° towards south (negative z direction) and west (negative x direction) to replicate the actual installation of PV Module for operation. Further, a computational domain around the PV module including the ground has been created and finally grids as in figure, (1b) are placed in the computational domain. The solar load is applied using the solar load model of ANSYS Fluent which takes the longitude, latitude, day and time of the location as input. The location of Jaipur (longitude: 74°, latitude: 27°), Rajasthan, India and time and date were set to 13:00 hours and 21th June, respectively for the steady state simulation. Figure 2 shows the solar heat flux distribution on the ground. The shadow of PV module appears on the ground and uniform distribution of the solar flux is available on rest of the area of the ground. It is also assumed that wind of 2 m/s blows from east direction (negative x direction). The soil is modeled by one dimensional conduction approach with an approximation that temperature at 20 m depth remain constant at 20^oC independent of surface temperature [4]. The rest boundaries of the computational domain are considered to be symmetric. The two
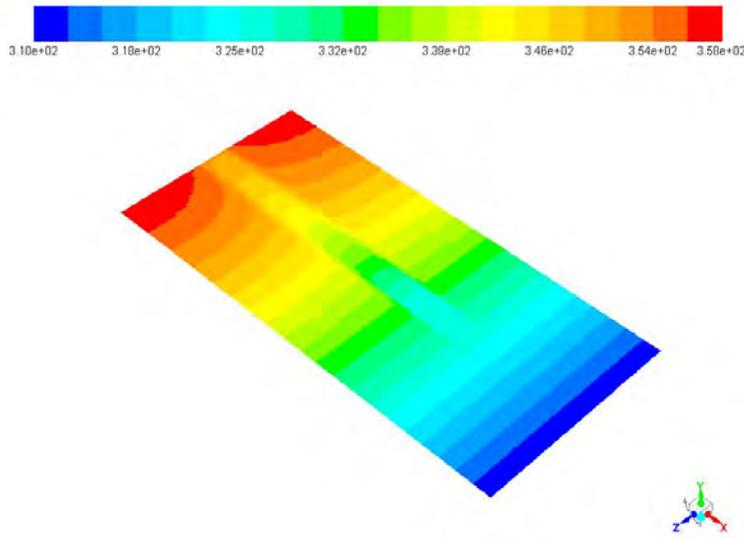
(a)
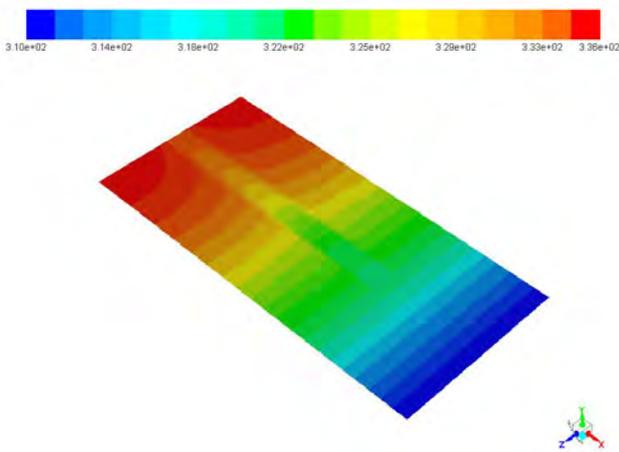
(b)

FIGURE 3: Temperature (K) contour at the Ground

equation $k - \varepsilon$ turbulent model and surface to surface radiation model have also been included in the simulation.

3 RESULTS AND DISCUSSIONS

The steady state simulation has been performed with fluid flow and heat transfer model including surface to surface radiation heat transfer module of ANSYS Fluent to study the temperature variation on the solar cell of PV module and underlying mechanism of heat transfer. The comparison of results of radiation model are made with results of without radiation model.

The temperature variations on the ground without and with radiation are shown in figure (3a) and figure (3b), respectively. The maximum temperatures obtained on the ground are 358 K and 336 K through simulation without and with radiation model, respectively while the temperature of the ground around the PV module installation are 335 K and 323 K, respectively. The temperature predicted by the simulation without radiation model is higher compared to with radiation model. The simulation with the radiation model predicts ground temperature more closely to the reported measured temperature i.e. around 320K [5].
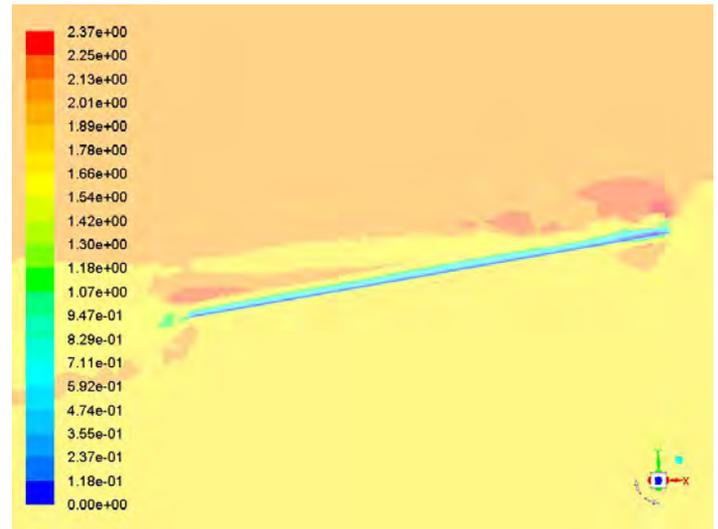
FIGURE 4: Velocity magnitude (m/s) contours around the PV module in z-plane

Figure 4 depicts the velocity magnitude contours around the PV module in the z–plane. The upstream undisturbed flow approaches to PV module and the flow gets disturbed at the tip of the PV module and flow velocity increases around (up and down) the PV module and the flow gets separated and then reattached after some distance downwards on PV module. A higher velocity is also seen at the end of the PV module above and away from the panel surface. This reveals that a stagnation fluid zone lies above the surface and flow glides on this stagnation fluid zone.

Figure 5 reveals the temperature contours on the solar cell layers of the PV module. In contrast to ground temperature , the solar cells temperature is higher in the simulation with radiation model than the simulation without radiation model. However, the temperature predicted with radiation model is more closer

(a)
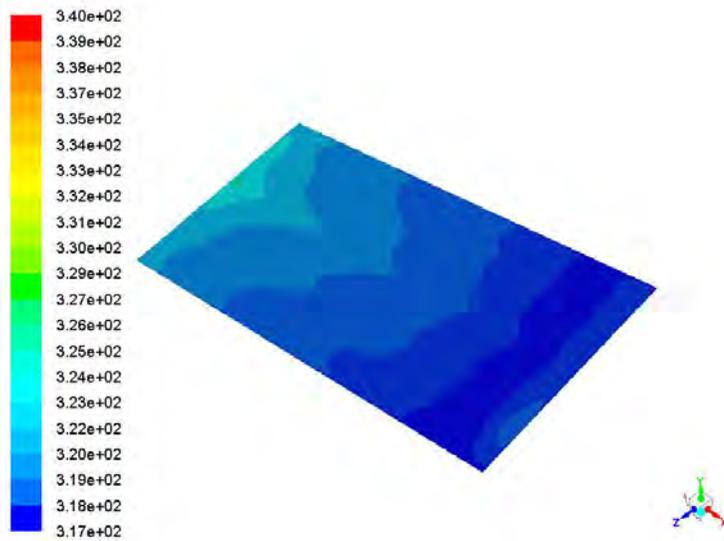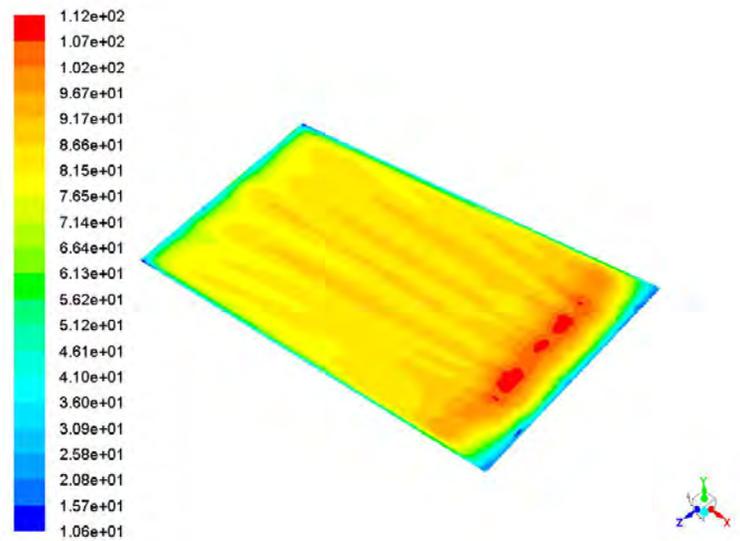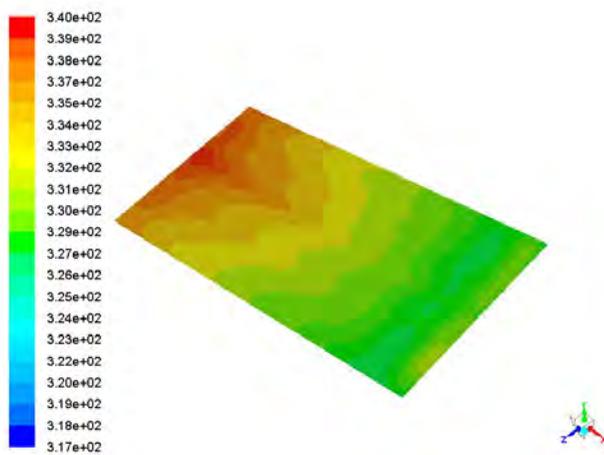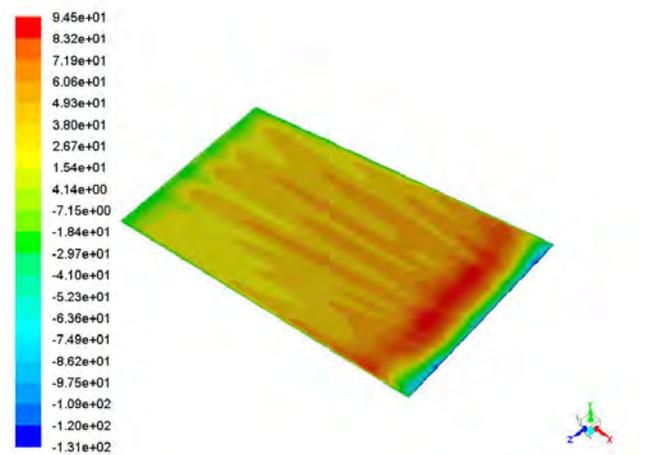
(b)

FIGURE 5: Temperature (K) contours on the layer of solar cell in PV module

(a)

(b)

FIGURE 6: Total heat flux (W/m^2) at the layer of Tedlar in PV Module

to the realistic temperature [6] which is around 70^oC. A strip of cooler zone perpendicular to velocity direction appears on the solar cell in both the simulations which may be due to flow reattachment of flow in this place. The higher temperature is observed at the end of the solar cell. This could be related to stagnation fluid zone appears above the surface of PV module in the the velocity contours graph (4).

It is interesting to know the behavior of the heat flux at the last layer of the PV module i.e. tedlar. The total heat flux contours on the tedlar are shown in figures (6a) and (6b) without and

with radiation model, respectively. The total heat flux is higher for the simulation without radiation model. There are positive values of total heat flux which indicates that flux enters in the PV module, however both in and out heat flux appear in the simulation with radiation model. The radiation heat flux always leaves from PV module through radiation heat transfer as appears from figure (7) since tedlar temperature is higher than the ground.
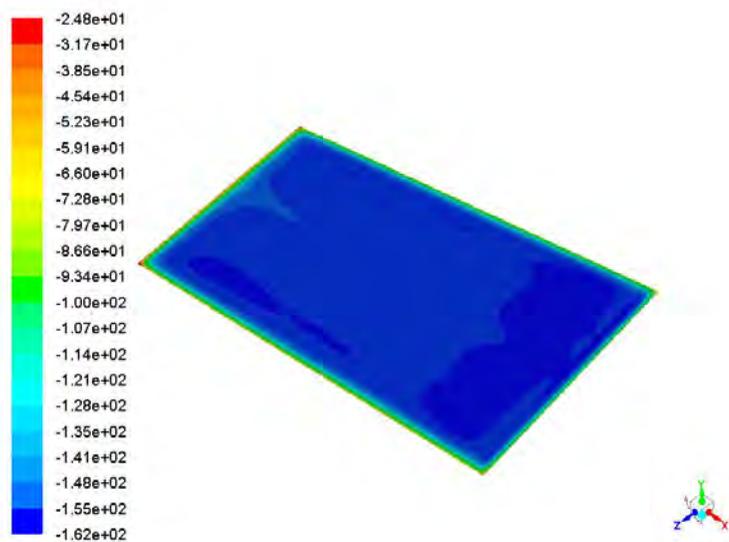
FIGURE 7: Radiative heat flux (W/m^2) at the layer of Tedlar in PV Module

4 CONCLUSIONS

A numerical experiment has been performed on the full–scale PV module under the practical condition with fluid flow and heat transfers model including surface to surface radiation model and the salient points have been concluded as follows.

1. The simulation results with radiation model predicts more accurate temperatures on the ground and at the solar cells of PV module.
2. The ground temperature predicted by radiation model is lower, however temperature at the solar cell is higher as compared to simulation results without radiation model.
3. A stagnation fluid zone appears above the surface of PV module that cause a higher temperature in that zone of PV module.
4. The total heat flux is unidirectional at tedlar in simulation without radiation model whereas both incoming and outgoing flux appears at the tedler with the simulation with radiation model.
5. The radiation flux always leaves from tedlar due to higher temperature than ground

REFERENCES

[1] Atkin, P., and Farid, M., 2015. "Improving the efficiency of photovoltaic cells using pcm infused graphite and aluminium fins". *Solar Energy, 114*, pp. 217–228.
[2] Kant, K., Shukla, A., Sharma, A., and Biwole, P., 2016. "Thermal response of polycrystalline silicon photovoltaic panels: numerical simulation and experimental study". *Solar Energy, 134*, pp. 147–155.
[3] Kalogirou, S. A., and Tripanagnostopoulos, Y., 2006. "Hybrid pv/t solar systems for domestic hot water and electricity production". *Energy Conversion and Management, 4*, pp. 3368–3382.
[4] Georgios, F., and Soteris, K., 2005. "Annual ground temperature measurements at various depths". In Proceedings of CLIMA, Lausanne, Switzerland.
[5] Tyagi, A., Singh, O. P., Singh, S. S., and Kumar, S., 2011. Climate of Jaipur. `http://amssdelhi.gov.in/news_events/Jaipur_climate.pdf`.
[6] Tiwari, G. N., Mishra, R. K., and Solanki, S. C., 2011. "Photovoltaic modules and their applications: A review on thermal modelling". *Applied Energy, 88*, pp. 2287–2304.

SEEC-2018-046

DEVELOPMENT OF AN INTEGRATED DILUTE ACID-LIME PRETREATMENT OF CHILI POST-HARVEST RESIDUE FOR BIOETHANOL PRODUCTION

Raveendran Sindhu*
[1]*Centre for Biofuels, National Institute for Interdisciplinary Science and Technology (CSIR-NIIST), Trivandrum - 695 019, India*
Email: sindhurgcb@gmail.com

Parameswaran Binod
[1]*Centre for Biofuels, National Institute for Interdisciplinary Science and Technology (CSIR-NIIST), Trivandrum - 695 019, India*
Email: binodkannur@gmail.com

Ashok Pandey
[3] *CSIR- Indian Institute of Toxicology Research (CSIR-IITR), 31 MG Marg, Lucknow-226 001, India*
Email: ashokpandey1956@gmail.com

Amith Abraham
[1]*Centre for Biofuels, National Institute for Interdisciplinary Science and Technology (CSIR-NIIST), Trivandrum - 695 019, India*
Email: amithabraham123@gmail.com

Athira Antony
[1]*Centre for Biofuels, National Institute for Interdisciplinary Science and Technology (CSIR-NIIST), Trivandrum - 695 019, India*
Email**:** athiraantony93@gmail.com

Edgard Gnansounou
[2]*Ecole Polytechnique Federale de Lausanne, Institute of Urban and Regional Sciences, GC A3, Station 18, CH-1015, Lausanne, Switzerland*
Email: edgard.gnansounou@epfl.ch

Anil Kuruvilla Mathew
[1]*Centre for Biofuels, National Institute for Interdisciplinary Science and Technology (CSIR-NIIST), Trivandrum - 695 019, India*
Email: anilaykara@gmail.com

ABSTRACT

Lignocellulosic biomass serves as a renewable substrate for the production of biofuels and other value added products. It is composed of cellulose, hemicelluloses and lignin which are connected by several intra- and inter-polymer linkages. Hence some kind of pretreatment to be carried out to make it accessible for enzymatic saccharification. Conventional pretreatment of lignocellulosic biomass is carried out by using either acid or alkali. During acid pretreatment, hemicelluloses is removed from the biomass in the liquid stream while in alkali pretreatment lignin is removed from the biomass in the liquid stream. An integrated process employing the benefits of acid and alkali pretreatment followed by enzymatic hydrolysis would be promising for better hemicelluloses and lignin removal.

Chili post-harvest residue is an underexploited lignocellulosic biomass and India has an availability of 0.5 million tons of this residue. Till date only few reports were available for its utilization for the production of bioethanol and other value added products. Some kind of pretreatment to be carried to make it accessible for enzymatic saccharification by removing hemicelluloses and lignin. Though several conventional as well as alternative strategies have been developed addressing biomass recalcitrance, most of them are a failure or economically nonviable as an industrial process.

The aim of the study was to develop an integrated dilute acid-lime pretreatment strategy for better hemicelluloses and lignin removal from the chili post-harvest residue for the production of bioethanol and to optimize various process parameters affecting pretreatment as well as characterization of the native and pretreated samples.

Keywords

NOMENCLATURE

CPHR   Chili post-harvest residue

IDALP   Integrated dilute acid lime pretreatment

INTRODUCTION

Depletion of fossil fuels and increase in environmental concerns like greenhouse gas emissions leads to search for alternative strategies of energy. Bioethanol serves as a potential alternative fuel. Lignocellulosic biomass serves as a potential renewable substrate for the production of bioethanol (Rezania et al., 2017). Usage of fossil fuels in automobiles release large amount of CO_2 which is a major cause of global warming.

Production of bioethanol from lignocellulosic biomass involves several unit operations like pretreatment, neutralization, enzymatic saccharification, detoxification and fermentation. One of the most energy intensive process is the pretreatment. Several research and developmental activities are going on in this direction to develop strategies which are economically viable. Most of the strategies currently in practice are energy intensive and economically nonviable.

The benefits of combined acid and alkali pretreatment was earlier reported by Zhou et al., 2013 for pretreatment of spent mushroom substrate for reducing sugar and biofertilizer production. The objective of the present study was to select the best dilute acid for integrated dilute acid - lime pretreatment of chili post-harvest residue (CPHR) and to optimize various process parameters affecting integrated dilute acid –lime pretreatment of CPHR (IDALP CPHR) and utilization of the hydrolyzate obtained after enzymatic saccharification for the production of bioethanol as well as characterization of native and the pretreated samples.

MATERIALS AND METHODS

Feed stock

Chili post-harvest residue (CPHR) received from Virudhanagar, Tamil Nadu, India was used in this study. The samples were dried and milled using a knife mill.

Screening of various acids for integrated dilute acid - lime pretreatment of chili post-harvest residue (IDALP CPHR)

Initial screening experiments were carried out with four different acids (H_2SO_4, HCl, HNO_3 and H_3PO_4) at an initial concentration of 2% w/w, biomass (solid) loading of 10% w/w and $Ca(OH)_2$ concentration of 2% w/w. Pretreatment carried out in a laboratory autoclave at 121°C for 60 min. After pretreatment the samples were used for hydrolysis after washing and drying.

Optimization of various process parameters affecting integrated dilute acid - lime pretreatment of chili post-harvest residue

Optimization of various process parameters affecting integrated dilute acid-lime pretreatment of CPHR was carried out by adopting a Taguchi design. The experiment consists of a total of 16 runs. The parameters selected were biomass (solid) loading, HNO_3 concentration, Ca $(OH)_2$ concentration and pretreatment time. Parameters like biomass loading, HNO_3 concentration, Ca $(OH)_2$ concentration and pretreatment time were selected at four levels.

Compositional analysis, characterization of native and pretreated biomass by SEM, XRD and FTIR analysis

Compositional analysis of native and pretreated samples was carried out by adopting NREL protocol (Sluiter et al., 2008). To investigate physical and chemical changes of lignocellulosic biomass before and after pretreatment, characterizations were performed. In addition to compositional data, physical attributions like morphological changes, cellulose crystallinity changes and FTIR responses were also monitored.

RESULTS AND DISCUSSION

Compositional analysis of native and pretreated chili post-harvest residue

Compositional analysis of the biomass revealed that the native biomass contains 39.95% cellulose, 17.85% hemicelluloses and 25.32% lignin. Control 1 (water alone) contains 41.05% of cellulose, 16.79% of hemicelluloses and 24.11% of lignin. IDALP CPHR contains 43.89% of cellulose, 10.27% of hemicelluloses and 14.37% of lignin. Mass balance analysis revealed a 34% loss of biomass during the pretreatment process. IDALP was found to be effective in removing hemicelluloses and lignin.

Screening profile of various acids for integrated dilute acid - lime pretreatment of chili post-harvest residue

Four different acids – H_2SO_4, HCl, HNO_3 and H_3PO_4 at 2% w/w were used for initial screening to select the best acid for IDALP of CPHR. Control experiments were carried out with water alone Initial screening were carried out with 10% w/w of biomass (solid) loading, dilute acid concentration of 2% w/w, lime concentration of 2%w/w and pretreatment time of 60 min in a laboratory autoclave at 121°C. Control samples were the pretreatment carried with water alone gave a reducing sugar yield of 0.05 g/g. H_2SO_4, HCl, HNO_3 and H_3PO_4 assisted lime pretreatment gave a reducing sugar yield of 0.253, 0.214, 0.284 and 0.204 g/g respectively. IDALP CPHR gave a better reducing sugar yield when compared to dilute acid pretreated alone or lime pretreated alone samples. Since HNO_3 assisted $Ca(OH)_2$ pretreated samples gave higher reducing sugar yield it was selected for further optimization of different process parameters affecting IDALP of CPHR by adopting a Taguchi design.

Effect of different process parameters on IDALP of chili post-harvest residue

Maximum reducing sugar yield (0.622 g/g) was observed in Run No: 6 where the conditions of pretreatment were $Ca(OH)_2$ concentration of 2% w/w, HNO_3 concentration of 5% w/w, biomass loading of 10% w/w and pretreatment time for 30 min.
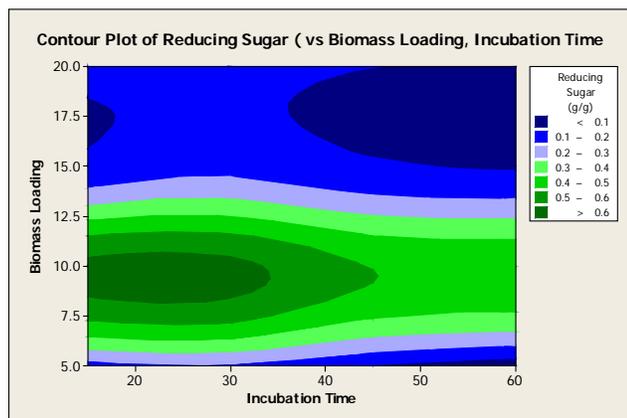
Fig.1. Contour plots showing interaction between pretreatment time and biomass loading on reducing sugar yield

Fig. 1 shows an interaction between pretreatment time and biomass loading. At low to middle levels of pretreatment time (15 – 30 min) the reducing sugar yield is high (0.60 g/g). It decreases with increase of pretreatment time (40 - 60 min). At low levels of biomass loading (5.0 – 7.5% w/w) the reducing sugar yield is low (0.40 g/g); it increases

with increase of increase of biomass loading (7.5 - 11.5%w/w). Maximum reducing sugar yield (0.60 g/g) was observed with middle levels of biomass loading (9.5 -10% w/w) and low to middle levels of pretreatment time (15 - 30 min).

Characterization of native and pretreated biomass by SEM, XRD and FTIR

Characterization of native and pretreated biomass were carried out by SEM, XRD and FTIR. The results indicate that there is difference between the native and pretreated samples. Fig.2 shows the scanning electron micrographs of native, hydrothermal, dilute HNO_3, $Ca(OH)_2$ and IDALP CPHR. The native samples showed a highly ordered and compact structure while the pretreated samples showed a highly distorted structure.
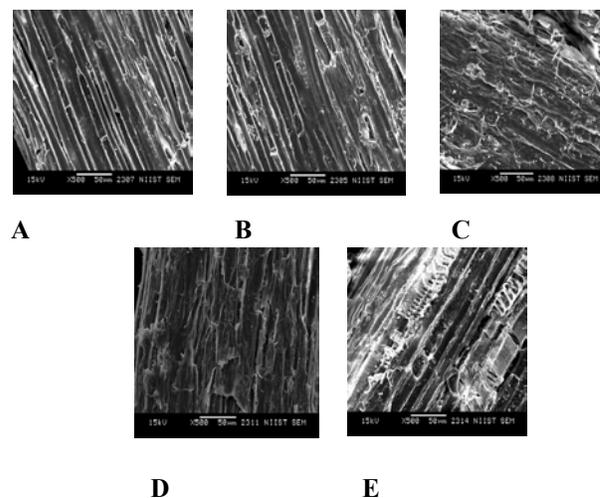
Fig.2. Scanning electron micrographs of native and pretreated samples (A-Native, B-Hydrothermal, C- Nitric acid, D- Lime and E-integrated dilute acid-lime)

CONCLUSION

Compositional analysis data revealed that hemicelluloses and lignin were removed during IDALP of CPHR. Maximum reducing sugar yield of 0.622 g/g was observed after optimization of various process parameters affecting IDALP of CPHR. To the best of our knowledge, this is the first report on IDALP of CPHR. Fine tuning of various process parameters will make the process economically viable.

Acknowledgments

References

[1] Zhou, H., Liu, J., Sun, L., Hu, Z., Qiao, J., 2013. Combined acid and alkali pretreatment of spent mushroom substrate for reducing sugar and biofertilizer production. Bioresour. Technol. 136: 257 – 266.

[2] Rezania, S., Din, M. F. M., Mohmad, S. E., Sohaili, J., Taib, S. M., Yusof, M. B. M., Kamyab, H., Darajeh, N., Ahsan, A., 2017. Review on pretreatment methods and ethanol from cellulosic water hyacinth. BioResources, 12: 2108 – 2124.

[3] Sluiter, A., B. Hames, R. Ruiz R, C Scarlata, J Sluiter, D. Templeton, and D. Crocker (2008) NREL Technical Report, NREL/TP-510-42618.

SEEC-2018-047

EFFECT OF EGR IN HCCI MODE OF COMBUSTION IN A FLEXIBLE LTC ENGINE

Uthanda Ganesh U
Department of Mechanical Engineering
Indian Institute of Technology Madras
Email: uthand.ganesh@gmail.com

Anand Krishnasamy
Assistant Professor
Department of Mechanical Engineering
Indian Institute of Technology Madras
Email: anand_k@iitm.ac.in

ABSTRACT

Low Temperature Combustion (LTC) is a emerging combustion strategy to simultaneously reduce nitric oxides (NOx) and smoke emissions to near zero level which are the major pollutants from the diesel powered vehicles. Homogeneous Charge Compression Ignition (HCCI) is one of the promising LTC strategy. Although, HCCI strategy has been extensively investigated for more than two decades, investigations on HCCI in a flexible LTC engine is very limited which could enable mixed mode combustion. The present work intends to optimize exhaust gas recirculation (EGR) concentration to address the major limitation in HCCI combustion interms of narrow load range. To improve the external mixture preparation in HCCI engine, a high pressure common rail injection system is used in the intake manifold for preparing homogeneous mixture. Experiments are initially conducted in an unmodified single cylinder diesel engine under conventional combustion mode to set the baseline reference data. Then the engine is modified as a flexible LTC engine which can run in any LTC mode including HCCI. With an existing engine compression ratio of 17.5, it is possible to run in HCCI mode only upto 20% of rated load, beyond that engine knocks severely. The major reason behind this is found to be a very early ignition at this higher compression ratio. To achieve higher loads the engine compression ratio is reduced to 15 and EGR is utilized upto 56%.. With these modifications the engine operating load range in HCCI is extended upto 40% of rated load. Near zero nitric oxide and smoke emissions are obtained in HCCI mode, however the brake specific fuel consumption and unburned emissions are found be higher as compared to conventional combustion.

Keywords
HCCI, LTC, EGR, Compression ratio, Emissions
.
NOMENCLATURE
HCCI	Homogeneous Charge Compression Ignition
LTC	Low Temperature Combustion
EGR	Ehaust Gas Recirculation
bmep	Brake Mean Effective Pressure
NTC	Negative Temperature Coefficient
NOx	Oxides of Nitrogen
CO	Carbon Monoxide
THC	Total Hydrocarbons
FSN	Filter Smoke Number

INTRODUCTION

The HCCI mode of combustion is achieved by compressing premixed fuel, air and recycled combustion products until the mixture auto ignites. As a result, ignition occur simultaneously at multiple locations inside the combustion chamber. Thus, HCCI combines the favourable features of conventional spark ignition (SI) and compression ignition (CI) engines interms of premixing fuel-air well before ignition and maintaining a higher compression ratio for thermal efficiency benefits. However, unlike SI and CI engines, HCCI eliminates the use of spark plug and fuel injector in the cylinder head.

HCCI combustion differs from that of SI combustion owing to the absence of flame front and devoid of localized high temperature zones. Because of overall lean mixture and lower temperatures, fuel economy is better in HCCI owing to lower heat losses. Combustion is induced inside the engine cylinder once the ignition temperature of 800 K is reached [1]. As the combustion

starts, temperature and pressure would increase but are found to be well below that required for the formation of nitric oxides [1]. Besides combustion duration is much shorter than in CI engines and thus, results in lower heat losses and higher thermal efficiency [1]. Further, it reduces overall vehicle cost owing to low pressure fuel injection system requirements and elimination of after treatment control requirements. Since the combustion temperatures remains low due to diluted homogeneous air and fuel mixtures, NOx and PM emissions decrease significantly compared to SI and CI engines.

Adapting Variable Compression Ratio (VCR) and exhaust gas recirculation (EGR) are some of the strategies that could help to achieve better HCCI combustion and address its challenges in terms of precise combustion timing control and lower operating load range [3]. HCCI engines are highly fuel flexible and can operate with gasoline, diesel and also, alternative fuels [15]. Most of the engines adopt HCCI in a mixed combustion mode, wherein, upto mid load conditions HCCI is utilized, while at higher loads the engines switch to conventional SI or CI mode of operation. Further, the engines start with conventional SI or CI mode before switching to HCCI mode for idle and low to part load operation.

METHODOLOGY

The base engine is a Kirloskar make, single cylinder air-cooled diesel engine whose technical specifications are provided in Table 1. To operate the engine under HCCI mode, suitable modifications are done in the intake and exhaust manifold. Subsystems such as air pre heater, fuel vaporizer, cooled EGR and a common rail injection system are fabricated and assembled in the intake/exhaust manifold to implement HCCI combustion.

Parameter	Specification
Displacement	662 cm^3
Stroke	110 mm
Bore	87.5 mm
Compression ratio	17.5:1
Rated output	4.4 kW at 1500 rpm
Rated speed	1500 rpm
Cooling system	Air cooled

TABLE 1: TECHNICAL SPECIFICATION OF TEST ENGINE

EGR System

A provision has been made in the exhaust manifold to re circulate exhaust gas (EGR) to the intake manifold to dilute the intake charge and thereby increase ignition delay and improve fuel-air mixing. It also provides control over combustion phasing in HCCI. When EGR is used the exhaust gas coming out of the engine is cut off

from the main exhaust blower and is drawn through a separate blower (refer Figure 1) designed to pump the exhaust gas. As the exhaust gas pressure is normally lower in the test engine which is of single cylinder, naturally aspirated type, a separate blower is required to maintain the required flow of exhaust gas into the intake system. The exhaust blower is coupled with a motor whose speed is controlled using an auto transformer to vary the flow rate. The main control valve is placed far from the engine so that back pressure can be eliminated. The exhaust gas from the blower is split into two paths to handle hot and cold EGR. For the cold EGR, a custom designed shell and type heat exchanger is utilized. To cool the exhaust gas water is fed into the shell side of the cooler by using a 0.5 HP motor. Thermocouples are placed at the inlet and outlet of the cooler to measure the temperatures of cooling water.
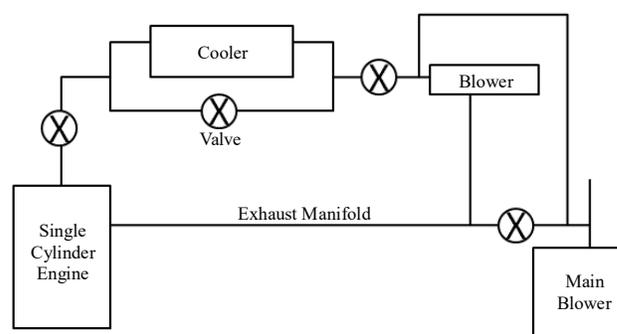
FIGURE 1: EGR LOOP

Parameter	Specification
Tube	11mm OD
Tube material	Admiralty Brass
Number of tubes	9
Tube sheet	Carbon steel
Baffle	SS304 – 3mm thick
Number of baffles	6
Tie rod	SS304 – 6mm diameter
Number of tie rods	4
End cover	MS
Shell side port	1" socket
Cover side port	1-1/2" socket
Overall size	100mm diameter x 1450mm long

TABLE 2: TECHNICAL SPECIFICATION OF COOLER

COMPARISON OF HCCI COMBUSTION WITH AND WITHOUT EGR

The engine performance and exhaust emissions trends in HCCI at 20% and 40% load with and without EGR are

presented and discussed next. The optimal EGR concentration at 20% and 40% load conditions are found to be 12.5 and 48.5 respectively.

Combustion Analysis

The heat release rates are compared between conventional and HCCI combustion in Figure 2. A distinct low temperature heat release is observed in HCCI indicating that the combustion mode is of low temperature combustion (LTC). Between the low temperature and high temperature heat release, there is a negative temperature coefficient (NTC) regime in HCCI. Further, unlike in conventional combustion, there is no diffusion phase heat release in HCCI combustion.
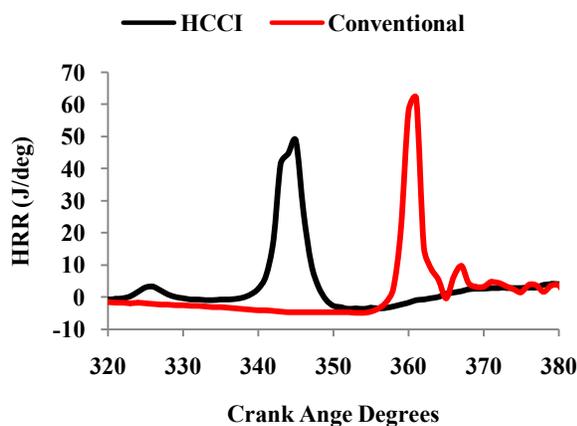
FIGURE 2: VARIATIONS OF HEAT RELEASE RATE IN CONVENTIONAL AND HCCI AT 20% LOAD
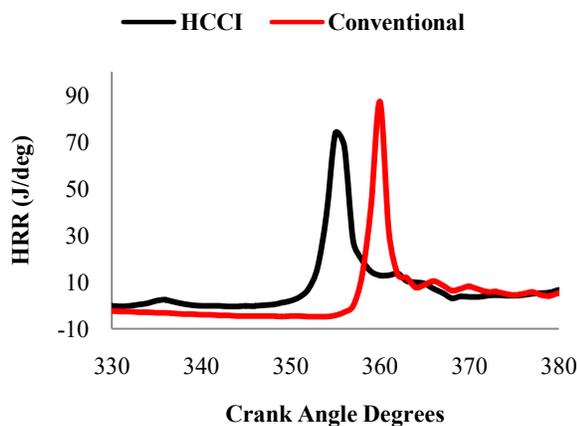
FIGURE 3: VARIATIONS OF HEAT RELEASE RATE IN CONVENTIONAL AND HCCI AT 40% LOAD

Performance Analysis

Figures 4 and 5 compares bsfc and brake thermal efficiency in HCCI with and without EGR. It is observed that the bsfc reduces and brake thermal efficiency increases with the addition of EGR. Thus, it is inferred that the

addition of EGR helps in achieving optimal combustion phasing wherein negative work is reduced and occurrence of peak pressures happen after TDC of compression stroke. This results in higher brake thermal efficiency and lower bsfc with EGR.
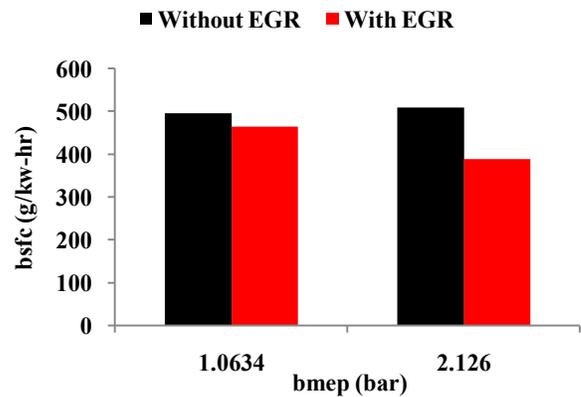
FIGURE 4: COMPARISON OF BSFC WITH AND WITHOUT EGR
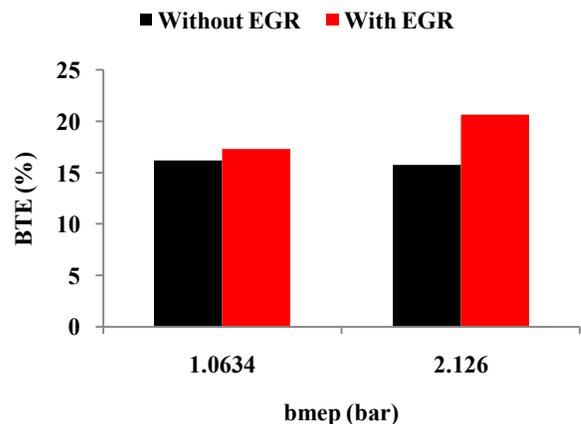
FIGURE 5: COMPARISON OF BTE WITH AND WITHOUT EGR

Emission Analysis

The engine out exhaust emissions such as NOx, Smoke, CO and THC are compared with and without EGR in HCCI in Figures 6 to 9. It is observed that CO emissions decrease with EGR addition primarily due to a better combustion phasing favoring more complete combustion. The NOx emissions decreases with EGR addition owing to lower in-cylinder temperatures due to higher specific heat of its inert constituents, THC emissions increase slightly for the same reason. The smoke emissions decreases with EGR addition especially at higher loads, owing to prolonged ignition delay resulting in better mixture preparation.
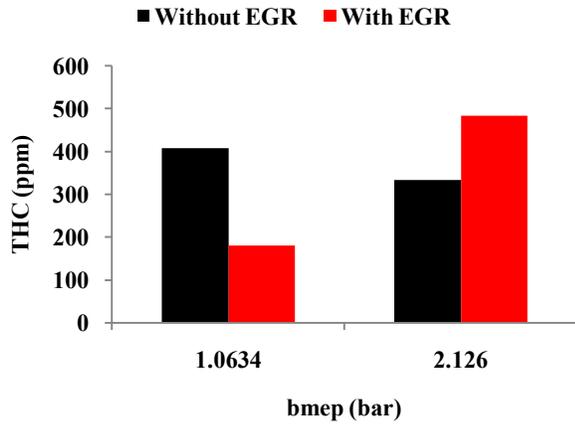
FIGURE 6: COMPARISON OF THC EMISSIONS WITH AND WITHOUT EGR

FIGURE 7: COMPARISON OF CO EMISSIONS WITH AND WITHOUT EGR
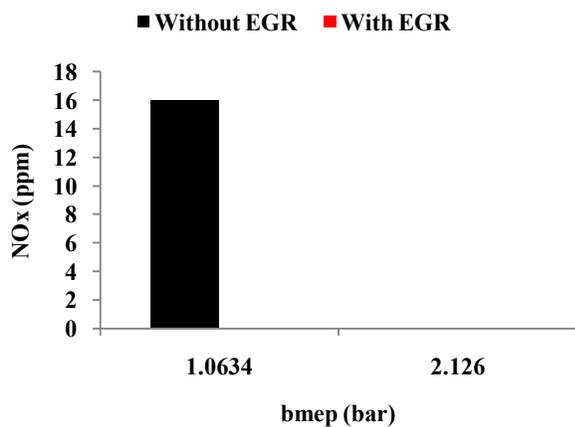
FIGURE 8: COMPARISON OF NOx EMISSIONS WITH AND WITHOUT EGR

FIGURE 9: COMPARISON OF SMOKE EMISSIONS WITH AND WITHOUT EGR

CONCLUSIONS

In the present research work, effects of optimizing EGR concentration on the performance and emission charcaterisitcs of a HCCI engine is investigated. The combustion, performance and emission parameters are compared between HCCI combustion mode with and without EGR at rated speed, varying load conditions. The important conclusions reached from this work are as follows:

- The appearance of distinct low temperature heat release and the absence of diffusion phase combustion are observed from the heat release rate plots of HCCI combustion at all the load conditions with the addition of EGR.
- By utilizing cooled EGR, the operating regime of HCCI is found to be extended upto 60% of full load primarily by avoiding very early ignition timing and un optimal combustion phasing.
- The addition of EGR to the intake charge in HCCI helps in achieving better combustion phasing and thereby increases brake thermal efficiency and reduces exhaust emissions.

ACKNOWLEDGMENTS

REFERENCES

[1] Mingfa Yao, Zhaolei Zheng, Haifeng Liu, Progress and recent trends in Homogeneous Charge Compression Ignition (HCCI) engines", Progress in Energy and Combustion Science 35 (2009) 398-437.
[2] Gregory E. Bogin, J. Hunter Mack, Robert W. Dibble, Homogeneous Charge Compression Ignition (HCCI) Engine", SAE paper 2009-01-1805.

[3] Daisuke Kawano, Hisakazu Suzuki, Hajime Ishii, Yuichi Goto and Matsuo Odaka, Yutaka Murata, Jin Kusaka, Yasuhiro Daisho, Ignition and Combustion Control of Diesel HCCI", SAE paper 2005-01-2132.

[4] S. Juttu, S. S. Thipse and N. V. Marathe, M. K. Gajendra Babu, Homogeneous Charge Compression Ignition (HCCI): A New Concept for Near Zero NOx and Particulate Matter (PM) from Diesel Engine Combustion", SAE paper 2007-26-020.

[5] Akhilendra Pratap Singh, Avinash Kuma Agarwal, An Experimental Investigation of Combustion, Emissions and Performance of a Diesel Fuelled HCCI Engine", SAE paper 2012-28-0005.

[6] Pranab Das, Mayur Selokar, P.M.V. Subbarao and J.P. Subrahmanyam, Effect of Injection Timing, Premixed Equivalence ratio and EGR on Combustion Characteristics of an HCCI-DI Combustion Engine Using In-Cylinder Dual Injection Strategy", SAE paper 2016-01-0752.

[7] D.Ganesh and G.Nagarajan, HCCI Combustion of Diesel Fuel with External Mixture Preparation", SAE paper 2009-01-0924.

[8] Yong Sun and Rolf D. Reitz, Modeling Diesel Engine NOx and Soot Reduction with Optimized Two-stage Combustion", SAE paper 2006-01-0027.

[9] Thomas W. Ryan III and Timothy J. Callahan, HCCI of Diesel Fuel", SAE paper 961160.

[10] Juttu, S., Thipse, S. S. and Marathe, N. V. and Gajendra Babu, M. K, Diesel HCCI Combustion Control Parameters Study using n-Heptane Reduced Chemical Kinetic mechanism", SAE paper 2008-28-0036.

[11] Malin Alriksson and Tanja Rente and Ingemar Denbratt, Low Soot, Low NOx in a Heavy Duty Diesel Engine Using High Levels of EGR", SAE paper 2005-01-3836.

[12] Suyin Gan, Hoon Kiat Ng, Kar Mun Pang, Homogeneous Charge Compression Ignition (HCCI) combustion: Implementation and effects on pollutants in direct injection diesel engines", Applied Energy 88 (2011) 559–567.

[13] S. Jayaraj, T.M Balaji, K. Mathivanan, An Experimental study of HCCI engine using multiple injection strategy with variable injection timing and variable injection", International Conference on Energy Efficient Technologies For Automobiles, ISSN: 0974-2115.

[14] Myung Yoon Kim, Jee Won Kim, Chang Sik Lee, and Je Hyung Lee, Effect of Compression Ratio and Spray Injection Angle on HCCI Combustion in a Small DI Diesel Engine", Energy & Fuels 2006, 20, 69-76.

[15] Kihyung Lee, Changsik Lee, Jeaduk Ryu and Hyungmin Kim, An Experimental Study on the Two-Stage Combustion Characteristics of a Direct-Injection-Type HCCI Engine", Energy & Fuels 2005, 19, 393-402.

Environmental Impact of tourism on Vembanad Lake

Joseph Chandy[1], Raghunathan Rajesh[2]

[1]Department of Mechanical Engineering, Rajiv Gandhi Institute of Technology,Kerala , India.
[2]Department of Mechanical Engineering, Rajiv Gandhi Institute of Technology,Kerala, India.

Abstract-Vembanad wetland is the largest wetland system in India which is the official site of the Ramsar convention on Wetlands. Human intervention on the lake is severe which affects the function, structure and entire composition of the Vembanad wetland system. There is a drastic growth in tourism sector in and around Vembanadu Lake for the past two decades. This paper focuses on the impact of tourism on Vembanad lake system and also to the environment. As a result of the tremendous growth of Backwater tourism in and around the Vembanad Lake, the waste composition has increased to a large extent. The major waste from tourism sector was identified through a questionnaire survey, on the peoples residing near the lake and these waste were quantified through different methods. The performance evaluation of the existing waste management system was conducted and found to be ineffective. Since a lack of a proper waste management system, this paper aims to propose a modified waste management system which is economically and socially beneficial. The economic analysis was done by conducting cost benefit analysis to the 4 alternatives and the existing system. These four alternatives were designed within the framework of the modified waste management system. The payback period of these alternatives and existing model were calculated and based on this, the most economical and social waste management system was proposed

Keywords-:backwater tourism,performance evaluation,waste management, cost benefit analysis,paybackperiod

1. INTRODUCTION

Vembanadu Lake spreads in Alappuzha, Kottayam and Ernakulum districts of Kerala which forms Vembanad Lake wetland system of an area of 2033.02km². In the past twenty years the growth of tourism sector in and around the Vembanad Lake is spectacular. Backwater tourism as emerged as the backbone of the tourism sector of Kerala state which leads to the tremendous increase of Houseboats in addition to many resorts which developed recently around the shore of lake. Kerala comes under the list of 50 places of Life time published by National Geographic Traveler scenic beauty of the region attracts the domestic as well as the foreign tourists. Kuttanad wetland system including Vembanad Lake which is now receiving global attention because of its unique feature which is below sea level permits the cropping of Rice in large quantity and permits the harvest of fish and an area which is thriving for the tourism where the nature beauty is at the peak among the Ramsar site.

Percentage of increase of foreign exchange earnings from tourism in Kerala in last decade is 68.9%. Rise of tourism sector results into shift of employment, one or two member from each house is now engaged in tourism industry as houseboat operators or other employment related to house boat and backwater tourism. This shift in employment sector from agricultural to the service sector is caused as a result of change in attitude and perception to the traditional occupation like agriculture. Shift of employment itself indirectly effects the agricultural production of the region. Uncontrolled growth in the number of the houseboat in Vembanadu wetland system affects the environment system of lake. This project focuses on the adverse effect of the backwater tourism growth on the environment system of wetland and livelihood of the area around the lake and to find out a proper waste management system in the region.

2. LITERATURE REVIEW

There has been an ample amount of literature in the domains of tourism and its causative factors from various studies conducted around the globe. Many of them are based on different aspects. By looking through the literature in environmental impact of tourism the commonality observed in the existing literature is that tourism can affect Socio-cultural of host community which includes changes in traditional lifestyles, value systems, family relationships, individual behavior and community structure. Even though the tourism sector in the region has greater economic benefits which are employment income and foreign generations there are also negative socioenvironmental impacts (Zacharias and Manalel,2010).Tourism development can be of benefit (e.g., job creation, image enhancement). However, it could also have negative impacts on the biophysical environment (e.g., soil pollution, water pollution, air pollution, ecosystem degradation) and social/cultural environment (e.g., loss of the traditional culture, increase in crime) if not well planned, developed, and managed (Mohammad, 2016) .In another one the impacts of tourism on environmental attributes such coral reefs, water, fisheries and beaches are discussed briefly. The impacts of tourism towards environmental attributes range derives from tourism activities such as boating, snorkeling, diving and fishing. Improper and irresponsible behavior of tourist is also believed to be a significant reason that contributes to detrimental effects on the environmental attributes (Murugadas and Badaruddin, 2014). The different mind-set of tourist derives from the different level of environmental literacy that they have. The concept environmental literacy that consists of not only knowledge on the environment and its issues but also includes disposition components of attitudes, sensitivity and motivation are discussed thoroughly. Intention to act or intended behaviour that is explored in this (Ferry, Lucky, Dietrich and LilikBudi, 2016).The link between the number of threatened plant species and tourism which was proxies by the number of international tourist arrivals (Muzafar and Radamd, 2016),). Tourism has been an important sector to both the developed and the developing economies. Although we recognized the great benefits of the tourism sector to the national income, the tourism activities have also been connected to the negative impact on the economy in particular to the environment. One crucial aspect of the negative impact as a result of increased tourism activities are on the loss of biodiversity .Tourism has an adverse effect on the environment in Eastern EU. Finally, short-run heterogeneous panel causality test results suggest that tourism,causes CO_2 emissions in Eastern EU while economic growth and CO_2 emissions cause tourism in Western EU. Overall, findings suggest that tourism plays an important role in accelerating economic growth however; its role on CO_2 emissions largely depends on the adaptation of sustainable tourism policies and efficient management (Alexandra, Christos, Nicolas, Dimitra, 2015).

On the other hand, protected riverside area can make rivers as a source of water, water transport and water tourism destination. Nowadays, water tourism is increasingly popular to people. Local residents should be given an understanding of the importance of tourism activities mainly based on the river environment and things that need to be done to support these activities. River cleanliness must be maintained and preserved (Tri Rahayuningsiha. Hariri and Lilik,2016) Another one puts forward a generic methodological scheme, based on Life Cycle Assessment (LCA) principles, in order to estimate the environmental load in areas of considerable tourism activity. A comparative assessment is realized for characteristic hotel categories. Their respective contribution to environmental burden attributed to tourists' transport and accommodation services is assessed. Up-market hotels impose larger absolute impacts on the environment, especially in the consumption of resources .LCA can play a crucial role in decreasing the complexity in the strategic planning of tourism, especially in local-to-regional areas of concentrated tourism activities (Orkut and Murat, 2014) Tourism is being considered as a development instrument in order to boost a country's economy and has become part of the global industry. However, tourism is also one of the actors that is responsible for environmental depletion, due to the constructions of buildings and tourism activities(Hsin and Shiann, 2013)

3.METHODOLOGY

Research is a process of arriving at an appropriate solution to a problem through a systematic approach .This systematic approach will be obtained through a well-defined research methodology. In

this project the methodology involves three phases. In phase-1, the problem was identified through a clear background study .after the problem identification a detailed literature survey is a need to define the problem. From the problem definition, the main objectives of the project were determined. As the first step the different types of waste generated from tourism, that affect the Vembanadu Lake was identified. In phase -2 the major waste from the generated waste should be identified. For this a questionnaire survey was conducted and the data was collected from the people residing near the shores of the Vembanadu Lake. In this phase the most predominant waste was determined and was estimated. In phase -3 the existing waste management for the major waste was studied and the performance evaluation was conducted. Based on the evaluation, modification was done to the existing waste management system. Different alternatives were identified and conducted a cost benefit analysis, to find out the best alternative in the waste management

4. RESULTS AND DISCUSSIONS

Rapid increase in house boats, hotels and resorts due to the fast growing back water tourism in Vembanadu Lake causes a tremendous increase in waste generation. Hence there is a lack effective of waste management system in Kumarakom. The main objectives were to identify and estimate the amount of major waste generated from tourism which affects the Vembanad Lake, to conduct a performance evaluation of the existing waste management system and to modify the existing system and conduct cost benefit analysis.

4.1 Questionaire Survey
A questionnaire survey was conducted as part of the study to understand the major waste from the listed ones and to evaluate about the existing waste management system. The questionnaire consists of 29 questions, out of which first 27 questions were using five scale and these questions were used to measure the effects of each waste components. 28 and 29 were used for rating the waste components for identifying the major waste. The survey was done with the people residing near Vembanadu Lake. Major waste generated from tourism was identified. Survey was conducted with 180 people residing in a stretch of 30km length and a width of 2km from the lake. The sampling technique used is area surveying. 3 respondents from $1Km^2$ area are selected. The number of household units who participated in the survey was 180. The respondents were approached individually at their homes to get their responses [3]. The major findings from the survey include different negative impacts of tourism and focus on the waste generation. By the help of this survey ,it has being identified that sewage from house boats, resorts and hotels and plastic waste dumped in boat jetties and small tourist spot are the major waste from tourism.

4. 2 Quantification Of Major Waste
The major waste from tourism is found to be sewage and plastic waste from houseboats, resorts and hotels. The quantity of waste generated from tourism is identified. The unavailability of pre-determined data of amount sewage and plastic generated was a limitation.So the quantification was a big task. The average estimation of waste generated was calculated by conducting a survey and field visits. Sewage from house boat is treated at DTPC sewage treatment plant and the sewage from resorts and the hotels is treated in their own plant. The quantity of sewage treated from house boats was obtained from DTPC sewage treatment log book, but the amount treated in resorts and hotels was not obtained, because they won't keep any records. Estimation of sewage is given below. Kumarakom, 103 registered house boats are there, as per the records given by the DTPC.The maximum amount of sewage is treated at the months of December and January.From the data an average of 65,520 litre of sewage is treated in every month.

To identify the amount of plastic waste generated in a month we conducted a survey and field visit to selected tourist spot. The survey was conducted for five consecutive days, at three times a day to get the exact amount of plastic items are dumped in six different spots. Table I shows the mean of the amount of plastic waste generated from the six tourist spot in Kumarakom, for five consecutive days The plastic waste we are considering are drinking water bottles, soft drink bottles, ice cream cups, plastic glass, are the main plastic waste in these tourist spot.

From the survey the amount of plastic waste generated from hotels and resorts was calculated. In a month approximately 4,665 kg of plastic is generated from the hotels and resorts in Kumarakom.It's

just an approximate amount, this can vary on seasons. From the 21 resorts and hotels these quantities of plastic waste is generated. In this we are considering only on drinking water bottles of 1 litre and ½ litre.in additional to these many other type of plastic waste can be generated such as ice-cream cups, plastic bags, and soft drink bottles so on. This waste can't be estimated due practical difficulties. Annually the least amount of plastic generated will be 55,985 kg from hotels and resorts

Table I
Quantity of main plastic waste generated at different tourist spot

Sources	Unit	Wt./No.	Mean Total(No:s)	Mean Wgt(Kg)
Water Bottles	No.s	27.98	112.2	3.13
Soft drink bottles	No.s	30.25	94.8	2.86
Ice-cream cups	No.s	5.97	73	0.435

4.3 Performance Evalution Of The Existing Waste Management System
The major waste from tourism are found to be sewage and plastic waste from houseboats, resorts and hotels. The present system of waste management in Kumarakom is not very efficient .The only way of treatment is done for sewage. The sewage from the hotels are treated in their own treatment plants. Most of the resorts and hotels have treatment plant. The sewage from house boats are treated in sewage treatment plant in DTPC, from the data obtained it is also ineffective. Out of the 103 registered house boats, only 70 of them is undergoing sewage treatment from the plant at DTPC .They are charging a minimum amount of Rs.1250/- monthly from these house boats.The existing system has a cash inflow of Rs.1, 26,500/- and has a payback period of 10.5 years. In the case of plastic waste there is no proper segregation from the panchayat or from the DTPC Kumarakom. The plastic waste are simply dumped in open spaces and also near the shore of the Vembanadu Lake. These waste are collected by some unauthorized people daily. There are a limited number of waste bins are situated at different locations. Most of these plastic waste are dumped in open spaces.
The performance of the waste management system in Kumarakom was also evaluated in the questionnaire survey. The questionnaire survey also consists of questions about the management of waste and the satisfaction of people towards the waste management. Out of 180 respondents, 73% of the respondents say that sewage treatment is ineffective and also 67.2%strongly agree that waste management system in Kumarakom is no properly managed. 69 %of respondents stated that cleaning is very important because their no collection or segregation process is taking place.

4.4 Modification of the Existing Waste Management System
The present waste management system in kumarakom has to be modified. From the performance evaluation of the existing system there should be proper way of collection and segregation of the waste. Sewage from house boats should be collected by some water transport and some fees should be collected from the house boats for treating the sewage, since most of the hotels have sewage treatment plant their isn't necessity of collecting sewage from the resorts and hotels .Since there isn't a proper management of plastic waste, the collection and segregation is also important .the establishment of collection bins at different spots are important for collection. These waste are should be collected by worker and to be segregated in a collection center and to be sold to get some benefit. This system has social benefit than economic benefit. The modified waste management system focuses only on two pre-dominant waste i.e. Plastic and sewage.by the questionnaire survey it has being already stated. he above frame work is used for modifying the existing waste management system. Here the sewage from the resorts, hotels and house boats are collected and then transported to the treatment plant. The treated sewage is flowed out to the Vembanadu Lake. Similarly the plastic waste from resorts, hotels and from other tourist spot should be collected accordingly and transported and segregated at suitable collection centre. This frame work will help to reduce the effects of plastics

and sewage. Within this frame work we implementing four models. Since this is a social issue, it has more social benefit than economic benefit. In this project we are dealing with four alternatives models from this frame work. For deciding the best alternatives we are conducting a cost benefit analysis for each alternatives. These alternatives will be made from this frame work. The implementation of this modified waste management system has both social and economic benefit.
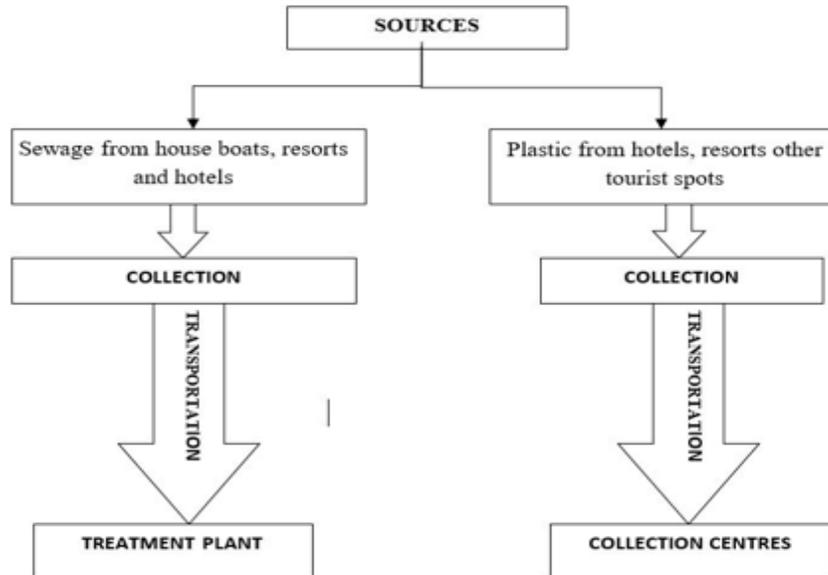
Fig. 1 Modified Frame work of the waste managemen System

4.4 Pay Back Period

The payback period can be calculated. For computing the payback period the fixed investment required for every model and cash flows from that model have to be calculated. For calculating fixed cost of alternative models the expenses related to machinery and other pre-operative expenses are estimated. Next step was to calculate the variable costs associated with different models. This calculation not only helps in DPP but also it will provide an idea about working capital requirements. Here the variable costs involves,labor payments,utilities paymentsand maintenance costs.After calculating the variable costs the total revenue that can be obtained from the models are calculated considering the price of outputs from the model. This total revenue is subtracted with current revenue to find out the additional revenue obtained from the models. Additional revenue is further subtracted with variable cost to calculate the additional cash inflow per year for a models.

Table II
Cost Benefit Analysis for Different alternatives

Model	A	B	C	D	E
Existing model	13,30,000	9,23,500	10,50,000	1,26,500	10.5
Alternative-1	Nil	Nil	Nil	Nil	Nil
Alternative -2	28,46,000	29,16,900	34,51,102	5,34,112	5.5
Alternative -3	38,31,000	33,12,900	28,39,893	Nil	infinite
Alternative-4	37,15,500	29,96,000	31,42,102	5,46,012	7.5

A-Total Fixed investment B-Variable cost per year C- Total revenue

D-Cash inflow E- Payback Period

Mathematically Fixed cost (A) = cost of machinery + installation charges Variable cost (B) = labor payments+ utilities payments+ maintenance costs Total revenue(C) = Sum of revenues obtained from all output products from the alternative Cash inflow per year (D) = Total revenue – Variable cost Pay Back Period (E) = Fixed Cost/Cash inflow All of these parameters for different models are calculated and the results are as shown in table –II. By conducting the cost benefit analysis for each alternative, the best alternative was found to be the second alternative.in this case the payback period was found to be 5.5 years. In these alternatives the sewage is not collected but these are directly treated from transporting the sewage from the house boat to the tank. In this the number of house boat treated should be noted, the first and the third alternative can't be implement because the total variable cost is more than the total revenue. The fourth alternative has a payback period of 7.5 years. In this alternative the collection is done properly as compared to the fourth alternatives. For an effective waste management the fourth alternative will be selected, because it provides both social and economic benefits. When compared to existing model, collection of sewage and plastic waste was not done.

5.CONCLUSION

Even though the tourism sector in the region has greater economic benefits which are employment income and foreign generations there are also negative socio-environmental impacts. To understand these impacts to the environment of the Vembanadu Lake and to find an action plan is a need to the society. To understand these impacts a questionnaire survey can be done. For this a questionnaire was developed on the basis of the sources which affect the environment. The predominant waste from tourism were identified through detailed literature survey, field visits and also by conducting a questionnaire survey. By studying the existing waste management system in Kumarakom, it was found to be in efficient. A modified system was proposed for the proper management of waste. A frame work was suggested for this purpose, which mainly include collection and transportation. Within this frame work four different alternatives were made. The four alternatives were proposed, on looking forward the social and economic benefit of these different system to the environment and to the society. The decision of finding the best alternative was done, by conducting cost benefit analysis.Since this is a social issue we have certain limitations for making the profit.

REFERENCES

Zacharias.S., James,M.C and Jose M.C (2010) Back Water Tourism in Kerala: Challenges and Opportunities, International Journal of Research (IJR) ,1,PP. 542-551.
Murugadas, R and Mohammedh,B(2014)Impacts of tourism on environmental attributes, environmental literacy and willingness to pay: A conceptual and theoretical review, Asia Euro Conference Procedia - Social and Behavioral Sciences ,144,PP.378 – 391
Habibullaha,M.S.,Dinb,B.H and Radamd,A (2016),A Cross-Country Analysis on the Impact of Tourism on Threatened Plant Species, Procedia - Social and Behavioral Sciences,224 ,PP.14 – 19
.Mohammad,D.L., and T.F Hilma (2016),Planning for Riverside Area as Water Tourism Destination to Improve Quality of Life Local, Procedia - Social and Behavioral Sciences, 234,PP.434 – 441.
Kim, K., Umanathb, N. S., Kim, J.Y., Ahrensc, F. and Kim, B. (2011) 'Knowledge complementarily and knowledge exchange in supply channel relationships', International Journal of Information Management, Vol. 32, No.1, pp.35-49.
Marra, M. Ho, W. and Edwards, J. S. (2011) 'Supply chain knowledge management: A literature review', Expert Systems with Applications, Vol. 39, No.5, pp.6103-6110
Zoltan,B., and Andras,T2015),Utilization of geo heritage in tourism development, Procedia - Social and Behavioural Sciences,188,316 – 324
Hsieha,H.K and Kungb K.L(2013)The linkage analysis of environmental impact of tourism industry, Procedia Environmental Sciences,17PP.658 – 665
D.D Dimitrovskia and Aleksandar, (2012), Rural tourism and regional development: Case study of development, Procedia Environmental Sciences, 14,PP.288 – 297
Victoria,K., and K. Wells et.al(2015)Heritage tourism, CSR and the role of employee environmental behavior, Tourism management,48PP,399-413.
Kuznets, C., L.Javier and Rey,J.M(2015) Tourism and solid waste generation in Europe, Article in press, waste management
Fery,K and Lucky,A(2016)Vulnerability assessment of small islands to tourism, Global Ecology and Conservation,6,PP.308–326.
Orkun,G.,Emel,L.,K.Murat(2014) A Strategic Environmental Management Model: Salt Lake Case, Procedia - Social and Behavioral Sciences, 150,PP.310 – 319.
M. Guerra and M. Dawson (2016)Boat-based tourism and bottlenose dolphins in Doubtful Sound, New Zealand: The role of management in decreasing dolphin-boat interactions, Tourism management,5,PP.3-9.

PROCESS SIMULATION OF
ALLOTHERMAL AIR-STEAM GASIFICATION OF BIOMASS IN ASPEN PLUS

Dr. Sreejith C. C
Department of Mechanical Engineering
Saintgits College of Engineering
Kottayam, Kerala, India
Email: ccsreejith79@gmail.com

Dr. C. Muraleedharan
Department of Mechanical Engineering
National Institute of Technology Calicut
Kozhikkode, Kerala, India
murali@nitc.ac.in

ABSTRACT

A model based on reaction kinetics is essential to capture the underlying kinetic effects in biomass gasification. The gasification process can be described better by incorporating drying and devolatilisation stages in the kinetic model. For this, a model which simulates the various process stages separately is inevitable. A possible option for the process splitting is simulation of gasification in process simulator Aspen Plus®. The formulation and simulation of a kinetic model for allothermal air-steam gasification in Aspen Plus is presented. The sensitivity of the variables including gasification temperature, air equivalence ratio and steam to biomass ratio on performance of gasification is predicted. The performance measures are H_2 concentration in the syngas, heating value and process energy and exergy efficiencies. The model is validated with published experimental results and the optimum values of the operating conditions are suggested.

Keywords: *Biomass gasification, kinetic model, H_2 concentration*

INTRODUCTION

Biomass gasification system is a thermo-chemical system exchanging heat and mass between the solid fuel and gasifying agent, and also among the intermediate products of gasification. Various chemical processes in biomass gasification are complicated and require the development of suitable mathematical models for its analysis. Models for biomass gasification can predict the mechanical and thermodynamic limits of energy conversion, and is beneficial for its design and scale up. Such models can evaluate the influence of the major input variables, such as sub-stoichiometric air supply rate, feed rate of biomass and its typology, rate of steam input and gasification temperature on the composition and heating value of the generated producer gas.

Aspen Plus models in biomass gasification

Aspen Plus (Aspen Technology Inc.) is a problem oriented input programme that is used to facilitate the simulation of physical, chemical and biological processes. Small sections of complex and integrated systems can be created and tested in Aspen Plus as separate modules before they are integrated. Many published on simulation of coal gasification models in Aspen Plus are available. Very few studies [1-5] are reported on Aspen Plus simulation of biomass gasification incorporating kinetic limitations of the individual chemical reactions involved. Some models were for specific gasifier designs such as bubbling fluidised bed [6], dual fluidised bed [7, 8] interconnected fluidised bed [8] and entrained flow bed. Majority of biomass gasification models [9-12] are based on thermodynamic equilibrium concept. The present model is unique in the sense that it incorporates the reaction kinetics and intermediate processes of biomass gasification by splitting the entire process into several sub-reactions accounting the respective rate costants.

MODELLING METHODOLOGY

The air-steam gasification process is divided into several sub-blocks performing specific operations such as drying, devolatilisation, partial combustion, char gasification and steam reforming. The model is formulated using wood sawdust as biomass material having chemical composition (wt.%) as Fixed Carbon: 11.7, Moisture: 7.7, Volatiles: 76.9, Ash: 3.7 and CHON: 46.9, 6.38, 46.5, 0.22. The pertinent chemical reactions involved in gasification [13, 14] are given in Tab. 1 along with the respective heat of reaction. The modelling framework is based on the following assumptions including (1) All the process blocks

except the kinetic blocks are zero dimensional (2) The product gases considered are CO, CO_2, CH_4, H_2 and $H_2O(g)$ neglecting higher order hydrocarbons being very small in concentration (3) Supply conditions of air and steam respectively are, 1 bar and 300 K, and 1 bar and 573 K (4) Pyrolytic tar is modelled as benzene (C_6H_6) neglecting other components such as naphthalene and phenols [15] and (5) All the streams obey RK real gas EOS.

Process description in Aspen Plus

Aspen Plus flow sheet developed is shown in Fig. 1. In general, biomass gasification consists of mainly the following processes.
(1) Drying of the feedstock,
(2) Primary pyrolysis generating light gases, char and tar in liquid form, (3) Partial combustion of char and gases generated from pyrolysis (4) Heterogeneous gasification reactions (5) Reforming of the gases with steam.
Biomass (7.7% moisture content) at a specific feed rate (1 kg/h on wet basis) is subjected to drying in the DRYREAC sub-block. DRYREAC simulates the drying process and the evaporated moisture is removed by DRYSEP, which is a FLASH SEPARATOR. The dried biomass is subjected to pyrolysis in DECOMP block which simulates its thermal decomposition. A RYIELD reactor which decomposes the biomass into char, gas and tar is introduced to simulate the actual process of pyrolysis. The yield of the pyrolysis products of wood sawdust is estimated as per the correlations suggested by Gomez-Barea *et al*. (2010). A calculator block based on FORTRAN subroutine is used for simulating the pyrolysis which will be executed before the RYIELD reactor. The pyrolysis products include char [16], tar (modelled as benzene) and gases (CO, CO_2, H_2 and CH_4). The char stream is assumed to be consisting of pure solid carbon and ash content of the dried biomass. The concentrations of the gas species is converted into mass fractions. The gases are separated from the output stream of the DECOMP block using PYSEP block. The solid yield (CANDASH) from the PYSEP contains the pyrolytic char. 25% the remaining char (CHAR) is removed as unconverted stream (UCCHAR), not participating in gasification which is achieved by a FSPLIT block. Remaining char is split into two streams to COMBUST block and to REFORM block, which is simulated using another calculation block defined in COMBSPLT. The gas mixture (VOLATILE) is fed into a chemical kinetic reactor, COMBUST (RPLUG reactor) which simulates the partial oxidation reactions R_1, R_7, R_8 and R_9. Tab. 1 provides the stoichiometry and rates of the reactions in terms of activation energy and pre-exponential factor. First order power law reaction scheme is employed for the estimation of the reaction rates. Products of partial combustion from COMBUST, tar (from PYSEP block), 70% of char, and steam are the inputs to another kinetic block, REFORM simulating the steam reforming, char

gasification, boudouard and tar reforming reactions (R_3-R_7 and R_{10}). Steam at 573 K and 1 bar is supplied to REFORM (RCSTR reactor) at predetermined feed rate maintaining the required Steam to Biomass Ratio (SBR). The model assumes the gas and liquid streams (tar) obey RK equation of state with Boston-Mathias modification. Twenty one material streams are used in the simulation.
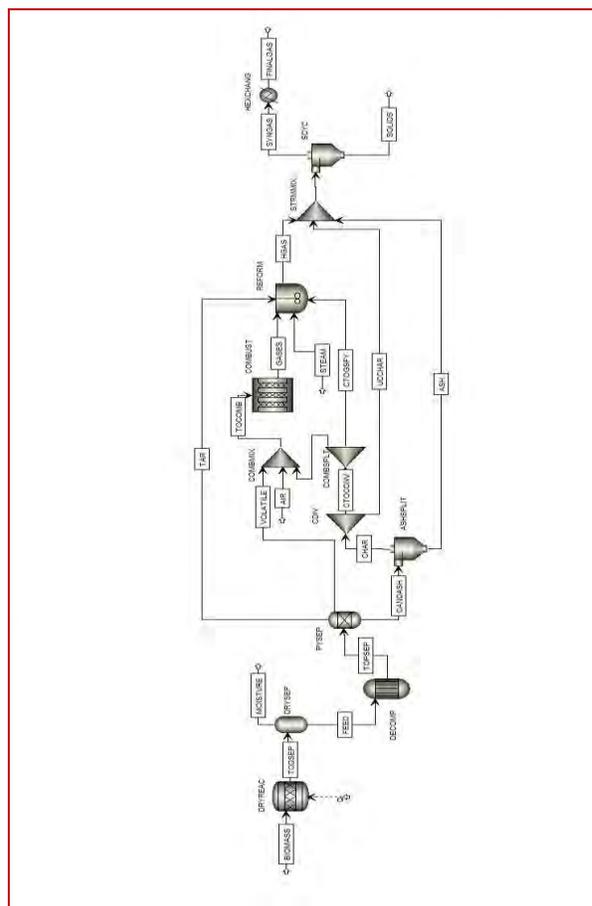
FIGURE 1. ASPEN PROCESS FLOW SHEET

Simulation of the model

The objective of the simulation model is to predict the sensitivity of the operational variables on the performance of air-steam gasification. A parametric study is carried out with the help of data analysing tool 'sensitivity analysis' in Aspen Plus to achieve this. Equivalence Ratio (ER), SBR and Temperature (T) are varied in the range 0.15-0.45, 0.25-2.5 and 600-1300 K, respectively. The criteria for comparison of gasifiers include concentration of H_2 (bio-hydrogen) in the producer gas (on dry basis) and its Lower Heating Value (LHV) and process energy & exergy efficiencies.

RESULTS AND DISCUSSION

Variation of H_2 concentration, LHV and process energy & exergy efficiencies with respect to the aforementioned process operational variables are discussed in this section. Simulations are carried out for 1 kg/h feed of biomass (with 7.7% moisture) at a char conversion efficiency of 75%.

Effect of gasification temperature

The effect of allothermal gasification temperature on H_2 concentration is depicted in Fig. 2. In the analysed range (600-1300 K), H_2 concentration increases with temperature, reaches a peak value and decreases with further increase in temperature. The maximum H_2 concentration is predicted at about 900-950 K for all the SBR values. The temperature enhances the rate of endothermic reactions (R_2, R_4, R_5 and R_{12}), and slows down that of exothermic reactions (R_3 and R_6) in the reformation block. SMR (R_5) and reforming of benzene (R_{12}) are much higher temperature processes prominent above 1000 K. H_2 production is controlled by the endothermic char gasification and reverse Water Gas Shift (WGS) reactions. It is inferred that above a temperature of 900-950 K, reverse WGS reaction dominates the combined effect of char gasification, Steam Methane Reforming (SMR) and benzene reforming reactions resulting in the reduction in H_2 concentration beyond 950 K.

Effect of steam to biomass ratio (SBR)

SBR is simulated in the range of 0.25-2.5, by varying steam supply rate to the reformation block and keeping the biomass feed rate constant. The concentration of H_2 in the dry syngas (see Fig. 2) is improved with steam addition. More steam improves the rates of heterogeneous gasification of char (R_2), WGS (R_6), and reforming reactions of methane (R_5) and benzene (R_{12}). Higher rates of these reactions result in improved H_2 concentration. The highest H_2 concentration achieved in the simulation range is 34.6% at T=900 K, SBR=2.5 and ER=0.15.
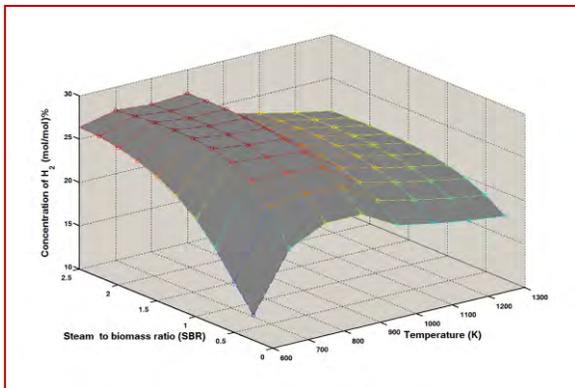
FIGURE 2. VARIATION OF H_2 CONCENTRATION WITH T AND SBR (ER=0.25)

Effect of equivalence ratio (ER)

Air input to the partial combustion block is increased to vary ER between 0.15 and 0.45, at constant steam input and constant biomass feed rate. Obviously, supply of more air shifts the whole reaction towards combustion yielding more CO_2 and H_2O (R_6, R_7 and R_9). Consequently, the gas mixture entering the reformation block would contain more amounts of CO_2, N_2 and H_2O than with lower ER values. The variation of the H_2 concentration is shown in Fig.3 for various SBR and ER values, keeping the temperature of the reformation block constant at 1000 K.

TABLE 1: KINETIC CONSTANTS OF REACTIONS IN BIOMASIFICATION

Reaction number	Reaction name	Kinetic parameters*		Reference
		E_a (kJ/mol)	k (1/s)	
R_1	Partial combustion	55.00	5.70E11	[17]
R_2	Char gasification	129.60	3420.00	[18]
R_3	Methane hydrogenation	129.60	3420.00	[18]
R_4	Boudouard	248.12	4364.00	[13]
R_5	SMR	2.4E5	3.30E10	[13]
R_6 (a)	WGS	0.282	5.00E12	[19]
R_6 (b)	Reverse WGS	0.238	9.50E10	[19]
R_7	Hydrogen oxidation	109.00	2.19E18	[20]
R_8	CO combustion	167.00	3.98E20	[20]
R_9	Methane combustion	202.38	1.58E19	[13]
R_{12}	Benzene reforming	1.96E5,	2.00E11	[13]

LHV of dry gas mixture

The reduction in concentrations of the combustible gases with air addition results in poor heating value gas at higher ER (for example, above an ER value of 0.4, maximum LHV is 4.03 MJ/Nm^3 only) values. As per the simulation results the two gases (CO and H_2) have comparable concentrations also. Moreover, maximum contribution of CH_4 to LHV is only 22% due to its low concentration in the dry gas mixture even though itsheating value is much higher. The favourable aspect of steam addition on H_2 and unfavourable aspect on CO concentrations result in subsided effect of SBR on LHV. The rate of increase in H_2 is much lower than the rate of decrease in CO while SBR is increased from 0.25 to 2.5. This is the reason for the slight reduction in LHV with

steam addition for air-steam gasification process which is illustrated in Fig. 4.
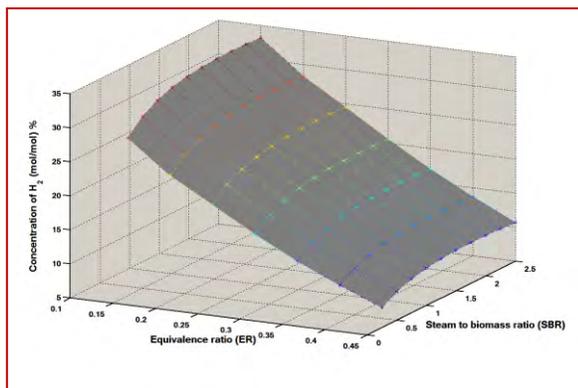
FIGURE 3 VARIATION OF H_2 CONCENTRATION WITH ER AND SBR (T: 1000 K)

Process efficiencies

Energy efficiency is another performance benchmark for steam-assisted gasification. On an average, the system is thermally efficient by 54.5% (see Fig. 5). The reduction in LHV reduces the process efficiency at higher air feed rates and with higher steam supply rate also. The maximum energy efficiency predicted is 83.4% at ER=0.15 and SBR=0.25 for a gasification temperature of 900 K.
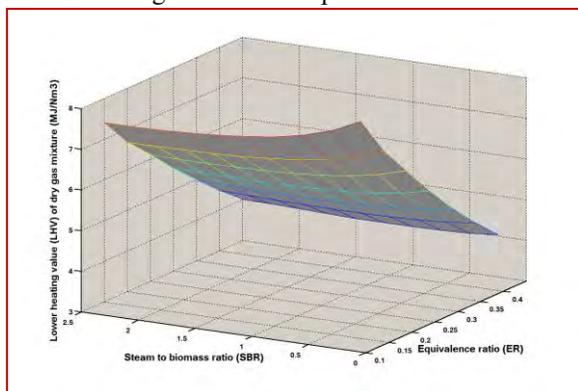
FIGURE 4 VARIATION OF LHV WITH ER AND SBR (T: 1000 K)

The second law thermodynamic efficiency (exergy efficiency) is computed following the exergy modelling procedure. The destruction in chemical and physical exergies during gasification process makes exergy efficiency lower than the corresponding energy efficiency. The two thermodynamic efficiencies are given in Tab. 2 for different operating conditions.

Optimum operating conditions

Maximum H_2 concentration achieved is 34.6% for air-steam gasification of sawdust which corresponds to a much

higher steam supply (SBR=2.5) rate. At this condition (T=900 K, ER=0.15 and SBR=2.5, moisture content=7.7%) LHV and consequently process efficiencies are lower than their corresponding maximum achievable values.
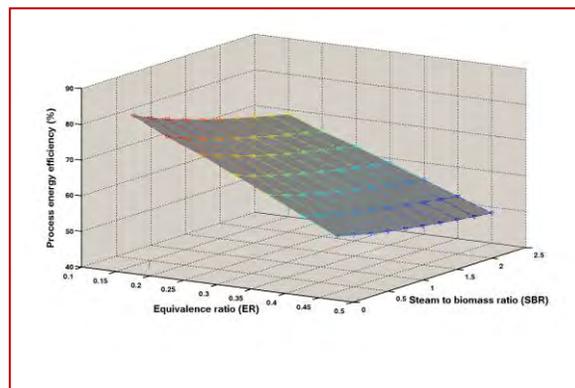
FIGURE 5 VARIATION OF ENERGY EFFICIENCY WITH ER AND SBR (T: 1000 K)

TABLE 2: ENERGY AND EXERGY EFFICIENCIES OF AIR-STEAM GASIFICATION FROM ASPEN PLUS MODEL SIMULATION

ER	SBR	T(K)	Energy efficiency (%)	Exergy efficiency (%)
0.25	0.5	1000	71.6	47.3
0.45	0.5	1000	54.4	29.8
0.25	1.5	1000	66.2	39.7
0.45	0.5	900	56.6	31.3
0.15	2.5	900	69.4	42.1

Thus, with regard to the highest bio-hydrogen concentration in the syngas mixture, the operating conditions where air-steam gasification can generate syngas containing 34.6% bio-hydrogen holding 7.57 MJ/Nm^3 heating value are suggested. The corresponding thermodynamic energy and exergy efficiencies are 69.4% and 42.1%, respectively. However, a SBR value above 1.5 is not recommended for steam-assisted gasification considering its energy efficiency. Thus, at ER=0.15 and SBR=1.5, the highest H_2 concentration predicted is 32.4% from this model.

EXPERIMENTAL VALIDATION OF THE SIMULATION RESULTS

The composition of the product gas is dependent on the type of the gasifier design. Thus, experimental results from BFB [21-23] as well as from fixed bed [24] gasifiers are utilised for the validation of the predicted results. The present model is developed for sawdust since the correlations for pyrolysis products are applicable to this

biomass only. In short, in addition to the chemical composition, correlations deduced for pyrolytic yields are executed as FORTRAN subroutines before the DECOMP block to simulate the model for gasification of various feedstocks. The regression equations are developed from the experimental data for pyrolytic yield from the biomass compounds. Comparison of the simulation results with the corresponding experiments [21-24] for air-steam gasification is illustrated in Fig. 6. The deviation of the simulation results from the corresponding experimental results is quantified as Root Mean Square Error (RMSE). The RMSE values estimated are 6.89, 4.62, 3.78, and 4.41, respectively for gasification of pine sawdust, pine bark, sewage sludge, and waste tire. The predicted results deviate slightly from the experimental results, however within satisfactory limits only.

Uniqueness of the model

The present model is based on the first order reaction scheme for all the major reactions involved in biomass gasification. Moreover, instead of the commonly discussed splitting of the biomass into its constitutive elements for simulating pyrolysis, this study simulates the actual pyrolysis process incorporating the yields of gas, steam, tar and char. The model can simulate the air-steam gasification with chemical composition and moisture of the feedstock, char conversion rate and the values of the operating conditions as inputs. The validation methodology is also unique since pyrolytic yields of the respective biomass compounds are incorporated based on the correlations deduced from experimental results.

CONCLUSIONS

A reaction kinetic model for air-steam gasification of wood sawdust is formulated and simulated in Aspen Plus environment incorporating the necessary chemical reactions involved in air-steam gasification. The influence of the major process variables on performance indicators of gasification are discussed. The gasification system may operate at low ER, higher SBR and medium temperature for augmentation of H_2 in the gas mixture. Maximum bio-hydrogen concentration predicted is 34.6% at T=900 K, ER=0.15, SBR=2.5 and moisture content=7.7%. The model is validated for gasification of woody and non-woody biomass materials. The results are found to be deviating slightly (RMSE ranging from 3.78-6.89), however within satisfactory limits only. The deviation of the results is attributed to the assumptions such as composition of tar and char, adiabatic condition of the process blocks and limitations of the correlations used for predicting pyrolytic products.
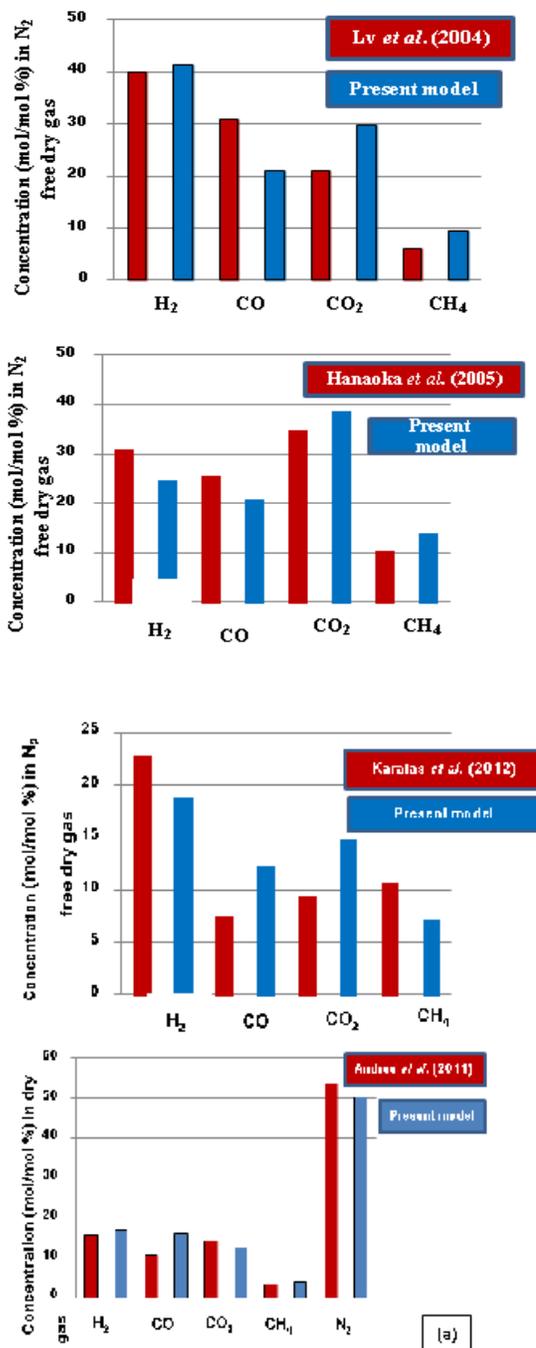
FIGURE 6. COMPARISON OF SIMULATION RESULTS WITH EXPERIMENTAL RESULTS FROM (A) [21] (BIOMASS: PINE SAWDUST, ER: 0.19, SBR: 2.7, T: 1023 K, MOISTURE: 8.0 %, CARBON CONVERSION: 80.6 %) (B) [22] (BIOMASS: PINE BARK, ER: 0.4, SBR: 5.84, T: 1173 K, [24] (BIOMASS: WASTE TIRE, STEAM/AIR: 0.25, T: 973 K, MOISTURE: 0.68 %, CARBON CONVERSION: 80%) MOISTURE: 6.5 %, CARBON CONVERSION: 70.3 %) (D) [23] (BIOMASS: SLUDGE, (A) ER: 0.3, SBR: 0.5, T: 1123 K, MOISTURE: 7.0 %, CARBON CONVERSION: 86.7 %

REFERENCES

[1] Wallman, P. H., Thorsness, C. B., and Winter, J. D., 1998. "Hydrogen production from wastes". Energy, 23(4), pp. 271-278

[2] Mathieu, P., and Dubuisson, R., 2002. "Performance analysis of a biomass gasifier". Energy conversion and management, 43(9), pp. 1291-1299

[3] Paviet, F., Chazarenc, F., and Tazerout, M., 2009. "Thermo-chemical equilibrium modelling of a biomass gasifying process using Aspen Plus". International Journal of Chemical Reactor Engineering, 7(1), A179

[4] Chen, C., Jin, Y., Yan, J. and Chi, Y., 2010. "Simulation of municipal solid waste gasification for syngas production in fixed bed reactors". Journal of Zhejiang University Science A, 11 (8), pp. 619-628

[5] Abdelouahed, L., Authier, O., Mauviel, G., Corriou, J. P., Verdier, G., and Dufour, A., 2012. "Detailed modeling of biomass gasification in dual fluidized bed reactors under Aspen Plus". Energy & Fuels, 26(6), pp. 3840-3855

[6] Nikoo, M. B., & Mahinpey, N. (2008). Simulation of biomass gasification in fluidized bed reactor using Aspen Plus. *Biomass and Bioenergy*, *32*(12), pp. 1245-1254.

[7] Murakami, T., Xu, G., Suda, T., Matsuzawa, Y., Tani, H., and Fujimori, T., 2007. "Some process fundamentals of biomass gasification in dual fluidized bed". Fuel, 86(1), pp. 244-255.

[8] Shen, L., Gao, Y., and Xiao, J., 2008. "Simulation of hydrogen production from biomass gasification in interconnected fluidized beds". Biomass and Bioenergy, 32(2), pp. 120-127

[9] Dong, C., Liang, H., Zhang, J., and Yang, Y., 2010. "Exergy evaluation of the biomass gasification system for varied fuel type". Proceedings of International Conference on Sustainable Power Generation and Supply, 1-6

[10] Zhang, Y., Xiao, J., and Shen, L., 2009. "Simulation of methanol production from biomass gasification in interconnected fluidized beds". Industrial & Engineering Chemistry Research, 48(11), pp. 5351-5359

[11] Atnaw, S. M., Sulaiman, S. A., and Yusup, S., 2011. "A simulation study of downdraft gasification of oil-palm fronds using ASPEN PLUS". Journal of Applied Sciences, 11(11), pp. 1913-1920

[12] Renganathan, T., Yadav, M. V., Pushpavanam, S., Voolapalli, R. K., and Cho, Y. S., 2012. "CO_2 utilization for gasification of carbonaceous feedstocks: A thermodynamic analysis". Chemical Engineering Science, 83, pp. 159-170.

[13] Ji, P., Feng, W., and Chen, B. 2009. "Production of ultra pure hydrogen from biomass gasification with air". Chemical Engineering Science, 64, pp. 582-92

[14] Inayat, A., Ahmad, M. M., Mutalib, M. I., and Yusup, S., 2012. Process modeling for parametric study on oil palm empty fruit bunch steam gasification for hydrogen production. Fuel Processing Technology, 93(1), pp. 26-34.

[15] Göransson, K., Söderlind, U., He, J., and Zhang, W., 2011. "Review of syngas production via biomass DFBGs".

Renewable and Sustainable Energy Reviews, 15(1), pp. 482-492

[16] Mullen, C. A., Boateng, A. A., Goldberg, N. M., Lima, I. M., Laird, D. A., and Hicks, K. B., 2010. "Bio-oil and bio-char production from corn cobs and stover by fast pyrolysis". Biomass and Bioenergy, 34(1), pp. 67-74

[17] Sommariva, S., Grana, R., Maffei, T., Pierucci, S., and Ranzi, E., 2011. "A kinetic approach to the mathematical model of fixed bed gasifiers. Computers & Chemical Engineering, 35(5), pp. 928-935

[18] Gerber, S., Behrendt, F., and Oevermann, M., 2010. "An Eulerian modeling approach of wood gasification in a bubbling fluidized bed reactor using char as bed material". Fuel, 89(10), pp. 2903-2917

[19] Lotrič, A., Sekavčnik, M., Kunze, C., and Spliethoff, H., 2011. "Simulation of water-gas shift membrane reactor for integrated gasification combined cycle plant with CO_2 capture". Strojniški vestnik-Journal of Mechanical Engineering, 57(12), pp. 911-926

[20] Groppi, G., Tronconi, E., Forzatti, P., and Berg, M., 2000. "Mathematical modelling of catalytic combustors fuelled by gasified biomasses". Catalysis Today, 59(1), pp. 151-162

[21] Lv, P., Chang, J., Wang, T., Fu, Y., Chen, Y., and Zhu, J., 2004. "Hydrogen-rich gas production from biomass catalytic gasification". Energy & Fuels, 18(1), pp. 228-233

[22] Andres, D. J. M., Narros, A., and Rodríguez, M. E., 2011. "Behaviour of dolomite, olivine and alumina as primary catalysts in air–steam gasification of sewage sludge". Fuel, 90(2), pp. 521-527

[23] Karatas, H., Olgun, H., and Akgun, F., 2012. "Experimental results of gasification of waste tire with air&CO_2, air & steam and steam in a bubbling fluidized bed gasifier". Fuel Processing Technology, 102, pp. 166-174

[24] Hanaoka, T., Inoue, S., Uno, S., Ogi, T., and Minowa, T., 2005. "Effect of woody biomass components on air-steam gasification". Biomass and bioenergy, 28(1), pp. 69-76

SEEC-2018-050

HIGH PERFORMANCE CROSS-LINKED POLY(VINYL ALCOHOL)/PIPERAZINE GLYCINATE POLYMER MEMBRANE FOR CO₂ GAS SEPARATION

Mridusmita Barooah
Department of Chemical Engineering
Research Scholar
m.barooah89@iitg.ernet.in

Dr. Bishnupada Mandal
Department of Chemical Engineering
HoD & Professor
bpmandal@iitg.ac.in

ABSTRACT

Global warming, a subject of increased emphasis in the recent years, is caused by the emission of greenhouse gases like CO_2 in the atmosphere. This work studies the synthesis, characterization and gas separation performance of CO_2 selective cross-linked poly (vinyl alcohol)(PVA)/piperazine glycinate(PG)/ polyethersulfone(PES) facilitated transport composite membranes synthesised via solution casting methodology. The synthesized membrane is characterized via Thermo gravimetric analysis (TGA), Differential scanning calorimetry (DSC), Fourier transform infrared spectroscopy (FTIR), X-ray diffraction (XRD) and FESEM. The effect of membrane performance on gas transport properties such as CO_2 and N_2 flux ($10^{-6} cm^3(STP)/cm^2.sec$), CO_2 and N_2 permeability (Barrer) ($10^{-10} cm^3(STP)cm/cm^2.sec.cmHg$), and CO_2/N_2 selectivity with variation in amine content, temperature, and gas relative humidity was thoroughly studied. The feed gas stream consisted of 20% CO_2 and 80% N_2 by volume. At $100^O C$ and 4.5 atm feed absolute pressure optimum performance was observed with CO_2 permeance of 38 GPU and CO_2/N_2 selectivity of 200 respectively.

Keywords : Polymeric membrane, Poly (vinyl alcohol), Piperazine glycinate, Permeability, CO_2/N_2 selectivity.

.
NOMENCLATURE

P_{CO2}/L	CO₂ Permeance
J_{co2}	CO₂ Flux
P_{CO2}	CO₂ gas permeability
P_{N2}	N₂ gas permeability
L	Thickness of the membrane
P_{fCO2}	Partial pressure in the feed side
P_{PCO2}	Partial pressure in the permeate side

INTRODUCTION

Greenhouse gases (GHGs) trap the heat radiating from the surface of earth when solar energy is being transmitted through the atmosphere thus increasing the global surface temperature. The Intergovernmental Panel on Climate Change (IPCC) has predicted that the sea level will rise by 0.09 to 0.88 meters from 1990 to 2100, which is a matter of serious concern. Post-combustion capture is important application because of its flexibility and easy addition to the operational units. Although conventional separation techniques such as absorption, cryogenic distillation and adsorption have huge applications, advanced technologies such as membrane separation have been extensively used due to advantages of less energy consumption, light weight, space efficiency and compact modular design[1-3]. Polymeric membranes are hugely applied due to its advantages of low cost and easy processability. However, it faces hiccup due to its trade-off limitation between permeability and selectivity as stated by the Robeson upper bound curve. This sometimes poses a great challenge for its

long term usability for industrial purposes. Incorporation of suitable amine carriers into the polymer backbone, crosslinking and blending of polymer matrix is useful for the enhancement of CO_2 transport property with increase in the stability throughout the membrane.[4] In this work, poly (vinyl alcohol) (PVA),a synthetic polymer having high hydrophilicity, good film-forming capability, enhanced chemical, thermal and mechanical properties is chosen as the polymer matrix for CO_2/N_2 separation.Piperazine glycinate (PG) salts are synthesized and added to the PVA aqeous solution. These salts act as the mobile carrier thereby leading to a considerable enhancement of the CO_2 transport properties as compared to pure PVA films.[5] In the synthesis process, novel cross-linked poly (vinyl alcohol) (PVA) membranes were doped with piperazine glycinate mobile carrier in different weight composition by solution casting methodology. The final polymer solution was cast over polyethersulfone (PES) support having a pore size of 0.03μm. 60mol% of formaldehyde (HCHO) was used as the cross-linking agent.

The CO_2 permeance and CO_2/N_2 selectivity can be defined by the following equations:

$$CO_2 \text{ permeance} = P_{CO2}/L = J_{CO2} / (P_{fco2} - P_{PCO2}) \quad (1)$$

$$CO_2/N_2 \text{ selectivity} = P_{CO2}/P_{N2} \quad (2)$$

Where P_{CO2}/L is the CO_2 permeance, GPU (1 GPU = 10^{-6} cm^3(STP)/ (s.cm^2.cmHg), J_{CO2} is the CO_2 flux, P_{co2} and P_{N2} is the CO_2 and N_2 gas permeability, L is the membrane selective layer thickness, P_{fCO2} and P_{pco2} are the partial pressure of CO_2 in the feed and permeate sides respectively.

Experimental section

Materials : Poly (vinyl alcohol) (99mol% hydrolyzed powder, Mw = 130,000), 2-methylimidazole [$C_4H_6N_2$] were procured from Sigma-Aldrich, USA. Formaldehyde solution (37wt % in H_2O), Glycine (Assay> 99%), piperazine (99%), Zinc nitrate hexahydrate [$Zn(NO_3)_2.6H_2O$], Methanol was purchased from Merck, India. All chemicals were used without any further purification. Microporous poly(ether sulfone) supports (thickness: 150 μm and pore size: 0.03 μm) were provided by Sterlitech USA. The feed gas (20% CO_2 and 80% N_2) used for the gas permeation analysis was procured from Vadilal Pvt. Ltd., India.

Synthesis of PVA/PG polymeric membrane: The PVA aqueous solution (12wt% solid weight) was prepared by continuously stirring at a temperature of 90°C which is maintained constant via oil bath. The PVA solution was cross-linked in formaldehyde at a ratio already optimized through our previous studies. Finally, the prepared PG salt

solution was added fixed in the weight ratio of 70 and 30 weight ratio of PVA solution to form the final cross-linked PVA/PG polymer solution. The air bubbles formed were removed by centrifugation at 10,000 rpm for 30 min. The final centrifuged solution was cast onto the porous PS support (average pore size: 0.03μm) kept over a glass plate. The thickness of the polymer film was maintained by the use of micrometer adjustable film applicator (GARDCO, Paul N. Gardner, USA).
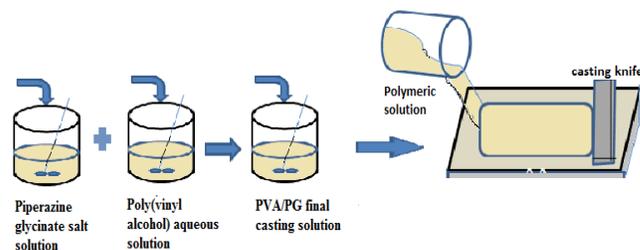
FIGURE 1: Synthesis procedure of PVA/PG polymer solution
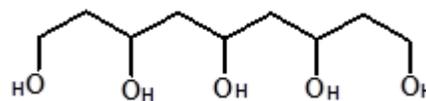
Poly (vinyl alcohol) (PVA)
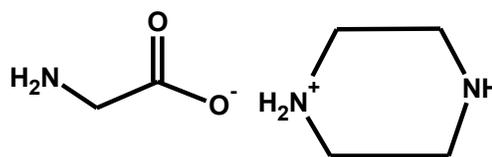
Piperazine glycinate (PG)

FIGURE 2: Chemical structure of PVA polymer and piperazine glycinate salt

Membrane Characterization: The synthesised membranes were characterized via various techniques. The thermal stability of the synthesized active layer was carried out using TGA/SDTA 851^e system (MATTLER TOLEDO, Switzerland). Nitrogen atmosphere was used for conduction of the analysis. DSC analysis was carried out using DSC 1/400 STAR^e system (METTLER TOLEDO, Switzerland) under nitrogen purge gas stream. The samples

were subjected to heating/cooling/heating cycle in the range from -30°C to 350°C at a scan rate of 10°C/min. The DSC curves were obtained from the second heating cycle.The functional groups present in the active layer of the prepared membranes were confirmed via Attenuated total reflection-Fourier transform infrared spectroscopy (ATR-FTIR) (SHIMADZU, IRAffinity 1, Japan). FTIR spectra were obtained in the range of wavenumber from 4000 to 400 cm^{-1} with 40 scans per sample and 4 cm^{-1} resolution.The crystal structure of all active layers was examined using Bruke D8, advanced X-ray diffraction measurement for 2θ angles between 10° and 60°. Cu Kα radiation of wavelength λ = 1.54056 A^{o} was considered.The morphology and distribution of the silica nanoparticles in the synthesized membrane were investigated via top surface and cross sectional views of FESEM imaging. To observe the membrane cross section, the samples were first fractured in liquid nitrogen and then sputter-coated with gold film prior to FESEM observation.

RESULTS AND DISCUSSIONS

TGA characterization: Thermo gravimetric analysis of the prepared PVA/PG polymer membrane is shown in Fig. 3. TGA plot indicates weight change of sample when heated at the rate of $10^{o}C$ min^{-1} rate. For, pure PVA/PEG blend membrane, the initial weight loss at a temperature below $120^{o}C$ is due to the loss of absorbed and bound moisture from atmosphere and other volatile matters. The weight loss in the second stage from $230^{o}C$-$320^{o}C$ is due to the eradication of hydroxyl groups and free amine groups. The final weight loss at $405^{o}C$ is attributed to the breakdown of the C-C polymer backbone.[1-2] The analysis showed a stable polymer with loss of weight in three distinct stages.
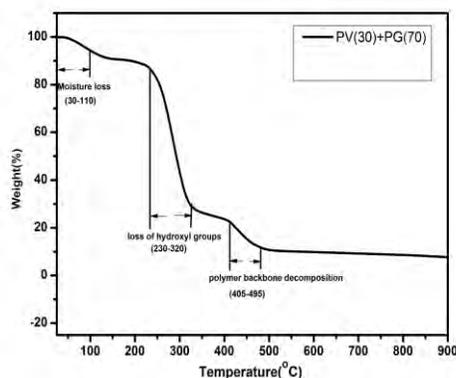
FIGURE 3: TGA characterization of the synthesised PVA/PG polymer membrane.

Effect of Temperature: The effect of temperature (°C) on CO_2 and N_2 flux, CO_2 and N_2 permeability, and CO_2/N_2 selectivity for pure PVA/PG/PES polymer membrane was investigated for temperature range from 25 to 80°C. The

pressure at feed and sweep side was maintained at 1.5atm and 1atm, respectively. The water flow rates at the feed and sweep sides were kept constant at 0.03 and 0.05ml/min, respectively. The gas flow rates of the feed gas (20% CO_2 balance N_2) and sweep gas (Ar) were kept constant at 30 and 40 ml/min, respectively. The effect of temperature on CO_2 and N_2 flux, CO_2 and N_2 permeability and CO_2/N_2 selectivity for the synthesized membrane is represented in Fig.4. It was observed that with the increase in temperature, the CO_2 flux, CO_2 permeance, and CO_2/N_2 selectivity increased gradually with the increase from room temperature to temperature as high as 90°C. At higher temperatures, the increased gradually becomes constant.[3] The N_2 gas undergoes separation only by solution diffusion mechanism. Hence, the N_2 flux, and N_2 permeance almost remained constant. The increase in CO_2/N_2 selectivity, CO_2 permeance and CO_2 flux is due to the enhanced rate of reaction between the CO_2 gas and amine carriers in presence of moisture and increase in temperature. For a active layer thickness of 18μm and temperature of $80^{\circ}C$, CO_2 permeance of 38 GPU along with CO_2/N_2 selectivity of 200 and a high CO_2 flux of 3000 was observed.
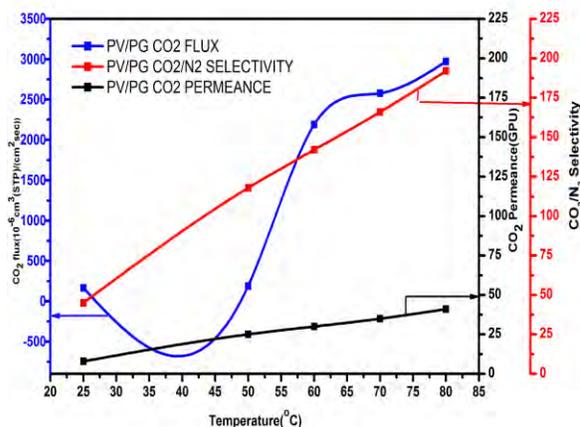
FIGURE 4: Effect of temperature on CO_2 permeance(GPU),and CO_2/N_2 selectivity for pure PVA/PG PM at feed absolute pressure=1.5 atm, sweep absolute pressure=1 atm, and water flow rates = 0.03/0.04 ml/min (feed/sweep).

ACKNOWLEDGMENTS

REFERENCES

[1] Mondal, A., Mandal, B., 2014. "Novel CO_2-Selective Cross-Linked Poly(vinyl alcohol)/Polyvinylpyrrolidone Blend Membrane Containing Amine Carrier for CO_2–N_2 Separation: Synthesis, Characterization, and Gas Permeation Study" .Ind. Eng. Chem. Res, 53, pp. 19736−19746.

[2] Mondal, A., Mandal, B., 2013. "Synthesis and characterization of crosslinked poly(vinyl alcohol)/poly(allylamine)/2-amino-2-hydroxymethyl-1,3-propanediol/polysulfone composite membrane for CO_2/N_2 separation." Journal of Membrane Science,446, pp. 383-394.

[3] Mondal, A., Barooah, M., Mandal, B., 2015. "Effect of single and blended amine carriers on CO_2separation fromCO_2/N_2mixtures using crosslinked thin-film poly(vinyl alcohol)composite membrane." Int. J. Greenh. Gas Control., 39**,** 27-38.

[4] Omidkhah M., Pedram MZ., Amooghin AE., 2013. "Facilitated Transport of CO_2 through DEA-Mediated Poly(Vinyl alcohol) Membrane Cross-Linked by Formaldehyde." J Membra Sci Technol 3:119.

[5] Chen,Y.,Ho.W., 2016. "High-molecular-weight polyvinylamine/piperazine glycinate membranes for CO2 capture from flue gas."Journal of Membrane Science, 514,pp. 376-384.

SEEC-2018-051

FOREST AND AGRICULTURAL BIOMASS FOR CLEAN ENERGY IN EUROPE AND INDIA

Narasinha J. Shurpali
Senior Scientist**,** Deaprtment of Environmental
and Biological Sciences, University of Eastern
Finland, FI-70211, Kuopio Finland,
Email: narasinha.shurpali@uef.fi

ABSTRACT

The EU and India share common goals of reducing their dependence on fossil fules and they have agreed to scale up their cooperation in science and technology for developing clean energy solutions from biobased resources. Through INDO-NORDEN, a joint research project involving Finland, Estonia and India, we showcase sustainable land use practices and processes for bioenergy production (solid, liquid and gas). Finland participates in this project as the coordinating unit with two field experiments – a recently clear-cut forest site and an agricultural field growing a mixture of legumes (red clover) and Timothy grass for examining the C and N dynamics in these ecosystems. Finland will also address the effects of biomass raw material on combustion processes. India and Estonia will explore the processes for increasing the yield of biobutenol and bioethanol using locally available agricultural restudies.

*Keywords***:** Finland, bioenergy, sustainability

INTRODUCTION

Finland is actively involved in developing bioeconomy, like most other Nordic countries [1]. The use of biomass from forests and agriculture in Finland is on the rise. Forests in Finland are being put to intensive biomass harvesting practices – collection of harvesting residues and stumps for bioenergy [2]. Howevere, we do not know much about these intensive harvesting processes in terms of how they impact the environment. Additionally, biogas production from agricultural wastes is a sources of renewable energy. However, we do not yet have a clear understanding of the life cycle analysis of biogas production, - especially if crop biomass is used with farm waste as a substrate in the biogas plant. It is hypotheisized that the addition of a legume crop (rich in nitrogen) as a cosubstrate in a biogas digester may enhance the biogas yield. As the crop production needs fertilisers, what happens to the fertilizers applied to the field? How large are the N_2O emissions from such fields? Does the biogas thus produced meet the overall sustainability standards?

Indian and Estonian partners participating in the project are developing processes in the lab for increasing the yield of biobutenol and bioethanol from agricultural residues in their respective countries [3,4]. India has a huge amount of rice and wheat residues left over in the field after harvest. This is generally burnt in the field leading to heavy environmental pollution. Why not use this bioresource for butenol production? Estonia has large amount of rye and barley residues. Can they be used for ethanol production? If yes, is such production cost effective? How can we make the process more commercial? These are the questions that will be addressed in the INDO-NORDEN project [5]. We present here research methods and preliminary results from the project work carried out in Finland during the growing season (May – Spetember) of 2017.

MATERIALS AND METHODS

The primary agricultural research site (Fig. 1) is located in the rural district of Maaninka, Eastern Finland (63° 9' 48.69" N, 27° 14' 3.29" E), about 45 km from UEF Kuopio campus. Long-term (reference period 1981-2010) annual air temperature in the region is 3.2°C and the annual precipitation is 612 mm. The soil type varies between loam and clay loam. The field is currently cultivated with a

perennial legume (red clover) and Timothy grass mixture. The crop receives an annual fertiliser application of 100 kg N in the spring (late May). The first cut is made in early July. After the first cut the site is divided into two parts along the NE-SW transect so that one part receives a second dose of inorganic fertilisers and the other is treated with the slurry (organic fertiliser) from the biogas digester maintained by Luke at the Maaninka research station. The crop reaches a height of about 60 cm at the peak vegetative growth prior to harvest. The second harvest is generally made at the end of August. After the second harvest, the crop restablishes owing to climatic conditions being still favorable for the crop growth. However, the crop growth remains stunted with a peak vegetation height of about 25 cm. The legume and grass mixture is left on the field for overwintering.

FIGURE 1. Eddy covariance measurements of CO_2 and N_2O exchange from a perennial legume crop in Finland

The aim of the agricultural study is examine the impact of organic and inorganic fertilisers on the growth and C and N dynamics of the legume grass mixture. A part of the harvested legume grass mixture serves as a substrate for the biogas plant fed with the farm waste. Is there any difference in the seasonal N2O fluxes from organic and inorganic fertilisers? Does the use of legume grass mixture as a substare enhance the biogas yield? The eddy covariance [6] measurements at this site include year-round, continuous and direct estimates of net ecosystem CO_2 exchange (NEE), nitrous oxide exchange and relevant soil, plant and micrometeorological data.

FIGURE 2. Eddy covariance measurements of CO_2 exchange from the floor of a clear-cut forest in Finland

At the forest site (Fig. 2), we are measuring year-round CO_2 exchange with the eddy covariance (EC) technique and soil GHG emissions using static chambers. The aim here is to investigate how the carbon balance of a clear-cut forest site differs from that of a standing forest. An adjacent, intact forest stand will serve as reference site for the study. We are measuring year-round CO_2 and N_2O fluxes with the EC technique.

RESULTS
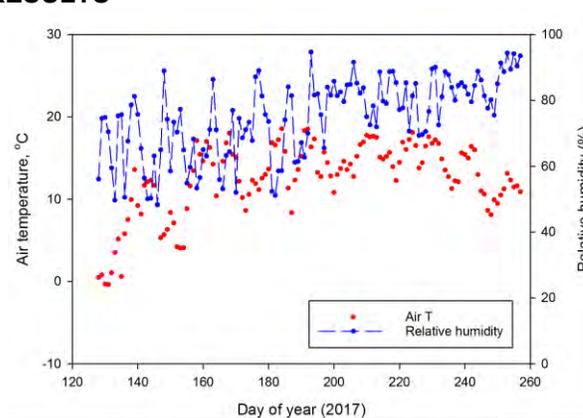
FIGURE 3. Daily average air temperature and relative humidity at the agricultural research site in Finland during the 2017 growing season.

The 1981-2010 30-year average temperature for May, July and September are 8.9, 17.0 and 9.4°C, respectively in the study region. The normal rain for the growing season is 318 mm. The seasonal pattern of daily air temperature and relative humidity are shown in Figure 3. The air temperatures varied between 10 and 20°C during May, reached a peak of 27°C during mid July in 2017.
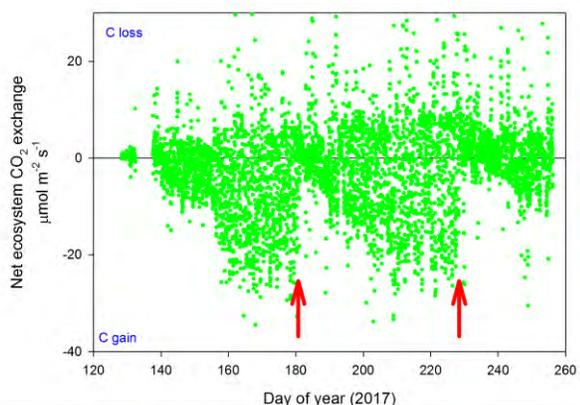
FIGURE 4. Seasonal CO_2 exchange (NEE) from a perennial legume crop in Finland during the 2017 growing season (the red arrows show the days of the year when the crop was harvested).

Eddy covariance measurements of NEE and N_2O exchange began in early May when the snow at the site had thawed in the spring. The perennial red clover and grass mixture that was sown in 2016 started its regrowth during this period. The crop was fertilised in late May. First harvest of the crop was performed in early July and the second harvest in late August. The NEE was close to zero early in the season. With increasing temperatures and radiation levels, the grass mixture enhanced its photosynethic activity to reach a peak in early June. The crop continued to sequester atmospheric CO2 until early July, when the crop was harvested for the first-cut biomass. The impact of this harvesting is evident in the NEE data shown in Figure 4. Soon after the crop harvest, the crop turned into a source of CO2 temporarily. The crop was fertilised with N fertilisers after the first-cut. With temperatures, soil moisture and PAR levels being favourable and with soil N high, the crop mixture began to produce tillers thus allowing a vigorous plant growth with a peak in the third week of July. The second-cut was performed during late August when the peak crop growth had plateaued. Soon after the second harvest, NEE declined sharply. Based on the data presented in Figure 4, on a seasonal basis, the crop accumulated more CO_2 than the amount the whole ecosystem released to the atmosphere.

CONCLUDING REMARKS

Further data analyses detailing the factors governing NEE, N_2O exchange and complete life cycle analysis of the crop production system are in progress. Studies that assess the environmental friendliness of bioresources will decide whether a given resource can be used sustainably as a renewable energy source.

REFERENCES

[1] http://www.bioeconomy.fi/facts-and-contacts/finnish-bioeconomy-strategy/

[2] Repo, A., Tuomi, M. and Liski, J. 2010. Indirect carbon dioxide emissions from producing bioenergy from forest harvest residues. GCB Bioenergy, doi:10.1111/j.1757-1707.2010.01065.

[3] Sukumaran RK, Surender VJ, Sindhu R, Binod P, Janu KU, Sajna KV, Rajasree KP, and Pandey A. (2010) "Lignocellulosic ethanol in India: Prospects, challenges and feedstock availability." Bioresource Technology 101 (2010): 4826-4833.

[4] Raud, M., M. Tutt, J. Olt and T. Kikas. "Effect of lignin content of lignocellulosic material on hydrolysis efficiency". Agronomy Research, 13.2: 405 – 412.

[5] Narasinha Shurpali, Binod Parameswaran, Merlin Raud, Olli Sippula, Perttu Virkajärvi, Jukka Pumpanen, Jorma Jokiniemi, 2017. "INDO-NORDEN – a consortium for developing holistic processes and land use practices for clean energy, Energy Procedia 125: 363–371

[6] Shurpali NJ, Rannik U, Jokinen S, Lind S, Biasi C, Mammarella I, Peltola O, Haapanala S,Virkajärvi P, Vesala T and Martikainen PJ. (2015) "Neglected diurnal variations are a cause for large uncertainties in global nitrous oxide emissions" Scientific Reports 6, Article number: 25739

Impact of different pre-treatment methods on the holocellulose content of finger millet stalk for biofuel production

Sumitha Banu J.[1*], Vijay S. Moholkar[1,2] and Arun Goyal[1, 3]

[1]*Centre for Energy, Indian Institute of Technology Guwahati, Guwahati-781039, India*
[2]*Department of Chemical Engineering, Indian Institute of Technology Guwahati, Guwahati-781039, India*
[3]*PAN-IIT DBT Center for Bioenergy, Department of Biosciences and Bioengineering, Indian Institute of Technology Guwahati, Guwahati-781039, India*

[*]*Corresponding author. Tel: +91 8011033882, E. mail: sumitha@iitg.ernet.in*

The predominant step in bioethanol production from lignocellulosic feedstock is pretreatment. Different pretreatment methods affect the lignocellulosic biomass in different ways. Comparison of pretreatment methods on any biomass with respect to total reducing sugar (TRS) is indirect. Structural composition of each pretreated sample needs to be analysed to understand the exact influence of each treatment on the biomass. Hence, this study focuses on comparison of various pretreatment methods such as oven heating, autoclaving, microwaving and ultra-sonication involving aqueous systems such as distilled water, 1% H_2SO_4 or 1% NaOH in concentrating the holocellulose content of finger millet stalk. Among all the chosen pretreatment methods, microwaving with distilled water was efficient in concentrating the holocellulose content to 76.7±0.2 wt% from 69.3±1.3 wt% of powdered raw finger millet stalk. Surface roughness rendered by microwaving pretreatment was visible in the FESEM image of pretreated biomass compared to the untreated biomass.

Keywords: Finger millet stalk, pretreatment method, holocellulose

EVAPORATION RATE ANALYSIS OF DIFFERENT FUEL BLENDS FOR LOW TEMPERATURE COMBUSTION ENGINE APPLICATIONS

Saurabh Kumar Gupta
Department of Mechanical Engineering
Indian Institute of Technology Madras
guptasaurabh365@gmail.com

Anand Krishnasamy
Department of Mechanical Engineering
Indian Institute of Technology Madras
anand_k@iitm.ac.in

ABSTRACT

As the global emission norms for automotive engines are becoming more and more stringent because of environmental concerns, an improved understanding about the fundamental processes which plays a role in emission formation is required. The rate at which the fuel evaporates is one such processes which affects the emission formation in a significant manner owing to its role in fuel-air mixing. Low Temperature Combustion (LTC) are emerging as the most promising strategies to simultaneously reduce oxides of nitrogen and particulate matter emissions along with maintaining higher thermal efficiecny. LTC strategies demand fuel blends of varying reacitvities to have a better control on combustion at varying loads. Understanding evaporation rate of possible fuel blends for LTC strategies is yet to be explored.

This study presents the fuel and evaporation rate characterstics of blends of commercial fuels (Gasoline and Diesel) as well as alternative fuels (Butanol and Ethanol) which are the potential fuel blends for LTC applications. The evaporation rate characterstics of all the fuel blends are carried out by using hanging droplet method. The obtained results show that diesel increases non evaporative part. Along with that multicomponent system behave differently compare to single one's.

Keywords: Evaporation Characteristics, Fuel Blends, Low Temperature Combustion, Alternative Fuels

.
NOMENCLATURE

D/ Do	Diameter/ Initial diameter
t	Time (sec)
K	Evaporation Constant

INTRODUCTION

The rise of civilization is closly related to the improvement of transportation. The internal combustion engines occupy a major role in that [1]. However, in the recent times the exhaust pollutants from the internal combustions are of seriuos concern owing to their global warming potential and human health problems. The countries all over the world have implemented stringent emissions norms to improve the air quality [2]. The engine out emissions could be reduced by utilizing after-treatment devices which are expensive or by in-cylinder control [1]. Low temperature combustion (LTC) is an in-cylider emission control strategy which has evolved based on the understanding of emission formation mechanisms. LTC is driven by the fuel chemical kinetics and is fuel flexible. LTC strategies demand fuels with varying reacitvities to widen the operating load range which could be achieved by the use of different fuels or by blending fuels of different reactivities [3].

Evaporation is an important mechanism in the internal combustion engines which helps to understand the mixture preparation, distribution and combustion [4]. Studies related to fuel evaporation rates at high pressure and high temperature conditions are well stablished for both single and multi component fuels such as biodiesel [5]. However, evaporation rate studies for different fuel blends which are of interest for LTC engine applications are scarce.

In this work, analysis of evaporation behaviour along with fuel characterstics is discussed for various commercial (Gasoline, Diesel) and alternative fuels (Ethanol, Butanol) and their blends. The results obtained form this study would provide improved understanding of evaporation rate

behaviour of fuel blends utilized for LTC engine applications.

EXPERIMENTAL SETUP AND TEST PROCEDURE

The present study involve fuel blends preparation, charaterisation and their evaporation rate estimation based on experiments.

Fuel Preparation and Characterization

Selected fuels are two commercial fuels (Gasoline and Diesel) and two alternative fuels (Butanol and Ethanol). The selection of fuels is based on the differences in their reactivities. Further, the selection of fuel blends are based on the base fuel evaporation behaviour. In case of diesel tests were performed at 10 and 20% by volume of diesel and in case of butanol, gasoline and ethanol 20, 50 and 80% of volume is tried. Blends are gasolinediesel (GD10, GD20), Butanol Diesel (BD10, BD20), Ethanol diesel (immisible), ButanolGaoline (BG20, BG50, BG80), Ethanol Gasoline (EG20, EG50, EG80) and Butanol Ethanol (BE20, BE50, BE80). GD10 represents 10% of diesel with 90% gasoline.

Engine fuel properties, viz. density, viscosity, surface tension are measured according to ASTM standards for the test fuel blends and are presented in Table 1. For fuel density measurement, Oscillatory U-tube method is used and for measuring viscosity rotating drum method is used. Surface Tension is measured with Attension Sigma 700 using Du Nuoy ring method.

TABLE 1: Fuel blends properties with base fuels.

Fuel	Density (g/cm^3)	Viscosity (mm^2/s)	Surf. Tension (mN/m)
Diesel	0.8175	2.999	24.679
Gasoline	0.799	0.43694	22.268
Butanol	0.8107	2.6311	22.283
Ethanol	0.7932	1.1656	20.35
GD10	0.8024	0.4864	22.565
GD20	0.8036	0.5216	22.853
BD10	0.8118	2.8457	22.86
BD20	0.813	2.9115	23.229
BG20	0.8055	2.0103	22.411
BG50	0.798	1.1613	21.802
BG80	0.8025	0.98321	21.84
EG20	0.7938	0.9791	20.774
EG50	0.7953	0.7263	21.093
EG80	0.7957	0.52404	21.608
EB20	0.7958	1.3449	21.209
EB50	0.8014	1.7269	21.903
EB80	0.8075	2.4112	22.145

Evaporation Characterisation

Various established techniques are available in the open literature for studying the single droplet evaporation behaviour. Among those, suspended droplet method is found to be more accurate and provides insight for both qualitative and quantitative nature of droplet evaporation [6]. Earlier similar technique has been used for studying fuel evaporation behaviour for Biodiesel, Diesel and respective blends [7]. To understand the evaporation behaviour of urea water solution for selective catalytic reduction (SCR) applications, similar kind of hanging droplet technique was used [6]. In suspended droplet technique, the presence of a suspender makes the method intrusive. To counter that care has been taken to minimize the effect of the suspender on evaporation behavior of the droplet by using a glass micro fiber [6, 8] of diameter about 25 microns as the suspender. Lower thermal conductivity of glass combined with very low cross sectional area helps in restricting heat conduction through the suspender and keeping it to a minimum. Use of a very fine suspender also leads to droplets retaining their spherical shape during evaporation [6].

The experimental setup contains a glass fiber fixed with clamps, a high speed camera and background light. Tests are performed at ambient conditions while placing droplets at fiber using syringe manually. Images of evaporating droplets were captured using a Photron fast cam mini, a high speed camera at a certain50 frame speed and are recorded in a computer. The light source used is an LED array.The complete test setup is presented in Fig 3 along with a representative suspended droplet. Captured images are post processed using an in house developed codes written in MATLAB. The diameter of the suspended droplet was retrieved from the image.
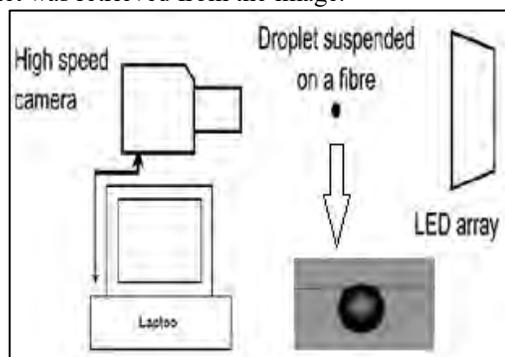
FIGURE 1. Experimental Setup for Evaporation Studies

To evaluate the evaporation rate of test fuel blends, D square (D^2) law is applied as provided in Equation 1 [9]. To get the evaporation rate plots of non-dimensional parameter $(D/D0)^2$ is plotted with (t/D_0^2) where „t‟ is time.

$$D^2(t) = D_0^2 - Kt \tag{1}$$

D is Diameter at time t, D_0 is initial diameter and K is the evaporation constant.

RESULTS AND DISCUSSIONS

Results are presented and are discussed next based on the test fuel blends. Evaporation charactersticsis represented as normalised diametric variation in form of $(d/do)^2$ versus t/do^2 which reflects the evaporation behavior and left over fuel.

Gasoline Diesel: Gasoline being a multicomponent system shows decresing evaporation rate with time but intial evaporation is very fast as compared to diesel which evaporates at a slower rate owing to the presence of heavier components. Both the fuels exhibit some non evaporative behaviour after a time frame. Similar trends are observed with fuel blends as well. Non evaporative volume increases proportionally with increase of diesel proportion and rate of evaporation at initial part is also affected with diesel proportion as shown in Fig. 2.
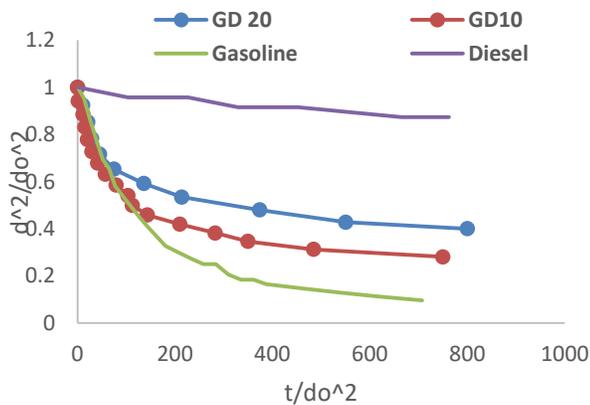
FIGURE 2. Evaporation Behaviour of Gasoline Diesel Blends

Butanol Diesel: In butanol-diesel blends butanol being a single component fuel shows a linear trend with higher evaporation rate as expected. Diesel fuel exhibits slower evaporation behaviour. Fig 3 shows that with an increase in the diesel blend percent the proportion of non evaporative component is increasing but it is not affecting the overall evaporation rate significantly.
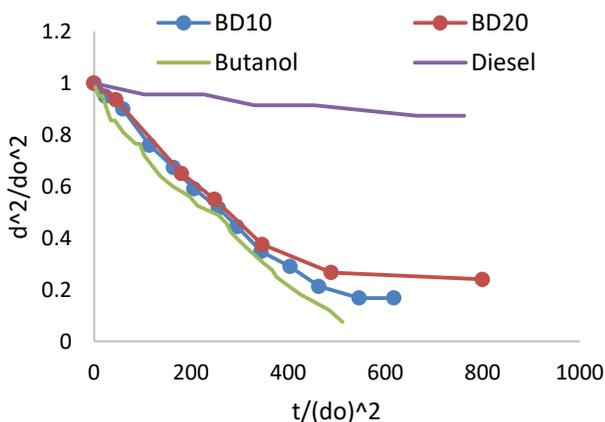
FIGURE 3. Evaporation Behaviour of Butanol Diesel Blends

Butanol Gasoline: In this blend system, butanol is a single component and gasoline is a multicomponent. Butanol being a single component shows a linear evaporation behavior and gasoline shows a decrease in evaporation rate with time. Their respective blends shows similar property as gasoline proportion increases the non evaporative part of system also increases. The evaporation rate of blends with upto 20 percent butanol in gasoline is not much affected as shown in Fig 4.
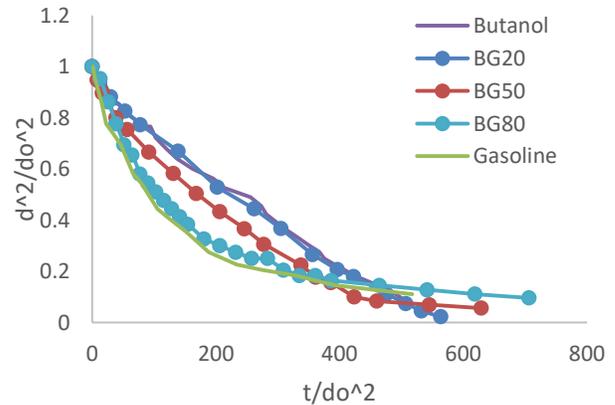
FIGURE 4. Evaporation Behaviour of ButanolGasoline Blends

Ethanol Gasoline: In this blend system, ethanol is a single component fuel which exhibit a linear evaporation behaviour initially but being hydrophilic it also contains a non evaporative part. Gasoline exhibit the evaporation rate as discussed earlier. Both the fuels have almost similar and a higher evaporation rate so their belnds lies in between due to thisplots are mjorly overlapping as shown in Fig 5.
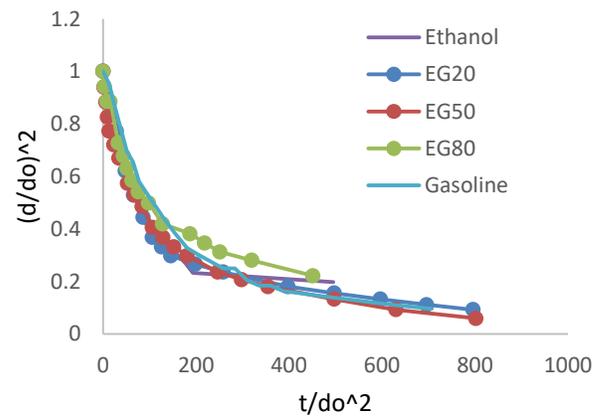
FIGURE 5. Evaporation Behaviour of Ethanol Gasoline Blends

Ethanol Butanol: Ethanol and butanol both are single component fuels whose evaporation rate are discussed earlier. For the blends, the evaporation rate comes in between. Also, it is observed that with an increase in ethanol content, the non evaporative component is reducing. Thus, the hydrophilic nature of ethanol is suppressed in presence other fuel as shown in Fig 6.
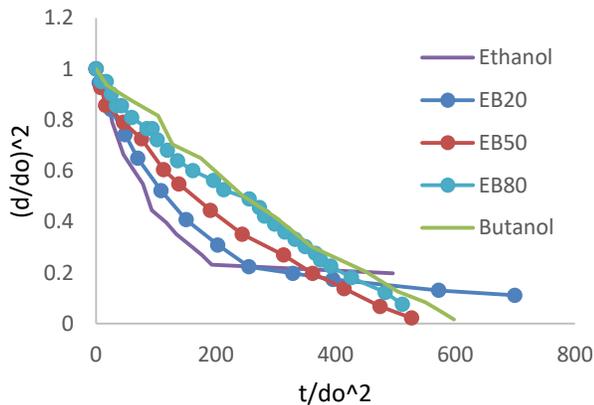
FIGURE 6. Evaporation Behaviour of Ethanol ButanolBlends

CONCLUSIONS

In the present work, evaporation rate behavior of potential fuels for LTC engines are studied. The major conclusions drawn form this work are as follows:

1- Evaporation behavior of single-single component blends (Ethanol-Butanol) or multi-multi component blends (Gasoline-Diesel) are varying linearly.
2- In case of blends of a single component and a multi component fuel, the evaporation rate behavior is not affected much for lower blend level (20%) (Butanol-Diesel, Butanol- Gasoline). This effect is not clear in ethanol gasoline blend due to similar evaporation behavior.
3- Addition of diesel increases the non evaporative part for blends (Butanol-Diesel and Gasoline-Diesel).
4- Blends helps in accomadating the hydrophilic nature as well (Ethanol-Gasoline, Ethanol-Butanol).
5- Lower density, viscosity and surface tension helps in evaporation. It also depends on fuel nature (Multicomponent or single component).

ACKNOWLEDGMENTS

REFERENCES

[1] Mathur, M.L., Sharma, R.P. A course in Internal Combustion Engine, 3rd ed., DhanpatRai& Sons, Delhi, Chap. 18, pp. 615.
[2] Pundir, B.P., IC Engines Combustion and Emissions, 1st ed., Narosa Publishing House Pvt Ltd, New Delhi, Chap. 6, pp.225-226.
[3] Anand, K., Ra, Y., Reitz, RD., and Bunting, B, 2011."Surrogate model development for fuels for advanced combustion engines". Energy Fuels 25: 1474 1484dx.doi.org/10.1021/ef101719a.
[4] Ghassemi, H.,Baek, S.W.,andKhan, Q.S., 2006."Experimental Study on Evaporation of Kerosene Droplets at Elevated Pressures and Temperatures". Combustion Science and Technology, 178:9, 1669-1684,DOI: 10.1080/00102200600582392
[5] Yogendra, D., Raghavan, V., and Mehta, P.S., 2015 " EvaporationCharacterstics of Karanja Biodiesel and its Diesel Blends". Energy Sources, Part A: Recovery, Utilisation and Environmental Effects, 37:15, 1597-1605, DOI: 10.1080/15567036.2011.629279.
[6] Mikhil, S., Anand, T.N.C., Bakshi, S., 2016. "Experimental Studies on Single Droplet Evaporation of Urea Water Solution (UWS) at Elevated Temperatures". ILASS – Europe 2016, 27th Annual Conference on Liquid Atomization and Spray Systems, 4-7 September 2016, Brighton, UK.
[7] Subbarayan, M.R., SenthilKumaar, J.S., and AnanthaPadmanaban, M.R.,2016. "Experimental investigation of evaporation rate and exhaustemissions of diesel engine fuelled with cotton seed methyl ester and its blend with petro-diesel". Transportation Research Part D 48, 369–377.
[8] Liu, Y.C., Xu, Y., Avedisian, C.T., Hicks, M.C., 2015. "The effect of support fibers on micro-convection in droplet combustion experiments" Proceedings of the Combustion Institute 35, 1709–1716.
[9] Turns, S.R., Introduction to mass transfer An Introduction to Combustion 2nd ed., McGraw Hill Singapore pp. 83-98.

AIR POLLUTION, RESPIRATORY INFECTIONS AND INNATE IMMUNITY

Gangamma S.
Environmental immunology laboratory, National Institute of Technology Karnataka, Surathkal, India,
ganganitk@gmail.com

ABSTRACT

According to a World health organization report, acute lower respiratory infections associated with ambient air pollution exposure causes significant mortality among children under five years of age. Similarly, exposure to indoor biomass fuel burning smoke causes respiratory diseases, especially respiratory infections among children. Several studies in India have identified S. pneumoniae is the major cause of respiratory infections and is followed by H. Influenzae type b and Staphylococcus aureus. Innate immune defense is important during initial stages of bacterial infection in the lung. Signaling molecules such as TNFα and IL6 produced by macrophages plays an important role in host immune response. Our experiments have shown that human macrophages exposed to air pollution particles are unable to produce cytokines de novo and are anergic to subsequent endotoxin or bacterial challenge. In summary, air pollution exposure induces high basal inflammation and inhibits a robust response of macrophage or monocyte to respiratory pathogens.

Keywords:Air pollution, respiratory infections, inflammatory cytokines

.

According to a World health organization[1] report, acute lower respiratory infections (ALRI) associated with ambient air pollution exposure causes significant mortality among children under five years of age. Similarly, exposure to indoor biomass fuel burning smoke causes respiratory diseases, especially respiratory infections among children. Lower respiratory tract infection is one of the leading causes of death among children under five years of age in India[2]. Several studies in India have identified *S. pneumoniae* is the major cause of respiratory infections and is followed by *H. Influenzae* type b and S*taphylococcus aureus*[3]. Viral isolation from respiratory samples is a difficult process compared to isolation of bacteria and this lead to underestimation of viral contribution to respiratory infection. Viral infection was identified in 49% of pneumonia cases in children.[4] In many studies, respiratory syncytial virus is identified as the most common organism followed by influenza viruses, parainfluenza viruses and adenovirus [4,5].

Innate immune defense is important during initial stages of bacterial infection in the lung [6,7.]. Alveolar macrophages and recruited monocytes are the dominant immune cells during the initial stages of bacterial infection. Signaling molecules such as TNFα and IL6 produced by macrophages plays an important role in host immune response. Inhibition of TNFα by vaccination promotes growth and survival of pneumococci [8]. When the bacterial count increases in the host tissues, macrophage and monocytes must send a signal (TNFα and IL6) of sufficient clarity to overcome the normal quiescent tissue homeostasis. However, high basal expression of inflammatory mediators due to air pollution reduces the clarity and effectiveness (Figure 1) of the macrophage and monocytes signaling. In Figure 1, THP-1cells were differentiated with PMA and were stimulated with air pollution particles (PM) for 5hrs. The supernatant was separated and TNF-α and IL6 were measured with ELISA. Endotoxin was measured using kinetic LAL assay. Quantiles, q1, q2 and q3 represents endotoxin levels in lowest 1/3- quantile ($< 26.75 Eu/m^3$), endotoxin levels in middle 1/3 (between 26.75 and 47.67 Eu/m^3) and endotoxin levels in last 1/3 (> 47.67 Eu/m^3).We have shown that human macrophages exposed to PM are unable to produce cytokines *de novo* and are anergic to subsequent endotoxin or bacterial challenge (Figure 2). In Figure 2, monocytes were stimulated with PM extracts for 24hrs. Cells were washed and rested for 2hrs. The cells were again stimulated with LPS (Sigma, India. 10ng/ml) alone or with cyclohexamide (Himedia, India) for 24hrs. Total RNA were isolated from cells and IL6 and TNF-α were estimated using RT-PCR (Life technology, India). However, interferon-γ treatment reverses the anergic response of monocytes. We have also studied the expression of host genes associated with viral entry and fusion in lung epithelial cells. Our results show that PM exposure enhances expression of host viral entry genes. In summary, air pollution exposure induces high basal inflammation and inhibits a robust response[9] of macrophage or monocyte to respiratory pathogens.
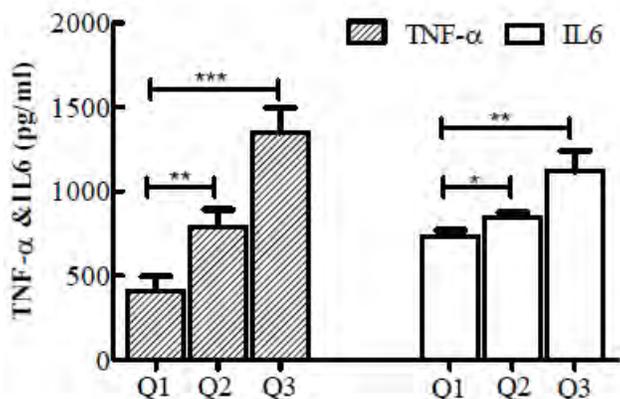
FIGURE 1. Airborne endotoxin levels influence TNF-α and IL6 production from differentiated THP-1 cells.
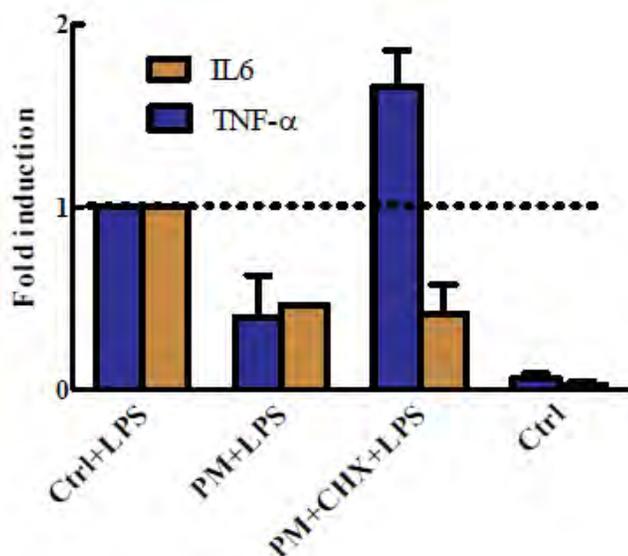
FIGURE 2. Cycloheximide treatment partially inhibits PM induced hypo-response (TNF-α) in peripheral monocytes.

REFERENCES

[1] WHO Ambient air pollution:2016."A global assessment of exposure and burden of disease". World Health Organization;2016.(www.who.int/iris/bitstream/ 10665 / 250141/1/9789241511353- eng.pdf accessed 08.11. 2016

[2] Bassani, D.G., Kumar, R., Awasthi, S., Morris, S.K., Paul, V.K., 2010. "The Million Death Study Collaborators: causes of neonatal and child mortality in India: a nationally representative mortality survey". Lancet.; 376,1853–60.

[3] Mathew, J., Singhi, S., Ray, P., Hagel, E., Saghafian-Hedengren, S., Bansal, A., Ygberg, S., Sodhi, K.S., Kumar, B.V., Nilsson, A.,2015. "Etiology of community acquired pneumonia among children in India: prospective, cohort study". J. Global Health 5, 1–9.

[4] Ruuskanen, O., Lahti, E., Jennings, L. C., Murdoch, D.R., 2011. "Viral pneumonia", Lancet: 6736 (10),61459-6

[5] McIntosh, K.., 2002. "Community acquired pneumonia in children", N Engl J Med, 346, 429-437

[6] Gangamma, S., 2012. "Airborne particulate matter and innate immunity activation". Environ. Sci. Technol. 46, 10879-10880.

[7] Gangamma, S., 2014. "Characteristics of airborne bacteria in Mumbai urban environment". Sci. Total Environ. 488-89, 70-74.

[8] van der Poll, T., Keogh, C.V., Buurman, W.A., Lowry, S.F., 1997. "Passive immunization against tumor necrosis factor-alpha impairs host defense during pneumococcal pneumonia in mice". Am J Respir Crit Care Med; 155, 603–08.

[9] Gangamma, S., Desai, S., Sowmiya, V., Seethalakshmi, V., Deepak, T.K., Vishnu Priya, D., Krishnaja, S., 2017. "Air Pollution and vulnerability to Respiratory infections: *InVitro* studies on particulate matter from Indian Cities". Am J. Respir. Crit. Care Med.;195, A6842

SEEC-2018-055

COMPARISON OF PERFORMANCE AND EMISSION CHARACTERISTICS OF DOUBLE CYLINDER FOUR STROKE CI ENGINE BETWEEN DIESEL AND NEEM BIODIESEL BLEND

Dr. S. S. Satputaley
Assistant Professor, Department of Mechanical Engineering,
St. Vincent Pallotti College of Engineering &
Technology, Nagpur, 441108 Maharashtra, India
Email: satputaley@gmail.com

Geo C John
Student, Department of Mechanical Engineering, St. Vincent
Pallotti College of Engineering &
Technology, Nagpur, 441108 Maharashtra, India
Email: geojohn411@gmail.com

Dr. Dhananjay B. Zodpe
Associate Professor, Department of Mechanical Engineering,
VNIT, Nagpur, 440010.
Maharashtra, India
Email: zodpedb@rediffmail.com

Bhoopendra Rajpoot
Student, Department of Mechanical Engineering, St. Vincent
Pallotti College of Engineering &
Technology, Nagpur, 441108 Maharashtra, India.
Email: bhoopendra12raj@gmail.com

Chetan Barapatre
Student, Department of Mechanical Engineering, St. Vincent
Pallotti College of Engineering &
Technology, Nagpur, 441108 Maharashtra, India
Email: cd12patre@gmail.com

Dr. N. V. Deshpande
Professor, Department of Mechanical Engineering, VNIT,
Nagpur, 440010.
Maharashtra, India
Email: nishu1952@yahoo.com

ABSTRACT

Due to increase in demand of alternative fuel in the recent years much research has been carried out to find the most worthy alternative fuel. Because of increased global warming activities and increased prices of fuels, the methyl ester of vegetable oil known as Biodiesel. It can be procured from vegetable oils (both edible and non-edible) and from animal fat [1].Biodiesel burns similar to that of pure diesel and also emitted less pollutants. Neem (Azadiractha indica) is one of the most proficient tree species. The seed of neem contain 30-40% oil and it has very high potential to be used as a biodiesel. This paper deals with performance and emission study on 10hp double cylinder CI engine using Neem biodiesel blend B20 and diesel fuel.

Keywords :- Biodiesel, Neem oil, Transesterification, emissions

1.0 INTRODUCTION

The prices of fuel are increase day after day in the world. So, ways and means have been sought for many years to be able to produce oil-substitute fuel. Biodiesel extracted from non-edible oil is one such renewable alternative under consideration [2]. Biodiesel (Greek, bio, life+ diesel from Rudolf Diesel) refers to a diesel-equivalent, processed fuel derived from biological sources.[3] Variety of oil rich trees are found in India such as Jatropha (Jatropha Curcus), Neem (Azadirachta Indica), Karanj, Palm, Mahua etc. where most of them are underutilized. Neem can grow in many different types of soil, but it thrives best on well drained deep and sandy soils. A mature Neem tree may produce 30-50 kg of fruit each year. By rough estimate India has nearly 20 million Neem trees. Indian Neem trees have a potentials to provide one million tonnes of fruits per year. Neem seeds yield 40-60% oil. Neem is a golden tree that has gained world-wide importance owing to its multiple uses. Besides agro forestry, it is used in pest control, toiletries, cosmetics, pharmaceuticals, plant and animal nutrition and energy generation [4].

2.0 BIODIESEL

The technical definition of biodiesel is "The mono alkyl esters of long chain fatty acids derived from renewable lipid feedstock such as edible or non-edible oils or animal

fats, for use in compression ignition (diesel) engines" (National Biodiesel Board, 1996). Biodiesel is made from virgin or used vegetable oils (both edible & non-edible and animal fats through transesterification and is a diesel substitute and requires very little or no engine modifications up to 20% blend and minor modification for higher percentage blends. The use of biodiesel results in substantial reduction of un-burnt hydrocarbons, carbon monoxide and particulate matters [5]. The edible, non-edible oils and animal fats used to produce biodiesel mainly have tricaylglycerol's TAGs chemically, TAG are classified as esters of fatty acids (FA) with glycerol (1-2-3-propanetriol). Now these TAG constitute of different FA (fatty acids) further each fatty acids attached to a glycerol. These FA present in TAG have different profiles or structures which further have an important role in deciding the physical and chemical properties of the FA which further influence the properties of corresponding animal fats, edible and non-edible oils [5].

2.1 NEEM OIL

Neem trees start bearing harvestable seeds within 3-5 years, and full production may be started in 10 years, and this will continue up to 150-200 years of age. A mature Neem tree may produce 30-50 kg of fruit each year. The fruit is a smooth (glabrous), olive-like drupe which varies in shape from elongate oval to nearly roundish, and when ripe is 1.4–2.8 centimeters (0.55–1.10 in) by 1.0–1.5 centimeters (0.39–0.59 in). The fruit skin (exocarp) is thin and the bitter-sweet pulp (mesocarp) is yellowish-white and very fibrous. The mesocarp is 0.3–0.5 centimeters (0.12–0.20 in) thick. The white, hard inner shell (endocarp) of the fruit encloses one, rarely two, or three, elongated seeds (kernels) having a brown seed coat as shown in figure 1.

FIGURE 1.NEEM FRUITS, NEEM KERNELS, NEEM KERNEL AFTER DRYING AND NEEM OIL

By rough estimate India has nearly 20 million Neem trees. Indian Neem trees have a potentials to provide one million tons of fruits per year and 0.1 million tons of kernels per years (assuming 10% kernel yield). Neem seeds yield 40-60% oil[7].

Making biodiesel, producing it on a large scale and using it to replace petro diesel is one among the most researched and anticipated developments of today[8].

2.2 NEEM BIODIESEL PRODUCTION

The most common method for biodiesel production is transesterification as shown in figure 2. It is also called alcoholysis which as the name suggests is the displacement of an alcohol from an ester by another alcohol i.e. basically conversion of one ester into other.

$$
\begin{array}{ccccc}
CH_2\text{-OOC-R1} & & R1\text{-COO-R} & & CH_2\text{-OH} \\
| & & | & & | \\
CH\text{-OOC-R2} + 3ROH & \underset{\text{Catalyst}}{\rightleftharpoons} & R2\text{-COO-R} & + & CH\text{-OH} \\
| & & | & & | \\
CH_2\text{-OOC-R3} & & R3\text{-COO-R} & & CH_2\text{-OH}
\end{array}
$$

Triglyceride   Alcohol   Alkyl Esters   Glycerol
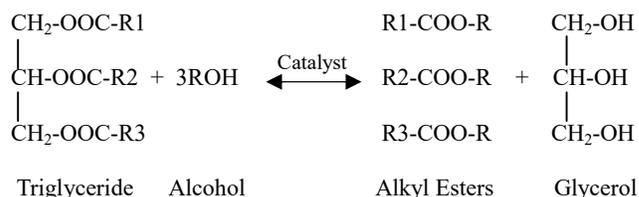
FIGURE 2.TRANSESTERIFICATION REACTION

In the process of transesterification a mixture of 100ml of neem oil and 25ml methanol is stirred and heated in the presence of 0.8gm of KOH as catalyst for one and a half hour at a temperature between 50 and 55°C. The obtained mixture of biodiesel and glycerol is kept for 8 to 10 hours to separate biodiesel and glycerol. The biodiesel (upper layer) is then separated from the raw glycerin (lower layer) by decantation. The crude biodiesel layer was needed to purify by washing with warm water. After the washing process, it was required to measure the pH of the biodiesel layer. When the pH of the biodiesel layer reached 7, the washing process was completed [6].

3.0 COMPARISON OF THE PROPERTIES OF NEEM BIODIESEL AND PURE DIESEL FUEL

The different physical and chemical properties of neem oil and neem biodiesel are tested in the chemistry lab of the institute using standard process of testing. The physical and chemical properties of neem biodiesel, diesel and ASTM biodiesel standards are compared and shown in Table 1.

Table 1: Properties of neem oil and its ester [9,10]

Properties	ASTM D-6751	Diesel	Neem oil	Neem biodiesel
Density (kg/m^3)	-	830	912–965	820–940
Viscosity at 40°C (cSt)	1.9-6.0	4.7	20.5–48.5	3.2–10.7
Calorific value(MJ/kg)	-	42	32–40	39.6–40.2
Flashpoint (°C)	>130	60	214	120
Cetane number	47 min	45	31–51	48–53

4.0 EXPERIMENTAL SETUP

The experimental investigation on performance and emission characteristics was carried out using a two cylinder four stroke water cooled CI engine make Mahinder Ltd., rated power of 10 BHP, at 1500 rpm. The experimental investigation was first carried out using diesel fuel and then using B20 and three sets of reading was obtained. The average of the three sets of reading is used to study the performance and emission characteristics of CI engine. The emitants HC, CO and CO2 was measured using calibrated AVL DIGAS 444 Exhaust gas analyser.

FIGURE 3. EXPERIMENTAL SETUP

1. U Tube Manometer, 2. Diesel Tank, 3. AVL Degas Analyser, 4. Air Chamber, 5. Fuel Burette, 6. Digital Temparature Measurement, 7. Rope Brake Dynamometer, 8. Brake Drum, 9. Calorimeter and 10. Exhaust Gas Pipe

5 RESULTAND DISCUSSION ON PERFORMANCE AND EMISSION CHARACHTERISTICS OF CI ENGINE USING NEEM BIODIESEL

With reference to the experiment carried out on CI engine using B20 blend of neem biodiesel and pure diesel is studied and compared in the paper. Some of the important parameters of CI engine based on performance and emission are discussed below.

5.1 BRAKE THERMAL EFFICIENCY (BTE):

Brake Thermal Efficiency is defined as break power of a heat engine as a function of the thermal input from the fuel. Based on experiment carried out, it can be observed that the break thermal efficiency using lower blends B20, is slightly higher as compared to diesel fuel for the Neem biodiesels as shown in figure 4. It is found that in the case of neem blend B20 the BTE is 35.04 which is higher than pure diesel fuel of BTE 34.08.
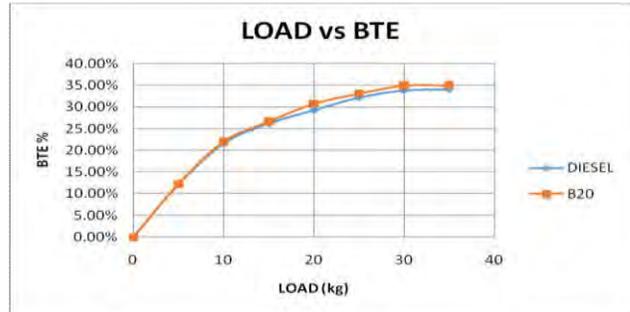
FIGURE 4. LOAD VERSES BRAKE THERMAL EFFICIENCY

5.2 BRAKE SPECIFIC FUEL CONSUMPTION (BSFC):

The properties of fuel such as the calorific value, density, and viscosity play a primary role in engine fuel consumption. From the data obtained, it is seen that the BSFC decreases with the B20 blend as compared to diesel as shown in figure 5, where B20 has 0.24 while diesel has 0.25.As load increases BSFC decreases as shown in graph.
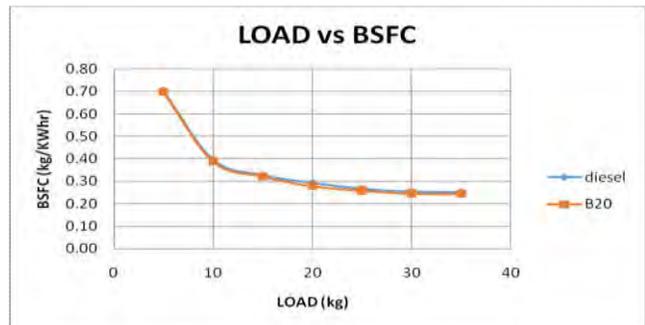
FIGURE 5. LOAD VERSES BRAKE SPECIFIC FUEL CNSUMPTION

5.3 HYDROCARBON (HC) EMISSION:

The values obtained from the experimentation shows that the HC emission reduces significantly on B20 blend as compared with diesel as shown in figure 6. The 20% neem biodiesel blend reduces HC emission by 9.87% which is due to higher oxygen content and Cetane number which reduces the ignition delay [11].
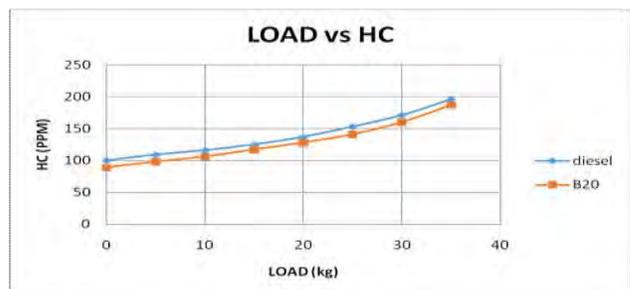
FIGURE 6. LOAD VERSES HYDROCARBON EMISSION

5.4 CARBON MONOXIDE EMISSION(CO):

The study on CO emission using B20 blends of neem and pure diesel show that the emission of CO of biodiesel is less a compared to the pure diesel fuel as shown in figure 7. It was observed that in neem blend of 20% the CO emission is 0.10% as compared to diesel fuel with CO emission of 0.18%. The biodiesel blended fuels provide lower CO emission than diesel fuel due to higher oxygen content and Cetane number [11].
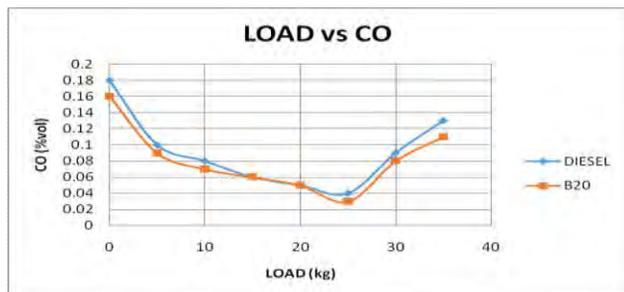

FIGURE 7. LOAD VERSES CARBON MONOXIDE EMISSION

5.5 CARBONDIOXIDE EMISSION (CO_2)

The study on CO_2 emission show that with B20 blend of neem biodiesel CO_2 emission is higher than pure diesel where B20 blend showsthat in neem blend of 20% the CO_2 emission 0.18% as compared to diesel fuel with CO_2 emission of 0.10%.The B20 blend of neem oil has higher CO_2 emission than diesel due to higher oxygen content.
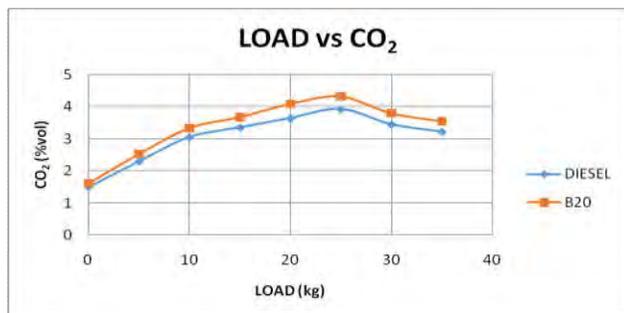
FIGURE 8. LOAD VERSES CARBON DIOXIDE EMISSION

6.0 CONCLUSION

The experiment on the performance and emission characterstics of double cylinder four stroke CI engine between diesel and neem biodiesel blend B20 is conducted and the following inferences are drawn.

➤ The brake thermal efficiency is seen to be slightly increasing for B20 blend of biodiesel.

➤ B20 blends shows decrease in BSFC than diesel fuel due to extra amount of oxygen present on the blend which is taking part in combustion process.

➤ B20 biodiesel blend exhibit lower HC emission compared to mineral diesel

➤ On B20 blends the amount of oxygen was sufficient for combustion of mixture leading to lower CO emission.Similar increasing pattern is observed for CO_2 emission as compared to CO emission.

From the above inferences, it can be stated that neem biodiesel blend B20 can be used as an alternative fuel for CI engine without any modification in present CI engines.

7.0 REFERENCES

[1] Wilson Parawira, "Biodiesel production from Jatropha curcas: A review" Scientific Research and Essays Vol. 5(14), pp. 1796-1808, 18 July, 2010

[2] Kywe, Tint Tint; Oo, Mya Mya, "Production of Biodiesel from Jatropha Oil (Jatropha curcas) in Pilot Plant", Proceedings of World Academy of Science: Engineering & Technology; Feb2009 Supplement, Vol. 50, p481, February 2009

[3] Hwai Chyuan Ong et.al. "Engine performance and emissions using Jatropha curcas, Ceiba pentandra and Calophyllum inophyllum biodiesel in a CI diesel engine", Elsevier, Energy 69 (2014) 427-445.

[4] Akshatha D.S, Manavendra.G, S.Kumarappa, "Performance evaluation of neem biodiesel on ci engine with diethyl ether as additive"International Journal of Innovative Research in Science, Engineering and Technology

[5] Kywe, Tint Tint; Oo, Mya Mya, "Production of Biodiesel from Jatropha Oil (Jatropha curcas) in Pilot Plant", Proceedings of World Academy of Science: Engineering & Technology; Feb2009 Supplement, Vol. 50, p481, February 2009

[6] Anindita Karmakar, Subrata Karmakar, Souti Mukherjee "Biodiesel production from neem towards feedstock diversification : Indian perspective", Renewable and Sustainable Energy Reviews 16 (2012) 1050 1060.

[7] Anindita Karmakar, Prasanta Kumar Biswas, Souti Mukherjee, "Environment-Congenial Biodiesel Production from Non-Edible Neem Oil.

[8] Hwai Chyuan Ong "Engine Performance and emissions using Jatropha curcas, Ceiba pentandra and Calophyllum inophyllum biodiesel in a CI diesel engine", Energy 69 (2014) 427-445

[9] A. Sanjid, "Production of palm and jatropha based biodiesel and investigation of palm-jatropha combined blend properties, performance, exhaust emission and noise in an unmodified diesel engine", Elsevier, journal of cleaner production 65 (2014) 295-303

[10] M.M. Rashed, M.A. Kalam, H.H. Masjuki, M. Mofijur, M.G. Rasul "Performance and emission characteristics of a diesel engine fueled engine with palm, jatropha, and moringa oil methyl ester", Elsevier, Industrial Crops and Products 79 (2016) 70–76.

Strain improvement of *Bacillus amyloliquefaciens* SS35 by UV and chemical mutagenesis for producing hyperactive mutant strain for improved β-glucanase and xylanase activities

*Shweta Singh and Arun Goyal

Carbohydrate Enzyme Biotechnology Laboratory, Department of Biosciences and Bioengineering, PAN-IIT DBT Center for Bioenergy, Department of Biosciences and Bioengineering Indian Institute of Technology Guwahati, Guwahati-781039, Assam, India

Corresponding author: E. mail: shweta.2014@iitg.ernet.in

The research on development of bioethanol is getting most attention worldwide mainly due to continuous depletion of fossil fuels and environmental pollution caused by them. The saccharification of lignocellulosic biomass by enzymes such as cellulases and hemicellulases for release of reducing sugars for their subsequent microbial conversion to bioethanol is the cost limiting step. Therefore, for reducing the cost of bioethanol production the strain improvement of cellulase producing microorganisms is of prime concern. The aim of present study was to improve the carboxymethyl cellulase activity from isolate *Bacillus amyloliquefaciens* SS35 [1] by UV and chemical (ethyl methane sulphonate) mutagenesis for efficient hydrolysis of the cellulosic biomass. The culture at 10^{-4} dilution was spread plated and exposed to UV light frequency at 0.6 J/cm^2 for 5s to 3h using direct plate irradiation method. The lethality rate 98.9% at 3h was obtained. 14 mutant colonies were qualitatively screened by 0.3% congo red. Out of 14, 4 UV mutant colonies showed increase in carboxymethyl cellulase activity grown in medium as described earlier [2] under batch fermentation at 40°C and 120 rpm for 48 h. Out of 4, the UV mutant colony no. 2 (UV2), as cell free supernatant gave specific activity (0.24 U/mg) against carboxymethyl cellulose which was 16.5% higher than the wild-type strain enzyme (0.206 U/mg). The enzyme from UV2 after partial purification by 90% ammonium sulphate saturation showed 1.9 (β-glucan), 2.3 (carboxymethyl cellulose) and 1.8 (Birchwood xylan) fold increase in β-glucanase, carboxymethyl cellulase and xylanase activities, respectively. UV2 was further subjected to chemical mutagenesis with ethyl methane sulphonate (EMS). At 2% EMS a lethality rate of 99.97% was obtained for UV2. 14 mutant colonies were qualitatively screened by 0.3% congo red. Two EMS mutant colonies out of 14, showed increase in carboxymethyl cellulase activity when grown in the medium as described earlier [2] under batch fermentation at 40°C and 120 rpm for 48 h. Out of 2, EMS mutant the colony no. 7, as cell free supernatant gave specific activity 0.26 U/mg against carboxymethyl cellulose which was 26% higher than the wild-type strain enzyme and 8% higher than that of UV2. The results on purification of enzyme from EMS mutant strain will be presented.

References

1. Singh, S., Moholkar, V. S. & Goyal, A. (2013) Isolation, identification, and characterization of a cellulolytic *Bacillus amyloliquefaciens* strain SS35 from Rhinoceros dung. *ISRN Microbiology*, 2013, Article ID 728134.

2. Singh, S., Moholkar, V. S. & Goyal, A. (2014) Optimization of carboxymethylcellulase production from *Bacillus amyloliquefaciens* SS35. *Biotech*, 4(4), 411-424.

AN EXPERIMENTAL INVESTIGATION OF NON-EDIBLE *PRUNUS ARMENIACA* (BITTER APRICOT) OIL BASED BIODIESEL FUELED IN CI ENGINE

Deepak Singh
Department of mechanical engineering
Dr. B R Amdekar NIT, Jalandhar

Email: deepmech777@gmail.com

S S Sandhu
Department of mechanical engineering
Dr. B R Amdekar NIT, Jalandhar

Email: sandhuss@nitj.ac.in

A K Sarma
Chemical conversion divsion
SSS - National Institute of Bio-energy, Kapurthala

Email: draksarma@gmail.com

ABSTRACT

Bio-fuels have been proven to be best alternative for the petroleum products due to its similar properties and renewablity. This work explorers the combustion, performance and emission characteristics of CI engine fueled with biodiesel produced from non-edible prunus armeniaca oil. The biodiesel has been produced by the process of transesterification with a new source of bitter apricot oil obtained from Himachal Pradesh, India. Further, Apricot methyl ester blends (AB10, AB20 and AB30) were investigated in CI engine to analyze its behavior. The experiment results shown that AB20 blend produces higher BTE with lower BSFC. As far as emission results are concerned, CO and UHC were reduced, but at higher load increase in NOx level was observed. The shorter ignition delay and higher cetane index of apricot biodiesel made peaks of cylinder pressure and HRR near to TDC.

Keywords: Apricot, biodiesel, fuel properties, combustion, performance, emission.

NOMENCLATURE
BTE- Brake thermal efficiency
BSFC- Brake specific fuel consumption
EGT- Exhaust gase temperature
CO- Carbon monoxide
UHC- Unburnt hybrocarbon
NOx- Oxides of nitrogen
CP- Cylinder pressure
HRR- heat release rate

INTRODUCTION

In the recent years, energy scarcity, hiking prices of petroleum products and stringent emission protocol encouraging the researchers to find out the replacement of fossil fuels [1][2]. In this context, straight vegetable oils are directly used as fuel in CI engine, but the higher kinematic viscosity, molecular weight and density lead to improper combustion inside the cylinder. As a result, engine parts get damaged after long run. So, many possibilities have been tried to reduce the kinematic viscosity and density of the vegetables oils like: dilution, pyrolysis and transesterification [3]. The transesterification process found to be best method for reduction of kinematic viscoty and density. In this process, the vegetable oil is reacted with alchoal in the presence of strong base catalyst like NaOH, KOH, sodium metal etc. to produce ester and glycerol. This esters is also known as biodiesel. The properties of the biodiesel are very close to properties of the petro-diesel. So, it can be used either directly or blended with diesel (B10, B20 and B30) to run the CI engine.

Many researchers reported that biodiesel fueled in CI engine improves engine performance and reduced exhaust emission like CO_2, CO, HC and Smoke. Further, many researchers used different feedstock (soyabean, sunflower, rapeseed, etc) to produced biodiesel [4][5]. In country like India where edible oils are not sufficient for consumption, so it is necessary to produce biodiesel from non-edible oil (kranja, Jatropha, mesoferia, etc)[6][7].

Keeping these things in mind, prunus armeniaca (non-edible) oil was used for the production of biodiesel. The properties of the obtained biodiesel have been measured as

per ASTM/EN standards. The biodiesel blends have been fueled in CI engine to know the effects on engine applications.

MATERIAL AND METHODS

In this study, non-edieble bitter apricot oil was collected from kullu-manali, Himcahal pardesh, India. The FFA of apricot oil was less than 5%, So one step transesterification process was used for the production of biodiesel.

EXPERIMENTAL METHODOLOGY

The detailed specifications of the CI engine shown in the Tab. 1. The engine is operated with varying load (0, 20, 40, 60, 80 and 100 % of full load) at a constant speed of 1500 rpm. The performance, combustion and emission characteristics of apricot biodiesel (AB100) and its blends (AB10, AB20 and AB30 were evaluated and compared with baseline diesel fuel or vice-versa. AVL DI 444 gas analyzer was used to measure the exhaust emission (CO, UHC and NOx).

Table 1. Engine specification

Maker	Kirloskar
Model	TV1
Type	Four Stroke, Water Cooled, Diesel Engine
Number of Cylinder	Single cylinder
Bore and Stroke	87.05 mm × 110 mm
Compression Ratio	17.5:1
Cubic Capacity	661
Rated Power	3.8 kW @ 1500rpm
Orifice Diameter	20mm
Inlet Valve Opens	4.5° before TDC
Inlet Valve Closes	35.5° after BDC
Exhaust Valve Opens	35.5° before BDC
Exhaust Valve Closes	4.5° after TDC
Fuel Injection	200 bar, 23° before TDC

RESULTS AND DISCUSSIONS

COMPATIBILITY OF BIODIESEL

There are some basic essential properties of biodiesel and its blends were measured as per ASTM/EN standards for the proper running of CI engine as shown in Table 1. The density and kinematic viscosity of apricot biodiesel and its blends are equivalent to diesel. The apricot biodiesel has higher cetane index as compared to diesel. Further, the flash point of biodiesel diesel is higher than diesel which indicates safe handling.

Table 2. Properties of the produced biodiesel and its blends

Properties	Diesel	AB100	AB10	AB20	AB30
Density kg/m3	850	880	853	856	859
Kinematic Viscosity (cSt)	2.6	4.9	2.83	3.06	3.29
Flash Point	65	115	70	77	85
Calorific value MJ/kg	42	39.95	41.79	41.59	41.38
Cetane Index	46	54	46.5	47.5	49

ENGINE COMBUSTION

In this section, combustion characteristics has been studied. The maximum heat release was extracted at 80 % load. So, this load was selected for the combustion characteristics in terms of cylinder pressure and heat release rate.
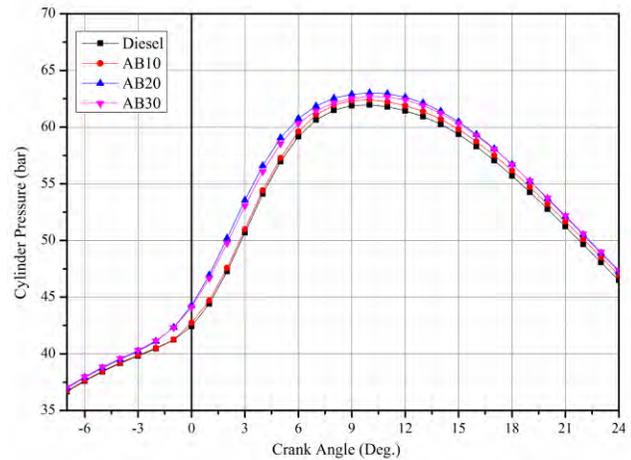
FIGURE 1. Cylinder pressure vs. Crank angle
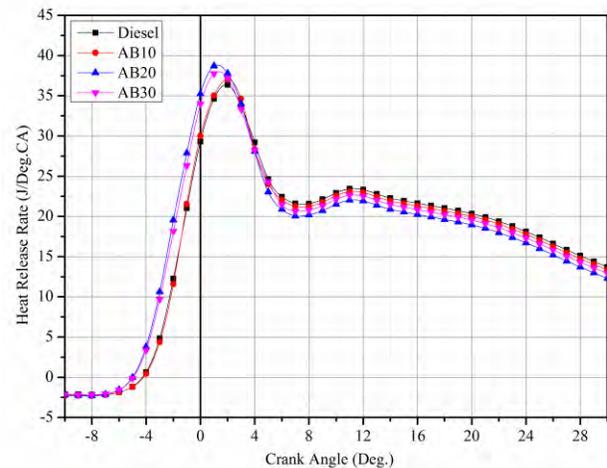
FIGURE 2. Heat release rate vs. Crank angle

Fig. 1 shows the cylinder pressure vs. crank angle at 80% load. Biodiesel blends have higher peaks of cylinder pressure as compared to diesel. Thus, more pressure energy can be converted into mechanical energy. Further, AB20 has highest peak of cylinder pressure as compared to diesel and other tested fuel. It is mainly due to biodiesel blends has higher cetane index and oxygen content which leads to ehance the combustion process.

Fig. 2 shows the heat release rate vs. crank angle at 80% load. It can be clearly observed that biodiesel blends have shorter ignition delay. It is mainly due to higher cetane index. As a result, the peaks of HRR are near to TDC. Thus, more conversion of energy taken placed in biodiesel blends.

ENGINE PERFORMANCE

In this section, engine performance chracteristics in terms of BTE, BSFC and EGT were evaluated.

Fig. 3 shows BTE vs. engine load. It can be clearly seen from the Fig. 3 that BTE increases as the load increases. Biodiesel and its blends have higher BTE as compared to diesel. AB20 has higher BTE among all the blends. This is mainly due to higher oxygen content and cetane index which improves the combustion quality. As discussed earlier, AB20 has higher peak of cylinder and HRR which also reflects the higher brake power output.
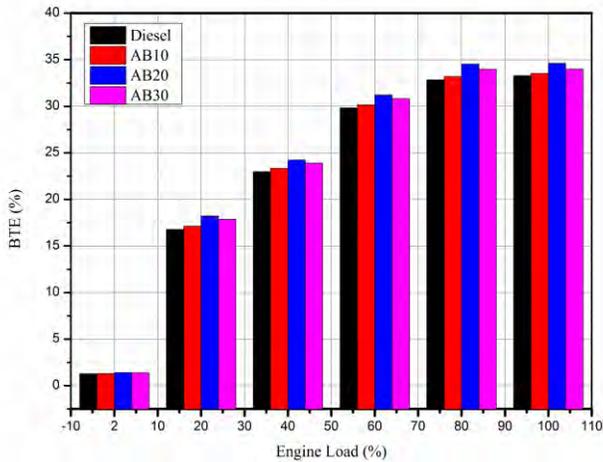
FIGURE 3. BTE vs. Engine load.

Fig. 4 shows the BSFC vs. engine load. It can be clearly seen from Fig.4 that BSFC decreases as the load increases. Biodiesel and blends have slight higher BSFC as compared to diesel. This is mainly due to low calorific value of biodiesel and its blends.

Fig. 5 represents EGT vs. engine load. It can be clearly seen from Fig 5. that biodiesel blends have lower EGT as compared to diesel which indicated that very less useful energy left at tail end. It is also supported from HRR peaks that reflected more heat energy conversion taken placed in biodiesel blends.
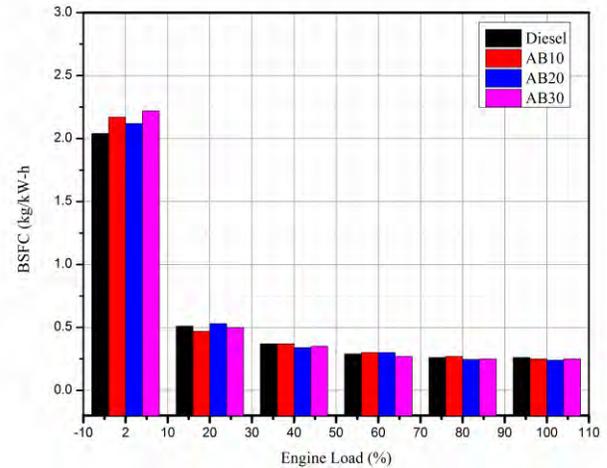
FIGURE 4. BSFC vs. Engine load
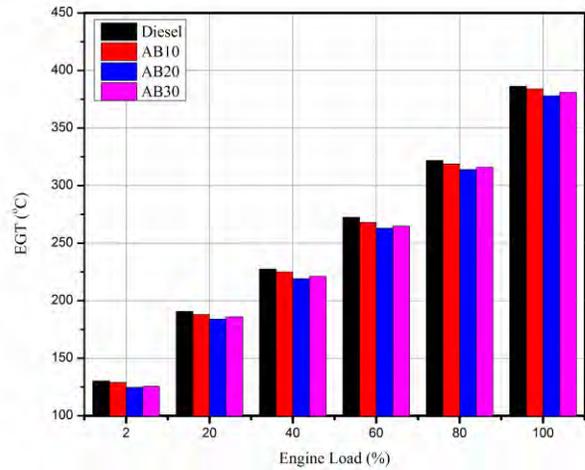
FIGURE 5. EGT vs. Engine load

ENGINE EMISSIONS

In this section, engine emission chracteristics in terms of CO, UHC and NOx were evaluated.

Fig. 6 represents the carbon monoxide w.r.to engine load. CO emission decreases as load on the engine increases. Biodiesel and its blends has lower CO emission as compared to diesel. AB20 shown the lowest CO emissions. It is mainly due to complete combustion taken placed inside the cylinder. Moreover, oxygen content and higher cetane index of biodiesel also enhance the combustion process.

Fig. 7 represents the hydrocarbon w.r.to engine load. It can be observed that HC emission decreases as the engine load increases. Biodiesel and its blends have lower UHC as compared to diesel. This is mainly due to complete combustion taken place inside the cylinder as discussed earlier. Further, AB20 blend has shown lower UHC emission
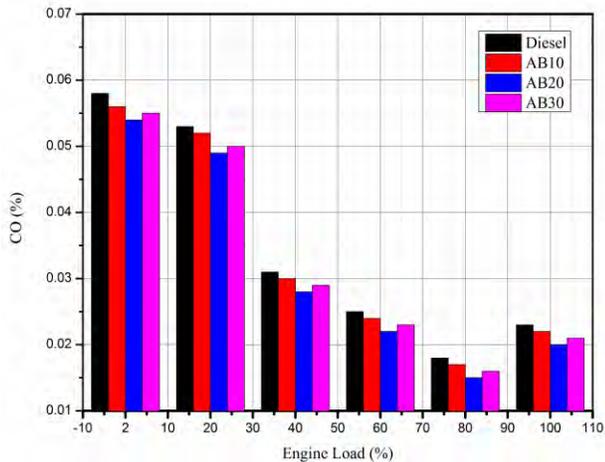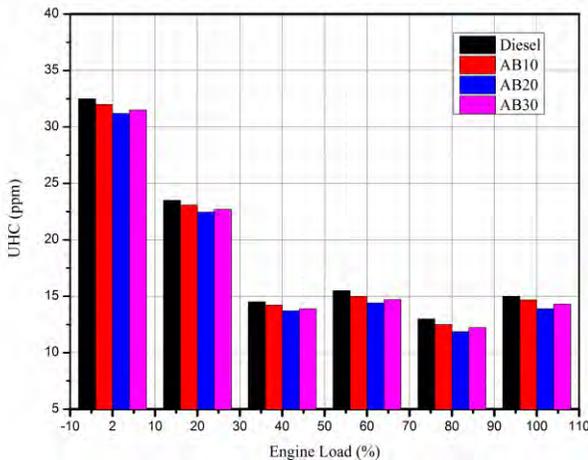
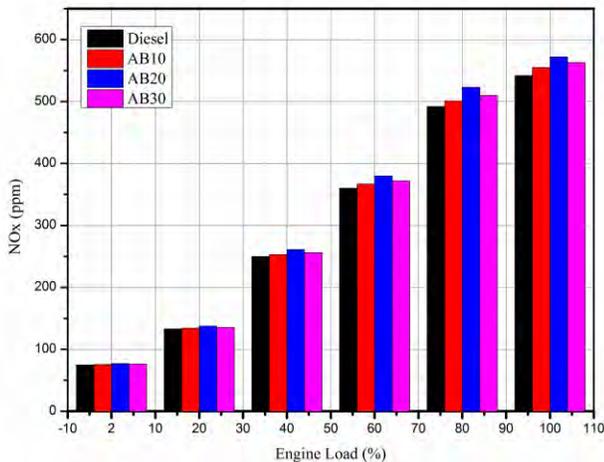**FIGURE 6.** CO vs. engine load

FIGURE 7. UHC vs. engine load

FIGURE 8. Oxide of nitrogen vs. engine load

Fig 8. represents the NOx w.r.to engine load. It has been obseved that NOx increases as engine load increases. Biodiesel and its blends have higher NOx level as compared to diesel. AB20 has the highest NOx level.

This is mainly due to higher oxygen content and higer cetane index of biodiesel that lead to complete combustion.

CONCLUSION

Prunus armeniaca (bitter apricot) oil is suitable for converting into methyl esters (biodiesel). The properties of the apricot biodiesel are found very close to petro-diesel. Further, the engine characteristics showed that apricot biodiesel blends improved BTE with low BSFC. The exhaust emissions (CO and UHC) were reduced, but higher NOx level was observed. It was concluded that AB20 blend found to be most effective blend among all the tested fuels.

ACKNOWLEDGEMENT

REFERENCES

[1]   E. Sadeghinezhad, S. N. Kazi, A. Badarudin, C. S. Oon, M. N. M. Zubir, and M. Mehrali, 'A comprehensive review of bio-diesel as alternative fuel for compression ignition engines', *Renew. Sustain. Energy Rev.*, vol. 28, pp. 410–424, 2013.

[2]   M. Ozcanli, C. Gungor, and K. Aydin, 'Biodiesel Fuel Specifications : A Review', *Energy Sources*, vol. 7036, no. March, pp. 37–41, 2013.

[3]   T. Ito, Y. Sakurai, Y. Kakuta, M. Sugano, and K. Hirano, 'Biodiesel production from waste animal fats using pyrolysis method', *Fuel Process. Technol.*, vol. 94, no. 1, pp. 47–52, 2012.

[4]   O. Özener, L. Yüksek, A. T. Ergenç, and M. Özkan, 'Effects of soybean biodiesel on a DI diesel engine performance, emission and combustion characteristics', *Fuel*, vol. 115, pp. 875–883, 2014.

[5]   M. Canakci, A. N. Ozsezen, and A. Turkcan, 'Combustion analysis of preheated crude sunflower oil in an IDI diesel engine', *Biomass and Bioenergy*, vol. 33, no. 5, pp. 760–767, 2009.

[6]   A. K. Agarwal and A. Dhar, 'Experimental investigations of performance, emission and combustion characteristics of Karanja oil blends fuelled DICI engine', *Renew. Energy*, vol. 52, pp. 283–291, 2013.

[7]   M. Mofijur, H. H. Masjuki, M. A. Kalam, M. A. Hazrat, A. M. Liaquat, M. Shahabuddin, and M. Varman, 'Prospects of biodiesel from Jatropha in Malaysia', *Renew. Sustain. Energy Rev.*, vol. 16, no. 7, pp. 5007–5020, 2012.

SEEC-2018-058

EFFECT OF VARYING SPEED AND LOAD ON PERFORMANCE AND EMISSION CHARACTERISTICS OF MULTI-CYLINDER COMPRESSION IGNITION ENGINE FUELED WITH DIESEL/ARGEMONE MAXICANA BIODIESEL BLENDS

Mandeep Singh
Mechanical Department/National Institute of
Technology Jalandhar
Email: mandeepsingh.nitj@gmail.com

Sarbjot Singh Sandhu
Mechanical Department /National Institute of
Technology Jalandhar
Email:sandhuss@nitj.ac.in

ABSTRACT

In this study, the performance and emission characteristics of diesel engine fueled with diesel/argemone biodiesel blends have been evaluated. An experiment was conducted on an indirect injection (IDI) compression ignition (CI) engine using diesel and diesel/argemone biodiesel blends. The result shows that with an increase in Argemone biodiesel blend ratio (up to B30) the performance characteristics such as brake thermal efficiency, brake specific fuel consumption get improved and result in significant reductions in CO and HC emissions. However, an increase in CO_2 and NOx emissions was observed for all biodiesel blends. The blends showed deterioration in brake thermal efficiency and brake specific fuel consumption at partial loads and high speed.

Keywords: Indirect injection, Performance, Emission, Argemone biodiesel
.

NOMENCLATURE

B10 10% biodiesel blended with 90% diesel
B20 20% biodiesel blended with 80% diesel
B30 30% biodiesel blended with 70% diesel
B40 40% biodiesel blended with 60% diesel
BTE Brake thermal efficiency
BSFC Brake specific fuel consumption
IDI Indirect Injection
CI Compression ignition
AOME Argemone oil methyl ester.
DI Direct injection
HC Hydrocarbon
CO Carbon monoxide
CO2 Carbon dioxide
NOx Oxides of Nitrogen
ppm Parts per million
rpm Revolution per minute

FFA Free fatty acid

INTRODUCTION

Energy transformation is the power muscle which has kept the human civilization transforming and evolving. Current era utilizes fossil fuels, coal and natural gas for transformation of energy. As these sources are non-renewable, their utilization can create serious energy security problems [1]. Also, it has been estimated by many studies that end of fossil fuel era is not so far [2]. Combustion of fuel-air mixture inside combustion chamber emits various acidic oxides of Sulphur, nitrogen and carbon. These oxides when react with water results in acid rain impacting both natural areas and built environment. These acids dissolve carbonates from monuments and sculptures made up of marble and limestone. In the developing countries like India, there are many places (Delhi, Patna, Gwalior, Raipur, Ahmedabad, Lucknow etc.) that are in the list of world's top polluted cities [3]. Though the government has taken many initiatives to control the pollution level, even than not able to attain desired targets. Therefore, to address energy-environment issues; biofuels are constantly tried by researches as a fuel in internal combustion engines.

Most of the previous investigations show that biodiesel blending (up to a certain extent) improves the combustion process resulting in higher brake thermal efficiency and reduced brake specific fuel consumption [4]. It also results in a reduction of emissions such as CO, HC, PM and SO_2 [5]. However, the increase in CO2 and NOx emissions were observed by Lin(2007) [6] due to a 10-11% increase in oxygen content that leads to complete combustion and conversion of CO to CO2 thereby increasing the cylinder temperature, resulting in higher NOx emissions. However, it is believed thatfuels having higher viscosity than diesel (such as biodiesels)show good result in IDI engines as

compared to DI engines.This is due to the cumulative effect of two factors. First, mixingof oil and air is better due to turbulence in the pre-combustionchamber. Second, NOx formation is reduced as less air isavailable in the secondary combustion chamber and the temperature of the main cylinder is also less as compared to a DI engine [7].

Argemone Maxicana oil (toxic and adulterer to mustard oil) is a non-edible oil having low free fatty acid content and is easily available in India. But there has been no comprehensive study on the performance and emission characteristics of Argemone oil methyl ester (AOME) in any multicylinder IDI engine. In the previous studies, limited experimentation has been carried out with AOME. The results show significant improvement in performance and emission characteristics [8]. In this study, biodiesel was produced from crude argemone maxicana oil by transesterification. This study aims to investigate the properties of biodiesel/diesel and performance and emission characteristics of a multicylinder IDI engine operating on biodiesel–diesel blends and comparing these results with diesel.

T1	Cooling water inlet temp to engine	F2	Air Consumption
T2	Cooling water outlet temp to engine	F3	Engine water flow
T3	Calorimeter Inlet water temp	F4	Calorimeter water flow
T4	Calorimeter Outlet water temp	Wt	Load Sensor
T5	Exhaust gas Temperature before Calorimeter	P	Cylinder pressure and injection pressure sensor
T6	Exhaust gas Temperature after Calorimeter	N	Speed Sensor
F1	Fuel consumption	R1/ R2	Rotameter for flow of water in engine and exhaust gas calorimeter.
DAQ	Data acquisition system		

FIGURE 1. SCHEMATIC DIADRAM OF ENGINE

2. Experimental setup and methodology

The experiment was performed on a four cylinder, four stroke, variable speed indirect injection (IDI) compression ignition (CI) engine. A schematic diagram of engine test bed is shown in figure 1 and the detailed engine specifications are listed in table 1. The engine was loaded with SAJ make AG80 eddy current type of dynamometer.

The setup has a stand-alone panel box consisting of air box, fuel tank, manometer, fuel measuring unit, transmitters for air and fuel flow measurements. The air flow rate was measured with orifice meter and manometer, pressure transmitter and the fuel consumption rate was measured with glass fuel metering column and DP transmitter (Range 0-500 mm water column). Type K-Chromel (Nickel-Chromium / Nickel-Alumel) were used to measure gas temperature at engine exhaust, calorimeter exhaust, water inlet of calorimeter, water outlet of calorimeter and ambient temperature. The signals were interfaced with a computer through data acquisition system

TABLE 1. ENGINE SPECIFICATION

Make	Tata Engineering Ltd
Model	Tata Indica
Details	4-Cylinder, 4-stroke IDI
Bore and Stroke	75 mm × 79.5 mm
Comprerssion ratio	18.5:1
Cubic capacity	1405
Rated power	52 KW @ 4000 rpm
Max torque	122.5 Nm @ 2500 rpm
Orifice diameter	48 mm
Cooling	Water
Speed type	Variable

(DAQ). Exhaust emissions like CO, CO2, HC and NOx were measured with the AVL 4000 Di-gas analyzer. The detailed specifications of gas analyzer are shown in the table 2. The basic properties of tested fuels such as Kinematic viscosity, density and calorific value were

TABLE 2. SPECIFICATIONS OF EMISSION ANALYZER

AVL DiGas 4000	Measurement range	Resolution
CO	0-10% Vol	0.01% Vol
HC	0-20,000 ppm	1 ppm
NOx	0-5,000 ppm	1 ppm

measured with Ostwald viscometer, automatic density meter and bomb calorimeter respectively.

Range of engine was studied to make an appropriate combination of load and speed (figure 2). To conduct the
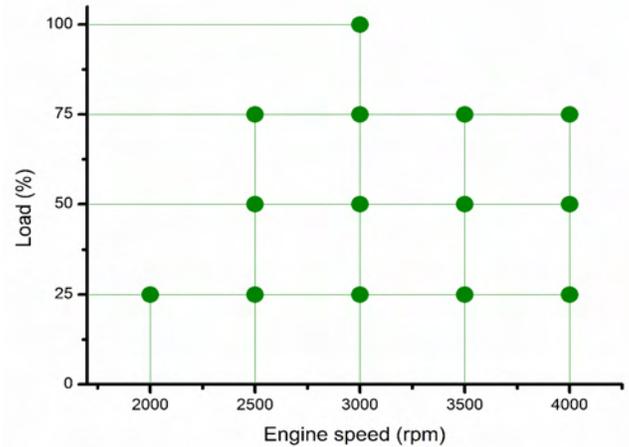
FIGURE 2. ENGINE RANGE CALCULATIONS

investigation engine was gradually throttled from 2000 to 4000 rpm (at an interval of 500) under four different conditions (i) No load (ii) 25% load (iii) 50% load (iv)
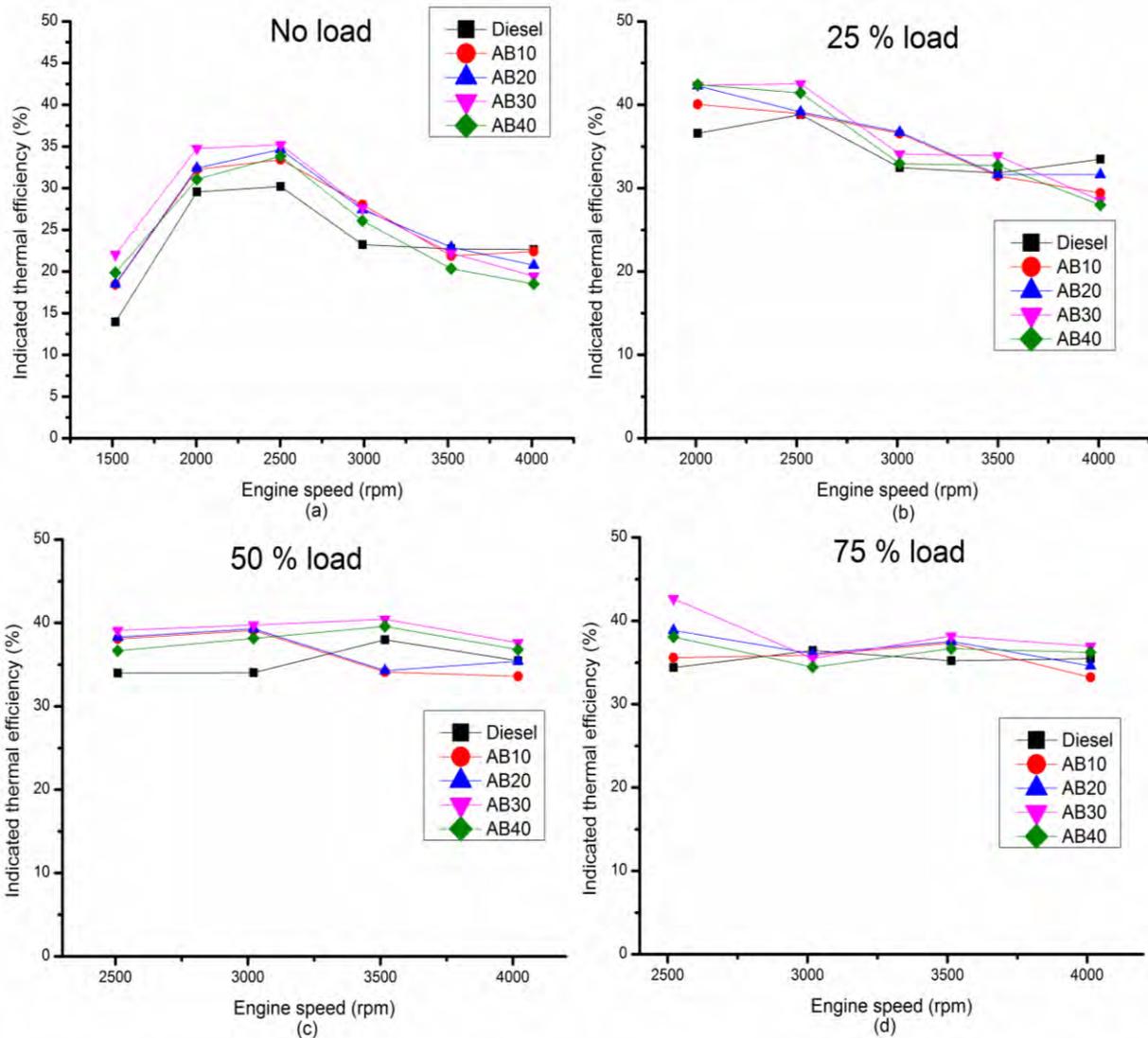
FIGURE 3. INDICATED THERMAL EFFICIENCY

352

75% load. The operation of engine was limited to 75% load condition as engine could not be loaded at 100% load beyond 3000 rpm. During experimentation, all the temperatures (T1, T2, T3, T4, T5 and T6) were allowed to stabilize before logging the data in "Engine soft". Each fuel sample was tested three times in an engine and mean values were used for analysis.

3. Experimental Results and discussion

Based on the experimental results the effect of diesel/AOME blends on engine performance (thermal efficiency, specific fuel consumption and indicated mean effective pressure) and emission (NOx, CO_2, CO and HC) characteristics are analysed in this section. In addition to this, comparison of various properties of AOME and its blends with diesel are also discussed.

3.1 Fuel properties

The various physicochemical properties of AOME and blends of AOME/diesel have been shown in table . It was found that blends of AOME/diesel have slightly lower calorific value as compared to diesel. This is expected as

biodiesel consists of long chain alkyl esters. The density and viscosity of AOME blends is also higher when compared with diesel. High density means- for the same volume, more energy content is available. Therefore, lower heating value of AOME can be compensated up to some extent by high density. The biodiesel blends used in the experimentation had a viscosity in conformance with ASTM standards.

3.2 Performance and emission characteristics

3.2.1 Indicated Thermal efficiency

In this study, it was observed that, with the increase in biodiesel blends up to AB30, ITE increases [Figure 3(a-d)], except at lower loads (no load & 25% load) and high speed (3500-4000). This increase in ITE is the result of extra oxygen present in biodiesel blends that helps in combustion. Another reason could be due to increased lubricity of biodiesel blends [9]. With higher blends (AB40), the thermal efficiency trend was reversed which could be due to decreased heating value of fuel and thus increase in fuel consumption.
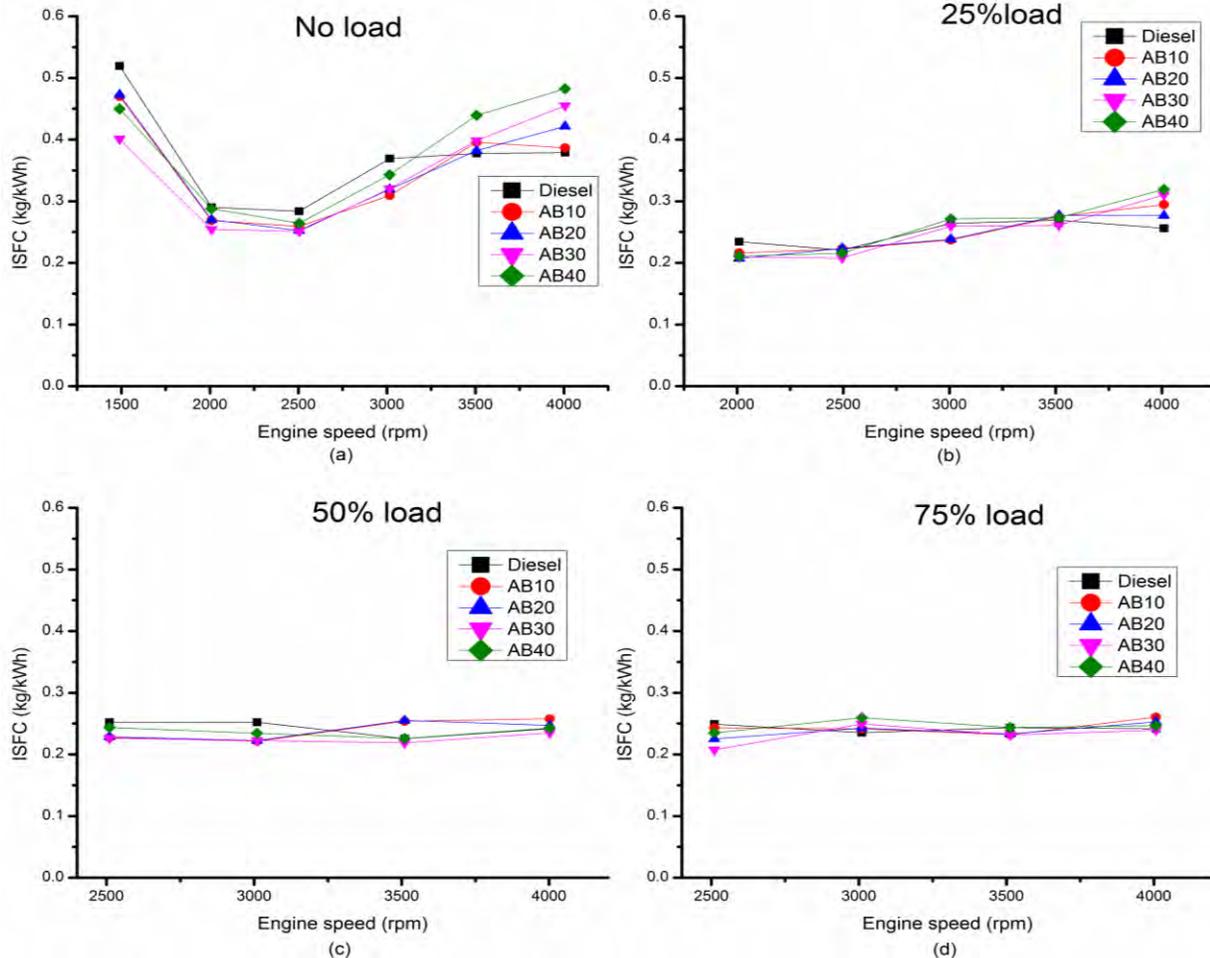
FIGURE 3. INDICATED SPECIFIC FUEL CONSUMPTION

TABLE 3. PROPERTIES OF DIESEL/ARGEMONE BIODIESEL BLENDS

Property	Diesel	AB10	AB20	AB30	AB40	AB100	ASTM Std
Density 15 ° C (Kg/m^3)	820	824.5	829	833.5	838	865	-
Calorific value (MJ/Kg)	42	41.57	41.14	40.71	40.2	37.5	-
Viscosity 40 °C (c St)	3.55	3.907	4.264	4.621	4.978	6.54	1.9-6
Flash point	56	69.7	83.4	97.1	110.8	193	130 min
Copper strip corrosion test	-	Passed	Passed	Passed	Passed	Passed	-

3.2.2 Specific fuel consumption

Specific fuel consumption is an important parameter, to observe how efficiently the fuel is being utilized in an engine to produce useful work [10]. The present work (Figure 4) shows that ISFC decreases with an increase in
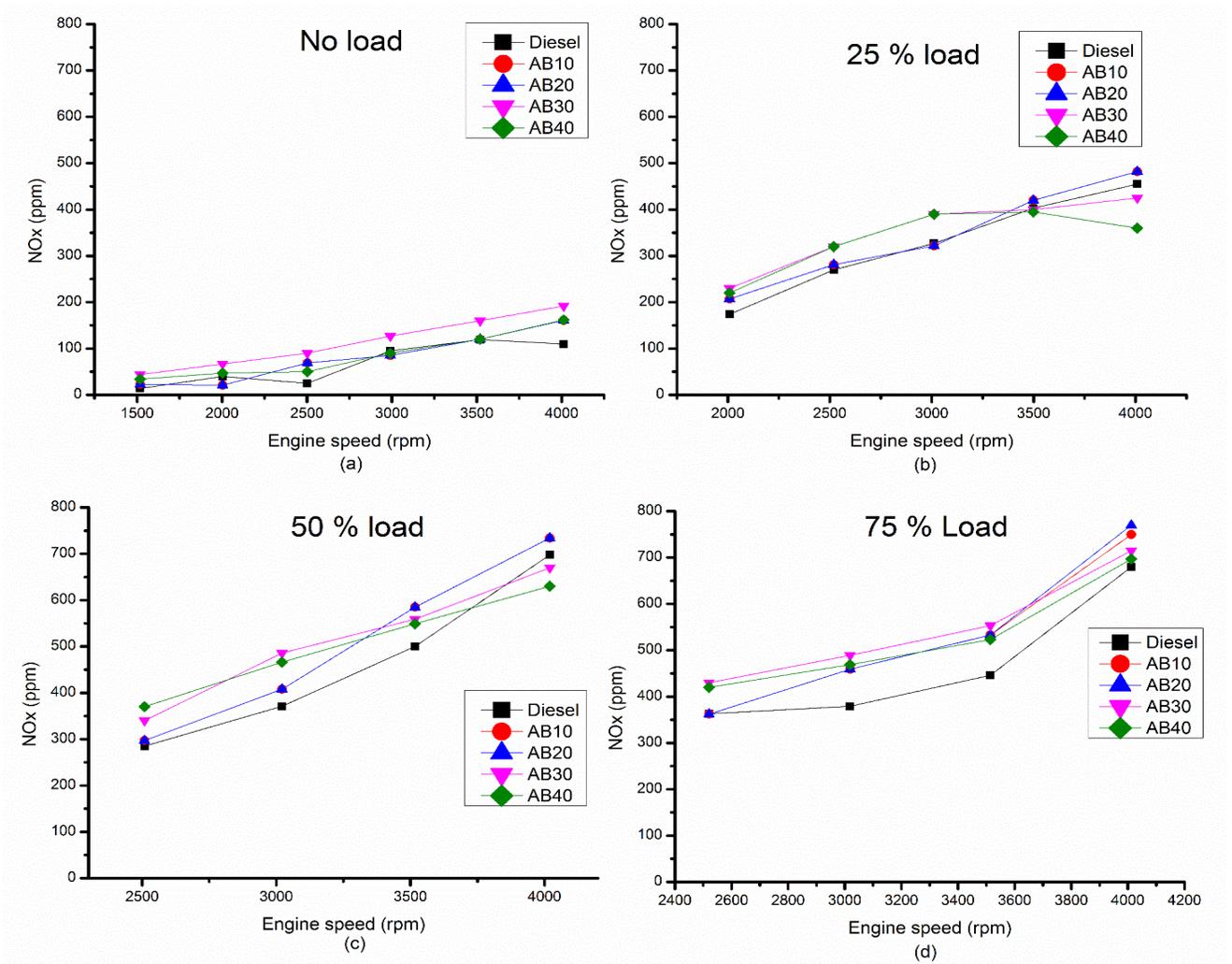
FIGURE 5. NO$_X$ VARIATION OF VARIOUS BLENDS WITH DIFFERENT ENGINE LOAD AND SPEED (RPM)

biodiesel blend ratio up to 30%; thereafter an increase is observed. In general, it is believed that for conventional diesel fuel, specific fuel consumption is inversely proportional to the heating value of hydrocarbon fuel [11]. However, though biodiesel and its blends have lower calorific value than conventional diesel, even then they show lower specific fuel consumption. This is attributed to higher oxygen content, in the chemical structure of Methyl esters (Biodiesel) [12]. As a result, AB 30 shows minimum ISFC at almost all the observation points. However, this increased oxygen content is only beneficial to some extent, as higher oxygen content results in reduction in calorific value. Therefore, AB40 (CV lower than AB30) shows higher ISFC as compared to AB30.

3.2.3 Nitrogen Oxide

Figure 5 (a-d) shows NOx emission (ppm and g/kWh) for diesel and various blends of diesel/argemone biodiesel.

Literature shows an increase in NOx emissions with biodiesel as a fuel [13,14]. The reason mentioned is the presence of oxygen and higher cetane number which leads to higher NOx levels. The present work also shows the correlation between NOx emission and increasing fraction of biodiesel in diesel. AB30 shows maximum NO_x emission (Figure 5(a-d)) as compared to diesel and other diesel/AOME blends. High density and more oxygen content are the probable reason for this increase in NOx. Higher density of biodiesel blends results in larger mass flow rate for the same volume of fuel and more oxygen is responsible for complete combustion that results in high in-cylinder temperature.

3.2.4 Carbon monoxide

CO formation is the result of incomplete combustion of HC fuels.
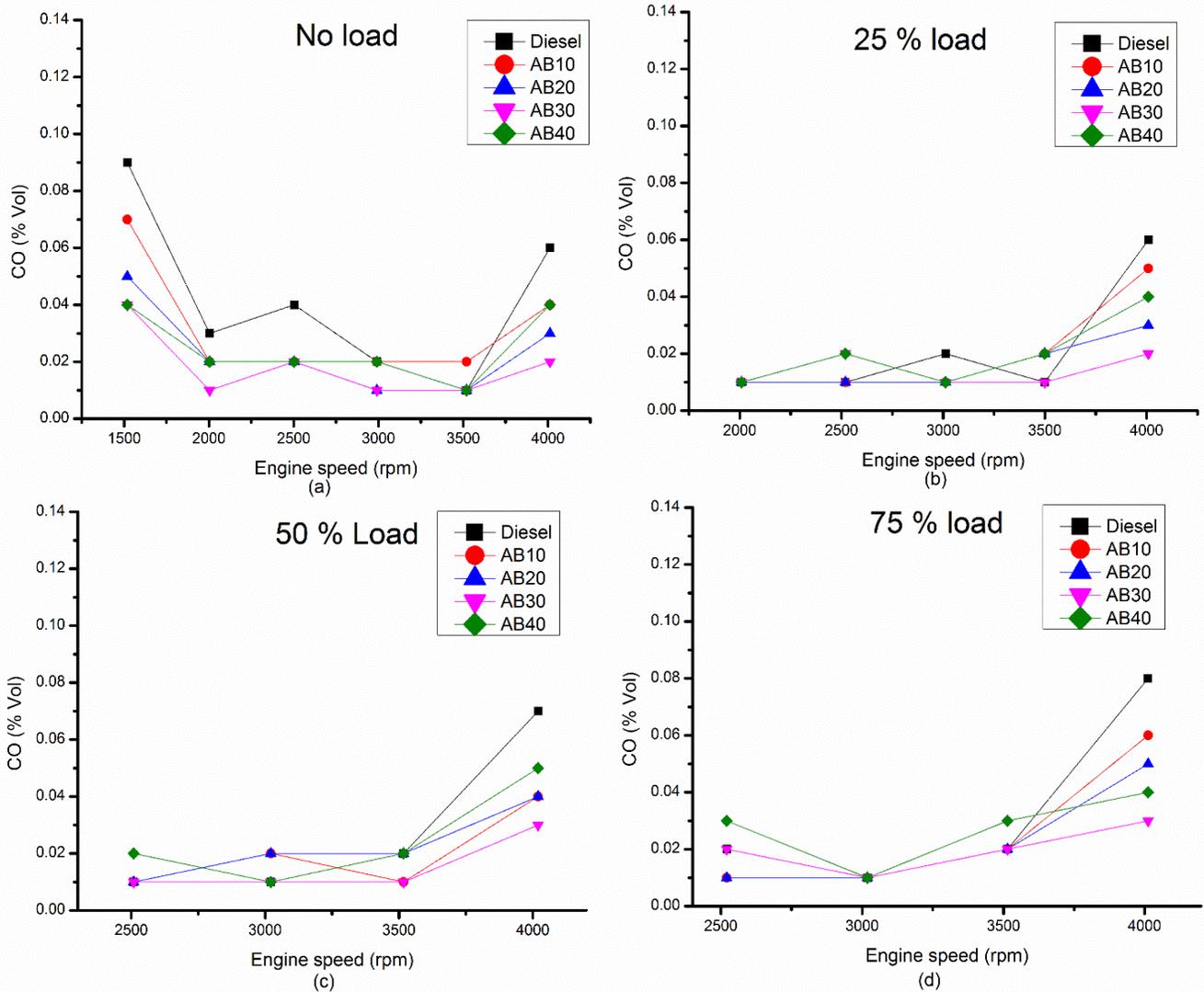
FIGURE 6. CO VARIATION OF VARIOUS BLENDS WITH DIFFERENT ENGINE LOAD AND SPEED (RPM)
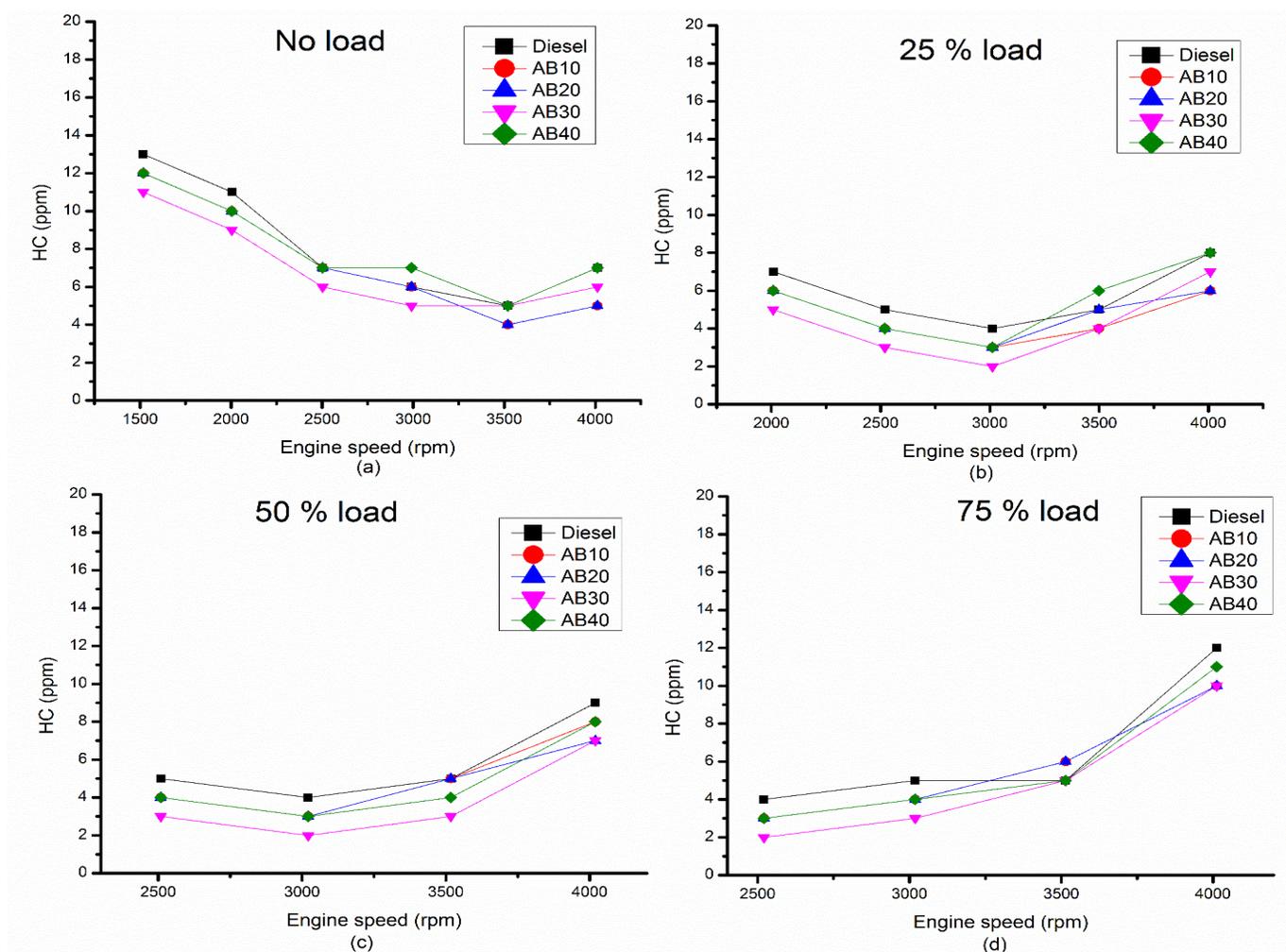
FIGURE 6. CO VARIATION OF VARIOUS BLENDS WITH DIFFERENT ENGINE LOAD AND SPEED (RPM)

In general, it is believed that lowering the A/F ratio results in increased CO emissions [15]. This exertion shows that CO emissions decrease with increasing biodiesel fraction in the diesel (Figure 6). Oxygen present in the molecules of AOME is one of the probable reasons for the improvement in combustion and decrease in CO emissions. Storey et al. [16] suggested advancement in injection timing using biodiesel, which could be another reason for the decrease in CO. Therefore, AB30 showed the lowest CO emission at all observation points. Higher blend, AB40 has the highest oxygen content, among all blends, but its lower calorific value and higher viscosity lowers the combustion temperature. Also, higher blends of biodiesel/diesel have low volatility as compared to diesel, hence an enhancement in CO emissions was observed for AB40.

A/F ratio decreases with an increase in load and speed. Therefore, an enhancement in CO emission was noticed with increase in load and speed. Similar such trends were obtained by Raheman and Phadatare [17]. Further, it has

also been observed from figure 6 (a-d) that CO emissions are high at high speed as time available for combustion is reduced.

3.2.5 Unburnt hydrocarbons

A number of investigations conclude that HC emissions decrease with increase in biodiesel content in the diesel [18,19]. This study shows the similar trend for HC emissions (ppm & g/kWh). AB 30 shows minimum UHC, at almost all the observation points as shown in figure 7 (a-d). This is attributed to higher oxygen content in the molecules of AOME. Higher blend, AB40 shows enhancement in HC emission as biodiesel is less volatile and more viscous than diesel which results in poor

356

atomisation of the fuel leading to increase in CO emissions.

Conclusions

In this study, experimentation was conducted on multicylinder, IDI, compression ignition engine. Diesel and various blends of AOME & diesel were prepared and tested in engine. To investigate the effect of operating conditions of engine on performance of diesel/biodiesel blends; tests were performed at no load, 25%, 50% and 75% load conditions by varying speed from 2500-4000 rpm at individual load. Following conclusions can be drawn from the series of experimentation performed.

- Engine operating conditions have a significant effect on engine performance and emission characteristics. It was observed that diesel/ AOME blends show better results at higher loads as compared to lower load condition. Moreover, biodiesel blends show poor performance at lower loads and high speed conditions.

- Due to high density, oxygen content and viscosity of AOME the performance of engine gets improved. Therefore, all the tested blends AB10, AB20, AB30 and AB40 show better performance and emission characteristics than conventional diesel.

- Among all the blends, AB30 shows maximum ITE and minimum ISFC. In addition to this, exhaust emissions such as HC and CO are also minimum for AB30 blend. However, AB30 blend shows higher emissions of CO_2 and NOx as compared to diesel and other tested blends.

- Reduction in NOx and CO_2 emissions were observed for AB40 fuel when compared with AB30. In essence, this reduction is due to lower calorific value of the blend that results in higher fuel consumption. AB 40 shows improvement in performance and emission characteristics as compared to diesel but deterioration in performance characteristics when compared with AB30.

The present analysis reveals that AB30 can be utilized in an engine with the advantage of higher thermal efficiency and lower CO and HC emissions. The engine fuelled with AB30 does not require any hardware modification.

REFERENCES

[1] Tilman, D., Socolow, R., Foley, J. A., Hill, J., Larson, E., Lynd, L., and Williams, R., 2009. "Beneficial biofuels—the food, energy, and environment trilemma". Science, 325(5938), 270-271.

[2] All fossil fuel reserve and consumption data from CIA World Factbook.

[3] Chakrabarti, P. D. 2001. "Urban crisis in India: new initiatives for sustainable cities". Development in practice, 11(2-3), 260-272.

[4] Sik, L.C., Park S. W. and Kwon S., 2005. "An experimental study onthe atomization and combustion characteristics of biodiesel-blended fuels." Energy Fuels, 19(5), 2201-2208.

[5] Oner, C., and Ehmus, A. S., 2009. "Biodiesel production from inedible animal tallow and an experimental investigation of its use as alternative fuel in a direct injection diesel engine". Appl. Energy, 86(10), 2114–2120.

[6] Ya-fen L., Greg Wu Y. P., and Chang, C.T., 2007. "Combustion characteristics of waste-oil produced biodiesel/diesel fuel blends". Fuel, 86(12), 1772–1780.

[7] Hossain Abul, K., and Davies, P. A., 2012. "Performance, emission and combustion characteristics of an indirect injection (IDI) multi-cylinder compression ignition (CI) engine operating on neat Jatropha and karanja oils preheated by jacket water". Biomass Bioenergy, 46, 332–342.

[8] Kumar, G., 2014. "Studies on Argemone maxicana oil for its usage as biodiesel". Int. J. Pharma Bio Sci., 5, 528–532.

[9] Mustafa, C., 2007. "Combustion characteristics of a turbocharged DI compression ignition engine fueled with petroleum diesel fuels and biodiesel". Bioresource technology 98(6), 1167-1175.

[10] Pulkrabek Willard W (2004). Engineering fundamentals of the internal combustion engine. *Prentice Hall*.

[11] Cardone, M., Prati M., Rocco V., et al., 2002. "Brassica Carinata as an alternative oil crop for the production of biodiesel in Italy: engine performance and regulated and unregulated exhaust emissions". Environ Sci Technol 36(21), 4656–62.

[12] Ramadhas, A.S, Muraleedharan C. and Jayaraj S. 2005. "Performance and emission evaluation of a diesel engine fueled with methyl esters of rubber seed oil". Renewable energy 30(12), 1789-1800.

[13] Xue, J., Grift, T.E. and Hansen, A.C., 2011. "Effect of biodiesel on engine performances and emissions Renew. Sustain". Energy Rev 5(2), 1098–1116.

[14] Gumus, M. and Kasifoglu, S. 2010. "Performance and emission evaluation of a compression ignition engine using a biodiesel (apricot seed kernel oil methyl ester) and its blends with diesel fuel". Biomass and bioenergy 34(1): 134-139.

[15] Tashtoush, G, Al-Widyan, M.I. and Al-Shyoukh A.O., 2003. "Combustion performance and emissions of ethyl ester of a waste vegetable oil in a water-cooled furnace". Applied Thermal Engineering 23(3), 285-293.

[16] Storey, J,M., Lewis S.A., West, B.H. et al. 2005. "Hydrocarbon species in the exhaust of diesel engines equipped with advanced emissions control devices". *CRC*, projet no. AVFL- 10b-2.

[17] Raheman, H. and Phadatare, A.G. 2004. "Diesel engine emissions and performance from blends of karanja methyl ester and diesel". Biomass and Bioenergy 27(4), 393-397.

[18] Buyukkaya, E., 2010. "Effects of biodiesel on a DI diesel engine performance, emission and combustion characteristics". Fuel 89(10), 3099-3105.

[19] Chauhan, B.S., Kumar, N. and Cho, H.M., 2012. "A study on the performance and emission of a diesel engine fueled with Jatropha biodiesel oil and its blends". Energy 37(1), 616-622.

SEEC-2018-059

REMOVAL OF METHYLENE BLUE DYE FROM WASTE WATER BY pH SENSITIVE HYDROGEL

Rinki Singh
Centre for Biosciences & Biomedical Engineering
Indian Institute of Technology Indore, Indore 453552,
India
Email: phd1501171003@iiti.ac.in

Sudeshna Chattopadhyay[*]
Centre for Biosciences and Biomedical Engineering,
Discipline of Physics
Discipline of Metallurgy Engineering and Materials
Science
Indian Institute of Technology Indore, Indore 453552,
India
[*] Corresponding author
Email: sudeshna@iiti.ac.in,
chattopadhyay.sudeshna@gmail.com

ABSTRACT

Hydrogels have gained importance in many applications like medical, pharmaceutical, environmental remediation, etc. because of its softness, hydrophilic nature and presence of chelation group. In this report, we are exploring the role of a pH sensitive hydrogel as an adsorbent of toxic dyes for environmental remediation specifically for waste water treatment. The biocompatible pH sensitive hydrogel composed of acrylic acid and vinylsulfonic acid was prepared by free radical polymerization reactions. The prepared hydrogel was then characterized by Fourier transform infrared (FTIR) spectroscopy and Field emission scanning electron microscopy (FESEM) techniques. FTIR studies confirmed the formation of Poly (acrylic-co-vinylsulfonic) acid hydrogel from its monomers. The morphology of the hydrogel corresponding to its pH sensitivity, was explored by FESEM analysis. The prepared hydrogel shows important application in waste water treatment, through significant dye adsorption capacity/performance.

Keywords: *Hydrogel, Environmental Remediation, Dye Adsorption*
.

INTRODUCTION

Hydrogels have gained importance in a wide variety of applications in medical, pharmaceutical, environmental remediation and related fields.[1] Hydrogels are basically defined as three-dimensional polymeric networks cross-linked by a chemical bond, hydrogen bonding, ionic interaction, hydrophobic interaction which can absorb a large amount of water without dissolving into it. Their hydrophilic nature, softness and presence of chelation groups in the polymeric network make them suitable materials for biomedical devices, tissue engineering, drug delivery, food, pharmaceutical industry, wastewater treatment, etc.[2-5]

Stimuli-responsive hydrogels have gained great attention, as these hydrogels show dramatic changes in volume and properties in response to external stimulus such as temperature, pH [the acidity or the alkalinity of any solution can be indicated by the term of pH which stands for the power of the hydrogen ions H^+, pH is related to the concentration (or more strictly the activity) of hydrogen ions], ionic strength, electric field etc. Their ability to swell and shrink according to the condition makes them interesting for use as intelligent materials (smart gels).[6-8]

pH is also an important limiting chemical factor for aquatic life. If the water in a stream is too acidic or basic, the H^+ or

OH⁻ ion activity may disrupt aquatic organisms' biochemical reactions by either harming or killing the stream organisms. Wastewater pH has been identified as one of the parameters which influence effective wastewater treatment.[9] The effective treatment of chemical contaminations of water in the environment has become one of the major issues of public interest due to their toxicity. The presence of dyes is responsible for ecological problems in aquatic environment and toxic to humans if they are introduced into the food chain and ingested beyond prescribed concentration.

There are many kinds of technologies which are used for dye removal from wastewater, such as membrane separation, chemical oxidation, coagulation and flocculation, photocatalytic degradation and adsorption. Adsorption technology is mainly considered to be an effective method for quickly lowering the waste concentration in the effluent. Hydrogel is known as one of the cost effective adsobants for dye removal.[10-12]

pH sensitive polymer/hydrogel contains acidic (carboxylic and sulfonic acid) or basic (ammonium salt) groups that either accept or release protons in response to pH change. Because of the presence of ionic and non-ionic groups in these type of hydrogels, they have the property to adsorb ionic dyes and thus, are useful for waste water treatment.[13-15] Among the various dyes, methylene blue (MB) is a thiazine cationic dye which is applied to leather, wool, silk, paper, plastic as well as for the production of ink, copying paper and cotton mordant with tannin. The color removal process in the textile industries generates effluents polluted with methylene blue dye which is toxic and mixes in the water causing mutation, allergic dermatitis, cancer, skin irritation, eye burns in human and animals, diarrhea and vomiting.[16]

In this study, we report the preparation and characterization of a biocompatible poly (acrylic-co-vinylsulfoinc acid) hydrogel whose adsorption capacity of methylene blue dye displays its potential application in waste water treatment.

METHODOLOY
Materials

The poly (acrylic-co-vinylsulfoinc acid) hydrogel (PAAVSA) were prepared using Acrylic acid (AA) (Sigma-Aldrich), Vinyl sulfonic (VSA) (Sigma-Aldrich) acid monomers, along with appropriate initiator and crosslinker using free radical polymerization reaction technique[6] . The optimum weight ratio of the AA-to-VSA mixture was determined/adjusted to achieve the better performance of the hydrogel in terms of its dye adsorption capacity. Methylene blue (MB) dye (Sigma-Aldrich) was used to analyse and quantify the dye adsorption capacity of the prepared hydrogel. 0.04 mM methylene blue dye aqueous solution of 50 ml volume were used for dye adsoprption measurements at different pH values.

Experimental Techniques

FTIR spectra of dried hydrogel was recorded with Tensor 27, BRUKER Fourier Transform IR (FTIR) spectrometer using KBr disc in the range of 4000-400 cm^{-1} .The morphology of the prepared hydrogel at different pH solution was studied by Field Emission Scanning Electron Microscopy (FE-SEM, Supra55 Zeiss).

The characteristic properties of the hydrogel were explored by quantifying the swelling behavior of the PAAVSA by calculating the swelling ratio.[6]

$$\text{Swelling ratio (Q)} = [(W_s - W_d)/W_d] \text{ X } 100 \text{ \%} \quad (1)$$

Where, W_s and W_d are the weights of swollen and dried hydrogels, respectively.

The concentration of adsorbed MB dye was determined by using UV–Vis spectrophotometer (Perkin Elmer lamda-35) with spectral range of 200 – 800 nm.

The experiments for dye adsorption by PAAVSA hydrogel were carried out at different pH of the dye solution. The percentage dye adsorption by PAAVSA was calculated by using formula:[17]

$$\text{Dye Adsorption} = [(A_0 - A_t)/A_t] \text{ X } 100 \text{ \%} \quad (2)$$

Where, A_0 and A_t are the UV-Vis absorbance of the dye solution at the initial stage and absorbance of the supernatant liquid collected at different time interval, at different stage of adsorption, respectively.

RESULTS
Spectroscopic Analysis
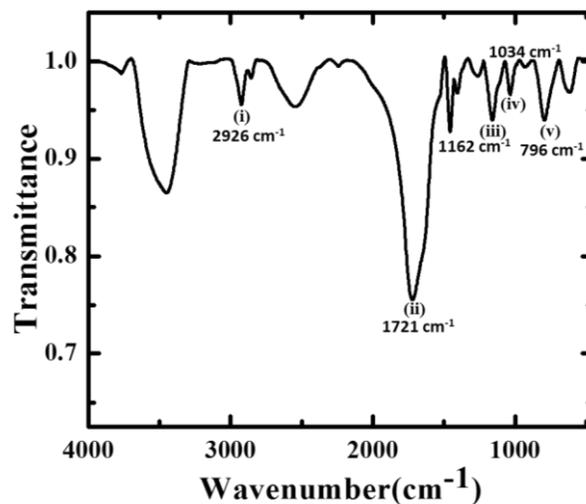
FIGURE 1: FTIR spectra of Poly (acrylic-co-vinylsulfonic)acid hydrogel (i) CH stretching, AA (ii) CO stretching of COOH, AA (iii) SO_3^-, VSA (iv) S=O, VSA (v) C-S stretching, VSA

The FTIR spectrum shown in Fig.1, displayed absorption peaks at 2926 cm^{-1} (CH stretching of AA), 1721 cm^{-1} (CO stretching COOH, AA), 1162 cm^{-1} (SO_3^-, VSA), 1034 cm^{-1} (S=O, VSA), 796 cm^{-1} (C-S stretching, VSA), which indicate the formation of the desired hydrogel from acrylic acid and vinylsulfonic acid monomers.

Morphology

Fig.2, shows the SEM morphologies of the poly(acrylic-co-vinylsulfonic) acid (PAAVSA) hydrogel, exposed to different pH solution. SEM images confirm that the PAAVSA hydrogel exhibits large porosity for high pH values, indicating enhanced surface induced activity towards neutral to alkaline dye solution..
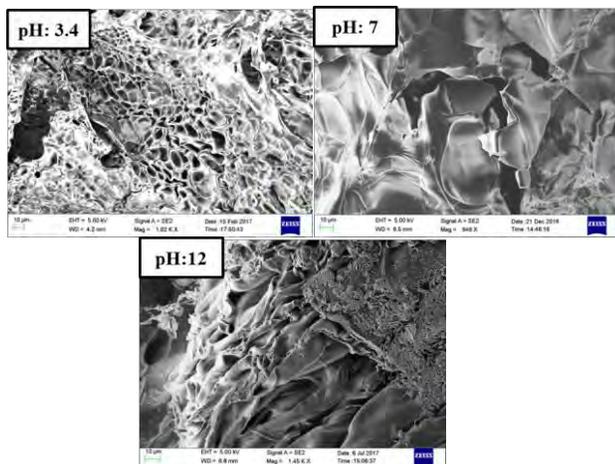
FIGURE 2: Characteristic SEM images of Poly (acrylic-co-vinylsulfonic) acid hydrogel at different pH solutions

Dye Adsorption Properties

The poly(acrylic-co-vinylsulfonic) acid (PAAVSA) shows the distinct swelling behavior of hydrogel at different pH. The results revealed (shown elsewhere[18]) that the hydrogel is pH sensitive and with the swelling ratio becoming higher, more than 7000%, at high pH values (neutral to basic range).

Dye adsorption studies indicated that the Poly (acrylic-co-vinylsulfonic) acid hydrogel has the ability to adsorb methylene blue dye from the aqueous solution. Fig.3 clearly depicts that the capacity of methylene blue dye adsorption is increased at pH-7 and pH-12, relative to the

acidic solution (pH 3). The observed increase in MB uptake at pH-7 and pH-12 is very much consistent with the high porosity of the hydrogel at pH 7 and pH 12 with respect to pH 3.4 (as shown in Fig.2). Generally, the industry generated waste water, which contains dyes, is alkaline in nature (i.e., high pH values)[19], and in that respect the PAAVSA shows its potential application in waste water treatmet through its significant dye removal capacity.
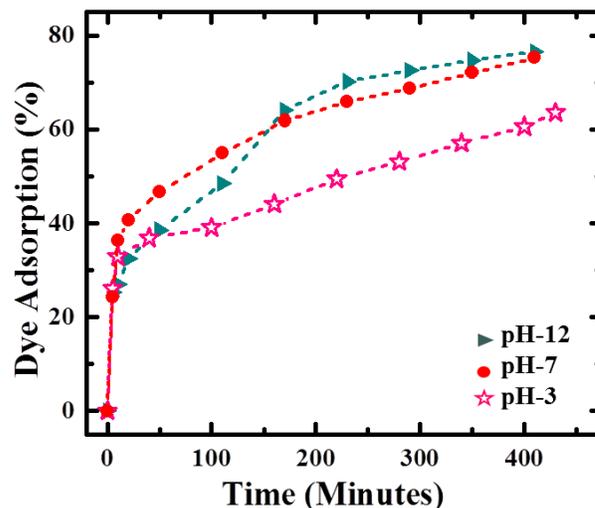
FIGURE 3: Effect of different pH solution on adsorption rate of MB dye with time

Dye adsorption mechanism has been explored by thorough investigation and using the theoretical model to get the quantitive explanation of the dye adsorption rate of the hydrogel[20-22] to determine the performance of PAAVSA in comparison to other studies, for its potential application in waste water treatment.

CONCLUSION

Poly (acrylic-co-vinylsulfonic) acid (PAAVSA) prepared by free radical polymerization method shows its pH sensitive hydrogel properties through its distinct swelling behavior at different pH. The dye adsorption study, along with the FESEM characterization show that the said hydrogel removes the cationic dye MB from aqueous solution very efficiently. The maximum observed dye adsorption occurred at alkaline pH which makes this biocompatible hydrogel a potential adsorbent for the dye containing wastewater treatment.

REFERENCES

1. L. Yahia, N. Chirani, L. Gritsch, F. L. Motta and S. Fare, 2015." History and applications of hydrogels".Journal of Biomedical Sciences, **4,** pp.

2. X.-Z. Zhang, Y.-Y. Yang, T.-S. Chung and K.-X. Ma, 2001." Preparation and Characterization of Fast Response Macroporous Poly(N-isopropylacrylamide) Hydrogels".Langmuir, **17,** pp., 6094-6099

3. G. A. Mahmoud, S. F. Mohamed and H. M. Hassan, 2015." Removal of methylene blue dye using biodegradable hydrogel and reusing in a secondary adsorption process".Desalination and Water Treatment, **54,** pp., 2765-2776

4. E. Caló and V. V. Khutoryanskiy, 2015." Biomedical applications of hydrogels: A review of patents and commercial products".European Polymer Journal, **65,** pp., 252-267

5. Z. Li, Y. Wang, N. Wu, Q. Chen and K. Wu, 2013." Removal of heavy metal ions from wastewater by a novel HEA/AMPS copolymer hydrogel: preparation, characterization, and mechanism".Environmental Science and Pollution Research, **20,** pp., 1511-1525

6. T. Hussain, M. Ansari, N. M. Ranjha, I. U. Khan and Y. Shahzad, 2013." Chemically Cross-Linked Poly(acrylic-co-vinylsulfonic) Acid Hydrogel for the Delivery of Isosorbide Mononitrate".The Scientific World Journal, **2013,** pp., 9

7. R. Yoshida and T. Okano, in Biomedical Applications of Hydrogels Handbook, eds. R. M. Ottenbrite, K. Park and T. Okano, Springer New York, New York, NY, 2010, pp. 19-43.

8. C. M. Schilli, M. Zhang, E. Rizzardo, S. H. Thang, Y. K. Chong, K. Edwards, G. Karlsson and A. H. E. Müller, 2004." A New Double-Responsive Block Copolymer Synthesized via RAFT Polymerization: Poly(N-isopropylacrylamide)-block-poly(acrylic acid)".Macromolecules, **37,** pp., 7861-7866

9. H. K. Mandal, 2014." Influence of wastewater pH on turbidity".International Journal of Environmental Research and Development, **4,** pp., 105-114

10. M. Rafatullah, O. Sulaiman, R. Hashim and A. Ahmad, 2010." Adsorption of methylene blue on low-cost adsorbents: a review".Journal of Hazardous Materials, **177,** pp., 70-80

11. N. Sezgin and N. Balkaya, 2016." Adsorption of heavy metals from industrial wastewater by using polyacrylic acid hydrogel".Desalination and Water Treatment, **57,** pp., 2466-2480

12. M. Mohammed, A. Shitu and A. Ibrahim, 2014." Removal of methylene blue using low cost adsorbent: a review".Research Journal of Chemical Sciences , **4,** pp., 91-102

13. Y. Liu, Y. Zheng and A. Wang, 2010." Enhanced adsorption of Methylene Blue from aqueous solution by chitosan-g-poly (acrylic acid)/vermiculite hydrogel composites".Journal of Environmental Sciences, **22,** pp., 486-493

14. R. Dhakar, A. Gupta, S. Maurya and R. Singh, 2010." pH-sensitive interpenetrating hydrogel for eradication of Helicobacter pylori".International Journal of Pharmaceutical Sciences and Nanotechnology, **3,** pp., 924-932

15. B. L. Rivas and L. N. Schiappacasse, 2003." Poly (acrylic acid-co-vinylsulfonic acid): Synthesis, characterization, and properties as polychelatogen".Journal of Applied Polymer Science, **88,** pp., 1698-1704

16. A. Youssef, M. Al-Awadhi and M. Akl, 2014." Solid phase extraction and spectrophotometric determination of methylene blue in environmental samples using bentonite and acid activated bentonite from Egypt".Journal of Analytical & Bioanalytical Techniques, **5,** pp., 1

17. H. Zhao, T. Jiao, L. Zhang, J. Zhou, Q. Zhang, Q. Peng and X. Yan, 2015." Preparation and adsorption capacity evaluation of graphene oxide-chitosan composite hydrogels".Science China Materials, **58,** pp., 811-818

18. R. Singh and S. Chattopadhyay." A pH sensitive hydrogel and its application in disease detection". pp.

19. Z. Wang, M. Xue, K. Huang and Z. Liu, in Advances in treating textile effluent, InTech, 2011.

20. C. Zhou, Q. Wu, T. Lei and I. I. Negulescu, 2014." Adsorption kinetic and equilibrium studies for methylene blue dye by partially hydrolyzed polyacrylamide/cellulose nanocrystal nanocomposite hydrogels".Chemical Engineering Journal, **251,** pp., 17-24

21. I. Tsibranska and E. Hristova, 2011." Comparison of different kinetic models for adsorption of heavy metals onto activated carbon from apricot stones".Bulgarian Chemical Communications, **43,** pp., 370

22. E. Demirbas, M. Kobya, E. Senturk and T. Ozkan, 2004." Adsorption kinetics for the removal of chromium (VI) from aqueous solutions on the activated carbons prepared from agricultural wastes".Water SA, **30,** pp., 533-539

SEEC-2018-060

STUDY ON IMPORTANCE OF SO$_x$, NO$_x$ & Hg CONTROL IN THERMAL POWER PLANTS AND THEIR IMPACTS ON ECOSYSTEMS: A REVIEW

Nidhi Malik
Department of Environmental Science & Engineering
Indian Institute of Technology
(Indian School of Mines),
Dhanbad- 826004, Jharkhand
Email: nidhimalik8@gmail.com

Suresh Pandian Elumalai
Department of Environmental Science & Engineering
Indian Institute of Technology
(Indian School of Mines),
Dhanbad- 826004, Jharkhand
E-mail: espandian@iitism.ac.in

Abstract: *Air pollution is an emerging issue in Asia. In particular, emission of sulphur dioxide and nitrogen oxides have been rising steadily over the last few decades. Rapid growth of cities together with expansion of industries and transport systems has made the Asian region increasingly exposed to these emissions. If this keeps on increasing at the same rate, the impacts like atmospheric acid deposition affecting the chemistry of soil and surface water and accelerating their acidification in Europe and North America will become apparent in large part of Asia. This paper presents the complete information on importance of SO$_x$, NO$_x$ and Hg control in thermal power plants. It has been concluded that more emphasis is required on SO$_x$ & NO$_x$ emissions control from coal based TPPs which are a major energy contributor to bring long term benefits to ecosystems apart from regulating ambient air quality. Also, in order to regulate SO$_x$ & NO$_x$ via NAAQs, deposition must be related to ambient air quantities. More deposition-to-response relationships are needed to identify a level of pollutant exposure that is still protective of ecosystems and to link the ecosystem response to depositional levels.*

Keywords: Nitrogen oxides (NO$_x$), Sulfur oxides (SO$_x$), Acid deposition, Thermal Power Plants (TPPs).

INTRODUCTION

Acidic deposition is the most widely acknowledged form of atmospheric deposition, with well-known effects on lakes, streams, and forests. In addition to contribution to acidic deposition, nitrogen emissions and subsequent deposition can affect aquatic resources by contributing to their over-enrichment with nutrients. In India, air-quality standards are set to protect ecosystems from damage caused by gas-phase nitrogen (N) and sulfur (S) compounds, but not from the deposition of these air pollutants to land and water. Though, emissions of NO$_x$ and SO$_x$ to the atmosphere contribute to total nitrogen (N) and sulfur (S) deposition, leading to acidification, N enrichment, and S-induced mercury methylation in sensitive ecosystems throughout the world. Here, we synthesize recent scientific literature on the ecological effects of N and S air pollution. Acidification is caused by both wet depositions via precipitation and dry deposition of gases and particles of N and S from the atmosphere. Furthermore, toxic air contaminants like mercury, are also emitted primarily by coal-fired utilities, and may be carried thousands of miles before entering lakes and streams as mercury deposition. S deposition can stimulate microbes to methylate mercury (Hg), a process that introduces Hg into the food chain and leads to its bioaccumulation, which is one of the reasons mercury deposition is included in this discussion. The main effects associated with NO$_x$ and SO$_x$ are illustrated in Figure 1.
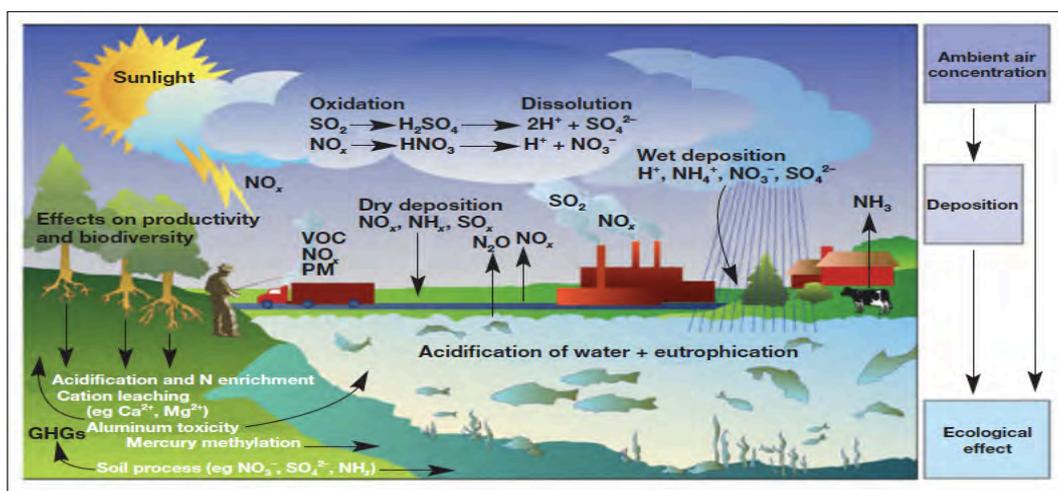
FIGURE 1: SIMPLIFIED DIAGRAM OF THE ECOLOGICAL EFFECTS CAUSED BY NITROGEN AND SULPHUR AIR POLLUTION.
[VOC = volatile organic compound; PM = particulate matter; GHGs = greenhouse gases.]
(Source: TL Greaver et al., 2012)

Effects of Particulate Matter (PM), from Thermal Power Plants (TPPs) is well established as well as Fly Ash Control using Electrostatic Precipitator and their disposal management are in place for a long time in India. However, less emphasis is given on acid causing gaseous pollutants which are by-products of coal combustion in TPPs. Till date we were visualizing the environmental impacts of power plants only for PM and Fly Ash Utilization but now weightage has been given to NO_x and SO_x to keep the ambient levels at certain limits. Though introduction of new rules for limiting NO_x, SO_x and mercury (Hg) at stacks of Indian TPPs are likely to bring long term benefits to the ecosystems apart from regulating ambient air quality. India being the 4th largest economy has a fast growing market whose 75% of energy needs are contributed by coal based Thermal Power Plants (TPPs), so it is vital to understand the hidden costs of air pollution from coal fired TPPs. According to a report, the total installed capacity is expected to increase three times from 159 GW in 2014 to 450 GW in 2030; under the proposed list of power plant projects "[1]". The PM, SO_2 & NO_x emissions will also increase in the same period. Many studies have been carried out globally to study the emissions from thermal power plants and their impact on ecosystem and a few has been summarized as below:

TABLE 1: LITERATURE REVIEW

S. No.	Author	Title	Focus of Study	Impacts on Ecosystem
1.	Arndt et al., 1997	Sulfur dioxide emissions and sectorial contributions to sulfur deposition in Asia	SO_2	In this paper, the emissions calculated were used along with the ATMOS long-range transport model to calculate sulfur deposition in Asia and it was concluded that present situation in Asia is that sulfur deposition at levels sufficient to cause ecosystem damage (as estimated by critical loads for Asia) are calculated for vast regions in Asian countries including parts of India. Acid deposition problems throughout Asia are anticipated as a result of the rapid expansion in energy consumption in the region.
2.	Sophia Mylona , 1996	Sulphur dioxide emissions in Europe 1880–1991 and their effect on sulphur concentrations and depositions	SO_2	According to this study, historical emission inventories for acidic precursors were compiled to correlate long term pollution trends with ecosystem change. In Europe as a whole, coal combustion remained the major emission source throughout the century. Emissions are principally in the form of sulphur dioxide, so that comparable concentrations of particulate sulphate in low emission regions indicate the importance of long range transport. Assuming a constant ecosystem sensitivity throughout the period, it was concluded that depositions sufficient to cause ecosystem damage may have occurred before 1880 in many areas of north-western and central Europe.
3.	Qian et al., 2017	Monitoring effects of SO_2 emission abatement on recovery of acidified soil and stream water in Southwest China	Sulphates, Nitrates and other major ions	It showed the clear effects of emission abatement on recovery of acidified soils and stream water. With decrease in SO_2 emission after 2006, a significantly decreasing trend of S deposition was detected during 2008-13. Since, soil acidification is still very serious, shown by quite low pH in soil water, future emission abatement of both SO_2 & NO_x should be strengthened.
4.	Charles T. Driscoll et al., 2007	Mercury Contamination in Forest and Freshwater Ecosystems in the North-eastern United States	Mercury	It showed that globally, coal-fired power plants are the largest single category of Hg emissions, with 1450 metric tons per year, comprising about 50% of anthropogenic sources. Forested regions with a prevalence of wetlands and of unproductive surface waters promote high concentrations of mercury in freshwater biota and thus are particularly sensitive to mercury deposition. Through fish consumption, humans and wildlife are exposed to methylmercury, which markedly bio-accumulates up the freshwater food chain. The analysis suggest decreased Hg deposition will result in lower Hg levels in biota, although significant time lags may exist in many ecosystems.
5.	Andy Haines et al., 2007	Policies for accelerating access to clean energy, improving health, advancing development, and mitigating climate change	Access to clean energy and public health	In this paper, they presented evidence about the connections between energy use (or lack of it) and adverse effects on population health. The absence of reliable access to clean energy and the services it provides imposes a large disease burden on low-income populations and impedes prospects for development. Furthermore, current patterns of fossil-fuel use cause substantial ill-health from air pollution and occupational hazards. Impending climate change, mainly driven by energy use, now also threatens health. Policies to promote access to non-polluting and sustainable sources of energy have great potential both to improve public health and to mitigate (prevent) climate disruption. The need for policies that prevent dangerous anthropogenic interference with the climate while addressing the energy needs of disadvantaged people is a central challenge of the current era.

FINDINGS:

1. **Comparison of Environmental Standards:** The emission standards laid down by Government of India for thermal power plants for existing and older thermal power plants are much more relaxed – allowing for up to six times higher counts in cases of SO_x (Sulphur Oxides) and NO_x (Nitrogen Oxides). Even if we go by the standards followed in

European Union which themselves are termed to be one of the most relaxed, the Indian standard seems to be considerably laxer. The European Union (Large Combustion Plants) Regulations 2012 classifies thermal power units into Schedule I (units before January, 2016) and Schedule II (later January 2016). For the older units which were in operation before 2003, the emission standards are relaxed up to 800 mg/Nm^3 for SO_x and 450 for NO_x, but with an additional condition that they do not operate more than 1,500 operating hours per year as a rolling average over a period of five years.

TABLE 2: STACK EMISSION STANDARDS (mg/Nm^3) FOR COAL BASED TPPS
(*Source: CPCB vide Notification No. S.O. 3305(E) dated 07.12.2015*)

Pollutants	*Before December 31, 2003* shall meet limits within 2 years from date of notification		*After 2003 to 2006* shall meet limits within 2 years from date of notification		*From January, 2017* all units which have been accorded environmental clearance and are under construction
	<500 MW	*≥500 MW*	*<500 MW*	*≥500 MW*	
PM	100		50		30
SO₂	600	200	-	200	100
NOx	600		300		100
Hg	-	*0.03*	*0.03*		*0.03*

2. **Trends in Coal Consumption; SO₂ & NO₂ concentrations in India:** Among fossil fuels, especially the use of coal doubled from 2005 to 2013 and oil consumption increased by 50% and it was also found that coal-based thermal power plant clusters were responsible for more than 75% of total SO_2 emissions in all 23 Indian states they analysed, and for more than 90% in 16 Indian states; also an estimated 75 - 90% of sulphates and 50% nitrates are formed from SO_2 and NO_x emissions originating from the stacks of thermal power plants "[2]".

(a)

(b)

(c)
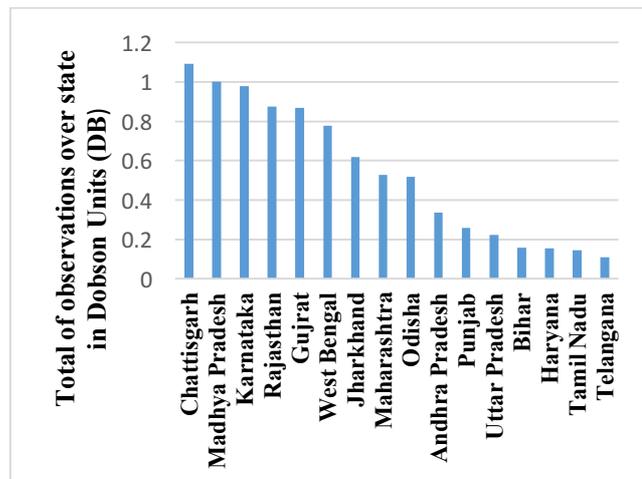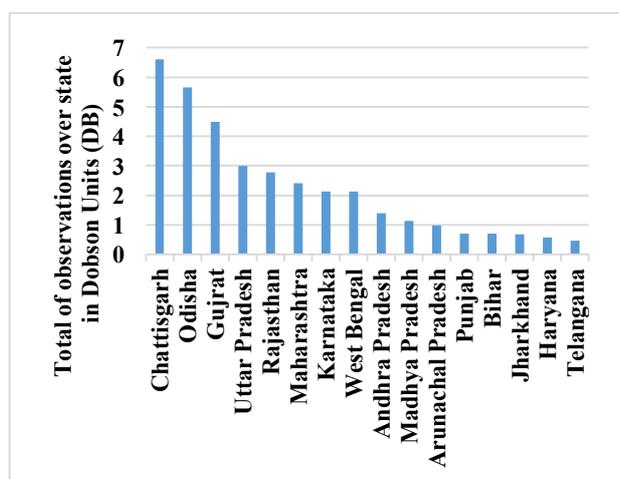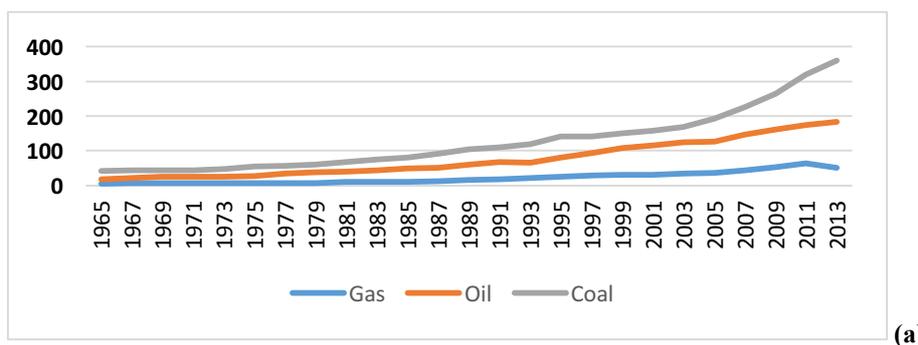
FIGURE 2: (A) FOSSIL FUEL CONSUMPTION IN INDIA, (B) SO₂ INCREASE 2009 TO 2015, (C) NO₂ INCREASE 2009 TO 2015
(Source: Greenpeace India report, May 2016)

3. Environmental impacts with increase of SO_x, NO_x & Hg:

- **Acidification:** Acidity develops naturally in soil, but this process is both altered and accelerated by acid deposition from anthropogenic sources. The biological effects of acidification on terrestrial ecosystems are often attributable to aluminium (Al) toxicity and the decreased ability of plant roots to take up nutrient base cations as acid deposition lead to an increase in H^+ ions in the soil, resulting in decreased soil pH and increased mobilization of aluminium in soils, affecting the soil water solution "[3]". Surface water acidification from atmospheric deposition affects aquatic biota by altering surface-water chemistry and can cause the loss of acid-sensitive biota; the greater the acidification, the more species are lost "[4]". Although both N and S deposition can cause aquatic acidification, S deposition is generally the primary cause of chronic acidification, with secondary contributions from N deposition.

- **Nutrient effects of N deposition:** The contribution of N deposition from the atmosphere to total N load varies among ecosystems; it is the main source of new N to most high-elevation lakes and headwater streams "[5]". High elevation areas are vulnerable due to increased acidic cloud deposition and decreased soil depth to buffer acid inputs.
The onset of NO_3^- leaching is one of the best documented biogeochemical indicators that a terrestrial ecosystem is receiving more N than it is able to retain "[6]". The productivity of some freshwater ecosystems is also N limited. Nitrogen deposition can alter aquatic species assemblages and cause eutrophication of aquatic ecosystems to the extent that N is the growth-limiting nutrient.

- **S-induced mercury methylation:** Mercury leads to bioaccumulation and bio-magnification through food chain in fish, humans and other animals only in its methylated form "[7]". Sulfur reducing bacteria in aquatic sediments convert inorganic mercury to methylmercury which has led researchers to establish that reductions in sulfur dioxide emissions and a resulting reduction in sulfate deposition will abate mercury concentrations in wildlife. Consequently, with decrease in level of sulfates in aquatic systems, sulfur reducing bacteria will reduce less sulfur, and this will in turn lead to less inorganic mercury being methylated.

CONCLUSIONS AND POLICY IMPLICATIONS:

Coal based TPPs remains the major energy contributor for power generation in India and therefore should be subjected to tighter emission standards, similar to those found in emerging economies (like China) and developed economies (like EU, Australia, and USA). In India, the amount of power generated from coal will remain high at least through 2030 "[8-9]", and unless a better way is proposed to manage pollution from the coal-fired thermal power plants, the environmental effects and human health costs will be high.

Key scientific research areas that will be important for policy making involve the protection of ecosystems from acidification and nutrient effects caused by atmospheric deposition. First, more deposition-to-response relationships are needed, to identify a level of pollutant exposure that is still protective of ecosystems.

NH_x is currently unregulated as a "criteria" air pollutant under the NAAQS, yet it acts in combination with NO_x to cause nutrient effects, and with NO_x and SO_x to cause acidification. Approaches will need to be developed that consider how a given quantity of NH_x deposition relates to total N deposition or acidic deposition, to determine how much can occur while still ensuring protection of sensitive ecosystems. Finally, in order to regulate NO_x and SO_x via the NAAQS, deposition must be related to ambient air quantities.

REFERENCES:

1. Conservation Action Trust of India (CAT) Report, 2014: Coal Kills (Health Impacts of Air Pollution from India's Coal Power Expansion).
2. Greenpeace India Report, May 2016: "Out of Sight- How Coal Burning Advances India's Air Pollution Crisis."
3. Cronan, Christopher S., and David F. Grigal., 1995. "Use of calcium/aluminum ratios as indicators of stress in forest ecosystems." *Journal of Environmental Quality* 24.2: 209-226.
4. Driscoll, Charles T., et al., 2001. "Acidic Deposition in the Northeastern United States: Sources and Inputs, Ecosystem Effects, and Management Strategies: The effects of acidic deposition in the northeastern United States include the acidification of soil and water, which stresses terrestrial and aquatic biota." *AIBS Bulletin* 51.3: 180-198.
5. Fenn, Mark E., et al., 2003. "Nitrogen emissions, deposition, and monitoring in the western United States." *AIBS Bulletin* 53.4: 391-403.
6. Aber, John D., et al., 2003. "Is nitrogen deposition altering the nitrogen status of northeastern forests?." *AIBS Bulletin* 53.4: 375-389.
7. Scheuhammer, Anton M., et al., 2007. "Effects of environmental methylmercury on the health of wild birds, mammals, and fish." *AMBIO: A Journal of the Human Environment* 36.1: 12-19.
8. Prayas, 2011. Thermal Power Plants on the Anvil: Implications and Need for Rationalisation. Prayas Energy Group, Pune, India.
9. Prayas, 2013. Black and Dirty e the Real Challenges Facing India's Coal Sector. Prayas Energy Group, Pune, India.

SEEC-2018-061

INFLUENCE OF TRACE METALS ON METHANE FORMATION FROM INORGANIC CARBON IN MICROBIAL ELECTROCHEMICAL SYSTEMS

C. Nagendranatha Reddy
Department of Environmental Science and
Engineering, Kyung Hee University, Seocheon- dong,
Yongin-si, Gyeonggi-do 446-701, Republic of Korea
Email: nagreddy16987@gmail.com

Booki Min
Department of Environmental Science and
Engineering, Kyung Hee University, Seocheon- dong,
Yongin-si, Gyeonggi-do 446-701, Republic of Korea.
E-mail address: bkmin@khu.ac.kr.

ABSTRACT

The enzymatic process of biomethane generation is influenced by the availability of trace metals on the biocatalyst's metabolic activity. The functional role of important trace metals viz., magnesium (Mg_2^+), iron (Fe_2^+), nickel (Ni_2^+) and zinc (Zn_2^+) in regulating the CH_4 production potential of a biocatalyst was evaluated under varying concentrations [trace metals concentrations (TM1 and TM2)]. The optimum concentrations were evaluated preliminarily and compared with the control (with no trace metals) conditions for enhanced conversion efficiency. The optimum concentrations (TM2 operation) of trace metals enhanced the CH_4 production and currents generation by 3 and 0.7 folds when compared to control operation. Cyclic voltammogram profiles depicted increment in redox catalytic currents during TM2 operation and also supports the involvement of reducing equivalents towards the CH_4 generation. Further studies viz., enzymes activity, volatile fatty acids generation and microbial community analysis would depict the clear understanding of biocatalyst's function at varied concentrations of trace metals during CH_4 generation. Optimum concentrations of trace metals showed an enhanced CH_4 production efficiency of the biocatalyst due to its role as a component of ferredoxin and hydrogenase related to energy metabolism and are also essential for the cell growth of many microorganisms.

***Keywords*:** Microbial electrochemical system; Trace elements; Biomethane; Inorganic carbon (CO_2)

1. INTRODUCTION

With the upsurge in global demand for clean and green energy, biomethane produced using inorganic carbon (CO_2) as feed stock in microbial electrochemical system serves as a promising prospect for future use [1]. The process of utilizing methanogens in the biocathode for production of CH_4 is called bioelectromethanogenesis. The basic understanding of biocatalyst behavior and shift in metabolic pathways will play a significant role in enhancing the generation of CH_4. Hence, any factor that affects the growth and metabolic activities of the bacteria responsible for the digestion of the organic matter can limit the biogas production and efficiency of the system. Growth factors such as trace metals have a direct effect on the growth of the microbial biomass and ultimately the biogas production [2]. Trace metals are required for the activation or function of many enzymes and co-enzymes related to energy metabolism and are also essential for the cell growth of many microorganisms. Several studies have been reported pertaining to the influence of different trace metals on anaerobic fermentation and H_2 production processes [3,4]. However, the optimum concentrations of various trace metals were inconsistent for MES system studies because the requirement of metal ions varies depending on various operational conditions.

Hence, the present study evaluated the biochemical function of four different trace metals in regulating the CH_4 production process with respect to the bioprocess parameters. Preliminary analysis depicted the influence of trace metals concentration on biomethane and voltage generations.

2. Proposed Pathway

Each of the trace metals has a specific biochemical function in the cell during the metabolic pathway and the change in its concentration may alter that metabolic function. Fe is the most abundant metal, followed by Ni and Mg, and smaller amounts of Zn (Fig. 1). Fe is primarily present as Fe-S clusters used for electron transport and catalysis. Almost every metalloenzyme involved in the methanogenic pathway contains multiple Fe_2S_2, Fe_3S_4, or Fe_4S_4 clusters. The first enzyme in the CO_2 reduction pathway, formylmethanofuran dehydrogenase (Fmd) can bind uptonine Fe_4S_4 clusters: one cluster in the Mo/W-pterin binding subunit and up to eight additional clusters in polyferredoxin [5,6].

Ni is either bound to Fe-S clusters or in the center of a porphyrin unique to methanogens, cofactor F430. It is likely that Fmd can bind additional Fe_4S_4 clusters. Ferredoxins that transfer electrons from H_2 to other methanogenesis enzymes require additional Fe in the form of two Fe_4S_4 clusters. All hydrogenases involved in methanogenesis are Ni-Fe enzymes that oxidize H_2 and reduce ferredoxin, coenzyme F420, and other electron carriers [7]. The four different types of Ni-Fe hydrogenases involved in methanogenesis all contain abundant Fe. The

energy-converting membrane associated hydrogenase contains three Fe_4S_4 clusters and a Ni-Fe active site and can contain additional polyferredoxin subunits with 6, 10, or 14 Fe_4S_4 clusters [7,8]. Another Ni-Fe hydrogenase is used to reduce coenzyme F420. Coenzyme F420, a flavin derivative that plays a critical role in two intermediate electron transfer steps in methanogenesis, is reduced with H_2 by the cytoplasmic hydrogenase Frh. The Frh enzyme complex contains a Ni-Fe active site and four Fe_4S_4 clusters, and forms large aggregates, multiplying its metal requirements approximately eight fold. Under conditions of Ni limitation, some methanogens without cytochromes substitute Frh for a Ni-free Fe hydrogenase (Hmd) to decrease Ni requirements. The Ni-free Fe hydrogenase has a significantly lower Fe requirement, using only two Fe atoms per complex. When formate is used as an electron source instead of H_2, Frh is replaced by formate dehydrogenase (Fdh), which contains one Mo/W-pterin cofactor, two Zn atoms and between 21 and 24 Fe atoms[6,7].

Zn occurs as a single structural atom in several enzymes. Heterodisulfide reductase (Hdr) is a Fe-S and Zn containing enzyme that catalyzes the reduction of heterodisulfide (CoM- S-S-CoB) to form HS-CoM and HS-CoB in the second to last step in methanogenesis. In methanogens without cytochromes, Hdr has three subunits (HdrABC) whereas methanogens with cytochromes have a two-subunit protein (HdrDE) [9]. HdrABC contains seven Fe_4S_4 clusters and one structural Zn atom and forms a tight complex with the Ni-Fe hydrogenase Mvh, which contains one Ni-Fe active site, one Fe_2S_2 cluster, two Fe_4S_4 clusters, one Fe_3S_4 cluster, and polyferredoxin with 12 Fe_4S_4 clusters. HdrDE contains three Fe_4S_4 clusters, one heme b cofactor, and one structural Zn atom. Methanophenazine is in turn reduced by the Ni-Fe hydrogenase Vht/Vho, which contains one Ni-Fe center, two b-type hemes, one Fe_3S_4 cluster, and two Fe_4S_4 clusters. Methyl coenzyme Mreductase (Mcr), common to all methanogenic pathways, catalyzes the final step in methanogenesis: the reduction of CH_3-S-CoM to CH_4 and the formation of CoM-CoB heterodisulfide with electrons derived from HS-CoB. The crystal structure of Mcr has been solved and contains two coenzyme F430 Ni tetrapyrroles. Methanogens actively transport Ni and Co using ATP-dependent uptake systems in order to fulfill enzymatic requirements. When grown on acetate, methanogens use two metalloenzymes for the conversion of the methyl group from acetate to CH_3-H_4SPT, which differ from those used in CO_2 reduction and methylotrophic pathways. The most metal rich aceticlastic enzyme is CO dehydrogenase/acetyl-CoA synthase (Cdh), which cleaves the methyl group off of acetyl-CoA and transfers it to CH_3-H_4SPT. The Cdh complex contains one Fe4S4 cluster bridged to a Ni-Ni site, four Fe_4S_4 clusters and a $NiFe_4S_4$ cluster, and reduces a $2\times[Fe_4S_4]$ ferredoxin. The CO_2 by-product of Cdh is converted to bicarbonate by a Fe-containing carbonic anhydrase (CA) instead of the Zn-form, which is commonly in CAs from other species. Overall, the metal content of enzymes involved in

aceticlastic methanogenesis is similar to the H_2/CO_2 pathway [6]. Mg is also an active site component of several enzymes and acts as a transporter molecule of adenosine triphosphate (ATP) in the cell [5].
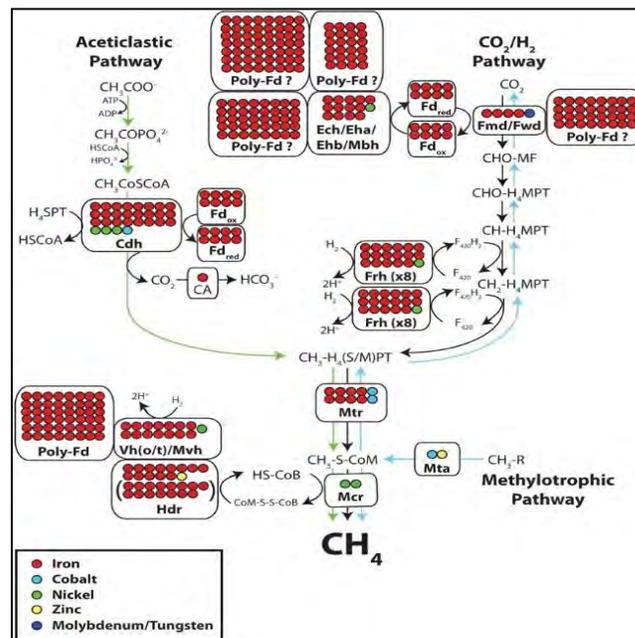
Figure 1. Schematic representation of pathways with respect to trace metals involvement

3. Experimental methodology

3.1 Bioreactor construction and Inoculum source
Single chambered MES system was fabricated using Perspex material with a total/working volume of 500/350 ml was used for the experiments. Carbon fiber brush (5X3 cm length/diameter) were used as anode and cathode electrodes and were connected to the keithley and external power pack with the help of stainless steel wires and the Ag/AgCl was used as a reference electrode (+196 mV vs. SHE) for measuring cathode potential and during electrochemical analysis. The bioreactor was operated at 150 rpm and 33ºC in a batch mode with a supplemental voltage of 1.0 V. The effluent of anaerobic digestion (Suwon Wastewater Treatment Plant; South Korea) was used as source of inoculums for biomethane generation. Initially, the bicarbonate was used for enriching the hydrogenotrophic methanogens followed by CO_2 gas to carry out the actual experiments.

3.2 Experimental Design
The operational solution were prepared by mixing the seed sludge with growth media (GM) at a ratio of 1:1 (based on volume). GM solutions, were prepared as follows: phosphate buffer, 50 mM/L; NH_4Cl, 0.53 g/L; $CaCl_2 \cdot 2H_2O$ 0.08 g/L; $MgCl_2 \cdot 2H_2O$ 0.1 g/L; trace elements solution, 1 ml. The trace elements solution consists of HCl 5.1 ml/L; $FeCl_2 \cdot 4H_2O$, 1500 mg/l; H_3BO_3, 60 mg/l; $MnCl_2 \cdot 4H_2O$, 100 mg/l; $CoCl_2 \cdot 6H_2O$, 120 mg/l; $ZnCl_2$, 70 mg/ l; $NiCl_2 \cdot 6H_2O$, 25 mg/l; $CuCl_2 \cdot 2H_2O$, 15 mg/l; $NaMoO_4 \cdot 2H_2O$, 25 mg/l in TM1 operation but whereas the

concentrations of ., magnesium (Mg_2^+), iron (Fe_2^+), nickel (Ni_2^+) and zinc (Zn_2^+) were varied and supplemented as 100, 600, 16 and 12 mg/l respectively in the TM2 operation. Solutions in the MEC reactors were replaced, when current generations were decreased [10,11]. The CO_2 was sparged at 1 atm pressure into the headspaceof the biuoreactor and the gas omposition is evaluated periodically to review the conversion of CO_2 to CH_4 under external potential application.

3.3 Analysis

The experiments were carried out and the preliminary analysis carried out were voltage and currents generation, cyclic voltammetry, Biogas composition, pH and SCOD concentration. Further detailed analysis viz., enzymes activity, Volatile fatty acids generation and microbial community analysis would aid in understanding the biocatalyst's metabolic function during operation under varying metal concentrations for CH_4 formation.

4. Results and Discussion

4.1 Biogas composition and currents generation

After stable biofilm formation and reaching a steady state, the bioreactor was fed with sludge seed, phosphate buffer and CO_2 gas supplemented without and with (different trace metals concentrations; TM1 and TM2) trace metals. The biogas composition showed higher methane generation with TM2 (14.22 %) operation followed by TM1 (8.1 %) and Control (5.7 %) operations (Fig. 2).
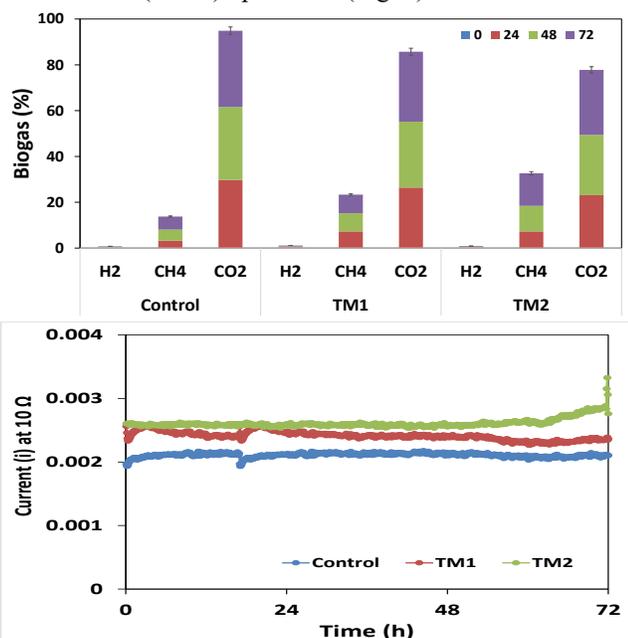
Figure 2. (a) Biogas (%) composition, and (b) Currents profile of MES bioreactor operated at varying trace metal concentrations.

This shows the 3 folds increase in CH4 generation when compared to control operation signifying the importance of optimum trace metals in the enzymatic functioning of biocatalyst. However, the CO_2 concentration showed decrease in the composition in TM operations when

compared to control. The hydrogen generation showed to be very fewer in overall composition. The CO_2 concentration was found to be maximum because of incomplete conversion of CO_2 to CH_4.

The control operation showed the lower currents of 0.002 A but whereas TM1 and TM2 operations showed 0.0025 and 0.0027 A. The TM2 operation depicted increment in the final hours of the operation. This voltage with TM2 operation may show increment with respect to number of cycle's operation. The difference in the voltage generation by the presence of trace metals in the TM1 and 2 operations depicts the significance of trace metals in the biocatalyst's metabolic function towards higher process efficiency.

4.2 Cyclic Voltammetric profiles

Voltammograms visualized a marked variation in redox catalytic currents (RC: reduction currents, OC: oxidation currents) with the function of varying trace metal concentration in comparision to control operation (Fig. 3).
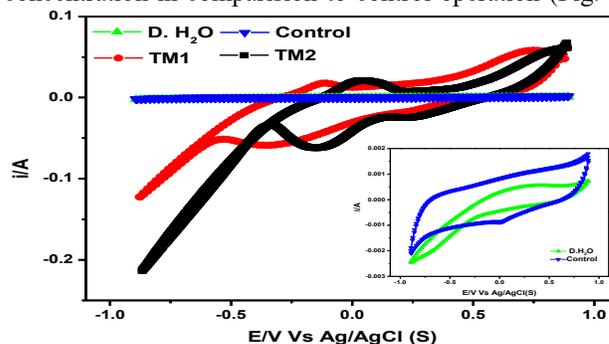
Figure 3. Cyclic voltammetric profiles with respect to control and 2 different concentrations of trace metals

Relatively, higher redox catalytic currents were observed with TM2 operation (OC/RC: 0.061/-0.213 A) in comparison to TM1 (0.061/-0.13 A), Control (0.0018/-0.002 A) and D. H_2O (0.0007/-0.002 A) operations. TM operations showed gradual increment in redox catalytic currents after introducing varying trace metal concentrations to the MES system indicating the direct positive effect that might have entrusted the biocatalyst capability towards CH_4 generation. The OC of TM1 and 2 operations are similar while the RC of Control and D.H_2O are similar. The trace metals at optimum concentrations enhance the overall activity of biocatalyst thereby producing more CH_4 from the CO_2.

4.3 SCOD Concentration and pH

The biocatalyst activity is also evaluated by the decrease in Cod concentration with respect to time intervals during the operation. But, in this case the organic carbon is devoid in the inlet. But, the SCOD concentration showed slight increment depicting the fermentation of complex molecules to simpler sugars or conversion of CO_2 to acetate or formate under external potential application.
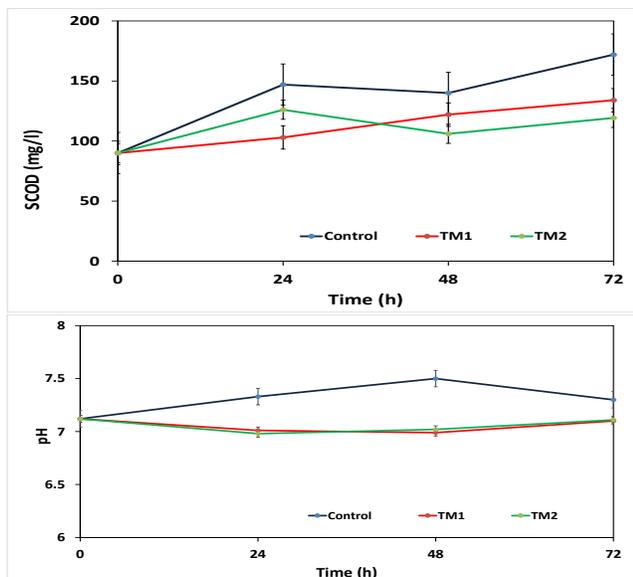
Figure 4. (a) SCOD concentration (mg/l), and (b) pH profiles of MES bioreactor operated at varying trace metal concentrations.

Initially, the SCOD concentration was 90 mg/l but as the time progresses, the Control operation showed higher SCOD concentration of 172 mg/l followed by TM1 (134 mg/l) and TM2 (120 mg/l) operations (Fig. 4). The TM2 operation showed to increase SCOD concentration till day1 and decreased thereafter.

Along with SCOD, the pH profiles were also evaluated to study the metabolic shifts. Changes in pH can alter the several physiological parameters, including internal pH, concentration of ions, membrane potential, proton shuttling, formation of volatile fatty acids (VFAs) and CO_2 dissolution depending upon the organism and hence it is one of the important governing parameters to be considered during bioreactor operation

Except control operation, the two experimental conditions showed similar patterns of redox change until the end of cycle. But the pH during control operation showed increment till 2nd day and further decreased by the end of 3rd day . The buffer is maintain the pH near to 7 during the TM1 and 2 operations whereas the metabolic shifts with control operation are to be evaluated using the VFAs qualitative and quantitative data.

5   Conclusion

The present study proposed and demonstrated the influence of trace metals on the generation of biomethane by utilizing CO_2 as a feed stock. The CH_4 generation showed 3 fold increase when the optimum concentrations of trace metals were used for the operation. The results suggests to overcome the thermodynamic and transport system barriers.

References
1. Sadhukhan, J., Lloyd, J.R., Scott, K., Premier, G.C., Yu, E., Curtis, T., Head, I.M., 2016. A critical review of integration analysis of microbial electrosynthesis (MES) systems with waste biorefineries for the production of biofuel and chemical from reuse of CO2. Renewable and Sustainable Energy Reviews. 56, 116-132
2. Sibiya, N.T., Tesfagiorgis, H.B., Muzenda, E., 2015. Influence of Nutrients Addition for Enhanced Biogas Production from Energy Crops: A Review. 7th International Conference on Latest Trends in Engineering & Technology (ICLTET'2015) Nov. 26-27, 2015 Irene, Pretoria (South Africa)
3. Choong, Y.Y., Norli, I., Abdullah, A.Z., Yhaya, M.F., 2016. Impacts of trace element supplementation on the performance of anaerobic digestion process: A critical review. Bioresource Technology. 209, 369-379
4. Ortner, M., Rameder, M., Rachbauer, L., Bochmann, G., Fuchs, W., 2015. Bioavailability of essential trace elements and their impact on anaerobic digestion of slaughter house waste. Biochemical Engineering Journal. 99, 107-113
5. Srikanth, S., Venkata Mohan, S., 2012. Regulatory function of divalent cations in controlling the acidogenic biohydrogen production process. RSC Advances. 2, 6576-6589.
6. Glass, J.B., Orphan, V.J., 2012. Trace metal requirements for microbial enzymes involved in the production and consumption of methane and nitrous oxide. Frontiers in Microbiology. 3, 1-20.
7. Thauer, R.K., Kaster, A.-K., Goenrich, M., Schick, M., Hiromoto, T., Shima, S., 2010. Hydrogenases from methanogenic archaea, nickel, a novel cofactor and H_2 storage. Annu. Rev. Biochem. 79, 507-536.
8. Anderson, I., Ulrich, L.E., Lupa, B., Susanti, D., Porat, I., Hooper, S.D., Lykidis, A., Sieprawska-Lupa, M., Dharmarajan, L., Goltsman, E., Lapidus, A., Saunders, E., Han, C., Land, M., Lucas, S., Mukhopadhyay, B., Whitman, W.B., Woese, C., Bristow, J., Kyrpides, N., 2009. Genomic characterization of Methanomicrobiales reveals three classes of methanogens. *PLoSONE.* 4, 5797.
9. Hedderich, R., Hamann, N., Bennati, M., 2005. Heterodisulfide reductase from methanogenic archaea: a new catalytic role for an iron sulfur cluster. *Biol. Chem.* 386, 961-970.
10. Choi, K.S., Kondaveeti, S., Min, B., 2017. Bioelectrochemical methane (CH_4) production in anaerobic digestion at different supplemental voltages. Bioresource Technology. 245, 826-832.
11. Kondaveeti, S., Min, B., 2015. Bioelectrochemical reduction of volatile fatty acids in anaerobic digestion effluent for the production of biofuels. Water Research. 87, 137-144.

SEEC-2018-062

3D LASER SCANNING FOR ESTIMATION OF LARGE SCALE BUILDINGS' ROOFTOPS BASED SOLAR ENERGY IN URBAN ENVIRONMENTS

Dr. Rama Rao Nidamanuri*, Dr. Ramiya, and Dr. V K Dadhwal
Department of Earth and Space Sciences
Indian Institute of Space Science and Technology
Department of Space, Government of India
Thiruvananthapuram 695 547
*Email: rao@iist.ac.in

ABSTRACT

The present and future demands of urban environments in India require quantification and efficient utilization of renewable energy resources. Within the urban environment, solar energy is the most important resource, as it is easy to obtain, renewable, and produces negligible waste. Huge demand of housing and industrialization has lead to the existence of open spaces a precious little in Indian urban environments and the possibility to have large scale solar installations at a single location is unviable. In dense urban areas, building roofs have been considered one of the abundant sources of space for solar panel installations. The ongoing government schemes aimed at encouragement and financial benefits to people going for solar panel installations in India are aimed at a high level of energy efficiency and a large degree of local renewable energy generation. In India, the number of building rooftops based solar energy installations is increasing although most of them at small scale at present. Especially, the effective implementation goals of smart urban environments requires detailed quantification, mapping and geometrical characterization of builds and rooftops. Very high resolution multispectral remote sensing has been successfully used for building detection and there are numbers of studies which have extracted building footprints from the perspective of the estimation of solar energy. However, the precise quantification and positioning of solar panels require height, area and orientation of the buildings at a scale amenable to operational requirements of average building level solar panel installations.

3D laser scanning or LiDAR (Light Detection and Ranging) is an active remote sensing technology that captures surface topography in 3D by scanning mechanism. Because of its acquisition mechanism of scanning, LiDAR data is an unstructured 3D point cloud consisting of millions of unclassified points. Efficient processing and reconstruction of LiDAR data for 3D building modelling, true to measurements, can be used for estimation and visualization of various buildings' topographical features such as slope, aspect, and angles, for accurate calculation of area available and the amount solar irradiance. The objective of this work is to demonstrate and implement a methodology for 3D building detection and topographical assessment of buildings' rooftops using high resolution airborne LiDAR remote sensing point cloud for assessing buildings' rooftops based solar energy. The methodology include density reduction and filtering, ground point density estimation, 3D segmentation, point clod labeling, classification and buildings reconstruction. Various statistical and machine learning algorithms have been applied on the builds detection and 3D characterization. Experiments have been performed on benchmark airborne 3D LiDAR remote sensing datasets encompassing various types of buildings and rooftops. Results indicate accurate quantization of buildings' rooftops and geometrical orientations at sub-building scale.

SEEC-2018-064

REVIEW: LASER IGNITION WITH LIQUID FUELS

Shrimantini S. Patil
Research Scholar
Mechanical Engineering Department
College of Engineering, Pune.
Email: Shrimantini.irwadkar@gmail.com

Dr. M.R. Nandgaonkar Associate Professor
Mechanical Engineering Department College of
Engineering, Pune. mrn.mech@coep.ac.in

ABSTRACT

With the developing industrialisation and economy sustainable energy and environment degradation problems have been becoming more and more serious. It is important and challenging job to design energy efficient combustion systems with least pollutants and also understand the interaction of combustion products with chemical species present in atmosphere. Higher thermal efficiencies due to lower heat loss to combustion chamber was the goal of current modern combustion systems. For this purpose innovative (non conventional) ignition techniques such as a laser induced ignition methods have become an attractive field of research in order to replace conventional spark ignition system. The fundamentals of laser induced ignition and recent developments of laser ignition for gaseous fuels have been previously reviewed. Therefore the objective of this study is primarily to examine and review the developments and studies of laser induced ignition with liquid fuel for development of future combustion related applications. Laser induced ignition experimentation have been carried out by many researchers on liquid fuels such as gasoline, wet ethanol, bio ethanol, butanol, bio ethyl-tertiary-butyl ether (ETBE), kerosene , Jet A1, (Gas to liquid) GTL kerosene, Exxsol D80.

Keywords: Laser Ignition, Liquid fuels, Droplet ignition,

INTRODUCTION

Combustion system play a important role in the society, representing the primary source of equipment for transportation and energy production in industry and also

one of the principle source of different pollutants. For this reason, even a slight improvement in its emission control and limitation will impact considerably on the reduction of overall emissions from the environment and increase in efficiency. The lean or low temperature combustion of an internal combustion engine is a key issue to improving thermal efficiency to prevent global warming and preserve fossil fuels. However current engines cannot be operated sufficiently lean or at low temperatures due to ignition related problems such as sluggish flame initiation, flame propagation along with potential misfiring [4]. Lean and low temperature combustion requires a stronger ignition system than conventional spark ignition method, which was invented more than centuries ago. Most of the problems listed above could potentially be solved by the use of laser induced spark ignition because it has many potential benefits. Due to limited sources of fossil energy carriers and a increasing global demand of energy, for this study emphasis is given on use of alternative liquid fuels for laser induced ignition. [7].

FUNDAMENTALS OF LASER IGNITION

Laser ignition is one of alternative system to the conventional spark ignition system. It is accomplished without electrodes, increasing its lifetime significantly longer. It also allow ignition in multiple locations inside the combustion chamber to shorter the combustion time of

Lean mixtures. Laser ignition of reactive mixture can be divided into four categories.
1. Thermal initiation: by the absorption of laser radiation through rovibrational molecules. It

utilizes infrared laser energy to vibrationally and/or rotationally excite a specific highly absorbing species within the combustible mixture to induce ignition. Ignition takes place when the target absorber transfers sufficient energy to the combustible mixture to cause auto ignition.[3-13].

2. Non-resonant breakdown initiated by multiphoton ionization and followed by electron cascade breakdown. It occurs when a laser pulse of sufficient peak power is focused to a sufficiently small spot whereby the electrical field component of the focused light is strong enough to influence the gas molecules and initiate the electron breakdown of the gas [3-11-13].

3. Resonant breakdown initiated by photodissociation and followed by electron cascade breakdown. The dissociated atoms or molecules are then resonantly ionized via multiphoton ionization by continued laser illumination. The electrons generated by the resonant ionization gain energy via the inverse Bremsstrahlung photon absorption process can induce breakdown via the electron cascade process [3-11-13].

4. Photochemical ignition through radical production by photolysis. It occurs when the high energy photon dissociates a molecule allowing the ionized constituents to react with the surrounding gases. [3-11-13].

Laser induced spark ignition or non resonant breakdown which is similar to spark ignition system. The process begins with multi-photon ionization of few gas molecules which releases electrons that readily absorb more photons via the inverse bremsstrahlung process to increase their kinetic energy. Electrons liberated by this means collide with other molecules and ionize them, leading to an electron avalanche, and breakdown of the gas [13].

ALTERNATIVE LIQUID FUELS

Today, the reserves of petroleum based fuels are being rapidly depleted. It is well known that the future availability of energy resources has increased the need for the utilization of alternative fuels like, ethanol, bio –ethanol, ethyl-tertiary butyl ether (ETBE), butanol and blend of these fuels, kerosene, GTL kerosene, Exxosol D80. Ethanol is becoming a promising biofuel due to higher flame propagation velocity than gasoline, lower combustion temperature which allows higher thermal efficiencies by reducing heat loss to the combustion chamber walls. Ethanol has greater enthalpy of vaporization, large octane number and smaller stoichiometric air/fuel ratio compared with gasoline [1-7-13]. Principally spark ignition engines are capable of using longer chained butanol, ethers (ETBE) One approach to reduce exhaust emissions

from airplane is the use of synthetic fuels such as GTL (gas to liquid) fuels. To produce GTL kerosene natural gas is converted first into a synthetic gas. Then liquid hydrocarbons are built by adding oxygen into and water vapor to this synthetic gas[2-3].

HIGH SPEED IMAGING

Investigation of the effect of water concentration on combustion characteristics of wet ethanol ignited using Nd:YAG laser have been carried out by Kazi Mostafizur et al. Flame kernel development, ignition delay, laminar burning velocity was determined by investigating the primary combustion pressure history. Images of flame were taken to determine the ignition delay. Stirring duration is important to determine the homogeneity of wet ethanol. It is investigated from flame growth images that with addition of 10 to 20% water, flame luminosity, flame propagation speed, flame growth rate, all increases. But with 30% and 40 % addition of water, flame becomes darker and contains granular orange luminescence, which causes reduction in flame propagation velocity due to dilution effects and chemical influence of water. With higher water concentrations, water ethanol interactions become more significant, ethanol molecules get trapped in the large cavities within the water structure, which leads to reduced flame propagation velocity of mixture. Laminar burning velocity is highest at ϕ =1.0 and for unhydrous ethanol and 10% addition of water. The laser ignition delay was shorter with water addition for 10% and 20% which gives rise to larger initial flame kernels. This was happened because generation of OH* was enhanced with presence of water, which accelerated the initial combustion reactions. But with further increase in water addition, the physical and chemical influence of water increases radical concentration and mixture reactivity leading to smaller flame kernels. For all equivalence ratios ranging from $0.7 \leq \phi \leq 1.2$ formation of front lobe were found evident [1]. Which indicate that laser ignition can generate consistent spark and flame kernel with wet ethanol fuel.

Experimental investigation and spectroscopic diagnostics of laser induced air breakdown and kerosene, Jet A-1 spray ignition have been done to get the amount of laser pulse energy absorbed by air breakdowns. It was found that from average pulse energy of 193.1mJ only a small fraction of 24.7mJ remained in air breakdown. Transient morphologies of air breakdowns and kerosene breakdowns were compared. Air breakdown has constantly defined surface. After 30 μs the air breakdown became invisible. Air breakdown firstly shrinks and then formation to a disc takes place. In contrast, the spray breakdowns did not shrink but became blurred and fibrous after 3-4 μs. With steadily decreasing

intensities they became invisible after 90 μs, that is three times later than air breakdown [3]. Due to fibrous shapes , formation of evoking flame kernels takes place. The plasma formed was no more bright, hence the combustion became weaker.

Droplet breakup mechanisms have been observed for kerosene and jet A1-1 fuel. At 5mm distance to the focal point droplets deformed to discs and disintegrated to very small secondary droplets. This mechanism resembles the catastrophic breakup mode, which occurs for Weber number of We ≥ 350. Second mechanism observed was resonant mechanism, 10mm below focal point, which occurs for the We ≤ 12. Catastrophic breakup is crucial mechanism for spray ignition. Secondary droplets evaporates very fastly than initial droplet, so the spark get quickly surrounded by the air fuel vapor during Catastrophic breakup mechanism. Hence such mechanism is supportive to the fuel ignition. Resonant breakdown appear only behind the shock fronts of spherical blast waves hence Weber number concept can not be adopted to unsteady flow fields. From calculations it was observed that postshock velocities becomes zero within 10 μs while droplet disintegration in resonant breakdown occurred after 200 μs. Hence its application for postshock flow of spherical blast waves becomes limited[5].

Formaldehyde laser induced fluorescence (LIF) detection and droplet ignition experiments with their comparisons have been carried out on GTL kerosene, Jet A-1, Exxsol D80 fuels. The laser induced fluorescence intensities of liquid GTL kerosene and Exxsol D80 are on a lower level than that of Jet A-1. In some droplet ignition mechanisms background emission was observed first followed by formaldehyde LIF after a time delay. For this experimentation of kerosene background substraction have been performed to derive correct igntition delay times based on formaldehyde LIF (cool flame). For GTL kerosene authors found a cool flame ignition delay time of 624ms, while for Exxsol D80 and Jet A-1 it was 1467ms and 1699ms, respectively. The differences for the starting time of hot ignition around 1050ms and ignition temperatures near 700K was observed [2].

ENGINE STUDIES USING LASER IGNITION:
There has been little information concerning experimental research carried out directly addressing the potential benefits of laser ignition as applied to automotive engines and combustion systems.
One of the earliest application of the laser ignition techniques in a gasoline engine was demonstrated by Nicolaie et.al.[8]. A Dacia Logan vehicle produced by renault with gasoline indirect injection engine was fully operated with laser spark plugs using Q-switched Nd: YAG/Cr^{4+}:YAG lasers. In first set of experiments

coefficient of variability (COV) were measured at medium speed. At 1500 rpm engine speed the improvement of COV of maximum pressure was around 15 % in comparison with Spark plugs. There was decrease in CO by 18% to 25%, HC reduction by 14% to 17% , and in case of NO$_x$ an increase by 2% to 8% in comparison with classical ignition.[8].
The variation of difference in BSFC of laser ignition and spark ignition was determined at air-fuel ratio λ=1.0 ,2000 rpm engine speed depending on the BMEP of 2 bar to 8 bar. Smaller specific fuel consumption was measured for laser ignition as comparison with classical ignition at all engine loads. The 3 % difference of BSFC was found at low engine load of 2bar (BMEP). At high loads the percentage difference of BSFC was very small. The COV IMEP was 32 % smaller for laser ignition than classical ignition at air-fuel ratio λ 1.2 and 2bar (BMEP).These differences were very important as they were directly related with emissions like CO and HC[8].
An investigation by Adrian[9] focused on by considering the duration of combustion as heat release at an angles at which 10% and 90% of the total heat obtained from the burning was released. Author found for shorter combustion duration when using laser ignition , which lead to increase in engine efficiency, and decrease in level of detonation for 4bar and 5bar BMEP. The combustion duration with laser ignition was at least 30% lower than classical ignition at 5 bar [9]. From above experimentations we can conclude there is a direct impact of laser ignition on engines efficiency , BSFC and HC,CO emissions.

Josef et.al.[7] performed ignition tests on a single cylinder spark ignition research engine at part load operating point and for relative air fuel ratio with port fuel injection by using gasoline EN228, ethanol E100, butanol B100 and ETBE as fuel. The paper described systematically the differences between spark and laser ignition with respect to the thermodynamics of the combustion process and the emissions. The temperature of the aspirated mixture was calculated from the measured volumetric efficiency and the measured cylinder pressure. Due to the different values of heat of vapourisation and the stoichiometric air/fuel ratio of the investigated fuels, a more or less intense mixture cooling observed. Authors found moderate cooling of 11K for ethanol, 2 K for ETBE, and temperature increase of 7K for butanol. These values found was significantly less than the theoretical values, (for example for ethanol at λ 1.4 it is approximately 60 K). These lower values caused the wall film formation on the surfaces of inlet port and the inlet valve discs, resulting in heat fluxes between the structure and the liquid film. Incomplete fuel evaporation at inlet valve closing was assumed because butanol has lower vapor pressure.

In general for engines operating with alcohol fuels the emissions are remarkable lower. Fluid properties, burn rate and the peak temperatures are the important parameters for emissions. The extinction of flame determines the amount of hydrocarbon emissions. Therefore a high laminar flame speed such as alcohol fuels, and a fast burning of the mixture at high temperatures are favorable. As compared to gasoline, ethanol was found with less emissions, HC 37%, NO_x 87%, CO_2 92 % for stoichiometric combustion[7].

CONCLUDING REMARKS

In this paper, work carried out using laser induced ignition with liquid fuels have been reviewed. The feasibility of using laser induced ignition with liquid fuels for automotive engine applications, gas turbine applications, combustion in boilers have wide scope of experimentations to be carried out. It can be concluded that enhancement to the lean burn and low temperature combustion process for liquid fuels will be achieved with laser induced ignition and also through multipoint combustion at multiple locations.

One of the main advantage of laser ignition is a rapid ignition of a homogeneous air-fuel mixture, especially at lean operation and higher residual gas content.

Moreover there is need for the technology development in the combustion chamber window (crucial for the succesful ignition) and plays important role in cost optimization.

Finally, due to the promising characteristics of laser ignition and continuous reduction in laser equipment costs, the future research on the subject may yield systems with significant applications in combustion systems.

REFERENCES

[1] Kazi Mostafijur Rahman, Nobuyaki Kawahara, Kazuya Tsuboi, 2016. "Combustion characteristics of wet ethanol ignited using a focused Q-switched Nd:YAG nanosecond laser". Fuel 165, (2016), October, pp. 331–340.

[2] A. Burkert, W Paa, 2016. " Ignition delay times of single kerosene droplet based on formaldehyde LIF detection". Fuel 167(2016), November ,pp 217-279.

[3] Gregor C.Gebel, Thomas Mosbach, Wolfgang Meier, 2015. "Optical and spectroscopic diagnostic of laser-induced air breakdown and kerosene spray ignition". Combustion and Flame 162 (2015), December, pp. 1599-1613.

[4] Cangsu Xu, Donghua Fang, Qiyuan Luo, 2014. " A comparative study of laser ignition and spark ignition with gasoline-air mixtures". Optics & Laser Technology 64 (2014), June, pp. 343-351.

[5] Gregor C.Gebel, Thomas Mosbach, Wolfgang Meier, 2013. "An experimental investigation of kerosene droplet breakup by laser- induced blast waves". Journal of Engineering for Gas Turbines and Power (ASME), (2013) January Vol. 135/ 021505-1.

[6] Caroline L. Genzale, Lyle M Pickett, Alexandra A, 2011. "Laser ignition of multi injection gasoline sprays". SAE International (2011), December, doi: 10.4271/2011-01-0659.

[7] Josef Graf, Thomas Lauer, Bernhard Geringer, 2012. " laser ignition of alternative liquid fuels", Research ignition, MTZ peer review, December, Vol. 73, MTZ 0512012.

[8] Nicolaie Pavel, Adrian Birtas, Gabriela Croitoru, 2017. "Laser ignition of a gasoline engine automobile". Laser Ignition Conference © OSA 2017, Romania.

[9] Adrian Birtas, Niculae Boicea, Gabriela Croitoru, 2017. " Combustion characteristics of a gasoline-air mixture laser ignition". Laser Ignition Conference © OSA 2017, Romania.

[10] Gabriela Croitoru, Onna Valeria Grigorge, Nicolaie Pavel, 2017. " Aspects of air-breakdown with a high peak power passively Q-switched Nd: YAG/Cr^{4+} :YAG laser". Laser Ignition Conference © OSA 2017, Romania.

[11] Mohamed H. Morsy, 2012. " Review and recent developments of laser ignition for internal combustion engines applications". Renewable and Sustainable Energy Reviews 16, (2012), June, pp 4849-4875.

[12] Steven A.O'Briant, SreenathB.Gupta, SubithS.Vasu, (2016). "Review: laser ignition for aerospace propulsion". Propulsion and Power Research 5(1), February, pp. 1-21.

[13] Tran X. Phuoc, 2006. " Reviwe- Laser- induced spark igntition fundamental and applications". Optics and laser in Engineering 44(2006), February, pp.351-397.

[14] Tran X. Phuoc,White FP 1999. " Laser induced spark ignition of CH_4/air mixtures". Combustion and Flame 119 (1999)January,pp 203-218.
.

SEEC-2018-065

AN INVESTIGATION OF THE SUPPLEMENTARY SOURCE OF POTABLE WATER BY ATMOSPHERIC VAPOR CONDENSATION AND ITS QUALITY CONTROL

Dinesh Kumar and Akhilesh Tiwari
Department of Applied Sciences
IIIT Allahabad, Deoghat Jhalwa
Allahabad 211015, India
Email: atiwari@iiita.ac.in

Kuldeep Srivastava
Information System and Services Division,
India Meteorological Department,
Ministry of Earth Sciences,
Mausam Bhavan, Lodhi Road,
New Delhi- 110003, INDIA
Email: kuldeep.srivsatava@imd.gov.in

ABSTRACT

The water vapour in Earth's atmosphere is available as fresh water, which can be considered as an alternative source of water obtainable as potable water, especially in Indian Coastal states. In order to extract water from atmospheric humid air, and make it qualitatively pure for drinking purpose, we have to develop alternative cost effective ways. This study was conducted to develop a cost effective technique for the condensation of water vapour from humid air, and to make it fit for drinking. This energy efficient and portable technique will help us to fulfill the needs of water.

Keywords: condensation, humid air, potable water, atmosphere
.

NOMENCLATURE

L is the lenth of the plate
ρ density of water
ρ_v density of vapour
k thermal conductivity
g gravity
μ viscosity of fluid
υ kinematic viscosity
T   atmospheric temperature
T_s saturation temperature
T_w wall temperature
H   enthalpy of the vapour
h_{loc} local heat transfer coefficient
h_m mean heat transfer coefficient
T_D dew point temperature
Φ humidity

L_w water productivity
E   effecience of dehumidification
α convection heat transfer coefficient
V velocity of fluid
D hydraulic diameter

INTRODUCTION

Within a century, the world population has increased from 1 billion to over 7.2 billion people. This growth should not stop and the population in 2050 is estimated at 9.6 billion. Thus, issues of resources and particularly that of water stocks arise. Indeed, current drinking water reserves will be insufficient to enough for the whole world [1-3]. It is therefore necessary, as is the case in energy for example, to find new ways to produce water. The condensation of water naturally present in the air could be a solution to this problem.

The atmosphere contains more than $12.9 \times 10^{12} \mathrm{m}^3$ of renewable water. In this study, our objective is to investigate the possibility of using TEC devices to retrieve water condensate from humid air in the areas, where there is high mean relative humidity during the whole year such as in coastal regions. Usually, These devices meant for cooling, which can create a surface below dew point, and can help to condense the water on the cold surface. But, the issues

which one has to overcome upon are, would this technique be effective and sustainable. And how to improve the TEC devices to maximize the amount of water that can be condensed?

To address these concerns, we have proposed a prototype device, which has produced water condensate with a controlled flat surface of regulated temperature. The metrological data has been studied for two different Indian states, one where there is a high relative humidity and another in semi arid regions with low relative humidity during the year. Also, the analysis will be done on the data, if this solution to condense drinking water is effective, i. e. if the amount of water produced will be considerable after the cost analysis. At the end we will seek the solutions to maximize the production of drinking water by changing device parameters.

EXPERIMENTAL MATERIALS AND METHODS

Creating a surface below the dew point will induce the condensation process. A prototype device has been developed for the condensation of the water vapour from humid air. This device is capable of tuning temperature on the flat surface below dew point for different temperature different temperature between saturation temperature and dew point.The drop wise or film wise condensation is produced on the basis of surface geometry and choice of material used. It is well known that drop wise condensation recovers more water because of higher heat transfer coefficient, which is 4 to 10 times more than film wise condensation.
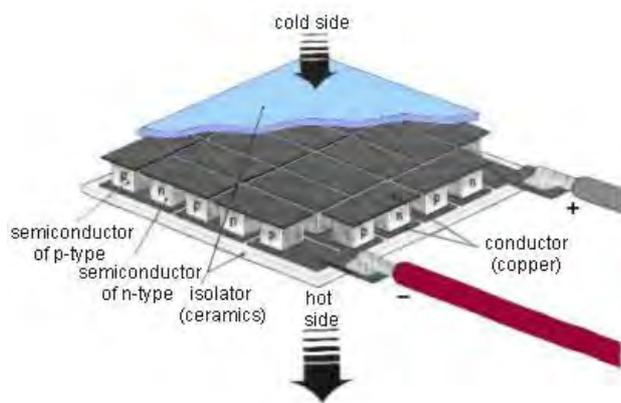
FIGURE 1: SCHEMATICS OF THE PELTIER DEVICE.

SALIENT FEATURES:

❖ Peltier element is made up of p-type and n- type semiconductors.
❖ p-type and n-type semiconductors connected in series.
❖ These semiconductors pallets are sand-witched between two thin ceramic plates.
❖ On current conduction One end of the Peltier element will become hot and another end will be cool.
❖ On changing the polarity of current the hot and cold sides will change.
❖ Hot end is connected with a heat sink to dissipated the thermal heat.
❖ Cool end may be connected with plates, to cool below the dew point, for the occurrence of condensation process.

NUSSELT'S THEORY

Nusselt's theory is the heat transfer phenomena by condensation process and it is dimensionless parameter characterizing convective heat transfer and define as [3] :

$$N_u = \frac{\alpha L}{k}$$

MEAN HEAT TRANSFER COEFFICIENT

According to the Nusselt's theory the mean heat transfer coefficient on a vertical plate which has lenth L are given below.

$$h_m = \frac{1}{L}\int_0^L h_{lco}\ dz = 0.943\left[\frac{\Delta H\rho(\rho-\rho_v)gk^3}{\mu(T_s-T_w)}\right]^{1/4}$$

REYNOLDS NUNBER

The flow pattern of different fluids in different situations.Laminar flow means low Reynolds number below certain threshold and turbulent flow means heigh Reynolds number above certain threshold [4].
It is defined as Re_D:

$$Re_D = \frac{\rho V}{\mu} = \frac{VD}{\nu}$$

DEW POINT TEMPERATURE

Dew point temperature at which the air must be cooled to became saturate with liquid water [5].
It is represented by T_D :

$$T_D = \left(\frac{\Phi}{100}\right)^{1/8}(112 + 0.9\ T) + (0.1T - 112)$$

WATER PRODUCTIVITY

Generated liquid water is defined as [6]

$$L_w = \frac{H_x^\Phi - H_x^{100\Phi}}{100} \times E$$

RESULTS AND DISCUSSIONS

The data given in the plots are from Jodhpur district of Rajasthan State in India. The data was taken from the Indian Metrological Department, New Delhi. It can be easily seen from the plots (Figures 2) that the temperature difference between the dew point temperature and ambient temperature is not very high and it may be possible to produce water condensates from the humid air by creating a surface of low temperature below dew point. And this may be possible for more than six months in a year. This is possible in the semi arid regions of the country also. The coastal regions have more possibility, where there is a scarcity of potable water and average relative humidity will be better during the day. The figure 3 and 4 depicts the mean average maximum and minimum ambient temperature variation with relative humidity with respect to the months in a year. The mean relative humidity during the year from July to September is more than 60 %, which may be used as a favourable condition for condensation phenomenon. The difference of temperature between the ambient minimum/ maximum temperature and dew point temperature is closer also during this period.
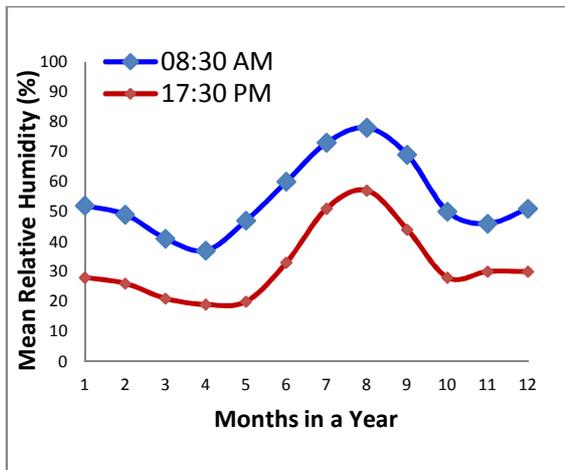
FIGURE 2. PLOT SHOWS MONTHS IN A YEAR VERSUS THE MEAN RELATIVE HUMIDITY IN TWO TIMES AT A DAY TIME IN UTC AT 3 (i.e. 08:30 IST) AND 12 (i.e. 17:30 IST).

The condition of condensation has been fulfilled by this cooled surface, and the temperature of this surface has to be below the dew point. The higher temperature difference between the dew point and the ambient temperature will produce more water condensate on the condensing surface.

We can see in the above diagram that the water production increases with the temperature difference between the dew point and the temperature of the cooled surface at atmospheric temperature T=50°C. The surface area of the cooling plate here is the same as previously (1m²). We can notice that the amount of compensated water increases to 200kL/h at a temperature difference of 20 degree C [9].
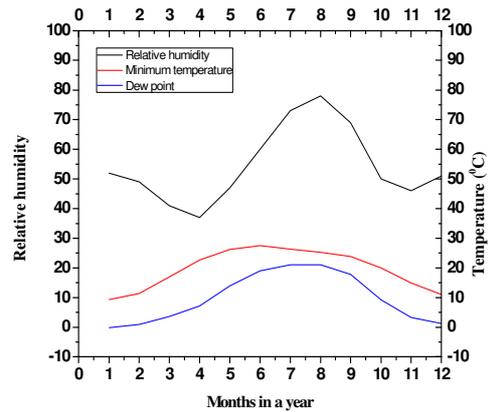
FIGURE 3. PLOT SHOWS THE MONTHS IN A YEAR VERSUS THE VALUES OF MEAN RELATIVE HUMIDITY, MINIMUM AMBIENT TEMPERATURE AND DEW POINT TEMPERATURE.
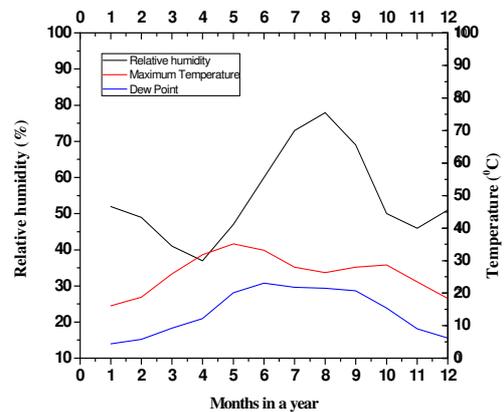
FIGURE 4. PLOT SHOWS THE MONTHS IN A YEAR VERSUS THE VALUES OF MEAN RELATIVE HUMIDITY, MAXIMUM AMBIENT AND DEW POINT TEMPERATURE.
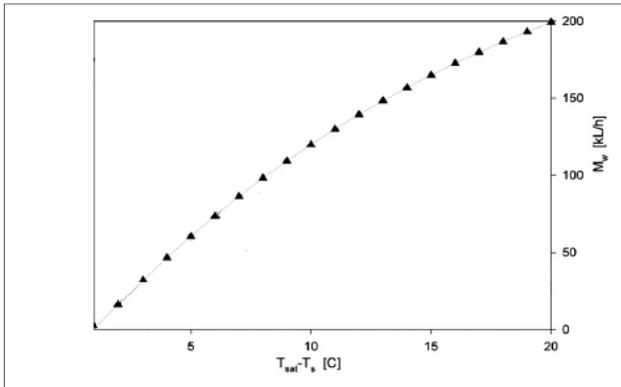
FIGURE 5. AMOUNT OF FRESHWATER PRODUCED
AS A FUNCTION OF THE TEMPERATURE
DIFFERENCE BETWEEN THE DEW POINT AND THE
SURFACE TEMPERATURE AT AMBIENT
TEMPERATURE T = 50°C [1].

CONCLUSION

The technique proposed in this study will be a beneficial tool to produce water condensate for our daily. The production of condensed water with thermoelectric cooling devices may be sustainable solution to respond to the future problem of potable water. Further, detailed study is required to analyze cost based study for different regions of the country, where the environmental conditions are favorable for condensation. Also more rigorous technological cost analysis and water quality assessment may be done to reduce the price of potable water using the TEC technology

ACKNOWLEDGMENTS

REFERENCES

[1] D. Milani, A.Abbas, D.Al Bakri. 2006. Sustainable solutions to our water crisis: generating freshwater from "thin air", The University of Sydney, Thesis

[2] Akhilesh Tiwari. 2011. Characterization of mass transfer by condensation on a horizontal plate, Université Blaise Pascal, Thesis

[3] Nusselt WA, 1916, The surface condensation of water vapour, *Zieschrift Ver. Deut. Ing.,* 60, 541-546

[4] Schlichting Herrmann,, Gersten Klaus. 2000..Boundary-Layer Theory,,Springer-Verlag Berlin Heidelberg, 2000, ISBN: 978-3-540-66270-9

[5] Martin Wanielista, Robert Kersten and Ron Eaglin. 1997. Hydrology Water Quantity and Quality Control. John Wiley & Sons. 2nd ed

[6] Hellstrom, B. .1969. Potable Water Extracted from the Air – Report on Laboratory Experiments, *Journal of Hydrology* **9**(1), 1-19

SEEC-2018-066

AN INDIGENOUSLY DESIGNED SOLAR DRIER FOR A NOVEL READY TO EAT CHEESE VARIENT PROCESSING

Minakshi Chakraborty[1]
Dept of Food Technology
and Biochemical Engineering,
Jadavpur University, Kolkata 700032
minakshichakraborty09@gmail.com

Debabrata Bera[3] *
Dept of Food Technology
and Biochemical Engineering
Jadavpur University, Kolkata 700032
beradebabrata@yahoo.co.in

Bedotroyee Chowdhury[2]
Dept of Food Technology
and Biochemical Engineering,
Jadavpur University, Kolkata-700032
bedotroyeechowdhury@yahoo.in

Lakshmishri Roy[4]
Dept.of Food Technology,
Techno India, Kolkata 700091
lakshmi1371@gmail.com

ABSTRACT

Increasing population and high cost of fuelsave created opportunities for using alternate energies for processing of foods. Solar processing is an emerging sustainable energy technology that provides good quality foods at low or no additional fuel costs. The present investigation is an attempt to design and explore solar drier for traditional and ethnic food i.e Churpi cheese and Bandel cheese .They are found in Nepal and Eastern- India, Bandel, West Bengal respectively. Objective was to modify these two traditional cheeses and produced a nutritive, value added, ready to eat cheese by applying a solar drying process. Drying was accomplished in an indigenously designed solar dryer maintained at around 70^0C, to reduce 80% moisture content. Solar drying technology was used, as its cost effective and minimizes micro and macro nutrients losses during drying process. Physical properties and proximate composition of ready to eat cheese were analyzed. The sensory panel of this cheese rated more acceptable.

*Keywords:*Ready to eat Cheese, Solar Drying, Bandel Cheese.

INTRODUCTION

Bandel cheese is the traditional cheese originated in an erstwhile Portuguese colony, Bandel located in eastern India (West Bengal). The two varieties of bandel cheese available in West Bengal, include smoked and non-smoked [13]. The variety is highly aromatic and fresh as it is sold in circular flats straight away after production [13]. Bandel cheese can be well salted to be stored. But these techniques, however were not beneficial in terms of product shelf life, and taste. To increase the shelf life, removal of moisture from the foods is important. Hence drying/dehydration of cheese to a Churpi like proto type may be a promising option that needs to be investigated, standaridized and adopted for enhancing its shelf life and there by improving the economic prospects and global availability of this traditional, local cheese variety.

Churpi as referred to in Tibetan and Nepali languages and by a slag in Mongolia, is a delicious dried cheese variant having a consistency ranging from soft to slightly hard, color white to orange, taste and odor, sour to pungent, pH 5.97 to 7.0 It is largely consumed in the Himalyian highland region though its industrial production is not yet standardized [1]. Churpi has two variety soft Churpi [2] and hard churpi [3]. Soft churpi is an excellent source of protein,[4].

Drying of agricultural products under direct sunlight is the traditional way of preservation of food. The process of dehydration alone contributes up to 30 % of the total cost of processing of most fresh produce. Thus, the cost of dehydration and energy consumption and quality of dried products play very important role in choosing an appropriate drying process.Traditional sun drying takes place by putting the products under the direct and indirect sunlight by covering the products by transparent or non-transparent covers [5]. Hence a solar drier could be a preferred option Advantages of solar drying include: no fuel dependence, negligible operating cost, reduced environmental impact, sustainable form of energy, allows

longer storage, reduced drying duration and less chance of food spoilage.

The process of drying in the solar dryer is facilitated by circulation of hot air, the spreading density of the product, the nature of pretreatment as well as the nature of the product to be dried itself. The time taken for drying is also determined by the factors such as the initial moisture content and the desired final percentage moisture of the product.

The objective of this study was, Invention of ready to eat churpi cheese varient by applying an eco-friendly technology (solar drying) without affecting the nutritional characteristics of bandel cheese. Major design parameters considered during designing of the drying chamber include:quantity of product, capacity of dryer effective circulation, vent, loading and unloading of materials, thermodynamic aspects etc. Effect of parameters on drying were studied and the kinetics of the drying phenomena modeled. Resultant Bandel cheese, a churpi prototype is likely to possess an increased shelf life and reduced storage and transportation cost, increased scope of marketability in national and international market. Overall adoption of this process may have a positive impact on the employability of local population and thereby promote their socio economic upliftment.

MATERIALS METHOD

Step 1: Solar drier *Design Calculations:*

Angle of Tilt (β) of Solar Collector/Air Heater:
It was calculated using: $\beta = 10^0 + lat\varphi$, where $lat\varphi$ is the latitude of the collector location, the latitude of Kolkata is 23 ^{0}N. Hence, $\beta = 10^0 + 23^0 \approx 35^0$

Insulation on the Collector Surface Area was obtained using: $Ic = H_T = HR = 4120 \times 1.1139 = 4589.27$ Whr/m^2/day, where average daily radiation on horizontal surface is; H = 4120 Whr/m^2/day and average effective ratio of solar energy on tilted surface to that on the horizontal surface R is 1.1139

Calculations pertaining to determination of Collector Area and Dimension [14]. Shown in Eqn.(1)

$$v = 4.48\sqrt{\frac{h(T_1 - T_a)}{(T_a + 273)}} \qquad (1)$$

v = velocity m/s
h = height of collector = 43.11cm = 0.4311 m
l = collector length m = 60.96 cm = 0.6096 m
$\emptyset$ = collector tilt angle = 35^0
T_1 = collector outlet temperature ^{o}C = 70^{0}C

T_a = ambient temperature ^{o}C = 30^{0}C
For T_1 T_a, The mass flow rate of air M_a was determined by taking the average air speed V_a = 1.263 m/s. The air gap height was taken as 5cm = 0.05m and the width of the collection assumed to be 60cm = 0.6m. Thus,
Volumetric flow rate of air V'_a = $V_a \times 0.05 \times 0.6$, V'$_a$ = $1.263 \times 0.05 \times 0.6 = 3.768 \times 10^{-2}$ m^3/s
Thus **mass flow rate of air**: Ma = $v_a\rho_a$

Density of air ρ_a is taken as 6.38 kg/m^3,
$M_a = 3.768 \times 10^{-2} \times 6.38 = 24.04 \times 10^{-2}$ kg/s, Therefore, **Area of the collector A_C**
$A_C = (24.04 \times 10^{-2} \times 1005 \times 40)/(0.5 \times 4589.27) = 4.211$ m^2
The length of the solar collector (L) was taken as;
L = A_c/B = 4.211/0.6 = 7 m, Length of the drier is taken as 8.77 m.
Hot air was passed from solar collector to the bottom of dryer. This hot air is diverted by placing a barrier at the bottom of dryer to get proper heat distribution.

Step 2: Preparation of churpi like product:
Bandel cheese were cut into small pieces and immersed in water for 8 to 10 hours for desalination. After every 4hours interval, water was removed and refilled with fresh water to improve the desalination process. After desalination it was macerated and kneaded into a smooth paste. The resultant slurry paste was then placed in perforated cheese cutter and manually pressed. The cheese strands obtained thereafter were placed in the indigenously designed solar dryer.

Step 3: Solar drying:
Cheese strands were spread on the racks of solar drier (Locally Made). Solar energy was set at 70^{0}C temperature. The drying was continued for 5hours.
Every15,30,45,60,90,120,150,180,240,300 minutes interval moisture loss was measured. Moisture ratio(MR) was calculated using the equation [6]. Shown in Eqn (2).

$$MR = \frac{M_t - M_e}{M_0 - M_e} \qquad (2)$$

Where, MR= Moisture Ratio, M_t = moisture constan at any time, M_0 = Initial moisture constant, Me = Equilibrium moisture content.
The initial moisture content of cheese slurry was found to be 70%. The experiment were conducted at 70^{0}C until the equilibrium moisture was achieved. Taking natural logarithm on both sides establishes a straight line relationship between logarithm of moisture ratio (lnMR) and time (t) was plotted an equation [6]. Shown in Eqn (2).

$$\ln MR = \ln\frac{8}{\pi^2} - \frac{\pi^2 2D_e t}{4L^2} \qquad (3)$$

The diffusion coefficient is calculated by the method of slope. From the slope of the plot of lnMR versus time at different temperatures.

According to, Newton kinetic model.,[8],Shown in Eqn. (5)

$$MR = \exp(-kt) \quad (5)$$

Handerson drying kinetic models.[7], Shown in Eqn. (6)

$$MR = a\exp(-kt) \quad (6)$$

Page drying kinetic models. [12], Shown in Eqn.(7)

$$MR = \exp(-kt^n) \quad (7)$$

Following Newton and Handerson Pubis model we got , k = -slope. Following page model we got, $k = e^x$.(Tab.1.)

Step 4: Evaluation of physical properties of the processed cheese:
Water absorbtion capacity [9] and Bulk density[10] was measured.The pH of the sample was estimated using pH meter.

Step 5: Evaluation of proximate composition:
Analysis of samples for protein,moisture, total solid, fat,ash content were carried out in triplicate using standards methods[10]. Fats were determined by Soxhlets methods [11]. Protein was determine by Lowry method [11].

Step 6: Sensory evaluation:
Taste panel evaluation of dried cheese from all the samples was conducted using a panel of 15 judges who were regular cheese eaters using a 9-point hedonic scale, where 1 and 9 represent dislike extremely and like extremely respectively.

RESULT AND DISSCUSSION

1. **Designed solar drier**

FIGURE 1. SOLAR DRIER

The designed solar dryer can captured about 134kw solar energy par day in Kolkata (West Bengal).

2. Drying characteristics for solar dried cheese:

TABLE 1: MODEL CONSENT WITH R^2 VALUE.

Model	Temp(^{0}C)	Constant	R^2 value
Newtons	70	K=-0.007	0.872
Page	70	K=0.12 n=1.22	0.962
Handerson-pubis	70	K=-0.006 a=1.53	0.872

± Standard deviation of three replicates.

Tab.1. shows that R^2 value is highest for page model ,that indicates the Page models is best fitted for drying of modified bandel cheese.
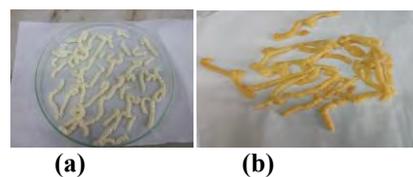
(a)   **(b)**
FIGURE 2. (a) BEFORE DRYING, (b) DRIED CHEESE

TABLE 2: PHYSICAL CHARACTERSTICS OF READY TO EAT CHEESE.

Property	Dried Cheese
Bulk-Density (gm/ml)	0.1±2.36
Water-Absorbtion Capasity(gm/ml)	1.5±1.36
PH	6.09±0.36

Solar dried cheese had the low bulk density.The pH of products is an important factor which affects their shelf–life.The pH of solar dried cheese was 5.19±0.17 which indicates the product is not easily spoiled by neutrophilic bacteria.(Tab.2.)

3. Results of Proximate composition.
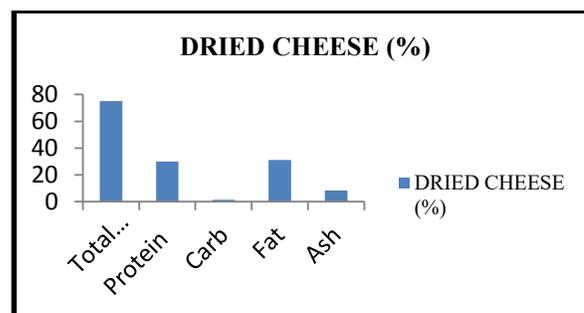
Result were mean± SD. Values were in triplicate
FIGURE 3. RESULTS OF PROXIMATE COMPOSITION.

Fig.3. revealed that the moisture content of wet cheese was higher, on drying moisture content comes down 25% and total solid was 75%. The contents of other component, namely fat 31.2%, protein 30.1%, carbohydrate 1.5%, ash 8.5%

4.Sensory evaluation results

TABLE 3.SENSORY EVALUATION

Dried cheese	Appearence	color	taste	odour[ns]	Overall acceptibility
Solar dried	7.41	7.00	7.95	6.26	8.5

± Standard deviation of three replicates.[ns] Not significantly different (P>0.05)

Tab.3. Shows sensory evaluation scores for ready to eat cheese or solar dried cheese in terms of color, taste, odour and overall acceptability the dried cheese were acceptable by the panelist.There were significant differences (p<0.05)in the sensory attributes of the final samples except odour.

CONCLUSION

The study indicated that the conventional solar system had important effect towards preservation of cheese. In solar dryer, trays gained heat, then transferred the heat by conduction to the product, increased their temperature, then lost moisture. On the other hand the installtion cost of solar drier was also less so this will be beneficial for the small scale industry.Though the solar drying takes several hours to dry but compared to other conventional drying this method was environment friendly,safe,produces no green house gases. Apart from this solar dryer prevent destruction of micro and macro nutritents.On the other hand the composition of dried cheese turned out to be nutritionally significant because it contained higher percentage of calorie, fat, protein. Presence of high protein and calorie increased the health benefit.The study also included that it will be a instant source of energy as it served as ready to eat form.

Reduction of moisture improved the shelf life and reduced the storage and transportation cost. As the bandel cheese is available in Indian market at very low price so the production of dried cheese wiil also be less expensive.

This study was a small initiation towards sustainable technology development for preparation of ready to eat food at economic cost by applying a solar drying technology.

ACKNOWLEDGEMENT

REFERENCES

[1] Prasant., Tomar, S.K., Singh, R., Gupta, S.C., Arora, D.K., Joshi, B.K., Kumar, D., 2009. "Phenotype and Genotype Characterization of Lactobacilli from Churpi Cheese". Dairy Science Technology, 89, pp. 531-540

[2] Tamang,J.P., Sarkar, P.K., 1988. "Traditional Fermented Food and Beverages of Darjeeling and Sikkim- A Review". Journal of science Food And Agriculture, 44, pp. 375-385

[3] Dahal , N.R., Karki, T.B., Swamylingappa,B., Li,Q., and Gu,G., 2005. "Traditional food and beverage of Nepal. A Review". Food Review International, 1(21), pp.1-25

[4] Tamang, J.P., Dewans., Thappa., Olasupo, N.A., Schillinger,U., Holazapfel,W.H.,Wijaya,A., 2000. " Identification and Enzymatic Profile of Predominant Profile of Prediminant Lactic Acid Bacteria Isolated From Soft Variety Churpi a Traditional Cheese Typical Of Sikkim Himalyas". Food Biotechnology, 14(1-2), pp. 99-112.

[5] Bahnasaway, A.H., Shenana, M.E., 2004. "A mathametical model of direct sun and solar drying of some fermented dairy products(Kishk)". Journal of Food Engineering, 61, pp.309-319.

[6] Saxena, J., Dash, K.K., 2015. "Drying Kinetics and Moisture Diffusity Study of Ripe Jackfruit". International Food research journal, 22(1), pp.414-420.

[7] Henderson, S.M., and Pabis, S., 1961. " Grain drying theory I.Temparaure effect on drying coefficient". Journal of Agricultural Engineering Research, 6(3), pp.169-174.

[8] Westerman,P.W., White,G.M., Ross, I. J., 1973. "Relative humidity effect on the high temperature drying of shelled corn". Transaction of the ASAE, 16(6), pp.1136-1139.

[9] Sosulski, F.W., 1962. " The centrifuge method for determining flour absorptivity in hard red spring wheats". Cereal Chemestry, 39, PP. 344.

[10] AOAC International Arhington, 1990. Official Methods of Analysis of the Association of Analytical Chemists. 15th ed.

[11] Official Method of analysis of AOAC International. Maryland.U., 2005. Assosication of Official Agricultural Chemist- AOAC. 18th ed.

[12] Page,G.E., 1949."Factors influencing the maximum of air drying shelled corn in thin layer". M.Sc.Thesis, Purdue University,Indiana,USA.

[13] Dutta.R., 2013. All you wanted to know about local cheese- kalimpong to bandel, The Telegraph, Calcutta, India.May.https://www.telegraphindia.com/1130503/jsp/entertainment/story_16852993.jsp

[14] Oguntola,J.A., Colin,N.N., Olayinka,A., Design and construction of a domestic passive solar food dryer.

SEEC-2018-067

LASER IGNITION FOR INTERNAL COMBUSTION ENGINES: A REVIEW

Sanket Mulye
Department of Mechanical Engineering,
College of Engineering, Pune.
mulyesanket@gmail.com

Milankumar Nandgaonkar
Department of Mechanical Engineering,
College of Engineering, Pune
mrn.mech@coep.ac.in

ABSTRACT

The research in internal combustion engines is now majorly aimed at improvement in performance and reduction of emissions. The spark ignition engines are equipped with electric spark plug as a source of initiation of ignition. It suffers from issues like durability, possibility of flame quenching etc. especially in case of modern high power density engines. Hence, a new ignition concept called laser ignition is proposed. It uses a nano second pulse laser, the beam from which is converged using a converging lens resulting in irradiance of the order of 10^{12}-10^{13} W/cm^2 at the focal point which acts as a source of ignition. It offers several advantages arbitrary positioning of laser plasma, absence of flame quenching, easy possibility of multi point ignition, ability to burn ultra- lean air fuel mixture thereby reducing NO$_x$ etc. In present paper, initially the advantages of laser ignition over electric spark plug are discussed. The mechanisms of laser ignition and their relative merits and demerits are then discussed. Studies done by several researchers on laser ignition of gaseous fuels in constant volume combustion chamber are reviewed and the general trends are discussed. Though the utility of laser ignition is well established in CVCC studies, there are many challenges in the practical implementation such as particulate deposits on optical window, need high frequency compact lasers etc. They are discussed and few studies carried out on engine and their key results are also discussed.

Keywords: laser, constant volume combustion, electric spark, plasma, emissions.
.

INTRODUCTION

The trend in the automotive engine research is towards maximizing the fuel economy and minimizing the emission. Especially the emission norms are getting stringent which underline need for emission reduction. The emphasis is given on reduction of NO$_x$ emissions. There are two major areas of research: the improvement in the combustion and the use of after treatment devices. The improvement in combustion can be achieved by replacement of fuel or improving the engine design. Researchers are attempting biodiesel, alcohols, dimethyl ether, hydrogen as a replacement to conventional automotive fuels. The technologies such as EGR, catalytic converter, SCR (Selective Catalytic Reduction) are also used to reduce the tail pipe emissions.

Nowadays, the attempts are made for downsizing the engines by increasing the power density. In spark ignition engines, electric spark plug is used as means of initiation of combustion. But, electric spark plug suffers from disadvantages like possibility of flame quenching, erosion of spark plug electrodes etc. Also, the energy input to the spark plug increases with increase in pressure of charge at the end of compression stroke. Hence, a new combustion concept called laser induced ignition is proposed. In this method, a laser beam having a pulse width of the order of nanoseconds is focused using a converging lens. It will generate a plasma at a focal point whose intensity is of the order of 10^{12} - 10^{13} W/cm^2. It acts as a source for initiation of combustion.

Laser combustion has several advantages over electric spark plug which includes arbitrary positioning of laser plasma in combustion chamber, precise ignition timing, easy possibility of multipoint ignition and ability of

burning ultra-lean air fuel mixtures. The precise ignition timing and multi point ignition will result in more complete combustion. The laser beam can be split into multiple beams by using the optics which doesn't require physically multiple spark plugs. The ultra-lean combustion results in lower combustion temperature and thereby minimizing NO_x emissions. The energy input to the electric spark plug increases with increase in pressure of charge at the end of compression stroke. Also, higher combustion pressure will result in reduction of the life of spark plug. The unique feature of laser ignition is that the energy required for combustion reduces with increase in initial pressure. Since laser spark plug is not directly interacting with combustion gases, erosion of electrodes will not occur.

LASER COMBUSTION MECHANISMS

The laser combustion can occur by four mechanisms: Thermal ignition, photochemical ignition, resonant ignition and non-resonant (laser spark) ignition [1]. They are explained in the following section:

Thermal ignition

In this mechanism, the concentrated laser beam results in formation of plasma. The thermal energy of the plasma results in increase of kinetic energy of gas molecules which results in breaking of bonds and there by a combustion. In thermal ignition, the ignition plasma should have a sufficient energy to break the chemical bonds. But, in practice, getting a sharp flame kernel is difficult. It forms a wide heating zone. This reduces the intensity of beam at focal point. Hence, some external substance can be added which will absorb the energy of plasma. The added substance should have a strong absorption at the wavelength of the laser used.

Photochemical ignition

In this mechanism, the laser energy results in dissociation of fuel molecules and forms radicals. If the rate of formation of radicals is sufficiently higher than the rate of their recombination, then it will result in formation of reactive species which causes combustion reaction. The photochemical ignition requires a close match between wavelength of incoming laser beam and target molecule's absorption wavelength. Hence, a laser of a specific wavelength is to be used depending upon type of gaseous fuel used. Since the photon energy at visible and near-IR wavelengths is smaller than the dissociation energy of most gases, photochemical ignition generally requires a UV lasers.

Resonant ignition

In resonant ignition, non-resonant multiphoton dissociation of some of the gas molecules occurs in a gas mixture. Further, resonant photoionization of one or more atoms generated by photo dissociation occurs. These processes results in formation of seed electrons which can readily absorb more energy by reverse bremsstrahlung effect and lead to plasma formation which acts as source of ignition. This process is efficient compared to non-resonant ignition as major portion of plasma is used to heat up the plasma.

Non-resonant/ laser induced spark ignition

The process of breakdown is initiated by the multiphoton ionization of few gas molecules which releases electrons. These electrons readily absorb more photons by inverse bremsstrahlung process which increases their kinetic energy. These electrons, in turn, collide with other gas molecules and ionize them. This results in electron avalanche and causes breakdown of the gas. The spark generated by this method emits energy in the form of heat, light, and shock wave to the surrounding gaseous mixture. If the energy of the spark is sufficiently large, then it can form a flame kernel which grows and causes the combustion of the fuel.

LASER COMBUSTION STUDIES IN CONSTANT VOLUME CHAMBER

In literature, numerous studies are available which are carried out to measure minimum ignition energy, the pressure-time characteristics, and visualization of flame kernel development by high speed photography. The conditions of pressure and temperature which will be there in engine cylinder at the end of compression stroke before spark occurs can be simulated in a constant volume combustion chamber. But, it is very difficult to difficult to simulate the turbulence in engine cylinder. Hence, most of the experiments are done keeping the air fuel mixture stagnant before combustion.

Gaseous fuels are attractive as internal combustion engine fuels, since they have wide ignition limits and capability to form homogeneous mixtures. Among gaseous fuels, Compressed Natural Gas (CNG) which contains approximately 96% of CH_4 and bio-methane are considered very important in terms of engine application. They represent an immediate advantage over other hydrocarbon fuels leading to lower CO_2 emissions due to their lower carbon to hydrogen ratio. Compared to gasoline, CH_4 has wider flammability limits and better antiknock characteristics, yet lower flame speed that can be enhanced by adding small amount of hydrogen. Researcher have studied combustion characteristics for different fuels like methane, CNG, hydrogen, LPG etc. Some researchers have tried multicomponent fuels like methane-hydrogen, CNG-hydrogen.

Hassan Mohamed et al. [2] studied combustion characteristics of methane-air mixture with laser induced spark ignition in a constant volume combustion chamber. They varied initial pressure, equivalence ratio and spark energy to explore flame behavior. The experiments were

carried out on hexahedral combustion chamber. The chamber had two glass windows with high power coating serving as entrance and exit for laser beam and other two for taking shadowgraphs. Ignition kernel exhibited nearly separated two kernels, one of which grown back towards the origin of ignition laser. Eventually after a short time, the two flame kernels separated into two flame fronts propagated individually. Lower initial mixture pressure and higher spark energy resulted in shorter flame initiation period and faster flame propagation. The ratio of the flame initiation period to combustion time decreased as the mixture became leaner. The laser ignition required higher energy than the electric discharge, however, the difference decreased toward the lean and rich flammability limits.

Kazantsev et al. [3] experimentally studied ignition of a CH_4: O_2 mixture by a laser spark excited in the reactor volume. It is found that the spark initiates a feebly radiating incomplete combustion wave, which is much faster than the combustion wave, but is substantially slower than the detonation wave. With a delay of 500–700 μs, a bright optical flash occupying the entire chamber volume is observed, which indicates fast (involving branching chain reactions) ignition of the gas mixture. The propagation velocity of the primary wave gradually increases with distance from the spark initiator, reaching a value of the order of 4-5 × 10^4 cm/s, which is much higher than the propagation velocity of the combustion wave in a CH_4: O_2 mixture, but much lower than the velocity of the detonation wave.

Phuoc [4] measured laser-induced breakdown thresholds of combustion gases. He experimentally found breakdown threshold laser intensities of air, O_2, N_2, H_2 and CH_4 using a Q-switched Nd–YAG laser operating at 532 nm and 1064 nm and 5.5 ns pulse for the range of pressure from 150 to about 3040 Torr. The data shown a P^{-n} pressure dependence which was in good agreement with the electron cascade process for creating gas breakdown. The decrease in ignition energy with increase in initial chamber pressure was also reported by Weinrotter et al. [5]. For 1064 nm laser beam, except for hydrogen, the pressure dependence was found to be similar for all gas with n is about 0.4. For 532 nm, the pressure dependence was much stronger showing the important effect of the diffusion loss. Phuoc et al. [6] experimentally investigated Laser-induced spark ignition of CH_4-Air mixtures using Q-switched, Nd: YAG laser, single mode, 5.5 ns pulse duration at 1064 nm wavelength. They found the sufficient laser irradiance for ignition in the order of 10^{12} to 10^{13} W/cm^2. Phuoc [7] also studied single-point versus multi-point laser Ignition. He reported experimental Measurements of combustion times and pressures for single point and two-point laser ignition of CH_4/air and H_2/air mixtures. It was found that multi-point ignition increases combustion pressure and shortens combustion time significantly. This benefit could be a

potential ignition approach for fuel-lean and high-speed combustion applications.

Srivastava et al. [8] carried out flame kernel characterization of laser ignition of natural gas–air mixture in a constant volume combustion chamber. The experiments were conducted at 10 bar chamber pressure and 373 K chamber temperature. The temporal variation of the flame kernel development in various directions with time inside the combustion chamber for different air–fuel ratios is analyzed by interrogation of different images. The flame kernel propagation distance was found to be consistently decreasing with leaner mixtures. A clear trend towards longer combustion duration with leaner CNG–air mixtures was observed. It was noticed that the peak cylinder pressure decreased for leaner mixtures.

Lee et al. [9] analyzed combustion and flame propagation characteristics of LPG and gasoline fuels by Laser Deflection method. They found increase in the flame propagation speed for both LPG and gasoline with decrease in ambient pressure. The maximum flame propagation speed appeared at the stoichiometric condition for LPG, but at equivalence ratio of 1.1 for gasoline. The flame speed of LPG was faster than that of gasoline at the range of lean or stoichiometric equivalence ratios. However, at the range of rich equivalence ratio conditions, the speed of flame propagation for the gasoline was superior to that of LPG. For LPG, as the initial temperature increased, the flame propagation was faster than the gasoline, while the time that the maximum pressure occurred was advanced.

The parametric study of laser ignition of hydrogen air mixture was carried out by Dharamshi [10] to study effect of focal length of convex lens, initial pressure, initial temperature, and location of plasma in a combustion chamber. By initial chamber filling pressure, the peak excess pressure during the combustion was increased. The MPE required to ignite hydrogen air mixtures reduced as the initial chamber temperature increased. Sharp fall in combustion duration was observed as the plasma position was moved towards the center of the CVCC. However, the value of peak excess pressure remained unchanged. The combustion duration for different focal lengths showed dependence on focal spot diameter and energy density at the focal point. MPE required to ignite hydrogen air mixture reduced upon decreasing the converging lens focal length. The similar trend was observed by Srivastava et. al. [11] for CNG – air mixtures ignited by laser ignition.

LASER COMBUSTION STUDIES ON ENGINES

The implementation of laser ignition in engines took a lot of time and till today it is done successfully at very few places for research purpose. The optical window which will withstand the engine conditions without getting covered with particle deposits, the availability of compact

high frequency lasers which can be mounted on engine cylinder are few of the challenges in the implementation of laser ignition. The cost and durability of commercial laser ignition system will decide its future implementation on mass basis.

Ranner et al. [12] studied the cleaning of optical window mounted on a 1.8 kW single cylinder engine and ignited by laser ignition. With cyclic 5-ns laser shots through the window, the pass-through stayed essentially free of deposits provided the energy was around 10 mJ/mm^2. In addition, even single shots with a higher flux were enough to remove a relatively thick layer of deposits at once.

Srivastava et al. [13] studied effect of laser pulse energy on laser ignited engine fueled with natural gas. The increase in maximum cylinder pressure, maximum rate of heat release was observed with increase in laser pulse energy which was attributed to reduction in ignition delay period. A marginal increase in brake power and consequently a reduction in BSFC was observed. NO_x emissions increased with increase in laser pulse energy.

Agarwal et al. [14-15] implemented laser ignition system on a single cylinder hydrogen fueled engine. They studied effect of compression ratio and spark energy on particulate emissions. They found increase in particulate emission with increase in load. With increase in compression ratio and spark energy the particulate emission increased. The spark energy is found to have significant effect on particulate emissions. Increase in particulate emission by increasing spark energy was attributed to higher heat release rate which encouraged combustion of lubricating oil on cylinder wall. They also compared the particulate emissions from laser ignited engine with spark ignition engine operating under same conditions. They found that spark ignition emits significantly less particulates. They highlighted the need of improvement in thermal stability of lubricating oil to withstand higher heat release rates in case of laser ignited engines.

CONCLUSION

The laser ignition has several advantages over electric spark ignition especially its ability to burn ultra-lean air fuel mixture thereby reducing combustion temperature and hence NO_x. CVCC experiments clearly indicate superior combustion characteristics compared to electric spark plug. But, this technology is in research phase for over four decades and not yet commercialised for automotive engines. The self-cleaning of optical window due to laser spark is really encouraging. Recently it is implemented on engines by few researchers but the results of increasing particulate emissions can pose a new challenge to commercialisation. So, this technology is still in research phase and will take some time to mature and commercialise.

REFERENCES

[1] Tran X. Phuoc, 2006. "Laser-induced spark ignition fundamental and applications". Optics and Lasers in Engineering, Vol. 44, pp. 351–397.

[2] Hassan Mohamed, Young-Sung Ko, Keum-Joong Yoon, and Suk-Ho Chung, 1999. "An Experiment on the Combustion Characteristics with Laser-Induced Spark ignition". KSME International Journal, Vol. 13, No. 1, pp. 82-89.

[3] S. Yu. Kazantsev, I. G. Kononov, I. A. Kossyi, N. M. Tarasova, and K. N. Firsov, 2009. " Ignition of a Combustible Gas Mixture by a Laser Spark Excited in the Reactor Volume," Plasma Physics Reports, Vol. 35, No. 3, pp. 251–257.

[4] Tran X. Phuoc, 2000. "Laser spark ignition: experimental determination of laser-induced breakdown thresholds of combustion gases". Optics Communications, Vol.175, pp. 419–423.

[5] Martin Weinrotter, Herbert Kopecek, Ernst Wintner, Maximilian Lackner and Franz Winter, 2005. "Application of laser ignition to hydrogen–air mixtures at high pressures". International Journal of Hydrogen Energy, Vol. 30, pp. 319–326.

[6] Tran x. Phuoc and Fredrick P. White, 1999. "Laser-Induced Spark Ignition of CH4/Air Mixtures". Combustion and Flame, Vol. 119, pp. 203–216.

[7] Tran X. Phuoc, 2000. "Single-Point Versus Multi-Point Laser Ignition: Experimental Measurements of Combustion Times and Pressures". Combustion and Flame, Vol. 122, pp. 508–510.

[8] Dhananjay Kumar Srivastava, Kewal Dharamshi, and Avinash Kumar Agarwal, 2011. "Flame kernel characterization of laser ignition of natural gas–air mixture in a constant volume combustion chamber". Optics and Lasers in Engineering, Vol. 49, pp. 1201–1209.

[9] Ki Hyung Lee, Chang Sik Lee, and Gyung-Min Choi, 2002. " Analysis of Combustion and Flame Propagation Characteristics of LPG and Gasoline Fuels by Laser Deflection method". KSME International Journal, Vol. 16, No. 7, pp. 935- 941.

[10] Kewal Dharamshi, and Avinash Kumar Agarwal, 2014. "Parametric study of a laser ignited hydrogeneair mixture in a constant volume combustion chamber". International Journal of Hydrogen Energy, Vol. 39, pp. 20207–20215.

[11] Dhananjay Kumar Srivastava, Ernst Wintner, and Avinash Kumar Agarwal, 2014. "Effect of focal size on the laser ignition of compressed natural gas–air mixture". Optics and Lasers in Engineering, Vol. 58, pp. 67–79.

[12] Helmut Ranner, Pratush Kumar Tewari, Heinrich Kofler, Maximilian Lackner, Ernst Wintner, Avinash

Kumar Agarwal, and Franz Winter, 2007. "Laser cleaning of optical windows in internal combustion engines". Optical Engineering, Vol. 46(10), Paper No. 104301.

[13] Dhananjay Kumar Srivastava, Ernst Wintner, and Avinash Kumar Agarwal, 2014. "Effect of laser pulse energy on the laser ignition of compressed natural gas fueled engine". Optical Engineering, Vol. 53(5), Paper No. 056120.

[14] Avinash Kumar Agarwal, Akhilendra Pratap Singh, and Anuj Pal, 2017. "Effect of laser parameters and compression ratio on particulate emissions from a laser ignited hydrogen engine". International Journal of Hydrogen Energy, Vol. 42 (15), pp. 10622-10635.

[15] Akhilendra Pratap Singh, Anuj Pal, Neeraj Kumar Gupta, and Avinash Kumar Agarwal, 2017. "Particulate emissions from laser ignited and spark ignited hydrogen fueled engines". International Journal of Hydrogen Energy, Vol. 42 (24), pp. 15956-15965.

SEEC-2018-069

SIMULATION AND EXPERIMENTAL INVESTIGATION OF MELTING PROCESS IN SPHERICAL PCM CAPSULES USED FOR LOW-TEMPERATURE THERMAL ENERGY STORAGE SYSTEMS

Vivek Tiwari
Mechanical Engineering Department, Birla Institute of Technology & Science, Pilani, Rajasthan 333031, India
Email: p2016414@pilani.bits-pilani.ac.in

Kedar Haradas Patil
Mechanical Engineering Department, Birla Institute of Technology & Science, Pilani, Rajasthan 333031, India
kedarhpatil93124@gmail.com

P. Srinivasan
Mechanical Engineering Department, Birla Institute of Technology & Science, Pilani, Rajasthan 333031, India
psrinivasan@pilani.bits-pilani.ac.in

ABSTRACT

Thermal energy storage is a good solution to bridge the gap between energy supply and energy demand. Low-temperature PCM materials have the major disadvantage of low thermal conductivity which can be rectified to an extent by using the additional surface area by enhancing heat transfer rate. In this paper, the study is performed by Modeling and simulation of transient thermal energy storage of PCM capsule. The result shows fast melting in finned PCM capsule in comparison to unfinned PCM capsule.

A key feature of this paper is that this research finding can be used to minimise charging time of Spherical PCM based thermal energy storage system.

Keywords Thermal energy storage (TES), Latent heat thermal energy storage (LHTES), Computational fluid dynamics (CFD), Phase change materials (PCM).

NOMENCLATURE

C_p	Specific heat capacity
k	Thermal conductivity
R	radius (m)
t	time (s)
T	Temperature (K)
T_m	Melting temperature (K)

Abbreviations
PCM   Phase Change Material.

TES   Thermal Energy Storage
OD   Outer diameter (m)

Greek letters
ρ   density (kg/m^3)
μ   Viscosity (kg $m^{-1} s^{-1}$)
λ   Heat of fusion (kJ/Kg)

INTRODUCTION

Low-temperature PCM materials have many advantages like physical and chemical stability, cyclic stability, good thermal behavior, adjustable transition zone, non-corrosive and low or no sub-cooling. While the major disadvantage with Low-temperature PCM materials is low thermal conductivity [1]. Additional surface areas (fins) are used to enhance heat transfer rate.

TABLE 1: PCM MATERIAL (SUNTECH PI16 PARAFFIN WAX) [3]

Melting Temperature, T_m (K)	**316 – 329**
Heat of fusion λ (kJ/Kg)	266
Specific heat capacity C_p (kJ/kg K)	2.51 (Liquid) 2.95 (Solid)
Thermal conductivity, k (W/m K)	0.24 (Liquid) 0.24 (Solid)
Density, ρ (kg/m^3)	760 (Liquid) 818 (Solid)

Liquid Viscosity (kg/ms)	1.90
Molecular weight (g/mol)	332

Borosil 4260 round bottom flask [2] of capacity 150ml (OD=75mm & Height=137mm) is considered an experiment as spherical PCM capsule shell. In the simulation, Borosil round bottom flask is assumed to be a perfectly spherical shell. Paraffin wax (Suntech PI16 Paraffin Wax) is considered for simulation as well as experiment. Properties of Paraffin wax is defined in tab 1.

R. VELRAJ et al. 1997 considered water bath setup for PCM capsule charging [4]. In their paper, the PCM capsule is heated with constant wall temperature. In our experiment setup, water bath with a glass window is taken. Borosil flask filled with a PCM material (PCM capsule) is immersed in a water bath. Electric water heater is used as an external heat source to charge PCM capsule. Thermocouple record temperature inside water bath and send a signal to data acquisition system. Data acquisition system alternately switches on and switch off water heat to maintain the set temperature. The stirrer is also used to maintain uniform temperature all over the water bath. Images from glass window are taken and with the help of image processing, melt fraction area is determined at different time intervals.

1. PCM Spherical Capsule
2. Water bath with glass window in front
3. Thermocouple
4. Water heater
5. Stirrer
6. Data acquisation system & Controller
7. Computer

FIGURE 1. EXPERIMENTAL WATER BATH SETUP FOR SPHERICAL PCM CAPSULE

MATHEMATICAL MODEL

The objective of this work is to improve the performance of encapsulated PCM system with the help of fin models. Governing equations are solved by FEM method using a commercial solver COMSOL MULTIPHYSICS 5.2. For this purpose, a transient two-dimensional axis-symmetric numerical model is developed. Simulations are carried out

for two different geometries viz. unfinned PCM Capsule and finned PCM Capsule. In case of finned PCM capsule, three annular fins made of a copper material (Properties of fin material is defined in tab 2) are attached to the inner spherical surface of the capsule with the angle of separation of 45^0. Length of the fin is 18.75 mm & width is 2 mm. The diameter of PCM capsules is 75 mm as shown in fig 2. Effect of gravity is taken into consideration. To simplify the model, following assumptions are taken.

- All thermos-physical properties of paraffin (thermal conductivity, density, specific heat capacity, dynamic viscosity) are assumed to be constant for respective phases viz. solid and liquid.

- Only radial and axial variation in heat transfer through the system is considered.

- Because of small volume and low Rayleigh's number, no convective heat transfer mode is considered during simulation.

- Effect of volume expansion of solid and liquid phases for the PCM material is neglected.

- The thermal resistance of Borosil flask is neglected in the simulation.

TABLE 2: FIN MATERIAL (COPPER)

Thermal conductivity, k (W/m K)	**400**
Sp. heat capacity C_p (J/kg K)	385

FIGURE 2. MODEL A) UNFINNED B) FINNED

Meshing is done taking free triangular shape with an element size extra fine as shown in fig 3.

FIGURE 3. MESHING FOR FINNED PCM CAPSULE

(a) AT 0 SEC

(b) AT 3600 SECS

(c) AT 5000 SECS

FIGURE 4. TEMPERATURES CONTOUR (K) FOR A) UNFINNED B) FINNED PCM CAPSULE AT (A) 0, (B) 3600, (C) 5000 SECONDS OF THE CHARGING TEST WITH CONSTANT TEMPERATURE WALL TEMPERATURE.

Figure 4 shows a variation of temperature throughout the PCM capsule at different time intervals for both unfinned and finned models. Figure 5 shows variation in melting fraction at different time intervals for both models. Improvement in heat transfer because of fins is observed through simulation.

FIGURE 5. MELT FRACTION VS TIME (S) FOR UNFINNED AND FINNED PCM CAPSULE

REFERENCES

[1]   T. Markandeyulu, J. Krishna Devanuri, and K. Kiran Kumar, "On the Suitability of Phase Change Material (PCM) for Thermal Management of Electronic Components," *Indian J. Sci. Technol.*, vol. 9, no. S1, pp. 1–4, 2016.

[2]   "Borosil Catalogue," *BOROSIL GLASS WORKS LTD., India*. [Online]. Available: www.borosil.com/doc_files/Binder1.pdf. [Accessed: 28-Sep-2017].

[3]   S. HIMRAN, A. SUWONO, and G. A. MANSOORI, "Characterization of Alkanes and Paraffin Waxes for Application as Phase Change Energy Storage Medium," *Energy Sources*, vol. 16, no. 1, pp. 117–128, 1994.

[4]   C. F. and K. S. R. VELRAJ, R. V. SEENIRAJ, B. HAFNER, "Experimental analysis and numerical modelling of inward solidification on a finned vertical tube for a latent heat storage unit," *Sol. Energy*, vol. 60, no. 5, pp. 281–290, 1997.

PERFORMANCE AND COMPATIBILITY TEST OF BIODIESEL FROM WASTE COOKING OIL IN IC ENGINE: A NOBLE TRANSESTERIFICATION APPROACH

Vipasha Bihone
University of Petroleum and Energy Studies
bihone.vipasha@gmail.com

Shanmathi Sridharan
University of Petroleum and Energy Studies
shanmi92@gmail.com

ABSTRACT

The energy consumption around the globe is surpassing human population. Increased emission of harmful greenhouse gases and depletion of fossil fuel reserves, have waved an alarming signal and brought out the utter need of alternate energy sources. Bio diesel is known to have replaced commercial diesel engines due to its renewable, non-toxic nature. It emerges on a worldwide level in light of its earth supportable attributes. Moreover, biodiesel prove to have minimized greenhouse gases, such as CO, CO_2, SO_2. One way of producing bio-diesel is by Trans-esterification of waste cooking oil (WCO) .Waste Cooking Oil is trans-esterified in the presence of acid or alkaline catalyst. Fatty Acid Methyl Esters so obtained have proven to be a vital alternate fuel sources which can be used in CI engines. The aim of this study is to concentrate on the performance, combustion and emission characteristics of CI engines using Fatty Acid Methyl Esters and to bring out new ways of using mixes of FAME with diesel extensively in place of diesel. The production technique plays a vital part in physiochemical properties of Fatty Acid Methyl Esters so delivered. Trans-esterification techniques may include ultrasonic Tran esterification, hydro-dynamic cavitation, magnetic stirring Trans-esterification. This study employs Trans-esterification using magnetic stirrer technique. Performance and Emission analysis of FAME have been discussed in the later segment.

Keywords FAME, WCO

NOMENCLATURE
  A) FAME: Fatty Acid Methyl Esters.
  B) WCO: Waste Cooking Oil

INTRODUCTION

The energy conservation around the globe is expected to surpass the population growth. An increment in 53% of global energy and 39% of greenhouse emission is expected by the early 2030's. And, depletion of petroleum reserves have waved an alarming signal and brought out the utter need for alternative energy sources. More the energy consumption, more are the chances of a polluted ecosystem. Hence, dream of a healthy environment persists to be the field of interest.

Widely available diesel engines find their utility in heavy engines due to high thermal efficiency, high output power and reduced emissions of Carbon Mono-oxide (CO) and other Hydro Carbons (HC).   However, diesel engine has been categorized to be carcinogenic by the International Agency for Research in Cancer (IARC). Besides, the release in excess Hydrocarbons lead to global warming which is a serious threat these days [1]. The steadily developing human population and relating monetary improvement of humankind have caused constant surge in vitality request of the world. The aforementioned facts have just provoked the world to search for exchange wellsprings of vitality to balance the fuel emergency in future. Biodiesel made from different renewable resources have proved to be a viable alternative for use as fuel in Compression Ignition (CI) engines pertaining to its non-toxic, biodegradable, less inflammable nature. In addition to this, bio diesel have a relatively lower sulfur content, flash point, aromatic content, cetane number as compared to commercial diesel. Biodiesel is mono alkyl esters of long chain fatty acids. By a compound procedure named "Trans esterification" biodiesel is delivered from vegetable oil and utilized as a part of Compression Ignition (CI)

engines. The cost of bio-diesel from cooking oil can be unexpectedly high due to high cost of cooking oil. Hence, Waste Cooking Oil (WCO) is used as an alternative these days. In Trans esterification process, tri-glycerides present in vegetable oil, are made to react with alcohol in presence of alkali or base catalyst. Methanol, due to its low cost, is most commonly used alcohol. Products so obtained, Fatty Acid Methyl Esters is referred as biodiesel. Glycerin is obtained as the by-product which can be further utilized in producing industrial lubricants, lotions, preserving food items etc. Owing to fast reaction rates, base catalyzed trans-esterification is the most commonly used. Sodium Hydroxide or Potassium Hydroxide is the usually used base catalyst. Acid catalysts, on the other hand are given the least attention pertaining to their low reaction rates. However, they are unreactive to free unsaturated fats already present in feed stock oil.

SEEC-2018-071

ENERGY ANALYSIS OF MULTIPHASE FLOW IN FLAT PLATE SOLAR COLLECTORS

MohitMurarka
Department of Energy
Tezpur University
murarkaenergy@gmail.com

Dr. Biraj Kumar Kakati
Department of Energy
Tezpur University
bkakati@tezu.ernet.in

Dr. R.Anandalakshmi*
Department of Chemical Engineering
IITGuwahati
anandalakshmi@iitg.ernet.in
*Corresponding Author

ABSTRACT

This paper presents thermodynamic modelling and energy analysis of multiphase flow in a flat plate solar collector, which engages mixture of refrigerants as working fluids. In this study, a mixture of R32 and R123 in four varying proportions as a working fluid were considered and compared based on energy balance analysis. This non-conventional collector involves multiphase flow due to low boiling temperature of the refrigerant fluids, which are preferable compared to conventional working fluids in terms of latent heat storage, enhanced heat transfer coefficient and freeze protection. In this study, the size of the solar collector required for a preferred inlet and outlet temperatures of the working fluid has been reported. The variation of fluid mean temperature, heat gain rate, heat transfer coefficient and mixture quality along the length of the collector tube has also been investigated for all considered refrigerant mixtures. Simulations were performed for a solar insolation of 850 and 700 W/m^2 at a mass flow rate of 0.001 and 0.05 kg/s. The purview of non-conventional collectors in both domestic and industrial applications has increased manifold over conventional collectors.

*Keywords***:**
Flat plate solar collectors, multiphase flow, refrigerant mixtures, fluid mean temperature, heat gain rate, heat transfer coefficient, mixture quality

NOMENCLATURE

A	Solar collector surface area, m^2
S	Absorbed flux by the collector, W/m^2
I_T	Falling flux on the collector, W/m^2
D	Diameter, m
G	Mass velocity, kg/m^{2}s
h	Enthalpy per unit mass, J/kg
Pr	Prandtl number
Re	Reynolds number
q	Heat gain per unit length of the tube, W/m
T	Temperature, K
ΔT_g	Gliding temperature difference, K
U_L	Overall heat loss coefficient of the solar collector, W/m^2
x	Mixture quality
X_{tt}	Martinelli parameter
1	10% R32 and 90% R123
2	20% R32 and 80% R123
3	30% R32 and 70% R123
4	40% R32 and 60% R123

GREEK SYMBOLS:

η	Efficiency
α	Heat transfer coefficient, W/m^2 K
μ	Viscosity, kg/m s
ρ	Density, kg/m^3

SUBSCRIPTS:

l	Liquid State
v	Vapor State

INTRODUCTION

Solar energy is one of the most encouraging options in reducing the usage of fossil fuels and pave the way for solution of numerous environmental problems such as

global warming, air pollution, acid rain, ozone layer depletion and many others [1].

Solar, geothermal and industrial waste heat are immense source of low grade thermal energy, which can be extracted using refrigerants as working fluids [2]. Refrigerants generally have a low boiling point and a high heat capacity, which enableless mass of refrigerant to transfer large amount of heat very efficiently. As compared to refrigerants that are in use, mixtures of refrigerants can result in improvement of capacity control and thus opens up wide area of both domestic and industrial applications [3]. Refrigerants based solar thermal collectors comprehend of multiphase flow [1-6] and their use in heat pump [3-4], electricity generation [2], stirling engine [5] and many other industrial processes have been both theoretically and experimentally analyzed.

Refrigerants have better thermodynamic and transport properties. However, according to new environmental regulations, the refrigerant fluids should also possess null ODP and low GWP. Along with these requirements, the refrigerants fluids should be non-flammable, non-toxic and low cost. Rossato et al. [6] made an attempt to determine the properties of low GWP R1234ze (E) and R32and their application as working fluids.

In this direction, size of the solar collector required for a preferred inlet and outlet temperatures of the working fluid has been determined. Also, fluid mean temperature, heat gain rate, heat transfer coefficient, mixture quality along the entire length of the collector tube with a mixture of R32 and R123 (at different proportions) as working fluids have also been investigated based on energy balance.

MATHEMATICAL MODELLING

The following mathematical model of serpentine flat plate collector was used to determine the length of tube, L
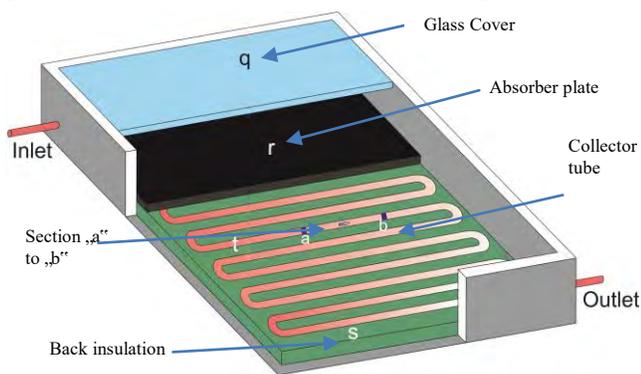
FIGURE 1. SCHEMATIC OF SERPENTINE TUBE FLAT PLATE SOLARCOLLECTOR

required to increase the temperature of the refrigerant fluid mixtures from 283 K (inlet) to 363 K (outlet) at steady state and uniform heat flux conditions. The transport and

thermodynamic properties were calculated using REFPROP 9.0 [7]. It is assumed that heat transfer coefficient varies along the length of the tube. The pressure drop and variation in heat loss coefficient with respect to temperatureare neglected.

The optical efficiency (η_0) of the system relates the total falling flux on the glass cover, I_T and the total absorbed flux by the system, S using Eqn. (1) [8]:

$$S = \eta \tag{1}$$

The useful heat gain per unit length available to be transferred to the fluid from the tube in the flow direction is given by the following Eqn. (2) [8]

$$q = \tag{2}$$

In Eqn. (2), the collector efficiency factor F' is given by [8]

$$\overline{\hspace{4cm}} \tag{3}$$

In Eqn. (3), F is the plate effectiveness and is given by Eqn. (4) [8]

$$\frac{^0/_2}{^0/_2} \qquad \text{where} \qquad \sqrt{\underline{\hspace{1cm}}} \tag{4}$$

The energy balance for a section of collector tube, (position „a" to position „b") as seen in Fig. 1, assuming thermodynamic equilibrium between two phases (liquid and vapour), is given by Eqn. (5) [8]

$$\dot{m}\big[x \qquad\qquad \big]$$
$$\big[x \qquad\qquad \big] \quad q\Delta z \tag{5}$$

Equation (5) can also be used for single phase flow by substituting x=0 for liquid phase and x=1 for vapour phase. If the whole collector length is divided into N sections ofΔz, the total length, L of the collector is given by Eqn. (6)

$$\Sigma \tag{6}$$

In Eqn. (3), α is heat transfer coefficient which varies with temperature and phase of the flow.

SINGLE PHASE FLOW:

The thermodynamic properties such as viscosity, specific heat, thermal conductivity, enthalpy were estimated using REFPROP 9.0 for liquid/vapour phases and the single phase heat transfer coefficient (α_l/α_v) was calculated using Eqns. (7-9) [4].

$$Re = \frac{GD}{\mu_l} \qquad \text{Where } G = \frac{4\dot{m}}{} \qquad (7)$$

$$Pr_l = \frac{\mu_l}{} \qquad (8)$$

$$\frac{}{} \qquad (9)$$

MULTIPHASE FLOW:

The gliding temperature range was calculated from REFPROP 9.0 and the Eqns. (10-12) were used to calculate the multiphase heat transfer coefficient, α [4].

$$Re = \frac{G(\;)}{\mu_l}; \qquad Pr_l = \frac{\mu_l}{} \qquad (10)$$

$$\left(\;\right)/_x \quad \rho/_\rho \quad /_\mu \qquad (11)$$

$$- \quad 1/_X \qquad (12)$$

DISCUSSION OF RESULTS

The mathematical model was developed in MATLAB (R2016a). In order to verify the model, the simulations were carried out for the refrigerant mixture of R134a and R123 with the operating parameters considered by [4]. The results are in good agreement and the validation is not shown for the brevity of the article. In this study, four mixtures of R123 and R32 (1, 2, 3 and 4) were considered as possible working fluids and energy analysis was done. The solar collector is of standard case [8] and the design parameters and operating conditions are given in Table 1.

TABLE 1: DESIGN PARAMETERS AND OPERATING CONDITIONS FOR THE COLLECTOR

Ambient temperature, T_a	280 K
Plate width, δ	0.5 mm
Plate material thermal conductivity, k	385 W/m K
Tube inner diameter, D_i	0.01m
Tube inner diameter, D_o	0.012 m
Tube spacing, W	0.15 m
Incoming solar radiation, I_T	850/700 W/m^2
Optical efficiency, η	0.82
Collector loss coefficient, U_L	6 W/m K
Refrigerant mass flow rate, $\dot{m}$	0.005/0.01 kg/s
Tube inlet temperature T_{in}	283 K

Figure 2 shows the variation of fluid mean temperature along the length of tube. It is noted that the refrigerant fluid mixtures enter the tube at 283 K and at operating pressure of 600 kPa and solar insolation of 850 W/m^2 with mass flow rate of 0.005 kg/s. Three regions of temperature rise (single phase liquid, multiphase and single phase vapour) can be clearly seen from Fig. 2. The final temperature of the fluid is 363 K in each case. Figure 3 represents the heat

gain rate per unit length for all the four mixtures considered. As the mean temperature of fluid increases, there is a decrease in the rate of heat gain per unit length. The decrease in the heat gain rate is due to increase in the convective heat loss with fluid mean temperature. It is also
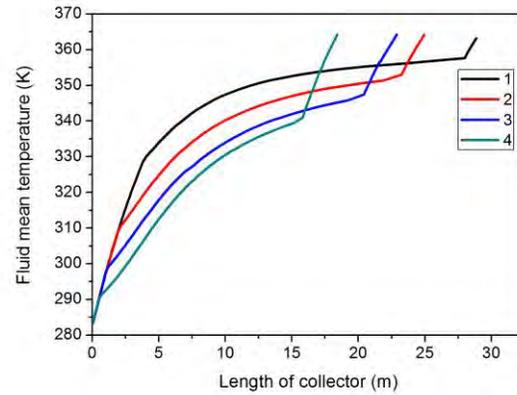
FIGURE 2. FLUID MEAN TEMPERATURE ALONG THE LENGTH OF THE COLLECTOR FOR DIFFERENT REFRIGERANT MIXTURES
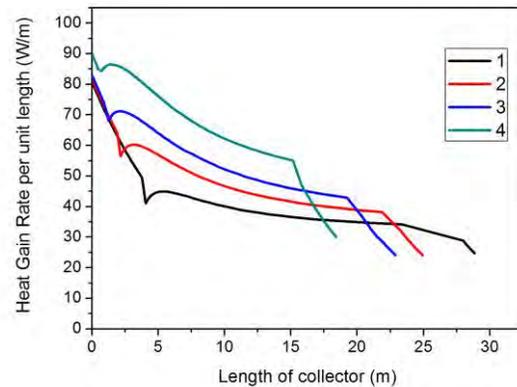
FIGURE 3. HEAT GAIN RATE ALONG THE LENGTH OF THE COLLECTOR FOR DIFFERENT REFRIGERANT MIXTURES

seen that the decrease in heat gain rateis not gradual. This is due to the fact that the heat transfer coefficient changes with change in temperature. The variation of the heat transfer coefficient along the length is shown in Fig. 4. The value remains almost constant in the single phase region (liquid and vapour) but there is a gradualincrease in the multiphase region. Towards the end of multiphase region, it decreases gradually due to dry out [1].

Figure 5 shows the variation of mixture quality along the length of the collector. It is seen that a portion of the length required to increase the temperature of the fluid to the onset of gliding temperature and the length to increase the temperature to the end of gliding temperature range are different for different mixtures (1, 2, 3 and 4). In the rest

of the tube length, temperature of the working fluid further increases to the final value of 363 K.
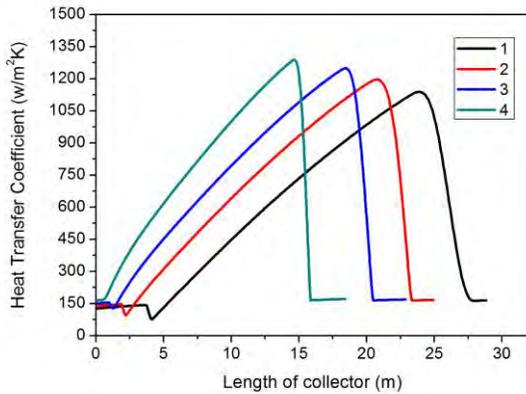
FIGURE 4. HEAT TRANSFER COEFFICIENT ALONG THE LENGTH OF THECOLLECTOR FOR DIFFERENT REFRIGERANT MIXTURES
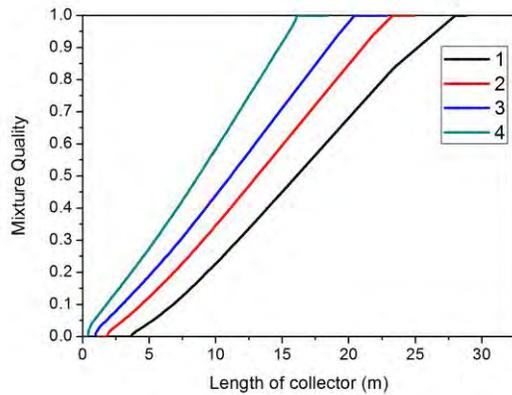
FIGURE 5. MIXTURE QUALITY VS TUBE LENGTH FOR DIFFERENT MIXTUR

Refrigerant mixtures (1, 2, 3 and 4) were compared in terms of tube length and collector efficiency for two different insolations and mass flow rates in Tab. 2.

TABLE 2: LENGTH OF THE COLLECTOR AND COLLECTOREFFICIENCY FOR DIFFERENT REFRIGERANT MIXTURES AT VARIOUS SOLAR INSOLATIONS AND MASS FLOW RATES

I_T	850				700			
$\dot{m}$	0.01		0.005		0.01		0.005	
Mixture	t		T		t		t	
1	55.3	32.4	28.9	31.0	99.9	21.8	52.1	20.9
2	48.7	38.7	25.0	36.9	79.4	28.1	41.0	27.3
3	44.6	42.5	22.9	41.4	69.5	33.1	35.6	32.3
4	36.0	54.6	18.4	53.3	50.2	47.8	25.7	46.3

CONCLUSIONS

Energy analysis for multiphase flow in a serpentine flat plate collector was done. A mixture of two refrigerants, R32 and R123 with varying concentrations was considered. It is found that the length of the collector tube required decreases from 28.9 m to 18.4 m with the increase in concentration of R32. It is also seen that the multiphase heat transfer coefficient and collector efficiency increases with the concentration of R32.It is suggested that mixture of refrigerants can be used in solar collectors to get the combined effect of multiphase and gliding temperature effect. The saturation temperature range, fluid properties and environmental impact are to be given most importance during selection of working fluids.

REFERENCES

[1] Helvaci, H.U. and Khan, Z.A., 2015. "Mathematical modelling and simulation of multiphase flow in a flat plate solar energy collector". Energy Conversion and Management, 106, Dec, pp.139-150.
[2] Garg, P., Kumar, P., Srinivasan, K. and Dutta, P., 2013. "Evaluation of isopentane, R-245fa and their mixtures as working fluids for organic Rankine cycles". Applied Thermal Engineering, 51(1), pp.292-300.
[3] Kruse, H., 1981. "The advantages non-azeotropic refrigerant mixtures for heat pump application." International Journal of Refrigeration, 4(3), May, pp.119-125.
[4] Aziz, W., Chaturvedi, S.K. and Kheireddine, A., 1999. "Thermodynamic analysis of two-component, two-phase flow in solar collectors with application to a direct-expansion solar-assisted heat pump". Energy, 24(3), Dec, pp.247-259.
[5] Der Minassians, A. and Sanders, S.R., 2009. "Multiphase stirling engines". Journal of Solar Energy Engineering, 131(2), pp.021013.
[6] Rossato, M., Da Silva, J.D., Ribatski, G. and Del Col, D., 2017. "Heat transfer and pressure drop during condensation of low-GWP refrigerants inside bar-and-plate heat exchangers". International Journal of Heat and Mass Transfer, 114, pp.363-379.
[7] Lemmon E, Huber M, McLinden M N. REFPROP. Standard reference database 23. REFPROP, NIST, Version. 9.0; 2010.
[8] Duffie, J.A. and Beckman, W.A., 2013. Solar engineering of thermal processes, 4th ed., John Wiley & Sons, Hoboken, New Jersey, (Chap. 5, pp. 222;Chap. 6, pp. 254-268).

DISTILLERY'S BY PRODUCT IN PRODUCTION OF COST EFFECTIVE BAKERY ITEMS

Puja Mukherjee[1],
Dept.of Food and Biochemical Engineering,Jadavpur University,Kolkata
pmpujamukherjee068@gmail.com

Debabrata Bera [2],
Dept.of Food and Biochemical Engineering,Jadavpur University,Kolkata
beradebabrata@yahoo.co.in

Lakshmishri Roy [3*]
Dept.of Food Technology,Techno India,Kolkata
lakshmishri371@gmail.com

ABSTRACT:

Increasing dependence on non-renewable energy resources has resulted in the escalation of bioethanol industry growth. Consequently the phenomenal quantity of ethanol industry processing residues is predicted to create a significant impact on its future. DDGS i.e. distillers dried grain with solubles is the nutrient rich non fermentable residue of this industry which is produced significantly. Thus research in the novel utilization of these residues i.e. for human consumption is becoming imperative. This study examined the effects of DDGS substitutions in various proportions and evaluated the cookies baking behaviour. Types of blended cookies were prepared with whole DDGS flour ranging from 50 and 70%. These cookies were evaluated for physical, textural and organoleptic attributes. Textural measurements showed that hardness of cookies decreased with the addition of DDGS flour. Sensory data indicated that the texture of DDGS cookies with up to 70% was acceptable. Results are indicative of the alternative novel mode of utilization and revenue generation of the alcohol industry waste. Further modification of the waste DDGS is bound to enhance the marketability and techno economic feasibility of the DDGS substituted bakery product.

Keywords: DDGS flour, novel use, cookies, hardness, waste, techno economic feasibility

INTRODUCTION

Distiller's dried grains with solubles (DDGS) are the major by-products of ethanol industry. It is generally used for animal and poultry feed "[2]". In India, bio ethanol production increased from about 52.8 million of gallons in 2007 to over 225 million of gallons in 2016 "[8]". The use of DDGS as human food is insignificant though it is very high in nutrients content approximately 3 fold high "[5]". The process for making ethanol currently is mainly by dry grind method i.e. grinding (dry milling), slurring, cooking, and liquefaction, scarification, fermentation, distillation, and coproduct recovery. During coproduct recovery the non-volatile components following the distillation steps are known as whole stillage, which is centrifuged and produced liquid thin stillage and solid fraction, distiller grain (DG). The thin stillage is concentrated by evaporation into condensed distiller solubles (CDS) also known as syrup. While DS, DG, or their combination known as wet distiller grains with solubles (WDGS). Then WDGS is dried and yields distiller dried grain with solubles (DDGS) and carbon di oxide. Because of dry grind processing the cost of DDGS is low than wet milling processing "[3]". Hence it can be used to produce various products.
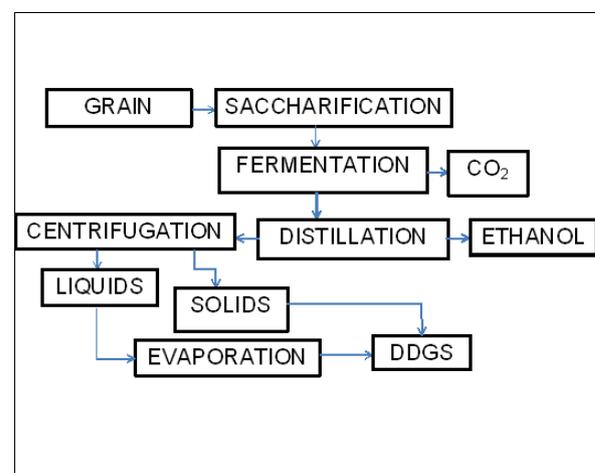
FIGURE 1. FLOW DIAGRAM OF PRODUCTION OF ETHANOL AND IT'S BY PRODUCTS

Cookies are bakery products gaining popularity amongst all age groups due to taste, crispness, and eating convenience. Generally, cookies are prepared from white flour (Maida). To increase its nutritive value, cookies are prepared with fortified or composite flour. Composite flour has an economic value in developing countries because it encourages use of locally grown crops and waste materials as flour. A number of studies have shown the improved nutritive values of cookies by incorporating navy bean, sesame seed, corn fiber, soy protein and fiber, chickpea, lentil, barley, soybean, maize, and barley. "[1]"

Likewise to utilise the nutritional benefits of DDGS, cookies were prepared from DDGS flour containing various proportions. The purpose of this study was to exploring the alternative utilization of alcohol industry waste i.e.DDGS to produce value added product. And analysis of the physicochemical and sensory attributes of DDGS flour-substituted cost effective cookies.

MATERIALS & METHODS

Materials

The sample of rice DDGS was collected from IFB Agro industry private Ltd, Kolkata. The samples were stored in zip lock plastic packets at room temperature. Wheat flour, butter, sugar, emulsifier and salt were purchased from a local market (Kolkata, India). All the trials were conducted in triplicate at room temperature.

Methods

Preparation of DDGS Flour: DDGS is a mixture of various particle sizes. So, it is important to analyse the particle size distribution (PSD). Particle size affects the flowability and acceptability of baked products which is incorporated with DDGS "[6]". To get uniform particle size, the flour was passed through 150-micron sieve and stored at room temperature till further analysis.

Proximate and Biochemical Composition: Compositional analysis of the flours, (white flour and DDGS) for moisture, fat, ash, fiber, carbohydrate and protein content was performed by the AOAC methods. "[6-7]"

Cookie Formulation: Cookies were made from white flour to serve as a control. The DDGS flour was mixed with white flour at different ratios (50:50, 70:30) to prepare cookies. The cookies were prepared using the following ingredients: flour (100 g), shortening (butter) (28.44 g), sugar (57.7 g), sodium bicarbonate (1.1 g), salt (0.93g) and water (7.11 ml). Shortening and sugar were mixed to form a cream, then added to the mixture of flour, sodium bicarbonate, and salt and mixed thoroughly to form dough. The dough was kneaded and refrigerates for 30 minutes and cut into circular shapes using cookie cutter. Baking was carried out at 180°C for 15 min. Cookie samples were cooled and stored in airtight containers for further analysis.

Textural Analysis Hardness and fracturability of the baked cookies was measured using a texture analyzer (TA-XT.plus) in a compression mode with a p/5 cylinder probe. Pre-test, test, and post-test speeds were 1.00, 0.5, and 10 mm/s, respectively.

Sensory Evaluation Cookies made from white flour and DDGS flours were subjected to sensory evaluation as shown in Tab 3, using 11 panellists drawn within the University community. The cookies were evaluated for appearance, colour, taste, texture, odour, overall rating, and anything dislike. The ratings were on a 9-point hedonic scale ranging from 9 (like extremely) to 1 (dislike extremely). All panellists were regular consumers of cookies. Water at room temperature was provided to rinse the mouth between evaluations. The control was cookies made from 100% white flour.

RESULTS & DISCUSSIONS

Proximate and Biochemical Composition of DDGS and Wheat Flour

The chemical compositions of white flour and DDGS flour used for cookies preparation are shown in Tab 1. DDGS flour was found to have high crude protein, crude fat, crude fiber, and ash content in comparison with white flour.

TABLE 1: RESULTS OF PROXIMATE COMPOSITION OF WHITE FLOUR AND DDGS FLOUR

	White flour (%)	DDGS flour(%)
Moisture	15	9.39
Ash	0.8	5.29
Crude fat	2	11.2
Crude protein	10	35
Crude fibre	10	5
Carbohydrate	15	8

Texture Analysis

Texture result of the two types of cookies prepared from blend of white flour and DDGS flour is shown in Tab 2. The hardness decrease with blend of 70:30 DDGS flour substitution in cookies. Therefore, the reduction of

gluten in cookie dough by substituting with DDGS flour resulted in retarding the formation of gluten matrices, which contributed to the substantial decrease in hardness.

TABLE 2: RESULTS OF TEXTURE PROFILE ANALYSIS OF COOKIES

	Control	50:50	50:70
Hardness	3599.25	3586.43	2806.88
Fracturability	3462.40	3747.25	3721.08
Adhesiveness	- 2.2	-7.87	-0.713
Springiness	0.16	0.462	0.602
Cohesiveness	0.09	0.03	0.015
Gumminess	28.46	116.60	57.092
Chewiness	4.14	89.05	34.35
Resilience	0.01	0.020	0.009

[a] control cookies

[b] 5:3 – cookies   **[c] 7:3 – cookies**

Sensory Evaluation

The sensory scores of white flour and DDGS composite cookies are shown in Tab 3. According to the results presented, there was a significant decrease in taste and overall acceptability of white flour and DDGS composite cookies. Colour, aroma, and texture of

cookies prepared from blend containing DDGS flour up to 70% level are accepted. The sensory score for taste decreased due to addition of DDGS flour. The after taste is bitter. The overall acceptability score is not too good due to bitter taste. If we modify this DDGS sample then we can improve the taste and overall acceptability.

TABLE 3: RESULTS OF SENSORY EVALUATION OF COOKIES

	Control	50:50	50:70
Appearance	8	7	7
Colour	7	6	6
Taste	8	2	2
Texture	7	5	7
Odour	7	3	5
Overall retain	8	3	4
Anything you dislike	no	bitter taste	bitter taste

CONCLUSION

There are several challenges in incorporating DDGS in food products. Incorporation of DDGS affects the sensory characteristics of the final products. In most of the cases the products attained darker colours with increased substitution of DDGS and the mode of drying undertaken during DDGS preparation affected the taste. The flavour of the product is also affected due to the presence of fats, pigments etc. Also the components of DDGS lacks gluten and hence do not impart the same functionality of texture and intermediate processing quality attributes to the bakery products as the conventionally employed flour. These issues make it pertinent for meticulous incorporation and modification of DDGS to suit to the requirements of the final product. Parallely this study revealed that the phenomenally available low cost alcohol industry waste i.e. DDGS flour is a good source of protein, fiber, and fat as compared with white flour, thereby, making it an effective cost effective nutritional alternative source . Though the score of overall acceptability decreased due to bitter taste of DDGS, but if we modify the properties of DDGS flour then we can get products of good sensory appeal and increased overall acceptability.

Thus, the use of DDGS flour in Bakery products like cookies holds promising scope for preparation of cost effective processes to ensure sustenance of the bakery industry.

ACKNOWLEDGMENTS

REFERENCES

1. Arti Chauhan1, D.C. Saxena1 and Sukhcharn Singh1*, 2016, "Physical, textural, and sensory characteristics of wheat and amaranth flour blend cookies", Cogent Food & Agriculture, 2: 1125773

2. Faye M.Dong, Barbara A. Rasco and Sahl. S.Gazzaz, 1987, "A protein quality assessment of wheat and corn distillers' dried frains with solubles", Cereal chemistry, 64(4), 327-332.

3. Jianchun Han & Keshun Liu, 2010, "Changes in composition and amino acid profile during dry grind ethanol processing from corn and estimation of yeast contribution toward DDGS proteins", Journal of agricultural and food chemistry, 58, 3430–3437.

4. Keshun Liu, 2008, "Particle size distribution of distillers dried grains with solubles (DDGS) and relationships to compositional and color properties", Bioresource Technology, 99, 8421–8428.

5. Weijie Xu, Narendra Reddy, and Yiqi Yang, 2007, "An acidic method of zein extraction from DDGS", Journal of agricultural and food chemistry, 55, 6279 – 6284.

6. AOAC International: Arlington, VA, 2002. AOAC (Association of Official Analysis Chemists). AOAC Official Methods of Analysis.

7. AOAC International (AOAC). 2003. Official Methods of Analysis of the Association of Analytical Chemists, 17th edn., The Association, Gaithhersburg.

8. Ethanol Industry Outlook, 2016, RFA analysis of public and private data sources, Fueling a High Octane Future. http://www.ethanolrfa.org/resources/industry/statistics/#1454099103927-61e598f7-7643

SEEC-2018-074

NUMERICAL INVESTIGATION ON THERMAL PERFORMANCE OF TRAPEZOIDAL FINNED FLAT PLATE SOLAR AIR COLLECTORS

Devanshu Nema
Department of Chemical Engineering
IIT Guwahati
n.devanshu@iitg.ernet.in

Dr. R. Anandalakshmi
Department of Chemical Engineering
IIT Guwahati
anandalakshmi@iitg.ernet.in

ABSTRACT

In this study, a detailed numerical model of a trapezoidal finned flat plate solar air collector was developed to investigate the solar heat energy harnessed by the operating fluid. The model was used to analyse both the temperature rise of the operating fluid with respect to time and the variation of the temperature with location inside the solar collector. The optimum number of trapezoidal fins to be used in order to achieve a desired temperature rise of the fluid while maintaining a minimum pressure drop was calculated. The finding shows that air based solar heat collectors with trapezoidal fins can be effectively used in both domestic and industrial needs for heating and drying applications where heated air is required at 40-50°C.

***Keywords*:** Flat plate solar collector, trapezoidal fin, heating, drying
.

NOMENCLATURE

A	Area of heat transfer, m^2
L,B	Length and breadth of solar collector, m
C	Specific heat of solid, J/kg K
C_p	Specific heat of fluid, J/kg K
D	Duct depth, m
D_h	Hydraulic diameter, m
H	Fin height, m
m	Mass, kg
m_{flow}	Mass flow rate, kg/s
R	Conduction heat transfer resistance, m^2 K / W
T	Temperature, K
t	Fin thickness, m

GREEK SYMBOLS

α	Absorptivity
β	Tilt Angle of Collector
γ	Reflectivity
ε	Emissivity
τ	Transmissivity

SUBSCRIPTS

a	Air Gap
ab	Absorber
c	Glass cover
f	fluid
fi(n)	nth fin node
fib,fie	fin base and fin end
ib,it	insulation bottom and insulation top
1	top
2	bottom

INTRODUCTION

Solar energy has emerged to be one of the most widely used renewable energy sources. One of its direct applications include solar air heaters which are commonly used for space heating, grain drying, hot air generation, steam generation etc. Concentrating solar heaters are used when the desired temperature is quite high as compared to non-concentrating type or flat plate type where the temperature is quite less (~375K). Several improvements in design of flat plate type collectors were attempted to increase the heat transfer and one such heat transfer augmentation techniques is use of longitudinal finned absorber plates. Flat plate solar collectors are the most popular air heaters because of their simple and low cost designs and easy installations.
.

Improvements in the design of flat plate solar air collectors with the help of longitudinal finned absorber plates have gained considerable attention in the recent past [1-4]. Garg *et al.* [1] proved that finned type solar air heaters yielding energy efficiencies ranging from 45 to 61% can compete with other high performance collectors. Naphon [2] analyzed the performance of double pass solar air heater with longitudinal fins and reported that the thermal efficiency is directly proportional to height and number of the fins whereas entropy generation is inversely to the same. Doost et al. [3] compared the performance of rectangular, trapezium, triangular and double-pass longitudinal fins air heaters. An analytical investigation on thermal and thermo hydraulic performance of offset finned solar air heater has been reported by Rai et al. [4]. However, the effect of longitudinal finned absorber in single pass solar air heater is still scanty. The aim of this article is to find out optimum number of trapezoidal fins for a desired temperature rise of the fluid while maintaining a minimum pressure drop in a single pass solar air heater for its application in heating and drying

MATHEMATICAL MODELLING

The solar collector was modelled using two dimensional mesh. The flow was assumed to be laminar for mass flow rate of 0.03 kg/s. Equations were derived using energy balance such that the difference between the input and output heat transferred is the accumulation of heat in the various collector components. Equations (1)-(9) [5] shown below were discretized using Finite Volume Method and solved using implicit method. The major assumption while simulating the system is that there was negligible heat loss from the sides in comparison to heat loss from top and bottom and negligible heat transfer along the length of the collector. It is also assumed that the solar radiation was uniformly distributed over the collector surface. Radiation was assumed to play a significant role in the air gap however it was neglected in the flow region i.e. in between absorber and insulation as convection was dominant in this regions due to fluid flow. Heat conduction of ambient air was also neglected.
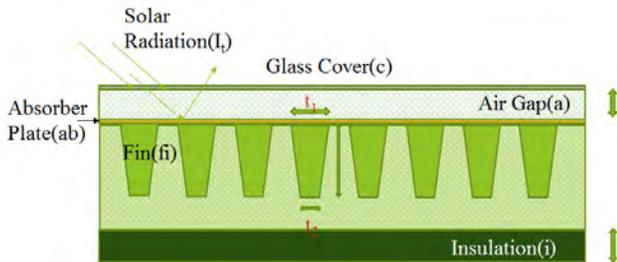
FIGURE 1: SCHEMATIC DIAGRAM OF FLAT PLATE COLLECTOR

1. Glass Cover

$$m_c C_{pc}\left(\frac{dT_c}{dt}\right) = A[h_{c-am}(T_{am} - T_c) + h_{c-a}(T_a - T_c) + h_{r1}(T_{ab} - T_c) + I_t\alpha_c] \tag{1}$$

2. Air gap

$$m_a C_{pc}\left(\frac{dT_a}{dt}\right) = A[h_{c-a}(T_c - T_a) + h_{a-ab}(T_{ab} - T_a)] \tag{2}$$

3. Absorber

$$m_{ab} C_{pab}\left(\frac{dT_{ab}}{dt}\right) = A[h_{a-ab}(T_a - T_{ab}) + h_{r1}(T_c - T_{ab}) + I_t\alpha_{ab}\tau_c] + R_{ab-fi}(T_{fib} - T_{ab}) \tag{3}$$

4. Fin Base

$$m_{fib} C_{pfib}\left(\frac{dT_{fib}}{dt}\right) = R_{ab}(T_{ab} - T_{fib}) + A_{fib}h_{fi-f}(T_f - T_{fib}) + R_{fib-fi}(T_{fi} - T_{fib}) \tag{4}$$

5. Fin end

$$m_{fie} C_{pfie}\left(\frac{dT_{fie}}{dt}\right) = R_{fie-fi}(T_{fi} - T_{fie}) + Ah_{fi-f}(T_f - T_{fie}) \tag{5}$$

6. Along the fin

$$m_{fi(n)} C_{pfi(n)}\left(\frac{dT_{fi(n)}}{dt}\right) = A_{fi(n)}h_{fi-f}(T_f - T_{fi(n)}) + R_{fi(n)-fi(n+1)}(T_{fi(n+1)} - T_{fi(n)}) + R_{fi(n)-fi(n-1)}(T_{fi(n-1)} - T_{fi(n)}) \tag{6}$$

7. Fluid

$$m_f C_{pf}\left(\frac{dT_f}{dt}\right) = A[h_{ab-f}(T_{ab} - T_f) + h_{fi-f}(T_{fi} - T_f) + h_{f-it}(T_{it} - T_f)] + m_{flow}C_{pf}(T_{f-in} - T_f) \tag{7}$$

8. Insulation top

$$m_{it} C_{pit}\left(\frac{dT_{it}}{dt}\right) = Ah_{f-it}(T_f - T_{it}) + R_i(T_{ib} - T_{it}) \tag{8}$$

9. Insulation bottom

$$m_{ib} C_{pib}\left(\frac{dT_{ib}}{dt}\right) = Ah_{am-ib}(T_{am} - T_{ib}) + R_i(T_{it} - T_{ib}) \tag{9}$$

SIMULATION DETAILS
COLLECTOR SPECIFICATION

The design parameters and operating conditions of the collector were similar as given by Bhattacharyya et al. [5] except the fin thickness the fins are trapezoidal in shape with base thickness of 0.002/0.003 m and end thickness of 0.001/0.0015 m.

HEAT TRANSFER CORRELATIONS

The heat transfer coefficients between the glass cover, the insulation plate and the ambient was calculated by summing up the contributions from both convection and radiation. Convective heat transfer coefficient was calculated using the following Eqn. (10) [6]

$$Nu = 0.86 * Re^{1/2} * Pr^{1/3} \tag{10}$$

Radiation heat transfer coefficient was estimated as follows,

$$h_r = \frac{\sigma \varepsilon_c (T_c{}^4 - T_{sky}{}^4)}{T_c - T_{sky}} \qquad (11)$$

where T_{sky} is determined by Swinbank formula [6].

The following correlation estimates the heat transfer coefficient during natural convection [6]

$$Nu = 1 + 1.44 \left[1 - \frac{1708 (\sin 1.8\beta)^{1.6}}{Ra \cos \beta} \right] \left[1 - \frac{1708}{Ra \cos \beta} \right]^+ + \left[\left(\frac{Ra \cos \beta}{5830} \right)^{1/3} \right]^+ \qquad (12)$$

To measure the heat transfer coefficient between absorber plate and glass cover due to radiation the following relation was used,

$$h_{r1} = \sigma \frac{(T_{ab}{}^2 - T_c{}^2)(T_{ab} - T_c)}{\left(\frac{1}{\varepsilon_c} + \frac{1}{\varepsilon_{ab}} - 1 \right)} \qquad (13)$$

The coefficient of heat transfer for convection between absorber, fins and insulation top in developing laminar region was estimated using the correlation proposed by Edward *et al.* [7] ,

$$Nu = 7.54 + \frac{0.03 \left(\frac{D_h}{L} \right) RePr}{1 + 0.016 \left[\left(\frac{D_h}{L} \right) RePr \right]^{2/3}} \qquad (14)$$

Whereas for fully developed laminar flow regime the convection heat transfer coefficient was given by Heaton *et al.* [8].

$$Nu = \frac{h_i D_h}{k_f} = Nu_\infty + \frac{0.019 \left(Re \, Pr \left(\frac{D_h}{L} \right) \right)^{1.71}}{1 + 0.00563 \left(Re \, Pr \left(\frac{D_h}{L} \right) \right)^{1.17}} \qquad (15)$$

SOLAR RADIATION MODEL

The following data of solar radiation in W/m^2 was obtained after studying solar radiation in Guwahati region. The data were taken from morning to evening between 9 am to 4 pm .The collector was aligned at 32° from the horizontal in accordance with the solar radiation data.
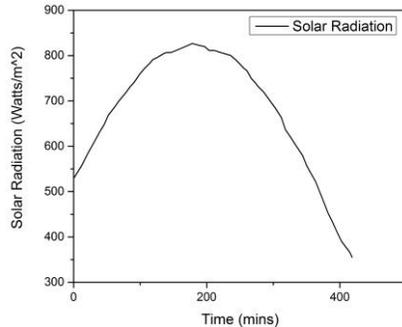
FIGURE 1: DATASOLAR RADIATION IN GUWAHATI REGION (26.11°N, 91.72°E).

RESULTS AND DISCUSSION

The present study was performed for food drying and pre-heating applications of solar air heating collector. Several grid optimization tests were performed and it was found that the simulation is sufficiently accurate for 50 grids. The present code was validated with Garg *et al.* [1] and the validation is not shown here for the brevity of the article.

OUTLET TEMPERATURE FOR VARIOUS FINS THICKNESS

In order to achieve a desired outlet temperature ($50°C$) required in various food drying and preheating processes optimum number of trapezoidal fins were calculated by performing simulations at fin thickness of $t_1 = 0.002$ m & $t_2 = 0.001$ m and $t_1 = 0.003$ m& $t_2 = 0.0015$ m for a mass flow rate of 0.03 kg/s and fin heights of 0.07m and 0.10 m. The results were shown in the Figs. 3 and 4. Due to
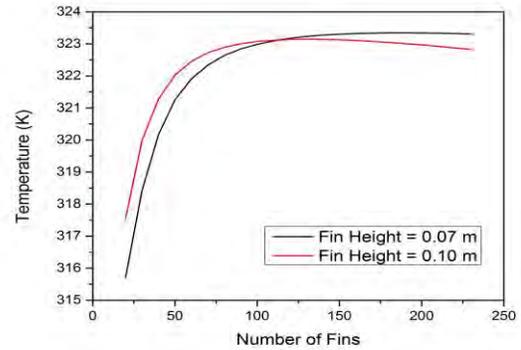
FIGURE 2: VARIATION OF OUTLET TEMPERATURE WITH NUMBER OF FINS FOR FIN THICKNESS $t_1 = 0.002$ m AND $t_2 = 0.001$ m.
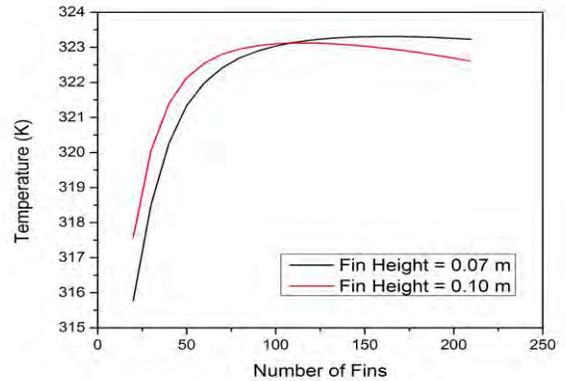
FIGURE 4: VARIATION OF OUTLET TEMPERATURE WITH NUMBER OF FINS FOR FIN THICKNESS $t_1 = 0.003$ m AND $t_2 = 0.0015$ m

High thermal conductivity of aluminium fins used in the present analysis, rise in the temperature was observed with increase in number of fins initially. However, since the specific heat of aluminium was also high, so with the increase in volume of the fins the outlet temperature started

decreasing. Further it was also observed that the outlet temperatures of fins of thickness t_1=0.003 m & t_2=0.0015 m were higher than the fins of thickness t_1=0.002 m & t_2= 0.001 m and this is because for the former case the interfacial area of contact of the fins with the fluid is greater than the latter. The outlet temperatures of the fluid in a trapezoidal finned air collector configuration were also compared with rectangular finned configuration [5] and it was found that the trapezoidal finned one resulted higher temperature rise.

PRESSURE DROP FOR VARIOUS FINS THICKNESS
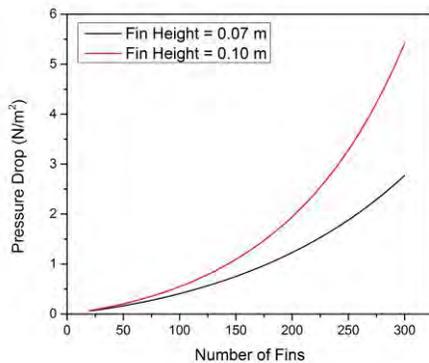
FIGURE 5: PRESSURE DROP V/S NUMBER OF FINS FOR FIN
THICKNESS t_1=0.002 m AND t_2 = 0.001 m.
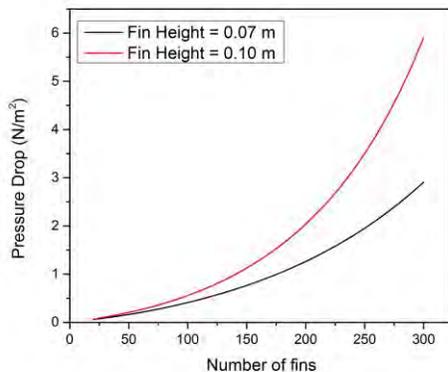
FIGURE 6: PRESSURE DROP V/S NUMBER OF FINS FOR FIN
THICKNESS t_1=0.003 m AND t_2 = 0.0015 m.

Pressure drop was observed to increase with number of fins and was observed to be maximum for 0.1m height. The pressure drop variation for fin thickness t_1=0.002 m & t_2=0.001m and t_1=0.003 & t_2=0.0015m were calculated for flow rate of 0.03 kg/s and were shown in Figs 5 and 6. It was noted that pressure drop in the case of trapezoidal fins were significantly lower than the rectangular fins case [5] for same operating conditions. This was mainly due the fact that trapezoidal fins provide larger area of flow for the fluid in comparison to the rectangular fins for the same number of fins used.

CONCLUSIONS

The results obtained from the simulations were analyzed and it was found that the outlet temperature for the case of fin thickness t_1=0.003 & t_2=0.0015 m was comparatively higher than the other. The optimum number of fins for trapezoidal finned solar air heater is suggested to be 100 number of fins of height 0.07m to attain higher outlet temperature and minimum pressure drop

REFERENCES

[1] Garg, H.P., Jha, R., Choudhury, C. and Datta, G., 1991. Theoretical analysis on a new finned type solar air heater. *Energy*, *16*(10), pp.1231-1238.
[2] Naphon, P., 2005. On the performance and entropy generation of the double-pass solar air heater with longitudinal fins. *Renewable Energy, 30*, pp. 1345-1357.
[3] Assadi, M. K., Doost, A. K., Hamidi, A. A., Mizani, M., 2011. Design, construction and performance testing of a new system for energy saving in rural buildings. *Energy and Buildings, 43,* pp. 3303-3310.
[4] Rai, S., Chand, P., Sharma, S. P., 2017. An analytical investigations on thermal and thermohydraulic performance of offset finned absorber solar air heater. *Solar Energy, 153,* pp. 25-40.
[5] Bhattacharyya, T., Anandalakshmi, R. and Srinivasan, K., 2017. Heat Transfer Analysis on Finned Plate Air Heating Solar Collector for its Application in Paddy Drying. *Energy Procedia*, *109*, pp.353-360.
[6] Duffie, John A., and William A. Beckman. *Solar engineering of thermal processes*. John Wiley & Sons, 2013.
[7] Edwards, D.K., Denny, V.E. and Mills, A.F., 1978. Transfer processes. an introduction to diffusion, convection and radiation. *Series in Thermal and Fluids Engineering, New York: McGraw-Hill, and Washington: Hemisphere Publication Co., 1978, 2nd ed., 1.*
[8] Heaton, H.S., Reynolds, W.C. and Kays, W.M., 1964. Heat transfer in annular passages. Simultaneous development of velocity and temperature fields in laminar flow. *International Journal of Heat and Mass Transfer*, *7*(7), pp.763-781.Misc., A., 2013.
[9] Miscellaneous Title,www.url.com, May

SEEC-2018-075

EFFECT OF HYDROGEN SUBSTITUTION IN DUAL FUEL CI ENGINE ON ENGINE PERFORMANCE AND PARTICULATE EMISSIONS

Priybrat Sharma
School of Engineering
Indian Institute of Technology Mandi
Email: priybrat_s@students.iitmandi.ac.in

Atul Dhar
School of Engineering
Indian Institute of Technology Mandi
Email: add@iitmandi.ac.in

ABSTRACT

The effect of hydrogen energy substitution on engine performance and Particulate emissions in a dual fuel engine is studied experimentally. Hydrogen is inducted through the intake port into the engine. Engine load is varied as 25, 50 and 75%. in all the investigations. Hydrogen energy share is varied as 0, 5, 10 and 20 %. The results show a marginal decrease in engine performance in terms of brake thermal efficiency. The hydrogen substitution is effective in reducing the particulate emissions. Considerable reduction in course and accumulation mode particles is observed.

Keywords: Hydrogen; Dual-fuel mode; Engine Performance; Particulate Matter; Emissions.

INTRODUCTION

There is an increasing stress on conventional fuel sources due to growing demand for energy. This has thrust the research towards renewable and alternative fuel sources. Hydrogen is one such alternative fuel with extremely clean combustion and the possibility of production through renewable energy route [1].

Hydrogen can be adapted as both primary or secondary fuel for internal combustion engines. In dual fuel compression ignition engines, hydrogen is preferred as a secondary fuel. It is known to improve the combustion efficiency of the engines due to its higher flame velocity, high diffusivity in the air and extremely wide flammability limits. Additionally, high auto-ignition temperature of 858 K makes it ideal for application in compression ignition engines. However, it offers low energy density, restricting its application as the primary fuel [2]. The improved combustion efficiency reflected as reduced emissions and increased the overall efficiency of the engine. However, the amount of diesel energy replacement with hydrogen is significantly restricted by the possibility of pre-ignition due to localised hot spots and detonation due to extended delay period [3–5]. Literature sparsely presents a reduction in engine performance on hydrogen substitution. Christodoulou et al. reported deterioration in engine performance at low speed due to a decrease in hydrogen combustion efficiency [6]. The reduction of engine performance corresponds to a dilution of charge due to the molar heat capacity of hydrogen being higher than atmospheric nitrogen [7]. The thermal loss also increases with hydrogen addition as it causes the heat flow to rise [8].

In this study, an effort has been made to investigate the effect of hydrogen substitution on particulate matter emissions and engine performance conditions at various hydrogen energy substitution (HES) ratios.

EXPERIMENTAL SETUP

The experiments are performed on Kirloskar TV 1 single cylinder water cooled engine, modified to run in dual fuel mode. Table 1 elucidates the technical specifications of the engine. The engine is mounted on a universal engine mounting test bed and coupled to a three-phase asynchronous vectorial servo motor. Figure 1 shows the detailed schematic layout of the test setup. Port fuel injection of hydrogen and direct injection of diesel is done to achieve dual fuel combustion in the setup. Hydrogen is supplied from 130 bar pressurised industrial gas cylinder, which is reduced to 3 bar using a double-stage pressure regulator. Needle valves are used to control the flow of hydrogen through the system safely. A Coriolis mass flow meter (Bronkhorst mini CORI-FLOW M14) is used to

detect and log the mass flow rate of hydrogen gas. On the engine end, port fuel injector (AFS Gs-60-05-5H) is mounted on the intake manifold, and hydrogen injection is timed using an in-house developed engine control and data acquisition system. TSI Engine Exhaust Particle Sizer (EEPS model 3090) is used for measurements of particulate matter (PM) number and mass distribution with particle size. A 10 disk thermo-diluter samples the exhaust gets at a primary dilution of 166.5, and then further dilution of 2.5 times is done by adding clean air through HEPA air filter. EEPS through a cyclone receives the sampled exhaust at a dilution factor of 462.5:1. It classifies the particles into 32 size channels using electrical mobility principle. This study reports data average over 60 seconds. Further, the device also integrates the size distribution data and gives total mass concentrations.

Table 1 Detailed specification of the test engine.

Engine Parameter	Specification
Make and model	Kirloskar, Model TV1
Engine type	Single-cylinder, 4-stroke, CI diesel engine
Rated power	5.2 kW (7 BHP) @1500 rpm
Type of cooling	Water cooled
Swept volume	0.661 Litre
Bore X Stroke	87.5 X 110 mm
Clearance volume	40.1 cc
Compression ratio	17.5:1
Speed	1500 rpm, constant
Injection pressure	270 bar at Full Load
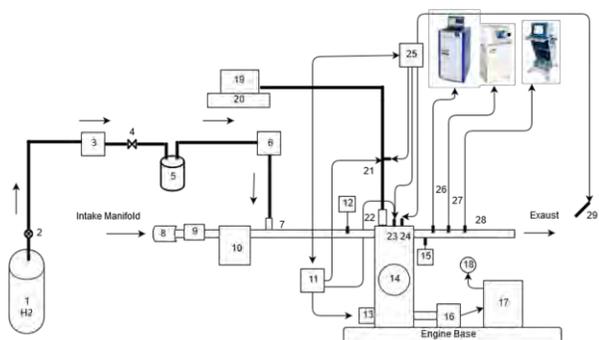
1. Hydrogen Gas Cylinder
2. Pressure Regulator of Hydrogen
3. Hydrogen Mass Flowmeter
4. Needle Valve
5. Flame Trap
6. Flame Arrestor
7. Hydrogen Injector
8. Air Filter
9. Air Mass Flowmeter
10. Air surge tank
11. Engine Control System
12. Air Intake Temperature Measurement
13. Optical Encoder
14. Kirlosker TV1 Engine
15. Air Exhaust Temperature Measurement
16. Transient Dynamometer
17. VDF Drive
18. Test Bed Control system
19. Fuel Tank
20. Load Cell for Fuel Measurement
21. Fuel Line Pressure Sensor
22. Diesel Injector
23. In-Cylinder Pressure Sensor
24. Single Axis Accelometer
25. Data Aquisition and Analysis System
26. FTIR Emission Analyser
27. Exaust Emission Particle Sizer
28. Compact Exaust Analyser
29. Microphone

Figure 1 Schematic diagram of the test setup.

In this study, the engine is run at the constant speed of 1500 RPM, while the engine load and Hydrogen energy share (HES) is varied. The engine has a valve overlap period of 9° CAD after IVO till EVC at 4.5° ATDC. So the hydrogen injection was started at 14.5° ATDC with a margin of 10° CAD for safety purpose. Even though the total available injection duration is 190° CAD till IVC but throughout the experimentation hydrogen injection period was kept constant to 90° CAD (10 ms @1500 RPM), i.e. till 75.5° BBDC. Such injection strategy allows for the maximum hydrogen to enter the cylinder with assured reliability. The hydrogen line has an injection pressure of 3 bar and the needle valve placed after the flame trap is used to control the flow rate of hydrogen. Table 2 shows the test matrix used in the investigation.

Table 2 Engine Experiment Test Matrix.

Load %	Hydrogen Energy Replacement level	Gaseous fuel replacement flow rate required (g/min)	Engine Torque (Nm)
25	0%	0	7.5
	5%	0.17	7.5
	10%	0.35	7.5
	20%	0.7	7.5
50	0%	0	15
	5%	0.23	15
	10%	0.46	15
	20%	0.92	15
75	0%	0	22.5
	5%	0.3	22.5
	10%	0.6	22.5
	20%	1.18	22.5

RESULTS AND DISCUSSION

The effect of hydrogen substitution on engine performance is studied in terms of brake thermal efficiency (BTE) and brake specific energy consumption (BSFC). The particulate emissions are reported as particle number and particulate size distribution.

Brake thermal efficiency (BTE) and Brake specific energy consumption (BSFC)

Figure 2 illustrates the comparisons of brake thermal efficiency (BTE) and brake specific energy consumption (BSFC) at different loads with varying levels of HES. The engine performance is strongly dependent on combustion performance, which appears to deteriorate with hydrogen substitution at tested loads. The reduced combustion efficiency of hydrogen causes a reduction in P_{max}, which results in a decrease of BTE and increase in BSFC at all tested loads. The reduction is marginal, as at 25 and 50 % loads BTE reduces by a maximum of 5 % where else BSFC

increases by 5 %. At 75 % load, the effect reduces further as only maximum 3 % deteriorating is observed in BTE and BSFC at 20 % HES. Zhou et al., concur with the findings and suggested that higher wall heat flux of hydrogen flame compared to diesel cause higher thermal losses, which also contributed to decreased engine performance [9].
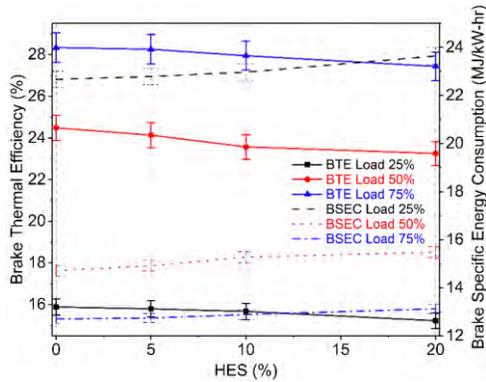
Figure 2 Effect of HES on BTE and BSEC.
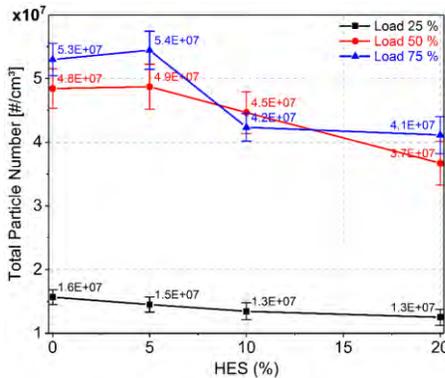
Figure 3 Effect of HES on the total particulate number (PN).

Particulate matter (PM)

Figure 3 illustrates the effect of HES on total particle number at 25, 50 and 75 % loads. Particle number (PN) and size distribution are measured using electro-mobility principle at steady engine conditions. The use of gaseous fuel influences soot formation by changing charge carbon content per unit mass, by the thermal effect on flame temperature and by changing reaction rate or path due to chemical interaction. The effect of charge dilution is predominating at low load throughout the range of HES test, resulting in 20 % reduction of PN from diesel-only operation value of 1.57×10^7 Particles/cm^3. While at higher loads, the PN increases at 5 % HES by 0.5 and 2.7 %, respectively. On increasing HES further the particulate number drops, indicating that the initial increase is due to incomplete oxidation of pyrolysis products from diesel. The quantity of hydrogen available for inhibition of soot particles formation rate is less at 5% HES, and it gets consumed in the initial stages of high-temperature combustion by interacting with

OH and H radicles. In Figure 4 (b) and (c), accumulation mode particles show a slight increase over pure diesel operation at 5% HES, which validates the reasoning.

(a)

(b)

(c)
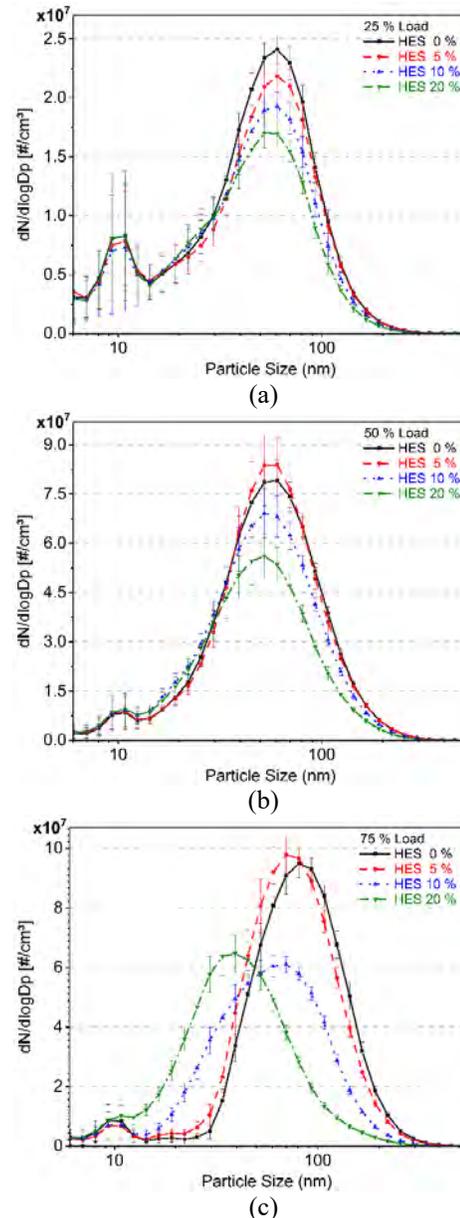
Figure 4 Effect of HES on Particle size distribution at engine loads (a) 25%, (b) 50% and (c) 75 %.

Lognormal bimodal curves in Figure 4 represents the effect of HES on particle size-number distribution at different loads. The first and second mode in the graphs depict the nucleation mode (5 to 50 nm) and the accumulation mode particles (50 to 1000 nm), respectively [10]. Nucleation mode particles tend to be more at lower loads due to longer ignition delay and lower in-cylinder temperature. While at higher loads, accumulation mode particles are more due to short ignition delay period, which

causes the diffusion combustion phase to increase, allowing the formation of larger particles. Figure 4 (a), (b) and (c) make this increase in large sized particles evident. The accumulation mode particle distribution peak value increases from around 2.4×10^7 Particles/cm^3 at 25% load to 7.60×10^7 and 9×10^7 Particles/cm^3 at load 50 and 75 %, respectively at 0% HES.

Literature suggests that premixing of gaseous fuel increases the premixed combustion phase, which causes heightened nucleation mode particle emissions [11].Hydrogen addition reduces the soot nucleation and surface growth rate during combustion by its chemical effect on sooty C_2H_2 and C_2H_4 flames, rather than dilution or cooling effect. Hydrogen when participating in combustion consumes OH radicles, inhibiting the formation of poly-aromatic hydrocarbons (PAH), which leads to a reduction in particle size and PN [12]. Therefore in Figure 4, the second mode peak shifts towards the first peak as HES is increased. The change from accumulation mode to nucleation mode is more drastic at higher load as compared to the small shift observed at lower loads (50 % and 25 %). In Figure 4 (c), the peak of accumulation mode particle concentration with 0% HES is around 50 nm particle diameter range, but on 20% HES it shifts to 40 nm range. This change occurs possibly due to hydrogen stopping the soot formation in surface growth stage by inhibiting the hydrogen abstraction and soot addition to the PAH molecules. Effectiveness on hydrogen in particulate size and number reduction is proven very well in most cases except 5 % HES at 75 % load.

CONCLUSIONS

Following conclusions are drawn from the investigations:

1. At low and mid loads hydrogen substitution cause the engine efficiency to decrease marginally. Dilution effect of hydrogen predominates at such load conditions.
2. Maximum reduction of 5 % in BTE is observed at 50 % load with 20% HES. Correspondingly the BSFC also increases by 5 %.
3. Particulate matter shows reduction with increasing HES after 5%. At 25% load, 20% HES results in 20 % reduction of PN. Hydrogen influences the soot formation by changing carbon content per unit mass of the air-fuel mixture.
4. At mid and high load initially with 5 % HES the PN increases due to competition for oxygen in after burning phase.
5. Hydrogen addition at higher loads reduces the larger particles in 100 to 560 nm size range.

REFERENCES

[1] T. V Johnson, "Diesel Emissions in Review," *SAE Int. J. Engines*, vol. 4, no. 1, pp. 143–157, 2011.

[2] B. Prasath, E. Leelakrishnan, and N. Lokesh, "Hydrogen Operated Internal Combustion Engines– A New Generation Fuel," *Ijetae.Com*, vol. 2, no. 4, pp. 52–57, 2012.

[3] S. Verhelst and T. Wallner, "Hydrogen-fueled internal combustion engines," *Prog. Energy Combust. Sci.*, vol. 35, no. 6, pp. 490–527, 2009.

[4] S. Szwaja and K. Grab-Rogalinski, "Hydrogen combustion in a compression ignition diesel engine," *Int. J. Hydrogen Energy*, vol. 34, no. 10, pp. 4413–4421, 2009.

[5] R. Morgan, P. Atkins, A. Atkins, C. Lenartowicz, and M. Heikal, "Effect of Hydrogen Fumigation in a Dual Fueled Heavy Duty Engine," 2015.

[6] F. Christodoulou and A. Megaritis, "Experimental investigation of the effects of separate hydrogen and nitrogen addition on the emissions and combustion of a diesel engine," *Int. J. Hydrogen Energy*, vol. 38, pp. 10126–10140, 2013.

[7] H. Pan *et al.*, "Effect of hydrogen addition on criteria and greenhouse gas emissions for a marine diesel engine," *Int. J. Hydrogen Energy*, vol. 39, no. 21, pp. 11336–11345, 2014.

[8] K. S. Varde and G. A. Frame, "Hydrogen aspiration in a direct injection type diesel engine-its effects on smoke and other engine performance parameters," *Int. J. Hydrogen Energy*, vol. 8, no. 7, pp. 549–555, 1983.

[9] J. H. Zhou, C. S. Cheung, and C. W. Leung, "Combustion, performance, regulated and unregulated emissions of a diesel engine with hydrogen addition," *Appl. Energy*, vol. 126, no. x, pp. 1–12, 2014.

[10] H. Burtscher, "Physical characterization of particulate emissions from diesel engines: A review," *J. Aerosol Sci.*, vol. 36, no. 7, pp. 896–932, 2005.

[11] M. Raj Saxena and R. Kumar Maurya, "Effect of premixing ratio, injection timing and compression ratio on nano particle emissions from dual fuel non-road compression ignition engine fueled with gasoline/methanol (port injection) and diesel (direct injection)," 2017.

[12] P. PANDEY, B. PUNDIR, and P. PANIGRAHI, "Hydrogen addition to acetylene–air laminar diffusion flames: Studies on soot formation under different flow arrangements," *Combust. Flame*, vol. 148, no. 4, pp. 249–262, Mar. 2007.

SEEC-2018-076

VIBRATION ANALYSIS OF HYDROGEN FUMIGATED DIESEL ENGINE

Sarthak Nag
Renewable Fuels and Internal Combustion Laboratory
Indian Institute of Technology Mandi, India
Email: iamsarthaknag@gmail.com

Priybrat Sharma
Renewable Fuels and Internal Combustion Laboratory
Indian Institute of Technology Mandi, India
Email: priybratsharma@gmail.com

Atul Dhar
Renewable Fuels and Internal Combustion Laboratory
Indian Institute of Technology Mandi, India
Email: add@iitmandi.ac.in

Arpan Gupta
Acoustics and Vibration Laboratory
Indian Institute of Technology Mandi, India
Email: agupta@iitmandi.ac.in

ABSTRACT

Vibration analysis for the hydrogen fumigated compression ignition engine have been carried out to study the engine vibration. The experiment was performed for the load of 25%, 50% and 75% with timed manifold injection. Hydrogen energy share was varied as 5%, 10% and 20%. A single axis accelerometer was mounted on the head of the engine to measure the uprooting force. The findings were then compared with the vibrations of neat diesel. Root mean square of vibration signal has been calculated for the same. The vibrations exhibited by hydrogen fumigated CI engines were less as compared to the diesel engine. The acceleration results further suggest that addition of hydrogen would reduce the mechanical failures due to vibrations at lower loads. The results were in agreement with combustion and total noise. This work provides insight into the development of hydrogen-fuelled CI engines due to low vibrations and motivates us to find their potential for a cleaner environment.

Keywords: vibration analysis, hydrogen fumigation, dual fuel engine.
.

NOMENCLATURE
IC   Internal Combustion

CAD   Crank angle degree
HRR   Heat release rate
CI   Compression ignition
HES   Hydrogen energy share

INTRODUCTION

IC Engines are an integral part of our day-to-day life. A major percentage of the vehicles use IC Engines as the power source for transportation. However, diesel engines have a reputation of excessive vibrations ever since Noise, vibration and harshness has become a critical part of an automobile [1]. Vibrations in an IC engine is a critical factor for engine's life and performance. Automotive engine's vibrations mainly depends on number of cylinders, balancing of the type of engine supports and engine operating conditions such as speed, load, kind of fuel, injection timing of fuel etc [2].

To reduce the vibrations in a CI engine, there is a need to understand the major physics behind its mechanisms. Vibration analysis requires study of various pressure fluctuations happening inside cylinder. Therefore, measurements from in-cylinder pressure transducers are critical in the vibrational study.

Hydrogen is a promising fuel and is known to be a high-quality energy carrier [3-5]. It has a high auto-ignition temperature making it suitable for CI engine, but also requires a secondary fuel to initiate combustion [3]. The clean burning nature of hydrogen makes it an ideal fuel for future use [6]. Hence it becomes critical to study the vibration characteristics and knocking of hydrogen fumigated CI engines [7].

The objective of this study is the vibration analysis of hydrogen fumigated CI engine. The authors have measured the acceleration on the head of the cylinder using single axis accelerometer. In-cylinder pressure is also measured using a pressure sensor. The relation between in-cylinder pressure and vibrations produced in the engine are discussed. The study has been carried at three loading conditions (25%, 50%, 75%) and four HES values (0%, 5%, 10%, 20%). The study concludes that the vibrations reduce as the hydrogen is added in the CI engine.

MATERIALS AND METHODS

Experimental setup:

The test setup was designed to study the hydrogen fumigated CI engines. Kirloskar TV-1 diesel engine was modified to incorporate hydrogen fumigation near the intake valve. Table 1 shows the specifications of the engine. Hydrogen was injected using port fuel injector. Figure 1 shows the schematic diagram of the test setup. For the vibration measurements, a single axis accelerometer was mounted on the head of the engine. Figure 2 shows the mounting position of the accelerometer [2]. In-cylinder pressure transducer was also used to measure in-cylinder pressure variations.
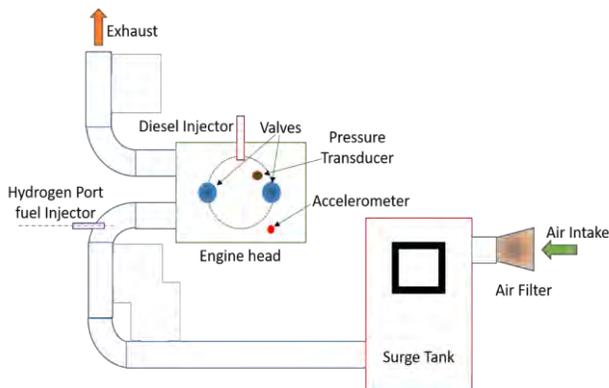
FIGURE 1. Schematic diagram of the test setup.

Operating Procedure:

The engine was allowed to run until its steady state was reached. The load was initially set at 25%, and the HES was varied as 0%, 5%, 10% and 20%. The load was then increased to 50%, and experiments were held till steady state was reached. The same was done again for 75%. At each operating point, the experiment was carried twice. Data

were recorded for 2000 cycles, and one cycle consisted of 5000 data points. The pressure and accelerations were then averaged over a single cycle for each operating point.

TABLE 1: SPECIFICATIONS OF TEST ENGINE

Cycle	4 Stroke
Cylinders	1
Swept Volume	661 cc
Stroke length	0.11 m
Bore diameter	0.0875 m
Speed	1500 rpm
Compression Ratio	17.5:1
Power	5.2 kW
Loading Device	AC transient dynamometer
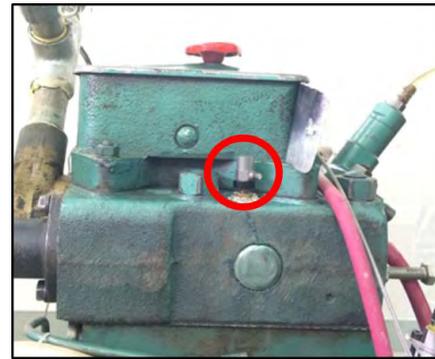
FIGURE 2. Accelerometer mounting position on the test engine.
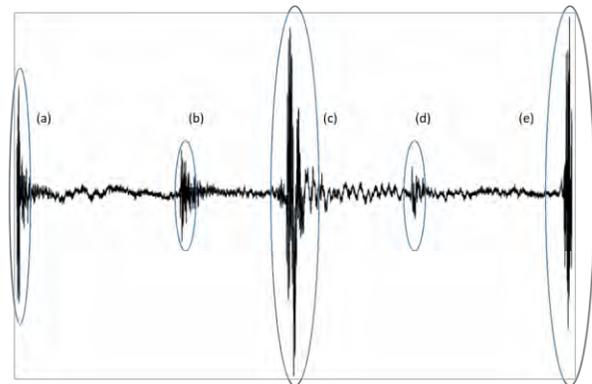
(a): Exhaust valve closes (4.5° aTDC); (b): Inlet valve closes (35.5° aTDC); (c) Combustion; (d) Exhaust valve opens (35.5° bBDC); and (5) inlet valve opens (4.5° bTDC)

FIGURE 3. Noticeable vibration peaks during testing

RESULTS AND DISCUSSION

Figure 3 shows the noticeable vibration peaks captured by accelerometer during experiments. The description of the peaks is in the text box below figure 3. The amplitude of peak (a) and (e) is comparatively higher when compared to

counterparts (b) and (d). This may be due to the very short time difference between these events (~9° CAD). The vibration produced due to these two events may constructively amplify one another and produce intense harshness.
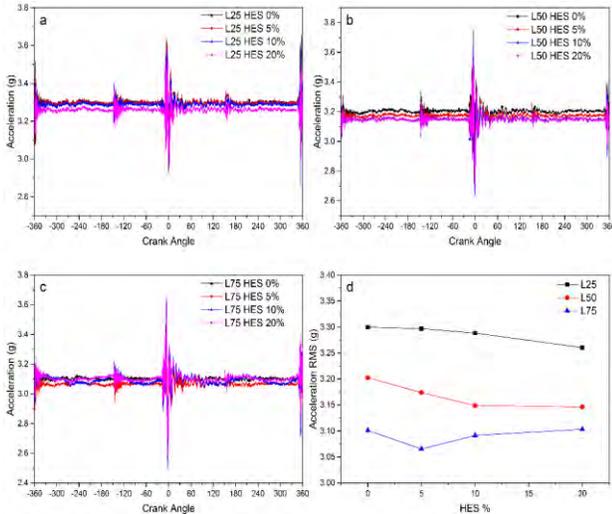
FIGURE 4. Acceleration vs Crank angle variation for (a) 25% load; (b) 50% load; (c) 75% load. (d) RMS value for acceleration at HES values for different loads.

Figure 4 shows the acceleration at different HES values at loads of 25%, 50% and 75%. At 25% load, there is a noticeable dip in engine vibration as the HES value is increased. The trend is similar for load 50%. However, at the load conditions of 75%, there is a rise in acceleration value after the HES 5% value. To further study the reasons for this behaviour, the in-cylinder pressure is studied. Figure 5 shows the in-cylinder pressure variation and acceleration for three load cases. Addition of hydrogen (load 25%) decreases the pressure inside the cylinder. This is due to the reduction of volumetric efficiency and available oxygen for combustion due to its replacement by hydrogen. This effect is called dilution effect [3]. The low in-cylinder pressure will have a lesser impact on the structural integrity of the engine (Fig. 5a). The similar trend can be seen for load 50% case (Fig. 5b) where the pressure reduces as the HES is increased.

However, for the loading case of 75%, the rise in the vibrations due to hydrogen addition can be due to the knocking phenomenon. Knocking phenomenon was quite visible at 75% load. The reason behind this may be improved combustion efficiency of hydrogen under higher mean in-cylinder gas temperature. The higher mean temperature leads to the growth of various flame fronts colliding into each other which leads to increased vibration in the engine block. The knocking is quite visible in Fig. 5c pressure curve.
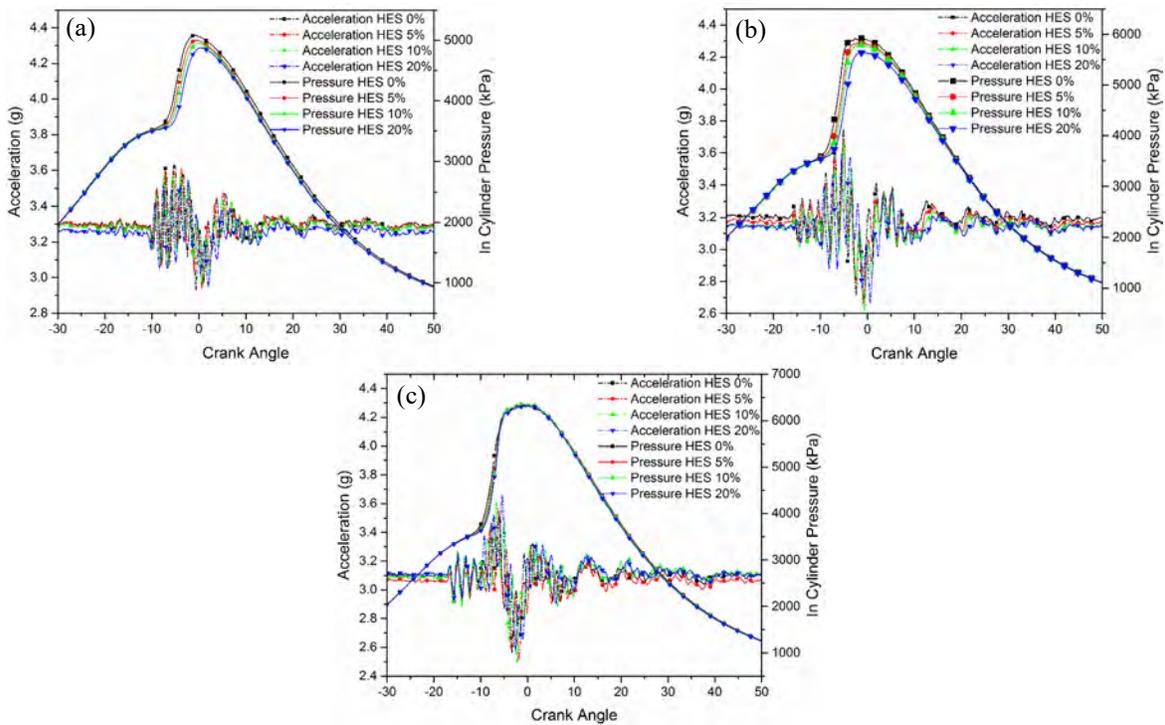
FIGURE 5. In-cylinder pressure variation and engine acceleration plotted against zoomed crank angle degrees for (a) Load 25%; (b) Load 50% and (c) Load 75%.
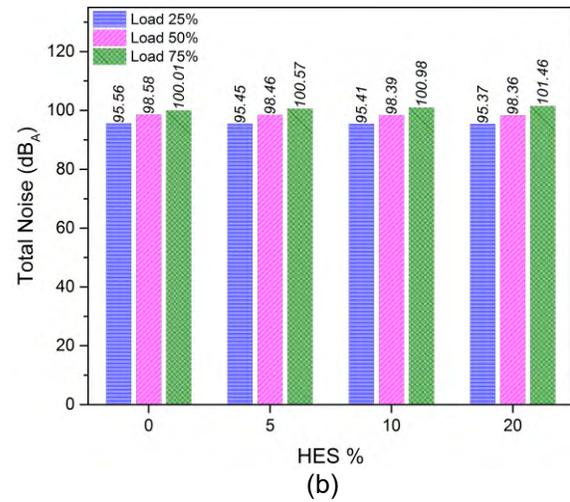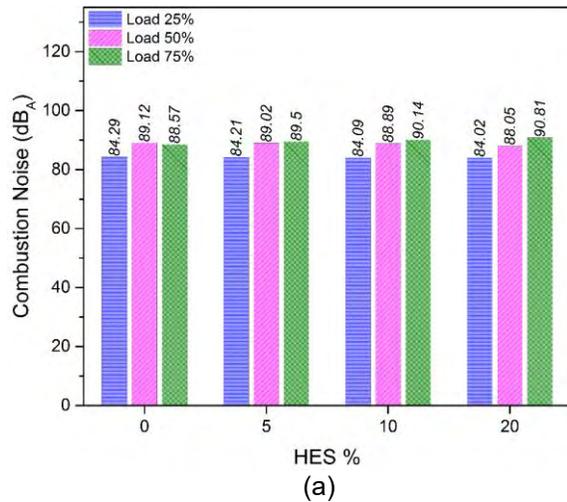
FIGURE 6. (a) Combustion noise measured using in-cylinder pressure transducer (b) Total noise as measured using microphone

Figure 6 (a) and (b) shows the combustion noise and the total noise during the experiment respectively. For the 25% and 50% loading condition, the combustion as well as total noise decreases due to the aforementioned dilution effect. But for the 75% loading case, the phenomenon of knocking increases both the combustion as well as total noise due to hydrogen addition. These results are in agreement with the increased vibrations in the engine due to hydrogen addition.

CONCLUSION

The vibrations on the hydrogen fumigated CI engine were experimentally studied. The experiments were conducted on 3 different loads and HES substitution was carried upto 20%. In-cylinder pressure was also measured. The major conclusions were:

- Due to the dilution effect of hydrogen, the cylinder pressure decreased when HES was increased. The reduced in-cylinder pressure lead to lower vibrations in engine block. This effect was substantial upto 50% load conditions.
- At the increased load of 75%, the knocking phenomenon was prominent which lead to the increase in engine vibrations. This was due to higher mean cylinder temperature.
- Combustion and total noise levels from the engine are in agreement with the level of vibrations produced in the engine.

REFERENCES

[1] Omar, F. K., Selim, M. Y., & Emam, S. A. (2017). Time and frequency analyses of dual-fuel engine block vibration. Fuel, 203, pp. 884-893.

[2] Szwaja, S., Bhandary, K. R. and Naber, J. D. (2007). Comparisons of hydrogen and gasoline combustion knock in a spark ignition engine. International Journal of Hydrogen Energy 32, no. 18: 5076-5087.

[3] White, C.M., Steeper, R.R. and Lutz, A.E. (2006). The hydrogen-fueled internal combustion engine: a technical review. International journal of hydrogen energy, 31(10), pp.1292-1305.

[4] Veziro, T.N. and Barbir, F. (1992). Hydrogen: the wonder fuel. International Journal of Hydrogen Energy, 17(6), pp.391-404.

[5] Verhelst, S. (2014). Recent progress in the use of hydrogen as a fuel for internal combustion engines. international journal of hydrogen energy, 39(2), pp.1071-1085.

[6] Bose, P.K. and Banerjee, R. (2012). An experimental investigation on the role of hydrogen in the emission reduction and performance trade-off studies in an existing diesel engine operating in dual fuel mode under exhaust gas recirculation. Journal of Energy Resources Technology, 134(1), p.012601.

[7] Zhen, X., Wang, Y., Xu, S., Zhu, Y., Tao, C., Xu, T. and Song, M. (2012). The engine knock analysis–an overview. Applied Energy, 92, pp.628-636.

SEEC-2018-077

Effect of Cetane Improver on Performance, Combustion and Emission of CI Engine Fuelled With Eucalyptus Oil Based Hybrid Micro-emulsion Biofuel

Mukesh kumar[1], Himansh Sexena[2], Prof. M.P. Sharma[3], Dr. Pramod kumar[4], Dr. A.K. Sharma[5]

[1]Assistant Professor, Department of Mechanical Engineering , C.E.C, Landran, Mohali, Punjab, India,
[2]Research Scholar, Department of Mechanical Engineering , NIT Jalandhar Punjab, India
3Professor and Head, Biofuel Research Laboratory, Alternate Hydro Energy Centre, Indian Institute of Technology Roorkee, India
[4]Associate Professor, Department of Mechanical Engineering, NIT Jalandhar Punjab, India
[5]Scientist E, SSS-NIBE Kapurthala, Punjab, India

mukeshiitr13@gmail.com, himansh.rmu@gmail.com

Abstract:

Vegetable oil based micro-emulsion technique has a positive attraction due to its inherent features such as short production time and during combustion no chemical reaction and less pollution production. In the present study eucalyptus oil, 1- butanol and anhydrous ethanol is used to form microemulsion based hybrid biofuel (MHBF) and overcome its poor cetane number issue through cetane improver Ethylenediamine (EDA) because low cetane number of any fuel delayed the self-ignitability of fuel. So the present study is focused on the effect of EDA on physical and chemical properties of MHBF and performance, combustion and exhaust emission of four-stroke single cylinder CI engine at the constant speed (1500 rpm). Also, the experiment was conducted for comparison of MHBF with B_{20}, B_{100}, and petro-diesel. EDA was added in the concentration of 500, 1000 and 2000 ppm in MHBF to study its effects. The addition of EDA had increased the CN without causing any negative effect on other chemical properties of MHBF. The CI engine performance results has shows that MHBF with EDA, brake thermal efficiency was comparable with B_{20} and petro-diesel while higher to B_{100} and brake specific fuel consumption (BSFC) was higher to B_{20} and petro-diesel and lower to B_{100}. MHBF with highest EDA decreases the delay period and smoothen the combustion. Also, MHBF with EDA produced a very low amount of oxides of nitrogen (NOx) and less reduction in unburned hydrocarbon (UHC) with the highest amount of EDA. Nevertheless, carbon monoxide (CO) emissions increased with highest EDA concentration. So these are the positive signs to move ahead on this work.

Keywords: Micro-emulsion, Ethylenediamine, CI Engine, Butanol, Ethanol,

SEEC-2018-078

SUSTAINABLE VALORIZATION OF ORGANIC MUNICIPAL SOLID WASTE TO BIOBASED PRODUCTS

A.Naresh Kumar
Bioengineering and Environmental Sciences Lab,
EEFF Department, CSIR-Indian Institute of
Chemical Technology (CSIR-IICT),
Hyderabad- 500007, India.

S. Venkata Mohan*
Bioengineering and Environmental Sciences Lab,
EEFF Department, CSIR-Indian Institute of
Chemical Technology (CSIR-IICT),
Hyderabad- 500007, India.
E-mail: vmohan_s@yahoo.com
svmohan@iict.res.in

ABSTRACT

Minimizing the dependency on fossil-based resources and reducing the solid wastes generation represent the main challenges for the modern society. Organic municipal solid waste (OMSW) is considered as potential feedstock to harness the energy, fuels and platform chemicals. The present study was evaluated with the re-engineering of anaerobic fermentation process for the production of various biobased products viz., reducing sugars, short chain fatty acids (SCFA), medium chain fatty acids (MCFA) and biohydrogen using OMSW. Initially, saccharification of OMSW was evaluated to convert the polysaccharides into reducing sugars using novel bioelectro-saccarification systems. Resulting sugars were used as a substrate in acidogenic fermentation process to produce SCFA and MCFA along with biohydrogen as co-product. The results enumerate the advantages of integrated multistage process for the production of various biobased products by simultaneously addressing the current solid waste practices in the framework of biorefinery.

Keywords: *Municipal Solid Waste, Reducing Sugars, Biohydrogen, Short-Chain carboxylic acids, Medium Chain Fatty Acids*

INTRODUCTION

The rapid growth of human population and urbanization is leading towards massive waste generation. Proper waste management practices are essential to eliminate the further environmental degradation and transition to a sustainable society (Pradel et al., 2016). Conventional solid waste management practices are eliminating the potential of valuable feedstock to harness the biobased products and with simultaneous emissions of greenhouse gases (Bing et al., 2016). Consequently, waste management practices need to be developed for the extraction of valuable resources from waste and their simultaneous remediation (Rong et al., 2017). Among the biological routes, acidogenic fermentation is economically viable and promising technology, thus compatible with various composite waste (high strength) biodegradation with concurrent production of biohydrogen (H_2) and short chain fatty acids (SCFA) (Venkata Mohan et al., 2016). Theoretically, 1 Kg COD gives 624.96 g of acetic acid (acetic acid pathway), 385 g of propionic acid (propionic acid pathway) 916 g of butyric acid (butyric acid pathway) (Dahiya et al., 2015). Currently, commercial production of SCFAs is mostly accomplished by chemical routes (Dahiya et al., 2015). The application of OMSW to produce SCFA offers alterative sustainable bioprocesses and also decreases the carbon foot prints. To consolidate the perceptions of OMSW, the present study was investigated to develop a sustainable integrated bioprocess for the high rate reducing sugars (RS) production followed by utilization of resulted sugars for the production of SCFA, MCFA and biohydrogen (H_2).

Materials and Methods

Biocatalyst

The anaerobic mixed consortium acquired from full scale anaerobic effluent treatment plant, Hyderabad was used as parent inoculum for all the reactors. Prior to inoculation, parent biomass was washed twice with phosphate buffer (50 mM: 5,000 rpm, 28±2°C) followed by heat-shock pretreatment (heating the sludge at 80°C) for one hour. The resulting culture was inoculated with designed synthetic wastewater for 24 h (32 ± 2^oC) in anaerobic conditions (Venkata Mohan et al., 2009).

Reactor Configuration

Anaerobic bioreactors were fabricated using borosilicate glass bottles with the total/working volume of 0.5/0.4 L. The reactors were operated in suspended growth configuration and batch mode of operation for 10 cycles with 48h of hydraulic retention time (HRT). Each batch comprised of 20 min of fill phase, 47 h of react phase, 20 min of settle phase and 20 min of decant phase in sequencing mode of operation (Dahiya et al., 2015). To remove the traces of oxygen present in the reactor nitrogen gas was sparged prior to starting of cycle. The reactors were kept in suspension mode during REACT phase (47h) by continuous mixing (120 rpm; $28 \pm 2oC$). During the start up, reactors were inoculated with 10% of heat pretreated inoculum.

Results and Discussion
Pretreatment of OMSW

Vegetable waste fraction of biogenic municipal solid waste (OMSW) was considerable potential to produce soluble RS of 8.2 g/l. Physicochemical pretreatment with dilute acid (1% HCl) accelerated its solubility and resulted maximum RS concentration (42.2 g/l) (Fig 1). In this context, to increase the RS solubilization, single (physical/ chemical) and combined pretreatments (physicochemical) were evaluated. Relatively, physicochemical pretreatment with dilute acids (combined with 1% HCl/H_2SO_4 autoclaving at 121^oC) resulted in higher RS solubilization (RS: 42.2/40.8 g/l) followed by alkaline (1% $NaOH/Ca(OH)_2$: 36.5/32.1 g/l). On the other hand, single physical pretreatment (without acid, only autoclaving at 121^oC for 15 min), resulted in comparatively lower RS solubilization (28.3 g/l). Dilute acid pretreatment in combination with thermal treatment is regarded as a promising pretreatment for carbohydrate rich biomass (Liu et al., 2012). The composition of sugars with dilute acids physicochemical (1% HCl $/H_2SO_4$ (v/v)) follows viz., glucose: 26.1/25.2g/l, fructose:7.8/7.5 g/l, galactose:3.8/6.58 g/l, maltose:3.2/3.1 g/l and ribose:1.5/1.45 g/l respectively. On the other hand, physicochemical pretreatment with dilute alkali (1%NaOH/Ca(OH)₂ (v/v)) resulted low sugar concentrations viz., glucose: 22.4/18.8 g/l, fructose: 6.1/5.7 g/l, galactose: 4.1/ 3.8 g/l, maltose: 2.8/2.6 g/l and ribose: 1.1/1.2 g/l.
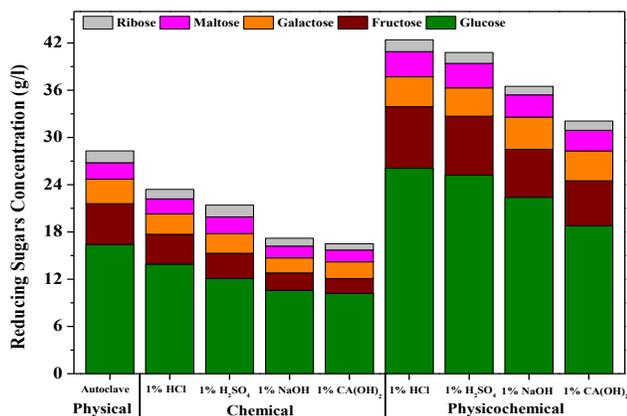
Fig 1: Reducing sugars composition with respect to method of pretreatment

Short Chain Fatty Acids (SCFA)

Organic solid waste biomethanation process can be amended to produce SCFA such as acetic acid (C2), propionic acid (C3) and butyric acid (C4), etc. SCFAs also known as short chain carboxylic acids (SCA) known as platform chemicals and it can be used directly for industrial applications or can be converted into other valuable compounds (alcohols/chemicals. Experimental results for SCFA production using OMSW illustrated variations in production and composition of total SCFA with the function of initial pH and operation time. Relatively, bioreactor operated with pH 6 resulted in higher concentration of SCFA (13.4 g/l) followed by pH 10 (10.8 g/l), pH 7 (7.12 g/l) and pH 4 (5.6 g/l).

Short Chain Fatty Acids

Distribution analysis of produced SCFA plays important role to understand the fermentative process performance. Operational pH plays key factor determining the product spectrum and microbial specific conversion. Majorly, depicted SCFA profiles were viz., acetic acid, propionic acid, butyric acid and isovaleric acids (C2-C5) (Fig. 2). Among all the produced SCFA, acetic acid concentration was relatively higher (7.3 g/l) followed by butyric acid (2.6 g/l), propionic acid (1.3 g/l) and isovaleric acid (2.2 g/l) in pH 6 conditions. In case of pH 10, acetic acid was found to be relatively high (5.2 g/l) followed by butyric acid (1.7 g/l), propionic acid (1.3 g/l) and isovaleric acid (2.6 g/l). Interestingly, alkaline conditions favored the high rate production isovaleric acid than corresponding other pH conditions. This ascribed to favoring of system buffering conditions for the process of chain elongation from acetic acid to isovaleric acid (Jankowsk et al., 2015). Neutral pH conditions favored for the maximum production of acetic acid (3.6 g/l) followed by propionic acid (2.5 g/l), but comparatively lower concentrations of butyric acid (0.86 g/l) and isovaleric acid (0.15 g/l) were resulted than other pH operations. In case of pH 4, distinct variations in the SCFAs composition were illustrated than corresponding pH 6, 7 and 10. pH 4 system SCFA profiles were found to be dominated with butyric acid (2.5 g/l) followed by acetic acid (1.6 g/l), propionic acid (0.92 g/l) and isovaleric acid (0.6 g/l).
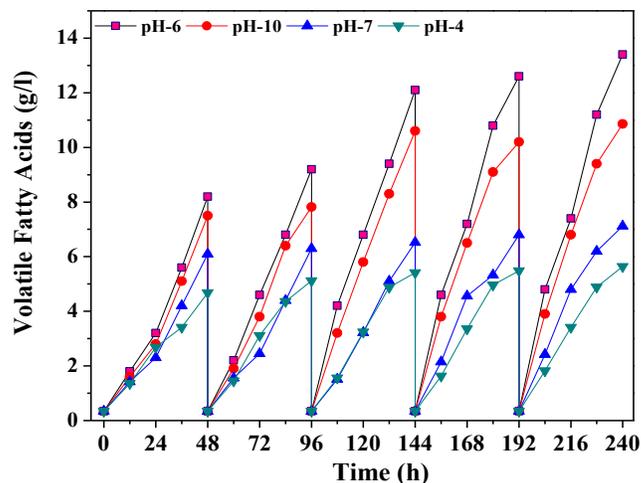
Fig 2: Volatile fatty acids concentration with the function of operation time

Degree of Acidification

Degree of acidification (DOA) signifies the system's production capability in terms of SCFA accumulation. DOA was calculated with respect to individual SCFAs viz., acetic acid, propionic acid, butyric acid, valeric acid concentrations and also with the mixture of all SCFAs (Dahiya et al., 2015). Significant variations in the DOA were depicted with the course of pH variation and fermentation time. Higher DOA was documented with pH 6 operation (54.1%), followed by pH 10 (43.5%), pH 7(30.2%) and pH 4 (26%). Higher acetic acid concentration in system operated with pH 6, 10 and 7 contributed to higher degree of acidification, while in case of pH 4 system butyric acid contributed major portion of DOA. Nature of substrate and its biodegradability majorly contributes in comprehensive yield of the acidogenic process and degree of acidification (DOA).

Buffering Capacity

Buffering capacity (BC) analysis enumerates the functional role of pH in the fermentation process and also helps in understanding the several interdependent and complex sequential biochemical reactions. It was observed that all the systems pH was towards acidic, that signifies the accumulation of SCFA in the bioreactor and its correlation with resulted buffering profiles. Maximum buffering was documented with pH 10 system (0.036 βmol) followed by pH 6 (0.034 βmol), pH 7 (0.028 βmol) and pH 4 (0.021 βmol). Higher alkaline conditions and simultaneous production of SCFA might have helped the good buffering conditions in pH 10. In case of pH 4 system, drop in the pH was rapid, although system gained good BC, this ascribed to liberated CO_2 from the substrate metabolism might have assisted as buffering agent in the form of bicarbonate (HCO_3).

Substrate Degradation

Substrate degradation (based on the RS and soluble COD removal (SCOD)) showed significant variations in the SCFA production with respect to system pH condition. Comparatively, higher substrate degradation efficiency (RS/SCOD removal) was documented with pH 6 operation (71/66%) followed by pH 10(63/62%), pH 7 (61/58%) and pH 4 (59/54%) respectively. Favoring of system buffering condition (pH 6) might have induced the higher substrate degradation. Moreover, the concentration of dissolved organic matters (DOM) also plays a significant role in the acidogenic process performance and SCFA production. Initially, during first few cycles of operation (96h), RS degradation was lower (pH 6:65%, pH 10:61%, pH 7:46% and pH 4: 47%) and thus resulted lower SCFA production. Additionally, with the course of cycles operation (240h) system attained stabilized performance and resulted higher substrate degradation was documented with the pH 6:71% followed by pH 10:63%, pH 7: 61% and pH 4: 59%).

Although substrate degradation varied marginally in the pH 7 and pH 10 (61/63%), but substantial SCFAs concentrations were resulted (pH 7/10: 6.6/10.8 g/l). This signifies the consumption of produced SCFA towards the bio-methane production, thus correlate well with the resulted biogas profiles.

Conclusion

The present study demonstrates the influence of various saccharification methods for the production of reducing sugars from OMSW. Acidogenic fermentation of the resulting RS for the production SCFA, MCFA and biohydrogen facilitates a new dimension of biobased products synthesis from OMSW. Complexity of substrate and varying initial pH conditions significantly influenced the products profiles during the acidogenic fermentation. The SCCA and MCFA obtained during the process can either be used as platform chemicals or reutilized in other processes rendering sustainability and economic viability to current solid waste management practices.

References

1. Bing, X., Bloemhof, J, M., Ramos, T, R, P., Povoa, A, P, B., Jack, C, Y, W., Vorst, G.A.J.V. 2016. Research challenges in municipal solid waste logistics management. Waste Management 48, 584-592
2. Dahiya, S., Sarkar, O., Swamy, Y, V., Venkata Mohan, S. 2015. Acidogenic fermentation of food waste for volatile fatty acid production with co-generation of biohydrogen. Bioresour Technol. 182, 103-113
3. Sarkar, O., Butti, S, K., Venkata Mohan, S. 2017. Acidogenesis driven by hydrogen partial pressure towards bioethanol production through fatty acids reduction. Energy 118, 425-434
4. Pradel, M., Aissani, L., Villot, L., Baudez, J, C. Laforest, J, C. 2016. From waste to added value product: towards a paradigm shift in life cycle assessment applied to wastewater sludge-a review. Journal of Cleaner Production. 131, 60-75.
5. Rong, L., Zhang, C., Jin, D., Dai, Z. 2017. Assessment of the potential utilization of municipal solid waste from a closed irregular landfill. Journal of Cleaner Production. 142, 413-419
6. Venkata Mohan, S., 2009. Harnessing of biohydrogen from wastewater treatment using mixed fermentative consortia: process evaluation towards optimization. Int. J. Hydrogen Energy 34, 7460-7474.
7. Venkata Mohan, S., Goud, R. K. 2012. Pretreatment of Biocatalyst as Viable Option for Sustained Production of Biohydrogen from Wastewater Treatment, in Biogas Production: Pretreatment Methods in Anaerobic Digestion (ed A. Mudhoo), John Wiley & Sons, Inc., Hoboken, NJ, USA.
8. Venkata Mohan, S., Nikhil, G, N., Chiranjeevi, P., Reddy, C, N., Rohit, M, V., Kumar, A, N., Sarkar, O. 2016. Waste biorefinery models towards sustainable circular bioeconomy: Critical review and future perspectives. Bioresour Technol. 215,2-12

SEEC-2018-079

Influence of Photosynthetic efficiency and Quantum Yield on Lipid profile of *Chlorella sorokiniana* SVMBIOEN2

M V Rohith
Bioengineering and Environmental Sciences Lab,
EE&FF Department, CSIR-Indian Institute of
Chemical Technology (CSIR-IICT),
Hyderabad- 500007, India
Email: rohit761@gmail.com

S Venkata Mohan*
Bioengineering and Environmental Sciences
Lab, EE&FF Department, CSIR-Indian
Institute of Chemical Technology (CSIR-IICT),
Hyderabad- 500007, India,
Email: vmohan_s@yahoo.com

ABSTRACT

Microalgae are biotechnologically exploited for commercial interests in the areas food, feed and biofuel sector. Microalgae have intrinsic ability to harness energy from sunlight and photosynthetically valorize CO_2 into various biobased products viz., triacylglycerols (TAGs), mono/poly-unsaturated fatty acids (MUFA, PUFA) etc. Microalgae have adapted to grow in various nutritional environments due to their metabolic versatility and resilience. In the present study, performance of isolated strain Chlorella sorokiniana SVMBIOEN2 was evaluated using design of experiments (DOE) methodology towards enhanced lipid/TAG production. Various triggering factors for synthesis of long chain fatty acids were studied to understand multi-parametric stressors and gain insights on underlying fatty acid (FA) synthesis mechanism.

Keywords: Microalgae, Lipids, Triacylglycerols (TAG), Mixotrophic, Heterotrophic
.

INTRODUCTION

Microalgal triacylglycerols (TAGs) are increasingly deliberated as sustainable feedstock for the commodity markets (i.e. food, chemical and biofuel) [1]. Microalgae operate as green cell factories and have higher photosynthesis rates compared to agricultural crops. For enhancing the efiicienc of microalgae cultivation, two stage operation is considered as cost effective strategy for higher biomass and lipid producitivities. The operational strategy strongly affects the product titres and ultimately techno economic feasilibility of the process while upscaling. TAG production is usually carried out in a two-step batch process in which first stage is biomass production under nitrogen sufficient conditions, in second stage, stress condition are provided by N depletion to trigger lipid production. Batch cultivation in second stage is desirable for ensuring TAG productivity of upto 30% w/w [2]. However, after reaching a maximum lipid within the first days of cultivation, TAG productivity decreases, due to a declining photosynthetic activity during N-starvation. Thus it is important to understand the dynamics of photosynthetic activities taking place during TAG synthesis to optimize and enhance the lipid production. At lab-scale, optimal conditions that influence TAG productivities are light, temperature, salinity, carbon etc. have been achieved with some microalgal species [3]. However, optimal factors vary from species to species depending on the diversity and strain characteristics. After reliable optimization and validation in lab scale systems, outdoor pilot-scale studies are essential to identify technical and process bottlnecks that should be tackled before scaling up.

Chlorella species are mainly cultivated under mixotrophic and heterotrophic conditions for higher biomass and lipid productivities. Also, systems biology of algae is now considered pre-requisite for gaining insights into total metabolic blueprint of algal bioprocess. Special interest is focused on production of food grade/edible oils, lipid powders from microalgae due to the versatile fatty acid profile with high MUFA and PUFA content [4]. In this study, the isolated strain *Chlorella sorokiniana* SVMBIOEN2 was evaluated using Design of Experiments (DOE) methodology using Taguchi Orthogonal array for optimization of conditions for enhanced TAG and long chain fatty acid production.

MATERIALS AND METHODS

The strain *Chlorella sorokiniana* SVMBIOEN2 was isolated from Nacharam Cheruvu and identified by 18S rRNA gene sequencing. The obtained sequence was submitted to Genbank with accession number KM677935 and strain deposited in NCIM cuture collection (Accession no. 5561). Isolated strain was cultivated in mixotrophic mode (7.5 g/l COD) for until maximum biomass growth was obtained. In the stress phase, Taguchi orthogonal array (OA) methodology was implemented to study specific influence of eight important factors (light, pH, temperature, sailinity, carbon concentration, nitrates, phosphates and trace metal concentration) on neutral lipid (TAG) production using three levels of factor (2^1 x 3^7) variation with L18 experimental matrix experimental trials. Except for salinity (2^1), all other factors were assigned with three levels. In the designed OA, each column consisted of a number of conditions depending on the levels assigned to each factor and the diversity of factors can be studied by crossing OA of control factors (**Table 1**).

Table 1: List of factors selected for optimization

	Level 1	Level 2	Level 3
Salinity (g/l)	0	5	
Carbon (g/l)	0	5	20
Phosphate (mg/l)	0	500	1000
Nitrate (mg/l)	0	100	200
Metal	Iron	Manganese	Zinc
Temp	10	25	35
pH	6	7	8.5
Light (µE/sec)	0	60	200

DESIGN OF BIOREACTORS

The experiments were conducted on 500ml Borosil bottles with the modular design for provision of air sparging unit fixed in the bottle cap for gas diffusion. LED lighting was supplied for 60µE/m^2/sec and 200 µE/m^2/sec condition. Modular cooling unit was designed for low temperature conditions. Aeration was provided using aquarium pumps for mixing and CO_2 supply in the form of air.

EXPERIMENTAL METHODOLOGY

Mixotrophically grown *Chlorella sorokiniana* SVMBIOEN2 strain (7.5 g/l COD) for 8 days in BG-11 media was inoculated into specific stress conditions based on their factor level. The total/working volume of the reactor was 300/500 ml. The cultivation was performed for a period of 12 days (HRT) and different parameters like biomass and lipid productivity, protein, carbohydrate and lipid content, nutrient removal and Chlorophyll fluorescence kinetics were analyzed. Ampicillin (0.2 mg/ml) was added to avoid bacterial growth during cultivation. Light intensity was measured using Extech Light meter. The 18 experimental conditions were designated as E1 to E18 based on their respective factor level.

RESULTS AND DISCUSSION

GROWTH PHASE

The *Chlorella sorokiniana* SVMBIOEN2 strain was cultivated in mixotrophic conditions initially for a period of 8 days and maximum biomass of 6.2 g/l was obtained. The maximum total chlorophyll (48.9 µg/mg), protein (288 mg/g) and carbohydrates content (267 mg/g) was achieved. Nitrogen and Phosphorus removal of 88% and 79% was observed. The total lipid percentage was found to be 16.9% with 4.9% of neutral lipid content. The Quantum yield (QY) was found to be 0.69 in biomass phase. The QY for healthy physiological state of algae is in the range of 0.5 to 0.7 [5]. Maximum Chlorophyll fluorescence was also increased from 40x10^3 to 140x10^{3}AU which is directly associated to biomass growth (**Fig 1**). Mixotrophic condition is known for achieving higher biomass concentrations due to the presence of glucose and CO_2 as carbon source resulting in greater carbon influx into the algal cells. Subsequently, chlorophyll, protein and carbohydrate content was found to be gradually increasing which are biological markers for algal growth and healthy cell physiology [6,7]. Later, After obtaining maximum biomass after 16 days, the biomass was concentrated and then inoculated into stress conditions into 18 different conditions.

OPTIMIZATION OF STRESS PHASE

The mixotrophically grown biomass was then served as inoculum for stress conditions designed by Taguchi DOE methodology. The different factors at three levels lead to diverse metabolic profiles based on their nutrient composition. Initially, 9 of the 18 set of conditions were operated namely E1, E2, E3, E6, E9, E11, E16, E17, E10 and classified into autotrophic and mixotrophic conditions based on presence or absence of glucose.

From the operated conditions, maximum biomass was obtained in E9 condition (2.9 g/l) followed by E16 (2.5 g/l) and E6 (1.25 g/l) conditions. The presence of carbon (20g/l), phosphate (1 g/l) and optimal (60µE/m^2/sec) of light might be influenced for biomass growth. Absence of nitrate content may have led to decrease in biomass from biomass phase to stress phase (6.2 to 2.9 g/l).
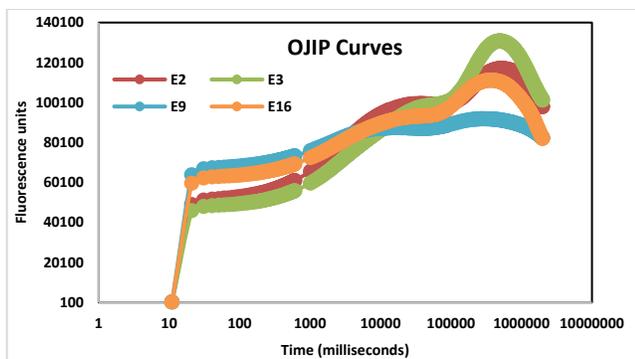
Fig 1: Photosynthetic efficiency in growth phase measured OJIP curves

The total/neutral lipid content was found to be maximum (34/16%) in E16 (29/19%) mixotrophic condition followed by E11 autotrophic condition and E6 (22.5/14.9%) mixotrophic conditions. Quantum yield (QY) and fluorescence kinetics showed altered physiological condition due to stress parameters. QY decreased from 0.69 to 0.45 in E9 condition where maximal lipid was observed. Chlorophyll concentration is directly proportional to nitrogen and absence of Nitrogen in E9 condition may have led to low QY and fluorescence. QY decreased from 90×10^3 to 25×10^3 AU. Presence of optimal conditions close to native habitat of microalgae has favoured maximal lipid production in E9 condition and predominant stress was due to N deprivation. Presence of High carbon concentration was known to influence rapid lipid synthesis in this condition.

Lipid productivity was found to be highest (422g/kg DCW) in E16 mixotrophic condition due to high biomass content. Predominant factors for E16 condition are salinity (5g/l, pH 6 and Temp 35°C) followed by E9 mixotrophic (306g/kg DCW). High carbon concentration was dominant influencer for lipid induction in E9 condition [8].

CONCLUSIONS

The E16 and E9 conditions were found to be optimal conditions for enhanced lipid productivity due to relative higher biomass in stress phase. The influencing factors for neutral lipid/ TAG induction are carbon, salinity, pH and temperature which led to enhanced lipid prodcuctivties. Further validation of optimized conditions needs to be performed for scale up studies. The oil thus produced can be used for edible oil or biodiesel purposes based on the fatty acid satuaration. This sustainable algal cultivation may be upscaled to enable Bioeconomy and integrated with closed loop biorefinery for sustainable economics.

ACKNOWLEDGMENTS

REFERENCES

[1] Draaisma RB, Wijffels RH, Slegers PM, Brentner LB, Roy A, Barbosa MJ (2013) Food commodities from microalgae. Curr Opin Biotechnol 24:169–177

[2] Benvenuti G, Bosma R, Klok AJ, LAmers PP, Barbosa MJ, Wijffels RH (2015) Microalgal triacylglycerides production in outdoor batch operated tubular PBRs. Biotechnol Biofuels 8:100H.W. Yen, S.H. Ho, C.Y. Chen, J.S. Chang, CO_2, NOx and SOx removal from flue gas via microalgae cultivation: A critical review, Biotechnol. J. 10 (2015) 829–839.

[3] Ho SH, Chang JS, Lai YY, Chen CNN (2014) Achieving high lipid productivity of a thermotolerant microalga Desmodesmus sp. F2 by optimizing environmental factors and nutrient conditions. Bioresour Technol 156:108–116

[4] Klok AJ, Lamers PP, Martens DE, Draaisma RB, Wijffels RH (2014) Edible oils from microalgae: insights in TAG accumulation. Trends Biotechnol 32:521–528

[5] P. Cardol, G. Forti, G. Finazzi, Regulation of electron transport in microalgae, Biochim. Biophys. Acta - Bioenerg. 1807 (2011) 912–918.

[6] S. Venkata Mohan, M.V. Rohit, P. Chiranjeevi, R. Chandra, B. Navaneeth, Heterotrophic microalgae cultivation to synergize biodiesel production with waste remediation: Progress and perspectives, Bioresour. Technol. 184 (2015) 169–178

[7] W.C., Chang, H.Q., Zheng, C.N.N. Chen, Comparative transcriptome analysis reveals a potential photosynthate partitioning mechanism between lipid and starch biosynthetic pathways in green microalgae, Algal Res. 16 (2016) 54–62.

[8] P. Chiranjeevi, S. Venkata Mohan, Optimizing the Critical Factors for Lipid Productivity during Stress Phased Heterotrophic Microalgae Cultivation, Front. Energy Res. 4 (2016) 1–10.

SEEC 2018-080

SUSTAINABLE BIOSEQUESTRATION OF CO_2 : CAPACITIVE BIOCATHODES INFLUENCE ON REGULATION OF MICROBIAL ELECTROSYNTHESIS

J. Annie Modestra
Bioengineering and Environmental Sciences Lab,
EE&FF Department, CSIR-Indian Institute of
Chemical Technology (CSIR-IICT),
Hyderabad- 500007, India

S Venkata Mohan*
Bioengineering and Environmental Sciences Lab,
EE&FF Department, CSIR-Indian Institute of
Chemical Technology (CSIR-IICT),
Hyderabad- 500007, India,
Email: vmohan_s@yahoo.com

ABSTRACT

In view of the ongoing climate change associated with the increasing levels of CO2 emissions, microbial electrosynthesis systems (MES) are emerging as potential routes for sequestration of CO2 with simultaneous production of biobased products. In MES, formation of electrotrophic bacteria as biofilm on electrodes surface regulates entire bio-electrochemical reduction reaction. In this context, a study was designed by opting carbon cloth (CC), stainless-steel mesh (SS), combination of CC-SS and hybrid combination of CC-SS and activated carbon (AC), as electrode materials during MES. Hybrid combination (CC-SS-AC) yielded higher carboxylic acids production, current density, bicarbonate removal and lower resistance followed by CC-SS, CC and SS. Higher productivity obtained with CC-SS-AC might be attributed to porous and biocompatible nature of electrode materials favouring the enrichment of electroautotrophic bacteria. Current study offers development of novel hybrid electrode combination for enrichment of electroautotrophic biocatalyst towards enhanced bio-electrochemical reduction of CO2 with simultaneous biobased products synthesis.

Keywords: *Bioelectrochemical system, biocathodes, electroautotrphs, electrochemical impedance, biobased products*

INTRODUCTION

Continous rise in CO_2 emissions associated with depletion in fossil reserves for energy generation, developed a quest to serach for energy efficient and environmentally benign technologies for sequestering CO_2 with simultaneous production of biobased products [1]. In this context, microbial electrosynthesis systems (MES) are emerging as promising and potential routes for sequestration of CO_2 with simultaneous production of biobased products [2,3]. Various parameters such as biocatalyst, applied potentials, pH, electrode materials, reactor design etc. will essentially govern the fate of product synthesis in MES [4]. Among these, electroautotrophy has a key function in conjunction with electrode materials in MES, as the formation of electrotrophic bacteria as biofilm on the surface of electrodes (biocathodes) regulates entire bio-electrochemical reaction [5-7]. In BES, electrode serves as electron donor, which is governed by several properties of electrode viz., electrode material, composition, biocompatibility, mechanical strength, porosity, impurities, anti-corrosive, increased surface area, metal catalyzed etc. which enables the surface catalyzed bio-electrochemical reduction reactions towards the synthesis of based products. Considering the importance of electrode materials essential for biofilm formation (electroautotrophs), present study is designed by opting carbon cloth (CC), stainless steel mesh (SS), combination of CC and SS and a hybrid material composed of CC, SS and activated carbon (AC), as electrode materials during MES. Biochemical and electrochemical parameters were comparatively analyzed for four different electrode material combinations to evaluate the optimum biocatahode electrode material for higher productivity during MES operation.

Materials and Methods

Biocatalyst

Indigenous mixed anaerobic bacteria obtained from full scale anaerobic reactor treating wastewater is used as the parent inoculum. Bacteria used as biocatalyst is different at

anode and cathode chambers. Anode chamber of BES was inoculated with anaerobic and untreated parent inoculum enriched in synthetic wastewater containing glucose (1.5 g/l) as carbon source. While in the case of cathode chamber, parent inoculum was subjected to acid pretreatment (pH 3 with HCl) to enrich acidogenic bacteria and to eliminate non-spore forming hydrogen consuming methanogenic bacteria. The resulting culture was subjected to a headspace gas mixture of H_2 and CO_2 (80:20) to selectively enrich homoacetogenic bacteria [5, 3]. This homoacetogenic bacteria is ultimately used as biocatalyst at cathode chamber.

Reactor Configuration

A double chambered BES was designed and fabricated using Schott-Duran glass bottles with a total/working volume of 2.5/2.0 l. BES consisted of an anode and a cathode chamber separated by a proton exchange membrane. Non-catalyzed graphite plate was used as electrode at anode in BES. While in the case of cathode, four different electrode materials viz., carbon cloth (CC), stainless steel (SS-mesh), combination of CC-SS and hybrid combination of CC-SS along with activated carbon (CC-SS-AC) were used as electrode materials to aid in efficient biofilm formation for enabling surface catalyzed electrochemical reactions. Copper wires were used to establish contact with electrodes. Proper leak proof sealing was done to ensure anaerobic environment at both the chambers.

Experimental Operation

BES was operated with four different electrode materials at cathode with a polarized potential of -0.8V vs Ag/AgCl (S) chronoamperometrically using a potentiostat-galvanostat system (EC-Lab). Performance was assessed in terms of carboxylic acids production, alcohols synthesis, bicarbonate reduction and pH change. Drop in carboxylic acids concentration and reductive catalytic currents were used an indicator for feed change. Experiment was carried out in fed batch mode with each cycle operated for a retention time of 72 hrs.

Results and Discussion

Acetic acid production

Experiments were conducted by applying a potential of -0.8 V vs Ag/AgCl (S) on bio-cathode considering it as working electrode against anode as counter electrode and Ag/AgCl (s) as reference electrode through a potentiostat-galvanostat system. CO_2 as sole carbon source was supplemented in the form of sodium bicarbonate with a pH of 8.0. While in the case of anode chamber, untreated culture was used as biocatalyst and glucose as carbon source. The reducing equivalents generated through the metabolic activity of anodic bacteria will be driven towards cathode with the aid of applied potential for the reduction

of CO_2 into carboxylic acids. A maximum of 4.3 g/l of acetic acid was produced in BES operated with hybrid electrode combination (CC-SS-AC) followed by CC-SS with a maximum yield of 4.11 g/l, CC (3.21 g/l) and SS (2.9 g/l) (Fig.1). This variation in yeild with different electrode materials might be attributed to the enrichment of bacterial biofilm that will enable surface catalyzed bio-electrochemical reactions. Comapartively, lower productivity observed with SS might be attributed to the electrolysis at electrode surface that is in support with the rise in pH that generates hydroxide ions.
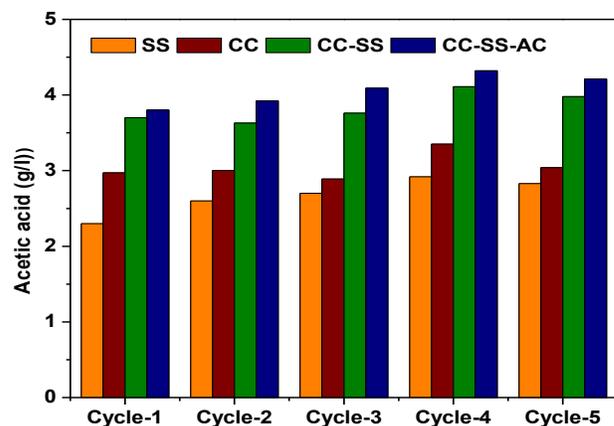
Fig.1 Acetic acid production of all the biocathodes for five cycles of operation

Total Carboxylic acids and alcohols production

Study depicted the bio-electrochemical synthesis of a mixture of carboxylic acids upon CO_2/bicarbonate reduction. Higher carboxylic acids production is observed in hybrid electrode combination (CC-SS-AC; 4.8 g/l) followed by CC-SS (4.5 g/l), CC (3.9 g/l) and SS (3.3 g/l). Carboxylic acids were bioelectrochemically synthesized by utilizing bicarbonate as sole carbon source along with an applied potential as driving force for directing the reducing equivalents. Among the mixture of carboxylic acids synthesized, acetic acid concentration was high followed by butyric acid. In addition, ethanol was also detected in small quantities in BES operated with hybrid combination and CC, which might be ascribed to the reduction of synthesized carboxylic acids towards alcohols synthesis. This is also in agreement with the observed pH profiles, where alcohol synthesis was initiated in associated with higher carboxylic acids accumulations. A gradual increment in concentration of carboxylic acids was noticed till 60 h followed by a decrement at 72 h. The decrement in carboxylic acids concentration might be due to the reduction of C2-C4 compounds towards alcohols synthesis.

Bicarbonate reduction

Bicarbonate concentration was observed to decrease with the increase in time for each cycle operation. Samples were collected at regular time intervals for each cycle operation

to monitor the changes in bicarbonate concentration. High reduction in bicarbonate reduction was depicted during BES operated with hybrid combination (CC-SS-AC) followed by CC-SS, CC and SS. This depicts the utilization of bicarbonate as inorganic carbon substrate by the enriched biocatalyst. Prevalence of alkaline range of pH also favored dissolution of bicarbonate in catholyte which in turn aided in the utilization of bicarbonate for carboxylic acids synthesis.

Variation in pH
During bioelectrochemical synthesis, variation in pH is noticed throughout the cycle with respect to carboxylic acids and alcohols production. Initially, all BES systems were operated at pH 8. A drop in pH is noticed from 6h in all the BES operated with various electrode materials (CC-SS-AC: 7.2; CC-SS: 7.1; CC: 7.1; SS: 7.4). Maximum drop in pH was noticed in hybrid combination (CC-SS-AC; 6.3) followed by CC-SS (6.23), CC (6.1) and SS (7), which is in congruence with ethanol production observed in hybrid combination at favourable pH conditions. Thereafter, a rise in pH is observed in all the BES, which might be ascribed to the utilization of carboxylic acids towards alcohols synthesis or as carbon source by other bacterial population.

Conclusions
This study demonstrates the efficacy of hybrid electrode combination as potential biocathodes with capacitive nature that would support electrophy towards enhanced biobased products synthesis. Various biobased products viz., carboxylic acids and alcohols were synthesized during bio-electrochemical reduction of CO_2. Study revealed the importance of electrode materials that enable electrotrophic biofim formation towards enhanced electron transfer and product synthesis. Study unraveled the potential of BES in not only synthesizing multi-carbon biobased products, but also efficient electrotrophic biofilm development deciphering the role of electrode materials as capacitive biocathodes.

REFERENCES
[1] S. Venkata Mohan, J. A. Modestra, K. Amulya, S. K. Butti, G. Velvizhi, Trends in Biotechnol. 34 (2016a) 506-519
[2] S. Venkata Mohan, G. Velvizhi, J.A. Modestra, S. Srikanth, Renew. Sustain. EnergyRev. 40 (2014) 779–797.
[3] R.C. Franca, A. Azapagic, J. CO2 Util. 9 (2015), 82-102.
[4] J. Annie Modestra, B. Navaneeth, S. Venkata Mohan, Journal of CO_2 Utilization 10 (2015) 78–87.
[5] K.P. Nevin, Appl. Environ. Microbiol. 77 (2011) 2882–2886.
[6] J. Annie Modestra, S. Venkata Mohan, Journal of CO_2 Utilization 20 (2017) 190-199.
[7] S. Venkata Mohan, S. K. Butti, K. Amulya, S. Dahiya, J. A. Modestra, Trends in Biotechnol. 34 (2016b) 852-855.

SEEC-2018-081

CONTINUOUS MODE OPERATION WITH WASTEWATER: INFLUENCE ON MFC PERFORMANCE WITH MEMBRANE VARIATION

Kuchi Swathi
Bioengineering and Environmental Sciences Lab, EEFF Department, CSIR-Indian Institute of Chemical Technology (CSIR-IICT), Hyderabad- 500007, India.

Sai Kishore Butti
Bioengineering and Environmental Sciences Lab, EEFF Department, CSIR-Indian Institute of Chemical Technology (CSIR-IICT), Hyderabad- 500007, India.

Omprakash Sarkar
Bioengineering and Environmental Sciences Lab, EEFF Department, CSIR-Indian Institute of Chemical Technology (CSIR-IICT), Hyderabad- 500007, India.

S. Venkata Mohan*
Bioengineering and Environmental Sciences Lab, EEFF Department, CSIR-Indian Institute of Chemical Technology (CSIR-IICT), Hyderabad- 500007, India.
E-mail: vmohan_s@yahoo.com

ABSTRACT

The present study evaluates the efficiency of continuous flow microbial fuel cells (MFC) for bioelectricity production in concurrence with waste remediation. Three single chambered air cathode MFCs were operated with membranes (Nafion 117 and Terry cotton) and without membrane in continuous mode using synthetic wastewater as substrate. Power density and COD removal efficiency ($€c$) obtained was observed to be high with nafion (100 mW /m^2; 50 %) followed by membraneless (62 mW/m^2; 47 %) and Terry cotton (25 mW/m^2; 39 %) respectively. The study infers that Nafion reported higher efficiency compared to Terry cotton and membranless, since it has high proton transfer efficiency. With respect to economics and real field adaptability membranless MFC is considered to be feasible and hence can be easily upscaled with continuous mode of operation.

Keywords: *Continuous microbial fuel cell, power density, coulombic efficiency, wastewater remediation*

INTRODUCTION

Microbial fuel cell (MFC) is the most prominent bioelectrochemical technology for energy generation. MFCs are hybrid bio-electrochemical device that directly converts chemical energy into electrical energy uisng microorganisms i.e. biocatalyst. The e^- and H^+ thus released during substrate degradtion develops the bipotential thus generating electricity. MFC also use wastewater as a susbstrate to harness bioenergy is considered as a prominent technique for its clean, sustainabl and renewable in nature [1].

MFCs can be operated in batch and continuous mode, wherein each of these has a direct impact on the number of electrons participating in redox reactions and on the microbial colonization on the electrode surface. Each mode of operation, influences the ratio of substrate to product concentration in the system thereby affecting the microbial activity and hence on power output [2]. In batch mode of operation, the catabolic activity of the microorganism reduces with the depletion of substarte and nutrients after certain time interval. However, in continuous MFCs the constant inflow of the substrate will replace the nutrient depleted medium that supports the microbial activity and hence for persistent power production. The other advantages are composition of the substrate could be optimized for maximum productivity, the growth of the biocatalyst are determined with respect to kinetics, high productivity per unit volume could be achieved, etc. The present study operates the MFC in contious mode of operation.

The other influencing factors of MFCs include electrode materials, reactor configuration, partial substrate utilization, biocatalyst activity, membranes etc [3]. Membranes is one of the factor on power production in MFCs, since the reducing equivalents generated during the microbial degradation of organic matter in the anodic chamber . The protons migrates to the cathode chamber through the membrane and electrons pass through the circuit and both get reduced in the cathode chamber [4]. Hence membrane also has a pivotal role in the operation of MFCs but due to its cost and long term problem associated with Nafion it is need to find alternative.

In this context, the present study is carried out to evaluate the performance of MFC in continuous mode of operation using different kind of membrane viz., Nafion and Terry cotton and membraneless. Three MFCs such as Nafion (MFC_N), membranless (MFC_{ML}) and Terry cotton (MFC_T) was operated in contious mode. The study evaluates the performance of all the three setup of MFCs with bioelectrogenic, bioelectrochemical activities and wastewater analysis.

Materials and Methods
MFC Construction
Three single chambered microbial fuel cells (Block shaped) identical in size and shape were fabricated using polytetraflouroethylene with total/working anode volume of each cell is (40/36ml). The fuel cells are designed to place the anode completely inside the reactor to provide anaerobic condition and cathode exposed to air. Non-catalyzed graphite with active surface area of 16 cm^2 is used as anode and the same was with cathode with surface area of 25 cm^2. Ag/AgCl-3.5 M KCl (±197 mV vs. SHE) is used as a reference electrode to measure the anode and cathode potentials respectively. Each cell is designed to have provisions for sample port, continuous inflow and outflow of the effluent and output of the wires. Of three MFC's, two are integrated with membranes (Nafion 117 and Terrycotton) and the other without membrane.

Operation
Anode chamber of MFC's were inoculated with (10% w/v) of the filtered sludge collected from anaerobic effluent treatment plant. Designed synthetic water (DSW) (Ref) with COD (5 g/l) of glucose is used as anolyte and fed into each reactor individually in a continuous mode with Inflow of the anolyte is from the bottom of the reactor in the upward direction through gravitational pressure, with continuous inflow the utilized effluent moves out from the top of the reactor, which helps to retain the microbes in active phase. Cells were operated at room temperature and pH of the anolyte was adjusted to 7.0 ± 1 using orthophosphosric acid/0.1 N NaOH for a better results. The system was operated in a continuous mode by connecting to a 20 l storage tank individually to each cell with the help of silicon tubes for continuous flow of effluent at a flow rate of 48 ml/hr. After 15 days of continuous operation in the open circuit, the constant behavior of the cells is observed with stable OCV and after which cells were operated in a closed circuit condition by connecting to a resistor.

Measurments & Calculations:
pH, VFA and COD removal are analyzed for samples collected at various intervals of time using standard methods. COD removal efficiency of each cell was calculated using [5].

$$E_{COD} = (C_{SO}\text{-}C_{ST})/ \ C_{SO} \ x \ 100 \qquad [Eq\text{-}1]$$

In the above equation C_{SO} is the Initial COD concentration (mg/lit) of the substrate and C_{ST} is the COD concentration (mg/lit) at a defined time (t).

Bioelectrochemical Anaysis
Performance of each individual cell is evaluated in terms of power generation (P), voltage (V) and current (I) production. Voltage is monitored regularly for every 300sec by kethley and is also measured by using multimeter at regular time intervals. Cyclic voltammetric studies were carried out at multiple scan rates (100mV/s-0.5mV/s). Polarization of cells at varied external resistances 30- 0.05 kΩ was performed using a variable resistor and multimeter

RESULTS AND DISCUSSION
Bioelectrogensis
MFCs were optimized with an organic loading range (OLR) of 3g/l glucose. Initially the performance of the cells was unstable but with time i.e. after 15 days of operation the cells has shown consistent improvement and also stabilization in terms of COD removal and stable voltage was observed which indicates the stable biofilm formation. The maximum open circuit voltage (OCV) recorded with MFC_N, MFC_{ML}, MFC_T was 510 mV, 420 mV and 307 mV. The maximum current and power density obtained with 1kΩ of external resistance in MFC_N is 3.5 mA and 100 mW/m^2 follwed by MFC_{ML} (2.6 mA, 69 mW/m^2) and MFC_T (1.9 mA, 25 mW/m^2) (Fig-1). The continuous mode of operation showed good power production due to the constant availabity of substrtae and nutrients therby increasing the cell density. MFC_N effective proton mobility resulting enhanced performance However with respect to cost and economy, memebranless MFC (MFC_{ML}) is considered to be feasible for upscaling.

Electrochemical Behavior of MFCs:
Cyclic Voltammetric studies carried out to understand the bioelectrochemical behavior of MFC_N, MFC_T and MFC_{ML}. The reducing equivalents obtained during the microbial metabolic activities tends to move towards the anode under applied voltage conditions thus generates a voltammogram.

CV profiles (*vs* Ag/AgCl) of three MFCs has shown visible and significant variations in discharge of reducing equivalent with and without membrane. Maximum oxidative currents of 4.54 mA, 4.01 mA and 3.0 mA were observed with MFC_T, MFC_{ML} and MFC_N respectively. The oxidative catalytic currents obtained with MFC_T and MFC_{ML} were almost identical and higher when compared to MFC_T which might be due to the effective electron ransfer from the biocatlyst to the electrode. The reductive catalytic current observed with MFC_N, MFC_T and MFC_{ML} were as follows 6.42 mA, 3.69 mA and 3.0 mA. The high reductive currents with MFC_N attribute to the effective migration of protons from the anode to cathode. The high reductive with MFC_N is due to the effective oxidation and reduction (ORR) in the cathode chamber. The membranelss MFC also reported good performance due to the proton mobility in the anolyte.
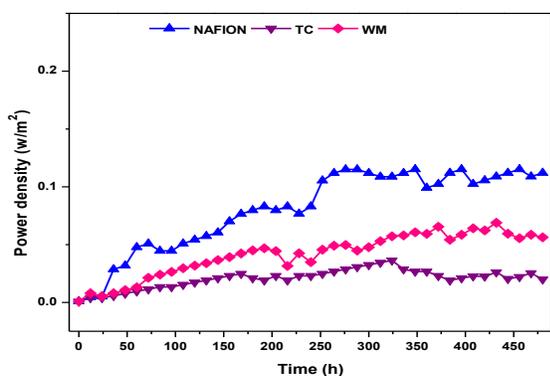
Fig. 1. Stable power density curves with respect to time in MFC_N, MFC_{ML}, MFC_T

Substrate removal efficiency

The substrate removal efficiency in continuous mode of operation with three MFCs (MFC_N, MFC_{ML}, MFC_T) was elucidated. MFC_N has shown highest COD removal of 50% $\pm$ 0.5 followed by 44% $\pm$ 0.5 with MFC_{ML} and 39 % $\pm$ 0.5 with MFC_T and remained constant with all the MFCs throughout the operation. This stable performance is due to continuous flow of the substrate with simultaneous removal of the effluent. The organic substrate present in anode region of MFC was utilized during the metabolic activity of the biocatalyst resulting in release of e^- and H^+. The protons thus migrates into the cathode chamber thereby catalyzing the reduction reactions. Although MFC_N and MFC_{ML} has shown identical performance to COD removal but the performance of electrogenic activity was observed to be less due to the losses of reducing equivalents. Moreover with respect to economics MFC_{ML} is considered more feasible for large scale applications.

CONCLUSION

The study concludes that continuous flow microbial fuel cells showed effective bioelectrogenic and bioelectrochemical activities due to the availability of continues substrate and nutrients .The study infers that continues mode of operation can be used as an persistent technology for energy generation and waste remediation. With respect to membrane and membraneless operation , Nafion reported that higher performance due to the effective transfer of protons to the cathode chamber. However, membraneless MFC has shown good COD removal efficiency which infers that the system could be effective for wastewater treatment . Moreover the cost efficient, easy operation and compatibility favours this system towards large scale applications.

Acknowledgement

REFERENCES:

[1] Venkata Mohan, S., Veer Raghavulu, S., Dinakar Peri, Sarma, P.N., 2008. Integrated function of microbial fuel cell (MFC) as bio-electrochemical treatment system associated with bioelectricity generation under higher substrate load. Biosens. Bioelectron.24 (1) 41-47.

[2] Kyoung-Yeol, K., Wulin, Y., Patrick J. E., Logan, B.E., 2016 Continuous treatment of high strength wastewaters using air-cathode microbial fuel cells. Bioresour Technol. 221, 96-101

[3] Jung, R. K ., Chen, G.S., Euno, H, S., Logan, B.E., 2007. Power Generation Using Different Cation, Anion, and Ultrafiltration Membranes in Microbial Fuel Cells. Environ Sci Technol. 41(3), 1004-1009

[4] Shanthi Sravan, J., Butti, S.K., Verma, A., Venkata Mohan, S., 2017. Phasic availability of terminal electron acceptor on oxygen reduction reaction in microbial fuel cell. Bioresour Technol. 242: 101-108

[5] Pasupuleti, S.B., Srikanth, Pant, D., Venkata Mohan, S., 2015. Continuous mode operation of microbial fuel cell (MFC) stack with dual gas diffusion cathode design for the treatment of dark fermentation effluent. International Journal of Hydrogen Energy. 40 (36), 12424-12435.

SEEC-2018-082

BIOBASED SUCCINIC ACID PRODUCTION: STRAIN ISOLATION AND OPTIMIZATION OF PROCESS

K. Amulya
Bioengineering and Environmental Sciences Lab,
EE&FF Department, CSIR-Indian Institute of
Chemical Technology (CSIR-IICT),
Hyderabad- 500007, India.

S. Venkata Mohan*
Bioengineering and Environmental Sciences Lab,
EE&FF Department, CSIR-Indian Institute of
Chemical Technology (CSIR-IICT),
Hyderabad- 500007, India.

E-mail: vmohan_s@yahoo.com

ABSTRACT

In the present work, potential succinic acid (SA) producing bacteria from natural ecosystems was isolated. In particular, the SA producer strain, with an attractive substrate utilization spectrum were tested for its ability to synthesize succinic aid by optimizing the process parameters. Design of experimental (DOE) methodology using Taguchi orthogonal array (OA) was applied to evaluate the influence and specific function of six important factors (carbon source, carbon concentration, applied potential, pH, concentration of neutralizing agent ($MgCO_3$) and CO_2 partial pressures) on the SA production. Three levels of factor (2^1X3^5) variation were considered with symbolic arrays of experimental matrix [L_{18}–18 experimental trials]. All the factors were assigned with three levels except applied potential.

Keywords: *Succinic Acid, Municipal Soild Waste, bioelectrochemical system, Taguchi methodology, Orthogonal array (OA), Optimization.*

INTRODUCTION

Twentieth century saw the advent of organic chemicals and fuel manufacturing industry based on petroleum feed stocks, while in the 21st century we see the development of chemicals and fuels based on renewable or bio-based feed stocks. In both scenarios the driving force is the demand for energy [1]. We are now in an era where fossil fuels are diminishing at a rapid rate, where there is an ever-growing energy demand and renewable sources of energy are sought with increasing vigour. Apart from the diminishing fossil fuels another problem that the world is is the enormous quantities of waste being generated. Million tons of waste is generated worldwide every year, making its management and treatment a challenging ordeal. Waste takes many forms, from household or kitchen wastes, municipal solid wastes, industrial wastes to gases emitted from industries especially CO_2 [1]. Considerable effort has been put into managing these wastes over the past few years. Apart from treatment, the focus has also been on developing several sustainable technologies that could wring the value of waste by producing industrially important bio-based chemicals, bio-based materials and bio-fuels that not only reduce our dependency on fossil based fuels and products but also help in mitigating environmental pollution [2]. The production of bio-based products has been so far limited to only high monetary value products. However, the advancements in science and technology allows the economic production of other bio-based products from wastes that have equal monetary value and more importantly have a wide range of applications. Of all the chemicals that are being manufactured, succinic acid production through fermentation is being pursued with a great deal of interest because of its potential as a platform chemical for the production of various value-added derivatives [3]. Succinic acid and its derivatives hold applications as surfactants, detergents, electroplating, food, pharmaceuticals, antibiotics, amino acids and vitamins. However, the cost of bio-based succinic acid production is not yet competitive with petrochemical-based alternatives such as maleic anhydride due to the use of expensive carbon and nitrogen sources. One possible way to reduce the cost of succinic acid production process is the use of municipal solid waste as a source of carbon and CO_2 during microbial fermentation.In this dimension, the current works aims to use wastewaters as a substrate and CO_2 to produce succinic acid by anaerobic fermentation and comparative evaluation with production in a bio-electrochemical system (BES under small applied voltages. This work seeks to

investigate how a broad range of parameters interact to influence succinic acid production by employing the Taguchi Design of experiments (DOE) methodology.

Materials and Methods
Taguchi's DOE methodology
DOE methodology by Taguchi approach was employed in this study to optimize critical factors pertaining to succinic acid production with the function of electron donor. The performance is measured by the deviation of a characteristic from its target value and a loss function [L(y)] [5]. Taguchi method involves establishment of large number of experimental situations described as OAs to reduce errors and to enhance the efficiency and reproducibility of the laboratory experiments. Six factors Viz., type of carbon source, carbon concentration, applied potential, pH, concentration of neutralizing agent ($MgCO_3$ and CO_2 partial pressures, which significantly influence the production performance were considered (Table 1). In the next step, experimental matrix was designed and the data analysis procedure had to be defined.

In this study, three levels of factor variation were considered and size of the experimentation was represented by experimental matrix [L_{18}–18 experimental trials] with a layout of $2^1 X\ 3^5$. All the factors were assigned with three levels except iron applied potential. A two phase experimental methodology was employed for the production of succinic acid. During phase-I, H_2 gas was used as electron donor and in phase-II succinic acid production was carried out in a bioelectrochemical system with. Experiments were carried out in fed batch mode with each cycle operated for a retention time of 48hrs.

Table 1 Selected factors and assigned levels

S.No	Factor	Level 1	Level 2	Level 3
1	Electron donor	H_2 Gas	Applied Potential	-
2	Carbon source	Glucose	Fructose	Sucrose
3	Carbon Concentration	20 g/l	30g/l	40g/l
4	CO_2 supply	0.06 MPa	0.08 MPa	0.1 MPa
5	Concentration of $NaHCO_3$	8 g/l	10g/l	12 g/l
6	pH	6.5	7	7.5

Biocatalyst
IICTSVM1 strain isolated from ruminal contents of cattle was used for succinic acid production in all experiments. Rumen and rumen contents were obtained from 4 different freshly slaughtered cattle. An aliquot (1g) from each sample was inoculated in 20 ml of tryptic soy broth (TSB) (Himedia) for the growth of seed cultures. These cultures were incubated overnight at 37°C in anaerobic conditions and were then serially diluted (up to 10^{-7}) in phosphate-buffered saline solution (PBS). Twenty microliters of each PBS dilution was spread on selective isolation media (20 g/L glucose, 5 g/L peptone, 10 g/L yeast extract,3g/L K_2HPO_4, 1g/L NaCl, 1g/L $(NH_4)_2SO_4$, 0.2 g/L $CaCl_2$. $2H_2O$, 0.2g/L $MgCl_2$. $6H_2$,1g/L Na_2CO_3 and 12 g/L bacteriological agar, pH 6.5). The plates were incubated at 37°C overnight in anaerobic chamber (Coy, USA). After incubation, single colonies were randomly isolated on the basis of their colony morphology (i.e., shape, edge, color, elevation, and dimension) by repetitive streaking on the same isolation media. After obtaining pure colonies, preliminary fermentation screening to select the best succinic acid producing bacteria was performed. The best strains were then identified by 16S ribosomal RNA (rRNA) gene sequencing.

Reactor Configuration
For phase-I experiments, the organisms were grown in 250 ml glass bottles sealed with butyl rubber stoppers with 200 ml of selective isolation medium (sterilized for 15 min at 121^0C, 15 psi) supplemented with required amount of carbon source. The nitrogen headspace was replaced by CO_2. Cystenie HCL and thioglycollate were added to maintain reducing conditions. The reduced medium was inoculated with 2% (v/v) inoculum. For phase-II experiments a double chambered BES was designed and fabricated using Schott-Duran glass bottles with a total/working volume of 2.5/2.0 l. BES consisted of an anode and a cathode chamber separated by a proton exchange membrane. Non-catalyzed graphite plates were used as electrodes at both anode and cathode chambers to aid in microbial electron transfer reactions. Copper wires were used to establish contact with electrodes. Proper leak proof sealing was done to ensure anaerobic environment at both the chambers. Polarized potential of -1.6 V vs Ag/AgCl (S) was applied using a potentiostat-galvanostat system (EC-Lab).

Analytical methods
The dry cell weight (DCW) was computed from a curve relating optical density at 600 nm (OD600) to dry weight. Samples were collected every 6 h during cultivation to evaluate product formation. 1 ml of

fermentation broth was centrifuged (12,000 rpm, 5 min) to separate bacterial cells and the supernatant was filtered through a 0.2 µm syringe filter to detect succinic acid, carbon and other organic acids in high pressure liquid chromatography (HPLC). HPLC analysis was performed by injecting 20 µL of filtered supernatant onto Shimadzu LC10A system with C18 reverse phase column (250×4.6 mm dia; 5 µm particle size, flow rate, 0.6 ml/min) using filtered milliQ water as mobile phase and a refractive index detector for detection.

Results and Discussion

The bacterial diversity of the enriched cultures was evaluated using a culture-dependent approach to isolate and select succinic acid (SA) producing microorganisms. The selective culture dependent approach used in this work enabled for the isolation of facultative anaerobic and/or microaerophilic bacteria from rumen samples characterized by the presence of fermentative microorganisms and, in particular, potential SA-producing microbes. A total of 28 bacteria were isolated and grouped on the basis of their colony and microscopic morphologies. Among these bacteria, 10 strains were capable of producing SA of which three potential strains were selected and identified by 16S rRNA gene sequencing. Optimizatin studies were carried out using IICTSVM1 strain.

During phase-I operation with H_2 gas as electron donor, significant increase in cell densityand succinic acid production were observed. In all the experimental sets succinic acid production increased till 24th h and then showed a very slight decrement thereafter (Fig 1). Maximum succinic acid production of 21 g/l was observed in experimental setup 8. Cell growth increased drastically during the initial hours and reached its maximum in the first 12 h. After 12 h, cell growth gradually declined. The carbon consumption also increased with time and residual amount was left by the end of the cycle in all the experimenrtal sets. Acetic Acid, formic acid and traces of propionic acid were the by products observed. As fermentation progresses, organic acids accumulate as a result of the decrease in pH by the end of the cycle in all the experimental sets.
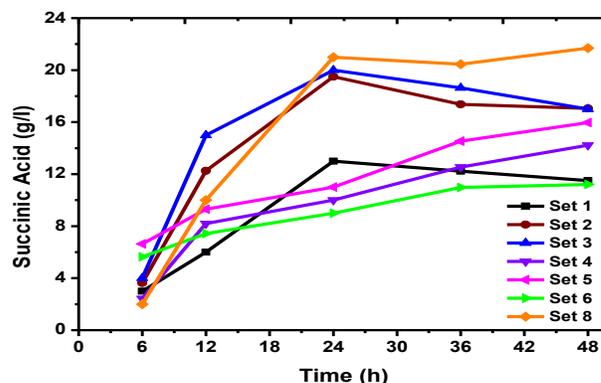
Fig1: Succinic acid production profiles in phase-1 operation

Conclusions

In this paper, the culture conditions related to succinic acid production were optimized.During batch fermentation, CO_2 partial pressures, carbon source and its concentration and pH had significant effect on the product yield. In phase-I operation, sucrose as the carbon source at a concentration of 30 g/l, at pH 6.5 and CO_2 partial pressure of 0.1 Mpa was observed to be the optimum condition for succinic acid production. In conclusion, the ecological strategy employed in this study enabled the isolation of new bacterial strains that are able to synthesize SA from various carbon sources. Furthermore, carbon dioxide was fixed during the fermentation process, which provides the potential to reduce greenhouse gas emissions, lower costs, and recycle wastes during chemical production.

REFERENCES

[1] S. Venkata Mohan, J. A. Modestra, K. Amulya, S. K. Butti, G. Velvizhi, Trends in Biotechnol. 34 (2016), 506-519

[2] S. Venkata Mohan, G. Velvizhi, J.A. Modestra, S. Srikanth, Renew. Sustain. EnergyRev. 40 (2014), 779–797.

[3] Cheng K.K, Zhao X.B, Zeng J, Zhang J.A. Biofuels, Bioproducts and Biorefining 6 (2012), 302-318.

[4] Cok, b., Tsiropoulos, i., Roes, A.L., Patel, M.K., Biofuels, Bioprod. Bioref. 8. (2013), 16–29.

[5] Venkata Mohan, S, Venkateswar Reddy. M Bioresource technology, 128 (2013), 409-416.

SEEC-2018-083

CYANO-PHOTO BACTERIAL SYNERGISTICS FOR SELF-SUSTAINED MULTIPLE BIOFUELS PRODUCTION

J. Shanthi Sravan
Bioengineering and Environmental Sciences Lab,
EEFF Department, CSIR-Indian Institute of
Chemical Technology (CSIR-IICT),
Hyderabad- 500007, India.

Manupati Hemalatha
Bioengineering and Environmental Sciences Lab,
EEFF Department, CSIR-Indian Institute of
Chemical Technology (CSIR-IICT),
Hyderabad- 500007, India.

S. Venkata Mohan*
Bioengineering and Environmental Sciences Lab, EEFF Department,
CSIR-Indian Institute of Chemical Technology (CSIR-IICT), Hyderabad- 500007, India.
E-mail: vmohan_s@yahoo.com; svmohan@iict.res.in; Tel: 0091-40-27161765

ABSTRACT

The study focuses on synergistics of oxygenic photosynthesis (cyanobacteria; cathode) and anoxygenic photosynthesis (photobacteria; anode) in a dual-chambered bioelectrochemical system (BES) for valorizing multiple products taking advantage of photosynthetic apparatuses. Photosynthetic cyanobacteria as biocathode replace expensive and/or toxic catalysts, since they can act as efficient in situ oxygenators to facilitate cathodic reaction. The experiments were performed in fed-batch mode using designed synthetic wastewater as substrate (organic loading: 1500 mg/L) in both anodic and cathode chambers (retention time: 72 h). The isolated pure cultures (anode and cathode) were captured digitally using SEM and TEM images for their structural analysis. The performance of BES was analyzed electrochemically with cyclic voltamograms, Tafel slopes, K_{app} and OJIP curves. The air-dried biomass (cathode) was analyzed for chemical bonding (FT-IR, XRD, Raman) and composition (EDAX, CHNS). The Cyano-Photosynthetic Bacterial synergistic process provides the advantage of harnessing biomass, bioenergy, biofuel along with wastewater treatment and CO_2 sequestration.

Keywords

Cyanobacteria; Bioelectrochemical systems; Biomass; CO_2 sequestration; Lipids; Hydrogen

INTRODUCTION

Integration strategies in BES exploiting microbial transformations towards bioenergy and biofuel generation are considered a novel approach. Photosynthetic microorganisms are a key in sustaining life in various fields of energy sector and could be integrated with Cyanobacteria, known to exploit the natural mechanism of photosynthesis by utilizing sunlight and CO_2 sequestration towards bioenergy generation. Cyanobacteria have characteristics well-suited for wastewater treatment with high nutrient removal capacity by accumulating inorganic phosphorus and nitrogen. The growth can happen in highly adverse conditions and the resultant biomass can also be easily harvested by sedimentation. Cyanobacteria production with wastewater provides an option of obtaining economically feasible biofuels such as biodiesel, biohydrogen benefiting the wastewater treatment plants. Integration of cyanobacteria is of particular interest in BES, because of the multiple benefits such as providing dissolved oxygen, nutrient removal, CO_2 sequestration and biomass production. The application of photosynthesis at cathode can replace the energy intensive mechanical aeration as reported in the fuel cell research. Alternatively, using photosynthetic bacteria as anodic biocatalyst can perform anoxygenic photosynthesis (without O_2 generation) at anode. Photosynthetic bacteria under anoxygenic photosynthesis exhibit strong electrochemical catalysis of organic compounds in the anode of a BES and cyanobacteria have inbuilt capability of producing oxygen through oxygenic photosynthesis upon illumination.

In this context, the synergy between photosynthetic bacteria and cyanobacteria in BES towards harnessing bioenergy along with other biofuels was studied. The influence of cyanobacteria as biocathode on valorizing multiple products while eliminating the toxic TEA and energy intensive aeration process at cathode can result in self-sustained and eco-friendly processes. For this purpose, photosynthetic double-chambered BES employing pure cultures of cyanobacteria (cathode) and photosynthetic bacteria (anode) was designed to evaluate their synergic association and influence on the production of multiple biobased products.

MATERIAL AND METHODS
BES Setup
A Dual-chambered Bioelectrochemical system (BES) was constructed. PEM of appropriate dimensions was used as separator between the two chambers, which individually act as anode and cathode. Hybrid Carbon cloth and stainless steel mesh was used as electrodes in both anode and cathode chambers. Copper wires were used to maintain contact with the electrodes for external electrical contact. Each chamber was specifically designed for batch mode of operation having inlet and outlet ports.

Biocatalyst
Pure cultures of Photosynthetic bacteria and Cyanobacteria isolated from mixed consortium and grown in specific media were used as biocatalysts in anode and cathode chambers respectively. The synergetic association and influence on bio-electrogenesis and other metabolic processes were evaluated.

Operation of BES
BES operation was initiated by inoculating anodic chamber with photosynthetic bacteria (10% V/V of reactor) and cathode chamber with cyanobacteria (10% V/V of reactor) enriched in DSW with organic load of 1500 mg/L at pH 7.0. Before start up and every feeding event, anode chamber was sealed and sparged with nitrogen gas (99.9%; 5 min) to maintain anoxygenic photosynthetic activity, whereas cathode chamber was exposed to ambient air to allow CO_2 biosequestration. Both the anode and cathode chambers were operated with DSW under photo-mixotrophic conditions (3000±200 Lux) in fed batch mode. Drop in power output was considered as an indicator for the feed replacement. The performance of the system was studied at an organic load of 1500 mg/L in DSW with HRT of 72 h at ambient temperature (28±2°C). Mixing of anolyte and catholyte was ensured with magnetic stirrer.

Bioprocess monitoring
Physicochemical parameters like pH, EC and COD were analyzed to follow influence of O_2 on system performance. COD, VFA, nitrates, phosphates, bicarbonates, pH and EC were periodically monitored using standard methods. H_2 production (anode) and Dissolved oxygen (DO) (cathode) was estimated using a gas sensor (ATMI GmBH Inc.) and DO sensor (HACH) respectively. At the end of each cycle, biomass (anode and cathode) was estimated in terms of dry cell weight (mg/L), total bacteriochlorophyll (Bchl) of anodic biomass along with lipids, carbohydrate and protein using standard methods.

Bio-electrochemical analysis
Bioelectrochemical behaviour in terms of open circuit voltage (OCV), current density (CD), power density (PD), Cyclic Voltammetry (CV), electron discharge rates (K_{app}) and Tafel slopes were studied. All electrochemical assays were performed with anode as working electrode and cathode as counter electrode against Ag/AgCl (3.5M KCl) reference electrode.

Bio-electrokinetics (OJIP curves)
OJIP studies for qualitative analysis of chlorophyll (Chl a) fluorescence induction kinetics for photosystem II (PS II) was evaluated and was compared to the quantitative data.

Analysis
SEM and TEM images of isolated pure cultures (anode and cathode) were captured digitally for the analysis of size and shape. The air-dried biomass obtained (cathode) at the end of each cycle analyzed with FTIR, XRD, Raman, EDAX and CHNS for chemical bonding and composition.

RESULTS AND DISCUSSION
Photo-Bioelectrogenic activity: The OCV of BES was monitored at start-up phase which stabilized at 410-425 mV. The potential difference is also a critical parameter in studying the synergistic influence of the biocatalysts on bioenergy generation. Polarization for the double chambered BES was performed at stabilization in order to obtain the cell design point. The change in PD and V with respect to external load was plotted against CD. CV's were taken in both open and closed circuit mode of operation at multi-scan rates (100-0.05 mVS^{-1}). Profiles showed proportional increase in oxidation and reduction currents (mA) with respect to scan rates. First order derivative for CV's at 30 $mV.S^{-1}$ was plotted to analyze rate of change of biocatalytic current (i) with respect to electrode potential E (di/dE) and the corresponding redox shuttlers during electrochemical interactions were analyzed. The tafel analysis drawn from CV provides direct evidence to quantitatively compare the electrometabolic activity in terms of electron discharge rates and synergistic bioenergy yields. K_{app} was derived from Laviron equations under varied microenvironments.

$$E_{pc} = E^{0'} + RT/\alpha nF \ln RTK_s/ \alpha nF - RT/\alpha nF \ln v \quad (1)$$

$$E_{pa} = E^{0'} + RT/(1-\alpha)nF \ln RTK_s/ (1-\alpha)nF + RT/(1-\alpha)nF \ln v \quad (2)$$
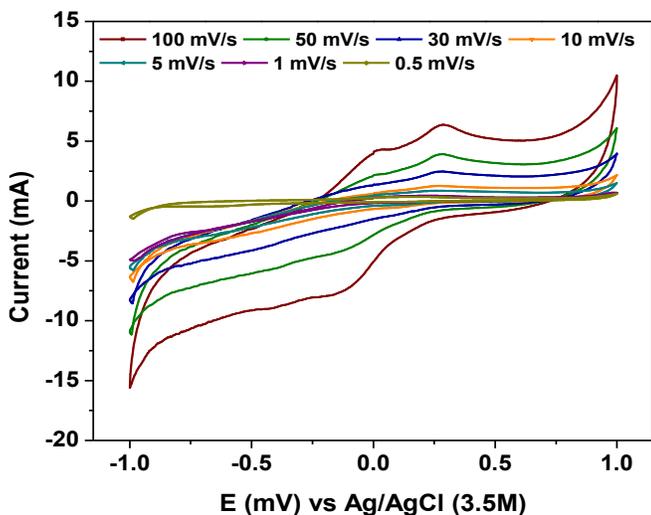
Fig 1: Cyclic voltammogram profiles depicting the photobacteria and cyanobacteria synergistics

Dissolved Oxygen (DO): O_2 liberated at cathode was measured in terms of DO. The metabolite products released after metabolism of anolyte gets reduced at cathode through oxygen reduction reactions (ORR). During operation the catholyte DO varied between 4.0 mg/L to 4.1 mg/L which correlated with the growth of cyanobacteria.

Biohydrogen (Anode): Photosynthetic bacteria (anode chamber) utilizes carbon source and generates H^+ and e^-. Presence of anaerobic conditions in anode chamber facilitated production of VFA and H_2. During initial phase of operation (12h) VFA was found to be high (1150 mg/L) and decreased to 958 mg/L by the end of experiment (48h).

Biomass: Anodic biomass was monitored spectrophotometrically at an absorbance of 600 nm. At the start of experiment initial biomass was 0.105 and it increased to 0.497 and later decreased to 0.300 by the end of cycle. Availability of carbon source, nutrients enhanced biomass growth along with metabolic and electrogenic activity. The decrement in biomass may be due to pH drop which resulted in acidic environment. Cathodic biomass was dependant on chlorophyll, at initial stages it was found to be 0.09 mg/L and increased to 0.19 mg/L which later showed a decrement by the end of cycle which was due to nutrient availability.

Chlorophyll: Bacteriochlorophyll was estimated which was well correlated with biomass. At the start of experiment bacteriochlorophyll was 0.036 and increased to 0.144 later decreased to 0.016 by the end of the cycle. Nutrient and carbon availability also enhanced the bacterial activity. The decrement in bacteriochlorophyll was due to pH drop which resulted in acidic environment hindering the bacterial photosynthetic activity. Cyanobacterial chlorophyll was estimated using ethanol and HCl method

which showed an increment form 0.1% to 0.35% of total weight of biomass and later decreased correlating well with biomass growth.

Lipids (Cathode): Lipids of cathodic biomass were estimated at the end of cycle using Bligh and dyer method. The total and neutral lipids were found to be 36% and 15% respectively.

Treatment efficiency: Anodic COD and cathodic bicarbonate removal were estimated using APHA standard methods, which showed a COD removal of 44% and bicarbonate removal of 28%. The removal efficiency indicated that nutrients are utilized for growth and metabolic processes of the photosynthetic cultures.

CONCLUSIONS

The dependence of anoxygenic photosynthetic bacteria and oxygenic cyanobacteria in a synergistic interaction can be a good option in environmental sustainability. Anoxygenic photosynthesis (anode) provides oxidative microenvironment for substrate degradation and oxygenic photosynthesis (cathode) creates reductive microenvironment while replacing the mechanical aeration by *in situ* generation of O_2 as TEA. The syntrophic strategy resulted in multiple benefits of harnessing bioelectricity, sequestering CO_2, O_2 generation, bioenergy, and bioproducts along with treatment.

ACKNOWLEDGEMENTS

REFERENCES

[1] Venkata Mohan, S.; Modestra, J. A.; Amulya, K.; Butti, S. K.; Velvizhi, G. A circular bioeconomy with bio-based products from CO2 sequestration. Trends Biotechnol. 2016, 34 (6), 506−519.

[2] Venkata Mohan, S.; Srikanth, S.; Chiranjeevi, P.; Arora, S.; Chandra, R. Algal biocathode for in situ terminal electron acceptor (TEA) production: Synergetic association of bacteria−microalgae metabolism for the functioning of biofuel cell. Bioresour. Technol. 2014, 166, 566−574.

[3] Xiao, L.; He, Z. Applications and perspectives of phototrophic microorganisms for electricity generation from organic compounds in microbial fuel cells. Renewable Sustainable Energy Rev. 2014, 37, 550− 559.

[4] Chandra, R.; Sravan, J. S.; Hemalatha, M.; Butti, S. K.; Venkata Mohan, S. Photosynthetic Synergism for Sustained Power Production with Microalgae and Photobacteria in a Biophotovoltaic Cell. Energ. Fuel. 2017, 31, 7635−7644.

[5] Pisciotta, J. M.; Zou, Y.; Baskakov, I. V. Role of the photosynthetic electron transfer chain in electrogenic activity of cyanobacteria. Appl. Microbiol. Biotechnol. 2011, 91, 377−85.

DRYING OF MORINGA OLEFERA LEAVES IN MIXED MODE AND INDIRECT FORCED CONVECTION SOLAR DRYERS

D.V.N.LAKSHMI
DEPARTMENT OF MECHANICAL ENGINEERING,NIT DURGAPUR
Research scholar
Email: lakshmiratan2311@gmail.com

Prof . P. MUTHUKUMAR
DEPARTMENT OF MECHANICAL ENGINEERING
IIT GUWAHATI
Professor
Email: pmkumar@iitg.errnet.in[*]

Dr. APURBA LAYEK
DEPARTMENT OF MECHANICAL ENGINEERING, NIT DURGAPUR
Associate professor
E-mail: apurba.layek@me.nitdgp.ac.in

ABSTRACT

In this study, a parallel flow mixed mode and indirect forced convection solar dryers have been developed and tested for drying of Moringa oleifera leaves. Dryers performance were compared with open sun drying conditions. Six kg of Moringa oleifera leaves have been dried from initial moisture content of 4.29 (g .water /g. dry matter) (d.b) to final moisture content of 0.07 (g .water /g. dry matter) (d.b) within 4 hr, 6.5 hr and 10 hr respectively in the mixed mode solar dryer, indirect forced convection solar dryer and under open sun drying. Measured average air temperature in the mixed mode and indirect forced convection solar dryers were 49.8 °C and 41.7°C, respectively. The drying efficiency of the mixed mode and indirect forced convection solar dryers were found to be 18.9 % and 14.3%, respectively.

Keywords:** **Moringa Oleifera; Mixed mode solar dryer, Indirect forced convection solar dryer, Dryer efficiency.

INTRODUCTION

India is blessed with many medicinal herbs and spices. The domestic demand of these medicinal plants is increasing rapidly. Total consumption of herbal raw drug in the country for the year 2014-15 has been estimated as 5, 12,000 MT with corresponding trade value of ₹ 5,500 crores. Moringa olefera (Drumstick) trees are cultivated largely in tropical countries. This tree is known as magical tree due to its high medicinal properties. Moringa leaves contain vitamin, protein, iron, and calcium [1]. The dried moringa leaves powder contains high nutrients compared to fresh leaves. Any freshly harvested agricultural products have high moisture content and the risk of spoilage is very high as compared to dried products. After harvesting, for long-term storage, the medicinal herbs should be processed. Drying is one of the common techniques is used for storing the medicinal herbs for longer life. Due to improper drying methods, the medicinal products lose their colour and nutrients. Further, longer drying time also causes micro orgasm growth. Drying at controlled conditions increases the product quality. Solar drying of medicinal herbs is one of the promising solutions to overcome the above said issues. Mohamed et al. [2] developed a forced convection solar dryer with the auxiliary heater for drying of citrus aurantium leaves (bitter orange). They studied the drying behaviour of citrus leaves by varying the air flow rate and temperature and observed that the drying air temperature has a significant effect compared to the air velocity. Akipinar et al. [3] studied the drying behaviour of mint leaves in a forced convection solar drying and open sun drying conditions. The experimental data fitted to ten drying kinetic models. They found that Wang and Singh model was best suited for forced convection and open sun drying conditions. Premi et al .[4] studied the drying behaviour of Moringa

Olefera leaves in a convective dryer in the temperature range of 50°C - 80°C at a constant velocity 0.4 m/s and observed that the product dried at 60°C has good color compared to others. El-Sebaii et al. [5] investigated the drying performance of indirect forced convection solar dryer for drying of thymus and mint. Fourteen drying kinetic models applied to the experimental data and found that Midilli Kucuk model for drying of mint and page and modified page models for drying of thymus were suited. Fevzi et al. [6] developed a drying kinetic model to study the drying behavior of sweet basil. The solar air heater with fins was used for drying. The experiments were carried out by varying the mass flow rates from 0.012 kg/s to 0.033 kg/s. They found that by increasing the mass flow rate of air, the drying time reduces and the solar air heater efficiency increases. Safa Mghazli et al. [7] studied the drying kinetics of rosemary leaves in an indirect forced convection solar dryer. The experiments were performed at four different temperatures (50, 60, 70 and 80 °C) and two flow rates (300 m³/h and 150 m³/h). The experimental data were fitted to nine thin layer drying models and found that Middili Kucuk model was best suited one.

From the literature, it is observed that most of the researchers dried medicinal leaves using either hybrid type or conventional dryers. Limited research works have been reported on the drying of Moringa Olefera leaves by using the solar dryer. The objective the present work is to develop mixed mode and indirect forced convention solar dryers with double pass counter flow solar air heaters for drying the medicinal herbs and spices under the climatic conditions of Guwahati, India. The performance of the mixed mode solar dryer (MFSD) is also compared with indirect forced convection solar dryer (IFSD).

EXPERIMENTAL SETUP

In the present work, mixed mode and indirect forced convection solar dryers with double pass counter flow solar air heaters have been developed for drying of high value medicinal Moringa Olefera leaves under the climatic conditions of Guwahati, India. The schematic of a mixed mode forced convection solar dryer is shown in Fig.1. The main components of the solar dryer are solar air heaters, blower, and drying chamber. In the experimental setup, two double pass counter flow solar air heaters (SAH) are connected in series for supplying the heated air to the solar dryer. Two solar air heaters are identical having same dimensions 2.04 m (length) * 1.04 m (width) * 0.02 m (depth) and mounted 25° to the south to maximize the solar radiation based on the geographical position. Both the solar air heaters have a black coated GI plate of 1 mm thickness as absorber plate.

The specifications of the solar air heaters are shown in Table.1. The absorber plate consisting of 4 horizontal fins

spaced at equal distance on the plate. The ambient air enters from the SAH1 above the absorber plate (front pass). The heated air then enters below the absorber plate and then passes into the SAH2.The heat transfer fluid (HTF), air enters into the mixed mode solar dryer. The drying chamber is of rectangular shape and fabricated with mild steel dimensions of 2 m × 0.85 m × 0.4 m. The drying chamber consists of six trays of size 0.8 m × 0.6 m × 0.025 m are placed in two stages of each with 3 trays. The gap between the two stages is 0.15 m. The trays are made of wooden frame and aluminium mesh. The temperature at different locations of the solar air heaters and in the solar dryer was measured with the help of T-type thermocouples connected to a data logger. Solar radiation intensity was measured with the help of a pyrano meter in hourly basis. The weight of the moringa leaves was measured in the interval of 30 min. with a digital electronic weighing balance accuracy 0.01 g. The schematic of the indirect forced convention solar dryer (IFSD) is similar to MFSD. However, in IFSD, there is glazing on the top of the solar dryer. Experiments have been performed using both the dryers (MFSD and IFSD). Fig.2 shows the pictorial view of MFSD set up.

Tab.1.SPECIFICATIONS OF THE COUNTER FLOW DOUBEL PASS SOLAR AIR HEATER

Sl. no	Collector component	Specifications
1	Collector type	Double pass flat plate counter flow solar air heater with horizontal fins.
2	Absorber plate	1 mm thick GI plate black coated
3	Glazing	Normal window glass 4 mm thickness
4	Base plate	Aluminum 0.2 mm thickness
5	Insulation	Glass wool 25 mm thickness
6	Drying chamber	Mild steel with thickness 1.2 mm, Size: 2 m × 0.85 m × 0.4 m
7	Number of trays	6
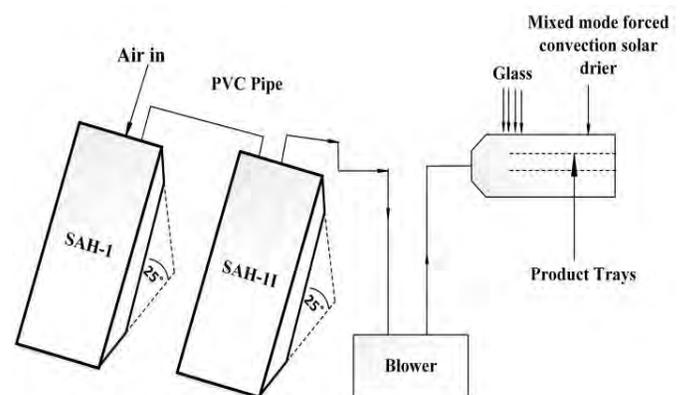
FIG.1: SCHEMATIC OF MIXED MODE FORCED CONVECTION SOLAR DRYER
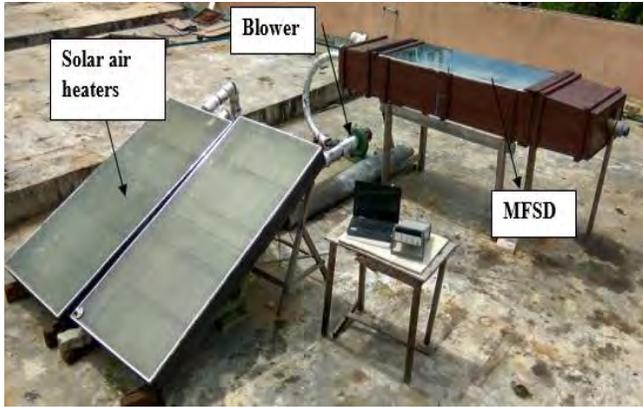
Fig.2 Pictorial view of MFSD setup

Drying Analysis

The moisture ratio of the product was calculated using the Eqs. 1 and 2 [3].

$$MR = \frac{M_t - M_e}{M_o - M_e} \quad (1) \qquad MR = \frac{M_t}{M_o} \quad (2)$$

The relative humidity fluctuates continuously during the experiment. So, the moisture ratio was calculated using Eq. 1 (neglecting the equilibrium moisture content M_e). M_t is the moisture content at time t (%) and M_o is the initial moisture content (%). The mass of water evaporated from the product was calculated by using Eq. 3, where m_p is the mass of the product (kg) and M_i and M_f are initial and final moisture contents of the product on wet basis.

$$m_w = \frac{m_p (M_i - M_f)}{100 - M_f} \quad (3)$$

Eq. (4) is used for estimating the energy input to the dryer. A_{SAH1}, A_{SAH2} and A_{dryer} (m²) are areas of solar air heaters and dryer, respectively. I is the average solar radiation intensity and PB is power consumed by the blower (W)

$$E_{MFSD} = \left[\left(A_{SAH1} + A_{SAH2} + A_{dryer} \right) * I + PB \right] * t_{MFSD} \quad (4)$$

$$E_{IFSD} = \left[\left(A_{SAH1} + A_{SAH2} \right) * I + PB \right] * t_{IFSD} \quad (5)$$

The dryer efficiency is defined as the ratio of amount of energy required to remove moisture from the product to energy input to the dryer.

$$\eta_{MFSD} = \frac{m_w * h_{fg}}{E_{MFSD}} \quad (6)$$

$$\eta_{IFSD} = \frac{m_w * h_{fg}}{E_{IFSD}} \quad (7)$$

Where, m_w is the mass of water evaporated (kg) and h_{fg} is the latent heat of vaporization (kJ/kg).

RESULTS AND DISCUSSION:

The experiments were carried out with mixed mode and indirect forced convection solar dryers, and also under open sun for drying of moringa olefera leaves. The dryer was operated 1 hr before the start of the experiment for achieving steady-state conditions. After reaching the steady state condition, the product was loaded into the solar dryers. Fig.3 represents the variation of the ambient temperature, solar air heater outlet temperature, average temperature of the mixed mode dryer and incident solar radiation intensity with respect to time. The solar radiation intensity was measured within the interval of 15 min and found the maximum value of 605.5 W/m² at 12.45 PM. The average outlet solar air heater temperature was 59.8°C. From Fig.4, it was observed that the temperature inside the mixed mode solar dryer was high compared to the indirect solar dryer due to extra glazing on the MSFD. The inside average temperature of the air was 49.8 °C for MFSD and 41.7°C for IFSD, respectively.
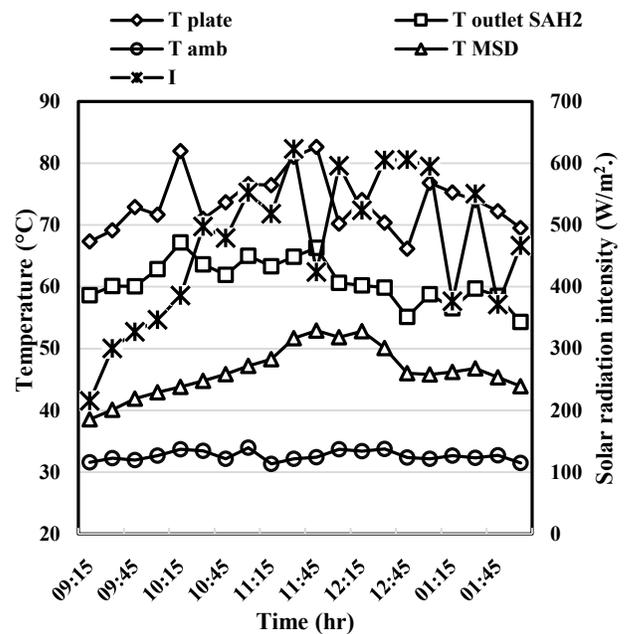
FIG.3 VARIATION OF TEMPERATURE AT DIFFERENT LOCATIONS OF MIXED MODE SOLAR DRYER AND SOLAR INTENSITY

Relative humidity (RH) plays an important role in the drying process. The average relative humidity of the MSFD, and IFSD were found 24.5 % and 32.8% respectively. Six kg of fresh moringa leaves were placed on the six trays in equal amount. A sample of 50 g of leaves was kept in a small tray to measure the moisture loss in the MSFD and ISFD.

Similarly, another sample of 50 g was placed under open for sun drying. The leaves were dried from the initial moisture content 4.29 (g water /g dry matter) d.b to final moisture content 0.07 (g water /g dry matter) d.b (shown in Fig. 5). The drying time was taken for moringa leaves in the MSFD was 4 hr and ISFD was 6.5 hr. In case of open sun drying, the final moisture content of 0.1 g water /g dry matter (d.b) was attained in 10 hr. The dryer efficiencies of the MSFD and ISFD were compared under the average solar radiation intensity of 472 W/m^2. The mass of water evaporated from 6 kg of moringa leaves was 4.7 kg. The average power consumed by the blower was 250 W. By applying the Eqs. 6 and 7, the efficiency of the MFSD and IFSD were estimated as 18.9% and 14.2%, respectively.
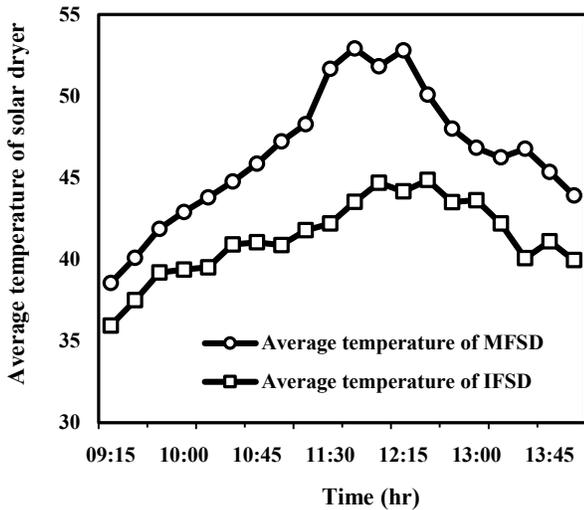
FIG.4. VARIATION OF AVERAGE TEMPERATURE INSIDE THE MFSD AND IFSD WITH DRYING TIME.

CONCLUSION:

Parallel flow mixed mode and indirect forced convection solar dryers have been fabricated and tested for drying of Moringa Oleifera leaves. Important observations made from the experimental studies are follows;

- The moringa olefera leaves has been dried in the mixed mode solar dryer (MFSD) within 4 hr and in the indirect forced convection solar dryer (IFSD), it took 6.5 hr. Under open sun drying, the drying operation was completed in 10 hr.
- Incomparison with open sun drying, MFSD reduces the drying time by 150 %. Further, quality of the dried sample FROM MFSD and ifsd look much better than the open sun drying.
- The drying efficiencies of the mixed mode and indirect forced convenction solar dryers were estimated as 18.9% and 14.2%.

- The dryer efficiency of the system can be improved by integrating thermal energy storage system.
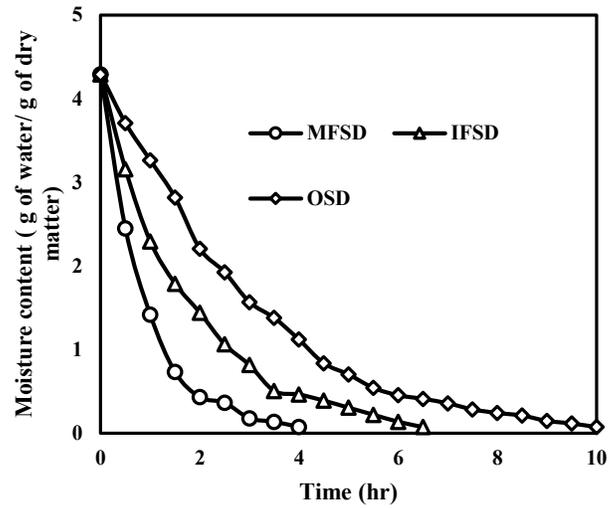
FIG.5.VARIATION OF MOISTURE CONTENT ON DRYBASIS WITH TIME

REFERENCES:

'[1] Fahey, J.W. 2005. "Moringa oleifera: A Review of the medical evidence for its nutritional, therapeutic, and prophylactic properties." Part 1. Trees for Life.
[2] Ait Mohamed .L, KouhilaM, Jamali A, Lahsasni S,Kechaou N, and Mahrouz M, 2005. "Single layer solar drying behaviour of Citrus aurantium leaves under forced convection" Energy Conversion and Management 46, November, pp 1473–1483.
[3] Kavak Akpinar .E 2010. "Drying of mint leaves in a solar dryer and under open sun: Modelling, performance analyses". Energy Conversion and Management 51, June, pp. 2407–2418.
[4] Monica Premi, Sharma H K, Sarkar B C and Singh C 2010. "Kinetics of drumstick leaves (Moringa oleifera) during convective drying. African Journal of Plant Science. 4 (10), October pp. 391-400.
[5] El-Sebaii A.A., Shalaby S.M. 2013. "Experimental investigation of an indirect-mode forced convection solar dryer for drying thymus and mint". Energy Conversion and Management, 74, June, pp 109–116.
[6] Fevzi Dulcimer, Hakan Kara kaya, Aydın Durmus. 2016, "Drying kinetics of sweet basil". Renewable Energy 93, February, pp77-86.
[7] Safa Mghazli ,Mourad Ouhammou, Nadia Hidar, Lamyae Lahnine, Ali Idlimam,Mostafa Mahfouz, 2017."Drying characteristics and kinetics solar drying of Moroccan rosemary leaves". Renewable Energy 108, February, pp 303-310.
(MFSD) is also compared with indirect forced convection solar dryer (IFSD).

SEEC-2018-087

LIFE CYCLE AND TECHNO-ECONOMIC ASSESSMENTS OF DOMESIC AND COMMERCIAL LPG COOK-STOVE WITH PROUS RADIANT BURNER

Lav Kumar Kaushik
Department of Mechanical Engineering,
Indian Institute of Technology Guwahati
Email: l.kaushik@iitg.ernet.in

Sunita Deb
Center for Energy,
Indian Institute of Technology Guwahati
Email: sunitadeb@iitg.ernet.in

P. Muthukumar
Department of Mechanical Engineering,
Indian Institute of Technology Guwahati
Email: pmkumar@iitg.ernet.in ; pmkumariitg@gmail.com

ABSTRACT

The present assessments compare the life cycle energy and cost of the LPG operated cook-stoves with Porous Radiant Burners (PRBs) developed by IIT Guwahati research team [1,2] with its conventional counterparts (CBs). Life Cycle Energy Efficiency (LCEE) has a surplus of 7-11.6% and 24.6% for commercial and domestic PRB stove, respectively. Techno-economic Assessment (TEA) of commercial LPG stove with PRB showed maximum annual saving (at 10 kW input power) of Rs. 73,219/- and the cumulative present worth of annual savings over the life as Rs. 5,46,192/-, which are much higher than the capital cost of the cook-stove. The calculated Internal Rate of Return (IRR) has been found to be 619.3% which is much higher than rate of return (8%). Similarly, the payback period has been found less than 2 month, which is very small considering the life of the cook-stove (10 years) at 10 kW input power. For domestic PRB stove (1-3 kW) corresponding results are Rs. 2,204/-, Rs. 18,037/-, 227.6% and less than 6 month, respectively.

Keywords: Porous Radiant Burner (PRB), Life Cycle Energy Assessment (LCEA), Controlled Cooking Test (CCT), Techno-economic Assessment (TEA)

INTRODUCTION

In India, residential LPG consumption amounts 17.3 Million Tons Per Annum with 22.93 crore active consumers, which works out to an estimated ~71% of national LPG coverage [3]. The Indian finance ministry allocated Rs. 21,803/- crore for subsidizing LPG during 2016-17 and with 10% annual consumption growth, it may increase rapidly [4]. Because of massive active consumers, a stove with improved performance will lead to significant reduction in LPG consumption and associated pollution. In order to minimize the financial burden on the government and environmental pollution, developing efficient and environmental friendly burner technology for cooking stove is a major challenge for scientific society.

Available LPG operated domestic cook-stoves (1-3 kW) not only in India but throughout the globe have thermal efficiency in the range of 60-65% and also have high emissions (CO: 220-550 ppm and NO_x: 5-25 ppm) [1]. Similarly, for commercial cook-stove (5-10 kW) these values are 30-45%, 355-1165 ppm and 28-110 ppm respectively [2]. Such a low thermal efficiency and high emissions are due to free-flame combustion in conventional combustion burners. Utilizing the concept of Porous Media Combustion (PMC), the research team at IIT Guwahati has developed self-aspirated LPG stove with Porous Radiant Burners (PRB) burners for domestic and commercial applications.

It is evident from the published literature from IIT Guwahati research team [5,6] that the LPG stoves with PRB have the great potential for the replacement of its conventional counterparts for domestic and commercial cooking applications. However, no systematic investigation has been made on the commercial viability of LPG stove

operating with Porous Radiant Burner (PRB). To ascertain their sustainability in the commercial market, their life cycle assessment has been performed in present work.

EXPERIMENTAL SETUP AND LIFE CYCLE ASSESSMENT

Two commercial and domestic LPG cook-stoves of input power range 5-10 kW and 1-3 kW respectively, of which one is the stove with conventional burner (CB) and other with PRB [1,2], have been tested for their energy requirements. PRB stove comprises two zones, the preheating zone made of alumina (Al_2O_3) porous matrix and the combustion zone comprising silicon carbide (SiC) porous foam. The state-of-the art LPG stove with PRB have improved thermal efficiency and lower pollutant emissions. The thermal efficiency and emission values for domestic cook-stove with PRB are 71-75% , CO: 30-140 ppm, and NO_x: 0.2-3.5 ppm, respectively and for commercial cook-stove these values are 45-55%, 60-190 ppm, and 2-10 ppm, respectively.

Life cycle performance analysis is accomplished on a functional unit. For a commercial cook stove with 9.5 kg of LPG consumption in one day is considered as a functional unit (based on the data collected from IIT Guwahati canteen). Similarly for domestic cook-stove daily heat energy requirement per household has been determined by Controlled Cooking Test (CCT) and further used as functional unit.

Controlled Cooking Test (CCT): CCT involves the preparation of typical meals based on daily average food intake, as suggested in National Sample Survey [7]. The experiment was performed in a simulated household surrounding using domestic CB and PRB stoves. Three menus (A, B and C: given in appendix A) were prepared after conducting a small query in the families of rural and urban household. While conducting the experiments, the cooking time and amount of LPG consumed for preparation of the dishes were recorded.

TABLE 1: TIME AND LPG CONSUMED FOR PREPARING DISHES IN PRB STOVE

Dish	Time (min)			LPG (g)		
	A	B	C	A	B	C
1	22	12	17	42.29	20.98	33.78
2	8	9	21	16.37	18.32	34.95
3	14	20	29	25.23	34.98	56.98
4	26	29	18	43.46	48.98	34.25
5	33	35	31	54.98	58.13	51.4
6	7	9	6	11.86	15.23	11.35
7	5	4	-	9.3	7.8	-
Total	**115**	**118**	**122**	**203.49**	**204.42**	**222.71**

From the results listed in Table 1 and similar results obtained for stove with CB, the average amount of fuel consumed by menu A, B and C was calculated. This gives the daily heat energy requirement per household. The average heat energy requirement per household for daily cooking activities is estimated as 13306 kJ and 9283 kJ for stoves with CB and PRB, respectively.

Life Cycle Energy Efficiency (LCEE): The standardized life cycle assessment methodology (ISO 14040-14043) has been adopted in the current work for Life Cycle Energy Analysis (LCEA) and restricted only to energy aspects. To compute the energy efficiency, 'total energy demand' concept has been used and the calculated values were based on the 'net calorific value (NCV)' of energy sources considered. During LCEA, LCEE has been determined by using eqn. (1-4).

$$LCEE = \frac{FEC}{E_p + E_t} \qquad (1)$$

$$FEC = m_f \times NCV \times \eta_{th} \qquad (2)$$

$$E_p = m_f \times NCV \qquad (3)$$

$$E_t = m_f(e_E + e_R + e_B + e_T) \qquad (4)$$

Where, FEC =final energy consumption (kJ), m_f = mass of LPG (kg), E_p = primary energy (kJ), E_t = Secondary total energy (kJ), e = specific energy required for LPG (kJ/kg), subscript E = Extraction, R = Refinery, B = Bottling, T = Transportation.

Techno-economic Assessment (TEA): TEA is used for evaluating the economic feasibility of a specific product by comparing the cost benefit of a new product with an existing one, which provides the same service. Economic analysis includes capital cost, life cycle cost and annual saving. Present worth of annual saving is expressed as a function of time, internal rate of return, and payback period. The parameters and equations used for monetary cost estimation are summarized as follows:

(i) Capital Cost (C): capital needed to purchase a stove.
(ii) Annual operating cost (C_{op}): where C_M is maintenance cost, m_f is daily fuel requirement and C_F is fuel cost for commercial and domestic stove given in eqn. (6) and (7).

$$C_{Op} = C_F + C_M \qquad (5)$$

$$C_F = \frac{ET}{\eta_{th} \times NCV} \times C_f \qquad (6)$$

$$C_F = m_f \times C_f \times Yearly\ operating\ day \qquad (7)$$

Where, ET = Total net energy required for cooking (kJ/year), and C_f = specific fuel cost (Rs/kg).

(iii) Cook-stove emission cost ($C_{emission}$): For its calculation, environmental loading unit (ELU) for emissions was used [8]. Emissions from cooking stoves on yearly basis were calculated based on Eqn. (8).

$$E_i = P_i \times C_i \times Yearly\ oerating\ hours \quad (8)$$

Where, E_i = emission of pollutant i, C_i = pollutant concentration (mg/kWh), P_i = Input power (kW)

(iv) Life cycle cost (C_{LS}): It is the sum of the actual capital cost ($\frac{C}{LS}$), the operating cost (C_{op}), and $C_{emission}$ cook-stove emission cost.

$$C_{LS} = \frac{C}{LS} + C_{op} + C_{emission} \quad (9)$$

Eqs. (5-9) were used to calculate the cost of individual stove and later the cost parameters of the PRB and CB stoves were compared with the help of the following equations.

(v) Annual saving (S): it is the life cycle cost difference between stove with PRB and CB.

$$S = (C_{LS})_{Stove\ with\ PRB} - (C_{LS})_{Conventional\ Stove} \quad (10)$$

(vi) Net Present Value (NPV): It is used to analyse an investment decision and positive NPV is used as the base to accept a proposed investment. NPV was calculated by considering interest and inflation rate, with the help of the following equation.

$$P_a = \frac{F_a}{(1+f)^n} \times \frac{1}{(1+i)^n} \quad (11)$$

$$NPV = \sum_{n=0}^{N} P_a \quad (12)$$

Where, i = interest rate, P_a = Present worth, F_a = future worth, f = inflation rate, N = life of cook-stove and n is a positive integer

(vii) Internal Rate of Return (IRR): It is used for measuring the profitability of potential investment. IRR is a discount rate that makes the net present value (NPV) of all cash flows from a particular project equal to zero.

(viii) Payback method: Payback period (N_{PB}) is the ratio of amount of initial investment and estimated annual net cash flow. While operating the stove, when Running Total (RT) is zero it gives the number of year required to recover all the invested money.

$$RT = C - S \times N_{PB} \quad (13)$$

RESULTS AND DISCUSSIONS

Results for LCEE and TEA of commercial and domestic cook-stoves are given in following section:

Commercial stove (5-10 kW) with PRB and CB: Energy flow diagrams have been prepared for both the stoves with input power of 5-10 kW, which portrays the impact of burner efficiency on the life cycle energy flow stream of cooking fuel. Fig. 1 shows the energy flow diagram at 10 kW input power and Fig. 2 shows that the LCEE variation for PRB stove is 38.2% to 36.7%, whereas for conventional stove, it is varied from 31.4% to 25.1% for the same input power range of 5-10 kW.
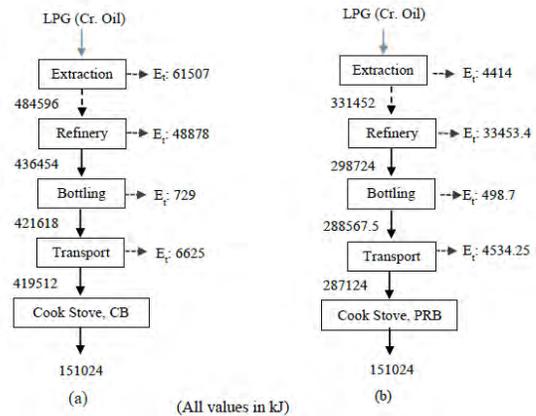
FIGURE 1. ENERGY FLOW DIAGRAM AT 10 kW INPUT POWER
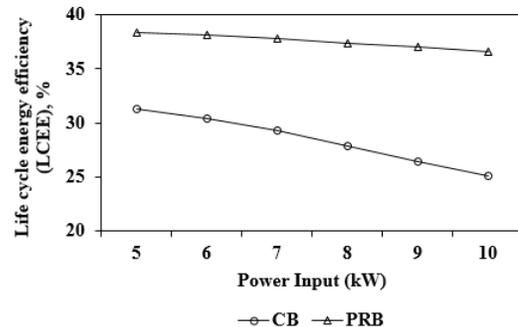
FIGURE 2. VARIATION OF LCEE WITH INPUT POWER

The life cycle cost of the LPG cooking stove with PRB can be reduced to a great extent with an annual saving of Rs. 42,580/- and Rs. 73,219/- as compared to conventional stove at 5 and 10 kW, respectively. The cumulative present worth of annual savings over the life of the PRB cook-stove has been estimated for 5-10 kW input power, and found to be Rs. 3,48,455/- to maximum Rs. 5,46,192/- at 5 and 10 kW respectively, which are much higher than the capital cost of the PRB cook-stove (Rs. 11920/-). The calculated payback period over the operating range is less than 4 month, which is very small considering the life of the cook-stove (10 years). IRR variation over the operating range has been found to be 362.2%-619.3%, which is much higher than the rate of return (8%).

Domestic cook-stove (1-3 kW) with PRB and CB: Based on functional unit selected for CCT, the estimated LCEE are 50.8 % and 26.3% for stove with PRB and CB, respectively. Monetary costs through TEA have been calculated based on Eqs. 5-13, and the results presented in Table 2. Replacement of stove with PRB results in an annual saving of about Rs. 2204/-. Table 3 shows the calculated value of the annual saving, the present worth of the annual saving and the cumulative present worth of the annual saving for each year of life of the cook-stove with PRB. With 5% inflation rate and 8% interest rate, the cumulative present worth of the annual savings for PRB stove over the life has been found as Rs. 18,037/- and the investment for the PRB stove is only just Rs. 990/-.

TABLE 2: TEA OF DOMESTIC COOK-STOVE

Parameters	Conventional stove	Stove with PRB
S (Rs.)	1200	990
C_L (years)	10	10
Annual financial appraisal		
C_F (Rs.)	6818	4822
C_M (Rs.)	60	20
C_{OP} (Rs.)	6878	4842
C_{LS} (Rs.)	7449	5245
S (Rs.)	-	2204
IRR	-	227.6%
N_{PB}	-	< 6 month

TABLE 3: ANNUAL SAVING OF DOMESTIC STOVE

Year	Annual savings (Rs.)	Present worth of annual saving (Rs.)	Present worth of cumulative saving (Rs.)
1	2204	2041	2041
2	2314	1984	4025
3	2430	1929	5954
4	2551	1875	7829
5	2679	1823	9652
6	2813	1773	11425
7	2954	1723	13148
8	3101	1676	14824
9	3256	1629	16453
10	3419	1584	18037

PRB stove has a high *IRR* value of 227.6%, as the initial investment and average total annual cost saving for PRB stove are Rs. 990/- and Rs. 2204/- respectively. At this rate, the PRB stove is expected to earn Rs. 2.3/- out of each Rs. 1/- invested (yearly). The payback period of less than six months shows recoupment of the original capital invested.

CONCLUSIONS

In order to compare the energy saving and economic impact of the newly developed LPG cooking stove with PRB with its counterpart CB, a comparative scientific investigation has been carried out by using LCEA and TEA. Based on the selected functional unit, commercial LPG stove with PRB offers a maximum surplus of 11.6 % LCEE, annual saving of Rs. 73,219/- with high *IRR* (619.3%) and a payback period of less than 4 month, over its operating range, which ascertain its sustainability in the commercial market. Similarly, use of domestic cook-stove with PRB results in 30.3 % saving of fuel, 30 % saving in time and 84.5% and 91.4 % reduction in CO and NO_x emission on daily basis, respectively. Rs. 2,204/- reduction in the life cycle cost, Rs. 18036/- cumulative present worth of annual savings and payback period of less than 6 month with an *IRR* of, 227.6% confirmed that PRB operated domestic cook stoves can be a favorable alternate for the currently used conventional one.

REFERENCES
[1] Mishra, S.C., Muthukumar, P., Mishra, N.K., 2015. Self-Aspirated LPG domestic cooking stove with a two-layer porous radiant burner. Patent No: 543/KOL/2015.
[2] Mishra, S.C., Muthukumar, P., Mishra, N.K., Panigrahi, S. Medium-Scale Self-Aspirated Improved Air Entrainment LPG Cooking Stove with a Two-Layer Porous Radiant Burner. Patent No: 201631037245.
[3] LPG profile (data on LPG marketing as on 01/01/2017), Petroleum Planning & Analysis Cell, Ministry of Petroleum & Natural Gas, India.
[4] Statement on subsidies and subsidy related schemes, Expenditure Profile 2017-2018, India (http://indiabudget.nic.in/ub2017-18/eb/stat7.pdf)
[5] Mishra, N.K., Mishra, S.C., Muthukumar, P., 2015 "Performance characterization of a medium-scale liquefied petroleum gas cooking stove with a two-layer porous radiant burner". Applied Thermal Engineering, 89, pp. 44-50.
[6] Mishra, N.K, Muthukumar, P., 2018. "Development and testing of energy efficient and environment friendly porous radiant burner operating on liquefied petroleum gas". Applied Thermal Engineering, 129, pp. 482-489.
[7] NSS 68th Round, Report No. 558: Household Consumption of Various Goods and Services in India, 2011-12.
[8] Steen, B., 1999. EPS, Version 2000 – models and data of the default method (Chalmers University of Technology, CPM Report).

APPENDIX A: ESTIMATION OF DAILY FOOD INTAKE BY HOUSEHOLDS AND MENUS FOR

ESTIMATING THE AVERAGE HEAT ENERGY REQUIREMENT

Table: Estimation of daily food intake by households

India: Daily average food consumption/ HH $= \{(r_i \times 4.9) \times .69) + (u_i \times 4.6) \times .31)\} \times \frac{12}{365}$

Main Ingredients	Per capita per month consumption [7]		Daily food consumption/HH
	Rural (r_i)	Urban (u_i)	
Rice (g)	5976	4487	875
Cereal (g)	4288	4011	665
Pulses (g)	783	901	130
Milk (ml)	4333	5422	736
Edible oil (g)	674	853	115
fish & meat (g)	597	642	965
Vegetables (g)	6760	6.842	1073
Tea (g)	79.925	95.32	14

[1](4.9, 4.6), and (.69, .31) are Urban and rural household size and % population in India, respectively.

Table: Menus for estimating the average heat energy requirement

Dish	Menu A	Menu B	Menu C
Dish 1	Rice (875 g + 3 kg water), boiled, open vessel	Rice (875 g + 3 kg water), boiled, cooker	'Khichdi' (rice 500 g + pulse 130 g + 3 kg water), boiled, cooker
Dish 2	Pulse 'dal' (130 g + 676 g water), boiled, cooker	Pulse 'dal' (130 g + 676 g water), boiled, Cooker	Vegetables 'Mix veg' (1073 g + 40 g oil), fried, open vessel
Dish 3	Vegetables 'Cabbage' (1073 g + 30 g oil), fried, open vessel	Vegetables 'Cauliflower' (1073 g + 40 g oil), fried, open vessel	'Kheer' (milk 636 ml + 375 g rice), boiled, open vessel
Dish 4	Chicken (965 g + 85 g oil), fried, open vessel	Fish curry (965 g + 75 g oil), open vessel	Fish (965 g + 75 g oil), fried, open vessel
Dish 5	Leaf bread 'chapatis' (665 g wheat), hot plate cooking	Fried Leaf bread 'parathas' (665 g wheat), hot plate cooking	Fried Leaf bread 'Chapatis' (665 g wheat), hot plate cooking
Dish 6	Milk 636 ml, boiled, open vessel	Milk 736 ml, boiled, open vessel	Tea-5 cups (14 g + 75 g sugar + 100 ml milk), boiled, open vessel
Dish 7	Tea-5 cups (14 g + 75 g sugar + 100 ml milk), boiled, open vessel	Tea-5 cups (14 g + 75 g sugar), boiled, open vessel	-

SUSTAINABLE URBAN STORMWATER MANAGEMENT:
A case for Tumakuru local planning area, Karnataka, India

Mahalakshmi Karnad
R V College of Architecture, Bengaluru
Landscape Architect
Email: lakshmikarnad@gmail.com

Dr. Meenakshi Dhote
School of Planning and Architecture, New Delhi
Environmental planner
Email:meenakshidhote@gmail.com

Abstract:

Along with the growing awareness towards environmental degradation and resource depletion, the need to find indigenous sustainable solutions is called for and it is in this context that one of the traditional water management systems in Karnataka is reviewed through the lens of ecosystem services. Traditional systems when engulfed by urban development lose their intended use and generally get deteriorated and misused. By identifying and understanding the ecosystem services provided by these traditional systems, we can mainstream them into urban planning process inorder to derive the benefits therein. The research reveals that Traditional drainage network provides for regulating, cultural and supporting services in an agrarian landscape and affirms the significant role and opportunity that they provide for urban stormwater management. Based on the ecosystem services provided by TDN, certain restoration, planning and management measures for urban stormwater management are proposed which aid in providing urban ecosystem services. This approach integrates TDN into urban planning process, manage urban stormwater and contribute positively to urban environment.

Keywords

Ecosystem services, Traditional drainage network, Stormwater management, Urban planning

Introduction

Rapid growth of urban population in most Indian cities has put tremendous pressure on many natural resources, water in particular. Indian cities not only need fresh potable water supply but also have to deal with waste water. The awareness towards environmental degradation and resource depletion has been amplified by consequences of global warming and climate change and the need to find indigenous sustainable solutions is called for at local levels. It is in this context that one of the traditional water management systems in Karnataka is reviewed through the lens of ecosystem services for better understanding. Classification and assessment of ecosystem services provides for a scientific basis for actions needed to enhance the conservation and sustainable use of ecosystems and their contributions to human well-being [1].

Ecosystem services and sustainable development

Ecosystem services are the benefits people obtain from ecosystems. These include provisioning services such as food and water; regulating services such as regulation of floods, drought, land degradation and disease; supporting services such as soil formation and nutrient cycling; and cultural services such as recreational, spiritual, religious and other nonmaterial benefits [1]. These benefits from ecosystem services which arise from managed as well as natural ecosystems sustain human existence [2] and any progress towards sustainable development needs to ensure sustainable management and use of these ecosystems and their services [1].

Urban ecosystem services

Ecosystem services derived from urban systems are termed as urban ecosystem services [2]. Urban ecosystem service flows generate both positive and negative impacts on the environment. While parks, urban forests and green belts provide positive ecosystem services like air and water purification, wind and noise reduction amongst others, polluted air and water from urban areas increase pressure on ecosystems of the surrounding regional landscapes [3]. When urban systems are managed more equitably and the loss of ecosystem services is purposefully addressed, the benefits to human well-being can be substantial [3]. Any planning and management efforts should minimize the negative impacts while maximizing the positive ones.

Study area

Tumakuru is a Class I city with a population of 3.05 lakh [4] and located 70km from Bengaluru, the state capital of Karnataka. Historically, the city has been a large trading

center for agricultural commodities from the surrounding areas [5]. Due to its proximity to Bengaluru, the city has, over time, developed as an industrial center for medium and small scale industries and ancillary units located in and around the city. It is also a growing educational center with multiple professional and para-medical institutions within the city limits. In recent years the city has grown extensively showing high decadal growth and its growth is expected to continue [6]. In 2015,Tumakuru Urban Development Authority (TUDA) has proposed Revised Master Plan 2031 comprising a conurbation area of 131 sq. km and Local planning area of 310 sq.kms including the green belt.

The geographic location of Tumakuru city is on latitude $13^{o}34$'E and longitude $77^{o}1$'N, at an average elevation of 822m. It is located on the Southern Karnataka Plateau and is classified under eastern dry climatic zone. It receives an average annual rainfall of 650mm, has gentle slopes with well drained red loamy soils [7]. In terms of its drainage, the city is located close to the main basin divide ridges that divide the three river basins, namely Pennar, Lower Cauvery and Lower Tungabadhra, and the runoff from the city drains into river Shimsa, a tributary to river Cauvery. Owing to the low rainfall and its topographic location, the city is dependent on rainwater and ground water for its water needs as it does not have any perennial surface water source.

Stormwater management and Traditional drainage network (TDN)

Owing to its geographical location in the rain shadow area of the Western Ghats and its position close to basin divide on upper catchment region of Cauvery basin, Tumakuru city falls under the semi-arid zone and rainwater was the main source of fresh water until few decades ago. Scarcity of water had made the people realise its significance and water conservation and management techniques have been in practice from a long period of time, mainly for agricultural and domestic purposes in this region [5]. One such significant tradition has been the construction of tanks or *kere* wherein series of check dams or embankments were built in succession across various drainage order streams inorder to impound runoff during rainy days (Fig.1). These check dams followed the terrain and natural drainage pattern. Local terminologies for these tanks can be associated with their drainage order [8]. Tanks on I order streams called as *kunte*, tanks on II and III order streams called as *katte* and tanks on higher order streams called as *kere* (Fig.2). There existed an overflow system from the upper level tank to the lower tank within the series. The rain water received into each tank depends upon the overflow from the higher level tank, the over land flow from the valley areas and the runoff from the side slope catchment areas. A tank has three main components: Catchment area, the tank bed and the command area. Location of the settlements was in relation to the tank and

most settlements were located on higher ground close to the embankment of a tank. The cultivation pattern followed the topography of the valley and the side slopes. Coconut plantation was predominant in the valley areas as the soil moisture is high due to series of tanks in the valley [8]. Side slopes were cultivated with rain fed crops and the command area of large tanks had irrigated cultivation. These interconnected series of tanks built over time since 5th century AD [9] and their drainage channels are collectively termed as Traditional drainage network (TDN). The traditional drainage network addressed conservation of water by i) reducing the surface runoff velocity and impounding the runoff water close to source of rainfall ii) detaining water for percolation and ground water recharge iii) retaining water for reuse in agriculture and domestic purposes iv) Conserve soil and reduce soil erosion . There are 84 tanks in the Tumakuru local planning area across various drainage orders (Tab.1). 66% of the number of tanks is across I and II order streams having a 19% in water spread area. The tanks across V order streams which are 9% in number provide for 40% of water spread area.
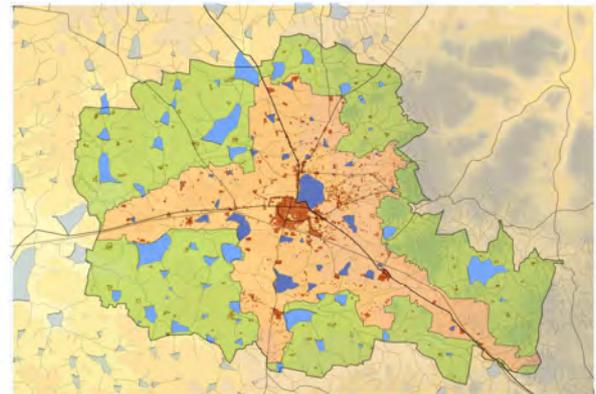
FIGURE 1: Tank series within Tumakuru LPA
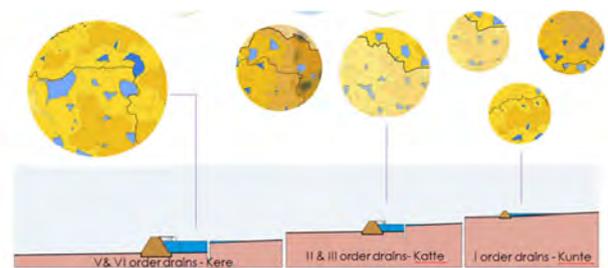
FIGURE 2: Local terminologies and drainage order

Over the years, there has been a neglect of the TDN owing to various reasons. The institutional setup for maintenance of TDN changed from Panchyats and nirgantis to government departments like the Public works department, Minor irrigation departments etc. This disconnected the maintaining agency from onsite issues and was a centrlised

system of maintenance which was not effective [8]. Change in crop cultivation under the green revolution adopted crops with higher water requirements and this was made possible by private irrigation source like wells and tube wells in the valley areas [9]. This private source of ground water reduced the dependency of the farmer on the tank water and eventually there was a slack in the maintenance of the tanks. Without annual maintenance, the upstream tanks silted up and its storage capacity decreased.

TABLE 1: Relating drainage order and tank distribution_2005

Drainage Order	Number of Tanks	Percentage	Average water spread area in Hectares	Percentage
I	25	30%	8.2	10%
II	30	36%	6.9	9%
III	17	20%	12.5	15%
IV	3	4%	1.1	2%
V	8	9%	33	40%
VI	1	1%	19.8	24%
Total	84			

Ecosystem services of TDN
Establishing ecosystem services of Traditional drainage network will signify its role in water resource management and its benefits to the environment. It will also provide a supporting tool for policy planners to integrate TDN within the master plan proposals.
Tumakuru region has red loamy soil which has low water holding capacity but well drained soils with good permeability and infiltration capacity range of 1.5 to 2.5 cm/hr. [8]. This factor facilitates ecosystem function of filtering the rainwater by soil and recharging ground water aquifers through infiltration of impounded water in the tanks. This amounts to regulating services by regulating provision of fresh potable ground water. In addition, the gentle to very gentle slopes of this well drained topography facilitates base flow from percolated water and there is a substantial increase in soil moisture in the valley areas [8]. This has made possible to grow coconut plantations in dry zone. This amounts to regulating service of modifying soil moisture which our ancestors took benefit to grow coconut and arecanut plantations in the valley areas. The numerous check dams at frequent intervals, especially across the lower orders drainage streams act as silt traps. They reduce runoff velocity which in turn reduces soil erosion from the valley floors and conserves soil. Due to the semi-arid climate, the rate of evapotranspiration is high in this region. The impounded water and the water spread participate in evapotranspiration and regulate the micro-climate of the area which is a much desired effect.
The importance of water and rainfall is embedded into the cultural practices of the local people. When a tank is full,

local people offer religious prayer in a gesture of gratitude and the tank shore becomes a social space for religious activities. Tanks and their drainage streams are seasonal in their operation. During the dry seasons, the tank bed of the smaller tanks are dry and the tank bed is used by residents as play area or as exhibition or *Jatre* grounds. These amounts to the cultural services provided by TDN.
The tank bed is de-silted every year and the soil is used to make earthen pots and bricks, supporting livelihood of people [9]. The shore line of the tanks vary based on the intensity of rainfall over the year and the foreshore supports grass pastures which are used for livestock grazing. The water impounded in tanks across higher order is stored and used for cultivation in the command area. The natural streams support vegetation on its banks due to the availability of soil moisture. This vegetation provides for native biodiversity habitats along the streams. These various services provide for supporting services which aid in soil conservation, primary production and regulating services.

These ecosystem services provided by traditional drainage network (Tab.2) were efficiently taken advantage of by our ancestors primarily for agricultural purposes. It is due to these services that there was sustainable agricultural production in the semi-arid region of Tumakuru which even today is a market for various agricultural products from its hinterland.
Due to the development of Tumakuru settlement, the agricultural lands are converted into urban plots and infrastructure corridors. In urban areas, there is no direct dependency on the tanks for its benefits due to the change in land use and the TDN is deteriorating and misused. Many tank beds have been allocated for various other land use like vegetable market and road and rail transportation corridors. In addition, the conventional stormwater management practices in the study area of constructing concrete stormwater drains over the natural streams and eventually connecting them to sewer pipes have altered the flow of runoff and denied the tanks of runoff water from their catchment areas. The proposed Master Plan 2031 too has failed to address TDN within an integrated framework and has looked at tanks as isolated pockets of open spaces. There are no guidelines or recommendations with respect TDN, except for buffer areas around tanks and drains, in the proposed Master Plan 2031 for Tumakuru local planning area.
If the TDN is dysfunctional, so will the ecosystem services provided by them. The TDN has provided ecosystem services and it was utilised for anthropogenic benefits by our ancestors for sustainable agricultural practices. There is an imperative need to examine various benefits that urban areas can take advantage of these ecosystem services and accordingly develop restoration, planning and management proposals for sustainable stormwater management and urban development.

TABLE 2: Ecosystem services facilitated by TDN

Influencing factor		Ecosystem Function	Ecosystem Services
Well drained loamy soil. Good permeability and infiltration range.	i	Ground water recharge due to impoundment of runoff water	Regulating services
Dry climate High rate of evapotranspiration	ii	Microclimate regulation due to presence of water spread	
Gentle to very gentle slopes Well drained loamy soils	iii	Substantial increase in soil moisture due to base flow from percolated water	
Check dam/Embankment at frequent intervals	iv	Reduces runoff velocity which in turn reduces soil erosion from valley floors and conserves soil	
Tanks are only source of surface water	v	Social space for community/religious activities	Cultural services
Smaller tanks are seasonal in operation	vi	Dry tank bed is used as playground or *maidan* for community activities	
Seasonal variation in shoreline due to difference in rainfall intensity over the year	vii	Supports grass pastures on its foreshore for livestock grazing	Supporting services
Annual de-silting of tank bed	viii	The soil is used by potters and to make bricks	
Higher order streams on gentle slopes and embankment across them	ix	Runoff water is stored for irrigation in the command area	
Natural streams with native vegetation along the banks	x	Reduce runoff velocity due to rough surface of conveyance and encourage percolation along drains. Supports vegetation due to soil moisture	

TABLE 3: Sustainable stormwater management strategies for Tumakuru local planning area

Ecosystem Services	Ecosystem Function	Restoration, Management and Planning measures
Regulating services	i	* Separating overland flow from sewer lines and ensuring runoff water reaches tank bed. *Maintaining natural streams and their levels.
	ii	
	iii	*Land use zoning in valley areas can have institutional lands and large residential plots *Land area downstream of the bund to be zoned for large parks, urban forests and other green areas
	iv	*Catchment level measures to reduce soil erosion and runoff pollution. *Regular desilting and maintenance of tank beds
Cultural services	v	*Passive recreational zones along the tank and stream buffer areas. *Drytank beds can be multifunctional during summer months. *Encouraging community participation in the health and maintenance of the TDN
	vi	
Supporting services	vii	*Encourage native vegetation along the foreshore and buffer areas.
	viii	*Desilted soil can be used to create landscape mounds within park areas
	ix	*Large tanks having perrinial water can be identified as biodiversity parks *Encourage native habitats
	x	*Grassed swales supported with vegetated banks *Variation in measures as per stream order *Encourage native habitats

Strategies for sustainable urban stormwater management

Water in arid and semi-arid areas is a valuable resource and urban stormwater needs to be managed as an urban resource. In the context of TDN, a basic stormwater infrastructure is in place and master plan proposals need to strengthen and integrate this with the objective of deriving urban ecosystem services. Strategies for sustainable urban storm water management (Tab.3) can be categorized under three issues: i) *Restoration measures:* Immediate priority is to restore the TDN and establish its ecosystem services. Separating overland flow from sewer lines and ensuring that runoff water reaches the tank is a primary measure. ii) *Management measures:* It is absolutely vital to keep the TDN functional if the intention is to integrate and derive urban ecosystem services. Regular desilting of tank beds, keeping the natura streams clean and maintaining overflow weirs are some of the measures. iii) *Planning measures*: There is tremendous opportunity here to develop TDN as an ecological infrastructure for the city. This can be multi-functional blue-green corridors dotted with tanks providing ample urban ecosystem services which are mutually beneficial to people and the environment.

Conclusion

The Traditional drainage network provides for regulating, cultural and supporting services in an agrarian landscape. If these ecosystem functions and their services are maintained and integrated into urban planning process, there is a possibility to derive urban ecosyem services. There exist a tremendous opportunity to build upon the TDN and develop ecological infrastructure for the city which can be beneficial to both people and the urban environment. An economic valuation of the urban ecosystem services provided by such an ecological infrastructure can further support the cause in terms of valuation.

References

[1] Millennium Ecosystem Assessment, 2003. Ecosystems and Human well-being: A framework for assessment, Island Press, Washington, DC.

[2] Wratten,S. et. al., 2013. Ecosystem services in agricultural and urban landscapes, Wiley-Blackwell, Sussex

[3] Millennium Ecosystem Assessment, 2005. Ecosystems and Human well-being: Synthesis, Island Press, Washington, DC.

[4] Census of India, 2011. Government of India.

[5] Government of Karnataka, 1969.Tumkur District Gazetteer.

[6] Administrative Staff college of India. Hyderabad, 2012. City Sanitation Plan:Tumkur, CMAK, Bangalore.

[7] Central Ground Water Board, 2012. Ground water information booklet: Tumkur district, Government of India

[8] Reddy, Somashekar. 1991. Forfeited Treasure: A study of the status of irrigation tanks in Karnataka, Prarambha, Bangalore.

[9] Dikshit. GS, GR. Kuppuswamy & SK. Mohan, 1993.Tank irrigation in Karnataka: A historical survey, Gandhi Sahitya Sangha, Bangalore

SEEC-2018-090

REMOVAL OF MICRO-POLLUTANTS FROM WATER USING MODIFIED UF-MEMBRANE

VISHALKUMAR VERMA
Chemical Engineering Department
IIT Guwahati, Assam
verma.vishalkr@gmail.com

SENTHILMURUGAN SUBBIAH
Chemical Engineering Department
IIT Guwahati, Assam
senthilmurugan@iitg.ernet.in

PUJA SINGH
Chemical Engineering Department
BIT Mesra, Ranchi
pujasingh8541.ps@gmail.com

ABSTRACT

This study investigates the efficiency of a sericin modified ultrafiltration membrane for removal of micro-pollutants (i.e. diclofenac sodium) from aqueous phase. The modified UF-membrane was able to provide 100% removal of drug for initial 1000mL, 850mL, 750mL, 500mL, and 350 mL of volume filtered at each consecutive 5 cycles and more than 50 % removal was observed at each cycle of 3 litre. Diclofenac sodium interaction with active sericin layer was investigated using ATR-Fourier transform infrared spectroscopy, isothermal titration calorimeter and X-ray diffractometer. Sericin and diclofenac sodium interaction was exothermic in nature, while hydrogen bonding and electrostatic interaction were found to be predominant driving force. ITC analysis exhibited a binding affinity (K_b) value of $3.52 \times 10^4 \pm 3.3$ and one binding site $(n \approx 1)$ per molecule at 27 °C, revealing moderate binding of diclofenac sodium to the sericin protein.The results suggest that modified UF-membrane exhibited high separation efficiency for selected drug and can be used for longer duration.

***Keywords:** **Diclofenac sodium, micro-pollutants, polymeric membrane, Silk Sericin, Ultrafiltration**
.*

INTRODUCTION

Micro-pollutants are unwanted organic or mineral substances, which are persistent, toxic and bio-accumulative in nature. They include metals/metalloids, drugs/pharmaceutical waste, organic products, household waste (solvents containing chlorine or bromine), and other industrial products. Among these, the presence of pharmaceuticals in water has been persistent and matter of great concern owing to their bio-accumulative nature [1].

Since, removal of these substances during municipal waste water treatment has been found to be incomplete[1-2]. Many studies report the adverse effects of pharmaceuticals to the aquatic organisms and non-target organisms including microbes and fish [3-4]. Though the toxic effect of these micro-pollutants on human being are still not well defined, still it has been a topic of debate recently and presence of pharmaceutical drug remnants may be harmful to humans in long run. Due to profound use of diclofenac (NSAID) an unusual high death rate among three species of vulture in India and Pakistan was reported [5]. Toxic effect of NSAIDs has been shown to significantly affect the growth of several microbes and aquatic organisms [6].

Most of the available drinking-water treatment processes has not been crafted to tackle micro-sized pharmaceutical pollutants that may be present in source water. Current treatment methods involves processes like conventional treatment, Advance Oxidation process (AOP), adsorption with activated carbon and membrane filtration [7]. Coagulation and flocculation have been reported to be largely ineffective in removing pharmaceuticals [8], AOP such as ozonation, UV/H_2O_2, UV/O_3, UV/TiO_2, and UV/Fenton are very effective in removal of pharmaceutical compounds from drinking water [9]. However, these process may lead to formation of potentially harmful by-products, incomplete degradation products, cause interference of

radical scavengers and are not cost effective [10]. Adsorption with activated carbon has been reported to have high removal of pharmaceutical compounds [8]. Major issue with activated carbon is high energy requirement during carbonization and pyrolysis of raw material [11].

Water treatment by membrane techniques is cost-effective, feasible process and can be better alternative for the traditional treatment systems since their high efficiency meets the high environmental standards [12]. NF (nano-filtration) and RO (revrese osmosis) have proved to be quite effective filtration technologies for removal of micro-pollutants. Removal of pharmaceuticals by NF-membrane has been reported for sulfamethoxazole, carbamazepine, and Ibuprofen [13]. Reverse osmosis has been found to be highly effective with varying degree of rejection (from 45-90%) [14], despite all these reports, trace quantities of some target compounds always breach RO membranes and complete removal is still a distant dream.

Although membrane processes are quite effective in removing huge loads of micro-pollutants, membrane modification is still required to treat newly emerging micro-pollutants. Hence, the current scenario forced us to explore new methods for modification of membrane technology to specifically target these micro-pollutants. Sericin is a globular protein with physicochemical properties like hydrophilicity, amphoteric, antioxidant, antimicrobial and are non-toxic nature [15]. These inherent properties make it very suitable as a polymer to be used for membrane modification. We have come up with a novel method for coating of polymeric UF membrane with sericin protein for removal of dissolved micro-pollutants from aqueous environment.

The current study focuses on evaluation of sericin modified ultrafiltration membrane (SER-modified UF membrane) for removal of drug based micro-pollutants. We have used a non-steroid anti-inflammatory drug-diclofenac sodium (DICNa) as a model drug to inspect the efficiency of modified membrane. Interaction of DICNa with sericin active layer on membrane surface was investigated using different analytical methods like ATR-Fourier Transform Infrared Spectroscopy (ATR-FTIR), Isothermal Titration Calorimeter (ITC) and X-ray Diffractometer (XRD). This work will provide a better solution for removal of drug-based micro-pollutants from aqueous solution using modified membrane filtration process to meet the requirements of safe drinking water.

EXPERIMENTAL SECTION

Materials:
The Polypropylene hollow fibre UF-membrane used in the this study was modified using a novel coating method devised by Mr. Vishal Kumar Verma and Dr. S Senthilmurugan, Chemical Engineering Department, IIT-Guwahati. The sericin modified (SER-modified) UF-membrane had an active layer of Silk Sericin on membrane surface.

The model target drug used in this study is a widely used NSAID-Diclofenac Sodium, obtained from Sigma-Aldrich Chemicals Pvt. Limited. The chemical formula of diclofenac sodium is $C_{14}H_{10}C_{l2}NNaO_2$, and the molecular weight is 318.14. The protonation constant (pKa) value is 4.15 hence at pH < 4.15, it exists in uncharged form, and are anionic with the increasing pH (i.e., deprotonation of carboxyl functional groups). All other chemicals (i.e., Ethanol, Acetonitrile, NaOH, HCl, Phosphoric Acid, Sodium-di-hydrogen phosphate) used in the study were of analytical/HPLC grade and procured from Merck®, India Ltd.

Methods:

Membrane Performance and Removal of Diclofenac Sodium:

We used a laboratory-scale dead-end filtration set-up for analyzing removal capacity of modified UF-membrane. The set-up mainly consists of low-pressure pump, feed tank equipped with stirrer, temperature controller, pressure dampner and a UF-membrane casing. Diclofenac sodium was fed in to the UF-membrane assembly at 2L/Hr feed flow rate and 1ppm fixed initial concentration. Permeate samples were taken at regular intervals of time and analysed to determine the removal efficiency.

The samples obtained in each experiment were analysed using HPLC instrument (Shimadzu, model UFLC SPD-20A) equipped with a reverse-phase C-18 column (5 μm, 4.6 mm ×250 mm) and UV-Detector to quantify the concentration of drugs in permeate and feed samples. The mobile phase was composed of Acetonitrile and phosphate buffer pH 2.5 in 70:30 (v:v) proportions. The flow rate was 1 mL/min, the detection wavelength 254 nm and the injection volume 10 μL. Each result is the mean of 3 measurements.

Methods used to Study Sericin and Diclofenac sodium Interaction:

ATR-Fourier Transform Infrared Spectroscopy
ATR-FTIR spectra (4000–400 cm–1) were acquired using ATR spectrophotometer (model, Spectrum TWO from PerkinElmer) to confirm adsorption of diclofenac on membrane surface and complex formation with sericin.
Isothermal Titration Calorimeter (ITC)
The heat of adsorption during complex formation was measured by ITC using MicroCal iTC-200 (MicroCal, Northampton, MA, USA). 20 μM of sericin protein was filled in the sample cell and titrated with 5 mM of diclofenac

sodium drug at 27 °C. Typically, 25 consecutive injections of 1.5 μL in two minute interval were injected into the sample cell with adequate mixing.

X-ray Diffractometer

Amorphous and crystalline structure of sericin, diclofenac sodium, and complex were examined using XRD and analyzed for any change noticed after complex formation using an X-ray diffractometer (XRD; make, Bruker; model, D8 Advance) with step size of 0.05 deg/sin the range of 2θ = 5–80° under the acceleration voltage of 40 kV and 40 mA.

RESULT AND DISCUSSION

Membrane Performance and Removal of Diclofenac Sodium:

The performance of SER-modified UF-membrane for removal of DICNa was assessed at a fixed flow rate of 2L/Hr with fixed feed concentration of 1ppm. Experiments were conducted at normal room temperature (30ºC) and pH of 7.5. Modified membrane was tested for consecutive 5 cycles of adsorption and desorption for diclofenac sodium and removal efficiency is shown in Fig.1.
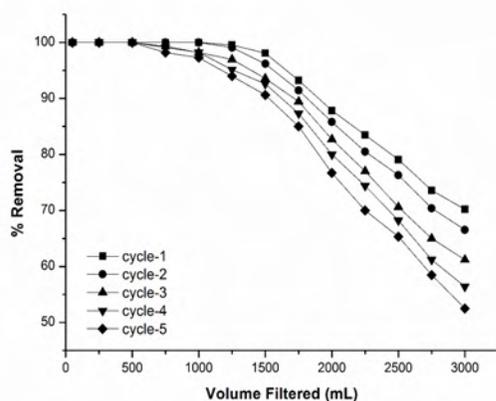
FIGURE 1. REMOVAL EFFICIENCY OF MODIFIED UF-MEMBRANE FOR CONSECUTIVE 5 CYCLES USING DICLOFENAC SODIUM AQUEOUS SOLUTION AT PH 7.5 AND TEMPERATURE 30ºC

A total of 3-liter volume was passed through UF-membrane and the results obtained were analysed. As the figure shows the removal percentage decreases slightly with each cycle which may be attributed to permanent deformation of some binding sites on protein layer. Still the membrane was able to remove more than 100% of drug for 1000mL, 850mL, 750mL, 500mL, and 350 mL volume filtered at each consecutive 5 cycles. At the end of each cycle membrane was washed with alkaline (1M NaOH) solution at pH 11 and temperature 40°C to regenerate the active layer of protein on membrane surface. At each cycle, removal efficiency was decreased further but still more than

50 % removal was observed at each cycle of 3000 litre. This shows that membrane regeneration gradually decreases with each cycle, exhausting some of the binding sites at each level. Experiments were also conducted at different temperature (20, 30 and 40ºC) and pH (5, 7 and 8) and it was found that removal efficiency improvised marginally at lower pH and temperature.

Sericin and Diclofenac Sodium Interaction Study:

ATR-Fourier Transform Infrared Spectroscopy:

The ATR-FTIR Spectra of SER-coated hollow fibre, diclofenac sodium and sericin coated hollow fibre after filtration was analysed for binding confirmation and to study molecular interaction between DICNa and SER-coated membrane surface (see fig.2).
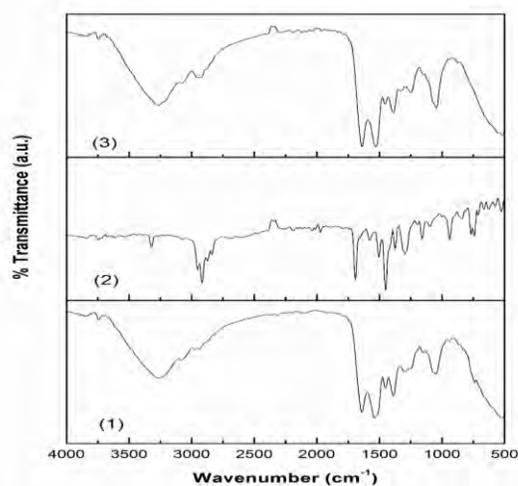
FIGURE 2: ATR-FTIR SPECTRA OF (1) DICNa (2) SER-MODIFIED MEMBRANE AND (3) SER-MODIFIED MEMBRANE AFTER FILTRATION

Sericin coated hollow fibre shows characteristic peaks for polypropylene at 2952, 2916, 2872, 2839 cm^{-1}, NH and OH stretch peak for sericin at 3320 cm^{-1}, amide I and II peaks at 1690 and 1577 cm^{-1}, sericin CH, OH bending and C-OH stretching at 1450 and 1096. When modified PP-HF was analysed after filtration we found diclofenac characteristic peak at 1638 cm^{-1}, while DICNa carbonyl peak shifted to 1525 and 1457 cm^{-1} and C-Cl peak disappeared at 740 cm^{-1}. The FTIR analysis clearly shows interaction between DICNa and active sericin layer on the membrane surface. Since in the pH range (pH 5–10) of this study, DICNa exists in anionic form (pH > pKa) and hence the electrostatic interaction between carboxylic group of DICNa drug and positive amide group of sericin ascertain binding of drug on to the membrane surface.

Isothermal Titration Calorimetry:

The ITC thermogram of DICNa titration with sericin has shown best fitting in one set of binding model after subtraction of buffer and shows the presence of single binding site in sericin for DICNa with exothermic pattern in thermogram (fig.3). ITC analysis also revealed the binding affinity (Kb) value 3.52 x 104 ± 0.33 at 27°C that conclude moderate binding of DICNa to the sericin protein. ITC analysis can reveal the driving force of corresponding interaction based on binding thermodynamics. If $\Delta H<0$, $\Delta S<0$, driving force is van der Waal's and hydrogen; if $\Delta H>0$, $\Delta S>0$, hydrophobic interaction is dominant while $\Delta H<0$, $\Delta S>0$ signify the dominancy of electrostatic force [16]. Therefore, negative values of ΔH and ΔS also has revealed that hydrogen bonding and electrostatic interaction are the predominant driven force in present binding. Thermodynamic parameters of drug binding with Sericin protein has been listed in table 1.

TABLE 1: THERMODYNAMIC PARAMETERS OF THE SERICIN AND DICLOFENAC SODIUM INTERACTION OBTAINED BY ITC AT 27°C TEMPERATURE.

	Stoichiometry (n)	K_b (mole^{-1})	ΔH (Kcal/mol)	ΔS (Kcal/mol.K)	ΔG_{app} (Kcal/mol)
SER-DICNa interaction	0.81± 0.031	3.52E4± 3.3	-3.57 ±0.33	-11.70	8.13
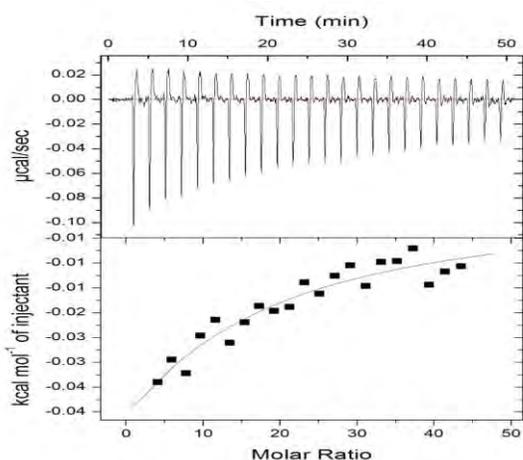
FIGURE 3: ITC THERMOGRAM FOR DICNa-SERICIN INTERACTION

X-ray Diffractometer:

The XRD analysis for Sericin revealed a large diffraction peak at around 2θ=21.15°, the broad curve indicates amorphous nature (fig.4). This peak is characteristic of the β-sheet structure due to intermolecular hydrogen bonding between the hydroxyl groups of the amino acid present in Sericin [17]. Diclofenac sodium XRD peaks shows its characteristic crystallinity and was found to be in good agreement with previous reported literatures [18]. The Sericin-diclofenac sodium complex XRD plot was found to be crystalline in nature and retained most of the diclofenac sodium characteristic peaks hence depicting adsorption of diclofenac sodium on to sericin.
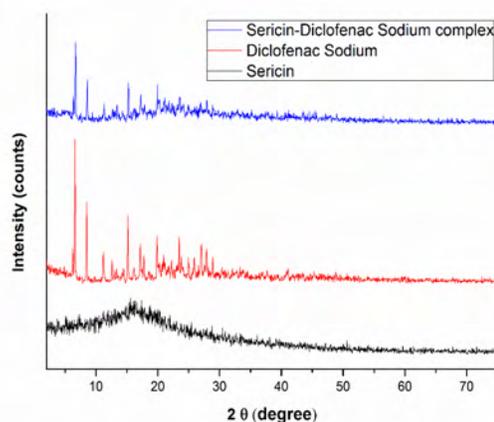
FIGURE 4: XRD PROFILE FOR DICLOFENAC SODIUM, SERICIN AND SERICIN-DICLOFENAC COMPLEX

CONCLUSION

In this work, the sericin-modified UF-membrane was assessed for its capacity to remove a model drug diclofenac sodium from water. The modified UF membrane life cycle was evaluated using repetitive cycles of filtration. The results suggest that regeneration of active binding sites gradually decreases with each filtration cycle. However, the modified membrane removal efficiency was still higher for evaluated 5 cycles of operation. Diclofenac sodium interaction with sericin was investigated and sericin-diclofenac binding and complex formation was established using FTIR, ITC and XRD analysis. We hope this study will help in modification of existing filtration processes and provide a better solution for removal of drug based micro-pollutants from aqueous solution.

REFERENCES

[1] Heberer, T., 2002. "Occurrence, fate, and removal of pharmaceutical residues in the aquatic environment: a review of recent research data". Toxicol Lett. Elsevier, 131(1), pp. 5–17.

[2] Kolpin, D. W., Furlong, E. T., Meyer, M. T., Thurman, E. M., Zaugg, S. D., Barber, L. B., 2002. "Pharmaceuticals, hormones, and other organic wastewater contaminants in U.S. stream, 1999-2000: A national reconnaissance". Environ Sci Technol, 36(6), pp. 1202–11.

[3] De Lange, H. J., Noordoven, W Murk, A.J., Lürling, M., Peeters, E., 2006. "Behavioural responses of< i> Gammarus pulex</i>(Crustacea, Amphipoda) to low concentrations of pharmaceuticals". Aquat Toxicol, 78(3), pp. 209–16.

[4] Owens, B., 2015. "Pharmaceuticals in the environment". Pharm J, 294(7850), pp. 205–7.

[5] Oaks. J.L., Gilbert, M., Virani, M.Z., Watson, R.T., Meteyer, C.U., Rideout, B., 2004. "Diclofenac residues as the cause of vulture population decline in Pakistan". Nature, 427(6975), pp. 630–3.

[6] Pomati, F., Netting, A. G., Calamari, D., Neilan, B. A., 2004. "Effects of erythromycin, tetracycline and ibuprofen on the growth of Synechocystis sp. and Lemna minor". Aquat Toxicol, 67(4), pp. 387–96.

[7] Gadipelly, C., Pérez-González, A., Yadav, G. D., Ortiz, I., Ibáñez, R., Rathod, V.K., 2014. "Pharmaceutical Industry Wastewater: Review of the Technologies for Water Treatment and Reuse". Ind Eng Chem Res, 53(29), pp. 11571–92.

[8] Westerhoff, P., Yoon, Y., Snyder, S., Wert, E., 2005. "Fate of endocrine-disruptor, pharmaceutical, and personal care product chemicals during simulated drinking water treatment processes", Environ Sci Technol, 39(17), pp. 6649–63.

[9] von, Gunten, U., Hoigne, J., 1994 "Bromate formation during ozonation of bromide-containing waters: Interaction of ozone and hydroxyl radical reactions". Environ Sci Technol, 28(7), pp. 1234–42.

[10] Boorman, G. A., Dellarco, V., Dunnick, J. K., Chapin, R. E., Hunter, S., Hauchman, F., 1999. "Drinking Water Disinfection Byproducs: Review and Approach to Toxicity Evaluation". -Environ Heal Perspect, 107(Suppl 1), pp. 207–17.

[11] Tiek, Wong, K., Yoon, Y., Jang, M., 2015. "Enhanced recyclable magnetized palm shell waste-based powdered activated carbon for the removal of ibuprofen: Insights for kinetics and mechanisms". PLoS One, 10(10), pp. e0141013.

[12] Owen, G., Bandi, M, Howell, J. A., Churchouse, S. J., 1995. "Economic assessment of membrane processes for water and waste water treatment". J Memb Sci, 102, pp. 77–91.

[13] Vergili, I., 2013. "Application of nanofiltration for the removal of carbamazepine, diclofenac and ibuprofen from drinking water sources". J Environ Manage, 30(127), pp. 177–87.

[14] Yangali-quintanilla, V., Maeng, S. K., Fujioka, T., Kennedy, M., Li. Z., Amy, G., 2011. "Nanofiltration vs. reverse osmosis for the removal of emerging organic contaminants in water reuse". Desalin Water Treat, 34(1–3), pp. 50–6.

[15] Nagura, M., Ohnishi, R., Gitoh, Y., Faculty, O., Science, T., October, R., 2001. "Structures and Physical Properties of Cross-Linked Sericin Membranes". J Insect Biotechnol Sericol, 70(2), pp. 149–53.

[16] Du, X., Li, Y., Xia, Y-L., Ai, S-M., Liang, J., Sang, P., 2016. "Insights into Protein-Ligand Interactions: Mechanisms, Models, and Methods". Int J Mol Sci, 17(2), pp.144.

[17] Gupta, D., Agrawal, A., Rangi, A., 2014. "Extraction and characterization of silk sericin". Indian J Fibre Text Res, 39(4), pp. 364–72.

[18] Zhao, Y., Liu, F., Qin, X., 2017. "Adsorption of diclofenac onto goethite: Adsorption kinetics and effects of pH". Chemosphere, 180(Supplement C), pp. 373–8.

SEEC-2018-092

BIOMASS DIRECTED DEVELOPMENT OF NOBLE METAL NANOSCAFFOLDS FOR APPLICATIONS IN BIOTECHNOLOGY

Sanjam Chandna , Aman Bhardwaj and Jayeeta Bhaumik*
Center of Innovative and Applied Bioprocessing (CIAB), Department of Biotechnology
Knowledge City, Sector 81, Mohali 140306, Punjab, India
Email id: sanjamchandna7@gmail.com, jayeeta@ciab.res.in

Lignin is one of the major components of agricultural waste. Lignin mainly contains polyphenols which can act as reducing, stabilizing and capping agents during the synthesis of noble metal nanoparticles (MNPs) namely silver and gold nanoparticles. Lignin was therefore utilized in the synthesis of silver and gold nanoparticles with optimum size. The metal nanoparticles were characterized by various analytical techniques such as absorption spectroscopy, DLS, SEM and FTIR. These nanoparticles were evaluated for their anti-oxidant potential, therapeutic potential and catalytic efficiency. The therapeutic potential was evaluated after conjugation of various therapeutic dyes on these nanoparticles and the catalytic efficiency was evaluated after enzyme immobilization and degradation of organic pollutants (such as dyes). By this means, lignin waste generated from agricultural biomass as well as from various industries can be transformed into valorized products.

SEEC-2018-093

SOOT FORMATION IN PREMIXED C₂H₄ FLAME WITHIN HIGHLY CONDUCTING AND RADIATING POROUS BURNER

Snehasish Panigrahy
Department of Mechanical Engineering
Indian Institute of Technology Guwahati, Guwahati – 781039, India
Email: snehasishiit@gmail.com

ABSTRACT

In this article the influence of porous media combustion on the soot formation mechanism in premixed fuel-rich ethylene-air flame is investigated. Towards solving macroscopic transport equations along with quasi-steady radiative transfer equation, a thermal non-equilibrium numerical model of the porous inert burner (PIB) is coupled to a discrete sectional method based soot kinetic mechanism containing 156 chemical species and 5600 reactions. The results show that the PIB not only reduces the CO emission, but also can minimize the soot generation and delay the soot inception as compared to the premixed free flame (FF) combustion. In PIB the maximum soot particle diameter formed is found to be 10 nm smaller than that of FF case. Furthermore, the agglomeration process of PAHs producing large soot particles are also suppressed by the PIB.

Keywords: Combustion, Porous inert burner, Radiation heat transfer, Soot formation, PAH.

NOMENCLATURE

C	Specific heat (J/kg·K)
d_p	Pore diameter (m)
G	Emissive power (W/m²)
$THRR$	total heat release rate (J/cm³·s)
h	Heat transfer coefficient (W/m²·K)
q_R	Radiative heat flux (W/m²)
V_i	Species Diffusion velocity (m/s)
Y	Species mass fraction

Greek symbols

ε	Emissivity
φ	Equivalence ratio
ξ	Porosity
Γ	Extinction coefficient (m⁻¹)
λ	Thermal conductivity (W/m·K)
σ	Stefan-Boltzmann constant (w/m²·K⁴)
ω	Scattering albedo

Superscripts

m	Indices for discrete polar angles
R	Related to radiation

Subscripts

g	gas phase
N	North face
s	Solid phase
S	South face

INTRODUCTION

Combustion resulting pollutions, such as carbon monoxide, nitric oxides, and soot particulates produced because of burning of petroleum product poses adverse effects on human health and on environment. Therefore, in this direction to reduce harmful pollutants from the combustion devices substantial amount of research has been conducted for the development of ecological combustion techniques. Porous inert burner (PIB) is one such technology, that make use of heat recirculation mechanism of highly conducting and radiating porous media for offering reduced amount of CO and NOx pollutants as well as higher thermal efficiency than that of conventional burners [1, 2]. However, in spite of the harmful effect of soot particles on public health and environment, no studies have been performed regarding soot particle growth process in the PIB. This is because of the problems arises in conducting

experiments for visualizing and measuring the soot particle evolution inside the porous matrix, as well as because of complication in numerical simulation associated to interpreting the soot formation process in such environment of highly coupled convection, conduction, and radiation heat transfer inside the PIB.

The purpose of this article is therefore, to examine the effect of PIB on the formation of soot inside a SiC based porous matrix. To understand the soot growth process within the PIB, the variations of soot volume fraction, particle number density, soot particle diameter, and mole fraction profiles of some major soot precursors such as benzene, naphthalene and pyrene along the flame axis and at the burner exit are compared to that of premixed FF combustion condition at the same input conditions. The conceptual diagram of the analyses is illustrated in Fig.1.
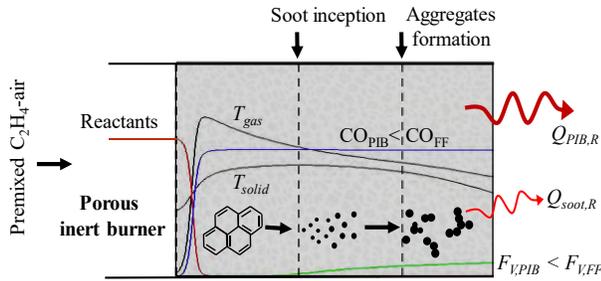
FIGURE 1. Soot growth process within PIB.

NUMERICAL METHOD

As illustrated in Fig. 1, the computational domain consists of a 1-D planer PIB with thickness equal to $L=0.03$ m. Rich C_2H_4-air mixture is introduced to the porous burner inlet at pressure of 1 atm and temperature of 298.15 K. Eventually the combustion spreads throughout the PIB, and depending on the velocity and equivalence ratio the flame become stable at a particular location inside the burner. The heat release generated in the combustion zone manifests the convective heat transfer from the gas to the solid porous matrix, which increases the solid-phase temperature (T_s) in the downstream region of the reaction zone. In the upstream section of the PIB, the heat recirculation caused by the conduction and radiation feedback from the downstream flame region increases the solid-phase temperature, that subsequently preheats the incoming C_2H_4-air mixture elevating the unburnt gas-phase temperature (T_g).

In the present study, the FDM based local thermal non-equilibrium numerical model employing the convective heat transfer between gaseous and solid-phase, the solid matrix conduction and the radiation source information of the porous matrix are integrated to the premixed laminar code Cantera [3] for solving the governing equations such as, mass continuity equation, conservation of chemical species equation, gaseous and solid energy equations. The effect of radiation from H_2O, CO_2 species and soot particles are

calculated considering optical thin model [4]. To understand the effect of the PIB on soot formation, in this study a comprehensive kinetic mechanism [5] comprising of 156 chemical species and 5600 different reactions is used. The discrete sectional method based soot kinetic model used in this study combines a gas-phase mechanism, which contains 97 species and heavy PAHs, and a detailed soot chemistry [6] consisting of 59 pseudo species (BINs) for describing the soot evolution mechansim.

Continuity equation:

$$\frac{\partial(\xi\rho_g)}{\partial t} + \frac{\partial(\xi\rho_g u)}{\partial x} = 0 \tag{1}$$

Species conservation equation, for ($k=1,......,K$):

$$\xi\rho_g\left(\frac{\partial Y_k}{\partial t} + u\frac{\partial Y_k}{\partial x}\right) = -\frac{\partial}{\partial x}\left(\xi\rho_g V_k Y_k\right) + \xi\dot{\omega}_k W_k \tag{2}$$

Gas phase energy equation:

$$\xi\rho_g C_g\left(\frac{\partial T_g}{\partial t} + u\frac{\partial T_g}{\partial x}\right) + h_V(T_g - T_s) + \xi\sum_{k=1}^{K}\rho_g Y_k C_{g,k} V_k\frac{\partial T_g}{\partial x}$$
$$+ \xi\sum_{k=1}^{K}\dot{\omega}_k h_k W_k = \xi\frac{\partial}{\partial x}\left(\lambda_g\frac{\partial T_g}{\partial x}\right) + \frac{\partial\dot{Q}_{g,R}}{\partial x} + \frac{\partial\dot{Q}_{soot,R}}{\partial x} \tag{3}$$

Solid phase energy equation:

$$(1-\xi)\rho_s C_s\frac{\partial T_s}{\partial t} - h_V(T_g - T_s)$$
$$-(1-\xi)\lambda_s\frac{\partial^2 T_s}{\partial x^2} + \frac{\partial q_R}{\partial x} = 0 \tag{4}$$

Under the optical thin and grey gas approximation, considering radiative heat transfer from major radiating chemical species like H_2O, and CO_2, as well as from soot particles, the radiative source terms is given by,

$$\frac{\partial\dot{Q}_{g,R}}{\partial x} + \frac{\partial\dot{Q}_{soot,R}}{\partial x} = 2\sigma\left(T^4 - T_0^4\right)\sum_k p_k\kappa_{p,k} \tag{5}$$

The temperature dependent Planck mean absorption coefficient for all species is computed by,

$$\sum_k p_k\kappa_{p,k} = p\left[X_{CO_2}\kappa_{p,CO_2}(T) + X_{H_2O}\kappa_{p,H_2O}(T)\right] + f_v\kappa_{p,soot}(T)p \tag{6}$$

The $\kappa_{p,k}$ of each species is estimated based on polynomial lines as described in ref. [7], and $\kappa_{p,soot}(T)$ is calculated as,

$$\kappa_{p,soot}(T) = \left[-3.75\times10^5 + 1735T(x)\right]\ \text{m}^{-1} \tag{7}$$

In this equation 3 the volumetric radiative source term from the porous matrix is calculated as,

$$\frac{\partial Q_{s,R}}{\partial x} = \Gamma\left(1-\omega\right)\left(I_b^4 - G\right) \qquad (8)$$

where ω is the scattering albedo, Γ is the extinction coefficient, $I_b = \dfrac{\sigma T^4}{\pi}$ is the blackbody intensity based on the local absolute temperature T and G is the incident radiation. In any given direction $\hat{s}$, the radiative transfer equation can be written as,

$$\frac{\partial I^m}{\partial x} = \hat{s} \cdot \nabla I^m = -\Gamma I^m + \Gamma S \qquad (9)$$

where I is the radiation intensity, and S is the source term. Equation 11 is solved using the FVM, and further details on the finite volume discretization to solve the RTE can be found in our previous study [1, 2]. The boundary intensities I_b^m at the inlet and outlet walls of the PM are calculated from the following,

$$I_b^m = \varepsilon \frac{\sigma T_{s,wall}^4}{\pi} + $$
$$\left(\frac{1-\varepsilon}{\pi}\right) 2\pi \sum_{m=1}^{M} I^m \left| \cos\theta^m \sin\theta^m \left(\sin\Delta\theta^m\right)\right| \qquad (10)$$

The various material properties and correlation for convective heat transfer coefficient h_V between gas- and solid phase of the SiC matrix required for solving the present numerical model is taken from ref. [2].

RESULTS AND DISCUSSION

The computed axial gas and solid-phase temperature profiles of the burner for the combustion of fuel-rich premixed C_2H_4-air mixture are presented in Fig. 2, where the sharp decrease in gas temperature can be observed in down-stream section of the PIB caused by the radiation losses mainly from the highly conducting and radiating SiC porous matrix and secondary from the soot particles. In addition, the sooting behavior of flame inside the burner in terms of soot volume fraction (F_V) is shown in Fig. 2 as function of axial distance of the PIB. Moreover, for the sake of assessment, the FF temperature distribution and F_V profile of premixed C_2H_4-air combustion in gas environment are demonstrated along with its combustion inside the burner at the same equivalence ratio of $\varphi = 2.4$, and input gas flow velocity of $V_{0L} = 0.1198$ m/s. The gas-phase temperature decreases more quickly inside the PIB than that of free flame temperature, which subsequently slows the growth in soot volume fraction along the PIB axis. Furthermore, the lower temperature at the down-stream region of the PIB is answerable for the later manifestation of the soot volume fraction which is controlled by bigger BINs generation, that

starts at ≈ 4.0 mm further down-stream from the soot initiation area of the FF condition (Fig. 2).
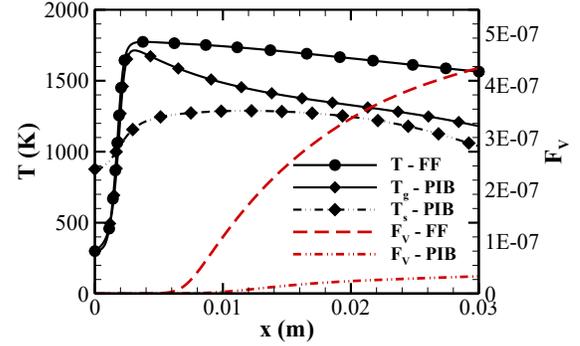
FIGURE 2. Comparisons of axial gas and solid-phase temperature profiles and soot volume fractions
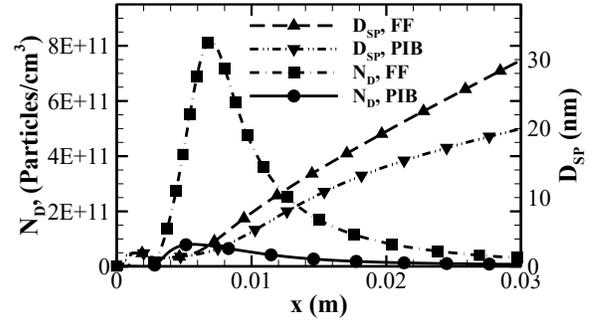
FIGURE 3. Comparisons of particle number densities and soot diameters as a function of burner distance

In Fig. 3 the number densities and soot particle diameter are plotted along the burner axis for the combustion of rich C_2H_4-air mixture inside the PIB and in FF case at $\varphi = 2.4$ and $V_{0L} = 0.1198$ m/s. In the case of PIB the noticeable decay in N_D profile and slower evolution of soot size D_{sp} along the flame axis as compared to FF case is apparent from the Fig. 3. It is also perceived that, within the burner the number density attains its peak value more quickly as compared to that of FF case. This is due to the fact that, the prior dissolution of nucleation process inside the burner affected by the lower gas-phase temperature, reduces the growth rate of particle number density, as presented in Fig. 3. To explore the effect of the porous media combustion on PAH and soot formation, the concentration profiles of some major soot precursors such as benzene (C_6H_6), Naphthalene ($C_{10}H_8$), Pyrene ($C_{16}H_{10}$), and the mole fraction profiles of different BINs generated along the PIB axis for both PIB and FF cases are compared in Fig. 4 and 5 respectively. It can be observed that, rich C_2H_4 flame inside the burner produces larger amount of PAHs (C_6H_6, $C_{10}H_8$, $C_{16}H_{10}$) than that of FF condition at the same input condition. The higher concentration of PAHs in the PIB is due to the presence of higher amount of acetylene (C_2H_2) produced in the down-stream region of the PI. Moreover, Fig. 4 demonstrates that, concentrations of all the PAHs

follow rise-decay profile for the combustion of C_2H_4-air mixture in the FF condition, whereas, in the case of PIB, after achieving the maximum values the mole fractions of the PAHs is observed to stay almost constant throughout the PIB.
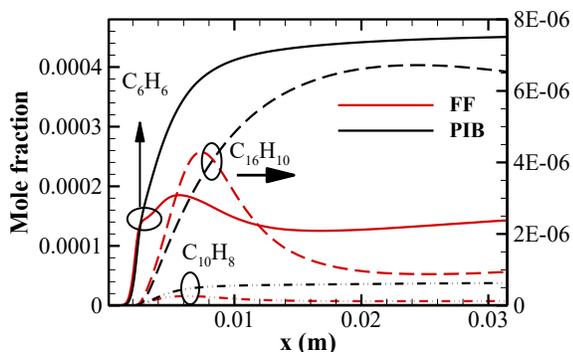
FIGURE 4. concentration profiles of major PAHs
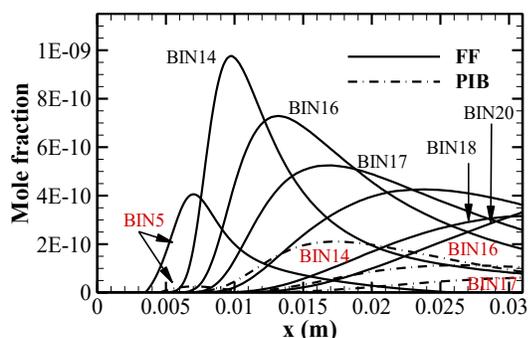
FIGURE 5. BINs concentrations along the flame axis

The coagulation and agglomeration process of PAHs to produce bigger soot particles are also depressed by the lower temperature profile and less prolonged presence of free radicals in the down-stream region of the PIB, that ultimately results in lesser amount soot production in the PIB than that of FF case. To support this information, in Fig. 5 the concentrations of various soot particles (BIN5 - BIN13) and aggregates (BIN14 - BIN20) in terms of different BIN classes are reported for both PIB and FF cases under the same input operating condition of $\varphi = 2.4$ and V_{0L} = 0.1198 m/s. The mole fractions of all the BINs produced in the C_2H_4-air flame inside the PIB along the PIB axis are found to be very much less than that of the FF values. Fig. 5 also displays that, with the combustion of fuel-rich C_2H_4-air mixture within the PIB instead of its combustion in FF condition, production of large aggregates beyond BIN17 totally disappear. Furthermore, in case of PIB the soot particles and the aggregates are developed at higher elevation above the burner, and they attain their highest at further down-stream side of the burner than that of the FF combustion.

CONCLUSION

The evolution mechanism of soot due to the combustion of fuel-rich C_2H_4-air mixture within a highly conducting and radiating SiC PIB was analysed. The results for premixed FF condition were also compared to that of PIB to establish the superiority of the porous media combustion towards the formation of soot aerosols. The gas temperature inside the burner decreases more rapidly than the FF temperature, which delayed the increase of F_V and delayed the appearance of the soot particulates. Furthermore, along the burner axis noticeable decline in particle density profile and slower growth of soot particle size were observed. The mole fractions of all the BINs generated within the PIB were observed to be very much less as compared to the FF case. The soot and the aggregates were developed at higher height above the burner, and they attained their highest values at further downstream side of the PIB than that of FF case.

REFERENCES

[1] Panigrahy, S., Mishra, N.K., Mishra, S.C., Muthukumar, P., 2016. "Numerical and experimental analyses of LPG (liquefied petroleum gas) combustion in a domestic cooking stove with a porous radiant burner". Energy, 95, pp. 404-14.

[2] Panigrahy, S., Mishra, S.C., 2016. "Analysis of combustion of liquefied petroleum gas in a porous radiant burner". Int. J. Heat Mass Transfer, 95, pp. 488-98.

[3] Goodwin, D., Malaya, N., Moffat, H., Speth, R., 2014. Cantera: An Object-Oriented Software Toolkit for Chemical Kinetics, Thermodynamics, and Transport Processes. https://code.google.com/p/cantera/.

[4] Liu, Y., Rogg, B., 1991. "Modelling of thermally radiating diffusion flames with detailed chemistry and transport". EUROTHERM Seminars, 17, pp. 114–27.

[5] Franzelli, B., Cuoci, A., Stagni, A., Ihme, M., Faravelli, T., Candel, S., 2017. "Numerical investigation of soot-flame-vortex interaction". Proc. Combust. Inst, 36, pp. 753-61.

[6] Saggese, C., Ferrario, S., Camacho, J., Cuoci, A., Frassoldati, A., Ranzi, E. et al., 2015. "Kinetic modeling of particle size distribution of soot in a premixed burner-stabilized stagnation ethylene flame". Combust. Flame, 162, pp. 3356-69.

[7] Cosilab Documentation, 2017. "1D premixed flames and counterflow diffusion flames", Section B.1.

NON CONVENTIONAL ENERGY SOURCES USED IN LIQUID DESICCANT

DEHUMIDIFICATION AND REGENERATION

Geleta Fekadu
Department of Mechanical & Industrial
Engineering, IIT, Roorkee-247667, India
Email: gelefeke@gmail.com

Sudhakar Subudhi
Department of Mechanical & Industrial
Engineering, IIT, Roorkee-247667, India
Email: subudhi3@gmail.com

ABSTRACT

Recent demand for primary energy utilization is increasing in the world for application of thermal comforts. Supply-demand on energy sector is concerning issues today for development while urbanization and population are increasing, it desires intensive investigation for promising an energy which is renewable, eco-friendly, and cost-effective. The aim of this paper is to use solar energy to reactivate diluted solution of $CaCl_2$-H_2O used for dehumidification of process air. The experimental set up was done in IIT Roorkee, Department of Mechanical and Industrial Engineering East Block which encompasses of viz. dehumidifier, solar collector, PHE, and Agilent data acquisition. A 40% by mass of $CaCl_2$-H_2O solution, the experiment conducted using a flow rate of 2.5LPM, solar heated water for regeneration in PHE after dehumidification of process air was done, and a minimum RH reduction was observed due to low in RH of ambient air.

Keywords: Solar energy, Dehumidification, liquid desiccant, Regenerator

NOMENCLATURE

ASHRAE	American Society of Heating, Refrigerating, and Air-Conditioning Engineers
BPE	Boiling point elevation
$CaCl_2$-H_2O	Calcium Chloride Solution
CO_2	Carbon dioxide
GHG	Greenhouse gas
HCOOK	Potassium formate
IIT	Indian Institute of Technology
LiCl	Lithium Chloride
LiBr	Lithium Bromide
LPM	Liters per minute
$MgCl_2$	Magnesium chloride
PHE	Plate heat exchanger
RH	Relative humidity
TEG	Tri-Ethylene Glycol

1. INTRODUCTION

In the era of primary demands of energy utilization is increasing in the world for the application of thermal comforts due to global warming. So supply- demands on energy is concerning issues today for one country's development, urbanization and increase in population are happening, it desires intensive investigation for promising an energy which is renewable, eco-friendly, cost-effective is vital. Fast depletion of conventional energy resources and thermal human comfort condition is getting higher because of increase in world population is becoming a major global environmental issue now today [1].

Thermal human comfort condition leads to increase in massive consumption of energy consequently contributing to environmental problems. Building sector: commercial and residential consumes more percentages of energy. So, electrical energy is required in most cases used to function heating or cooling air conditioning systems.

In some areas peak or higher eclectic power consumption was observed during summer. This leads large consumption of fossil fuels for power generations. Using non-renewable energy leads to higher emissions of GHG like CO_2 [2].

To alleviate/lessen energy consumption in the building sector and improve GHG, by ensuring good thermal comfort for the occupant in their locals is mandatory. So the use of renewable energy and development of clean, efficient and eco-friendly is recommended to develop one counter'. Among these technologies, liquid desiccant technology is cited for problems as a possible solution. Use of available

resources and developing systems to satisfy needs is indicated in Fig.1.
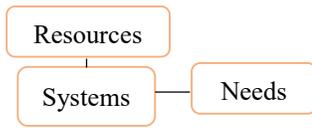
FIGURE 1. THREE BLOCK DIAGRAM TO USE AVAILABLE RESOURCES

Desiccant dehumidification system is energy efficient and allow a better indoor air quality. Desiccant dehumidification is profitable in handling humidity (latent heat), easy to be reactivated with low-grade energy, like solar energy.

The exploitation of heat produced by solar collectors is a motivating option for thermal driven desiccant air conditioning processes. It is a good solution to promising to lessen environmental impact. Internationally energy consumption is more depends on fossil fuels viz. petroleum, natural gas and coal those energies are depreciating from time to time and increase in price addition to an environmental problem. These issues make of energy, environment and technology are interrelated as shown in the Fig. 2.

These situations have become global economic, political, and technological issues. Hand in hand solutions for these problems are a must to attain a common goal.
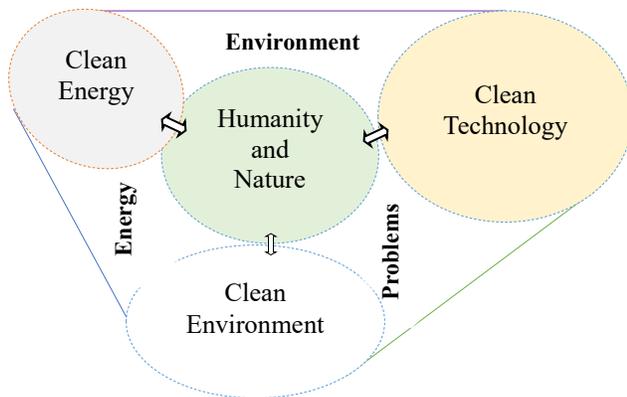
FIGURE 2. ENERGY, ENVIRONMENT AND TECHNOLOGIES RELATIONSHIP BETWEEN NATURE AND HUMANITY SURVIVAL [3]

1.2 Thermal Comfort Factors and Initiators

ASHRAE defines comfort is "the condition of mind that expresses satisfaction with the thermal environment; it requires subjective evaluation". A number of variables and parameters that affect heat dissipation from the body (thus also thermal comfort) can be categorized into three sets: which is indicated in Fig.3. For controlling of indoor air temperature and relative humidity for the human comfort divides the building's cooling load into the sensible and latent load respectively [3].

The latent load is more dominant in hot and humid environments and there is an essential for air conditioning system to effectively handle the latent loads. Fig.4 are initiators for renewable energy developments for various application like air conditioning.
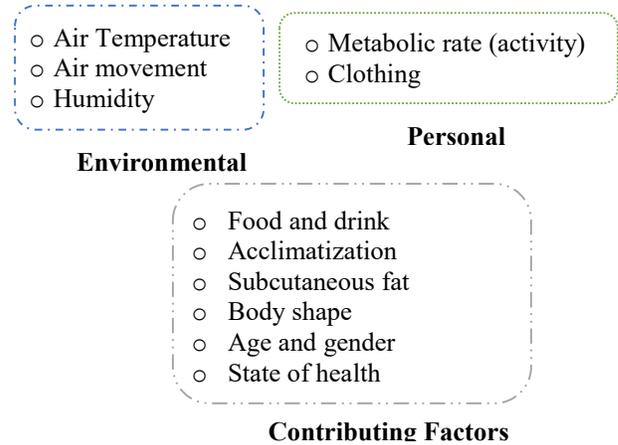
FIGURE 3. FACTORS HUMAN THERMAL COMFORT
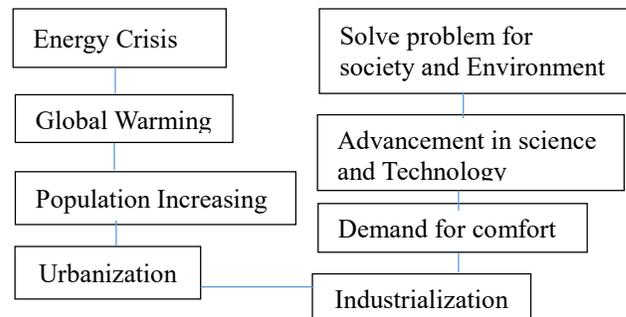
FIGURE 4. TERMS INITIATE FOR RESEARCH

2. DESICCANTS

A desiccant a substance that is natural or synthetic has capable of showing a strong attraction for moist air. It is either liquid or solid, some of the desiccants and their respective costs are shown in the Fig.5 and Tab.1.
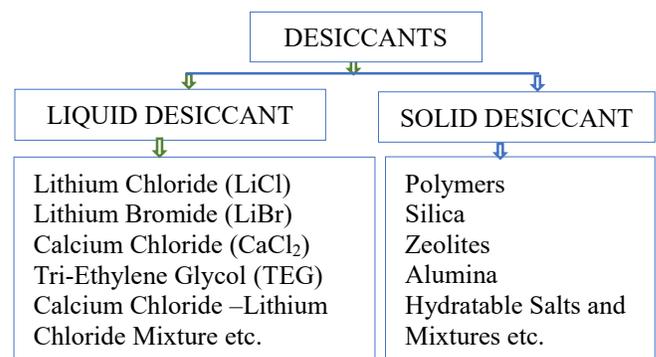
FIGURE 5. SOME EXAMPLES OF DESICCANTS [4]

TABLE 1. PRICES OF A COMMONLY USED SOLID DESICCANT FORM OF SALTS AS ASIAN SUPPLIER IN 2009 [4].

Liquid Desiccants	Salt forms	Price per metric ton (USD)
LiCl	anhydrous	7400
$CaCl_2$	Dehydrate	284
LiBr	anhydrous	3660
$MgCl_2$	hexahydrous	155
TEG	-	-
HCOOK	-	Cheaper
$CaCl_2$-LiCl	-	lower by 30% than LiCl

2.1 Liquid Desiccant Materials Properties

The strength of a liquid desiccant can be measured by its equilibrium vapor pressure, which is water vapor pressure that is in equilibrium with the liquid desiccant material. The vapor pressure exponentially increases with the temperature of the water or desiccant and also increases as the water is absorbed by the desiccant, that is, equilibrium vapor pressure will be higher for a dilute liquid desiccant than a concentrated one [5-8].

Some other parameters which indicate desiccant materials performance are: Energy storage density, the temperature for regeneration, BPE, Availability, low vapour pressure, low crystallization point and high density and being cost effective. A good desiccant should have the following properties: large saturation absorption capacity, low regeneration temperature, low viscosity, high heat transfer, non-volatile, non-corrosive, odourless, Non-toxic, Non-flammable, Stable and inexpensive Cost [9-10].

2.3 Major Applications

Some spaces, control temperature and humidity are required in order to avoid growth of fungi and bacteria which affects human health. Some main applications of liquid desiccant dehumidification viz.: residential, supermarkets, theatres, hospitals, hotels, office buildings, indoor swimming pools and pharmaceutical manufacturing plants.

3. METHODOLOGY

3.1 Experimental Procedure

The experimental set up was done on the roof of the building of IIT Roorkee, Department of Mechanical and Industrial Engineering East block was indicated in Fig.8. dehumidifier, regenerator, Marquise Shaped Channel Flat Plate Solar Collector (Fig.6 and Fig.7), flow meter, pumps, fan, and thermal hygrometer- mode l605i, thermocouples, and data logger and it was shown fig 9. Dehumidifying process air using a $CaCl_2$ solution of concentration 40% by mass. Solar energy is used to reactivate the solution to continuously operate. The water passing through collector is getting heat and used for regeneration and solar collector temperature data was taken by the data logger and the graph

is drawn using excel to analysis the results. The dehumidification and regenerator were plotted in the graph to analyze the experimental results.
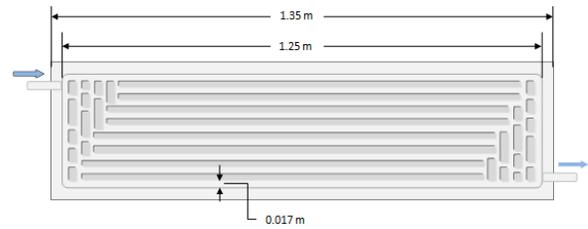
FIGURE .6 MARQUISE SHAPED CHANNEL FLAT PLATE SOLAR COLLECTOR.
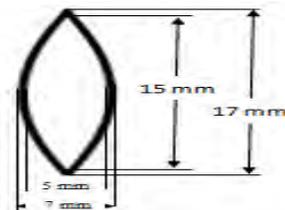
FIGURE.7 MARQUISE SHAPED CHANNEL.
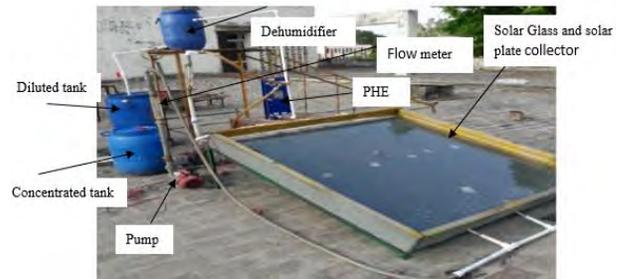
FIGURE 8. PHOTOGRAPHIC VIEWS OF EXPERIMENTAL SET-UP.
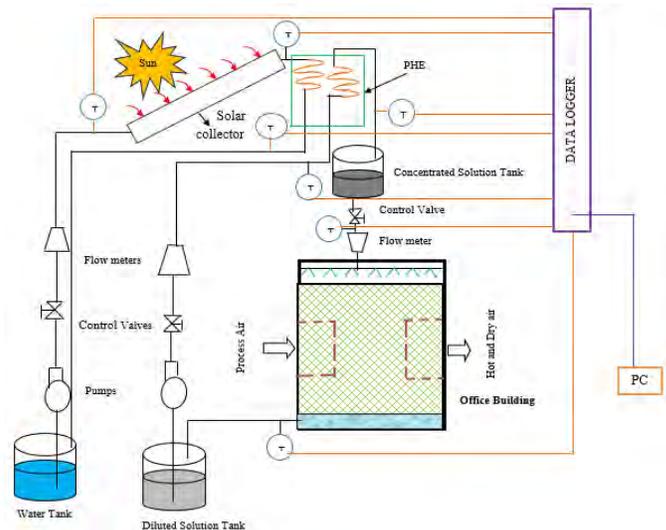
FIGURE 9. SCHEMATIC LINE DIAGRAM FOR THE EXPERIMENT.

3. RESULTS AND DISCUSSIONS

The solar assisted regeneration for dehumidification is used for air conditioning was done to observe and analyze the visibility of solar energy to regenerate desiccants and to work continuously for house comfort. The experiment was done in the month of May after running the experiment for two hours from11:00am to 1pm and the average data was used where the maximum solar radiation is seen and the average data was taken. The water and $CaCl_2$ solution flow rate were maintained at 2.5 LPM are used.
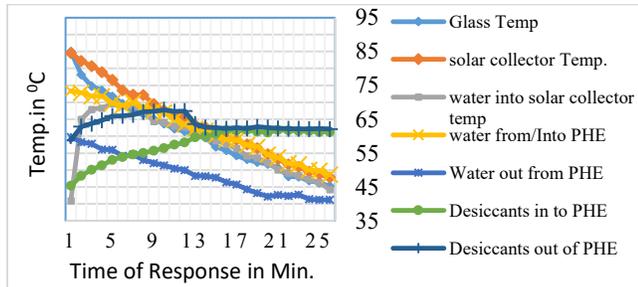
FIGURE 5. SOLAR COLLECTOR TEMPERATURE, WATER TEMPERATURE AND DESICCANT REGENERATED IN PHE.

From Fig. 10. desiccant regeneration is higher for one hour and stable after one hour and the desiccant temperature into PHE is also increasing simultaneously for one hour and almost stable after one hour. The plate temperature, glass temperature and water out of PHE is higher for one hour and decreasing slowly. Whereas the water into glass solar collector temperature is increasing initial.
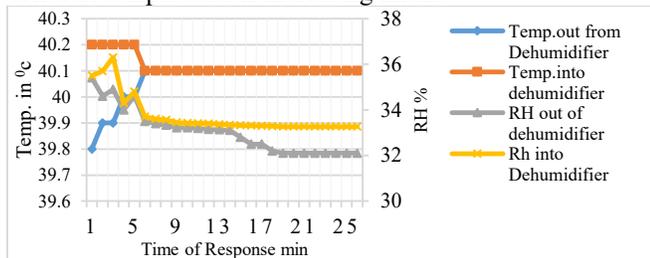
FIGURE6. RELATIVE HUMIDITY AND TEMPERATURE DISTRIBUTION IN DEHUMIDIFIER.

From the Fig.11. temperature into the dehumidifier is higher in the initial 40 minutes and whereas the temperature out is getting lower and becomes almost stable after one-hour experimental running. The humidity of process air entering to the dehumidifier is getting lower from the first running and increasing in the reduction of humidity from the process air due to the absorption by the $CaCl_2$ solution. So, RH from the dehumidifier is lower as compared to process air.

CONCLUSIONS

Experimental set up using 40% by mass of $CaCl_2 \cdot H_2 0$ is installed at Department of Mechanical and Industrial Engineering, IIT Roorkee. The Marquise Shaped Channel Flat Plate Solar Collector solar assisted regeneration for

dehumidification is used. The desiccant regeneration is higher for one hour and then stable. Also, the desiccants temperature into PHE is also increasing for the first one hour and then almost stable. RH leaving from the dehumidifier is lower as compared to entering but lower RH% reduction is observed due to lower RH in ambient air.

REFERENCES

[1] K. Gommed, G. Grossman, Experimental investigation of a liquid desiccant system for solar cooling and dehumidification, Solar Energy 81 (2006) 131-138.

[2] P. Bourdoukan, E. Wurtz P. Joubert, Experimental investigation of a solar desiccant cooling installation, Solar Energy 83 (2009) 2059–2073.

[3] Enteria N, Yoshino H, Mochida A, Takaki R, Satake A, Yoshie R, Mitamura T, Baba S. Synergization of clean energy utilization, clean technology development and controlled clean environment through the thermally activated desiccant cooling system. In: Proceedings of the 2nd international conference on energy sustainability; 2008.

[4] Afshin M. Selection of the liquid desiccant in a run-around membrane energy exchanger M.Sc. thesis]. Saskatoon: University of Saskatchewan; 2010. (ttp://ecommons.usask.ca/handle/10388/etd 05262010-175310).

[5] Sanjeev Jain, P.K. Bansal, Performance analysis of liquid desiccant dehumidification systems, International Journal of Refrigeration 30 (2007) 861- 872.

[6] ASHRAE Handbook-Fundamentals. Sorbents and desiccants. Atlanta, GA: American Society of Heating, Refrigeration and Air-Conditioning Engineers, Inc.; 2005

[7] Ertac Hurdogan, Orhan Buyukalaca, M. Tolga Balta, Arif Hepbasli, Tuncay Yılmaz, Experimental exergoeconomic assessment of a desiccant cooling system, Energy Conversion and Management 69 (2013) 9–16.

[8] S. Bouzenada, C. Mc Nevinb, S. Harrison, A. N. Kaabid, An experimental study on the dehumidification performance of a low- flow falling-film liquid desiccant air-conditioner, Procedia Computer Science 52 (2015) 796 – 803.

[9] W. Kessling, E. Laevemann and C. Kapfhammer, Energy storage for desiccant cooling systems component development, Solar Energy Vol. 64, Nos 4–6, (1998) 209–221.

[10] A.S.A.Mohamed, M.S.Ahmed, A.A.M. Hassan, M.Salah Hassan, Performance evaluation of gauze packing for liquid desiccant dehumidification system, Case Studies in Thermal Engineering 8 (2016) 260–276

SEEC-2018-095

THERMODYNAMIC ANALYSIS OF LIGNITE GASIFICATION IN THE DOWNDRAFT GASIFIER

Darshit S. Upadhyay
Mechanical Engineering Department,Institute of Technology, Nirma University - Ahmedabad
Email: darshit.upadhyay@nirmauni.ac.in

Anil Kumar V. Sakhiya
Mechanical Engineering Department,Institute of Technology, Nirma University - Ahmedabad
Email: anilkumar.sakhiya@gmail.com

Krunal R. Panchal
Mechanical Engineering Department,Institute of Technology, Nirma University - Ahmedabad
Email: 16mmet11@nirmauni.ac.in

Rajesh N. Patel
Mechanical Engineering Department,Institute of Technology, Nirma University - Ahmedabad
Email: rnp@nirmauni.ac.in

ABSTRACT

Thermodynamic analysis such as energy and mass balance and exergy efficiency were carried out for different particle size of lignite in present work. A pilot scale 10 kW_e downdraft gasifier was used. Six particle sizes of lignite such as 13-16 mm, 16-19 mm, 19-22 mm, 22-25 mm, 25-28 mm and 28-31 mm were identified for thermodynamic analysis. Mass balance closure (MBC) and energy balance closure (EBC) were found in the range of 0.95-1 and 0.90-0.95 respectively. Exergy efficiency was remaining in the range of 23.66 % - 29.64 % for all selected particle sizes. Exergy efficiency was found maximum with 22-25 mm particle size of lignite.

Keywords: Lignite, Downdraft gasifier, Particle size, Energy and mass balance, Exergy efficiency

INTRODUCTION

Energy is the most crucial component of infrastructure for the growth and welfare of a nation. As a developing country, around 70 % population in India lives in villages. Out of this, about 77% villages which are either fully or partially electrified are getting unreliable or limited access and poor quality of power [1]. The major problem occurring in electrification of villages is the high cost of supplying electricity due to considerable losses in transmission and distribution. Furthermore the cost of grid extension in remote areas is economically unfeasible. The share of electricity generation from coal is about 59.9% [2]. India has about 308.802 billion tonnes of coal reserves. Lignite reserves was estimated around 44.59 billion tonnes as per the geological survey of India [3]. But still the lignite resources is not exploited much due to its poor quality (high moisture content, high ash content and low calorific value) and stability issues occurring during storage [4].

The objective of the current work focuses on investigating the thermodynamic analysis of lignite as feedstock for the gasifier with different particle sizes. The particle sizes on which the experiments were conducted are 13-16 mm, 16-19 mm, 19-22 mm, 22-25 mm, 25-28 mm and 28-31 mm [5]. In the present work, influence of different particle sizes of lignite on the downdraft gasifier performance in terms of mass balance, energy balance and exergy analysis is reported.

EXPERIMENTAL SETUP

The experiments were carried out in a pilot-scale 10kW_e downdraft gasifier as shown in Fig. 1. It consists of downdraft gasifier (reactor), gas conditioning system (water scrubber, saw dust filled surge tank and fabric filter) and flow measuring device. [5]. The K type (Chromel-Alumel) thermocouples were used for measuring the temperature of various zones of a gasifier. The gas flow rate was measured using an orifice meter (error within $\pm 3 Nm^3\ h^{-1}$). The gas analysis was carried out on gas chromatography (GC 2010, Shimadzu) to measure concentration of CO, CO_2, H_2, N_2 and CH_4 gases [6].
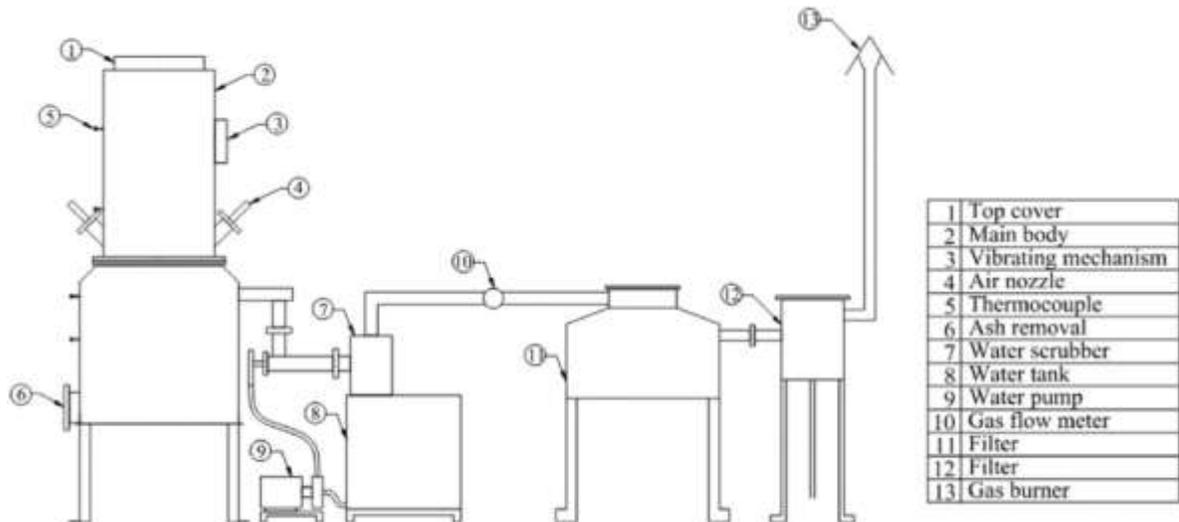
FIGURE 1. SCHEMATIC DIAGRAM OF THE 10 KWE DOWNDRAFT GASIFIER SYSTEM

TABLE 1: MASS BALANCE OF THE LIGNITE GASIFICATION

Particle Sizes (mm)	Inputs (kg h^{-1})			Outputs (kg h^{-1})					MBC ratio
	Fuel	Air	Total	Dry gas	Char	Water	Ash	Total	
13-16	10.67	18.31	28.98	24.86	0.30	1.80	1.65	28.61	0.98
16-19	10.55	18.23	28.78	23.77	0.28	1.82	1.63	27.50	0.95
19-22	10.25	18.01	28.26	24.03	0.27	1.89	1.57	27.76	0.98
22-25	10.01	17.66	27.67	22.99	0.23	1.79	1.54	26.55	0.95
25-28	9.86	17.45	27.31	23.05	0.22	1.73	1.48	26.48	0.96
28-31	9.72	17.10	26.82	23.14	0.15	1.68	1.46	26.43	0.98

MASS BALANCE

The conservation of mass must be satisfied in the gasifier system. The basic mass balance equation used for the gasification process is:

$$m_{fuel} + m_{air} = m_{gas} + m_{char} + m_{tar} + m_{ash} + m_{water} \quad (1)$$

where m_{fuel} and m_{air} in the above equation (Eqn. (1)) represents the fuel consumption rate of lignite and mass flow rate of air in a gasifier respectively. m_{char}, m_{tar}, m_{ash} and m_{water} represents the mass flow rate of producer gas, char, tar, ash and water formed in the gasification process respectively. The fuel consumption was calculated by marking the initial position and final position of the feedstock in a reactor and taking the bulk density of the feedstock measured using the test method IS 7190-1974 [5]. The mass flow rate of producer gas calculated by using following equation:

$$m_{gas} = \frac{m_{fuel} \times (Gas\ yield\ (Nm^3\ kg^{-1}))}{Gas\ production\ time(hr)} \quad (2)$$

The mass of char and ash was measured by weighing the material formed at the ashpit (below grate) of the gasifier. The mass of
water represents the moisture content of producer gas. The material formed at the bottom of the gasifier. The mass of water represents the moisture content of producer gas. The

water represents the moisture content of producer gas. The mass balance for different particle sizes is shown in Tab. 1. As mass of tar content in producer gas was very less, it was neglected. Mass of fuel, air and dry gas were decreased as particle size increased. It is due to the fact that smaller particle size has higher surface area which may react with larger quantity of air. Water content in producer gas with all particle sizes was not uniform. It is because of different relative humidity content during various experiments. Ash content is highly depending on fuel consumption. Char content decreased with increasing of particle size of lignite. MBC ratios for all selected size of lignite were in the range of 0.95 to 1.

ENERGY BALANCE

The Energy balance was carried out by using the following equation:

$$E_{fuel} + E_{air} = E_{gas} + E_{char} + E_{tar} + E_{ash} + E_{water} + E_{losses} \quad (3)$$

Where, E_{fuel} and E_{air} represents the energy inlet of a gasifier respectively. E_{gas}, E_{char}, E_{ash}, E_{water} and E_{losses} represents the energy outlet to the gasifier. The energy rate of the fuel was calculated using following equation:

$$E_{fuel} = m_{fuel} \times LHV_{fuel} \qquad (4)$$

Where, m_{fuel} is the lignite consumption of a gasifier, LHV_{fuel} is the lower heating value of lignite. Gas compositions were obtained by gas chromatograph and LHV was calculated by using formula given by T Reed [6]. The energy content of the air flow is calculated using the equation (Eqn. (5)):

$$E_{air} = m_{air} \times Cp_{air}(T_{air} - T_{ref}) \qquad (5)$$

Where, m_{air} represents the mass flow rate of air and Cp_{air} is the specific heat of air, T_{air} and T_{ref} (298.15 K) are the inlet air temperature and reference temperature respectively. The total energy of producer gas includes the physical energy and its chemical energy. The following equation (Eqn. (6)) was used to calculate the chemical energy of the producer gas:

$$E_{gas-chemical} = m_{gas} \times \frac{LHV_{gas}}{\rho_{gas}} \qquad (6)$$

Where, ρ_{gas} represents the producer gas density, LHV_{gas} represents the heating value of producer gas. The physical energy of producer gas was calculated using equation:

$$E_{gas-physical} = m_{gas} \times h_{gas} \qquad (7)$$

Where, h_{gas} represents the specific enthalpy of producer gas. The specific enthalpy of the producer gas was calculated by using the correlation as in Eqn. (8) between enthalpies and mole fractions of the gas components i.e. N_2, H_2, CO_2, CH_4 and CO:

$$h_{gas} = \sum_{i=1}^{n} h_{oi} + y_i h_i \qquad (8)$$

Where, h_{oi} and h_i represents the specific enthalpy of dead state and enthalpy at a specific temperature respectively for i^{th} component of gas, y_i represents the mole fraction of various gas components. The energy content of char and ash were calculated using Eqn. (9) and Eqn. (10) respectively.

$$E_{char} = m_{char} HHV_{char} \qquad (9)$$
$$E_{ash} = m_{ash} Cp_{ash} dT \qquad (10)$$

Where, Cp_{ash} is specific heat of ash and it is calculated using the following correlation:

$$Cp_{ash} = K_0 + K_1 T^{-0.5} + K_2 T^{-2} + K_3 T^{-3} \qquad (11)$$

Where, the coefficients of the Eqn. (11) are taken from the literature [8]. Energy of fuel is depending on LHV and fuel consumption.

As LHV remains same for different particle sizes of lignite, hence energy of fuel depends only on fuel consumption. It was observed that the energy from ash found higher when smaller size lignite used as a feedstock. It is due to the fact that smaller particle size of lignite produces higher ash. ECB ratio was found in the range of 0.90 to 0.95.

EXERGY ANALYSIS
Exergy analysis was carried out for the gasification process of lignite with various particle size. Exergy efficiency or second law efficiency is defined as a ratio of exergy of producer gas to sum of exergy of lignite and gasification medium (air). The equation used for calculating the second law efficiency is:

$$\eta_{ex} = \frac{\emptyset_{gas}}{\emptyset_{lignite} + \emptyset_{medium}} \qquad (12)$$

In current analysis, air was used as an oxidizing medium. The air was supplied to the gasifier at atmospheric condition; hence its exergy was neglected. Total exergy is defined as:

$$\emptyset_{x,total} = \emptyset_{x,t-mech} + \emptyset_{x,chem} \qquad (13)$$

The specific thermo-mechanical exergy for different gas species can be calculated using Eq. (14).

$$\emptyset_{x,t-mech} = (h - h_o) - T_o(s - s_o) \qquad (14)$$

Where, h and s represents the enthalpy and entropy at the specified temperature and specified pressure, while h_0 and s_o are dead state enthalpy and entropy respectively (T_o = 298.15 K, P_o =1 atm).
To calculate standard chemical exergy of ideal gas fluid, following Eq. (15) was used:

$$\emptyset_{x,chem} = \sum_i x_i \emptyset_{ch,i} + RT_o \sum_i x_i \ln x_i \qquad (15)$$

where, x_i represents mole fraction of ith species and R is the universal gas constant (R=8.314 $g\ mol^{-1}$), $\emptyset_{ch,i}$ is standard chemical exergy of ith species in $kJ\ kmol^{-1}$. The standard chemical exergy of various gases is reported in literature [10]. The standard chemical exergy of lignite can be calculated using Eqn. (16) [11].

$$\emptyset_{fuel} = (LHV_{fuel} + 2442 \times W_{fuel})\beta \qquad (16)$$

Where, LHV_{fuel} is the lower heating value of the lignite and W_{fuel} is the mole fraction of the moisture present in lignite, β is the ratio of standard chemical exergy to LHV of lignite which is expressed by:

$$\beta = \frac{1.0438 + 0.1882\frac{m_H}{m_C} - 0.2509\frac{m_O}{m_C}\left[1 + 0.7256\frac{m_H}{m_C}\right] + 0.383\frac{m_N}{m_C}}{1 - 0.3035\frac{m_O}{m_C}} \qquad (17)$$

Where, m_H, m_c, m_o and m_N are mass fraction of hydrogen, carbon, oxygen and nitrogen of lignite. Thermo-mechanical and chemical exergy for different particle size of lignite is shown in figure 2. Exergy of different particle size of lignite remains constant as exergy doesn't depend on size of feedstock. Thermo- mechanical efficiency is generally dependent on enthalpy and entropy of the producer gas. Higher temperature in combustion zone with smaller particle size of lignite was responsible for higher thermo-mechanical exergy of 13-16 mm lignite and lesser for 28-31 mm lignite size. lignite and

TABLE 2: ENERGY BALANCE OF THE LIGNITE COAL GASIFICATION

Particle Size (mm)	Energy in (MJ/hr)			Energy Out (MJ/hr)					EBC
	Fuel	Air	Input	Producer Gas	Char	Ash	Water	Output	%
13-16	164	0.257	154.01	137.54	3.64	0.125	3.34	144.64	93.92
16-19	162	0.293	162.29	139	3.65	0.123	4.01	146.78	90.44
19-22	157.44	0.271	159.85	136.36	3.34	0.119	5.01	144.82	90.59
22-25	153.75	0.257	154.01	134.60	3.17	0.117	4.59	142.47	92.51
25-28	151.44	0.243	151.68	128.93	5.23	0.112	3.72	137.99	90.97
28-31	149.3	0.242	149.54	126.23	4.91	0.110	3.73	134.98	90.26

lesser for 28-31 mm lignite size. Chemical exergy was generally depending on exergy of individual producer gas species. As combustible product such as H_2, CO in producer was higher with 22-25 mm particle size of lignite feedstock, its chemical exergy was found higher comparatively. Thermo-mechanical and chemical exergy curves were intersected on 22-25 mm lignite size, shown optimum particle size of lignite among selected particle sizes of lignite which was shown in figure 2. This result was inline with higher exergy efficiency as per figure 2 and higher cold gas efficiency [7] for 22-25 mm lignite particle size. Exergy efficiency was calculated and remains in the range of 23.66% - 29.64 % for all selected particle sizes of lignite.

CONCUSIONS

Energy and mass balance were carried out for six different particle sizes of lignite. Closure ratio of energy and mass balance were found in the range of 0.90-0.95 and 0.95-1 respectively. Exergy efficiency was in the range of 23.66% - 29.64 %. 22-25 mm particle size of lignite has maximum exergy efficiency among selected feedstocks.

ACKNOLEDGEMENTS

Authors are thankful to Dr. Vimal R Patel for giving valuable suggestions in thermodynamic analysis.

REFERENCES

[1] Deen Dayal Upadhyaya Gram Jyoti Yojana (2017) http://www.recindia.nic.in/ddugjy. Assessed on 21st August 2017

[2] Government of India, Ministry of Power, Central Electricity Authority, New delhi; 2017, http://www.cea.nic.in/reports/ monthly/ executivesummary /2017/exe_summary-01.pdf, pg-39; Assessed on 23rd August 2017

[3] Annual report, Ministry of coal, Government of India; 2016-17, http://coal.nic.in/sites/upload_files/coal/files/coalupload_/chap1AnnualReport1617en.pdf Assessed on 16th July 2017
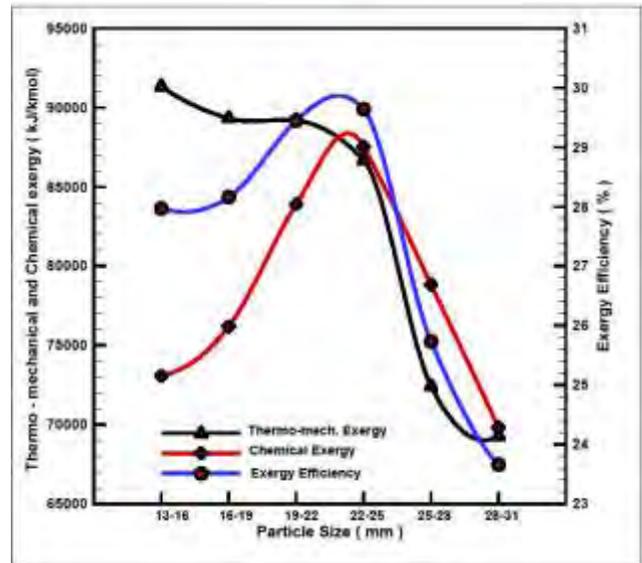
FIGURE 2. THE THERMO-MECHANICAL AND CHEMICAL EXERGY OF LIGNITE FOR DIFFERENT PARTICLE SIZES.

[4] Mike CF, Theovan L (2017) A review of the history of coal exploration, discovery and production in Indonesia: The interplay of legal framework, coal geology and exploration strategy, International Journal of Coal Geology; 178:56-73.

[5] Patel VR, Upadhyay DS, Patel RN (2014) Gasification of lignite in a fixed bed reactor: Influence of particle size on performance of downdraft gasifier. Energy; 78:323-32.

[6] Reed TB, Das A. Handbook of biomass downdraft gasifier engine systems. SERI 1998

[7] Patel VR, Patel DR, Varia NA, Patel RN (2017) Co-gasification of lignite and waste wood in a pilot-scale (10 kWe) downdraft gasifier. Energy; 119:834-44.

[8] Cengel YA, Boles MA.(1994) Thermodynamics: an engineering approach. New York: McGrawHill, Inc.;

[9] Truls G (2009).The introduction to the concept of exergy and energy quality. Norway : Springer ;

[10] Kotas TJ.(1985) The exergy method of thermal plant analysis. London: Butterworths

SEEC-2018-096

Kinetic Modelling and Experimental Study of Small Esters: Methyl Acetate and Ethyl Acetate

Ahfaz Ahmed, S. Mani Sarathy

Clean Combustion Research Center, King

Abdullah University of Science and Technology-

Saudi Arabia

Marco Mehl, Scott Wagnon, William J. Pitz

Lawrence Livermore National Laboratory,

Livermore, United States of America

Nitin Lokachari, Henry Curran

Combustion Chemistry Center,

National University of Ireland,

Galway, Ireland

Abstract

A detailed chemical kinetic mechanism comprising methyl acetate and ethyl acetate has been developed based on the previous work by Westbrook et al. [1]. The newly developed kinetic mechanism has been updated with new reaction rates from recent theoretical studies. To validate this model, shock tube experiments measuring ignition delay time have been conducted at 15 & 30 bar and equivalence ratio 0.5, 1.0 and 2.0. The new mechanism shows significant improvement in prediction of experimental data over earlier model across the range of experiments.

***Keywords**: Esters, Ignition delay, kinetic modelling*

1 Introduction

Global energy trends show continuous increase in consumption of bio-based fuels for transportation sector [2]. This trend supports growing efforts to mitigate climate change by offsetting the consumption of fossil fuels. At present, a wide variety of bio- based fuels are proposed as alternatives to fossil fuels. Esters represent one such an important class of bio-derived fuels with potential to supplement gasoline as well as diesel fuel supply. While longer chain esters such as methyl oleate, methyl linoleate etc. are found suitable for diesel engine applications [3], smaller esters with higher RON values are found suited to gasoline range applications [4]. In principle, esters can be synthesized using various feasible

pathways including vegetable oils, animal fats [5], algae [6] etc. Esters as a bio-based fuel makes an attractive alternative to fossil fuels due to its suited combustion properties and with proven synthesis pathways. However in the literature, there has been more focus on larger esters [3] and studies on combustion characteristics of smaller esters are limited. In past a couple of flame studies have been conducted with these fuels by Gasnot *et al.* [7], Dayma *et al.*[8] and Badawy *et al.*[9] in which various parameters like flame speeds, low pressure oxidation were investigated, Gasnot *et al.* [7] also proposed a kinetic model. There have been a few studies investigating ignition behavior of these fuels, Zhang *et al.* [10] studied high temperature ignition of methyl acetate in a shock tube and developed a kinetic mechanism. Kumegh *et al.* [11] also studied the high temperature ignition of methyl acetate and ethyl acetate in a shock tube, and proposed a kinetic model entailing these fuels. There is another work by Yang *et al.* [12] studying pyrolysis and oxidation of methyl acetate in low pressure flames, a mechanism was also proposed. There have been some other attempts to study these fuels blends in engines [13, 14] as well. Additionally, there have been some theoretical studies discussing the rates of H atom abstraction from fuel [15], decomposition of fuel [16] and fuel radicals [17].

In this study, a detailed chemical kinetic model for methyl and ethyl acetate has been developed. This model is advanced from the mechanism proposed for laminar premixed flames by Westbrook and coworkers in 2009 [1]. Acetates studied in this work are both high RON fuels

with suitable physical and chemical properties [Table 1] to be considered as potential fuels in advanced gasoline engines [4]. Shock tube experiments measuring ignition delay time have been conducted at 15 & 30 bar and equivalence ratio 0.5, 1.0 and 2.0. Another set of experiments measuring laminar burning velocity have also been performed on a heat flux burner at atmospheric pressure over wide range of equivalence ratios. The model developed in this work shows good agreement with ignition data across the temperature and equivalence ratio range respectively.

Fuel	RON	MON	Density [Kg/m3]	LHV [KJ/Kg]
Methyl acetate	120	120	927.4	17.9
Ethyl acetate	118	120	894.6	21.34

Table 1: Properties of Methyl acetate and Ethyl acetate[4]

2 Experiments

2.1 High Pressure Shock Tube [HPST]

The high temperature (1000-1400 K) ignition delay data in HPST has been measured behind reflected shock wave at 15 and 30 bar and equivalence ratio 0.5, 1.0, 2.0. This shock tube is made of 9 m long section of steel with uniform cross-section of 63.5 mm inner diameter. The length of shock tube is divided into three sections; driver section [3 m], driven section [5.7 m] and a section with double diaphragm. This double diaphragm section [30 mm] separates the driver and driven section and enables improved control of the generated shock wave. In this study helium or mixture of helium and nitrogen is used as driver gas in the shock tube during the experiments. During experiments, pressure-time histories are measured using the Kistler 603B pressure transducer mounted on the end wall. The ignition delay in the HPST is defined as the time interval between two sharp pressure rises; one of them due to the shock wave reaching the end-wall and other due to initiation of ignition. The acceptable error for the measured pressures behind the reflected shock wave was ±0.5 bar. The NUI Galway HPST has been further discussed in detail in Nakamura et al.[18]

3 Kinetic Modelling

Detailed chemical kinetic mechanism has been developed for methyl and ethyl acetate based on previous work by Westbrook et al [1]. The former mechanism has been updated with additional reaction rates and reaction classes based on theoretical calculations and structurally similar molecules. In present work Aramcomech 2.0 [19] has been used as the base chemistry.

3.1 Methyl acetate

Kinetic reaction scheme of methyl acetate comprises of H abstraction reactions followed by decomposition of fuel and fuel radical. Rates of H abstraction reaction by OH

and HO_2 are calculated in this work by Dr. Carlo Cavallotti [politecnico di Milano] at CCSD(T) energy levels. However H abstractions by H, O, CH_3 are taken from Tan et al. [15]. The fuel decomposition rates are taken from Peukert et al. [16] and the fuel radical decomposition reaction rates are from another study by Tan et al. [17]. In the reaction scheme the decomposition of fuel and the fuel radicals lead to formation of formaldehyde and some unstable radicals eventually producing CH_3, CO and CO_2 as shown in Fig.1. Further consumption of formaldehyde and other products has been dealt in the base chemistry reactions.
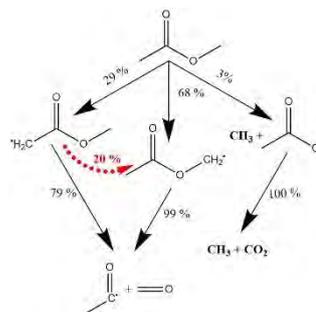
FIGURE 1: REACTION PATH ANALYSIS OF METHYL ACETATE AT 10% OF FUEL CONVERSION TIME. P=15 BAR, 1200 K AND PHI =1.

3.2 Ethyl acetate

The kinetic mechanism of ethyl acetate involves additional reaction pathways as compared to methyl acetate, owing to its relatively larger size. Its oxidation chemistry comprises of unimolecular fuel decomposition and H abstraction reactions by various radicals from fuel. The unimolecular decomposition of ethyl acetate has been studied by Swihart et al.[20] using pulsed laser powered homogeneous pyrolysis. They utilized this technique for studying rates of gas phase decomposition reactions. The measurements revealed that the major products of breakdown are acetic acid and ethene. The chemistry of acetic acid involves H atom abstraction followed by fuel radical decomposition. The ethene chemistry is described in detail within the base chemistry and is not discussed here. Some other minor products were also observed as a
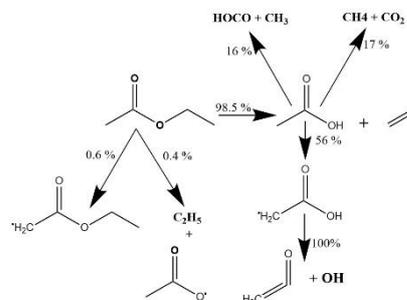
FIGURE 2: REACTION PATH ANALYSIS OF ETHYL ACETATE AT 10% OF FUEL CONVERSION TIME. P=15 BAR, 1200 K AND PHI =1.

result of abstraction of primary, secondary H atoms and breakage of methyl, ethyl groups from the fuel molecule. The fuel radicals produced after H atom abstractions along with products of decomposition of C-H bond further

undergoes radical decomposition to produce smaller radicals. Figure 2 describes major reaction pathways in the oxidation chemistry of ethyl acetate. The kinetic mechanism developed in this work only deals with high temperature chemistry as both the experiments discussed in this work are conducted in the high temperature region. The thermodynamic properties are retained from the previous work [1] The transport parameters are recalculated in this work using correlations from Wang *et al*. [21] and Dooley *et al*. [22].

4 Results

The proposed kinetic mechanism has 1958 species and 8098 reactions. Aramcomech 2.0 [19] has been used as base mechanism and all the species with 6 carbon and less have been retained to allow complete account of reactivity. As explained in the experimental sections, ignition and burning velocity data have been acquired at NUI Galway and Lund University, respectively. In this section comparison of developed mechanism is presented with experimental data. The simulations have been performed using Chemkin Pro 18.1. Shock tube simulations were performed with closed homogenous batch reactor model. The ignition delay simulations for methyl acetate and measured data is shown in Fig. 3 and 4. It is evident that the newly proposed model captures the ignition data quite well across all equivalence ratios, pressure and temperature ranges. While the model detailed in [1] under predicts the ignition across all conditions. Comparisons of ignition data and simulations for ethyl acetate is presented in Fig. 5 and 6. Here the old model by Westbrook et al. under predicts the ignition delay at high temperature and over predicts ignition delay at temperatures lower than 1150 K.
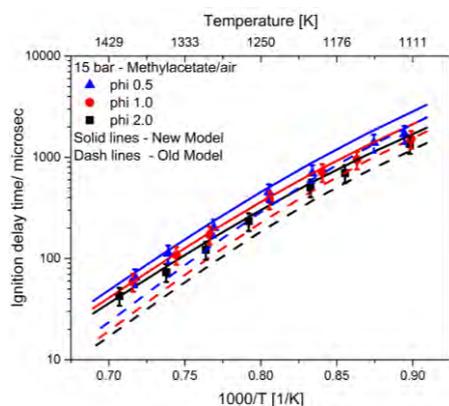
FIGURE 3: COMPARISON OF METHYL ACETATE IGNITION DELAY DATA WITH PROPOSED MODEL AND MODEL BY WESTBROOK ET AL.
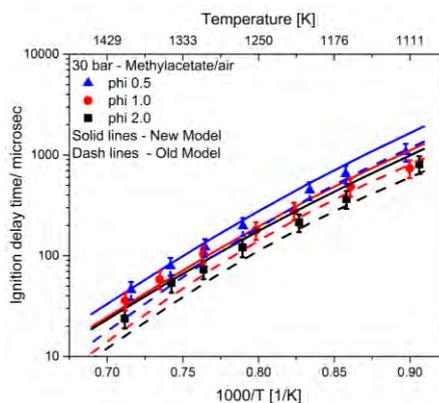
FIGURE 4: COMPARISON OF METHYL ACETATE IGNITION DELAY DATA WITH PROPOSED MODEL AND MODEL BY WESTBROOK ET AL.
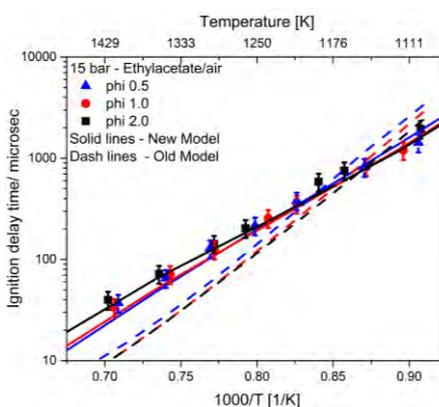
FIGURE 5: COMPARISON OF ETHYL ACETATE IGNITION DELAY DATA WITH PROPOSED MODEL AND MODEL BY WESTBROOK ET AL.
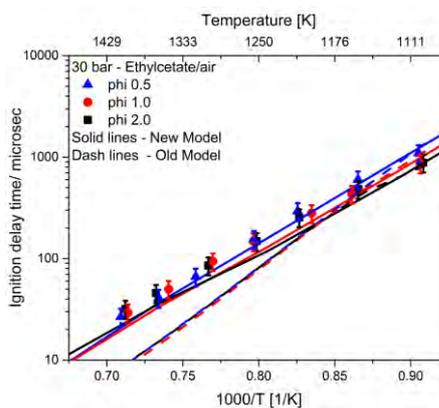
FIGURE 6: COMPARISON OF ETHYL ACETATE IGNITION DELAY DATA WITH PROPOSED MODEL AND MODEL BY WESTBROOK ET AL.

5 Conclusions

A detailed mechanism for small esters, methyl acetate and ethyl acetate has been developed. Experiments were conducted to measure ignition delay time at NUI Galway. Comparisons between the model and experimental data is conducted and model was found to agree well with the experimental data over the entire experimental range. The

modifications made in the mechanism could not be presented here due to limitation of space. The corresponding author could be contacted for obtaining the mechanism and thermochemistry data files.

References

[1] C.K. Westbrook, W.J. Pitz, P.R. Westmoreland, F.L. Dryer, M. Chaos, P. Osswald, K. Kohse-Höinghaus, T.A. Cool, J. Wang, B. Yang, N. Hansen, T. Kasper, A detailed chemical kinetic reaction mechanism for oxidation of four small alkyl esters in laminar premixed flames, Proc. Combust. Inst. 32 (2009) 221-228.
[2] 2017.
[3] J.Y. Lai, K.C. Lin, A. Violi, Biodiesel combustion: advances in chemical kinetic modeling, Prog. Energy Combust. Sci. 37 (2011) 1-14.
[4] R.L. McCormick, G.M. Fioroni, L. Fouts, J. Yanowitz, E. Polikarpov, K. Albrecht, D.J. Gaspar, J. Gladden, A. George, Selection Criteria and Screening of Potential Biomass-Derived Streams as Fuel Blendstocks for Advanced Spark-Ignition Engines, SAE Int. J. Fuels Lubes 10 (2017).
[5] G. Knothe, J. Krahl, J. Van Gerpen, The biodiesel handbook, Elsevier2015.
[6] T.M. Mata, A.A. Martins, N.S. Caetano, Microalgae for biodiesel production and other applications: a review, Renew. Sustain. Energy Rev. 14 (2010) 217-232.
[7] L. Gasnot, V. Decottignies, J. Pauwels, Kinetics modelling of ethyl acetate oxidation in flame conditions, Fuel 84 (2005) 505-518.
[8] G. Dayma, F. Halter, F. Foucher, C. Mounaim-Rousselle, P. Dagaut, Laminar Burning Velocities of C4–C7 Ethyl Esters in a Spherical Combustion Chamber: Experimental and Detailed Kinetic Modeling, Energy & Fuels 26 (2012) 6669-6677.
[9] T. Badawy, J. Williamson, H. Xu, Laminar burning characteristics of ethyl propionate, ethyl butyrate, ethyl acetate, gasoline and ethanol fuels, Fuel 183 (2016) 627-640.
[10] Z. Zhang, E. Hu, C. Peng, X. Meng, Y. Chen, Z. Huang, Shock Tube Measurements and Kinetic Study of Methyl Acetate Ignition, Energy & Fuels 29 (2015) 2719-2728.
[11] B. Akih-Kumgeh, J.M. Bergthorson, Experimental and Modeling Study of Trends in the High-Temperature Ignition of Methyl and Ethyl Esters, Energy & Fuels 25 (2011) 4345-4356.
[12] X. Yang, D. Felsmann, N. Kurimoto, J. Krüger, T. Wada, T. Tan, E.A. Carter, K. Kohse-Höinghaus, Y. Ju, Kinetic studies of methyl acetate pyrolysis and oxidation in a flow reactor and a low-pressure flat flame using molecular-beam mass spectrometry, Proc. Combust. Inst. 35 (2015) 491-498.
[13] F. Contino, F. Foucher, C. Mounaïm-Rousselle, H. Jeanmart, Experimental Characterization of Ethyl Acetate, Ethyl Propionate, and Ethyl Butanoate in a Homogeneous Charge Compression Ignition Engine, Energy & Fuels 25 (2011) 998-1003.

[14] R. Chandra, R. Kumar, Fuel Properties of Some Stable Alcohol–Diesel Microemulsions for Their Use in Compression Ignition Engines, Energy & Fuels 21 (2007) 3410-3414.
[15] T. Tan, X. Yang, C.M. Krauter, Y. Ju, E.A. Carter, Ab Initio Kinetics of Hydrogen Abstraction from Methyl Acetate by Hydrogen, Methyl, Oxygen, Hydroxyl, and Hydroperoxy Radicals, The Journal of Physical Chemistry A 119 (2015) 6377-6390.
[16] S.L. Peukert, R. Sivaramakrishnan, M.-C. Su, J.V. Michael, Experiment and theory on methylformate and methylacetate kinetics at high temperatures: Rate constants for H-atom abstraction and thermal decomposition, Combust. Flame 159 (2012) 2312-2323.
[17] T. Tan, X. Yang, Y. Ju, E.A. Carter, Ab Initio Unimolecular Reaction Kinetics of CH2C(=O)OCH3 and CH3C(=O)OCH2 Radicals, The Journal of Physical Chemistry A 119 (2015) 10553-10562.
[18] H. Nakamura, D. Darcy, M. Mehl, C.J. Tobin, W.K. Metcalfe, W.J. Pitz, C.K. Westbrook, H.J. Curran, An experimental and modeling study of shock tube and rapid compression machine ignition of n-butylbenzene/air mixtures, Combust. Flame 161 (2014) 49-64.
[19] Y. Li, C.-W. Zhou, K.P. Somers, K. Zhang, H.J. Curran, The oxidation of 2-butene: A high pressure ignition delay, kinetic modeling study and reactivity comparison with isobutene and 1-butene, Proc. Combust. Inst. 36 (2017) 403-411.
[20] M.T. Swihart, R.W. Carr, Pulsed laser powered homogenous pyrolysis for reaction kinetics studies: Probe laser measurement of reaction time and temperature, International journal of chemical kinetics 28 (1996) 817-828.
[21] H. Wang, M. Frenklach, Transport properties of polycyclic aromatic hydrocarbons for flame modeling, Combust. Flame 96 (1994) 163-170.
[22] S. Dooley, M. Uddi, S.H. Won, F.L. Dryer, Y. Ju, Methyl butanoate inhibition of n-heptane diffusion flames through an evaluation of transport and chemical kinetics, Combust. Flame 159 (2012) 1371-1384.

SEEC-2018-098

NIACIN PRETREATMENT OF ANODE FOR INCREASED POWER GENERATION IN MFC

Aradhana Singh
University School of Environment Management
Guru Gobind Singh Indraprastha University
Email: as.280591@gmail.com

Anubha Kaushik
University School of Environment Management

Guru Gobind Singh Indraprastha University
Email: aks.es.10@gmail.com

ABSTRACT

The study reports comparison of two Microbial fuel cells (MFC), one with pretreated anode electrode(TE) and other without any pretreatment serving as control electrode (CE) for power production. Niacin was used to pretreat the electrode (TE) by simple absorption technique. It was absorbed on graphite brush electrode for 24 hours which was then used in double chambered microbial fuel cell (DMFC). It was found that power density was two times higher in MFC with TE as compared to the MFC with CE. Internal resistance was also lower in TE MFC.

Keywords: *Microbial Fuel Cells, Power Production, Niacin, Pretreated Anode Electrode.*

INTRODUCTION

Microbial fuel cell (MFC) technology is of great relevance in present day world as it addresses the problems related with two key issues i.e. wastewater treatment and electricity generation. The conventional units of wastewater treatment require a high amount of energy and also produce a large amount of sludge which requires further treatment. MFC has a marked advantage over the traditional units as it does not require external energy, rather, it uses the energy already present in the waste, treats the waste and does not produce any sludge. MFC is a new ecofriendly technology which is renewable and has lot of potential to serve the energy demands of the present society. It utilizes the available energy present in the waste for producing electricity. This new technology works on the principle of natural ability of microbes to release electrons and protons to the outside. Some microbes are itself able to release electrons directly outside the membrane: *Geobacter* (Bond et al., 2003) and *Shewanella* (Li et al., 2008). While in some microbes electron transfer is mediated with the help of mediators like Methylene blue and Neutral red. Before taking MFC on commercial state there are many parameters which needs to be scaled up like design, architecture, electrode materials, substrates, catholytes etc. One component of MFC that is

electrode has been modified by researchers in a manner to increase its stability as well as efficiency. Of all the known materials and designs used in MFC, graphite brushes (Logan et al., 2007) reported to give excellent results because of its high surface area. Increasing its efficiency will be of great importance to the system. This study is focused on examining the effect of pretreatment of anode on power production. In this work Niacin has been used to pretreat the anode material. Its effect was examined in pretreatment of electrodes by simple absorption technique. Niacin (Pyridine-3-carboxylic acid) also known as nicotinic acid is a precursor of NAD and NADP. NAD and NADH help in transfer of electrons in many redox reactions. This property helps us in choosing niacin as a modifier in our traditional graphite electrode. NAD also helps in breaking down protein, fat, carbohydrate, alcohol into simpler forms, which is an excellent property for a microbial fuel cell. More the degradation of these larger compounds into simpler form more will be the availability of these substrates to the microorganisms. Niacin is easily soluble in water and can easily be absorbed on graphite brushes. Earlier effect of niacin and other vitamins has been examined in hydrogen production (Li et al., 2011). They found that there was significant increase in hydrogen production when these vitamins were present in growth medium.

METHODS AND MATERIALS

To perform the study, two units of double chamber microbial fuel cell (DMFC) of 1liter working volume was fabricated carrying distillery wastewater as substrate. The molasses based distillery wastewater was collected from a local distillery plant in Faridabad. Table 1 outlines the characteristics of the distillery wastewater which was used in the present study. Pressmud, a waste from a sugar industry

was used as a source of microbial inoculum since it is rich in many nutrients that can favor good microbial growth. Nafion 117 membrane was used as separator between the two chambers. Graphite brushes were used as electrode in both the units. These electrodes were pretreated with Niacin which was absorbed on graphite brush electrodes for 24 hours and then used in DMFC. In both units of MFC, graphite brushes of size 15*9(L*b) was used as anode and cathode. It was autoclaved for 15 mins for sterilization and then used as such (CE) in the first unit of MFC. While in second MFC the graphite brushes to be used as anode was dipped in Niacin solution for 24 hours and then air dried for 1 hour (TE). After then it was used in DMFC.

TABLE 1: DISTILLERY WASTEWATER CHARACTERISTICS

Parameters	Value
pH	4.79
Conductivity (mS)	14.34
COD (mg/L)	67200
TDS (ppm)	11.89
Salinity (ppt)	19.59
ORP (mV)	-467.8

RESULTS AND DISCUSSIONS

POWER DENSITY

This work has been conducted to check the effect of Niacin absorption as a pretreatment method for electrode. The power density for MFC with TE has been found to be $180.6mW/m^3$ while for MFC with CE it is $94.8mW/m^3$. Figure 1 represents the power curve graph for both the units i.e. MFC with TE and MFC with CE. The graph clearly indicates the differences in maximum value of curve in both the MFC. The maximum curve is nearly two fold in MFC with TE as compared to MFC with CE.

POLARIZATION

Polarization is performed to determine the internal resistance of MFC. It gives an idea of the losses of electrons during migration of same from microbes to the anode and ultimately to the cathode. In the present experiment, it was found that internal resistance for MFC with TE (1063.5ohms) came lower as compared to MFC with CE (1194.7ohms) that is proved in Figure 2. This indicates that the electrons are less deprived in MFC with TE.
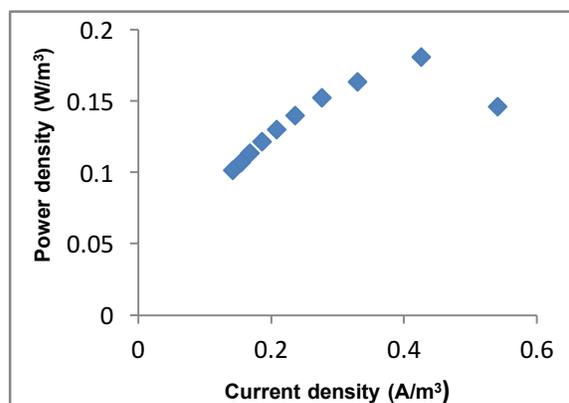
Fig.1.1 POWER GRAPH OF MFC WITH TE
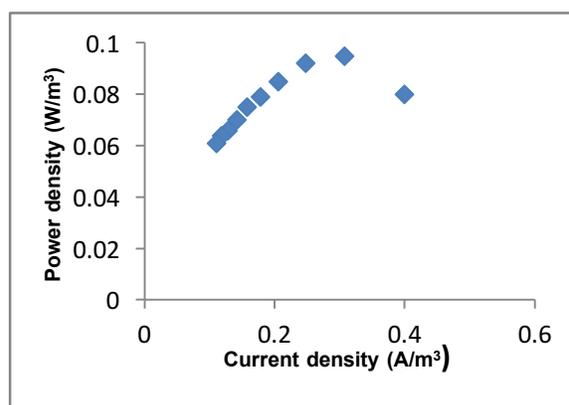
Fig.1.2 POWER GRAPH OF MFC WITH CE
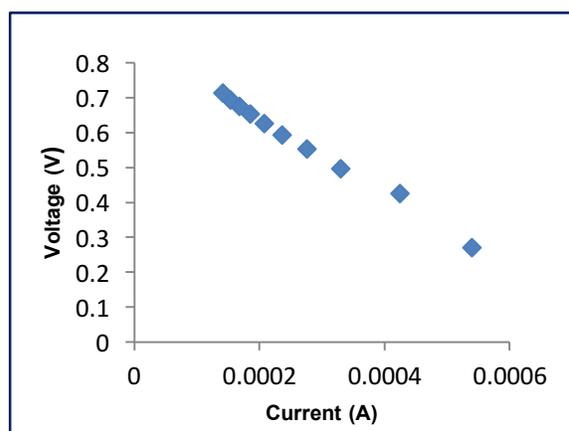
Fig.2.1 POLARIZATION BEHAVIOUR OF MFC WITH TE
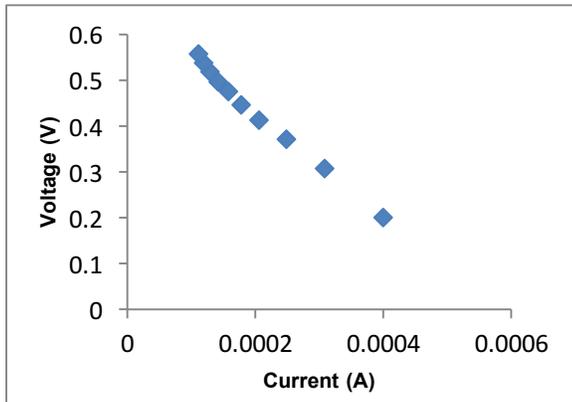
Fig.2.2 POLARIZATION BEHAVIOUR OF MFC WITH CE

CONCLUSION

The above study clearly indicates the impact of Niacin absorption on electrode as a pretreatment technique. The difference in power density was nearly two-fold. More study could be done following the same technique using other compounds. Further application of the present study becomes pertinent in resolving problems related with energy security and wastewater management.

REFERENCES

1. Bond, D.R., Lovley, D.R., 2003. Electricity production by *Geobacter sulfurreducens* attached to electrodes. Appl Environ Microbiol. 3, 1548-55
2. Li, D.L., Xu, M.Y., Sun, G.P., 2008. Electricity generated by *Shewanella decolorationnis* S12 in microbial fuel cell. Microbiology. 35, 777-81
3. Li, X., Shi, H., Wang, Y., Zhang, S., Chu, J., Zhang, M., Huang, M., Zhuang Y., 2011.Effects of vitamins (nicotinic acid, vitamin B1 and biotin) on phototrophic hydrogen production by Rhodobacter Sphaeroides ZX-5.International Journal of Hydrogen Energy. 36, 9620-9625
4. Logan,B.E., Cheng, S., Watson, V., Estadt, G., 2007. Graphite fiber brush anodes for increased power production in air-cathode microbial fuel cells. Environ. Sci. Technol. 9, 3341-3346

SEEC-2018-100

BIOETHANOL PRODUCTION FROM THE MICROWAVE ACID HYDROLYSATE OF RED MACROAGLAGE *EUCHEUMA DENTICULATUM*

Lee Keat Teong
School of Chemical Engineering, Universiti Sains Malaysia, 14300 Nibong Tebal, Pulau Pinang, Malaysia
Email: ktlee@usm.my

Teh Yong Yi
School of Chemical Engineering, Universiti Sains Malaysia, 14300 Nibong Tebal, Pulau Pinang, Malaysia
Email: yongyiteh92@gmail.com

ABSTRACT

This study aims to produce bioethanol from macroalgae hydrolysate obtained from microwave-assisted acid hydrolysis with sulfuric acid concentrations of 0.1 and 0.2 M, reaction temperatures of 150–170 °C and a heating time of 10 min. The main components of carrageenan in macroalgae can be hydrolysed and fermented with baking yeast. Higher yield of bioethanol and shorter optimum time taken were attained when dilute sulphuric acid was added.

***Keywords*:** Macroalgae, Microwave-assisted acid hydrolysis, Bioethanol

INTRODUCTION

The overall global primary energy consumption increased progressively. Concurrently, the global energy landscape is changing concomitant with the shifting of the world's economic centre of gravity. Energy consumption in Asia Pacific rose sharply, contributing highest 2.1 % of annual growth rate in 2016 [1]. Indeed, the rapid growth and improving prosperity have prompted the global energy to be consumed largely by fast-growing emerging economics. In the milieu of economical and environmental concern, extensive academic and industrial research on biofuels is being undertaken.

Liquid biofuels such as bioethanol can be produced when carbohydrates of biomass are metabolized by fermenting microorganisms. The bioethanol production process represents a carbon cycle [2]. The biomass would utilize sunlight and carbon dioxide that released during a vehicle's fuel combustion in order to synthesis organic molecules, particularly carbohydrate and lipids, for biofuel production.

It is noteworthy that chemical composition of macroalgae is significantly different from microalgae and lignocellulosic biomass. Macroalgae have a variety of carbohydrates depending on their species, including manan, ulvan, carrageenan, agar, laminarin, monnitol, alginate and fucoidin [3,4]. Therefore, being such abundant in carbohydrates, macroalgae can be hydrolysed into fermentable sugars and converted to bioethanol by natural microorganims. However, the complex and diverse carbohydrate composition of seaweed has impeded the feasibility of bioethanol recovery [5]. Thus, hydrolysis is required to break down the structural cell-wall polysaccharides of macroalgae to monosaccharide for the subsequent fermentation.

The conventional methods used for hydrolysis are enzymatic hydrolysis and/or chemical hydrolysis. Enzymatic hydrolysis is a mild approach to convert storage carbohydrate in macroalgae biomass into simple fermentable sugars. However, the longer completion time of the process and costly commercial enzyme make the process not economically feasible. Hence, chemical hydrolysis using acid (eg. H_2SO_4, HCl, HNO_3) or alkali (NaOH, KOH) is preferred and widely applied in order to disrupt the network of intra and interchain hydrogen bonds and decrystallize cellulose [6-9]. According to Lenihan et al. [10], the higher temperature with longer heating time accelerated the degradation of carbohydrates to by-products, consequently reducing the formation of reducing sugars. Thus, microwave heating can be the alternative way

to addressing these problems as well as present a faster and more efficient method [11-13]. Variables such as heating temperature (150, 160 and 170 °C) and acid concentration (0.1M and 0.2M) will be optimized in order to obtain highest bioethanol yield.

MATERIAL AND METHODS

In this study, red macroalgae *E. denticulatum* was chosen as raw material.

The fermentation was conducted according to the method described by Tan and Lee [14]. Yeast (*Saccharomyces cerevisiae*) was precultured overnight in 50 mL of sterile YEPD medium containing 1 % (w/v) yeast extract, 2 % (w/v) peptone, 2 % (w/v) galactose and 0.175 % (w/v) potassium dihydrogen phosphate. The preculture was incubated in a shaking incubator (IKA, Germany) at 35 °C with shaking at 130 rpm for 24 hours. Yeast cells were harvested by centrifugation (10000 xg, 5 minutes, 5 °C) and washed with 1% (v/v) phosphoric acid three times to remove the residual sugars in the medium.

The hydrolysate obtained from microwave-assisted acid hydrolysis [15] was diluted 2-fold with sodium acetate buffer (50 mM, pH 4.8). The aforementioned mixture was incubated with inoculum prepared (yeast loading varied from 10.80 to 12.30 g/L). The fermentation was performed in a shaking incubator (IKA, Germany) at 35 °C at a shaking speed of 130 rpm for 72 hours. Five-hundred-microlitre sample was taken from fermentation broth and centrifuged at 10000 xg for 5 minutes. The supernatant obtained was analyzed for bioethanol and sugar content by using GC-FID and HPLC, respectively.

The reducing sugars contents in hydrolysate were determined by a high performance liquid chromatography (HPLC) system (Agilent series 1260 infinity) which was equipped with a 385 Evaporative light scattering detector (ELSD) and a 300 mm × 7.7 mm Hi-Plex Ca column. The HPLC-ELSD's spray chamber and detector temperature (nebulizer and evaporator) were set at 50 and 80 °C, respectively. The system was run at a flow rate of 0.6 mL/min using deionized water as the mobile phase. Purified nitrogen was used as a carrier gas (70 psi) for the detector and 20 µL of sample was injected for each analysis.

The measurement of by-product content was carried out with Agilent series 1260 infinity high performance liquid chromatography system which was equipped with a UV detector and a Poroshell 120 EC-C18 2.7 µm column at 250 nm (range: 0 - 400 nm). The mobile phase used was a solution of methanol: deionized water = 20: 80 (v/v) at a flow rate of 0.3 mL/min.

Quantitative analysis was performed using a calibration with internal standard of known concentrations. The yield of reducing sugars was calculated as follows [14]:

$$\text{Yield (\%)} = \frac{\text{Concentration of sugar}}{\text{Initial concentration of substrate}} \times 100$$
(1)

The bioethanol was analyzed by a gas chromatography (GC-FID, Clarus 500, Perkin Ekmer, USA). The column used was a DB-Wax capillary column (30 m length, 0.25 mm ID, 0.25 µm, Agilent, USA). The detector and injector were set at 250 and 220 °C, respectively. The oven was set to isothermal at 150 °C for 5 minutes. Helium was used the carrier gas and 2 µL of sample was injected for each analysis. Quantitative analysis was performed using a calibration with internal standard of known concentrations. Bioethanol yield and percent theoretical yield were calculated based on the following equations, respectively [14,16].

$$Y_{P/S} = \frac{[EtOH]_{max}}{[Sugar]_{ini}}$$
(2)

$$Y_{\%T} = \frac{Y_{P/S}}{0.51} \times 100$$
(3)

where $Y_{P/S}$ is ethanol yield (g/g), $[EtOH]_{max}$ is the highest ethanol concentration achieved during fermentation (g/L), and $[Sugar]_{ini}$ is the total initial sugar concentration at onset of fermentation (g/L), $Y_{\%T}$ is percent theoretical yield (%), 0.51 is the maximum ethanol yield per unit of hexose sugar from glycolytic fermentation (g/g), P = Product and S = Substrate.

RESULTS AND DISCUSSION

The composition of cell wall of red macroalgae includes cellulose and long-chain structural polysaccharides carrageenan consisting of β-D-galactose and α-D-galactose. In order to cleave 1,4-glycosidic bondsin polysaccharides, conventional thermal heating requires a higher temperature to deliver heat from the surface to center of a material compared than the required reaction temperature, which is comparatively slow and inefficient. As a result, the longer heating time gives rise to a dramatic reduction of reducing sugars but higher content of by-products. Contrarily, in this study, microwave irradiation produces uniform and controlled heating, producing higher yield of fermentable sugars and bioethanol with low content of by-products. Higher yield of bioethanol and shorter optimum time taken were attained when dilute sulphuric acid was added.

CONCLUSIONS

This study successfully demonstrated that the yield of bioethanol has been improved for microwave-assisted acid hydrolysis compared to conventional acid hydrolysis. Thus, this study has elucidated the scalability of microwave-assisted heating and paved the way for utilizing macroalgae as an excellent alternative biofuel.

ACKNOWLEDGMENTS

REFERENCES

[1] BP Statistical Review, 2017. "BP Statistical Review of World Energy", London, UK.

[2] RFA, 2017. "Building Partnerships and Growing Markets: Ethanol Industry Outlook", Renewable Fuels Association, USA.

[3] Jung, K. A., Lim, S., Kim, Y. and Park, J. M., 2013. "Potentials of macroalgae as feedstocks for biorefinery", Bioresource Technology, 135, pp. 182-190.

[4] Lobban, C. S. and Wynne, M. J., 1981. "The Biology of seaweeds", 1st ed., Blackwell Scientific Publications.

[5] Wei, N., Quarterman, J. and Jin, Y., 2013. "Marine macroalgae: An untapped resource for producing fuels and chemicals", Trends in Biotechnology, 31(2), pp. 70-77.

[6] Abd-Rahim, F., Wasoh, H., Zakaria, M. R., Ariff, A., Kapri, R., Ramli, N., Liew, S. L., 2014. "Production of high yield sugars from Kappaphycus alvarezii using combined methods of chemical and enzymatic hydrolysis. Food Hydrocolloids", 42, pp. 309-315.

[7] Bensah, E. C. and Mensah, M., 2013. "Chemical pretreatment methods for the production of cellulosic ethanol: technologies and innovations", International Journal of Chemical Engineering, 2013, pp. 1-21.

[8] Xiang, Q., Lee, Y. Y., Pettersson, P. O. and Torget, R.W., 2003, "Heterogeneous aspects of acid hydrolysis of α-cellulose", Application of Biochemical and Biotechnology, 105, pp. 505-514.

[9] Dekker, R. F. H. and da Silva, G. V. J., 2005, "Purification and structural characterization of $(1{\rightarrow}3;1{\rightarrow}6)$-$\beta$-d-glucans (botryosphaerans) from *Botryosphaeria rhodina* grown on sucrose and fructose as carbon sources: a comparative study", Carbohydrate Polymers, 61, pp. 10-17.

[10] Lenihan, P., Orozco, A., O'Neill, E., Ahmad, M. N. M., Rooney, D. W. and Walker, G. M., 2010, "Dilute acid hydrolysis of lignocellulosic biomass", Chemical Engineering Journal, 156, pp. 395-403.

[11] Yuan, Y. and Macquarrie, D. J., 2015. "Microwave assisted acid hydrolysis of brown seaweed *Ascophyllum Nodosum* for bioethanol production and characterization of alga residue", ACS Sustainable Chemistry and Engineering, 3, pp. 1359-1365.

[12] Macquarrie, D., Clark, J. H. and Fitzpatrick, E., 2012, "Review: The microwave pyrolysis of biomass", Biofuels Bioproducts and Biorefining, 6(5), pp. 549-560.

[13] Budarin, V. L., Zhao, Y., Gronnow, M. J., Shuttleworth, P. S., Breeden, S. W., Macquarrie, D. J. and Clark, J.H., 2011., "Microwave-mediated pyrolysis of macro-algae", Green Chemistry, 13, pp. 2330–2333.

[14] Tan, I. S., and Lee, K. T., 2016., "Comparison of different process strategies for bioethanol production from *Eucheuma cottonii*: An economic study", Bioresource Technology, 199, pp. 336-346.

[15] Teh, Y. Y., Lee, K. T., Chen, W.-H., Lin, S.-C., Sheen, H.-K., Tan, I. S., 2017, "Dilute sulfuric acid hydrolysis of red macroalgae *Eucheuma denticulatum* with microwave-assisted heating for biochar production and sugar recovery", Bioresource Technology, In press.

[16] Keating, J. D., Robinson, J., Bothast, R. J., Saddler, J. N. and Mansfield, S. D., 2004. "Characterization of a unique ethanologenic yeast capable of fermenting galactose", Enzyme Microbiology Technology, 35, pp. 242-253.

SEEC-2018-102

ASSESSMENT OF INDOOR PARTICULATE POLLUTION IN A LECTURE HALL COMPLEX

Veerendra Sahu*
Department of Civil engineering,
Indian Institute of Technology
Roorkee India
Email: veerendraideal@gmail.com

B. R. Gurjar
Department of Civil engineering,
Indian Institute of Technology
Roorkee India

Komal Jayaswal
Department of Civil engineering,
Indian Institute of Technology
Roorkee India

ABSTRACT

Air quality inside learning environment of schools and colleges is vital for students' health and their academic performance. This study aims to assess the particulate pollution in Lecture hall complex of a technical institute situated at Roorkee city in north India. Coarse, fine and submicron particles (PM_{10}, $PM_{2.5}$ & PM_1) concentration was monitored in indoor as well as the outdoor environment of the complex. The hourly average concentrations for PM_{10}, $PM_{2.5}$ & PM_1 was found in the range of 137-141, 70-86 and 44-67 µg/m3, respectively. Indoor-Outdoor ratio of PM concentrations for all microenvironments was found greater than 1. Fractional analysis of various PM sizes has describe the contribution of different PMs from various indoor and outdoor sources. Results of the present study would find implication in exposure analysis and help the regulating authority to develop the policy framework on indoor air quality.

Keywords: *IAQ, Particulate Pollution, Air Quality*

INTRODUCTION

Air quality of the indoor environment directly influence the human health, people spend almost 80 to 90% of their time in different indoor environments which highlights the importance of the assessment of indoor air quality (IAQ). Indoor pollutant sources, building materials, ventilation and designs of the urban building affect the air quality inside its microenvironments [1]. Poor Indoor Air Quality (IAQ) inside homes, offices, schools and colleges has also been linked to increases in sick building syndrome along with losses in productivity and performances in schools /colleges and offices [2]. Particulate matter (PM) concentration, being the criteria air pollutants, is one of the indicator for indoor as well as outdoor air quality. Various physical and chemical characteristics of PM are potential contributors to adverse health effects. Large number of epidemiologic studies addressed the adverse health effects of both short-term and long-term exposure to PM concentration [3, 4].

Air quality in libraries, lecture halls, laboratories and other microenvironments of schools and colleges where the students spend most of the time of the day, is very important for healthy learning environment and worthy academic performance [5].

Therefore, the aim of the present study is to assess the indoor Air Quality (IAQ) as indoor particulate matter concentration in order to find out the spatial variations of particulate pollution in Lecture hall complex of Indian Institute of Technology Roorkee.

METHODOLOGY

Site description:

Indian Institute of Technology (IIT) Roorkee is one of the premium technical institute of India, Established in 1847 at Roorkee city of Uttarakhand (29° 51′ 52″ N, 77° 53′ 47″ E). New Lecture hall complex (NLHC) of IIT Roorkee was selected as study site for this study. NLHC is a three story building, have 18 large lecture halls of occupancy of around 150-200 at each hall, 15 tutorial class rooms and other facility rooms. All the lecture halls are equipped with air conditions, wall fans and selling fans but due the frequent window opening the ventilation of the halls are categorized as mixed kind of ventilation (natural and mechanical both).

Monitoring:

PM_{10}, $PM_{2.5}$, and $PM_{1.0}$ measurements were made for eight hours on five consecutive days in lecture halls at a sampling rate of 5 min using environmental dust monitors

(GRIMM make, Model 1.109). Continuous Monitoring was performed from 10AM to 6PM in lecture halls at each floor of the NLHC except top floor due to the different design and occupancy of the top floor classrooms.

The sampling procedure involved conducting three to five indoor measurements and the instrument was located at the height of 1.3m above the floor and at least 1m away from the wall. Inlet head was positioned as close as possible to the breathing zone for the occupants. Outdoor monitoring was also performed continuously for 24 hours, to develop the Indoor-Outdoor relationship during the period of occupancy.

This 31-channel dust monitors work on the principle of light scattering by drawing air at a sample flow rate of 1.2 L/min and detects the particle in the size range of 0.3–25μm then convert to mass using well-established conversion equations [6].

Results and Discussion

Indoor Particulates Concentrations: The hourly average concentrations for PM_{10} (141±26 μg/m^3) was found highest in lecture hall at 1st floor whereas $PM_{2.5}$, and $PM_{1.0}$ concentrations (86±10 and 67±9 μg/m^3, respectively) were highest at second floor. The 8-h average outdoor PM_{10}, $PM_{2.5}$, and $PM_{1.0}$ concentrations were 96.7± 3.7, 56.9± 2.8, and 40.1±2.6 μg/m^3, respectively. Spatial variation of particulate pollution at different floor of the NLHC can be relate to the variation in occupancy and ventilation. Table 1 shows the 8-hourly average values of different PM types in lecture halls at floor and the variation of concentration for PM shown in figure 1.

TABLE 1: Concentration of different PM types in studied indoor environments

PM Concentration in indoor environment(μg/m3)											
	PM10				**PM2.5**				**PM1**			
Site	Mean	Max	Min	SD	Mean	Max	Min	SD	Mean	Max	Min	SD
Ground Fl	139.2	169.4	87.1	25.4	82.7	108.1	74.4	13.5	61.5	88.9	51.2	10.8
1st Floor	141.1	186.9	97.6	25.7	70.3	101.6	69.5	11.3	44.1	84.2	51.6	12.0
2nd Floor	137.2	207.8	89.8	35.0	86.3	84.6	58.6	10.4	66.9	57.9	34.6	9.1
Outdoor	96.7	101.7	92.4	3.5	56.7	60.6	53.8	2.7	39.8	43.6	37.3	2.6
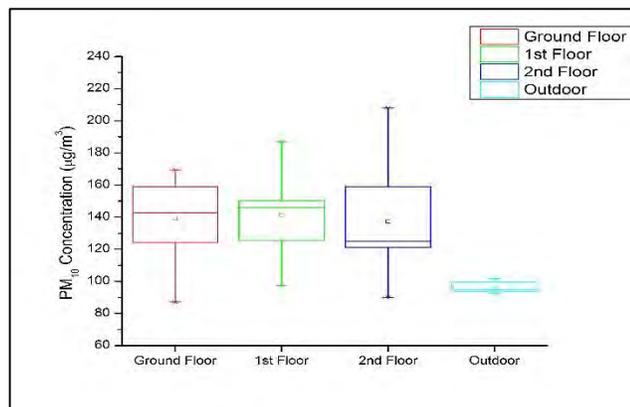
FIGURE 1a. Concentration variation for PM_{10}
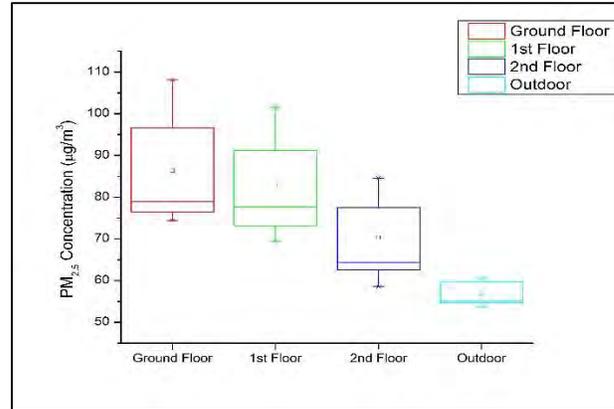
FIGURE 1b. Concentration variation for $PM_{2.5}$
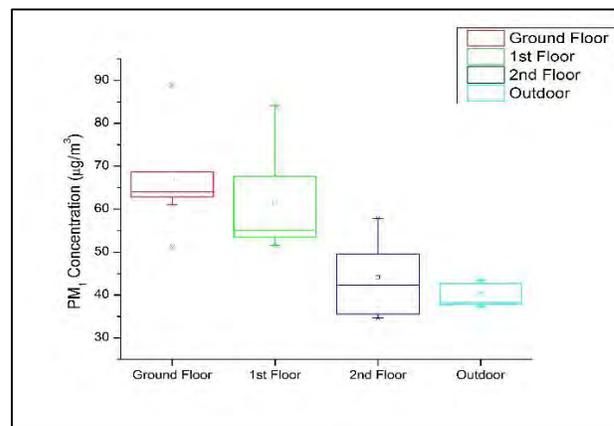
FIGURE 1c. Concentration variation for PM_1

I/O relationship:

Indoor-Outdoor ratio of PM_{10}, $PM_{2.5}$, and $PM_{1.0}$ was calculated for all the selected lecture halls to understand the contribution from various indoor activities and the infiltration of particles from the outdoor environment. The hourly average outdoor concentrations of various PM fractions, was used to calculate the I /O ratio for different PM types in the studied indoor environments during working hours (Fig. 2). I/O ratio for various PM types was found in the range of 1.43- 1.54 at Ground floor, 1.10-1.44 at 1st floor and 1.41-1.67 2nd floor. I/O ratio shows the decline trend from Ground floor to first floor. Highest I/O ratio for $PM_{2.5}$ and $PM_{1.0}$ was found at 2nd floor whereas it was for PM_{10} at Ground floor.

These observations suggest that the outdoor infiltration and the indoor activities are responsible for the higher I /O in indoor environments. In line with the previous findings [7,8], the key parameters, which are supposed to regulator the I /O ratio of PM in our study, are the air exchange rate between the indoor and the outdoor air and the particle resuspension. The results of several other studies also exhibited the varying range of I /O ratio as 0.5 to 2.0 in

different indoor environments in the absence and presence of indoor sources, respectively [9,10].
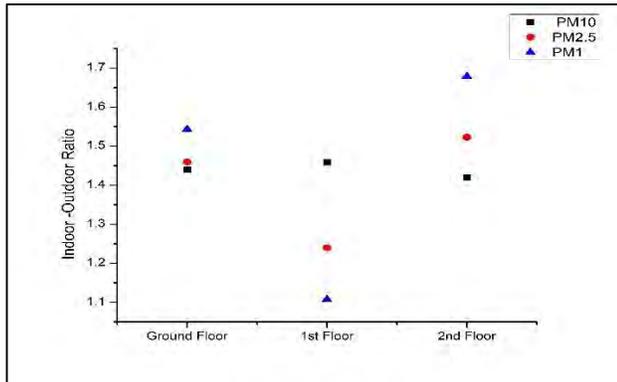
FIGURE 2. I/O ratio of PM10, PM2.5, and PM1.0

Proportion of PM fractions:

Fractional analysis of various PM sizes has also been carried out to understand the contribution of different PMs from various indoor and outdoor sources. Figure 3 shows the proportion of different PM fractions in all the selected indoor environments and during outdoor measurements. Together, the PM2.5 (17 %) and PM1.0 (41 %) contributes ~58 % of the total PM10 concentration in outdoor ambient air, leaving only 41 % for PM2.5–10.

By looking at the indoor concentrations separately at different floor, PM fraction at Ground floor's lecture hall shows nearly identical proportions as were outdoors even though having mixed ventilation. The sum of PM2.5 and PM1.0 contributed ~59 % of total PM as opposed to ~58 %in outdoors, this can be expected given the frequent opening of doors/windows, allowing free movement of outdoor air. Whereas the fractional variation PM Concentration is of different order for 1st and 2nd floor's lecture hall.
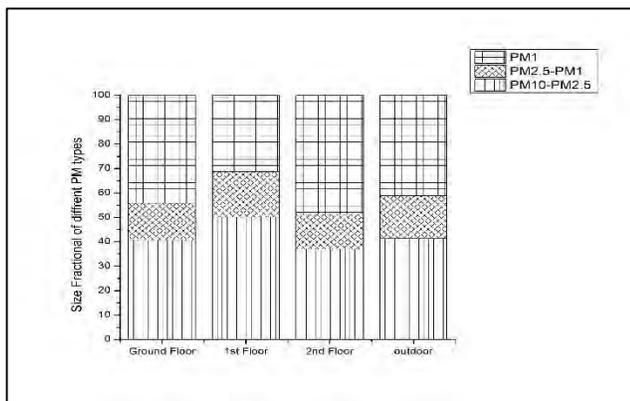
FIGURE 3. Proportion of PM concentrations in various size ranges

CONCLUSION

Higher concentration of coarse particles was found at first floor of NLHC whereas the concentration of fine particles was higher at 2nd and 3rd floor. Which shows the spatial variation of indoor particle concentration in lecture hall complex. I/O ratio of different PM types also followed the spatial variation which depicts the variation of IAQ in lecture hall at different floor of the complex. Ventilation of the lecture hall also affect the I/O ratio of PM concentration. Overall the fine fraction particles was found higher compare to coarse fraction.

REFERENCES

[1] Olesen, B.W., 2011. Standards for Ventilation and Indoor Air Quality in relation to the EPBD. REHVA Eu HVAC J, pp.28-32.

[2] Mohd Aris, M.S., 2013. An assessment of indoor air quality at two contrasting location and building ventilation types in London (Doctoral dissertation, King's College London (University of London).

[3] Zeka, A., Zanobetti, A. and Schwartz, J., 2005. Short term effects of particulate matter on cause specific mortality: effects of lags and modification by city characteristics. *Occupational and Environmental Medicine*, *62*(10), pp.718-725.

[4] Brook, R.D., Rajagopalan, S., Pope, C.A., Brook, J.R., Bhatnagar, A., Diez-Roux, A.V., Holguin, F., Hong, Y., Luepker, R.V., Mittleman, M.A. and Peters, A., 2010. Particulate matter air pollution and cardiovascular disease an update to the scientific statement from the American Heart Association.Circulation, 121(21), pp.2331-2378.l medicine, 62(10), pp.718-725

[5] Daisey, J.M., Angell, W.J. and Apte, M.G., 2003. Indoor air quality, ventilation and health symptoms in schools: an analysis of existing information. Indoor air, 13(1), pp.53-64.

[6] http://www.dustmonitor.com/Occupational/1107.htm

[7] Goyal, R. and Khare, M., 2009. Indoor–outdoor concentrations of RSPM in classroom of a naturally ventilated school building near an urban traffic roadway. Atmospheric Environment, 43(38), pp.6026-603

[8] Chithra, V.S. and Nagendra, S.S., 2014. Characterizing and predicting coarse and fine particulates in classrooms located close to an urban roadway. Journal of the Air & Waste Management Association, 64(8), pp.945-956.

[9] Morawska, L., He, C., Hitchins, J., Gilbert, D. and Parappukkaran, S., 2001. The relationship between indoor and outdoor airborne particles in the residential environment. Atmospheric Environment, 35(20), pp.3463-3473

[10] Hussein, T., Hämeri, K., Aalto, P., Asmi, A., Kakko, L. and Kulmala, M., 2004. Particle size characterization and the indoor-to-outdoor relationship of atmospheric

aerosols in Helsinki. Scandinavian journal of work, environment & health, pp.54-62.

SEEC-2018-104

EXTERNAL RESISTANCE REGULATES LACTIC ACID PRODUCTION IN MICROBIAL CATALYZED ELECTROCHEMICAL SYSTEMS

G. Velvizhi
Bioengineering and Environmental Sciences Lab,
EEFF Department, CSIR-Indian Institute of
Chemical Technology (CSIR-IICT),
Hyderabad - 500007, India.

Manupati Hemalatha
Bioengineering and Environmental Sciences Lab,
EEFF Department, CSIR-Indian Institute of
Chemical Technology (CSIR-IICT),
Hyderabad - 500007, India.

J. Shanthi Sravan
Bioengineering and Environmental Sciences Lab,
EEFF Department, CSIR-Indian Institute of
Chemical Technology (CSIR-IICT),
Hyderabad - 500007, India.

R.S. Shravani
Institute of Bioinformatics and Applied
Biotechnology
Electronic city, Phase I,
Bangalore – 560100, India.

S. Venkata Mohan*
Bioengineering and Environmental Sciences Lab, EEFF Department,
CSIR-Indian Institute of Chemical Technology (CSIR-IICT), Hyderabad- 500007, India.
E-mail: vmohan_s@yahoo.com; svmohan@iict.res.in; Tel: 0091-40-27161765

ABSTRACT

Lactic acid production was evaluated in a microbial catalyzed electrochemical system (MCES) by regulating the external resistance in a closed circuit mode of operation. The study was performed in a single chamber (SC) and double chamber (DC) MCES system with 3 g/l of glucose as substrate and 10 % of lactic acid bacteria (LAB) isolated from the curd. The SC and DC reactors were operated initially with OC mode and after stabilization polarization conferred CDP at 400 Ω resistance. The observed external resistance has effectively regulated the anodic fermentation in both the chambers with nearly 40% increment in lactic acid than OC indicating effective electron flux in the system. SC showed increment in lactic acid production by 30% when compared to DC, inferring distribution of net electron flux to both electrodes in a single system whereas in DC the electrons pass to a separate chamber as electricity.

Keywords

Electron flux; Microbial fuel cell; Lactic acid Production; Potential gradient; Redox mediators; Cell design point (CDP).

INTRODUCTION

Lactic acid has widespread applications and also has the potential for production of biodegradable and biocompatible polylactic acid (PLA) polymers that drive the current market expansion. Production of lactic acid can be achieved either by chemical synthesis routes or biological fermentative routes. The chemical synthesis route is energy intensive and expensive whereas the biological fermentation routes offers advantages of using cheap renewable substrates and low energy consumption while producing optically pure D- or L-lactic acid using pure lactic acid bacteria as biocatalyst. The major bottleneck in the biological fermentation processes is low productivity and longer durations of operation. Hence to overcome these limitations, several strategy such as fed-batch fermentation, repeated fermentation, and continuous fermentation, high cell densities (HCDs) via immobilization and integrated-membrane fermentation reactor systems are practiced [1]. The present study use MCES as an integrating electrochemical and biological fermentation as a novel strategy for enhancing the production of lactic acid.

MCES is capable of harnessing electrons from microbial electrometabolic activities to generate bioelectric currents and biobased chemicals [2]. Regulation of electron flux during bacterial metabolism with electrode involvement in

microenvironment is one of the important factor in MCES. The regulation of anode potential is usually carried out by poising external potential and alternatively it can also be controlled by applying external resistance [3-5]. In this context, the present study evaluates two MCES systems for the production of lactic acid in a SC and DC systems using glucose as substrate and pure lactic acid bacteria isolated from curd as biocatalyst. The study was initially operated in the open circuit mode and after stabilization the system was operated with closed circuit operation with an external resistor to evaluate the lactic acid production efficiency.

MATERIALS AND METHODS
MCES Setup
A single chamber (SC) and double chamber (DC) MCES with three electrode setup was designed and fabricated using schott-duran glass bottles (working/total volume - 200/250 ml). The reactors were designed with a provision for electrode placement and sampling ports. Leak proof sealing was employed to maintain anaerobic microenvironment. Carbon cloth-Stainless steel mesh (CC-SS) hybrid electrodes with the dimension of 5×3×1 cm was used as anode and carbon cloth (CC) as cathode electrodes. Cathode was considered the working electrode while anode as counter electrode against Ag/AgCl (3.5M KCl) as the reference electrode, anode as counter electrode and cathode as working electrode. The electrodes were intertwined with stainless steel wire as current collector.

Biocatalyst
Pure srains of lactic acid bacteri was isolated from curd. 1g of curd sample were taken aseptically and subjected to 10-fold dilution, 0.1 ml of diluted sample was inoculated on MRS agar plates under anaerobic condition and incubated at 32^0C for 48 hours. The different morphological colonies were isolated and pure cultures were maintained in MRS agar slant at 4^0C. The isolated colonies were transformed to MRS broth and purified by streaking twice on MRS agar. The individual bacterial colonies were stored in 0.8% MRS agar overlaid with 50% glycerol at -20^0C. The colonies were grown in MRS broth for 24 hr and used as incoculum for the experiments.

Operation of MFC
In DC-MCES, anode chamber was fed with 10% of isolated LAB and design synthetic wastewater with glucose (3g/l) as a substrate. The cathode chamber was fed with distilled water which was continuously oxygenated. SC-MCES was fed with 10% of isolated LAB in designed synthetic wastewater with glucose (3g/l) as a subsatrte. The reactor was operated wth a retention time of 48 hr.

Analysis
Lactic acid production was analyzed through HPLC with UV detector (Perkin Elmerseries 200) at 214 nm using RP-18 column (120 x 4.6 mm). Open circuit voltage (V) was recorded using a data acquisition system (Keithley Instruments, Inc. OH). Cyclic voltammetry (CV) was used to study the electrochemical behaviour of biocatalyst during stabilized phase of operation using potentiostat-glavanostat system to get mechanistic insights into the electrochemical reactions. Biochemical parameters viz., pH, ORP, VFA and COD reduction were estimated according to the standard methods. Buffering capacity analysis was performed using auto titrator (Mettler – Toledo).

RESULTS AND DISCUSSION
Lactic acid production
The SC and DC reactors were operated initially in open circuit mode for assessing the performance of the both MCES. After stabilization, polarization studies were performed and the circuit was closed with cell design point at 400 Ω resistor. SC-MCES reported maximum lactic acid production of 0.8 g/l in the open circuit mode (OC) and DC-MCES reported 0.75 g/l at 4 h which was gradually observed to decrease till 20 h of operation. In the closed circuit operation, SC-MCES reported 1.2 g/l and DC-MCES reported 0.9 g/l (Fig 1and 2). The study infers that CC operation reported higher lactic acid production than OC due to continuous and controlled electron flux in the system, since the external resistance triggered the enrichment of electrochemical active bacteria (EAB) due to regulation of anode potential. Lactic acid production was also supported by variation in pH and biomass growth at 4th h. The pH dropped from 6.7 to 5.5 till 6th h and gradually increased to 7.1 at the end of operation and the same was supported by the biomass growth.
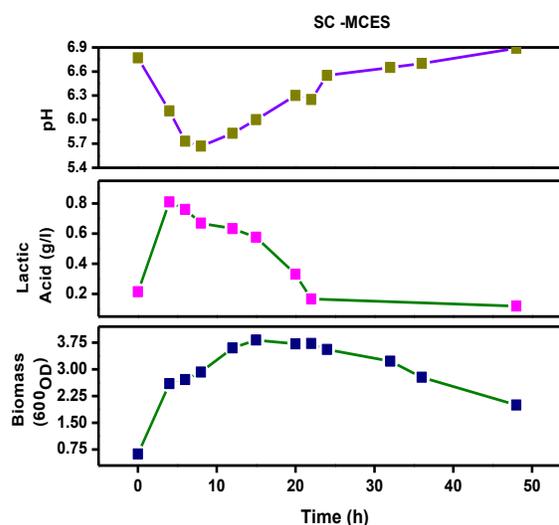
FIGURE 1: The profile specifies pH change, lactic acid production and biomass with respect to time for Closed circuit operation Single chamber MCES.
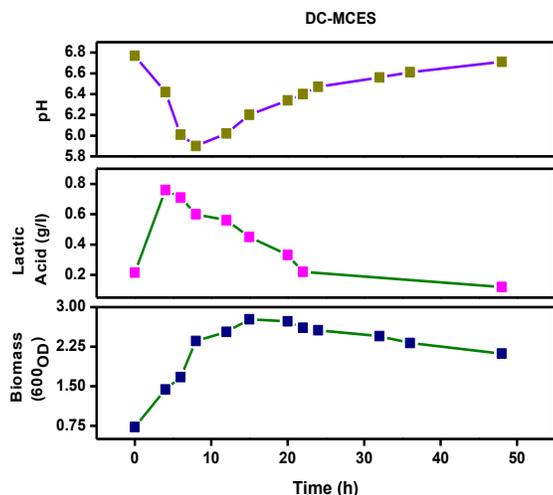
DC-MCES

FIGURE 2: The profile specifies pH change, lactic acid production and biomass with respect to time for Closed circuit operation for Double chamber MCES

Electrogenic Activity

The OCV of DC-MCES was stabilized at 600 mV and SC-MCES at 320 mV. Electrogenic activity was observed to gradual increase for both the systems till 10th h of operation and thereafter was observed to be stable till the end of operation. After stabilization, polarization studies were performed with a varying resistor from 0.05-30 kΩ and cell design point (CDP) was observed at 400 Ω resistor with a power density of 40 mW/m$^{2.}$ The external resistance of 400 Ω was used to regulate the electron flux in CC mode of operation. Lactic acid bacteria belong to Fe(III) reducing bacteria, and the existence of Fe(III) oxides could induce effective electrically conductive network which results in efficient electrogenic activity [6].

Substrate removal efficiency

Closed circuit operation reported enhanced substrate degradation in both systems, DC-MCES-CC reported COD removal efficiency of 50 % and SC-MCES-CC reported COD removal efficiency of 60% (Fig. 2). Nearly 20% increase was observed in CC mode of operation in comparison to OC mode of operation. The study infers that the LAB are capable of degrading glucose and simultaneously produce electricity in both MCES systems. The coupled action of electrode assembly as solid electron acceptor as well as bacteria as biocatalyst in the closed circuit documented significant substrate degradation in comparison to the open circuit. The direct electron flux between the external resistors regulates the anodic potential for effective substrate degradation. The presence of electrode and circuit mode also reported the enhanced biomass growth and enhanced the lactic acid production and electrogenic activity.

CONCLUSIONS

Microbial catalyzed electrochemical systems reported enhanced lactic acid production in closed circuit operation in comparison to open circuit, due to effective distribution of net electron flux between the electrodes. The study infers that continuous flux of electrons in the system activated the electrochemical active bacteria on the electrode as biofilm without any external energy as input in the closed circuit operation. The presence of electrode assembly stimulates the fermentation and enhances the synergetic interactions between the biocatalyst and the electrode resulting to higher lactic acid production.

Acknowledgement

REFERENCE

[1] Rahman, K., A., Tashiro, Y and Sonomoto, K., 2013. " Recent advances in lactic acid production by microbial fermentation processes". Biotechnolgy Advances 31, pp 877 -902.

[2] Venkata Mohan, S., Velvizhi, G., Modestra, J.A., Srikanth, S., 2014. "Microbial fuel cell: critical factors regulating bio-catalyzed electrochemical process and recent advancements". Renewable Sustainable Energy Rev. 40, 779–797.

[3] Srikanth, S., Venkata Mohan, S., Sarma, P.N., 2010. "Positive anodic poised potential regulates microbial fuel cell performance with the function of open and closed circuitry". Bioresour. Technol. 101, 5337–5344.

[4] Nikhil G,N, Venkata Subhash, G, Yeruva, D,K,. Venkata Mohan,S., 2015. "Closed circuitry operation influence on microbial electrofermentation: Proton/electron effluxes on electro-fuels productivity." Bioresource Technology 195,pp 37–45

[5] Yu,T., Li,D., Song,H., Yan,X., Chen.W,N. 2016. "The effect of external resistance on biofilm formation and inte rnal resistance in Shewanella inoculated microbial fuel cells". *RSC Adv.*, 6, pp 20317-20323.

[6] Wang, M., Yang, Z., Xia, M., Fan, L., Zhang, X., Wei, S., Zou.T., 2017. "Performance Improvement of Microbial Fuel Cells by Lactic Acid Bacteria and Anode Modification". Environmental Engineering Science 34, 251-257, DOI: 10.1089/ees.2016.0110

SEEC-2018-105

HARNESSING MICROBES FOR GENERATION OF CLEAN FUEL AND GREEN CHEMICAL

Sanjukta Subudhi*

Environmental and Industrial Biotechnology Division (EIBD), The Energy and Resources Institute Darbari Seth Block, Habitat Place Lodhi Road, New Delhi - 110 003, Tel: +91-11-24682100 and +91-11-41504900, Fax: +91-11-24682144 and +91-11-24682145, India

* Presenting author: Dr. Sanjukta Subudhi, Senior Fellow
(ssubudhi@teri.res.in, sanjuktasubudhi@yahoo.com)

Current global energy demand is relying mostly on crude oil reserves and the demand is projected to rise further owing to the rising global population. Fossil based sources are also being used extensively for synthesis of industrial important platform chemicals. Fast depletion of limited fossil fuel sources including rising Green House Gas (GHG) emissions, raised global concern not only for energy security but also for environmental protection. In view of this, production of clean energy and green chemicals from alternate sustainable sources that do not compete for feed, has become the major focus for national policies across the globe. This eventually prompted scientists worldwide to explore for environment friendly alternate renewable sources for production of clean fuel and green chemical. In this regard, bio based production of clean biofuel and green chemical through the employment of specific microbes considered more significant. These microbes have enormous potential to serve as cell factory for production of clean fuel and green chemical from non-fossil based non-edible feedstock such as; organic waste , lignocellulosic biomass including waste agricultural residues.

Among various biofuel forms, fermentative hydrogen production by microbes considered as one of the cleanest forms of energy. This is because of the fact that hydrogen has highest gravimetric energy, generates clean water when burns and can be generated by microbes at ambient condition from non-edible feedstock such as lignocellulosic biomass. Further microbes also play key role in synthesis of industrial important chemicals. One of such industrially important chemical is lactic acid that has got wide applications in food, textile, chemical, cosmetic and pharmaceutical industries. Currently lactic acid is mostly produced by chemical synthesis process from petrochemical resources and is not considered environmental friendly. Fermentative lactic acid production from non edible biomass sources is environmental friendly and do not compete with edible feedstock.

Lignocellulosic biomass is abundant and offer as good feedstock for microbial production of fuel and chemical. However, major challenge lies in utilization of C_5 sugar component of this biomass. Only few of the microbes encompass C_5 fermentation pathway and crux lies in isolation and selection of unique microbes for these processes that can ferment C_5 as well as C_6 sugars. This presentation will highlight on fermentative production of hydrogen and lactic acid from second generation lignocellulosic biomass.

SEEC-2018-107

EFFECTS OF INTAKE AIR AND FUEL PREHEATING FOR IMPROVING DIESEL ENGINE OPERATION PARAMETERS RUNNING WITH METHYL ESTER (BIODIESEL) BLENDS

Menelik Walle Mekonen
Mechanical Engineering Department
Institute of Technology Guwahati
menelik@iitg.ernet.in

Niranjan Sahoo
Mechanical Engineering Department
Institute of Technology Guwahati
shock@iitg.ernet.in

Santosh Kumar Hotta
Mechanical Engineering Department
Institute of Technology Guwahati
h.santosh@iitg.ernet.in

ABSTRACT

In this study preheated methyl ester biodiesel oil properties and its effects on engine performance parameters and emission levels on diesel engine were examined for a variations of fuel inlet temperature from 54 to 126 ^0C for increments of 12 ^0C with variation of engine load to see its effects and found optimal preheating temperature which resulted comparable oil properties and engine parameters with diesel fuel. Apart from preheated methyl ester, experiments also executed the intake air heated at different temperatures in order to find the optimum level of from the ranges between 33 ^0C to 65 ^0C. The experimental results showed that increasing fuel inlet temperature the viscosity and density properties of biodiesel decrease significantly and improved engine performance and emission parameters with a variation of load due to better fuel atomization of lower viscosity of methyl ester oil. It was seen that among the various preheating temperature, heating biodiesels at 114^0C temperature, bring down their viscosity and density within a standard range and close to that of mineral diesel fuel at 40^0C. The viscosity and density Palm Oil Methyl Ester (POME) oil are considerably reduced to be 3.74 mm^{2}s^{-1} and 871 kg.m^{-3} at 114^0C respectively, which are very close to diesel fuel viscosity 3.35 mm^{2}s^{-1} at 40^0C and density 842 kg.m^{-3} at 15^0C. The engine performance (brake specific fuel consumption, brake thermal efficiency, and exhaust gas temperature) and combustion (peak cylinder pressure, the rate of heat release rate and ignition delay period) parameters were improved run with preheated POME oil at 114^0C fuel inlet temperature and their blends with diesel and closer to diesel fuel. The results also showed that preheating intake air plays a massive effort for improvement of performance, combustion and emission parameters of diesel engine compared with without intake air preheating at 34 ^0C. The test results also showed that BSFC and BTHE were improved with increases of intake air temperature, and in-cylinder peak pressure increased and ignition delay period decreased with increases in intake air temperature. And, intake air preheat may be proved to be one of the effective solutions to emission control. In this study due to a number of pages' limitation, we cannot able to include emission analysis results. In summary from our experimental investigation of combined effects Methyl ester and intake air preheating may be proved valuable option for the application of existing diesel engines run with biodiesel blends as diesel fuel.

.

Keywords: Fuel Preheating, Intake Air Preheating, Diesel Engine, POME

NOMENCLATURE
BSFC   Brake Specific Fuel Consumption
BTHE   Brake Thermal Efficiency
ID   Ignition Delay
PCP   Peak Cylinder Pressure
POME   Palm Oil Methyl Ester
PPOME Preheated Palm Oil Methyl Ester

INTRODUCTION

Nowadays, in all over the world alternative fuels sources of methyl ester biodiesel oils are receiving a lot of attention and applied in many countries as a diesel fuel in a diesel engine to overcome the rapid depletions, price hikes and pollutions of mineral diesel fuel. The concerns of these, so far enormous experimental research studies have been conducted on many aspects to improve the parameters of existing diesel engine running with biodiesel diesel bends or pure methyl ester biodiesel. Thus the use of pure biodiesel

in a diesel engine without any modification on biodiesel or fuel injection system leads poor engine performance, combustion and emission parameters because of high kinematic viscosity and density which causes poor fuel atomization and mixing, and incomplete combustion [1-3]. Hence, the direct use methyl ester biodiesel in diesel engine attained improper homogeneity in charge and fuel atomization, resulted in the to decrease the overall efficiency of diesel engine compared with run with fossil diesel fuel. This experimental work is focused to investigate the effects preheating of methyl ester biodiesel for reduction of their high viscosity, high density, and cold flow properties and for improving fuel atomization and mixing, and combustion efficiency. In addition, the impacts of intake air preheating for maximization of performance and combustion parameters, and reductions of emission concentrations of a diesel engine running with pure methyl ester and their blends with diesel fuel also examined.

Numerous efforts have been made by scholars, scientist and researchers for improving operation diesel engine running with biodiesel blends, preheated biodiesel blends with air inlet preheating and without air preheating. The majority of previous studies on diesel engine run at different fuel inlet temperature of various biodiesel [4−5]. They found that the kinematic viscosity and density a value of pure biodiesel B100 oils was decreased with an increased the heating temperature, and their values at higher temperatures were close to diesel fuel. A few earlier studies indicated that preheated biodiesel in compression ignition engine resulted in improved engine performance parameters and reduced emission concentration compared with without preheating case [6-8] However, the literature shows limited analysis on the use of preheating biodiesel in diesel engines. A few types of research have been conducted on the effect of preheating intake air on diesel engine performance and emission analysis in diesel engine [9-11]. They found that the BSFC and BTHE significantly improved with intake air preheating temperature. However, there are not extensive studies on combined effects of fuel and intake air preheating on a diesel engine, it is hard to make a conclusion regarding diesel engine performance and combustion analysis about a combined result in past literature.

THE OBJECTIVE OF THE STUDY

The primary aim of this experimental study is to evaluate the combined effects fuel and intake air preheating on performance parameters, combustion and emission characteristics of a diesel engine running with POME biodiesel blends.

EXPERIMENTAL SETUPS AND PROCEDURES

The experiments are carried out at the rated speed of 1500 rev/min with variable load conditions. A separate fuel and air preheater arrangement is made to preheat the POME

biodiesel oil and air. The POME is heated to (54, 66, 78, 90, 102, 114 and 126 ^{0}C), and intake air is heated at exhaust temperature of (34, 41, 49, 61 ^{0}C) with a variation of engine load (10%, 30%, 50%, 70% and 90%). Experiments are conducted at all temperatures. Performance, emissions and combustion parameters are analyzed and compared with mineral diesel fuel. In this study, among a few techniques, preheating option is applying for improving the existing problems of POME biodiesel oil for reducing its kinematic viscosity and density. For this regards, a simple counter flow shell and tube type heat exchanger are designed and fabricated considering Tubular Exchanger Manufacturing Associations (TEMA) and America society of mechanical engineers (ASME) codes [12]. The experimental analysis was carried out on single cylinder cylinders, four strokes, variable compression direct injection diesel engine.

RESULTS AND DISCUSSION
Effect of Preheating on Fuel Property of POME
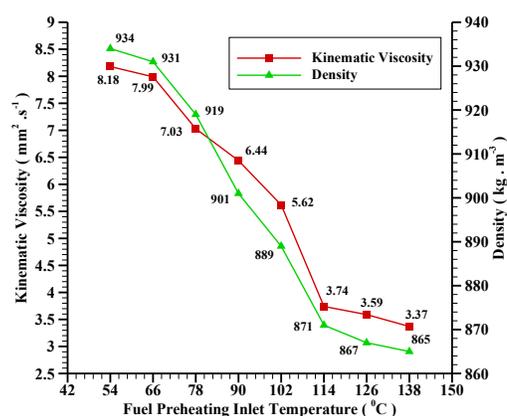
FIGURE 1. Variations of kinematic viscosity and density of POME with fuel inlet preheating temperature.

The Palm Oil Methyl Ester B100 biodiesel used in this study, have relatively higher kinematic viscosity and density values compared with diesel fuel. POME oil needs to meet minimum Biodiesel standards which are widely known EN 14214, ASTM D 6751, and IS 15607 to solve fuel atomization and spray characteristics problems, caused by high fuel viscosity, high density and surface tension leading poor engine performance characteristics and pollution [13]. Hence, in this study the important properties (viscosity and density) of POME oil is attempted to improve using a heating technique. It is clearly seen in Fig. 1, when fuel inlet temperature is at 54 ^{0}C, the viscosity and density values were (8.18 mm^2 s^{-1}) and (934 kgm^{-3}) for POME oil respectively. When the temperature increased to 66 ^{0}C, the corresponding numbers were (7.99 mm^2 s^{-1}) and (931 kg m^{-3}), respectively. However, when the oil heated at 114 ^{0}C, the values were (3.74 mm^{2}s^{-1}) and (871 kgm^{-3}) respectively and the two important properties are within ASTM, EN and IS standards (Kadu and Sarda 2010). It is almost horizontal for

preheated POME oil after 114^{0}C. When the fuel preheating temperature increases beyond 114 ^{0}C, the preheated POME oil in fuel mixture started to vapor and make vapor lock in the fuel line. Hence, among the various preheating temperature heating the POME oil at 114^{0}C, brings down the viscosity and density values, and close to diesel fuel.

Effect of Preheat POME on Performance Parameters

The various performance parameters of brake Specific fuel consumption (BSFC) and brake thermal efficiency (BTHE) with engine load for different test fuels are discussed as follows. The BSFC for various test fuels (diesel fuel, unheated POME biodiesel, preheated POME biodiesel at (90 and 102 ^{0}C) has shown in Fig. 2. Results clearly indicated that BSFC for different tested fuels are decreases as the load is increases. It also shown that, BSFC for POME oil decreased with heating and decreased with increased fuel preheating temperature over the given load range due to poor mixture formation as a result of high viscosity and density. The BSFC of Preheated POME biodiesel at (90 and 102 ^{0}C) is lower than unheated POME, but closer to diesel fuel [14]. The BSFC for diesel fuel diesel fuel was lower compared all other tested fuel over load rage. At 90 ^{0}C and 102 ^{0}C preheated fuel temperature for POME biodiesel at 90 % load, the BSFC decreased from (0.467423 to 0.385401 kg/kW-hr.) and (0.467423 to 0.361805 kg/kW-hr) respectively with unheated POME biodiesel. While the BSFC for diesel fuel (D100) was 0.304224 kg/kW hr. Hence, the poor properties of biodiesels are improved and closer to diesel fuel, and offered comparable engine performance parameter using a preheating.
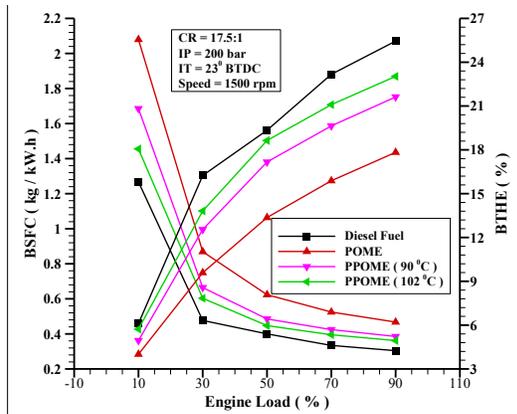
FIGURE 2. Variations of BSFC and BTHE for different test fuels in diesel engine with engine load.

Figure 2 also show the brake thermal efficiency (BTHE) for various test fuels with variation of preheating fuel temperature under varying loads as shown in Fig.2. BTHE of unheated as well as preheated POME oil was found lower than diesel. The possible reasons are higher fuel

viscosity. Higher fuel viscosity results in poor atomization and larger fuel droplets followed by inadequate mixing of biodiesel oil droplets and heated air. However, BTHE for preheated POME oil at 90^{0}C and 102^{0}C respectively were higher than unheated POME oil over the load ranges. The reason for this behavior may be improved fuel atomization because of reduced fuel viscosity [15]. At 90 ^{0}C and 102 ^{0}C preheated fuel temperature for POME biodiesel at 90 % load, the BTHE increased from (17.83 to 21.62%) and (17.83 to 23.03 %) compared with POME100 respectively. Although the BTHE for diesel fuel (D100) was 25.45 %. Hence, the poor properties of biodiesels are improved and closer to diesel fuel, and offered comparable parameters. Test results (data) indicated that preheating increases the thermal efficiency preheated POME biodiesel at full engine load. This is a good indication of improvement of spray characteristics and atomization due to preheat.

Effect of Preheat intake air on Performance Parameters
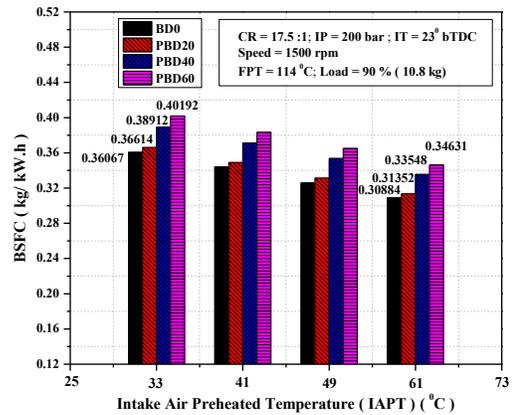
FIGURE 3. Variations of BSFC for different test fuels in diesel engine with intake air preheating temperature.

The experimentation is carried out to find the effect of intake air preheating on engine performance parameters. For these analyses, intake air preheating at different temperatures (33, 41, 49 and 61^{0}C) at constant 90 % load condition for induction of diesel fuel (BDO), and preheated POME at 114 ^{0}C fuel inlet temperature before blend with diesel fuel (PBD20, PBD40 and PBD60), respectively.

Figure 3 showed that, the BSFC for each fuel decrease with increasing intake air preheating due a decreased ignition delay and improved combustion efficiency. For 90% load the minimum BSFC is attained at a preheating of 61°C and values were (0.30884, 0.31352, 0.33548 and 0.34631 kg/Kw.hr), where the BSFC was seen maximum at 33^{0}C and the value being (0.36067, 0.36614, 0.38912 and 0.40192 kg/Kw.hr). The average percentage decrease in BSFC for 61°C to be (14.37, 14.37, 13.78 and 13.84%) when compared to the conventional engine without preheating intake air at 33^{0}C.
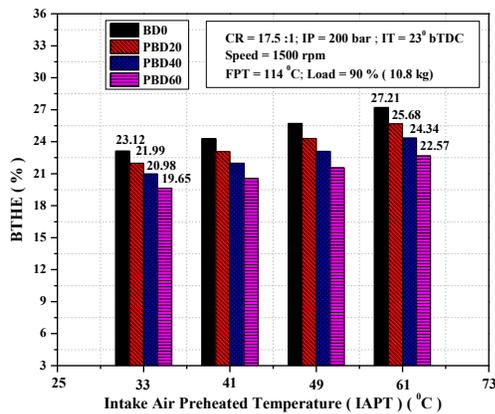
FIGURE 4. Variations of BTHE for different test fuels in diesel engine with intake air preheating temperature.

The trends of BTHE for diesel fuel and various preheated biodiesel blends with intake air preheating temperatures are opposite to that of the graphs of BSFC. Figure 4 shows the variation in BTHE with an increase in the intake air preheating temperature for diesel fuel and different amount of preheated biodiesel-diesel blend inducted. The test results showed that BTHE increases with increasing intake air preheating temperature. It is seen in Fig. 4, the BTHE for different tested fuels is increased with increased intake air temperature from (33^0C) without preheating intake air to (41, 49 and 61^0C) intake air preheating temperatures. For 90 % load, the maximum efficiency obtained is (27.21, 25.68, 24.34 and 22.57 %) at a preheating temperature of 61°C where the minimum was found at 33^0C and to be (23.12, 21.99, 20.98 and 19.65 %), respectively for BD0, PBD20, PBD40 and PBD60 blends. The percentage increase in efficiency for this condition is (17.69, 16.78, 16.02 and 14.86 %) when compared to the conventional engine with stock intake air operation or without preheating intake air.

Effect of Preheat Intake Air on Combustion Characteristics

The primary purpose of preheating intake air is to improve combustion efficiency due to shortening of ignition delay. Figure 5(a-b) shows the peak cylinder pressure for various ted fuels was increased with engine load due to a high air-fuel mixture formation at high load. Results also that, increasing intake air temperature helps to an increased peak pressure of the cylinder. For 90% load, the maximum PCP is attained at a preheating of 61°C and values were (60.7, 62.4, 64.2, 64.6 and 65.6 bar), where the PCP was seen minimum at 33^0C and the value being (59.2, 61.3, 62.1, 63.6 and 64.1 bar). The average percentage increase in PCP for 61°C was to be (2.53, 1.79, 3.38, 1.57 and 2.34%) when compared to without preheating intake air at 33^0C.

Figure 6 shows a variation of ignition delay for various test fuels with engine load at 33 0C and 61^0C intake air

preheated temperature. Result revealed that the ignition delay period for all tested fuel decreased with engine load as well as intake air preheating temperature. This is because increased intake air temperature the overall combustion efficiency increased due to better mixing characteristics of high-temperature air with inducted vaporized fuel.
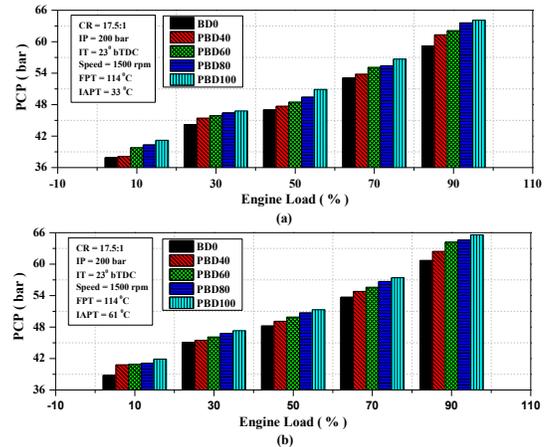
FIGURE 5. Variations of PCP for test fuels in a diesel engine with load with and without intake air preheating.
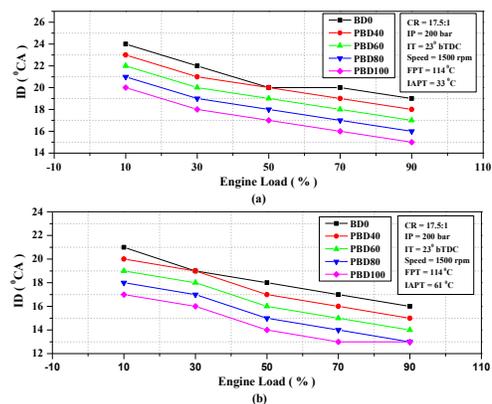
FIGURE 6. Variations of ID for test fuels in a diesel engine with load with and without intake air preheating.

CONCLUSIONS

The aim of this paper is to investigate the influences of fuel and intake air preheating in diesel engine run with different test fuels of biodiesel-diesel blends. It was seen that the fuel property of POME oil (kinematic viscosity and density) was decreased with increased fuel inlet preheating temperatures, and at maximum preheating fuel, the temperature was close to diesel fuel. Increased fuel preheating temperature improved engine performance parameters (BSFC and BTHE) compared to unheated POME under varying loading conditions. Preheating intake air at different also improved engine overall efficiency. Increased intake air temperature decreased brake specific fuel consumption, and increased brake thermal efficiency,

peak cylinder pressure, and reduced ignition delay period. Hence, as per our experimental finding, we can suggest a combined fuel and intake air preheating technique help to improve the existing diesel engine performance and combustion parameters using a different percentage of biodiesel-diesel blended fuels.

REFERENCES

[1] Bari, S., Yu, C.W. and Lim, T.H., 2002. Performance deterioration and durability issues while running a diesel engine with crude palm oil. *Proceedings of the Institution of Mechanical Engineers, Part D: Journal of Automobile Engineering*, *216*(9), pp.785-792.

[2] Kegl, B., Kegl, M. and Pehan, S., 2016. *Green diesel engines*. Springer London Limited.

[3] Yoon, S.H., Park, S.H. and Lee, C.S., 2007. Experimental investigation on the fuel properties of biodiesel and its blends at various temperatures. *Energy and Fuels*, *22*(1), pp.652-656.

[4] Aksoy, F., Baydir, S.A. and Bayrakçeken, H., 2009. An investigation on the effect in the viscosity of canola and corn oil biodiesels at a temperature range of 0 to 100 C. *Energy Sources, Part A: Recovery, Utilization, and Environmental Effects*, *32*(2), pp.157-164.

[5] Bari, S., Lim, T.H. and Yu, C.W., 2002. Effects of preheating of crude palm oil (CPO) on injection system, performance and emission of a diesel engine. *Renewable Energy*, *27*(3), pp.339-351.

[6] Agarwal, D. and Agarwal, A.K., 2007. Performance and emissions characteristics of Jatropha oil (preheated and blends) in a direct injection compression ignition engine. *Applied thermal engineering*, *27*(13), pp.2314-2323.

[7] Kalam, M.A. and Masjuki, H.H., 2004. Emissions and deposit characteristics of a small diesel engine when operated on preheated crude palm oil. *Biomass and Bioenergy*, *27*(3), pp.289-297.

[8] Shahadat, M.M.Z., Nabi, M.N., Akhter, M.S. and Tushar, M.S.H.K., 2008. Combined Effect of EGR and Inlet Air Preheating on Engine Performance in Diesel Engine. *International Energy Journal*, *9*(2).

[9] Yilmaz, N., 2012. Performance and emission characteristics of a diesel engine fuelled with biodiesel–ethanol and biodiesel–methanol blends at elevated air temperatures. *Fuel*, *94*, pp.440-443.

[10] Torregrosa, A.J., Olmeda, P., Martin, J. and Degraeuwe, B., 2006. Experiments on the influence of inlet charge and coolant temperature on performance and emissions of a DI Diesel engine. *Experimental Thermal and Fluid Science*, *30*(7), pp.633-641.

[11] Cao, E., 2009. *Heat transfer in process engineering*. McGraw Hill Professional. Chap. 6-7, pp 115-215.

[12] Kakac, S., Liu, H. and Pramuanjaroenkij, A., 2012. *Heat exchangers: selection, rating, and thermal design*. CRC press. Chap.2, pp 33-70.

[13] Kegl, B., Kegl, M., and Pehan, S. (2016). *Green diesel engines*, Springer.

[14] Aksoy, F., Baydir, S. A., and Bayrakçeken, H. (2009). "An investigation on the effect in the viscosity of canola and corn oil biodiesels at a temperature range of 0 to 100 C." *Energy Sources, Part A: Recovery, Utilization, and Environmental Effects* 32(2): 157-164.

[15] Qi, D. H., Lee, C. F., Jia, C. C., Wang, P. P., and Wu, S. T. (2014). "Experimental investigations of combustion and emission characteristics of rapeseed oil–diesel blends in a two cylinder agricultural diesel engine." *Energy conversion and management* 77: 227-232.

SEEC-2018-109

DEVELOPMENT OF 4-STROKE SINGLE CYLINDER METHANOL FUELLED DIRECT INJECTION SPARK IGNITION ENGINE

Shivashish Kumar Gupta
Engine Research Laboratory
Department of Mechanical Engineering
Indian Institute of Technology Kanpur
Kanpur-208016, India
Email: kgshiva@iitk.ac.in

Avinash Kumar Agarwal
Engine Research Laboratory
Department of Mechanical Engineering
Indian Institute of Technology Kanpur
Kanpur-208016, India
Email: akhips@iitk.ac.in

Prashumn Wrekkonge
Engine Research Laboratory
Department of Mechanical Engineering
Indian Institute of Technology Kanpur
Kanpur-208016, India
Email: prashumn@iitk.ac.in

Tushar Agarwal
Engine Research Laboratory
Department of Mechanical Engineering
Indian Institute of Technology Kanpur
Kanpur-208016, India
Email: tushara@iitk.ac.in

ABSTRACT

Vehicular emissions are a major concern in today's world. With the Paris Climate agreement, other Government initiatives and more stringent norms set by Pollution Control Board, it is the need of the hour to find a suitable solution to reduce the vehicular emissions, provide a cleaner environment and a sustainable future for automotive industries. In order to meet such stringent pollution control norms, more and more efforts are required to develop alternatives to conventional fossil fuels. Amongst the alternative fuels, alcohol based fuels (methanol and ethanol) and hydrogen have been the most attractive ones. Methanol, having higher research octane number, thus providing higher thermal efficiency and a significant reduction in NOx and CO emissions as compared to simple gasoline fuelled engine, is really lucrative to be accepted as an automotive fuel. On the other hand, very high latent heat of vaporization, corrosive nature and increased formaldehyde emissions are some of the major concerns to be taken care of, before incorporating it as a viable alternative. Methanol's very high latent heat of vaporization poses a strong challenge in order to decide the mode of injection and ignition while operation. Two major possibilities for methanol injection are multi-port fuel injection (MPFI) and direct in-cylinder injection (DI). Both the methods, MPFI and DI, have their own pros and cons and each need to be evaluated thoroughly, based on physical and chemical properties of methanol, before choosing one over the other. In this paper, we will discuss some of the critical features of direct in-cylinder injection (DI) of methanol, and to what extent, does it fulfills the requirements for methanol to be used as a successful alternative to conventional fossil fuels. The conclusion would then be utilized to build an experimental setup for testing a single cylinder spark ignition engine on 100% methanol, using an open-ECU.

Keywords: DI, MPFI, Open ECU, Methanol.

INTRODUCTION

Due to environmental concerns, stricter pollution norms and increased global warming, efforts are being made in finding out cleaner and more environment friendly fuels, which can provide better fuel efficiency, while at the same time does not require much structural changes within the engine. Conventional fossil fuel like gasoline is increasingly used for powering light-duty vehicles. The exponentially depleting fossil fuel resources are constantly

questioning the sustainability of conventional fossil fuels and their continuation to remain a primary source of energy for automotive industry. Moreover, the pollution control norms related to CO, HC, SOx and NOx emissions are being revised and made stricter in quick successions, eventually resulting in higher processing cost for fuels, installation of expensive catalytic convertors or particulate filters in the exhaust system etc. to meet the pollution norms. Introducing cleaner and environment friendly alternative fuels is one of the key solutions. Alcohol based fuels, like methanol & ethanol, hydrogen fuel cells and electric powered vehicles are some of the alternatives that have caught the eye of researchers in recent times.

Methanol can be produced from coal, biomass, biogas etc. It has higher hydrogen-to-Carbon ratio and higher research octane number resulting in reduction in HC emissions and better fuel efficiency as compared to gasoline. Nearly all the regulated pollutants like NOx, SOx, CO etc. will be substantially reduced, as compared to conventional fossil fuels, with methanol used as an automotive fuel.

Direct in-cylinder injection of methanol is chosen over port-fuel injection due to very high latent heat of evaporation of methanol, making it difficult for cold starting purposes using port-fuel injection. Direct in-cylinder injection accompanied by a spark plug ensures maximum utilization of fuel and promises better combustion performance as compared to port-fuel injection. Since, the fuel will be directly injected into the cylinder, stratified charge combustion may be utilized for part load operations, to achieve better fuel economy and lower HC, NOx and CO emissions over port-fuel injection, owing to overall lean burning mixtures. This is similar to gasoline direct injection (GDI) technique, which utilizes stratified charge combustion by achieving various strata of different air-fuel ratios within the combustion chamber, thus allowing better fuel economy at part load operation without compromising with power output during full load operation. Direct injection of methanol also ensures better response time for change in injection and spark timings. Considering direct injection over port fuel injection, a high pressure (~100 bar) fuel injector and fuel pump will be required. Moreover, the engine cylinder head needs to be modified to accommodate the high pressure fuel injector along with the spark plug. Owing to the corrosive nature of methanol, special care needs to be taken for piston rings, gaskets, seals, etc. and appropriate material must be used to avoid any corrosive damage.

In the present study, we wish to set-up an experimental test-bench to conduct experiments on a 4-stroke, single cylinder, gasoline fuelled, spark ignition engine, using 100% methanol as fuel. The study aims at successfully running the engine on 100% methanol, generating the base fuel maps for methanol and fine-tuning the engine parameters like spark timing, fuel injection timing etc. by using an open-ECU. Having achieved the same, we intend to incorporate appropriate catalytic converters in the exhaust tailpipe to reduce the NOx and formaldehyde emissions.

EXPERIMENTAL SETUP

To perform the experiments, we will be using Royal Enfield 500 cc Classic 4-stroke, gasoline fuelled spark ignition engine, coupled to a Dynomerk eddy-current dynamometer, with load and speed control flexibility. Engine and dynamometer are coupled using direct chain-sprocket coupling. The engine will be controlled using Performance electronics PE3 SP000 open-ECU (engine control unit).

To analyze the real-time in-cylinder combustion data, we will be using AVL combustion analyzer, with current clamps used to tap low-voltage sensor data. This would help us generate pressure-crank angle curve along with spark timing and fuel injection timing, hence providing us with the data required to build base fuel-maps for gasoline. Subsequently, we will tweak the gasoline fuel maps to fine-tune the engine parameters optimized for 100% methanol to work as fuel.

In order to achieve high fuel injection pressure, HP injection valve HDEV 5.2 will be used. It can provide flow rates up-to 1500 cm^3/min at 100 bar pressure. The injector is methanol compatible and provides multi-hole fuel injection with a spray angle varying from 8° to 20°. Along with this, HDP 5-LW, high pressure fuel pump, with integrated control valve, will be used, which allows pressures up-to 500 bar.
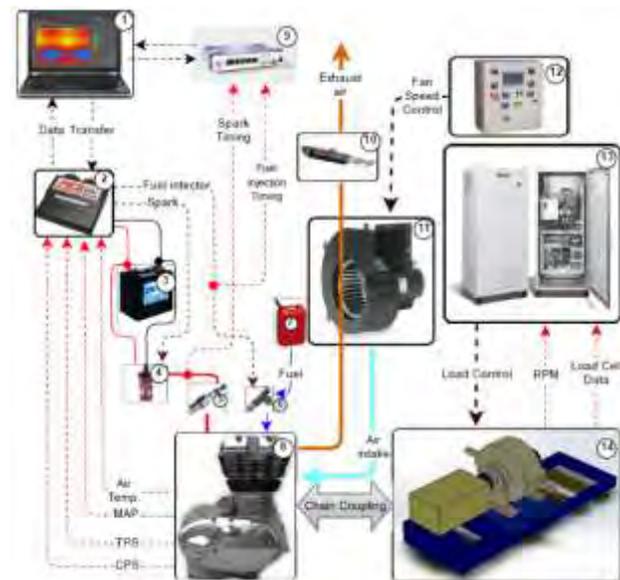
1- Computer interface, 2- Open-ECU, 3- Battery, 4- Laminar Flow Element, 5- Spark plug, 6- Fuel injector, 7- Fuel Tank, 8- Test engine, 9- Data acquisition system, 10-Exhaust tailpipe, 11- Intake air-filter, 12- Cooling fan controller, 13- Dynamometer controller, 14- Dynomerk eddy-current dynamometer

FIGURE 1: Schematic of the experimental setup for generating fuel-maps for methanol

CONCLUSION

The experiments will be performed on a 4-stroke, single-cylinder, gasoline fuelled, spark ignition (SI) engine. The engine will be spark ignited along with direct fuel injection (DISI). The objective of the study is to convert a 4-stroke, single cylinder, SI engine on 100% methanol using direct injection of methanol. An open-ECU will be used to control the engine parameters like fuel injection timing, spark advance etc. and eventually generate the fuel-maps with methanol as the only fuel.

Finally, the study aims to prove the feasibility of methanol to replace conventional fossil fuel (gasoline) for automotive vehicles, achieving substantially lower emissions (CO, NOx and HC) without any compromise with the power or torque output.

REFERENCES

[1] L. Bromberg, D. R. Cohn, 2008. "Effective octane and efficiency advantages of direct injection alcohol engines", MIT Laboratory for Energy and the Environment Report.

[2] Wyszynski, L., Stone, C., and Kalghatgi, G., 2002, "The Volumetric Efficiency of Direct and Port Injection Gasoline Engines with Different Fuels," SAE Technical Paper 2002-01-0839.

[3] George, S., Schock, H., Gray, C., Hamady, F. et al., 2001, "Design of a High Compression, Direct-Injection, Spark-Ignition, Methanol Fueled Research Engine with an Integral Injector-Ignition Source Insert," SAE Technical Paper 2001-01-3651.

SEEC-2018-110

DEVELOPMENT OF 4-STROKE SINGLE CYLINDER METHANOL FUELLED PORT FUEL INJECTION SPARK IGNITION ENGINE

Prashumn Wrekkonge
Engine Research Laboratory
Department of Mechanical Engineering
Indian Institute of Technology Kanpur
Kanpur-208016, India
Email: prashumn@iitk.ac.in

Avinash Kumar Agarwal
Engine Research Laboratory
Department of Mechanical Engineering
Indian Institute of Technology Kanpur
Kanpur-208016, India
Email: akhips@iitk.ac.in

Shivashish Kumar Gupta
Engine Research Laboratory
Department of Mechanical Engineering
Indian Institute of Technology Kanpur
Kanpur-208016, India
Email: kgshiva@iitk.ac.in

Tushar Agarwal
Engine Research Laboratory
Department of Mechanical Engineering
Indian Institute of Technology Kanpur
Kanpur-208016, India
Email: tushara@iitk.ac.in

ABSTRACT

Vehicular emissions are a major concern in today's world. With the Paris Climate agreement, other Government initiatives and more stringent norms set by Pollution Control Board, it is the need of the hour to find a suitable solution to reduce the vehicular emissions, provide a cleaner environment and a sustainable future for automotive industries. In order to meet such stringent pollution control norms, more and more efforts are required to develop alternatives to conventional fossil fuels. Amongst the alternative fuels, alcohol based fuels (methanol and ethanol) and hydrogen have been the most attractive ones. Methanol, having higher research octane number, thus providing higher thermal efficiency and a significant reduction in NOx and CO emissions as compared to simple gasoline fuelled engine, is really lucrative to be accepted as an automotive fuel. On the other hand, very high latent heat of vaporization, corrosive nature and increased formaldehyde emissions are some of the major concerns to be taken care of, before incorporating it as a viable alternative. Methanol's very high latent heat of vaporization poses a strong challenge in order to decide the mode of injection and ignition while operation. Two major possibilities for methanol injection are multi-port fuel injection (MPFI) and direct in-cylinder injection (DI). Both the methods, MPFI and DI, have their own pros and cons and each need to be evaluated thoroughly, based on physical and chemical properties of methanol, before choosing one over the other. In this paper, we will discuss some of the critical features of direct in-cylinder injection (DI) of methanol, and to what extent, does it fulfills the requirements for methanol to be used as a successful alternative to conventional fossil fuels. The conclusion would then be utilized to build an experimental setup for testing a single cylinder spark ignition engine on 100% methanol, using an open-ECU.

Keywords: MPFI, single cylinder spark ignition, Open ECU, methanol.

INTRODUCTION

Due to concerns of environmental preservation and global warming, strong efforts are being made to find out the environment friendly alternative fuels, which produce lower emissions, have better fuel economy and require minimalistic structural changes in the engine. Apart from the environmental pollution caused by the Carbon monoxide (CO), unburnt hydrocarbons (HC), oxides of Nitrogen (NOx) and oxides of Sulphur (Sox) emmisions,

the depletion of the fossil fuels is also a major concern. Also, due to the stringent emission norms, the processing cost of these fuels is rising. In order to minimize the emmisions, a shift towards alternative fuels such as alcohol based fuels is being made.

Gasoline engines are highly popular in powering light duty vehicles such as motorcycles and two wheelers Methanol has a production advantage that it can be produced from any resource which can be utilized to form the synthesis gas, such as biomass, agriculture and timber waste, municipal waste etc. Methanol has a higher Hydrogen to Carbon ratio, which results in reduction of the HC emmisions. The octane number of methanol is higher and hence there is reduction in the knock. However, a lot of factors have to be considered before using methanol as a fuel in SI gasoline fuelled engine such as higher latent heat of vaporization, lower calorific value, lower stoichiometric air fuel ratio and the corrosive nature of the fuel.

Multi- port fuel injection requires minimum changes in the engine and no modification of the cylinder head is required. As compared to the direct injection, low pressure fuel pumps and fuel injectors are required in case of MPFI and there is less complexity involved compared to the DI. . Also, as the fuel and air are better mixed, the partially rich zones are reduced there is more reduction in NOx formation as compared to DI. However, the higher latent heat of vaporization poses a challenge during the cold start of the engine because the pre ignition temparatures are reduced due to higher latent heat of vapourisation. Also the evaporation of the fuel will be limited due to the high latent heat of vaporization., and hence the cold starting of the engine is a trouble, but the modification of spark parameters can aid the cold start. Apart from this, methods such as external heating aids and the fuel modifications can also be employed in order to overcome the challenges associated with the cold start. Another factor to be considered is the corrosive nature of methanol, which requires the changes in the materials and appropriate coating of the piston rings.

In this study, experimental setup is made for a single cylinder, four stroke, spark ignition engine using 100% methanol in port fuel injection. The base fuel maps for 100% methanol are generated and the parameters such as spark timimg and injection timing are modified using open engine control unit (ECU) in order to achieve more power and better efficiency. The appropriate catalytic converters are then applied in order to reduce the NOx and HC emmisions

EXPERIMENTAL SETUP

To perform the experiments, we use the Royal Enfield classic 500 cc engine, which is a four stroke, spark ignited, gasoline fueled engine. This is an air cooled engine with

wet sump lubrication and two valves per cylinder. This engine is coupled to the Dynalec dynamometer, which is an eddy current type dynamometer. The engine is coupled to the dynamometer using chain sprocket coupling and is mounted on a three-axis adjustable cast iron bed.

The initial experiments are conducted on the engine using the base fuel maps for gasoline. The real time combustion data is analyzed using AVL indi-micro combustion analyzer. The spark plug and the injector data is tapped using the current clamps. Also, a spark plug pressure transducer is used to analyze the pressure inside the cylinder. This data is used to generate the spark timing and injection timing tables at various load vs. rpm conditions along with the crank angle vs pressure plots. The base fuel maps for the gasoline are obtained and accordingly fed in the PE SP3 000 open ECU, made by Performance Electronics. The fuel maps for 100% methanol are then obtained and fine tuned by tinkering with the above maps.

Apart from this, methanol compatible fuel injector and fuel pump is required. Bosch EV 14 fuel injector series, which is 100% methanol compatible and operates at 3 bar pressure is used and Bosch FP300 100% methanol compatible fuel pump is used along with a Bosch Mini 2 pressure regulator.

In the initial stages with methanol fuel, the engine is first run on gasoline fuel in order to raise the temperature and then methanol is used, in order to overcome cold starting challenges.
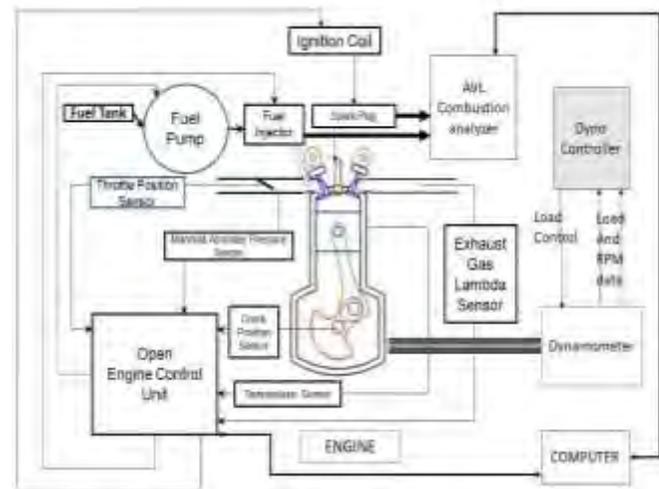
FIGURE 1: Schematic of the experimental setup for 4-stroke single cylinder methanol fuelled port fuel injection Spark ignition Engine

CONCLUSIONS

The experiments are performed on a single cylinder, port fuel injection, spark ignition motorcycle engine using

100% methanol as a fuel. The main objective of the experiments is to convert the gasoline based 4-stroke two wheeler engine to 100% methanol based engine with as low modifications as possible. An open ECU is installed on this engine to tune this engine on 100% methanol based fuel.

Finally, it is aimed to be proved that methanol can be used as an alternative fuel in light duty vehicle engines such as two/ three wheeled vehicles and motorcycles. The use of methanol results in lower HC and NOx emmisions compared to gasoline.

REFERENCES

[1] Tiegang Hu,Yanjv Wei, Shenghua Liu, Longbao Zhou, 2007 "Improvement of Spark-Ignition (SI) Engine Combustion and Emission during Cold Start, Fueled with Methanol/Gasoline Blends", Energy & Fuels 2007, 21, 171-175.

[2] Melissa S. Pike, Timothy J. Guglielmello, Jeffrey W. Hodgson, 1993 "Development of a Cold-Start Device for Methanol-Fueled Engines", SAE Paper No. 932772, Society of Automotive Engineers, 1993.

SEEC-2018-111

REMOVAL OF PHARMACEUTICALS IN SMBR AT VARYING HRT AND DYNAMICS AND DIVERSITY OF THE BACTERIAL COMMUNITY.

B. TIWARI[a], Y.OUARDA[a], A Azais[a], P. DROGUI[a*], R.D. TYAGi[a*], M.A. VAUDREUIL[b], G.BUELNA[c], S. SAUVÉ[b], R. DUBÉ[c]

[a] Eau, Terre et Environnement – INRS

[b] Université de Montréal

[c] Centre de recherche industrielle du québec (CRIQ)

*rd.tyagi@ete.inrs.ca , patrick.drogui@inrs.ca

Abstract

In this study, the removal of 4 types of pharmaceuticals compounds, namely: ibuprofen, carbamazepine, estradiol and venlafaxine in submerged membrane bioreactor system (SMBR) were evaluated using synthetic wastewater at HRT duration of 6, 12 and 18 h. Study on bacterial community dwelling in MBR was performed. The removal rate of ibuprofen (>90%), estradiol (>90%) and venlafaxine (<10%) were similar at varying HRT. The carbamazepine shows negative removal at HRT duration of 12 and 18h. In spite of high removal, the clogging of the membrane was frequent, which was evident by the increase in transmembrane pressure (TMP) to 40KPa in one week of operation. The removal of pharmaceuticals was almost uniform in all the treatment condition, however, clogging of MBR was decreased with increased HRT, which was due to the slow biomass generation rate at long HRT. The results on the metagenomics will be discussed in presentation.

Keywords: Pharmaceuticals, Submerged membrane bioreactor system (SMBR), Hydraulic Retention time (HRT).

Introduction

Research advancement and discoveries in the field of medical science and concomitant increase in population lead to high demand for production of pharmaceuticals. These pharmaceutical (biologically active) compounds were not fully metabolized by the body and thus excreted out in wastewater. These compounds remains unchanged during wastewater treatment plant operation and enters into the receiving environment via the discharge of treated water [1]. Persistence of pharmaceutical compounds in aquatic environment becomes a major concern because they deteriorate the water quality and impart toxic effects on living organisms. Published studies on removal of pharmaceuticals from wastewater revealed that membrane bioreactor (MBR) could be an efficient treatment process for pharmaceuticals removal [2]. Membrane bioreactor (MBR) offers flexibility in the management of operating conditions and allows the application of high biomass concentration and long sludge/solid retention time. High biomass concentration in MBR could promote removal of micro-pollutant via adsorption, which in turn increases the required contact time of pharmaceuticals with the degrading microbial community. High SRT facilitates the proliferation of microbial community dwelling in sludge, which enhances the production of the microbial catabolic enzyme in the bioreactor that ultimately enhances the efficiency of biological degradation of drug residues and their metabolite.

Microbial community is the essential component of WWTP due to their involvement in nutrient and pollutant removal. In biological treatment of wastewater containing pharmaceuticals, the analysis of microbial community is necessary because presence of pharmaceuticals in wastewater treatment process may lead to (i) hinder growth of microorganisms, (ii) development of antibiotic resistance, (iii) shift and drift in microbial community, (iv) consequent change in biodegradation or treatment efficiency, and (v) formation of toxic intermediates [3].. Therefore, a systematic research study is required on the understanding of dynamics of the microbial communities and consequences on the treatment process. In present study, the removal of 4 types of pharmaceuticals compounds, namely: ibuprofen, carbamazepine, estradiol and venlafaxine in submerged membrane bioreactor system (SMBR) were evaluated using

synthetic wastewater at HRT duration of 6, 12 and 18 h. Study on bacterial community dwelling in MBR was performed in order to get the in-depth knowledge of composition and diversity of microbial community that is responsible for biological transformation of pharmaceuticals to simpler and less toxic products.

Material and Methods

Preparation of synthetic wastewater and pharmaceuticals stock

Synthetic solution was prepared by diluting the already prepared 20X mineral stock solution with distilled water, then by adding glucose and pharmaceutical stock solution (2ppm) to achieve desired COD, and pharmaceutical concentration. The synthetic wastewater contained $(NH_4)_2SO_4$ -353.57; KH_2PO_4 - 92.19 $MgSO_4$ -34.68; $CaCl_2.2H_2O$ - 22.10; $FeCl_3$ - 11.63; $CuSO_4$ - 0.07 $Na_2MoO_4.2H_2O$ - 0.10; $MnSO_4.H_2O$ - 0.12; $ZnCl_2$ - 0.23; $CoSO_4.7H_2O$ -0.48; Na_2CO_3- 428.60; $C_6H_{12}O_6$- 938.35 in mg L^{-1} range. Pharmaceutical compounds was purchased from Sigma Aldrich (purity 99%). Stock solution of pharmaceuticals (2 ppm) was prepared by dissolving a known mass of pharmaceutical in distilled water. The stock solution of pharmaceutical pollutants was stored at 4°C and utilized within 30 days. The concentration of estradiol, ibuprofen, and carbamazepine chosen for study was 10 μg L^{-1} and 200 ng L^{-1} for venlafaxine.

Experimental conditions

The study was performed by using a submerged membrane bioreactor (MBR) with a working volume of 5.0 L in continuous mode Membrane bioreactor was initially inoculated with activated sludge obtained from (Canada Victoriaville, Quebec, Canada) municipal wastewater treatment plant. A synthetic effluent prepared daily was fed in membrane bioreactor. The pH and temperature of the MBR was 7±0.5 and 20°C±1°C, respectively in order to provide a favorable environment condition for the growth of micro-organisms.

In order to assess the influence of Hydraulic retention time (HRT), three HRT duration of 6h, 12h and 18h was chosen. The choice of HRT duration were based on the fact that longer HRT, resulting in lower organic loading rate that could decreases sludge viscosity and reduce fouling of membrane. Desired HRT in the MBR system was achieved by controlling the influent flow rate.

Microbial community analysis

A critical study of microbial community dwelling in MBR was performed by taking different samples of the mixed liquor at different operating conditions (i.e., HRT duration) before, during and after the treatment. The bacterial community study was performed with the tools of next generation sequencing. For microbial community analysis, sludge samples was collected from MBR and pretreated before genomic DNA isolation. Pretreatment was performed to ensure the removal of humus and other impurities Pretreatment process involves centrifugation of sludge at 8000 rpm for 10 min at 20°C followed by washing with mili-Q water. Genomic DNA extraction was performed using the Power soil DNA isolation Kit from MoBio laboratories, Inc. PCR-amplification of the V1-V3 regions of 16S rRNA, libraries preparation and Illumina MiSeq PE 250 bp paired-ends sequencing reactions was performed by the technical staff of Centre d'Innovation Génome Québec, Canada. The data obtained from sequencing tools was analyzed by performing alignment, clustering, and phylogenetic tree using USERACH v10 software.

Analytical Methods

Samples of influent and effluent of membrane bioreactor was collected twice in a week and acidified immediately after each collection by concentrated H_2SO_4 for COD, N-NH$_4$ and PO$_4^-$ estimation. COD analysis was performed by protocol prescribed by CEAEQ, 2014, Ammonia nitrogen (NH$_4$-N) and orthophosphate are analyzed simultaneously online by colorimetry (QuikChem® 10-107-06-2 Method-B and Method QuikChem® 10-115-01-1-B LACHAT Instrument. The analysis of pharmaceutical pollutant was carried out using Liquid chromatography and tandem mass spectrometry analysis (LC-MS/MS) (Thermo Scientific TSQ Quantiva Triple-Stage Quadrupole Mass Spectrometer) with a reverse phase column and Solid phase extraction (SPE) process.

Result and discussion

The starting phase of MBR was carried out for a period of 60 days. The initial concentration of total suspended solid and volatile suspended was 7.5 and 5.017 g L-1. The high biomass concentration of 16.5 g L -1 was achieved after 40 days of operation at HRT of 12h. The COD removal was 90% in the starting phase and continued with constant removal rate. Table 1.1 demonstrate the stable performance of MBR in terms of COD, ammonium nitrogen and orthophosphate removal. No suspended matter was detected in the effluent of MBR throughout the process. The retention rate of sludge is very high (99.99%), demonstrating a very high separation S / L by the membrane module.

The study of effect of HRT was carried out with 3 HRT duration (6, 12 and 18h). The concentration of pharmaceuticals in influent and effluent of the MBR were measured. During the HRT duration of 6 h the high removal (>90%) of compound ibuprofen and estradiol was achieved (Figure 1), However the removal of carbamazepine was > 5% (Figure 1.). The high removal of ibuprofen and estradiol might be due to their high sorption potential to sewage sludge and hydrophobicity. In spite of high removal, the clogging of membrane was frequent which was evident by increase in TMP to 40KPa in one week of operation. The clogging of membrane was reduced slight at 12h HRT. However the removal rate of pharmaceuticals at 12 h HRT were similar to the result obtained at 6h HRT (Figure 1). The concentration of carbamazepine in effluent of 12h HRT was 5% higher than the influent concentration. The negative removal is probably due to the desorption of carbamazepine residues from sludge. Some studies reported that the negative removal of carbamazepine is due to reconversion of carbamazepine glucuronide into parent compound [4], however, since this work is conducted using synthetic wastewater, the probability of presence of metabolites (glucuronide) and by-products was negligible. The removal rate of venlafaxine were similar in all the treatment condition i.e., at 6, 12 and 18h HRT however the removal rate was >10% (Figure 1). Although the removal of pharmaceutical at 18h HRT were similar to previously studied HRT, a reduction in membrane fouling rate was achieved during treatment. During the treatment at HRT of 18h the clogging start after 30 days of operation. The low removal of venlafaxine and carbamazepine might be due to their stable chemical structure and hydrophilic nature.
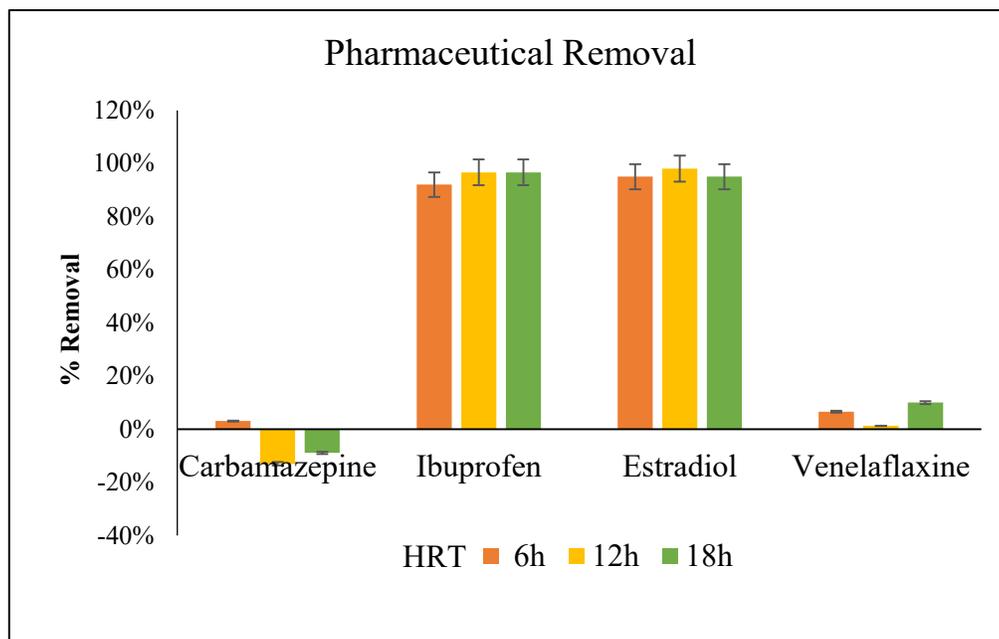
FIGURE 1: REMOVAL OF PHARMACEUTICALS AT VARYING HRT DURATION IN SMBR.

Parameters	Influent	Effluent	Removal %
COD (mg L^{-1})	1000	80	92
Ammonium (mg N L^{-1})	46.57	3.68	93.8
Phosphates (mg P L^{-1})	15.63	11.13	30.5

TABLE 1.1: PERFORMANCE OF MBR

The work was focused on the study of efficiency of membrane bioreactor for the treatment of a synthetic wastewater containing pharmaceuticals. Membrane bioreactor was efficient in removal of COD, ammonium nitrogen and phosphorus were removed. The removal of pharmaceuticals was almost uniform in all the HRT condition, however, clogging of MBR was decreased with increased HRT, which due to the slow biomass generation rate at long HRT. It is concluded that an intermediate HRT of 12h could be utilized for better performance of MBR. The result on microbial community will be presented in Conference.

Acknowledgement

References

1. Al Aukidy, M., Verlicchi, P., & Voulvoulis, N. (2014). A framework for the assessment of the environmental risk posed by pharmaceuticals originating from hospital effluents. *Science of the Total Environment*, *493*, 54-64.
2. Alrhmoun, M., CASELLAS, M., & DAGOT, C. Hospital Wastewater Treatment by Membrane Bioreactor: Performance and Impact on the Biomasses. *TC*, *14*, 5-20.
3. Amend, A. S., Seifert, K. A., & Bruns, T. D. (2010). Quantifying microbial communities with 454 pyrosequencing: does read abundance count?. Molecular Ecology, 19(24), 5555-5565.
4. Vieno, N., Tuhkanen, T., & Kronberg, L. (2007). Elimination of pharmaceuticals in sewage treatment plants in Finland. *Water research*, *41*(5), 1001-1012.

SEEC-2018-112

Experimental and Modeling Studies on the Degradation of Lignin and Enzymatic Hydrolysis of Cellulose to Fuel Products

Ashwin Gaikwad
Department of Chemical Engineering
Visvesvaraya National Institute of Technology,
Nagpur
Email: ashwin2781@gmail.com

ABSTRACT

An experimental-theoretical investigation on pretreatment and enzymatic hydrolysis of biomass is presented under various operating conditions in the reactor. Pretretment of Bambusa Bambos was analysed at different particle sizes and mixing conditions in the reactor and further processing of biomass was analysed through modeling and simulations of enzymatic processes. Michaelis-Menten kinetics including inhibitions is presented to quantify the product formation at various particle sizes of microcrystalline cellulose. A particle size of 0.4 μm and a mixing speed of 200 rpm shows higher degradation (64%) of lignin. The model simulations for the enzymatic hydrolysis of microcrystalline cotton cellulose (10 and 20 mg/ml) were performed for the average particle size ranging from 0.78−25.52 μm. A highest glucose yield (99.8%) was observed for the 0.78 μm particle size in 100 h of enzymatic hydrolysis. Thus, through this analysis more efficient production processes can be devised for the sustainable production of lignocellulosic fuels.

***Keywords:** Particle size, Cellulase, Enzymatic hydrolysis*

NOMENCLATURE

C_1 Concentration of glucose (mmol/L)
C_2 Concentration of cellobiose (mmol/L)
$[C_i]$ Concentration of cellulose fragment of degree of polymerization i (mmol/L)
DP   Degree of polymerization of cellulose
E_{endo} Total concentration of endoglucanase (mg of protein/ml)
E_{exo} Total concentration of exoglucanase (mg of protein/ml)
$E_{\beta-G}$ Total concentration of β-glucosidase (mg of protein/ml)
k_1, k_2 Rate constant of E_{endo} and E_{exo} respectively (hr^{-1})
k_{f1}, k_{b1} Forward and backward rate constant for endoglucanase (hr^{-1})
k_{f2}, k_{b2} Forward and backward rate constant for exoglucanase (hr^{-1})

$k_{G3}, k_{G3'}$ Forward and backward rate constant for β-glucosidase (hr^{-1})
K_{M1}, K_{M2}, K_{M3} Michaelis-Menten constant of E_{endo}, E_{exo} and $E_{\beta-G}$ respectively (mmol/L)
K_{G1}, K_{G2}, K_{G3} Inhibition constant of E_{endo}, E_{exo} and $E_{\beta-G}$ by glucose, respectively (mmol/L)
K_{C1}, K_{C2} Inhibition constant of E_{endo} and E_{exo} by cellobiose, respectively (mmol/L)
N_o Total concentration of molecular unit $\left(= \sum_i \{i[Ci]\} = \text{Constant}\right)$ (unit mmol/L)

INTRODUCTION

Enzymatic hydrolysis and fermentation are considered to be most promising conversion processes for the production of cellulosic fuels in terms of energy efficiency and environmental issues in the current scenario. Pretreatment of lignocellulosic biomass (LB) is one of the essential step in the biofuels production. Different pretreatment technologies have been studied by numerous investigators for the lignin degradation [1]. Among all the techniques, fungal pretreatment is becoming important as it is less energy intensive and more environmental friendly compared to other pretreatment techniques. In the present investigation lignin degradation of LB-*Bambusa Bamboo* and enzymatic hydrolysis of cellulose to glucose for bioethanol production is presented through experimental-theoretical investigation. Particle size of substrate is a major factor that affects the performance of fungal pretreatment. Large particle size may not allow the penetration of fungi into LB and hence smaller particle size exhibits enhanced delignification rates. In order to maximise the lignin degradation, effect of particle size of substrate was investigated. Apart from particle size, mixing is an important operating parameter that can influence the delignification of lignocellulosic biomass in several ways. Mixing is required to ensure the sufficient contact between the reactants, thus enhancing the mass transfer rates within the reaction vessel. However, excessive mixing can deactivate the enzyme and lower rates of delignification can be achieved due to the shear generated by mixer.

Recently, Gaikwad et al., have performed the enzymatic hydrolysis of Avicel PH 101 and analysed the effects of mixing on the kinetics and dynamics of the enzymatic hydrolysis for biofuels production [2, 3]. It was demonstrated that vigorous mixing has negative impact on the enzymatic process and lower mixing was more beneficial for glucose and reducing sugar production in batch as well as continuous stirred tank reactor.

The refined cellulose produced in the first step, i.e., after the lignin degradation by laccase can be processed further for the conversion of cellulose to glucose through the enzymatic hydrolysis in batch reactor. As the enzymatic hydrolysis of cellulose is a surface phenomena, available surface area of cellulose must be the most influential structural features of biomass. It not only influences cellulase adsorption on the cellulose surface and subsequent enzymatic breakdown, but also reduces the probability of competition to the substrate by the inhibitors [4]. Accessibility of the cellulose can also be correlated to other properties of the substrate such as cellulose crystallinity or *DP*. However, some previous investigations have shown that pore volume and particle size [5] are the two main features of the cellulosic biomass that affects enzymatic hydrolysis. Thus, effect of particle size of LB and mixing in batch reactor was quantified on both the pretreatment and enzymatic hydrolysis.

EXPERIMENTAL TECHNIQUES

MICROORGANISM AND INOCULUM PREPARATION

The laccase producing fungal strain *P. ostreatus* (white-rot fungi) was procured from the NCIM, Pune, India. All the media components were obtained from Central Chemical Laboratory, Nagpur, India. For media preparation, 24 gm of commercial potato dextrose broth and 20 gm agar powder was added to 1 litre of distilled water. The media was sterilized by autoclaving it at 121˚C for 20 minutes. Sterile media was inoculated by the fungal strain, *P. ostreatus*. The culture was kept at 26˚C for 7 days inside the incubator to maintain the environment for fungal growth. The growth of *P. ostreatus* was observed after five days of inoculation.

FUNGAL PRETREATMENT

In an Erlenmeyer flask, 3 g of *Bambusa bamboos* of different particle sizes (45, 70, 90, and 105 μm) was added to prepare 100 ml solution of woody biomass for studying the effect of particle size on fungal growth and lignin degradation. Mixing effects were studied by operating the process at no mixing (0 rpm) and vigorous mixing (200 rpm) condition. For moistening the substrate, 10 ml of mineral salt solution was added in the flask. The mineral salt solution was prepared by adding 0.3 g of NH_4Cl, 0.2 g of KH_2PO_4, 0.1 g of $MgSO_4$ and 1 g of $CaCO_3$ per liter of distilled water. The initial pH and moisture content of solution was adjusted to 5.8± 0.2 and 70% respectively. To sterilize the medium, solution was autoclaved at 121ºC and 15 lbs pressure for 20 min. The sterile medium was

inoculated with two plugs (6 mm diameter) of *P. ostreatus* from a seven-day old fungal culture plate stored at 4ºC. The reaction flasks were incubated at 25± 2˚C for 28 days under static condition in the dark. During the incubation, white rot fungi secrets the enzyme laccase. The laccase present in the broth further oxidizes the lignin present in lignocellulosic substrate, *Bambusa bamboos*. During the experiment, 1ml of the sample was taken out at regular interval of time for 24 hours of incubation for analyzing the laccase activity and total phenolic compounds formed during the delignification process.

Estimation of Total Phenolic Content

The measurement of concentrations of phenolic compounds was carried out through Folin-Ciocalteu assay as described below.

Folin-Ciocalteu assay: The total phenolic content (TPC) in samples was determined using the Folin–Ciocalteu assay [6]. A sample of 15 μl, taken during the delignification process was diluted with distilled water (240 μl). Thereafter, 15 μl of Folin–Ciocalteu reagent of 0.25 N was added into the sample solution. The resultant mixture was incubated for 3 min, and thereafter 30 μl of Na_2CO_3 of 1 N was added into the final mixture. Further, the mixture was incubated for 120 min at room temperature in the dark. The samples were analysed by measuring the absorbance at 765 nm by using UV spectrophotometer. Absorbance values were compared against a standard curve of gallic acid and results were reported as mg of gallic acid equivalents.

MATHEMATICAL MODEL

KINETIC MODEL FOR ENZYMATIC HYDROLYSIS

The mechanism of binding of cellulase to cellulose can be described though a multistep reaction scheme as shown below. As cellulase is a mixture of enzymes (endo-, exo-, β−glucosidase), a combination of all these enzymes is necessary for the complete hydrolysis of microcrystalline cotton cellulose.

Non–competitive inhibition:For non–competitive case, the proposed reaction mechanism is described as

$$E_{Cel} + C_i \underset{k_{b1}}{\overset{k_{f1}}{\longleftrightarrow}} \left(E_{Cel} \bullet C_i\right) \overset{k_1}{\longrightarrow} E_{Cel} + C_j + C_{i-j}, \tag{1}$$

$$E_{Cel} + C_2 \underset{k_{C2}}{\overset{k_{C1}}{\longleftrightarrow}} \left(E_{Cel} \bullet C_2\right), \tag{2}$$

$$E_{Cel} + C_1 \underset{k_{G2}}{\overset{k_{G1}}{\longleftrightarrow}} \left(E_{Cel} \bullet C_1\right), \tag{3}$$

$$E_{Cel} \bullet C_i + C_1 \underset{k_{G2}}{\overset{k_{G1}}{\longleftrightarrow}} \left(E_{Cel} \bullet C_1 \bullet C_i\right), \tag{4}$$

$$E_{Cel} \bullet C_1 + C_i \underset{k_{b1}}{\overset{k_{f1}}{\longleftrightarrow}} \left(E_{Cel} \bullet C_1 \bullet C_i\right), \tag{5}$$

$$E_{Cel} \bullet C_i + C_2 \underset{k_{C2}}{\overset{k_{C1}}{\longleftrightarrow}} \left(E_{Cel} \bullet C_2 \bullet C_i\right), \tag{6}$$

$$E_{Cel} \bullet C_2 + C_i \underset{k_{b1}}{\overset{k_{f1}}{\longleftrightarrow}} \left(E_{Cel} \bullet C_2 \bullet C_i\right). \tag{7}$$
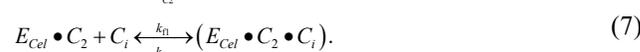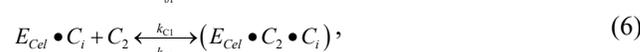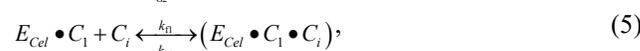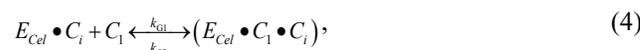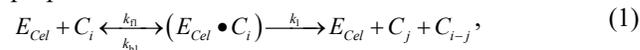
In the reactions 2–8, k_1, k_{f1}, k_{b1}, k_{G1}, k_{G2}, k_{C1}, k_{C2} are the rate constants for E_{Cel} and are independent of the degree of polymerization i. C_j and C_{i-j} are end products with degree of polymerization i and $(i-j)$, respectively. Using the

continuity equation for equations (1–7) and rearranging the terms leads to the following expression [2]

$$\frac{d[C_1]}{dt} = V_{1Max} \frac{\left(2\sum_{j=i+1}^{\infty} C_j\right)}{\left(K_{M1} + \sum_{i=2}^{\infty}(i-1)C_i\right)\left(1 + \frac{C_1}{K_{G1}} + \frac{C_2}{K_{C1}}\right)}.$$

(8)

Where $K_{M1} = \dfrac{k_{b1} + k_1}{k_{f1}}$, $K_{G1} = \dfrac{k_{G2}}{k_{G1}}$, $K_{C1} = \dfrac{k_{C2}}{k_{C1}}$, and $V_{1Max} = k_1 \times [E_{Cel}]$.

Competitive inhibition: For competitive inhibition, it is assumed that only C_1 and C_2 inhibit the enzyme and no enzyme–inhibitor–substrate complex is formed.

For glucose ($i=1$),

$$\frac{d[C_1]}{dt} = V_{1Max} \frac{\left(2\sum_{j=i+1}^{\infty} C_j\right)}{\left(K_{M1}\left(1 + \frac{C_1}{K_{G1}} + \frac{C_2}{K_{C1}}\right) + \sum_{i=2}^{\infty}(i-1)C_i\right)}.$$

(9)

DEGREE OF POLYMERIZATION

The Degree of Polymerization (*DP*) of the cellulose can be determined as number–average (*DP*$_n$), weight-average (*DP*$_w$), or viscosity-average (*DP*$_v$). The knowledge of *DP* of cellulose at various time intervals helps to determine the extent of scission of β−1, 4−glycosidic bonds by the enzymes. The *DP*$_n$ can be expressed as [2-3]

$$DP_n = \frac{\sum_{i=1}^{\infty}(i[C_i])}{\sum_{i=1}^{\infty}[C_i]} = \frac{N_O}{\sum_{i=1}^{\infty}[C_i]},$$

(10)

where $N_O = \sum_{i=1}^{\infty}(i[C_i]) = \text{Constant}$

$$\frac{d}{dt}\left(\sum_{i=1}^{\infty}[C_i]\right) = -\frac{d}{dt}\left(\sum_{i=1}^{\infty}\{(i-1)[C_i]\}\right) = N_o \frac{d}{dt}\left(\frac{1}{DP_n}\right).$$

(11)

RESULTS AND DISCUSSION

EFFECT OF PARTICLE SIZE ON LIGNIN DEGRADATION

In this study, different particle sizes (45, 70, 90 and 105 μm) were utilised to capture the effect of particle size on lignin degradation of lignocellulosic biomass *Bambusa bamboo*. As the percent lignin degradation was calculated from TPC determined during the progress of lignin degradation, changes in the concentrations of TPC captured at regular interval of time are presented in figure 5. It was observed that highest yield of TPC was observed for 45 μm particle size and it decreases with the increase in particle size of the *Bambusa bamboo*. The corresponding values of TPC for different particle sizes are then applied for lignin degradation calculations and the observed results are plotted as shown in figure 1. The amount of lignin degraded was highest for the smallest particle size (45 μm) whereas the bigger size particles shows lower degradation of lignin. The initial weight of lignin was 617.5 mg (3000 mg of *Bambusa bamboo*) which was converted into total phenolic compounds by laccase and it was found that the initial lignin was reduced to 222.72 mg at the end of 30 days of incubation.

EFFECT OF MIXING ON LIGNIN DEGRADATION

The percent lignin removal was analyzed for 0 rpm (no mixing) and 200 rpm (high mixing) and the results for reduction in lignin component of *Bambusa bamboo* by laccase are shown in figure 2. At higher mixing speed i.e., 200 rpm, TPC formed were 1.5 times more than that of no mixing condition at the end of 28 days of incubation. Mixing at 0 rpm helps to liberate 4.2 μg/ml of gallic acid equivalent of TPC whereas at 200 rpm, 6.59 μg/ml of gallic acid equivalent of TPC was obtained after 28 days of incubation. As greater yield of total phenolic compounds was obtained at higher mixing speed, more amount of lignin degradation was achieved at 200 rpm.

EFFECT OF PARTICLE SIZE ON GLUCOSE YIELD

The enzymatic hydrolysis of microcrystalline cotton cellulose of concentration 10 and 20 mg/ml was analysed by using kinetic model (eqn. 8 and 9). For the cellulosic particles of size 0.78−25.52 μm, the model simulations were performed by using the K_M and V_{Max} available in the literature [7]. As shown in figure 3 (a) and (b), a highest glucose concentration of 9.98 and 14.96 mg/ml was observed for the average particle size of 0.78 μm for the cellulose concentration of 10 and 20 mg/ml respectively for the case of competitive inhibition. This may be due to the fact that, tiny particles have larger surface area per unit volume and, therefore more cellulose can be accessed by the enzyme at a faster rate. For the case of non–competitive inhibition, the simulations were performed for the same concentrations under consideration. As can be seen from the figure 3 (a) and (b), again a highest glucose yield was observed at the substrate concentrations of 10 and 20 mg/ml for the smallest particle size of 0.78 μm.

Effect of Particle Size on DP

The *DP* of different particle sizes have been analysed cotton cellulose under competitive and non-competitve inhibition. For the concentration of 20 mg/ml, the cotton polymers were showing (fig. 5 (a) & (b)) reduction in *DP* from 250 to 41–40 for the particle size of 25.52 μm whereas, for the particle size of 6.08 to 2.07, the *DP* decreases upto 23–20 in 100 h of enzymatic hydrolysis under competitive inhibition. For the concentration of 10 mg/ml, reduction in particle size from 6.08 to 2.07 leads to decreases in DP from 12–10 in 100 h of hydrolysis. Under non-competitve inhibition the results were obtained at same initial concentrations. For the concentration of 20 mg/ml, the initial *DP* was considered to be 250, which then decreased approximately up to 41−40 and 16−15 for the particle size of 25.52 μm and 0.78 μm respectively. The *DP* of cotton decreases with decrease in particle sizes. For the concentration of 10 mg/ml, even lower values of *DP* were found. At this concentration, *DP* drops down to 30−29 for the particle size of 25.52 μm whereas for the smallest particle size (i.e., 0.78 μm) it drops down to 8−7 which is shown in figure 6 (a) & (b).

FIGURES
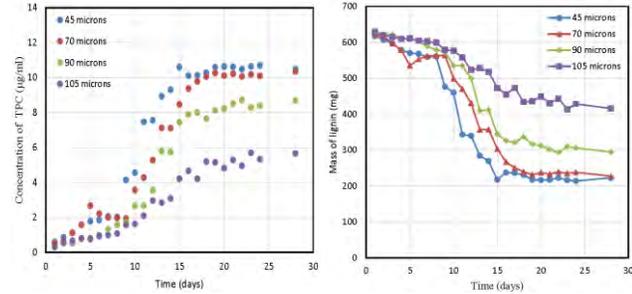
FIGURE 1: Effect of particle size of *Bambusa bamboo* on TPC and lignin degradation of *Bambusa bamboo*.
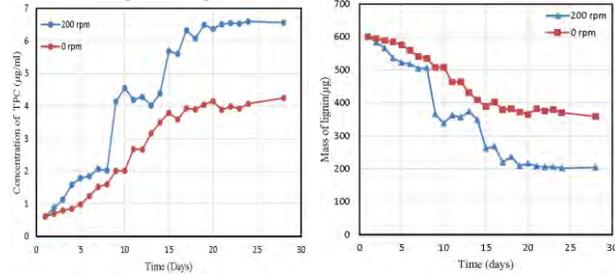
FIGURE 2: Effect of mixing on the TPC and lignin degradation of *Bambusa bamboo* in batch reactor.
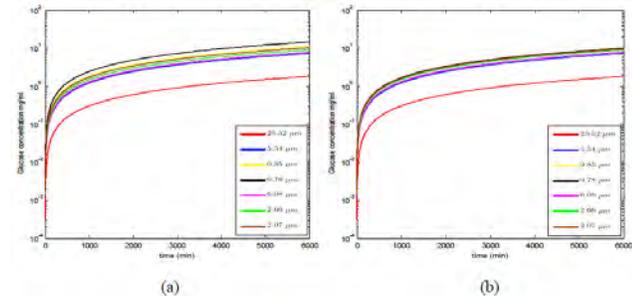
FIGURE 3. Effect of particle size on glucose yield under competitive inhibition obtained from model simulation (eqn. 9) for the initial cellulose concentration of (a) 20 mg/ml and (b) 10 mg/ml.
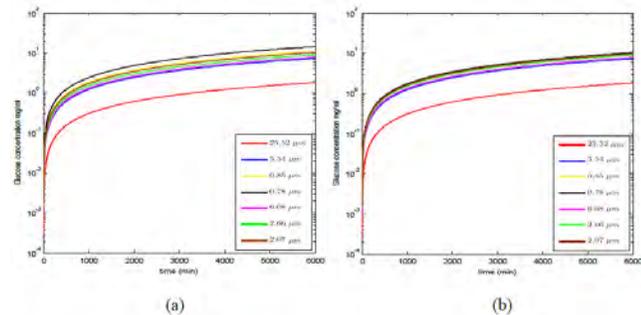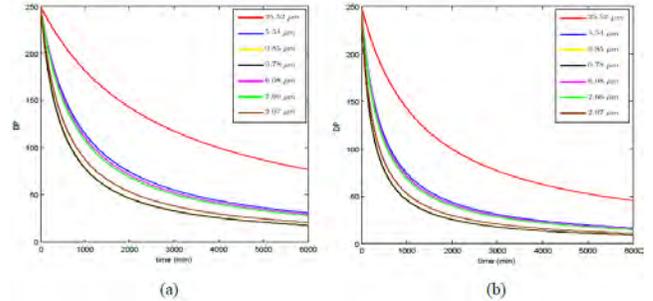

FIGURE 4. Effect of particle size on glucose yield under non–competitive inhibition obtained from model simulation (eqn. 8) for the initial cellulose concentration of (a) 20 mg/ml (b) 10 mg/ml.
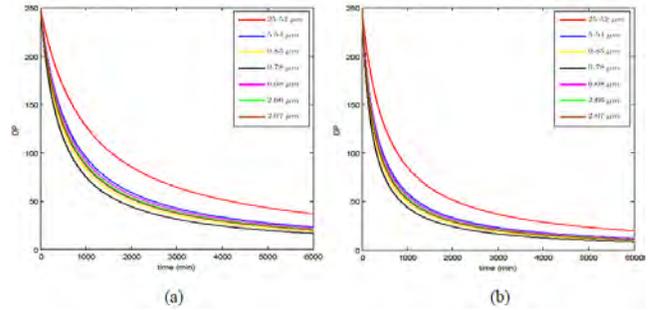
FIGURE 5. Effect of particle size on *DP* under competitive inhibition obtained from model simulation for the initial cellulose concentration of (a) 20 mg/ml (b) 10 mg/ml.

FIGURE 6. Effect of particle size on *DP* under non–competitive inhibition obtained from model simulation for the initial cellulose concentration of (a) 20 mg/ml (b) 10 mg/ml.

REFERENCES

[1] Chakraborty, S., Gaikwad, A., 2012. "Production of Cellulosic Fuels". PNAS, India, 82(1), 59–69.

[2] Gaikwad, A., Chakraborty, S., 2013. "Mixing Effects on the Kinetics of Enzymatic Hydrolysis of Avicel for Batch Production of Cellulosic Ethanol". Ind. Eng. Chem. Res., 52(11), 3988–3999.

[3] Chakraborty, S., Gaikwad, A., Aniket, 2010. "Mixing Effects in Cellulase-Mediated Hydrolysis of Cellulose for Bio-Ethanol Production". Ind. Eng. Chem. Res., 49, 10818−10825.

[4] Yang, B., Wyman, C. E., 2006. "BSA treatment to enhance enzymatic hydrolysis of cellulose in lignin containing substrates". Biotechnol. Bioeng., 94(4), 611−617.

[5] Grethlein, H. E., 1985. "The Effect of Pore Size Distribution on the Rate of Enzymatic Hydrolysis of Cellulosic Substrates". Nat. Biotechnol., 3, 155−160.

[6] Granato, D., Karnopp, A. R., Van Ruth, S. M., 2015. "Characterization and comparison of phenolic composition, antioxidant capacity and instrumental taste profile of juices from different botanical origins". J. Sci. Food Agric., 95(10), 1997–2006.

[7] Yeh, A., Huang, Y. C., Chen, S. H., 2010. "Effect of particle size on the rate of enzymatic hydrolysis of cellulose". Carbohydr. Poly., 79, 192–199.

SEEC-2018-114

EXPERIMENTAL STUDY ON PYROLYSIS OF COAL BY THERMOGRAVIMETRIC ANALYSIS (TGA) UNDER DIFFERENT TEMPERATURE CONDITIONS.

Krishna Kant Dwivedi
National Institute of Technology
Durgapur, West-Bengal India-713209
Email: kkdwivedi44@gmail.com

P.K.Chatterjee
Energy and ResearchTechnology Group
CSIR-CMERI, Durgapur
Email: pradipcmeri@gmail.com

Malay Kr Karmakar
Energy and Research Technology Group
CSIR-CMERI, Durgapur
Email: malaycmeri@gmail.com

A.K.Pramanick
National Institute of Technology
Durgapur, West Bengal India-713209
Email: akpramanick@yahoo.com

Abstract - In this study the pyrolysis characteristics of four different particle size (25-36, 36-52, 52-72, 100-150 μm) coal samples is performed by using thermogravimetric analysis (TGA). The experiments are conducted in nitrogen atmosphere for four different heating rates (50, 100, 160, 200 K/min) and temperature ranging from 30 ᵒC to 950 ᵒC. The peak temperature, mass loss, maximum mass loss rate for all different particle size coal samples are evaluated. All thermogravimetric (TG) and differential thermogravimetric (DTG) curves shows that the overall pyrolysis can be divided into different stages according to temperature profiles and each stage has its unique characteristics.The characteristic parameters of different particle size coals increased significantly with increasing the heating rate.Coal pyrolysis in this experiment can be divided in to three stage: moisture release, devolatilization and char gasification in higher temperature zone. The results might have important implication for understanding the mechanism of pyrolysis of coal in nitrogen environment.

Keywords : Pyrolysis, coal, thermo gravimetric, heating rate, Nitrogen environment.

.

NOMENCLATURE

TGA   Thermogravimetric Analysis.
DTG   Differential Thermogravimetric.

INTRODUCTION

The thermal decomposition of coal particles is an important part and also an essential step in the gasification of coal. Pyrolysis is one of the most important thermal conversion processes and it is also the first step in the process of combustion and gasification. Large amounts of clean solid, liquid and gas products can be obtained from pyrolysis process, such as high heating value semi-char and hydrogen enriched gaseous products. For determine the pyrolysis behaviour of solid fuels like coal, thermo-gravimetric analysis (TGA) is one of the most prevalent method. It is also used to study the physical and chemical properties of samples as a function of temperature [5]. Many co-processing studies have been performed with thermo-gravimetric analysis in both co-pyrolysis and co-gasification [9,7,4,10]. Two types of process occurs when coal is heated. First is depolymerisation in this stage gas,water vapour and tar are formed and second is repolymerization in which char formed [4]. Thermal analysis method is widely used for research of combustibility and oxidation behaviours of coal. When thermal curves of different coals varied a lot, the practical combustibility of them is different, when the curves are close to each other, the practical combustibilities are normally the same. The current work focus on pyrolysis of coal with different particle size on different heating rate.

The pyrolysis of coal is chemically complex as it involves simultaneous chemical reaction process and also used to determine the physical and chemical properties of different particle size coal samples as a function of temperature. Coal conversion heavily relies on coal reactivity. The reactivity of Coal basically affected by several factors like thermo-chemical processing condition, coal rank as well as particle size. By coupling pyrolysis and gasification process in any fluidized bed reactors to produce the syngas is one of the most efficient coal utilization technology. The main objective of the present work is to experimental study of physic-chemical and thermal characteristics of coal in nitrogen environment at four different heating rates (50, 100, 160, 200 K/min). So proposed study could increases the use of coal, minimise wastages, pertaining the storage of coal.

MATERIALS METHODS

SAMPLE-PREPARATION- Four different coal samples are collected from Eastern Coalfield Limited Ranigunj (West-Bengal) for this experiment. Collected coal samples are kept for sun drying for 2-3 days. Sun dried sample is grinded using mortar and pestle. The fine powder is allowed to pass through a 105 lm sieve to confirm the uniform particle size distribution. These different particle size coal samples are crushed and sieved to obtain four different particle size (25-36, 36-52, 52-72, 100-150 μm) suitable for TGA pan and kept in air tight bag.

PROXIMATE & ULTIMATE ANALYSIS- Proximate & analysis of coal samples has been carried out from CSIR-Central Institute of Mining & Fuel Research (CIMFR), Dhanbad (Jharkhand) according to American standard for testing and materials (ASTM) D-5373 standard. Table 1 table 2 Shows the proximate and ultimate analyses for these coal samples.

TABLE 1: PROXIMATE ANALYSIS (%).

Sample	Volatile Matter	Ash	Moisture	Fixed Carbon
Coal	20.4	11.23	3.7	48.6

Table 2: ULTIMATE ANALYSIS (%).

Sample	C	H	N	S	O
Coal	76.4	4.5	1.0	0.2	10.4

EXPERIMENTAL APPARATUS AND PROCEDURE-

All TGA experiments has been carried out by using NETZSCH (TG 209 F3 Tarsus) thermal analyzer in nitrogen environment with a purge flow rate of 20 ml/min. At the beginning of each experiment, 10.0 g of the coal sample is placed on an Al_2O_3 crucible in the heating zone of the TGA. During the experiment Different heating rates (50, 100, 160, 200 K/min) are used.

RESULTS & DISCUSSION

PHYSICO-CHEMICAL CHARACTERISTICS OF THE MATERIALS- For estimate the physical and chemical properties of coal samples proximate and ultimate analysis has been carried out. Proximate analysis results shows that moisture, volatile matter, fixed carbon and ash contents are 3.7 %, 20.4 %, 48.6 % and 11.23 % respectively as shown in Table 1 and ultimate analysis shows the amount of carbon contents (76.4%) as shown in Table 2. The results are good with standard daviation.

THE INFLUENCE OF HEATING RATE ON THE PARTICLE SIZE OF COAL SAMPLE- The mass loss (TG) curves and the differential mass loss (DTG) curves for coal samples at four different heating rate (50, 100, 160, 200 K/min) from 30 ºC to 950 ºC in nitrogen gas atmosphere are shown from Figure 2-5. For these all four heating rate the weight loss of coal particle is due to water releases and second due to devolatilization. Different curves for weight loss versus temperature is shown in Figure 2-5. The thermal degradation takes place towards the right as the heating rate continuously increases. From DTG curves (Figure 2-5) we can examine the influence of different heating rates. It is found that the maximum rate of degradation at active pyrolysis stage are increasing with increasing with increasing the heating rate because at maximum heating rate, thermal energy gained by coal samples. Possible devolatilization for least amount of adsorbed gases and very light hydrocarbons might have occurred below 250 ºC.
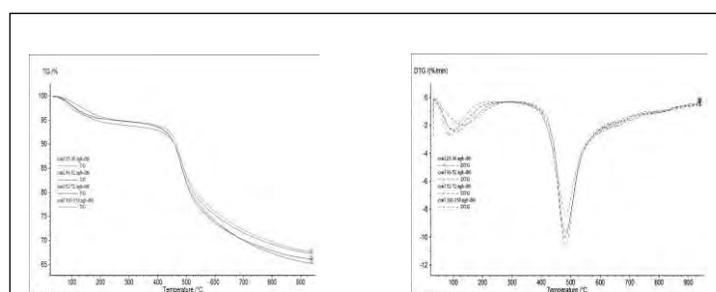
FIGURE 1. TG & DTG CURVES FOR HEATING RATE OF 50 K/MIN.
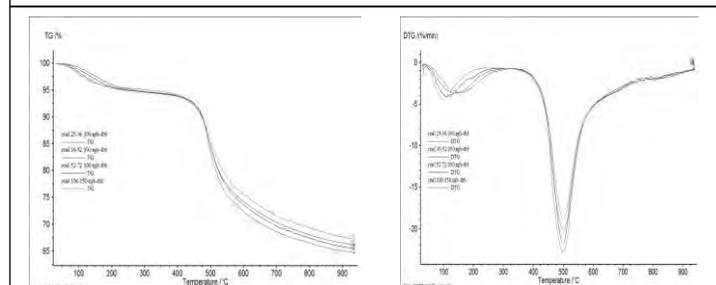
FIGURE 2. TG & DTG CURVES FOR HEATING RATE OF 100 K/MIN.
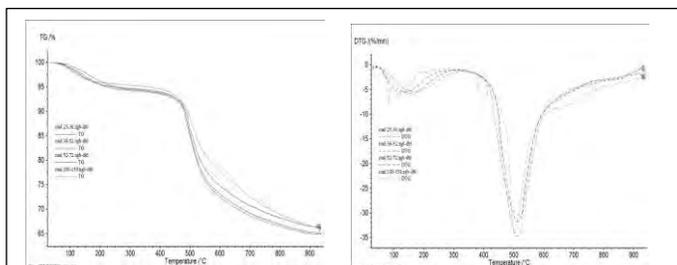
FIGURE 3. TG & DTG CURVES FOR HEATING RATE OF 160 K/MIN.
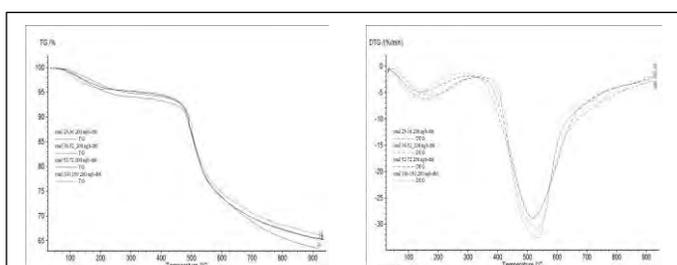
FIGURE 4. TG & DTG CURVES FOR HEATING RATE OF 200 K/MIN

EFFECT OF PARTICLE SIZE-

In general the coal pyrolysis is affected by coal particle size. To explore the effect of coal type different experiments are performed on four different heating rate (50, 100, 160, 200 K/min.) for different particle size (25-36, 36-52, 52-72, 100-150 μm) as shown in Figure 1-5. During the experiments it is observed that with increasing the particle size, pyrolysis of coal also affected in terms of weight loss with respect to temperature and time. To further illustrate the effect of coal particle size on coal pyrolysis reaction, some characteristics parameters also consider during this experiments such as initial temperature (T_s), final temperature (T_f) and peak temperature (T_p).The initial temperature of different coal particle size decreases from 535 ºC to 612 ºC.

CONCLUSION

A thermo-gravimetric analyser has been used to determine the pyrolysis characteristics for different particle size (25-36, 36-52, 52-72,100-150 μm) coal samples. Experiments has been carried out to obtain the effect of coal type, heating rate. The results shows that the pyrolysis characteristic of coal varied from its coalification and chemical composition. TG and DTG curves for all coal samples shows three pyrolysis stages including slow pyrolysis and fast pyrolysis stage. The ignition temperature of coal samples is affected by some volatile matter. The general thermal zones of coal samples can be observe by using TG and DTG curves. For all heating rate the maximum weight loss is found between the temperature range 100-400 ºC. The order of reactivity of different particle size samples are still increases with increases the particle size respectively and it seems reasonable to reburn with large particle size in a circulating fluidized bed gasifier. The characteristics for all DTG curves for different heating rate during main combustion stage are caused by feedstock properties of coal samples. In other words, the pyrolysis behavior of coal can be determined in terms of the weight percentages of coal samples.

REFERENCES

[1] JunqingCai,J.,Wang,Y.,Zhou,L.,Huang,Q.(2008), Thermogravimetric analysis and kinetics of coal/plastic blends during co-pyrolysis in nitrogen atmosphere, Fuel Processing Technology, 89, pp.21–27.

[2] Li,Q., Zhao,C., Chen, X., Wu,W. and Li,Y.(2009) Comparison of pulverized coal combustion in air and in O2/CO2 mixtures by thermo-gravimetric analysis, Journal of Analytical and Applied Pyrolysis, 85, pp. 521-528.

[3] Yanfen, L. and Xiaoqian, M. (2010) Thermogravimetric analysis of the co combustion of coal and paper mill sludge, Applied Energy, 87, pp. 3526–3532.

[4] Seo,D.K., Park,S.S., Kim,Y.T., Hwang, J and Yu,T. (2011) Study of coal pyrolysis by thermo-gravimetric analysis (TGA) and concentration measurements of the evolved species, Journal of Analytical and Applied Pyrolysis 92, pp.209–216.

[5] Kelebopile, L., Sun, R. and Liao, J.(2011) Fly ash and coal char reactivity from Thermo-gravimetric (TGA) experiments, Fuel Processing Technology ,92, PP. 1178–1186.

[6] Yan, B., Xu , P., Guo, c .y., Jin, Y., Cheng, Y. (2012) Experimental study on coal pyrolysis to acetylene in thermal plasma reactors, Chemical Engineering Journal 207–208, pp.109–116.

[7] C. Naveen and M. Premalatha (2014) Thermo gravimetric and kinetic studies on dried solid waste of post methanated distillery effluent under oxygen and nitrogen atmosphere, Bioresource Technology, 174, pp.126–133.

[8] Wang,G.G., Zhang,J.G., Shao,J.G., Sun,H., and Zuo, H.G.(2014) Thermogravimetric Analysis of Coal Char Combustion Kinetics, Journal of Iron and Steel Research, 21(10), pp.897-904.

[9] Zhang, Y., Guo, Y., Cheng, F., Yan, K., Cao, Y. (2015) Investigation of combustion characteristics and kinetics of coal gangue with different feedstock properties by thermogravimetric analysis, Thermochimica Acta, 614, pp. 137–148.

[10] Yuanyuan Zhang,Y., Zhang,Z., Zhu,M., Cheng, F. and Zhang,D.(2016), Interactions of coal gangue and pine sawdust during combustion of their blends studied using differential thermogravimetric analysis, Bioresource Technology, 214,pp.396–403.

SEEC-2018-115

PERFORMANCE ANALYSIS OF SOLAR AND NATURAL GAS BASED BUILDING COOLING SYSTEM

Gaurav Singh
Department of Mechanical Engineering
Indian Institute of Technology Ropar, 140001,
Punjab
Email: gaurav.singh@iitrpr.ac.in

Ranjan Das
Department of Mechanical Engineering
Indian Institute of Technology Ropar, 140001,
Punjab
Email: ranjandas@iitrpr.ac.in

ABSTRACT

This paper demonstrates the impact of implementing a vapor absorption-based building cooling system in an office building using Energy Plus simulation. The designed system operates with two modes, the first one with solar collector, and the second one with natural gas-fired water boiler. To fully meet the system requirement, auxiliary electric heating arrangement is provided in the solar collector mode, whereas, no auxiliary heating is needed in the gas-fired mode. Results show a quantitative performance of this system with these two modes of operation in terms of the coefficient of performance, the energy consumption pattern, and other factors related to thermal comfort. It is found that both systems are although feasible to satisfy the building cooling need, but, the natural gas-fired system is a better alternative towards reducing the air pollution due to stubble burning and system's dependency on conventional electric grid.

Keywords: building cooling, solar collector, natural gas boiler, vapour absorption

.
NOMENCLATURE

$c_{p,w}$	Specific heat of water, kJ/(kg·K)
COP	Coefficient of performance
CFM	Cubic feet per minute
f_{pl}	Part load factor
$\dot{m}_a$	Mass flow rate of air, kg/Sec
$\dot{m}_w$	Mass flow rate of water, kg/Sec
ΔP	Pressure difference, Pa
Q_e	Chiller evaporator load, W
Q_f	Fan energy consumption, W
Q_g	Heat supplied to the generator, W
$Q_{w,h}$	Energy consumption in water heater, W
$SHGC$	Sensible heat gain coefficient
t	Time, s
$T_{g,i}$	Water temperature at generator inlet, ˚C
$T_{g,o}$	Water temperature at generator outlet, ˚C
T_o	Water outlet temperature to the heater, ˚C
T_i	Water inlet temperature to the heater, ˚C
$T_{w,i}$	Water inlet temperature to the evaporator, ˚C
$T_{w,o}$	Water outlet temperature from the evaporator, ˚C
U	Overall heat transfer coefficient, W/(m^2·K)
VLT	Visible light transmittance
V_t	Volume of water tank, m^3
$\eta_{w,h}$	Efficiency of water heater
η_f	Fan efficiency
ρ_a	Density of air, kg/m^3
ρ_w	Density of water, kg/m^3

INTRODUCTION

In the present era, building cooling systems are the major source of energy consumption among all other building components [1]. Conventionally, electrically

operated vapor compression systems are used which consume considerable energy. Electricity is mainly derived from thermal power plants which are again based on fossil fuels. Additionally, in many parts of the country, the issue of stubble burning is responsible for poor air quality [2]. Therefore, the design and development of a building cooling system based on renewable energy addressing the environmental challenges becomes important. Towards this direction, vapor absorption system-based building cooling systems offer a feasible alternative to vapor compression-based cooling systems.

In vapor absorption systems, heating energy either in the form of hot water or hot steam is required in the generator. This energy can be supplied either by solar energy or waste heat available from exhaust of any industrial process. Temperature of heating energy supplied either by hot water or steam may vary from 70°C to 150°C [3]. A good number of studies on vapour absorption-based cooling systems are reported. Ravikumar et al. [4] studied a solar-assisted absorption system that emphasised that evaporator design has more effect on system performance. Study shows that absorption system based on only solar collectors will not fulfil the system requirements due to associated intermittency [5]. Performance analysis of absorption system from different heat sources hot water, hot air, and hot steam is carried out by Kaynakli et al. [6]. Xu et al. studied the performance of a solar-driven vapour absorption system with varying collector area, generator temperature, and tank volume [7]. Use of natural gas as a heating source in conjunction with solar collector is found to be possible for operating absorption system, because of availability and low cost of gas [8].

It becomes apparent from the literature that a quantitative assessment between solar and natural gas driven vapour absorption building cooling system is not yet done. Thus, in this work, a simulation study is performed using Energy Plus software [9] on a reference small office building situated in warm and humid climate zone of India. For supplying heat energy to the generator, two different plant modes are considered. In the 1st mode, hot water is supplied with the aid of flat-plate solar collector plant. With this, an auxiliary heater is also coupled in series to address the conditions of solar unavailability. In the 2nd mode, hot water is supplied through a natural gas fired boiler. Further description of the system is given below.

BUILDING AND SYSTEM DESCRIPTION

A small office reference building with single zone has been studied in this work which comprises a single floor with total floor area of 1,000 m^2 [10]. The construction of building envelope is taken as per the energy conservation building code (*ECBC*) guidelines [11] as shown in Table 1 and the geometry of building is shown in Fig. 1. The location of building is taken for warm and humid climate in India [12]. Office working hours is taken as 9 am-5pm.

TABLE 1: Building input and output parameters

Input/Output variables	Description	Unit value	ECBC [11] values
Exterior Wall	Outside insulation + Gypsum plaster + Brick 2× 100mm + Gypsum plaster	U Value = 0.419 W/(m^2·K)	0.440
Roof	Outside insulation + Gypsum plaster + 100 mm light weight concrete + Gypsum plaster	U value = 0.428 W/(m^2·K)	0.409
Window	Single Glazing	U value = 3.004 W/(m^2·K), $SHGC$ = 0.296, VLT = 0.751	U= 3.30, $SHGC$ = 0.25, VLT= VLT=0.76
Occupancy Density	Not applicable (NA)	10 m^2/Person	NA
Lighting Power Density	NA	10 W/m^2	NA
Electric Equipment Power Density	NA	80 W/Person	NA
Ventilation	NA	20 *CFM*/Person	NA
Window to Wall Ratio	Area covered by window	40%	NA
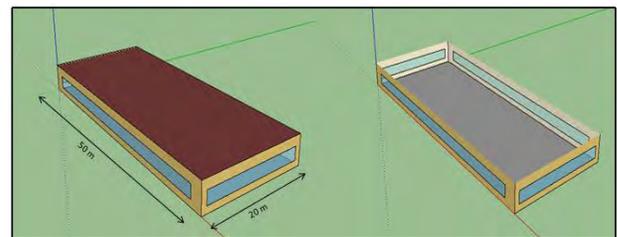
FIGURE 1. 3-D Model of Building Geometry

The present system involves an absorption chiller with water cooled condenser and other components are similar to a conventional heating ventilation and air-conditioning system. Absorption chiller supplies chilled water at the temperature of 7.22 °C to the cooling coil installed in the system. A fan is installed in front of cooling coil which supplies cooled and dehumidified air at 15 °C to the air conditioning space of the office building for maintaining comfort conditions. It is well-known that in the absorption chiller, some kind of heating energy has to be supplied in the generator portion. For this purpose, in the 1st mode (Fig. 2), a flat-plate solar collector loop of total collector

area 375 m^2 is installed on the roof of building. Since, the heat supplied by the collector may not be sufficient and invariably subjected to weather conditions, thus along with this, an auxiliary electric water heater is also provided for continuous operation of the system. This collector loop supplies hot water at the 80°C to the generator side of the absorption chiller. In the 2nd mode (Fig. 3), a natural gas operated boiler is coupled in place of solar collector loop which supplies hot water at 80°C to the generator side. In this boiler, natural gas is supplied from biomass or any other potential source, and the boiler efficiency is considered as 85% [8].
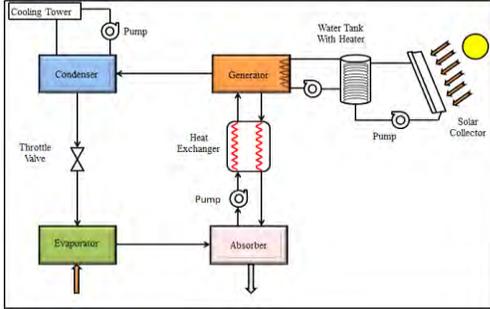
FIGURE 2. Schematic of First Mode of Operation

Using the prescribed data, Energy Plus solves energy equations for different components to yield output parameters of interest such as, *COP*, heating rate, and temperature outcomes. Results based on the present analysis are discussed next. *COP* of the system from derived simulation results is calculated as [7],

$$COP = \frac{Q_e}{Q_g} \qquad (1)$$

where, Q_e is chiller evaporator load and Q_g is the heat supplied to the generator. These are computed in the following manner,

$$Q_e = \dot{m}_w c_{p,w}\left(T_{w,i} - T_{w,o}\right) \qquad (2a)$$

$$Q_g = \dot{m}_w c_{p,w}\left(T_{g,i} - T_{g,o}\right) \qquad (2b)$$

For a given generator inlet temperature, $T_{g,i}$ Energy Plus evaluates the value of generator outlet temperature, $T_{g,o}$ based on the imposed load. The annual energy consumption by each component is evaluated by solving the pertinent energy equation.
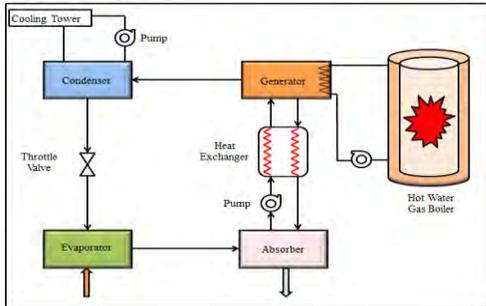
FIGURE 3. Schematic of Second Mode of Operation

For instance, the energy consumption by water heater used in the 1st mode of operation is computed as shown below,

$$Q_{w,h} = \frac{\eta_{w,h} \times V_t \times \rho_w \times c_{p,w}\left(T_o - T_i\right)}{t} \qquad (3)$$

where, $\eta = 0.96$ is the efficiency of the heater, whereas, $V_t = 15$ m^3 is the tank volume simulated by the Energy Plus. In Eq. (3), t is the total time in seconds the water heater is operated. Similarly, the fan power consumed in the 2nd mode of operation is calculated in the following manner,

$$Q_f = \frac{\left(f_{pl} \times \dot{m}_a \times \Delta P\right)}{\left(\eta_f \times \rho_a\right)} \qquad (4)$$

where, $\Delta P = 900$ N/m^2, $\eta_f = 0.70$. In Eq. (4), f_{pl} is part load factor is related to is the ratio of the given and design air mass flow rates. Power consumption by other equipments can be computed using the methodology discussed in Energy Plus documentation [9]. Results are discussed next.
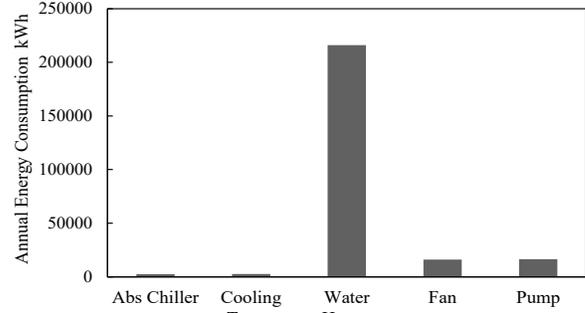
FIGURE 4. Energy Consumption for Solar Mode

RESULTS AND DISCUSSION

To find out the energy consumption pattern in various components involved in different operating modes, simulations were carried out for warm and humid climatic zone. Results obtained from simulation were analyzed and further details of output results are given below.

Solar Collector and Auxiliary Heater Mode

In this section, energy consumption pattern of different installed components is shown in Fig. 4. Total annual electric energy consumption of the system for fulfilment of the system requirement (1,80,696 kWh) is 2,53,586 kWh. Out of this, absorption chiller electric consumption is 2,404 kWh because the pump consumes less power than compressor. Fan energy consumed for the transportation of cooled and dehumidified air into the building space is 16,076kWh. In this mode, total 3 pumps are used in condenser, solar collector, and for hot water circulation. Total energy consumption of these 3 pumps (other than the chiller pump) installed in the system is 16,506 kWh. Total heating energy required for the generator side of the absorption chiller is 3,27,000 kWh that has to be supplied with by combined solar collectors and auxiliary heater. Solar energy contribution towards the total requirement of the system is 1,11,000 kWh. As an auxiliary heater is installed in the system for improvement of reliability of the

system and further energy consumed in the auxiliary water heater for fulfilment of the requirement is 2,16,000 kWh. *COP* of the system obtained from the simulation results is 0.55 that is in accordance with literature [3]. In this total mode, electric energy consumption is the major portion of energy that is consumed in the auxiliary heating requirement.
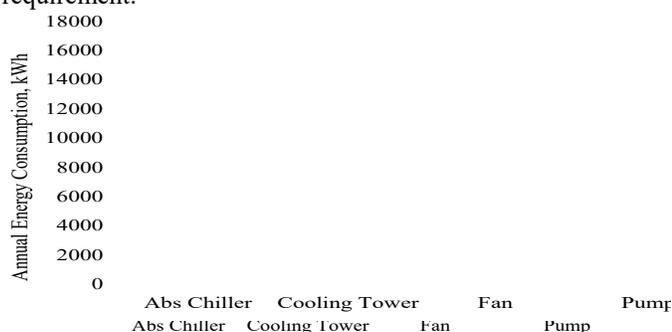
FIGURE 5. Energy Consumption for Natural Gas Mode

Natural Gas Fired Boiler Consisting Mode

The energy consumption pattern of different components for mode-2 is shown in Fig. 5. It is seen that total annual energy consumption is 27,909 kWh, out of which absorption chiller consumption is 2,416 kWh. Total thermal load removed from the space in this case is 1,83,687 kWh. Fan energy consumption is 16,305 kWh. In this system, two water circulation pumps are installed Total energy consumption by pumps is 6,588 kWh. In this case total heating energy required in the generator side is from boiler is 3,32,381 kWh. Here, full energy is supplied by natural gas fired boiler. Total heating energy supplied to the boiler is 3,55,351 kWh. In this case too, *COP* of the system obtained is found as 0.55.

Conclusion

This study shows the performance of a vapor absorption based building cooling system. Two different modes involving solar and natural gas are studied using Energy Plus simulations. It is found that in the solar collector mode, the electric energy consumption is very high. But, in terms of *COP* and heating rate requirement, both systems perform in a similar manner. The use of natural gas derived through biomass gasification is encouraged in the present building cooling system to reduce the adverse consequences of stubble burning. The present work can be extended to a combined solar and natural gas based building cooling system.

ACKNOWLEDGMENTS

REFERENCES

[1] Chinnakani, K., Krishnamurthy, A., and Moyne, J., 2011. "Comparison of Energy Consumption in HVAC Systems Using Simple ON-OFF, Intelligent ON-OFF and Optimal Controllers". IEEE Power and Energy Society General Meeting, Detroit, MI, USA.

[2] Lohan, S.K., Jat, H.S., B., Yadav, A.K., Sidhu, H.S., Jat, M.L., Choudhary, M., Peter, J.K., and Sharma, P.C., 2018. "Burning Issues of Paddy Residue Management in North-West States of India". Renewable and Sustainable Energy Reviews, 81 (1), January, pp. 693-706.

[3] Alobaid, M., Hughes, B., Calautit, J.K., O'Connor, D., and Heyes, A., 2017. "A Review of Solar Driven Absorption Cooling with Photovoltaic Thermal Systems". Renewable and Sustainable Energy Reviews, 76, March, pp. 728-742.

[4] Ravikumar, T.S., Suganthi L, and Samuel, A.A., 1998. "Exergy Analysis of Solar Assisted Double Effect Absorption Refrigeration System". Renewable Energy, 14 (1-4), May-August, pp. 55-59.

[5] Saleh, A., and Mosa, M., 2014. "Optimization Study of a Single-Effect Water–Lithium Bromide Absorption Refrigeration System Powered by Flat-Plate Collector in Hot Regions". Energy Conversion and Management, 87, July, pp. 29-36.

[6] Kaynakli, O., Saka, K., and Kaynakli, F., 2015. "Energy and Exergy Analysis of a Double Effect Absorption Refrigeration System Based on Different Heat Sources". Energy Conversion and Management, 106, December, pp. 21-30.

[7] Xu, Z.Y., and Wang, R.Z., 2017. "Comparison of CPC Driven Solar Absorption Cooling Systems with Single, Double and Variable Effect Absorption Chillers". Solar Energy, 158, December, pp. 511-519.

[8] Gomri. R., 2013. "Simulation Study on the Performance of Solar/Natural Gas Absorption Cooling Chillers". Energy Conversion and Management, 65, January, pp. 675-681.

[9] Energy Plus 8.7 Open Source Software, https://energyplus.net/downloads, accessed: 01.11.2017

[10] Technical Report, 2011. U.S. Department of Energy Commercial Reference Building Models of the National Building Stock, National Renewable Energy Laboratory, 1617 Cole Boulevard, Golden, Colorado 80401.

[11] Energy Conservation Building Code User Guide, 1st ed., 2009, Bureau of Energy Efficiency, New Delhi, India.

[12] Weather data by location, https://energyplus.net/weather-location/asia_wmo_region_2/IND//IND_Chennai-Madras.432790_ISHRAE , Energy Plus weather file source. accessed: 01.11.2017

SEEC-2018-116

PERFORMANCE OF ALUM & POLYALUMINUM CHLORIDE AS EFFICIENT COAGULANTS FOR FLUORIDE REMOVAL IN BATCH AND CONTINUOUS REACTORS

Swati Dubey
Department of Chemical Engineering, Malaviya National Institute of Technology, Jaipur, India 302017
Email: swatidubey2021@gmail.com

Madhu Agarwal
Department of Chemical Engineering, Malaviya National Institute of Technology, Jaipur, India 302017
Email address: madhunaresh@gmail.com

A.B. Gupta
Department of Civil Engineering, Malaviya National Institute of Technology, Jaipur, India 302017
EmailL abgupta.ce@mnit.ac.in

Yogendra Solanki
Department of Chemical Engineering, Malaviya National Institute of Technology, Jaipur, India 302017
Email: yogendra201292@gmail.com

ABSTRACT

In this study, performance of alum and polyaluminum chloride(PACl) for fluoride removal has been compared in batch and continuous modes. Experiments were performed to determine the optimum doses of coagulant for bringing the fluoride (<1.5 ppm) and aluminum(0.2 ppm) within acceptable limits. The residual turbidity and TDS was found to be higher in case of alum as compared to PACl representing less efficient settling of suspensions, primarily comprise of alumino-fluoro complexes. In addition to this, water treated with PACl contains relatively low soluble salts compared to alum & also requires lesser lime for pH compensation due to its lower acidity. It was also observed that the PACl treated water contains less residual aluminium(0.34ppm) compared to alum (0.46 ppm) when initial fluoride concentration of water was 4 ppm. In batch mode, residual Al was found to be 0.182ppm(alum) & 0.143ppm(PACl), after subsequent microfiltration which conform to the Al standards in defluoridated water.

Keywords: Fluoride, alum, polyaluminum chloride, batch, continuous

.

NOMENCLATURE

PACl- Poly aluminum chloride
Alum- Aluminum sulphate

ά   There are two arguments for each entry of the nomenclature environment, the symbol and the definition.

INTRODUCTION

Exposure to fluoride through drinking water above the permissible limit causes severe dental and skeletal fluorosis [1]. Skeletal Fluorosis can cause pain and stiffness in joints as well as deformities such as crippling, kyphosis, and genu varum. The World Health Organization recommends an upper limit of 1.5 mg/L for fluoride in drinking water [2].

Various processes such as coagulation, precipitation, adsorption, ion exchange electrocoagulation, reverse osmosis, and nano-filtration have been adopted for defluoridation of drinking water [3,4]. The techniques used for defluoridation of water, are mainly dependent on either adsorption or precipitation. Activated alumina process based on adsorption and widely used in the field has the major disadvantage of leaving residual aluminium in excess of 0.2 mg/L in the treated water. The essential requirement of electricity and exorbitant cost of RO process make it unsuitable for community supplies in developing countries like Africa, India etc. and it cannot compete economically with general field processes used for defluoridation [5]. Electrocoagulation is an effective process for defluoridation but when it is operated in a continuous mode to serve relatively large communities, there is a problem of high turbidity in the treated water [6]. The Nalgonda Defluoridation Technique which is based on coagulation is considered to be the most economical and simple method for bringing the fluoride content to acceptable limit in drinking water and is reported to

have high removal efficiency [7]. Aluminium salts such as sulphates or chlorides, lime and bleaching coagulants are added to the raw water in a batch process followed by rapid mixing, flocculation, sedimentation and filtration. Lime facilitates complete hydrolysis of alum forming dense aluminium hydroxide flocs for rapid settling while retaining a minimum residual alkalinity of 1 to 2 meq/l and pH between 6.5 and 8.5 in treated water [8].

Nalgonda technique, being a batch process, suffers from a limitation in terms of the amount of water being treated. Another limitation of the technique is the high amount of residual aluminium left in the treated water, which is due to high concentration of suspended solids that primaril1y comprise alumino-fluoro complexes not being able to settle under plain sedimentation [9]. We expected that shifting the process to continuous mode may enhance the treatment capacity significantly and it would be able to serve relatively larger communities. Shifting of the system to continuous mode had the risk to result in increase in the treated water turbidity as the settle ability suffers in such systems compared to the batch mode. It was further perceived that the low turbidity of the raw groundwater may not permit efficient sweep floc mechanism, the major mode of action of alum, resulting in high concentration of suspensions of alumino-fluoro complexes. Thus the present study focuses on the use of Polyaluminium chloride (80% and 100% doses), which promotes bridging action for the removal of suspensions and hence expected to work well at low raw water turbidity levels. Aluminium salts such as alum, poly aluminium chlorides etc. are widely used as coagulants for the removal of organic and inorganic pollutants in water and wastewater [20]. Poly Aluminium Chloride (PACl) can be an effective coagulant for the removal of fluoride from water with higher removal efficiency [10].

It was reported by George et al. 2010 that despite close controls exercised in laboratory conditions, the Nalgonda process cannot meet the standards for residual aluminium in drinking water and the majority of aluminium remains in colloidal suspensions, which required filtration through a 0.2 micron filter to meet the above requirement [3]. The present study shows the experimental results of both batch and continuous mode Nalgonda process with a subsequent step of filtration through 0.2 micron filter.

Material and Methods
Chemicals
All chemicals used for the study, namely, sodium fluoride (NaF), aluminium sulphate ($Al_2(SO_4)_3.16H_2O$), lime were of analytical grade obtained from Merck. Polyaluminium chloride solution (KANPAC 10 HB) was obtained from Aditya Birla group, with Aluminium content of 10.2% as Al_2O_3 as per the specifications provided by the supplier.

Analytical Methods
The residual fluoride in treated water was analyzed using fluoride ion selective electrode (Orion Star A 214) and coupled to a standard electrode as reference. The residual aluminium content in the treated samples was determined by Atomic Absorption Spectroscopy (LABINDIA Analytical AA8000).

Batch Study for fluoride removal
Batch experiments were carried out on conventional Nalgonda process for varying raw water fluoride concentrations at recommended doses of alum (80% & 100%) and equivalent PAC (80% & 100%) in terms of aluminium. The 1000 ml of known fluoride concentration solution was taken in a beaker and dose of alum/PAC and lime was added to it as per the specifications of Nalgonda process. The content of beaker was then flash mixed at 100-130 rpm for initial 10 minutes followed by slow stirring at 7-10 rpm for 20 minutes. After the settlement for 30 min, the supernatant was analyzed for residual fluoride and aluminum. Treated water was analyzed for various parameters to derive the efficiency of fluoride removal and its quality was also assessed in terms of residual aluminium.

Continuous flow Nalgonda Process
In order to increase the throughput of the process, a defluoridation set-up was fabricated for carrying out the Nalgonda defluoridation experiments in continuous mode as shown. Alum/PACl and lime solutions of specific concentrations were added to designated tanks to deliver the doses prescribed in the Nalgonda defluoridation table given by Nawlakhe et al. (1975) [11]. The flow rate of the chemicals was maintained using the peristaltic pump. The dosage of PAC was kept equivalent to that of alum in terms of aluminium. Apart from equivalent doses, another set of experiments with lower dose at 80% of the aforementioned prescribed doses was also run in order to determine the optimum dose for fluoride removal. Lime was added to maintain a desirable pH (6.5-8.5) for floc formation. Being relatively less acidic, the PAC required half of the amount of lime as that for alum for pH maintenance.

Results and Discussion
Defluoridation efficiency
In the conventional batch Nalgonda process, treatment with recommended doses as per Nawlakhe et al. (1975) as well as 80% of these recommended doses of alum and lime resulted in acceptable levels of 1.5 mg/L of residual fluoride in the water as depicted in Fig. 1 respectively which indicate almost comparable performance of the two systems in terms

of fluoride removal though alum appeared to have a slight edge over PAC [11]. In order to increase the throughput of the process, a defluoridation set-up was fabricated for carrying out the Nalgonda defluoridation experiments in continuous mode and the results are shown in Fig. 2. From the results, it can be observed that residual fluoride was less for 80% doses than for 100 % dose. Both alum and PACl were efficient for defluoridation at 80% as well as 100% dose, indicating that the Nalgonda process recommends higher dose of chemicals than what is actually required stoichiometrically for defluoridation. Parthasarathy & Buffle 1986 reported that monomeric Al species react almost instantaneously with fluoride ions and polymeric species act much more slowly [13]. The polymeric aluminium hydroxides $Al_n(OH)_{3n}^0$ serve as sites for complexation of fluoride in the fluoride removal mechanism. These precipitating aluminium hydroxides $Al_n(OH)_{3n}^0$ acquire charges by adsorbing and desorbing H^+ ions and form positively and negatively charged particles depending upon the pH of the aqueous medium (pH$_{pzc}$ in 7.5 to 8.5 pH range). At lower pH all surface hydroxyl groups are positively charged in protonated form and electrostatic interactions are responsible for surface adsorption of negatively charged ions on to the hydroxide particle [14]. Both these chemicals follow the aforementioned basic mechanism for defluoridation and hence were expected to produce similar results. However, the marginal difference in residual fluoride was perceived due to difference in turbidity resulting from suspensions of alumino-fluoro complexes, which may have different settling properties as the mechanism for their removal would be different as explained in the subsequent section. This was further expected to result in differences in residual aluminium in the two systems. To assess the above hypothesis, suspensions were dissolved with HNO_3 and the samples were re-analyzed for total residual fluoride. The results are shown in Fig. 3. From Figure 3, it can be seen that PACl has comparable fluoride removal efficiency to alum at both 100% as well as 80% of the recommended doses. The residual fluoride is within the acceptable limit (<1.5 mg/L) for drinking water on treatment with either alum or PACl. It can be also seen that the fluoride removal is better at higher initial concentrations of fluoride in raw water.The residual turbidity was a cause of high concern as this comprised predominantly alumino-fluoro complexes, which may induce high residual Al in treated water, thus a filtration step was added in sequence [15]. More fluoride was found in suspension form in water treated with alum due to high turbidity.
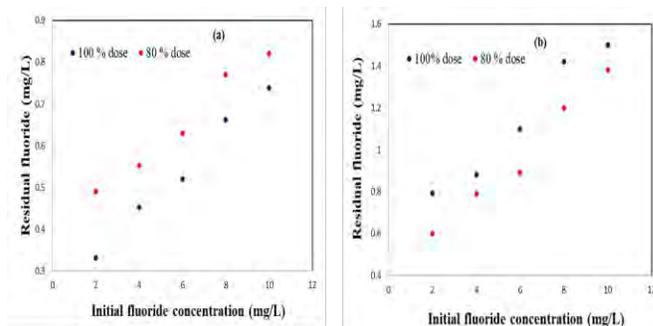
FIGURE 1 Comparative fluoride removal efficiency of (a) alum and (b) PAC at 80% and 100% doses in batch mode
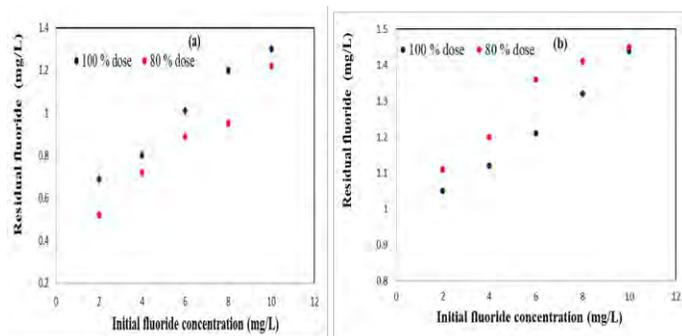
FIGURE 2 Comparative fluoride removal efficiency of (a) alum and (b) PAC at 80% and 100% doses in continuous mode
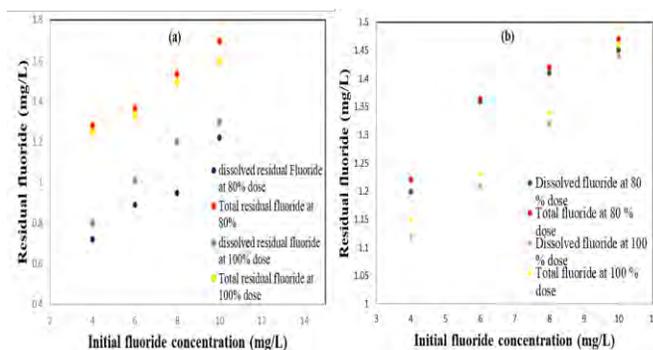
FIGURE 3 Total & dissolved fluoride of (a) alum and (b) PAC at 80% and 100% doses

Membrane Filtration

The samples were filtered using microfiltration membrane having 0.2 micron pore size. Vacuum was applied while filtering the samples through 0.2 micron pore size microfiltration membrane. Table 1 shows that the samples treated with PACl show better results through the membrane as compared to those treated with alum. This can be attributed to the fact that PACl treated samples are less turbid due to fewer suspensions as compared to those produced by alum. This gives the advantage of introducing lesser load on the membrane which in turn will lead to

increased life of the membrane and less frequency of cleaning of the membrane.

The aluminium Al^{3+} ions that occur in their hydrated form in water have a primary hydration shell with six octahedrally coordinated water molecules, e.g. $Al(H_2O)_{63}^{+}$. Hem & Roberson 1967 described the behavior of aluminium hydroxide precipitates during the hydrolysis mechanism with respect to varying pH of the aqueous solution [16]. The acceptable limit of aluminium in drinking water is 0.2 mg/L. Since Nalgonda technique uses aluminium sulphate for fluoride removal, so a part of the dose used remains in the water in dissolved form and also in suspension with fluoride in the form of flocs. So, membrane filtration is necessary to remove these suspensions.

S. No.	Treating Agent	Sample Detail	Aluminium content (mg/L)
1.	Alum	Before filtration	0.46
2.	Alum	After filtration through 0.2 µm membrane	0.182
3.	PACl	Before filtration	0.34
4.	PACl	After filtration through 0.2 membrane	0.143

Without filtration the content was much beyond the acceptable limit, but after filtration through 0.2 µm pore size microfiltration membrane, the residual aluminium contents are within the acceptable limit (0.2 mg/L) for aluminium in drinking water. This establishes that microfiltration is sufficient to reduce the residual aluminium content to acceptable limits in treated samples after treatment with either alum or PACl.

REFERENCES

[1] M.E. Kaseva, Optimization of regenerated bone char for fluoride removal in drinking water: A case study in Tanzania, J. Water Health. 4 (2006) 139–147. doi:10.2166/wh.2005.062.

[2] H.G. Gorchev, G. Ozolins, WHO guidelines for drinking-water quality., WHO Chron. 38 (2011) 104–108. doi:10.1016/S1462-0758(00)00006-6.

[3] S. Dubey, M. Agarwal, A.B. Gupta, A study on the characterisation of the species formed during fluoride removal through coagulation Swati Dubey and Madhu Agarwal *, Interdiscip. Environ. Rev. 18 (2017) 143–154.

[4] S. Dubey, M. Agarwal, A.B. Gupta, Coagulation process for fluoride removal by comparative evaluation of Alum & PACl coagulants with subsequent membrane microfiltration, Int. J. Environ. Technol. Manag. (2017).

[5] S.S. Waghmare, T. Arfin, Fluoride Removal By Industrial , Agricultural and Biomass Wastes As Adsorbents : Review, Int. J. Adv. Res. Innov. Ideas Educ. 1 (2015) 628–653.

[6] C.Y. Hu, S.L. Lo, W.H. Kuan, Effects of co-existing anions on fluoride removal in electrocoagulation (EC) process using aluminum electrodes, Water Res. 37 (2003) 4513–4523. doi:10.1016/S0043-1354(03)00378-6.

[7] Z. He, H. Lan, W. Gong, R. Liu, Y. Gao, H. Liu, J. Qu, Coagulation behaviors of aluminum salts towards fluoride: Significance of aluminum speciation and transformation, Sep. Purif. Technol. 165 (2016) 137–144. doi:10.1016/j.seppur.2016.01.017.

[8] S. Dubey, M. Agarwal, A.B. Gupta, R.K. Dohare, S. Upadhyaya, Automation Control in Defluoridation Water Treatment Plant, (2016).

[9] S. Dubey, M. Agarwal, A.B. Gupta, RECENT DEVELOPMENTS IN DEFLUORIDATION OF DRINKING WATER IN INDIA, in: V.P. Singh, S. Yadav, R.N. Yadava (Eds.), Environ. Pollut., Springer International Publishing, 2018: pp. 310–322.

[10] P. Sharma, M. Agarwal, A.B. Gupta, Polyaluminium Chloride- An Alternative to Alum for Defluoridation, Int. J. Adv. Res. Sci. Eng. 4 (2015) 323–327.

[11] W.G. Nawlakhe, K.R. Bulusu, Nalgonda technique – a process for removal of fluoride from drinking water., Water Qual. Bull. 14 (1989) 218–220.

[12] N. Parthasarathy, J. Buffle, Study of interaction of polymeric aluminium hydroxide with fluoride, Fluoride. 64 (1986) 24–29.

[13] N. Parthasarathy, J. Buffle, Study of polymeric aluminium(III) hydroxide solutions for application in waste water treatment. Properties of the polymer and optimal conditions of preparation, Water Res. 19 (1985) 25–36. doi:10.1016/0043-1354(85)90319-7.

[14] A.J. Vučina-Vujović, I.A. Janković, S.K. Milonjić, J.M. Nedeljković, Influence of AlOOH nanoparticles on the oxidation of iodide by persulphate, Colloids Surfaces A Physicochem. Eng. Asp. 223 (2003) 295–300. doi:10.1016/S0927-7757(03)00197-3.

[15] G.I. Muthu, V. Vinodhini, P.C. Padmapriya, G. Sathiyanarayanan, K. Sabumon, An improved method for defluoridation, Indian J. Environ. Health. 45 (2003) 65–72.

[16] J.D. Hem, C.E. Roberson, Form and Stability of Aluminum Hydroxide Complexes in Dilute Solution, USGS Water Supply Pap. 1827–A (1967) 55.

STOCHASTIC MMC MODELLING OF TURBULENT PILOTED JET DIFFUSION FLAME

Sanjeev Kumar Ghai
Department of Mechanical Engineering
Indian Institute of Technology Kanpur
Kanpur, U.P. - 208016
Email: snjv@iitk.ac.in

Santanu De
Department of Mechanical Engineering
Indian Institute of Technology Kanpur
Kanpur, U.P. - 208016
Email: sde@iitk.ac.in

ABSTRACT

The turbulent piloted flame DME-D has been studied numerically using Reynolds-averaged Navier-Stokes (RANS) based stochastic multiple mapping conditioning (MMC) method. A sinle reference variable is used whose mapping function represents the cumulative probability distribution of the mixture fraction for non-premixed combustion investigated in the present study. The Curl's mixing model, originally developed for the conventional PDF method has been adapted for the MMC approach. A reduced mechanism has been used to model the chemistry which consists of 28 species and 24 step reactions. Computed results for mixture fraction and reactive scalars are found to be in excellent agreement with the published experimental data.

Keywords: Turbulent diffusion flames; multiple mapping conditioning; stochastic processes.

INTRODUCTION

Probabilistic methods such as probability density function (PDF) [1] methods have a great advantage for modelling turbulent combustion processes because they allow direct closure for calculation of the chemical source term. But these approaches are computationally expensive as compared to mixtures fraction based approaches such as the flamelet model [2] and the conditional moment closure (CMC) method [3]. PDF methods are generally more universal and provide relatively better agreement with experimental measurements for most of the flames. On the other side, conditional methods are restricted to cases that do not exhibit large fluctuations around the conditional mean and predictions of flames with significant local extinction/re-ignition tend to be less satisfactory. Stochastic multiple mapping conditioning (MMC) approach [4] has recently emerged as an alternate model for simulation of turbulent combustion, which is claimed to be [5, 6] computationally cheaper compared to the PDF methods.

Despite conditional approach, MMC has the capabilities to capture complex phenomenon such as extinction/re-ignition at a comparatively modest cost w.r.t to PDF methods. In recent times MMC has been successfully applied to piloted turbulent jet diffusion flame of Sandia flame series D-F [5-7]. In the present work, the turbulent piloted flame DME-D is being investigated following RANS-MMC approach. The objectives of this work are to ascertain the capability of the MMC approach and to assess the performance of the small-scale mixing model within the MMC framework.

MATHEMATICAL FORMULATION

MMC approach has the inherent capability to consider multiple fluctuations of several key quantities by the introduction of reference variables such as mixture fraction, reaction progress variable etc. To consider more than one key quantity, one has to increase the dimensionality

of the reference space which has also increased the computation cost. The concept behind the MMC methodology is that the large scale turbulent fluctuations and small scale mixing employed in reference space are imitated by the use of reference variables in the reference space, ξ, whose PDF is well known in advance. In this work to reduce the computation cost, a single reference variable, ξ^*, is used whose mapping function X (ξ) represents the mixture fraction Z. In the stochastic implementation, the reference variable, ξ^*, is assumed to be Gaussian distributed. A separate equation for the evolution of the reference variable, ξ^*, is solved that ensures closeness of the cumulative distribution function of X (ξ) of the reference variable, ξ^*, with mixture fraction Z. The corresponding sets of equations for a stochastic particle method are:

Transport in physical space

$$dx^* = U(\xi^*; x^*; t)dt$$

Transport in reference space:

$$d\xi^* = A^o(\xi^*; x^*; t)dt + b(\xi^*; x^*; t)dw^*$$

Transport in mixture fraction space:

$$dZ^* = S^* dt$$

Transport in composition space:

$$dY_I^* = (W_I^* + S_I^*)dt$$

Where $2B = b^2$, x^* is location, ξ^* is reference variable, A^o is the drift coefficient, B is the diffusion coefficient, Y_I^* is the species concentration, S_I^* is the mixing operator and W_I^* is the chemical source term. The superscript '*' is used to differentiate the values linked to stochastic variables. The detailed derivations of these equations may be found in [4].

NUMERICAL APPROACH

The turbulent piloted flame DME-D has been considered in the present work. The central jet has a diameter of 7.45mm. The jet has 20% DME and 80% air with a stoichiometric mixture fraction of Z_{st}=0.351. The flame is stabilized by the hot combustion products issued from an annular pilot surrounding the central jet. The pilot consists of burnt gases resulting from combustion of lean C_2H_2/air mixture and has a temperature of 1800 K. The inner and outer diameters of the pilot are 8 and 18.2 mm, respectively. The hot pilot is surrounded by the cold coflowing stream of air. Here, we have simulated the DME-D flame with a jet velocity of 45.9 m/s and Reynolds number of 29300. The velocities of pilot and coflow streams are 1.1 m/s and 0.9 m/s, respectively. More details are available in [8].The boundary conditions used for all the variables at the exit section, outer radius and along the axis are the outflow, Neumann and symmetric conditions respectively. The stochastic MMC model is fully coupled to a RANS solver for the flow field. The standard k–ε model with the following set of constants has been used: C_μ = 0.09, $C_\varepsilon 1$ = 1.53 and $C_\varepsilon 2$ = 1.85. A reduced chemical mechanism, with 28 species and 24 reactions [9,10], has been used. In the present set of simulations, the mixing model constant C_ϕ = 3 and the minor time scale Cmin =0.25 have been used. A cylindrical coordinate system is used, where the computational domain extends 50D and 15D in the axial- (z) and the radial (r) directions, respectively. The domain is discretized in 100 cells in each direction. For the stochastic MMC method, 50 stochastic particles per cell have been used. The maximum and minimum numbers of particles within one CFD cell are restricted to 75, and 25, respectively. The grid sensitivity study is also carried out on the flow field and the predictions are found to be independent of the further refinement of the mesh.

RESULTS AND DISCUSSIONS

In this section, we will present the numerical simulation results for piloted turbulent DME jet diffusion flame using RANS-MMC approach.

Figure 1 reprsents radial profiles of velocity at different axial location for DME-D. The results are predicted very well over the entire domain and the jet decay rate is accurately captured by the RANS-MMC.
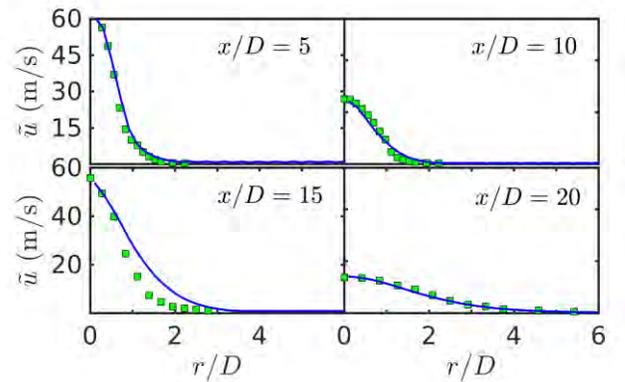
Figure 1: Radial profiles of axial velocity at different axial locations. Square represents experimental data [8] and blue solid line RANS-MMC.

Figure 2 represents the radial profiles of CO_2 mass fraction at different axial locations and the results for the reactive scalar CO_2 agree reasonably well at all the downstream positions of the jet. Morever, some what broader profile is observed in simulation as compare to experiments.

CONCLUSIONS

A coupled RANS-MMC simulation has been performed for the turbulent diffusion flame DME-D. Reduced chemistry for the chemical kinetics with 28 species and 24 step reactions has been used. The results are found to be in excellent agreement for the DME flame. However, further investigations are needed for other flames of the series which exhibit significant local extinction and reignition such as flame F and G.
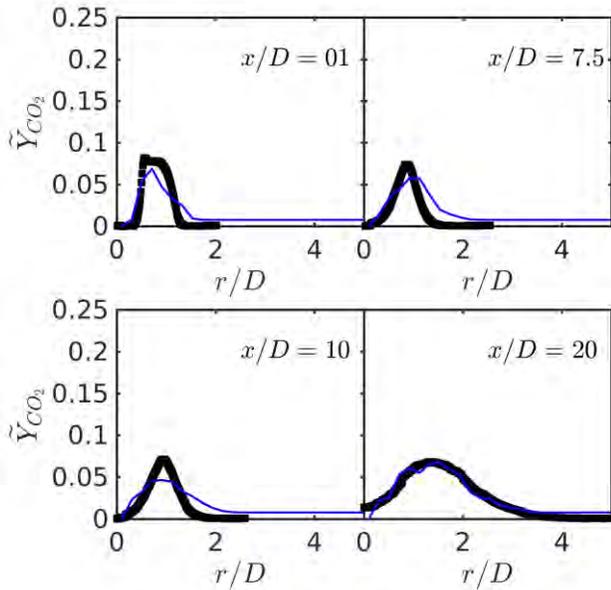
Figure 2: Radial profiles of CO_2 mass fraction at different axial locations.

ACKNOWLEDGMENTS

REFERENCES

[1] S.B. Pope, Progress in Energy and Combustion Science, 11 (1985) 119-192.

[2] N. Peters, Progress in Energy and Combustion Science, 10 (1984) 319-339.

[3] A.Y. Klimenko, R.W. Bilger, Progress in Energy and Combustion Science, 25 (1999) 595-687.

[4] A.Y. Klimenko, S.B. Pope, Physics of Fluids, 15 (2003) 1907-1925.

[5] K. Vogiatzaki, S. Navarro-Martinez, S. De, A. Kronenburg, Flow Turbulence and Combustion, 95 (2015) 501-517.

[6] C. Straub, S. De, A. Kronenburg, K. Vogiatzaki, Combustion Theory and Modelling, (2016) 1-19.

[7] K. Vogiatzaki, A. Kronenburg, S. Navarro-Martinez, W.P. Jones, P Combust Inst, 33 (2011) 1523-1531.

[8] F. Fuest, G. Magnotti, R.S. Barlow, J.A. Sutton, P Combust Inst, 35 (2015) 1235-1242.

[9] C.J. Sung, C.K. Law, J.Y. Chen, Combustion and Flame, 125 (2001) 906-919.

[10] G.T. Chin, J.-Y. Chen, V.H. Rapp, R.W. Dibble, Development and Validation of a Reduced DME Mechanism Applicable to Various Combustion Modes in Internal Combustion Engines, Journal of Combustion 2011 (2011) .

SEEC-2018-118

DEFLUORIDATION OF DRINKING WATER BY INORGANIC POLYMER COAGULANT

Yogendra Singh Solanki[1], Madhu Agarwal[1], Sanjeev Gupta[2], Pushkar Shukla[2], A.B Gupta[3]
[1]Department of Chemical Engineering, Malaviya National Institute of Technology, Jaipur,
India 302017
[2] Grasim Industries Limited (Aditya Birla Group), Bharuch, Gujrat India
[3]Department of Civil Engineering, Malaviya National Institute of Technology, Jaipur,

India 302017

ABSTRACT

Fluoride contamination of water is a major problem in India. World Health Organization(WHO 2004) recommends an upper limit of 1.5 mg/L fluoride in drinking water. Present study reveals performance evaluation studies of Inorganic Polymer coagulant (IPC) at different concentration of alumina and basicity in the fluoride removal from drinking water. The amount of IPC was decided according to the Al_2O_3 amount present in alum dose recommended in batch Nalgonda de-fluoridation technique. The effects of coagulant dosage (IPC) at different pH and initial concentration of fluoride, on fluoride removal has been studied. Synthetic sample having Fluoride concentration 3 mg/L were treated at optimized dosage and residual fluoride was reduced to 1.1 to 1.4 ppm with different IPC samples. Residual aluminium in treated water was well within WHO norms for drinking water. Optimum pH for fluoride removal was 6.5 and there was deterioration in performance of IPC at both lower and higher pH.

Keywords: Alum, Nalgonda, IPC, de-fluoridation, coagulation, fluoride

NOMENCLATURE

IPC   : Inorganic polymeric coagulant
UHB   : Upper high basicity.

HB   : High basicity

MB   : Medium basicity

INTRODUCTION

Fluorides occurs mainly as sellaite (MgF_2), fluorspar (CaF_2), cryolite (Na_3AlF_6) and fluoroapatite [$3Ca_3(PO_4)_2$ $Ca(F,C_{12})$]. Hence, fluoride will be present in groundwater when conditions favour their dissolution or high fluoride containing effluents are discharged to the water bodies from industries [1]. In India various states namely Assam, Andhra Pradesh, Bihar, Delhi, Rajasthan, Gujarat etc. to have high fluoride concentration in water.

The presence of high fluoride content in drinking water makes bones and teeth brittle, harder and dense due to deposition of fluoride as calcium fluorapatite. World Health Organization (WHO 2004) recommends an upper limit of 1.5 mg/L fluoride in drinking water [2-3]. Fluoride is required in small amount (1.0-3.0 mg/day) on daily basis for prevention of dental problems but taken in large amount can cause dental fluorosis, skeletal fluorosis (Fluorosis is a common symptom of high fluoride ingestion manifested by mottling of teeth in mild cases and embrittlement of bones and neurological damage in severe cases [6], osteoporosis, arthritis, brittle bones, cancer, infertility, brain damage, Alzheimer syndrome, and thyroid disorder, etc. Fluoride can be harmful or beneficial depending upon the amount taken. Human intake of fluoride is mainly from groundwater [7]. Effects of fluoride concentration in drinking water are depicted in Table 1 below.

Table 1: Effects of fluoride in water on human health [6]

Fluoride concentration (mg/L)	Effects
<1.5	Safe limit
1.5–3.0	Dental fluorosis (discoloration, mottling and pitting of teeth)
3.0–4.0	Stiffened and brittle bones and joints
4.0–6.0 and above	Deformities in knee and hip bones and finally paralysis making the person unable to walk or stand in straight posture, crippling fluorosis.

Different techniques viz. precipitation, adsorption, coagulation, membrane separation have been used previously for De-fluoridation of drinking water. The Nalgonda De-fluoridation Technique is considered to be the most economical and simple method for bringing the fluoride content to acceptable limit in drinking water and is reported to have high removal efficiency. The Nalgonda process (Nawlakhe et al.,1975) was originally developed on the basis of laboratory tests and field studies at NEERI and uses high dosages of alum varying from 145 to 1600 mg/L for treating raw water fluoride levels of 2 to 10 mg/L at varying alkalinity[4-5].

2. MATERIALS AND METHODS

2.1 Chemicals

All chemicals used for the study, namely, sodium fluoride (NaF), aluminium sulphate $(Al_2(SO_4)_3.16H_2O)$, calcium carbonate $(CaCO_3)$ were of analytical grade obtained from Merck. IPC samples of different grades were provided by Grasim Industries Limited (Aditya Birla Group) IPC specifications are shown in Table below:

Table 2: Characterization of Inorganic polymeric coagulant

Coagulants Name	Al_2O_3 (%)	Basicity (%)	Chloride (%)	Sp. Gravity
IPC-UHB	22.06	88	7.8	1.31
IPC- HB	13.7	63	16.2	1.30
IPC -MB	17.18	45	20.8	1.32

2.2 Experimental:

Synthetic solutions of different concentrations of fluoride in raw water were prepared in laboratory. The dose of IPC variants were kept such that Alumina content would match with that of Alum dose prescribed in Nalgonda Technique originally given by Nawlakhe et al. Initially pH was varied from 5 – 8. Residual Fluoride and pH were checked using Fluoride Ion Selective Electrode (Thermo-Orion Versastar) and pH meter (Hanna) respectively. The concentration of residual Aluminium ion in treated water was determined by Ferron-Ascorbic acid colourometric method on UV Visible Spectrophotometer (Shimadzu).

3. RESULTS AND DISCUSSION

3.1. Effect Of pH On Removal Efficiency

The removal efficiency of fluoride by UHB, HB and MB IPC in a pH range of 5–8 is illustrated in Fig. 1. The optimum pH for fluoride removal was observed to be in pH 6.5. With pH increasing from 6.5 to 8, the removal efficiency of fluoride by all the three variants saw a significant decrease from approx 65 % to 29 %.

Table 3: Residual aluminium in optimize dose of different variants of IPC at 3 ppm initial fluoride concentration

Coagulant name	Coagulant dose in term of alumina (mg/L)	Residual fluoride (mg/L)	Residual aluminium (mg/L)
IPC-UHB	43.0	1.1	0.14
IPC-HB	59.8	1.4	0.10
IPC-MB	35.0	1.1	0.05
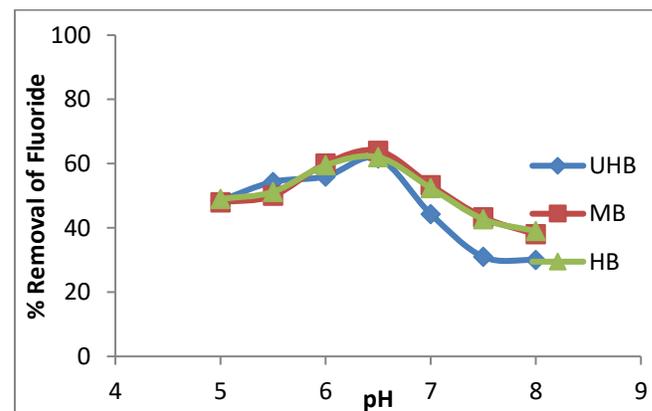
Fig.1: Effect of pH on de-fluoridation efficiency of IPC variants

3.2. Effect Of Coagulants Dose On Removal Efficiency @ 3 mg/L Fluoride Conc.

Figure 2 reveals the effect of coagulant dose at pH 6.5 with different variants of IPC. It was observed that MB IPC was most efficient in fluoride removal at 35 mg/L to achieve a residual fluoride conc. of 1.1 mg/L, it was closely followed by UHB IPC (43.07).
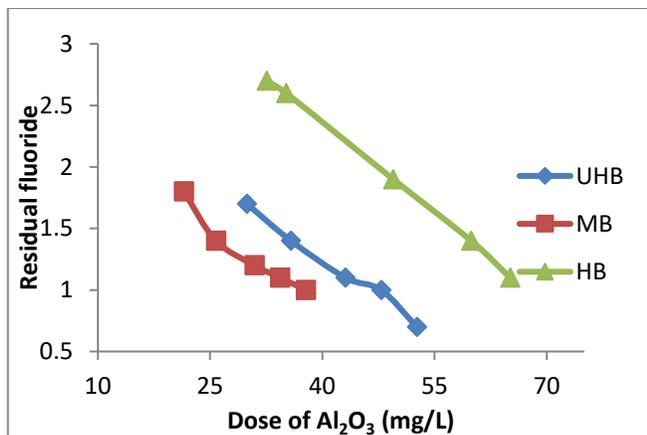
Fig.2: Comparative analysis of different variants of IPC v/s residual fluoride

3.3 Total Dissolved Salts

An upper limit of 500 mg/L is prescribed for drinking water as per IS 10500. Both, alum and IPC add to the TDS of the samples. As compared to alum (in Nalgonda technique), IPC leads to lesser increase in the TDS of the sample. IPC being partially hydrolysed polymeric compound caused less drops in pH and thus requires less amount of lime for neutralisation. This ultimately causes less increase in overall TDS of treated water. (Figure 3)
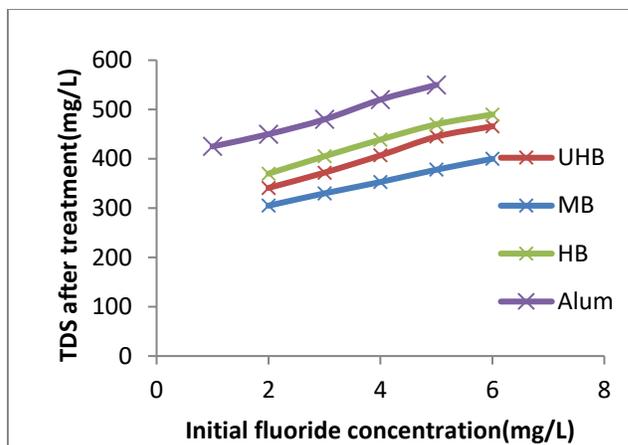
Fig.3: TDS (mg/L) after treatment with Alum and IPC variants

CONCLUSION

IPC is an efficient alternative to alum for use in Nalgonda Technique, Medium basicity IPC was found to be most efficient in removing Fluoride followed by UHB and HB was found to be least effective. TDS of water treated with IPC has TDS well within the limits of 500 mg/L as prescribed by IS 10500, the same was not the case with Alum. In all experiments, residual aluminium was found to be within WHO prescribed limits thus making it a safer de-fluoridating agent.

ACKNOWLEDGMENTS

REFERENCES

[1] Dissanayake, C.B., 1991. The fluoride problem in the groundwater of Sri Lanka environmental management and health. Int. J. Environ. Stud. 19, 195–203.

[2] World health organization (WHO), Guidelines for drinking-water quality, guidel drink qual, Third ed., Inc. First Second Addenda, vol. 1, World health organization, Geneva, 1997. (Recomm.) http://www.who.int/water_sanitation_health/dwq/gdwqvol32ed.pdf.

[3] WHO, 1985. Guidelines for Drinking Water Quality, vol. 3. World Health Organization, Geneva, pp. 1–2.

[4] Nawlakhe, W.G. and Bulusu, K.R. "Nalgonda technique – a process for removal of fluoride from drinking water." Water Quality Bull. 14 (1989): 218-220.

[5] Nawlakhe, W.G., Kulkarni, D.N., Pathak, B.N., and Bulusu, K.R. "Defluoridation of Water by Nalgonda Technique." Indian Journal of Environmental Health 17, no. 1 (1975): 26.

[6] Kofi Annan, United Nations Secretary General. 2003.

[7]. S. Chidambaram, A. L. Ramnathan and S. Vasudevan, Fluoride Removal Studies in Water Using Natural Materials, Water SA, 29(3), 339-343 (2003).

[8] Bhattacharjee S, Zhao Y, Hill JM, Percy ME, Lukiw WJ. Aluminum and its potential contribution to Alzheimer's disease (AD). Frontiers in Aging Neuroscience. (6) 62-67 (2014)

SEEC-2018-119

QUASI-STEADY STATE REDUCED ORDER MOVING BOUNDARY MODEL OF ORC HEAT EXCHANGER FOR MEDIUM TEMPERATURE SOLAR-THERMAL SYSTEMS

Rudrodip Majumdar
Department of Energy Science and Engineering,
IIT Bombay, Mumbai-400076,
Institute PDF
Email: rudrodip@iitb.ac.in

Sandip K. Saha
Department of Mechanical
Engineering,
IIT Bombay, Mumbai-400076,
Assistant Professor
Email: sandip.saha@iitb.ac.in

ABSTRACT

Moving boundary methods are efficient in tracking of the continuously moving phase change boundary and are particularly for the dynamical simulation of transient models that describe the evaporation process. Even a simplified quasi-steady version of such low order fast models is capable of tracking phase change boundaries without the requirement of well-formulated starting solutions. In the present study, a simplified quasi-steady state reduced order model is utilized to investigate moving boundary characteristics in a narrow tube of heat exchanger that carries organic refrigerant as working fluid (R134a) in the medium solar thermal applications (~ 200 °C). The study brings forth the changes in wall segment temperatures of the subcooled, two-phase and superheated regions for the tube carrying the refrigerant, with changing average heat transfer fluid (HTF) temperature that changes with the solar radiation incident on the solar collectors. The study also investigates the variation in refrigerant mass flow rates with varying temperature of a commercialized heat transfer fluid (Duratherm FG) that exchanges energy with the narrow tube containing organic refrigerant and estimates suitable mass flow ranges for different steady state bulk heat transfer fluid temperatures.

Keywords: Reduced Order Model, Heat Exchanger, Phase Change Boundary, Solar Thermal.

NOMENCLATURE

D	Diameter of tube (m)
h	Enthalpy (J/kg)
L	Length (m)
$\tilde{T}$	Average temperature (K or °C)
$\dot{m}$	Mass flow rate (kg/s)
$\tilde{P}$	Power (W)
p	Pressure (Pa)
T	Temperature (K or °C)
t	Time (s or min)

Greek Symbols

α	Heat transfer coefficient (W/m^2.K)

Subscripts

1	Subcooled region
2	Two-phase region
3	Superheated region
12	Interface 1-2
23	Interface 2-3
l	Saturated liquid
g	Saturated gas
HTF	Heat transfer fluid
i	Inner side of the tube
in	Inlet of tube
o	Outer side of the tube
out	Outlet of tube
lower	Lower end of the limit
r	Reservoir
rfg	Refrigerant
sat	Saturation
upper	Upper end of the limit
wall	Wall

INTRODUCTION

In the present study, a simplified quasi-steady state reduced order model [1, 2] is utilized to investigate moving boundary characteristics in a narrow tube of heat exchanger that carries organic refrigerant as working fluid (R134a) in the medium solar thermal applications (~ 200 °C) as schematically represented in Fig. 1. The schematic conceptualization of the phase change boundary can be seen in Fig. 2.

For computational investigation, the length of the heat exchanger has been assumed to be 15 m. The inner and outer diameters of the pipe that carries the ORC working fluid (R134a) are 5.08 and 6.033 cm respectively. For the current study thermal performance optimization of the heat exchanger has not been performed. However, the working fluid mass flow rates can be varied such that at least 200-500 kW$_t$ electricity can be generated by using a medium sized turbine with isentropic efficiency in the range of 65-70%. The subcooled refrigerant entering the heat exchanger unit is assumed to be pressurized at a pressure of 3 MPa.
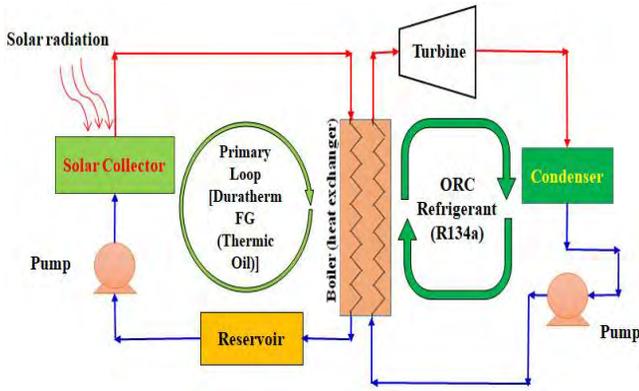
FIGURE 1. Schematic diagram of the primary and secondary loops of an ORC based medium temperature solar thermal power plant

Parabolic trough solar collector in the solar thermal power plant (fig. 1) is modelled by following the configuration as described in the published literatures [3, 4]. The different values of HTF temperature at the solar collector exit corresponding to different solar radiation levels are calculated by using a HTF mass flow rate of 13.8 kg/s. The profile of the average heat transfer fluid temperature (T_{HTF}) with the changing levels of solar radiation incident on the solar collectors is presented in Fig. 3.
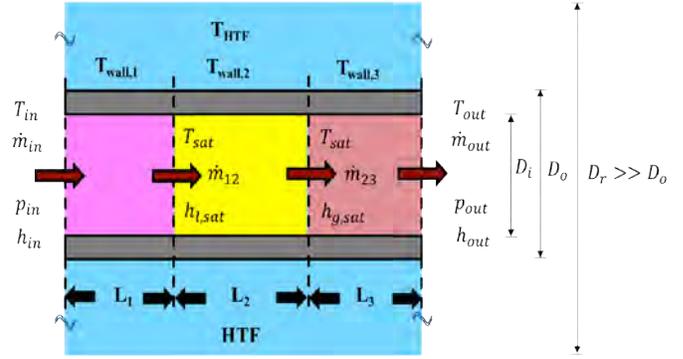
FIGURE 2. Schematic diagram of the tube placed in the thermic oil reservoir ($D_r >> D_o$), that carries R134a as the working fluid (From left to right, the colored zones represent (i) sub-cooled region, (ii) two-phase flow region and (iii) superheated region, respectively).
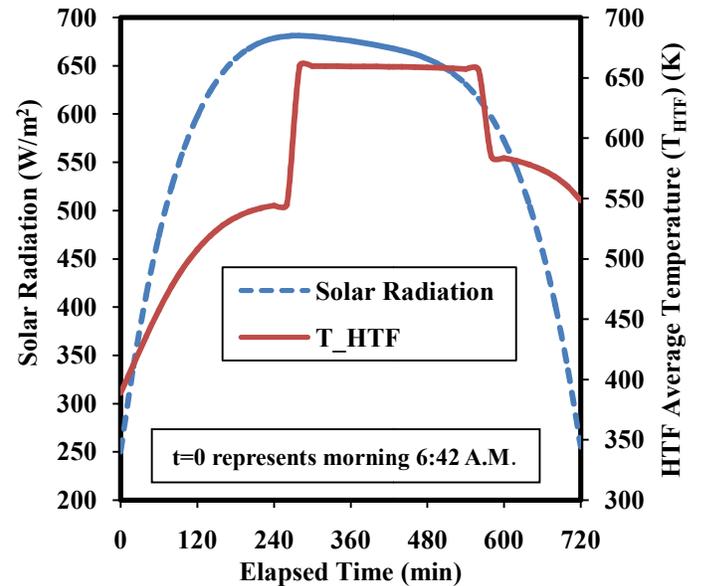
FIGURE 3. Variation of temperature of the heat transfer fluid Duratherm FG (T_{HTF}) with the changing solar radiation power ($\tilde{P}$)

GOVERNING EQUATIONS

A simplified steady state differential energy balance for the subcooled, two-phase and superheated regions can be written from the time-dependent energy equations available in published literature [1, 2], pertaining to the respective regions. In the subcooled region, the energy balance equation at steady state effectively becomes,

$$\dot{m}_{in}h_{in} - \dot{m}_{12}h_l(p) + \pi D_i \alpha_{i1} L_1 \left(T_{wall,1} - \widetilde{T_{rfg,1}} \right) = 0 \qquad (1).$$

For the two-phase region, energy balance equation reduces to,

521

$$\dot{m}_{12}h_l(p) - \dot{m}_{23}h_g(p) + \pi D_i \alpha_{i2} L_2 (T_{wall,2} - \widetilde{T_{rfg,2}}) = 0 \qquad (2)$$

For the superheated region, the energy balance leads to,

$$\dot{m}_{23}h_g(p) - \dot{m}_{out}h_{out} + \pi D_i \alpha_{i3} L_3 (T_{wall,3} - \widetilde{T_{rfg,3}}) = 0 \qquad (3)$$

Similarly, at steady state, the energy balance equations for the wall for three different regions can be easily written as follows:

(a) In the subcooled region,

$$\pi D_i \alpha_{i1} L_1 (\widetilde{T_{rfg,1}} - T_{wall,1}) \qquad (4)$$
$$+ \alpha_o \pi D_o L_1 (T_{HTF} - T_{wall,1}) = 0$$

(b) For the two-phase region,

$$\pi D_i \alpha_{i2} L_2 (\widetilde{T_{rfg,2}} - T_{wall,2}) \qquad (5)$$
$$+ \alpha_o \pi D_o L_2 (T_{HTF} - T_{wall,2}) = 0$$

(c) For the superheated region the expression turns out to be,

$$\pi D_i \alpha_{i3} L_3 (\widetilde{T_{rfg,3}} - T_{wall,3}) \qquad (6)$$
$$+ \alpha_o \pi D_o L_3 (T_{HTF} - T_{wall,3})$$
$$= 0$$

All the sysmbols carry the meaning as indicated in **Nomenclature.**

RESULTS AND DISCUSSIONS

Solar radiation data collected in Greater Noida on June 4, 2016 are used as the input data for the solar collector model. The wall segment temperatures of the subcooled, two-phase and superheated regionsfor the tube carrying the refrigerant are shown in Fig. 4. In the current study, the pressure is assumed to be constant at 3 MPa, over the length of the aforesaid tube (*i.e.* $p_{in} = p_{out}$), and any change in pressure in the axial direction is neglected. This ensures that the superheated steam at 3 MPa exits the tube with a significantly high outlet temperature (T_{out}) and outlet enthalpy (h_{out}) and enters the turbine.

The refrigerant R134a is an isentropic fluid. Additionally, a sufficient temperature margin has to be taken into account for the condenser and the pump units respectively. Keeping in mind all the associated constraints and system requirements, the outflow of the refrigerant is assumed to be a dry steam at 70°C at the turbine outlet.

The wall segment temperatures are dependent on the physical properties of the fluids involved, the total length , the inner diameter as well as the thickness of the tube and

the refrigerant (ORC working fluid) mass flow rate. For the calculation of the heat transfer coefficients of the single-phase regions, Dittus-Boelter equation [5] is used, whereas Donowski-Kandlikar parameterized correlation [6] is employed to determine heat transfer coefficient of the two-phase region corresponding to a reasonable average void fraction value of 0.665.

For a very high heat flux coming from the HTF and very high mass flux of the refrigerant, the average heat transfer coefficient in the subcooled region has been calculated to be 6071.67 $Wm^{-2}K^{-1}$. The heat transfer coefficient of the two-phase region corresponding void fraction value of 0.665 has been calculated to be 25058.38 $Wm^{-2}K^{-1}$. The average heat transfer coefficient in the superheated region has been calculated to be about 1471 $Wm^{-2}K^{-1}$. The outer heat transfer coefficient of 397 $Wm^{-2}K^{-1}$has been obtained from the website of Duratherm fluids [7].
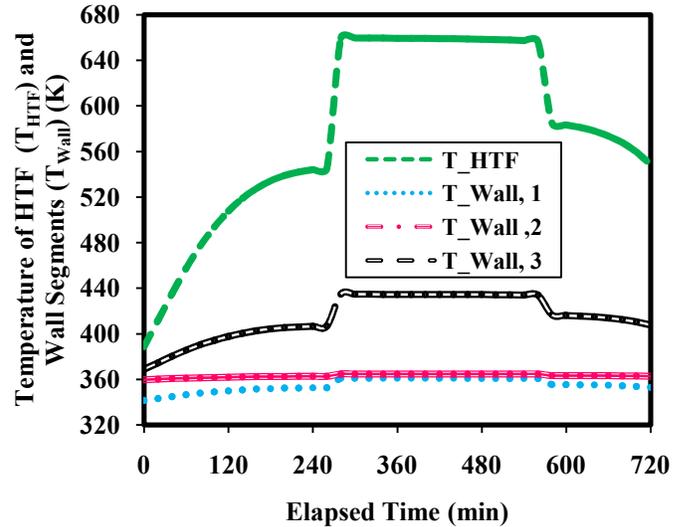
FIGURE 4. Variation of temperature of the wall segments ($T_{wall,1}$, $T_{wall,2}$, $T_{wall,3}$) with the changing temperature of the heat transfer fluid Duratherm FG (T_{HTF})

The wall temperature in subcooled region is found to be the lowest for all the levels of solar radiation, whereas the wall temperature in superheated region remains the hottest, as can be seen from Fig. 4. As the heat transfer fluid temperature of increases, the difference between the wall temperatures of the superheated and the subcooled regions, as well as that between the superheated and the two-phase phase regions also increase.

The study also brings forth the variation in refrigerant mass flow rates with varying bulk temperature of a commercialized heat transfer fluid (Duratherm FG) that exchanges energy with the narrow tube containing organic refrigerant and estimates suitable mass flow ranges for

different steady state bulk heat transfer fluid temperatures, as can be seen from Fig. 5.

It is found that the wall temperatures of interest and the refrigerant mass flow rates become very high with higher values of HTF temperature. Thus, feasible operating region has to be chosen carefully for practical purposes, considering the system specifications.
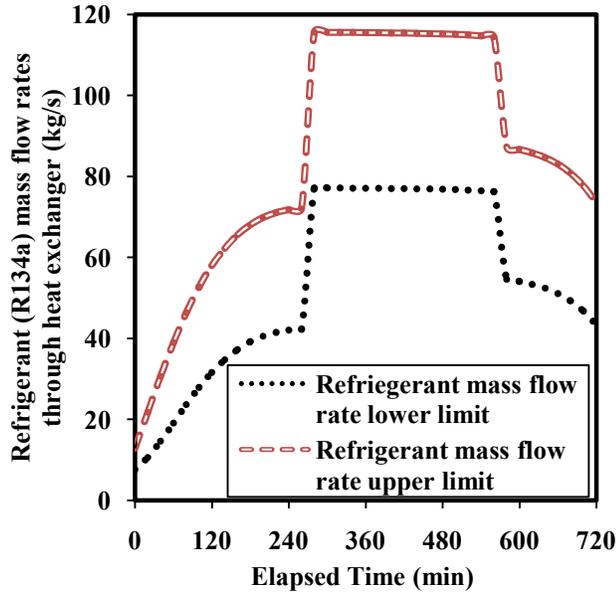
FIGURE 5. Variation of the ORC refrigerant (R134a) mass flow rate with changing temperature of the heat transfer fluid Duratherm FG (T_{HTF})

CONCLUSIONS

In this work, the effect of changing HTF bulk temperature on the wall temperature distributions in a narrow tube is investigated computationally, to understand the moving boundary phase change characteristics of the ORC working fluid in a solar thermal heat exchanger. The required mass flow rate of the ORC refrigerant has also been studied by considering a suitable length of the subcooled region that essentially prevents the system from entering into a state devoid of subcooled refrigerant supply. In future, finer transient characteristics can be explored by incorporating axial variation in the heat transfer fluid temperature profile in shell and tube heat exchanger and by introducing time-dependent fluctuations in the subcooled refrigerant flow at the heat exchanger entry.

ACKNOWLEDGMENTS

REFERENCES

[1] J.M. Jensen, H. Tummescheit, Moving boundary models for dynamic simulations of two–phase flows, Modelica 2002, The Modelica Association, March 18-19, 2002.

[2] E.W. Grald, J.W. MacArthur, A moving boundary formulation for modeling time-dependent two-phase flow, Int. J. Heat and Fluid Flow, 13 (1992) 266-272.

[3] K.M. Powell, T.F. Edgar, Modeling and control of a solar thermal power plant with thermal energy storage, Chemical Engineering Science, 71 (2012) 138–145.

[4] O. Behar, A. Khellaf, K. Mohammedi, A novel parabolic trough solar collector model – Validation with experimental data and comparison to Engineering Equation Solver (EES), Energy Conversion and Management, 106 (2015) 268–281.

[5] Dawid Taler and Jan Taler, Simple heat transfer correlations for turbulent tube flow, E3S Web of Conferences **13**, 0200 (2017).

[6] Vincent D. Donowski and Satish G. Kandlikar, Correlating evaporation heat transfer coefficient of refrigerant R-134a in a plate heat exchanger, Mechanical Engineering DepartmentRochester Institute of Technology Rochester, NY, 1999.

[7] https://durathermfluids.com/calculators/heat-transfer-coefficient/

SEEC-2018-120

STABILITY ANALYSIS OF AN OIL BASED THERMOCLINE ENERGY STORAGE SYSTEM

Advaith S
Interdisciplinary Center for Energy Research
IISc Bangalore
advaiths@iisc.ac.in

Ambuj Punia
Mechanical engineering
IISc Bangalore
Ambuj0809@gmail.com

Utpal Kumar Chetia
Mechanical engineering
IISc Bangalore

Nikhil Dani
Interdisciplinary Center for Energy Research
IISc Bangalore

Kamanio Chattopadhyay
Materials engineering
IISc Bangalore

Saptarshi Basu
Mechanical engineering
IISc Bangalore
saptarshibasukol@gmail.com

ABSTRACT

Oil based thermal energy storage system offers a higher energy storage density as compared to other solar energy storage techniques like Solar PV etc. The present paper focuses specifically on the practical viability thermocline storage system. A lab scale setup has been developed at Thermal Energy Research Laboratory Indian Institute of Science Bangalore. The experimental study investigates the stability of high temperature oil based thermocline storage system.The thermocloine restablise itself just after the interaction of hot fluid with the cold one. Once the restablisation phenomena was found to be complete, a stable thermocline is observed for more than two hours. This stability of thermocline act as an energy storage system from which useful work can be extracted at will or when there is no sunlight.

Keywords:*Thermocline, Energy Storage, Solar thermal*
.

INTRODUCTION

The demand of energy for the sustenance of human life is increasing day by day. In order for us to cope up with the ever increasing energy demand, our dependence on fossil fuels needs to be shifted towards the renewable sources of energy. Another reason for this shift is the increase in global warming due to heavy utilization of fossil fuels. The effects of global warming can be seen easily these days and the situation is critical. Solar energy can be a very good substitute for replacing our dependency on fossil fuels. But the problem with solar energy is that, it is not available during night. Solar thermal thermocline energy storage system shows a promising future in terms of economics and delivery of useful work at will. Thermocline energy storage system consists of a cylindrical tank where hot and cold fluids are stored in the same tank. The hot and cold fluids are separated from each other due to density difference. In this way a temperature difference is created, which acts as a driving potential for the energy extraction.

Many studies have been conducted on thermocline energy storage system. Galione et.al[1] developed a new PCM based thermocline storage concept. Under the study they did the numerical simulations for the number of cycles after which the energy given and retrieved becomes periodic. For a multilayer PCM and solid filler system proved to give better results than single PCM and MULTI PCM storage systems. Oro et.al[2] compared a fully filled water tank with a PCM + water filled tank for charging and discharging process. Thermal stratification was used to analyse the performance of two tanks. Various dimensionless numbers and other parameters like MIX number, Richardson number, energy and exergy efficiency etc were used to identify the thermal stratification. Flueckiger et.al[3] developed a new thermocline model based and implemented on the system based simulation of 100 Mwe for 1 year. The system efficiency for a year long based simultion was found to be greater than 99% for a thermocline storage period of 6hrs everyday with charging and discharging. Wu et.al[4] evaluated the discharge efficiency based on different configurations of concrete in the storage system like channel embedded structure, parallel plate structure, round bundle structure, packed bed structure. Out of the 4 structure mentioned, packed bed storage system gave a better discharge efficiency. Qin et.al[5] proposed 4 criterions to minimize the widening of thermocline thickness. For criterion 2, when hot fluid displaces the cold fluid, the flow velocity should be less than the critical value, for criterion 3, when cold fluid displaces hot fluid from top, the flow velocity mus be greater than the critical value. criterion 4, if mobility ration is less than 1, then thermocline is stable else unstable. So as far as the study of thermocline is concerned, major studies have been conducted only on the numerical evaluation of thermocline stability. So a need arise to practically investigate the behaviour of the abovementioned storage unit taking oil as the HTF and also the storage medium.

EXPERIMENTAL SETUP AND PROCEDURE

The current study focuses on the stability of the thermocline energy storage system. The operational cycle of a thermocline consists of 2 phases, charging and discharging. During the charging phase, cold fluid from the bottom is extracted and passed through a heat exchanger thereby extracting heat from the solar field. The fluid thus becomes hot and comes back to the storage tank. When the storage tank is filled with hot fluid, it marks the end of the charging process. During discharging we extract energy from the storage tank. So, hot fluid is taken from the top of

the storage tank and the energy is delivered to the required space for applications. The fluid after delivering energy comes back to the storage system from the bottom. When the storage tank is full of cold fluid, it marks the end of discharging phase. During the charging and discharging phases, the interphase between the hot and cold fluid moves down and up respectively. This application of thermocline eliminates the need for two-tank energy storage system.

The current system is a lab scale setup used to store energy by thermocline phenomenon. It consists of an inventory tank to store the storage media, from where the pump will transfer it to the thermocline tank. Next to the inventory tank is the heat receiver, where the storage media like oil will come and gets heated up in the heat receiver section also. Heat receiver is a cylindrical container mounted with jacketed heaters to heat the oil. The from the heat receiver the oil goes to the thermocline storage tank which is fitted with the optical axis window for outside inspection. There is another diversion of pipeline just before entrance to the storage tank, towards the heat exchanger system to reject excess heat to the ambient. The heat exchanger has been designed keeping in view other heat transfer fluids, which will serve as a future scope of study. Figure 1. shows the experimental setup with its corresponding nomenclature. The heat transfer fluid used in the setup is HYTHERM-600 oil. The properties of HYTHERM-600 are given in Table 1. Initially the cold fluid is transferred to the cylindrical storage tank with the help of a high temperature based pump and it is ensured that the storage tank is half full of cold oil(at room temperature). After ensuring the same, the heaters inside the inventory tank are switched on, and the oil is heated to the desired temperature. The temperature of the oil inside the inventory tank is controlled using variac. The temperature is measured with the help of thermocouples(K-type) placed at different locations according to the need. For example, as we are concerned with the stability of the thermocline, more number of thermocouples are placed axially inside the storage tank. After getting the desired temperature of the oil, the hot oil is filled slowly from the top of the thermocline storage tank through a honeycomb structure in order to minimize the distortion of the thermocline. A stable thermocline starts to form and the storage tank is filled upto top with the hot oil. The pump is then stopped such that there is no flow inside the thermocline storage tank. Figure 2. shows the thermocline formation with hot and cold fluids.
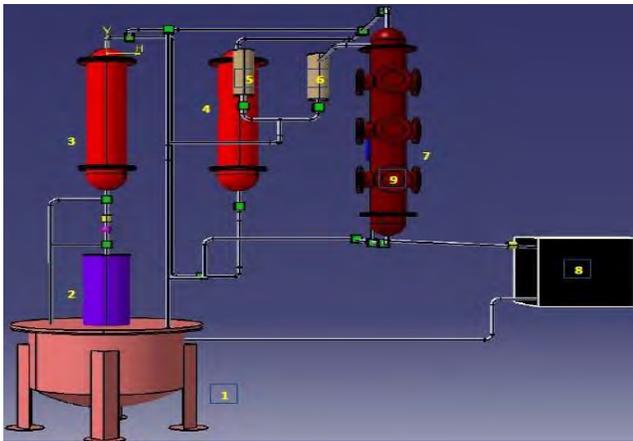
Figure 1. Schematic of the thermocline energy storage system developed at Thermal Energy Research Laboratory. (1) Inventory Tank, (2) Pump, (3 & 4) Heat receiver (5 & 6) Surge Tank (7) TES, (8) Optical Window (9) Heat exchanger
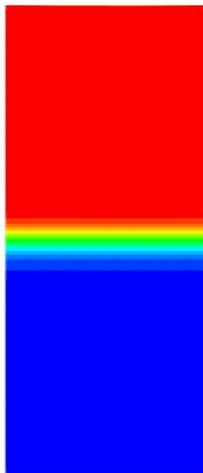
Figure 2. Thermocline formation showing the upper hot and bottom colder fluids. The in between interface degradation is under study.

RESULT AND DISCUSSION

A comprehensive study on the stability of thermocline energy storage system has been performed with the help of a laboratory based experimental setup. Figure 3 shows the results of the experimental study done taking oil as the heat transfer fluid. The experimental results shows the initial degrading of the thermocline for the initial 1/3rd of the time going from from 140°C to 75°C. The degradation can be attributed majorly to the losses due to ambient and axial conduction inside the oil. After the degradation phenomenon, at around 40 min, the graph shows fluctuations in the thermocline formation explanation of which needs further detailed study. The thermocline finally comes to a halt and then stabilises itself for the rest of the duration of experimentation. So overall, initially a

rapidly degrading thermocline was formed which after a temperature difference of around 65°C stabilised itself and again a new thermocline was found to be established for a temperature difference of 40°C. This newly formed thermocline is found to be stable for a much longer duration of time.

Table 1. Various properties of HYTHERM-600

Properties	HP Hytherm 600
Kinematic Viscoslty @ 40 °C, Cst	27-38
Flash Point (Coc), °C, Min	220
Specific Heat Kcal/Kg °C	0.741
Thermal Conductvity , Kcal/Hr-Mt °C	0.1

If we are considering even the temperature of thermocline from 75°C to 35°C we still have a temperature difference of 40°C, from which we can extract useful energy. This much amount of useful energy can be used for building applications or hydronic systems like in integration with heats pumps of higher COP.
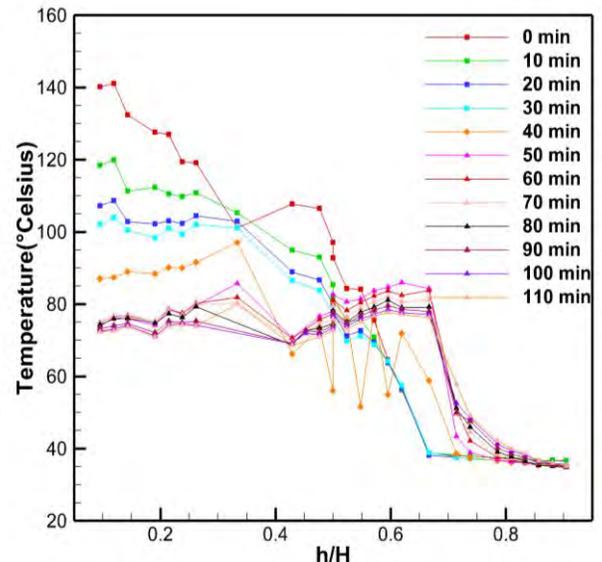
Figure 3. Profile of the thermocline using HITHERM-600.

CONCLUSIONS

An experimental study of an oil based thermocline energy storage system has been performed. Under the experimental investigation, it is found that the thermocline degrades at a much faster rate during the initial 1/3rd time. The reason for the same can be due to losses to environment or some other phenomena like viscous fingering inside the thermocline system. After the initial degration for the abovementioned duration, the thermocline restablised itself and we found a well established

thermocline interface for the rest of the time. This stability of thermocline is well suited for low temperature applications like building thermal energy storage.

Future scope of work includes the understanding of the sudden degradation of the thermocline from 140°C to 75°C, various factors impacting its stability. Apart from this various modelling based studies have been done taking molten salt as the HTF and also the storage medium. We would like to conduct the same experimentation with molten salts and further different combinations of salts with heat transfer enhancement is also taken into consideration for future work.

ACKNOWLEDGEMENTS

REFERENCE

1. P.A. Galione, C.D. Pérez-Segarra, I. Rodríguez, A. Oliva, J. Rigola, Multi-layered solid-PCM thermocline thermal storage concept for CSP plants. Numerical analysis and perspectives, Applied Energy 142 (2015) 337–351.
2. Eduard Oró, Albert Castell, Justin Chiu, Viktoria Martin, Luisa F. Cabeza, Stratification analysis in packed bed thermal energy storage systems, Applied Energy 109 (2013) 476–487.
3. Scott M. Flueckiger, Brian D. Iverson, Suresh V. Garimella, James E. Pacheco, System-level simulation of a solar power tower plant with thermocline thermal energy storage, Applied Energy 113 (2014) 86–96.
4. Ming Wu, Mingjia Li, Chao Xu, Yaling He, Wenquan Tao, The impact of concrete structure on the thermal performance of the dual-media thermocline thermal storage tank using concrete as the solid medium, Applied Energy 113 (2014) 1363–1371
5. Frank G.F. Qin, Xiaoping Yang, Zhan Ding, Yuanzhi Zuo, Youyan Shao, Runhua Jiang, Xiaoxi Yang, Thermocline stability criterions in single-tanks of molten salt thermal energy storage, Applied Energy 97 (2012) 816–821

SEEC-2018-122

Numerical study of mist jet impingement cooling of an isothermal flat plate at low superheat.

Vikash Kumar Singh Chauhan
Reserach Scholar
Department of Mechanical Engineering
National Institute of Technology, Manipur
Email: vksc@nitmanipur.ac.in

Dr. Dushyant Singh
Assistant Professor
Department of Mechanical Engineering
National Institute of Technology, Manipur
Email: dushyant@nitmanipur.ac.in

ABSTRACT

In the present study results of numerical investigation of air water mist jet cooling of an isothermal flat plate is presented. Separate parallel offset inlets were considered for air and water as of an air atomized nozzle. Low mass loading fraction of liquid with droplet size, d_o=32 µm is considered to be co flowing with annular air jet of $Re_{d(hyd)}$=4500 and impinging on a flat isothermal plate maintained at 40ºC placed at 5d from the nozzle exit. Results of Volume of Fluid, mixture and Eulerian Multiphase model were compared with experimental results of Quinn et al.[28]. It was observed that Eulerian multiphase model predicts the heat transfer results most closely than the available multiphase models.

Keywords >: *Mist, Jet Cooling, Flat plate, Numerical study, Water, Multiphase Models*

.
NOMENCLATURE
d=Outer diameter of the annular jet (m)
d_i=Inner diameter of the annular jet (m)
d_w= Diameter of the central water jet (m)
d_{hyd}=Hydraulic diameter of the jet (m)
$\dot{m}_w$= Mass flow rate of water (kg/hr)
$\dot{m}_a$= Mass flow rate of air (kg/hr)
f=Mist loading fraction or mass loading fraction of water
h=Heat transfer coefficient (W/m²k)
H=Nozzle to plate spacing (m)
r= Radial distance from the jet axis (m)
ρ=Density (kg/m³)
τ =Shear stress tensor (N/m²)
F=Acting forces on the body (N)

INTRODUCTION
The cooling of industrial products by jet cooling process has been used in industries for a while. It has been observed that enhancement in jet cooling is almost linear with the mass flow rate of the flowing gas [1-2]. With h/d=8, Kanamori et al. [3] have concluded that by increasing the Re_d from 25,000 to 50,000 the improvement in heat transfer rate is only 50 percent. However they also reported that by adding only 200 millilitre of water per hour have increased the heat transfer rate by 100% for Re_d of 25,000 and 200% for the Re_d of 50,000.

Mist jets have been used in the cooling of electronic components[4-5].Okhubo and Nishio[6] and Sozbir and Yao [7] have studied the mist quenching of glass sheets using mist cooling and concluded that very thin tempered glass can be made in order of few millimeters. Li et al. [8] and Wang and li [9]   studies have been done on cooling of turbines using mist flow. Babic et al. [10], An et al. [11] and Tan et al. [12] reported the feasibility of use of mist jet cooling as an alternative to cooling fluid in the machining processes whereas Liu et al. [13] have studied the characteristics of mist jet cooling in pressurized die casting process. Zhang et al. [14] have studied the mist cooling during neurosurgical bone grinding to reduce the thermal shock to the nerve cells and enhance visibility during surgical operations. Pais et al. [15] conducted experiments with air atomized spray jet to study the heat transfer from a heated plate of different surface roughness. Yang et al. [16] reported the heat flux to be an order of magnitude higher than that of pool. Sozbir et al.[17] reported in his study that heat transfer coefficient and Leidenfrost temperature increases with the increase in the air velocities and the liquid loading fraction. Agrawal et al. [18] studied transient mist cooling and reported that increase in the initial temperature increases the rewetting temperature and wetting delay however the rewetting velocity decreases. Graham and Ramadhyani [19] concluded with their study of air-water and air-methanol mist jet cooling that surface average heat flux as high of 6,00,000 W/m²can be removed from the target surface at temperatures of 70ºC for air methanol mist and 80ºC for air water mist. Lyons et al. [20]

concluded that convective heat transfer rate increase with increase of water loading fractions.

Quinn et al. [21] reported that the mist jet profile and the air jet profile collapses to same level at certain r/d however for higher mist loading fractions the collapse occurs at higher r/d. In another study [22] they concluded that due to mist droplets evaporation is significant the mist jet behaves like an air jet of lower temperature however when the mist loading is increased and due to saturation of the jet no further cooling is observed. Vouros et al. [23] reported that heat flux from the target affect the jet formation and the mist droplets near at the stagnation region. Nguyen and Zhang [24] and Jiang et al. [25] studied numerically the effect of mist cooling on the grinding wheel. Pakhomov and Terekhov [26] conducted computational study of mist jet cooling and observed cooling enhancement with increasing the Re_d, mass flux of water and droplet size whereas increase in h/d results in decrease in the heat flux. They further studied the effect of confinement on the mist jet impingement on the flat plate [27] and observed that the confinement only effect the heat transfer if h/d ratio is very small for both single and two phase flow.

To the best of my knowledge the study of feasibility of different Multiphase models in Eulerian Framework has not been studied for the air water Mist jet cooling on flat plate.

PROBLEM STATEMENT

In the present study cooling of a heated flat surface by an externally mixing mist nozzle has been investigated numerically. Figure 1 shows the axis symmetric geometry of the domain to be studied. Air atomized nozzle of Quinn et al. [28] is considered for the numerical study.
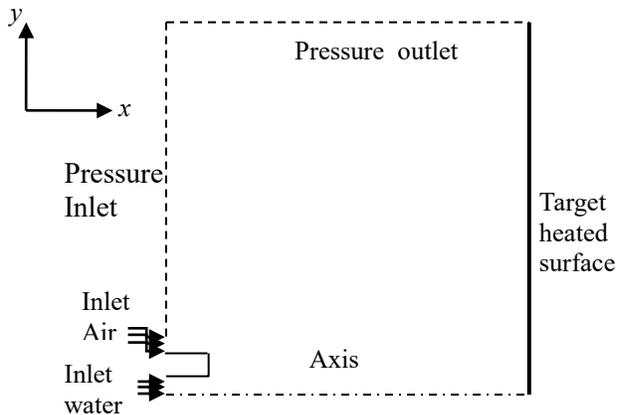
Figure 1:-Geometry of the Domain

The Reynolds number of 4500 of the jet is defined on the basis on the hydraulic diameter of the air jet .

$$\text{Re}_{d(hyd.)} = \frac{\rho_g V_g d_{hyd.}}{\mu_g} \tag{1}$$

The mist loading fraction is defined as

$$f = \frac{mass\ flowing\ rate\ of\ water}{mass\ flowing\ rate\ of\ air} = \frac{\dot{m}_w}{\dot{m}_a} \tag{2}$$

GOVERNING EQUATIONS

The conservation equations for mass momentum and energy are given by

$$\nabla \cdot \vec{v} = 0 \tag{3}$$

$$\nabla \cdot (\rho \vec{v} \vec{v}) = -\nabla p + \nabla \cdot (\bar{\bar{\tau}}) + \rho \vec{g} + \vec{F} \tag{4}$$

$$\nabla \cdot (\vec{v}(\rho H + p)) = \nabla \cdot (k_{eff} \nabla T + (\bar{\bar{\tau}}_{eff} \cdot \vec{v})) + S_h \tag{5}$$

The jet impingment heat transfer study by singh et al. [29] was considerd for the turbulence modelling and for multiphase models the ANSYS Fluent theory guide [30] was followed.

NUMERICAL METHODOLOGY

In the present numerical study an axisymmetric, incompressible, steady state, numerical simulations was carried out using the commercial CFD package ANSYS Fluent. To solve continuity momentum and energy equations pressure based solver used. For spatial discretization of convective terms first order upwind scheme was used. Realizable k-ε turbulence model among was used for the turbulence modeling with enhanced wall treatment function for the near wall flows[31]. Air and water was considered as primary and secondary phases respectively.

BOUNDARY CONDITIONS

- **Inlet Water**. Uniform velocity distribution was considered for the study at 25°C.

- **Inlet air**. Velocity inlet for the gas phase with Uniform velocity distribution at 25°C.

- **Heated Target surface**. An isothermal wall is considered as the target flat surface with no slip flow condition.

- **All open domain**. Pressure inlet and pressure outlet are the open sides of the domain with zero initial gauge pressure as show in Figure 1.

- **Axis**. The boundary along the x-axis was considered as axis of the domain.

GRID INDEPENDENCE TEST

Mesh with dimensions (x,y) 151×76, 204×110, 204×157, 257×110, 323×119 were used for the grid independence test with eulerian multiphase model with realizable k-ε turbulence model $Re_{d(hyd)}$ = 4500 and h/d = 5.
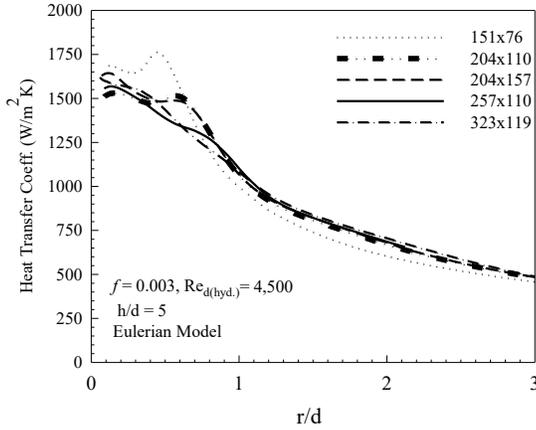
Figure 2:-Grid Independence Test

Sufficient grid refinement was done near the target heated plate to capture satisfactory y^+ value less than unity. The grids 257×110 and 323×119 shows similar results and therefore 257×110 was selected for the study.

RESULTS AND DISCUSSION

The results of heat transfer coefficient on the plate is plotted agains the non dimensional radial distance r/d.
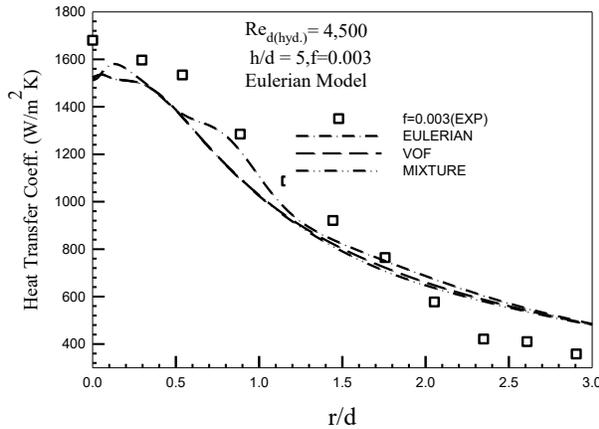
Figure 3:-Comparision of the Multiphase models for heat transfer results

It was reported that the results of the Eulerian Multiphase model shows the most near results to the experimatal values.The countours of the velocity mangnitute of the air and water are shown in figure 4 it can be observed that the water particles are being accelerated
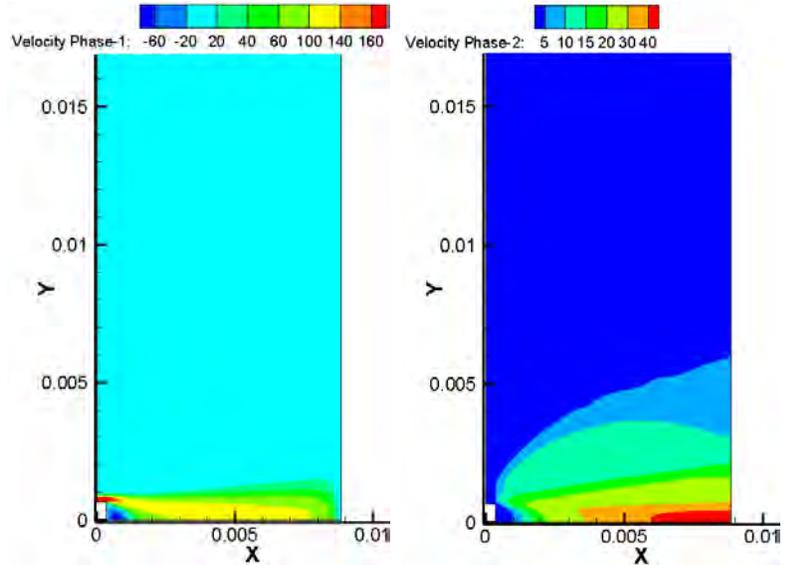
Figure 4:-Contours of Velocity for air and water.

as they move away from the nozzle whereas the air particles velocity reduces.This also confirms the transfer of momentum from the air to the liquid.

REFERENCES

[1] Singh, D., Premachandran, B., & Kohli, S. (2015). Effect of nozzle shape on jet impingement heat transfer from a circular cylinder. *International Journal of Thermal Sciences*, *96*, 45-69.

[2] Singh, D., Premachandran, B., & Kohli, S. (2015). Circular air jet impingement cooling of a circular cylinder with flow confinement. *International Journal of Heat and Mass Transfer*, *91*, 969-989.

[3] Kanamori, A., Hiwada, M., Mimatsu, J., Sugimoto, H., &Oyakawa, K. (2009). Control of impingement heat transfer using mist. *Journal of Thermal Science and Technology*, *4*(2), 202-213.

[4] Bar-Cohen, A., Sherwood, G., Hodes, M., & Solbreken, G. (1995). Gas-assisted evaporative cooling of high density electronic modules. *IEEE Transactions on Components, Packaging, and Manufacturing Technology: Part A*, *18*(3), 502-509.

[5] Mudawar, I., Bharathan, D., Kelly, K., & Narumanchi, S. (2009). Two-phase spray cooling of hybrid vehicle electronics. *IEEE Transactions on Components and Packaging Technologies*, *32*(2), 501-512.

[6] Ohkubo, H., & Nishio, S. (1988). Mist cooling for thermal tempering of glass. *JSME International Journal. Ser. 2, Fluids engineering, heat transfer,*

power, combustion, thermophysical properties, *31*(3), 444-450.

[7] Sozbir, N., & Yao, S. C. (2004). Experimental investigation of water mist cooling for glass tempering. *Atomization and Sprays*, *14*(3).

[8] Li, X., Gaddis, J. L., & Wang, T. (2003). Mist/steam cooling by a row of impinging jets. *International Journal of Heat and Mass Transfer*, *46*(12), 2279-2290.

[9] Wang, T., & Li, X. (2008). Mist film cooling simulation at gas turbine operating conditions. *International Journal of Heat and Mass Transfer*, *51*(21), 5305-5317.

[10] Babic, D., Murray, D. B., & Torrance, A. A. (2005). Mist jet cooling of grinding processes. *International Journal of Machine Tools and Manufacture*, *45*(10), 1171-1177.

[11] An, Q. L., Fu, Y. C., & Xu, J. H. (2011). Experimental study on turning of TC9 titanium alloy with cold water mist jet cooling. *International Journal of Machine Tools and Manufacture*, *51*(6), 549-555.

[12] Tan, X., Zhang, J., Liu, B., & Zhu, X. (2013). Experimental investigation on heat transfer enhancement of mist/air impingement jet. *Science China Technological Sciences*, *56*(10), 2456-2464.

[13] Liu, G. W., Morsi, Y. S., & Clayton, B. R. (2000). Characterisation of the spray cooling heat transfer involved in a high pressure die casting process. *International journal of thermal sciences*, *39*(5), 582-591.

[14] Zhang, L., Tai, B. L., Wang, A. C., & Shih, A. J. (2013). Mist cooling in neurosurgical bone grinding. *CIRP Annals-Manufacturing Technology*, *62*(1), 367-370.

[15] Pais M. R. ,Chow, L. C., & Maheikey, E. T. (1992). Surface roughness and its effects on the heat transfer mechanism in spray cooling. *Journal of Heat Transfer*, *114*, 211.

[16] Yang, J., Chow, L. C., & Pais, M. R. (1996). Nucleate boiling heat transfer in spray cooling. *Journal of Heat Transfer*, *118*(3), 668-671.

[17] Sozbir, N., Chang, Y. W., & Yao, S. C. (2003). Heat transfer of impacting water mist on high temperature metal surfaces. *Tran. ASME Journal of Heat Transfer*, *125*(1), 70-74.

[18] Agrawal, C., Lyons, O. F., Kumar, R., Gupta, A., & Murray, D. B. (2013). Rewetting of a hot horizontal surface through mist jet impingement cooling. *International Journal of Heat and Mass Transfer*, *58*(1), 188-196.

[19] Graham, K. M., & Ramadhyani, S. (1996). Experimental and theoretical studies of mist jet impingement cooling. *Journal of Heat Transfer*, *118*(2), 343-349.

[20] Lyons, O. F., Quinn, C., Persoons, T., & Murray, D. B. (2012). Heat transfer and flow in an atomizing mist jet: a combined hot film and shadowgraph imaging approach. In *Journal of Physics: Conference Series, 395(1),* (Vol. 395, No. 1, p. 012173).

[21] Quinn C., Persoons T. Murray D.B., (2013)., heat transfer profiles of an impinging atomizing water-air mist jet, 8thWorld Conference on Experimental Heat Transfer, Fluid Mechanics, and Thermodynamics.

[22] Quinn C., Murray D.B., Persoons T. (2014)., The effect of liquid mass flow rate on heat transfer for an air-water atomizing mist jet, in: 15th International Heat Transfer Conference, IHTC-15, pp. 1–13.

[23] Vouros, A., Vouros, A., &Panidis, T. (2016). experimental study of a water-mist jet issuing normal to a heated flat plate. thermal science, 20(2), 473-482.

[24] Nguyen, T., & Zhang, L. C. (2005). Modelling of the mist formation in a segmented grinding wheel system. *International Journal of Machine Tools and Manufacture*, *45*(1), 21-28.

[25] Jiang, F., Wang, H., Wang, Y., & Xiang, J. (2016). Simulation of Flow and Heat Transfer of Mist/Air Impinging Jet on Grinding Work-Piece. *Journal of Applied Fluid Mechanics*, *9*(3).

[26] Pakhomov, M. A., &Terekhov, V. I. (2010). Enhancement of an impingement heat transfer between turbulent mist jet and flat surface. International Journal of Heat and Mass Transfer, 53(15), 3156-3165.

[27] Pakhomov, M. A., & Terekhov, V. I. (2011). The effect of confinement on the flow and turbulent heat transfer in a mist impinging jet. International Journal of Heat and Mass Transfer, 54(19), 4266-4274.

[28] Quinn, C., dilute impinging air-water mist jet at low wall temperatures. *International* Murray, D. B., & Persoons, T. (2017). Heat transfer behaviour of a *Journal of Heat and Mass Transfer*, *111*, 1234-1249.

[29] Singh, D., Premachandran, B., & Kohli, S. (2013). Numerical simulation of the jet impingement cooling of a circular cylinder. *Numerical Heat Transfer, Part A: Applications*, *64*(2), 153-185.

[30] Fluent, I. N. C. (2015). FLUENT 15.6 user's guide. *Fluent documentation*.

[31] Garbero, M., Vanni, M., & Fritsching, U. (2006). Gas/surface heat transfer in spray deposition processes. *International journal of heat and fluid flow*, *27*(1), 105-122.

SEEC-2018-125

NUMERICAL INVESTIGATION OF EFFECT OF METHANE ADDITION ON COMBUSTION AND EMISSION CHARACTERISTICS OF COMPRESSION IGNITION ENGINE IN DUAL FUEL MODE

Gaurav Tripathi
School of Engineering
IIT Mandi
Email: g_tripathi@ students.iitmandi.ac.in

Priybrat Sharma
School of Engineering
IIT Mandi
Email:priybrat_s@students.iitmandi.ac.in

Atul Dhar
School of Engineering
IIT Mandi
Email: add@iitmandi.ac.in

ABSTRACT

In this paper, Converge CFD is used to simulate the effect of methane addition in CI engine at different conditions. Simulation results after validation are used for studying the effect of increasing methane share on the performance and emission characteristics of the engine at different load conditions. Simulation results indicate that lower methane addition results in improvement of combustion and emission characteristics in comparison to higher methane addition. Higher methane energy supplementation results in higher NOx, soot and HC emission while peak pressure decreases.

Keywords: dual fuel, spray parameters, emission reduction.

NOMENCLATURE

aTDC   After Top Dead Center
bTDC   Before Top Dead Center
CA   Crank Angle

INTRODUCTION

Currently, petroleum fuel is the primary source of energy for internal combustion engine. However, petroleum fuel is finite in quantity. There are estimated 1000 billion barrels of petroleum reserves worldwide, and it is predicted that they will be consumed in about 40 years [1]. Hence there is a need to save petroleum fuel, and the most viable alternative is to harvest cleaner renewable fuels. Amongst such fuels Hydrogen, methane and hydrogen-methane mixture are promising alternative gaseous fuels. Use of methane in IC engine offers many advantages such as its application in IC engine require minimum modifications; methane also has lean burn capability and high thermal efficiency. Bates et al. report that use of natural gas results is efficient in reduction of HC and CO emission compare to gasoline engine [2].

Karagoz et al. investigated the effect of natural gas and diesel fuel on combustion, performance and emission characteristics of CI engine. They report that with an increase in methane addition BSFC and HC and NOx emission increases, and BTE decreases while CO emission at lower supplementation levels decreases, but as the methane energy share is enhanced, it increases [3].

This paper presents a numerical model developed to analyse the effect of methane supplementation on combustion and emission characteristics of dual fuel engine.

METHODOLOGY

ConvergeCFD is used to simulate the methane diesel combustion in CI engine during the closed cycle. Experimental data published in literature is used to validate the simulation results of Converge CFD. Validated model is used for varying methane substitution and changing spray parameters. A 45° angular slice of the cylindrical domain is considered instead of the complete cylinder to save computational time; periodic boundary conditions are applied on inter-sector boundaries.

Grid independency study is performed on the model using base grid sizes of 1.8 mm, 2.3 mm and 3.0 mm. For each grid, size pressure is plotted in fig 1(a). Fig 1(a) shows that refining the grid size from 3 mm to 2.3 mm improves the match of the experimental results with numerical results to a great extent. Where else refining the mess size further from 2.3 mm to 1.8 mm results in no significant improvement in the match for validation but the computation time increases from 8 hrs to 14 hrs. Hence to achieve better computational efficiency, 2.3 mm grid size is considered for all simulations.

Verbiezen et al., experimental result is used to validate the simulation results obtained from the developed model [4]. Comparison of the experimental data and numerical model data is shown in fig 1(b), and a good match is observed between the two, proving the validity of the model developed. Engine specification is given in Table 1.

TABLE 1: ENGINE SPECIFICATION IN MODEL

S. No.	Parameter	Specification
1	Engine type	6-cylinder 4-stroke direct injection diesel engine
2	Bore (mm)	130
3	Stroke (mm)	146
4	Displacement	1.939
5	Piston bowl shape	Bathtub
6	Piston bowl diameter (mm)	84

(a)

(b)
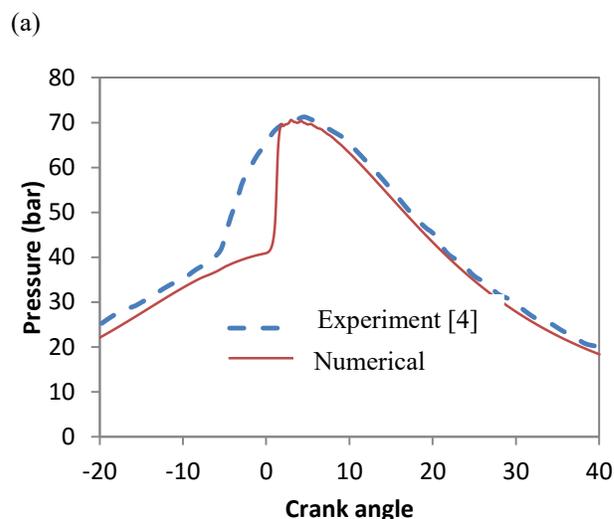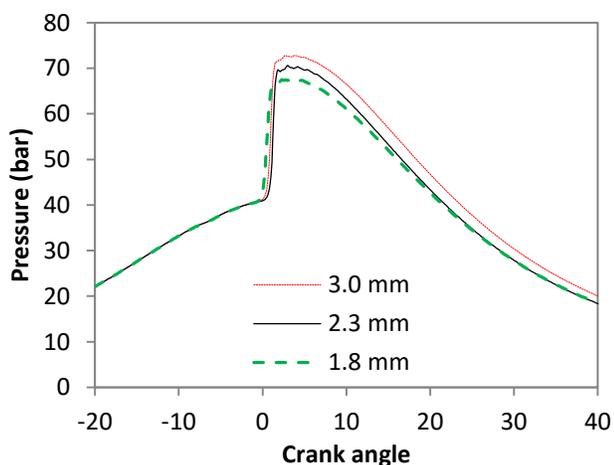
FIGURE 1. (a) PRESSURE TRACE FOR DIFFERENT GRID SIZE (b) COMPARISON OF PRESSURE WITH EXPERIMENTAL DATA FOR VALIDATION.

RESULT AND DISCUSSION

In this numerical study, the effect of 10, 25 and 50% methane substitution on combustion and emission characteristics of CI engine has been observed in dual fuel mode. Here methane addition is done by constant energy supplementation method and the mode of supplementation considered is port fuel injection.

EFFECT OF METHANE ADDITION ON PRESSURE AND HEAT RELEASE RATE

With methane energy supplementation, pressure drops (fig 2a) as methane has high specific heat capacity and it burns slowly. The decrease in the peak pressure signifies a decrease in knocking tendency. With the increase in methane energy substitution peak of heat release rate (HRR) curve decreases (fig 2b) because methane burns gradually. So the heat release is uniform with crank angle. Gradual heat release signifies enhanced combustion phasing and results in increased brake thermal efficiency.

EFFECT OF METHANE ADDITION ON INJECTION PRESSURE AND INJECTION VELOCITY

With methane energy supplementation, diesel fuel injection velocity decreases (fig 3) because the amount of diesel injected for same duration decreases. With the decrease in injection velocity of diesel fuel the in-cylinder pressure and peak heat release rate decreases due to reduced mixing of diesel spray with the premixed charge.

(a)
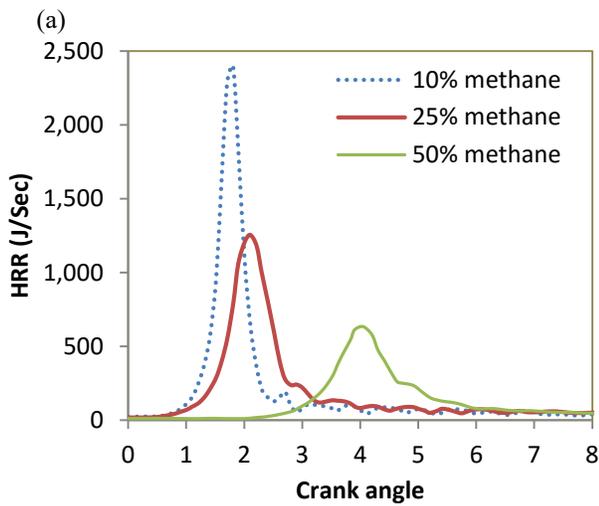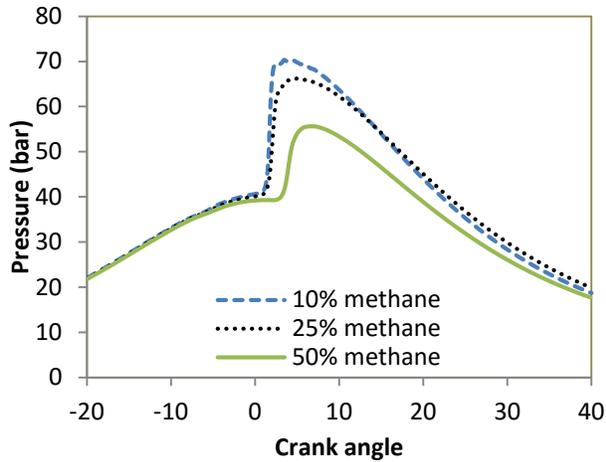
(b)

FIGURE 2. (a) COMPARISON OF PRESSURE FOR VARYING METHANE PERCENTAGE AND (b) HRR VARIATION WITH METHANE PERCENTAGE
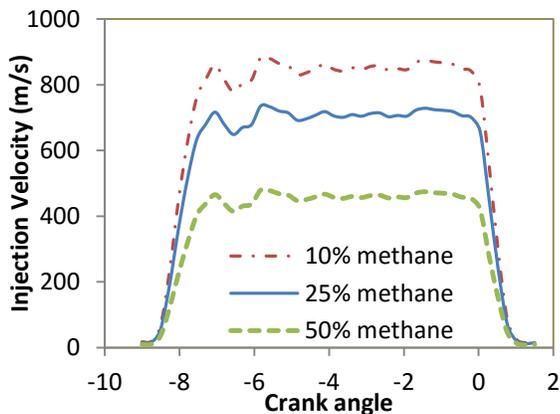
FIGURE 3. INJECTION VELOCITY WITH METHANE PERCENTAGE

EFFECT OF METHANE ADDITION ON HC AND SOOT EMISSION

With methane energy supplementation, hydrocarbon emission increase (fig 4a) because methane supplementation reduces the oxygen available for the combustion. Since gaseous fuel burns efficiently compared to liquid fuel, therefore the CO emission decreases with increase in methane. However, more increase in methane (up to 50%), increases the CO emission again due to reduced levels of oxygen (fig 4b).

(a)
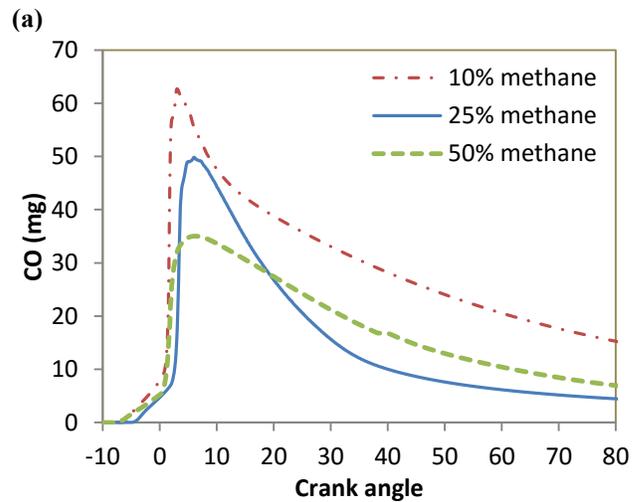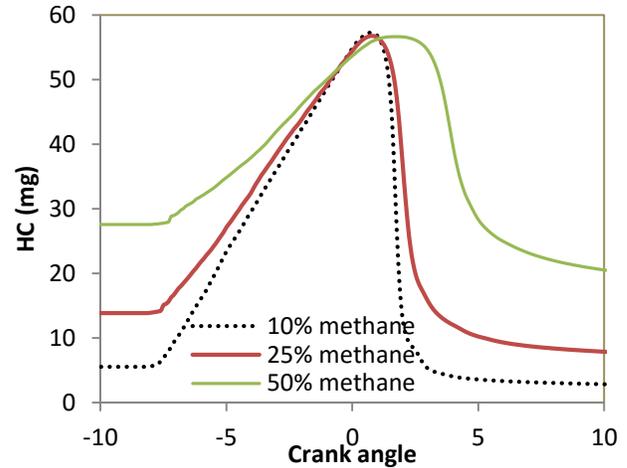
(b)

FIGURE 4. (a) HC VARIATION FOR VARYING METHANE PERCENTAGE AND (b) CO VARIATION FOR VARYING METHANE PERCENTAGE

EFFECT OF METHANE ADDITION ON NOx AND SOOT EMISSION

Gaseous fuels mix readily in the combustion chamber due to high diffusivity and enhance the combustion, resulting in higher combustion temperature. Higher combustion temperature causes higher NOx emission (fig

5a). Therefore, with an increase in methane substitution combustion efficiency decreases, leading to decrease in combustion temperature causing NOx emission to decreases. Enhanced methane substitution on 50%, results in higher soot emissions (fig 5b) due to competition for oxygen between methane and diesel. Where else with 25% methane addition, a decrease in soot emission is observed because of the faster flame speed of methane compared to diesel.

1. Higher addition of methane results in reduced peak pressure and peak heat release rate.
2. Increase in methane supplementation results in higher hydrocarbon emission.
3. NOx emission increases up to 25% methane addition, then decrease.
4. 25% methane energy supplementation is an optimum value for reduced soot and CO emission.

REFERENCES

[1] US Department of Energy, EIA/IEA International Energy Annual, Energy Information Administration. US Department of Energy, Washington, DC, 2002, http://www.eia.doe.gov.

[2] Bates, G. J., Germano, S., 1994. Vehicle tail pipe emissions e a comparison of natural gas and petrol injection. In: Maryland: SAE Fuels & Lubricants Meeting & Exposition;, SAE paper 942042.

[3] Karagöz, Y., Sandalcı, T., Koylu, U.O., Dalkılıç, A.S. and Wongwises, S., 2016. Effect of the use of natural gas–diesel fuel mixture on performance, emissions, and combustion characteristics of a compression ignition engine. *Advances in Mechanical Engineering*, *8*(4), p.1687814016643228..

[4] Verbiezen, K., Donkerbroek, A.J., Klein-Douwel, R.J.H., Van Vliet, A.P., Frijters, P.J.M., Seykens, X.L.J., Baert, R.S.G., Meerts, W.L., Dam, N.J. and Ter Meulen, J.J., 2007. Diesel combustion: In-cylinder NO concentrations in relation to injection timing. Combustion and Flame, 151(1), pp.333-346

(a)

(b)

FIGURE 5. (a) NOx EMISSION VARIATION FOR VARYING METHANE PERCENTAGE (b) SOOT EMISSION VARIATION FOR VARYING METHANE PERCENTAGE

CONCLUSIONS

Converge CFD tool is used to study the effect of methane injection, compression ratio and spray parameters on performance and soot emission characteristics of the engine in dual fuel mode. Following conclusions are drawn from the investigation:

SEEC-2018-126

NUMERICAL SIMULATION OF TWIN FLUID FLOW BLURRING ATOMIZATION CONCEPT USING LARGE EDDY SIMULATION

Raju M
Department of Mechanical and Aerospace
Engineering
Indian Institute of Technology, Hyderabad
Email: me14resch11006@iith.ac.in

Pankaj S Kolhe
Department of Mechanical and
Aerospace Engineering
Indian Institute of Technology,
Hyderabad
Email: psk@iith.ac.in

ABSTRACT

Atomization process is about converting volume of fluid into a multiplicity of small droplets, and twin fluid atomizers are more efficient in this aspect if the uninterrupted fluid flows are involved. The present numerical study is focusing on atomization of liquids (ethanol and water) by air with flow blurring injector at air to liquid ratio by mass of 2. The numerical simulation was carried out with commercial solver Ansys Fluent by using multiphase volume of fluid method (VOF) with large eddy simulation(LES). The uniform grid of minimum cell size of 2.5 micron was chosen after grid analysis of different sizes. The difference in air penetration length in the fuel tube, drop size distributions was observed through the numerical simulations for ethanol and water.

Keywords: Flow Blurring Atomizer, ALR ratio, Spray, LES-VOF.

NOMENCLATURE

ALR	Air to Liquid Ratio
CFL	Courant-Friedrich-Lewy number
LES	Large Eddy Simulation
FB	Flow Blurring
VOF	Volume of Fluid

INTRODUCTION

In order to reduce the environmental pollutions and to find the alternative solutions to the fossil fuels, research is going around the world. The major source of energy in the world is from different combustion process by using liquid, solid and gaseous fuels. Researchers find the biomass energy in the world such as Ethanol, plant oils, etc. as alternative liquid fuels for future [1]. The literature for spray characterization of bio-fuels through numerical analysis is limited. Spray plays an important role in liquid fuel combustion for stability limits, combustion efficiency, and pollutant emission levels. "Airblast atomizers" or "twin fluid atomizer" have many advantages over "pressure atomizers" or "conventional atomizers" or "single fluid atomizer" especially in their application to gas turbine combustion of high pressure ratio [2].

Ganan-Calvo introduced the Flow blurring twin atomization concept for twin fluid atomization, which has many advantages over other atomizer such as more atomization efficiency, uniform drop, and smaller spray size compared to other conventional atomization concept. The experimental and numerical analysis for FB atomization concept are limited.

Flow Blurring twin fluid atomization

The configuration of the FB twin fluid atomizer is as shown in Fig 1, proposed by Ganan-Calvo [3]. In FB atomization concept the air comes at very high velocity component in radially inward direction (perpendicular to designed liquid flow direction) just upstream of injector dump plane (orifice exit plane), which creates the finer spray. When the gap (h) between the orifice and liquid tube is less than quarter of the orifice diameter or internal diameter of the liquid tube (d), stagnation bubble forms just upstream of the orifice, which diverts the air flow backward in the fuel tube as well as through orifice creating internal and external mixing. Note that, here h/d and mass flow rate of air dictates the radially inward component of velocity, responsible for creating the recirculating bubble region inside liquid tube. Internal mixing occurs due to the backward air flow, creating bubbles that burst as they pass through orifice exit leading to a fine spray. H/d ratio plays an important role as it controls whether flow focusing or flow blurring configuration is exhibited. Note that, h/d ratio greater than 0.25 leads to the flow focusing configuration as shown in Fig 1(a), whereas h/d ratio is less than 0.25 gives the flow blurring concept as shown in Fig 1(b). The Flow blurring concept of twin fluid atomization is an example for prompt atomization as described in reference [4].

d=liquid tube inner diameter = injector orifice diameter
h=spacing between liquid tube exit and orifice disc dump plane
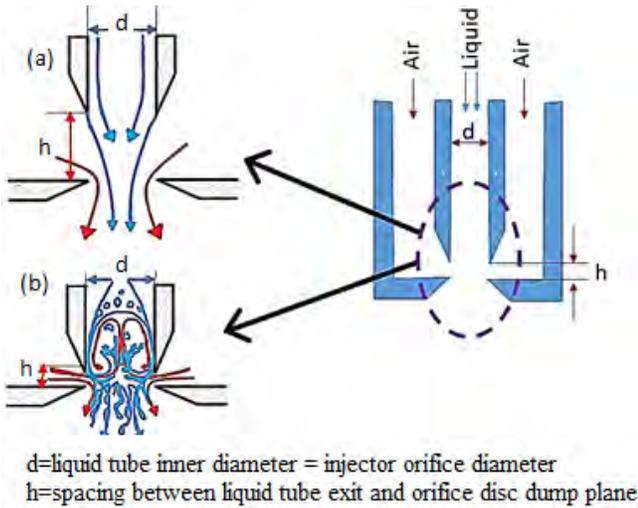
FIGURE 1. FLOW BLURRING TWIN FLUID ATOMIZATION CONCEPT (a) FLOW FOCUSING, (b) FLOW BLURRING BASED ON h/d RATIO.

Simmons et al [5] carried out the comparative study between the airblast and flow blurring injectors, and their results showed that for FB injectors nearly uniform radial distribution with smaller sauter mean diameter (SMD) is obtained compared to the airblast injectors, which is very essential for liquid fuel atomization in combustion systems. Agrawal and group [5]–[8] as well as Azevedo & group[9]–[12] have carried out in depth analysis of spray characterization and its application to combustion systems for fuel flexibility. The penetration length measurement in the liquid tube were experimentally carried out by Agrawal *et al* [6] to study the effect of ALR on penetration length and spray quality. The penetration length through the numerical simulation was studied and reported in reference [14], but spray characteristics were not studied.

Objective of this study is to look into the impact of difference in thermos-physical properties of ethanol and water on spray formation and its statistical description. Mass flow rates were kept constant for air and liquid at 0.333 gm/s and 0.166 gm/s respectively. Note that orifice and fuel tube inner diameter is 1.5 mm, and inner and outer diameter for annular passage for air are 2 mm & 4.5 mm respectively.

NUMRICAL ANALYSIS

Governing Equation

The interface of the gas and liquid was tracked by the solution of the continuity equation for the volume fraction of the phase as shown in Eqn. (1).

$$\frac{1}{\rho_q}\left[\frac{\partial(\alpha_q\,\rho_q)}{\partial t} + \nabla.\left(\propto_q\,\rho_q\,\overrightarrow{v_q}\right)\right.$$
$$\left. = \sum_{p=1}^{n}(\dot{m}_{pq} - \dot{m}_{qp})\right] \tag{1}$$

Where $\dot{m}_{qp}$ is the mass transfer from phase q to phase p and $\dot{m}_{0pq}$ is the mass transfer from phase p to phase q.

Where volume fraction of all the phases is constrained as,

$$\sum_{q=1}^{n}\propto_q = 1 \tag{2}$$

A single momentum equation shown in Eqn. (3) is solved in the whole flow domain while using VOF model and is expressed as

$$\frac{\partial(\rho\vec{V})}{\partial t} + \nabla \cdot (\rho\vec{V}\vec{V})$$
$$= -\nabla p + \nabla$$
$$\cdot \left[\mu\left(\nabla\vec{V} + \nabla\overrightarrow{V^T}\right)\right] + \rho\vec{g}$$
$$+ \vec{F} \tag{3}$$

The momentum equation, is dependent on the volume fractions of all phases through the properties ρ and μ. The volume fraction equation was solved by explicit time discretization. Courant-Friedrich Lewy number *(*CFL) number plays a very important role in explicit time discretization for stability condition. The simulations for this numerical studies were carried out with a CFL number as 0.25. The time step has adopted based on variable time stepping method for fixed CFL number. The standard Smagorinsky-Lilly model is considered for LES.

The geometric reconstruction algorithm, which represents the interface between the two phases using a piecewise-linear profile, was used to determine the face fluxes for the VOF model. It assumes that the interface between the two-fluids has a linear slope within each cell and uses this property to calculate the advection of fluid through the cell faces using a geometric reconstruction scheme. The boundary condition for the numerical simulations is shown in Fig.3.
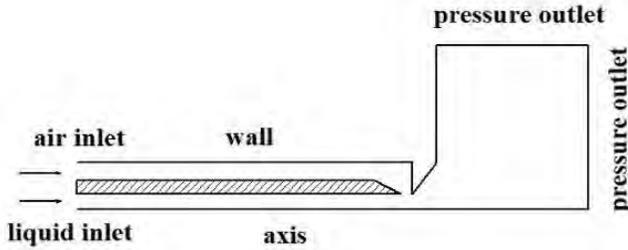

FIGURE 2. BOUNDARY CONDITION FOR THE NUMERICAL SIMULATION

TABLE 1: GRID DETAILS

Case	Cell Counts	Minimum Cell size(micron)
1	83408	18.75
2	333632	9.37
3	1334528	4.68
4	5338112	2.34
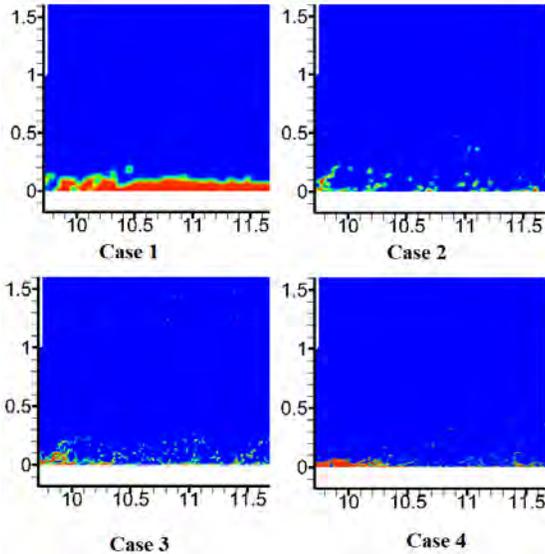
FIGURE 3. VOLUME OF FLUID FOR WATER AT DIFFERENT GRID SIZES

The numerical simulation was carried for different grid cases as shown in Table 1 before finalizing the grid for all the cases. Note that case 4 was used for the final simulations.

RESULT AND DISCUSSION

Numerical Simulations were carried out for ethanol and water at atomizing air to liquid ratio of '2' by mass.
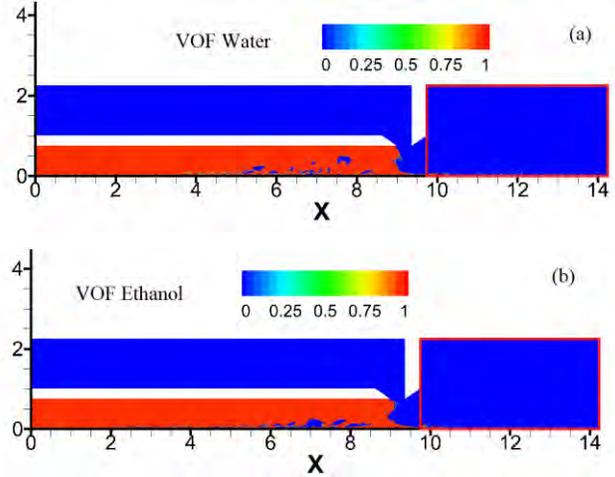
FIGURE 4. CONTOUR OF VOLUME OF FLUID

(A) WATER (B) ETHANOL

The statistics of the drops on the axisymmetric plane is calculated through image process techniques using Matlab Software. The droplet diameters were calculated just 0.375 mm downstream from the nozzle exit which is highlighted in red color rectangle in Fig.4(a) and Fig.4(b) zoomed view as show in Fig 5. The drop size threshold drop diameter is 50 microns. The penetration length in the liquid tube is less for ethanol compared to water because of difference in thermo-physical properties and flow velocities. However, the number of drop are more in ethanol, which can be seen from the drop statistics shown in Fig.6. This can be attributed to higher volumetric flow rate for ethanol compared to water for same ALR where mass flow rate of air is kept constant.
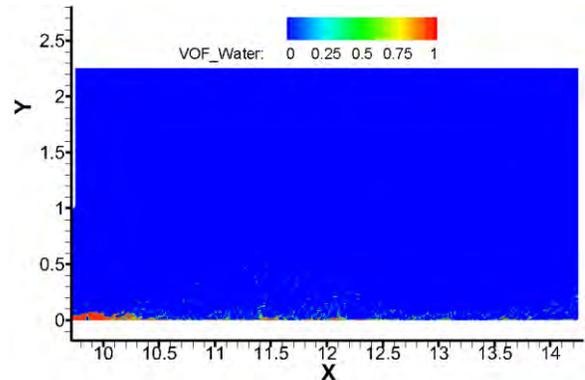
FIGURE 5. AREA CHOSEN FOR DROPLET CALCULATION
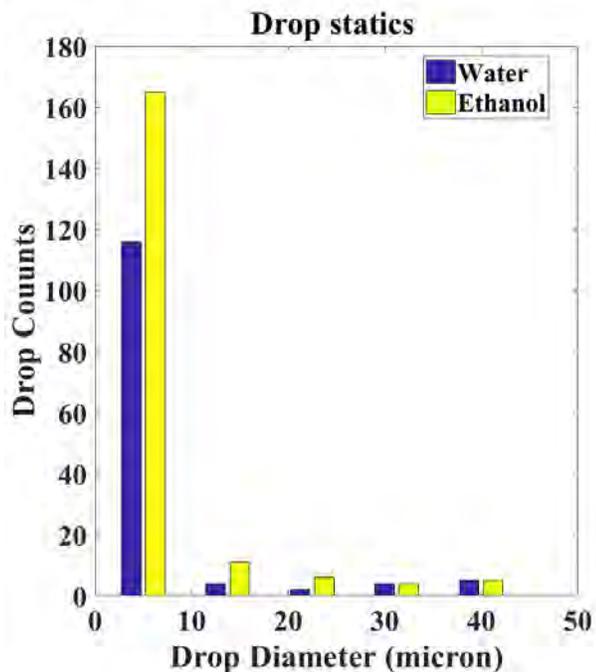
FIGURE 6. DROPLET STATICS FOR WATER AND ETHANOL

CONCLUSIONS

The main important points from predictions using numerical simulations are as follows.

- Owing to lower density of ethanol, volumetric flow is more for same ALR and mass flow rate. Consequently droplets population density observed is more in case of ethanol. Besides, lower surface tension for ethanol allows to form more smaller droplets as observed.

- For same ALR and liquid mass flow rates, momentum for ethanol is more compared to water and hence bifurcated air flow penetration in liquid tube is lower for ethanol.

- Complicated flow recirculation pattern observed warrants 3D LES simulations, which would make sure the vorticity estimation is more accurate allowing precise representation of the flow field just upstream of orifice exit, which is influencing the spray quality.

ACKNOWLEDGMENTS

REFERENCES

[1] M. Balat and G. Ayar, "Biomass energy in the world, use of biomass and potential trends," *Energy Sources*, vol. 27, no. 10, pp. 931–940, 2005.

[2] A. H. Lefebvre, "Airblast atomization," *Prog. Energy Combust. Sci.*, vol. 6, no. 3, pp. 233–261, 1980.

[3] A. M. Gañán-Calvo, "Enhanced liquid atomization: From flow-focusing to flow-blurring," *Appl. Phys. Lett.*, vol. 86, no. 21, pp. 1–3, 2005.

[4] A. Lefebvre, D. Ballal, and D. Bahr, *Gas turbine combustion: alternative fuels and emissions*. 2010.

[5] B. M. Simmons, H. V. Panchasara, and A. K. Agrawal, "A Comparison of Air-Blast and Flow-Blurring Injectors Using Phase Doppler Particle Analyzer Technique," *Vol. 2 Combust. Fuels Emiss.*, pp. 981–992, 2009.

[6] S. R. Agrawal, L. Jiang, A. K. Agrawal, and K. C. Midkiff, "High-Speed Visualization of Two-Phase Flow inside a Transparent Fuel Injector," no. 2005, 2013.

[7] L. Jiang and A. K. Agrawal, "Investigation of glycerol atomization in the near-field of a flow-blurring injector using time-resolved piv and high-speed visualization," *Flow, Turbul. Combust.*, vol. 94, no. 2, pp. 323–338, 2015.

[8] L. Jiang, A. K. Agrawal, and R. P. Taylor, "Clean combustion of different liquid fuels using a novel injector," *Exp. Therm. Fluid Sci.*, vol. 57, pp. 275–284, 2014.

[9] C. de Azevedo, F. D. S. Costa, and H. da S. Couto, "Initial Study of a Blurry Injector for Biofuel," *Bibdigital.Sid.Inpe.Br*, pp. 1–10, 2011.

[10] C. G. De Azevedo, J. C. Andrade, and F. D. S. Costa, "Characterization of a Blurry Injector for Burning Biofuels in a Compact Flameless Combustion Chamber," no. 2009, 2012.

[11] C. G. de Azevedo, J. C. de Andrade, and F. de S. Costa, "Experimental valuation diagnostics of hydrous ethanol sprays formed by a blurry injector," *J. Aerosp. Technol. Manag.*, vol. 5, no. 2, pp. 197–204, 2013.

[12] C. G. de Azevedo, J. C. de Andrade, and F. de Souza Costa, "Effects of injector tip design on the spray characteristics of soy methyl ester biodiesel in a blurry injector," *Renew. Energy*, vol. 85, pp. 287–294, 2016.

[13] C. G. de Azevedo, J. C. de Andrade, and F. de Souza Costa, "Effects of injector tip design on the spray characteristics of soy methyl ester biodiesel in a blurry injector," *Renew. Energy*, vol. 85, pp. 287–294, 2016.

[14] N. J. Vardaman and A. K. Agrawal, "Computational Analysis of Two-Phase Mixing Inside a Twin-Fluid, Fuel-Flexible Atomizer," pp. 1–10, 2017.

PARAMETRIC STUDY AND PHASE ANALYSIS OF CATHODIC ACTIVE MATERIALS OF SPENT LITHIUM-ION BATTERY

Sandeep Anwani, Ravi N. Methekar

Visvesvaraya National Institute of Technology, Nagpur

ABSTRACT

Ever increasing demand of lithium ion batteries generates huge amount of e-waste after their useful life. An eco-friendly disposal method needs to be devised to dispose these batteries. Recycling is one of the best options from an environmental point of view and also it will ensure sustainable metal supply. Recycling process consists of peeling, dissolution and extraction steps. Phase analysis and variation of parameters of peeling and dissolution steps have been studied here. The peeling efficiency of cathode active materials has been enhanced to 82% using solvent like NMP with ultrasonic cleaning. Optimal parametric values have been identified for higher dissolution efficiency. The dissolution efficiency was found to be 95.15% with operating temperature of 90^0C, 2 molar sulfuric acid, and solid to liquid ratio of 10 g/l with particle size less than $25\mu m$. High peeling and dissolution efficiencies will result in the higher metal extraction efficiency.

Keywords: *Spent batteries, recycling of batteries, parametric study*

INTRODUCTION

Lithium-ion batteries have been extensively in use from last two decades and considered to be the best power source for many portable devices as well as for the transport applications that can operate at higher voltage and higher energy density. In the last decade (2000-2010) the production of lithium-ion batteries has increased at an alarming rate of 800% world-wide [1]. It is expected that there will be huge growth of LIB industry close $32 billion by 2020 [2]. However, due to huge demand and usages, there is large amount of lithium-ion batteries to be disposed off after their useful life. Spent lithium ion batteries, however cannot be disposed off into the landfills because of safety and economic reasons. Also spent lithium-ion batteries are rich source of lithium, cobalt, manganese, nickel, aluminium, copper etc. Sometimes the metal concentrations in the spent lithium-ion battery are higher than they found in the natural ores. On the other hand, lithium shortage may inevitable in few decades. Hence, recycling/or recovering of the major metal contents are critical to prevent adverse environmental impacts and also to ensure sustained material supply.

Several researchers are presently working in the field of recycling of spent lithium ion batteries. The recycling process of spent lithium ion batteries can be broadly categorized into pyrometallurgy, hydrometallurgy and bio-hydrometallurgy processes. Pyrometallurgy processes faces the disadvantages like emission of toxic gases, higher cost of recycling. A bio-hydrometallurgy process takes longer time for treatment and also the microbes are very difficult to incubate [3]. For high recovery of metal contents from the spent lithium–ion battery, hydrometallurgical process is considered to be more suitable among all the available processes. In hydrometallurgical process, acidic or alkaline leaching is carried out for extraction of valuable materials followed by chemical precipitation and separation. The strong acids like sulphuric, hydrochloric, nitric or phosphoric acid [4-8] or weak acids like citric, formic, tartaric, succinic, lactic or oxalic acids [1, 9-12] are used in the hydrometallurgical process. It is reported in the literature that the leaching efficiency using the strong acids lies in the range of 85-99% whereas for weak acids lies in the range of 70-99%. Leaching efficiency consist of efficiencies of all the steps incurred in extraction of the valuable metals. However, very few literature reports the efficiency of each step incurred. In general, extractions of valuable materials from the spent lithium ion battery consist of three main steps viz.1) peeling of active cathode materials from the cathode electrode 2) dissolution of active materials into the acid and 3) extraction of valuable materials from the dissolved active materials using chemical precipitation. Efficiency of each of the

above mentioned step will greatly impact on the overall efficiency of extraction of the valuable materials. Hence, it is extremely important to enhance the efficiency of all the steps.

In this paper, the efficiency of peeling of materials has been studied and enhanced by using various techniques such ultrasonic cleaning, solvent like N-Methyl-2-pyrollidone (NMP) and operating temperature. The obtained active materials contains various phase like oxide, dioxide, and carbonate. These phases play significant role while selecting the acids as well as the reducing agents and hence it is extremely important to know these phases before going for the dissolution process. Here, a XRD (X-Ray diffractometer) analysis of the spent active material is carried out to know materials phases along with ICP-OES (Inductively Coupled Plasma Optical Emission Spectroscopy) and SEM (Scanning Electron Microscopy) for percentage metal content as well as morphology of the materials. The dissolution efficiency is also enhanced by optimizing the parameters like molarity of the acid, particle size of the active materials, operating temperature and solid to liquid ratio.

MATERIALS AND METHODS

The spent lithium ion battery used in mobile phone in general weighs around 20g and made from steel casing, cathode, anode, separator, connectors and electron conductors. The cathode and anode is mainly made up from $LiCoO_2$ amorphous powder and carbon black powder layered around aluminium and copper foil respectively with the help of binder. In this paper, only extraction of valuable materials from cathode is studied. The chemicals used were all analytical grades.

Peeling of active cathode materials

First, a battery is fully discharged manually and then dismantled to separate out various components like cathode, anode, separator, current collectors and connectors from the casing. The cathode strip is weighed (6.4g) and cut into small pieces. Then the pieces of cathode are dipped into 40ml NMP solvent. The conical flask containing the NMP solvent and cathode pieces are then subjected to ultrasonic cleaning for about 5 minutes. Then the aluminium pieces which was separated from cathode materials due to ultrasonic cleaning is collected and separate out. The solution deprived off the aluminium, is centrifuged to separate out the active cathode materials from NMP solution. The solid untreated active material is then dried at 700^0C for 5 hrs in muffle furnace. Then this material is ball milled to reduce the particle size up to less than 25μm. The entire peeling procedure is shown in Fig. 1. This material is called as active material from spent lithium ion battery.

Dissolution of active cathode materials

Once we found out the weight percentage of various metals of the active materials and morphology

using SEM, a phase analysis was carried out using XRD. 2gm of sample materials are then taken for the dissolution process. In dissolution, appropriate amount of sulfuric acid with optimal molarity is added in a conical flask with stiochiometric quantity of oxalic acid and sodium carbonate. Then the conical flask is subjected to magnetic stirring for 2 hrs at 90^0C. Once the dissolution is over, the solution is filtered. The gouge materials are separated, dried and weighed. The dissolution efficiency is then calculated as the ratio of weight of gouge materials and initial sample weight. To optimise the dissolution process, the parameters like molarity of acid, particle size, operating temperature, and solid to liquid ratio are varied and various runs of experiments are carried out.

RESULTS AND DISCUSSION
Peeling efficiency

Peeling efficiency of the cathode active materials from the cathode electrode is enhanced by using the NMP solvent with ultrasonic cleaning. In ultrasonic cleaning, pressure in the solvent goes to negative and mass of tiny vacuum gets generated in the solvent. Thus the bubble of solvent formed bursts and cathode material peels off from the aluminium foil [13]. The dissolution of binder will be caused by NMP solvent. It is found that the peeling efficiency of the material is 82% which is in well agreement with literature [13].

Phase analysis of the active materials

It is important to analyse the phases present in the active cathode materials so that the types of bonds structure would be known. This information will help in finding the right acid for leaching. Tab. 1 shows the XRF analysis of the untreated cathode materials. The XRF analysis shows that the cobalt, manganese and lithium metals are present in the significant amount as transition metals. Once we got to known the metal contents, a XRD analysis is carried out for knowing the phase of the valuable metals. XRD analysis shows that the lithium cobalt oxide is present in a significant amount along with cobalt (II, III) oxide. As the Co (II) oxide is unstable, we need to add some reducing agent while dissolution of the materials. Magnesium aluminium silicate, phosphorus pentoxide, ferroferric oxide are also present in small quantity. The XRD graph is shown in Fig. 2. Morphological study of the active materials is carried out using SEM analysis shown in Fig.3. It is found that the active material sample is having amorphous goblet like structure with sufficient porous nature.

Parametric study of the dissolution efficiency

To enhance the dissolution efficiency, the operating parameters are optimized. The operating parameters like temperature, particles size, molarity of the acid used, and solid to liquid ratio are varied. The range of variations is fixed from the literatures. Tab. 2 shows the operating parameters matrix for optimization as well as corresponding dissolution efficiency. The

maximum dissolution efficiency is achieved equal to 95.15 % at the temperature of 90⁰C, particle size less than 25µm, 2 molar sulfuric acid and solid to liquid ratio of 10 g/l. We found that the dissolution efficiency increases with increase in temperature, decrease in particle size, increase in molarity of the acid with certain upper level, and decreases with solid to liquid ratio. The results of parameter optimization are in well agreement with literature [1, 5-8].

CONCLUSIONS

Heavy consumptions of Li-ion batteries and its subsequent disposal to landfills or incineration adversely impact the environment. A method needs to device to dispose these huge amounts of e-waste of LIBs economically and effectively. Peeling and dissolution processes of the recycling of the spent battery have been studied using sulfuric acid as a lixiviant. The study shows that the peeling efficiency can be enhance by using solvent like NMP with ultrasonic cleaning. A detailed study of the operating parameters has been carried out, which shows that the dissolution efficiency of 95.15% can be achieved under the optimized operating condition. As the dissolution efficiency has been increased, the overall recovery of valuable materials from the spent active cathode materials can be increased.

FIGURES AND TABLES

FIGURE 1. SCHEMATIC OF PEELING PROCESS
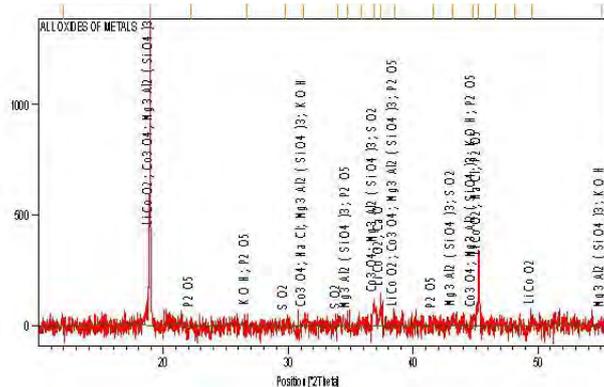
FIGURE 2. XRD OF ACTIVE CATHODE MATERIALS
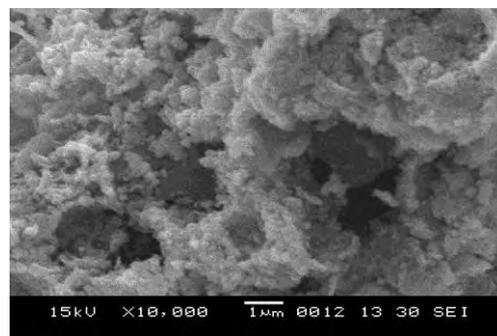
FIGURE 3. SEM OF ACTIVE CATHODE MATERIALS

TABLE 1. XRF OF ACTIVE CATHODE MATERIALS

Metal	Weight %	Metal	Weight %	Metal	Weight %	Metal	Weight %	Metal	Weight %
Li	6.3	Cu	0.6	K	0.02	Si	0.09	Fe	0.11
Co	45.1	Al	0.67	Ca	0.03	Cl	0.02	Zr	0.01
Mn	11.8	P	0.32	Na	0.23	Ti	0.02	Nb	0.01
Ni	0.30	S	0.16	Mg	0.41	Cr	0.09	O2	rest

TABLE 2. OPERATING CONDITION MATRIX FOR OPTIMIZATION AND DISSOLUTION EFFICIENCY

Molarity (M)	Temperature (⁰C)	Particle Size <(µm)	Solid to liquid ratio(g/l)	Dissolution Efficiency %
2	90	25	10	95.15
2	90	90	10	82.15
2	60	25	10	79.50
2	75	25	10	87.00
1	90	25	10	93.50
2	90	90	20	46
2	90	25	20	53.5
1.5	90	25	10	94.02

REFERENCES

[1] Li Li., Fan E., Guan Y., Zhang X., Xue Q., Wei L., Wu F., Chen R., 2017, "Sustainable Recovery of Cathodic Materials from spent li-ion batteries using lactic acid leaching system", ACS Sustainable Chem. Eng, 5(6), May, pp 5224–5233.

[2] Zhang X., Cao H., Xie Y., Ning P., An H., You H., Nawaz F., 2015, "A closed process for recycling $LiNi_{1/3}Co_{1/3}Mn_{1/3}O_2$ from the cathode scraps of lithium-ion batteries: Process optimization and kinetics analysis", Sep. Purif. Technol, 150, July, pp 186-195.

[3] Jha M. K., Kumari A., Jha A. K., Kumar V., Hait J., Pandey B. D., 2013, "Recovery of lithium and cobalt from waste lithium ion batteries of mobile phone", Waste Management, 33 (9), May, pp 1890-1897.

[4] Zhang P., Yokoyama T., Itabashi O., Suzuki M.T., Inoue K.,1998, "Hydrometallurgical process for the recovery of metal values from spent lithium ion spent batteries", Hydrometallurgy, 47, July, pp 259–271.

[5] Castillo S., Ansart F., Laberty-Robert C., Portal J., 2002, "Advances in the recovering of spent lithium battery compounds", Journal of Power Sources , 112, July, pp 247–254.

[6] Lee C., Rhee K., 2003, "Reductive leaching of cathodic active materials from lithium ion battery wastes", Hydrometallurgy, 68, September, pp 5 – 10.

[7] Shin M.S., Kim N., Sohn J., Yang H.D., Kim H.Y., "Development of a metal recovery process from Li-ion battery wastes", 2005, Hydrometallurgy, 79, July, pp 172–181.

[8] Meng Q., Zhang Y., Dong P., 2017, "Use of glucose as reductant to recover Co from spent lithium ions batteries", Waste Management 64, June, pp 214–218.

[9] Li-Po He., Shu-Ying Sun., Yan-Yu Mu., Xing-Fu Song., Jian-Guo Yu., 2017, "Recovery of Lithium, Nickel, Cobalt, and Manganese from Spent Lithium-Ion Batteries Using L-Tartaric Acid as a Leachant", ACS Sustainable Chem. Eng., 5 (1), October, pp 714–721.

[10] Li L., Wenjie Q., Zhang X., Lu J., Chen R., Wu F., Amine K., 2015, "Succinic acid-based leaching system: A sustainable process for recovery of valuable metals from spent Li-ion batteries", Journal of power sources, 282, May , pp 544-551.

[11] Chen X., Luo C., Zhang Z., Kong J., Zhou T., 2015, "Sustainable Recovery of Metals from Spent Lithium-Ion Batteries: A Green Process", ACS Sustainable Chem. Eng., 3 (12), October , pp 3104–3113.

[12] Nayaka P.G., Pai V.K., Santhosh G., Manjanna J., 2016, "Recovery of cobalt as cobalt oxalate from spent lithium ion batteries by using glycerin as leaching agent", Journal of Environmental Chemical Engineering, 4, May, pp 2378–2383.

[13] Li-Po H., Shu-Ying S., Xing-Fu S., Jiang-Guo Y., 2015,"Recovery of cathode materials and Al from spent lithium-ion batteries by ultrasonic cleaning", Waste Management, 46, December, pp 523-528.

DYNAMIC ANALYSIS OF DUAL CHAMBER CONTINUOUS MICROBIAL FUEL CELL

Ashish Yewale[1], Ravi N. Methekar[2], Shailesh Agrawal[3]

Visvesvaraya National Institute of Technology, Nagpur

1: ayewale07@gmal.com,
2: methekar.vnit@gmail.com
3: sgagrawal28783@gmail.com

ABSTRACT

Growing demand of energy and fast depletion of non renewable energy sources, challenge scientific community to find alternate solutions to satiate the energy demand of the society. Microbial fuel cell (MFC) is one of the technologies, where electricity is generated from waste-water or organic waste and clean water come out as a by-product. Commercial success of this technology is heavily depends on the understanding physics of the system. Dynamic analysis of various potential manipulated variables like flow rate of substrate, coolant and voltage of the cell is carried out in steady state as well as transient state. It is found that the MFC power demonstrate linear relationship with flow rate of substrate as well as coolant flow rate, however it demonstrate highly nonlinear relationship with voltage applied with input multiplicity.

Keywords: MFC, Dynamic Analysis, Step function

NOMENCLATURE

a	Anode
b	Tafel coefficient
c	Cathode
R	Gas constant (J/mol.K)
F	Faradays constant (coloumb/mol)
C_{sb}	Bulk substrate concentration (kg/m^3)
C_s	Film substrate concentration (kg/m^3)
$C_{sb,0}$	Initial substrate concentration (kg/m^3)
C_{CO2b}	Bulk CO_2 concentration (kg/m^3)
C_{CO2}	Film CO_2 concentration (kg/m^3)
M_W	Mass flow of coolant (kg/hr)
V_L	Bulk liquid volume (m^3)
A_m	Membrane area (m^2)
Ds	Diffusivity of substrate (m^2/day)

D_{CO2}	Diffusivity of CO_2 (m^2/day)
L_l	Diffusional sublayer thickness (m)
T	MFC chamber temperature (K)
T_0	Initial temperature (K)
T_{cool}	Coolant temperature (K)
ϑ_{in}	Inlet flow rate (m^3/hr)
ϑ_{out}	Outlet flow rate (m^3/hr)
$C_{p,lact}$	Specific heat of lactate (J/kg.K)
C_{pwater}	Specific heat of water (J/kg.K)
ρ_{lact}	Density of lactate
ΔG	Gibbs free energy (J/mol)
ΔH	Enthalpy change (J/mol)
d_m	Membrane thickness (m)
d_{cell}	Distance between electrode (m)
k_{aq}	solution conductivity (mS/m)
k_m	Membrane conductivity (mS/m)
i,I	Current (mA)
$i_{0,ref}$	exchange current density (mA/m^2)
η	Activation over potential (mV)
t	Time (hr)

INTRODUCTION

Water and fossil fuel scarcity are among the most serious challenge faced by the scientific community now days. Over a billion of people around the world do not have proper clean water for drinking. Millions of people die every year because of water related diseases. Further, combustion of fossil fuel release green house gases in the environment, which makes health problem even complex for the humankind. Therefore it is very important to find the new ways to produce energy from renewable energy sources and make the water potable with less amount of energy consumption. Microbial fuel cell (MFC) is one of the technologies, where electricity

is generated from waste-water or organic waste and clean water come out as a by-product. MFC is an electrochemical device that converts organic matter directly into the electricity with high efficiency. Despite its wide range of potential applications and ease of feed stocks, commercialisation of this technology did not realized till now [1]. The major limitations for the commercialization are the scale up of the process [2] and continuous operations. To have smooth continuous operation for longer time, it is extremely important to understand the dynamics of the system. Dynamics of the system can be understood by performing exhaustive experiments and analysing the data thus obtained. But performing exhaustive experiments is a time consuming as well as expensive task. The other approach is to model the system to understand the dynamics.

In literature very few researcher worked on the modeling of continuous microbial fuel cell (CMFC). Although batch modeling of MFC have been reported earlier, a very few studies have focused on understanding the dynamics of the system. First dynamic study was carried out by Zhang et al. [3], and there model is based on electron transfer using mediator. Later, Picioreanu et al. [4] modeled the bio-film development on the anode electrode in MFC. Marcus et al. [5] and Pinto et al. [6] developed 1-D model for multispecies electron donor and acceptor for bio-film anode based on the material balance, Ohm's law and Nernst-Monod kinetics to describe the rate of electron donor oxidation. In 2017, Esfandyari et al. [7], developed batch process model considering direct electron transfer through bio-film to the electron acceptor.

In this paper, we will present the steady state as well as dynamic characteristics of the manipulated variables on the outputs of the MFC i.e. power and operating temperature. Dynamic analysis will provide deeper insights of the various physical phenomena of the microbial fuel cell.

MATHEMATICAL MODEL OF THE DUAL CHAMBER CONTINUOUS MFC

The operating principle of the MFC involves transport of ions as well as bio-chemical reactions. In this fuel cell we are taking lactate as a substrate at the anode. The substrate at the anode gets diffuse through the bulk to the biofilm attached to the anode of the cell. Microbes present in the biofilm at the anode consume the substrates and produces electrons and protons. The electrons then back diffuses toward the current collector and flows through external circuit producing power. The protons migrate through membrane called as proton exchange membrane to the cathode chamber where redox reaction takes place between the electrons from the external circuit, migrated protons and supplied oxygen producing water. These phenomena are captured through the mathematical model. In this paper, we used the model presented by Esfandyari et al. [7]. This is a one dimensional batch model. We converted this batch model into continuous model by adding the equations for continuous flow of substrate and CO_2. The temperature is maintained by providing the jacket to the cell from outside. The coolant flow equation for extraction of heat from the cell is also added. For sake of brevity, we are presenting here only modified equations; however other equations used in the model can be found in Esfandyari et al. [7].

Model assumptions:
1) MFC is considered as lumped parameter system
2) The electrical resistance of electrodes and membrane is neglected
3) pH of the substrate is maintained at neutral condition

Half reaction at anode is given as

$$C_3H_6O_3 + 3H_2O \rightarrow 3CO_2 + 12H^+ + 12e^- \tag{1}$$
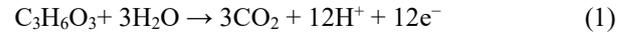
Half reaction at cathode is given as

$$O_2 + 4H^+ + 4e^- \rightarrow 2H_2O \tag{2}$$

Change in concentration of substrate in the bulk of the liquid is given as

$$\frac{d\left(C_{sb}(t)\right)}{dt} = \frac{1}{V_L(t)}\left(\frac{-A_m D_s}{L_l}(C_{sb}(t) - C_s(t))\right) + \left(\frac{C_{sb,0}\vartheta_{in}}{V_L(t)}\right) - \left(\frac{C_{sb}\vartheta_o}{V_L(t)}\right) \tag{3}$$

The first term on the right hand side is diffusion rate of substrate from bulk, second term represents inlet flow rate of substrate, and the last term denotes outlet flow rate of the substrate from the anode chamber.

Change in concentration of CO_2 in the bulk of liquid is given as

$$\frac{d\left(C_{co_2}(t)\right)}{dt} = \frac{1}{V_L(t)}\left(\frac{-A_m D_{co_2}}{L_l}\left(C_{co_2 b}(t) - C_{co_2}(t)\right)\right) - \left(\frac{C_{co_2 b}\vartheta_{out}}{V_L(t)}\right) \tag{4}$$

The first term on the right hand side is the diffusion term and second is the outlet flow rate from the cell.

Heat balance equation around the cell is given as

$$\frac{d(T(t))}{dt} = \left(\frac{\vartheta_{in}C_{sb,0}T_0 C_{p,lact}}{\rho_{lact}V_L(t)C_{p,lact}}\right) - \left(\frac{\vartheta_{out}C_{sb,0}T(t)C_{p,lact}}{\rho_{lact}V_L(t)C_{p,lact}}\right) + \left(\frac{M_w C_{p,water}(T_{cool} - T(t))}{\rho_{lact}V_L(t)C_{p,lact}}\right)$$
$$+ \left(\frac{I(\eta_a + \eta_c)}{\rho_{lact}V_L(t)C_{p,lact}}\right) - \left(\frac{\left[\left(\frac{\Delta H_a - \Delta G_a}{nF}\right) + \left(\frac{\Delta H_c - \Delta G_c}{nF}\right)\right]I}{\rho_{lact}V_L(t)C_{p,lact}}\right) \tag{5}$$

The first term on right hand side is the heat coming in with substrate flow rate, second term is the heat going out with substrate outlet flow rate, third term is heat transfer rate between cooling water and MFC, fourth term represents heat generated because of current production and fifth term is heat due to reactions.

The cell voltage obtained from continuous MFC is given as

$$E_{out} = E_{thero} - \frac{b}{2.303} \sinh^{-1}\left[\frac{i}{2i_{0,ref}}\right] - \left(\frac{d_m}{k_m} + \frac{d_{cell}}{k_{aq}}\right)i - \frac{RT}{nF}\ln\left(\frac{\frac{nFD_sC_{sb}}{L_l}}{\frac{nFD_sC_{sb}}{L_l} - i}\right)$$

(6)

Solution procedure

The data for the base case considered in this paper is given in Tab. 1. This model consists of eleven ordinary differential equations with one algebraic equation. Equation number 6 is solved for current after setting the voltage of the cell. After obtaining the cell current, all eleven differential equations are solved for required time period. Here it is important to note that the cell voltage has been fixed to a particular value and then current is obtained at operating condition. Due to this solution approach, trial and error method of solution has been avoided.

Model validation

We have validated developed batch model with literature. As mentioned earlier, the batch model equations are taken from Esfandyari et al. [7]. Hence this model is validated with the work of Esfandyari et al. [7] as well as Picioreanu et al. [4] for some key dynamics of the system like substrate consumption, current produced. Fig. 1 shows the dynamics of the above mentioned variables with the work of Picioreanu et al. [4]. It is found that the key dynamics are qualitatively in well agreement with the work of Picioreanu et al. [4].

RESULTS AND DISCUSSION
Steady state response

The impact of manipulated variables like inlet flow rate of substrate, coolant flow rate and cell voltage is studied in steady state as well as transient state. In steady state one manipulated variable is changed and fixed to a particular value, keeping all other variables at the base case. The values of the interested output are noted down when system reached steady state. In this way the impact of all the manipulated variables are studied as shown in Fig 2. It is observed that the power demonstrate linear relationship with inlet flow rate of substrate and temperature of the cell is increased slightly. Voltage of the cell demonstrates highly nonlinear relationship with power of the cell having input multiplicity.

Transient response

In transient analysis, the cell is subjected to step change in manipulated variables such as inlet flow rate of substrate, coolant and applied voltage. Fig.3 shows the step change response of inlet flow rate of substrate to

the power and temperature of the cell. It is observed that power shows first order dynamics with flow rate of the substrate and not significant change is observed on the cell temperature. As the flow rate get increase, the faster diffusion of substrate takes place and hence there is significant amount of substrate is available in the biofilm to consume by the microbes. As the consumption of substrate increases, amount of electrons produced will also be increases, which result in increase in power of the cell. At this point, it is unclear that why temperature is not showing significant change. Fig.4 shows step change response of the voltage on the power of the cell. It is observed that voltage is inversely proportional to the power of the cell, as the operating base case lies on the right hand side of the peak power of the steady state. Voltage dynamics is very fast as compared to the other key dynamics of the system like consumption of substrate, diffusion of substrate and hence instantaneous change in the power of the cell is observed.

CONCLUSIONS

Continuous model of the microbial fuel cell has been developed from the batch model given by Esfandyari et al. [7]. The batch model is validated with available literature qualitatively and found that it there is well agreement qualitatively. A novel method for the solution of MFC model is presented. The steady and transient dynamics of the MFC is studied and it is found that power of the cell exhibit linear relationship with substrate flow rate and nonlinear relationship with applied voltage. Voltage show input multiplicity with power. Power can be controlled with substrate flow rate with linear controller and with applied voltage by nonlinear controller.

FIGURES AND TABLES
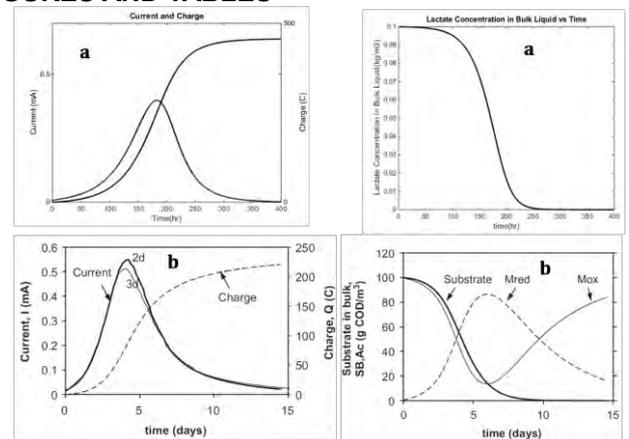
FIGURE 1. QUALITATIVE VALIDATION OF BATHCH MODEL WITH LITERATURE, A) TRENDS FROM MODEL SIMULATION, AND B) TRENDS FROM LITERATURE
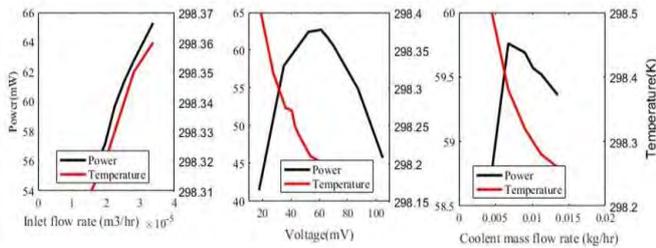
FIGURE 2. STEADY STATE PROFILE OF THE POWER AND TEMPERATURE OF THE CELL WITH MANIPUALTED VARIABLES
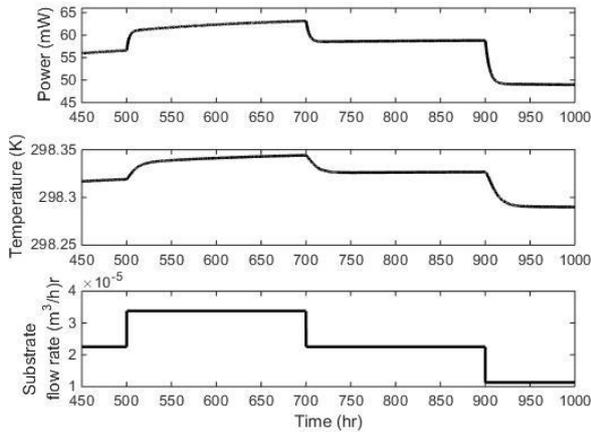
FIGURE 3. DYNAMIC RESPONSE OF SUBSTRATE FLOW RATE ON THE POWER AND TEMPERTURE
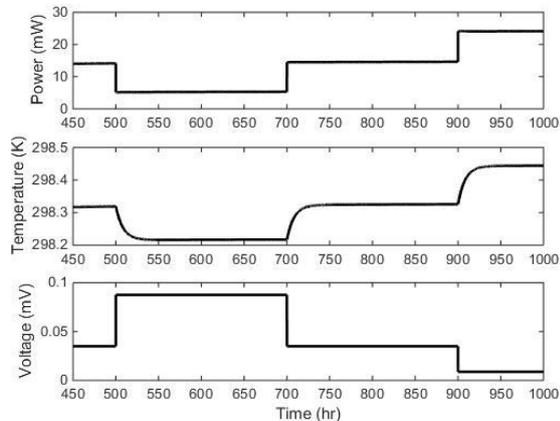
FIGURE 4. DYNAMIC RESPONSE OF VOLTAGE ON THE POWER AND TEMPERTURE

TABLE 1. DATA FOR THE BASE CASE

Input variable	values
$C_{sb,0}$ (kg/m³)	0.1
M_W (kg/hr)	9×10^{-3}
ϑ_0 (m³/hr)	2.25×10^{-5}
T_{cool} (K)	298
T_i (K)	303

REFERENCES:

[1] Chouler J., Padgett G. Cameron Petra, Preuss Kathrin, Titirici M., Ieropoulos I., Lorenzo M, 2016. "Towards Effective Small Scale Microbial Fuel Cells for Energy Generation from Urine", Electrochimica Acta 192, January, pp 89–98

[2] Choi S., 2015"Microscale microbial fuel cells: Advances and challenges", Biosensors and Bioelectronic, 69, February, pp 8-25

[3] Zeng Y., Choo Y., Kimb B., Wu P., 2010. "Modelling and Simulation of Two-Chamber Microbial Fuel Cell", Journal of Power Sources, 195,July, pp. 79-89

[4] Picioreanu C., Head I., Katuri K., Loosdrecht M. van, Scott K., 2007. "A Computational Model For Biofilm-Based Microbial Fuel Cells" , Water Research,41,May, pp. 2921-2940

[5] Marcus A., Torres C., and Rittmann B., 2007. " Conduction-Based Modeling of the Biofilm Anode of a Microbial Fuel Cell" , Biotechnology and Bioengineering, 98 (6),June, pp. 1171-1182

[6] Pinto R., Srinivasan B., Manuel M., Tartakovsky B., 2010. "A Two-Population Bio-Electrochemical Model Of A Microbial Fuel Cell", Bioresource Technology, 101(14), February, pp. 5256-5265

[7] Esfandyari M., Fanaei M., Gheshlaghi R., and Mahdavi M., 2017. "Mathematical Modeling of Two-Chamber Batchmicrobial Fuel Cell With Pure Culture of Shewanella", Chemical Engineering Research and Design, 7, October pp. 34-42.

SEEC-2018-130

Kinetics, isotherm and thermodynamic studies for immobilised lipase from *Yarrowia* lipolytica MTCC 9520 using chicken tallow oil on surface functionalised mesoporous activated carbon

Radha P.[1], Jiny George[1], Deepika S.L[1], Sindhu V.[1], Muthamilselvi P.[2], Ramani K.[1*]
[1]Department of Biotechnology, School of Bioengineering, SRM University, Kattankulathur- 603 203.
[2]Department of Chemical Engineering, School of Bioengineering, SRM University, Kattankulathur- 603 203.
Correspondence:
Radha P. – radha.p@ktr.srmuniv.ac.in
Ramani K. – ramani.k@ktr.srmuniv.ac.in

ABSTRACT

Lipase from *Yarrowia lipolytica* MTCC 9520 produced using chicken tallow oil (CTO) was adsorbed onto Surface Functionalised Mesoporous Activated Carbon (SFMAC). To determine the optimum conditions for the immobilization of lipase onto SFMAC, the study was performed by varying the time, pH, enzyme loading and carbon mass. The feasible conditions for immobilization of lipase were found to be: time – 4hrs; pH- 5.5; enzyme loading – 500U/mL; carbon mass – 0.5g. The adsorption data will be illustrated using isotherm models like Langmuir, Freundlich, Dubinin-Radushkevich, Temkin, Kiselev, Frumkin, Harkins-Jura, Fowler-Guggenheim, Halsey and Jovanovic models to understand the dynamic mechanism of immobilization. Also, the thermodynamic parameters and non-linear models of pseudo first order and second order will be investigated to analyze the experimental data and to determine the rate-limiting steps.

Keywords: Chicken tallow oil, Surface functionalised mesoporous activated carbon, Adsorption isotherm, Pseudo first order and second order.

NOMENCLATURE

A_0 - Initial lipase activity, U/ml
A_t - Lipase activity after immobilization
M - Mass of immobilized matrix
Q_e - Amount of solute is adsorbed per unit weight of adsorbent at equilibrium
C_e - Equilibrium concentration of the solute in the bulk solution
Q_m - Maximum adsorption capacity
K_L - Constant related to the free energy of adsorption
K_F - Constant indicative of the relative adsorption the capacity of the adsorbent

n - Constant indicative of the intensity of the adsorption

q_D - Dubinin–Radushkevich isotherm constant

B_D - Free energy of sorption per mole of sorbate
θ - Fractional coverage
R - Universal gas constant.
T - Temperature
ΔQ_{Temp} - Variation of adsorption energy
K_{Temp} - Temkin equilibrium constant.
K_1 - Kiselev equilibrium constant,
K_n - Constant of complex formation
W - Interaction energy between adsorbed molecules
q_{jova} - Maximum adsorption capacity in Jovanovic model
K_{jova} - Jovanovic isotherm constant.

INTRODUCTION

Lipases (triacylglycerol acyl hydrolase, EC 3.1.1.3) are enzymes that catalyze the hydrolysis of long-chain triglycerides under physiological conditions [1-3]. These enzymes have the ability to drive several reactions like esterification, transesterification, aminolysis and oxymolysis in an environment with low water content [4-6].These enzymes possess excellent characteristics such as high tolerance to extreme pH, temperature and organic solvents which provides high stability in non-aqueous media for biodiesel transesterification reactions [7,8]. In general, a significant mechanism of action of lipases is the interfacial activation. Most lipases have α-helical oligopeptide structure covering their active site in the form of lid or flap, thus making them obscure to the substrate. In the absence of hydrophobic interface, the active site is concealed from the reaction medium and the enzyme is in "closed conformation". However in the presence of a hydrophobic interface, the lipase changes its conformation and thus, exposing the active site to hydrophobic phase, that is "open conformation" [9-11]. Practical use of lipases in pseudo homogeneous reaction systems presents several technical difficulties such as contamination of the product

with residual enzymatic activity and economic cost [12]. In order to troubleshoot the problems, the enzyme is usually immobilized, so that it can be reused to reduce the cost and also to improve the quality of the product. Immobilization refers to the localisation or confinement of an enzyme onto a support material. The choice of support is based on several factors such as mechanical strength, microbial resistance, thermal stability, chemical functionality, hydrophobic or hydrophilic character, ease of regeneration, loading capacity and cost [13]. Adsorption is the attachment of enzyme on the surface of carrier particles by weak forces such as van der Waals or dispersion forces. Moreover, this method is easy, cost-effective, involves no toxic chemicals and the resultant immobilized enzyme doesn't experience internal mass transfer limitations unlike other techniques [14].

Amongst the support materials studied till date, porous inorganic substrates with the high specific surface area and large porous volume were reviewed for immobilisation of the enzyme [15-19]. Activated carbon is capable of providing a buffering condition to impart structural stability during immobilization [20]. The sustained stability of an enzyme on to mesoporous activated carbon (MAC) was one of the main issues for most industrial applications since the reduction in the operational stability was caused by the strains induced on active sites by the periodic application. The enrichment of reactive groups onto the surface of the matrix by functionalization of mesoporous activated carbon (SFMAC) by using glutaraldehyde led to increasing stabilisation of enzymes because it permits a more intense multipoint covalent attachment [21-24]. Prior to glutaraldehyde activation, the MAC undergoes amino-functionalization by ethylenediamine. Surface Functionalized Mesoporous Activated Carbon (SFMAC) is a potential support for the covalent interaction followed by the physical adsorption of the lipase. On comparing, the immobilization efficiency of SFMAC was higher than MAC and other reported support materials [25].

In this research study, chicken tallow oil has been used as a substrate for production of lipase and process conditions were optimized. Tallow can be used for the production of biodiesel same way as oils from plants since, tallow is derived from animal by-products, which have little to no value and thus, avoiding food to fuel controversies.

Yarrowia lipolytica MTCC 9520 lipase was immobilized on SFMAC as an enzyme carrier. The techniques of immobilization for lipase enzyme on SFMAC were physical adsorption and covalent bond. In addition, the kinetics rate model and isotherm studies of the immobilized enzyme on the support material will be discussed [26]. An adsorption isotherm is characterized by constant values which express the surface properties and affinity of the adsorbent. Over the years, a wide variety of equilibrium isotherm models like Langmuir, Freundlich, Dubinin-Radushkevich, Temkin, Kiselev, Frumkin, Harkins-Jura, Fowler-Guggenheim, Halsey and Jovanovic

models have been formulated [27]. Further, the immobilization mechanisms of lipase onto SFMAC for kinetic rate models will be examined. Pseudo first order and second order models will be investigated to analyze the experimental data and to determine the rate-limiting steps [25]. Thermodynamic parameters will also be analyzed for sorption kinetics since the temperature has a pronounced effect in adsorption [27]. The main objective of the present work is to study immobilized lipase on SFMAC by determining its kinetics and isotherm models, which will further be used as an efficient catalyst in the transesterification reaction of biodiesel in future studies.

FIGURES AND TABLES:

TABLE 1: LIPASE OPTIMISATION CONDITIONS

Parameter	Optimal conditions
pH	5.5
Time (hours)	72
Temperature (°C)	35
Inoculum percentage (v/v)	10
Substrate concentration (v/v)	1
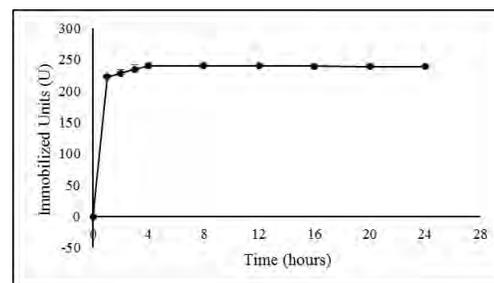
FIGURE.1- OPTIMISATION OF TIME
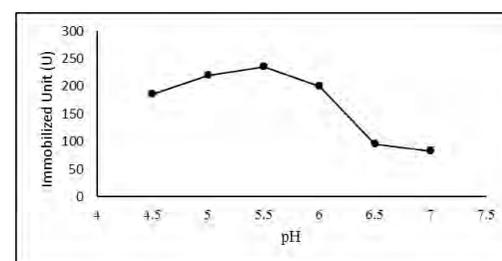
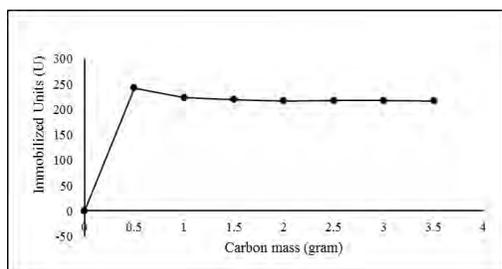FIGURE. 2- OPTIMISATION OF pH
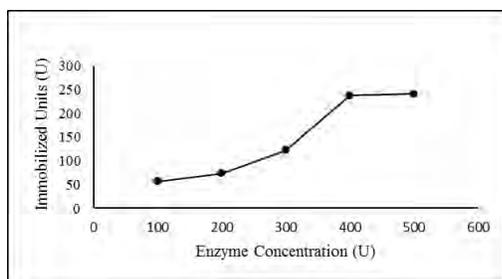
FIGURE.3- OPTIMISATION OF ENZYME CONCENTRATION

FIGURE.4- OPTIMISATION OF CARBON MASS

EQUATIONS:

Lipase activity, U/mL =

$$\frac{N*Vol.of\ NaOH*1000*Vol.of\ the\ sample}{Time\ of\ incubation} \tag{1}$$

Langmuir model,

$$\frac{Q_e}{Q_m} = \frac{K_L C_e}{1 + K_L C_e} \tag{2}$$

$$R_L = \frac{1}{(1 + K_L C_0)} \tag{3}$$

Freundlich model,

$$q_e = K_F C_e^{\frac{1}{n}} \tag{4}$$

Halsey model,

$$K_F = \frac{q_m}{C_0^{\frac{1}{n}}} \tag{5}$$

Dubinin– Radushkevich model,

$$\ln(q_e) = \ln(q_D) - 2B_D RT \ln\left(1 + \frac{1}{C_e}\right) \tag{6}$$

Temkin model,

$$\theta = \frac{RT}{\Delta Q_{Temp}} \ln K_{Temp} C_e \tag{7}$$

Kiselev model,

$$K_1 C_e = \frac{\theta}{(1-\theta) + (1 + K_n \theta)} \tag{8}$$

Frumkin model,

$$\frac{\theta}{1-\theta} e^{-2a\theta} = KC_e \tag{9}$$

Harkins – Jura model,

$$q_e = \left(\frac{A_{HJ}}{B_{HJ} - \log C_e}\right)^{\frac{1}{2}} \tag{10}$$

Fowler–Guggenheim model,

$$K_{FG} C_e = \frac{\theta}{1-\theta} \exp\left(\frac{2\theta W}{RT}\right) \tag{11}$$

Jovanovic model,

$$q_e = q_{jova}\left(1 - e^{K_{jova} C_e}\right) \tag{12}$$

REFERENCES:

1. Guncheva, M., & Zhiryakova, D. (2011). Catalytic properties and potential applications of Bacillus lipases. *Journal of Molecular Catalysis B: Enzymatic*, *68*(1), 1-21.
2. Sharma, R., Chisti, Y., & Banerjee, U. C. (2001). Production, purification, characterization, and applications of lipases. *Biotechnology advances*, *19*(8), 627-662.
3. Stergiou, P. Y., Foukis, A., Filippou, M., Koukouritaki, M., Parapouli, M., Theodorou, L. G., ... & Papamichael, E. M. (2013). Advances in lipase-catalyzed esterification reactions. *Biotechnology advances*, *31*(8), 1846-1859.
4. Adlercreutz, P. (2013). Immobilisation and application of lipases in organic media. *Chemical Society Reviews*, *42*(15), 6406-6436.
5. Kapoor, M., & Gupta, M. N. (2012). Lipase promiscuity and its biochemical applications. *Process Biochemistry*, *47*(4), 555-569.
6. Mendes, A. A., Oliveira, P. C., & de Castro, H. F. (2012). Properties and biotechnological applications of porcine pancreatic lipase. *Journal of Molecular Catalysis B: Enzymatic*, *78*, 119-134.

7. Hasan, F., Shah, A. A., & Hameed, A. (2006). Industrial applications of microbial lipases. *Enzyme and Microbial technology*, *39*(2), 235-251.

8. Villeneuve, P., Muderhwa, J. M., Graille, J., & Haas, M. J. (2000). Customizing lipases for biocatalysis: a survey of chemical, physical and molecular biological approaches. *Journal of molecular catalysis B: enzymatic*, *9*(4), 113-148.

9. Verger, R. (1997). 'Interfacial activation'of lipases: facts and artifacts. *Trends in Biotechnology*, *15*(1), 32-38.

10. Reis, P., Holmberg, K., Watzke, H., Leser, M. E., & Miller, R. (2009). Lipases at interfaces: a review. *Advances in colloid and interface science*, *147*, 237-250.

11. Bastida, A., Sabuquillo, P., Armisen, P., Fernandez-Lafuente, R., Huguet, J., & Guisan, J. M. (1998). A single step purification, immobilization, and hyperactivation of lipases via interfacial adsorption on strongly hydrophobic supports. *Biotechnology and bioengineering*, *58*(5), 486-493.

12. Al-Zuhair, S. (2007). Production of biodiesel: possibilities and challenges. *Biofuels, Bioproducts and Biorefining*, *1*(1), 57-66.

13. Karube, I., Yugeta, Y., & Suzuki, S. (1977). Electric field control of lipase membrane activity. *Biotechnology and bioengineering*, *19*(10), 1493-1501.

14. Jegannathan, K. R., Abang, S., Poncelet, D., Chan, E. S., & Ravindra, P. (2008). Production of biodiesel using immobilized lipase—a critical review. *Critical Reviews in Biotechnology*, *28*(4), 253-264.

15. Mateo, C., Palomo, J. M., Fernandez-Lorente, G., Guisan, J. M., & Fernandez-Lafuente, R. (2007). Improvement of enzyme activity, stability and selectivity via immobilization techniques. *Enzyme and microbial technology*, *40*(6), 1451-1463.

16. Zhao, D., Huo, Q., Feng, J., Chmelka, B. F., & Stucky, G. D. (1998). Nonionic triblock and star diblock copolymer and oligomeric surfactant syntheses of highly ordered, hydrothermally stable, mesoporous silica structures. *Journal of the American Chemical Society*, *120*(24), 6024-6036.

17. Ying, J. Y., Mehnert, C. P., & Wong, M. S. (1999). Synthesis and applications of supramolecular-templated mesoporous materials. *Angewandte Chemie International Edition*, *38*(1-2), 56-77.

18. Kamori, M., Hori, T., Yamashita, Y., Hirose, Y., & Naoshima, Y. (2000). Immobilization of lipase on a new inorganic ceramics support, toyonite, and the reactivity and enantioselectivity of the immobilized lipase. *Journal of Molecular Catalysis B: Enzymatic*, *9*(4), 269-274.

19. Mitchell, S., & Pérez-Ramírez, J. (2011). Mesoporous zeolites as enzyme carriers: synthesis, characterization, and application in biocatalysis. *Catalysis today*, *168*(1), 28-37.

20. Ramani, K., Boopathy, R., Mandal, A. B., & Sekaran, G. (2011). Preparation of acidic lipase immobilized surface-modified mesoporous activated carbon catalyst and thereof for the hydrolysis of lipids. *Catalysis Communications*, *14*(1), 82-88.

21. Kandasamy, R., Kennedy, L. J., Vidya, C., Boopathy, R., & Sekaran, G. (2010). Immobilization of acidic lipase derived from *Pseudomonas gessardii* onto mesoporous activated carbon for the hydrolysis of olive oil. *Journal of Molecular Catalysis B: Enzymatic*, *62*(1), 58-65.

22. López-Gallego, F., Montes, T., Fuentes, M., Alonso, N., Grazu, V., Betancor, L., ... & Fernández-Lafuente, R. (2005). Improved stabilization of chemically aminated enzymes via multipoint covalent attachment on glyoxyl supports. *Journal of Biotechnology*, *116*(1), 1-10.

23. Jal, P. K., Patel, S., & Mishra, B. K. (2004). Chemical modification of silica surface by immobilization of functional groups for extractive concentration of metal ions. *Talanta*, *62*(5), 1005-1028.

24. Mendes, A. A., Giordano, R. C., de LC Giordano, R., & de Castro, H. F. (2011). Immobilization and stabilization of microbial lipases by multipoint covalent attachment on aldehyde-resin affinity: Application of the biocatalysts in biodiesel synthesis. *Journal of Molecular Catalysis B: Enzymatic*, *68*(1), 109-115.

25. Ramani, K., Karthikeyan, S., Boopathy, R., Kennedy, L. J., Mandal, A. B., & Sekaran, G. (2012). Surface functionalized mesoporous activated carbon for the immobilization of acidic lipase and their application to hydrolysis of waste cooked oil: isotherm and kinetic studies. *Process biochemistry*, *47*(3), 435-445.

26. Gilani, S. L., Najafpour, G. D., Moghadamnia, A., & Kamaruddin, A. H. (2016). Kinetics and isotherm studies of the immobilized lipase on chitosan support. *Int J Eng Trans A. 2016b*, *29*(10), 1402-1414.

27. Muthamilselvi, P., Karthikeyan, R., & Kumar, B. S. M. (2016). Adsorption of phenol onto garlic peel: optimization, kinetics, isotherm, and thermodynamic studies. *Desalination and Water Treatment*, *57*(5), 2089-2103.

SEEC-2018-131

CHICKEN TALLOW OIL, AN ECONOMICAL SUBSTRATE FOR BIOSURFACTANT PRODUCTION USING *YARROWIA LIPOLYTICA* MTCC 9520: PRODUCTION AND CHARACTERIZATION

Radha P.[1], Priya Suhazsini[1], Keerthana Prabhu[1], Anjali J.[1], Ramani K.[1*]

[1]Department of Biotechnology, SRM University, Kattankulathur, Tamil Nadu, India

Correspondence:

Radha P. - radha.p@ktr.srmuniv.ac.in

Ramani K. – ramani.k@ktr.srmuniv.ac.in

ABSTRACT

The poultry industry is one of the fastest growing agro sectors and produces an overwhelming amount of wastes. Recently, the valorization of such wastes has gained a scientific momentum in cost-cutting strategies. In this study, chicken tallow oil is used as a cheap substrate by Yarrowia lipolytica MTCC 9520 for production of biosurfactant. Biosurfactants are amphiphilic compounds produced by several microorganisms on the living surface, microbial cell surface, or are released extracellularly. Reduced surface tension, low toxicity, optimal activity in varied conditions, biodegradability and production from several different substrates are major advantages of bio processed surfactants. The product properties were determined using emulsification index, surface tension, and critical micelle concentration. Also, the physiochemical and chemical properties of the biosurfactant were characterized using TGA, DSC, FT-IR, ^{13}C NMR, $^{1}HNMR$, and GC-MS analysis. The optimal parameters such as time, substrate concentration for increased yield and biosurfactant stability were studied.

KEYWORDS: *Yarrowia lipolytica* MTCC 9520, Biosurfactant, Characterization

NOMENCLATURE

E_{24}	Emulsification Activity
CMC	Critical Micelle Concentration
^{1}H NMR	Proton Nuclear Magnetic Resonance
^{13}C NMR	Carbon Nuclear Magnetic Resonance

INTRODUCTION

Recently, there has been an exponential growth in population and the demand for sustenance. The poultry industry is one of the largest growing agricultural sectors resulting in an overwhelming increase in degradable biological wastes. Effective use of by-products has an influence on the economy and environment pollution of the country. Nonutilization of by-products can lead to loss of possible revenue as well as increase the cost of disposal of such products [1]. A by-product of the poultry industry, Chicken tallow are potentially an excellent source of animal fats and oil which will boost up the commercial values of these cheap and underutilized fatty raw material. The

recovery of high value-added products such as microbial enzymes, including secondary metabolites such biosurfactants can be important applications [2, 3].

Biosurfactant is surface active amphiphilic bio-molecules with diverse structures and that are produced by several microorganisms, such as bacteria, yeasts, and filamentous fungi. These secondary metabolites comprise hydrophobic and hydrophilic moieties, that are classified according to their chemical structures, including glycolipid and lipopeptides as their important classes [4]. These biomolecules play an important role in the survival of these microorganisms, as they enhance the solubility of water-insoluble compounds. These compounds also facilitate biological processes such as cell adhesion and aggregation, biofilm formation and single cell oil production [5]. Microbial surfactants have various advantages over synthetic surfactants, for instance, low toxicity, high biodegradability, selectivity and specificity and the ability to be produced from renewable substrate [6].

A greater part of biosurfactants has been extensively premeditated based on their production, structures, and properties reportedly produced by *Bacillus* and *Pseudomonas* [7-10]. However, due to pathogenic nature of some microorganism, the applications of these products have been limited. On the other hand, yeast species such as *Candida, Wickerhamomyces,* and *Yarrowia* have a greater advantage of GRAS (Generally Regarded as Safe) status for biosurfactant production [11-13].

Yarrowia lipolytica is nonconventional, aerobic, dimorphic yeast found in environments containing hydrophobic substrates, fats, and oils. This strain is used in my biotechnological and industrial purposes for obtaining products like citrate, for bioremediation and production of biosurfactant [14-16]. This myriad of probable applications has resulted in exploitation of the strain for various purposes such as the production of lipase and biosurfactant. The obtained biosurfactant help in emulsification of the hydrophobic substrate during fermentation [17].

This paper aims to investigate the physiochemical characterization of a biosurfactant produced by an oleaginous yeast *Yarrowia lipolytica* MTCC 9520 under optimized feasible parameters such as time and substrate concentration. The physiological surface activity of the biosurfactant was assessed using emulsification index, surface tension, and CMC (Critical Micelle Concentration) analysis. The structural characterization of the biosurfactant was studied by FT-IR, GC-MS, ^{1}H NMR and ^{13}C NMR. The zeta potential was observed to analyse the ionic nature of the biosurfactant. .Additionally, the thermal properties of the biosurfactant produced was investigated using TGA (Thermo gravimetric analysis) and DSC (Differential Scanning Calorimetric) analysis.

FIGURES AND TABLES

TABLE 1: EMULSIFICATION INDEXES DURING DIFFERENT TIME INTERVALS OF PRODUCTION.

Time (Hours)	E24 %
24	4
48	27
72	48
96	56
120	33
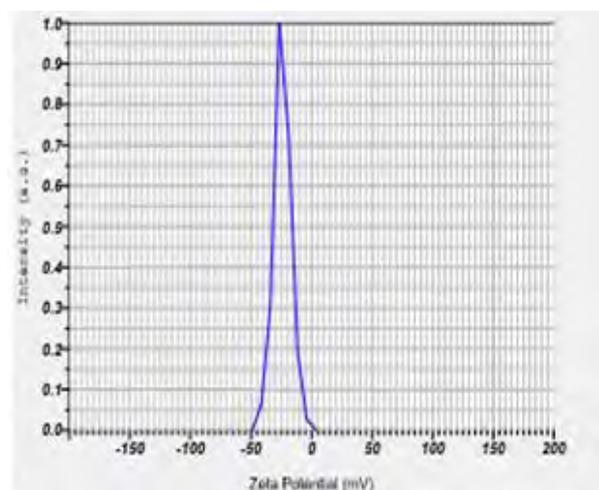
FIGURE 1: ZETA POTENTIAL ANALYSIS
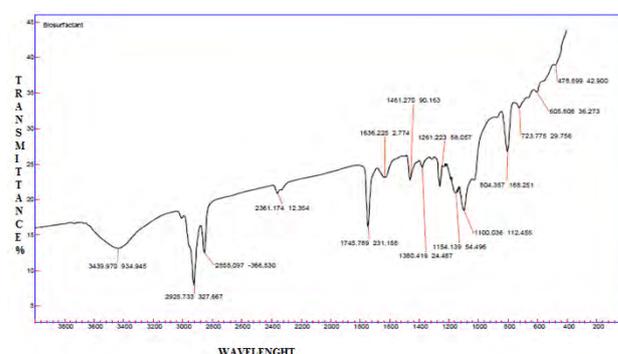
FIGURE 2: FT-IR ANALYSIS
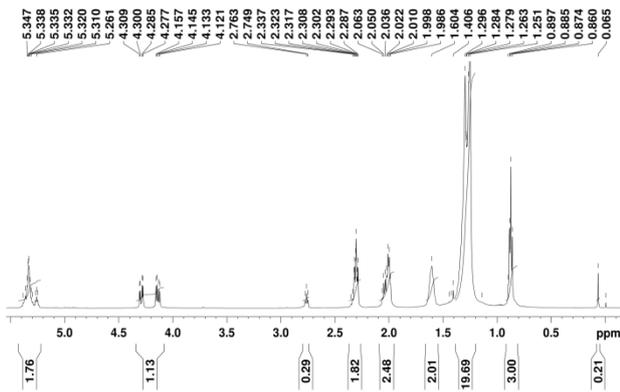
FIGURE 3: ^{1}H NMR OF BIOSURFACTANT.
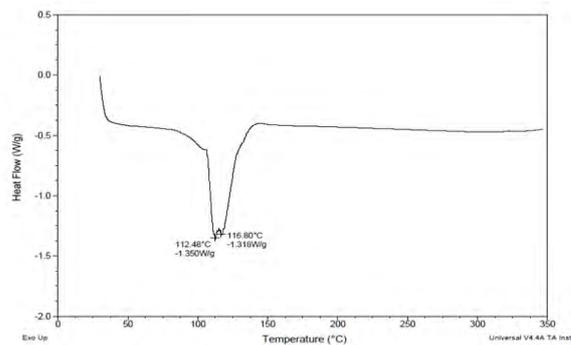
FIGURE 6: DIFFERENTIAL SCANNING

CALORIMETRY (DSC) ANALYSIS
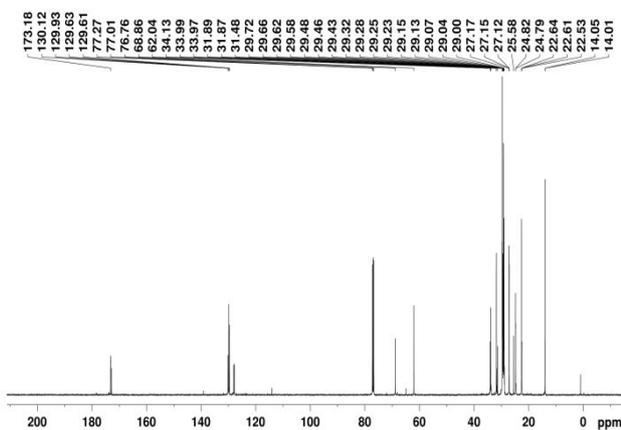
FIGURE 4: ^{13}C NMR OF BIOSURFACTANT
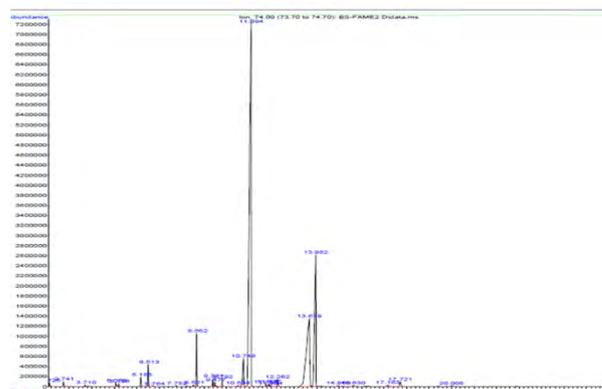
FIGURE 7: GC- MS ANALYSIS OF
BIOSUTFACTANT

EQUATION

The emulsification activity (E_{24}) was measured using the method described by Cooper and Goldenberg [18].

$$E24 \% = \frac{Height\ of\ emulsion\ layer}{Total\ height\ of\ mixture} \times 100 \qquad (1)$$

ACKNOWLEDGEMENT
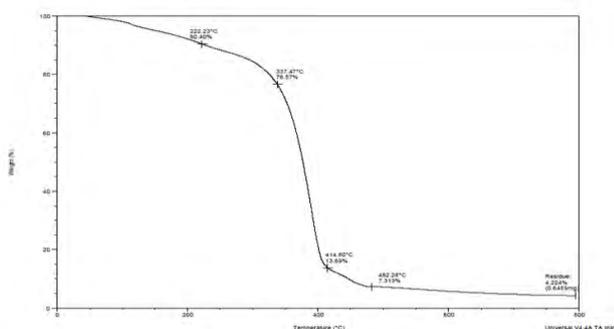
FIGURE 5: THERMOGRAVIMETRIC ANALYSIS
(TGA) OF BIOSUFACTANT

of Biotechnology, School of Bioengineering, and SRM University.

REFERENCE

[1] Jayathilakan K, Sultana Khudsia, Radhakrishna K, Bawa A S, 2012. Utilization of byproducts and waste materials from meat, poultry, and fish processing industries: a review. J Food Sci Technol 49(3); 278–293.

[2] K. Ramani, S. Chandan Jain, A.B. Mandal, G. Sekaran, 2012. Microbial induced lipoprotein biosurfactant from slaughterhouse lipid waste and its application to the removal of metal ions from aqueous solution. Colloids and Surfaces B: Biointerfaces 97, 254–263.

[3] S. Papanikolaou, I. Chevalot, M.G. Panayotou, M. Komaitis, I. Marc, G. Aggelis, 2007. *Yarrowia lipolytica* and Its Multiple Applications in the Biotechnological Industry.Electron. J. Biotechnol. 10 425–435

[4] E.J. Gudiña, V. Rangarajan, R. Sen and L.R. Rodrigues, 2013.Potential therapeutic applications of biosurfactants.Trends Pharmacol. Sci., 34,667.

[5] I.N.A. Van Bogaert, J. Zhang and W. Soetaert, 2011. Jatropha Oil Derived Sophorolipids: Production and Characterization as Laundry Detergent Additive Process. Biochem., 46, 82.

[6] I. M. Banat, 1995. Characterization of biosurfactants and their use in pollution removal: State of the art. ACTA Biotechnol., 15, 251–267.

[7] J. D. Desai and I. M. Banat, 1995. Microbial production of surfactants and their commercial potential.Microbiol. Mol. Biol. Rev. 61, 47–64.

[8] A. Fiechter, 1992. Biosurfactants: moving towards industrial application Trends Biotechnol., 1992, 10, 208–217

[9] E.J. Gudiña, J.F.B. Pereira, L.R. Rodrigues, J.A.P. Coutinho and J.A. Teixeira,2012. Isolation and study of microorganisms from soil samples for application in microbial enhanced oil recovery Int. Biodeterior. Biodegrad., 68 (2012) 56.

[10] E.J. Gudiña, A.I. Rodrigues, E. Alves, M.R. Domingues, J.A. Teixeira and L.R. Rodrigues, 2015. Bioconversion of agro-industrial by-products in rhamnolipids toward applications in enhanced oil recovery and bioremediation.Bioresour. Technol., 177, 87.

[11] N.M. Ramos, P.F.F. Amaral, M. Nele and M.A.Z Coelho, 2012. Renewable resources for biosurfactant production by *Yarrowia lipolytica* . G.C. Fontes Braz. J. Chem. Eng., 29, 483.

[12] A. Daverey and K. Pakshirajan,2010. Sophorolipids from *Candida bombicola* using mixed hydrophilic substrates: production, purification, and characterization. Colloids Surf. B Biointerfaces, 79,246.

[13] Karla S. Teixeira Souza, Eduardo J. Gudina, Z˜elia´ Azevedo, Victor de Freitas, Rosane F. Schwan, L´ıgia R. Rodrigues, Disney R. Dias, Jose A. Teixeira, 2017. New glycolipid biosurfactants produced by the yeast strain *Wickerhamomyces anomalus* CCMA 0358. Colloids and Surfaces B: Biointerfaces.

[14] J.-M. Beckerich, A. Boisramé-Baudevin, and C. Gaillardin, 1998.*Yarrowia lipolytica*: a model organism for protein secretion studies.International Microbiology, vol. 1, no. 2, pp. 123–130.

[15] S. V. Kamzolova, N. V. Shishkanova, I. G. Morgunov, and T. V. Finogenova, 2003.Oxygen requirements for growth and citric acid production of *Yarrowia lipolytica*. FEMS Yeast Research, vol. 3, no. 2, pp. 217–222.

[16] C. Madzak, C. Gaillardin, and J.-M. Beckerich, 2004. Heterologous protein expression and secretion in the non-conventional yeast *Yarrowia lipolytica*: a review.Journal of Biotechnology, vol. 109, no. 1-2, pp. 63–81.

[17] A. Beopoulos, J. Cescut, R. Haddouche, J.-L. Uribelarrea, C. Molina-Jouve, and J.-M. Nicaud, 2009. *Yarrowia lipolytica* as a model for bio-oil production. Progress in Lipid Research, vol. 48, no. 6, pp. 375–387.

[18] David G. Cooper* and Beena G. Goldenberg, 1987. Surface-Active Agents from Two *Bacillus* Species. Appl Environ Microbiol, 53(2): 224–229.

EFFECTS OF EXCESS AIR SUPPLY ON STACK EMISSION FOR MAJOR AIR POLLUTANTS IN A TYPICAL INDIAN COAL FIRED POWER PLANT

Biswajit Mohanty
Department of Environmental Science and Engineering
Indian Institute of Technology (ISM), Dhanbad,Jharkhand, India, 826004
Email: bmpp105@gmail.com

Suresh Pandian Elumalai
Department of Environmental Science and Engineering
Indian Institute of Technology (ISM), Dhanbad,Jharkhand, India, 826004
Email: espandian@iitism.ac.in

ABSTRACT

This study is carried out to determine the effect of excess air supply on stack emission for major air pollutants in typical Indian power plant consuming F1 grade coal with a coal feed rate of 150000 kg/hour. In this research work, mass emission factors for CO_2, SO_2, and nitric oxide (NO) are computed based on the input data, such as chemical composition of the coal used at the power plants and the actual air used during combustion. These calculations are based on theoretical ideals and do not take account for the control devices. The operative combustion temperature is assumed to be 1200 K.The concentrations of CO_2, SO_2, PM in stack emission decreases from 181690 mg/m³, 1357 mg/m³ and 30008.9 mg/m³ to 118744 mg/m³, 887 mg/m³ and 19880 mg/m³ respectively when the excess air supplied is increased from 0% to 50%. At the same time the concentration of NO in stack emission increses from 0 mg/m³ at theoretical air supply to 868 mg/m³ when 50% excess air is supplied.There is a comparison between the concentration of pollutant in stack emission and stack emission standard and miligrams of pollutants needs to be captured per meter cube of flue gas also calculated to develop a basic idea of pollution control requirments in power plants in India according to MoEF&CC.This study found that approximately 17% excess air needs to be supplied to boiler for best results in terms of over all air pollution control in thermal power plants in India. This study results can be used to optimize the excess air supply in coal fired power plants and the study may be expanded by considering all types of coal available, pollution control devices and type of combustion technology.

1.INTRODUCTION

India is now facing great challenges resulting from climate change and air pollution, driven by the processes of industrialization andurbanization. Coal fired powerplants are the major energy production units which are dominated over others in Indian power sectors contributing about 68.9 % of total energy [1]. There are six different grades of coals which are utilised in power sector of India named D1, D2, D3, E, F1 and F2 [2].These six different coal types have different emission potentials. Excess air supply limits the production of incomplete combustion products such as CO, but at the same time increases the production of oxides of nitrogen.When excess air supply increases, the flue gas flow rate increases to the control devices, though concentrations of major pollutants such as sulphur dioxide, particulate matter and carbon dioxide decreases in flue gas.Every pollution control device has a life period of its own in terms of cubic metres of flue gas cleansing capacity so when flue gas flow rate increses to control device its life decreses.In this work, the mass emissions factors are theoretically calculated using basic principle of combustion and then emissions are calculated for 100 kg of F1 grade coal. Assuming a coal feed rate of 150000 kg/hr. the flue gas compositions are estimated and compared with standard prescribed in Environmental (protection) Rules 2015 [3].The required efficiencies for pollution control devices

and amount of pollutants needs to be captured are calculated so as to meet norms prescribed by MoFF&CC at different excess air conditions [3].

2. MATERIALS AND METHODS

2.1 EXCESS AIR, THEORETICAL AIR, FLUE GAS COMPOSITION CALCULATION [4]

From the elemental analysis of the coal, the percentage of carbon, hydrogen, nitrogen, oxygen, ash, and moisture in the coal is known. Let C be the mass of the carbon, S of thesulphur, H of the hydrogen, O_2 of the oxygen, and N_2 of the nitrogen,

Then Oxygen (O_r) required to burn one kilogram (kg) of coal

$$O_r = C (32/12) + H (16/2) + S (32/32) - O_2 \qquad (1)$$

Air mass required for O_r kg of oxygen = (O_r/ mass fraction of O_2 in the air) = O_r/ 0.233 $\qquad (2)$

If E is the percentage of excess air used in the furnace to burn the coal, the air mass used

$$Air\ (used) = (1 + E)\ O_r/\ 0.233 \qquad (3)$$

Knowing the air mass used to burn one kg of coal, mass of O_2 and N_2 are calculated as

$$O_2 \text{ in the air used} = (1 + E)\ O_r \qquad (4)$$

$$N_2 \text{ in the air used} = 0.767(1 + E)O_r/0.233 \qquad (5)$$

Mass of CO_2, SO_2, NO, and H_2O are calculated by mass balance as

$$CO_2 = C (44/12) \qquad (6)$$

$$SO_2 = S (64/32) \qquad (7)$$

$$H_2O = H (18/2) \qquad (8)$$

2.2 CONCENTRATION OF NITROGEN

The actual mechanism, whereby atmospheric nitrogen is oxidized, goes through a complex chain of reactions initiated by oxygen atoms. Generally accepted principal reactions [5] for 'thermal NO' formation are as follows.

$$O + N_2 \rightarrow NO + N \qquad (9)$$

$$N + O_2 \rightarrow NO + O \qquad (10)$$

$$N + OH \rightarrow NO + H \qquad (11)$$

Present estimates give the equilibrium concentrations of NO assuming long residence time as found in large boilers. The oxidation of nitrogen is represented by the overall balance [6].

$$N_2 + O_2 \rightarrow 2NO \qquad (12)$$

A simple stoichiometric calculation gives the equilibrium NO concentration as

$$\chi_{NO} = K_{10.1}\ (\chi_{N_2})^{0.5}\ (\chi_{O_2})^{0.5} \qquad (13)$$

Where χ_{NO} is the species concentration and $K_{10.1}$ isan equilibrium constant that depends upon the temperature of the gas. At 1200 K, $K_{10.1} = 0.00526$ [6].

3. RESULT AND DISCUSSION

3.1 COAL PROPERTIES, AIR REQUIREMENT AND FLUE GAS COMPOSITION

In first step of calculation, an F1 grade coal used in a thermal power plant having coal feed rate 150000 kg/hr, is considered. The properties of this type coal and major air pollutants emitted from burning of 100kg of coal is tabulated (Table 1&2).

When there is no excess air supply there is no emission of NO .There are chances of incomplete combustion only if the theoretical air is supplied for combustion, so for the complete combustion of fuel excess air is supplied (Table 3).

3.2 FLUE GAS COMPOSITION AND COMPARISON WITH MOEF&CC STANDARD

Different amount of air supplied with fuel (theoretical and excess 10% to 50%) so as to determine the major pollutant concentration (Table 4) and the amount of emissions are compared with existing emission standards of Environment (Protection) Amendment Rules 2015 by MoEF &CC (Table 5).

3.3 DETERMINATION OF EFFICIENCIES OF CONTROL DEVICE AND AMOUNTS OF POLLUTANTS CAPTURED

We have the inlet loading, which is the stack emission as per our calculation and the outlet loading is specified by the MoEF&CC, India. By considering the inlet and outlet loading we can determine the required efficiencies for control device.From the result we can also calculate the amount of excess air suitable for combustion and the amount of pollutants captured also tabulated (Table 6).

TABLE 1: PROPERTIES OF F1 GRADE COAL [7]

Grade of coal	C %	H%	S%	N_2%	O_2%	Ash %	M%	NCV (Kcal/Kg)	UHV (Kcal/Kg)
F1	41.87	3.33	0.56	0.94	6	34.07	7.8	4137	3122

TABLE 2: AIR REQUIREMENT AND FLUE GAS COMPOSITION OF F1 GRADE COAL

Grade of coal	Amount of coal (in Kg)	Theoretical Air required (in Kg)	Theoretical O_2 required (in Kg)	CO_2 (in Kg)	N_2 (in Kg)	SO_2 (in kg)
F1	100	573.199	120.37	153.52	452.82	1.12

TABLE 3: AMOUNT OF EXCESS AIR SUPPLIED FOR COAL COMBUSTION

	With 10%	With 20%	With 30%	With 40%	With 50%
Kg of Air per 100 Kg of Fuel	57.32	114.64	171.96	229.28	286.60
Kg of O_2 per 100Kg of Fuel	13.29	26.59	39.89	53.19	66.49
Kg of N_2 per 100Kg of fuel	44.01	88.03	132.04	176.06	220.08

TABLE 4: STACK GAS COMPOSITION FOR MAJOR AIR POLLUTANTS BASED ON EXCESS AIR SUPPLIED

Percentage of excess air	Total air volume (m^3)	Carbon dioxide %	Sulphur dioxide %	PM (mg/m^3)	NO (in ppm)
0	839.84	9.2	0.047	30060	0
10	928.90	8.36	0.042	27500	615.03
20	1017.96	7.63	0.039	25100	854.21
30	1106.96	7.01	0.036	23080	1009.57
40	1196.02	6.49	0.033	21360	1128.20
50	1285.08	6.04	0.031	19880	1227.05

TABLE 5: COMPARISON OF MAJOR AIR POLLUTANT CONCENTRATION WITH MOEF&CC STANDARD [3]

Percentage of excess air	carbon dioxide (mg./m^3)	sulphur dioxide Emission (mg/m^3)	Sulphur dioxide Standard (mg/m^3) ($\geq$500MW)	PM (mg/m^3) Emission	PM Standard (mg/m^3)	NO in (mg/m^3) Emission	NO Standard (mg/m^3)
0	181690	1357		30060		00	
10	164274	1227		27500		459	
20	149956	1119		25100		619	
30	137851	1029	200	23080	50	725.4	300
40	127586	953		21360		804.3	
50	118744	887		19880		868.9	

TABLE 6: REQUIREMENT EFFICIENCY OF CONTROL DEVICE TO MEET MOEF&CC NORMS 2015 AND AMOUNT OF POLLUTANTS CAPTURED

Percentage of excess air	CO_2 Captured at 90% efficiency (mg/m^3)	SO_2 Control Efficiency(≥500MW) (%)	SO_2 Captured (in mg/m^3)	PM Control Efficiency (%)	PM Captured (in mg/m^3)	NO_X Control Efficiency (%)	NO_X Captured (in mg/m^3)
0	163521	85.26	1156.97	99.83	30008.90		
10	147846	83.70	1026.99	99.81	27447.75	34.64	158.99
20	134960	82.16	919.37	99.80	25049.92	51.53	318.99
30	124065	80.56	828.96	99.78	23029.92	58.64	425.39
40	114827	79.01	752.99	99.76	21308.74	62.70	504.29
50	106869	77.45	686.99	99.74	19828.31	65.47	568.89

4.CONCLUSION

This research work studied the impacts of excess air supplied during coal combustion in Indian thermal power plants. The results have shown that the percentage of CO_2 in flue gas decreases from 9.20% (no excess air) to 6.04% (at 50% excess air). SO_2 decreases from 0.047% to 0.031% and PM concentration decreases from 30060 mg/m^3 to 19880 mg/m^3, whereas the NO_x concentration increase up to 1277.05 ppm which was just 0 ppm at theoretical air supply. The feasibility on carbon capture will decrese with decresed CO_2 % and same is true with FGD for SO_2 removal. In this study, where F1 grade coal used at a feed rate of 150000 kg per hour, approximately 17% excess air is used for minimization of major air pollutants concentrations in stack emission.

.

5. REFERENCES

[1] B. K. Sharma, K. K. Sharma, Narendra Singh, Rajesh Kumar, 2017, "CO_2 Base line data base for Indian power sector", user guide, version 12, Central Electricity Authority, India, www.cea.nic.in, May.

[2] Coal India Limited, 1993, "Coal atlas of India", Central Mine Planning &Defense Institute (CMPDI), Ranchi-834008.

[3] Ministry of Environment, Forest and Climate Change, Government of India, 2015, "Environmental (Protection) Amendment Rules, 2015", www.moef.nic.in .

[4] Moti L. Mittal, Chhemendra Sharma, and Richa Singh, 2010, "Estimates of Emissions from Coal Fired Thermal Power Plants in India".

[5] Zeldovich, J., 1946 "The oxidation of Nitrogen in Combustion and Explosions", ActaPhysicochimica URSS, 21, 557.

[6] Hanby, V.I., 1994, "Combustion and Pollution Control in Heating Systems", Springer-Verlag.

[7] Central Institute of Mining and Fuel Research (CIMFR), Jharkhand, India, "Elemental analysis of D, E, and F grade coal" (personal communication).

SEEC-2018-134

Clean and Green Energy from Gravitational Forces – A Novel Approach

Anasuya Nagaraju[a], SasidharJangam[a, b,]
[a] SLNS Renewable Energy Technology Pvt Ltd, Bangalore 560017, INDIA
[b]Department of Mechanical Engineering, Faculty of Engineering, Christ University, Bangalore 560074, INDIA

Abstract

The energy demand between 2012 and 2040 is expected to grow nearly half worldwide. The Energy Information Administration (EIA) expects developed countries demand will rise 18% while for the developing countries (India, South Africa, South East Asian Countries, etc.) demand jumps 71%. But this increase in clean energy demand can't be met with the conventional energy sources as they are not only non renewable but also pollutant. Because of this reason the demand for the clean energy technologies is increasing rapidly. The majority of the conventional energy sources (fossil fuels) are pollutant and exhaustible. On the other side the renewable energy sources like solar energy, wind energy, biomass, etc., are non-pollutant and abundantly available but the efficiency is quite low when compared to the conventional energy sources because they are seasonal and partial.

To meet the world's energy demand, there is a massive demand for the new renewable energy technologies. These new renewable sources of energies should be abundantly available for all the seasons round the clock throughout the calendar. Our new renewable energy technology (Indian Patent No: 2017 4 1 037588) makes use of gravitational energy to generate electricity with basic mechanical, hydraulic and electrical principles. This new renewable technology is not only simple, eco-friendly (absolute zero pollutants) but also scalable.

Acknowledgements

Key Words

Renewable Energy, Non-Renewable Energy, Gravitational Forces.

***Corresponding Author: SasidharJangam, Tel: +91 888 4639 888.
  E-mail address: sasidhar.jangam@gmail.com
  Category: Oral presentation

SEEC-2018-135

LPG COMBUSTION PHASE CONTROL IN LEAN STRATIFIED SPARK IGNITION ENGINE

Sanguk, Lee	**Sangjae, Park**	**Choongsik, Bae**
Department of Mechanical Engineering	Department of Mechanical Engineering	Department of Mechanical Engineering
KAIST, KOREA	KAIST, KOREA	KAIST, KOREA
Email: sulee@kaist.ac.kr	Email: psangj9@kaist.ac.kr	Email: csbae@kaist.ac.kr

ABSTRACT

The emission regulation for transportation industry is becoming stricter especially in automobile industry due to the increased concerns of air pollution. To satisfy this strict regulation, Researchers who involved in engine field are trying to improve the emission characteristics. Most of them are not only focused on the catalyst systems, but also on the in-cylinder combustion technique. This research adopted the lean stratified combustion mode which has a high potential of low fuel consumption. Although lean stratified combustion can catch the high fuel economy, the emission problem can be happened especially on Particulate Matter(PM) emission. To avoid this PM emission, air and fuel mixture should be ignited after proper mixing time. However, if the mixing time is increased too much, combustion stability was decreased and, maximum Heat Release Rate (HRR) is decreased. Due to these reasons, combustion phase is located very advanced position. Therefore, the objection of this research is that locate the combustion phase in proper position without deterioration of combustion stability and emission characteristic. To reach this objection, this paper applied the intake air control strategy. The results showed that the in-cylinder ambient pressure affects the combustion phase location and its maximum value of HRR. The main reason of this effect was come from the level of the in-cylinder charge density.

***Keywords*:**   Internal Combustion Engine, Lean Stratified Combustion, LPG, Charge Density, Combustion Phase,

NOMENCLATURE

CAD	Crank Angle Degree
IMEP	Indicated Mean Effective Pressure
BTDC	**Before Top Dead Center**
BBDC	**Before Bottom Dead Center**
ATDC	**After Top Dead Center**
AFR	**Air to Fuel Ratio**
SI	**Spark Ignition**
CA50	**Crank Angle Degree with 50% mass burn**
LPG	**Liquefied Petroleum Gas**

INTRODUCTION

Recently, the fine dust problem has been issued since not only due to the air pollution concerns but also to decreased visible distance issue. Globally, there are many regulations for the vehicle emission to keep the clean atmosphere state or to make it better. The regulations are still continuously becoming stricter than those before. To satisfy the harsh emission regulations, novel combustion modes have been appeared since early stage of this. The one possible technique is lean stratified combustion mode that is able to operate with high fuel economy[1]. High fuel economy is achieved with Wide Open Throttle (WOT) operation. Conventional SI engine mostly control the air quantity to ignite the flame in the condition of stoichiometric AFR because the fuel quantity is determined with respect to air quantity. Due to this throttle valve intervention in intake

air flow, pumping loss is bigger than WOT operation condition. In the other hand, lean stratified combustion engine does not control the intake air quantity. It means that there is no throttle valve intervention in intake air flow. The difference between conventional combustion mode and lean stratified combustion is the level of fuel distribution. Conventional combustion mode in SI engine is homogeneous combustion which is the fuel and air are mixed with high homogeneity. However, in case of lean stratified combustion mode, the fuel and air distribution has not high homogeneity but high stratification. In detail, flammable fuel and air mixture is formed near the spark plug in the state of rich mixture. In contrast, most of lean mixtures are located in-cylinder everywhere except near the spark plug. Therefore, Flame kernel is created by the spark ignition, and subsequently, the flame propagates from rich mixture to lean mixture. As mentioned before, the biggest reason of high fuel economy is small pumping loss with WOR operation. Despite the high fuel economy, the combustion phase of lean stratified combustion mode is largely advanced compare to ideal combustion phase. If ignition was made on more retarded time than usual, the fuel will be dissipated more than before. Eventually, Total amount of fuel which is participate in combustion will decreased as retardation of the ignition timing. Additionally, the form of spray is important in lean stratified combustion mode. The retardation of fuel injection will decrease the combustion stability due to the high in-cylinder flow and pressure. With these reasons, combustion phase is located in more advanced location than ideal case. This paper aim to modify the combustion phase to theoretically ideal location about 0 -10 CAD ATDC. Typically, CA50 could be interpreted as a location of combustion phase, and intake air control strategy was applied to control the CA50 location. Mostly, lean stratified combustion is adopted in low-load condition. because the vehicle already equipped with the throttle valve for high-load condition, so that it could be strategic solution with an economic approach.

METHODOLOGY

FUEL

In this research, n-butane was selected as an experimental fuel. The most important reason of choice is that n-butane have higher vapor pressure than gasoline. Lean stratified combustion mode has limit of short mixing time between fuel and air and it causes the PM emission problem. Therefore, n-butane was chosen as a fuel because this fuel can be easily vaporized. Secondly, n-butane has high heat of vaporization feature. This advantage could be worked as one way to decrease the NO_X emission. When n-butane injected in-cylinder, it immediately vaporized and caused the charge cooling effect. It can bring the drop of combustion temperature. The drop of temperature can be interpreted as an improvement of NO_X emission characteristic. Lastly, n-

butane has lower contents of carbon. Because n-butane has only four carbon atoms in a molecule, it has less C-C bond compared to gasoline. The lower contents of carbon imply the possibility of CO_2 emission decrement.

EXPERIMENTAL SETUP

To check the throttle operation effects in lean stratified combustion engine, engine performance test was conducted in single cylinder research engine. The research engine is SGDISI (Spray-guided Direct Injection Spark Ignition) engine. The spark plug was able to install from base location to 4mm more deeper place in direction of center of chamber to compensate for the spray contraction effect[2]. In case of injector, outwardly opening piezo injector installed in the center of engine head. The compression ratio of research engine is 12:1 and, bore x stroke is 85mm x 88mm respectively. Measurement for combustion phenomenon was done by pressure data which was detected by pressure sensor (6052c) made by KISTLER. Data acquisition systems were composed of personal DAQ 3000 board and DASY LAB software. To figure out the emission characteristics, exhaust gas analyzer (Horiba's MEXA 1500d) was installed at the exhaust pipe, furthermore, particulate mass (AVL's SMOKE meter) meter was installed. The engine controller (ZB-00-13, Zenobalti. Co) was used to control the injection and spark timing in response to detected signal by 1800ppr (pulse per revolution) encoder. More detail specification of the engine and system configurations are described in Table 1

TABLE 1 : RESEARCH ENGINE SPECIFICATION

| Single-Cylinder IC research engine specification	
Bore x Stroke	85 x 88 [mm]
Compression Ratio	12 : 1
Engine Type	Spray guided Direct Injection SI
Spark Plug	Base – 4mm (possible to change)
Intake Valve	11ATDC
Exhaust Valve	34 BBDC – 10 ATDC
Injector	Outwardly opening piezo injector

RESULT

To find out the intake air control strategy effect, the value of air excess ratio was swept from 2.6 to 1.5. Injection timing was swept from 46 – 32CAD BTDC and, ignition timing was adopted depend on the injection timing condition.

The HRR and in-cylinder pressure results are depicted in FIGURE 1. In FIGURE 1, all cases have same injection and ignition timing. As the lambda decreased, in-cylinder pressure and maximum HRR were decreased. These phenomena can be interpreted as an effect of the low charge density. The case of lower air-excess ratio has lower amount

of air in cylinder. In other words, within the same compression ratio, in-cylinder ambient pressure will drop. Therefore, the combustion will start at lower ambient pressure condition than the case of higher air-excess ratio. The flame propagation speed was decreased as ambient pressure decrease. It affects the decrement of maximum HRR value. However, even though the total HRR was decrease, actual work conversion was increased due to the retardation of combustion phase location.
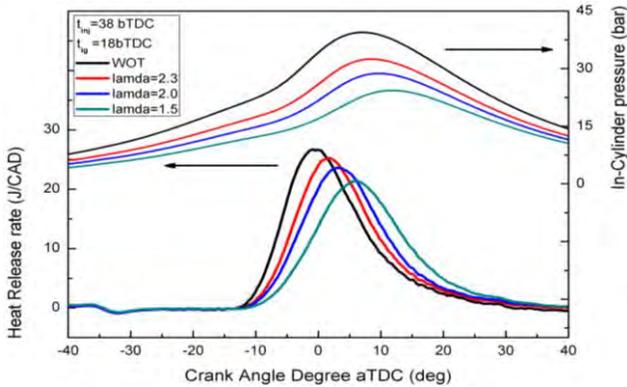
FIGURE 1. HEAT RELEASE AND IN-CYLINDER PRESSURE WITH DIFFERENT AIR-EXCESS RATIO
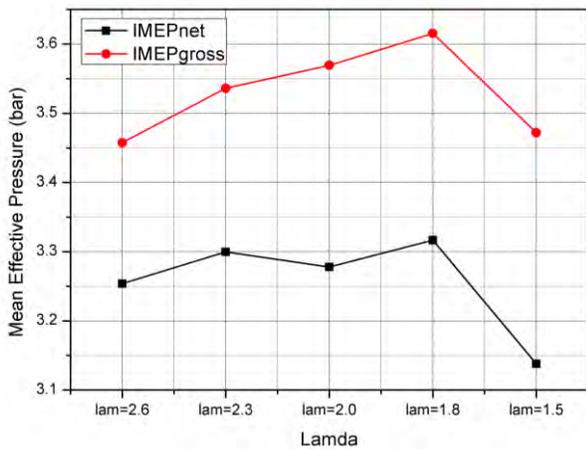
FIGURE 2. MAXIMUM IMEP & GMEP IN EACH CASE

As the inhaled-air reduced, the maximum HRR was continuously decreased due to the low charge density effect. On the other hand, $IMEP_{net}$ and $IMEP_{gross}$ show the increasing trend as decreased air-excess ratio until the value of 1.8. These phenomena were happened due to the combustion phase optimization. In case of high air-excess ratio, bigger portion of combustion was generated than lower air-excess ratio case in compression stroke process.

Therefore, there were many negative work than that of lower air-excess ratio case. Despite of the big increasing gradient in $IMEP_{gross}$ graph in FIGURE 2, the actual $IMEP_{net}$ increasing gradient is not that big. This gradient difference comes from the pumping loss increment. If more intake air restriction was applied in intake air flow, the pumping loss will continuously increase. After the case of air-excess ratio 1.8, both $IMEP_{net}$ and $IMEP_{gross}$ was dropped dramatically. This is the worst case of scenario because the maximum HRR was deteriorated too much, and also combustion phase was located too much retard position. Additionally, pumping work is maximized than the other case.

CONCLUSION

This research was conducted to control the combustion phase location in lean stratified combustion engine. The intake air quantity control strategy was adopted by controlling the throttle valve angle. The key conclusion is followed:

1. The combustion phase is located at the retarded position as decrease the air-excess ratio. Due to the decrement of charge density, combustion start at the lower ambient pressure, and flame propagation speed is decreased. Therefore, the location of combustion phase is retarded.

2. As air excess ratio keep decreased, the maximum HRR is decreased. However, $IMEP_{net}$ and $IMEP_{gross}$ showed increasing trend. This is the effect of combustion phase optimization, but the gradient is different. The reason of difference comes from the existence of pumping work.

In this paper, we find out the possibility of combustion phase change by doing only intake air quantity control. With this finding, we planned to apply the Late Intake Valve Closing (LIVC) system in leans stratified combustion mode because LIVC can decrease the charge level without the pumping work.

REFERENCES

[1] Internal Combustion Engine Fundamentals, International Edition, Automotive Technology Series, McGRAW-HILL, John B. Heywood, Chap. 3, 37-40
[2] ILASS-Asia, 2017, Spray distortion effect on particulate emission in stratified combustion of n-butane, S.Park et al, See also ILASS-Asia 2017

STUDY OF NOZZLE WITH DIFFERENT NPR AND THEIR EFFECT ON IR SIGNATURES

Bhanu Mahesh
Aerospace Engineering Department
Indian Institute of Technology-Kharagpur
bhanumahesh1993@iitkgp.ac.in

Awanish Pratap Singh
Aerospace Engineering Department
Indian Institute of Technology-Kharagpur
awanishsingh009@iitkgp.ac.in

Dr. Ratan Joarder
Aerospace Engineering Department
Indian Institute of Technology-Kharagpur
jratan@aero.iitkgp.ernet.in

ABSTRACT

Many of the Super Power Nations consider stealth technology as the technological leap for the nation in defense and is useful during the warfare. Aircrafts are detected by Radar (or RCS), IR Signature, Visual and aural means. Detection of aircraft, by means of IR signature had been an immense threat since the development of the Man-portable air-defense system (MANPADS). Reducing the IR signature directly affects the Survivability of the aircraft in warfare. IR Signature mostly depends on nozzle shape and atmospheric conditions, where the study of different nozzle shapes and curvatures has been already performed in the past. The study remains critical and important with respect to different Nozzle Pressure Ratios (NPR). To calculate the IR signature, the temperature and species concentration were calculated at known pressure conditions. Finally, the Lock-on range will be calculated for different NPR.

Keywords: IR Signature, Exhaust Plume, Species concentration, Nozzle Pressure Ratio, Lock-on Range.
.

NOMENCLATURE

RCS	Radar Cross Section
IR	Infrared
NPR	Nozzle Pressure Ratio
SAM	Surface to Air missiles
K_b	Boltzmann constant
UAV	Unmanned Aerial Vehicle
η	Wavenumber

INTRODUCTION

During the World War-2, the use of aircraft tracking and detection has been an essential requirement to survive in the hostile regions, which later causes the technological advancements such as the stealth capabilities of Aircraft's and IR Signature detection [1,2]. The development of portable IR seeker with modern detector has made it easier to detect aircraft and rotorcraft flying at low altitudes [3]. Survivability is an important aspect of warfare because aircraft/helicopters are crucial to mission objectives. Therefore, to improve the survivability of aircraft, the development of technologies to reduce the susceptibility related IR signals of aircraft remains critical. Consequently, IR signature analysis is important to increase aircraft/helicopter survivability.

As the aircraft itself is an intrinsic source of IR energy, and due to the reasonably good propagation of IR signature, it clearly indicates the potential threat by even relatively simple, accurate short-range missile guidance. Moreover, due to that, the majority of aircraft/helicopters lost in tactical warfare have been destroyed by heat-seeking missiles. Further, passive detection and tracking are tactically superior to active, for comparable detection range. With increasing sensitivities of IR detectors, analysis of passively emitted IR signatures has emerged as an important component of stealth technology [4].

Modern military aircraft, despite the efforts of their designers, are abundant sources of IR energy. The principal heat source is the propulsion system, as jet engines have an

efficiency far below 100%, a considerable amount of energy is thrown away, advertising the aircraft's position [5]. The IR signatures of an aircraft are generated by the engine/nozzle, heating due to the exhaust gas, aerodynamic surface heating, surface emission, anti-icing and de-icing systems, and reflection of the sun and the moon [6,7]. However, the most intense IR source in an aircraft is the tailpipe (afterburner off).

The IR spectrum covers the range, 0.77–1000 μm; i.e., between the visible and microwave radiation. However, mainly two atmospheric windows where the transmittance is high, 3–5 and 8–12 μm, are used for surveillance and tracking respectively. Outside these windows, attenuation of IR is high, due to the role of CO_2 and H_2O (vapor) in absorption and scattering [8]. The 3–5 μm window corresponds to higher peak emission temperature (~ 723.15 K), and is better suited for detecting hot spots. The 8–12μm band has lower peak emission temperature (~290.15 K), and is generally used for emissions from larger surfaces at lower temperatures [9].

IR signature is generally reduced in order to increase the survivability of the aircraft; the present study will show the effects of nozzle pressure ratio and examine the IR signature and Lock-on range. This study was performed by using commercial software Ansys Fluent. The density-based Navier-Stokes equation was used, the thermal flow field and the distribution of chemical species within a plume, which are essential for the analysis of IR signatures, were calculated.

The study has been performed to reduce aircraft plume IR signatures, Thompson and Birk [10] published a test report that investigated how an IR suppressor affected the infrared signatures generated by exhaust gas. Decher [11] analyzed the link between the shape of a nozzle outlet and IR signals. Mahulikar et al. [12–17] conducted research quantifying aircraft infrared signatures for numerical calculation, and also examined the effects of atmospheric transmission and radiance on aircraft infrared signatures. However, as per author's knowledge, previous studies have mostly been based on fixed nozzle pressure ratios, without altitude change effects, on the conventional circular nozzle shape and associated simplified plume model. Detailed analyses of IR signatures based on the thermal flow field information obtained with accurate CFD method for various NPR was studied.

METHODOLOGY

To analyze the characteristics of the thermal flow fields at the rear side of the engine, the nozzle parameters were taken from [3]. In the present study, a convergent nozzle for a jet engine of UAV cruising at Mach 0.8 was considered. The nozzle inlet area (A_i) is 0.18232m², the outlet area (A_0) is 0.12617 m² and the length of the nozzle (L) is 0.964m. The mass flow rate (ṁ) at the nozzle inlet is 17.19 kg/s and

the specific heat ratio (ϒ) is 1.3477 for the combustion gases. The static pressure (P), static temperature (T) and the Mach number at the nozzle inlet is 104740Pa, 629.86K and 0.4454 respectively.

The nozzle inlet and outlet cross-section were created circular in shape, and the flow generated by high-pressure, high-temperature gases consist of various complicated flow features and their interaction like shocks and expansion waves, wall boundary layers were generated. To capture the nozzle exhaust flows effectively the domain was set to 30 and 50 times of the diameter of the nozzle inlet (D_i) in the radial and axial directions respectively. The no-slip flow condition with adiabatic thermal boundary condition was applied to the nozzle wall. Later, the pressure inlet boundary condition was maintained as per engine parameters, while, the pressure outlet boundary condition was maintained according to atmospheric pressure at the corresponding altitude as shown in Fig.1. In this study, engine parameter was kept fixed where the altitude was changed, to change the outlet atmospheric pressure and temperature which results in a change in NPR at International Standard Atmosphere (ISA); an in-house MATLAB code was written to show this variation and also use it for further analysis, which is shown in Fig.2.

A two-dimensional structured computational grid of 37,014 nodes was used. The species concentration for this study was used similar to the An et al. [3] and was set according to the Fig.1, and the flow fields were captured in the 2-D simulation in Ansys Fluent. Jet-A fuel $(C_{11}H_{22})$ with complete combustion was used with a mole fraction, at the nozzle inlet, consisting of N_2-74%, H_2O-13% and CO_2-13%. The results for the nozzle exhaust plume have been solved in the Ansys Fluent using a standard k-ε turbulence model [18], which is known suitable for jet flows, with valid turbulence intensity parameters and the Fick's Law was used to calculate the mass diffusion of chemical species.
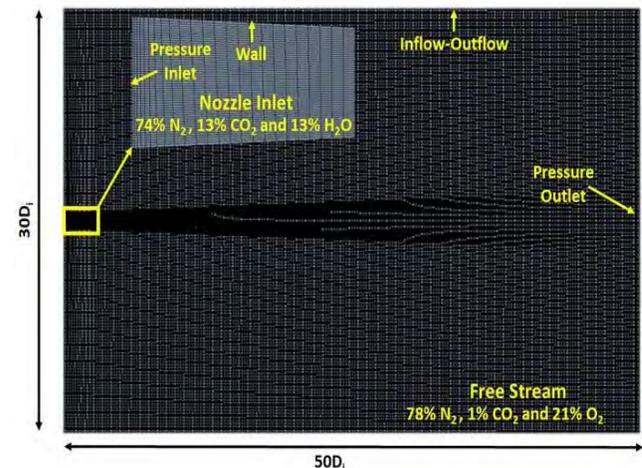

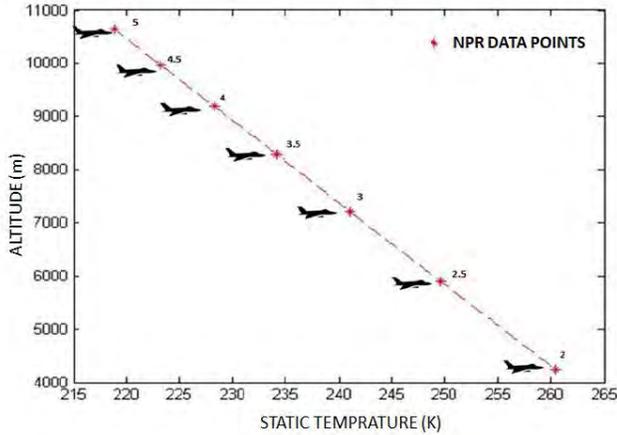**FIGURE 1.** NUMERICAL BOUNDARY CONDITIONS

FIGURE 2. CHANGE IN NPR WITH ALTITUDE

RESULTS AND DISCUSSION

A verification study was performed with Ref. [3] to check the accuracy of the present computational work by following the validation and verification study described by Ref. [19]. In Fig.3 (a) it can be seen that NPR of 2.5 is giving the similar result as it was performed by Ref. [3].

The computational results for the circular nozzle of an aircraft cruising at a speed of Mach 0.8 at different altitude were performed. It can be seen in Fig 3(a) and 3(b) that average temperature at the exit of the nozzle is reducing with an increase in NPR. The average reduction in temperature at the nozzle exit was observed due to less atmospheric temperature and presence of shock diamonds. Due to series of shock diamonds at higher NPR, the free-stream flow gets disturbs due to the presence of higher pressure gradient, which helps in mixing of exhaust jet flow with surrounding cold atmospheric air. The species concentration of CO_2, which is the main source of IR signature, is also calculated along the centreline of the nozzle exhaust. From Fig.4 it can be stated that the concentration of CO_2 in the exhaust gas is reduced after a certain length, where it is also shown that for lower NPR, CO_2 concentration was reducing earlier than higher NPR's. These results of thermal flow field analysis of exhaust gas will be further used for the calculation of IR Signature and subsequently the lock-on range R_{LO}.

CALCULATION OF IR SIGNATURE AND LOCK-ON RANGE

The radiative heat transfer equation (RTE) which governs the radiation intensity I_η for a medium at any position $\vec{r}$ along a path $\vec{s}$ through an absorbing and emitting medium is given by [20,21]

$$\frac{d I_\eta (\vec{r},\vec{s})}{dx} = -k_{a,\eta} I_\eta (\vec{r},\vec{s}) + k_{a,\eta} I_{b,\eta} (\vec{r}) \qquad (1)$$

Where, scattering is neglected in this study. In the above equation $k_{a,\eta}$ is absorption coefficient at wavenumber η.
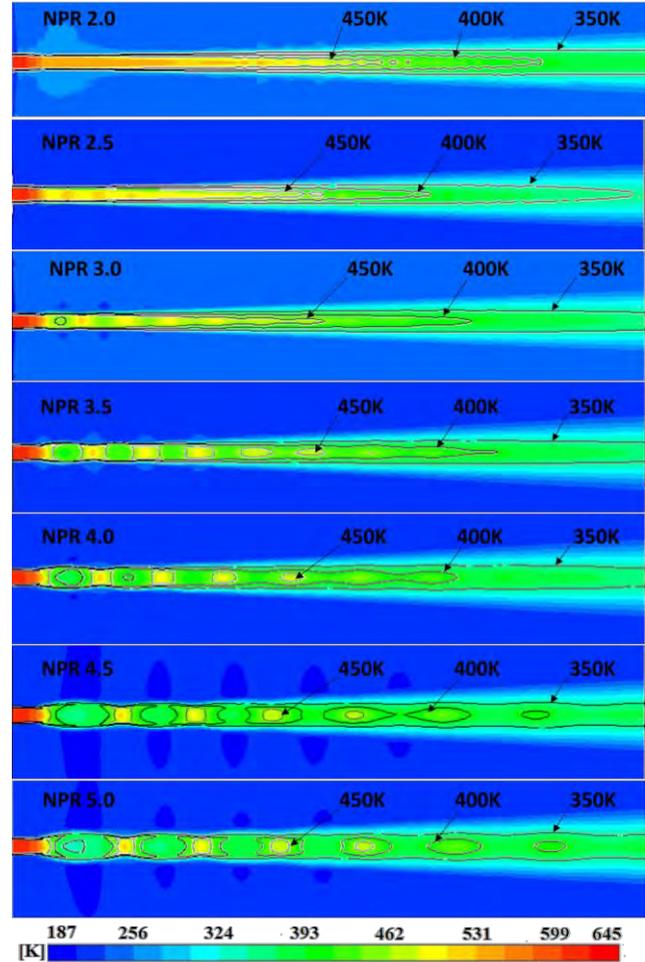
(a)
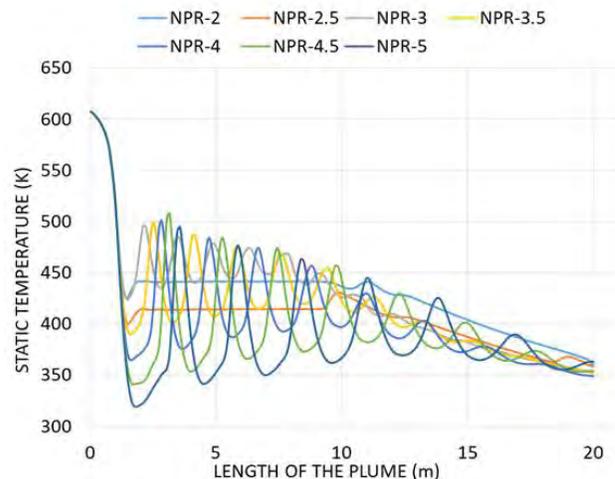
(b)

FIGURE 3. (a) TEMPERATURE CONTOUR, **(b)** TEMPERATURE VARIATION ALONG THE CENTER-LINE, OF EXHAUST PLUME AT DIFFERENT NPR.
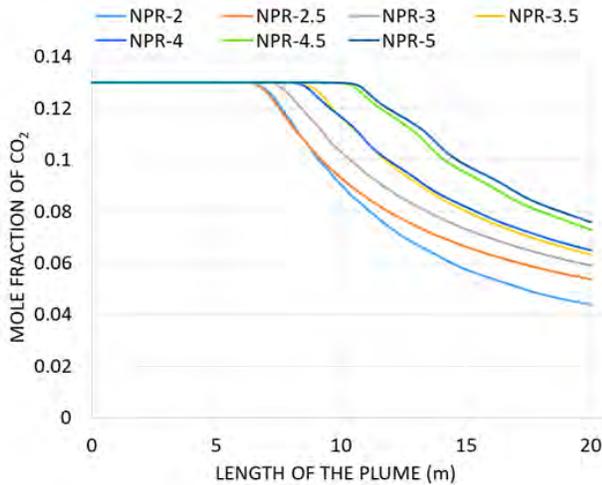
FIGURE 4. VARIATION OF MOLE FRACTION ALONG THE CENTER-LINE, OF EXHAUST PLUME AT DIFFERENT NPR.

The lock on range is given by

$$R_{lo}^2 = \frac{I_\eta \ \tau_a}{\left(\frac{S}{N}\right).NEI} \qquad (2)$$

Where, τ_a is the atmospheric transmission efficiency, (S/N) is Signal to Noise Ratio and NEI is Noise Equivalence Irradiance of a typical seeker missile.

SUMMARY AND CONCLUSION

This study is intended to calculate the IR Signature and Lock-on range with change in altitude at different NPR (2 to 5). Generally, IR signature depends on temperature, species concentration, and pressure. To calculate the IR signature, the temperature and species concentration was calculated at known pressure conditions, which later will be used to calculate Lock-on range, which will be presented in the final version of the paper or during the conference.

REFERENCES

[1] F. Simmons, Rocket Exhaust Plume Phenomenology, American Institute of Aeronautics and Astronautics, Inc., Washington, DC, 2000.

[2] J. Richard D. Hudson, Infrared System Engineering, 2006.

[3] C.H. An, D.W. Kang, S.T. Baek, R.S. Myong, W.C. Kim, S.M. Choi, Analysis of Plume Infrared Signatures of S-Shaped Nozzle Configurations of Aerial Vehicle, J. Aircr. 53 (2016) 1768–1778.

[4] G.A. Mahulikar, S.P., Sonawane, H.R., and Rao, Infrared Signature Studies of Aerospace Vehicles, Prog. Aerosp. Sci. 43 (2007) 218–245.

[5] C. Kopp, Heat-Seeking Missile Guidance, Aust. Aviat. (1982).

[6] D. Howe, Introduction to basic technology of Stealth aircraft: Part 1-Basic considerations and Aircraft Self-Emitted Signals, J. Eng. Gas Turbine Power. 113 (1991) 629–641.

[7] G.A. Rao, S.P. Mahulikar, Integrated review of stealth technology and its role in airpower, Aeronaut. J. 106 (2002) 629–642.

[8] G. DA Burch DE, Laboratory measurment of the Infrared absorption by H2O and CO2 in regions of weak absorption, SPIE - Int. Soc. Opt. Eng. 142 (1978) 16–24.

[9] S.P. Mahulikar, S.K. Sane, U.N. Gaitonde, A.G. Marathe, Numerical studies of infrared signature levels of complete aircraft, Aeronaut. J. 105 (2001) 185–192.

[10] J. Thompson, A.M. Birk, M. Cunningham, Design of Infrared Signature suppressor for the Bell 205(UH-1H) Helicopter Part 1 : Aerothermal Design", in: Proc. 46th Annu. Can. Aeronaut. Sp. Inst. Conf., 1999.

[11] R. Decher, Infrared emissions from turbofans with high aspect ratio nozzles, J. Aircr. 18 (1981) 1025–1031.

[12] A. Rao, S. Mahulikar, Aircraft Powerplant and Plume Infrared Signature Modelling and Analysis, in: 43rd AIAA Aerosp. Sci. Meet. Exhib., American Institute of Aeronautics and Astronautics, Reston, Virigina, 2005.

[13] S.P. Mahulikar, P.S. Kolhe, A.G. Rao, Skin-Temperature Prediction of Aircraft Rear Fuselage with Multimode Thermal Model, J. Thermophys. Heat Transf. 19 (2005) 114–124.

[14] G.A. Rao, S.P. Mahulikar, New criterion for aircraft susceptibility to infrared guided missiles, Aerosp. Sci. Technol. 9 (2005) 701–712.

[15] A.G. Rao, S.P. Mahulikar, Effect of Atmospheric Transmission and Radiance on Aircraft Infared Signatures, J. Aircr. 42 (2005) 1046–1054.

[16] S.P. Mahulikar, A.G. Rao, P.S. Kolhe, Infrared Signatures of Low-Flying Aircraft and Their Rear Fuselage Skin's Emissivity Optimization, J. Aircr. 43 (2006) 226–232.

[17] S.P. Mahulikar, G.A. Rao, S.K. Sane, A.G. Marathe, Aircraft plume infrared signature in nonafterburning mode, J. Thermophys. Heat Transf. 19 (2005) 413–415.

[18] D.C. Wilcox, Turbulence Modeling for CFD, 3rd ed., D C W Industries, 2006.

[19] W.L. Oberkampf, T.G. Trucano, Verification and validation in computational fluid dynamics, Prog. Aerosp. Sci. 38 (2002) 209–272.

[20] R. Joarder, G.C. Gebel, T. Mosbach, Two-dimensional numerical simulation of a decaying laser spark in air with radiation loss, Int. J. Heat Mass Transf. 63 (2013) 284–300.

[21] A.P. Singh, U.P. Padhi, H. Tummalapalli, R. Joarder, Investigations on Ignition of Atomized Fuel-Air Mixtures and Liquid Fuel Column-air Combinations by Low Energy Laser Pulses, in: Asia-Pacific Conf. Combust., The Combustion Institute, Sydney, 2017.

INFLUENCE OF CONCENTRATION AND TEMPERATURE ON TRANSPORT PROPERTIES IN

CATION-EXCHANGE MEMBRANE

Fasil Qayoom Mir
Department of Chemical Engineering,
National Institute of Technology Srinagar,
Srinagar-190006, Jammu & Kashmir, India
Email: mirfasil@nitsri.net

Babar Ahmad
Department of Mechanical Engineering,
National Institute of Technology Srinagar,
Srinagar-190006, Jammu & Kashmir, India

Anupam Shukla
Department of Chemical Engineering,
Indian Institute of Technology Delhi,
Hauz Khas, New Delhi 110016, India

ABSTRACT

The functional properties, such as electric resistance and limiting current of homogeneous Selemion CMV cation exchange was measured. A four-probe electrode system was used in a two-compartment cell to measure electric resistance of CMV membrane in aqueous NaCl solutions of two different concentrations (0.017 and 0.1M) at two temperatures (25 and 32 °C) using impedance spectroscopy. Electric resistance of the membrane increased with decrease in both the salt concentration and temperature. A small increase in temperature (7 °C) reduced resistance by about half indicating that selection of appropriate temperature can result in substantial saving in energy required. Limiting current was obtained from I-V curves using multi-step chronoamperometry and linear sweep voltammetry at three different temperatures (25, 35, 45 °C) in 0.1 M NaCl. I_{lim} values obtained from I-V curves were close to the values (less than 10% difference) obtained from LSV. I_{lim} increased by 79% on increasing temperature by 20 °C. Transition time was measured using chronopotentiometry in 0.1 M NaCl solution at three different temperatures (25, 35, and 45 °C) in the six compartment cell. Transition time also increased on increasing temperature. The average transition time were found to be 7.48, 9.99 and 13.05 at 25, 35, 45 °C when 20 mA/cm^2 current densities was applied in 0.10 M NaCl. The increase in transition time also supports increase in conductivity of diffusion boundary layer at membrane.

Keywords: Ion-exchange membrane, Electric resistance, Transition time
.

INTRODUCTION

CMV membrane is a reinforced, standard grade membrane with low resistance and high selectivity, used commonly for concentration or desalination purposes. Homogeneous Selemion CMV cation exchange membrane (Asahi Glass Co., Japan) was used for determining important functional properties of membrane such as electric resistance and limiting current. These functional properties have strong influence on the overall performance of processes, like membrane electrolysis, fuel cell [1], diffusion dialysis [2] and electrodialysis in which ion exchange membranes are being used. Some efforts were made about two decades ago to study the membrane resistance at low salt concentrations [3-4]. However, the dominant view believed membrane resistance to be independent of electrolyte concentration and the value obtained at standard concentration [5-11] was used for design of applications. Recent studies report drastic increase in membrane resistance at low salt concentrations [12-14]. In biological fuel cells, sharp increase in resistance of ion exchange membrane is reported [15].

Other properties of membrane are significantly affected at low salt concentration [8, 13].

RESULTS AND DISCUSSION

A four-probe electrode system was used in a two-compartment cell to measure electric resistance of CMV membrane in aqueous NaCl solutions of two different concentrations (0.017 and 0.1M) at two temperatures (25 and 32°C) using impedance spectroscopy. Electric resistance of the membrane, determined from impedance measurement and given in Table 1, increased with decrease in both the salt concentration and temperature.

Table 1 Variation of areal resistance of CMV membrane (in Ω-cm^2) with concentration of NaCl solution and temperature.

Concentration	Areal Resistance (Ω-cm^2)	
(M)	25°C	32°C
0.017	7.08	3.88
0.1	3.10	1.95

A small increase in temperature (7°C) reduced resistance by about half indicating that selection of appropriate temperature can result in substantial saving in energy required. limting current (I_{lim}) was obtained from I-V curves using multi-step chronoamperometry at three different temperatures (25, 35, 45°C) in 0.1 M NaCl. I_{lim} was also measured using linear sweep voltammetry (LSV) at same conditions. Fig. 1 shows the I-V and LSV curves in 0.1 M NaCl solution at three temperatures (25, 35 and 45°C). I_{lim} values obtained from I-V curves were close to the values (less than 10% difference) obtained from LSV. I_{lim} increased by 79% on increasing temperature by 20°C. Transition time was measured using chronopotentiometry in 0.1 M NaCl solution at three different temperatures (25, 35, and 45°C) in the six compartment cell where the test membrane was isolated from the electrode processes. Transition time also increased on increasing temperature shown in Fig. 2. The average transition time obtained were 7.48, 9.99 and 13.05 at 25, 35, 45 °C when 20 mA/cm^2 current densities was applied in 0.10 M NaCl. The increase

in transition time also supports increase in conductivity of diffusion boundary layer at membrane.

Since I_{lim} is the maximum current at which process can be operated, appropriately elevated temperature can reduce both the size of the equipment (since I_{lim} increases) and the energy requirement (lower electric resistance) for operations using ion exchange membrane at low ionic concentration. I_{lim} and transition time increased on increasing temperature which indicated that operation at elevated temperature can be done at higher current densities and could be used to balance the negative effect of lower ionic concentration.

(a)

(b)
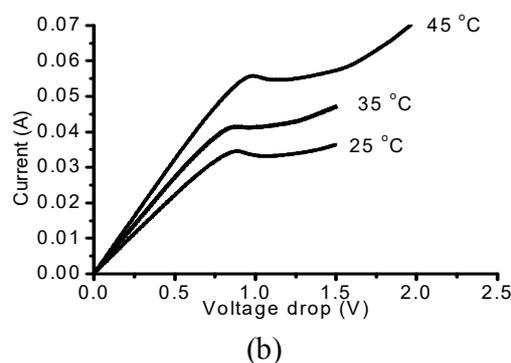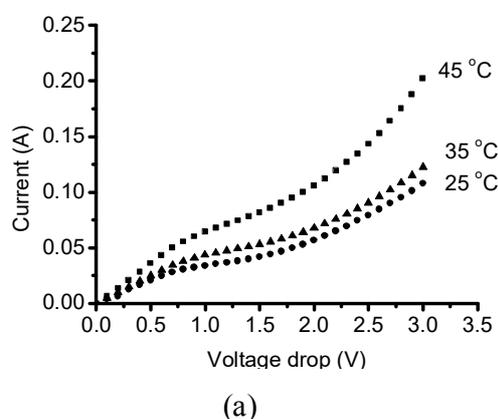
Fig.1 Effect of temperature on (a) current-voltage curves and (b) LSV curves for CMV membrane in 0.10 M NaCl.
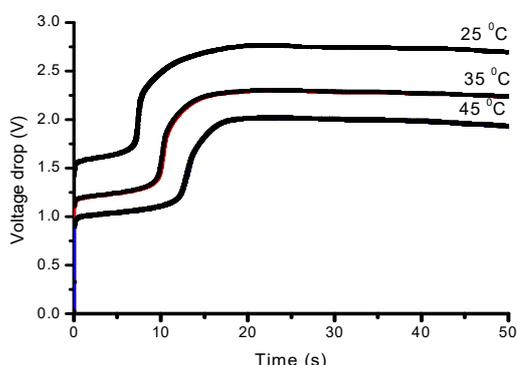
Fig.2 Chronopotentiometeric curves for CMV membrane at 20.23 mA/cm^2 applied current densities in 0.10 M NaCl.

CONCLUSION

Impedance measurement showed that electric resistance of CMV membrane reduced by half on small increase (7°C) in temperature in low concentration (0.017 M) NaCl solution increased with decrease in both the salt concentration and temperature. Thus selection of appropriate temperature can result in substantial saving in energy required. I$_{lim}$ values obtained from current voltage curves were close to the values obtained from LSV. I$_{lim}$ and transition time increased on increasing temperature which indicated that operation at elevated temperature can be done at higher current densities and could be used to balance the negative effect of lower ionic concentration.

REFERENCES

1. G.G. Scherer, Ber. Bunsenges. Phys. Chem. **94** (1990) 1008-1014.
2. Y. Kobuchi, H. Motomura, Y. Noma and F. Hanada, J. Membr. Sci. **27** (1986) 173-179.
3. V.I. Zabolotsky, V.V. Nikonenko, J. Mem. Sci. **79** (1993) 181–198.
4. K. Urano, Y. Masaki, M. Kawabata, Desalination **58** (1986) 171–176.
5. J.W. Post, J. Veerman, H.V.M. Hamelers, G.J.W. Euverink, S.J. Metz, K.Nymeijer, C.J.N. Buisman, J. Mem. Sci. **288** (2007) 218–230.
6. F. Suda, T. Matsuo, D. Ushioda, Energy **32** (2007) 165–173.
7. P. Dlugolecki, K. Nijmeijer, S. Metz, M. Wessling, J. Mem. Sci. **319** (2008) 214–222.
8. J. Veerman, J.W. Post, M. Saakes, S.J. Metz, G.J. Harmsen, J. Mem. Sci. **310** (2008) 418–430.
9. M. Turek, B. Bandura, P. Dydo, Desalination **221** (2008) 462–466.
10. J.N. Weinstein, F.B.J.W. Leitz, Science **191** (1976) 557–55.
11. P. Długołecki, B. Anet, S. Metz, K. Nijmeijer, M. Wessling, J. Membr. Sci. **346 (1)** (2010**)** 163−171.
12. S. M. Hosseini, S. S. Madeaeni, A. R. Khodabakhshi, Sep. Sci. Technol. **47** (2012) 455−462.
13. G. M. Geise, D. R. Paul, B. D. Freeman, Prog. Polym. Sci. (2013) DOI: 10.1016/j.progpolymsci.2013.07.001.
14. F. Harnisch, U. Schroder, F. Scholz, Environ. Sci. Technol. **42** (2008) 1740–1746.
15. F.G. Wilhelm, N.F.A. van der Vegt, M. Wessling, H. Strathmann, J. Electroanal. Chem. **502** (2001) 152–166.

SEEC-2018-138

Production of carbon nanostructures in coal char, oil and gases from low and medium rank Indian coals via microwave assisted pyrolysis using Fe as susceptors

B. Rajasekhar Reddy
Department of Chemical Engineering
Ph.D. Scholar
Email: rajasekharreddy104@gmail.com

R. Vinu
Department of Chemical Engineering
Associate Professor
Email: vinu@iitm.ac.in

ABSTRACT

In this study, the production of nanostructured char from low and medium rank Indian coals is demonstrated via microwave assisted pyrolysis by using iron (Fe) particles as susceptor. The experiments were performed in a bench scale pyrolysis reactor at 560W and 420W microwave power up to a temperature of 800 ^{0}C. The effect of coal:susceptor composition on the quality of biochar was evaluated using a range of characterization techniques like scanning electron microscopy, transmission electron microscopy, porosimetry, X-ray diffraction and Raman spectroscopy. The addition of Fe as the susceptor resulted in formation of nanoparticles and nanotubes of average diameter in the range of 30-120 nm and 20-50 nm, respectively. Microwave pyrolysis produced different carbon shell morphologies including nanotubes, nanoflakes and amorphous carbon were observed. The biochar obtained by the addition of Fe susceptor was rich in carbon content. Besides coal char, coal-oil and non-condensable gases were also characterized by their composition. The major organic compounds in coal oil included monoaromatics, naphthalene derivatives, polyaromatics, simple phenols and aliphatic hydrocarbons. Pyrolysis gas was rich in H_2 and CO. Thus, microwave pyrolysis is shown to be a promising technique to tailor the morphological features of biochar by using metallic susceptors, and produce good quality of coal oil and gases.

Keywords:

Pyrolysis, microwave, Indian coal, nanotube

REFERENCE

[1] Debalina, B.; Reddy, B.R.; Vinu, R. Production of carbon nanostructures in biochar, bio-oil and gases from bagasse via microwave assisted pyrolysis using Fe and Co as susceptors, J. Anal. Appl. Pyrol. 2017, 124, 310-318.

SEEC-2018-139

EMBODIED ENERGY OF MATERIALS IN BUILDING ENVELOPE FOR SUSTAINABLE BUILDINGS

Smitha J. S.
Department of Civil Engineering,
Pillai HOC College of Engineering
and Technology,
Mumbai University
Email: smitha@mes.ac.in

Dr.Tejaswini D. Nalamutt
Department of Civil Engineering,
Pillai HOC College of Engineering
and Technology,
Mumbai University
Email: ntejaswini@mes.ac.in

Dr.Shrikant Charhate
Department of Civil Engineering,
Pillai HOC College of Engineering
and Technology,
Mumbai University
Email: scharhate@mes.ac.in

ABSTRACT

Sustainable buildings are energy efficient constructions that consume low enery during their construction phase and operational phase. Energy utilised in the construction stage of a building can be measured in terms of Embodied Energy (EE). It depends on the materials selected for construction and is influenced by factors like their manufacturing process, distance of travel between location of manufacture and construction site and the type of fuel used in the whole process. With certain amount of care excercised during the design and planning stages of a building, the energy requirement for construction can be reduced. Knowledge of EE coefficient of various construction materials helps to choose the right materials with low EE in a sustainable construction. In this study EE for different building materials used in masonry work in Mumbai is evaluated and compared. Variation in EE of the building with alternative materials is analysed.

Keywords: Embodied Energy, Process Analysis, Building materials.
.
NOMENCLATURE

Kg   Kilogram
cum   Cubic meter
MJ/Kg Megajoules per Kilogram
MJ/cum Megajoules per cubic meter

INTRODUCTION

Building construction has become inevitable today as it is the primary requirement for any industrial, commercial or residential system. The volume of construction activities taking place in the country, especially in cities is huge. Hence utilization of energy by construction sector is substancial. Unscientific use of energy has caused much harm to the environment and led to problems like energy resource depletion, greenhouse gas emission, climate change and increase in temperature [1,2]. We should become environmentally responsible and adopt sustainable building techniques. The building envelope is the physical separator between the interior and exterior of a building. Changing the design or improving the building envelope of a structure can alter its energy efficiency [3].

The estimation of total energy flow of a building, including direct and indirect energy utilization is termed as Life cycle energy analysis. It includes (i) Embodied energy (EE) (ii) Operational energy (OE) (iii) Maintenance energy and (iv) Demolition energy [4]. Energy utilised for manufacturing process, construction activities and transportation is embedded in the building materials. All energy that goes into making of building materials, its conveyance and construction activities sum up to form the EE of the building [5]. The total energy required for the functioning of the building including heating, lighting and ventilation is called Operational Energy [6]. Energy used for maintenance of the building after construction stage is called Maintenance energy [7]. Energy requirement for demolition and waste disposal of the building at the end of useful life is Demolition energy [4]. In countries like India this need not be considered as there is no system of

demolishing buildings after its intended life period. A lot of research has been carried out in the field of Operational Energy and many innovations were made to lower it. Significance of EE was noticed only recently. Embodied energy of a building is the total energy consumed during the construction stage, including energy for extraction of raw materials, manufacturing process, transportation and erection at site.

Selection of suitable building materials plays an important role in reduction of EE of the structure. Construction in Mumbai is mainly of RCC framed structure with masonry partition walls. There is no suitable replacement for RCC, regarding its structural properties and economic efficiency. So considering RCC as the basic structural component, the different materials available for construction of building envelope may be analyzed. Three common materials used in masonry walls, which are manufactured in Mumbai are selected for this study – bricks, solid concrete blocks and hollow concrete blocks.

METHODOLOGY TO EVALUATE EE

The Embodied Energy calculation is a very complex process and involves tedious calculations. EE is usually expressed in Mega Joules per unit mass or volume of the building material and can be better expressed as a range of values [8]. It's unit is MJ/Kg or MJ/cum [8,9].

Steps in analysing EE

The steps followed for evaluation of EE are:
- Select system boundaries.
- Identify the feasible method for assessment of EE.
- Calculation of Embodied Energy Coefficients of construction materials.

System boundary for the analysis should be defined to understand which processes need to be considered. Cradle-to-Gate, Cradle-to-Grave, Cradle-to-Cradle and Cradle-to-Site are the different system boundaries defined [5]. In this study, the system boundary is taken as Cradle-to-Site, as it takes into account energy consumption from extraction of raw materials till transportation to site.

The different methods for determining the EE are Statistical analysis, Process-based analysis, Input/ Output analysis and hybrid methodology which combines process-based analysis with I/O analysis [5,6]. In this study, process analysis is selected as this method is more realistic and feasible in Indian conditions [9]. This method identifies different stages of procurement, production and transportation of materials and analyse its energy consumption.

From energy requirement for the processes, per unit weight, EE coefficient of the material can be calculated in MJ/Kg [10]. EE coefficient can be evaluated for each and every construction material.

Total EE is calculated as the product of EE coefficient and quantity of material used for any item of civil work. Embodied Energy of the Building is evaluated as a sum of EE of all the activities in a building project.

EE COEFFICIENTS

EE calculation is dependant on manufacturing process and the location considered. The values obtained are process specific and location specific. For the same construction material, if the process considered is similar in that case, the EE values can be expressed in terms of its ranges.

In Mumbai, typically the bricks are manufactured using clay and rice husk as raw materials in clamp kilns using anthracite coal as fuel. EE coefficient of bricks is calculated considering the energy requirement for extraction of raw materials, transportation of clay to clamp, transportation of rice husk to clamp, transportation of coal, burning of coal in Clamp kiln and transportation of bricks to construction site. The average transporation distance considered in this study is 30 Km.

Energy details of solid concrete block and hollow concrete blocks are obtained from a manufacturing unit in Mumbai, which is completely mechanised and use electricity for working. The raw materials used in manufacture of cement concrete blocks are cement, crushed sand and 10mm aggregate. Manufacturing procedure for solid and hollow blocks is the same, but the shape and weight per block is different. As the raw materials used (crushed sand, aggregate and cement) are not natural, hence energy required for manufacturing and transportation of these materials needs to be calculated.

Electricity consumpsion can be obtained from meter readings. Daily energy consumption and production is used to get energy per unit weight. Diesel used by the shifting machineries in the factory as well as the trucks for transportation to site are considered.

EE OF MASONRY WALL

For construction of masonry walls cement-sand mortar is used in addition to bricks or blocks. Activities like mixing of mortar, lifting and shifting of materials and laying of masonry work at site are considered to be done manually. Therefore EE of masonry work can be obtained by adding EE of sand and cement as per proportion of mortar, to that of bricks or blocks as calculated above. The standard unit of masonry work is cum and hence EE of masonry shall be calculated in MJ/cum.

EE OF MASONRY WORK FOR A MULTISTORIED BUILDING

To compare the effect of building materials on EE of a building, case study of a building under construction in

Mumbai is considered. The building is fourteen storied with floor area 520 square meter per floor. The quantity of masonry work for the case study building is calculated considering 150 mm thick walls; as bricks and blocks of thickness 150 mm (6") has been analysed. Quantity of masonry work per floor is 90.375 cum and for entire building is 1265.25 cum. Total EE for masonry work of the building is calculated as the product of quantity of masonry work and EE in MJ/cum of that masonry.

RESULTS AND DISCUSSIONS

By analyzing the different processes involved in manufacture, EE coefficients of the basic building units of masonry are worked out. EE coefficient of bricks is found to be 1.65 MJ/Kg for Mumbai location. EE coefficient of solid concrete blocks is 0.51 MJ/Kg and for hollow concrete blocks is 0.54 MJ/Kg.

Total energy requirement of the material can be classified into energy required for different processes. Energy consumption in different stages of manufacturing process is represented in Fig.1.
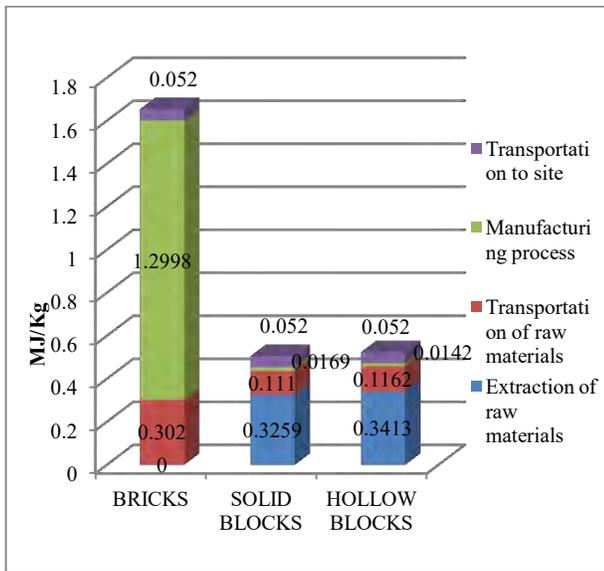
FIGURE 1. Energy consumption in different stages

It can be observed that EE coefficient of bricks is more than three times that of concrete blocks. This is mainly due to the use of coal for burning bricks. In countries where biomass, which is a renewable souece of energy, is used for burning bricks the environmental impact will be lesser [11]. The main source of energy in the manufacturing of solid blocks is electricity, which is very energy efficient. Thus it can be observed that the type of fuel or the source of energy is a deciding factor of the EE coefficient. In Fig.2, contribution of different source of energy to EE of the material is shown.
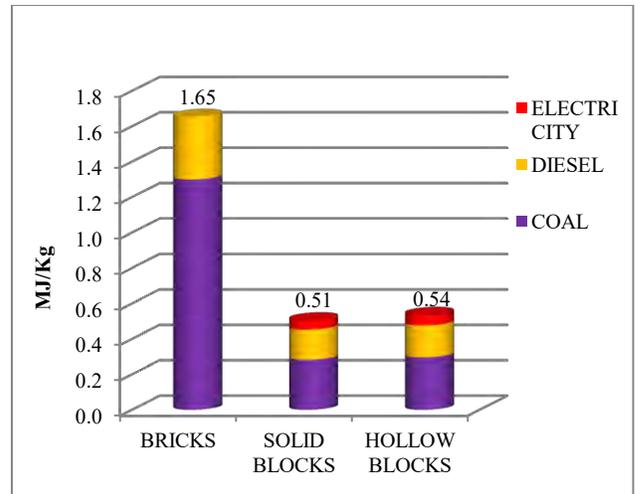
FIGURE 2. Energy expended by different energy sources

EE of brick masonry is highest with 2524.49 MJ/cum, owing to the high EE coefficient of bricks. For solid blocks and hollow blocks, there was only a slight variation in the values of EE coefficients in MJ/Kg. Difference of EE in MJ/cum of solid block masonry and hollow block masonry is observed to be more. This is because weight per unit volume is lesser for hollow blocks due to the air pockets in its design. Weight of the structure can also be reduced by using hollow block. EE of solid block masonry and hollow block masonry are 1266.83 MJ/cum and 962.807 MJ/cum respectively. A graphical comparison is given in Fig.3.
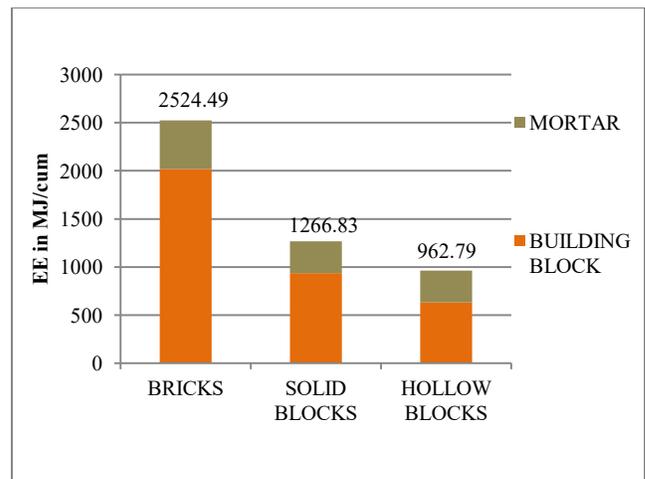
FIGURE 3. Comparison of EE of masonry works

In the case study building the masonry walls were constructed of Solid concrete blocks. The contribution of masonry work to the total EE of building is 1602854.25MJ. If bricks were used, then EE of masonry work would have been 3194109.35MJ. By using hollow concrete blocks, the EE of masonry work would have been reduced to

1218191.50MJ. The three cases are graphically represented in Fig.4.
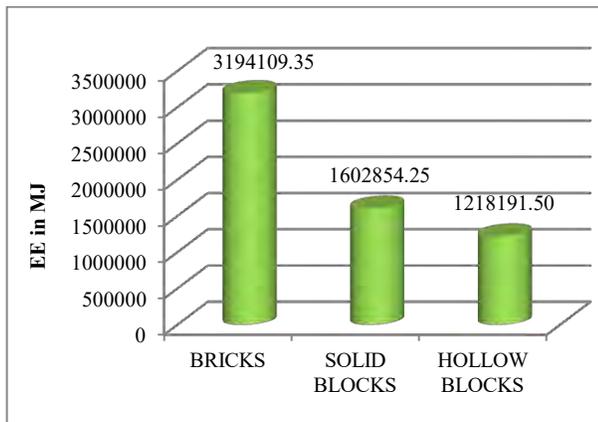
FIGURE 4. Total EE of different masonry works

CONCLUSIONS

EE is lowest when hollow blocks are used and highest when bricks are used in masonry. The difference in EE while considering the case of a building is huge when compared to difference in EE of basic construction materials. For a multistoried building of fourteen floors, it was observed that when bricks are replaced by solid concrete blocks in masonry work, the decrease in EE is 1591255 MJ. If hollow blocks are used EE can be further decreased by 384662 MJ. The difference in EE using bricks and hollow blocks is 1975918 MJ. That is, upto 1.976 Terra Joules of energy can be saved by choosing the right material for masonry in one building. Taking into account, the total volume of construction work carried out, the energy that can be saved is huge.

For sustainable development, EE of buildings should be kept as low as possible. Total EE of a building is the sum of EE of all the activities like foundation, RCC framework, masonry, plastering, flooring, painting, doors and windows etc. Each activity can be analysed based on the materials used. It will be easy for designing and planning sustainable buildings if there is a database of EE coefficients in our country. Inputs from all research works may be summarised to form the database..

REFERENCES

[1] B.V. Venkatarama Reddy and K.S. Jagadish, 2003. "Embodied energy of common and alternative building materials and technologies", Energy and Buildings, 35, January pp. 129–137

[2] Ashok Kumar, D. Buddhi and D. S. Chauhan, 2012. "Indexing of Building Materials with Embodied, Operational Energy and Environmental Sustainability with Reference to Green Buildings", Journal of Pure and Applied Science & Technology, 2(1) , January, pp. 11-22

[3] Sunil Kumar Sharma, 2013. "Zero Energy Building Envelope Components: A Review", International Journal of Engineering Research and Applications, 2(3), March, pp. 662-675

[4] T. Ramesh, Ravi Prakash and K.K. Shukla, 2010. "Life cycle energy analysis of buildings: An overview", Energy and Buildings 42, May, pp. 1592–1600,

[5] G. P. Hammond and C. I. Jones, 2008. "Embodied energy and carbon in construction materials", Proceedings of the Institution of Civil Engineers – Energy 161 (2), May, pp. 87-98, See also http://opus.bath.ac.uk/

[6] Manish Kumar Dixit, José L. Fernández-Solís, Sarel Lavy and Charles H. Culp, 2010. "Identification of parameters for embodied energy measurement: A literature review", Energy and Buildings 42, May, pp. 1238–1247

[7] T. Ramesh, Ravi Prakash and K.K. Shukla, 2013. " Life Cycle Energy Analysis of a Multifamily Residential House: A Case Study in Indian Context", Open Journal of Energy Efficiency, 2, March pp. 34-41

[8] K.I. Praseeda, B.V. Venkatarama Reddy and Monto Mani, 2016. "Embodied and operational energy of urban residential buildings in India", Energy and Buildings 110, September, pp. 211–219

[9] K.I. Praseeda, B.V. Venkatarama Reddy and Monto Mani, 2014. "Embodied energy assessment of building materials in India using process and input–output analysis" Energy and Buildings, 86, October, pp. 677–686

[10] Ashish Shukla, G.N. Tiwari and M.S. Sodha, 2009. "Embodied energy analysis of adobe house", Renewable Energy 34, June, pp. 755–761

[11] Chameera Udawattha and Rangika Halwatura, 2016. "Embodied energy of mud concrete block (MCB) versus solid block and cement blocks", Energy and Buildings 126, April, pp.28–35

ADSORPTIVE REMOVAL OF ACID RED 3BN BY COCONUT SHELL ACTIVATED CARBON

Neha Pandey[1], Chandrakant Thakur[2*]
Department of Chemical Engineering
National Institute of Technology Raipur
Raipur, Chhattisgarh, India
Email: nehapandey61093@gmail.com[1], cthakur.che@nitrr.ac.in[2]

ABSTRACT

Treatment of aqueous dye solution of Acid Red 3BN dye was studied using activated carbon by adsorption. Activated carbon was prepared from coconut shell by steam activation. The adsorptive response of acid red 3BN onto the biomass (coconut shell) activated carban were study in batch experiment. The experimental results showed that the removal efficiency of dye onto activated carbon were maximum at the natural pH of acid red 3BN aqueous solution. Experimental parameters, such as initial concentration, contact time and adsorbent dosage were optimized. The adsorption procedure on activated carbon was mosty controlled by inter particle dispersion mechanism. Thermodynamic investigations proposed that adsorptive response was an endothermic and unconstrained process.

Keywords< Adsorption, Acid red 3BN, Activated carbon

INTRODUCTION

Wastewater produced from different industries makes extreme unfavorable impacts to nature prompting ecosystem lopsidedness. The textile industry, which is one of the biggest water customers worldwide, produces wastewater containing various organic agents such as dyes, dyeing aids, and sizing agents, that should be of concern in discharging into environment[1]. The degradation of dyes is should have been considered in the destruction of textile wastewater because of aesthtic decay and additionally the obstruction of sagacity of dissolved oxygen and sunlight into water bodies, which seriously influences aquatic life[1-2].

If the adsorption system planned as of now it will create astounding quality effluent. Most commercial system utilize activated carbon as sorbent to expel dyes in wastewater because of it's magnificent adsorption capacity commercial activated carbon is viewed as the best material for controlling the organic contaminated wastewater[4].

Objective of the present study was to thermodynamic study of the coconut shell activated carbon as a conceivable adsorbent for treatment of acid red 3BN dye aqueous solution. Study on three essential process parameters like initial concentration, contact time and adsorbent dosage had been done and decolorization of acid red 3BN has taken as responses.

EXPERIMENT PROCEDURE
Reagent

Coconut shell steam activated carbon was purchased from Merck India limited. All the reagents used for this experiment were of analytical grade and used without further purification. Distilled water was used for all the experiments. The pH was adjusted by addition of sodium hydroxide (0.1 M) and sulfuric acid (0.1 M). Acid red 3BN (LOBA Chemie, India, and LR grade) was chosen as the target compound, and its chemical structure is as follows:
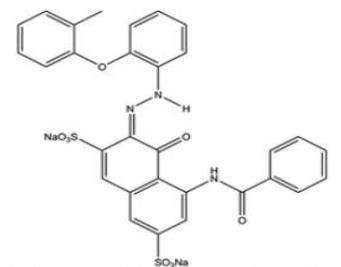
FIGURE 1. STRUCTURE OF ACID RED 3BN.

Adsorption

The dynamic stuies was performed utilizing 250-mL conical shaped flasks which were contained 100 mL dye solution of concentration (100 ppm), kept up at desired temperature and pH. An equivalent amount of adsorbent was added into every individual flasks. The flasks were agitated in an orbital shaker at a speed of 100 rpm. The percentage of decolorization was calculated using the following equation:

$$\% \, Decolorization = \left[\frac{C^{\circ} - C}{C}\right] \times 100 \qquad (1)$$

where C° and C are the initial and final lead concentrations (ppm), respectively. All the experimental run were performend two times, and average values were accounted. The parameters considered for batch experiments were initial concentration of aqueous solution of Acid red 3BN, adsorbent(Activated carbon) dose, contact time and pH.

RESULT AND DISCUSSION

Effect Of Contact Time

In order to adsorptive response of the percentage of decolorization and the equilibrium time for optimum take-up and to know the efficiency of the sorption procedure, the adsorption of Acid Red 3BN by activated carbon was done under contact times from 0 to 360 min, shown in Fig. 2. The decolorrization efficiency of dye increases gradually with increasing contact times and reaches equilibrium at around 240 min at which point the majority of dye is removed[4-6]. Now, the measure of dye being adsorbed onto the coconut shell AC was in a condition of kinetic equilibrium with the measure of dye desorbtion from the adsorbent. As per the removal, the equilibrium time is same as of now for whatever remains of the batch experimental run to ensure that equilibrium is reached.
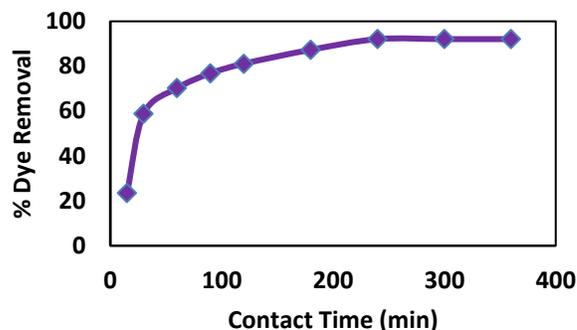
FIGURE 1. THE EFFECT OF CONTACT TIME ON THE DECOLORIZATION OF ACID RED 3BN. (CONDITIONS: INITIAL DYE CONCENTRATION 100 PPM; DOSAGE PH 7; AGITATION SPEE= 100 RPM; OF ADSORBENT = 2.5 gm; CONTACT TIME = VARIABLE).

Effect Of Adsorbent Dosage

The adsorbent dosage was varied from 0.0 to 3.0 g/L, kept all other variable steady. As shown in Fig. 3, the percentage of decolorization increments up to adsorbent dosage of 1 g/L. This might be ascribed to an expanded sorbent surface area and accessibility of more adsorption destinations coming about because of the extra dosage of the adsorbent[5-7]. The percentage of decolorization increases from 18% to 92% with an increase in the amount of adsorbent from 0.5 to 3.0 g, respectively.
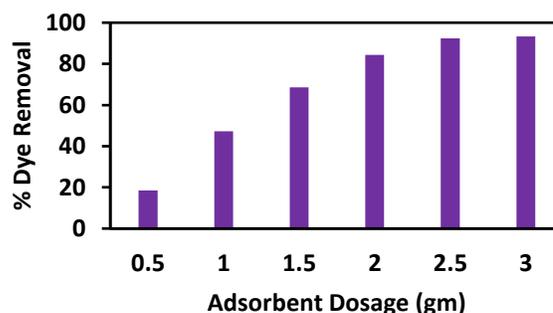
FIGURE 3. THE EFFECT OF ADSORBENT DOSAGES ON THE DECOLORIZATION OF ACID RED 3BN. (CONDITIONS: INITIAL DYE CONCENTRATION 100 PPM; AGITATION SPEE= 100 RPM; TIME = 240 min; CONTACT PH 7; DOSAGE OF ADSORBENT = 2.5 gm = VARIABLE).

CONCLUTION

On the basis of the outcomes acquired, it can be concluded that the coconut shell AC worked as potential adsorbents for the removal of acid red 3BN from aqueous media.

REFERENCES

[1] Gupta, V.K., Agarwal, S., Saleh, T.A., 2011. "Synthesis and characterization of alumina-coated carbon nanotubes and their application for lead removal". J. Hazard. Mater., *185*, pp.17–23.

[2] Li, Y., Wang, S., Wei, J., Zhang, X., Xu, C., Luan, Z., Wu, D., Wei, B., 2002. "Lead adsorption on carbon nanotubes". Chem. Phys. Lett., 357, pp.263–266.

[3] Sekar, M., Sakthi, V., Rengaraj, S., 2004. "Kinetics and equilibrium adsorption study of lead(II) onto activated carbon prepared from coconut shell". J. Colloid Interf. Sci., 279, pp. 307–313.

[4] O'Connell, D.W., Birkinshaw, C., O'Dwyer, T.F. 2008. "Heavy metal adsorbents prepared from the modification of cellulose: A review". Bioresour. Technol., 99, pp.6709–6724.

[5] Acharya, J., Sahu, J.N., Mohanty, C.R., Meikap, B.C., 2009. "Removal of lead(II) from wastewater by activated carbon developed from Tamarind wood by zinc chloride activation". Chem. Eng. J., 149, pp. 249–262.

[6] Thakur, C., Srivastav,a V.C., Mall, I.D., Hiwarkar, A.D., 2017. "Modelling of binary Isotherm behavior for the adsorption of catechol with phenol and resorcinol onto Rice Husk Ash". Indian Chemical Engineers.,

[7] Thakur, C., Dembla, A., Srivastava, V.C., Mall, I.D., "Removal of 4-chlorophenol in sequencing batch reactor with and without granular-activated carbon", 2014. Desalination and Water Treatment, 52, pp. 4404–4412.

COMPARATIVE STUDY ON CHARACTERISTICS OF COMPRESSION IGNITION ENGINE IN DUAL FUEL MODE EMPLOYING GASOLINE/BUTANOL AND DIESEL

Mohit Raj Saxena
Department of Mechanical Engineering
Indian Institute of Technology Ropar, Rupnagar-140001, India
Email: mohitraj@iitrpr.ac.in

Rakesh Kumar Maurya,* Geo Alex
Department of Mechanical Engineering
Indian Institute of Technology Ropar, Rupnagar-140001, India
Email*: rakesh.maurya@iitrpr.ac.in

ABSTRACT

This study investigates the performance and emission characteristics of compression ignition engine in dual fuel operation employing gasoline/butanol and diesel. The intake manifold of the conventional diesel engine is modified and a solenoid based injector is installed in the intake manifold to operate the engine in dual fuel mode. A separate port fuel injector controller is developed and used for injecting the required quantity of gasoline/butanol in the manifold. All the experiments are performed at different fuel premixing ratio (on the energy basis) at the constant engine speed of 1500 rpm. Results reveal that the dual fuel operation has lower brake thermal efficiency (BTE) in comparison to neat diesel fuel operation and decreases with fuel premixing ratio (especially at 25% and 50% engine load condition). Results also depict that dual fuel compression ignition operation has higher HC and CO emissions while NO_x and particle emissions reduce for dual fuel operation.

Keywords: Dual fuel, Butanol, Gasoline, Diesel engine
.

INTRODUCTION

The application of diesel engine in small passenger cars or in power generators is increasing day by day because of their higher power output, more fuel economy, lower hydrocarbon, and greenhouse gas (i.e. carbon dioxide (CO_2)) emissions. However, diesel engines emit particulate matter and oxides of nitrogen in higher concentration from the exhaust. These emissions have a fatal effect on the human health as well as on the environment. Degradation of the environmental conditions and the crises of depilation of fossil fuel resources motivated the engine community researchers to investigate an alternative renewable fuel or different combustion strategy for a diesel engine. In past decades, several renewable fuels were investigated for diesel engine application [1-2]. Alcohol fuels were intensively investigated by the researchers because of their inherent properties [1]. Alcohol fuels have higher oxygen content which leads to improve the combustion characteristics, have potential to reduce smoke, particulate matter and NO_x emissions from diesel engine [1, 3]. However, alcohol fuels are considered as more suitable fuel for spark ignition (SI) engines because of their higher octane number (i.e. more resistant to auto-ignite). Alcohol fuel can also be used in the diesel engine either by making blend of alcohol and diesel with suitable additives and directly injected into the cylinder (by direct injection technique) or by separately injecting the alcohol or any other low reactivity fuel in the intake manifold and direct injection of diesel-like fuels (which is termed as dual fuel compression ignition engine). Dual fuel compression ignition (CI) engine may combine the advantage of SI engine (i.e. premixing of fuel may lead to reduce the formation of particulate matter) and CI-engine (can be operated at higher compression ratio and no throttling loss occurs which may lead to higher thermal efficiency). Several studies have been found which explore the different aspect of dual fuel compression ignition engine [4-8]. These studies mainly investigated the performance, combustion and emission characteristics of dual fuel CI-engine. Butanol has more favorable properties for a diesel engine in comparison to ethanol and methanol.

Butanol has higher cetane number as compared to methanol and ethanol. In addition, it is easily miscible with diesel fuel (that means no further additives are required to avoid the fuel layers separation). The typical properties of the alcohol fuels are available in the study [1]. To the best of the author's knowledge, no literature was found on particle emission for butanol-diesel dual fuel operation. This study presents the performance and emission characteristics (including particulate emissions) of dual fuel engine employing port injection of gasoline/butanol and direct injection of diesel fuel for different fuel premixing ratios.

EXPERIMENTAL SETUP

For this study, a single cylinder CI- engine is modified to run in dual fuel combustion mode. The engine is coupled to an eddy current dynamometer. To operate the engine in dual fuel mode, intake manifold of the engine is modified and a port fuel injector is installed in the intake manifold to inject gasoline/butanol separately. The gasoline/butanol is injected into the intake manifold typically at 2.5 bar injection pressure at 273° bTDC during dual fuel operation.
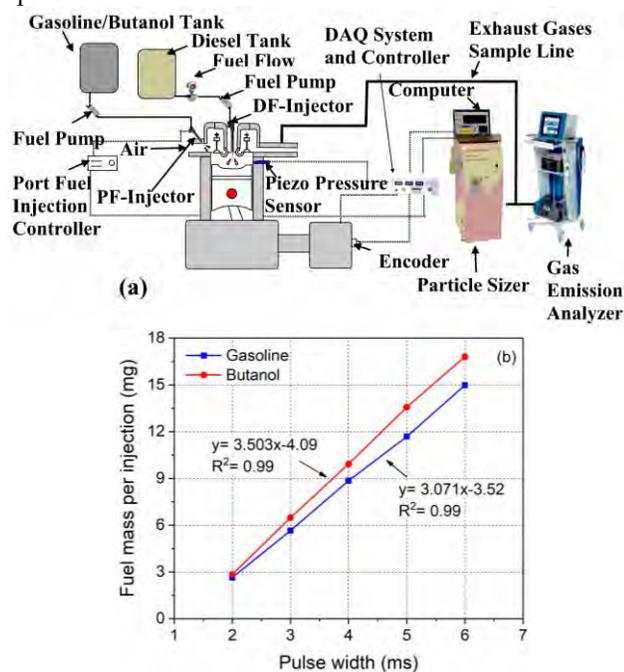
FIGURE 1. (a) Schematic diagram of experimental setup (b) Calibration curve for port injector of gasoline and butanol

The mechanically operated fuel injection system is used for injecting the diesel fuel directly into the cylinder during dual fuel operation. Diesel is injected at 23° bTDC with an injection pressure of 200bar. A fuel transmitter is installed between the diesel fuel tank and a fuel injector for the measurement of mass flow rate of fuel. The detail specification of the engine setup is available in the

previous study [6]. Gaseous and particle emissions are measured by gas emissions analyzer (Manufacturer: AVL, Austria, Model: CDS450) and differential mobility spectrometer (Manufacturer: Cambustion, UK, Model: DMS500) respectively. The calibration curve for port fuel injector and typical experimental setup is presented in figure1. Fuel premixing ratio is used for characterizing the contribution of fuel energy and is evaluated by using equation 1.

$$Premixing\ ratio\ (\%) = \frac{m_x \times LHV_x}{m_x \times LHV_x + m_d \times LHV_d} \times 100$$
(1)

Where 'x' could be gasoline or butanol, 'm' is the mass of injected fuel, 'LHV' is the lower heating value and,'d' represents for diesel.

RESULTS AND DISCUSSION

This section presents and compares the performance and emissions characteristics of dual fuel CI-engine employing port injection of gasoline/butanol and direct injection of diesel fuel. In this extended abstract, performance characteristics include only the brake thermal efficiency (BTE) and brake specific fuel consumption (BSFC). Emission characteristics include the concentration of gaseous (i.e. hydrocarbon (HC), carbon monoxide (CO), nitrogen oxide (NO_x)) as well as particle emissions.

Performance characteristics of dual fuel engine

This section presents the performance characteristics of gasoline/butanol-diesel dual fuel CI-engine. Figure 2(a) indicates that with an increase in the engine load, BTE increases and BSFC decreases for all the premixing ratios. BTE is a function of engine operating load. BTE increases with engine load due to the reduced ratio of friction to brake power. The interaction between these factors results in lower BSFC. Another major factor is with an increase in the engine load, combustion phasing advances which leads to increase the expansion ratio and results in higher BTE. At 25% and 50% engine load condition, the BTE slightly increases for 20% gasoline-diesel premixing ratio. However, with further increase in the premixing ratio, BTE decreases. Gasoline has the higher latent heat of vaporization, premixing of gasoline leads to reduce the mean in-cylinder temperature which results in more retarded combustion phasing. Therefore, more fraction of charge will burn during the diffusion combustion phase which results in lower BTE. At 100% engine load condition, the BTE slightly increases with gasoline/diesel premixing ratio up to 60%. With further increase in premixing ratio, BTE starts decreasing. Figure 3 represents the comparison of BTE and BSFC at 50% engine load condition for gasoline-diesel and butanol-diesel dual fuel operation. It can be observed from the figure that for lower fuel premixing ratio, butanol-diesel dual fuel operation has slightly higher BTE in comparison to gasoline-diesel dual fuel operation. A possible reason for this observation is

butanol is an oxygenated fuel which may lead to improve the combustion characteristics. Another possible reason is butanol has higher auto-ignition temperature in comparison to gasoline which leads to increase the ignition delay period. Therefore more amount of charge will burn during the premixed combustion phase which results in higher BTE. With further increase in the premixing ratio, BTE rapidly starts decreasing.
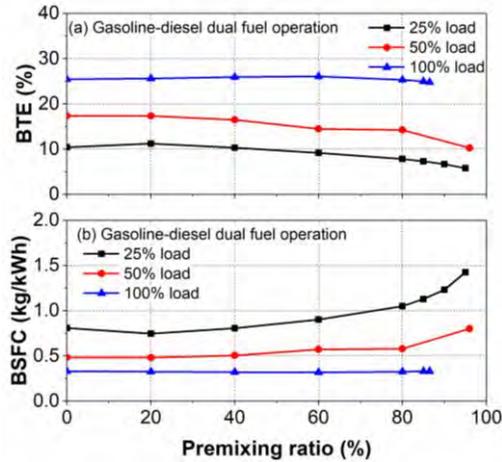
FIGURE 2. (a) Effect of fuel premixing ratio on BTE; (b) Effect of fuel premixing ratio on BTE at different engine loads
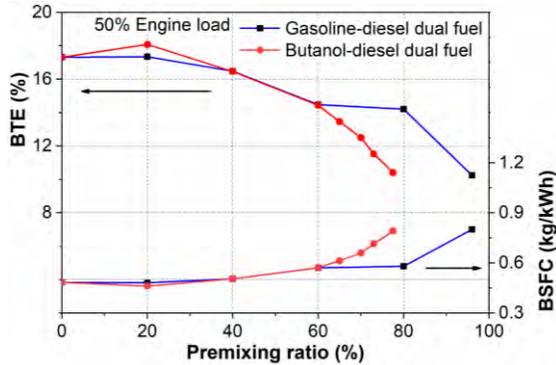
FIGURE 3. Effect of fuel premixing ratio on BTE and BSFC for gasoline/butanol-diesel dual fuel operation

Figure 3 depicts that for butanol-diesel dual fuel operation, with further increase in the premixing ratio from 60%, BTE rapidly start decreasing. Butanol has the higher latent heat of vaporization in comparison to gasoline thus, further increase in the butanol-diesel premixing ratio leads to more retard combustion phasing and lower mean gas temperature (because of more fraction of charge will burn during the expansion stroke) which results in lower BTE. Therefore, the BTE will depend on the factor which is dominating.

Emission characteristics of dual fuel engine

In this section, an emissions characteristic of gasoline/butanol-diesel dual fuel operations for different fuel premixing ratios is presented. In this extended abstract, the emissions characteristics at 50% engine load are only presented. Figure 4 demonstrated the variation of CO, HC, and NO_x emissions with fuel premixing ratio at 50% engine load condition for gasoline/butanol-diesel dual fuel operation. The figure depicts that with an increase in the fuel premixing ratio, the CO and HC emissions are increasing while NO_x emissions are reduced with the fuel premixing ratio.
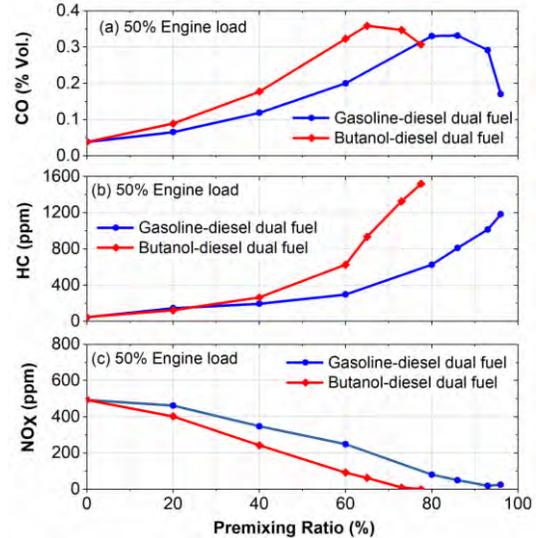
FIGURE 4. Variation of CO, HC, and NOx emission with gasoline/butanol-diesel premixing ratio

Higher HC and CO emissions could be due to different possible reasons. Higher HC emissions could be due to some fraction of gasoline/butanol-air directly release in the exhaust and results in higher HC emissions. It also may be due to some fraction of gasoline/butanol-air trapped on the crevices, which may lead to higher HC and CO emissions due to incomplete combustion. Another possible reason is due to premixing, the charge becomes lean which is difficult to be oxidized and may also lead to higher HC and CO emissions [5, 6]. However, figure 4(a) also reveals that after certain fuel premixing ratio, the CO emission start decreasing and this trend is similar for both the dual fuel operations. Figure 4(a) and 4(b) depicts, the HC and CO emissions are higher for butanol-diesel dual fuel operation in comparison to gasoline-diesel dual fuel operation. It is mainly due to the lower fuel reactivity (of butanol) and mean gas temperature which leads to comparatively lower combustion efficiency and results in higher HC and CO emissions. With an increase in the fuel premixing, the NO_x emission decreases and this trend is similar for both the dual fuel operations. Premixing of low reactivity fuel leads to reduce the mean in-cylinder combustion temperature (due to retard combustion phasing). Lower mean in-cylinder combustion temperature leads to reduce the NO_x emissions. Figure 5 represents the variation of total, nucleation, and accumulation mode particle concentration with fuel premixing ratio. It has been observed from the

figure that the total particle concentration reduces with an increase in the fuel premixing ratio up to a certain limit after that it starts increasing. Formation of particles is mainly dependent on the local fuel-air equivalence ratio. Increase in the fuel premixing ratio leads to enhance the fuel and air mixing (i.e. reduces the local fuel rich cores) which results in reduced particles formation. With further increase in the fuel premixing ratio, the total particle concentration starts increasing. In the total particle number concentration, nucleation mode particles are higher in concentration in comparison to accumulation mode particles (can be seen from figure 5(b) and 5(c)).
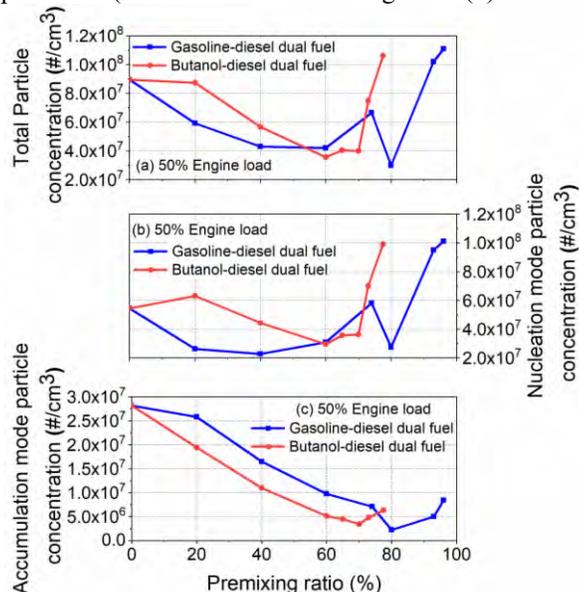
FIGURE 5. Variation of (a) total particle number; (b) nucleation mode; (c) accumulation mode particles concentration with fuel premixing ratio

Typically particles having a diameter less than 50nm are termed as nucleation mode particles while particles having a diameter more than 50nm are known as accumulation mode particles. Nucleation mode particles are higher in concentration for all the premixing ratios possibly due to nucleation, coagulation, and condensation of HC emissions in dual fuel operation. These particles are generated due to the comparatively reduced in-cylinder combustion temperature during the premixed combustion phase. The higher HC emission will produce the nucleation mode particles and led to raising the total particle concentration. Higher HC emissions with increase in premixing ratio can also be seen from figure 5(b). In addition, it also has been observed from the figure that the butanol-diesel dual fuel operation has higher particle emissions in comparison to gasoline-diesel dual fuel mode. Gasoline is more volatile and has a lower viscosity in comparison to butanol which led to enhance the fuel-air mixing thus results in improved combustion and will produce less nucleation size particles precursors and HC. Lower HC emissions with gasoline-

diesel dual fuel operation in comparison to butanol-diesel dual fuel operation can also be seen from figure 4(b). Butanol/diesel dual fuel operation has lower accumulation mode particles in concentration as compared to gasoline/diesel dual fuel operation (as shown in figure 5(c)).

CONCLUSION

This study presents the performance and emission characteristics of dual fuel CI-engine fuelled with a port injection of gasoline/butanol and direct injection of diesel fuel. Results demonstrated that with 20% fuel premixing ratio, BTE slightly increases. At 25% and 50% engine load condition, a further increase in premixing ratio reduces the BTE. However, for 100% engine load condition, the BTE slightly increases up to 60% fuel premixing ratio. During dual fuel operation, the CO and HC emissions were increasing with increase in the fuel premixing ratio, while NO_x and particle emissions were decreasing. This trend was similar for both the dual fuel operations. It also had been seen butanol/diesel has slightly higher BTE for lower fuel premixing ratio in comparison to gasoline/diesel dual fuel operation. Additionally, butanol/diesel dual fuel operation has higher CO, HC and particle emissions in comparison to gasoline/diesel dual fuel operation. Butanol/diesel dual fuel operation has lower accumulation mode particles in concentration as compared to gasoline/diesel dual fuel operation.

REFERENCES

[1] Geng, P., Cao, E., Tan, Q., & Wei, L. (2016). Effects of alternative fuels on the combustion characteristics and emission products from diesel engines: A review. Renewable and Sustainable Energy Reviews.

[2] Mahmudul, H. M., Hagos, F. Y., Mamat, R., Adam, A. A., Ishak, W. F. W., & Alenezi, R. (2017). Production, characterization and performance of biodiesel as an alternative fuel in diesel engines–A review. Renewable and Sustainable Energy Reviews, 72, 497-509.

[3] Saxena, M. R., & Maurya, R. K. (2016). Effect of butanol blends on nano particle emissions from a stationary conventional diesel engine. Aerosol Air Qual. Res, 16, 2255-2266.

[4] Bora, B. J., Saha, U. K., Chatterjee, S., & Veer, V. (2014). Effect of compression ratio on performance, combustion and emission characteristics of a dual fuel diesel engine run on raw biogas. Energy conversion and management, 87, 1000-1009.

[5] Wei, L., Yao, C., Han, G., & Pan, W. (2016). Effects of methanol to diesel ratio and diesel injection timing on combustion, performance and emissions of a methanol port premixed diesel engine. Energy, 95, 223-232.

[6] Saxena, M. R., & Maurya, R. K. (2017). Effect of premixing ratio, injection timing and compression ratio on nano particle emissions from dual fuel non-road compression ignition engine fueled with gasoline/methanol (port injection) and diesel (direct injection). Fuel, 203, 894-914.

[7] Bora, B. J., & Saha, U. K. (2016). Optimisation of injection timing and compression ratio of a raw biogas powered dual fuel diesel engine. Applied Thermal Engineering, 92, 111-121.

[8] Park, S., Cho, J., Park, J., & Song, S. (2017). Numerical study of the performance and NO x emission of a diesel-methanol dual-fuel engine using multi-objective Pareto optimization. Energy, 124, 272-283.

SEEC-2018-142

Analysis of flow in the dump combustion chamber with varied step angle

Tushar kant swain
School of Engineering,
Indian Institute of Technology Mandi,
Kamand, Mandi,175005.

Dr. P. Anil Kishan
School of Engineering,
Indian Institute of Technology Mandi,
Kamand, Mandi,175005.

Abstract: *Numerical simulations are carried out on the dump combustor with various step angles and the expansion ratio. The angles and aspect ratio are important for the recirculation zone in combustor. The simulations are carried out using RANS, $k - \omega$ turbulence model along with SST, species transport. The reattachment length increase with increase in step angle and primary recirculation zone is seen till 30^0 angle of the step. The presence of recirculation is to be known from the stream line, velocity and pressure distribution. The minimization of the total pressure loss is an important factor for the dump combustor analysis as well as the thrust.*

Keywords: ***Dump combustor, temperature, recirculation***

Introduction:

Dump combustor is considered as a generic combustion chamber for *various* practical devices like gas turbines, ramjet engines, power plants and jet stirred chemical reactors. The flow in the dump combustor is a complex phenomenon that is characterized by turbulent mixing of fuel and air, flow separation, recirculation zone and shear flow reattachment and other complex phenomenon for the combustion. The current study will try to reduce the fuel consumption for combustion by improving the mixing of fuel and air. Better the mixing, better the combustion efficiency. Drewry [1] has discussed the flow inside the dump combustor and suggested about the distinct regions in the flow namely are recirculation zone, reattachment of the flow and complete development of the flow inside the dump combustor. Hammad et al. [2] have discussed the effect of flow Reynolds number on reattachment length, developed length, and recirculating flow strength in the laminar axisymmetric sudden expansion flow. The reattachment of the flow and length are reported to be linear function of the Reynolds number. The strength of the recirculation is found to be nonlinear function of the Reynolds number. Yang and

Yu [3] showed that the maximum velocity fluctuation along the centerline occurred immediately after the reattachment. The shear layer, where the high gradient of mean velocity occurs, is associated with high energy levels. Higher turbulent kinetic energy is transported by both diffusion and convection in and out of the recirculation region.

Numerous works has been carried out on dump combustor. There is no complete understanding of the processes involving the turbulence and combustion within the combustor. The objective of these present numerical simulations is to analyze the flow field characteristics. An exclusive study is carried out on the step angle of backward facing step of the combustor and the aspect ratio of the combustor.

Combustor geometry

A Planar combustor with a step in the flow direction is used in this simulation. Combustor fuel is injected near to the shear layer where the flame is stabilized near the backward facing step. Fig (1) represents three dimensional schematic diagram of dump combustor. The inlet section has a width of 20 mm, backward facing width of 20 mm and overall length of the combustor chamber is 400 mm and 160 mm in lateral direction.

Fig 1: Schematic diagram for three dimensional dump combustor

The air is fed through the air inlet and fuel is injected from backward facing wall. The recirculation zone near to the facing wall helps in mixing of fuel and air efficiently. The flame gets stabilized and anchored near to the backward facing step.

Results and Discussion

(A)Validation:

The current model is simulated using continuity equation, momentum equation, energy equation, turbulence mode. The above three dimensional dump combustor has been validated with the reported results of Nemitallah et al. [4] (Fig 2.) for the axial velocities at X/H = 0.25. The axial velocity is first reduced due to the expansion over the step which is being represented by the recirculation zone due to the unfavorable pressure gradient. Fig 2 shows good agreement between the current and reported results. The reported results used the LES turbulence models whereas we have used the $k - \omega$ SST turbulence models. The figure [3] shows good agreement for the velocity profile at X/H=0.25 even though the turbulence models are different. Figure [3] shows the comparison between the various turbulence models used for the given combustor design. Even though the flow field predicted by various models matches well in the upper portion of the combustor, the flow field in bottom portion, after the dump is different.
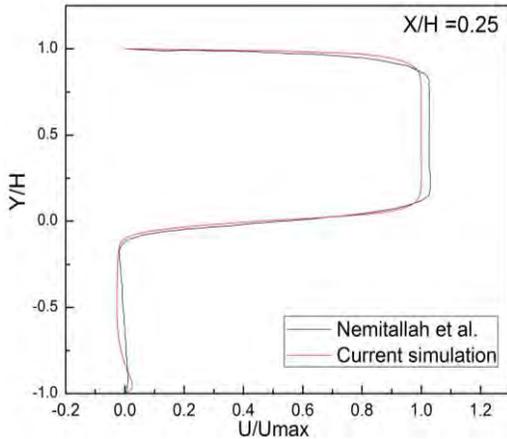
Fig 2: Velocity profile at normalized axial location X/H = 0.25.
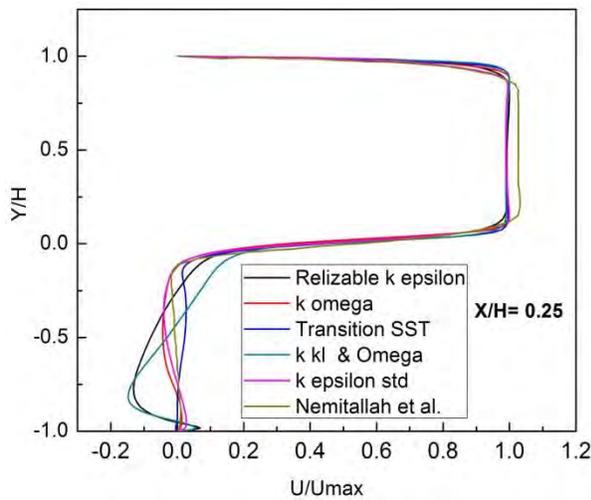
Fig 3: Velocity profile using various turbulence model at normalized axial locations at X/H = 0.25.

(B) Flow field

As it can be seen from Fig. 4 there are two eddies in the recirculation zone. At θ = 0° the primary eddy (PE) rotates in clockwise and constitute a part of the recirculation zone. The secondary eddy (SE) rotates in the opposite direction to the primary eddy. The size of the primary eddy and secondary eddy depends upon the backward step angle of the dump combustor. The backward step angle of the dump combustor is increased as

θ = 10°, 20°, 30° and 45°. From the fig 4 the axial velocity contours it can be seen that the primary eddy exists till θ = 20°. At θ = 30° and 45° secondary eddy predominantly seen as compared to primary eddy. Beyond θ = 30° the secondary prominently seen and helps in better mixing of fuel and air efficiently.
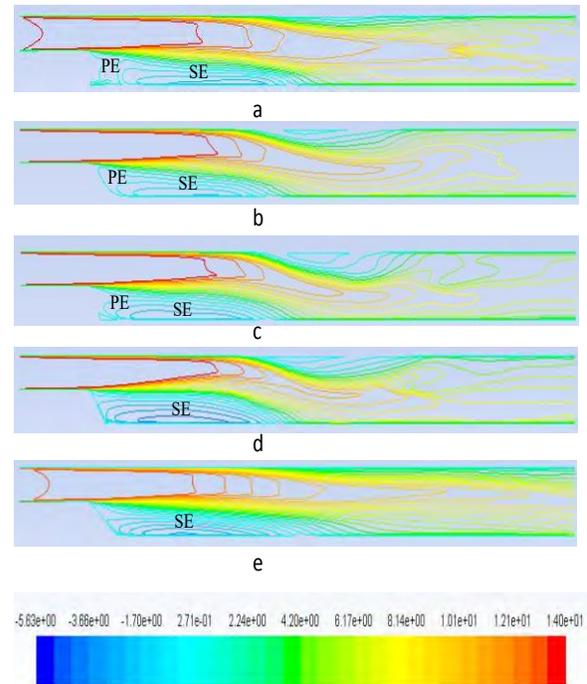
Fig 4: Contour plots of axial velocity for varied backward step angle for the dump combustor (a) θ = 0° (b) θ = 10° (c) θ = 20° (d) θ = 30° and (e) θ = 45°.

Figure 5 represents the line plots of the averaged axial velocity at different locations. It is seen two eddies inside the combustion chamber recirculation zone. The primary eddies and secondary eddies constitute the recirculation inside the dump combustor. The circulation of primary and secondary eddies are opposite in direction. Primary eddy have close proximity to the

backward step wall. The size of the primary eddies and secondary eddies is controlled by the step wall. If the varied step angle wall the primary eddies diminishes and the prominently seen the secondary eddies in the recirculation zone. Fuel will be injected near to the shear layer which will have better mixing of fuel and air. In the absence of primary eddies the mixing takes palace efficiently in comparison to the other case. Hence the varied angle of the step wall will enhance the mixing and improve the combustion in the combustion chamber.
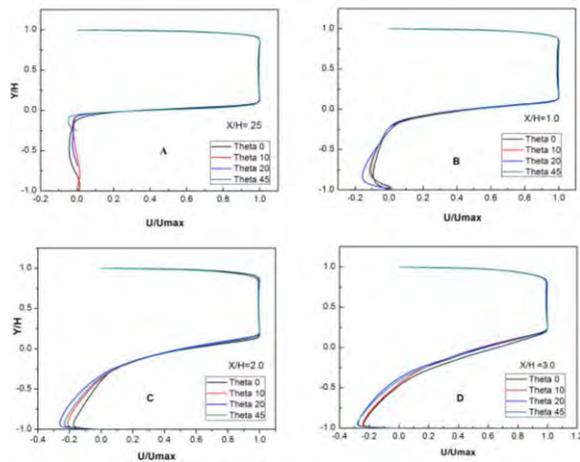
Fig 5: Average Velocity profile at different location of X/H (A) X/H= 0.25 (B) X/H = 1.0 (C) X/H= 2.0 (D) X/H = 3.0

Conclusion:

The current study gives information about the eddy in the dump combustor. At θ=0⁰ there is a presence of primary and secondary eddies. As the step angle θ increases beyond 30° there is absence of primary eddies. The secondary eddy helps in mixing of fuel and air efficiently and diffused to the downstream of the flow.

References:
1. J.E. Drewry, "Fluid dynamic characterization of sudden expansion ramjet combustor flow fields", AIAA Journal, 16(4), 1978, 313-319.
2. K.J. Hammad, M.V.Otugen, and E.B.Arik, "A PIV study of the laminar axisymmetric sudden expansion flow", Experiments in fluids, 26, 1999, 266-272.
3. B.T.Yang, and M.H.Yu, "The flow field in a sudden enlarged combustion chamber", AIAA Journal, 21(1), 1983, 92-97.
4. M.A. Nemitallah, G. Kewlani, S. Hong. S.J Shanbhogue, M. A. Habib, and A. F. Ghoniem, "Investigation of a turbulent premixedcombustion flame in a backward facing step combustor; effect of equivalence ratio", Energy 95, 2016, 211-222.

PARAMETRIC STUDY OF VARIATION IN HEAT FLUX IN SOLAR PARABOLIC TROUGH COLLECTOR

Prashant Saini
School of Engineering
IIT Mandi
prashantsaini9997@gmail.com

Satvasheel Powar
School of Engineering
IIT Mandi
satvasheel@iitmandi.ac.in

Atul Dhar
School of Engineering
IIT Mandi
add@iitmandi.ac.in

ABSTRACT

Utilization of concentrating solar power (CSP) technologies are increasing day by day in industries owing to its great potential to harness solar energy. Parabolic trough collector (PTC) is one of the best, economical and proven technology among the CSP Technologies. This paper discuss the methodology for obtaining the Non-Uniform heat flux at the bottom half of absorber tube of a solar parabolic trough collector. Variations in zenith angle of the sun throughout the day, leads to variations in the heat flux at the surface of absorber tube. This Non-uniformity of heat flux leads to the variation in the temperature profile curve on the surface of absorber tube. These variations are obtained by Monte Carlo Ray Tracing Method (MCRT Method) and FLUENT Software package.

Keywords

Irradiance, Monte Carlo Method, Solar Collector, Laminar flow

NOMENCLATURE

CSP   Concentrated Solar Power
PTC   Parabolic Trough Collector
MCRT   Monte Carlo Ray Tracing
HTF   Heat Transfer Fluid
HCE   Heat Collection Element

INTRODUCTION

Parabolic trough collector (PTC) is the most economical concentrator for the indirect generation of steam in solar thermal power plants. Parabolic trough concentrator is simple to manufacture as compared to dish type and compound type concentrators. It requires only single axis solar tacking system [1,2]. The basic schematic diagram of the PTC is given in fig. 1.
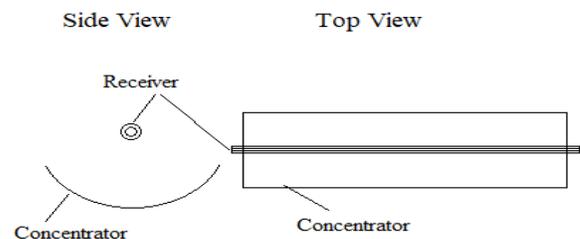
Figure 1. Schematic diagram of PTC.

By using parabolic trough collector, solar irradiance can be focused up to 40 - 50 times on absorber tube and hence, heat transfer fluid is heated (300-400°C) [3]. Normally, PTC consists of 3 parts, (i) parabolic reflector, which concentrates solar irradiance on Heat Collection Element(HCE). (ii) HCE, which is usually an absorption pipe made of copper or steel placed at the focus of parabola, (iii) the glass tube, which envelops the absorber tube [4]. The heat transfer fluid passes through the absorber tube and heats up. Parabolic trough collector has capability to achieve high temperature without much drop-in

efficiency. PTC is widely used in the process of electricity generation in thermal power plant despite high amount of losses incurred because of poor design of PTC. These losses reduce the efficiency of the PTC to greater extent [5, 6].

Variations in the Zenith angle of the sun results in the variation of solar irradiance. Due to variation in irradiance the heat flux on the surface of absorber tube also varies. This non-uniformity of heat flux results in non-uniform temperature profile across the absorber tube. There is circumferential variation of heat flux in the receiver. The bottom half of absorber tube receives the maximum solar flux, which leads to higher temperature rise in the bottom half compared to upper half of the absorber tube. In this study, modelling is performed using Fluent software. Simulation of heat losses (convection and radiation), mass flow rates, effect of wind speeds etc. helps us to understand how to eliminate these losses [7]. Figure 2 represent the losses in receiver. Simulation of PTC helps in calculation of heat losses and sizing of the power plant during its earlier design. These simulations also provide an idea how to improve the geometry or a system to minimize various types of heat losses and enhance the efficiency of the PTC [8].
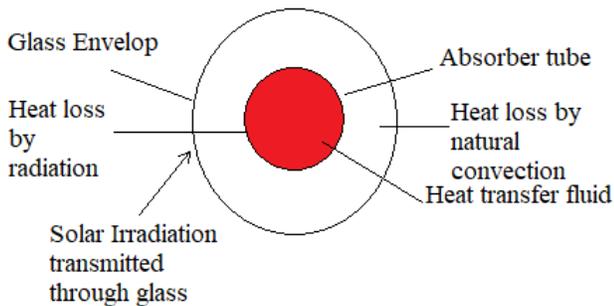
Figure 2. Schematic diagram of evacuated receiver

Computational Model
Physical Model
Schematic diagram of PTC and its receiver is shown in figure 3(a) and 3(b). Following assumptions are adopted to model the PTC:
   a. Both the ends of receiver are adiabatic.
   b. The incident angle modifier is considered as unity, that is true when the incident angle is at zero degree.
   c. Vacuum space present in between glass tube and absorber tube is able to eliminate the convection and conduction losses from the absorber tube.
   d. There should be negligible infrared radiation exchange in between the glass envelop and the absorber surface.
   e. The fluid flow is in steady state and incompressible.

   f. Infinite long absorber tube is considered to minimized the edge/end loss.
   g. Model is theoretically and physically symmetric along the y-z plane. The heat flux profile is symmetrical along the circumference of the absorber tube in y-z plane.
   h. The efficiency of the tracking is so good that the optical errors could be neglected.

(a)

(b)
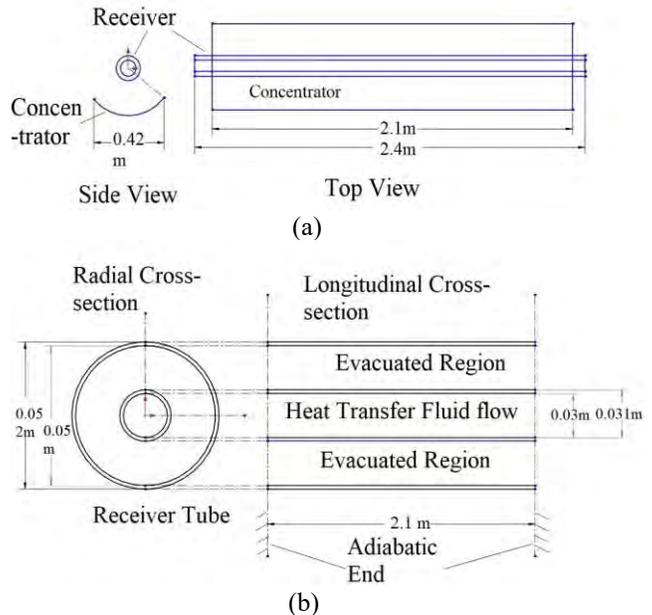
Figure 3. Schematic diagram of (a) PTC (b) receiver

Numerical approach and methodology:
- Ambient Temperature remains constant.
- Viscosity, density and other thermal properties were kept as constant.
- K-ε turbulent model with enhanced wall treatment is used.
- Incident angle modifier (k) is considered as unity, which is true at an incidence angle of zero.
- The vacuum inside the envelop of glass is able to prevent the convection and conduction losses, which occurs mainly from the surface of copper tube.
- There is negligible infrared radiation exchange in between the copper tube and the glass envelop.
- To make the flow incompressible the pressure is considered to be very low.
- Wall boundary condition: all walls are modelled as stationary wall with no slip condition. For the proper handling of viscous effect walls are properly closed and near-wall treatment is applied as a standard wall function.
- Outer surface of the copper tube: non-zero heat flux condition with zero wall thickness and no shell conduction.
- The solar energy flux distribution is calculated by using MCRT Method.

- Mass flow rate or velocity inlet remains constant.
- Coupled scheme is used as the solution method.
- Second order pressure and energy equation are used with pseudo transient condition.
- Second order turbulent kinetic energy and turbulent dissipation rate were used.
- Minimum iteration of 3000 is used for each case.
- Different optical specification of glass is as below:

	Type of Spectrum	Incident	Diffused
Reflectance, (r)	Visible	0.08	0.84
	Infrared	0.08	
Absorbtance, (α)	Visible	0.09	0.1
	Infrared	0.09	
Transmitance, (τ)	Visible	0.83	0.75
	Infrared	0.83	

The second order upwind differential scheme is used for the energy and momentum equations. The COUPLED scheme is used for the pressure-velocity interpolation because it is appropriately used to find the density variation with respect to increase in temperature and swirl flows due to gravity.

The convergence of the solution was monitored by keeping the residual target 10^{-5} except the energy equation, for that the target of 10^{-8} is used. Further an extra investigation is performed to ensure the appropriate convergence. The convergence difficulties occur due to the vacuum modeling by using pseudo fluid whose velocity components are kept as zero while the radiational effects are investigated by using the MCRT method [9].

Result and Discussion

3D view of temperature contour and Non-Uniform heat flux contour on the surface of receiver tube is shown in figure 4(a) and 4(b) below. The resultant Non-Uniform heat flux varies from 900 W/m^2 to 42 KW/m^2. The maximum heat flux is concentrated on the lower half of the receiver tube. The Non-uniformity of heat flux on the surface of absorber tube is observed as, the temperature on the surface of receiver changes not only longitudinally but also changes circumferentially.
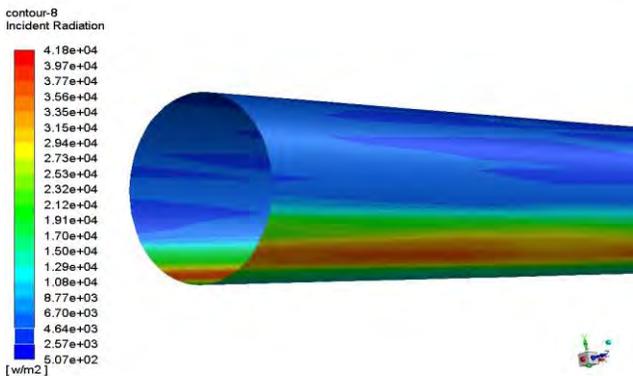
(a)
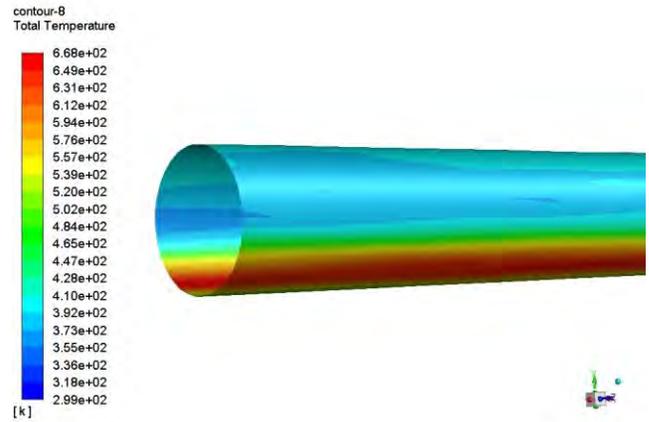
(b)
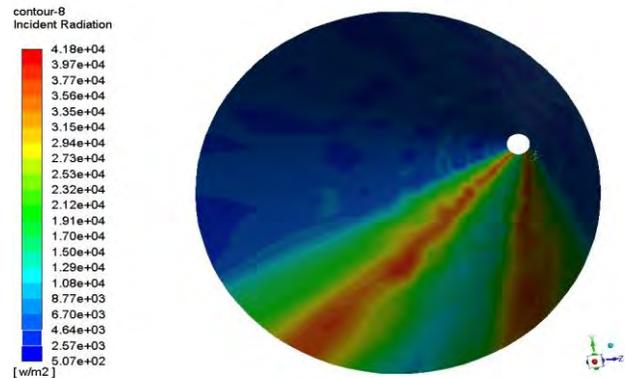
(c)

Figure 4. Three-Dimensional view of (a) Non-uniform heat flux (b) Temperature contour on receiver surface (c) Isometric view of receiver

Isometric view of inner side of absorber tube is shown in fig. 4(c), Which shows that the maximum heat flux is at the lower half of the receiver tube.
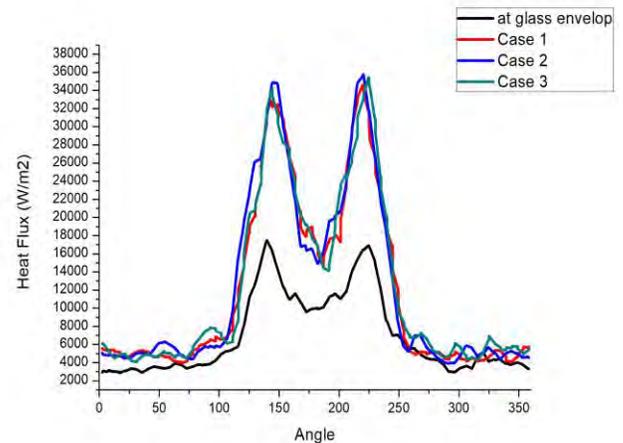
Figure 5. Solar energy flux distribution on the absorber tube with different case

Figure 5 represents the solar flux distribution at three different cases and these cases are as:

Case 1- no wall model case.

Case 2- no radiation (i.e. the conduction and convection occur in the receiver tube).

Case 3- unabridged model i.e. used all three modes of the heat transfer in tube (conduction, convection and radiation).

Trends observed the average temperature on the surface of absorber tube of cases (2 and 3) are higher than that of case 1. The temperature of heat transfer fluid varies from 300k to 668k with minimum flow rate of 0.1 m/sec. This Non-Uniformity of heat flux on the surface of absorber tube depends upon the geometrical configuration of the system.

Fig. 6 represent the temperature distribution in the angular direction in the three-different longitudinal location on the receiver tube (i.e. x = 0.5m, x = 1.0m and x = 1.5m). From this we saw that the temperature distribution increases as increase in the value of x and the temperature distribution on the surface of the absorber tube is almost symmetrical. And which look similar to the flux distribution on the surface of absorber tube. The temperature on the upper half of the receiver tube is slightly higher as compared to lower half of the receiver tube which is due to the natural convection by the temperature dependent property of the heat transfer fluid.
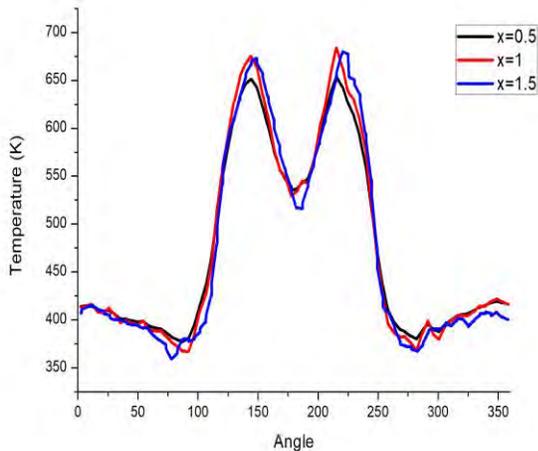
Figure 6. Temperature distribution on copper tube on angular direction

Fig. 7(a), 7(b) and 7(c) represents the increase in the temperature of three different fluid along with the length of the absorber tube at solar irradiance of 500 W/m^2, 800 W/m^2 and 1000 W/m^2. It shows that temperature of the

fluid rises along with the increase in the length of the tube.
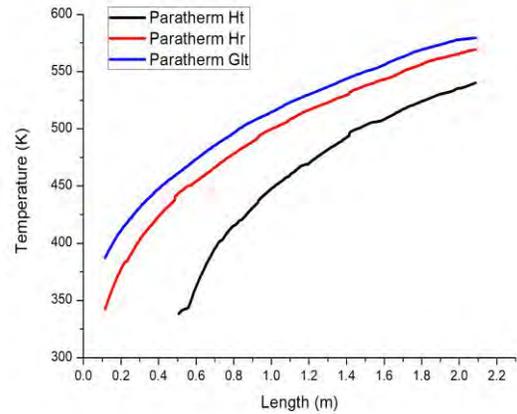
(a)
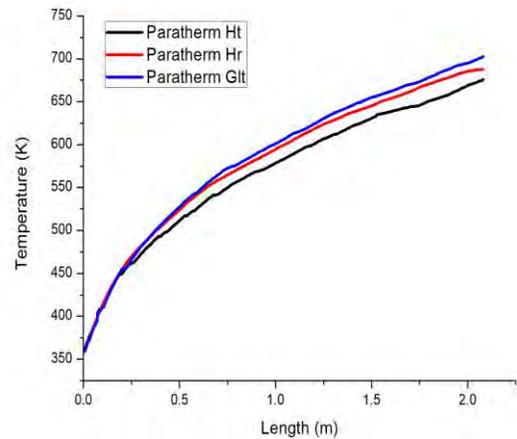
(b)
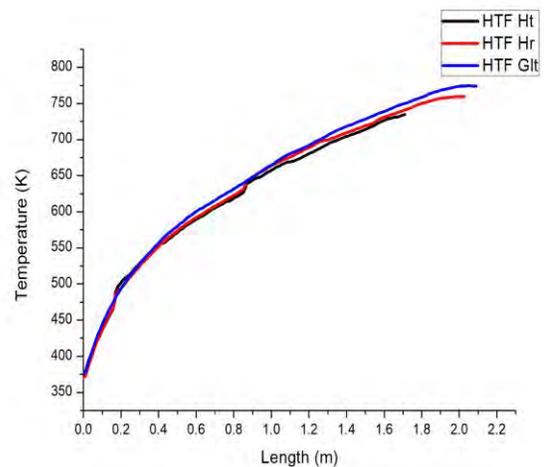
(c)

Figure 7. Temperature of different heat transfer fluid at (a) 500 W/m^2 (b) 800 W/m^2 (c) 1000 W/m^2
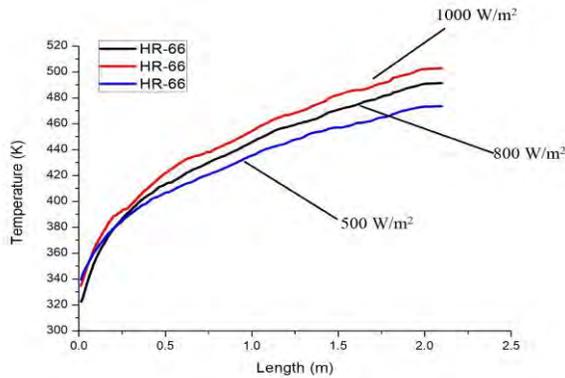
(a)
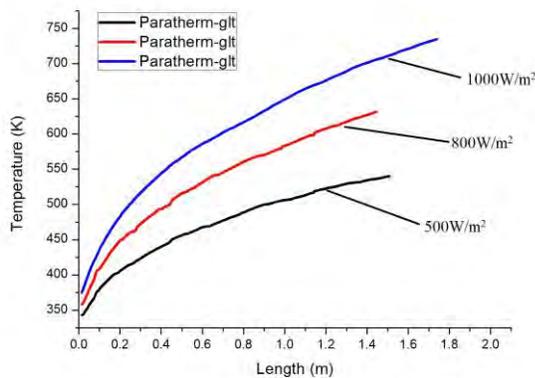
(b)

Figure 8. Temperature of heat transfer fluid (a) HR-66 (b) paratherm-glt at different solar radiation

Figure 8 (a) and 8(b) represents the variation in the temperature of the same heat transfer fluid at different solar irradiance. At different solar irradiance temperature profile on the surface of the absorber tube varies. This variation in the temperature profile leads the temperature variation in the heat transfer fluid.

Conclusions

Three-dimensional study of heat transfer characteristics on the surface of receiver tube of solar parabolic trough collector simulated by combining the Monte Carlo Ray Tracing (MCRT) method and FLUENT software has been performed. Three different models (i.e. no radiational model, unabridged model and no wall model) are modelled in the FLUENT to provide a further explanation of heat transfer mechanism from the receiver tube. Solar flux distribution on the absorber surface is obtained by using MCRT method under different conditions. Temperature distribution on the surface of absorber tube is almost symmetrical to variation of heat flux. Heat extraction from the receiver tube is highly dependent on the properties of heat transfer fluid and it increases with increase in solar irradiance.

References

[1] M. Islam, A. Karim, S. Saha, P. K. D. V Yarlagadda, S. Miller, and I. Ullah, "Visualization of thermal characteristics around the absorber tube of a standard parabolic trough thermal collector by 3D simulation," *Iccm*, 2012.

[2] A. A. Hachicha, I. Rodríguez, R. Capdevila, and A. Oliva, "Heat transfer analysis and numerical simulation of a parabolic trough solar collector," *Appl. Energy*, vol. 111, pp. 581–592, 2013.

[3] M. Günther, M. Joemann, and S. Csambor, "Advanced CSP Teaching Materials Chapter 5 Parabolic Trough Technology Authors," *2011*, pp. 1–43, 2011.

[4] M. Romero-alvarez and E. Zarza, "Concentrating Solar Thermal Power," vol. 20072827, no. September, 2007.

[5] H. Al-Ansary and O. Zeitoun, "Numerical study of conduction and convection heat losses from a half-insulated air-filled annulus of the receiver of a parabolic trough collector," *Sol. Energy*, vol. 85, no. 11, pp. 3036–3045, 2011.

[6] M. Yaghoubi, F. Ahmadi, and M. Bandehee, "Analysis of Heat Losses of Absorber Tubes of Parabolic through Collector of Shiraz (Iran) Solar Power Plant," *J. Clean Energy Technol.*, vol. 1, no. 1, pp. 33–37, 2013.

[7] Sargent & Lundy, "Assessment of Parabolic Trough and Power Tower Solar Technology Cost and Performance Forecasts Assessment of Parabolic Trough and Power Tower Solar Technology Cost and Performance Forecasts," *Rep. No. NREL/SR-550-34440*, no. October, p. 47, 2003.

[8] Z. D. Cheng, Y. L. He, J. Xiao, Y. B. Tao, and R. J. Xu, "Three-dimensional numerical study of heat transfer characteristics in the receiver tube of parabolic trough solar collector," *Int. Commun. Heat Mass Transf.*, vol. 37, no. 7, pp. 782–787, 2010.

[9] R. Forristall, "Heat Transfer Analysis and Modeling of a Parabolic Trough Solar Receiver Implemented in Engineering Equation Solver," no. October, p. 164, 2003.

FEASIBILITY STUDY OF BIOGAS INTERCHANGEABILITY

D. S. Yadav
Mechanical Engineering Department
Research Scholar
er.ds2009@gmail.com

B. Paul
Mechanical Engineering Department
Assistant Professor
bipaul@mnnit.ac.in

ABSTRACT

Energy saving and enviornment challanges for current situation for India. Biogas is one of the best option for save the Liqified Petroleum Gas (LPG) fuel which is used in domestic appliances. Mixing and substitute of biogas in place of LPG can increase the utilzation of renewable energy and reduce the pollution. According to the American gas association (AGA) and Weaver indices were investigated gas interchangeability of any gases substitute to other or replace. In this paper we investigates theoretical interchangeability of biogas into LPG or mixing into LPG. Minimum and maximum percentage of biogas mixed into LPG, Propane, Butane is 56-71%,48-65% and 61-74% respectively which is similar to the wobbe number of natural gas. The weaver indices of mixed gases (biogas and LPG) is interchangeable with natural gas but Propane, Butane, LPG is not interchangeable with biogas.

Keywords: interchangeability, biogas, LPG

NOMENCLATURE

H	High volumetric heating value
d	Specific gravity
s	Substitute gas
r	Reference gas
V_0	Theoretical air for complete combustion
D	Flame propagation velocity index
$\Phi (O_2)$	Volume fraction of oxygen in gas mixture
R	Ratio of number of atoms of H_2 in all forms of combination
N	Number of readily liberated atom of carbon per hundred molecules of gas
I_L	Lifting index
I_Y	Yellow tipping index
I_F	Flashback index
f	Primary air factor
Y	Yellow tip point
K	Lifting ultimate index

INTRODUCTION

Biogas is an important renewable energy resources in rural areas of India. At the end of 2015, about 20,700 lakh cubic meters of biogas is produced in the country which is equivalent to 5% of the total LPG consumption in India. Indian government had set a target to 6.5 lakh biogas plant in India under a program "The national biogas manure management program (NBMMP)" in 2012-2017. This program is being implemented by the State Nodal Departments, Khadi and village industries commission (KVIC) and Biogas Development and training Centers (BTDCs) [1].

Biogas is a type of gaseous fuel, that is mainly composed of 50-70% methane (CH_4) and 25-50% carbon dioxide (CO_2) and also traces small amounts of CO, H_2S, H_2, N_2 and so on. It is usually produced by anaerobic digestion bacteria using the organic fraction of animal manure, solid waste residue, sewage sludge from the waste treatment plants [2]. Interchangeability of biogas expresses the ability to substitute one kind of gaseous fuel replaced to another gaseous fuel without changing the material, efficiency, operational safety, performance and emissions. The main issue for interchangeability at low pressure atmospheric burners without involving other types of burner in different method of combustion [3]. Gas

interchangeability is not a new concept, it is began in 1926, when Wobbe presented a term Wobbe indices (WI) is directly proposnal to heating value and inversly proposnal to square root of specific gravity. These two paramters represent the gas quality of the interchangeability. American Gas Association (AGA) began a systmatic research on gas interchangeability and presented the two indices 'C' in 1933 for mixed gas research and 'I' in 1946 for interchangeability findout by multi-exponential method. In 1951, Weaver developed by using the multi-exponential method, furtherly, in which burning speed of mixed gas was taken for consideration [4]. Delbourg put forward new concept of 'combustion potential' in 1971, for developed a graphical method for gas interchangeability. Most researchers will work on the gas interchangeability of biogas and LPG. Merging non-upgraded and upgraded biogas into piped natural gas (PNG) investigate by Huang et al. [5], they found to be maximum mixing volume ratio of non-upgraded biogas 14.7% into PNG, when wobbe number and combustion potential are same as natural gas. Lee et al. [6] investigated the interchangeability of two kinds of Landfill gas (LFG) and LPG of their applicability to domestic appliances. Wai et al.[7] investigate theoretcal and experimental studies on biogas interchangeability, they found to change of biogas composition leads to issue the gas interchangeability. They also further investigated for biogas-LPG interchangeability of mixed gases according to AGA Bulletin 36 and Weaver. The qualities of mixed gases by varying the composition of methane (CH_4), carbon dioxide (CO_2), and propane (C_3H_8) or butane (C_4H_{10}) [8].

In this paper, we investigated the feasibility analysis of biogas interchangeability.

INTERCHANGEABILITY OF BIOGAS

Mixing the biogas into LPG gas can increase the utilization of biogas, reduce carbon intensity and promote renewable energy resources. Theoretical prediction of biogas interchangeability found with the help of three methods, method of Wobbe number (WN) and Combustion Performance (CP), method of American Gas Association (AGA) interchangeable indices, method of weaver index. When the constituents of the gas change, the heat value, density and combustion characteristics will vary as well. This will lead to variation in many factors, such as heat load, combustion stability, flame structure, CO emission, etc. Wobbe number (WN) and CP are used as the national standards to identify the gas interchangeability. However, in order to provide a more comprehensive analysis on interchangeability requirements, AGA indices are also calculated. AGA indices include lifting, flash-back and yellow indices in order to decide interchangeability. It is important to consider AGA indices as they not only provide interchangeability specifications but also provide specific gas quality. From table 1, the typical composition biogas, natural gas (12T reference gas), propane, butane, and LPG is taken consideration for study [5, 9].

METHOD OF WOBBE NUMBER AND COMBUSTION POTENTIAL

It is important criteria for gas interchangeability in combustion of burner one is Wobbe number (WN) other is combustion performance. Wobbe number is defined as the ratio of gas heating value H, and the square root of relative density $\sqrt{d}$. When the pressure is constant at the burner nozzle for the heat load of Q of gas appliances, then

$$WN = \frac{H}{\sqrt{d}} \qquad (1)$$

The wobbe number cannot exceed $\pm$ 5-10% in two gas interchangeability. It is not sufficient to identify the interchangeability of gas by WN, then other phenomena is combustion potential (CP). CP is a measurement of flame speed to be considered as another interchangeability factor. The calculation of CP is shown in Equations (2) and (3).

$$CP = \frac{\eta \left(1.0\, H_2 + 0.6(C_mH_n + CO) + 0.3CH_4\right)}{\sqrt{d}} \qquad (2)$$

$$\eta = 1 + 0.0054 O_2{}^2 \qquad (3)$$

METHOD OF AGA INTERCHANGEABILITY INDICES

Three interchangeable indices including lifting (I_L), flash-back (I_F) and yellow tip (I_Y) were suggested to judge interchangeability of substitute gas into reference gas only by AGA.
AGA interchangeable indices include the following:
1. Lifting index

$$I_L = \frac{K_a}{(f_r a_s / f_s a_r)(K_s - log(f_r/f_s))} \qquad (4)$$

Lifting is the movement of flame front downstream and away from burner port as a result of decreases in flame speed relative to flow velocity. This phenomena can cause the delayed ignition on burner or failed ignition. Lifting can also produced elevated carbon monoxide emissions.

2. Flash back index

$$I_F = \frac{K_s f_s}{K_r f_r} \sqrt{\frac{H_s}{39940}} \qquad (5)$$

3. Yellow tip index

$$I_y = \frac{f_s a_r Y_r}{f_r a_s Y_s} \qquad (6)$$

Yellow tipping phenomena generally comes in incomplete

combustion, it is the generation of soot particles with a flame that radiate incandescently, exhibiting a yellow colour [4, 5].

METHOD OF WEAVER INDEX

Although WN is frequently used and considered as the most effective method to judge the combustion stability, it lacks the ability to express combustion state such as lifted fire, flash, yellow tip, etc. The AGA method improves the justification creditability by referring to the lifted fire, flash and yellow tip indices to evaluate the interchangeability. However, the Weaver index is a more precise method by further considering flame speed and incomplete combustion indices besides all the AGA indices (Gas Technology Institute 2003). The best justification can be achieved by coupling the application of the single index with multiple indices. The Weaver index method evaluates the interchangeability by using a set of non-dimensional indices.

Weaver interchangeable index includes the following:

1. Index of interchangeability with respect to the heat rate

TABLE 1. COMPONENT AND PROPERTIES OF GASES

	Biogas	Natural gas	Propane	Butane	LPG
Component					
CH_4 (%)	60	100	0	0	0
C_2H_6 (%)	0	0	0	0	0
C_3H_8 (%)	0	0	100	0	40
C_4H_{10} (%)	0	0	0	100	60
CO_2 (%)	35	0	0	0	0
CO (%)	1.5	0	0	0	0
N_2 (%)	1.2	0	0	0	0
H_2 (%)	2	0	0	0	0
O_2 (%)	0.3	0	0	0	0
Higher heating value (MJ/m3)	23.08	37.77	95.65	126.21	113.98
High wobbe number (MJ/m3)	24.39	50.73	76.84	87.54	82
Specific gravity	0.9	0.555	1.55	2.079	1.876

$$J_H = \frac{H_s}{H_r}\sqrt{\frac{d_r}{d_s}} \tag{7}$$

For the complete interchangeable to substitute gas into reference gas, $J_H = 1$.

2. Index of interchangeability with respect to supply of air

$$J_A = \frac{V_{0s}}{V_{or}}\sqrt{\frac{d_r}{d_s}} \tag{8}$$

When $J_A = 1$, the total quantity of air required to burn each gas is the same for substitute and reference gas.

3. Index for flashback

$$J_F = \frac{D_s}{D_r} - 1.4J_A + 0.4 \tag{9}$$

For the gases that are exactly interchangeable with respect to flashback, $J_F = 0$.

4. Index for interchangeability with respect to lifting

$$J_L = J_A \frac{D_s}{D_r} \frac{1 - \emptyset(O_2)_s}{1 - \emptyset(O_2)_r} \tag{10}$$

For gases that are exactly interchangeable in this respect to lifting, $J_L = 1$.

5. Index for incomplete combustion of gas

$$J_i = J_A - 0.366\frac{R_s}{R_r} - 0.634 \tag{11}$$

For gases that are exactly interchangeable in this respect to incomplete combustion, $J_i = 0$.

6. Index of interchangeability with respect to yellow tip indices

$$J_Y = J_A + \frac{N_s - N_r}{110} - 1 \tag{12}$$

For gases that are exactly interchangeable in this respect to yellow tip, $J_Y = 0$

RESULTS AND DISCUSSSION

Out of three method of interchangeability, we have discussed only two method for the present study of biogas interchangeability.

RESULTS OF WOBBE NUMBER METHOD
According to interchangeability rules, biogas has a lower wobbe number than the other fuels so this is not interchangeable. Propane (WN = 76.84), Butane (WN = 87.54), LPG (WN = 82) can substitute in place of natural gas (50.73). Biogas is not substitute but can be mixed in gases to achieve a mixture which is acceptable in range of the reference gas (Natural gas). The minnimum and maximum allowable percentage of biogas mixed in given gases is x (0 < x < 1), then the wobbe number is accepeted in range of wobbe number of natural gas (WN = 45.67-

54.78). Then, Wobbe number of LPG, Propane, Butane respectively.

$$WN_{LPG} = \frac{113.98 - 90.9 * x}{\sqrt{1.876 - 1 * x}} \qquad (13)$$

$$WN_{prop} = \frac{95.65 - 72.57 * x}{\sqrt{1.55 - 0.65 * x}} \qquad (14)$$

$$WN_{buta} = \frac{126.21 - 103.31 * x}{\sqrt{2.079 - 1.179 * x}} \qquad (15)$$

After solving these equations gets minimum and maximum percentage of biogas mixed in gases. The theoratical value of biogas is mixed 57-71% into LPG, 48- 65% into Propane and 61-74% into Butane respectively. That means the minimum allowable percentage of biogas into LPG is 57% and maximum is 71%, which of wobbe number is near to natural gas, it is shown in figure 1.

RESULTS OF WEAVER INDICES METHOD

The weaver indices of biogas interchangeability, substituting biogas with propane, butane and LPG are given in table 3. Results of weaver indices, mixed biogas and LPG is interchangeable with reference gas as Natural gas, but pure propane, butane and LPG is not interchangeable with biogas and natural gas. The weaver indices of propane, butane, LPG value are exceeds the limit range of allowable value. Since these two mitxure of biogas and LPG have the same Wobbe number with natural gas. The value of J_H is near about to 1, which is range between in allowable range. All indices of mixed gases is not in range of allowable, the fuel is not adjested to natural gas.
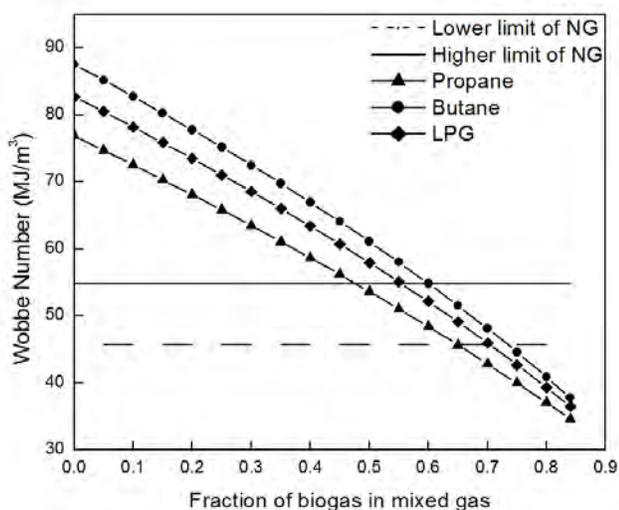
FIGURE 1. WOBBE NUMBER TO BIOGAS PERCENTAGE

TABLE 3. INTERCHANGEABILITY OF BIOGAS AND BIOGAS MIXED WITH LPG ACCORDING TO WEAVER INDEX

Weaver Indices	Biogas to LPG	Biogas to Propane	Biogas to Butane	Mixed (57 % biogas and 43 % LPG) to natural gas	Mixed (71 % biogas and 29 % LPG) to
J_H	3.398	3.157	3.597	1.08	0.902
J_A	3.380	3.177	3.566	1.05	0.881
J_F	-2.84	-2.548	-3.093	-0.152	0.037
J_L	5.07	4.764	5.347	0.9835	0.769
J_i	2.36	2.14	2.55	0.2	0.02
J_Y	4.75	4	5.29	1.09	0.57
Interchan- geable	No	No	No	No	Yes

REFERENCES

[1] Biogas production in India, 2015, www.factly.in/biogas-production.com
[2] C. G. Olmedo, A. R. Omez and R. Cartagena, 2014. "Energetic performance of landfill nad digester biogas in a domestic cooker". Applied energy, 134, pp. 301–308
[3] Guidebook to Gas Interchangeability and Gas Quality, August 2011
[4] E.R.Weaver, 1951."Formulas and graphs for representing the interchangeability of fuel gases". Journal of research of the national bureau of standards, 46(3), pp. 213–245
[5] X. Huang, S. Liu, W. Zhao, and A. Shukla, 2014. "Feasibility study on merging biogas into the natural gas pipe network in China". International Journal of sustainable energy, pp. 1–14
[6] C.E. Lee, C.H. Hwang, H.Y. Lee, 2008. "A study on the interchangeability of LFG-LPG mixed fuels with LFG quality in domestic combustion appliances", Fuel, 2008, 297-303
[7] W. Dai, C. Qin, Z. Lu, and C. Guo, 2011. "Theoratical predictions and experimental studies on biogas interchangeability". International conference on New Technology of Agriculture Engineering, May 27-29, pp. 706–709
[8] W. Dai, C. Qin,J.Tang, Z. Lu and Z. Li, 2011. "A study on the interchangeability of Biogas-LPG mixed gases with biogas and LPG qualities". pp. 280–283
[9] P. Boggavarapu, B. Ray, R.V. Ravikrishna, 2014."Thermal efficiency of LPG and PNG-fired burners: Experimental and Numerical Studies". Fuel, 115, pp. 709–715

SEEC-2018-145

Sustanaible hydrogen production from catalytic steam reforming of Acetic acid as model oxygenate of bio-oil using MoF derived nano Ni/ALC catalyst

Ankit Kumar , Dr.J.P.Chakraborty
Deapartment of chemical Engineering & technology IIT BHU
Email: ankit.rs.che14@iitbhu.ac.in,
jpc.che@itbhu.ac.in

Prof. A.S.K Sinha
Deapartment of chemical Engineering & technology IIT BHU
asksinha.che@itbhu.ac.in

ABSTRACT

Due to the fast declining of fossil fuels reourcess and growing concerns of global warming, climate issues have arouse the need of clean and renewable energy sources. Under such condition utilization of renewable resources like biomass has attracted more attention to the present researchers. Biomass derived biofuel (called bio-oil) by fast pyrolysis could be an efficient replace of fossil fuels. Acetic acid (AcOH) one of the major component of bio-oil was investigated for hydrogen production via steam reforming. In this study, Metal–Organic Framework (MOF) derived Nickel nano oxide particles supported on $Al_2O_2/La_2O_3/CeO_2$ (ALC) was synthesized and the catalytic activity and stability of the catalyst was evaluated. The catalyst was characterized by XRD, BET, HRSEM, HRTEM , TPR and Thermogravimetry.The conversion and H_2 yield of the synthesized catalyst were 100% and 86% respectively. The synthesized Catalyst relatively show stable activity behaviour up to a period of 28h.

Keywords>:*Hydrogen Production, Steam reforming, Bio -oil ,Acetic acid*

.

NOMENCLATURE

MOF   Metal Organic Frame work
ALC   Alumina-lanthana-Cerium

AcOH   Acetic acid

SRAA Steam reforming of acetic acid

1.INTRODUCTION

Hydrogen as a fuel is widely considered an emerging energy carrier and as a future transportation fuel. it presents several advantages, such as a high specific energy($\sim$120 MJ kg-1), formation of water as the only product during thecombustion process, among others [1]. Hydrogen production from renewable energy source like Biomass has gained great attention[2]. Bio-oil, generated from fast pyrolysis of biomass has been projected as a renewable sources to produce hydrogen by steam refroming because because it does not contribute to a net increase in atmospheric CO_2. In the present study bio-oil model compound Acetic acid, is one of the main components of bio-oil (up to 13 wt %) [3] has been selected to investigate the reaction mechanism for hydrogen production from steam reforming at different temperature on prepared heterogeneous catalyst via MOFs process. Steam reforming of acetic acid and the water gas shift reaction occur simultaneously in the reactor, the overall stoichiometry is represented by

$$CH_3COOH+2H_2O \longrightarrow 2CO_2+4H_2O \qquad (1)$$

Carbon dioxide and methane are two identical trends, a fact which implies that they may be produced according to the decomposition

$$CH_3COOH \longrightarrow CH_4+CO_2 \qquad (2)$$

Acetone is observed at low temperatures and low HAc conversion, and seems to be produces via the ketonization reaction

$$2CH_3COOH \longrightarrow (CH_3)_2CO+H_2O+CO_2 \qquad (3)$$
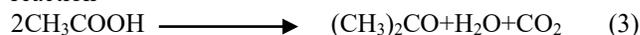
Carbon monoxide is also detected at high temperatures and its concentration increases with temperatures. A possible route of for CO production via decarboxylation reaction with cracking reaction

$$CH_3COOH+2H_2O \longrightarrow CO+CO_2+3H_2O \qquad (4)$$

WGS Reaction

$$CO+H_2 \longrightarrow CO_2+H_2 \qquad (5)$$
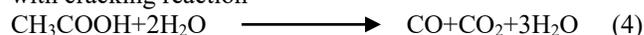
The acetic acid is unstable at high temperatue and prone to easily coke deposition on the catalyst surafec by thermal decomposition recation

$$CH_3COOH \longrightarrow C_2H_4, C_2H_6, C_3H_4, Coke\ldots. \qquad (6)$$
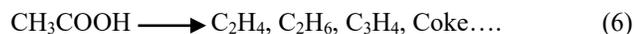
The severe hydrothermal process of SRAA makes catalyst easily deactivated due to carbon deposition and sintering of acticve metal [4] . Ni has been extensively used as an active metal for acetic acid steam reforming for its high activity. It shows high ability to both C-C and C-H rupture [5]

Metal–organic frameworks (MOFs) consist of Nickel as a metal in the ligand framework can potentially overcome the above disadvantages associated with the catalyst. These MOF based catalysts have signifcantly improved the efficiency, stability and the reusability of catalysts. However, in high temeperatue thermal reactions, direct use of MOFs as catalyst not possible due to their relatively limited thermal stability. To overcome these problems, researchers have prepared by combining with thermally stable support material like zeolite[6]. In the present study to investigate the MoF derived Nano Nickel particle supported on prepared Aumina-Lanthana-Ceria (ALC) thermally stable support was synthesized for acetic acid steam reforming. The catalytic activity were studied in a fixed bed flow reactor.

2. Experimental
2.1 Catalyst preparation
2.1.1 Synthesis of Support meterial
A high surface area aluminium hydroxide gel was prepared by neutralizing a concentrated solution of aluminium nitrate with ammonia solution at pH 9 and temperature 303 K. The hydro gel was aged for 24 h and then washed with distilled water until it was free of nitrate ions. Finally, it was dried in oven at 383 K and then calcined at 1073 K each for 8h to obtained γ -Al_2O_3 support. The γ -Al_2O_3 support was impregnated with the requisite amount of a dilute aqueous solution of lanthanum nitrate [La $(NO_3)_3.6H_2O$. 99.0%] to yield 3 wt% La_2O_3 in the final calatyst. This concentration was selected as it has been reported to be optimal in stabilizing the surface area of alumina against sintering [15]. The mixture was then dried over a bath with continuous stirring and finally dried in oven at 383 K and calcined at 1073 K each for 8hr. Ceria was then incorporated in to lanthana supported alumina by impregnation with the requisite amount of a dilute nitric acid solution of Cerium (IV) sulphate tetrahydrate (99+% Acros Organic) to obtain solids containing 9 wt. % CeO_2. The mixture was then dried over a bath with continuous stirring and then dried in oven at 383 K and calcined at 873 K each for 8h.

2.1.2 Synthesis of the Nano Nickel Particles
Stoichiometric ratios were used for the synthesis of the mano-metallic complexes.

$$NiCl_2 + 2(bpy) \longrightarrow Ni[(bpy)_2]Cl_2$$

1.47g of $NiCl_2$ and 3.54g of 2,2'-bipyridine ligand were dissolved in 2-propanaol 20 mL and 20 mL separately and dropwise mixed in a round bottom lab scale crystallizer with a flow rate of 0.33 mL/min. Solution stirred for 4

hours and temperature was maintained at 40 °C. Fine crystals of Ni-complex were separated, washed with ether to remove impurities. The yield was 80%. Stirring speed was kept 400rpm.

2.1.3 Synthesis of the Ni/ALC
In this case we took prepared requisite amount of Ni-complex dissolve in methanol solvent and the solution was impregnated with prepared $Al_2O_3/La_2O_3/CeO_2$ support to obtain final $conc^n$ of 15 wt% Ni (wt/wt) catalyst. After impregnation, the crystalline particles were dried for 12 hr (100 °C) and calcined at 550 °C for 4 hr in the tubular reactor after making pallets in the presence of controlled flow N_2 gas.

3. Characterization of Catalyst:
3.1 TGA analysis of nano Nickel (Nickel Complex):
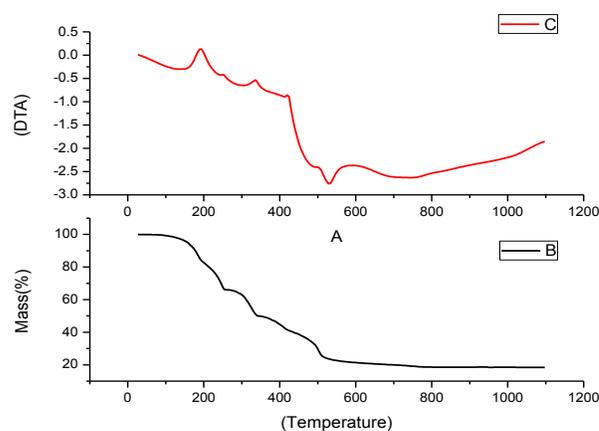
Figure. 1 TG and DTA curves of bis(bipyridine)nickel(II) chloride

Thermogravimetric analysis of Ni-Complex[Ni(2'2'-bipy)$_2$ Cl$_2$] was examined under inert atmosphere at a heating rate of 20 K/min. Nickel complex finally degrade to Ni(0) along with elimination of various volatiles by-products. The decomposition to Ni (0) proceeds by four steps. Early decomposition ~200 °C started probably with release of water coordination. The first step results in mass loss of 29.38% followed by three successive indistinctive steps showing elimination of bipyridine, hydrogen chloride and chlorine indifferent stages with mass loss of 19.32% and 24.45% giving final residue 18.32% that correspond to zero valent Nickel (ZVN) . On the other hand Hydrated $NiCl_2$ is found to be stable up to 400° C above which it decomposes in the presence of inert atmosphere by dehydrochlorination, dechlorination and partial oxidation [7].

3.2 XRD pattern of catalyst

Figure 2. depicts the XRD pattern of γ-Al_2O_3, $Al_2O_3/La_2O_3/$ CeO_2 (ALC), Ni-complex/ALC.
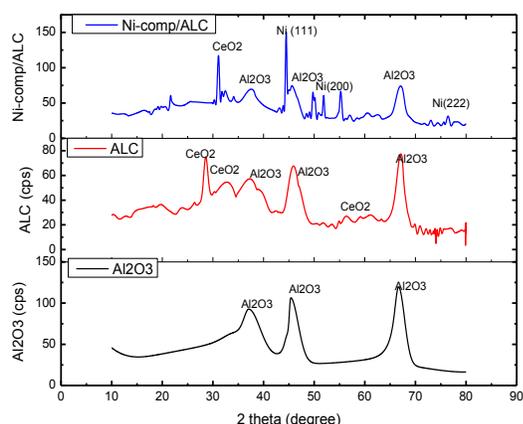
597

Figure. 2 Xray pattern of Support and catalyst

Species		Crystallite size (nm)	
	γ-Al_2O_3	CeO_2	Ni
Alumina Support	3.2	-	-
ALC support	3.2	3.1	-
Ni-Complex/ALC	3.2	3.1	5.5

Table 1: Crystallite size in support and catalyst

The d value and 2θ values for every peak of the support and catalysts were calculated and matched with the standard values reported for γ-Al_2O_3, La_2O_3 and Ni metal. The absence of diffraction peaks of La_2O_3 in all the samples indicates a high dispersion of lanthanum oxide in the support and the catalysts.

3.3 Surface area and pore size analysis

Support/Catalyst	Surface area (m²/g)	Pore Volume(cm³/g)	Pore size (nm)
γ- Al_2O_3	242	0.6077	11.33
Al_2O_3/La_2O_3/CeO_2 (ALC)	158	0.3673	13.07
Ni-complex/ALC	117	0.435	17.64

Table.1: Characteristics results of the calcined samples

Al_2O_3/La_2O_3/CeO_2 (ALC) has surface area 158 m²/g. As can be observed, the surface area was reduced with the introduction of nickel and/or ceria/lanthana on the supporting material. Whereas the pore volume was also significantly altered form γ- Al_2O_3 to final support (ALC).

The lower surface area can be ascribed to the fact that the internal surface area of the support pore system is probably covered by ceria/lanthana and nickel species adsorbed on alumina active sites forming a layer.

3.4. SEM images and EDX analysis:

SEM–EDX technique was carried out on the catalyst samples to have an idea on the textural properties and morphology of the catalyst samples. In Ni-/ALC catalyst, the observed particles with rod like particles and observed in a group of cluster high density and get agglomerated.

Element	Wt %	Atomic %
O K	32.37	51.44
AlK	41.70	39.29
LaL	0.38	0.07
CeL	7.44	1.35
NiK	18.11	7.84
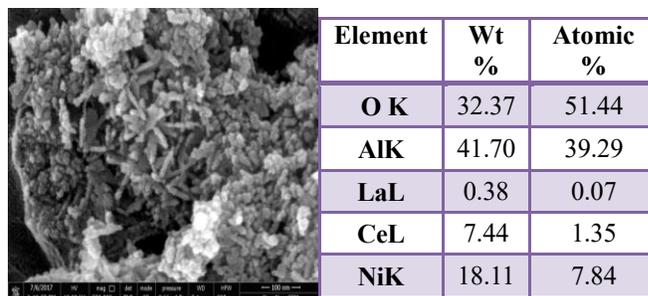
Figure 3 SEM image and EDAX analysis of Ni/ALC

3.5. TEM Analysis and particles size of samples:

TEM photographs and the morphologies of metal particles have been shown in figures 4. The sizes of the nano crystals obtained from the XRD diffraction patterns are in close agreement with the TEM studies, which shows that the sizes are nearly road type or like rice grain particles. The SAD patterns indicate that the particles are crystalline nature.
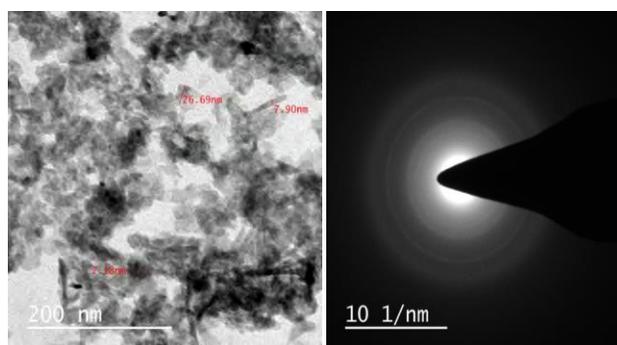
Figure 4.TEM images of Ni/ALC catalyst

4. Catalytic Activity

For this reforming test the synthesized catalysts were crushed and sieved to particles with diameter of 1.5-2.5mm. The particles were packed into a quartz fixed bed flow reactor in a physical mixture with inert same size The quartz reactor tube was 50 cm in length with a 10 mm of internal diameter and was held inside a temperature controlled electric furnace. A K-type thermocouple was located within the catalyst bed for controlling the overall

reaction temperature. The experiment were performed at steam to carbon ratio of 6.35 using a liquid feeding rate of 3ml/min and a WHSV =1.26h^{-1}. The product gas was allowed to pass through a condenser to condense the excess water and any condensable vapours and analyzed with two separate Gas chromatograph. H_2, N_2, CO, CH_4, and CO_2 in the gas were alayzed by a thermal conductivity detector (TCD) with Carosieve SII column and liquid product analyzed by Flame ionization detector (FID) with Porapak Q column.

5. Result and Discussion
5.1 Effect of reaction Temperature

The effects of reaction temperature on the conversion and selectivity of products gases were presented here in **Fig. 5** . It could be infered that reaction temperature had great influences on acetic acid conversion and seletivities to the products in the temperature range 300-700 °C. As expected, acetic acid conversion was increased with temperature and reached a complete conversion together with high Hydrogen yield about 63.69%. Besides this the higher CO_2 yield was also obtained apart from H_2 yield. At 300 °C, the conversion of acetic acid was just 15.60%, but it reached 98..09% at temperature 700 °C.
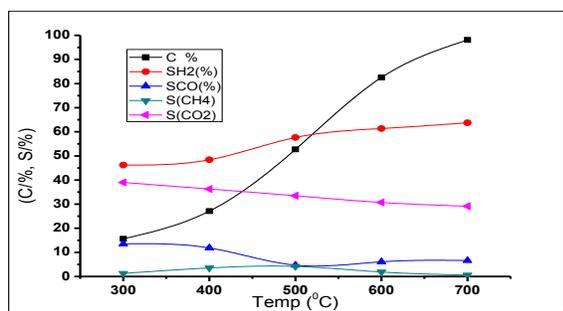
Fig 5. Effects of temperature on the conversion of acetic acid and Selectivities of the products. Experimental Conditios- S/C mol ratio 6.35:1; WHSV=1.26 h^{-1}; P=1 atm

At the same time, CO selectivity decreased from 13.6% to 4.7 % at 500 °C and slight increase at 600 °C. The cause of large amount of CO at low temperatute might be that Eqaution 1. (overall steam reforming recation) and Equation 5. (water gas shift reaction) could not occurred properly.The acetic acid and steam adsorbed on the catalyst surface could not be activated appropriately at low temperature. At 500° C the steam reforming and WGS reaction proceeded properly. As a consequences both the acetic acid conversion the selectivity of H_2 and CO_2 increased significantly. At temperature 700 C the catalyst showed the best performance. Acetic acid converted completely in o H_2 and CO_2 and reached maximum. While the selectivity to by-product of CH_4 was about 0.57 % due to thermal decomposition reaction or mathanation recation occurred during the reforming reaction.

5.2 Stability Test
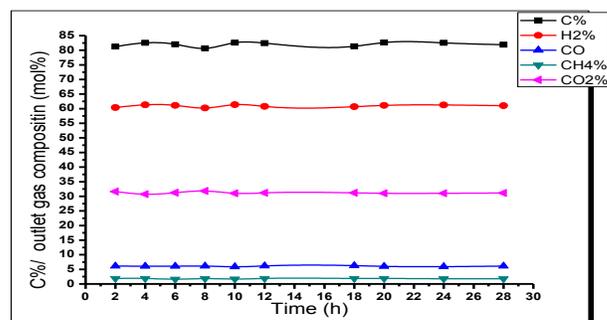
Fig. 6 stability test of 15Ni/ALC at 600 °C

Stability testing of 15Ni/ALC was carried out at 600 °C temperature with the same conditions of S/C ratio and wight hour space velocity for mor than 24h displayed in Figure 6. The carbon conversion and product mol% reatain almost same during the time interval. The catalyst showed a good stable behavior to coke deposition more than 24h.

6.Conclusion

The Ni-Complex/ALC supported catalyst showed high conversion and yield of SRAA and also showed maintained stability to the severe coke deposition of carbon up to 28h.

Acknowledgments

REFERENCES

[1] S.A. Chattanathan, S. Adhikari, N. Abdoulmoumine, Renew. Sustain. Energ. Rev.16 (2012) 2366–2372.

[1]   A. Kumar, J. P. Chakraborty, and R. Singh, "Bio-oil: the future of hydrogen generation."

[2]   F. Zhang, N. Wang, L. Yang, M. Li, and L. Huang, "Ni-Co bimetallic MgO-based catalysts for hydrogen production via steam reforming of acetic acid from bio-oil," in *International Journal of Hydrogen Energy*, 2014, vol. 39, no. 32.

[3] A. Remiro, B. Valle, A.T. Aguayo, J. Bilbao, A.G. Gayubo Fuel Process. Technol., 115 (2013), pp. 222–232.

[4] L. An, C. Dong, Y. Yang, J. Zhang, L. He, Renew. Energy, 36 (2011) 930-935. [10]

[5]   F. Zhang, N. Wang, L. Yang, M. Li, and L. Huang, "Ni-Co bimetallic MgO-based catalysts for hydrogen production via steam reforming of acetic acid from bio-oil," in *International Journal of Hydrogen Energy*, 2014, vol. 39, no. 32.

[6]   Corma, A., Garcia, H., & Llabrés i Xamena, F. (2010). Engineering metal organic frameworks for heterogeneous catalysis. *Chemical Reviews, 110*(8), 4606-4655.

[7] Mishra SK, Kanungo SB. Thermal degradation and decomposition of nickel chloride hydrate ($NiCl_2xH_2O$). J Therm Anal Calorim. 1992;38:2417–36.

SEEC-2018-146

UTILIZATION OF NANOPARTICLE-BASED SOLAR ENERGY SYSTEMS FOR IMPROVING THE OVERALL ENERGY EFFICIENCY OF BUILDINGS

Vishal Bhalla, Kapil Garg, Swapnil S. Salvi
Indian Institute of Technology Ropar
Rupnagar - 140001, Punjab, India
vishal.bhalla@iitrpr.ac.in kapil.garg@iitrpr.ac.in swapnil.salvi@iitrpr.ac.in

Venkataramana Badarla
Indian Institute of Technology Tirupati
Tirupati – 517506, Andhra Pradesh, India
ramana@iittp.ac.in

Deepak Fulwani
Indian Institute of Technology Jodhpur
Jodhpur - 342011, Rajasthan, India
df@iitj.ac.in

Vikrant Khullar
Thapar University
Patiala - 147004, Punjab, India
vikrant.khullar@thapar.edu

Madhukar M. Rao, Chakrapani A, Navaneeth Krishnan
CFD Virtual Reality Institute
Dharamsala, H. P., India
Madhukar.Rao@cfdvrinstitute.org   chakrapani@cfdvrinstitute.org
navaneeth.krishnan@cfdvrinstitute.org

Himanshu Tyagi *
Indian Institute of Technology Ropar
Rupnagar - 140001, Punjab, India
himanshu.tyagi@iitrpr.ac.in

* Corresponding Author: Tel: +91-1881- 242119, Fax: +91-1881- 223395

ABSTRACT

In developing countries like India and China, construction of buildings and usage by occupants consume upto one third of the total primary electricity. Rising incomes, urban migration, increasing incomes, population growth, growing electrification, transformation in lifestyle are some of the reasons which lead to this prediction in increase in energy consumption by buildings (both residential as well as commercial). Increase in requirement of comfortable living and working space necessitate the requirement of air-conditioned (heating during the winters and cooling during the summer). It is estimated that significant energy savings are possible from changes in building construction, climate sensitive design, use of locally appropriate material. Along with these measures it's also imperative to utilize clean and sustainable energy sources (such as solar energy) for meeting the energy demand of the building.

This paper considers the utilization of solar energy for meeting some of the energy requirements for a building envelope. In order to improve the overall efficiency of the solar collector, a nanofluid-based direct absorption system has been considered in this study. In such a collector, the solar irradiation is directly absorbed by the working fluid, which is a base fluid containing nanoparticles. The optical properties of these nanoparticles are a function of their size, shape and material properties. In this study the effects of aluminum nanoparticles have been considered. The results indicate that the solar collector has high efficiency and is able to meet the requirements of indoor space heating, for the designed area of solar collector.

Keywords: Solar energy; Heat transfer; Numerical modelling, Energy efficient Buildings, Solar collector, Nanoparticles.

INTRODUCTION

Energy plays a significant role for the existence of human life and primarily fossil fuels (coal, oil and natural gas) are used to provide required energy. Most of the energy is used for cooling and heating of the buildings (commercial and residential) because of climate change, social and economical changes, transformation of life style

etc. especially in developing countries like India and China.

For comfortable residential and commercial buildings, cooling and heating of the building is necessary. The typical energy breakdown by end-use for buildings is shown in Fig. 1. For most of these end-uses (such as lighting, fans, appliances, heating, cooling) electrical energy is required, for which fossil fuels have been used. The use of the depleting fossil fuels causes air pollution after burning. So, one should focus on the usage of clean and free energy (such as solar energy) resources for comfortable buildings. It has been estimated that around 5.6 million exajoules of sunlight incident on earth's surface, which is 1000 times the current global energy consumption [1]. The value of the incident solar radiation varies from one terrestrial location to another.
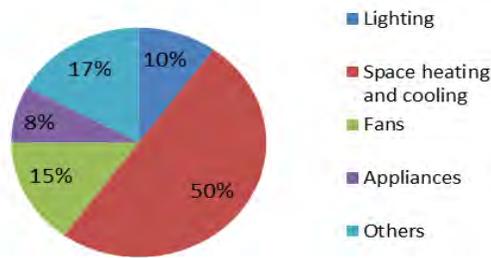
Figure 1 Energy breakdown by end use for buildings.

For the harnessing of the solar irradiation, solar thermal collectors have been used, which are a type of heat exchangers. These solar thermal collectors absorb the solar energy, convert it into heat and transfer the heat to the working fluid (air, water etc.). Shen et al. [2] have conducted an experimental study with unglazed solar thermal facade and have concluded that the integration of solar thermal facade and building affects the overall building energy performance. Li et al. [3] have numerically showed that 64.6 % heating demand and 20.2% of cooling requirement in buildings can be met by using solar energy. Tsalikis and Martinopoulos [4] have concluded that the use of a solar combo system for space and water heating, coupled with a small photovoltaic system can pro- vide enough energy for a building. They have suggested that the solar energy systems are capable of covering more than 76% of the total primary energy demand and in some cases up to 97%, while presenting a Discount Pay Back Period of less than 6 years (with a minimum of 4 in some cases) with an initial investment cost of 10000– 12250 €. Kyriaki et al. [5] have presented the overall evaluation of the solar thermal system and its contribution in the improvement of building's energy and environmental performance. They have concluded that with solar thermal systems there has 67% less CO_2 emission to the environment.

Some challenges are associated with the conventional surface absorber based collectors like: a) high

emission losses to the environment at high flux b) the material used to absorb the solar radiation gets damaged due to weather c) high thermal resistance in between absorber plate and the working fluid. In order to overcome these issues, the researchers and scientists suggested that the incoming solar radiation should get absorbed by the heat transfer fluid itself and the collectors are known as direct absorption solar collector (DASC) [6][7]. Tyagi et al. [8] have shown that with the addition of aluminium nanoparticles ($D = 5$ nm) in water, the absorptivity of water is increased by nine times and have concluded that on absolute basis the efficiency of DASC is 10% higher than the conventional solar collector. Taylor et al. [9], Otanicar et al. [10], Lenert and Wang [11], Khullar et al. [12], have concluded experimentally and numerically that the performance of nanoparticles-laden fluid based collector is dependent of the volume fraction of the nanoparticles.

From the literature, it has been found that DASC has high thermal efficiency and can be used to make the building's environment comfortable (for the heating and cooling purpose). In the current study, numerical analysis for an energy efficient building which utilizes solar thermal energy for heating purposes has been conducted. A novel design of solar collector – consisting of nanofluid-based direct absorption solar collector is analysed in detail. The results show that convective heat transfer coefficients as well as the volume fraction of nanoparticles (aluminium) play a very significant role in determining the overall efficiency of the solar collector.

HEATING OF BUILDING ENVELOPE DURING WINTER SEASON

A detailed analysis has been carried out for one of the city of Punjab– Rupnagar [13-15], for a particular month in winter season (December). An example of an office building is considered, located within Rupnagar. The heating of the indoor space is designed to be carried out with the help of solar energy. For this purpose a solar collector shall be placed on top of the building which will convert the solar irradiation into thermal energy (of the working fluid). Such a warm fluid will then be passed through a heat exchanger kept inside the indoor space in order to transfer its heat to the air. The fluid hence cooled, will return back to the solar collector and again be heated. This cycle will continue as long as the solar energy is available.

This section is divided into 2 parts. In the first part the problem formulation has been carried out where the details of the building, such as its dimensions, building materials and properties, ambient conditions, physical and meteorological conditions etc., have been described. In the second part, the full details of the results which are obtained by varying the important parameters and observing their effects on the performance of the solar collector (collector efficiency, fluid outlet temperature) and the loading of the building have been carried out.

Heating of interior space using solar collector (nanofluid-based direct absorption solar collector)

Figure 2 shows the schematic of the building envelope considered in these calculations. The roofs of the building as well as the 4 walls are exposed to the ambient conditions. The rooftop of the building contains the solar collector system. The purpose of this solar collector is to convert the solar irradiation into thermal again, which is then transferred by conduction and convection to the working fluid (usually water, in the present study it's a nanofluid). As shown in the figure, a large heat exchanger is placed inside the building which transfers the heat from the fluid to the indoor air and creates the comfortable conditions. Once the fluid transfers its heat to the air, it gets cooled down and returns back to the solar collector through the insulated pipes. Since the temperature of outside air during winters in Rupnagar are quite low (< 10 ^{o}C), the pipe carrying the fluid back to the solar collector is also insulated to improve the overall efficiency of the solar collector.
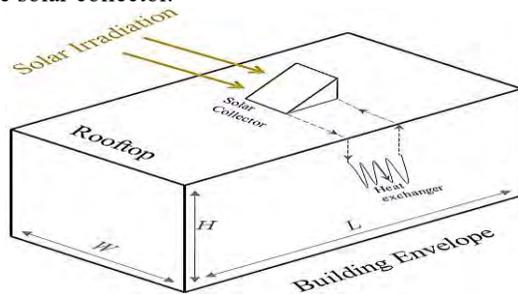
Figure 2 Schematic of the building envelope, showing the rooftop solar collector as well as the heat exchanger for space heating.

In the present calculation the following building parameters have been considered:

Location of building, Rupnagar   (31.1 ^{o}N, 76.5 ^{o}E)
Floor area of the building, A_f 3000 ft^2 (= 278.7 m^2)
Length of the building, L 100 ft (30.48 m)
Width of the building, W 30 ft (9.14 m)
Height of the building, H 10 ft (3.05 m)

The thermal properties of the building envelope material are as follows:

Building material   Brick and concrete
Thermal conductivity, k_{th} 0.7 W/mK
Density, ρ 1900 kg/m^3
Specific heat, C_p 0.84 kJ/kgK

The schematic of the nanofluid -based direct absorption solar collector considered in these calculations are shown in Fig. 3. As shown in the schematic the problem is assumed to be 2-dimensional (in x and y directions). The top glass cover is exposed to the ambient conditions (surroundings at a temperature of T_{out} = 10 ^{o}C, and a convective heat loss coefficient of h_{conv} = 5 W/m^{2}K). The solar irradiation incident on the top surface is assumed to be normally incident.

In the present model for the solar collector the following parameters have been assumed:

Basefluid:	Water
Type of nanoparticles:	Aluminum
Particle diameter, D	10 nm
Nominal particle volume fraction, f_v	0.05%
Incident flux (normal) on the top surface, q_o	700 W/m^2
Transmissivity of the glass cover, τ	0.9
Fluid inlet temperature, T_{in}	30 ^{o}C
Velocity of the fluid, U_o	0.5 cm/s
Collector height, h_o	2 cm
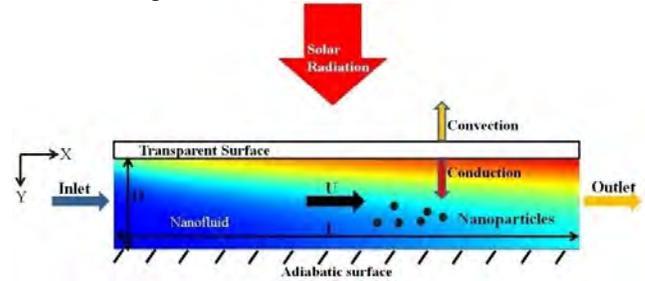
Figure 3 Schematic of the solar collector using nanoparticles.

This model is numerically solved using the 2-D heat transfer and 1-D radiative transport equations in MATLAB, using finite difference technique. The details of the equations and the numerical methods have been discussed elsewhere [8][11] and those details are not the focus of the current study. Three of the main equations used in the analysis are presented here, along with the results obtained by solving those governing equations.

The black body spectral intensity ($I_{b\lambda}$) incident on the solar collector is given by the following relation[8][11]:

$$I_{b\lambda}(\lambda, T) = \frac{2h'c_o^2}{\lambda^5 \left[\exp\left(\frac{hc_o}{\lambda k_B T_{solar}}\right) - 1 \right]} \quad (1)$$

The extinction coefficient ($K_{e\lambda}$) of the nanoparticles-laden fluid is calculated by adding the absorption coefficient ($K_{e\lambda}$) and the scattering coefficient ($K_{e\lambda}$), and the expression is given by the following relation [8]:

$$K_{e\lambda} = K_{a\lambda} + K_{s\lambda} \quad (2)$$

The 2-D heat transfer equation (shown below) is solved using finite difference method, by discretizing the temperature and intensity values across the x and y directions, for a given velocity of the fluid, U_o, [8].

$$k_{th}\frac{\partial^2 T}{\partial y^2} - \nabla q_r = \rho C_p U_o \frac{\partial T}{\partial x} \quad (3)$$

Once these equations are solved (by applying the suitable boundary conditions at the solar collector boundaries), the following results are obtained from the numerical model:

Design fluid mass flow rate, m = 0.2 kg/s
Collector length, l = 16 m

Collector width, $w_o = 1.1$ m

Total area of the collector, $A = 18.8$ m^2

Overall performance of the solar collector and heating load of the building

As can be seen from this Fig. 4, the incident solar energy on the top surface of the fluid corresponds to the solar blackbody radiation (T_{sun} = 5800 K). As the irradiation passes through the fluid, it is gradually absorbed. The absorption is also accompanied by scattering, and the sum together is denoted by extinction. Hence the extinction coefficient (K_e), can be expressed as the sum of absorption and scattering coefficients, $K_e = K_a + K_s$.
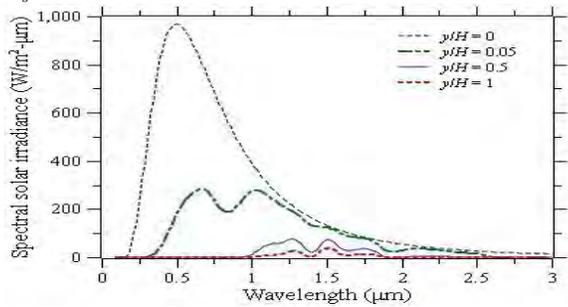
Figure 4 Spectral solar irradiance within the collector at various depths.

Fig. 5 depicts the effect of four different values of convective heat transfer coefficients. The heat transfer coefficient has a significant impact on the overall performance of the solar collector, as it directly affects the fluid temperature distribution. The temperature profile is highest when the heat transfer coefficient is low, and with gradual increase in the heat transfer coefficient, the temperature shows a uniform decrease.
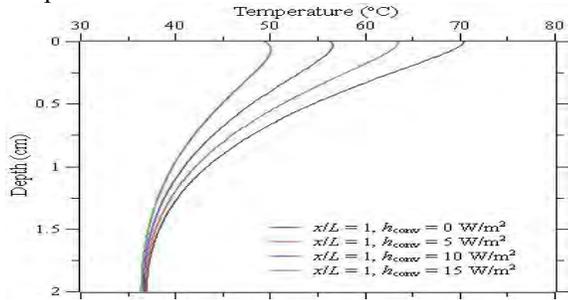
Figure 5 Temperature profile within the collector, at various convective heat transfer coefficients.

This impact can also be seen in the mean fluid outlet temperature, which is shown in Fig. 6. The 2 curves show much higher outlet temperatures compared to the pure fluid case. Also, the effect of convective heat transfer coefficient is quite visible, as there is an appreciable temperature dip (of about 10°C), when the convective heat transfer coefficient increased from 0 W/m^{2}K to 10 W/m^{2}K.

Finally the overall solar collector efficiency is shown in Fig. 7. All the curves are plotted as a function of

the ratio of the temperature difference (ΔT) and the incidence irradiation flux (G_T). As the ratio increases there is a corresponding decrease in the value of the solar collector efficiency. This is because at larger values of temperature difference, the amount of losses from the collector (both convective as well as radiative) tend to increase and as a result the efficiency tends to decrease. Interestingly, the first curve (corresponding to heat transfer coefficient of 0 W/m^{2}K) shows no variation with temperature difference.
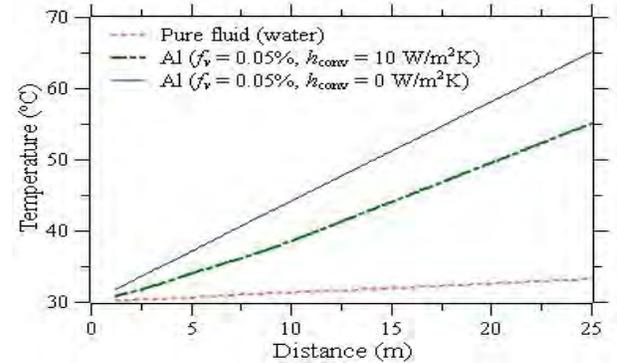
Figure 6 Fluid outlet temperature as a function of distance along the collector length.
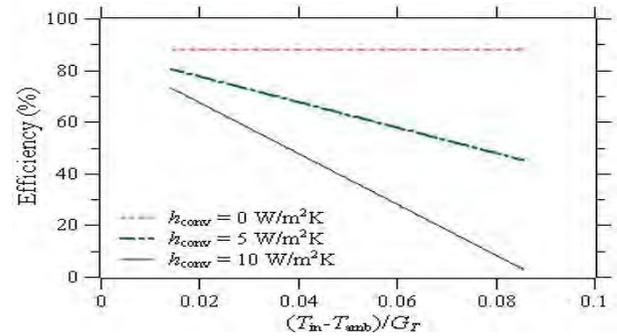
Figure 7 Collector efficiency as a function of temperature difference (for various convective heat transfer coefficients).

The results discussed in this section show that with the use of nanofluid-based direct absorption solar collectors efficient conversion of solar energy into thermal energy can be achieved.

CONCLUSION

The study shows the results of numerical analysis for an energy efficient building which utilizes solar thermal energy for heating purposes. A novel design of solar collector – consisting of nanofluid-based direct absorption solar collector is analyzed in detail. A typical building in one city (Rupnagar) is analysed in detail for a winter month (December). The results show that convective heat transfer coefficients as well as the volume fraction of

nanoparticles (aluminium) play a very significant role in determining the overall efficiency of the solar collector. The calculation results show the required are of the solar collector needed for the building, and also evaluated the efficiency of the solar collector. An improvement in the overall energy consumption by the building is observed, by reducing the dependence on electricity and increased reliance on clean energy sources (solar energy).

ACKNOWLEDGEMENT

REFERENCES

[1] Kondaraju, S., Jin, E. K., & Lee, J. S. (2010). Direct numerical simulation of thermal conductivity of nanofluids: the effect of temperature two-way coupling and coagulation of particles. International Journal of Heat and Mass Transfer, 53(5), 862-869.

[2] Shen, J., Zhang, X., Yang, T., Tang, L., Shinohara, H., Wu, Y., Wang, H., Pan, S., Wu, J., and Xu, P., 2016, "Experimental Study of a Compact Unglazed Solar Thermal Facade (STF) for Energy-Efficient Buildings," Energy Procedia, **104**, pp. 3–8.

[3] Li, L., Qu, M., and Peng, S., 2017, "Performance Evaluation of Building Integrated Solar Thermal Shading System : Active Solar Energy Usage," **109**, pp. 576–585.

[4] Tsalikis, G., and Martinopoulos, G., 2015, "Solar Energy Systems Potential for Nearly Net Zero Energy Residential Buildings," Sol. Energy, **115**(2015), pp. 743–756.

[5] Kyriaki, E., Giama, E., Papadopoulou, A., Drosou, V., and Papadopoulos, A. M., 2017, "Science Direct Energy and Environmental Performance of Solar Thermal Systems in Hotel Buildings," Procedia Environ. Sci., **38**(38), pp. 36–43.

[6] Otanicar, T. P., Phelan, P. E., and Golden, J. S., 2009, "Optical Properties of Liquids for Direct Absorption Solar Thermal Energy Systems," Sol. Energy, **83**(7), pp. 969–977.

[7] Khullar, V., Bhalla, V., and Tyagi, H., 2017, "Potential Heat Transfer Fluids (Nanoparticles-laden fluids) for Direct Volumetric Absorption-Based Solar Thermal Systems," J Therm Sci Eng Appl.(Article In Press)

[8] Tyagi, H., Phelan, P. E., and Prasher, R., 2009, "Predicted Efficiency of a Low-Temperature Nanofluid-Based Direct Absorption Solar Collector", *ASME Journal of Solar Energy Engineering*, Vol. 131(4), p. 041004.

[9] Taylor, R. a, Phelan, P. E., Otanicar, T. P., Walker, C. a, Nguyen, M., Trimble, S., and Prasher, R., 2011, "Applicability of Nanofluids in High Flux Solar Collectors Applicability of Nanofluids in High Flux Solar Collectors," J. Renew. Sustain. Energy, **23104**(3), pp. 23104-1-0-15.

[10] Otanicar, T. P., Phelan, P. E., Prasher, R. S., Rosengarten, G., and Taylor, R. a., 2010, "Nanofluid-Based Direct Absorption Solar Collector," J. Renew. Sustain. Energy, **2**(3), p. 33102.

[11] Lenert, A., and Wang, E. N., 2012, "Optimization of nanofluid volumetric receivers for solar thermal energy conversion", Solar Energy, Vol. 86, pp. 253-265.

[12] Khullar, V., Tyagi, H., Hordy, N., Otanicar, T. P., Hewakuruppu, Y., Modi, P., and Taylor, R. A., 2014, "Harvesting Solar Thermal Energy through Nanofluid-Based Volumetric Absorption Systems," Int. J. Heat Mass Transf., **77**, pp. 377–384.

[13] IMD (India Meteorological Department), Monthly mean maximum & minimum temperature and total rainfall based upon 1901-2000 data, http://www.imd.gov.in/section/climate/climateimp.pdf

[14] Solar Radiation Data for India, Solar Energy Centre, Ministry of New and Renewable Energy, http://mnre.gov.in/sec/solar-assmnt.htm

[15]http://www.synergyenviron.com/tools/solar-irradiance/india/

SHAPE-CONTROLLED SYNTHESIS OF CDS DECORATED ON REDUCED GRAPHENE OXIDE: A POTENTIAL PHOTOCATALYST FOR H2 PRODUCTION FROM WATER SPLITTING

1*·Zahoor Alam 2. Dr. Bhawna Verma
Department of Chemical Engineering IIT(BHU)
Varanasi
zahoor.rs.che14@iitbhu.ac.in
bverma.che@itbhu.ac.in

3. Prof. A.S.K Sinha
Department of Chemical
Engineering IIT(BHU) Varanasi
asksinha.che@itbhu.ac.in

ABSTRACT

In this study we have been synthesized reduced graphene oxide supported cadmium sulphide (CdS-rGO) by different preparation techniques i.e., hydrothermal and solid gas method. Prepared catalysts are potentially active in splitting of water to hydrogen under visible light. Microstructures of catalysts were determined by XRD, UV-VIS, SEM, TEM, HRTEM, and SAED .Reduced graphene oxide (rGO) use as a co-catalyst, it enhance the hydrogen production as well as durability of photocatalyst.Reduced graphene oxide has more negative work function (-4.2eV) than conduction band potential (-1.42eV) of CdS, so charge at conduction band migrates into the reduced graphene sheet and suppress the recombination of charge carriers, i.e., electron and hole recombination. Reduced graphene oxide (rGO) not only use to prevent the recombination of charge carriers but also provide active sites for reduction H+ ions into H_2.It is also seen that structure and morphology of photocatalyst also enhance the hydrogen production.

***Keywords** Photocatalyst,Graphene, Hydrogen, Charge recombination,Morphology*

NOMENCLATURE
1. SG   Solid-Gas method
2. HY Hydrothermal method

INTRODUCTION

Nowadays, energy crisis and global warming have been increasing constantly. To overcome these problems, there is a search about renewable energy resources. Hydrogen production by photocatalytic splitting of water is one of the methods to overcome the above mention problems.So there is need of stable and durable phtocatalyst.CdS has narrow band gap (2.42eV) and has more negative conduction band potential energy than reduction potential of H+[1] .To improve the activity of CdS, much more research was done on the catalyst morphology and crsytallinity.It is commonly opted that co-catalyst play an important role in transfer of photoinduced electrons and improve the stability and durability of catalyst.It is commonly opted that Co-catalyst play important role in transfer of photoinduced electrons and improve the activity, stability and durability of catalyst.Graphene oxide(GO), a graphene derivatives, is an electricalyy insulating material and usually exhibits a rich mélange of oxygen-containing groups such as carboxylic, hydroxyl, carbonyl and epoxide groups.The electrical conductivity of graphene oxide(GO) can be increased by reduction of and gfragmentary restoration of sp^2-hybridized network,the resulting products is also known reduced graphene oxide(rGO).However, the combination of CdS nanoparticles with (rGO) sheets, a good strategy to improve the photocatalytic perfomances of CdS.The electron accepting ability of rGO sheet can be used to enhance the elctron transport properties of CdS[2]

2.   **EXPERIMENTAL:**

(a)Synthesis of reduced graphine Oxide: Graphite oxide (GO) was prepared by modified Hammers method. Then prepared Graphite Oxide powder was added into distilled water and sonicated for 30 minutes to exfoliate the graphite oxide sheet and then ammonium nitrate was added into graphite oxide solution and stirred for one hour. As prepared solution was put into Teflon line stainless steel reactor and placed in an oven at 180 degree Celsius for 24 hours. Resulting solution was washed with water and dried at 70 degree for 24 hours.

(b) Preparation of Reduced Graphene Oxide supported Cadmium Sulphide in Aqueous Solution (CdS/rGO): Equal Amount of Cadmium Acetate $Cd(Ac)_2.2H2O$ and Thiourea CH_4N_2S along with 1.5 g of graphite oxide (GO) were dispersed in 150 mL of distilled water and mechanically mixing the solution for 2 hours and it placed into Teflon lined stainless steel reactor with 200 (mL) capacity. Then it was placed in an oven at 130 degree Celsius for 15 hours. Resulting products was washed with distilled water several times and it dried in an oven at 70deg for 24 hours.

(c)Preparation of Reduced Graphene oxide Supported Cadmium Sulphide by solid –gas method (CdS/rGO): In a typical synthesis, Firstly Cadmium Sulphate Powder and Graphite oxide were added into 200 mL of distilled water and stirred for 4 hours to make homogenous .Chemically prepared homogenous mixture dried in an oven for overnight. After that dried granules was placed into fixed bed tubular reactor and then reactor was purged with N_2 gas and thereafter Pure H_2S gas passed into fixed at 300 degree Celsius for 4 hours. Then resulting products was with water and dried.

Figure1: Experimental set up for Hydrogen production by Photocatalytic splitting of water.

3. ACTVITY MEASUREMENT

The photocatalytic reaction for hydrogen production was carried out in a semi –batch flat bottomed flask photorector (Pyrex glass)which shown in figure 1. A 100 W Oriel mercury –Xenon lamp was employed as light source.One gram of prepared photocatalyst (200 mesh size) was suspended into 250 mL of aqueous solution of 0.01M sulphide(Na_2S)and 0.004M (Na_2SO_3) as sacrificial agent.The 8.6 pH was maintained for the experiment by adding NaOH and acetic acid solution.

.

4.RESULTS AND DISCUSSION:
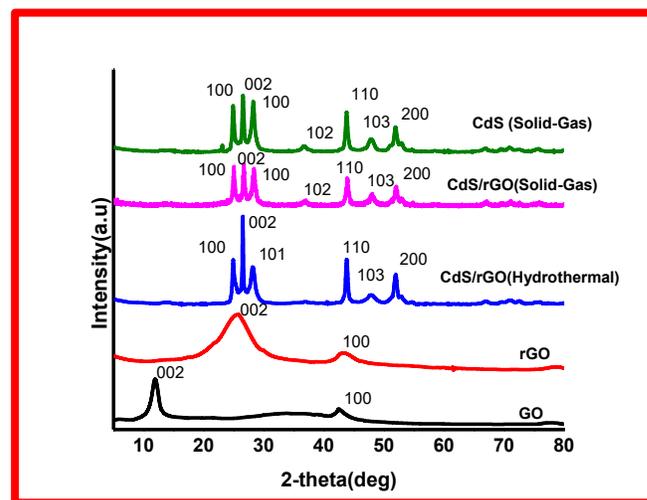
Figure2: XRD pattern ofGO,rGO,CdS/rGO(hydrothermal), CdS/rGO (Solid-gas) and CdS(Solid-Gas)

X-ray diffraction analysis of catalysts were carried out by an X-ray diifractometer (XRD Rigaku Ultima IV) with Cu Kα radiation ($\lambda=1.54056$ A^0).In X-ray diffraction Pattern, graphite oxide(GO) and reduced grapheme oxide (rGO) are shown in figure 2. A sharp diffraction pattern (002) appearing at 11.95^0 is attributed to GO. This confirmed that graphite was oxidised into Graphite oxide by expanding the d-spacing 3.4 A^0 to 7.4 A^0 . After reduction XRD peak at 23.79^0 appeared, which confirmed that some of the oxygen-containg functional groups has been removed.Incorpoaration reduced grapheme oxide (rGO)with CdS, all diifraction peaks of catalysts CdS/rGO(Hydrothermal) , CdS/rGO (Solid-gas) and CdS (SG) well matched with hexagonal structure of CdS with JCPDWIN (File No.653414).In figure2 it is also seen that incorpation of reduced graphene oxide with CdS, peak at 23.79^0 of reduced graphene oxide was dissapered, this peak shielded by the main peak of CdS at 25^0. It is also seen from XRD pattern, catalysts prepared by hydrothermal method, the growth of CdS particle preferentilly oriented along the c-axis{[3]. Reduced graphene oxide supported cadmium sulphide prepared by solid –gas method showed highly crystalline in nature and intensity of diffraction peaks of (100),(002)and (101) nearly equal.It means that the growth of this catalyst equal in all the three planes.
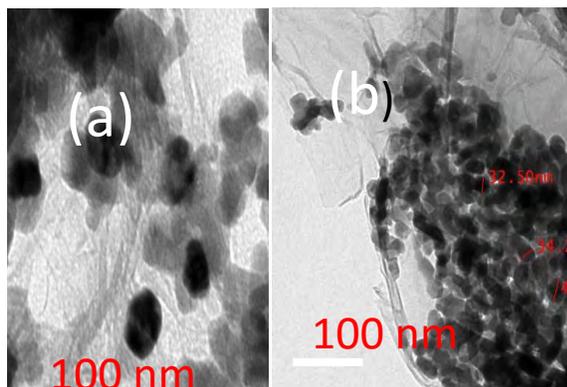
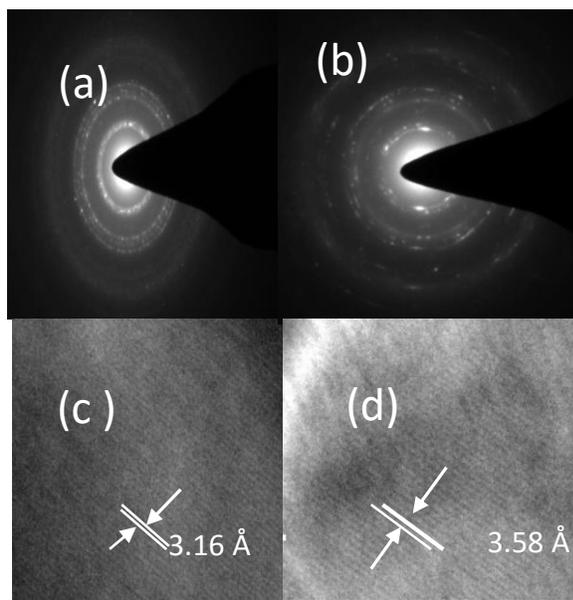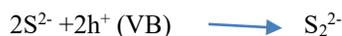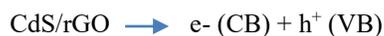Figure3: (a) and (b) shows TEM image of CdS/rGO(HY) and CdS/rGO (SG)

Figure 4. (a) and (b) shows SAED pattern of CdS/rGO (Solid-Gas) and CdS/rGO (HY), (c) and(d) shows lattice fringes of CdS/rGO (Solid-Gas) and CdS/rGO (HY)

The microstructure of as- prepared catalysts were examined with Trnasmission Electron Spectroscopy (TEM). TEM image of catalyst CdS/rGO

(HY) and CdS/rGO (SG) shown in figure 3. It is observed that CdS nanoparticle uniformally distributed on the surface of the reduced graphene oxide sheet.Selected area pattern and lattices fringe of prepared catalysts are shown in figure 4, it is clearly seen that d-spacing of catalyst CdS/rGO (HY) and CdS/rGO (SG) are measured nearly $3.16A^0$ and $3.58A^0$ respectively, which correspond to (101) and (100) reflection planes of hexagonal structure of CdS.

Photocatalytic activity:
The activity of catalyst as mL of H_2 produced at NTP for 2h of iiradiation is given in Table1.The reported value are average of number of repeated runs.No hydrogen was observed in the absence of light.Upon the iiradiation of light on photocatalyst,the reaction should proceed as follows:

$$CdS/rGO \longrightarrow e- (CB) + h^+ (VB)$$

$$2H_2O +2e^- \longrightarrow H_2 + 2OH-$$

$$SO32- + H2O +2h^+ (VB) \longrightarrow SO4^{2-} + 2H^+$$

$$2S^{2-} +2h^+ (VB) \longrightarrow S_2^{2-}$$

$$S_2^{2-} + SO3^{2-} \longrightarrow S_2O_3^{2-} + S2^-$$

$$SO_3^{2-}+S^{2-} +2h^+(VB) \longrightarrow S_2O_3^{2-}$$

It is also observed that catalayst prepared by solid gas method has more activity than catalyst preapared by hydrothermal because of higly crystalline nature of CdS/rGO (SG) and CdS particles is uniform distributed on rGO sheet

Table 1

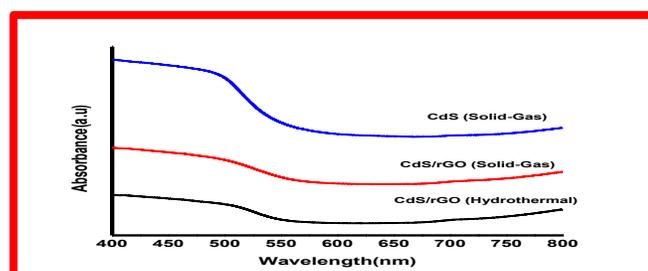| Catalyst	H_2 evolved for 2 h (mL gCdS^{-1}
CdS	5
CdS/rGO (HY)	12
CdS/rGO (SG)	18

Figure 5 Diffuse reflectance spectra of CdS/rGO(HY), CdS/rGO(SG) and CdS(SG)

The UV-vis diffuse reflectance spectra of prepared catalysts are shown in figure 5. Bare CdS(SG) shows sharp and continuous excition but in reduced graphene oxide supported cadmium sulphide (CdS/rGO) shows weak linear absorption because of there is a excess surface charges present in reduced graphene oxide(rGO).

5.CONCLUSION: In summary, Incorpation of reduced graphene oxide with CdS enhances the hydrogen production because rGO has electron accepting ability so it absosorbs electrons from the surface of CdS and prevent the charge recombination and also provide the active site for reduction hydrogen ions to hydrogen gas.

REFERENCES

1. Li Jia, Dong-Hong Wang, Yu-Xi Huang, An-Wu Xu, and Han-Qin Yu; Highly Durable N-doped reduced graphene/ CdS nanocomposite with Enhanced Photocatalytic Hydrogen Evolution from water under Visible light;J.Phys. C 2011,115,11466-11473

2. Anderia Morais, Claudia Longo, JoyceR.Araujo,Monica Barroso,James R.Durrant and Ana Flavia Nogueira; Nanocrystalline TiO$_2$/ reduced graphene oxide composite films as photoanodes for photoelectrochemical water splitting studies :the role of reduced graphene oxide; Phys.Chem.Chem.Phys 2016,18, 2608-2616

3. Yuexiang Li, Yuanfang Hu, ShaoqinPeng,Gongxuan Lu, and Shuben Li;Synthesis of CdS nanorods by an Ethylenediamine assisted hydrothermal method for photocatalytic hydrogen evolution; J.Phys.Chem.C 2009,113,9352-9358

4. Vaquero F,Navarro RM, Fierro JLG: Evolution of the nanostructures of CdS using Solvothermal synthesis at different temperature and its influence on the photoactvity for hydrogen production. Int J Hydrogen Energy 2016; 41 (27) 11558-67

SEEC-2018-148

Heat Transfer Characteristics of Nanoparticle Dispersed Nitrate salt-PCM For Thermal Energy Storage Applications

Sudheer R.
Department of Metallurgical & Materials
Engineering, National Institute of Technology
Karnataka
Email: sudheerrajagopalan@gmail.com

Prabhu K.N.
Department of Metallurgical & Materials
Engineering, National Institute of Technology
Karnataka
Email: knprabhu.nitk@gmail.com

ABSTRACT

Nano particle dispersed salt-PCMs have emerged to be better candidates for TES applications. In this work the carbon nano structures (0.1% by weight of PCM) of graphite, MWCNT and graphene were separately dispersed in potassium nitrate. Solidification of nanosalt-PCMs was analysed by employing the Fourier technique of computer aided cooling curve analysis method for a sample of size 1Kg. The solidification time of the PCM significantly decreased on nano particle addition indicating an enhancement in the heat removal rate. Graphite and MWCNT additions decreased the thermal diffusivity property of the base PCM while the graphene added PCM offered a higher thermal diffusivity. However, the benefits of addition of nanoparticles to the salt-PCM reduced on 10 successive thermal cycles. This deterioration of TES functions on thermal cycling is attributed to the agglomeration of nano particles.

Keywords: PCMs, Thermal energy storage, CACCA

.
NOMENCLATURE

LH   Latent heat
Δ Change in value**t**
t   solidification time

INTRODUCTION

Energy storage technologies have been widely appreciated as they offer an increase in the efficiency and decrease in cost of energy in sustainable energy systems. In order to achieve this, energy storage technologies require efficient materials and high energy densities. For this, heat transfer paths should be altered by modifying thermal conductivity, thermal diffusivity, heat capacity, contact resistance etc. in the concerned energy storage technique. Nitrate salt-PCM are good candidates as a thermal energy storage material in solar thermal systems. Modification of their TES functions with various additives can improve their prospects as a TES material. Characterization of PCMs has been solely performed using differential scanning calorimetry for many years. Its unsuitability in characterizing inhomogenous samples due the very small sample size, have surfaced in recent times [1]. Other methods like T-History method [2] and Computer Aided Cooling Curve Analysis (CACCA) method [3] can be employed to study large samples. This study uses CACCA method to assess the effect of nanoparticle additions on the solidification and other TES parameters of potassium nitrate.

EXPERIMENTAL

The salt-PCM (KNO_3) was separately mixed with the nano particles to study their respective effects on the TES parameters. The nanoparticles used were MWCNT (OD >50nm, ID 5-15nm,Length 10-20micron), Graphite (400nm, 50μm) and Graphene (Layer <3, Thickness 1-3nm, Scale 2-10μm). The PCM mass of 1kg was used in every trial into which the particle additives weighing 0.1% of the PCM weight were added. Every sample was melted and then solidified for 10 cycles to analyze the thermal-cycling effects on these inhomogeneous PCMs.
Computer aided cooling curve analysis performed in a cylindrical container with length to diameter ratio of 5. The calibrated k-type Inconel sheath thermocouples were used as the temperature sensors. The temperature data acquired from thermal analysis was later processed and analysed to

ACKNOWLEDGEMENT

REFERENCE

[1] Mehling. H., and Cabeza. L.F., 2008. Heat and cold storage with PCM: an up to date introduction into basics and applications, 2008 ed., Heat and Mass Transfer series 2008, Springer, pp. 57–102.

[2] Yinping, Z., Yi, J., and Yi, j., 1998. "A simple method, the T-history method, of determining the heat of fusion, specific heat and thermal conductivity of phase-change materials". Measurement Science Technology, 10, pp. 201–205

[3] Sudheer, R., and Prabhu, K.N., 2016. "A Computer Aided Cooling Curve Analysis method to study phase change materials for thermal energy storage applications". Materials and Design, 95, pp. 198–203.

SEEC-2018-149

COMPUTATIONAL STUDY OF PRE-IGNITION AND SUPER-KNOCK IN SI ENGINES

Mohammed Jaasim
Clean Combustion Research Center
King Abdullah University of Science and Technology
Email: mohammedjaasim.mubarakali@kaust.edu.sa

Hong G. Im
Clean Combustion Research Center
King Abdullah University of Science and Technology
Email:hong.im@kaust.edu.sa

ABSTRACT

Advanced spark ignition engine is necessary to improve the efficiency and operating load limits, which is limited by pre-ignition and super-knock. Full cycle three-dimensional pre-ignition simulations were performed using CONVERGE to understand the end-gas behavior during a pre-igntion event. Pre-ignition is initiated with a hot-spot and the local pressure near the end-wall is analyzed at eight locations (points A-H). The local pressure exhibit super-knock behavior with high pressure peaks accompanied with pressure oscillations. Knock intensity is higher at locations away from pre-ignition location when compared to locations closer to pre-ignition. Auto-ignition is induced in end-gas due to increasing end-gas temperature. Low temperature reactivity in end-gas is observed which is identified by strong formation of formaldehyde. Methods to simulate pre-ignition and techniques to analyze the results are proposed in the study.

Keywords: Pre-ignition, Super-knock, knock intensity.

INTRODUCTION

Efficiency demand of engines has increased in the last decade and the emission regulations imposed by governments pose a major challenge to automobile manufacturers [1]. Efficiency in spark ignition (SI) engines can be improved by operating at high compression ratios, but is limited due to the undesired auto-ignition of the fuel/air mixture, called knock, which causes a non-smooth operation of the engine [2-4]. The problem of knock is well known and can be abated by adjusting the spark timing during operation. Reduction of emissions can be achieved by downsizing of the engine and is a proven effective method [5] but is limited by pre-ignition, which is the ignition of the fuel/air mixture ahead of spark firing due to other sources [6]. Pre-ignition may be accompanied with large pressure peaks and severe oscillations, an event referred to as super-knock, which can damage the moving components of the engine [7-9].

The source of pre-ignition that triggers super-knock is not clearly known and various reasons such as hot-spots, engine oil droplets, fuel/oil droplets, carbon particles, etc., are reported to be the source of pre-ignition in literature [7, 10-12]. Super-knock behavior is anticipated to be the outcome of multiple in-cylinder auto-ignition of end-gas accompanied by detonation [13, 14]. Temperature stratification with local hot-spots is expected to trigger both pre-ignition and detonation [15]. The ignition delay sensitivity of the system is well known and various methods to predict the detonation are available in literature [16]. Zeldovich et al. [17] proposed a regime classification based on the uniformity of the initial mixture and classified the auto-ignition regimes into deflagration, spontaneous ignition and detonation regimes.

Pre-ignition in SI engine was previously investigated by the author and the location and time of initiation of pre-igntion was found to be of paramount importance that decides the fate of the cycle. Pre-ignition at late crank angles were found to exhibit super-knock and the end-gas temperature increased ~250 K for super-knock cycle when compared with a normal combustion cycle [18]. Different physical and chemical reasons are cited for pre-ignition and super-knock in the literature [6, 11, 19]. Contrary to pre-ignition, super-knock is mainly governed by the

chemical kinetics of the system. Although the probability of super-knock cycles occurrence is lower, solving the problem of super-knock is necessary to achieve higher efficiency in SI engines. The main aim of this study is to understand the end-gas behavior during a pre-ignition event that leads to super-knock through numerical simulations.

COMPUTATIONAL SETUP

Three dimensional full cycle pre-ignition simulations were performed using CONVERGE, a computational fluid dynamics code widely used for engine simulations. The mass, momentum, energy and species conservation are ensured in the code. A base mesh size of 4 mm was used in all three directions which is later refined locally using adaptive mesh refinement technique (AMR). AMR of level 5 is used to reduce the minimum cell size to 0.125 mm based on the criteria of 5K temperature difference between the neighboring cells (new_cell_size = base grid/$2^{level=5}$). The geometry and the mesh generated is shown Fig. 1. Second order spatial discretization and first order adaptive time marching is used to solve the governing equations. Kelvin-helmholtz spray break-up model is used to represent the spray break-up. In-cylinder turbulence was modeled using Reynolds-averaged Navier Stokes (RANS) based (RNG-k-epsilon) turbulence model and the heat loss from walls is modeled using Han model. Multi-zone combustion model based on well-stirred reactor assumption groups the cells based on temperature (5 K) and equivalence ratio (0.05), and maps back the compositional change and heat release at each time step. A small CFL numer of 1 is used to capture the pressure oscillations during super-knock. The readers may refer to [18] for detailed information about the models and the validation of modeling methodology used in the study.
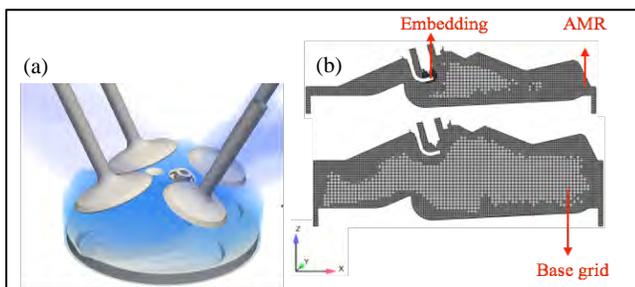

FIGURE 1: (a) GEOMETRY OF THE SI ENGINE, (b) MESH GENERATED FOR THE STUDY.

PROBLEM DESCRIPTION

Pre-ignition was initated using a hotspot of 1 mm radius placed over the piston closer to the end-wall at 20 CAD aTDC. The temperature of the hot-spot was maintained at 2000 K to initate a deflagrative pre-ignition front. The pressure was monitored at 8 locations along the circumference of the cylinder, points A-H, as shown in Fig. 2. The specifications and operating conditions of the study is provided in Tab. 1.
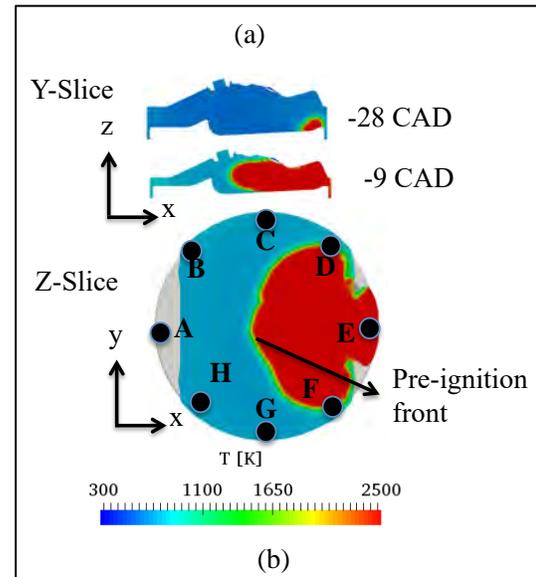
FIGURE 2: (a) Y-SLICE SHOWING HOTSPOT AND PRE-IGNITION FLAME FRONT, (b) LOCATIONS OF POINT A-F SELECTED FOR ANALYSIS.

TABLE 1: ENGINE SPECIFICATIONS AND OPERATING CONDITIONS FOR THE STUDY.

Parameters	Values
Bore	85 mm
Stroke	90 mm
Connecting rod length	138 mm
Compression ratio	9.5
Valves	2-intake, 2-exhaust valves
Spark plug energy	40 mJ
Spark time	0 CAD
RPM	1200
Intake temperature	300 K
Intake pressure	2 bar
Lambda (λ)	1
Fuel	*iso*-octane

RESULTS AND DISCUSSION

The methods to analyze the pre-ignition cycles are presented here. First, the local in-cylinder pressure is investigated in the points A-H. Some points exhibited strong pressure peaks accompanied with oscillations, a typical nature of super-knock, and some points did not exhibit super-knock. Local pressure is analyzed to study the intensity of knock along the circumference in close

proximity to the end-wall. The intensity of pressure oscillation varies between these points (A-H) along the circumference as shown in Fig. 3.
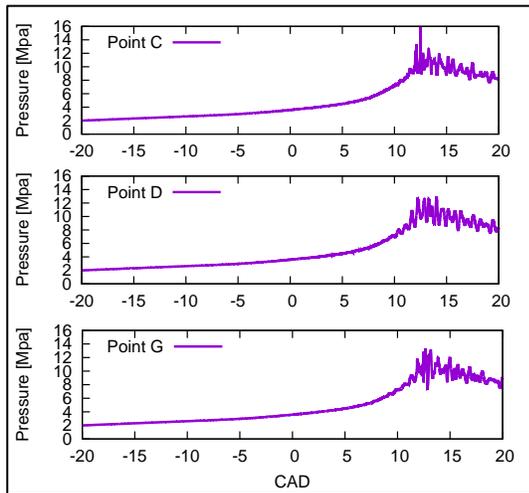
FIGURE 3: IN-CYLINDER LOCAL PRESSURE AT POINTS C, D AND G.

Knock Intensity

The knock intensity (KI) varies at point A-H based on the location in the cylinder. To calculate KI, first a three point moving average of pressure is obtained and is subtracted from the mean pressure of the cylinder which provides the knock signal. The difference between the maximum and minimum frequency of the signal provides the knock intensity. The calculated KI at points A-H is shown in Fig. 4. The points (D, E and F) closer to pre-ignition location exhibit low KI when compared to other points that are away from the pre-ignition location. This must be due to the time available to react for these points (A-C,G & H) in end-gas.
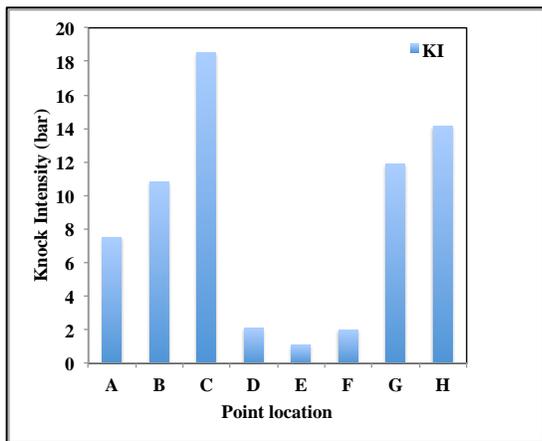
FIGURE 4: KNOCK INTENSITY AT POINTS A-H.

Deflagration and End-gas Auto-ignition

The pre-ignition deflagrative front initates auto-igniton in end-gas as shown in Fig. 5(a). The auto-ignition are due to increase in end-gas temperature and as a consequence low-temperature reactivity is induced in the end-gas. A strong formation of formaldehyde (CH_2O) which is an indicator of low-temperature reactivity is observed in the end-gas as shown in Fig. 5(b). This low-temperature reactivity is not observed in normal combustion cycles. The mass fraction of formaldehde formed during combustion duration is compared between a normal combustion cycle and pre-ignition cycle. A strong increase in fromaldehyde by a factor of 4 is observed for the pre-ignition cycles, which later favors auto-igniton that results in super-knock as shown in Fig. 6.
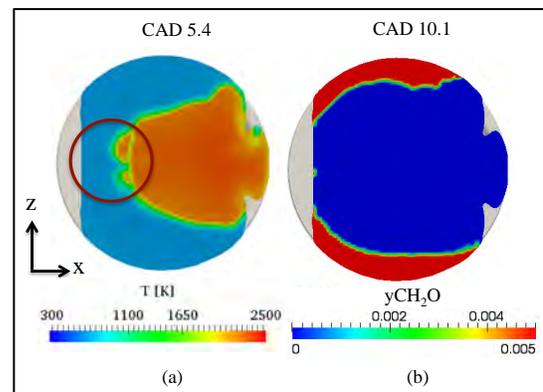
FIGURE 5: (a) END-GAS AUTO-IGNITION (CIRCLED),(b) FORMATION OF FORMALDEHYDE IN END-GAS PRE-IGNITION CYCLE.
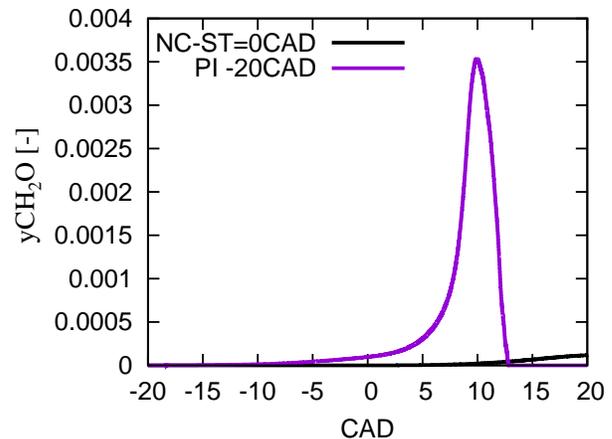
FIGURE 6: COMPARISON OF FORMALDEHYDE FORMATION BETWEEN NORMAL COMBUSTION AND PRE-IGNITION CYCLE.

CONCLUSIONS

Pre-ignition full cycle simulations were performed and the results were analyzed. In summary;

- The numerical methodology and models used are successful in capturing the auto-ignition events in end-gas.
- Strong pressure peaks and oscillations are observed for the points selected near end-wall.
- Knock intensity was lower for points near the pre-igniton location when compared to the points farther away to the pre-igniton location.
- Strong formation of formaldehyde is observed in the end-gas indicating low-temperature reactivity.

ACKNOWLEDGMENTS

REFERENCES

[1] WEC, G.T.S., 2011. "2050". World Energy Council. Londres.

[2] Chen, L., Li, T., Yin, T., Zheng, B., 2014. "A predictive model for knock onset in spark-ignition engines with cooled EGR". Energy Conversion and Management, 87, 946-955.

[3] Chen, Y., Raine, R., 2014. "Engine Knock in an SI Engine with Hydrogen Supplementation under Stoichiometric and Lean Conditions". SAE International Journal of Engines, 7(2014-01-1220), pp. 595-605.

[4] Da Silva, R., Cataluña, R., de Menezes, E.W., Samios, D., Piatnicki, C.M.S., 2005. "Effect of additives on the antiknock properties and Reid vapor pressure of gasoline". Fuel, 84(7), pp. 951-959.

[5] Leduc, P., Dubar, B., Ranini, A., Monnier, G., 2003. "Downsizing of gasoline engine: an efficient way to reduce CO2 emissions". Oil & gas science and technology, 58(1), pp. 115-127.

[6] Dahnz, C., Han, K.-M., Spicher, U., Magar, M., Schießl, R., Maas, U., 2010. "Investigations on pre-ignition in highly supercharged SI engines". SAE International Journal of Engines, 3(2010-01-0355), pp. 214-224.

[7] Gupta, A., Shao, H., Remias, J., Roos, J., Wang, Y., Long, Y., Wang, Z., Shuai, S.-J., 2016. "Relative Impact of Chemical and Physical Properties of the Oil-Fuel Droplet on Pre-Ignition and Super-Knock in Turbocharged Gasoline Engines". SAE Technical Paper.

[8] Wang, Z., Liu, H., Song, T., Qi, Y., He, X., Shuai, S., Wang, J., 2015. "Relationship between super-knock and pre-ignition". International Journal of Engine Research, 16(2), pp. 166-180.

[9] Wang, Z., Qi, Y., He, X., Wang, J., Shuai, S., Law, C.K., 2015. "Analysis of pre-ignition to super-knock: hotspot-induced deflagration to detonation". Fuel, 144, pp. 222-227.

[10] Kassai, M., Torii, K., Shiraishi, T., Noda, T., Goh, T.K., Wilbrand, K., Wakefield, S., Healy, A., Doyle, D., Cracknell, R., 2016. "Research on the Effect of Lubricant Oil and Fuel Properties on LSPI Occurrence in Boosted SI Engines". SAE Technical Paper.

[11] Mayer, M., Hofmann, P., Geringer, B., Williams, J., Moss, J., Kapus, P., 2016. "Influence of Different Oil Properties on Low-Speed Pre-Ignition in Turbocharged Direct Injection Spark Ignition Engines". SAE Technical Paper.

[12] Qi, Y., Xu, Y., Wang, Z., Wang, J., 2014. "The effect of oil intrusion on super knock in gasoline engine". SAE Technical Paper.

[13] Gao, Y., Chen, Z., "Autoignition and detonation development from a hot spot in hydrogen/air mixture". 26th ICDERS, 2017.

[14] Robert, A., Richard, S., Colin, O., Poinsot, T., 2015. "LES study of deflagration to detonation mechanisms in a downsized spark ignition engine". Combustion and Flame, 162(7), pp. 2788-2807.

[15] Sow, A., Lee, B.J., Im, H.G., "A Computational Study of the End Gas Autoignition and Shock Development by Flame Front and Local Hot Spot". 26th ICDERS, 2017

[16] Meyer, J., Oppenheim, A., 1971. "On the shock-induced ignition of explosive gases". Journal, 13(Issue), pp. 1153-1164.

[17] Zeldovich, Y.B., 1980. "Regime classification of an exothermic reaction with nonuniform initial conditions". Combustion and Flame, 39(2), pp. 211-214.

[18] Ali, M.J.M., Perez, F.E., Sivasankaralingam, V., Raman, V., Dibble, R., Im, H., 2017. "Effect of Location and Timing of Hotspots on Superknock during Pre-ignition". SAE Technical Paper.

[19] Hülser, T., Grünefeld, G., Brands, T., Günther, M., Pischinger, S., 2013. "Optical investigation on the origin of pre-ignition in a highly boosted SI engine using bio-fuels". SAE Technical Paper.

SEEC-2018-150

DRAFT: Exergy Analysis of Diesel Engine Running on Biofuel: A Review Study

Author name
Email:

Second Author
Name of Department/Division
Affiliation
Email address

ABSTRACT

As we know that the energy analysis which is based upon the first law of thermodynamics, plays a significant role in the performance of diesel engine, however, the analysis based upon the second law of thermodynamics is also important to know the real picture of engine operation. Analysis based upon the second law is known as exergy or availability. By applying the energy analysis we are able to know the quantity of energy flow in engine operation, there is no information about the quality of energy, losses of energy during the engine operation. Exergy analysis has the ability to answer all these questions related to the quality of energy, losses. Hence the present study is dedicated to review the previous research on the application of exergy analysis to the diesel engine. Special attention has been given to the diesel engine fuelled with biodiesel.
Keywords<Biodiesel, Diesel Engine,Exergy analysis, Second Law of thermodynamics >

INTRODUCTION

Diesel engine is being used in transportation section from so many years due to its high thermal efficiency compared to others engine. The performance analysis of the diesel engine has been done by applying the first law of thermodynamics however it's not sufficient to give the real picture of engine operation and the performance losses. Exergy analysis which is based upon the second law of thermodynamics capable to give the real picture of engine operation. Energy analysis gives the quantity of energy while exergy analysis tells about the quality of energy, where are the losses occurring, what are the causes of these losses. Hence exergy analysis is very important for the performance analysis of diesel engine. Present study is the

Brief review of the previous studies based on the application of exergy analysis to diesel engine. Special attention has been given to the diesel engine running on biodiesel. Following section is the chorological review of application of exergy analysis to diesel engine.

There is detailed review study was presented by the Caton [2000]. He has reported over the two dozens of studies on exergy analysis which include both SI (spark ignition) and CI (compression ignition) engine running on petroleum fuels. It was reported the variation of exergy performance parameters with the engine operating conditions. Numerical and experimental studies results were presented from the exergy analysis point of view. He presented the difference between the energy and exergy analysis of diesel engine. Another review paper on the exergy analysis studies was published by **Rakopoulos & Giakoumis (2006).** Their main focus was to present the difference between energy and exergy analysis application to internal combustion engine. They reported that combustion process is the main cause of irreversibilities in internal combustion engine operation.. They suggested that the variation in parameter i.e., equivalence ratio, cylinder wall insulation, increased turbocharging, higher compression ratio lead to increase the level of pressure and temperatures in the cylinder which lead to reduction in combustion irreversibilities. Canakci M & hosoz M [2006] they performed the exergy analysis of 4 cylinder turbocharged diesel engine fuelled with yellow grease methyl ester and soyabean oil methyl ester at various load condition for constant speed. The second law efficiency of the biodiesel blend is lower as compare to the first law efficiency. **Rakopoulos C.D., & Kyritsis C.D. [2006]** computed the exergy balance during combustion of hydrogen-enriched natural and landfill gas in single cylinder natural aspirated direct injection diesel engine by zero dimensional combustion model. It is reported with increase the hydrogen content of the fuel, there was reduction in combustion irreversibility, for mole fractions of hydrogen smaller than 10%. **Giakoumis [2007]**

investigated the influences of cylinder wall insulation strategy on the turbo charged diesel engine from the energy and exergy analyses perspective under transient operating conditions.. An analytical and computational study to examine the exergy destruction in turbocharged diesel engine was conducted by **Giakoumis et al., 2007.** They analyzed the turbocharged diesel engine under transient conditions. They reported that the exergy destruction is different in the steady and transient operation of the engine. it is recommended to recover the exhaust gas exergy, and heat loss exergy to improve the performance of engine. **9 Rakopoulos et al., [2008]** performed the computation investigation of combustion of hydrogen and natural gas mixture in diesel engine from the exergy analysis perspective. They employed the single zone combustion model. They reported the high exergetic efficiency by increasing the amount of hydrogen in the mixture, less exergy losses may the cause of higher exergectic efficiency.

M. et. al. [2008] conducted the exergy analysis of turbocharged diesel engine to identify the locations of exergy losses in various subsystem namely turbine, compressor, intercooler and the exergy efficiency of the overall system. The effect of inlet air temperature and pressure are reported on the second law efficiency and exergy destruction. The exergy efficiency of the engine is reported 40.5%. **Abassi et. al. [2010]** presented the influence of inlet charge temperature on the exergy analysis of DI diesel engine by using the computational model. They reported the reduction in exhaust gas exergy, low entropy production while high fuel consumption, lows work output with the increase of inlet temperature. They also reported that reduction in combustion irreversibilities was more than reduction in work output.

Giakoumis et al., [2007] They analyzed the turbocharged diesel engine under transient conditions. They presented the detailed contribution of various subsystem ie aftercooler, turbocharger, exhaust and inlet manifolds, in the exergy destruction or the irreversibilities during the combustion. Gokalp et al [2008]. compared the first and second law analyses if diesel fuel, marine fuel, and biodiesel for 4 cylinder direct injection diesel engine They reported higher thermal and exergetic efficiencies for the biodiesel blends as compared to marine and diesel fuel. To present the advantage of hydrogen as fuel Rakopoulos et al., [2008] performed the computation investigation of combustion of hydrogen and natural gas mixture in diesel engine from the exergy analysis perspective. They employed the single zone combustion model. They reported the high exergetic efficiency by increasing the amount of hydrogen in the mixture, less exergy losses may the cause of higher exergectic efficiency. Hakan Caliskan [2010] has reviewed the articles on the exergy analysis of diesel and petrol engine from 1963-2008. Author has include all types of engine turbocharged non-turbocharges. Azoumah, et al. (2009). Cotton seed oil, palm oil and diesel fuel blends are tested as fuel in exiting direct injection diesel from the energy and exergetic point of view. Second law efficiency decrease with increases the load however reverse result obtained for the thermal efficiency. The influence of variation of dead state temperature on the second law efficiency of 4 stroke 4 clyinder turbocharged direct injection diesel engine fuelled with HOME

was carried by Caliskan et al., [2009.] They carried out the experiment in different outdoor conditions to vary the dead state temperature. They reported the exergy efficiency ranged from 29.78% to 34.93% with the dead state temperature increment (-5 to 30 C). They mentioned the entropy generation rate from 0.18594 kW/K to 0.19406 kW/K with vary the dead state temperature from -5 to 30 C. Caliskan, H., Tat, M.E., Hepbasli, A. and Van Gerpen, J.H. (2010) They conducted the exergectic evaluation of the diesel engine fuelled with high oleic soyabean oil methyl ester at 1400 rev/min at full load condition and the performance was compared with the diesel and soya methyl ester from the second law analysis. Abassi et al., [2010] they conducted the numerically investigated the effect of injection system variation (nozzle hole, nozzle hole diameter and injection duration) on the energy and exergy analysis of DI diesel engine.
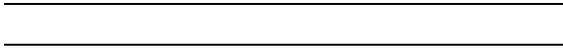
REFERENCES

[1] Author, A., Author, B., and Author, C., 1984. "Article Title". Journal Name, 1(5), May, pp. 1–3

[2] Book, A., ed., 2001. Book title, 1st ed., Vol. 5 of Series Title. Publisher Name, Publisher address, Chap. 3, pp. 1–3.

[3] Proceedings, IHMTC, ed., 2015. Volume Title, Vol. 1 of Proceedings Series, Organization Name, Publisher Name. See also http://www.ihmtc2015.com.

[4] Phdthesis, A., 2000. "Thesis Title". PhD Thesis, University of Higher Education, IIT. See also URL http://www.iit.edu.

[5] Misc, A., 2013. Miscellaneous Title,www.url.com, May

SEEC-2018-151

PERFORMANCE ANALYSIS OF PHASE CHANGE MATERIAL BASED SOLAR AIR HEATER

Soma Sekhar Reddy	**Vikram Soni**	**Arvind Kumar**
Dept. of Mechanical Engineering IIT Kanpur, Kanpur, UP,208016 India	Dept. of Mechanical Engineering IIT Kanpur, Kanpur, UP,208016 India	Dept. of Mechanical Engineering IIT Kanpur, Kanpur, UP,208016 India
sekhar@iitk.ac.in	vikrams@iitk.ac.in	arvindkr@iitk.ac.in

ABSTRACT

In this paper, the numerical study of solar air heater (SAH) is performed in the presence of phase change material (PCM). A macroscopic model for SAH is presented in which the complete set of coupled governing equations (mass, momentum, energy) is solved and the solar radiation heat transfer effect is considered by using discrete ordinates (DO) radiation model. The thermal performance of solar air heater with and without phase change material (PCM) is compared. Further, the effect of mass flow rate on the average outlet temperature is presented. The results provide insights for a PCM based SAH where the charging (melting) and discharging (solidification) cycle is affected due to incorporation of PCM and with changing mass flow rates.

*Keywords***:** Solar air heater, Phase change material, Thermal energy storage, Charging, Discharging

NOMENCLATURE

μ	Viscosity	Pa.s
c_p	Specific heat capacity	J/kg.K
k	Thermal conductivity	W/m.K
L	Latent heat of fusion	J/kg
H	Enthalpy	J/kg
ρ	Density	kg/m^3
T	Temperature	K
g	Acceleration due to gravity	m/s^2
$\vec{u}$	Velocity vector	m/s
f	Mass fraction of the liquid	

SUBSCRIPT

amb	Ambient
avg	Average
a	Amplitude
melt	Melting
max	Maximum
ref	Reference

ABBREVIATIONS

PCM	Phase change material
SAH	Solar air heater
CFD	Computational fluid dynamics

INTRODUCTION

Solar energy is one of the promising sources for meeting energy demand without having any detrimental effect on the environment. The intermittency of this renewable source of energy is always a concern in the development of energy storage devices. To deal with this issue the latent heat based thermal energy storage systems are being explored extensively for storing energy in regard to heating and cooling purpose applications. Various researchers like, Kalogirou et al. [1] and Tyagi et al. [2] have done the comprehensive review about various types of solar thermal collectors and their applications with and without thermal energy storage. It was observed that the phase change materials (PCMs), as latent heat storage, is

more efficient than sensible heat storage. Similarly, few analytical and computational studies have been performed (Yadav et al. [3], El-Sebaii et al. [4], Enibe et al. [5]) for the design of a solar air heater. Various models are tested for transient analysis and optimized model with the best results are realized for the two-dimensional flow through conventional solar air heaters. They provided the analytical expressions for the temperature of an air heater and storage material considering effect of various parameters on the thermal efficiency of the system. Further few experimental studies have been performed (Kabeel et al. [6] and Peng et al. [7]) considering various designs like a flat and v-corrugated plate, to analyse the heat transfer performance with and without PCM as thermal energy storage material. They discussed the effect of various parameters such as solar radiation, a temperature difference of air across the heater, convective heat transfer coefficient between the absorber plate and the flowing air were presented.

Overall, very few works are reported using numerical modeling to study the solar air heater integrated with phase change material. In this study, the numerical modelling of a solar air heater integrated with a layer of a paraffin wax as PCM is performed. The performance of solar air heater has been investigated with and without PCM layer below the absorber plate. Also, the effect of different mass flow rates on the thermal behaviour of SAH with PCM is analysed.

MATHEMATICAL AND NUMERICAL MODELLING

The schematic of the 2-D computational domain in the present study is shown in Fig.1. For the case of solar air heater (SAH), paraffin wax is considered as PCM, the PCM layer thickness is 20 mm and the height of the airflow duct is 50 mm in the SAH. The insulated boundary condition is employed except for inlet, outlet and top surface. The initial temperature of the SAH with and without PCM is considered as the ambient temperature which is taken as 301 K for the current numerical study. The thermo-physical properties of various materials used in this simulation are given in Table 1.
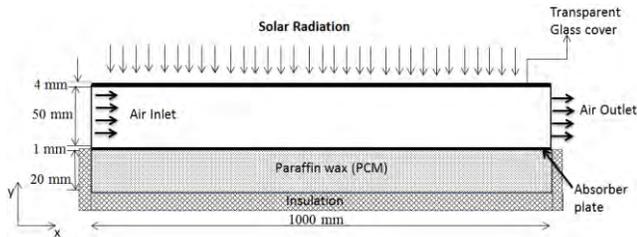

FIGURE 1. COMPUTATIONAL DOMAIN

Considering Newtonian, laminar and incompressible flow with no shrinkage, the appropriate governing equations (continuity, momentum, and energy) were solved by finite volume method using SIMPLE [8] algorithm in ANSYS Fluent v17.0 and additional subroutines are incorporated using UDFs (user-defined functions) for

defining the transient state boundary conditions [9]. An enthalpy porosity technique is used for modelling the solidification/melting process in PCM. The unstructured mesh is employed after performing mesh dependency for the numerical simulation with the fine grid in the domain. The convergence limit for residual continuity, velocity components, energy equations and discrete ordinate (DO) radiation intensity were taken as 10^{-5}, 10^{-5}, 10^{-6} and 10^{-5} respectively. Firstly, a separate validation case study is performed by simulating the copper as the absorber plate for the flat plate SAH without PCM. The conditions used for the validation case study are same as provided by kabeel et.al [6] and an acceptable agreement is observed.

TABLE 1: THERMOPHYSICAL PROPERTIES OF VARIOUS MATERIALS USED IN THIS STUDY [6]

Property	Paraffin wax	Air	Aluminum	Glass
ρ (kg/m^3)	810	1.225	2719	2500
K (W/mK)	0.21	0.0242	202.4	1.4
c_p (J/kg.K)	2100	1006.43	871	750
μ (Pa.s)	1.6×10^{-4}	1.78×10^{-5}	-	-
L (kJ/kg)	190	-	-	-
T_{melt} (K)	327	-	-	-

GOVERNING EQUATIONS

The governing equations are as follows

Mass conservation

$$\nabla . \vec{u} = 0 \tag{1}$$

Momentum conservation

$$\rho \frac{\partial \vec{u}}{\partial t} + \left(\rho \vec{u} . \nabla \right) \vec{u} = -\nabla p + \nabla .(\mu \left(\nabla \vec{u} + \left(\nabla \vec{u} \right)^T \right) + S_m \tag{2a}$$

$$S_m = 0 \qquad \text{(For air)}$$

$$= \rho \vec{g} \beta_T \left(T - T_{ref} \right) + \frac{A \left(1 - f_l \right)^2}{\varepsilon + f_l^3} \vec{u} \quad \text{(For PCM)} \tag{2b}$$

The mushy zone constant A is taken as 10^6 kg/m^{3}s for the present study and $\varepsilon = 0.001$ is used to avoid the zero in denominator. Boussinesq's approximation is used to account for the density change due to the temperature variation in PCM.

Energy conservation

The energy conservation equation is written as follows

$$\rho C_P \frac{\partial T}{\partial t} + \rho C_P \vec{u} . \nabla T = \nabla .\left(k \nabla T \right) + S \quad \text{(For air)} \tag{3}$$

$$\rho \frac{\partial H}{\partial t} + \nabla .\left(\rho \vec{u} H \right) = \nabla .\left(k \nabla T \right) + S_e \quad \text{(For PCM)} \qquad (4)$$

where S_e is a source term associated with the phase change phenomena and H is defined as follows

$$H = h + \Delta H \qquad (5)$$

where h is the total enthalpy of the material and it can be calculated as

$$h = h_{ref} + \int_{T_{ref}}^{T} c_p dt \qquad (6)$$

where ΔH is the latent heat content based on the fraction of the latent heat of fusion of the material, and is defined as

$$\Delta H = f_l L \quad for \quad T \geq T_m$$
$$= 0 \quad for \quad T < T_m \qquad (7)$$

where f_l is the liquid fraction during the phase change process between solid and liquid state. Once we get the liquid fraction value, then we can calculate the nodal temperature and phase of the material.

$$\rho_g c_g \frac{\partial T}{\partial t} = \lambda_g \left[\frac{\partial^2 T}{\partial x^2} + \frac{\partial^2 T}{\partial y^2} \right] + S_g \qquad (8)$$

(For glass and absorber plate)

where the source term, S_g in the energy equation is used for accounting the radiation heat transfer phenomenon, in which the radiation heat transfer effect is calculated by using discrete ordinates (DO) radiation model.

The transient variation of solar radiation G(t) falling at the top surface of the system at time t is considered as [10]

$$G(t) = I_{\max} \sin\left(\frac{\pi t}{12} \right), \, 0 \leq t \leq 12 \qquad (9)$$

The maximum solar radiation of 968 W/m^2 is considered in the present study and the solar radiation effect is considered from morning 6 am to evening 6 pm. The variation of the transient ambient temperature is mathematically modelled by using the following empirical relation

$$T_{amb}(t) = T_{avg} + T_a \cos\left(\frac{\pi(t-14)}{12} \right), \, 0 \leq t \leq 24 \qquad (10)$$

Where the average ambient temperature of 305 K and the amplitude of 6 K is considered in this study. The uniform mass flow rate is given at the inlet of the solar air heater and the gauge pressure is considered as zero at the pressure outlet. No slip boundary conditions are assumed at the fluid-solid interface.

RESULTS AND DISCUSSION

HEAT TRANSFER BEHAVIOUR

The transient thermal response of the absorber plate and outlet of the SAH is shown in Fig. 2. In the initial, the mass flow rate is taken as 0.02 kg/s. The thermal response behaviour of the absorber plate is same as of the solar radiation (Peak temperature = 370 K corresponding to the maximum irradiation). The transient temperature of the absorber plate with PCM is observed to be less as compared to the absorber plate without PCM. This is due to the reason that the PCM below the absorber plate also absorbs heat. A very interesting phenomenon is observed that the peak temperature of the absorber plate with PCM is not behaving same as of the absorber plate without PCM. A lag in achieving peak temperature is there in case of absorber plate with PCM due to availability of multiple heat absorbing materials (PCM, glass, air) in the domain.
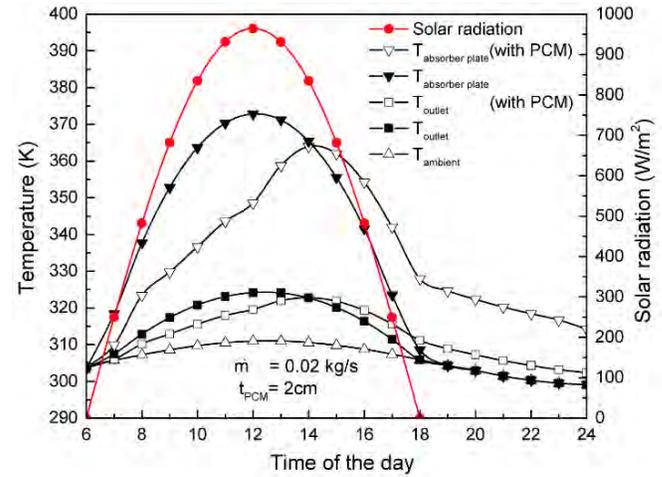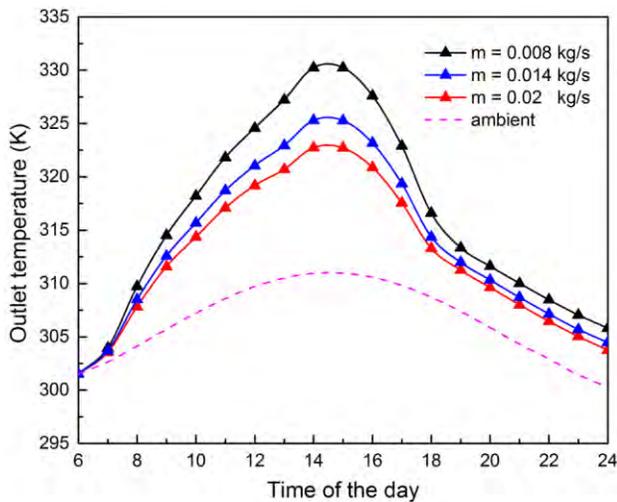

FIGURE 2. TRANSIENT TEMPERATURE VARIATION OF THE VARIOUS ELEMENTS OF FLAT PLATE SOLAR AIR HEATER WITH AND WITHOUT PCM.

Further, it is also observed that for the first few hours of the day, the outlet temperature of a SAH with PCM is low compared to without PCM. This is due to the fact that during initial stage the heat gets transferred to the PCM below the absorber plate. It leads to the availability of less heat for the air passing above the absorber plate. The outlet temperature of the SAH is maximum corresponding to the maximum solar radiation in case of absorber plate without PCM. But, in the case of absorber plate with PCM again a lag is noticed in achieving peak temperature. Also, the transient outlet temperature of the absorber plate with PCM is observed to be always greater than the absorber plate without PCM after 2:30 pm. This is due to the reason that during low solar radiation period, the air extracts stored heat from the PCM. There is release of latent heat from paraffin wax as it solidifies, which leads to heat transfer

from PCM to absorber plate and then to air. Due to this the outlet temperature increases and the same goes with the average temperature of the absorber plate.
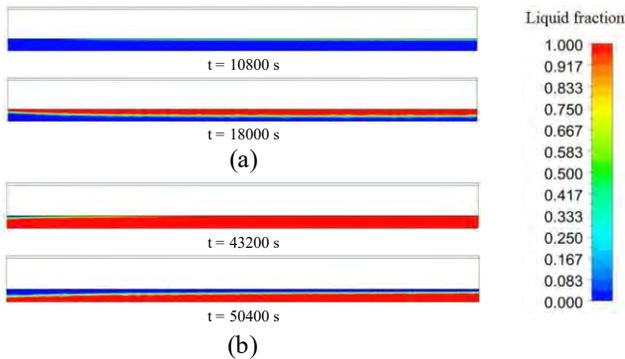
FIGURE 3. LIQUID FRACTION CONTOURS DURING MELTING AND SOLIDIFICATION FOR $m = 0.02$ kg/s.

FIGURE 4. TRANSIENT VARIATION OF OUTLET TEMPERATURE FOR VARIOUS MASS FLOW RATES OF AIR (SAH with PCM).

Figure 3 shows the charging and discharging behaviour of the PCM based SAH. The complete melting is observed in first 4 hours followed by sensible heating. Subsequently, the solidification phenomenon gets started when the solar radiation is about to cutoff. Further, the performance of the flat plate solar air heater is numerically investigated with and without using PCM for different mass flow rates (0.008, 0.014 and 0.02 kg/s) as shown in Fig. 4. It is observed that the increase in mass flow rate leads to decrease in the outlet air temperature. This is due the decrease in the interaction time of air with the absorber plate for heat transfer.

CONCLUSION

- The peak temperature of the absorber plate is observed to be non-identical for SAH with and without PCM.

- During initial stage of the process PCM based SAH provide less heat for the air passing above the absorber plate.

- There is heat transfer from PCM to the absorber plate due to loss of latent heat, which further absorbed by the air flowing above the absorber plate.

- The outlet temperature of the air decreases with increase in the mass flow rate of the air.

Overall, the insights from the study delineate the fact that the performance of the SAH with PCM is observed to be better as compared to without PCM with low mass flow rate.

REFERENCES
[1] Kalogirou, S. A. (2004). Solar thermal collectors and applications. Progress in energy and combustion science, 30(3), 231-295.
[2] Tyagi, V. V., Panwar, N. L., Rahim, N. A., & Kothari, R. (2012). Review on solar air heating system with and without thermal energy storage system. Renewable and Sustainable Energy Reviews, 16(4), 2289-2303.
[3] Yadav, A. S., & Bhagoria, J. L. (2013). Heat transfer and fluid flow analysis of solar air heater: a review of CFD approach. Renewable and Sustainable Energy Reviews, 23, 60-79.
[4] Aboul-Enein, S., A. A. El-Sebaii, M. R. I. Ramadan, and H. G. El-Gohary. "Parametric study of a solar air heater with and without thermal storage for solar drying applications." Renewable Energy 21[3], (2000): 505-522.
[5] Enibe, S. O. "Thermal analysis of a natural circulation solar air heater with phase change material energy storage." Renewable Energy 28.14 (2003): 2269-2299.
[6] Peng, D., Zhang, X., Dong, H., & Lv, K. (2010). Performance study of a novel solar air collector. Applied Thermal Engineering, 30(16), 2594-2601.
[7] Kabeel, A. E., Khalil, A., Shalaby, S. M., & Zayed, M. E. (2016). Experimental investigation of thermal performance of flat and v-corrugated plate solar air heaters with and without PCM as thermal energy storage. Energy Conversion and Management, 113, 264-272.
[8] Patankar, S. V. (1980). Numerical Heat Transfer and Fluid Flow, Hemisphere, London.
[9] ANSYS FLUENT. 17.0 Documentation.
[10] Reddy, K. S. (2007). Thermal modeling of PCM-based solar integrated collector storage water heating system. Journal of solar energy engineering, 129(4), 458-464.

PRODUCTION OF MICROBIAL LIPID FROM *YARROWIA LIPOLYTICA* MTCC 9520 BY VALORIZING CHICKEN TALLOW FOR BIODIESEL PRODUCTION: A MECHANISTIC STUDY

Radha P.[1], Ramani K.[1*]

[1] Assistant Professor, Department of Biotechnology, SRM University, Kattankulathur-603 203,

Tamil Nadu, India

Correspondence:

Radha P. - radha.p@ktr.srmuniv.ac.in

Ramani K. – ramani.k@ktr.srmuniv.ac.in

ABSTRACT

In recent years, biodiesel has become an essential alternative replacement for petroleum diesel due to its lower environmental effects and cost-effectiveness. Microbial lipid also is known as single cell oil(SCO) was recognized as a promising substitute produced by a range of oleaginous microorganisms through the fermentation process. In the present study, valorized poultry waste, i.e., chicken tallow was used as a carbon source for Yarrowia lipolytica MTCC 9520. The paper aims to explore the mechanistic information about SCO production and the optimal conditions required for achieving high productivity. Besides, the morphology of the cells with accumulated lipid was observed using SEM, Fluorescence microscopy, and FT-IR. Flow cytometry was performed for quantification lipid from biomass. Finally, the suitability of the derived SCOs as an alternate for biodiesel was preliminarily analyzed by elucidating its fatty acid composition through GC-MS analysis.

Keywords: Biodiesel, Single cell oil, Chicken tallow

NOMENCLATURE

SCO   Single Cell Oil

SEM   Scanning Electron Microscope

FT-IR   Fourier Transform Infrared Spectroscopy

GC-MS   Gas   Chromatography-Mass Spectrophotometry

TAG   Triacyl Glycerol

CDW   Cell Dry Weight

INTRODUCTION

Production of chemicals and fuels through sustainable microbial platforms is in advancement as petroleum reserves are depleting and environmental glitches are inflating throughout the world. [1]. Biodiesel is a thriving alternative to petroleum diesel produced by trans-esterification of triacylglycerides (TAGs) into fatty acid methyl esters that have put food and traditional oleo chemical industry sector under pressure [2,3]. As the majority of feedstocks for commercial biodiesel production are edible rapeseed oil, soybean oil, and palm oil. However, consumption of large amount vegetable oils as raw material for biodiesel production would result in a shortage of edible oils and leads to the soar of food price [4]. This resultant high cost of raw material (70-75%) has become one of the sturdy obstacle for its development

and wide applications [5,6] Adoption of animal fat, used frying oil, and waste cooking oil as feedstock is a good cost-cutting strategy, but these cannot meet the overwhelming needs for clean, renewable fuels [2,7]

Microbial lipids also referred as single cell oils (SCOs) provide a potential source for green and sustainable biodiesel production process, with no hostile impact on the food supply chain. Microbial lipids are renowned for their faster production rate, easier scale-up, less labor, more flexibility regarding season and climate [4, 8, and 9]. These lipids are produced by some oleaginous microorganisms (intracellular lipid accumulation levels are greater than 20% of dry cell weight), such as yeast, fungi, bacteria, and microalgae. Among the oleaginous microorganisms, Yeast species, such as *Rhodosporidium sp., Rhodotroula sp., Lipomyces sp.,* and *Yarrowia lipolytica*, are accumulating intracellular lipid upto 87% of CDW [2]. Depending on the strain and the applied cultivation method, microbial lipid bodies with varied character are being produced attributing to the diversified fatty acid composition. The oleaginous microorganisms under suitable culture conditions store lipids by processing carbon-rich substrate. The composition of microbial lipids is similar to vegetable oils, comprised of long chain saturated and unsaturated fatty acids. This similarity justifies the fact that microbial oils produced by these microorganisms can subsist as a prospective feedstock for biodiesel production [10].

Yarrowia lipolytica is one of the most extensively studied "non-conventional" oleaginous dimorphic yeast. [11, 12]. Assimilating hydrophobic substrates and ability to produce lipase, organic acids and secondary metabolites such as biosurfactant have extended its application to various fields [13]. Contemplation regarding both *de novo* and *ex novo* lipid accumulation and the underlying pathways responsible for such multiple aspects of applications have begun. More than 90% of accumulated lipid in *Yarrowia lipolytica* exists in triacylglycerol (TAG) form from this *de novo* fatty acid biosynthesis pathway. On the other hand, *Yarrowia lipolytica* can also use an *ex novo* process to accumulate intracellular lipids by incorporation of exogenous fatty acids and lipids. Significant progress has been achieved in understanding and engineering the *de novo* lipid biosynthesis in *Yarrowia lipolytica*. [14]. On the other hand; cost-effective production of biodiesel by employing this microbial lipid is not feasible while utilizing glucose as the carbon source. Consequently, the production of microbial lipid from wastes or renewable materials is highly in demand. The utilization of waste materials and by-products from various industries via microbial cell factories for biodiesel production provides a substantial leverage over conventional methods [15]. Amongst such types of waste materials, various low-or negative-cost hydrophobic compounds (e.g., animal waste fats, tallow derivatives, lards waste cooking oils and fats) are produced in high and continuously increasing concentrations with their disposal and valorization being a significantly distressing task Development of feasible ways of utilization and valorization of these crude fatty materials is indispensable [16].

The poultry industry is one of the fastest emerging segments of the agricultural sector. Nonutilization of by-products generated from poultry industries can lead to loss of possible revenue as well as increase the cost of disposal of such products. Chicken tallow is acquired (usually as a by-product) from chicken rendering and processing. Chicken tallow mainly consists of palmitic, stearic and oleic acids which are of analogous to the fatty acid composition of the feedstocks currently accomplished for biodiesel production.[17]. Hence, chicken tallow after its pre-processing was utilized as a renewable substrate for the production of microbial lipid and thereof for biodiesel synthesis.

The present study intended to analyze the biotransformation of chicken tallow into microbial lipids mechanistically. The *Yarrowia lipolytica* MTCC 9520 cells morphological changes during lipid accumulation process was explored with Fluorescence (Fig. 1) and Scanning Electron Microscope (Fig 2). The cell wall modification during lipid accumulation was analyzed by using FT-IR, a non-invasive technique (Fig.3). The role of bio emulsifier and lipase enzyme on the solubilization and hydrolysis of chicken tallow was studied. Quantification lipid content was carried out by estimating fluorescence intensity by using Flow Cytometry (Fig. 4). A batch kinetic study was carried out to analyze the time course of cell growth and lipid accumulation (Fig. 5) Further, GC-MS analysis was carried out to preliminarily check the candidature of the obtained microbial lipid as biodiesel via acid transesterification process to determine the fatty acid composition (Fig. 6).
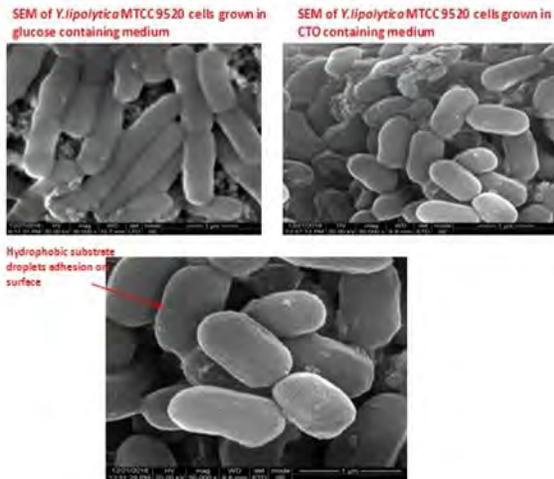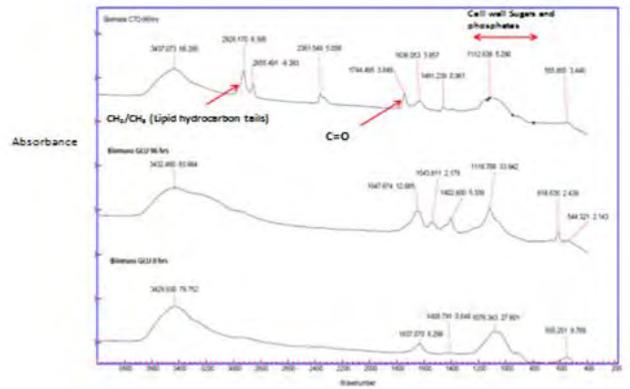
FIGURES

(A)
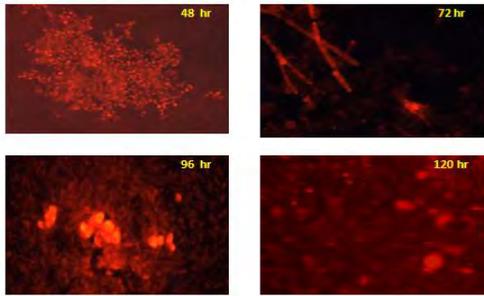
(B)
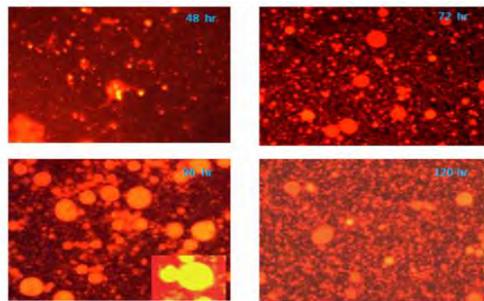
FIGURE 1. FLUORESCENCE MICROSCOPY
ANALYSIS OF *YARROWIA LIPOLYTICA*
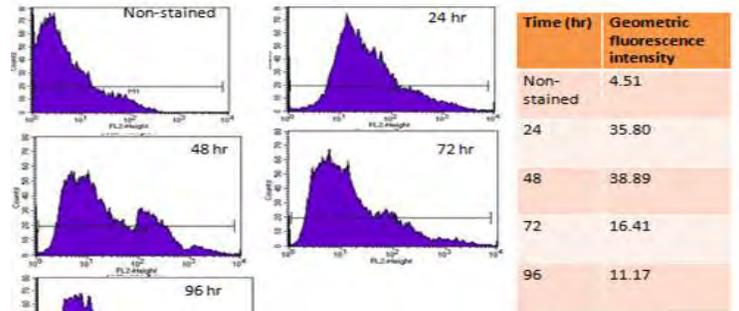MTCC 9520 (A) GLUCOSE MEDIUM (B)
CHICKEN TALLOW MEDIUM

FIGURE 2. SCANNING ELECTRON
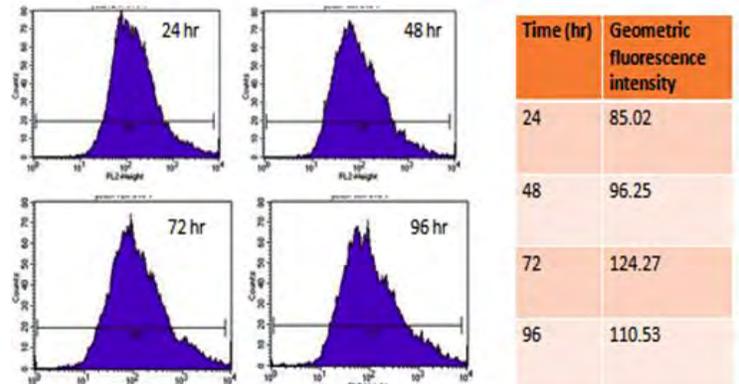MICROSCOPY ANALYSIS OF *YARROWIA
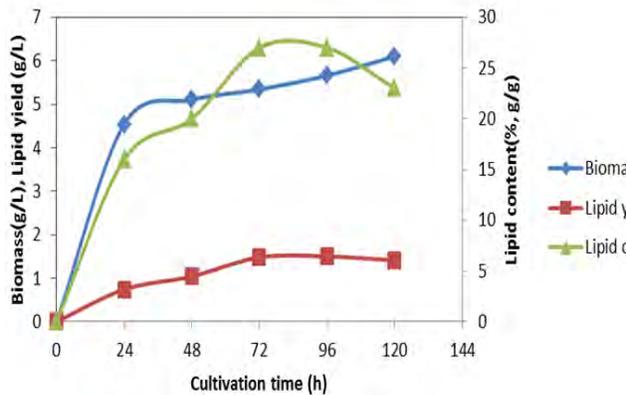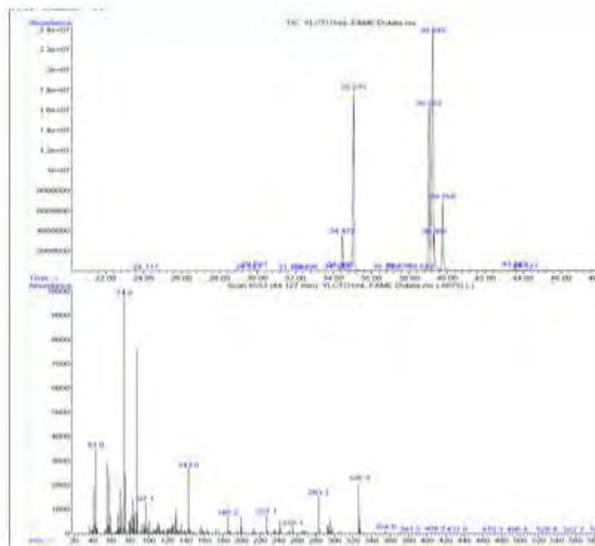LIPOLYTICA* MTCC 9520

FIGURE 3. FT-IR ANALYSIS

(A)

Time (hr)	Geometric fluorescence intensity
Non-stained	4.51
24	35.80
48	38.89
72	16.41
96	11.17

(B)

Time (hr)	Geometric fluorescence intensity
24	85.02
48	96.25
72	124.27
96	110.53

FIGURE 4. FLOW CYTOMETERY ANALYSIS
OF YARROWIA LIPOLYTICA MTCC 9520 (A)
GLUCOSE MEDIUM (B) CHICKEN TALLOW
MEDIUM

FIGURE 5. TIME COURSE OF CELL GROWTH AND LIPID ACCUMULATION OF YARROWIA LIPOLYTICA MTCC 9520

FIGURE 6. GC-MS ANALYSIS OF CHICKEN TALLOW DEREIVED YARROWIA LIPOLYTICA MTCC 9520 MICROBIAL LIPID

ACKNOWLEDGMENTS

REFERENCES

[1] Abghari, A. and Chen, S., 2014. *Yarrowia lipolytica* as an oleaginous cell factory platform for production of fatty acid-based biofuel and bioproducts. *Frontiers in Energy Research*, *2*, p.21.

[2] Tsigie, Y.A., Wang, C.Y., Truong, C.T. and Ju, Y.H., 2011. Lipid production from *Yarrowia lipolytica* Po1g grown in sugarcane bagasse hydrolysate. *Bioresource Technology*, *102*(19), pp.9216-9222.

[3] Sitepu, I.R., Sestric, R., Ignatia, L., Levin, D., German, J.B., Gillies, L.A., Almada, L.A. and Boundy-Mills, K.L., 2013. Manipulation of culture conditions alters lipid content and fatty acid profiles of a wide variety of known and new oleaginous yeast species. *Bioresource technology*, *144*, pp.360-369.

[4] Signori, L., Ami, D., Posteri, R., Giuzzi, A., Mereghetti, P., Porro, D. and Branduardi, P., 2016. Assessing an effective feeding strategy to optimize crude glycerol utilization as sustainable carbon source for lipid accumulation in oleaginous yeasts. *Microbial cell factories*, *15*(1), p.75.

[5] Tsigie, Y.A., Huynh, L.H., Nguyen, P.L.T. and Ju, Y.H., 2013. Catalyst-free biodiesel preparation from wet *Yarrowia lipolytica* Po1g biomass under subcritical condition. *Fuel processing technology*, *115*, pp.50-56.

[6] Subhash, G.V. and Mohan, S.V., 2015. Sustainable biodiesel production through bioconversion of lignocellulosic wastewater by oleaginous fungi. *Biomass Conversion and Biorefinery*, *5*(2), pp.215-226.

[7] Chang, Y.H., Chang, K.S., Lee, C.F., Hsu, C.L., Huang, C.W. and Jang, H.D., 2015. Microbial lipid production by oleaginous yeast *Cryptococcus sp.* in the batch cultures using corncob hydrolysate as carbon source. *Biomass and bioenergy*, *72*, pp.95-103.

[8] Tchakouteu, S.S., Kalantzi, O., Gardeli, C., Koutinas, A.A., Aggelis, G. and Papanikolaou, S., 2015. Lipid production by yeasts growing on biodiesel-derived crude glycerol: strain selection and impact of substrate concentration on the fermentation efficiency. *Journal of applied microbiology*, *118*(4), pp.911-927.

[9] Dobrowolski, A., Mituła, P., Rymowicz, W. and Mirończuk, A.M., 2016. Efficient conversion of crude glycerol from various industrial wastes into single cell oil by yeast *Yarrowia lipolytica. Bioresource technology*, *207*, pp.237-243.

[10] Rutter, C.D., Zhang, S. and Rao, C.V., 2015. Engineering *Yarrowia lipolytica* for production of medium-chain fatty acids.

Applied microbiology and biotechnology, *99*(17), pp.7359-7368

[11] Tsigie, Y.A., Wang, C.Y., Kasim, N.S., Diem, Q.D., Huynh, L.H., Ho, Q.P., Truong, C.T. and Ju, Y.H., 2012. Oil production from *Yarrowia lipolytica* Po1g using rice bran hydrolysate. *BioMed Research International*, *2012*.

[12] Saygün, A., Şahin-Yeşilçubuk, N. and Aran, N., 2014. Effects of different oil sources and residues on biomass and metabolite production by *Yarrowia lipolytica* YB 423-12. *Journal of the American Oil Chemists' Society*, *91*(9), pp.1521-1530.

[13] Rakicka, M., Lazar, Z., Dulermo, T., Fickers, P. and Nicaud, J.M., 2015. Lipid production by the oleaginous yeast *Yarrowia lipolytica* using industrial by-products under different culture conditions. *Biotechnology for biofuels*, *8*(1), p.104.

[14] Mlickova, K., Roux, E., Athenstaedt, K., dAndrea, S., Daum, G., Chardot, T. and Nicaud, J.M., 2004. Lipid accumulation, lipid body formation, and acyl coenzyme A oxidases of the yeast *Yarrowia lipolytica*. *Applied and environmental microbiology*, *70*(7), pp.3918-3924.

[15] Papanikolaou, S., Dimou, A., Fakas, S., Diamantopoulou, P., Philippoussis, A., Galiotou-Panayotou, M. and Aggelis, G., 2011. Biotechnological conversion of waste cooking olive oil into lipid-rich biomass using *Aspergillus* and *Penicillium* strains. *Journal of applied microbiology*, *110*(5), pp.1138-1150.

[16] Papanikolaou, S., Chevalot, I., Galiotou-Panayotou, M., Komaitis, M., Marc, I. and Aggelis, G., 2007. Industrial derivative of tallow: a promising renewable substrate for microbial lipid, single-cell protein and lipase production by *Yarrowia lipolytica*. *Electronic Journal of Biotechnology*, *10*(3), pp.425-435.

[17] Ito, T., Sakurai, Y., Kakuta, Y., Sugano, M. and Hirano, K., 2012. Biodiesel production from waste animal fats using pyrolysis method. *Fuel processing technology*, *94*(1), pp.47-52.

SEEC-2018-153

SIMULATION AND EXPERIMENTAL INVESTIGATION OF MELTING PROCESS IN SPHERICAL PCM CAPSULES USED FOR LOW-TEMPERATURE THERMAL ENERGY STORAGE SYSTEMS

Vivek Tiwari
Mechanical Engineering Department, Birla Institute of Technology & Science, Pilani, Rajasthan 333031, India
Email: p2016414@pilani.bits-pilani.ac.in

Kedar Haradas Patil
Mechanical Engineering Department, Birla Institute of Technology & Science, Pilani, Rajasthan 333031, India
kedarhpatil93124@gmail.com

P. Srinivasan
Mechanical Engineering Department, Birla Institute of Technology & Science, Pilani, Rajasthan 333031, India
psrinivasan@pilani.bits-pilani.ac.in

ABSTRACT

Thermal energy storage is a good solution to bridge the gap between energy supply and energy demand. Low-temperature PCM materials have the major disadvantage of low thermal conductivity which can be rectified to an extent by using the additional surface area by enhancing heat transfer rate. In this paper, the study is performed by Modeling and simulation of transient thermal energy storage of PCM capsule. The result shows fast melting in finned PCM capsule in comparison to unfinned PCM capsule.

A key feature of this paper is that this research finding can be used to minimise charging time of Spherical PCM based thermal energy storage system.

Keywords Thermal energy storage (TES), Latent heat thermal energy storage (LHTES), Computational fluid dynamics (CFD), Phase change materials (PCM).

NOMENCLATURE

C_p	Specific heat capacity
k	Thermal conductivity
R	radius (m)
t	time (s)
T	Temperature (K)
T_m	Melting temperature (K)

Abbreviations
PCM   Phase Change Material.

TES   Thermal Energy Storage
OD   Outer diameter (m)

Greek letters
ρ   density (kg/m^3)
μ   Viscosity (kg $m^{-1} s^{-1}$)
λ   Heat of fusion (kJ/Kg)

INTRODUCTION

Low-temperature PCM materials have many advantages like physical and chemical stability, cyclic stability, good thermal behavior, adjustable transition zone, non-corrosive and low or no sub-cooling. While the major disadvantage with Low-temperature PCM materials is low thermal conductivity [1]. Additional surface areas (fins) are used to enhance heat transfer rate.
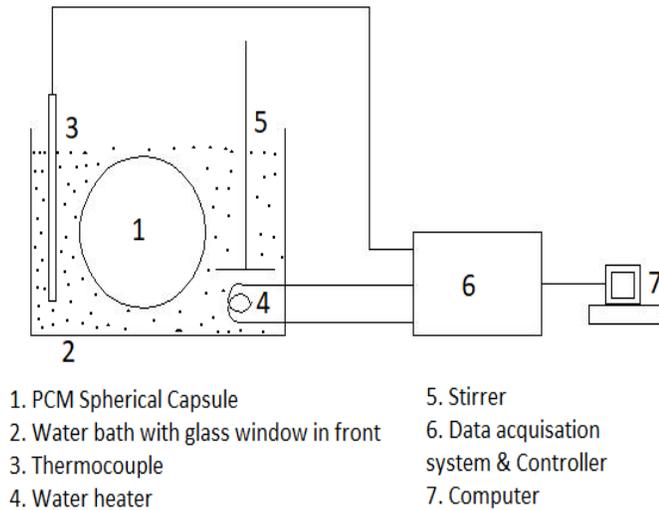
TABLE 1: PCM MATERIAL (SUNTECH PI16 PARAFFIN WAX) [3]

Melting Temperature, T_m (K)	**316 – 329**
Heat of fusion λ (kJ/Kg)	266
Specific heat capacity C_p (kJ/kg K)	2.51 (Liquid) 2.95 (Solid)
Thermal conductivity, k (W/m K)	0.24 (Liquid) 0.24 (Solid)
Density, ρ (kg/m^3)	760 (Liquid) 818 (Solid)

Liquid Viscosity (kg/ms)	1.90
Molecular weight (g/mol)	332

Borosil 4260 round bottom flask [2] of capacity 150ml (OD=75mm & Height=137mm) is considered an experiment as spherical PCM capsule shell. In the simulation, Borosil round bottom flask is assumed to be a perfectly spherical shell. Paraffin wax (Suntech PI16 Paraffin Wax) is considered for simulation as well as experiment. Properties of Paraffin wax is defined in tab 1.

R. VELRAJ et al. 1997 considered water bath setup for PCM capsule charging [4]. In their paper, the PCM capsule is heated with constant wall temperature. In our experiment setup, water bath with a glass window is taken. Borosil flask filled with a PCM material (PCM capsule) is immersed in a water bath. Electric water heater is used as an external heat source to charge PCM capsule. Thermocouple record temperature inside water bath and send a signal to data acquisition system. Data acquisition system alternately switches on and switch off water heat to maintain the set temperature. The stirrer is also used to maintain uniform temperature all over the water bath. Images from glass window are taken and with the help of image processing, melt fraction area is determined at different time intervals.

1. PCM Spherical Capsule
2. Water bath with glass window in front
3. Thermocouple
4. Water heater
5. Stirrer
6. Data acquisation system & Controller
7. Computer

FIGURE 1. EXPERIMENTAL WATER BATH SETUP FOR SPHERICAL PCM CAPSULE
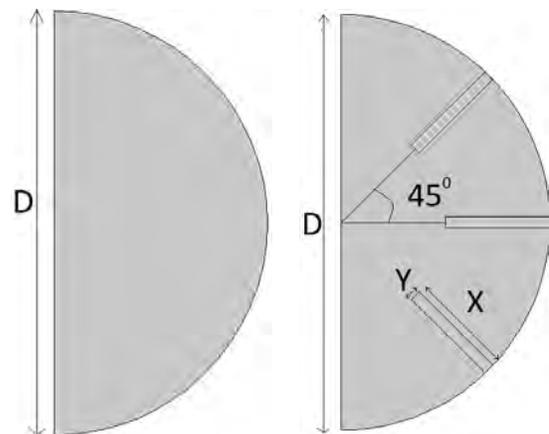
MATHEMATICAL MODEL

The objective of this work is to improve the performance of encapsulated PCM system with the help of fin models. Governing equations are solved by FEM method using a commercial solver COMSOL MULTIPHYSICS 5.2. For this purpose, a transient two-dimensional axis-symmetric numerical model is developed. Simulations are carried out for two different geometries viz. unfinned PCM Capsule and finned PCM Capsule. In case of finned PCM capsule, three annular fins made of a copper material (Properties of fin material is defined in tab 2) are attached to the inner spherical surface of the capsule with the angle of separation of 45^0. Length of the fin is 18.75 mm & width is 2 mm. The diameter of PCM capsules is 75 mm as shown in fig 2. Effect of gravity is taken into consideration. To simplify the model, following assumptions are taken.

- All thermos-physical properties of paraffin (thermal conductivity, density, specific heat capacity, dynamic viscosity) are assumed to be constant for respective phases viz. solid and liquid.

- Only radial and axial variation in heat transfer through the system is considered.

- Because of small volume and low Rayleigh's number, no convective heat transfer mode is considered during simulation.

- Effect of volume expansion of solid and liquid phases for the PCM material is neglected.

- The thermal resistance of Borosil flask is neglected in the simulation.
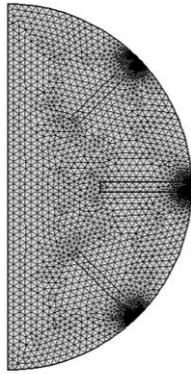
TABLE 2: FIN MATERIAL (COPPER)

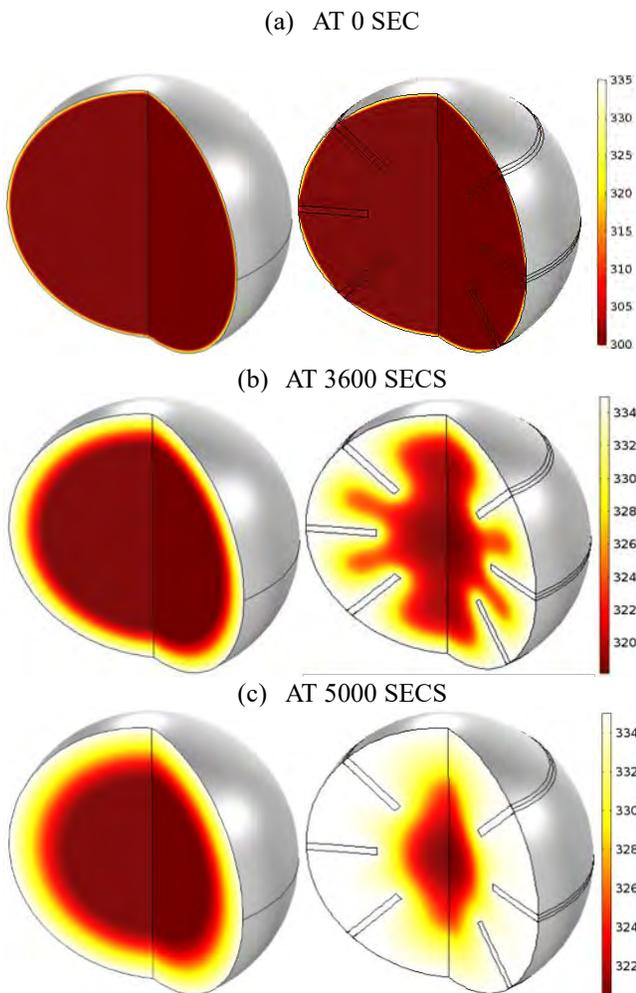|	
Thermal conductivity, k (W/m K)	**400**
Sp. heat capacity C_p (J/kg K)	385

FIGURE 2. MODEL A) UNFINNED B) FINNED

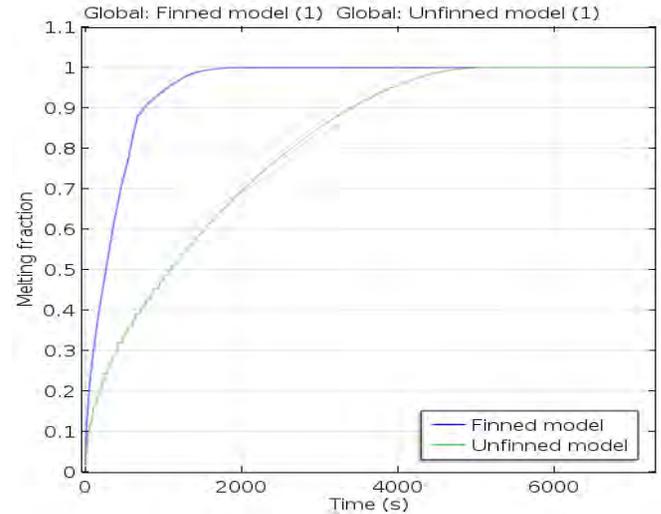Meshing is done taking free triangular shape with an element size extra fine as shown in fig 3.

FIGURE 3. MESHING FOR FINNED PCM CAPSULE

(a) AT 0 SEC

(b) AT 3600 SECS

(c) AT 5000 SECS

FIGURE 4. TEMPERATURES CONTOUR (K) FOR A) UNFINNED B) FINNED PCM CAPSULE AT (A) 0, (B) 3600, (C) 5000 SECONDS OF THE CHARGING TEST WITH CONSTANT TEMPERATURE WALL TEMPERATURE.

Figure 4 shows a variation of temperature throughout the PCM capsule at different time intervals for both unfinned and finned models. Figure 5 shows variation in melting fraction at different time intervals for both models. Improvement in heat transfer because of fins is observed through simulation.

FIGURE 5. MELT FRACTION VS TIME (S) FOR UNFINNED AND FINNED PCM CAPSULE

REFERENCES

[1]   T. Markandeyulu, J. Krishna Devanuri, and K. Kiran Kumar, "On the Suitability of Phase Change Material (PCM) for Thermal Management of Electronic Components," *Indian J. Sci. Technol.*, vol. 9, no. S1, pp. 1–4, 2016.

[2]   "Borosil Catalogue," *BOROSIL GLASS WORKS LTD., India*. [Online]. Available: www.borosil.com/doc_files/Binder1.pdf. [Accessed: 28-Sep-2017].

[3]   S. HIMRAN, A. SUWONO, and G. A. MANSOORI, "Characterization of Alkanes and Paraffin Waxes for Application as Phase Change Energy Storage Medium," *Energy Sources*, vol. 16, no. 1, pp. 117–128, 1994.

[4]   C. F. and K. S. R. VELRAJ, R. V. SEENIRAJ, B. HAFNER, "Experimental analysis and numerical modelling of inward solidification on a finned vertical tube for a latent heat storage unit," *Sol. Energy*, vol. 60, no. 5, pp. 281–290, 1997.

EFFECT OF COMPRESSION RATIO ON THE PERFORMANCE OF A CONSTANT SPEED SPARK IGNITION ENGINE OPERATING ON RAW BIOGAS

S. K. Hotta	**N. Sahoo**	**K. Mohanty**	**P. Mahanta**
Centre for Energy	Mechanical Engineering	Chemical Engineering	Mechanical Engineering
IIT Guwahati	IIT Guwahati	IIT Guwahati	IIT Guwahati
h.santosh@iitg.ernet.in	shock@iitg.ernet.in	kmohanty@iitg.ernet.in	pinak@iitg.ernet.in

ABSTRACT

In the present investigation, experiments were conducted in a 4.4 kW, single cylinder, water cooled, constant speed, spark ignition (SI) engine fuelled with raw biogas. The engine was operated with load a range of 6 to 77% and at four different compression ratios (10.52, 11.94, 13.96 and 15.29) of the engine. The effect of load level on the performance and emission characteristic of the engine at different compression ratios are analysed and presented in this paper. The brake power producing capability of the engine corresponds to CR 13.94 was maximum and found to be 3.01 kW with 76.27% of brake load. With increasing CR the engine becomes more stable and operated with an appreciable deviation in speed. Irrespective of engine loading condition, the minimum HC emission was observed at CR 15.29 and was found very between 23-144 ppm. The maximum NOx emission was detected at CR 15.29 and was found to very between 27-240 ppm.

Keywords: SI Engine, Biogas, Performance Analysis
.

1. INTRODUCTION

The increasing concern of energy security and environmental protection has stimulated the active research on improving fuel economy and reducing exhaust emission. To address this issues, the major research aspects of combustion and engine development has attracted the development of alternative fuelled engines. Liquid fuels like alcohols and vegetable oils, gaseous fuels such as natural gas, liquefied petroleum gas (LPG), hydrogen, biogas, and producer gas are promising alternative fuels. Very low levels of pollutant emission were reported when gaseous fuels are effectively utilized in spark ignition (SI) and compression ignition (CI) engines [1]. Gaseous fuels are quite acceptable for IC engine because of their wider range of flammability limit, higher hydro carbon ratio and capability to form homogeneous mixture [2-6]. Biogas is one such a renewable fuel and attractive source of energy produced from anaerobic digestion of organic matters. It consists of approximately 50-70% of methane (CH_4), 25-50% of carbon dioxide (CO_2), 1-5% of hydrogen (H_2), 0.3-3% of nitrogen (N_2) and traces of other impurities, notably hydrogen sulfide (H_2S). Typically, it consists of 60% of CH_4 and 40% of CO_2 [7-8]. The auto ignition temperature of biogas is very high, hence, it resist knocking which is desirable in SI engine. Since biogas has a higher anti nock index, biogas fueled SI engine can sustain high compression ratio (CR), which enhances the thermal efficiency of the engine [1-3, 9].

The performance and efficiency of a SI engine is mainly dependent on the combustion phasing and is influenced by factors such as compression ratio (CR), spark advance (SA) or ignition advance (IA), air-fuel ratio (AFR), exhaust gas recirculation (EGR), variable valve timing (VVT), combustion chamber design and composition of the fuel [1-3,10,12]. Out of which CR is the most important parameter for optimizing the efficiency,

emission and permitting combustion engines to conform future emission targets and standards. Proper control of ignition advance timing and CR can significantly improve the exhaust emission and the performance parameters for various kinds of operating fuels in IC engines. Increased compression ratios is an effective means of increasing the performance of biogas fueled engine when CO_2 is present in the biogas. However, the break mean effective pressure and break thermal efficiency increases steadily with compression ratios up to a critical value of 13:1 [13]. Operating with a variable compression ratio (VCR) Ricardo E6 single cylinder SI engine fueled with simulated biogas Hung and Crooks reported the effect of compression ratio with RAFR and carbon dioxide fraction of 0.97 and 37.5%, respectively. As reported break mean effective pressure (BMEP) and break thermal efficiency (BTE) values increase steadily with compression ratio up to a critical value of 13:1, above which there is a slight increase in these values. Although there is a slight increase in the BMEP along with the increase in the CR above 13:1, the additional indicated power (IP) do not compensate the mechanical losses arises due to friction. The traces of detonation were also observed at CR 15:1 [14]. In case of biogas fueled engine, the CR that can be employed should be higher than normal SI engine as the CO_2 present suppresses the knock. CR ranging from 11:1 to 13:1 reported suitable for operation without knock [3]. SI engine operated with biogas contains significant amount of CO_2 and N_2 which decreases the performance and increases the NOx emission as compared with natural gas and gasoline fueled engine [15].

In view of the current demand of energy utilization, fuel crisis, waste to energy conversion techniques and search of renewable resource of energy, the use of raw biogas as a standalone fuel in SI engine seems to be a good alternative solution. In order to make the raw biogas fueled SI engine more energy efficient, a detail investigation has been carried out to understand the effect of CR on the performance, combustion and emission characteristics of raw biogas fueled SI engine operating with a CR ranging from CR 10.52 to CR 15.29.

2. EXPERIMENTAL DETAILS
2.1 Selected Fuel and Their Properties
The fuel selected for the evaluation of the engine performance is the raw biogas produced by anaerobic digestion of cow dung and lignocellulos biomass produced in a Dinabandhu modeled biogas digester of 3 cubic meter capacity. The biogas produced from the digester is collected and stored in neoprene coated rubber fabric balloons connected in series. The stored biogas is then supplied to the engine by flexible pipes. The composition of the used fuel is analyzed each time before testing by using Thermo Fisher Scientific make gas chromatograph (GC). It has been observed that there is no substantial

change in the composition of the produced biogas unless until there is drastic change in environmental operating parameters or change in feed materials to the biogas digester. However, there is a little variation in the composition of the biogas with time according to the activities of the anaerobic bacteria. Tab. 1, describes some of the important properties of biogas used in the experiment.

TABLE 1. PROPERTIES OF THE USED FUEL

Properties	Biogas
Composition	CH_4- 55.6%[#], CO_2- 42.3[#] N_2- 2.1[#]
Density at 15^0C (kg/m3)	1.11[#]
Lower heating value (MJ/kg)	17[#]
Heat of vaporization (MJ/kg)	0.5
Stoichiometric A/F ratio	5.67*
Research octane number	110 [12]
Auto ignition temperature (^oC)	650 [12]
Flame Speed (cm/s)	25 [12]

* Calculated [#] Experimental value

2.2 Experimental Engine Test Rig
The experimental setup shown in Fig.1 consists of a Prakash made single cylinder, 990.6 CC, four stroke, water-cooled, constant speed, SI engine of rated power and speed of 4.4 kW and 1500 rpm, respectively. The engine was equipped with a unique governing system and a T-type mixture along with two throttle valve to control the mass flow rate of air and air-biogas mixture at all operating load to maintain the engine speed constant. The engine was coupled with a single phase, 3.5 kVA alternator to generate 230 V and 50 Hz frequency at 1500 rpm. For loading the engine crank shaft the output of the alternator was connected with a load panel consisting of 15 numbers of 200 Watt bulbs in series. To track the consumed current and output voltage of the alternator at a particular loading condition of the engine a voltmeter and an ammeter was connected inline before the load panel. The rated CR of the engine was 13.94 for biogas mode operation. But for the sake of analyzing the effect of CR on the performance and emission characteristics of a biogas fuelled constant speed SI engine, the CR ratio of the engine was varied manually by altering the clearance volume of the engine. Since the stroke volume (939.69 CC) and the piston cavity (51 CC) were known, the engine CR without any clearance slot was found to be 19.38. Therefore by adding copper slots of 2.65 mm thick and bakelite slots of 1.8 mm thick at different combinations the CR of the engine was varied for each test. The performance tests of the engine were conducted at four different CRs i.e., CR 10.52, CR 11.96, CR 13.94 and CR 15.29. The engine was well instrumented to track the operating parameters. The load on the engine was varied by applying electrical load on the alternator. For measuring the biogas flow rate a biogas flowmeter (make: Siya

Instruments, Model SI-6) was used. An air box was fabricated along with an orifice of 20 mm diameter and connected with an open U tube manometer; the pressure difference in the manometer column was later used to calculate the air mass flow rate. A diaphragm type piezo pressure sensor with built in amplifier and no noise cable is mounted on the engine head to measure the cylinder pressure during combustion. The optical crank angle encoder attached to the engine delivers a signal for each degree rotation of the crankshaft. The pressure and crank angle signals are then interfaced to the computer through piezo power unit to observe the pressure and crank angle signals as well as to measure the speed of the engine. The engine is connected to the Labview based software "Enginesoft" to record and analyze the data stored via a NI USB 6210 data logger. The emission analysis is carried out by using AVL DIAGAS 444N five-gas analyzer.
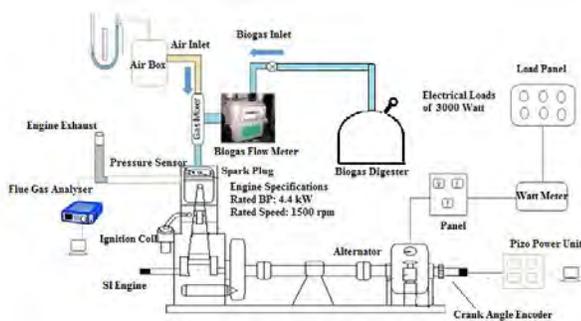
FIGURE 1. SCHEMETIC LAYOUT OF EXPERIMENTAL TEST RIG

3. RESULTS AND DISCUSSIONS

The performance parameters of the constant speed biogas fueled SI engine were evaluated for varying load conditions at four different compression ratios of CR 10.52, CR 11.96, CR 13.94 and CR 15.29. The average values of each engine performance parameter are presented below in detail.

3.1 Performance Analysis

Figure 1 shows the correlation between brake power (BP) (kW) and brake load (%) developed by the raw biogas fuelled SI engine operated with compression ratios 10.52, 11.96, 13.94 and 15.92. As observed, irrespective of the CR, the BP developed by the engine was increasing with progressive development of the load on the engine.

The maximum brake power output of the engine operated at CR 10.52, CR 11.96, CR 13.94 and CR 15.29 were found to be 1.94, 2.82, 3.01, and 2.92 kW with maximum brake load development of 50.40%, 73.33%, 78.20% and 76.27%, respectively. It was observed that with increasing CR the BP output of the engine increases but beyond CR 13.94 the BP of the engine starts decreasing.

The variations of the engine speed developed by the biogas fuelled SI engine operated at different CRs are shown in Fig. 3. It was observed that with progressive development of the engine load the speed of the engine starts deviating from its rated speed. However, these deviations are quite acceptable in CR 15.29, CR 13.96 and CR 11.94 where, the maximum deviation is only 9% from the rated speed. It was noticed that at CR 15.29, CR 13.96
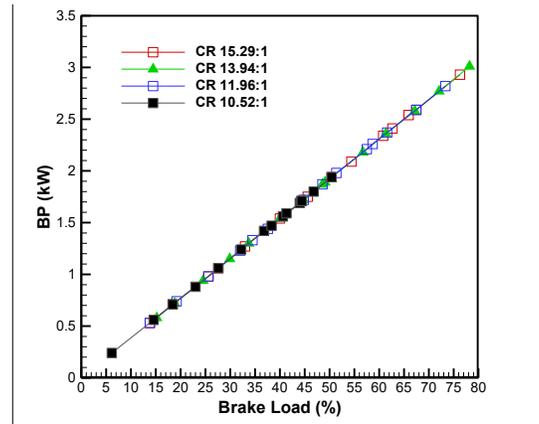

FIGURE 2. BRAKE POWER DEVELOPED BY THE ENGINE ON DIFFERENT COMPRESSION RATIOS
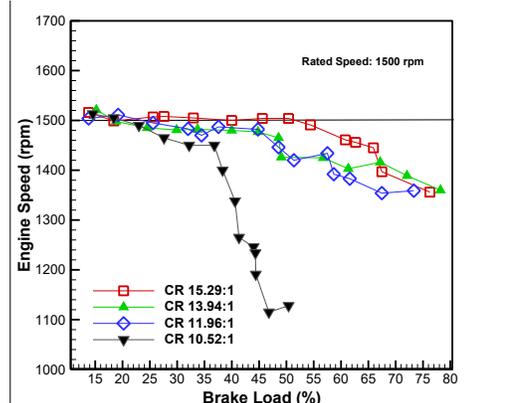

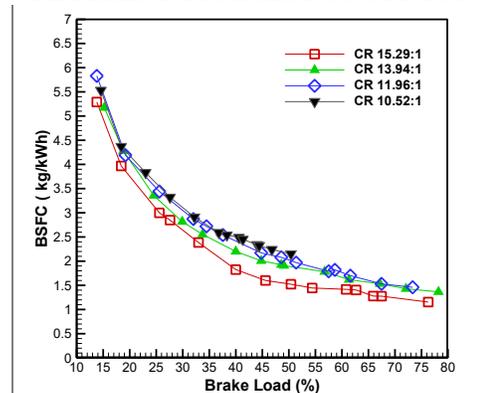FIGURE 3. SPEED DEVELOPED BY THE ENGINE AT DIFFERENT COMPRESSION RATIOS

FIGURE 4. BRAKE SPECIFIC FUEL CONSUMPTION OF THE ENGINE AT DIFFERENT CR

And CR 11.94 the speed remains almost constant (1500±50 rpm) up to 50% brake load and starts deviating after wards. But, at CR 10.52% the engine speed was found decreasing with increasing load on the engine. However, the minimum speed observed was 1128 rpm at 50% engine load and was the maximum developed brake load at CR 10.52. The same trend was also noticed by R. Chandra et al, [13]. With increasing CR the engine becomes more stable and operated with an appreciable deviation in speed.

Figure 4 shows the brake specific fuel consumption (BSFC) of the engine at different operating CRs. It was observed that with increasing CR the BSFC of the engine decreases. It was also observed that irrespective of CR the BSFC of the engine follows a decreasing trend along with progressive development of the engine load. At a particular loading condition (50% brake load) increasing the CR form 10.52 to 11.96, 11.96 to 13.94 and 13.94-15.29 reduced the BSFC by 8.37%, 4% and 21%, respectively. This is because, with increasing CR, the differential mass of fuel consumed is lesser than rise in BP and the mass fuel consumed to generate unit BP is comparatively lesser than at lower CR. Hence, The BSFC is reduced with increased CR.

Figure 5 shows the variation brake thermal efficiency (BTE) at different operating CR of the engine. It was observed that, the BTE of the engine increases with increasing CR. The maximum BTE of the engine was observed to be 18.36% at CR 15.29 and with brake load of 76.27%. It was also observed that, the BTE of the engine increases with increasing brake load of the engine.
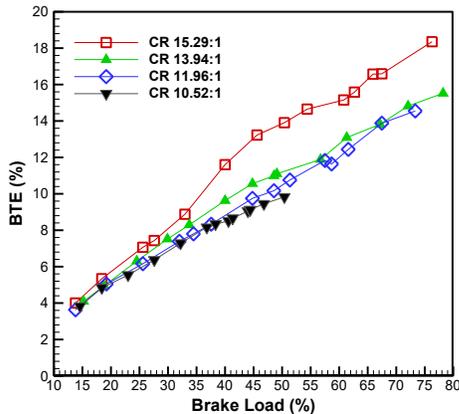

FIGURE 5. BRAKE THERMAL EFFICIENCY OF THE ENGINE AT DIFFERENT CR

3.1 Emission Analysis

The variation of hydrocarbon emission at different CRs of the biogas fuelled SI engine is shown in Fig. 6. It was observed that HC content in exhaust emission of the biogas fuelled SI engine was decreased with increased CR of the engine. It was also observed that with increasing

brake load the HC emission was increased. Irrespective of engine loading condition, the minimum HC emission was observed at CR 15.29 and was found very between 23-144 ppm.
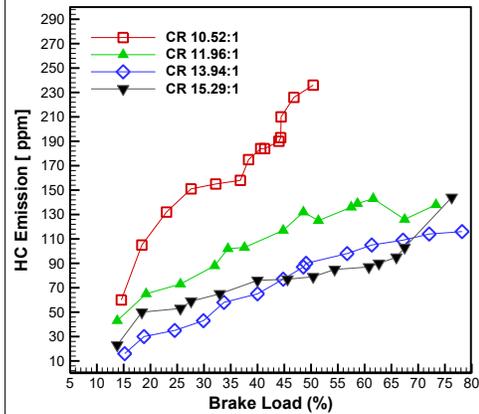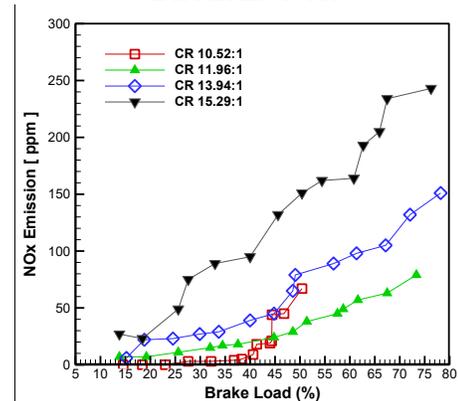

FIGURE 6. HC EMIISION OF THE ENGINE AT DIFFERENT CR

FIGURE 7. NO_x EMIISION OF THE ENGINE AT DIFFERENT CR

Fig. 7 shows the effect of compression ratio on the NO_x emission of a biogas fuelled SI engine. It was observed that with increasing CR and brake load on the engine the NO_x concentration in the exhaust emission of the biogas fuelled SI engine follows an increasing trend. The maximum NO_x emission was detected at CR 15.29 and was found to very between 27-240 ppm. The NO_x emission is strongly related to the lean fuel with high cylinder temperature or high combustion temperature. The cylinder temperature and combustion temperature increases with increasing CR and is higher in case of CR 15.29 as compared to other CRs. Because of this reason only the NO_x concentration is comparatively higher in CR 15.29.

4. CONCLUSIONS

Based on the experimental investigation carried out to investigate the effect of CR on the performance and emission characteristics of the raw biogas fueled, constant speed SI engine, the following conclusions are drawn.

The brake power producing capability of the engine corresponds to CR 13.94 was maximum and found to be 3.01 kW with 76.27% of brake load. With increasing CR the BSFC of the engine follows a decreasing trend and the BTE follows an increasing trend. The minim BSFC and the maximum BTE was found to be 5.29 kg/kWh and 18.36% at CR 15.29%. With increasing CR the engine becomes more stable and operated with an appreciable deviation in the rated speed. Irrespective of engine loading condition, the minimum HC emission was observed at CR 15.29 and was found very between 23-144 ppm. The maximum NO_x emission was detected at CR 15.29 and was found to very between 27-240 ppm.

ACKNOWLEDGMENTS

REFERENCES

[1] Porpatham, E., Ramesh, A. and Nagalingam, B. (2012) Effect of compression ratio on the performance and combustion of a biogas fuelled spark ignition engine, *Fuel*, 95, pp. 247-256.

[2] Porpatham, E., Ramesh, A. and Nagalingam, B. (2013) Effect of swirl on the performance and combustion of a biogas fuelled spark ignition engine, *Energy Conversion and Management*, 76, pp. 463-471

[3] Porpatham, E., Ramesh, A. and Nagalingam, B. (2008) Investigation on the effect of concentration of methane in biogas when used as a fuel for a spark ignition engine, Fuel, 87.8, pp. 1651-1659.

[4] Chandra R, Vijay V. K., Subbarao P. M. and Khura T. K. (2011) Performance evaluation of a constant speed IC engine on CNG, methane enriched biogas and biogas, *Applied Energy*, 30;88 (11), pp. 3969-77.

[5] Nathan S. S., Mallikarjuna J. M. and Ramesh A. (2010) An experimental study of the biogas–diesel HCCI mode of engine operation, *Energy Conversion and Management*. 31; 51 (7), pp. 1347-53.

[6] Hotta S. K, Singh R., Sahoo N., Mohanty K. and Mahanta P. (2015) Design of a venturi type biogas mixer for a four stroke spark ignition engine. *Proceedings of the 5th International Conference on Advances in Energy Research*, pp. 998-1005.

[7] Crookes, R. J. (2006) Comparative bio-fuel performance in internal combustion engines, *Biomass and Bioenergy,* 30(5), pp. 461-468.

[8] Huang, J. and Crookes, R. J. (1998) Assessment of simulated biogas as a fuel for the spark ignition engine, *Fuel*, 77(15), pp. 1793-1801.

[9] Porpatham, E., Ramesh, A. and Nagalingam, B. (2007) Effect of hydrogen addition on the performance of a biogas fuelled spark ignition engine, *International Journal of Hydrogen Energy*, 32(12), pp.2057-2065.

[10] Alagumalai, A. (2014) Internal combustion engines: Progress and prospects. *Renewable and Sustainable Energy Review,* 38:5, pp. 61-71.

[11] Mitzlaff V (1988) Engines for Biogas- theory, modification, economic operation, A publication of Deutsches Zentrum fur Entwicklungstechnologien, GTZ – GATE, Germany.

[12] Corti, E., Cavina, N., Cerofolini, A., Forte, C., Mancini, G., Moro, D., Ponti, F. and Ravaglioli, V. (2014) Transient spark advance calibration approach, *Energy Procedia*, *45*, pp.967-976.

[13] Chandra, R, Vijay, V. K., Subbarao P. M. and Khura T. K. (2011) Performance evaluation of a constant speed IC engine on CNG, methane enriched biogas and biogas, *Applied Energy,* 30;88 (11), pp. 3969-77.

[14] Huang, J. and Crookes R. J. (1998) "Assessment of simulated biogas as a fuel for the spark ignition engine, *Fuel.* 77(15), pp. 1793-1801.

[15] Surata, I. W., Nindhia, T. G.T., Atmika, I. K. A., Negara, D. N. K. P and Putra, I.W. E. P. (2014) Simple Conversion Method from Gasoline to Biogas Fueled Small Engine to Powered Electric Generator, *Energy Procedia*, 52, pp. 626–632.

EFFECT OF NANOPARTICLES ON BIOELECTRICITY GENERATION IN MICROBIAL FUEL CELL

S.M. Sambavi
Department of Mechanical Engineering,
SRM University, Ramapuram,
Chennai - 600 089.
Tamil Nadu, India.
Email: smsneka@gmail.com

P. Mullai
Department of Chemical Engineering,
Faculty of Engineering and Technology,
Annamalai University,
Annamalai Nagar - 608 002, Tamil Nadu, India.
pmullai@yahoo.in

ABSTRACT

Microbial fuel cell (MFC), a bioelectrochemical device in which microorganisms directly oxidize energy stored in organic matters to electricity under anaerobic condition, can be used to recover of energy from renewable sources[1,2]. In this experiment, a laboratory scale two chambered microbial fuel cell was designed and operated batch mode to find out the effect of initial substrate concentration (2,000 – 10,000 mg COD/L) and iron oxide nanoparticles concentration (0.01– 0.20 g/L) at constant pH of 5.5 at the room temperature of $30 - 35°C$ and constant for bioelectricity generation. In each chamber one electrode made of graphite plate was immersed. In the control test, with initial substrate concentrations of 2000, 4000, 6000, 8000 and 10000 mg COD/L, the recorded maximum COD removal efficiency was 76.5, 96.0, 85.0, 66.0 and 64.0%, respectively. The current generated under the applied external resistance of $R=100Ω$ for the said substrate concentrations was 7.77, 8.10, 7.98, 2.65, 1.25 mA, respectively. Among the five different initial substrate concentrations studied, 4000 mg COD/L was found to generate maximum electricity.

Iron is essential for the synthesis hydrogenase or other enzymes which in turn are very essential for the production of protons and electrons [3]. In this experiment, the substrate with the initial substrate concentration of 4000 mg/L which was found to be ideal was taken for the experiment to find out the effect of iron oxide nanoparticle concentration on COD removal efficiency and bioelectricity production. For the different iron oxide nanoparticles concentration such as, 0.010, 0.050, 0.100, 0.150 and 0.200 g/L, the corresponding COD removal efficiencies were 85.0, 93.0, 98.0, 75.0 and 68.0 %. For the same substrate concentration with five nanoparticle concentration the maximum potential recorded was 93.0, 850, 870, 567 and 140 mV, respectively at 36, 56, 71, 75 and 29 h. In the control the value of COD removal efficiency and potential recorded which was 96% and 810mV, respectively increased slightly to 98% and 870 mV after the addition of nanoparticles. The iron oxide nanoparticles used enhanced the electricity generation potential from 810 mV to 870 mV by 6.9%.

*Keywords***:** Microbial fuel cell, nanoparticles, current generation.
.

REFERENCES

[1] Venkatamohan, S., Mohanakrishna, G., Srikanth, S., and Sarma, P. N., 2008. "Harnessing of bioelectricity in microbial fuel cell (MFC) employing aerated cathode through anaerobic treatment of chemical wastewater using selectively enriched hydrogen producing mixed consortia." Fuel, 87, pp. 2667–2676.

[2] Sambavi,S.M.,2013 https://www.googlesciencefair.com/en/projects/ahJzfnNjaWVuY2VmYWlyLTIwMTJyRAsSC1Byb2plY3RTaXRlIjNhaEp6Zm5OamFFXVnVZMlZtWVdseUxUSXdNVEp5RUFzU0IxQnliMnBsWTNSRWTc4cUpBUXcM.

[3] Mullai, P., Yogeswari, M. K., and Sridevi, K., 2013. "Optimisation and enhancement of biohydrogen

production using nickel nanoparticles - A novel approach." Bioresource Technology, 141, pp. 212–219.

AXIAL DISPERSION IN A HYBRID UPFLOW ANAEROBIC SLUDGE BLANKET REACTOR TREATING PENICILLIN G WASTEWATER

P. Mullai
Department of Chemical Engineering,
Faculty of Engineering and Technology,
Annamalai University,
Annamalai Nagar – 608 002, Tamil Nadu, India.
Email: pmullai@yahoo.in

S.M.Sambavi
Department of Mechanical Engineering,
SRM University, Ramapuram, Chennai - 600 089,
Tamil Nadu, India.
Email: smsneka@gmail.com

ABSTRACT

The flow pattern in bioreactors is different from those of ideal reactors like the plug flow and the perfectly mixed flow reactors. The flow patterns have a great influence on the performance of the bioreactors. A closer look at a hybrid upflow anaerobic sludge blanket (HUASB) reactor on the startup and steady state operation indicate that its fluid flow can be explained with an axial dispersion model. The performance of the HUASB reactor was found out using this model. For four different OLRs such as 5.85, 11.46, 13.8 and 24.28 kg COD $m^{-3}d^{-1}$, the values of dispersion number obtained were 0.13, 0.23, 0.2 and 0.54, respectively. Further, for the said OLRs, the values of theoretical COD removal efficiencies respectively were 92.4, 82.0, 63.0 and 41.7%. As the values of percentage error calculated were less than 11%, the dispersion model was found to be a good representation of the flow in the HUASB reactor.

Keywords: HUASB reactor, residence time distribution, dispersion model
.

NOMENCLATURE

u   Mean flow velocity along reactor.
L   Length of axial travel in reactor.
k   Removal rate constant per unit time.
n   Order of the reaction.
τ Theoretical detention time (V/Q).
C_{Ao}&C_A Initial and final substrate concentrations, respectively.

INTRODUCTION

The mixing phenomena are important in the design of bioreactors, since the time spent in each of the environments that the bioreactor offers, and age of other elements that an element of fluid does contact, are of crucial importance in evaluating the bioreactor performances. The mixing phenomenon is of particular importance for design, modelling and operation, as well as for scale-up from laboratory to industry scale [1-5]. The study of flow pattern in the HUASB reactor, which has the positive features of both the AF and UASB reactor is difficult because of the coexistence of solids (bacterial colonies in the form of pellets, granules and flocs), wastewater and biogas. In this work, an attempt was made to characterise the liquid flow, in terms of an overall axial dispersion for the entire HUASB reactor. The axial dispersion is caused by turbulence, dead space and molecular diffusion.

MATERIALS AND METHODS
Substrate
Penicillin-G wastewater collected from J.K.Pharmachem Limited, Cuddalore was used as a substrate.

Inoculum
Sewage sludge and cow dung slurry were mixed and filtered and used as inoculum.

Hybrid Upflow Anaerobic Sludge Blanket (HUASB) Reactor
A laboratory scale hybrid upflow anaerobic sludge blanket reactor used in this study was made of perspex tube with an internal diameter of 10.4 cm and overall height of 60cm. The top third of the reactor (10cm) was filled with polypropylene spherical beads.

Experimental Procedure
Penicillin-G wastewater used as a substrate was diluted with demineralised water to a desired concentration. Thereafter, nutrients were added to the substrate to maintain a COD: N: P ratio of 100:5:1. Before feeding the influent, the pH was adjusted to 7.2 by adding sodium bicarbonate. The experiment was carried out with an organic loading rate (OLR) of 5.85 kg COD m^{-3} d^{-1} and continued till the chemical oxygen demand (COD) values reached a steady state. The experiments were repeated for three different OLRs such as 11.46, 13.8, and 24.28 kg COD m^{-3} d^{-1}. The pulse experiments were conducted on days 13, 33, 46, and 59 of the steady state operation of the HUASB reactor. Tracer concentration of the sample was measured by using a flame photometer.

RESULTS AND DISCUSSION
Residence Time Distribution
The residence time distribution studies were carried out at steady states on days 13, 33, 46 and 59 of the operation of the HUASB reactor with the OLRs of 5.85, 11.46, 13.8 and 24.28 kg COD $m^{-3}d^{-1}$. The residence time of a fluid element in a vessel is defined as the time interval between the moments of entering and leaving. The average theoretical residence time (τ_{th}) is defined as the volume (V) of the vessel over the volumetric flow through the vessel (v). For the three OLRs such as 5.85, 11.46 and 24.28 kg COD m^{-3} d^{-1}, the values of mean HRts were lower than the values of theoretical HRTs. The low HRT values indicated that there might be some dead zones and short circuiting caused by a large number of bubbles occasionally formed near the reactor inlet and also due to the existence of the packing media and accumulated biomass. Similarly, lower mean HRT values when compared to the theoretical HRT values were documented by Tay and Zhang [6] in

anaerobic filter (AF) and UASB reactors and Pires *et al.* [2] in UASB reactors.

Reactor Performance using Dispersion Model
Levenspiel [7] obtained the following general equation for any reactant following nth-order kinetics. When axial dispersion is predominant, the equation is

$$D\frac{\partial^2 C}{\partial X^2} - u\frac{\partial C}{\partial X} - kC^n = 0 \qquad (1)$$

The results obtained in the anaerobic treatment of penicillin-G wastewater were found best fitted with the first order kinetics (n=1). So the Eq. (1) with first order kinetics, solved by Danckwerts as given by Fogler [8] is adopted here to find out the performance of the HUASB reactor. The solution is

$$\frac{C_A}{C_{Ao}} = 1 - X_A = \frac{4a\exp\left(\frac{1uL}{2D}\right)}{(1+a)^2\exp\left(\frac{auL}{2D}\right) - (1-a)^2\exp\left(-\frac{auL}{2D}\right)} \qquad (2)$$

where

$$a = \sqrt{1 + 4k\tau\left(\frac{D}{uL}\right)}$$

Using the Eq. (2), the conversion values for the four different OLRs such as 5.85, 11.46, 13.8 and 24.28 kg COD $m^{-3}d^{-1}$ were 92.4, 82.0, 63.0 and 41.7%, respectively. The experimental and theoretical COD removal efficiencies are compared. The corresponding percentage errors obtained for the four different OLRs such as 5.85, 11.46, 13.8 and 24.28 kg COD m^{-3} d^{-1} were 8.45, 10.36, 8.25, 0.48%. As the values of percentage error calculated were less than 11%, the dispersion model was found to be a good representation of the flow in the HUASB reactor.

CONCLUSIONS
The mixing and fluid flow behaviour in the HUASB reactor was investigated at four different OLRs viz., 5.85, 11.46, 13.4 and 24.28 kg COD $m^{-3}d^{-1}$. The findings of the present work are as follows:
1. The dispersion numbers calculated were 0.13, 0.23, 0.2 and 0.54.
2. The axial dispersion model was found to be a good representation of the flow in the HUASB reactor.

REFERENCES

[1] Gavrilescu, M., Muntean, O., and Tudose, R.Z., 2000. "Stochastic modelling of axial dispersion in external-loop airlift bioreactors". Bioprocess Engineering, 23, pp. 543-549.

[2] Pires, E.C., Hanisch, W.S., and Andrade, M.A.N., 2000. "An original procedure for physical simulation of upflow anaerobic sludge blanket reactors". Bioprocess Engineering, 23, pp 389-395.

[3] Tilche, A., and Vieira, S.M.M., 1991. "Discussion report on reactor design of anaerobic filters and sludge bed reactors". Water Science and Technology, 24, pp. 193-206

[4] Li, S.N., Nan, J., Li, H.Y., Yao, M., 2015. "Comparative analyses of hydraulic characteristics between the different structures of two anaerobic baffled reactors (ABRs)". Ecological Engineering, 82, pp. 138 - 144.

[5] Ji, J.Y., Zheng, K., Xing, Y.J., Zheng, P., 2012. "Hydraulic characteristics and their effects on working performance of compartmentalized anaerobic reactor". Bioresource Technology, 116, pp. 47 - 52.

[6] Tay, J.H., and Zhang, X., 2000. "Stability of high rate anaerobic systems. I. Performance under shocks". Journal of Environmental Engineering, 126, pp. 713-731.

[7] Levenspiel, O., 1999. Chemical reaction engineering, 3 rd ed., John Wiley and Sons, New York.

[8] Fogler, H.S., 1986. Elements of chemical reaction engineering, 4 th ed., Prentice-Hall, New Jersey.

SEEC-2018-159

DEVELOPMENT OF INJECTION TECHNOLOGY FOR DIESEL AND GASOLINE ENGINES

Jai Gopal Gupta*
Department of Mechanical Engineering,
Govt. Women Engineering College, Ajmer,
Rajasthan,India
Email: jaigopalg@gmail.com
*corresponding author

Deeksha Kanwar
Department of Mechanical Engineering,
Govt. Women Engineering College, Ajmer,
Rajasthan,India
Email: deekshakanwar150@gmail.com

ABSTRACT

Fuel injection is the introduction of fuel in an internal combustion engine by the means of an injector in most commonly automotive engines. All diesel engines use fuel injection by design. Petrol engines can use gasoline direct injection, where the fuel is directly delivered into the combustion chamber, or indirect injection where the fuel is mixed with air before the intake stroke.

In petrol engines, fuel injection replaced carburetors from the 1980s onward. The primary difference between carburetors and fuel injection is that fuel injection atomizes the fuel through a small nozzle under high pressure, while a carburetor relies on suction created by intake air accelerated through a Venturi tube to draw the fuel into the airstream and the purpose of the fuel injection system is to deliver fuel into the engine cylinders, while precisely controlling the injection timing, fuel atomization, and other parameter.

.Keywords: History of Fuel Injection system, Development of injectors, Diesel injector, Gasoline injector

NOMENCLATURE

SPICA S.(Società Pompe Iniezione Cassani & Affini) was an Italian manufacturer of fuel injection systems.

INTRODUCTION

Herbert Akroyd Stuart developed the first device with a design similar to modern fuel injection, using a 'jerk pump' to meter out fuel oil at high pressure to an injector. This system was used on the hot-bulb engine and was adapted and improved by Bosch and Clessie Cummins for use on diesel engines (Rudolf Diesel's original system employed a cumbersome 'air-blast' system using highly compressed air[citation needed). Fuel injection was in widespread commercial use in diesel engines by the mid-1920s.

An early use of indirect gasoline injection dates back to 1902, when French aviation engineer Leon Levavasseur installed it on his pioneering Antoinette 8V aircraft

powerplant, the first V8 engine of any type ever produced in any quantity [1].

FIGURE 1. Hessalman Engine

Another early use of gasoline direct injection was on the Hesselman engine invented by Swedish engineer Jonas Hesselman in 1925 [2]. Hesselman engines use the ultra lean-burn principle; fuel is injected toward the end of the compression stroke, then ignited with a spark plug. They are often started on gasoline and then switched to diesel or kerosene [3].

Direct fuel injection was used in notable World War II aero-engines such as the Junkers Jumo 210, the Daimler-Benz DB 601, the BMW 801, the Shvetsov ASh-82FN (M-82FN). German direct injection petrol engines used injection systems developed by Bosch from their diesel injection systems. Later versions of the Rolls-Royce Merlin and Wright R-3350 used single point fuel injection, at the time called "Pressure Carburettor". Due to the wartime relationship between Germany and Japan, Mitsubishi also had two radial aircraft engines utilizing fuel injection, the Mitsubishi Kinsei (kinsei means "venus") and the Mitsubishi Kasei (kasei means "mars").

Alfa Romeo tested one of the first electronic injection systems (Caproni-Fuscaldo) in Alfa Romeo 6C 2500 with "Ala spessa" body in 1940 Mille Miglia. The engine had six electrically operated injectors and were fed by a semi-high-pressure circulating fuel pump system [4].

Development of Injectors

For different engines different Injection systems for fuel injection into the combustion chamber of all diesel engines (with the exception of some tractors and scale model engines).

Mechanical injection

The invention of mechanical injection for gasoline-fueled aviation engines was by the French inventor of the V8 engine configuration, Leon Levavasseur in 1902 [2]. Levavasseur designed the original Antoinette firm's series of V-form aircraft engines, starting with the Antoinette 8V to be used by the aircraft the Antoinette firm built that Antoinette (Levavasseur) Aircraft Engines (Fig. 2).

FIGURE 2. Antoinette (Levavasseur) Aircraft Engines

Levavasseur Aircraft also designed, flown from 1906 to the firm's demise in 1910, with the world's first V16 engine, using Levavasseur's direct injection and producing around 100 hp (75 kW; 101 PS) flying an Antoinette VII monoplane in 1907.

The first post-World War I example of direct gasoline injection was on the Hesselman engine invented by Swedish engineer Jonas Hesselman in 1925.[5] Hesselman engines used the ultra-lean-burn principle and injected the fuel in the end of the compression stroke and then ignited it with a spark plug, it was often started on gasoline and then switched over to run on diesel or kerosene. The Hesselman engine was a low compression design constructed to run on heavy fuel oils.

Direct gasoline injection was applied during the Second World War to almost all higher-output production aircraft powerplants made in Germany (the widely used BMW 801 radial, and the popular inverted inline V12 Daimler-Benz DB 601, DB 603, and DB 605, along with the similar Junkers Jumo 210G, Jumo 211, and Jumo 213, starting as early as 1937 for both the Jumo 210G and DB 601), the Soviet Union (Shvetsov ASh-82FN radial, 1943, Chemical Automatics Design Bureau - KB Khimavtomatika) and the USA (Wright R-3350 Duplex Cyclone radial, 1944). Immediately following the war, hot rodder Stuart Hilborn started to offer mechanical injection for race cars, salt cars, and midget racers,[6] well-known and easily distinguishable because of their prominent velocity stacks projecting upwards from the engines on which they were used.

The first automotive direct injection system used to run on gasoline was developed by Bosch, and was introduced by Goliath for their Goliath GP700 automobile, and Gutbrod in 1952. This was basically a high-pressure diesel direct-injection pump with an intake throttle valve. (Diesels only change the amount of fuel injected to vary output; there is no throttle.) This system used a normal gasoline fuel pump, to provide fuel to a mechanically driven injection pump, which had separate plungers per injector to deliver a very high injection pressure directly into the combustion chamber. The 1954 Mercedes-Benz W196 Formula 1 racing car engine used Bosch direct injection derived from wartime aircraft engines. Following this racetrack success, the 1955 Mercedes-Benz 300SL, the first production sports car to use fuel injection, used direct injection. The 1955 Mercedes-Benz 300SLR, in which Stirling Moss drove to victory in the 1955 Mille Miglia and Pierre Levegh crashed and died in the 1955 Le Mans disaster, had an engine developed from the W196 engine. The Bosch fuel injectors were placed into the bores on the cylinder wall used by the spark plugs in other Mercedes-Benz six-cylinder engines (the spark plugs were relocated to the cylinder head). Later, more mainstream applications of fuel injection favored the less-expensive indirect injection methods.

FIGURE 3. Chevrolet 1959 Corvette fuel injection

Chevrolet introduced a mechanical fuel injection option, made by General Motors' Rochester Products Division, for its 283 V8 engine in 1956 (1957 U.S. model year). This system directed the inducted engine air across a "spoon shaped" plunger that moved in proportion to the air volume. The plunger connected to the fuel metering system that mechanically dispensed fuel to the cylinders via distribution tubes. This system was not a "pulse" or intermittent injection, but rather a constant flow system, metering fuel to all cylinders simultaneously from a central "spider" of injection lines. The fuel meter adjusted the amount of flow according to engine speed and load, and included a fuel reservoir, which was similar to a carburetor's float chamber. With its own high-pressure fuel pump driven by a cable from the distributor to the fuel meter, the system

supplied the necessary pressure for injection. This was a "port" injection where the injectors are located in the intake manifold, very near the intake valve.

In 1956, Lucas developed its injection system, which was first used for Jaguar racing cars at Le Mans. The system was subsequently adopted very successfully in Formula One racing, securing championships by Cooper, BRM, Lotus, Brabham, Matra, and Tyrrell in the years 1959 through 1973 [7]. While the racing systems used a simple fuel cam for metering, a more sophisticated Mk 2 vacuum based shuttle metering was developed for production cars. This mechanical system was used by some Maserati, Aston Martin, and Triumph models between 1963 and 1975.[8]

During the 1960s, other mechanical injection systems such as Hilborn were occasionally used on modified American V8 engines in various racing applications such as drag racing, oval racing, and road racing.[9] These racing-derived systems were not suitable for everyday street use, having no provisions for low speed metering, or often none even for starting (starting required that fuel be squirted into the injector tubes while cranking the engine). However, they were a favorite in the aforementioned competition trials in which essentially wide-open throttle operation was prevalent. Constant-flow injection systems continue to be used at the highest levels of drag racing, where full-throttle, high-RPM performance is key [10].

In 1967, one of the first Japanese designed cars to use mechanical fuel injection was the Daihatsu Compagno. Another mechanical system, made by Bosch called Jetronic, but injecting the fuel into the port above the intake valve, was used by several European car makers, particularly Porsche from 1969 until 1973 in the 911 production range and until 1975 on the Carrera 3.0 in Europe. Porsche continued using this system on its racing cars into the late seventies and early eighties. Porsche racing variants such as the 911 RSR 2.7 & 3.0, 904/6, 906, 907, 908, 910, 917 (in its regular normally aspirated or 5.5 Liter/1500 HP turbocharged form), and 935 all used Bosch or Kugelfischer built variants of injection. The early Bosch Jetronic systems were also used by Audi, Volvo, BMW, Volkswagen, and many others. The Kugelfischer system was also used by the BMW 2000/2002 Tii and some versions of the Peugeot 404/504 and Lancia Flavia.

A system similar to the Bosch inline mechanical pump was built by SPICA for Alfa Romeo, used on the Alfa Romeo Montreal and on U.S. market 1750 and 2000 models from 1969 to 1981. This was designed to meet the U.S. emission requirements with no loss in performance and it also reduced fuel consumption.

Because mechanical injection systems have limited adjustments to develop the optimal amount of fuel into an

engine that needs to operate under a variety of different conditions (such as when starting, the engine's speed and load, atmospheric and engine temperatures, altitude, ignition timing, etc.) electronic fuel injection (EFI) systems were developed that relied on numerous sensors and controls. When working together, these electronic components can sense variations and the main system computes the appropriate amount of fuel needed to achieve better engine performance based on a stored "map" of optimal settings for given requirements [11].

Electric Fuel Injection

Because mechanical injection systems have limited adjustments to develop the optimal amount of fuel into an engine that needs to operate under a variety of different conditions (such as when starting, the engine's speed and load, atmospheric and engine temperatures, altitude, ignition timing, etc.) electronic fuel injection (EFI) systems were developed that relied on numerous sensors and controls.The first commercial EFI system was the Electrojector, developed by the Bendix Corporation and was offered by American Motors Corporation (AMC) in 1957 [15][16].

FIGURE 4. First Electrojector

The Rambler Rebel, showcased AMC's new 327 cu in (5.4 L) engine. The Electrojector was an option and rated at 288 bhp (214.8 kW) [12]. The EFI produced peak torque 500 rpm lower than the equivalent carburetored engine[9]. The Rebel Owners Manual described the design and operation of the new system (due to cooler, therefore denser, intake air[citation needed]) [13]. The cost of the EFI option was US$395 and it was available on 15 June 1957 [14]. Electrojector's teething problems meant only pre-production cars were so equipped: thus, very few cars so equipped were ever sold [15] and none were made available to the public [16]. The EFI system in the Rambler ran fine in warm weather, but suffered hard starting in cooler temperatures [14].

Chrysler offered Electrojector on the 1958 Chrysler 300D, DeSoto Adventurer, Dodge D-500, and Plymouth Fury, arguably the first series-production cars equipped with an EFI system. It was jointly engineered by Chrysler and Bendix. The early electronic components were not equal to the rigors of underhood service, however, and were too slow to keep up with the demands of "on the fly" engine control. Most of the 35 vehicles originally so equipped were field-retrofitted with 4-barrel carburetors. The Electrojector patents were subsequently sold to Bosch.

FIGURE 5. D Jetronic components

Bosch developed an electronic fuel injection system, called D-Jetronic (D for Druck, German for "pressure"), which was first used on the VW 1600TL/E in 1967. This was a speed/density system, using engine speed and intake manifold air density to calculate "air mass" flow rate and thus fuel requirements. This system was adopted by VW, Mercedes-Benz, Porsche, Citroën, Saab, and Volvo. Lucas licensed the system for production in Jaguar cars, initially in D-Jetronic form before switching to L-Jetronic in 1978 on the XK6 engine.

FIGURE 6. K Jetronic Components

Bosch superseded the D-Jetronic system with the K-Jetronic and L-Jetronic systems for 1974, though some cars (such as the Volvo 164) continued using D-Jetronic for the following several years. In 1970, the Isuzu 117 Coupé was introduced with a Bosch-supplied D-Jetronic fuel injected

engine sold only in Japan. In 1984 Rover fitted Lucas electronic fuel injection, which was based on some L-Jetronic patents, to the S-Series engine as used in the 200 model.

In Japan, the Toyota Celica used electronic, multi-port fuel injection in the optional 18R-E engine in January 1974 [17]. Nissan offered electronic, multi-port fuel injection in 1975 with the Bosch L-Jetronic system used in the Nissan L28E engine and installed in the Nissan Fairlady Z, Nissan Cedric, and the Nissan Gloria. Nissan also installed multi-point fuel injection in the Nissan Y44 V8 engine in the Nissan President. Toyota soon followed with the same technology in 1978 on the 4M-E engine installed in the Toyota Crown, the Toyota Supra, and the Toyota Mark II. In the 1980s, the Isuzu Piazza and the Mitsubishi Starion added fuel injection as standard equipment, developed separately with both companies history of diesel powered engines. 1981 saw Mazda offer fuel injection in the Mazda Luce with the Maz

Conclusion

We are in need of fuel injection system to utilize available fuel resourses without polluting the environment. Injection system revolutionised the automobile industry to a excellent way.

REFERENCES

[1] Hartmann, Gerard (2007-08-05). "Les moteurs et aéroplanes Antoinette" [Antoinette engines and aeroplanes] (PDF) (in French). hydroretro.net. Archived from the original (PDF) on 2014-12-14. Retrieved 2015-05-01.
[2] Lindh, Björn-Eric (1992). Scania fordonshistoria 1891-1991 (in Swedish). Streiffert. ISBN 978-91-7886-074-6.
[3] The Direct Injection Engine Will Likely Power Your Next Car". HybridKingdom.com. 2009. Retrieved 2015-05-01.
[4] 1940 6C 2500 Touring "Ala Spessa"" (in Italian). digilander.libero.it. Retrieved 2014-01-20.
[5] Lindh, Björn-Eric (1992). Scania fordonshistoria 1891-1991 (Scania: vehicle history 1891-1991) (in Swedish). Streiffert. ISBN 91-7886-074-1.
[6] Circle Track, 9/84, pp.82-3.
[7] "A short history of Lucas injection". lucasinjection.com. Retrieved 2015-05-01.
[8] "Petrol Injection Mk II". Lucas Service Training Centre. Retrieved 2015-05-01.
[9] Walton, Harry (March 1957). "How Good is Fuel Injection?". Popular Science. 170 (3): 88–93. Retrieved 2015-05-01.
[10] Davis, Marlan (October 2010). "What You Need To Know About Mechanical Fuel Injection". Hot Rod Magazine. Retrieved 2015-05-01.
[11] Faiz, Asif; Weaver, Christopher S.; Walsh, Michael P.; Gautam, Surhid P. (1996). Air pollution from motor vehicles; standards and technologies for controlling emissions. The World Bank. p. 133. ISBN 9780821334447. Retrieved 2017-08-26.
[12] Holder, William; Kunz, Phil (2006). Extreme Muscle Cars: The Factory Lightweight Legacy. Krause Publications. p. 16. ISBN 978-0-89689-278-1. Retrieved 2015-05-01.
[13] An Invitation to Happy Motoring... (Excerpts from the 1957 Rambler Rebel Owner's Manual)". AMX-files.com. Archived from the original on 2009-03-28. Retrieved 2015-05-01.
[14] Auto Editors of Consumer Guide (2007-08-22). "Rambler Measures Up". Retrieved 2015-05-01.
[15] Aird, Forbes (2001). Bosch fuel injection systems. HP Trade. p. 29. ISBN 978-1-55788-365-0.
[16] Kendall, Leslie. "American Musclecars: Power to the People". Petersen Automotive Museum. Archived from the original on 2011-10-27. Retrieved 2015-05-01.
[17] "Celica Parts Catalogue" (in Japanese). Toyota. Retrieved 2014-01-20.

SEEC-2018-160

Optimization of Biocrude Production from Bagasse by Hydrothermal Liquefaction using Factorial Model

A. Yerrayya*, A. Nikunj, S. R. Chakravarthy, R. Vinu

National Centre for Combustion Research and Development, Indian Institute of Technology Madras, Chennai - 600036, India

* Corresponding author: A. Yerrayya, E-mail: yerrayya503.nitw@gmail.com

Abstract

India is the second largest sugar producing country in the world after Brazil. It is producing nearly 15 % of sugar and 25% of the world's sugarcane production. India produces over 341.2 million metric tonnes (MMT) of sugarcane annually and an annual production of roughly 113 MMT of bagasse. Bagasse, the fibrous residue of sugar cane stalk that is obtained after crushing and extraction of juice. The bagasse is burned on site to generate heat and electricity. Till now bagasse is mainly used for generation of heat and electricity, this can also be used for production of valuable fuels and chemicals. Among the different thermochemical conversion techniques, hydrothermal liquefaction (HTL) is a promising one as it can be used to process the wet biomass, and still yield low oxygen containing bio-crude. HTL involves treating the feedstock at mild temperatures (200-350°C) at high pressures (50-200 bar) in sub-critical conditions in presence of water.

In this work HTL of bagasse was investigated for the production of high quality biocrude. The effect of different operating parameters on yield of biocrude and quality of biocrude were investigated to find the optimum operating conditions. The investigated parameters include reaction temperature, reaction time and amount of catalyst. Experiments were performed in a stirred batch reactor of 1.3 L volume by taking 30 g of bagasse. It was found that at the optimal conditions of 320°C, 180 bar, 15 min, and bagasse to water ratio of 1:10, high biocrude yield (8.9 wt.%) and high conversion (83.6 %) were obtained. The 2^3 -factorial design was used for modelling and optimization of the operating parameters. The optimal conditions found to be at the reaction temperature of 320°C, reaction time of 15 min and amount of catalyst of 3g, the yield of biocrude and HHV of biocrude was approximately 36.3 wt.% and 31 MJ/kg respectively. The biocrude composition results showed that the high amount of phenolics (49-52 %) were observed at 300°C, 30 min and amount of catalyst of 2.25 g, and 320°C, 15 min and amount of catalyst of 1.5g. This is mainly due to the decomposition of complex lignin structure. The high amount of esters (27.5-28.6 %) were observed at 280°C, 1.5 g of catalyst and the reaction time of 15 and 45 min. The observed compounds in esters were straight chain fatty esters such as hexadecanoic acid methyl ester, dodecanoic acid methyl ester, and octadecanoic acid methyl ester. These compounds are significant in biodiesel.

SEEC-2018-161

The effect of wind speed on the thermal profile of photovoltaic module under cloudy sky condition

Prakash Pratik
School of Computing & Electrical Eng.
Indian Institute of Technology, Mandi
Email: ppratik.iitmandi@gmail.com

Ankit Agarwal
School of Engineering
Indian Institute of Technology, Mandi
Email: ankit5agrwl@gmail.com

Kunal Ghosh
School of Computing & Electrical Eng.
Indian Institute of Technology, Mandi

Email: kunal@iitmandi.ac.in

Abstract

The operating temperature of the photovoltaic module has the significant effect on the thermal performance of the PV module. In this paper, a three-dimensional thermal model of poly-crystalline silicon PV module is developed to analyze the thermal characteristics of the module using finite element method. Using this model, the effect of wind speed on the thermal profile of PV module under cloudy sky condition is analyzed and simulated. In particular, the speed of the wind is varied from 1 m/s to 5 m/s. Based on the simulation results, we observe that, with an increase in wind speed, the operating temperature of the module decreases non-linearly. For wind speed of 1m/s, the average operating temperature of the module was 331.21 K, whereas, for wind speed of 5 m/s, the value was 314.82 K. From this result, we can also conclude that higher wind speed keeps the operating temperature of the module at a lower level, which can improve the electrical efficiency of the module.

Keywords: *PV module, Thermal model, Wind Speed, FEM Analysis*

NOMENCLATURE
T_a Ambient Temperature

T_{mod} Average Module Temperature

U_{POA} Solar Insolation Level

WS Wind Speed

h_c Heat Transfer Coefficient

Introduction

A solar photovoltaic (PV) module is used to convert solar energy into electrical energy directly. The operating temperature of the module significantly affect the performance of photovoltaic modules, with the power output decreasing by approximately 0.4 % of rated power for every degree increase in module temperature above standard testing condition (STC). The operating temperature of the module depends multiple factors such as solar insolation level, speed of the wind, ambient temperature and sky conditions i.e. cloudy or clear [1].

Previously, many research work has been done to analyse and predict the operating temperature of PV module under different climatic conditions. Mattei et al. 2005 analyzed the thermal as well as electrical performance of the PV module under different climatic conditions using energy balance equations [2]. Lee and Tay, 2012 analyzed the distribution of temperature in relevant layers of the PV module using finite element analysis [3]. Zhou et al., 2013 simulated and analyzed the distribution of temperature in cell layer and along the thickness of module by developing a three-dimensional thermal model under different climatic conditions and by varying the adjacent cell intervals [4].

In this paper, a three dimensional FEM based thermal model is developed. Based on the model, we have analysed the thermal profile of a PV module with varying condition of wind-speed. The

thermal model has developed based on the following assumptions:

- Steady state condition is assumed for thermal simulation.
- PV modules are under open-circuit conditions. This signifies that the total energy flux received due to the incident solar insolation is balanced by the losses due to the thermal processes, without contributing to the generation of electrical power.
- The solar energy flux absorbed by each of the constituent layers of the solar PV module is calculated by using resources available in PVLighthouse.
- The optical properties are assumed to be constant and independent of temperature.
- The thermal properties of the material are assumed to be constant, independent of temperature.
- To calculate the convective heat loss, Notton's equation is considered to determine the convective heat transfer coefficient (hc) [5].
- The variance in heat transfer coefficient for the front and the rear is accounted for by assuming that the rear hc is half of the front hc.
- The ambient temperature is considered to be the same and equal to 298K on all the sides of the module.
- Heat transfer due to radiation is modelled using discrete ordinates (DO) radiation model as supported by the software.
- The glass surface faces the sky while the backsheet is facing the ground. Therefore, the glass and the backsheet will radiate with respect to the sky and the ground respectively [9].
- The sky condition is presumed to be cloudy i.e. sky temperature is equal to ambient 298 K [8].
- The ground temperature is assumed to be equal to 298 K.

Results & Discussion

To analyse the effect of wind speed, we have varied the its speed from 1 m/s to 5 m/s and other climatic conditions solar insolation level and ambient temperature are kept constant at 1000 W/m^2 and 298 K respectively. The sky condition is chosen to be cloudy sky condition. Figure 1 represents the temperature distribution of backsheet layer for a particular climatic condition solar insolation level (U_{POA}) 1000 W/m^2, wind speed (WS) 2 m/s and ambient temperature 298K. We can conclude from the plot that the temperature of the central region is maximum and as we move towards the edge, we will observe a temperature gradient. The region near the aluminium frame is significantly at a lower temperature.
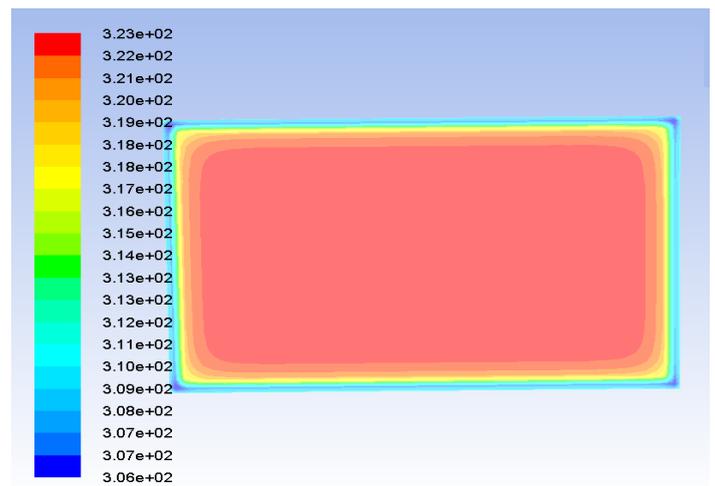

Figure 1: Thermal profile of a PV module at a wind speed of 2 m/s

Figure 2 represents the effect of wind speed on the difference in average module and ambient temperature. In the X-axis, we have varied the wind speed and on the Y-axis we have plotted, the difference in average module and ambient temperature. We can see from the graph that, as the wind speed is increasing from 1 m/s to 5 m/s, the difference in T_{mod} and T_a is decreasing non-linearly. The reason behind this decrement in temperature is, with the increase in wind speed convective heat transfer coefficient increases.
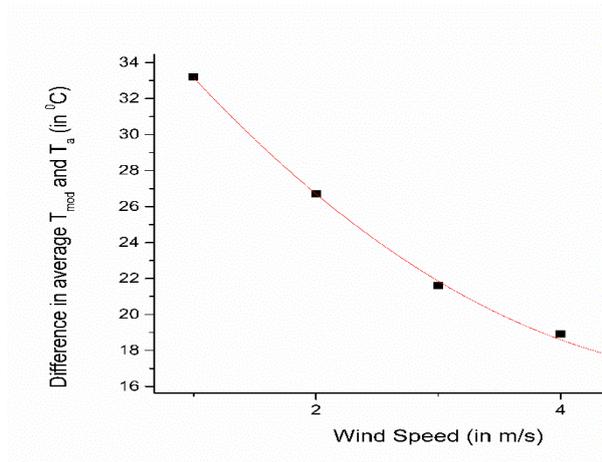
Figure 2: Temperature differential as a function of wind speed

Conclusion

In this paper, we have developed a three-dimensional thermal model of standard polycrystalline Silicon PV module. The analysis of effect of wind speed on the temperature profile shows that, with an increase in wind speed, the operating temperature of the module decreases non-linearly. Also, the central region of the module is at maximum temperature and region near the edge is at a lower temperature.

Reference

1. Skoplaki, E., & Palyvos, J. A. (2009). On the temperature dependence of photovoltaic module electrical performance: A review of efficiency/power correlations. *Solar Energy*, *83*(5), 614–624. https://doi.org/10.1016/j.solener.2008.10.008

2. Mattei, M., G. Notton, C. Cristofari, M. Muselli, and P. Poggi. 2006. "Calculation of the Polycrystalline PV Module Temperature Using a Simple Method of Energy Balance." *Renewable Energy* 31 (4): 553–567. doi:10.1016/j.renene.2005.03.010

3. Lee, Yixian, and Andrew A.O. Tay. 2012. "Finite Element Thermal Analysis of a Solar Photovoltaic Module." *Energy Procedia* 15 (2011): 413–420. doi:10.1016/j.egypro.2012.02.050

4. Zhou, J., Yi, Q., Wang, Y., & Ye, Z. (2015). Temperature distribution of photovoltaic module based on finite element simulation. *Solar Energy*, *111*, 97–103. https://doi.org/10.1016/j.solener.2014.10.040

5. Notton, G., C. Cristofari, M. Mattei, and P. Poggi. 2005. "Modelling of a Double-Glass Photovoltaic Module Using Finite Differences." *Applied Thermal Engineering* 25 (17–18): 2854–2877. doi:10.1016/j.applthermaleng.2005.02.008

6. King, D L, W E Boyson, and J A Kratochvil. 2004. "Photovoltaic Array Performance Model." *Sandia Report No. 2004-3535* 8 (December): 1–19. doi:10.2172/919131.

7. Schott, T., 1985. Operational temperatures of PV modules. In: Proceedings of 6th PV Solar Energy Conference, pp.392–396.

8. Jones, A.D., and C.P. Underwood. 2001. "A Thermal Model for Photovoltaic Systems." *Solar Energy* 70 (4): 349–359. doi:10.1016/S0038-092X(00)00149-3

9. Armstrong, S., and W. G. Hurley. 2010. "A Thermal Model for Photovoltaic Panels under Varying Atmospheric Conditions." *Applied Thermal Engineering* 30 (11–12). Elsevier Ltd: 1488–1495. doi:10.1016/j.applthermaleng.2010.03.012.

SEEC-2018-162

POLYMER BASED NANOCOMPOSITE MATERIALS AND DEVICES FOR PRACTICAL THERMOELECTRIC APPLICATIONS

Biswapriya Deb
CSIR-National Institue for Interdisciplinary Sciences and Technology, Trivandrum, Kerala, India
biswapriya.deb@niist.res.in

Vijayakumar C. Nair
CSIR-National Institue for Interdisciplinary Sciences and Technology, Trivandrum, Kerala, India
cvijayakumar@niist.res.in

T. P. Yuvaraj
GAIL (India) Limited, Noida, Uttar Pradesh, India
tpyuvaraj@gail.co.in

Jaivinder Singh
GAIL (India) Limited, Noida, Uttar Pradesh, India
jaivinderSingh@gail.co.in

I. Vijitha
CSIR-National Institue for Interdisciplinary Sciences and Technology, Trivandrum, Kerala, India
ivijitha@niist.res.in

Arjun P.
CSIR-National Institue for Interdisciplinary Sciences and Technology, Trivandrum, Kerala, India
arjun.nettur@gmail.com

Neethu Mukundan
CSIR-National Institue for Interdisciplinary Sciences and Technology, Trivandrum, Kerala, India
neethusangamithra1@gmail.com

ABSTRACT

Polymer based nanocomposite thermoelectric materials are a new class of functional materials that have an immense potential for commercial usage. Devices based on these materials typically operate <350 °C and could be used for on-the-spot sustainable power generation from thermal sources like hot water released by process plants, automotive exhausts and even human body heat. Despite considerable scientific knowhow generated in the last decade, the practical implementation of these devices needed to address important factors like adopting a materials/device fabrication scheme with better batch reproducibility, innovation in device design to maximize power conversion and finding the right interconnects for low-loss transport. In this work, the strength and limitations of several polymer-inorganic nanocomposite systems for thermoelectric practical operations are explored. The resulting hybrids exhibited a percolation threshold for conductivity for each combination that was obtained by varying polymer-nanocomposite weight ratio. Further device fabrication templates and future modification schemes will be discussed.

NOMENCLATURE

TE	Thermoelectric
ZT	Figure-of-merit
PEDOT	Poly(3,4ethylenedioxythiophene)
CNT	Carbon nanotube
TEM	Transmission Electron Microscopy
FTIR	Fourier Transform Infra Red
TGA	Thermal Gravimetric Analysis
TEG	Thermoelectric Generators

INTRODUCTION

The scavenging of waste heat using TE generators has become a promising method in the present situation of drastic increase in world's energy demand. The TE modules are solid-state devices, therefore have no moving parts and are silent, reliable, lightweight and durable. The efficiency of a TE device depends on their ZT, which is defined as in Eqn. (1), where α, σ, κ, and T are the Seebeck coefficient, electrical conductivity, absolute temperature, and thermal conductivity, respectively [1].

$$ZT = \frac{\alpha^2 \sigma}{\kappa} T \qquad (1)$$

A good TE material should have high electrical conductivity to minimize Joule heating, low thermal conductivity to prevent thermal shorting, and a high Seebeck coefficient for maximum conversion of heat to electrical power or electrical power to cooling.

In 1993, theoretical predictions performed by Hicks and Dresselhaus suggested that the TE efficiency could be significantly enhanced by quantum confinement of the electron charge carriers [2- 3]. That started a string of high quality scientific work based mainly on nanofabrication to reduce lattice thermal conductivity without altering electrical conductivity. Besides being readily processable and scalable compared to their inorganic counterparts, most conducting polymer has intrinsic advantage of having very low thermal conductivity. This is due to their phonon mean free path is comparable to the minimum separation between equivalent structural units [4]. Polymer nanocomposite based TE materials are a new class of functional materials that have immense potential for commercial usage. Devices based on these materials typically operate < 350 °C and could be used for on-the-spot sustainable power generation from thermal sources like hot water released by process plants, automotive exhausts, and even human/mammal body heat. Despite considerable scientific know-how generated in the last decade, the practical implementation of these devices needed to address essential factors like adopting a materials/device fabrication scheme with better batch reproducibility, innovation in device design to maximize power conversion and finding the right interconnects for low-loss transport.

Researchers are now actively pursuing to develop organic and polymer-based TE materials. Wang et al. [5] showed a blend of gold nanoparticle with polyaniline resulted in a three-fold increase in ZT compared to prisitine polyaniline. Kim et al. [6] showed reducing dopant volume is as important as optimizing carrier concentration when maximizing ZT. Implementing this strategy, with the dopant poly(styrenesulphonate) in poly(3,4-ethylenedioxythiophene), they achieved a ZT value of 0.42 at room temperature. In this report, we discussed several polymer-nanocomposite systems and explored their strengths and limitations for practical operations. The polymer components consisted of bithiazole based polymers, fused thiophenes, PEDOT and polyaniline, etc. while single/multi-walled CNTs and several important inorganic nanostructures (metal quantum dots, metal oxides, bismuth telluride, etc.) were used to form the desired composites. The composites were mostly prepared by physically mixing the constituents followed by thermal treatment and subsequent coating formation. The resulting hybrids exhibited a percolation threshold for conductivity for each combination that was obtained by varying polymer/nanocomposite weight ratio. From the output power measured from the fabricated devices, we show that apart from achieving the right balance of electrical/thermal conductivity and thermo e.m.f. the total device resistance played a crucial role.

MATERIALS AND METHODS

Synthesis of Bithiazole Based Polymer Nanocomposite. Bithiazole polymer was prepared by mixing monomer (103.5 mg, 0.125 mmol), 1,4- benzene dithiol (92.66 mg, 0.125 mmol) and Aliquat 336 (11 mg). Dry toluene was added to this reaction mixture followed by 2 M aqueous solution of potassium carbonate. Air was removed from the round bottom flask by freeze-thaw-pump method. Tetrakis(triphenylphosphine)palladium(0) (2.8879 mg, 0.0025 mmol, 0.02 equivalent) was added under nitrogen counterflow, and the reaction was refluxed at 100 °C. After 48 hrs, bromobenzene (1.96 mg, 0.012 mmol, 0.1 equivalent) was added to the reaction mixture, and 1 hr later phenyl boronic acid was added (1.5 mg, 0.012 mmol, 0.1 equivalent) and refluxed overnight to complete the end-capping reaction. To this 3 ml chloroform was added. To this, methanol (150 ml) was then added to precipitate the polymer which was filtered and dried. A 40 ml, 2 mM gold(III) chloride trihydrate solution was stirred rapidly along with refluxing. To this, a 4 ml of 1% sodium citrate dihydrate was quickly added and stirred well. The solution gradually changes to a purple colour as the citrate reduces the gold (III). The nanoparticles formed were centrifuged at 14000 rpm for 30 min. The settled particles were collected and washed with water for several times and dried to obtain gold nanoparticles. To prepare the polymer nanocomposite, the synthesized polymer was dissolved in 1, 2-dichlorobenzene and a suitable amount of the prepared nanoparticles were added, sonicated for 1 hr to obtain the polymer nanocomposite.

Synthesis of Fused Thiophene-Based Polymer Nanocomposite. Polymer/CNT nanocomposites were prepared by adding polymer and CNT in 1, 2-dichlorobenzene by varying the weight percent of CNT. The suspension was then sonicated for 60 min in a low-power sonic bath. An amount of 20 µL of solutions was drop casted on a glass substrate (precleaned with distilled water and isopropanol, followed by preheating for 15 min at 130 °C). A 0.05 M solution of metal salt in nitromethane was used for p-doping the nanocomposite. Samples were doped by soaking in the dopant solution for half an hour followed by annealing at 100 °C for 1 h.

RESULTS AND DISCUSSIONS

The polymer nanocomposite was prepared by the above-mentioned method. The formation of the nanoparticles and their incorporation within the bithiazole based polymer matrix were confirmed by TEM analysis. TEM images showed gold nanoparticles having nearly spherical shape spread within the polymer matrix.
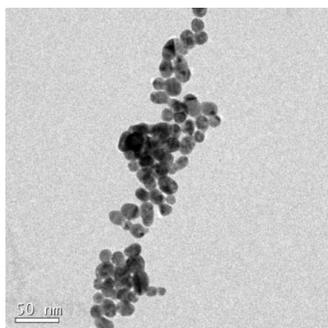
FIGURE 1. TEM image of bithiazole polymer/ gold nanoparticle composite

The FTIR spectra of fused thiophene polymer nanocomposite with CNT shows that the composite was a physical mixture of both since it contains the signature peaks of polymer and CNT. The thermal stability of the polymers was investigated by TGA, which was conducted with a heating rate of 10 °C/min in the presence of nitrogen. The TGA analysis shows that thermal stability of the polymer was enhanced after hybridization [7].

(a)

(b)
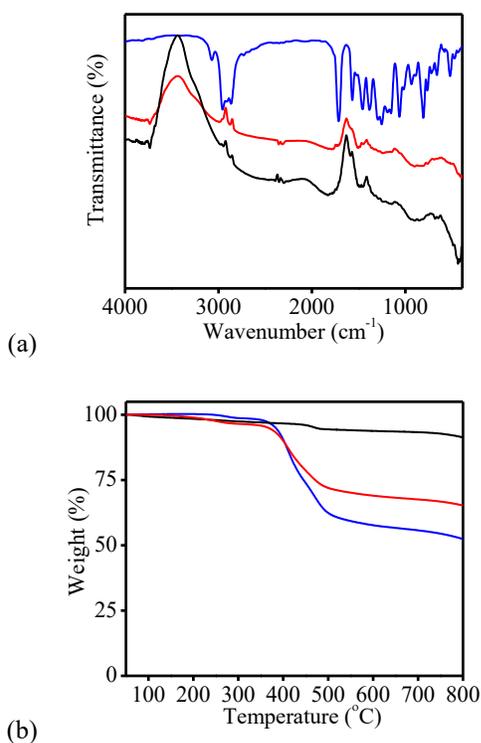
FIGURE 2. (a) FTIR spectra and (b) TGA plot of CNT (black), fused thiophene polymer (blue) and polymer nanocomposite (red).

The TE property studies were done using LSR-3 Seebeck instrument. The thickness of the films was measured using a stylus profilometer (Veeco Dektak 6M). For fused thiophene polymer nanocomposite, the conductivity at 30 °C, enhanced from 31.26 S/cm to 208.9 S/cm after doping. The doping may also increase the power factor of the composite to be greater than the power factor of either the polymer or the CNT separately. The polymer composite shows 38.7 times enhancement in power factor after doping. The doping treatment causes oxidization of polymer, and the polymer was doped with a positive charge (p-type doping). Also, such an enhancement in power factor arises as the doping affects the band structure. The highest efficient TE composite material in the present work includes fused thiophene based polymer nancomposite with CNT structures, which shows 80% ZT compared to the PEDOT based hybrid systems.

There are several reports on the power density obtained for polymer-based TEG. With a stack of 35 thermocouples, TEGs from organometallic polymers have achieved surface power densities of approximately 1 $\mu W/cm^2$ at a temperature difference of 25 K. For a PEDOT:tosylate- based TEG, the surface power density is around 0.27 $\mu W/cm^2$ (ΔT= 30 K). TE device with 4 thermocouples were fabricated with) PEDOT: poly(styrenesulphonate) /dimethyl sulfoxide as p-type and bismuth telluride as n-type. The substrate used is a combination of alumina and glass in which the junctions are placed on top the high thermal conducting alumina, and both the hot junction and cold junction were separated with low thermal conducting glass. The fabricated devices had a strip dimension of 12x4 mm^2. Silver and copper were used as the metal contacts between each monolegs. The device produces a current output of 118.3 μA and voltage output of 16.42 mV which gives a power output of 1.94 μW at 50 K.

REFERENCES
[1] Rowe, D.M., ed. 1, 2005. CRC Thermoelectrics Handbook: Macro to Nano, CRC Press, New York, Chap. 3, pp.1-7.
[2] Hicks, L.D. and Dresselhaus, M.S., 1993. "Thermoelectric Figure of Merit of a One-Dimensional Conductor". Physical Review B, 47(24), pp. 16631-16634.
[3] Hicks, L.D. and Dresselhaus, M.S., 1993. "Effect of Quantum-Well Structures on the Thermoelectric Figure of Merit". Physical Review B, 47(19), pp. 12727-12731.

[4] Bubnova, O., Khan, Z.U., Malti, A., Braun, S., Fahlman, M., Berggren, M., Crispin, X., 2011. "Optimization of the thermoelectric figure of merit in the conducting polymer poly(3,4-ethylenedioxythiophene)". Nature Materials, 10(6), May, pp. 429-433.

[5] Wang, Y., Liu, J., Zhou, J., Yang, R., 2013. "Thermoelectric Transport across Nanoscale Polymer-Semiconductor-Polymer Junctions". Journal of Physical Chemistry C, 117(47), October, pp. 24716-24725.

[6] Kim, G.H., Shao, L., Zhang, K., Pipe, K.P., , 2013. "Engineered Doping Of Organic Semiconductors for Enhanced Thermoelectric Efficiency". Nature Materials, 12(8),May, pp. 719-723.

[7] Vijayakumar, C., Bijitha, B., Kim, M.J., Takeuchi, M., 2011. "Noncovalent Functionalization of SWNTs with Azobenzene Containing Polymers: Solubility, Stability, and Enhancement of Photoresponsive Properties". Journal of Physical Chemistry C, 115(11), February, pp- 4533-4539.

CFD ANALYSIS OF GASIFICATION BASED COOK STOVE TO PREDICT THE TEMPERATURE VARIATION AND LOCAL CONCENTRATION OF VARIOUS EMITTING SPECIES

Ankur Kaundal
School of Engineering
IIT Mandi
ankur_kaundal@students.iitmandi.ac.in

Satvasheel Powar
School of Engineering
IIT Mandi
satvasheel@iitmandi.ac.in

Atul Dhar
School of Engineering
IIT Mandi
add@iitmandi.ac.in

ABSTRACT

Even today biomass holds substantial importance to cater day to day needs of people worldwide. Majority of biomass utilization for domestic applications takes place in the form of combustion, which is either an open fire or using conventional cook stoves. Inefficient and improper combustion leads to the emission of detrimental pollutants which pose serious threats to human lives. Gasification-based natural draft and forced draft cooking stoves are helpful in improving the overall performance and reducing the harmful pollutants. Use of primary as well as secondary air throughout the combustion chamber improves the efficiency of combustion and sidewise lowers the pollutants' emission. Furthermore buoyancy effects due to thermal draft in the chimney facilitate the incoming of air and sidewise keep the smoke and flue gases moving. This extended abstract presents the CFD results of wood combustion inside the cook stove and various contours corresponding to the mole fractions of different species emitting out of combustion.

Keywords

Thermal draft, pyrolysis gases, emitting species
.

INTRODUCTION

According to a recent report on global health observatory data from WHO [1] around three billion people globally rely on biomass namely wood, crop residues, dung cakes etc. to meet their day to day energy demands. Traditional cook stoves emit harmful pollutants like CO, NO, NO_2 and suspended particles containing polynuclear aromatic hydrocarbons. Smoke coming out of wood combustion consists of many harmful compounds viz. NO_x, SO_x, CO, Volatile Organic Compounds (VOC), Particulate Matter (PM), furans and dioxins [2]. Inhaling these compounds can put anyone on cardiovascular risks like cardiac arrhythmias, heart attacks and other respiratory diseases [3, 4, 5]. Fine PM which gets inhaled quite easily may lead to the destruction of alveolar wall and disturb the lung functioning. All these parameters affect the health of household members slowly and gradually. Hence it becomes quite important to design and fabricate cook stove so efficiently to improve the combustion characteristics and have control over emissions as well.

Presented work here shows the cook stove well equipped with primary and secondary air so that sufficient amount of oxygen is present throughout the combustion chamber. Chimney placed at the back generates pressure difference due to density variation and hence keeps smoke and flue gases moving and sidewise facilitates the incoming of primary and secondary air.

DESIGN AND SIMULATION MODEL

Figure 1a shows the external view of cook stove with front extension for wood inlet. Primary air is fed from the front whereas secondary air is fed from the sides. Chimney is located at the back. Figure 1b shows the combustion chamber which is the internal view of cook stove.
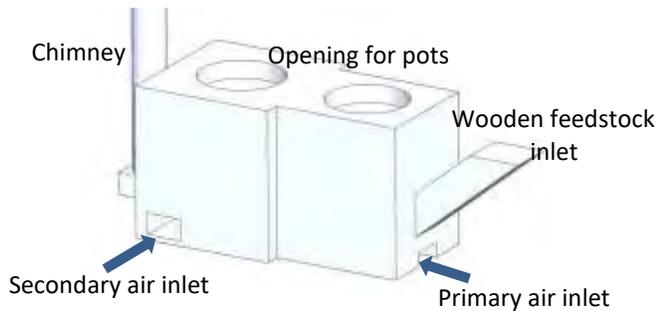
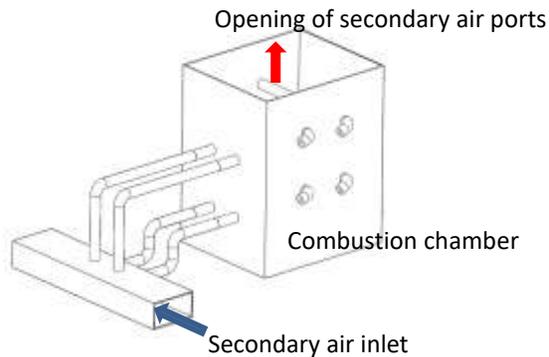Figure 1a: External view of cook stove

Figure 1b: Internal view of cook stove

 While starting the cook stove, first of all air in the chimney is heated up using some combustible substance like paper, through an opening left at the back to serve this purpose. Thermal draft established in the chimney sucks the air through primary and secondary air inlets. Furthermore when combustion starts, smoke and hot gases move out through this chimney and hence make the suction of air a continuous one. Primary air along with the application of heat is responsible for the release of pyrolysis gases from wood and is provided from the front. Secondary air reacts with these pyrolysis gases and results in flaming combustion. Hence the proper mechanism for intake of primary and secondary air is remarkably important for efficient working of cook stove. Secondary air once entered through respective inlet vent out in combustion chamber through multiple ports at various elevations to make uniform availability of oxygen for combustion.

Figure 2 shows the computational domain for CFD simulations of combustion chamber. Ansys Fluent 18.1 was used to simulate wood volatile combustion.
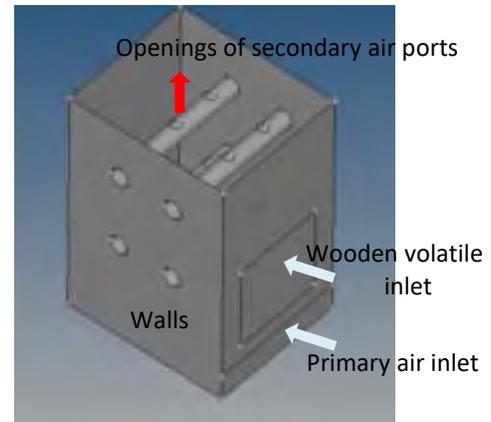
Figure 2: Computational domain for simulations

Validation

Geometry presented by Klason et al. [6] was used to validate the results. Figure 3 shows the same geometry which was replicated and simulated in Ansys Fluent 18.1. During simulations in Fluent, it was found that actual combustion starts at certain height above the wood volatile inlet. So to make the conditions realistic as used by Klason et al. [6], wood volatile inlet in our geometry was little beneath of the grate. Table 1 shows the values used for various mass flow inlets.
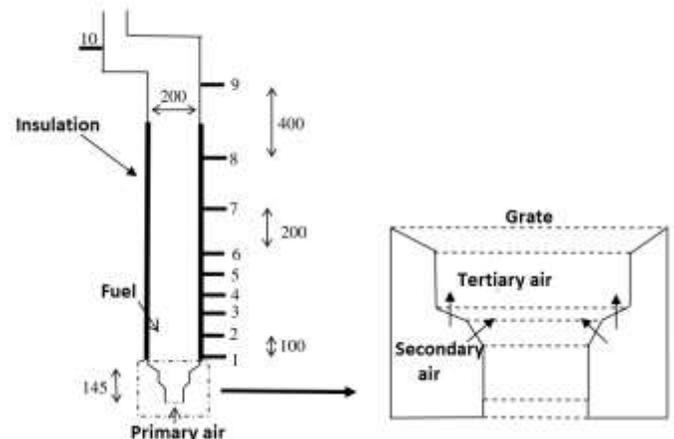
Figure 3: Geometry for validation of results [6]

Table 1: Mass flow rates of air and feedstock

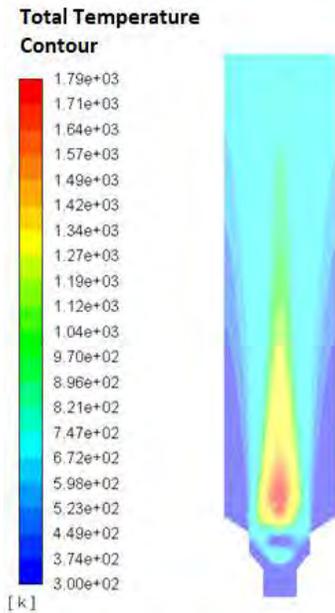| Mass flow rate of wood volatile	4.61×10^{-4} kg/s
Mass flow rate of primary air	5.81×10^{-4} kg/s
Mass flow rate of secondary air	1.18×10^{-4} kg/s
Mass flow rate of tertiary air	1.89×10^{-4} kg/s

Figure 4: Temperature contour in geometry used for validation

Figure 4 shows the temperature contours in simulated geometry. Figure 5 shows the temperature variation along the height of furnace in our case and also the results shown by Klason et al. It can be concluded that results are in close agreement with each other and hence same physics can be used to solve the problem shown in figure 2.
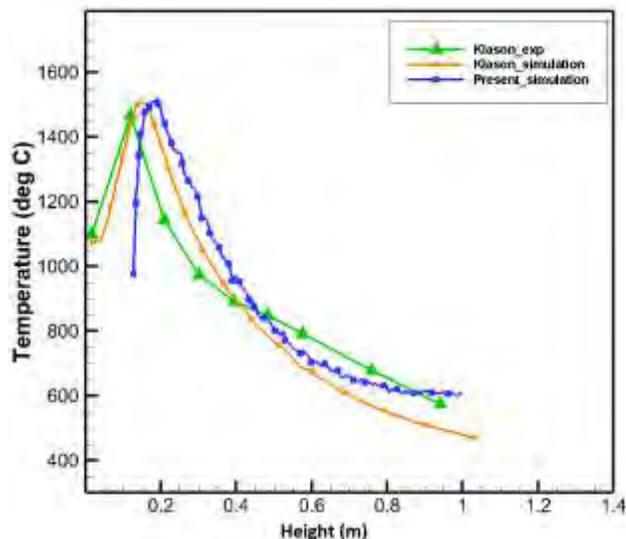

Figure 5: Validation of results

Simulation approach and boundary conditions to simulate the combustion in cook stove

Species transport model in Ansys Fluent 18.1 was used to simulate the wood volatile combustion. General conservation equation for species transport takes the form [7]

$$\frac{\partial}{\partial t}\left(\rho Y_i\right) + \nabla.(\rho \vec{v} Y_i) = -\nabla.\vec{J_i} + R_i + S_i$$

Where Y_i denotes the local mass fraction of ith species, R_i is the rate of production of species i by chemical reaction, S_i is rate of creation from dispersed phase or any other user defined media and J_i is the diffusion flux of ith species due to concentration and temperature gradient.

Eddy-dissipation model was used in which reaction rate is assumed to be controlled by turbulence.

Determination of wood burning rate

Wood burning rate was determined experimentally using the protocol mention in BIS norms [8] for testing of wood cook stoves. Accordingly, difference between the mass of packed cook stove before combustion and the mass of cook stove after combustion when normalized for one hour gives the wood burning rate.

Mass of packed cook stove, M_1= 24.945 kg
Mass of cook stove after combustion, M_2 = 24.275 kg
Time taken by complete combustion = 15 mins
Therefore, wood burning rate= $(M_1$- $M_2)$ x 60/15
$= 2.68$ kg/hr
$= 7.444$x 10^{-4} kg/s

Taking composition of wood as 50% carbon, 6% hydrogen and 44% oxygen, stoichiometric amount of air required to burn wood with mass flow rate of 7.444x 10^{-4} kg/s comes out to be 4.4068x 10^{-3} kg/s.

This amount of air has been divided into primary and secondary inlet in different ratios and hence used in simulations. Secondary air vents out through twelve holes and hence divided into twelve parts. Following table depicts the same.

Table 2: Mass flow rates of primary and secondary air

Primary to secondary air ratio	Primary air (kg/s)	Secondary air (kg/s)
50:50	0.002203	0.000184
20:80	0.00088	0.000294
10:90	0.0004407	0.00033

With reference to figure 2, various boundary conditions and respective values are shown in following table

Table 3: Boundary conditions

Description	Boundary Condition	Numerical Value
Wood volatile inlet	mass flow inlet	7.444×10^{-4} kg/s
Primary air inlet	mass flow inlet	As in table 2
Secondary air ports	mass flow inlet	As in table 2
Top surface	pressure outlet	Atm.
Walls	wall	Zero diffusive flux

RESULTS AND DISCUSSION

Problem was simulated in Ansys Fluent 18.1 for multiple cases with varying primary to secondary air ratio. Figure 6 shows the temperature contour for primary to secondary air ratio of 20:80.
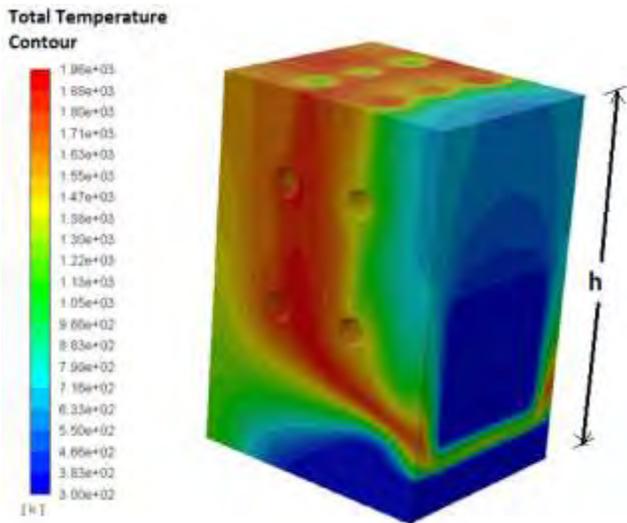
Figure 6: Temperature contours in combustion chamber

Following plots depicts the variation of temperature and different species along the height (h) of cook stove for varying primary to secondary air ratio.
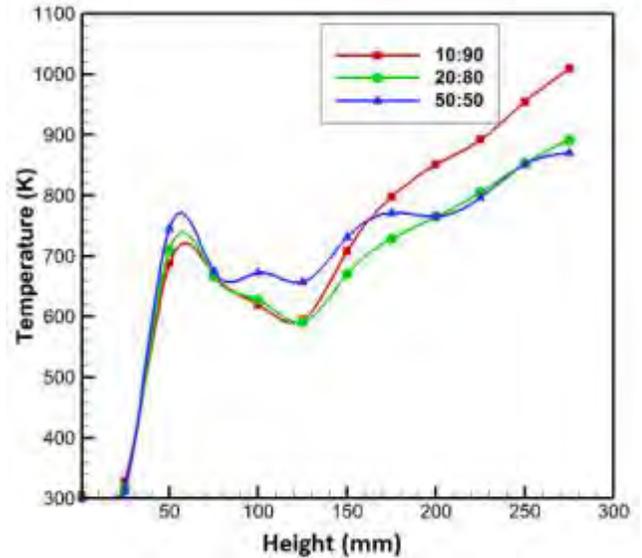
Figure 7a: Temperature variation along the height of cook stove
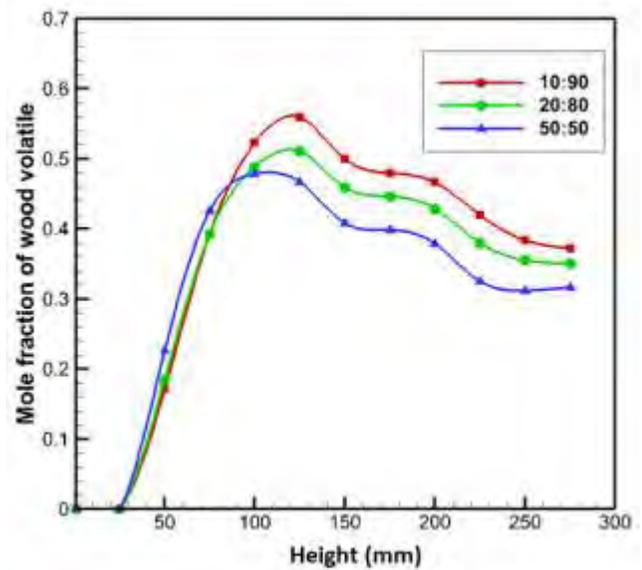
Figure 7b: Variation in mole fraction of wood volatile along the height of cook stove
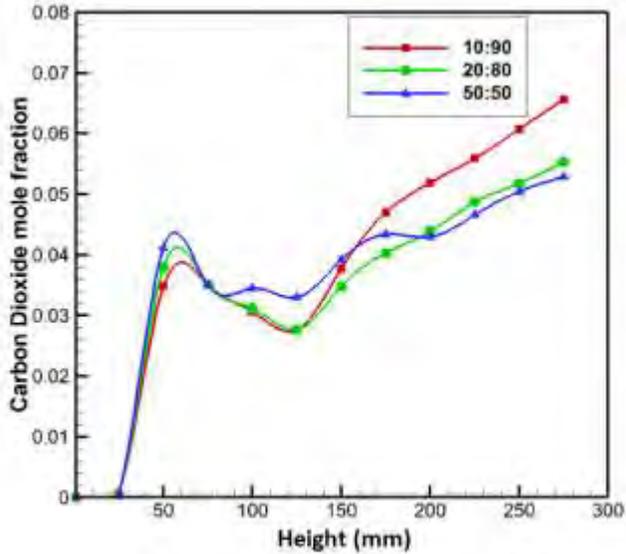
Figure 7c: Variation in mole fraction of carbon dioxide along the height of cook stove
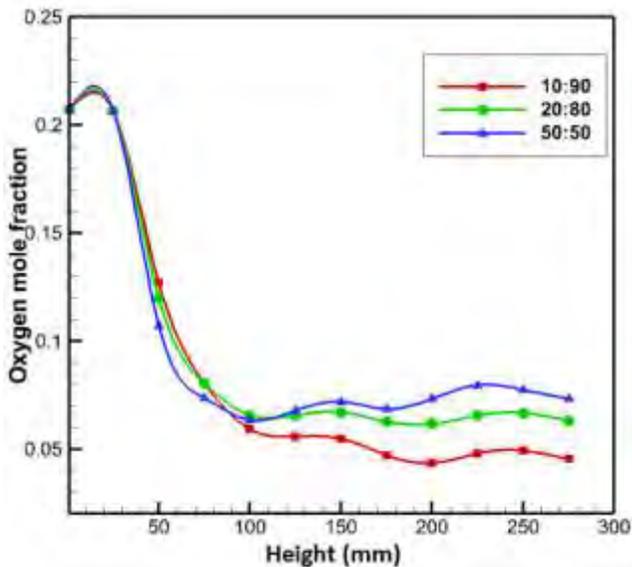

Figure 7d: Variation in mole fraction of oxygen along the height of cook stove

Temperature and mole fraction of species shown above are surface averaged values. Figure 7a shows the variation of temperature along the height of cook stove and it can be depicted that maximum temperature near the top surface is obtained for primary to secondary air ratio of 10:90. Similar trend has been obtained for carbon dioxide mole fraction as shown in figure 7c. Mole fraction of oxygen is decreasing along the height of cook stove for all cases. However 10:90 case shows the maximum utilization of supplied air with minimum excess air near the top surface as depicted in figure 7d. Figure 7b shows the variation of

mole fraction of wood volatile along the height of cook stove. Plot however shows little decrease towards the top surface, but there is underutilization of feedstock as mole fraction of wood volatile is 0.38 for 10:90 case and 0.32 for 50:50 case. Ideally it should approach zero for maximum utilization of feedstock. Hence 10:90 case shows best values of all parameters except wood volatile mole fraction. Simulation model needs to be modified so as to have better mixing of wood volatile and air and hence maximum utilization of feedstock.

CONCLUSION

Ansys Fluent provides a good platform to use species transport model to simulate the production of species through chemical reaction and hence their transport. Temperature profile and mole fraction of various species emitting out as a result of combustion of wood volatile can be used to design an efficient cook stove. In presented problem primary to secondary air ratio of 10:90 shows the best parameters among all except for feedstock utilization. Simulation geometry needs to be modified to have proper reaction between wood volatile and air so that the utilization of feedstock can be made to the fullest.

REFERENCES

1. Global Health Observatory (GHO) data, World Health Or-ganization, Indoor Air Pollution , See Also:
   http://www.who.int/gho/phe/indoor_air_pollution/en/
2. B Christoffer Boman, A Bertil Forsberg, Bengt G Jarvholm, Adverse health effects of ambient air pollution in relation to residential wood combustion in modern society" Scandinavian Journal of Work, Environment & Health, Vol. 29, No. 4 (August 2003), pp. 251-260
3. A. Kocbach Bølling, Joakim Pagels, Karl Espen Yttri, Lars Barregard, Gerd Sallsten, Per E Schwarze, Christoffer Boman, A. et al. Health effects of residential wood smoke particles: the importance of combustion conditions and physicochemical particle properties. Particle and. Fibre Toxicollogy. 6, 29 (2009).
4. Ostro , Bart et al, Rachel Broadwin, Shelley Green, Wen-Ying Feng, Michael Lipsett. "Fine Particulate Air Pollution and Mortality in Nine California Counties: Results from CALFINE." Environmental Health Perspectives 114.1 (2006): 29–33. Web.
5. Brook, R. D., e Barry Franklint al, Wayne Cascio, Yuling Hong, George Howard, Michael Lipsett, Russell Luepker, Murray Mittleman, Jonathan Samet, Sidney C, Ira T. . Air pollution, and cardiovascular disease: A statement for healthcare professionals from the expert panel on population

and prevention science of the American Heart Association. Circulation 109, 2655–2671 (2004).

6. Klason T, Bai X S, "Computational study of the combustion process and NO formation in a small-scale wood pellet furnace" vol 86, 1465-1474 (2007).

7. Species transport equations, Ansys Manual, See Also:
http://www.afs.enea.it/project/neptunius/docs/fluent/html/th/node128.htm

8. Portable Solid Bio-Mass Cookstove (Chulha), "Bureau of Indian Standards", Doc:MED 04(1157)C, ICS 97.040.20, February 2013

"Biodiesel production and utilization from Guizotia abyssinica (niger) seed oil using bio-alcohol produced from Eichhornia Crassipes as reactant"

[1]Bijit Sarma,[2]Dilip Kumar Bora, [3]Bichitra Bikash

[1,2]Dept of Mechanical Engineering, Assam Engineering College, Assam

[3]Dept of Mechanical Engineering ,Assam Down Town University

Abstract

In this study water hyacinth (Eichhornia crassipes) is used to produce bio-alcohol which is used as reactant for producing biodiesel from Guizotia abyssinica (niger) seed oil. In this study, water hyacinth (Eichhornia crassipes) was used as the source material for production of ethanol. The celluloses and hemicelluloses contained in water hyacinth plant were broken down by treatment with sulphuric acid and exposed to the effect of cellulase enzyme. These celluloses and hemicelluloses were converted by saccharification to fermentable sugars which were further fermented with the help of yeast in anaerobic conditions leading to the production of Ethanol. Further biodiesel was produced from niger (*Guizotia* abyssinica) seed oil using bio-ethanol produced from water hyacinth as reactant in presence of KOH as catalyst by the transesterification reaction. The physic-chemical properties of the biodiesel produced from niger seed oil was assessed and found comparable to the conventional diesel conforming to ASTM standard. Engine performance was carried out using biodiesel and its blends and it showed encouraging results for B_{20} (20% biodiesel) in terms of brake thermal efficiency, lower brake specific fuel consumption, lower emission of CO and lower emission of NO_x at higher load.

Keywords: Biodiesel, water hyacinth, niger

COMBUSTION DYNAMICS OF NANOPARTICLE LADEN JET FUEL

Khushboo Pandey
Interdisciplinary Centre for Energy Research
(ICER),Indian Institute of Science,
PhD
Email: 009khushboo@gmail.com

Saptarshi Basu
Department of Mechanical Engineering,
Indian Institute of Science,
Associate Professor
Email: saptarshibasukol@gmail.com

ABSTRACT

Multiscale combustion dynamics, shape oscillations, secondary atomization, and precipitate formation have been elucidated for low vapour pressure nanofuel [n-dodecane seeded with alumina nanoparticles (NPs)] droplets. Dilute nanoparticle loading rates (0.1%–1%) have been considered. Simultaneous high speed droplet shape and flame imaging is done. For nanofuels, intense heat release from the enveloping flame leads to the formation of micron-size aggregates (of alumina NPS) which serve as nucleation sites promoting heterogeneous boiling. In the present work, variation of flame dynamics and spatio-temporal heat release (HR) have been analysed using high speed OH* chemiluminescence imaging. Addition of alumina NPs enhances the heat absorption rate and ensures the rapid transfer of fuel parcels (detached daughter droplets) from droplet surface to flame front through secondary ejections. Therefore, average HR shows an increasing trend with particle loading rate (PLR). We have established the coupling mechanisms among heat release, shape oscillations, and secondary atomizations that underline the combustion behaviour of such low vapour pressure nanofuels.

*Keywords:*Combustion, low vapour pressure nanofuel, nanoparticles, secondary atomisation,

NOMENCLATURE

τ Thermal diffusive timescale,

INTRODUCTION

The American Society for Testing and Materials define nanomaterials as particles of length ranging from 1 to 100 nm in two or three dimensions [1]. NPs manifest different optical, chemical, and magnetic properties as compared to their respective bulk mediums resulting in custom engineered dispersions. Nanofuels are novel, and are stable suspensions of nanoparticles (NPs) in base fuels. Due to their higher energy density and combustion enthalpy, energetic metal particles are added to liquid fuels as "liquid fuel extender". Metals with high energy density like Aluminium, Iron, and Boron, can increase the combustion energy output of conventional fuels. NPs of metallic oxides, like cerium oxide, help in the reduction of soot emissions and pollutants like carbon monoxide and NOx because of their oxygen carrying ability and their capability to oxidize soot particles in their precursor stage. Nanofuels have also been shown to reduce ignition delay and increase ignition probability. Tyagi et al.[2] reported higher ignition probability of diesel blended with aluminium and aluminium oxide as compared to pure diesel. In a shock tube experiment employed for the study of n-dodecane blended with aluminium NPs, Jackson et al.[3] reported the reduced ignition delay for temperature above 1157 K. Reduction in ignition delays of ethanol and JP-8 with addition of aluminium NPs by 32% and 50%, respectively, was reported by Allen et al.[4] Rotavera et al.[5] found reduced soot formation in toluene combustion in the presence of nano-ceria (CeO_2).

For the present work, we have focussed on n-dodecane, a long chain hydrocarbon fuel of practical applicability with typically low vapour pressure (~17.65 Pa at room

temperature). For jet fuels, n-dodecane is one of the widely accepted surrogates of jet fuels and is shown to be useful for shock-tube experiments and ignition delay analysis. Alumina is a passive component which does not participate in reactions.Therefore, to understand atomization and heat release changes due to NP addition without affecting chemical kinetics, alumina NPs are utilised. Alumina NPs are added to the base fuel at dilute PLRs (0.1%−1%). For this experimental study, simultaneous high speed imaging of droplet shape and flame heat release (HR) has been conducted for the better understanding of the interlinked processes. Here we specifically elucidate the (i) global oscillatory behaviour of droplet shape, (ii) internal ebullition mechanism which induces secondary droplet atomization through two ejection modes and Rayleigh-Plateau ligament break-up, (iii) spatial HR fluctuations, and (iv) combustion residue analysis (for nanofuels).
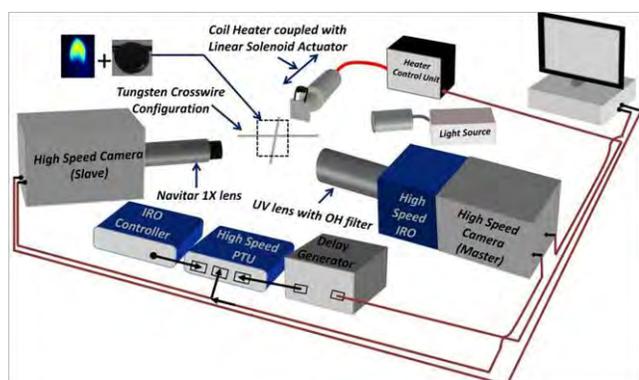
FIGURE 1 Schematic of the experimental setup comprising of high speed camera and chemiluminescence imaging systems for simultaneous capture of droplet shape and flame. Both imaging systems are synced with a droplet ignition apparatus. [6].

I. EXPERIMENTAL METHODOLOGY

A. NANOFUEL PREPARATION

The nanofuels are prepared with n-dodecane as the base fluid and aluminium oxide (alumina, Al_2O_3 ,spherical shape with an average size of 40 nm procured from Reinste Nano Ventures NPs)as the additive for the present experimental study. The stability of the nanofuel is ensured by adding a non-ionic surfactant (Tween 85; Polyoxyethylene sorbitan trioleate) with HLB value of 11. Five different functional droplet cases are considered: (i) Pure dodecane, (ii) dodecane with 0.1 wt. % (0.019 vol. %) alumina, (iii) dodecane with 0.25 wt. % (0.045 vol. %) alumina, (iv) dodecane with 0.5 wt. % (0.096 vol. %) alumina, and (v) dodecane with 1 wt. % (0.191 vol. %) alumina. These suspensions (base fluid and nanoparticles) were sonicated for nearly 30 min using an ultrasonic disruptor (Trans o sonic D120/P model) with 15 s alternate ON/OFF cycles (inherent settings of the sonicator).

B. EXPERIMENTAL SET-UP

FIGURE 1 shows the schematics of the experimental setup. Droplets (∼750−850 μm) are suspended at the junction of a 100 μm diameter tungsten crosswire arrangement in a pendant configuration. Heat loss effects are usually neglected for wires of diameter less than 100 μm[]. It is to be noted that the suspender's conductivity effect (if any) is present across all the experimental cases (pure and NP laden droplets).Therefore, on a relative basis, the physical arguments, combustion behaviour, nucleation, and bubble mechanisms along with key conclusions should remain largely unaltered. A coil heater coupled with a linear solenoid actuator (synced with imaging system through a delay generator) is incorporated to achieve fuel ignition under atmospheric pressure. The coil heater is triggered using an electronic TTL signal (of 200 ms period). The heater heats up the droplet during this period thus igniting it. Subsequent to ignition, the heater is retracted away from the initial position.

II. RESULTS AND DISCUSSIONS
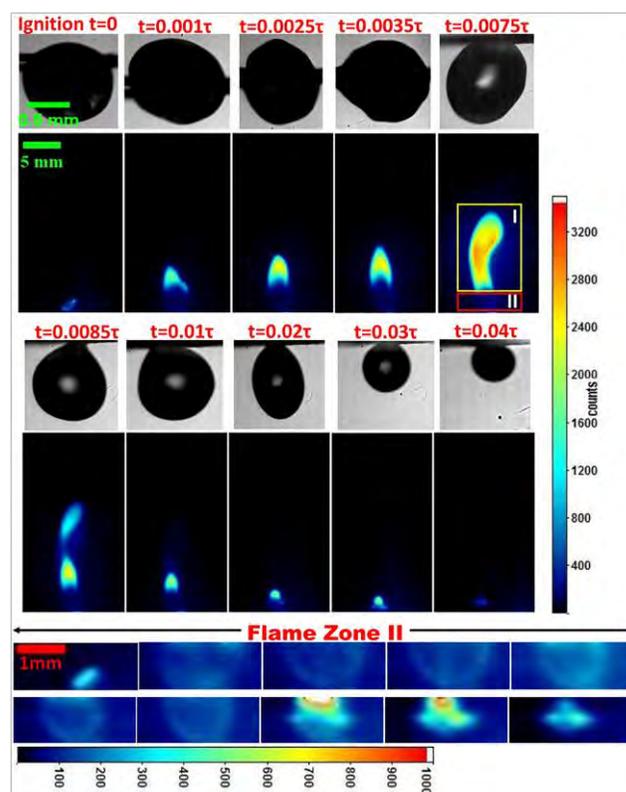
FIGURE 2 Simultaneous high speed imaging of surface oscillations and flame heat release for pure dodecane droplets at various time instants [6].

A. Combustion characteristics of pure fuel droplets

Pure dodecane droplet burns at a very slow rate exhibiting minimal shape oscillations and a long plume shaped diffusion flame (**FIGURE 2**). Pure dodecane droplets exhibit surface undulations for ignition for a period $\sim 0.1 t_{total}$ (t_{total} is the total droplet lifetime). This stage can be designated as the droplet heat-up period; the time span (around 5% to 10% of droplet lifetime) required for increasing the droplet temperature to the final wet bulb limit. Presence of surface undulations [**FIGURE 4**]. is attributed to the gradual change ($\sim 34\%$) in surface tension of dodecane from 0.025 N/m (at room temperature, 298 K) to 0.017 N/m (at wet bulb temperature of dodecane, 393 K). This period is followed by stage II of the quiescent droplet combustion process [**FIGURE 4**]. Interestingly, the bubble count due to boiling in pure dodecane is found to be minimal throughout the droplet lifetime.

B. Combustion characteristics of nanofuel droplets
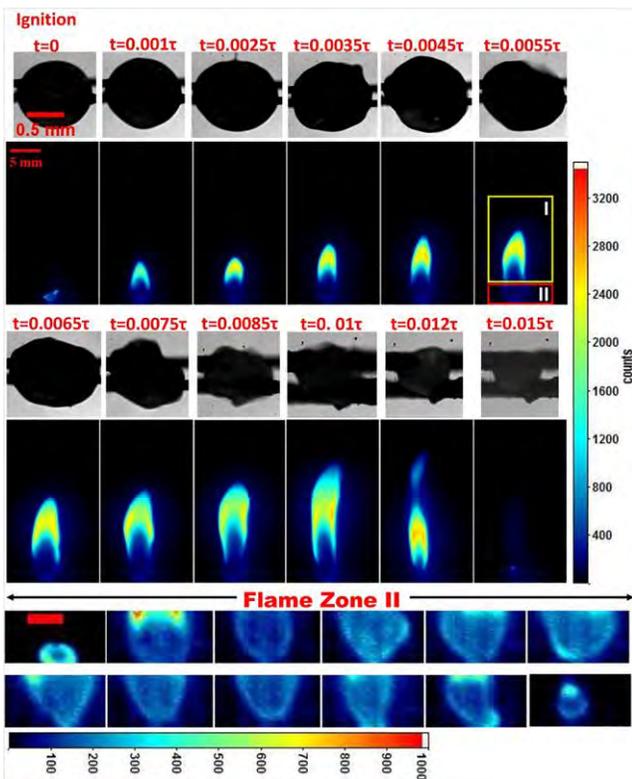
FIGURE 3 Simultaneous high speed imaging of shape oscillations and flame HR for PLR 1%. Flame zone II shows intense and localised fluctuations of the flame envelope due to ejection events. At the end stages, gelatinous mass is evidently present. The scale bar represents 2 mm [6].

Combustion of nanofuel droplets is accompanied with increase in bubble density (number of bubbles per unit droplet volume), bubble coalescence, and bubble expansion and expulsion resulting in droplet swelling and severe volumetric oscillations [**FIGURE 3** and **FIGURE 4**]. NP

agglomerates act as nucleation sites at multiple length scales which opens up heterogeneous boiling mode for nanofuels. Bubbles of various sizes are further ejected from the droplet surface as continuous localised and major ejections. These ejections (Mode1 and Mode 2, **FIGURE 5**) cause spatio-temporal fluctuations of droplet shapes. Disintegration of parent droplets into daughter droplets is a secondary pathway of fuel transfer from the droplet surface to flame front.
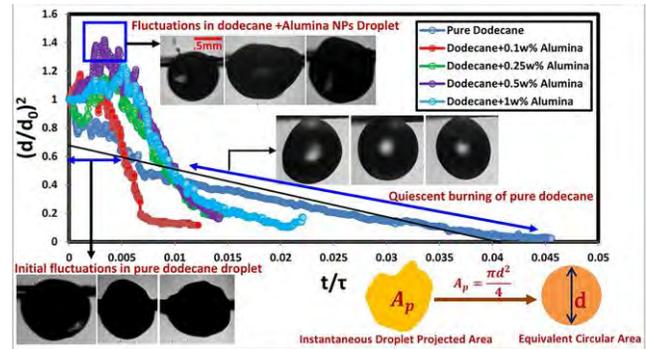
FIGURE 4 Temporal variation of the normalised droplet diameter showing linear regression for pure dodecane and heightened fluctuations for nanofuel droplets. Droplet lifetime is normalised by the thermal diffusive time scale τ.
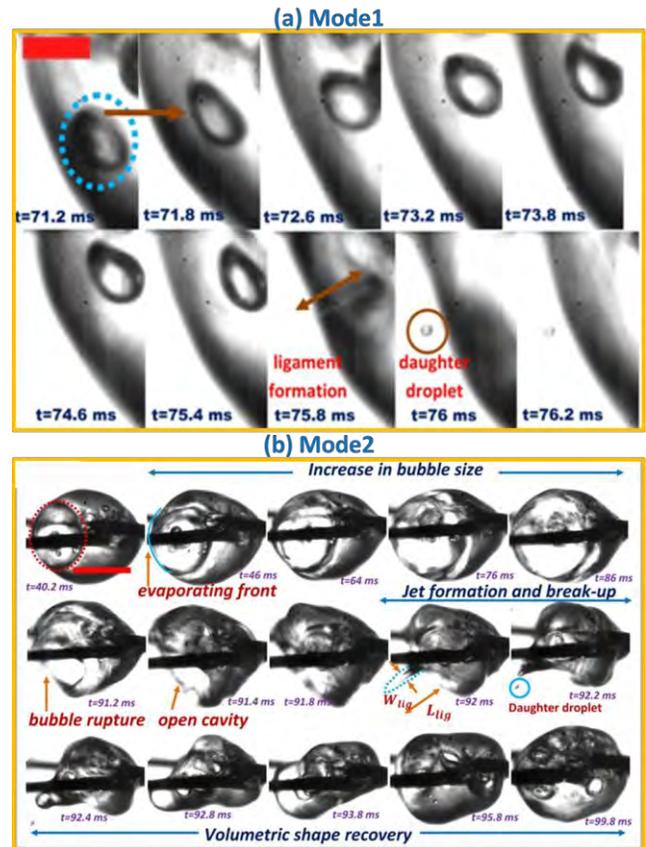

FIGURE 5 (a) High speed images of localised single bubble expulsion from the droplet surface with $\alpha_{local} \sim O(10^{-3})$

resulting in needle-shaped ligaments (L_{lig}) **(b)** Mode 2 ejection event, which exists mostly for PLRs > 0.1% . High speed images depicting bubble growth, bubble rupture, formation of an open cavity followed by jet formation and Rayleigh-Plateau ligament tip break-up (L_{lig}/W_{lig}) > π forming daughter droplets (d_d) and final volumetric recovery. The scale bar represents 0.5 mm **[6]**.

C. Flame dynamics of nanofuel droplets

To understand the influence of alumina NPs addition on flame dynamics and average heat release, the OH* emission signature is captured through high speed chemiluminescence imaging. Instantaneous fluctuation in local HR [**FIGURE 6**(a)] is the result of local flame perturbations arising from vigorous droplet shape deformation due to ejections. Whereas variation in average HR indicates global variation in the burning rate due to NP induced droplet heat absorption rate enhancement. Furthermore secondary atomization leads to an enhanced transfer of fuel daughter droplets to the flame front. Therefore, it increases the global fuel burning rate. In short, the enhancement of burning rate, reduced burning time and increased heat absorption (**FIGURE 6** (b)), culminates into an increase in average HR with PLRs.
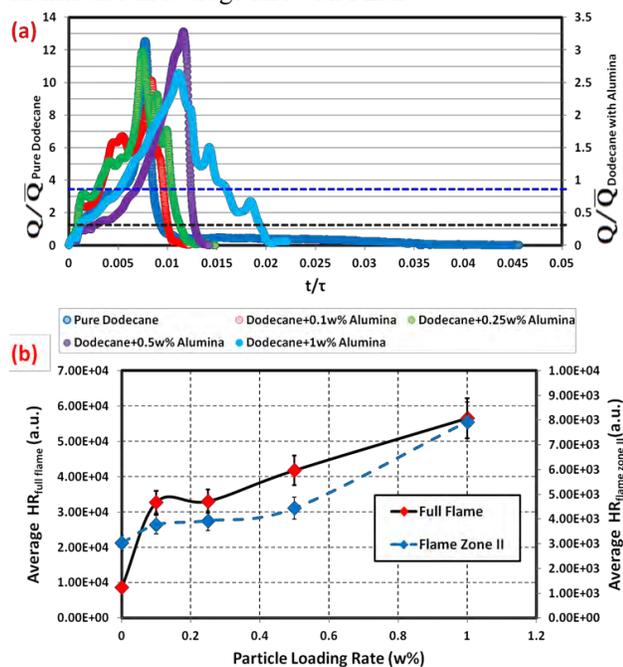
FIGURE 6 (a) Temporal history of normalised instantaneous heat release for all cases. **(b)** Average heat release (considering full and flame zone II) variation with PLR **[6]**.

CONCLUSION

The addition of alumina NPs induces the heterogeneous mode of boiling in the droplets. The formation of vapour bubbles followed by their growth, coalescence, and expulsion opens a pathway of secondary atomization in NP laden droplets. Flames corresponding to nanofuel droplets show ~2 times enhancement in heat release with respect to pure dodecane. Flames of NP laden fuel droplets exhibit a dominant frequency band ~(8 – 20 Hz) corresponding to buoyant flickering. In addition to the flame flicker, auxiliary oscillation modes are present. These modes correlate well with the droplet shape oscillations. These auxiliary oscillations arise due to interactions of the daughter droplets (via secondary ejections) with the flame envelope. The burning time of NP laden droplets is found to be nearly half of pure fuel droplets. We have reported the possible reasons for this reduction: (i) heat absorption rate enhancement, (ii) absorption of radiative energy by NPs from flame, and (iii) rapid transfer of fuel from the droplet surface to flame front through secondary ejections. These aforementioned enhancements increase the average HR of nanofuel droplets.
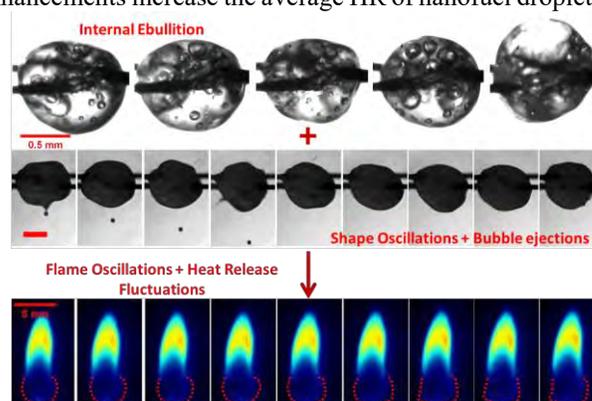
Figure 7 Pictorial representation of correlation of internal ebullition to shape oscillations and finally, to flame fluctuations.

REFERENCES

[1] E. ASTM, 2456-06 "Terminology for Nanotechnology.," ASTM Int. 2 (2006).

[2] H. Tyagi, P.E. Phelan, R. Prasher, R. Peck, T. Lee, J.R. Pacheco, P. Arentzen, Increased hot-plate ignition probability for nanoparticle-laden diesel fuel, Nano Lett. 8 (2008) 1410–1416.

[3] D. Jackson, D. Davidson, R. Hanson, Application of an aerosol shock tube for the kinetic studies of n-dodecane/nano-aluminum slurries, in: 44 Th AIAAASMESAEASEE Jt. Prop Conf Exhib., 2008.

[4] C. Allen, G. Mittal, C.-J. Sung, E. Toulson, T. Lee, An aerosol rapid compression machine for studying energetic-nanoparticle-enhanced combustion of liquid fuels, Proc. Combust. Inst. 33 (2011) 3367–3374.

[5] B. Rotavera, A. Kumar, S. Seal, E.L. Petersen, Effect of ceria nanoparticles on soot inception and growth in toluene–oxygen–argon mixtures, Proc. Combust. Inst. 32 (2009) 811–819.

[6] K. Pandey, K. Chattopadhyay, S. Basu, Combustion dynamics of low vapour pressure nanofuel droplets, Phys. Fluids. 29 (2017) 074102. doi:10.1063/1.4991752.

SEEC-2018-166

INFLUENCE OF EXIT-EXPANSION ANGLE ON GLOBAL FLOW-FIELD OF A DUAL- SWIRL INJECTOR

Aditya Potnis
Department of Mechanical Engineering,
IISc, Bangalore

Kuppuraj Rajamanickam
Department of Mechanical Engineering,
IISc, Bangalore

Saptarshi Basu
Department of Mechanical Engineering,
IISc, Bangalore
Email: sbasu@iisc.ac.in

ABSTRACT

In this study the influence of exit-expansion angle on the global flow field of a dual-swirl injector is investigated. Interchangeable flares with constant exit diameter and different diverging angles are used. High speed PIV with liquid spray is used to visualise the flow and velocity profiles. Characteristics of the recirculation zone (CTRZ) along with turbulent kinetic energy distribution are studied. Results show that the flare angle has a considerable effect on the flow downstream of the injector. The size and strength of CTRZ, and location of turbulent mixing zones changes drastically with small changes in the flare angle and above a critical value result in conical breakdown.

Keywords: Dual-swirl injector, Flare angle, CTRZ, High speed PIV, Conical breakdown

NOMENCLATURE

Ψ	Blockage ratio
Φ	Vane angle
Z	Number of vanes
S	Swirl number
lpm	Litres per minute
g/s	Grams per second
gph	Gallons per hour
PIV	Particle imaging velocimetry
TKE	Turbulent kinetic energy
CTRZ	Central toroidal recirculation zone
V_{axial}	Normalized Axial velocity
RMS	Root mean squared

INTRODUCTION

A swirl injector is integral to gas turbine combustor. Its function is to deliver atomized, well-distributed fuel to the combustor and to generate a recirculation zone for flame stabilization [1]. Swirl injector greatly influences emission characteristics of a combustor by controlling fuel spray distribution and its mixing. Emissions such as NOx and CO are a result of high temperatures caused by improper distribution of fuel, insufficient mixing, and incomplete combustion. A well-designed swirl injector should ensure clean and stable combustion as well as minimize emissions.

Spray produced by a dual swirl injector is influenced by a number of parameters; swirl sense (counter or co-rotating), swirl number, airflow distribution among swirlers, venturi or pre-filmer geometry, internal mixing length, exit expansion angle. Prior studies [2-6] done suggest that some geometric parameters have a more pronounced effect on the flow-field. Presence of venturi, vane angle, swirl sense and exit expansion angle are suggested to be major influencing parameters.
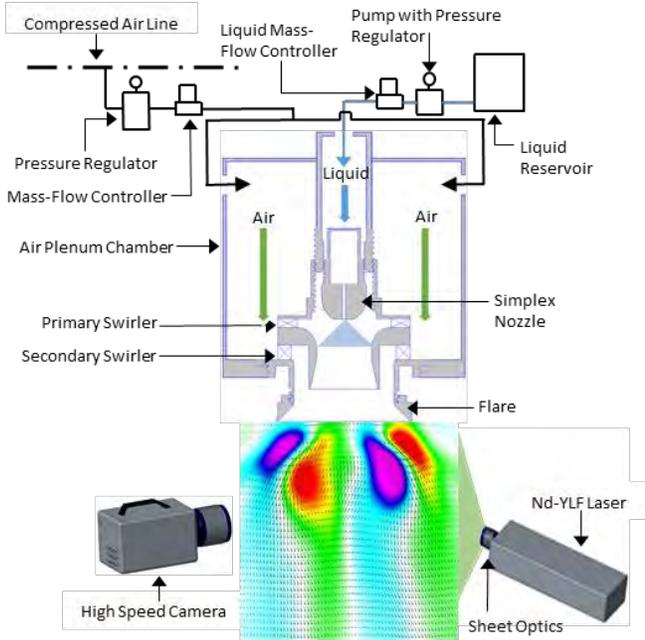
FIGURE 1. SCHEMATIC OF EXPERIMENTAL SETUP

Presently, the effect of exit expansion angle on the flow-field of a dual-swirl injector is investigated with the help of high speed PIV. The results show that there is a significant influence of the exit expansion angle on the CTRZ characteristics. Large angles cause the CTRZ to weaken drastically and results in flow unsuitable for flame stabilization in combustors.

EXPERIMENTAL SETUP

The experimental setup consists of dual-swirl injector and a simplex or pressure swirl liquid nozzle mounted vertically. The injector is manufactured by rapid prototyping using nylon based PLA. The dual-swirl injector has two radial swirlers arranged in counter-rotating configuration. Swirl number of individual swirlers is calculated using Eqn. (1), obtained by H.J. Sheen et al [6]. The primary and
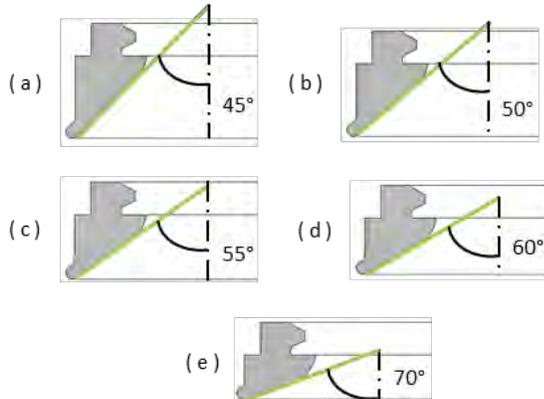

FIGURE 2. DESIGN OF FLARE GEOMETRY

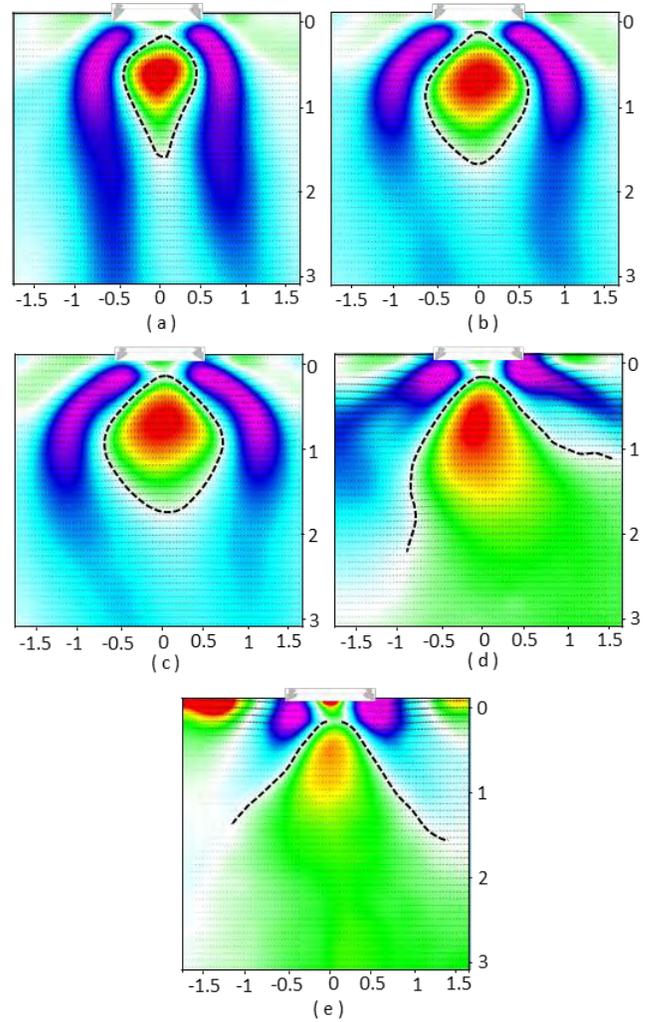a) CASE 1 b) CASE 2 c) CASE 3 c) CASE 4 d) CASE 5

FIGURE 3. AXIAL VELOCITY CONTOURS SHOWING CTRZ BOUNDARY
a) CASE 1 b) CASE 2 c) CASE 3 d) CASE 4 e) CASE 5

secondary swirlers have swirl numbers 0.77 and 1.14 respectively. The exit expansion angle of the injector is varied by using interchangeable flares attached using a screw thread. Four flare configurations with half angles 45°, 50°, 55°, 60° and 70° (Figure 2) are utilized. Exit diameter of the flares is kept unchanged at 45mm.

TABLE 1. CASES CONSIDERED

Case	Exit-Expansion Angle
1	45°
2	50°
3	55°
4	60°
5	70°

Working fluids used are air and water. Flow of air is controlled using a pressure regulator, and a mass-flow controller manufactured by Alicat Inc. Water flow is controlled using a needle valve and is measured using an inline rotameter. Air and water are supplied at a constant flowrate of 2900 lpm (56.56g/s) and 0.15lpm (2.5g/s) respectively.

Water is supplied to a simplex nozzle via a pump with differential pressure of 150 KPa. The simplex nozzle rated for 4 gph generates a hollow cone spray with spray angle of 90°. All experiments are carried out with non-reactive flow, at isothermal conditions in quiescent environment. A large collection chamber is used to collect spray produced by the injector. High-speed PIV is used to obtain flowfield downstream of the injector.

High-speed PIV system consists of a dual-pulsed high speed Nd:YLF laser (wavelength: 532nm, pulse energy: 30mJ) with sheet optics to obtain a thin sheet of 1mm thickness. A Photron SA5 high-speed camera high speed camera positioned orthogonally to the laser sheet is used to image the flow. 2000 double-framed raw images at 3500 Hz with a resolution of 1024x1024 are captured per case. A commercial PIV post processing package Davis 8.4 from Lavision GmbH is used to reconstruct vector fields from the raw images. PIV is carried out with droplets produced by injector; no external tracer particles are introduced.

$$S = 0.28 \cdot \left(\frac{1}{1-\Psi}\right) \cdot \left(\frac{tan\Phi}{1+tan\Phi.tan(\pi/Z)}\right) \quad (1)$$

Where $\Psi = \dfrac{Z.t}{2.\pi.R_{inner}.cos\Phi}$

RESULTS AND DISCUSSION

The global flow-field downstream of the dual-swirl injector is captured. In the following sections a detailed comparison of mean quantities in the flow-field as well as the distribution of turbulent kinetic energy is presented. Mean quantities are obtained from time-averaged reconstruction of instantaneous high speed PIV images. Length scales and velocity components have been normalised using exit diameter of flare (45mm) and average bulk axial velocity with respect to flare exit diameter (30.39 m/s).

Axial Velocity and extent of CTRZ

A strong swirling flow is observed which results in an adverse pressure gradient along the central axis of the swirler. This low pressure zone results in flow reversal and forms a recirculation zone. This zone is bounded by iso-surface of zero axial velocity and is known as CTRZ. A
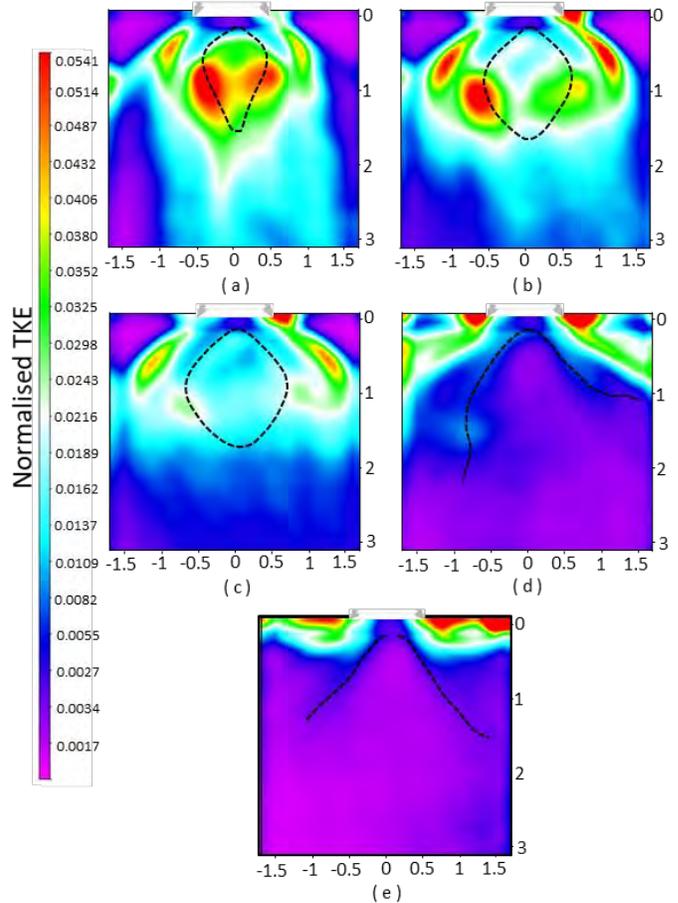
FIGURE 4. NORMALIZED TKE CONTOURS
a) CASE 1 b) CASE 2 c) CASE 3 d) CASE 4 e) CASE 5

well-defined CTRZ was observed for Case 1, Case 2 and Case 3.

Case 1, (Figure. 3 (a)), shows as a small but strong CTRZ with maximum V_{axial} of -0.71. Flow exiting the injector envelopes the CTRZ. This flow has annular-jet like structure and does not expand further downstream. This is due to the restrictive effect of the low-pressure region around the centreline. It is further elucidated by slight flow convergence observed downstream of the CTRZ.

Case 2 and case 3 show that the CTRZ widens in size (Figure 3 (b), (c)) and thus weakens; a result of mass continuity. As CTRZ weakens the enveloping flow experiences less inward-directed restoring force and it expands outwards. In the first 3 cases the enveloping flow showed some convergence downstream of the CTRZ, implying that a region of low pressure persists along the centreline. CTRZ for Case 2 and Case 3 has maximum reverse V_{axial} of -0.62 and -0.57 respectively.

A well-defined CTRZ structure was absent for case 4 and case 5 (Figure 3 (d), (e)). In case 4 the exiting flow had expanded to an extent that the low pressure was too weak to

overcome the outward momentum of the expanding flow. Maximum reverse V_{axial} for case 4 is -0.43.

For Case 5, the exiting flow was completely expanded. The low pressure zone along the centreline is weakest and exerts negligible restoring for on the flow exiting the injector does so at an angle of almost 180°. This type of flow has been termed as a conical breakdown. Maximum V_{axial} is noted to be -0.35 and is least amongst all cases considered.

Turbulent Kinetic Energy

Normalized TKE is calculated using post-processing software, Davis 8.4 from LaVision GmbH. Davis 8.4 uses RMS velocities obtained from PIV to compute TKE values. TKE contours show regions with maximum turbulence and therefore mark locations for mixing of air and dispersed liquid phase. High TKE values are observed at shear layer formed at CTRZ boundary [7] and enveloping flow and outer shear layer between enveloping flow and quiescent air.

Normalized TKE distribution for Case 1 (Figure 4 (a)) shows region of global maximum with peak value of 0.0537. It lies at the boundary of CTRZ and its enveloping flow. Besides global maxima, regions of local maxima exist in the outer shear layer between flow existing the injector and quiescent environment. Local maximum have value around 0.0480.

In Case 2 (Figure 4 (b)), loci of maximum TKE is similar to Case 1. Regions of local maxima are larger relative to Case 1. Global and local maxima are closer compared to Case 1. The CTRZ is larger and relatively less turbulent as a whole. Maximum TKE at CTRZ boundary and in the outer shear layer is greater than that for Case 1 with value 0.0596 and 0.0561 respectively.

Case 3 (Figure 4 (c)) shows that overall TKE has decreased. Global maxima is now located in the outer shear layer. Turbulence present in the CTRZ is much lower compared to both Case 1 and Case 2. Maximum normalized TKE in the outer shear layer is 0.0529 and at CTRZ boundary is 0.0368.

Case 4 and Case 5 (Figure 4 (d), (e)) have extremely weak flow recirculation. TKE around the centerline for Case 4 is much less and negligible for Case 5 when compared with previous cases. Maximum TKE is seen to be flare exit where flow interacts with quiescent air.

SUMMARY AND CONCLUSION

A detailed study on the effect of exit expansion angle on the flowfield of a dual-swirl injector was carried out. The exit expansion angle was controlled by using interchangeable flares. On increasing the flare angle, flow exits the injector at roughly the same angle as the flare. This can be explained by Coanda effect which causes the flow to adhere to the flare surface. Yet, on increasing angle above a

limit (Case 5) the flow exits at an angle greater than that of the flare. With increase in flare angle, CTRZ increased in size but weakened. Weakening of CTRZ resulted in lower reverse velocity. This caused the inner shear layer to be less energetic as evidenced by the shift in location of maximum TKE from the CTRZ boundary to outer shear layer.

The breakdown of CTRZ observed in Case 4 and Case 5 shows negligible recirculation with TKE concentrated near injector exit. Case 2 showed good recirculation with presence of high TKE at the CTRZ boundary and in the outer shear layer. This case is the ideal configuration for good mixing and flame stabilization.

In conclusion, the exit-expansion angle is an essential parameter for controlling flame stabilisation and mixing. Downstream flow is very sensitive to changes in this angle and small changes result in drastic changes in flow. This shows that further investigations into the flow dynamics of the dual-swirl injector need to be carried out. A well-designed flare will considerably improve combustion efficiency and reduce emissions and avoid unsuitable flow such as the one observed in Case 4 and Case 5.

REFERENCES

[1] Beér, J.M. and Chigier, N.A., 1972. Combustion aerodynamics. New York.

[2] Wang, H., McDonell, V.G., Sowa, W.A. and Samuelsen, S., 1994. Experimental study of a model gas turbine combustor swirl cup, part I: Two-phase characterization. Journal of Propulsion and Power, 10(4), pp.441-445.

[3] Wang, H.Y., McDonell, V.G. and Samuelsen, S., 1995. Influence of Hardware Design on the Flow Field Structures and the Patterns of Droplet Dispersion: Part I—Mean Quantities. ASME J. Eng. Gas Turbines Power, 117(2), pp.282-289.

[4] Ateshkadi, A., McDonell, V.G. and Samuelsen, G.S., 1998, January. Effect of hardware geometry on gas and drop behavior in a radial mixer spray. In Symposium (International) on Combustion (Vol. 27, No. 2, pp. 1985-1992). Elsevier.

[5] Estefanos, W., Tambe, S. and Jeng, S.M., 2015. A Study of the Mean and Dynamic Behavior of the Swirling Flow Generated by a Counter Rotating Radial-Radial Swirler Using a Water Test Rig. ASME Paper No. GT2015-43464.

[6] Sheen, H.J., Chen, W.J., Jeng, S.Y. and Huang, T.L., 1996. Correlation of swirl number for a radial-type swirl generator. Experimental thermal and fluid science, 12(4), pp.444-451.

[7] Rajamanickam, K. and Basu, S., 2017. Insights into the dynamics of spray–swirl interactions. Journal of Fluid Mechanics, 810, pp.82-126.

SEEC-2018-167

RESILIENCE OF THERMOCLINE TO FLOW DISTURBANCES IN A THERMAL ENERGY STORAGE SYSTEM

Sandeep Hatte
Department of Mechanical Engineering
Indian Institute of Science
Email: sandeephatte92@gmail.com

Bhaswati Gohain Barua
Department of Mechanical Engineering
Indian Institute of Technology Guwahati
Email: gb.bhaswati96@gmail.com

Vinod Srinivasan
Department of Mechanical Engineering
University of Minnesota
Email: vinods@umn.edu

Saptarshi Basu
Department of Mechanical Engineering
Indian Institute of Science
Email: sbasu@iisc.ac.in

ABSTRACT

Thermocline based thermal energy storage system (TES) is a low-cost solution to store energy in concentrated solar power (CSP) plants. The performance of these storage devices is subjected to the operating conditions (charging and discharging) and environmental boundary conditions. Due to variability of solar radiation throughout the day, TES system experiences variability in the heat loads during charging. In the present study, numerical simulations are conducted to analyze the effects of inlet flow disturbances on the performance of thermocline based thermal energy storage system. During charging, flow disturbances are introduced at different initial velocities from the inlet at colder temperature for a short duration. With time, disturbance grows in size and interacts with the thermocline causing mixing across the stratified medium. The abrupt mixing and thermocline oscillations come to rest and a new thermocline is formed at the end. The extent of mixing in the region of thermocline determines the thickness of newly formed thermocline. Relative increase in thermocline thickness which determines the performance of a TES system is observed to be a function of inlet flow disturbance velocity.

Keywords
Thermal energy storage, thermocline, flow disturbance
.

NOMENCLATURE

At	Atwood number $((\rho_c - \rho_h)/(\rho_c + \rho_h))$
D	Diameter of the tank, m
g	Acceleration due to gravity, m/s^2
H	Height of the tank, m
L_P	Penetration length, m
$L_p{}^*$	Non-dimensional penetration length, (L_P/H)
p	Pressure, Pa
T	Temperature, k
t	Time, s
v	Axial velocity, m/s
δ	Thermocline thickness, m
δ_0	Initial thermocline thickness, m
ρ	Density, kg/m^3
$\widetilde{\tau}$	Viscous stress tensor, Pa
τ	Time scale for Rayleigh-Taylor instability $((H/(\mathrm{At}_d\, g))^{1/2})$, s
τ^*	Non-dimensional time during disturbance evolution (t/τ)
θ	Non-dimensional temperature $((T - T_c)/(T_h - T_c))$
ω	Vorticity, 1/s

Subscripts

c	Cold fluid
h	Hot fluid
d	Disturbance fluid

INTRODUCTION

The intermittent supply of solar energy affects the performance of solar powered systems. For concentrated solar power (CSP) plants the demand of constant rated power is not met because of the variability in the solar radiation throughout the day and its non-availability during night. Thermal energy storage system is the solution to correct this mismatch between the demand and supply of energy in CSP plants [1]. During daytime, the heat transfer fluid (HTF), in present study; molten salt, heated in the solar field is directed towards the thermal energy storage system (initially filled with cold HTF). Single tank thermocline based thermal energy storage system is found to be cost efficient than using a two tank system [2]. In thermocline based system, the most common method of storing energy is by means of creating a sharp region of interaction between the hot and cold HTF. With an optimum flow rate of hot fluid from the top of the tank a thin region of interaction can be created with a sharp increase in temperature across the interface known as thermocline. Stability and the stratification of the thermocline are directly related to the performance of the thermal energy storage system, which are very sensitive towards the mixing caused by the incoming fluid. The inertia of the charging fluid (kinetic energy) and the restoring buoyancy force acting against it dictates the relative strength of the incoming fluid causing disruption of the thermocline, thereby decreasing the operational performance of the TES system.

. The stratification and performance of TES systems can be quantified in terms of the thickness of thermocline. The dynamic thickness of thermocline depends upon different operating parameters such as thermo-physical properties of the inlet charging fluid, hot-cold fluid temperatures [3-5]. The undesirable mixing caused by different flow instabilities reduce the performance of thermocline. For a colder fluid disturbance, the Rayleigh-Taylor instabilities cause the entrainment of cold fluid into the hot fluid and enhance the mixing across stratified interface [6]. Previous studies on the dynamic interaction of inlet flow disturbance and thermocline were focused on the effects of inflow temperature [7], oscillations in the thermocline region and the subsequent cyclic operations [8]. However, very few studies have explored the effects of the strength of inlet fluid disturbance on the performance of thermocline based thermal energy storage system. In the present study, the resilience of thermocline to inlet fluid flow disturbances of different initial velocity values is studied. The insights into the growth and evolution of disturbance fluid due to the presence of Rayleigh-Taylor instabilities, its interaction with the thermocline and the subsequent mixing dynamics causing the degradation of thermocline are presented in details.

PROBLEM DESCRIPTION

Dynamic interaction of inlet flow disturbance and thermocline is governed by the conservation of mass, momentum, and energy, as per the following mathematical formulations:

$$\frac{\partial \rho}{\partial t} + \nabla \cdot (\rho \vec{v}) = 0 \tag{1}$$

$$\frac{\partial}{\partial t}(\rho \vec{v}) + \nabla \cdot (\rho \vec{v} \vec{v}) = -\nabla p + \nabla \cdot \tilde{\tau} + \rho \vec{g} \tag{2}$$

$$\frac{\partial}{\partial t}(\rho E) + \nabla \cdot (\vec{v}(\rho E + p)) = \nabla \cdot (k \nabla T) \tag{3}$$

Temperature profile in the rectangular TES tank of dimensions 1000mm×1000mm is initialized as:

$$T(y) = T_c + \frac{T_H - T_c}{1 + e^{-m(y-n)}} \tag{4}$$

where, m: sharpness of the temperature rise; n: position of the thermocline (500mm), operating temperatures T_H and T_c are 650k and 550k respectively. A narrow axisymmetric part at the top (40mm) is considered as an inlet for the inception of disturbance fluid at temperature 645 k for a duration of 11s. At the end of 11s, the inlet flow is stopped and the subsequent phenomena of growth and interaction of disturbance with thermocline is studied for another 51s. A parabolic velocity profile is considered for the inlet fluid flow. In the present study, the strength of inlet flow disturbance is varied by varying the maximum inlet flow velocity values across 5 different cases as described in Tab. (1).

TABLE 1:

| Case number	Maximum inlet velocity (m/s)
1	0.06
2	0.12
3	0.18
4	0.24
5	0.30

Governing equations were numerically solved at each grid point in ANSYS FLUENT software [9]. The grid independence analysis was conducted for case 3 on three grids; coarse grid: 250×250, adopted grid: 500×500, and fine grid: 1000×1000. The average velocity and temperature values were obtained within an error of 1.5 % and 0.8 % respectively. A SIMPLE algorithm was used for the coupling of pressure and velocity. The scaled residuals of 10^{-5} were used for the convergence of mass, momentum, and energy equations. A time step of 0.01 was used for the entire simulations.

RESULTS

Time is non-dimensionalized by the time scale of Rayleigh-Taylor instability $\left(\tau^* = \frac{t}{\tau}\right)$.

Flow Disturbance-Thermocline Interaction

A disturbance fluid is inserted from the narrow region located at the top of the tank at a temperature 645k with a parabolic velocity profile. The Rayleigh-Taylor instabilities cause the rolling up of disturbance fluid as it moves downwards under the influence of gravity [6]. With time, the size and shape of the rolled up disturbance fluid structure changes before interacting with the thermocline as shown in Fig. (1).
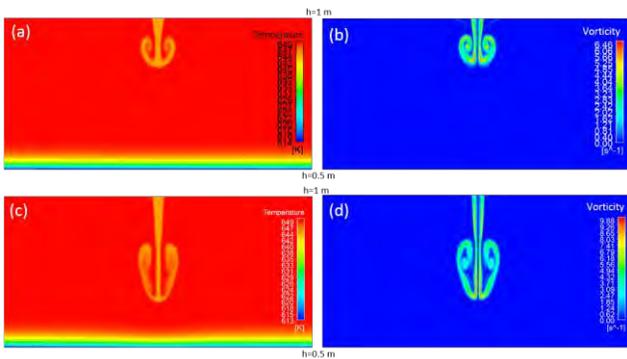
FIGURE 1. Growth of flow disturbance in the form of (a) temperature and (b) vorticity contours at $\tau^* = 0.45$; and (c) temperature and (d) vorticity at $\tau^* = 0.82$ for case 1.

During the interaction of disturbance fluid with thermocline, an opposing buoyancy force exerted by the high density fluid surrounding the flow disturbance retards its motion. The relative strength of buoyancy and inertia forces defined by Richardson number decides the maximum penetration of disturbance fluid in a TES system as shown in Fig. (2).
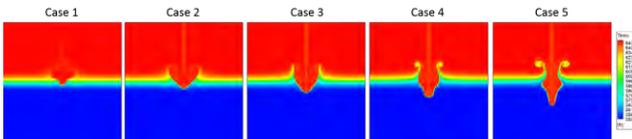
FIGURE 2. Contours of temperature at the instance of maximum penetration of disturbance fluid.

Fig. (3) shows the position of disturbance fluid in TES system for all 5 cases. It is to be noted that the maximum penetration length, defined by the first local maxima in Fig. (3) increases while the time instance of its occurrence decreases with increase in inlet velocity of disturbance fluid. The reference markings of the upper and lower limits of thermocline in Fig. (3) aids in understanding the

disturbance penetration dynamics with respect to thermocline position and thickness.
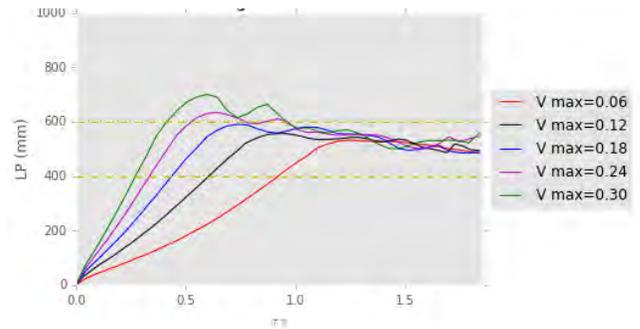

FIGURE 3. Track of inlet flow disturbance in TES system across all five cases

For case 1, disturbance fluid does not penetrate the thermocline and floats in the middle region of thermocline, while for case 5 disturbance fluid penetrates all the way below the thermocline and causes mixing between hot and cold fluid regions across the interface.

Thermocline Performance

As a result of the stable configuration of thermocline (positive density gradient in the direction of gravity) any kind of disturbance will eventually come to rest. But the extent of mixing in the region of thermocline dictates the formation of new thermocline. The axial temperature distribution of the new thermocline at the end of 60s is shown in Fig. (4).
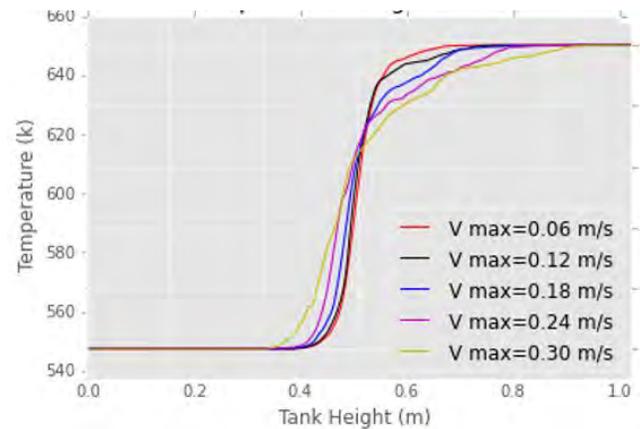

FIGURE 4. Axial distribution of temperature at 60s across all five cases

The widening of thermocline region (Fig. (4)) shows the increased degradation of thermocline with increase in inlet flow disturbance velocity. As described in Eqn. (1) the value of 'm' determines the sharpness of the thermocline. In the present study, the thickness of thermocline (δ) is defined as:

$$\delta = 4 \int_{y=0}^{y=H} \theta(1 - \theta)\, dy \qquad (5)$$

Fig. 5 shows the transient increase in thermocline thickness across all five cases. The small oscillation in the thermocline thickness values represent the unsettling of disturbance fluid and potential of mixing.
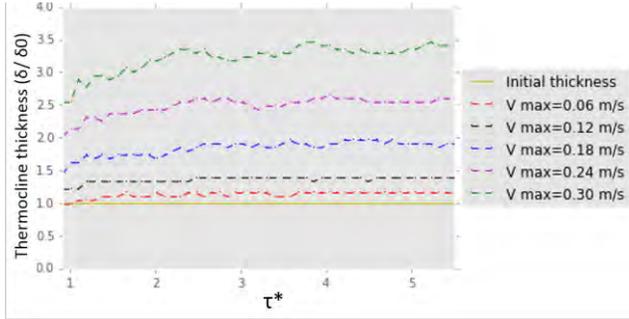

FIGURE 5. Transient variation of thermocline thickness across all five cases

With time as the mixing stops, the oscillations decay and thermocline thickness value saturates to a new value as seen in Fig. 5. The relative increase in thermocline thickness value $\left(\frac{\delta - \delta_0}{\delta_0}\right)$ at the end of 60s is observed to be correlated to the inlet flow disturbance velocity as;

$$\frac{\delta - \delta_0}{\delta_0} = 26.63 \times V_{max}^2 \qquad (6)$$

The potential of mixing during the interaction of inlet flow disturbance with thermocline can be quantified in terms of average vorticity at any time t in the TES tank as:

$$\bar{\omega}(t) = \frac{1}{H} \int_{y=0}^{y=H} \omega(t)\, dy \qquad (7)$$
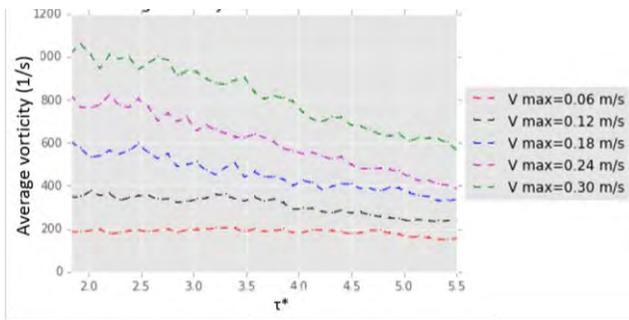
FIGURE 6. Transient variation of average vorticity in a thermal energy storage tank.

From Fig. (6) it is evident that the increase in values of average vorticity for higher inlet flow disturbance fluid velocity indicates the greater extent of mixing in TES tank.

With progressive time the average vorticity curve saturates to a minimum value showing the stability of the newly formed thermocline.

CONCLUSION

In the present study, the dynamic interaction of inlet flow disturbance and thermocline is studied in details. The effects of flow disturbances on the performance of thermocline TES are analysed by quantifying the response of thermocline in term of transient thickness variation, average vorticity variation and disturbance penetration dynamics. It is observed that the relative increase in thermocline thickness value is correlated to the velocity of inlet flow disturbance.

REFERENCES
[1] Gil, A., Medrano, M., Martorell, I., Lázaro, A., Dolado, P., Zalba, B., and Cabeza, L. F., 2010. "State of the art on high temperature thermal energy storage for power generation. Part 1-Concepts, materials and modellization". Renewable Sustainable Energy Review, 14, pp. 31–55.
[2] Pacheco, J. E., Showalter, S.K., and Kolb, W.J., 2002. "Development of a molten-salt thermocline thermal storage system for parabolic trough plants". Journal of Solar Energy Engineering, 124, pp. 153-159.
[3] Flueckiger, S.M., Yang, Z., and Garimella, S. V., 2013. "Review of Molten-Salt Thermocline Tank Modeling for Solar Thermal Energy Storage". Heat Transfer Engineering, 34, pp. 787–800.
[4] Qin, F.G.F., Yang, X., Ding, Z., Zuo, Y., Shao, Y., Jiang, R., and Yang, X., 2012. "Thermocline stability criterions in single-tanks of molten salt thermal energy storage". Appled. Energy, 97, pp. 816–821.
[5] Yang, Z., and Garimella, S. V., 2010. "Thermal analysis of solar thermal energy storage in a molten-salt thermocline". Solar Energy, 84 pp. 974–985.
[6] Manu, K.V., Deshmukh, P., and Basu, S., 2016. "Rayleigh–Taylor instability in a thermocline based thermal storage tank". International Journal of Thermal Science, 100 pp. 333–345.
[7] Manu, K. V., Anand, P., Chetia, U.K., Basu, S., 2015. "Effects of instabilities and coherent structures on the performance of a thermocline based thermal energy storage". Appled Thermal Engineering, 87, pp. 768–778.
[8] Hatte, S., Mira-Hernandez, C., Advaith, S., Tinaikar, A., Chetia, U.K., Manu, K.V., Chattopadhyay, K., Weibel, J.A., Garimella, S.V., Srinivasan, V. and Basu, S., 2016. "Short and long-term sensitivity of lab-scale thermocline based thermal storage to flow disturbances". Applied Thermal Engineering, 109, pp. 936-948.
[9] ANSYS, Fluent 15.7.0, (2014).

SEEC-2018-168

A QUALITATIVE STUDY OF HYBRID EFFERVESCENT-AIR BLAST ATOMIZER

Swapneel Roy	**Kuppuraj R**	**Saptarshi Basu**
Department of Mechanical Engineering	Department of Mechanical Engineering	Department of Mechanical Engineering
Indian Institute of Science	Indian Institute of Science	Indian Institute of Science
Email: swap.roy88@gmail.com	Email: kuppurajr@iisc.ac.in	Email: saptarshibasukol@gmail.com

ABSTRACT

Various industries such as food processing, spray drying etc., implement spray nozzles for fine atomization which can produce extremely small droplet size (≤10 μm). In addition to the droplet size, its momentum too has equal importance in high-speed combustion systems like scramjets, pulse detonation engines for rapid mixing. Many of the nozzles which adopt standalone techniques (pressure, air-assist) fail to produce finer size droplets. The focus of this study has been to hybridize two or more techniques to achieve the finer atomization. The combination of effervescent and co-axial external air has shown significant reduction in droplet sizes at lower pressure ranges in contrast to, more traditional atomization techniques. The proposed hybrid nozzle is discussed at length in this study.

Keywords>: *Effervescent atomization, hybrid atomizer*
.

NOMENCLATURE
<Times New Roman, 10 pt, left aligned.>.
EA   Effervescent Atomizer
EAA   Effervescent Air-assist Atomizer
HSA   Hybrid Swirl Air-assist Atomizer

INTRODUCTION
Conventional atomizers, used in combustion systems or in other industrial applications like airblast and pressure jet offer high momentum, but for the several limitations, the minimum droplet size is limited to ~40–50 μm [1]. In standalone airblast and pressure atomizing nozzles, even at very high air velocity/injection pressure, the liquid jet exhibits poor atomization performance very close to the injector. This phenomenon leads to bigger droplets in that zone. To meet the size requirements, studies have been carried out to promote atomization in these atomizers by supplementing with other non-traditional techniques. The main idea behind hybrid atomizer is to disrupt or reduce the intact portion of the liquid jet before it interacts with coaxial air flow.

Effervescent atomization is a method of twin fluid atomization that involves bubbling a small amount of gas into the liquid before it is ejected from the atomizer [1]. The principle of working is marginally different from internal and external mixing twin fluid air atomizing nozzles. Effervescent atomization technique was developed in late 1980s by Lefebvre and co-workers [2-5].

Advantages over conventional pressure, rotary and twin fluid atomizers [1]:
- good atomization can be achieved at injection pressures that are several times lower than those required by others type of atomizers
- gas flow rates are much smaller than those employed in most other forms of twin fluid atomization
- exit orifice are larger than those of other atomizer types having a comparable flow rate. This alleviates clogging problems and facilitates atomizer fabrication
- in combustion applications, effervescent atomizer produced sprays are conducive to lower pollutant emissions due to the presence of air in spray cone
- flow velocities in the discharge orifices are much lower than those encountered in conventional

atomizers because two-phase flows choke at significantly lower velocities than single phase flows. This reduces orifice erosion when handling liquids with solid suspensions. The device is simple, rugged and reliable. Requires little or no maintenance and can be operated at low cost [6].

EXPERIMENTAL SET-UP

The proposed hybrid nozzle combines the above-mentioned advantages of effervescent atomization with that of air-blast (co-axial flow) technique to achieve even smaller droplets through secondary atomization at nozzle exit plane. With the capability to operate in three different modes, the hybrid nozzle can produce droplets as required for the operation. Figure 1 shows the droplet size reduction for various mode of operation.

The atomizer consists of three distinct parts; namely, Aerator tube, Inner nozzle body and external air nozzle body. All parts are detachable for ease of maintenance. The aerator tube is a hollow 3 mm stainless steel tube of length 160 mm. The tube is blocked at the far end and is drilled with having 12-24 equidistant (at 10 mm apart) circular holes of 0.5mm. This tube in supplied with compressed air at 5 bar pressure. Air is only allowed to escape only through these passages (holes). This aerator tube is placed within the inner nozzle body and is tightly sealed to deny any leakages.

The inner nozzle body, with exit orifice (d_o) of 2mm and an inner tube diameter of 6mm, facilitates supply of liquid and external air conduits. The liquid surrounding the aerator tube forms a two-phase bubbly mixture when pressurized air is supplied through aerator tube. The bubbles in the two-phase mixture consequently burst upon exposure to atmospheric pressure. Based on the principle of effervescent atomization, it forms the integral part of this hybrid atomizer. This is the primary atomization stage of this atomizer.

The external air passages provided through the inner nozzle body make way to a detachable external stainless steel conical nozzle with an exit diameter of 10 mm. The volume between the inner and external bodies is filled with a honeycomb structure to maintain air flow to laminar regimes and support the inner tube concentrically. Both the exits of the nozzles meet at the same plane. Hence the external air meets the droplets at the exit of the inner tube. The external air mixing increases the momentum of the droplets providing a secondary break-up of droplets, increasing the velocity of jet flow and increasing the penetration length.
The internal air supply to aerator tube can be operated between 0-5 bar and this supply pressure can be varied to control the droplet size and velocity. The external air was

supplied at 400 lpm at a pressure of 10bar. The atomizer was operated within 0-10% air-to-liquid ratio.

The experimental diagnostics involved both global as well as local measurements. Global measurement was done with the help of high pulse rate LED strobe lamp synchronized with camera shutter. The images are acquired at 7500 frames/s at a different field of view (FOV). Large FOV (80 mm × 80 mm) yields a global picture of the spray, from which breakup length, spray spread, atomization quality of the droplets are quantified. The near-nozzle breakup, particularly bubble formation and breakup, jet oscillations are delineated with small FOV (40 mm × 40 mm). The droplets size information at various operating conditions of the spray is acquired with the help of long distance microscope (LDM). To acquire the time-frozen snapshot of the droplet contour, low pulse duration (5 ns) laser light is used as an illumination source. The LDM is coupled with 2 × magnification lens to focus onto a small region of the spray (1.5 mm × 1.5 mm). Further, the acquired images are post-processed in MATLAB to yield droplet size. Throughout the experiments, water flow rate is maintained constant, while air flow rate across aerator tube and outer nozzle body (coaxial air) is progressively varied in different proportions.

RESULTS

Droplet sizes (SMD) have shown significant drop for hybrid nozzles (EAA and HSA) in comparison to effervescent nozzle (EA) as shown in figure 1. With only efferverscent nozzle, the lowest SMD observed was 45 µm, while the SMD for hybrid nozzle the SMD dropped to 17 µm at comparable flow conditions. The effect of the secondary atomization is evident from figure 2. With increasing internal air pressure the droplet sizes decresases, consequently SMD diminish. It is also observed that the reduction in droplet size for effervescent atomizer (EA) stagnates much earlier than hybrid nozzles (EAA AND HSA), hence limiting further atomization. Secondary atomization in form of external air-assist at 400 lpm breaks down the droplets further while limiting occurrence of larger droplets as shown in figure 2, hence lowering SMD. At the same internal air pressure (2.6 bar) figure 2 shows a noticeable difference between three modes of nozzle operation, where large droplets of the order of 150 µm can still be observed for effervescent mode but with the addition of external air at 400 lpm, there seems to be an even spread of droplet size of much smaller droplet sizes (4-20 µm).

The nozzle has also been tested with both swirl and straight inlet ports. The droplet sizes were comparable but the angle of dispersion (cone angle) was significantly greater for the swirl vanes as shown in Table 1.
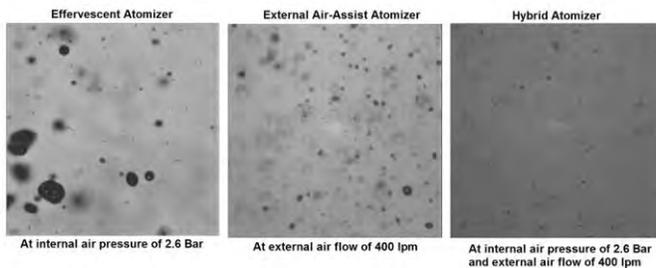
FIGURES
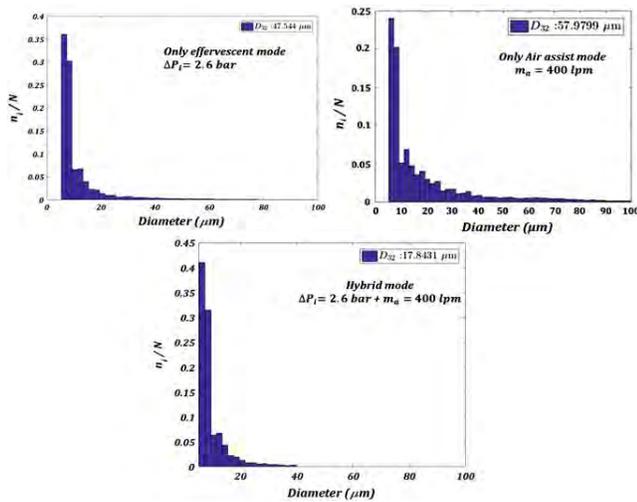
FIGURE 1. Drolpet distribution and SMD at various conditions
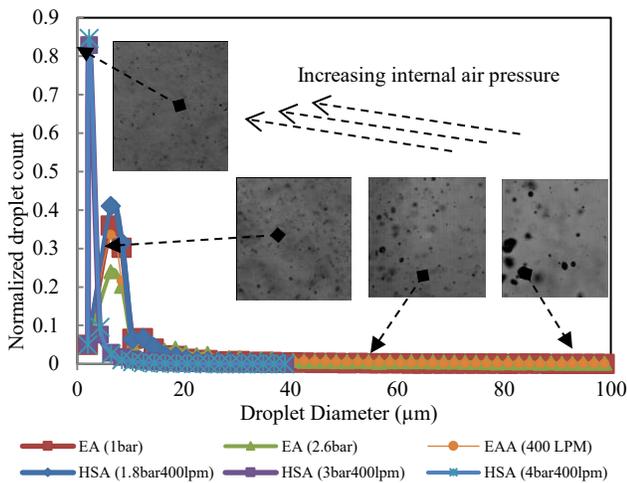
FIGURE 2. Normalized droplet count vs Droplet diameter- with increasing internal air pressure

FIGURE 3. Droplet size reduction in three modes

Table 1: Cone angles for various modes

Atomizer configuration		Cone Angle (degrees)
Effervescent (Mode 1)		22-30
External Air-assist (Mode 2)	No swirl	<20
	With swirl	>50
Hybrid (Mode 3)	No swirl	<20
	With swirl	>50

REFERENCES

[1] Chin, J. S., Lefebvre, A. H., "A Design procedure for Effervescent Atomizers", Journal of Engineering for Gas Turbines and Power, Transactions of the ASME, Vol. 117, APRIL 1995, pp. 266-271.

[2] Sovani, S.D., Sojka, P.E., Lefebvre, A.H., "Effervescent atomization", Progress in Energy and Combustion Science 27 (2001), pp. 483-521.

[3] Li, J., Lefebvre, A. H., Rollbuhler, J. R., "Effervescent Atomizers For Small Gas Turbines", International Gas Turbine and Aeroengine Congress and Exposition, The Hague, Netherlands, ASME, 1994.

[4] Lefebvre, A. H., "A novel method of atomization with potential gas turbine application", Indian Defence Science Journal, 1988; 38:353-62.

[5] Bayvel, L. P., Orzechhowski, Z., "Liquid Atomization", 1993.

[6] Jedelksy, J., Jicha, M., "Energy conversion during effervescent atomization", Fuel 111 (2013), pp. 836–844.

Gold Sponsors

TAFE

iNSERB India
Science and Engineering
Research Board (SERB)

Silver Sponsors

VOLVO

CATERPILLAR®

ONGC ENERGY CENTRE

TSI

Simpson & Co. Ltd

Tesscorn

Bronze Sponsors

Progress Rail
A Caterpillar Company

GAIL